Preface:

Sustainable development and its extensive domain affect every aspect of specialized activities including Civil Engineering with its vast and extensive scope. In this respect, protection of investments on concrete constructions on the one hand , and production and utilization of concrete materials in construction industry and its related issues like Analysis and Design, Durability, Strengthening, Maintenance, Quality Control, Environmental Considerations, Modern Constructional Technologies, Nano-Concrete, Concrete Constitutive Laws, on the other, have attracted the attention of researchers, planners and management authorities in various societies in considering concrete as an effective factor in the creation of sustainable development. Such characteristics have shaped a renowned, comprehensive and indispensable material from concrete, which plays an important role in various aspects of human life such as production, employment, environment and development in a rather significant manner. Behavioral complexities of this material, e.g. varying mechanical and physical properties exposed to diverse conditions, its behavior under different loading circumstances and development of properties like creep, shrinkage, dual action, bond between concrete and steel, slip, durability, corrosion etc, have all created a wide scope of research based on this material.

An in-depth knowledge and awareness of various scientific and technological developments on concrete and its related issues is conceivable only through an exchange of scientific and technical information by researchers and engineers across the globe. The Building & Housing Research Center, affiliated to the Ministry of Housing & Urban Development is honored to hold the 3rd International Conference on Concrete & Development, based on its functions and objectives. The Conference Secretariat at first stage received **195** Abstracts out of which **160** were accepted for preparation of full papers. At the second stage **143** Papers submitted by researchers from within the country and overseas, of which **101** (including **87** in English and **14** in Persian languages) were accepted by the Scientific Committee to be presented at Conference. The Conference CD-Proceeding totally includes **123** papers, out of which **17** Papers in Persian and **106** in English.

It is hoped that the proceedings will provide a fruitful background for up grading the Civil Engineering branch, with an emphasis on concrete materials and structures through an appropriate exchange of information between all researchers, scientists and industrial scholars.

We would like to take this opportunity to thank our esteemed keynote speakers and distinguished authors, as well as members of the Reviewing Committee for their invaluable contribution to the proceedings. A special note of acknowledgement is also due to the staff and personnel of the BHRC who worked tirelessly in laying the groundwork and carrying out the numerous tasks involved in the organization of the Conference.

Abbas Ali Tasnimi

Conference Secretary

Honorary President:	**M. Saeedi Kia**	**Minister of Housing and Urban Development**
Chairman:	**S. M. FatemiAghda**	**BHRC President**
Secretary:	**A.A. Tasnimi**	**Tarbiat Modarres University**

Scientific Committee

Prof. Ahmadi, Mohammad Taghi, Iran
Prof. Andrade, C, Spain
Prof. Bakens, Wim, Netherland
Dr. Bagheri, Ali Reza, Iran
Dr. Famili, Hormoz , Iran
Prof. Fourneir, B, Canada
Dr. Ghoddusi, Parviz , Iran
Prof. Gjorv, O, Norway
Prof. Habibi, Mohsen , Iran
Dr. Haj Kazemi, Hasan , Iran
Dr. Hariri, Mohammad Taghi, Iran
Prof. Hillemeier, I.B, Germany
Prof. Hooton, D, Canada
Prof. Haj Ebrahim Zargar, Akbar, Iran
Prof. Ichinose, Toshikasu, Japan
Prof. Joe, O, Japan
Prof. Kabayasava , Japan
Dr. Kazemi, Mohammad Taghi, Iran
Prof. Khalu, Ali Reza, Iran
Prof. Maheri, Mahmoud Reza , Iran
Prof. Milford, Rodney, South Africa
Prof. Moghaddam, Hasan , Iran
Dr. Marefat, Mohammad Sadegh , Iran
Dr. Nili, Mahmoud , Iran
Prof. Otani, Sh , Japan
Dr. Parhizkar, Tayebeh , Iran
Prof. Pahl, P.J, Germany
Prof. Rahaee, Ali Reza, Iran
Prof. Ramezanian Pour, Ali Akbar, Iran
Dr. Sarvghad Moghaddam, Abdolreza , Iran
Prof. Schiessel, p, Germany
Dr. Shayanfar, Mohsen Ali , Iran
Prof. Sheikh, Shamim, A ,Canada
Dr. Soltan Mohammadi, Masood , Iran
Prof. Stark, J, Germany
Dr. Taheri Motlagh, Ali , Iran
Prof. Tasnimi, Abbas Ali , Iran
Dr. Tadayon, Mohsen , Iran
Prof. Yokota, H, Japan
Dr. Zahedi, Morteza, Iran

Organizing Committee

Dr. S. M. FatemiAghda
Prof. A.A. Tasnimi
Dr. T. Parhizkar
Eng .Kh .Mokhtari
Dr. Gh. Raheb
Eng. M. Safdari
H .Alavi
D .Meshkini Teharni

Building and Housing Research Center
P.O. Box 13145-1696 Tehran. I. R. Iran
Tel : (+98)21-88267854
Fax : (+98)21- 88267854, 88259984
E-mail: iccd@bhrc.ac.ir
Website:www.bhrc.ac.ir

Table of Contents

CD2-KN01

A METHOD TO EVALUATE SEISMIC DEMANDS OF LOW-RISE RC BUILDINGS

Nanako Marubashi[1], Santiago Pujol[2], Toshikasu Ichinose[3], Mogens P. Nielsen[4]
[1]Assistant Professor, Yamaguchi University, Yamaguchi, Japan
[2]Assistant Professor, Purdue University, West Lafayette, Indiana, USA
[3]Professor, Nagoya Institute of Technology, Nagoya, Japan
[4]Emeritus Professor, Technical University of Denmark, Bygning, Denmark

ABSTRACT
A new methodology for design of low-rise RC building structures is proposed. This methodology uses base shear strength as the sole variable in the estimation of the maximum displacement demand. The formulation is applicable to 'asymmetric' ground motions exhibiting a large difference between the peak accelerations in opposite directions of motion, which result in larger inelastic displacement than symmetric ground motions. Conventional methods such as The Capacity Spectrum Method do not yield adequate results for such 'asymmetric' ground motions. The proposed method is effective if the period at the yield strength is smaller than 0.5 s, the base shear coefficient of the building is smaller than 0.4, and the ground motion is strong (PGA > 0.5g and PGV > 0.5 m/s).

Keywords: base shear strength, displacement demand, asymmetric ground motions

1. INTRODUCTION
The damage potential of ground motion is, arguably, estimated best in terms of the magnitude of the deformations induced on structures. In this article, we show results from analyses confirming that the correlation between an intensity measures commonly used to rank ground motion records, namely PGV, and displacement demand is poor. As a result, we concentrate on direct estimation of displacement demand, which is not only a good measure of damage potential but also the key parameter in the design and evaluation of building structures. Because there is much uncertainty in the problem, especially regarding the intensity of future ground motion, a simple method for estimation of displacement demand is preferable over a complex method. But simplicity ought not to compromise the quality of the answer. Several studies have proposed simplified procedures to estimate the maximum deformation of nonlinear single and multi-degree-of-freedom (SDOF and MDOF) systems. One of the most popular methods to estimate deformation demand of nonlinear structures was conceived by Freeman in 1975 [1]. It is known as The Capacity Spectrum Method and is used in design and evaluation provisions in the US (ATC-40, 1996 [2]) and Japan (Kuramoto, 2006 [3]). Although analytical studies have indicated the contrary, the available experience has not shown the results of the method to be inadequate. Its positive

record and its simplicity are the main reasons for its popularity among both academicians and practitioners. In this paper we take another look at the results obtained with the Capacity Spectrum Method (CSM). We do so motivated by the recent abundance of available ground motion records. Our computations show that the method is not sensitive to an attribute of strong ground motion that we have coined "asymmetry" for lack of a better term. By asymmetry we refer to the difference between the "positive" and "negative" peaks of a ground acceleration or velocity record. We quantify it using the absolute value of the ratio of the positive to the negative peaks. Our computations indicate that the response of nonlinear SDOF systems with short periods of vibration (T<0.6s) is in fact sensitive to asymmetry in the acceleration record.

In this article we propose a new design spectrum. The spectrum can be used to capture the effect of record asymmetry on structural response. It differs from the spectrum used in the CSM in that the one we propose refers to nonlinear response, rather than linear response. And it differs from other spectra for nonlinear response (Blume et al., 1961 [4]; Chopra 2006 [5]; Priestley 2007 [6]) in that we use base-shear strength, not initial period or frequency, as the independent variable (as the horizontal axis). We do not mean to suggest that response is not sensitive to initial period. What we are suggesting is simply that, for short-period structures, response is more sensitive to strength than to initial period.

2. METHODOLOGY

We study the potential effects of ground motion on structures by using SDOF systems (Figure 1a). Three hysteresis rules are considered as depicted in Figures. 1b, 1c and 1d. Figure 1b shows the force-displacement response for an elasto-plastic system, where Q_u is the yield force and K is the stiffness. The stiffness K is calculated using Eq. 1,

$$T = 2\pi\sqrt{m/K} \tag{1}$$

where m is the mass and T is the fundamental period. The force-displacement response of a rigid-plastic system is shown in Figure 1c. A rigid plastic system is simply a particular case within the elasto-plastic systems in which K is assumed to be infinite. We consider this case because the solution of the differential equation of motion for a system with infinite stiffness is simpler than the solution for a system with finite stiffness. Figure 1d shows the force-displacement response assumed for an oscillator with decreasing stiffness. Stiffness variations are computed using the formulation proposed by Takeda (1970) [7]. Fundamental period (T in Eq. 1) is computed the secant stiffness K shown in Figure 1d. The initial viscous damping factor is assumed 2% for the initial stiffness of each model. The damping coefficient is assumed to reduce in proportion to the tangential stiffness.

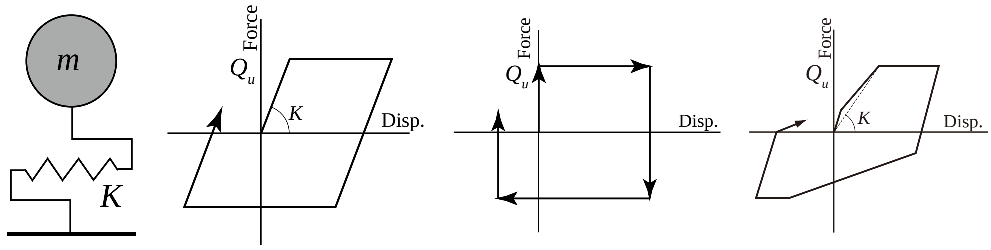

(a) SDOF **(b) Elasto-plastic** **(c) Rigid-plastic** **(d) Decreasing stiffness**

Figure 1. SDOF systems with various load-displacement responses

3. ASYMMETRY

The positive and negative peaks in ground acceleration and velocity records are different (Figure 2a, Erzincan 1992 record). The signs are a matter of convention. They are necessary but otherwise unimportant. We adopt the convention that accelerations and velocities are positive in the direction of the absolute acceleration or velocity maxima. The difference between the positive and negative peaks is usually ignored. To gain insight on the magnitude and the possible relevance of this difference, which we refer to as "asymmetry," we studied 2715 horizontal ground motion records published by PEER (2000) [8]. Figure 2b shows the ratio of the peak ground acceleration a_1 to the maximum acceleration in the opposite direction a_2 plotted against a_1. Ten percent of the records with a_1 exceeding 6 m/s^2 have a ratio a_1 / a_2 larger than 2.

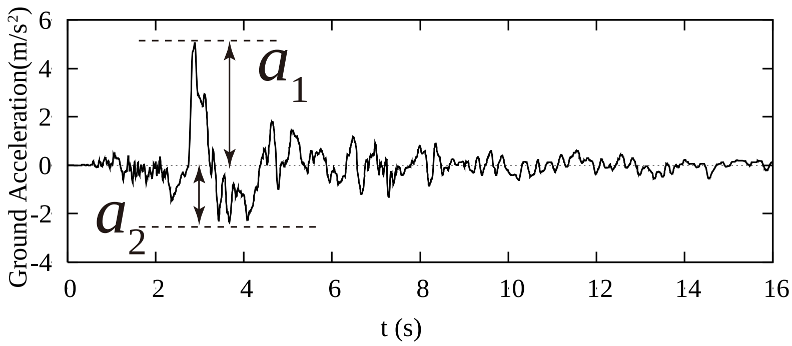

Figure 2. Erzincan 1992 record

To understand the effects of the asymmetry in records on system response we start by considering the simplified periodic motions shown in Figure 4. We consider three idealized acceleration records with equal (absolute) peak ground acceleration a_1: A1, A1.5, A2.5. The numbers following the letter A, which stands for "acceleration," are ratios of peak accelerations a_1/ a_2. Figure 2b indicates that ratios between 1 and 1.5 are common and a ratio of 2.5 is close to the upper bound for the records we have. Figures 4b and 4c show ground velocities and displacements computed by integrating the idealized signals A1, A1.5, and A2.5. Note that peak ground velocity and displacement decrease as we increase of the ratio a_1/ a_2.

Figure 5 shows linear response spectra computed for the idealized periodic motions shown in Figure 3 for a damping ratio of 10%. The spectra indicate that relative displacement and absolute acceleration tend to decrease with increases in the ratio of peak accelerations. In other words, the spectra would lead us to think that the "asymmetry" in the records we are considering is not detrimental, and in fact, one could argue that the spectra show it is beneficial.

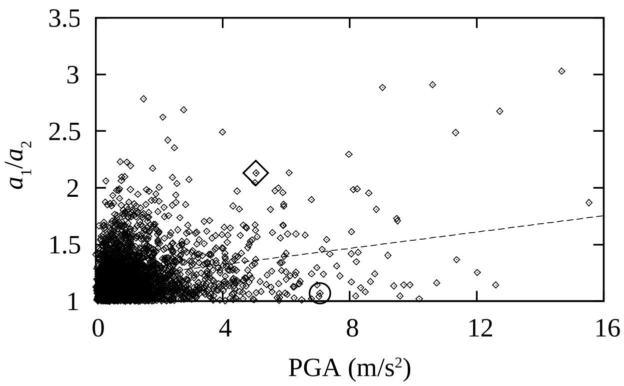

Figure 3. a_1/a_2 vs PGA (a_1)

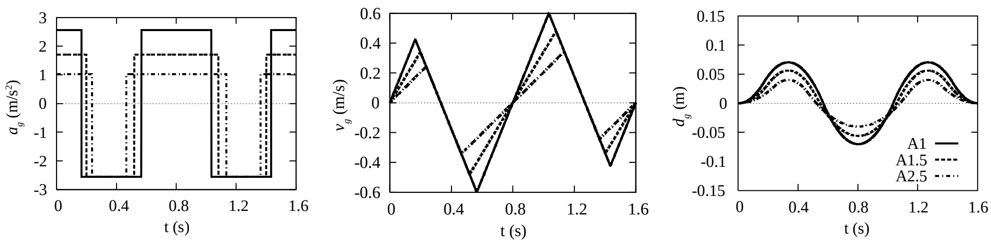

(a) Ground acceleration (b) Ground velocity (c) Ground displacement

Figure 4. Idealized records with asymmetric ground acceleration.

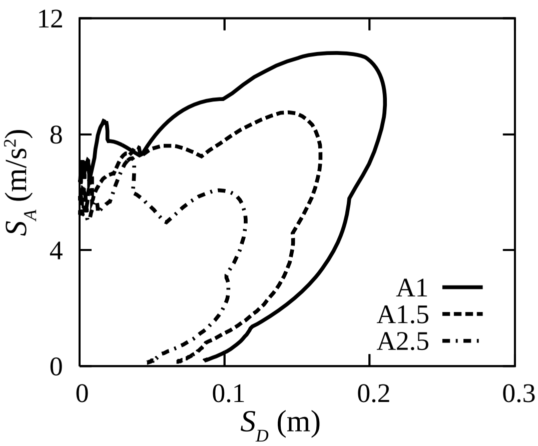

Figure 5. Linear response spectra computed for idealized records

4. COMPUTED RESPONSE TO IDEALIZED MOTIONS

Figure 6a shows absolute peak relative displacements computed for synthetic motions A1, A1.5 and A2.5 and for elasto-plastic oscillators with T = 0.2 s with base shear coefficients C_b ranging from 0 to 0.4. The computed relative displacement maxima are larger for the asymmetric records A1.5 and A2.5 than for record A1 for base shear coefficients exceeding approximately 0.1. Record A1, the symmetric record, has the same PGA, and larger PGV and response spectra (Figure 3b and 5a) than records A1.5 and A2.5. The peak ground velocity of record A2.5 is approximately half of the peak ground velocity of record A1, but the relative displacement computed for A2.5 is 1.5 times the displacement computed for A1 at Cb = 0.1. This observation indicates that there is no proportionality between peak ground velocity and displacement response for short-period structures. Elastic response spectra also fail to capture the effects of the asymmetry of the records considered (Figure 5). Estimates of displacement demand based on elastic spectra would, therefore, not include the effects of asymmetry.

Figure 6b shows the relationship between the base shear coefficient Cb and the absolute maximum relative displacements computed for elasto-plastic oscillators with T = 0.6 s. The asymmetry of the record seems not to impact negatively the computed relative displacements. We conclude that response is sensitive to asymmetry in the acceleration record for T < 0.6 s.

On the other hand, response is not as sensitive to asymmetry in the velocity record as it is to asymmetry in the acceleration record.

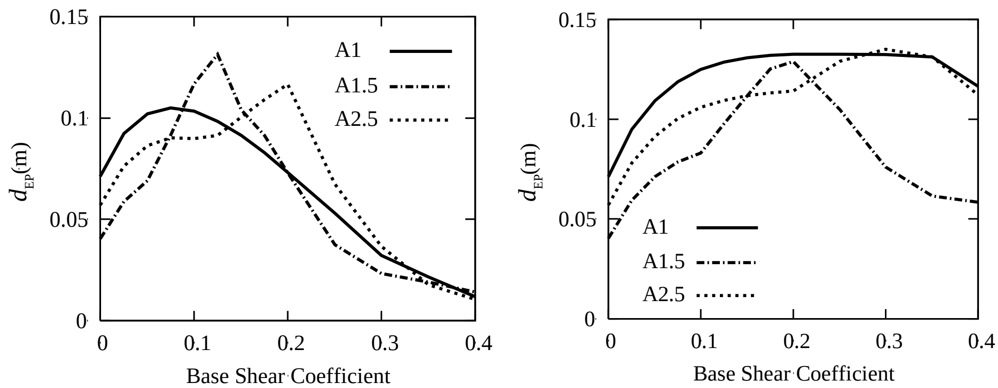

(a) Elasto-plastic systems with T=0.2s **(b) Elasto-plastic systems with T=0.6s**

Figure 6. Peak relative displacements computed for idealized records

5. COMPUTED RESPONSE TO RECORDED MOTIONS

In section 4 we considered the response of oscillators to idealized ground motion records. We now consider response to actual records. For illustration purposes we consider, initially, two records: 1992 Erzincan, Turkey, NS component, and 1992 Landers, Lucerne Station, component 275. Table 1 lists intensity measures for each record. Notice that the record for the Landers Earthquake has larger PGA, PGV and PGD. But, at the same time, the record for the Landers Earthquake has small asymmetry while the record from Erzincan has large asymmetry as indicated by the ratios of PGA to maximum ground acceleration in the direction opposite to that of PGA. Figure 7 shows computed displacement peaks for elasto-plastic oscillators with T = 0.2 and 0.6 s. and base shear coefficients ranging from 0 to 0.4. In all cases, the relative displacements computed for the record from Erzincan are larger than those for Landers. This trend is opposite to what would have been expected on the basis of the differences in PGA, PGV, PGD, and linear response spectra. This observation indicates that asymmetry is an important attribute in an acceleration record.

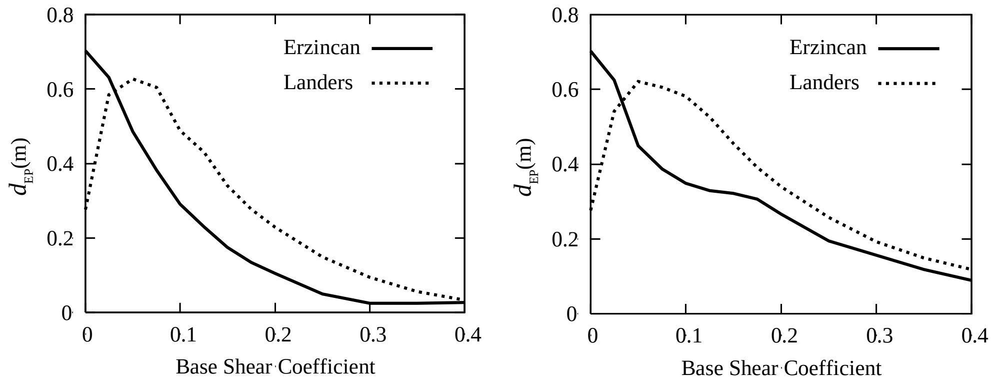

(a) Elasto-plastic systems with T=0.2s **(b) Elasto-plastic systems with T=0.6s**

Figure 7. Peak relative displacements computed for the Erzincan and Landers records

6. HOW ASYMMETRY IN THE ACCELERATION RECORD AFFECTS DISPLACEMENT RESPONSE

We think of the response of a sliding block (Figure 8a: a physical representation of a rigid-plastic system) to a simple idealized ground acceleration record (Figure 8c). The record is asymmetric and periodic, and features acceleration "pulses" in two directions ($a_1 = 3$ and $a_2 = -1$, positive values represents movement to the left). We assume that the block will move relative to the ground if the frictional resistance in terms of acceleration reaches its strength ($\mu g = 2$ in Figure 8b). When the ground starts to move, with an acceleration of $a_2 = -1$, the block will simply move with the ground, and the frictional resistance is $a_2 = -1$ (Figure 8d). When the ground experiences the first "positive" acceleration pulse $a_1 = 3$ (point 1 in Figure 8c), the block will try to follow the ground. But its "strength" is limited ($\mu g = 2$ in Figure 8d). So there will be sliding. We can compute the relative acceleration simply by subtracting the acceleration of the block from the acceleration of the ground: $a_1 - \mu g = 3 - 2 = +1$ (Figure 8b, the positive sign indicates relative motion to the right). When the ground returns to an acceleration of $a_2 = -1$ (point 2), the relative acceleration becomes $a_2 - \mu g = (-1) - 2 = -3$. The relative acceleration reverses. If we integrate relative acceleration we obtain relative velocity (Figure 8f). And we observe that the relative velocity will increase during the first positive acceleration pulse (that is, between points 1 and 2) and will start to decrease when the ground acceleration of the ground returns to $a_2 = -1$ and the relative acceleration changes in sign (point 2). Eventually the relative velocity returns to zero (point 3). At this point, the relative motion between block and ground ceases, and, therefore, the relative acceleration returns to zero. The acceleration of the block becomes equal to the acceleration of the ground ($a_2 = -1$) once again. The result of this process is a spike in the relative velocity record, which is zero elsewhere. This spike results in a permanent offset of the block with respect to its initial position (Δ_1 in Figure 8g). The magnitude of this offset is equal to the area under the spike in the relative velocity record. If a second positive acceleration pulse takes place (points 4 and 5 in Figure 8c), it will result in a second spike in the relative velocity and an additional offset (Figure 8g). The ground may go back to its original position (as in Figure 3c), but the block does not. The relative displacement (Δ_1 in Figure 8g) is maximum if the resistance is equal to a_2 ($\mu g = |a_2|$), as we observed in Figure 6a, unless the asymmetry is small ($|a_1 / a_2| \approx 1$). If the ground acceleration pulses did not have a preferred direction, the block would slide back and forth without accumulation of successive offsets. This analogy shows why asymmetry in the acceleration record may cause large relative displacements in inelastic systems.

7. THE STRENGTH SPECTRUM

We have shown that linear response spectra do not capture the effects of what we have called "asymmetry" in acceleration records. And we have shown that the effect of asymmetry can be significant for short-period structures (T < 0.6 s). To solve this conundrum we propose the direct use of nonlinear spectra. And to ease the transition from linear spectra to nonlinear spectra we propose a simplification. Figure 9 shows computed displacement maxima for rigid plastic and elasto-plastic oscillators with periods ranging from 0 to 0.6 s and base shear coefficients from 0 to 0.6. The values shown were computed for the Erzincan and Landers records. From these four Figures it is apparent that, for T < 0.6 s, response is more sensitive to base shear strength than to initial period of vibration. We therefore suggest that, for design or evaluation purposes, it would be sufficient to work with spectra computed for oscillators with a fixed average period (say T = 0.2 s) and varying base shear strength. We call such spectra (graphs showing maximum displacements of systems with T = 0.2 s vs. base-shear coefficient) "Strength Spectra."

In the following discussion, we refer to results obtained for the decreasing-stiffness system defined in Figure 1d with a base shear coefficient of 0.2. Those results were obtained for the 59 ground motion records with PGA > 0.5g and PGV > 0.5 m/s. Figure 10a compares the maximum displacements for systems with T = 0.2 s with maximum displacements for systems with T = 0.1 s and 0.5 s. The correlation coefficient is 0.97, indicating that the systems with T = 0.2 s provide a good estimate of the maximum displacement of systems with different periods (not exceeding 0.5 s). As we increased the base shear coefficient up to 0.4, the correlation coefficient decreased but was larger than 0.8. In contrast, Figures 12b and c show how intensity indicators, PGA and PGV, correlate with the computed displacement demand. It is clear that PGA is not a good measure of displacement demand. PGV is not very good, either. Note that the records in Table 2 include various ground motions with various dominant periods. We therefore conclude that the Strength Spectrum with T = 0.2 s can be used as an indicator of potential for seismic damage in low-rise buildings (T < 0.5 s) regardless of the characteristics of the ground motion if the ground motion is strong (PGA > 0.5g and PGV > 0.5 m/s) and the base shear coefficient of the building is smaller than 0.4. The same observation is also true for elasto-plastic systems.

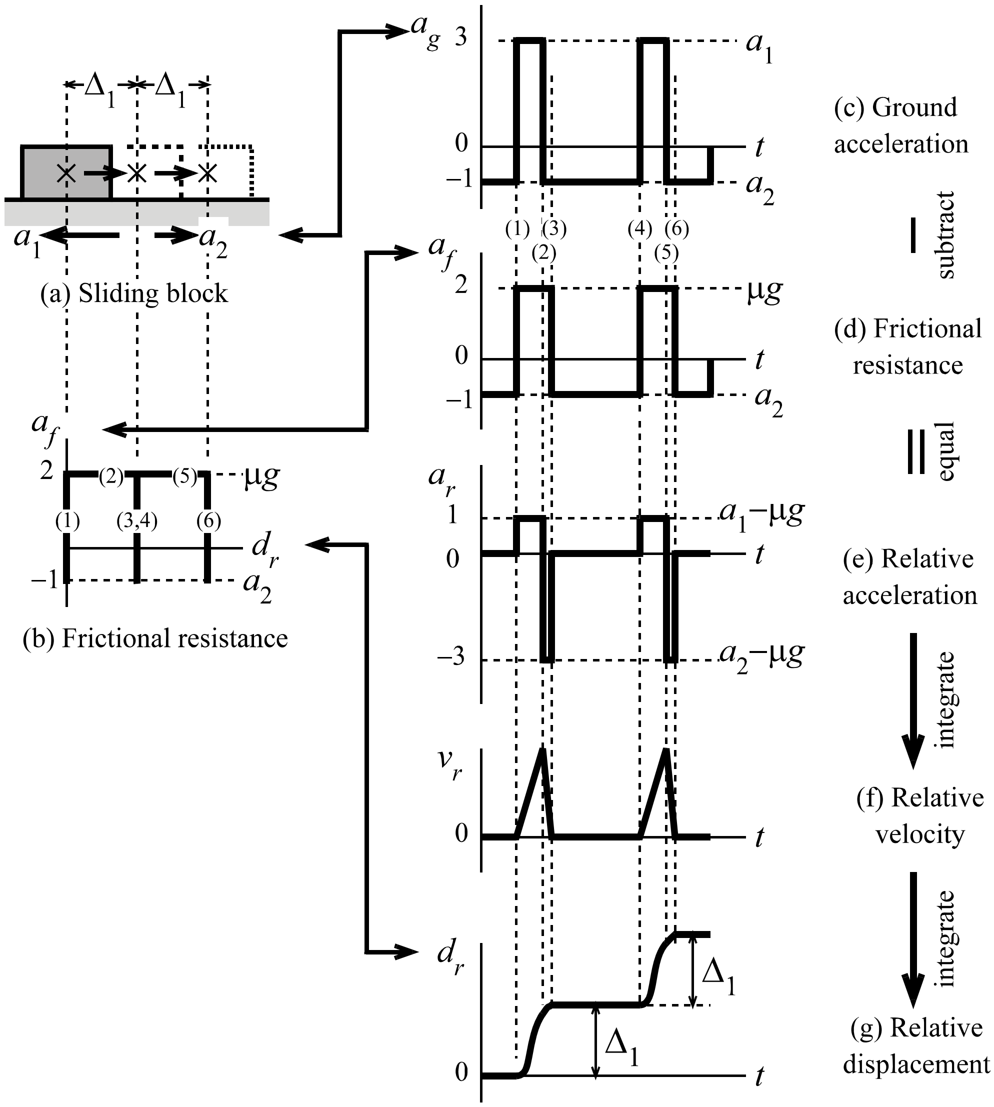

Figure 8. Response of a rigid-plastic oscillator to an idealized asymmetric record

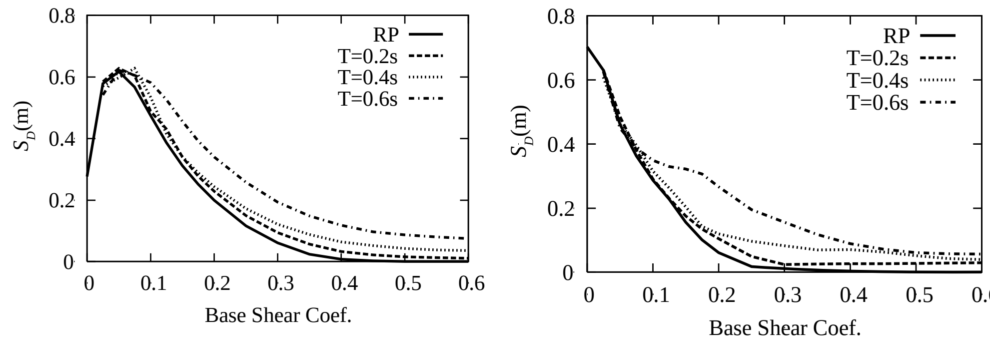

(a) Erzincan **(b) Landers**

Figure 9. Computed displacement maxima for rigid-plastic and elasto-plastic oscillators

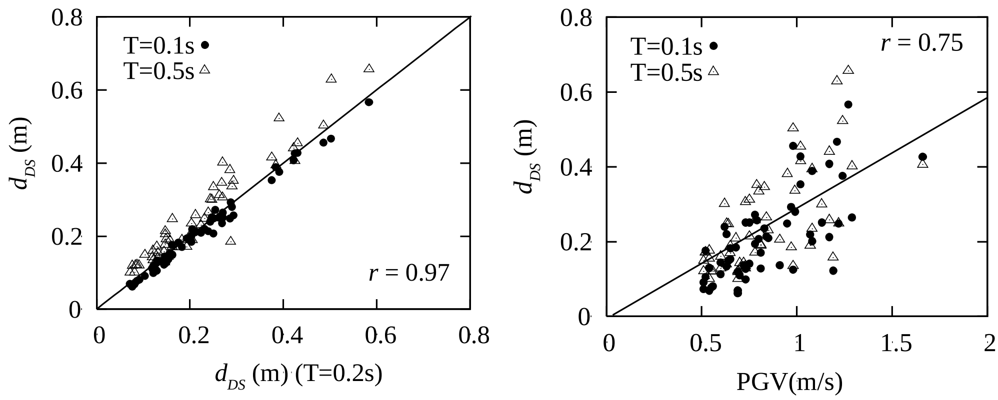

(a) Oscillators with T=0.2 sec **(b) PGV**

Figure 10. Maximum displacement of decreasing-stiffness oscillators with 0.1 < T < 0.5 s (*r*: correlation coefficient)

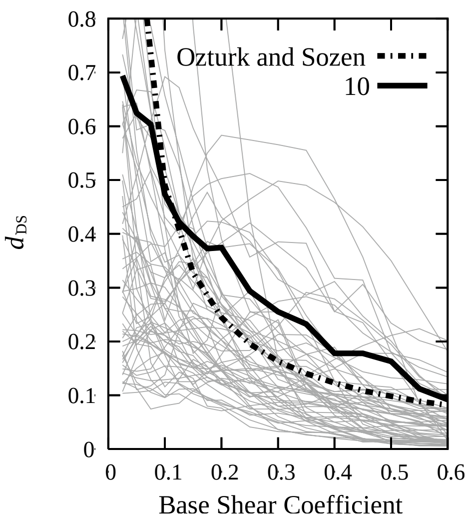

Figure 11. Strength spectra for decreasing-stiffness SDOF systems with T<0.5s

Figure 13 shows maximum displacements of decreasing-stiffness oscillators with T=0.2 s and various base-shear strengths. The 59 records satisfying PGA > 0.5g and PGV > 0.5 m/s were used again to generate this plot. The thick continuous line shows the tenth largest value of displacement response at each base shear coefficient considered. We consider that the data above this line are exceptionally large and should not govern the design. The thick broken line was obtained using the formulation proposed by Ozturk (2003) [9] for T = 0.2 s and PGV = 1.1 m/s, which is the mean plus one standard deviation for the peak ground velocities of the considered records. It is interesting that the line we computed matches reasonably well the one obtained using Ozturk's formulation although Ozturk calibrated his formulation using records from Turkey exclusively while we have used records from a number of locations.

We suggest that the spectra in Figure 13, which have been computed for T = 0.2 s, can be used to estimate the displacement demand for building structures with different initial periods not exceeding 0.5 s. For 0.05 < Cb < 0.4 and T < 0.5 s, we propose this envelope to be:

$$S_d = 0.6 - C_b \tag{2}$$

Where S_d is displacement demand for strong motion in meters and C_b is base shear coefficient. This demand may be reduced according to the soil condition and the seismicity of the region; matters outside the scope of this manuscript.

8. CONCLUSION

(1) Asymmetry in ground acceleration -as defined here- can cause large inelastic displacements in low-rise RC buildings.
(2) Elastic spectra do not capture the effects of asymmetry.
(3) A Strength Spectrum (a graph showing maximum displacements of nonlinear SDOF systems with T at yield = 0.2 s and various base shear coefficients) can be used as an indicator of potential for seismic damage in low-rise buildings (T at yield < 0.5 s) if the base shear coefficient of the building is smaller than 0.4 and the ground motion is strong (PGA > 0.5g and PGV > 0.5 m/s). The Strength Spectrum captures the effects of asymmetry in the ground motion.
(4) Strength Spectra can, therefore, be used as a new paradigm for design and evaluation of low-rise RC buildings (T at yield < 0.5 s).

References

1. Freeman, S. A., Nicoletti, J. P., and Tyrell, J. V., "Evaluations of existing buildings for seismic risk—a case study of Puget Sound Naval Shipyard, Bremerton, Washington," Proceedings of the U. S. National Conference on Earthquake Engineering, 1975, Berkeley, California.
2. Applied Technology Council (ATC), Seismic Evaluation and Retrofit of Concrete Buildings, 1996, volumes 1 and 2, Report No. ATC-40, Redwood City, CA.
3. Kuramoto, H., "Seismic Design Codes for Buildings in Japan" Journal of

Disaster Research, 2006, Vol.1 No.3, 16 p.
4. Blume J.A., Newmark N.M., Corning L.H., Design of Multi-storied Buildings for Earthquake Ground Motions, Portland Cement Association, 1961, Chicago.
5. Chopra, A. K., “Dynamics of Structures (3rd Edition),” Prentice-Hall, 2006.
6. Priestley, M.J.N., Calvi, G.M., and Kowalsky, M.J., Displacement-based Seismic Design of Structures. IUSS Press, 2007.
7. Takeda, T., Sozen M., and Nielsen N., “Reinforced Concrete Response to Simulated Earthquakes,” ASCE Journal of Structural Division, 1970, Vol. 96, No. ST12.
8. Peer strong motion database, 2000, http://peer.berkeley.edu/smcat/
9. Ozturk, B.M. (supervised by Sozen, M.A.), “Seismic Drift Response of Building Structures in Seismically Active and Near-Fault Regions,” Ph.D. Thesis, 2003, Purdue University.

WORLD RECORD: THE LONGEST CONCRETE PLATE WITHOUT JOINTS, WITHOUT CRACKS

B. Hillemeier & R. Wens[1], L. Hänisch[2]
[1]Technische Universität, Berlin, Germany
[2]Deutsches Elektronen Synchrotron, Hamburg, Germany

ABSTRACT

The German electron synchrotron DESY (Deutsches Elektronen-Synchrotron) in Hamburg is a centre for research into the structure of matter. DESY uses the accelerator PETRA (Positron-Elektron-Tandem-Ring-Anlage) as an intense synchrotron radiation sources for a broad spectrum of tests with electromagnetic radiation. The tests must take place on an extremely stiff and smooth concrete plate. The plate had to be 280 m long, 24 m wide and 1 metre thick. The plate should not get any joints and has to remain free of cracks because of the resistance demanded. The plate has to be produced monolithically, that is on behalf of the huge dimensions and properties world record. The positioning of the plate on a sliding bitumen layer and the use of steel fibre concrete have been the prerequisites for a successful performance under such challenging requirements.

1. INTRODUCTION

The German electron synchrotron DESY in the Helmholtz-Community in Hamburg, Germany, is one of the leading accelerator centres in the world. The accelerator PETRA is being improved to be the most brilliant worldwide storage ring-based X-ray radiation sources worldwide. This new light source of the superlative offers excellent conditions for top research with particularly intensive and sharp joint X-ray radiation. The decisive advantage is the capillary X-ray radiation of an especially high brilliance: Also, tiny tested materials can be examined and their pictures highly resolved in the order of their atoms.

Almost 300 m of the 2.3 km long Petra ring must be completely modified and a new experimentation hall had to be constructed. The basis of the hall is a 1 m thick concrete slab which carries the accelerator and the experiments. The slab is 24 m wide and 280 m long. It follows the circular shape of the accelerator ring. The concrete slab protects the highly precise measurement equipment from mechanical vibrations. The slab is decoupled from the building. It had to be built without joints and cracks. Therefore the slab had to be concreted without interruption. The evenness of the final floor slab was better than 4 mm/10 m. At a concentrated load of 1kN the floor slab may deform vertically only by 1 µm.

The unusually high requirements called for correct planning, faultless production, highly sophisticated quality assurance, and an experienced contractor.

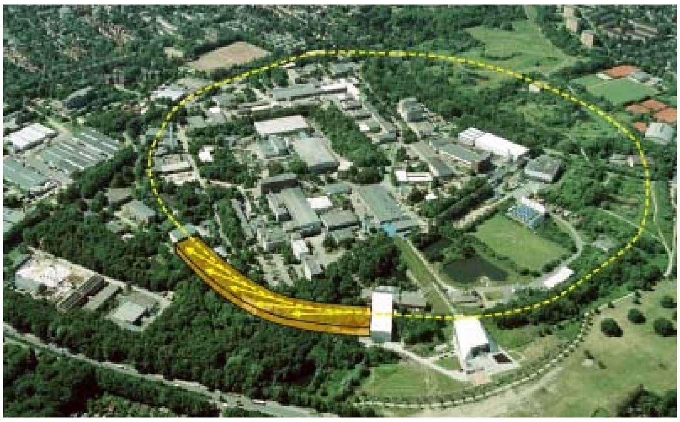

Figure 1. Aerial photo DESY with Petra ring. In the foreground the planned new experimentation hall (Photo: DESY)

2. PHILOSOPHY OF THE ENGINEERING DESIGN

The dimensioning of the floor slab was planned with the following considerations: A minimal deformation hindrance has been gained by applying a bituminous sliding layer despite not knowing initially the necessary minimum thickness. The slab starts shortening by cooling off after its maximum temperature gained by hydration heat. As a consequence it has to suffer a maximum tensile stress in its central cross section through each of the approximately 150 m long ends. If these tensile stresses remain below the tensile strength of the concrete, an additional mild reinforcement could be saved. The shortening of the slab has been expected to start three days after the beginning of concreting. For this circumstance a concrete mix had to be designed which produced a hydration temperature as low as possible while reaching a tensile strength of at least 2 N/mm^2 as early as possible. The mixture had to be proven in internal performance tests by the construction firm.

Because not all conditions and may be impacts could be foreseen for this special construction task nevertheless no crack has been allowed leading to a gaping joint in the concrete slab. Concerning these requirements the planned tensile strength of the young concrete had to be achieved for certain. The achievable tensile strength can only be guaranteed when steel fibres are mixed into the concrete. Steel fibres do not increase the tensile strength of the concrete, however, they guarantee it. This guarantee is reached only by a fibre content of approximately one volume per cent. For this reason we suggested 75 kg of steel fibres per cubic metre of concrete.

Micro cracks arise during the hydration process in the very young concrete. Late cracks arise by shrinkage at a higher age, by restraint and internal tensions. Micro cracks caused by autogenous shrinkage or by tensile stresses through hydration heat act later as crack starters when the plate is subjected to stresses by external loads. These fine micro cracks do not further enlarge if they are held small and locked by well bonding scraped fibres. To cope with the shrinkage crack formation in the very early age we chose scraped fibres with the best bonding performance in young concrete. The amount was 40 kg scraped fibres per cubic metre of concrete. For cracks arising later we chose crack bridging fibres with double bended ends, a

length of 50 mm, diameter 0.8 mm, and 35 kg per cubic metre of concrete.
Cracks have to be avoided primarily in the surface. Near the surface of a concrete the influences are more various and more intense than inside the structure. Therefore steel fibre concrete has been planned for the top 50 centimetres, for the upper half of the slab. The lower area got conventionally reinforced with a single reinforcing layer calculated for preventing crack widths bigger than 0.3mm. (Figure 2.)

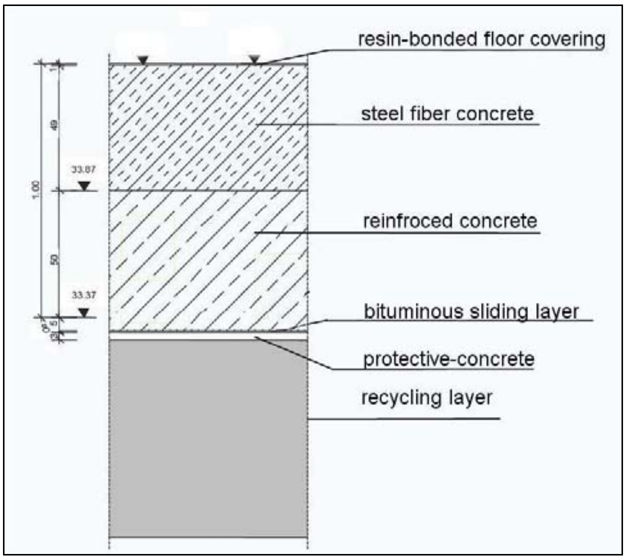

Figure 2. Layers of the floor slab

The centre of the 300 m long concrete slab was designed as a fixed symmetry centre. A 1 m deep trench was executed monolithically in the central section of the slab. Concreting had to be started from here in the two directions simultaneously.

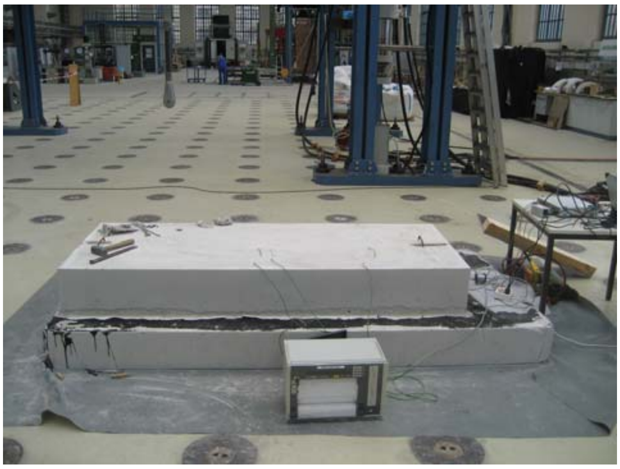

Figure 3. Test setup at the TU Berlin to check the sliding resistance of the bituminous sliding layer

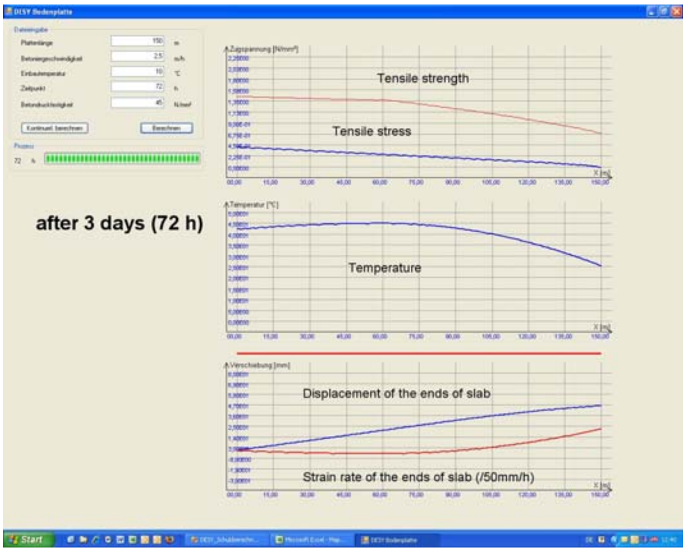

Figure 4. Calculated values for one half of the slab (zero on the horizontal axis is the centre of the slab)

3. SOLUTION METHOD

Long building structures traditionally get subdivided into sections by expansion joints. Because of the high requirements for the bending stiffness of the slab it had to be executed without joints. For a floor slab of such a huge length deformations are adding up in the decimetre range by loss of hydration heat and shrinkage. The foundation basement of the slab leads to a resistance against shortenings. Forces by friction or adhesion are caused in the plate. The not avoidable cracks normally get limited in width by a crack distributing reinforcement. As the requirements for this floor slab were extremely high this would have required an exceptionally high amount of steel reinforcement with a time consuming forming and placing.

A special cracking risk is gained by the hydration heat of the cement. Maximum temperatures of more than 50°C were expected. During cooling the concrete contracts and will crack if its deformation is hindered. To not hinder the deformation, we proposed to place the slab on a 3 mm thick sliding bituminous layer. Laboratory tests with a 1.5 mm thick bituminous layer proved the sliding performance to be not sufficient.

A temperature difference of only 10 K between surface and centre of the concrete slab theoretically leads to a temperature related crack in the surface. Water loss by drying of unprotected concrete yields to a shortening by shrinkage of about 0.4mm/m. Therefore the concrete slab had to be covered against drying after smoothing with a foil and had to be protected against cooling with a mat of foam with a chosen thickness of 10mm.

To optimize the slab construction not only technically but also economically we proposed to construct the slab in two fresh concrete layers.

The 49 cm thick upper layer has been made with steel fibre reinforced concrete with 1 Vol% fibre content with the concrete strength class C 30/37 (F1,6

XC1XM1 D_{max}=16) according to EN 206-1 „Concrete – Part 1: Specification, performance, production and conformity”. The 50 cm thick bottom layer was made with reinforced concrete strength class C 30/37 (XC1 D_{max}=32) according to EN 206-1 with a weak reinforcement for crack width smaller than 0.3 mm at the bottom according to DIN 1045-1 „Concrete, reinforced and prestressed concrete structures – Part 1: Design and construction“. Each concrete layer had to be cast in place while proceeding into both directions without interruption and without joints in one sequence. The top layer with steel fibre concrete was cast in place nearly 25 metres behind the front of the bottom layer.

In the steel fibre concrete an electromagnetic compatibility shielding (EMC Shielding) had to be installed with steel mats in a depth of 15 cm under the top edge of the floor slab. A 1 cm thick layer for wear made of epoxy resin produced the finish of the slab.

4. PRELIMINARY TESTS

4.1. Tests with Sliding Bitumen Layer

The bitumen sliding layer had to be executed as thick as necessary but as thin as possible so that no surplus bitumen would flow out at the sides of the floor slab. For the regulation of the different sliding resistance of differently thick bitumen layers corresponding tests were carried out at different temperatures at the TU Berlin.

The result of the experiments was a friction coefficient μ_R of 0.1 at 20°C with a 3 mm thick sliding layer made of bitumen 50/70 to EN 12591 "Bitumen and bituminous binders – Specification for paving grade bitumen". For a 1 mm thick layer a sliding resistance of μ_R > 0.4 was found.

On the construction site a bitumen sliding layer with an amount of 3 litres of bitumen per square meter got mechanically sprayed on the sub-concrete. This volume produced a nearly 3 mm thick layer. The extraordinary smoothness of the layer is shown in Figure 5.

Figure 5. The smoothness of the bitumen layer on top of the sub-concrete

For the bitumen sliding layer a friction coefficient μ_R=0.35 was set for the further static calculations.

4.2. Mix Design

In addition to constructive measures concrete technological parameters had to be assumed in order to reduce the crack width provoked by heat of hydration or by long term shrinkage. The high steel fibre content of 1 V-% in the upper part of the floor slab was an indispensable component of the quality concept. The slab should remain crack free in its early age and for its lifetime.

The concrete slab should be able to suffer shortening deformations three days after production. Consequently cement had to be chosen which builds up its tensile strength fast. In addition, the steel fibres had to be intensively connected to the hardened cement paste. Therefore minimum binder content is required. This demand stands contrary to the reduction of hydration heat. However, a rapid strength development is more important than a slightly elevated hydration temperature. A mix of CEM III A and fly ash was recommended.

For the assessment of the longitudinal deformations of the slab, the time dependent temperature development of the concrete was examined in polystyrene cubes under adiabatic conditions. The target consistency was 50cm spread on a flow table according to EN 12350-5 "Testing fresh concrete–Part 5: Flow table test". Preliminary tests were performed by the contractor Züblin for different concrete mixtures. The results of the selected mixture are shown in Table 1. Table 2 shows the main characteristic values of the selected mix.

The measurements of the temperature development led us to expect a temperature rise of about 40 K in the centre of the floor slab.

Table 1: Mixture

	C 30/37
CEM III/A 42.5 N	340 kg/m ^{3}
Fly ash	112 kg/m ^{3}
Maximum grain size	16 mm
	w/(c +0,4 f) = 0.43
Fibre mix	35 kg/m ^{3} DE 50/0,8 (Harex)
	40 kg/m ^{3} SF 01-32 (Harex)

To make the concrete pumpable, the content of ultra fines had to be sufficiently high. The components below 0.25 mm, (cement, fly ash, fine sand) should therefore be at least 400 kg/m^3. In preliminary tests the pumpability was proven also for the relatively high steel fibre content. The pumping of such a concrete is representing a special challenge.

Table 2: Test results (main characteristic values).

	Compressive strength $f_{c,\,cube}$ in N/mm²	Young's modulus in N/mm²	Fibre concrete class
1 d	7.5		
2 d	14.0		
3 d			1,0/0,6
7 d	33.0	28 000	
28 d	52.0	33 900	1,6/1,0

5. EXECUTION

5.1. Quality Assurance

Before the beginning of the challenging concreting task the companies involved trained their employees for the special site requirements.

The concreting concept and the quality system of the building contractor regulated the quality control during the execution. The quality was monitored additionally beyond this at particularly relevant stages upon request of the owner-builder. Controls of the preparations and equipment in the mixing plants before the beginning of the work as well as spot tests during the addition of the steel fibres were included.

Each mixing truck was checked on the construction site once again. Rejection criteria for concrete trucks were fresh concrete temperatures falling below 10°C and a spread on a flow table of more than 55 cm. Special emphasis was put on the compaction of the concrete embedding the EMC mats and on curing measures.

5.2. Concrete Production

The concrete supplier Holcim had to guarantee delivery of 160 m^3 per hour for the four concrete pumps. Holcim used four ready-mix concrete factories and one alternative factory with a corresponding stockpiling of the base materials. Twenty eight ready-mix trucks of 8m^3 each were used. An interruption of the concreting process was not foreseen and was not allowed under any circumstances.

The concrete factories put special emphasis on a high regularity of concrete production. Coping with the moisture content of the sand and the medium-sized aggregates was important. The target value of the spread at delivery was 52.5cm in order to not fall below the demanded consistency of 50 cm on the site.

The steel fibres were weighed and pre-packaged beforehand. The scraped fibres SF 01-32 were added to the empty transport vehicle by an elevator. After this the concrete was loaded. The steel fibres DE 50/08 were blown with an air stream device into the loaded ready-mix vehicle (Figure 6). A prolonged mixing time for the steel fibre concrete had to be taken into account in the delivery concept.

Vehicles with steel fibre concrete were indicated by a green arrow in the windshield to avoid false placement. The site foreman checked every vehicle again at the pump for its consistency by visual inspection.

Figure 6. Blow in of the steel fibres into the mixing vehicle

5.3. Placing the Concrete

The walls and the roof of the hall were completed except for the end walls before placing the concrete. Four concrete pumps and one reserve pump were used. Two pumps concreted the lower layer with normal reinforced concrete; the other two pumps concreted the steel fibre concrete for the top layer of the slab 20 m behind the leading edge of the lower layer. The concrete was pumped at the same time at both sides starting in the middle of the slab. The 7000 m^3 of concrete were placed within approx. 60 hours.

The compaction of the concrete was carried by immersion vibrators. The surface was levelled with a special levelling plank. After reaching the required degree of hardness the concrete surface was smoothed with a double slab machine.

As soon as the concrete was sufficiently set, it was covered with foil and a 10 mm thick insulating mat. The curing time was 31 days. The concrete was left in the side formwork for the complete curing time.

6. RESULTS

Immediately after the completion of work the monitoring of the strength and deformation behaviour of the slab began.

The floor slab behaved as calculated. The ends were shortened with a speed of 30 - 40 nm/s after three days. Each end shortened by about 40mm.

Figure 7. Surface finishing

Figure 8. One sided shortening of the floor slab by 38mm

The temperature from hydration heat and heat conduction was recorded continuously starting at the beginning of concreting in different places in the following four heights:

Sliding layer ± 0 cm (bottom contact zone)
Sliding layer + 10 cm
Sliding layer + 50 cm (slab centre)
Sliding layer + 90 cm (10 cm below slab surface)

Compared with the values determined in the laboratory the temperature rise inside the concrete slab increased at most 32 K. The reason was the low fresh concrete temperature and the cool weather during the execution. Figure 9 shows the typical temperature developments at different measuring points in one cross-section.

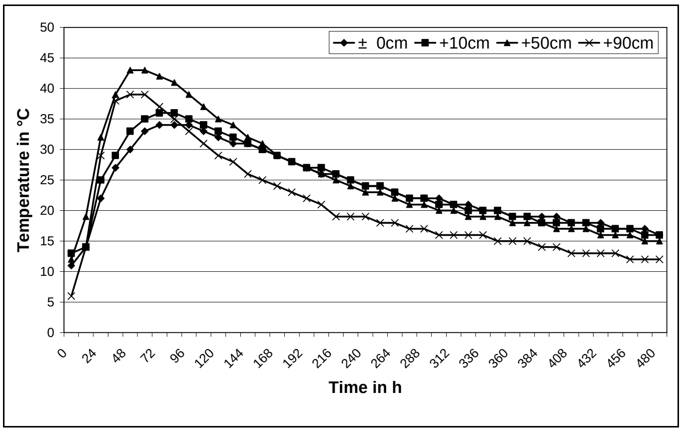

Figure 9. Temperature development in the concrete slab

After the length deformation stopped the floor slab was measured in a grid of 2.0m×2.0m. Such a high level of evenness was achieved that a planned additional levelling screed could most likely be foregone. Nevertheless the epoxy-layer has been performed.

Figure 10. The glass like surface of the finished concrete slab

Partners:
Züblin AG, Direction North, Hamburg
Holcim Concrete and Aggregates GmbH, Hamburg
GuD Consult, Berlin
IFDB, Berlin

REFERENCES

1. Blitzlicht, Deutsches Elektonen-Synchrotron, Mitglied der Helmholtz-Gemeinschaft, Hamburg, 2007.
2. Hillemeier, B., Wens, R., Hänisch, L., High Performance Concrete for Extreme Applications, Proceedings of the 2ND International Conference on Concrete Repair, Rehabilitation and Retrofitting (ICCRRR), 24-24 November, 2008, Cape Town, South Africa.
3. Schütte, Jens, Einfluss der Lagerungsbedingungen auf Zwang in Betonbodenplatten, Dissertation, Technische Universität Carolo-Wilhelmina zu Braunschweig, 1997.

SEISMIC UPGRADE OF CONCRETE COLUMNS

S.A. Sheikh and J. Liu
Department of Civil Engineering, University of Toronto, Toronto, Ontario, Canada

ABSTRACT
This paper presents a summary of the work from an extensive research program underway at the University of Toronto on strengthening deficient and repairing damaged concrete columns with fibre reinforced polymer (FRP) jackets. The specimens consisted of either a 305 mm square or 356 mm diameter and 1.47 m long column connected to a 508 × 762 × 813 mm stub. Each specimen was tested under lateral cyclic displacement excursions and simultaneous constant axial load to simulate seismic forces. Results indicate that added confinement with FRP at plastic hinge locations significantly enhanced ductility, energy dissipation capacity and strength of columns. Efficiency of FRP confinement was much superior in circular columns than in square columns. A procedure is presented for the design of confining FRP reinforcement in columns required to achieve a certain ductility performance given the applied axial load and the properties of the FRP.

Keywords: columns, confinement, ductility, earthquake, energy dissipation, retrofitting.

1. INTRODUCTION

Large inelastic deformation capacities of individual members allow entire structures to resist severe ground motion while dissipating significant levels of seismic energy. To ensure overall structural integrity, plastic hinge formation associated with lateral displacement excursions is preferred in beams and girders rather than in columns [1, 2]. However, plastic hinge development can occur in columns, particularly at the bases of multi-storey frames and bridges. Ductile behavior is essential at these crucial sites to prevent complete structural collapse under sustained loading. Many of the existing reinforced concrete structures do not have adequate amount of confinement reinforcement in potential plastic hinge regions of the columns and may result in brittle structural response during earthquakes. Destruction from the 1994 Northridge, 1995 Kobe and 2005 Kashmir earthquakes [3, 4, 5] has highlighted the worldwide vulnerability of reinforced concrete columns exposed to inelastic conditions. To provide additional confinement to these deficient columns, retrofitting with a fiber-reinforced polymer (FRP) jackets provides a very attractive solution due to their lightweight, high strength, and excellent corrosion resisting capabilities. The current design code provisions [1, 2] require large amounts of steel reinforcement placed at small spacing in critical regions of columns, which, quite often, makes construction very cumbersome and at times impractical. Use of external FRP shells with fibers aligned in the circumferential direction of the column can provide confinement and a stay-in-place formwork for new structures [6].

Many experimental studies [7– 14] have demonstrated that the confinement provided by the FRP wraps can significantly increase the energy absorption capacity and ductility of the columns under combined axial, flexural and shear loads, thereby increasing their seismic resistance. This paper presents selected results from an extensive experimental program in which similar large size square and circular columns were tested under simulated seismic load in exactly the same manner to provide comparable results to investigate different variables and design parameters. A design procedure is also presented which can be used to calculate the amount of confining FRP required for a certain ductility performance given the axial load on the column and the properties of the FRP. Initial focus of this research program was on square columns due to the fact that it presented a more challenging scenario due to inferior confinement efficiency in these columns compared with circular columns. A large number of well-instrumented square columns were tested in a similar manner under simulated earthquake loads and extensive data was used to develop analytical models and design procedures. Experimental work on circular columns has recently been completed on similar lines and analytical work is in progress. Results indicate that the amount of FRP reinforcement required in circular columns is about half of what is required in square columns for similar improvement in ductility.

2. EXPERIMENAL RESULTS AND DUCTILITY PARAMETERS

To develop a procedure for the design of confining FRP for concrete columns, an extensive review of the available test results was conducted. This review indicated that the results available were seriously limited. Although there exists a consensus that confining FRP can significantly enhance the seismic performance and ductility of circular, square or rectangular concrete columns, the test setups, loading histories, instrumentations, specimen details and ductility parameters used in the available experimental investigations were different from one program to another, making it difficult to evaluate these results on a common platform.

A test program was thus undertaken in which all the column specimens were similar and tested in exactly the same manner. Each specimen was comprised of a 305×305×1473 mm or 356 mm circular column connected to a 508×762×813 mm stub. The column part of the specimens was 1.47 m long. The corners of all square columns were rounded using concave wood sections, with a 16 mm radius, placed inside the forms during casting to facilitate FRP wrapping. The columns were characteristic of field members located in multi-storey building frames or in bridges between the points of maximum moment and contraflexure. All square specimens contained eight 20M longitudinal bars (ρ_l = 2.58 %) uniformly distributed around the column core creating a core area that was 77 % of the gross column area. Perimeter hoops laterally supported the four corner bars and internal hoops enclosed the four middle bars. The circular columns contained six 25M longitudinal bars (ρ_l = 3.01 %) and the ratio between the core area and the gross

column area was 74 %.
Each specimen was tested horizontally in the loading frame shown in Figure 1 under a constant axial load and applied lateral cyclic displacement excursions simulating earthquake forces. The specimens were subjected to transverse displacement excursions (Figure 2) using a displacement-control mode of loading until the specimen was unable to sustain the applied axial load. The retrofitted specimens were externally confined by different amounts of continuous CFRP or GFRP wraps. Table 1 lists the details of the square specimens considered in this study, while the test data of circular specimens is presented in Table 2. Throughout this experimental program the same types of CFRP and GFRP materials were used. The FRP properties varied only slightly from one batch to the other. The ultimate tensile strength and rupture strain of the CFRP fabric ranged from 912 to 962 N/mm width per layer and 0.0123 to 0.0142, respectively, while these values for the GFRP fabric were 518 to 647 N/mm width per layer and 0.0197 to 0.0228, respectively.

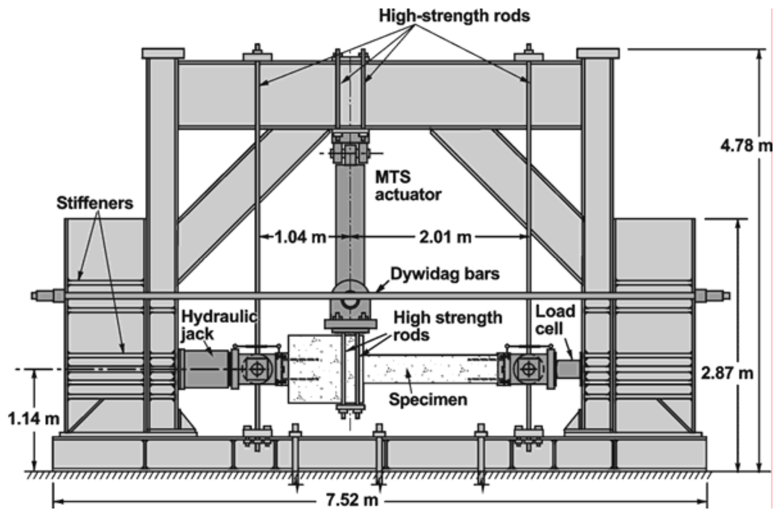

Figure 1. Schematic test setup

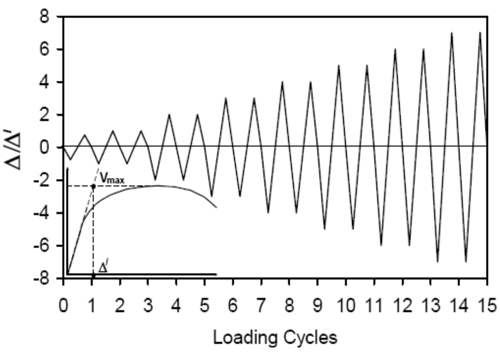

Figure 2. Lateral displacement excursions

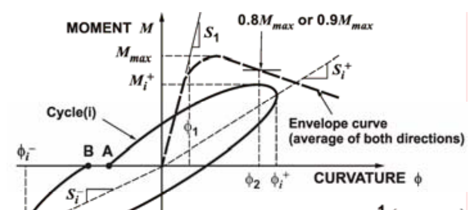

$$\phi_i = \frac{1}{2}(\phi_i^+ + \phi_i^-) \qquad M_{i,max} = \frac{1}{2}(M_i^+ + M_i^-) \qquad S_i = \frac{1}{2}(S_i^+ + S_i^-)$$

$$\mu_\phi = \frac{\phi_2}{\phi_1} \qquad N_\phi = \sum_{i=1}^{i=m}\frac{\phi_i}{\phi_1} \qquad E = \frac{1}{M_{max}\phi_1}\sum_{i=1}^{i=m} e_i \frac{L_f}{h}\left(\frac{S_i}{S_1}\right)\left(\frac{\phi_i}{\phi_1}\right)^2$$

Figure 3. Ductility parameters

2.1. Ductility Parameters

The design approach was developed on the pattern of the procedure for the design of steel confining reinforcement [15]. The parameters used for evaluating the ductile performance of a column included section and member ductility, energy dissipation capacity and the number of standard displacement excursions a column could sustain before failure. In evaluating the seismic performance of the columns and studying the effects of different variables, ductility and toughness parameters defined in Figure 3 were used [15]. These included curvature ductility factor μ_Φ, cumulative ductility ratio N_Φ, and energy-damage indicator E. Subscripts t and 80 indicate, respectively, the value of the parameter until the end of the test (total value) and the value until the end of the cycle in which the moment has dropped to 80 percent of the maximum value. The energy parameter e_i represents the area enclosed in cycle i by the M-Φ loop. Terms L_f and h represent the length of the most damaged region measured from the test and the depth of the column section, respectively. All other terms are defined in Figure 3. Table 1 and Table 2 list these ductility and toughness parameters for the columns considered in this analysis.

Sheikh and Khoury [15] observed that different ductility and toughness parameters were interrelated (Figure 4). In columns internally confined with steel, for $\mu_{\Phi 80}$ of 16, the values for $N_{\Phi 80}$ and E_{80} were found to be 64 and 575, respectively. A column with this level of deformability was defined as highly ductile. The section with a $\mu_{\Phi 80}$ value of 8 to 16 was defined as moderately ductile and the low ductility column had $\mu_{\Phi 80} < 8$. Figure 4 also shows the relationships between different ductility parameters of FRP-confined columns. Data from nine steel-confined columns reported by Sheikh and Khoury [16] and ten FRP-confined columns as listed in Table 1 are used to construct the figure.

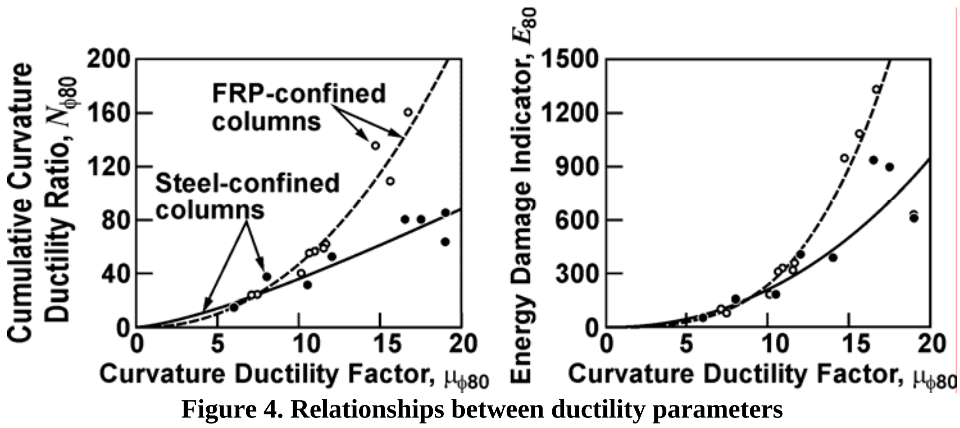

Figure 4. Relationships between ductility parameters

It is clear from Figure 4, that up to $\mu_{\Phi 80}$ of approximately 8, the relationships between various parameters for steel-confined and FRP-confined columns are very similar. For values of $\mu_{\Phi 80}$ larger than 8, the parameters $N_{\Phi 80}$ and E_{80} of the FRP-confined columns are significantly higher than those of the steel-confined columns with similar $\mu_{\Phi 80}$ values. For dissipating equal amount of energy, the FRP-confined columns require smaller curvature ductility factors than comparable steel-confined columns. This can be attributed to the different curvature distributions in the plastic hinge region and different plastic hinge lengths in these two types of columns. The FRP-confined columns require a curvature ductility factor of only 13.2 to dissipate the amount of energy as the steel-confined columns dissipate at $\mu_{\Phi 80}$ of 16. Similar trend is observed for cumulative curvature ductility ratio. The behavior of a FRP-confined column with $\mu_{\Phi 80}$ = 13 can thus be considered as highly ductile. The section with a $\mu_{\Phi 80}$ value of 8 to 13 is defined as moderately ductile and the low ductility column has $\mu_{\Phi 80} < 8$.

2.2. Effects of Different Variables on Column Performance

Based on the experimental results listed in Table 1 and Table 2, the most important variables identified to affect a column's ductility are the amount of FRP confining reinforcement, type of FRP and the level of axial load. The effect of these variables on column behavior is discussed in the following.

Amount of confining FRP – The effect of the amount of confining CFRP can be evaluated by comparing the moment vs. curvature behavior of two sets of columns, as presented in Figure 5. The first set (Figure 5a) includes square columns AS-1NS, ASC-2NS and ASC-6NS that were tested under an axial load of 0.33 P_o. All the columns in the second set (Figure 5b), AS-1NSS, ASC-4NS, ASC-3NS, and ASC-5NS, were tested under an axial load of 0.56P_o. The ductility parameters in Table 1 and the responses shown in Figure 5 clearly demonstrate the enhanced cyclic performance of the FRP-retrofitted columns. The behavior of columns improved progressively as the amount of confining CFRP increased. While Specimen AS-1NS tested under axial load of 0.33P_o failed following the 7th cycle, Specimen ASC-2NS and ASC-6NS confined by one and two layers of CFRP, respectively endured 15 and 20 load cycles, respectively. The columns tested under higher axial load, ASC-4NS, ASC-3NS, and ASC-5NS, were able to sustain 8, 11, and 15 load cycles, respectively while the control specimen AS-1NSS failed in the fourth cycle. The enhancements in curvature ductility of the columns were approximately proportional to the amount of confining FRP provided. Comparisons of the behavior of the GFRP-confined square columns and the control specimens as shown in Figure 6 and Table 1 also lead to the same conclusion. Figure 7, 8 and 9 show the behavior of eleven circular columns tested under an axial load of 0.27P_o, 0.40P_o or 0.56P_o. Seven columns were confined by CFRP or GFRP and others only had steel as lateral reinforcement. The test data of circular columns also demonstrated the enhancement of ductility by FRP confinement.

More over, addition of FRP confinement provided improvements in the performance of circular columns that were significantly better than those observed in square columns. It should be noted that minimal lateral steel reinforcement was used in all the FRP-confined columns with spacing approximately equal to the size of the column core. The confinement effectiveness of such reinforcement is known to be insignificant and is obvious from the behavior of control specimens AS-1NS, AS-8NS, AS-1NSS, P40-NF-5 and P56-NF-10.

Axial load level – Another important variable that determines the behavior of a column particularly with respect to ductility is the level of axial load applied. The effect of this parameter can be evaluated by comparing the behavior of several pairs of circular or square columns. As an example, Specimens ASC-2NS and ASC-4NS, which were almost identical in every aspect except for the different levels of axial load applied. An increase in axial load from $0.33P_o$ in ASC-2NS to $0.56P_o$ in ASC-4NS resulted in significantly less ductile behavior. The column resisting a high axial load experienced a decline in ductility ratio of approximately 60% and dissipated energy of about 75%. Its excursion limit was also reduced to 8 cycles from 15 for the specimen under lower axial load. Comparison of specimens ASG-2NSS, ASG-4NSS and ASG-3NSS shows that the effects of the higher axial load can be countered by an increase in the lateral FRP confinement. Specimen ASG-3NSS was strengthened with 4 layers of GFRP and tested at high axial load of 0.56 P_o. Moment curvature responses of ASG-2NSS and ASG-3NSS are very similar, with ASG-2NSS displaying a little more ductile behavior. Similar observations can also be found by comparison among CFRP confined circular columns P27-1CF-3, P40-1CF-8 and P56-2CF-13. The former two columns were confined by one layer of CFRP, while the last column was confined by two layers of CFRP. As the axial load increased from $0.27P_o$ in P27-1CF-3 to $0.40P_o$ in P40-1CF-8, the curvature ductility factor decreased from 25.6 to 9.6. On the other hand, P56-2CF-13, tested under a high axial load of $0.56P_o$ but confined by two layers of CFRP, showed a ductile behavior similar to P40-1CF-8.

Table 1: Ductility parameters of FRP-confined square columns

Researchers	Specimen	f_c' (MPa)	Lateral steel		Layers & type of FRP	Axial load level P/P_o		Ductility ratio	
			Size@ Spacing (mm)	ρ_s (%)			$\mu_{\Phi 80}$	$N_{\Phi 80}$	$N_{\Phi t}$
Iacobucci et al. [4]	AS-1NS [a]	31.4	US#3@300	0.61	0	0.33	5.3	8	24
	ASC-2NS	36.5	US#3@300	0.61	1CFRP	0.33	11.6	61	73
	ASC-3NS	36.9	US#3@300	0.61	2CFRP	0.56	10.9 [b]	56 [b]	56
	ASC-4NS	36.9	US#3@300	0.61	1CFRP	0.56	7.4 [b]	24 [b]	24
	ASC-5NS	37.0	US#3@300	0.61	3CFRP	0.56	15.6 [b]	109 [b]	109
	ASC-6NS	37.0	US#3@300	0.61	2CFRP	0.33	16.7 [b]	161 [b]	161
	AS-8NS [a]	42.3	US#3@300	0.61	0	0.56	2.6 [b]	5.4 [b]	5.4
Memon and Sheikh [5]	AS-1NSS [a]	42.4	US#3@300	0.61	0	0.56	2.6 [b]	5.4 [b]	5.4
	ASG-2NSS	42.5	US#3@300	0.61	2GFRP	0.33	11.5	59	79
	ASG-3NSS	42.7	US#3@300	0.61	4GFRP	0.56	10.6 [b]	55 [b]	55
	ASG-4NSS	43.3	US#3@300	0.61	2GFRP	0.56	7.1 [b]	24 [b]	24
	ASG-5NSS	43.7	US#3@300	0.61	1GFRP	0.33	10.1	40	47
	ASG-6NSS	44.2	US#3@300	0.61	6GFRP	0.56	14.7 [b]	135 [b]	135

[a] **Control steel-confined specimens.**
[b] **Reduction in capacity less than 20% for completed cycles.**

Table 2: Ductility parameters of FRP-confined circular columns

Researchers	Specimen	f_c' (MPa)	Lateral steel: Size@ Spacing (mm)	Lateral steel: ρ_s (%)	Layers & type of FRP	Axial load level P/P_o	$\mu_{\Phi 80}$	Ductility ratio: $N_{\Phi 80}$	Ductility ratio: $N_{\Phi t}$
Sheikh and Yau. [9]	S-3NT[a]	39.2	US#3@300	0.30	0	0.54	2.6	4[b]	4
	S-4NT[a]	39.2	US#3@300	0.30	0	0.27	3.6	7[b]	7
	ST-2NT	40.4	US#3@300	0.30	2GFRP	0.54	8.9[b]	38[b]	38
	ST-3NT	40.4	US#3@300	0.30	1CFRP	0.54	7.7[b]	38[b]	38
	ST-4NT	44.8	US#3@300	0.30	1CFRP	0.27	15.2[b]	83[b]	83
	ST-5NT	40.8	US#3@300	0.30	1GFRP	0.27	12.9[b]	89[b]	89
	ST-6NT	41.6	US#3@300	0.30	1CFRP	0.27	5.5[b]	21[b]	21
Sheikh and Liu (19)	P27-1CF-3	40.0	US#3@300	0.30	1CFRP	0.27	25.6	130	145
	P27-2GF-4	40.0	US#3@300	0.30	2GFRP	0.27	28.3	114[b]	114
	P40-NF-5[a]	40.0	US#3@300	0.30	0	0.40	2.2	5[b]	5
	P40-1CF-8	40.0	US#3@300	0.30	1CFRP	0.40	9.6	34[b]	34
	P40-1GF-9	40.0	US#3@300	0.30	1GFRP	0.40	19.4	61[b]	61
	P56-NF-10[a]	40.0	US#3@300	0.30	0	0.56	1.4	4[b]	4
	P56-2CF-13	40.0	US#3@300	0.30	2CFRP	0.56	10.9	49[b]	49
	P56-3GF-14	40.0	US#3@300	0.30	3GFRP	0.56	18.1	107[b]	107
	P56-4GF-15	40.0	US#3@300	0.30	4GFRP	0.56	15.2	163[b]	163

[a] Control steel-confined specimens.
[b] Reduction in capacity less than 20% for completed cycles.

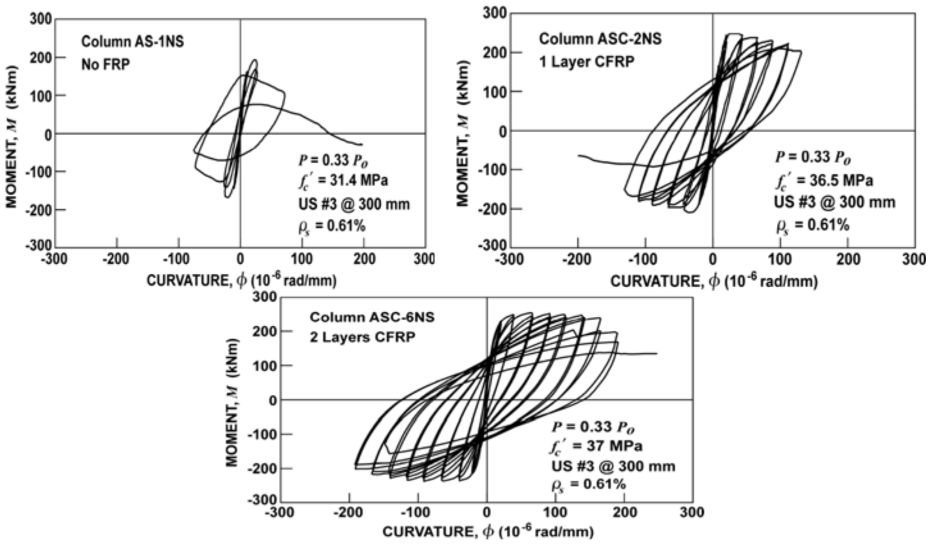

(a) Specimens tested under an axial load of 0.33 P_0

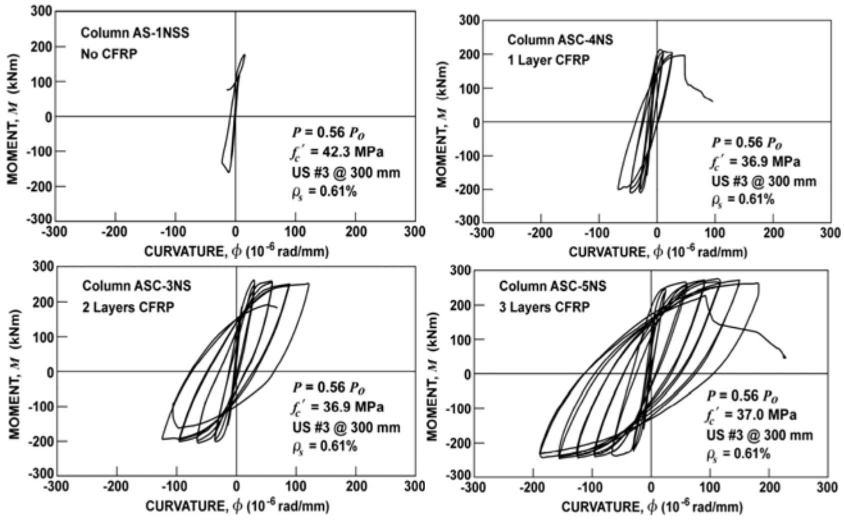

(b) Specimens tested under an axial load of 0.56 P_0

Figure 5. Behavior of CFRP-confined square specimens

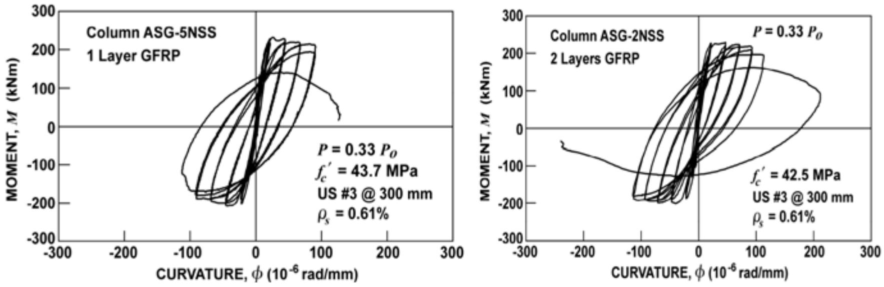

(a) Specimens tested under an axial load of 0.33 P_0

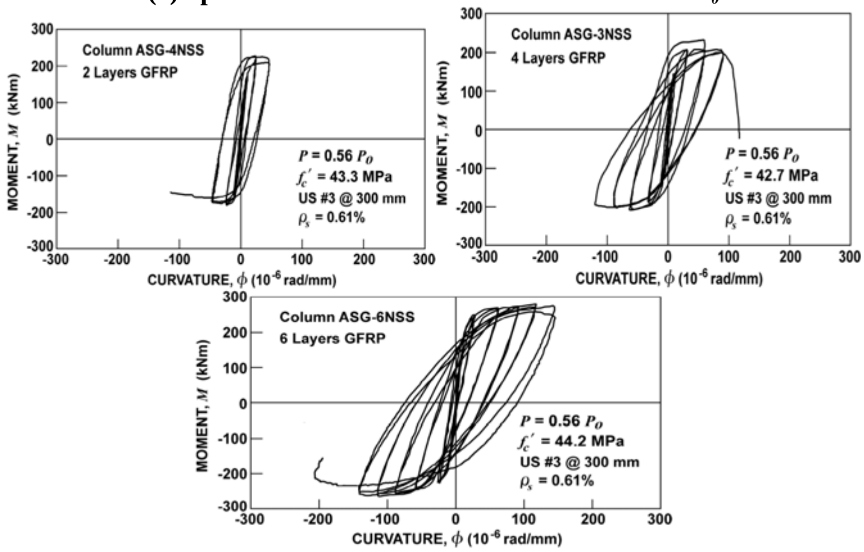

(b) Specimens tested under an axial load of 0.56 P_0

Figure 6. Behavior of GFRP-confined square specimens

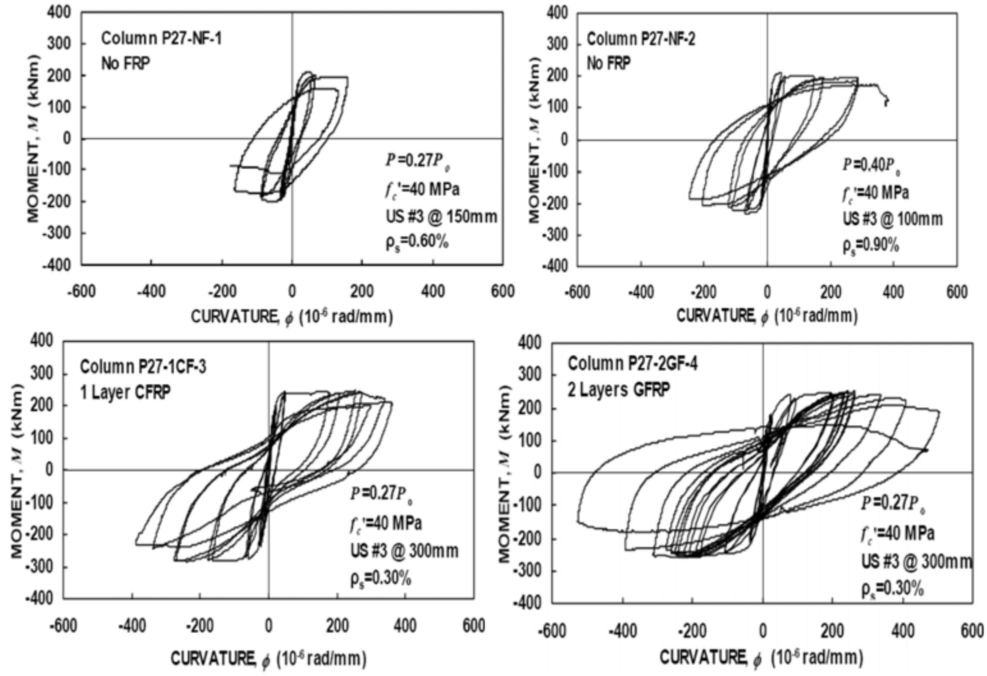

Figure 7. Behavior of circular columns under 0.27P_o

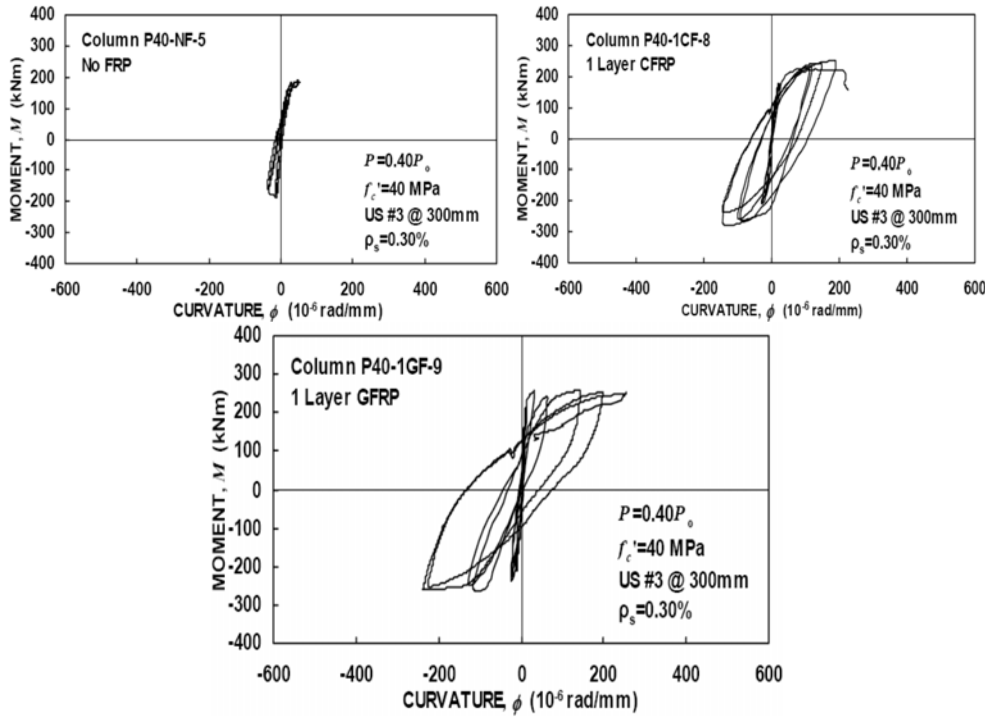

Figure 8. Behavior of circular columns under 0.40P_o

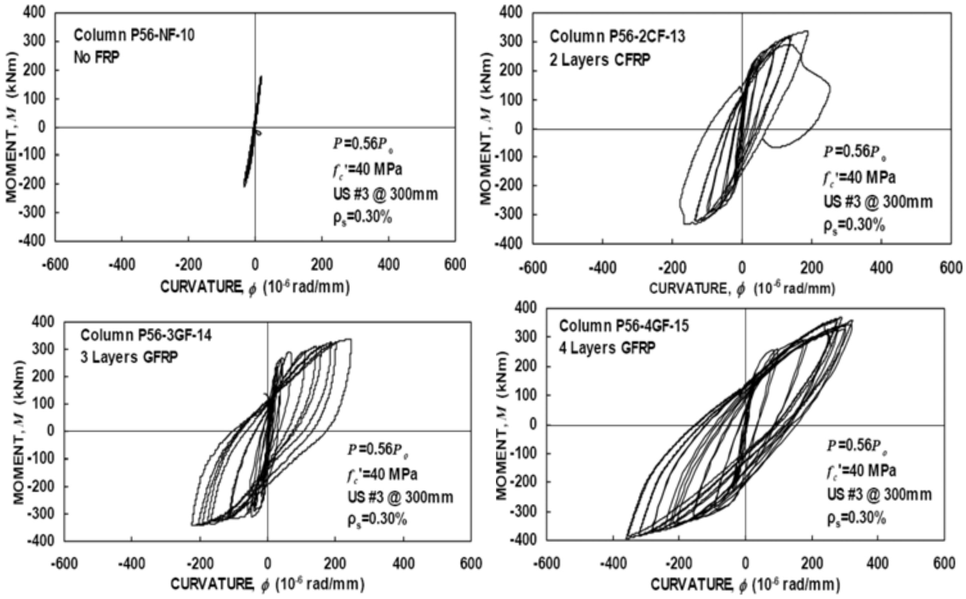

Figure 9. Behavior of circular columns under 0.56P_o

Type of confining FRP- The relative effectiveness of CFRP and GFRP in strengthening deficient columns can be evaluated by comparing the behaviour of four sets of square specimens: ASC-2NS and ASG-2NSS, ASC-3NS and ASG-3NSS, ASC-4NS and ASG-4NSS, and ASC-5NS and ASG-6NSS. The two columns in each set of specimens are similar in every aspect except that one column was confined by CFRP whereas the other one was confined by GFRP. The layers of the GFRP were twice as many as those of the CFRP. Comparisons of the ductility parameters given in Table 1 and the moment-curvature relationships in Figures 5 and 6 show that both columns in each set behaved in a similar manner and had comparable ductility parameters, indicating that the confinement effectiveness of two layers of GFRP is similar to that of one layer of CFRP. This behaviour was also observed in tests of circular columns. The specimens in each of the two pair of columns: ST-2NT and ST-3NT, and P27-1CF-3 and P27-2GF-4, are identical in all aspects except that one was confined by one layer of CFRP and another was confined by two layers of GFRP. As shown in Table 2 and Figure 7, the two columns in each set displayed very similar behaviour and had similar ductility levels and energy dissipation capacities. It is worth noting that in these tests, the ultimate tensile strength of the CFRP fabric was approximately 70% higher than that of the GFRP fabric. The stiffness of CFRP measured in terms of N/mm width per layer was about three times larger than that of GFRP. From these test results, it appears that the effectiveness of FRP in enhancing column ductility closely relates to its ultimate tensile strength.

3. DESIGN OF FRP CONFINEMENT

From the results discussed above, it can be concluded that the column ductility and

energy dissipating capacity increase as the amount of FRP confining reinforcement increases, whereas an increase in axial load level reduces column ductility. These effects are similar to those in steel-confined columns reported by Sheikh and Khoury [15]. While there are similarities between steel-confined and FRP-confined columns, major differences exist between these two types of columns that must be taken into account while designing confinement reinforcement. While the core concrete in steel-reinforced column is confined, the cover concrete outside the lateral steel is not. As the thickness of the cover concrete increases, the area of the confined concrete decreases and larger amount of confinement reinforcement is required to achieve a certain ductility performance. In FRP-confined columns, however, the entire cross section of the column is confined with the FRP wraps that are used externally. The thickness of the cover concrete thus has no effect on column behavior and is not a design parameter. Another important difference is the nature of the lateral confining pressure exerted by steel and FRP. In steel-confined columns subjected to large deformations, the confining pressure remains practically constant while the steel yields under hoop tension. In columns confined by FRP, on the other hand, the lateral confining pressure keeps increasing up to the rupture of fibers due to the linear elastic stress-strain characteristic of the FRP.
For square columns confined by FRP, Sheikh and Li [17] developed a procedure for the design of FRP confining reinforcement on the lines of a procedure Khoury and Sheikh [15] proposed for steel confined columns. In this procedure, the amount of required confinement is related to the level of axial load, lateral reinforcement configuration and ductility demand in terms of curvature ductility factor. The equation to calculate the number of layers of FRP wraps is given below (Eq.1).

$$n \cdot f_u = \beta \cdot h \cdot f_c^{'} \cdot \left\{ 1 + 13\left(\frac{P}{P_o}\right)^5 \right\} \frac{\mu_{\phi 80,in}^{\;\;1.15}}{29} \tag{1}$$

where $\mu_{\phi\, 80,in}$ is the increase in curvature ductility factor due to FRP confinement and

$$\mu_{\phi\, 80,in} = \mu_{\phi\, 80} - \mu_{\phi\, 80,con} \tag{2}$$

where
n = number of layers of FRP
f_{FRP} = tensile stress in FRP
h = cross sectional dimension of column
f_u = the ultimate tensile strength of the FRP obtained from tensile coupon tests
β = confinement efficiency parameter; equal to 0.25 for square columns
$\mu_{\phi\, 80}$ = curvature ductility factor of the FRP-confined specimen; and
$\mu_{\phi\, 80,con}$ = curvature ductility factor of the control reinforced specimen.

The simplified version of the above equation was given as

$$n \cdot f_u = \beta \cdot h \cdot f_c^{'} \cdot \left(6\frac{P}{P_o} - 1.4 \right) \frac{\mu_{\phi 80,in}}{18} \tag{3}$$

$$\geq \beta \cdot h \cdot f_c^{'} \cdot \frac{\mu_{\phi 80,in}}{18}$$

The experimental curvature ductility factors and analytical values obtained from Eq.1 and Eq.3 are compared in Figure 10(a). The average of the analytical curvature ductility factors using Eq.1is roughly equal to the average of the experimental values and the standard deviation from the mean is about 6%, whereas Eq.3 is more conservative and slightly underestimates the curvature ductility of the columns in most cases.

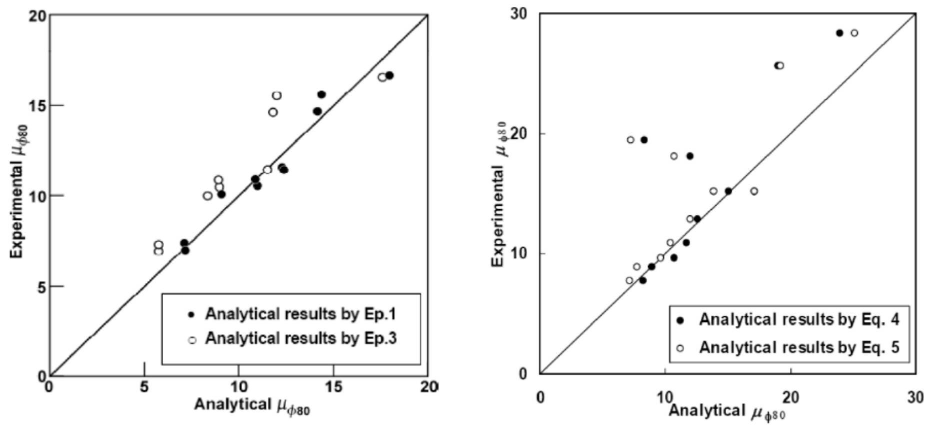

(a) Square columns (b) Circular columns

Figure 10. Comparison of experimental and analytical curvature ductility factors for square and circular columns

Equations 1 and 3 are applicable to square normal strength concrete columns confined by continuous FRP wraps with continuous longitudinal rebar in plastic hinge regions. For circular columns, following design equations were derived based on similar procedure and existing test data [18].

$$n \cdot f_u = 0.07 \cdot d \cdot f_c^{'} \cdot \left\{ 8.8\frac{P}{P_o} - 1.2 \right\} \frac{\mu_{\phi 80,in}^{\;1.15}}{29} \tag{4}$$

$$\geq 0.07 \cdot d \cdot f_c^{'} \frac{\mu_{\phi 80,in}^{\;1.15}}{29}$$

The simplified version of Eq.4 was given as

$$n \cdot f_u = 0.07 \cdot d \cdot f_c^{'} \cdot \left(9.2\frac{P}{P_o} - 1.4\right)\frac{\mu_{\phi 80,in}}{18} \quad (5)$$

$$\geq 0.07 \cdot d \cdot f_c^{'} \cdot \frac{\mu_{\phi 80,in}}{18}$$

where, d = diameter of circular column, and all the other parameters are the same as defined for Eqs.1 and.2. The validity of the design equation for circular column has also been shown by the comparison of analytical and experimental curvature ductility factors in Figure 10(b).

4. APPLICATION OF THE PROPOSED DESIGN APPROACH

The proposed method is applied to a 450 mm square column and a 500 mm diameter circular column, respectively. Both columns, with similar area of cross section, are reinforced with eight longitudinal bars of 25 mm diameter. The concrete compressive strength, steel yield strength and FRP rupture strength are assumed to be 35 MPa, 400 MPa and 900 N/mm width per layer, respectively. Figure 11 shows the number of layers needed as function of the column axial load for two values of ductility enhancement. Assuming that the original columns are capable of displaying a ductility factor of 4, enhancements of $\mu_{\Phi 80}$ by 4 and 9 would make the columns moderately and highly ductile, respectively. Addition of one layer of FRP would make the square column moderately ductile if the axial load is 0.5 P/P_o or lower. For this range of axial load, between 2 and 3 layers of FRP are needed to make the square column highly ductile.

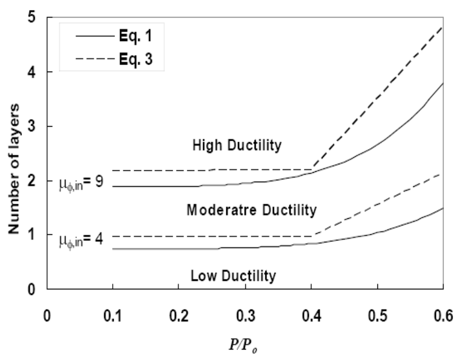

(a) Square column

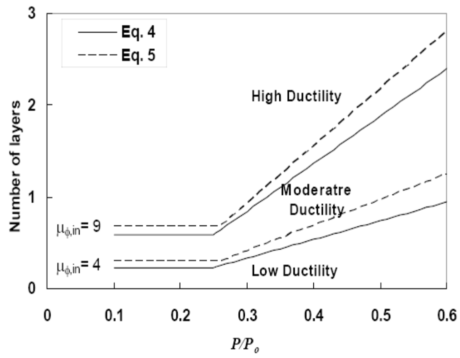

(b) Circular column

Figure 11. Application of the design procedure

As stated earlier, the results shown in Figure 11 demonstrate clearly that about half the number of FRP layers would be required for circular columns for similar ductility enhancements compare to equivalent square columns. It should be noted from Figure 11 that the simplified equation is significantly more conservative compared to the original equation particularly for high axial load levels.

5. CONCLUDING REMARKS

Selected results from an extensive experimental and analytical research program on seismic upgrade of concrete columns with FRP underway at the University of Toronto are presented. Columns tested under simulated earthquakes were either 305 mm square or 356 mm diameter circular in cross section and 1.47 m long. The experimental results show that variables that affect the ductility parameters of a column include confinement configuration, the level of axial load and the type and amount of confining reinforcement. Circular confinement is more efficient than square confinement. An increase in the level of axial load significantly reduces ductility and energy dissipation capacity of a column. The column performance in terms of ductility improves almost proportionally with an increase in the amount of FRP confinement while strength improvement is less than proportional. A performance-based approach is also briefly presented for the design of confining FRP reinforcement externally applied to square and circular concrete columns. The required amount of confining FRP increases with an increase in ductility demand, an increase in the level of axial load applied and reduced FRP strength.

ACKNOWLEDGMENTS

The authors wish to express their gratitude to Natural Sciences and Engineering Research Council of Canada and ISIS Canada, an NSERC Network of Center of Excellence for financing this work. The experimental work was carried out in the Structures Laboratories of the University of Toronto. Assistance of the technical staff is gratefully acknowledged.

REFERENCES

1. CSA-A23.3-04, *Design of Concrete Structures*. Canadian Standards Association, Rexdale, Ontario, Canada; 2004.
2. ACI Committee 318. *Building Code Requirements for Structural Concrete* (ACI 318-08). Farmington Hills (MI): American Concrete Institute; 2008.
3. Hall, J. F., ed., Northridge Earthquake of January 17, 1994, *Preliminary Reconnaissance Report*, EERI Publication No. 94-01, Earthquake Engineering Research Institute, Oakland, CA, Mar. 1994, 104 pp.
4. Comartin, C. D.; Greene, M.; and Tubbesing, S. K., The Hyogo-Ken Nanbu Earthquake: Great Hanshin Earthquake Disaster, January 17, 1995, *Preliminary Reconnaissance Report*, EERI Publication No. 95-04, Earthquake Engineering Research Institute, Oakland, CA, Feb. 1995, 116 pp.
5. Sheikh, S. A., Performance of structures during the Kashmir (Pakistan) Earthquake of 8 October 2005, *Proceedings of Ninth Canadian Conference on Earthquake Engineering*, Ottawa, Canada, June 26-29, 2007.
6. Sheikh, S. A., Jaffry, S.A.D. and Cui, C., Stay-in-place GFRP forms for Concrete Columns, *Canadian Journal of Civil Engineering*, National Research Council, Canada, 2007; 34 (3): 389-402.
7. Iacobucci, R., Sheikh, S.A., and Bayrak, O. Retrofit of Square Columns with Carbon Fiber Reinforced Polymers for Seismic Resistance. *ACI Structural Journal*, 2003; 100 (6): 785-794.

8. Memon, M.S. and Sheikh, S. A., Seismic Resistance of Square Concrete Columns Retrofitted with GFRP, *ACI Structural Journal,* 2005, 102 (5): 774-783.
9. Sheikh, S. A. and Yau, G., Seismic Behavior of Concrete Columns Confined with Steel and Fiber-Reinforced Polymers. *ACI Structural Journal*, 2002; 99 (1): 72-80.
10. Saadatmanesh H., Ehsani M. R. and Jin, L., Repair of Earthquake-Damaged RC Columns with FRP Wraps. *ACI Structural Journal*, 1997; 94 (2): 206-215.
11. Ma, R., Xiao Y. and Li, K. N. Full-Scale Testing of a Parking Structure Column Retrofitted with Carbon Fiber Reinforced Composites. *Journal of Construction and Building materials*, 2000; 14 (2): 63-71.
12. Ghosh, K. K. and Sheikh, S. A., Seismic Upgrade with CFRP of Columns Containing Lap Spliced Rebars", *ACI Structural Journal*, 2007, 104 (2), 324-333.
13. Ozbakkaloglu, T. and Saatcioglu, M. Seismic Performance of high-Strength Concrete Columns Cast in Stay-in-Place FRP Formwork. *Proceedings of 13th World Conference on Earthquake Engineering*, 2004, Vancouver, Canada.
14. Hosseini, A., Khaloo, A.R. and Fadaee, S. Seismic Performance of High-Strength Concrete Square Columns Confined with Carbon Fiber Reinforced Polymers (CFRP). *Canadian Journal of Civil Engineering*, 2005; 32 (3): 569-578.
15. Sheikh, S. A., Khoury, S. S., A Performance-Based Approach for the Design of Confining Steel in Tied Columns. *ACI Structural Journal*, 1997; 94 (4): 421-431.
16. Sheikh, S. A. and Khoury S. S., Confined Concrete Columns with Stubs. *ACI Structural Journal*, 1993; 90 (4): 414-431.
17. Sheikh, S. A., and Li, Y., Design of FRP Confinement for Square Concrete Columns. *Engineering Structures*, 2007; 29(6): 1074-1083.
18. ISIS Design Manual 4, Version 2, *FRP Rehabilitation of Reinforced Concrete Structures*, ISIS Canada Research Network, Winnipeg, Manitoba, Canada, 2008,178 pp.
19. Liu, J. and Sheikh, S. A., Seismic Behavior of Steel-confined and FRP-confined Circular Concrete Columns, *Research Report*, Department of Civil Engineering, University of Toronto, 2009, (in preparation).

CD2-KN07

SIMULATION AND BEHAVIOR OF CORROSION DETERIORATED REINFORCED CONCRETE MEMBERS

M. A. Shayanfar[1], A. Safiey[2]
[1]School of Civil Engineering., Iran University of Science and Technology, Tehran, Iran
[2]Moshanir Consultant Engineers, Park Prince Buildings, Tehran, Iran

ABSTRACT
Several reinforced concrete (RC) infrastructures are now crumbling from corrosion of steel bars in concrete. The paper presents the recent advancements in analytical simulation of corrosion aftereffects on behavior of RC members. The model juxtaposes the experimental findings with analytical relationships. The implementation of the model into a nonlinear finite element formulation as well as the experimental and analytical backgrounds are discussed. The abilities of the resulted program have been studied by modeling some experimental specimens showing a reasonable agreement between the analytical and experimental findings.

Keywords: reinforced concrete, corrosion, bond-slip, nonlinear finite element method, tension stiffening

1. INTRODUCTION
The integrity of many RC buildings and infrastructures are compromised due to some dangerous effects of the aggression of the corrosive agents. To evaluate the effects of these types of the damages on the total behavior of reinforced concrete structures, the nonlinear finite element models for reinforced concrete need an improvement to take the effects of corrosion of the steel bars into account. A survey on the literature reveals that there is a knowledge gap in this area of researches; relatively few studies addressed explicitly analytical modeling of corroded reinforcements in RC members. The amalgamation of the available analytical models is presented by Table 1. All of the reviewed models have their own advantages and disadvantages. Some of them sound to be more valuable from engineering point of view while the others seem to be more complicated and suitable at elemental level. The common point of these models is application of especial elements between concrete and reinforcement to represent the bond-slip behavior and associated damages as results of the corrosion of reinforcements.
Corrosion of steel reinforcements in the RC structures diminishes the total load bearing capacity of RC structures. This happens not only by means of depletion of rebar cross-sectional area, but also by bond deterioration as reported by some of the researchers, e.g. [6]. Tension-stiffening phenomenon in reinforced concrete is developed as a result of steel and concrete bond that occurs between the tensile cracks. Therefore, degrading effects of corrosion to the bond between steel and concrete could be taken into consideration more effectively by a proper tension

stiffening model. This would be a more practical method to solve the problem than utilization of link elements between steel bar and concrete. For this purpose at first step, a comprehensive experimental program including 58 cylindrical reinforced concrete specimens under various levels of corrosion is conducted. Some of the specimens (44) are located in large tub containing water and salt (5% salt solution). An electrical supplier has been utilized for the accelerated corrosion program. Afterwards, the tensile behavior of the specimens was studied by means of the direct tension tests. For each specimen, the tension-stiffening curve is studied at various load levels. Average crack spacing, loss of cross-section area due to corrosion, the concrete contribution to the tensile response for different strain levels, and maximum bond stress developed at each corrosion level are studied, and their appropriate relationships are proposed. Afterwards based on the experimental program and some analytical relationships, a new bond-slip-tension-stiffening model considering the effects of corrosion of reinforcement was developed. It is implemented into nonlinear finite element relationships as a part of a hypoelastic model of reinforced concrete. Finally, the performance of the program in handling nonlinear analysis of corroded reinforced concrete members is validated.

Table 1: Amalgamation of current literature

Researchers	Subject of simulation	Framework for constitutive relations	Corrosion and bond-slip representation
Coronelli and Gambarova [1]	RC beam	Incremental stress–strain relation for concrete, with smeared rotating cracks	Link element
Dekoster et al. [2]	RC beam	Elasto-plastic and damage Mechanics	Special link element called "rust"
Lundgren [3]	Direct tension test specimens	Theory of plasticity	Special layer of elements between steel and concrete
Lee et al. [4]	RC beam	Incremental stress–strain relation for concrete	Bond element
Amleh and Ghosh [5]	Direct tension test specimens	Elastic and plastic Model	Pressure–overclosure relationship

2. EXPERIMENTAL PROGRAM

A total of 58 specimens have been prepared for the experimental program. Specimens were divided into 7 types according to their sizes (see Table 2). From each type, 2 specimens (totally 14) were used as control and were not placed in the corrosive conditions. The rest of the specimens (totally 44) have been kept in the corrosive environment until the expected level of corrosion achieved. Subsequently, all of the specimens including non-corroded samples were tested by direct tension test on the embedded rod. Medium strength concrete (26 MPa) was used. The mean value of physical and mechanical properties of each type of rebars and concrete were measured (see [7] for details). Concrete cylinder specimens had a constant 500 mm length and variable diameter (60, 100, 150 mm). One deformed steel reinforcement has been embedded in the middle of the concrete cylinder. This steel bar was extended adequately outside the two ends of the specimen. The specimen diameter and reinforcement diameter have been chosen in a manner to facilitate the feasible study of the effects of some important parameters such as clear concrete cover, ratio of clear concrete cover to rebar diameter, and ratio of rebar diameter to reinforcement ratio. For the construction of the specimens, 500 mm long rubber molds have been used. The molds have been set on a special chassis vertically. Steel reinforcement has been placed in the middle of the specimens to pass through the existing socket on an especial chassis at the end area. This set has been placed on a vibration table and the ready mixed concrete has been cast in mold layer by layer. After 24 hours, the molds have been opened and the specimens were cured in the ambient temperature for 28 days. The exposed parts of the reinforcement and the end areas of the RC specimens at the top and bottom surface were coated by epoxy. The extended steel bar outside the concrete was covered by two layers of tape, electrical tape followed by duct tape. The specimens have been immersed into a fiberglass tub containing a solution of water and salt (5%). An electric supplier has been utilized to subject the specimens to voltage of 24 V and current density of 8 A. The direction of the electric current was set so that the reinforcement served as the anode while the bare metal wire which was spread over the specimens served as cathode (see Figure 1). The duration of the accelerated corrosion procedure was estimated by Faraday's law to reach the required corrosion levels; with periods ranging from one day to one month. The actual values of degree of corrosion were calculated by breaking the specimens to retrieve the reinforcing bar after completion of the tests. The reinforcement bar for each specimen was cleaned and carefully scrubbed with a wire brush to assure that the bar was free from any adhering corrosion products. Special attention had been paid not to alter the base metal. The reinforcing bar was then carefully weighed to determine the actual corrosion degree.

Two special metal plates were fabricated, and each one was affixed to the top and the bottom of the specimens by three screws for measurement of specimen axial deformation. The LVDT (Linear Voltage Differential Transducer) system was employed to measure axial deformations. One gage was attached to the top plate and another one to the bottom plate for this purpose; the values of axial deformation of the specimen in each stage of loading were recorded by connecting them to the data logger apparatus. To measure reinforcing steel elongation, a displacement gage was affixed to the reinforcing bar at the top and another one at the bottom, connected to another LVDT system. The axial tensile forces were applied by a hydraulic jack and measured by a load cell connected to the top bracket. The axial load values were measured continuously by a data logger equipment (see Figure 2). The axial forces were increased to reach yielding capacity of the steel reinforcement; the tests were ceased by the onset of plastic deformations, and the number of transversal cracks and minimum and maximum crack spacing were recorded for each specimen. Eventually, actual degrees of the corrosion were measured for the corroded RC specimens as described earlier.

Figure 1. Accelerated corrosion program [7]

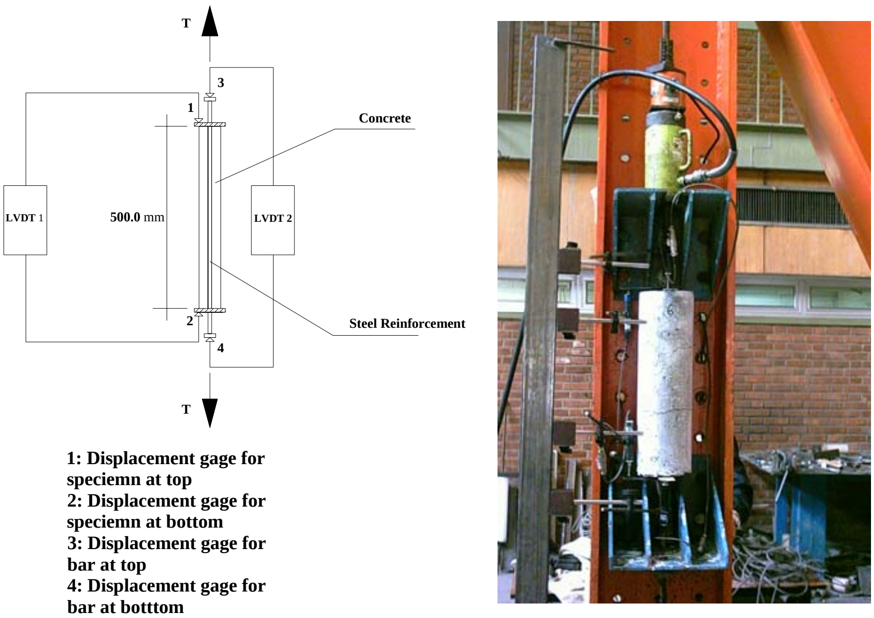

(a) Schematic representation **(b) Photo**

Figure 2. Details of the direct tension tests [7]

Table 2. The specimens overview [7]

Type	Specimen	c (mm)	ρ	c/d
1	S12-60	24	0.04	2.0
2	S12-100	44	0.0144	3.67
3	S18-60	21	0.09	1.167
4	S18-100	41	0.0324	2.278
5	S18-150	66	0.0144	3.67
6	S25-100	37.5	0.0625	1.5
7	S25-150	62.5	0.0278	2.5

The Corrosion levels, ultimate crack spacing, concrete stress contribution, bond strength, specimens' total applied tensile load versus average reinforcement strain and effect of corrosion on the cross-section area of the reinforcement are studied for specimens. The results of the experimental investigation reported elsewhere [7]. Some of the empirically obtained formulas are summarized by Table 3.

Table 3: Review of some proposed relationships [7]

Parameter	Formula
Average Final Crack Spacing	$S_m = 2.35c.\begin{cases} 1 & C_w = 0 \\ 1.533 - 0.3\dfrac{c}{d_0} + 4.2(\dfrac{C_w.d_0}{9c})^2 & C_w > 0 \end{cases}$
Steel reinforcement yield strain	$\varepsilon_y = \dfrac{f_y}{E_s}.\begin{cases} 1 & C_w = 0 \\ 0.907 - 0.757\dfrac{C_w d_0}{9c} + 0.0087\dfrac{c}{d_0} & C_w > 0 \end{cases}$
Reinforcement cross-sectional area	$A_s = A_{s0}.\begin{cases} 1 & C_w = 0 \\ 1.2 - 0.35\dfrac{C_w d_0}{9c} - 0.08\dfrac{c}{d_0} & C_w > 0 \end{cases}$
Ultimate bond strength	$f_{bu} = \dfrac{0.4c}{d_0}\sqrt{f_c}$

3. MODELING STRATEGIES

In tension, the model adopts a macroscopic approach that is directly integrated into the concrete law. It simulates implicitly the reinforcing bar-concrete interaction using tension-stiffening factors adjustable according to the nature of specimen that vary as a function of the member strain, clear concrete cover, bond-slip behavior, degree of steel bar corrosion and amount of steel reinforcements. The tension-stiffening curve consists of two distinct states, namely “multiple cracking state” and “final cracking state.” Therefore, the uniaxial tensile stress-strain curve of a RC element could be divided into three states (see Figure 3-a): (a) “uncracked state” (path OA), (b) “multiple cracking state” (path AB) and (c) “final cracking state” (path BC). The numerical strategy of the proposed model is to discretize the tensile stress-strain curve by a set of discrete points called “principal points.” Those are connected by straight line to form a polygon similar to Figure 3-b. The number of “principal points”, N, is a constant value for a specific RC element during each analysis. This value probably differs from a RC element to another, depending on its characteristics; the minimum value of N is 4; because at least for describing the reinforced concrete tensile stress-strain curve, three lines are necessary. The computed stress and strain values corresponding to “principal points” are stored in two separate vectors, namely: $\{esm\}$ and $\{scm\}$; the dimensions of these two vectors are equal to the number of “principal points,” N. The value of tensile stress corresponding to the specific tensile strain could be calculated by a linear interpolation. This concept and a sample for interpolation between the "principal points" are represented in Figure 3-b. For $i=1$, the values $esm(i=1)$ and $scm(i=1)$ are equal to zero. When $i=2$, the values $esm(i=2)$ and $scm(i=2)$ are equal to ε'_{cr} and f'_t; when i exceeds 2 the "multiple cracking state" is started and this state lasts until the value of a becomes less than $0.5S_m$. The values of stress and strain corresponding to the "principal points" in "multiple cracking state" is calculated by the following formulas:

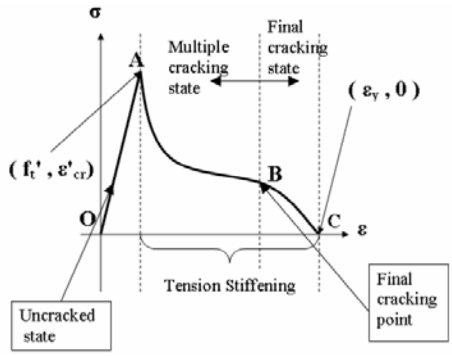

(a) Schematic representation of tension stiffening curve

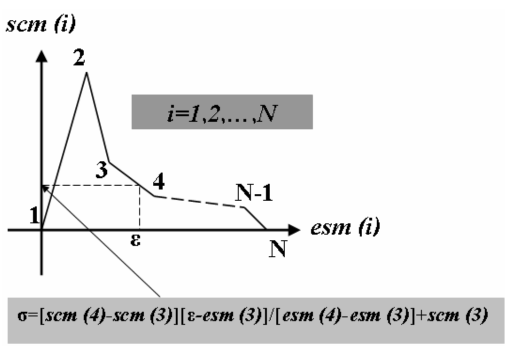

(b) Idealization of RC tensile behavior and a sample for linear interpolation between principal points

Figure 3. Tension-stiffening [8]

$$esm(2<i<N-1)=\left(\frac{1+n\rho}{n\rho}\frac{\cosh(ka)}{\cosh(ka)-1}-\frac{\sqrt{1+.5\cosh(2ka)-\frac{.75\sinh(2ka)}{ka}}}{(\cosh(ka)-1)n\rho}\right).(\varepsilon'_{cr}(\exp(-550.esm(i)-\varepsilon'_{cr}))) \quad (1)$$

$$scm(2<i<N-1)=\left(\frac{\sqrt{1+.5\cosh(2ka)-\frac{.75\sinh(2ka)}{ka}}}{\cosh(ka)-1}\right)(f'_t(\exp(-550esm(i)-\varepsilon'_{cr}))) \quad (2)$$

The derivation processes of above equations are presented in [8]. Parameter a is the half of the spacing between the two faces of two adjacent cracks in a tensile member. The value of $2a$ for the first "principal point" of "multiple cracking state" ($i=3$) is equal to element length perpendicular to crack direction, L. For the second point of "multiple cracking state", $i=4$, the value of parameter $2a$ is bisected and it gets the value of $L/2$. For the next points this procedure will be continued until a becomes less than half of the average final crack spacing (S_m); at this point ($i=N-1$) which is called "final cracking point," the "multiple cracking" curve is completed. At "final cracking state," the curve corresponding to this part is idealized by a line which is defined by two points, namely, "final cracking point" ($i = N - 1$) and "ultimate tensile point" ($i = N$). At this stage, $\{esm\}$ and $\{scm\}$ vectors are computed by these two formulas:

$$esm(i = N - 1) = \varepsilon_y - \frac{f_{bu}\Psi.S_m}{A_s E_s .2\sqrt{3}} \tag{3}$$

$$scm(i = N - 1) = 0.577 f_t' \exp(-550(esm(i) - \varepsilon_{cr}')) \tag{4}$$

For simplicity and due to the lack of information about corrosion effect on "final cracking state," the "final cracking state" is neglected for corroded RC elements, therefore, Eqs. (3) and (4) change to:

$$esm(i = N - 1) = \varepsilon_y \quad , \quad scm(i = N - 1) = 0 \tag{5}$$

and the "final tensile point" is calculated by:

$$esm(i = N) = \varepsilon_y \quad , \quad scm(i = N) = 0 \tag{6}$$

A comparison between Eqs. (5) and (6) shows that the elements $i = N - 1$ and N has the same values for the corroded RC elements, leading to removal of the "final cracking state."

4. APPLICATION

The proposed tension-stiffening model is implemented into a nonlinear finite element analysis program which is called HODA. In this section, the abilities of the developed program on the analysis of field corroded RC beam specimens are verified.

The history, capabilities, element library, constitutive models and limitations of HODA nonlinear finite element analysis program used in this study are discussed elsewhere [9]. This program can depict, through the entire monotonically increasing load range, the static and reversed cyclic response of any plain, reinforced or prestressed concrete structures that is composed of thin plate members. This includes beams, slabs (plates), shells, folded plates, box girder, shear walls, or any combination of these structural elements. Time-dependent effects such as creep and shrinkage can be also studied. The element library includes membrane, plate bending, facet shell, one-dimensional bar, and boundary elements. The facet element has been used for modeling the RC beams. The program employs a layered finite element approach. The structure is idealized as an assemblage of thin constant thickness plate elements with each element subdivided into a number of imaginary layers. Each layer is assumed to be in plane stress condition, and can be in any state - uncracked, partially cracked, fully cracked, non-yielded, yielded, and crushed- depending on the stress or strain conditions. Analysis is performed using an incremental-iterative tangent stiffness approach, and the stiffness of the element is obtained by adding the stiffness contributions of all layers at each Gauss quadrature point. Appropriate convergence/divergence criteria are utilized to stop the iterations in each load step as soon as a required degree of accuracy has been attained. Concrete are assumed to be as a stress-induced orthotropic material. The hypoelasticity constitutive relationship developed by Shayanfar has been used for modeling of the uncracked concrete. Smeared crack approach has been adopted for modeling of the cracked concrete. Thorenfeldt, et al. relationship which is able to accurately represent the family of stress-strain curves for different strength concretes including the high strength concrete is employed. In this research, the program has been modified to include tension-stiffening effect considering bond-slip and corrosion effects in reinforced concrete structures. The steel reinforcement is treated in HODA program as an elasto-plastic-strain-hardening material. A slightly modified form of the biaxial strength envelope curve developed by Kupfer, et al. is used in the program built up in the present study [9 and 10].

Three reinforced rectangular beams with f_c' equal to 70.1 MPa –that are almost high strength type concrete- were tested by Lee, et al [4]. Three beam specimens of their tests, namely BCD1, BCD2 and BCD3 are investigated in this study. The beams were 250x200 mm^2 in cross-section and they were supported over a clear span of 2000 mm (see Figure 4). It was subjected to two concentrated loads. The details of the reinforcement layout and the geometry of the beams are shown in Figure 4. The material properties of the concrete and the steel reinforcement are given in Table 4. The rate of reinforcement corrosion of each specimen is available on Table 5. Because of symmetry of load and geometry of the beams, only one-half of the beams are modeled in the finite element idealization. The beam specimen is discretized into 120 facet shell elements as illustrated in Figure 4. Plane stress conditions are assumed, therefore only one layer of concrete is sufficient. The longitudinal reinforcements are modeled using discrete bar elements without any flexural stiffness and are lumped in single bars at the reference surfaces. A 4x4 Gauss quadrature is used for estimating the integrations involved. The vertical loads are applied in 30 load steps with smaller increments of loads being applied just before the beam reaches its ultimate load stage. It would improve the rate of convergence of the solution and the accuracy in predicting the failure load. The smeared fixed crack model is used for crack modeling. All of the elements classified into two groups according to their tensile behavior; first group consists of reinforced elements with “tension-stiffening” behavior according to the proposed model; second group, consists of elements without reinforcement and their tensile stress-strain curves are described by linear “tension-softening” behavior. The first group ultimate tensile strain is equal to reinforcement yielding strain, while for the second group, it was chosen near to the strain calculated by a simple formula proposed by Shayanfar et al. [11]; this formula defines the RC element ultimate tensile strain as function of element size in a very simple manner. This is used to remedy mesh size dependency in a nonlinear finite element formulation for reinforced concrete structures.

The analytical and experimental load-deflection curves for the beams BCD1 to BCD3 are plotted in Figure 5. The analytical results are a little bit stiffer than the experimental results and in good agreement with experimental findings. The stiffer response of model can be related to non-uniform corrosion, pitting, and longitudinal cracking due to rebar corrosion and the other items that arise from haphazard nature of corrosion and cracking phenomenon in RC members.

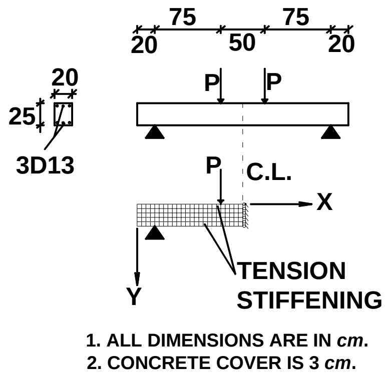

Figure 4. BCD1, BCD2 and BCD3 experimental details and finite element idealization

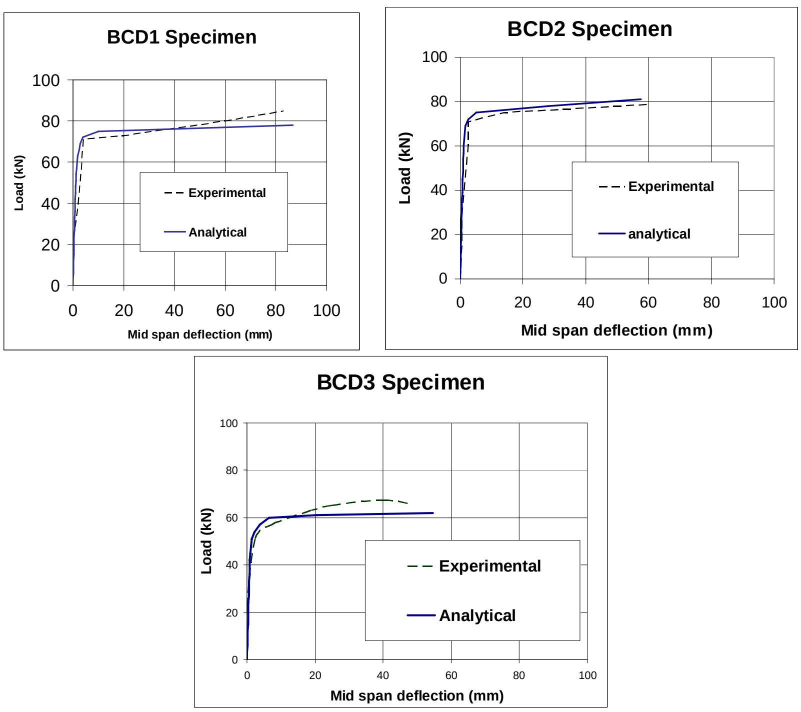

Figure 5. Experimental and analytical comparison

Table 4: Material properties of RC beams

Properties	Beams
$A_s\,(mm^2)$	256.46
$f_c\,(MPa)$	70.1
$E_0\,(MPa)$	38500
ε_c	0.002
ε_{cu}	.004 (Assumed value)
$f_t'(MPa)$	3.67
$f_y\,(MPa)$	359.4
$E_s\,(MPa)$	197000
$E_s^*\,(MPa)$	1300 (Assumed value)
ε_{su}	0.15
$E_b\,(MPa/mm)$	450 (Assumed value)

Table 5. Rate of corrosion in RC beams

Beams	$C_w\,(\%)$
BCD1	3.8
BCD2	7.9
BCD3	25.3

5. CONCLUSION AND SUMMARIES

The conclusions drawn from experimental investigation, which is presented with more details in [7], could be summarized as follows: The tensile behavior of reinforced concrete considering corrosion effects was studied experimentally. The specimen properties were chosen in a manner to reflect the effects of the governing parameters in the tensile behavior of the reinforced concrete specimens. The following conclusions are drawn:

1. (a) The ultimate crack spacing for non-corroded specimens mainly is related to the clear concrete cover of specimens. (b) This length will be increased for corroded specimens by increasing the degree of corrosion and appearance of longitudinal cracks. (c) This is merely related to the decline of the bond between concrete and steel reinforcement demanding for greater length to transfer tensile forces from the steel to the concrete.
2. The study of the specimens concrete stress contribution versus steel reinforcement average strain reveals that the tension stiffening of reinforced concrete is very sensitive to the degree of reinforcement corrosion. Severe corrosion results in bond breakdown between concrete and steel reinforcement; nearby no contribution of the concrete in the tensile response

beyond cracking (tension cut-off) could be expected for specimens in such condition. The lower levels of the reinforcement corrosion have considerable impacts on the stiffness and the ultimate strain of the tension-stiffening curve. The ultimate tensile strain of these curves for non-corroded specimens is close to the reinforcement yielding strain, but it will be reduced nearby to the strain corresponding to the tensile strength of concrete by increasing the levels of corrosion. The study on total applied tensile forces versus the average reinforcement strain curves also shows that the corrosion will decrease concrete stress contribution in cracking states.

3. The study of ultimate average bond strength deterioration of specimens and loss of cross-section area of reinforcement as result of corrosion reveals that the ratio of clear concrete cover to the size of the reinforcement has an important role in controlling these two important effects of corrosion.
4. Some empirical formulas for prediction of some of the studied parameters (e.g. ultimate crack spacing) were proposed and compared with the experimental findings of a similar program. Acceptable correlations were observed between the results of these two research programs.

Moreover, a new semi-analytical model describing the tension-stiffening phenomena considering bond-slip behavior and corrosion is represented; see also [8]. The model splits the tension-stiffening curve into two states, namely: "multiple cracking state" and "final cracking state." The proposed procedure predicts the "final cracking point" by an experimental criterion by setting a lower bound for the average final crack spacing parameter. Another novel aspect of the tension-stiffening model is the discretization of the tension-stiffening curve by a set of points called "principal points" and using linear interpolation technique for computing tensile stress corresponding to a specific tensile strain. This model has been implemented into the HODA program. This program utilizes the hypoelastic model and the smeared crack approach. The model has been tested by means of analyzing three field RC beams; the RC beams have the same geometry and material property but different rates of tensile rebar corrosion. The analytical responses using HODA program reveals good agreements with the experimental findings. The principal features of this paper in a quick view are:

1. Without using any special element between concrete and steel by only modifying the tension-stiffening curve depending on the rate of steel bar corrosion, the corroded RC elements can be modeled with a reasonable accuracy. This method is applicable for a vast variety of steel reinforcement corrosion rates.
2. A new bond-slip-tension-stiffening algorithm has been introduced.
3. Ductility and the failure points of the corroded reinforcements RC members have been predicted reasonably by the means of a simple nonlinear finite element model.

REFERENCES

1. Coronelli, D. and Gambarova, P. (2004), "Structural assessment of corroded reinforced concrete beams: Modeling Guidelines", *J. of Str. Eng., ASCE,*

130(8), 1214-1224.

2. Dekoster, M., Buyle-Bodin, F., Maurel, O. and Delmas, Y. (2003), "Modeling of the flexural behavior of RC beams subjected to localized and uniform corrosion", *Eng. Str.*, **25**, 1333-1341.
3. Lundgren, K. (2001), "Bond between corroded reinforcement and concrete", Report No.00:3, Department of Structural Engineering, Chalmers University of Technology, Gotenberg, Sweden.
4. Lee, H.S., Noguchi T., and Tomosawa F. (2000), "Analytical evaluation of structural performance of reinforced concrete beams considering degree of reinforcing bar corrosion", *Proceedings of Fourth International Conference on Repair, Rehabilitation and Maintenance of Concrete Structures and Innovations in design and Construction, Seoul, Korea*, **SP 193-46**, 779-789.
5. Amleh L., and Ghosh A. (2006), "Modeling the effect of corrosion on bond strength at the steel–concrete interface with finite-element analysis", *Can. J. Civ. Eng*. 33: 673–682.
6. Amleh, L., and Mirza, M.S. (1999), "Corrosion influence on bond between steel and concrete", ACI Str. J., 96(3), 415-423.
7. Shayanfar, M. A., Ghalehnovi, M., and Safiey, A., "Corrosion effects on tension stiffening behavior of reinforced concrete," *Computers and Concrete: An International Journal*, Vol.4, No.5, pp.403-424, 2007.
8. Shayanfar, M. A., and Safiey, A., "A new approach for nonlinear finite element analysis of reinforced concrete structures with corroded reinforcements," *Computers and Concrete: An International Journal*, Vol. 5, No. 2, pp. 155-174, 2008.
9. Shayanfar, M. A. (1995), "Nonlinear finite element analysis of normal and high strength concrete structures", PhD thesis, McGill University, Montreal, Canada.
10. Shayanfar, M. A., and Safiey, A., "Hypoelastic modeling of reinforced concrete walls," *Computers and Concrete: An International Journal*, Vol. 5, No. 3, in press, 2008.
11. Shayanfar, M.A., Kheyroddin, A., and Mirza, M.S. (1997), "Element size effects in nonlinear analysis of reinforced concrete members", Com. & Str., 62(2), 339-352.

CD3-KN02

INTERNATIONAL TRENDS IN BUILDING & CONSTRUCTION RESEARCH & DEVELOPMENT

W. Bakens,
Secretary General CIB, International trends in Building & Construction Research & Development

1. BACKGROUND AND INTRODUCTION

CIB-the International Council for Research and Information in Building and Construction –is the world's foremost network of organizations and persons in this area. Its objective is to stimulate the worldwide exchange information and cooperation in international projects, on all aspects of building and construction,

- with activities in the areas: technology, design and process for buildings and the built environment
- with members from research, academia, industry and other built environment stakeholders
- operating through experts commission, priority themes, student chapters and special interest clubs

Two groupings of worldwide / international trends and developments:

- of a more general nature and related to developing governmental policies
- related to priority themes for building and construction R&D.

2. TRENDS IN B&C R&D OF A MORE GENERAL NATURE

1 In many developed countries, with a built environment that is more or less "ready": Lessening of political interest in B&C R&D and withdrawing of government as subsidizer of collective research, resulting in:
- growing impact of industry stakeholders
- growing focus in R&D on industry requirements / applicability of R&D / innovation
- increasing commercial pressures on B&C R&D institutes / slimming or even disappearing B&C R&D institutes.

In CIB we see this reflected in the form of a growth since a few years especially of industry members and through a former emphasize in CIB Meetings on academic discussions being replaced by ones on practice oriented projects.

2 In Europe: R&D programs directed and financed from Brussels, resulting in:
- EU cooperation ànd competition in programs, but now also between institutes beyond programs; resulting for example in regional cooperation / mergers or specialized (expensive) international R&D laboratories, with Brussels'subsidies.

In CIB we are realizing that we are in fact competing with such funded EU R&D programs and we notice that no longer our growth in membership is originating from Europe but from the other regions in the world.

3. WORLDWIDE B&C R&D PRIORITY THEMES=CIB PRIORITY THEMES

1 SBC-Sustainable Building and Construction CIB started with SBC as a Priority Theme in 1995, but after more then 10 years it is still that important worldwide as a "driver" of R&D. Dominant developments in the SBC area over these years include"

-changing focus: from an emphasize on "simple" topics like energy, waste pollution and recycling, via a more holistic but also complex approach looking for balance between social, economic and environmental sustainability, now "back to a "relative simple" approach again with an emphasize on topics like energy (again, but far more ambitious) and climate change (both mitigation and adaptation).

-SBC becomes a strategic priority in other parts of the world, for example in China-SBC/Green Building becoming a necessity in main stream construction practice, resulting for example in the need for assessment/labeling/certification systems.

CIB Priority Theme since 1995: SB Agenda, SB Conference series, various Commissions, partnership with the UN.

2 RC-Revaluing Construction There is an acknowledged need in many countries to develop towards a substantially different and high performing industry that is integrated and transparent in organization, that is pro-active, innovative and client and user oriented in attitude, that is perceived to be of high value to society and that attracts high quality and well educated employees.

- examples of national reform programs include: Rethinking Construction in the UK, PSIBouw in The Netherlands, CRC for Construction Innovation in Australia en various such programs in Scandinavian countries
- R&D themes in such national reform programs include: procurement and process (with assumed decisive roles for large public clients), with attention for example for LCC based procurement and performance procurement, and industrial production processes.

CIB Priority Theme since 2001: RC Agenda, various Commissions, RC Conference series

3 IDS-Integrated Design Solution in Construction After two decades of developments in international research now – since 1 or 2 years – a sudden exploding attention all over the world for the use of BIM - Building Information Models = all partners in a project (for example in one joint server) really sharing all information in one model throughout all phases of the project, based on IFC information standards. The technology for this seems to be more or less ready for application (or not yet?).
-the application of BIM will result in a substantially different process for

the planning, design, construction and management of buildings and infrastructural works; one that requires not only different information management, but also different liabilities, communication, procurement, culture etc.
-BIM will offer new possibilities for integrated CAD/CAM processes and create a new context for Automation and Robotics in Construction.
-the application of BIM is being made mandatory in the public procurement of buildings in some North European countries, but also by organizations like GSA in the USA.
IDS is a CIB Priority Theme since 2006 and is still in stage of program elaboration: first CIB IDS conference in Helsinki, Finland in June 2009

Summary trends in worldwide B&C R&D:

- in developed countries: growing role for the industry / growing emphasize on applicability of R&D outcomes, but also growing commercial pressures in some case resulting in slimming down or even disappearing B&C R&D institutes
- in Europe: development towards an international R&D market, with funding for collective R&D from Brussels = unique in the world
- surprisingly many similarities in defining Priority Themes, with today's B&C R&D in many countries being driven by priorities i) still for Sustainable Building and Construction but now with amongst other a strong focus on issues related to climate change and the built environment, ii) Revaluing Construction with its often very ambitious industry reform programs and with a lot of attention for applying new organizational models and iii) the aim for Integrated IT based Design Technologies with in this context the 'sudden" worldwide and often mandatory application of BIM.

Closing Remarks

Not one country has the resources to be leading all developments. For all countries the principle applies that 80 – 90% of needed new knowledge and technologies is being developed abroad.

State-of-the art knowledge and information on all such themes B&C R&D is being brought together in CIB and is being made accessible for all its members.

We live in fast changing world: one in which R&D has a great potential to be of value to all built environment stakeholders and one in which modern technologies can very substantially increase the performances of our industry.

It is important for the Iranian B&C R&D community to become engaged in CIB as actively as possible.

CD3-KN05

CONSTRUCTION INDUSTRY DEVELOPMENT IN DEVELOPING COUNTRIES; LESSONS AND OPPORTUNITIES

R. Milford
Immediate Past President, CIB, Programme Manager; Performance Improvement, Cidb

ABSTRACT

This paper deals with the development of the construction industry, with a particular focus on developing countries. The paper brings together some of the lessons learned from the national programmes around the world, and explores the opportunities for enhancing the role of research infrastructure and national laboratories in supporting such change.

The paper notes that in those countries that have adopted national initiatives to develop the construction industry, opportunities exist for the research infrastructure (the universities and research laboratories) to make a meaningful contribution to the development of the industry. In fact, it is likely that any national activity cannot succeed without the active support and participation of the research infrastructure. Specifically, research organisations underpin the development of the construction industry in any country.

Keywords: construction industry development, research

INTRODUCTION

Ladies and gentlemen.

My address deals with construction industry development, with a particular focus on developing countries. My aim is to:

- bring together some of the lessons learned from the national programmes around the world; and
- explore some of the opportunities for enhancing the role of research infrastructure and national laboratories in supporting such change.

WHAT IS CONSTRUCTION INDUSTRY DEVELOPMENT?

- Construction industry development is the deliberate and managed process to optimise the contribution of the construction industry in:

meeting national construction demand;

- promoting national social and economic development objectives;
- promoting industry performance and competitiveness; and
- providing improved value to clients.

This definition was crafted by, amongst others, Prof George Ofori, Jill Wells and Spencer Hodgson at the 1st Conference on Construction in Developing Countries in Arusha, Tanzania, September 1998, organised by TG29 of the CIB.

PARTICIPANTS IN CONSTRUCTION INDUSTRY DEVELOPMENT

This definition of construction industry development addresses the role and the contribution of all participants who add value to the delivery process;

- from project inception to project handover and maintenance; and includes
- the public and private sector clients, build environment professionals, constructors, materials manufacturers and suppliers, training delivery institutions, regulatory bodies and research institutions.

Furthermore, this definition does not differentiate between the local industry and the foreign industry – but in developing countries a component must clearly include a focus on the development of the local (or indigenous) industry.

AN INTERNATIONAL PERSPECTIVE

Internationally, several countries have established formal or informal national programmes to support the objectives of construction industry development. The ‘drivers’ that have led to the creation of theses national initiatives show both common elements and local dimensions.

Common elements include (after Roger Courtney, 2002):

- a recognition that construction accounts for a significant proportion of national economic activity and that the effectiveness of the sector has implications for other industries and for public services;
- a perception that construction, in contrast to other industry sectors, has not improved its use of labour and its overall productivity as much as other sectors in recent decades and that as a consequence its outputs are becoming relatively more expensive;
- a view that a key factor in the allegedly poor performance of construction is the number of different parties who have responsibilities within the construction process and therefore a desire to bring about a more integrated process; and
- overall, a view that construction should, by integrating its internal processes and adopting new information and production technologies, seek to become more similar to manufacturing sectors.

Before looking at these factors in more depth, it is useful to look at construction industry development from a developing country perspective.

A DEVELOPING COUNTRY PERSPECTIVE

Although many of the challenges facing the construction industry in developing countries are similar to those in developed countries (and hence much can be learnt from the initiatives in developed countries), there are also significant differences between the developed and developing countries. In particular, Ofori (1999, 2001) notes that:

- although construction may account for a significant proportion of national economic activity in developing countries, in many cases the indigenous industry is weak and under-developed, and much of the construction activity is undertaken by multinationals;

- the construction industry in many developing countries is facing reduced levels of demand as a result of adjustment programmes which invariably involve cuts in governments' capital investment; and
- with public funds under severe strain and chronically short, ways must be found to structure funding strategies which are suitable for the developing countries.

DRIVERS FOR CHANGE; LOCAL ELEMENTS

Other factors, or local elements, have been prominent in many countries which have created the need for a national or industry focus on the development of the industry, including:

- in the UK, major clients (notably utility companies that had been previously public sector organisations) wished to achieve better value from their investments in construction and sought new relationships and procedures to obtain this;
- in the UK also, the poor image of construction, as perceived by prospective employees and the Stock Market, caused firms to consider how new forms of operation could both provide more attractive employment conditions and higher levels of profitability;
- in Singapore, there was a realisation that the industry was heavily dependent upon relatively unskilled operatives, many from outside Singapore, and a principal focus of the review was therefore skills requirements and means of making more effective use of labour;
- in South Africa, the need to create an enabling environment for the transformation of the industry to create economic opportunities for all participants;
- in Hong Kong, some prominent defects in new construction works, such as inadequate foundations, had revealed shortcomings in quality practices, and – in the extreme – corrupt practices. Institutional arrangements for both procurement and in the carrying out of the works (e.g. the use of multi-layer sub-contracting) became a principal focus of the review;
- a desire to increase the international competitiveness of the construction sector, so that it could secure a higher proportion of business from other countries, was a factor in Hong Kong, Singapore and Australia.

It is seen from these examples that the focus of the development of the industry is very context specific, and depends on the needs of the country at a specific point in time.

NATIONAL PROGRAMMES

Internationally, the national programmes to support construction industry development broadly fall into three categories, namely:

- those that have established national initiatives to develop the construction sector, involving a wide range of actions (e.g. UK, Australia, Hong Kong, Singapore, South Africa, India, Denmark);

- those that have recognised many of the needs of construction industry development in research programmes and other activities, but have not brought these together in a national initiative (e.g. Finland, the USA, Sweden); and
- those that have no national programme, but have some activities that address construction industry development (e.g. France, Malaysia, the Netherlands, Chile, Japan).

These categories do not have sharp boundaries, and some countries (e.g. Denmark) might be placed in a different category.

My presentation to follow will only focus on national initiatives.

THE SOUTH AFRICAN EXPERIENCE

While the need for, and focus of, the development of the industry differs from country to country, it may be useful to reflect on some aspects from the South African experience in developing the construction industry.

The impetus to the start of the reform process in South Africa began before the democratic elections in 1994, in which political power was transferred from a minority to the majority.

But the passage of transfer of economic opportunities to the majority was not going to be easy. Prior to 1994, the black population was excluded from most economic and many social opportunities (including meaningful education and skills development). Amongst others, a clear need therefore existed to promote the development of black contractors and participants – most of which had been excluded from meaningful participation in the construction industry.

A DECLINING CONSTRUCTION INDUSTRY

While the need for transformation was clear–prior to 1994 (like many other countries), the demand for construction in South Africa was in decline, resulting in increased competition, shedding of labour and skills, limited recapitalisation of equipment, and so on.

Simply transferring economic opportunities from one sector to another was not a viable option, and the development of the industry depended on:

- growth in infrastructure investment - providing increased opportunities;
- growing the capacity of the industry to meet the increased demand – and particularly amongst the previously disadvantaged sector; and
- improving the performance of all participants to deliver value for money to clients and to meet socio-economic objectives.

THE SA GREEN AND WHITE PAPERS

The process for setting up the framework the development of the construction industry in South Africa included the development of a government Green Paper in 1997, a White Paper in 1999, and legislation for the establishment of the

Construction Industry Development Board (ci**d**b) in 2000.
The South African Green and White Papers parallel in many ways the frameworks developed in other countries, such as:

- the Latham and Egan Reviews in the UK;
- the Australian Construction Industry Development Agency (CIDA) and the National Building and Construction Committee (NatBACC) Action Agenda – Building for Growth; and, more recently
- Vision 2020 in Singapore.

THE CONSTRUCTION INDUSTRY DEVELOPMENT BOARD (SA)

The ci**d**b was established in South Africa in 2000, reporting to the Minister of Public Works, and currently has a staff complement of about 120 people, grouped around:

- corporate functions;
- registration of contractors and projects;
- procurement and delivery management;
- growth and contractor development; and
- performance improvement.

Again, the ci**d**b parallels in many ways the institutional structures developed in several countries, including:

- the Rethinking Construction, Constructing Excellence, Better Public Buildings and other initiatives in the UK;
- the performance improvement programmes of the Building and Construction Authority (BCA) of Singapore;
- the initiatives of the Construction Industry Development Board (CIDB) of Malaysia;
- the Australian Construction Policy Steering Committee (CPSC) Construct NSW and other initiatives of the government of New South Wales.

DRIVING CHANGE

Turning again to international experience, the ability and approach adopted to influence stakeholders under a national initiative varies significantly from country to country. However, there are many commonalities.
Firstly, internationally, many governments have assumed the lead responsibility for driving reform initiatives in the context of national socio-economic objectives.
Governments are more able to organise public sector clients around reform initiatives (*albeit* usually under the instructions of a higher authority), driving change within their own business functions (such as procurement reform), and driving change amongst their suppliers (largely through the procurement regime). On the other hand, there are only a few successful examples of private sector clients collectively driving change and reform initiatives amongst themselves or amongst their suppliers – other than amongst a small number of forward looking

committed private sector clients.
Similarly, there are few successful examples of construction industry suppliers collectively driving change amongst themselves – with the most notable examples being the benchmarking initiatives in the USA.

AFFECTING CHANGE
International experience has shown that effecting change at a national or sector level is complicated, resource intensive, and can only be achieved over a relatively long period of time (in some cases up to 10 years or even longer). Notwithstanding the huge challenges, numerous reform initiatives have been initiated around the world to support the necessary development of the construction industry – and many of these have shown progress towards their objectives for reform. An assessment of these reform initiatives (some of which themselves have been in existence for 10 years or longer) highlights key criteria for the success of such reform initiatives, and collectively these point towards a structured framework that can be adapted to national performance initiatives.

The international reform initiatives reviewed by the authors include, amongst others:

- the Rethinking Construction, Constructing Excellence, Better Public Buildings and other initiatives in the UK;
- the performance improvement programmes of the Building and Construction Authority (BCA) of Singapore;
- the Australian Construction Industry Development Agency (CIDA) and the National Building and Construction Committee (NatBACC) Action Agenda – Building for Growth;
- the Australian Construction Policy Steering Committee (CPSC) Construct NSW and other initiatives of the government of New South Wales;
- the initiatives of the Construction Industry Development Board (CIDB) of Malaysia;
- the recently initiated Process and System Innovation in Building and Construction (PSIB) programme in the Netherlands; together with
- a range of government and client driven initiatives aimed at furthering sustainable development, and in particular environmentally sustainable development.

Some key elements of these initiatives are described in the following sections.

LEADERSHIP
Without exception, the role of leadership by individuals and/or organisations has been fundamental to the success of every one of the more successful international reform initiatives. Common forms of leadership that are observed in the international reform initiatives include:

- Leadership by *government* (either individuals of government departments) – demonstrating commitment and willingness to the reform initiatives. Examples of such leadership by government include the procurement reform initiatives being carried out in the Office of Government Commerce (OGC) in the UK, the *Better Public Buildings* initiative in the UK, and the *Construction Client Charter* and *Demonstration Projects* initiatives in the UK.
- Leadership by influential forward thinking and progressive *private sector* organisations, and in particular private sector clients, is relatively common internationally. Examples include those initial private sector clients participating on the UK *Construction Client Charter*, and members of influential organisations such as the *World Business Council for Sustainable Development*.

OBJECTIVES CREATE THE FOCUS

Performance improvement programmes are generally driven by high level goals and objectives. For example, the Singapore programme to promote buildability derives from the national objective to limit the need for imported labour by improving productivity. Clarity on priority reform objectives is of the utmost importance to ensure focus, and is usually informed by policy, legislation and industry reviews. The objectives usually have to be cascaded out from higher level objectives to more manageable lower level objectives, which can them be prioritised. For example, the *Construct NSW* agenda set out an integrated framework of 20 strategies and 85 supporting actions to enable the government to achieve best value for money from its construction procurement, to support its economic and social goals through construction procurement and to assist the industry to achieve it potential. These strategies were then grouped under 8 headings-analogous to objectives – including:

- strategic information for decision making;
- business ethics and practices;
- security of payment;
- management and workforce development;
- continuous improvement;
- towards an ecological sustainable industry; and
- encouragement and recognition.

AWARENESS

Awareness creation and promotion is fundamental to furthering the objectives of reform initiatives, so as to continually reinforce the reform message, and to broaden the awareness and understanding of the reform initiatives. There are numerous examples of successful (and unsuccessful) awareness creation and promotion activities internationally, including:

- targeted awareness creation in the popular and technical press;
- award systems, such as the Considerate Contractor Scheme and the Prime Minister's Better Public Building Award in the UK;

- forums, benchmarking clubs, and demonstration projects, and
- periodic reporting, on the state of the industry or industry reform.

INFORMATION AND TOOLS

The development and dissemination of appropriate *information and tools* to support the attainment of reform objectives is a further key success factor, and as illustrated below can take various forms. Note, however, that many of the systems outlined below are in fact enforced through various instruments in many of the reform initiatives around the world, but the systems themselves provide a tool together with information to equip various stakeholders for change:

- *codes, standards and guidelines*, both voluntary and enforced through legislation;
- *best practices*, applicable to almost every reform initiative around the world;
- *management systems*, together with supporting implementation tools, specifying processes to be adopted and reported on, varying from full ISO 9000 and 14000 accreditation (which is currently required on selected projects in Singapore), to the management systems developed to target specific issues – such as the NSW Australia OHS&R Management Systems and Environmental Management Systems;
- *accreditation and rating systems* together with supporting implementation tools, such as the LEED environmental design accreditation of design professionals in the USA, the NSW Contractor Best Practice Accreditation System, and accreditation systems for buildings – predominantly environmental and quality systems;
- triple-bottom line *reporting schemes* and methods, which are becoming increasingly common around the world.

CAPACITY BUILDING

Capacity building is key to several of the international reform initiatives, including:

- formal training programmes for public sector officials that support reform initiatives;
- the establishment of public sector Centres of Excellence (such as the *OGC Programme and Project Management Centres of Excellence* in the UK), whose aim is to achieve significant improvement to central government capability to deliver successful programmes and projects;
- the sponsorship of formal and informal training programmes for private sector participants impacted on by reform initiatives.

In addition, many of these capacity building programmes in the public sector are supported by the development and implementation of performance management systems for public sector officials that are aligned to the reform initiatives.

ENFORCEMENT AND COMPLIANCE

All reform initiatives around the world are dependent to a greater or lesser degree on enforcement and compliance mechanisms. These mechanisms vary significantly, and include:

- *legislation* to seek compliance with minimum acceptable standards (such as safety and health, and certain environmental considerations). In NWS, legislation has also been introduced to effect the prompt payment of subcontractors;
- *procurement instruments*, which are one of the most powerful instruments used in all reform initiatives for effecting change amongst suppliers, i.e. clients (typically government clients) specifying their requirements (aligned with the reform objectives) for other parties wishing to do business with them –often requiring compliance with codes of conduct, standards, and guidelines, or the mandatory use of management systems;
- *registration and accreditation* of contractors, designers, etc. according to specified criteria for different types of activities – including "construction registers", which is typically implemented through legislative or procurement means; and
- *commitment to voluntary compliance* together with review mechanisms, to charters, codes of practice and/or conduct, management systems, reporting, including:
- the UK *Construction Client Charter Improvement Programme*, in which clients commit to continually improving their performance in 4 themes;
- the numerous environmental and social responsibility charters – such as the *Equator Principles* developed by leading international financiers; and the FIDIC *Integrity Management System*, adopted by the World Bank and others.

MONITORING, EVALUATION AND REVIEW

Regular monitoring, evaluation and review is an essential requirement for the successful implementation of any strategy, and is a key element of all international reform initiatives – and takes place at both the "macro-level" and the "micro-level". For example:

- at the "macro-level" the UK has instituted the *Construction Industry Indicators* and the *Quality of Life Indicators* – setting high-level performance targets for the industry together with ongoing monitoring against these targets; and
- at the "*micro-level*", the UK has initiated the OGC "*Gateway*" review process for acquisition programmes and procurement projects, and the CABE "Design Review" for buildings that will have a significant impact on their environment, while Singapore and Australia require closeout reviews of projects against certain criteria (which will also shortly be introduced in South Africa).

RESEARCH INFRASTRUCTURE

Turning now to the role of the research infrastructure in supporting national initiatives.

It stands to reason that research infrastructure, including national laboratories and academic institutions, can play a strong role in supporting the development of the construction industry and any national programmes. However, the relationship between the research infrastructure and national initiatives has not always been clear–often due to conflicting priorities and conflicting departmental reporting lines.

FUNDING STREAMS

The past 20 years or so has seen significant changes in the landscape impacting on national laboratories due to changing funding streams, impacting in particular on national laboratories in Europe, the UK, Australia and South Africa.

For example, in the built environment, the Building Research Establishment (BRE) was privatised in the middle of the change programme in the UK, notwithstanding a very strong link between the UK reform initiative being driven from the then Department of the Environment, Tourism and the regions (DETR) and the DETR being a principle funding agency of the BRE.

Similarly, although not linked to any national change initiative (but certainly linked with supporting governmental departmental needs and priorities), changes in funding streams from the Department of Transport in South Africa had a major negative impact on transportation and road engineering at the CSIR. Similarly, changes in funding priorities from the Department of Science and Technology resulted in the closure of the structural, materials engineering and other laboratories at the building research facilities at the CSIR in South Africa – and in all probability these facilities have been lost to South Africa (and in fact Africa) for good.

Clearly, if the national research infrastructure is to support national change initiatives supporting the development of the construction industry, then it has to be funded appropriately.

CONFLICTING PRIORITIES

However, changes in funding streams have also been associated with changes in research priorities initiated by the research institutions themselves or by government departments.

For example, in South Africa, which probably mirrors some countries in the rest of the world, we have seen changes in which the national laboratories were originally set up in the 1950s as "agencies" of government departments to support the developmental objectives of the government departments. With the withdrawal of government funding for research in the 1980s and 1990s, these laboratories followed a more market orientated and commercial approach – resulting in research directions being dictated by commercial opportunities. More recently, in the 2000s, the national laboratories have adopted an increasing blend of "science for science sake" in order to rebuild a deteriorated research base in these laboratories.

All these changes in South Africa, and in many parts of the world, have largely been driven by a disjuncture between:

- research funding streams often determined by departments of science and technology; and

- developmental objectives determined by government service delivery departments and/or industry.

LINKING RESEARCH TO DEVELOPMENT NEEDS

I have always held the view there has to be a close link between research institutions and national or industry policies and priorities – but these have to be appropriately funded through the same mechanism.

In South Africa, the ci**d**b (like some other countries in the world) have adopted an approach to consciously build capacity at selected departments within the research infrastructure in South Africa that is aligned with the objectives of construction industry development. It is our aim to build selected Centres of Excellence that can support the ci**d**b – but in reality this vision will only be realised when the ci**d**b is able to fund these Centres of Excellence on a sustainable basis. The ci**d**b is in the process of developing such funding models and funding streams.

SUMMARY

Ladies and gentlemen, it is not for me to pass comment on whether there is a need or an opportunity for a focused initiative on the development of the construction industry in any country – that needs a deep understanding of context specific issues in that country.

But, in those countries that have adopted national initiatives to develop the construction industry, opportunities exist for the research infrastructure (the universities and research laboratories) to make a meaningful contribution to the development of the industry. In fact, it is likely that any national activity cannot succeed without the active support and participation of the research infrastructure.

And where it is not necessary to have a national focus on the development of the industry, or where such national focuses have not been initiated, opportunities still exist for the research infrastructure to make a meaningful contribution to the development of the industry – *albeit* that it may be more difficult to do so.

Research organisations, such as those represented here today, underpin the development of the construction industry in any country.

CONCLUDING COMMENTS

In conclusion, I am proud to have been a President of the International Council for Research and Innovation in Building and Construction (CIB). The membership of the CIB currently numbers over 400 members originating in some 70 countries. CIB members include most of the major national laboratories and leading universities around the world in building and construction.

The CIB facilitates international cooperation and information exchange in building and construction research and innovation. Individually, and collectively, the members of CIB play an important role in many countries in supporting the development of the construction industry.

BIBLIOGRAPHY

1. Milford, R V, Hodgson, S, Chege, L and Courtney, R (2002). Construction

Industry Development: A Developing Country Perspective. CIB W107: Conference on Creating a Sustainable Construction Industry in Developing Countries. Stellenbosch, South Africa.

2. Milford, R V and Hodgson, S (2005). *Construction Safety, Health, Environment and Quality; A Framework for Performance Improvement in South Africa*. Rethinking and Revitalizing Construction Safety, Health, Environment and Quality. 4th Triennial International Conference, Port Elizabeth, South Africa.
3. Ofori G (1999). *Challenges of Construction Industries in Developing Countries: Lessons from Various Countries*. Construction Industry Development in the New Millennium. 2nd International Conference on Construction Industry Development, and 1st Conference of CIB TG 29 on Construction in Developing Countries, Singapore.
4. Ofori G (2001). *Challenges Facing Construction Industries in Southern Africa*. Keynote Address, Regional Conference on Developing the Construction Industries of Southern Africa. National Department of Public Works, Pretoria.

CD6-KN08

INTERNAL STEEL BRACING OF RC FRAMES

M.R. Maheri
Professor of Civil Engineering, Shiraz University, Shiraz, Iran

ABSTRACT

Steel bracing systems can be used effectively for seismic retrofitting of existing RC buildings as well as for seismic design of new buildings. Although adaptation of bracing to upgrade the lateral load capacity of existing RC frames has been the subject of a number of successful studies, guidelines for its use in newly constructed RC frames need to be further developed. This paper reports on some recent experimental and numerical work conducted by the author and his colleagues on internal bracing of RC frames using direct connections between the bracing system and the frame. The effects of X-bracing and knee bracing on enhancing the seismic capacity of the frames are investigated experimentally through pushover tests as well as cyclic tests. A compression release device has also been introduced and tested to enhance the seismic performance of the bracing system by avoiding the buckling of the compression member. An important consideration in the design of steel-braced RC frames is the level of interaction between the strength capacities of the RC frame and the bracing system. In this paper, results of experimental and numerical investigations aimed at evaluating the level of capacity interaction between the two systems are also discussed. It is found that the capacity interaction is due primarily to connections overstrength. Based on the numerical results the connection overstrength has been quantified and guidelines for the seismic design of the internally braced RC frames with direct connections are provided.

1. INTRODUCTION

Steel bracing is generally used to increase the lateral load resistance of steel structures. In recent years, the concept of steel bracing has also been applied to the retrofitting of reinforced concrete frames. Increased architectural flexibility, reduced weight of the structure, ease and speed of construction and the ability to choose more ductile systems can be considered as the main advantages of steel bracing in comparison with RC shear walls. Two bracing systems are generally used, external bracing and internal bracing. In external bracing, steel trusses or frames are attached either as a global external support to the building exterior or, more locally, to the face of individual building frames. A number of investigators have reported on the efficiency of external bracing in seismic retrofitting of existing RC buildings [1-4]. Architectural concerns and difficulties in providing appropriate connections between the bracing system and RC frames are two of the shortcomings of this method.

In internal bracing, steel bracing members are inserted in the empty space enclosed by columns and beams of RC frames. As a result, each unit frame is individually braced from within. The bracing may be attached to the RC frame either indirectly or directly. In the indirect internal bracing, a braced steel frame is positioned inside the RC frame. As a result, the transfer of load between the steel bracing and the concrete frame is carried out indirectly through the steel frame. Successful retrofits of existing buildings by indirect internal bracing using different forms of X, V and K concentric and eccentric braces have been reported in the literature [5-8]. In some repair and retrofitting cases, provision of the steel frame may be necessary to reduce the strength demand on an already damaged and weakened RC frame; however, in other instances the steel frame acts only as a costly connecting mechanism with inhibiting technical difficulties in fixing the steel frame to the RC frame.

To overcome the shortcomings of the indirect internal bracing, Maheri and Sahebi [9] first recommended using direct connections between the brace elements and RC frame without the need for an intermediary steel frame. In an experimental work, they showed the ability of this bracing system to enhance the strength capacity of RC frames.Later experimental work on directly braced model frames by Tasnimi and Masoomi [10] also showed the applicability of this method. Recent analytical work carried out by Abou-Elfath and Ghobarah [11, 12] on both concentric and eccentric direct internal bracing in non-ductile RC buildings also showed an improvement in the seismic performance, particularly when using eccentric bracing. In continuation of their previous work, Maheri et-al [13] conducted experimental investigations on pushover response of scaled RC frames; braced with both diagonal bracing and knee bracing systems. In this study the effectiveness of the two bracing systems in increasing some seismic performance parameters was shown. Also, in a theoretical study, Maheri and Akbari presented the behaviour factor, R, for this class of dual systems [14].

Appropriate design of direct connections between the bracing members and the RC frame is important to achieve the required lateral load capacity. Maheri and Hadjipour [15] proposed a connection that minimizes the eccentricity of the brace member force. This allows transferring the brace force to the corner of the RC frame without producing local damage in concrete members. Using the results of an experimental program conducted on a number of full-scale connections, they also presented design guidelines for the brace-frame connections in new construction. Recent experimental works by Youssef et-al [16] and Ghaffarzadeh and Maheri [17-19] have shown further that different directly-connected internal bracing systems can be used effectively in retrofitting of existing concrete frames as well as shear resisting elements for construction of new RC structures.

2. SEISMIC RESPONSE PARAMETERS OF X-BRACED FRAMES

2.1. Pushover Tests

In an experimental study, details of which are presented in reference [13], pushover tests were conducted on scaled models of ductile unit frames, directly braced by X steel braces. The objective of the study was to compare some seismic response and design parameters, including; load capacity, stiffness, toughness, ductility and performance factor of different unbraced and X-braced RC frames in order that suitability of the X bracing of RC frames could be investigated. Model unit frames constructed for experimental investigations were 1:3 scaled models of a typical 3mx3m unit ductile frame. For the purpose of comparison, RC beams and columns in all the model frames (braced or unbraced) had identical dimensions and reinforcement detail. The corresponding horizontal loads estimated for the ultimate capacity of the model frame and the bracing systems were, 33 kN for the unbraced frame and 79 kN for the X-bracing system alone. In total four model frames were constructed so that the repeatability of the tests could be verified. Two model frames (F1-P and F2-P) were identical unbraced frames and two models (FB1 and FB2) were identical X-braced frames. A detailed account of test set-up and observations are given in [13].

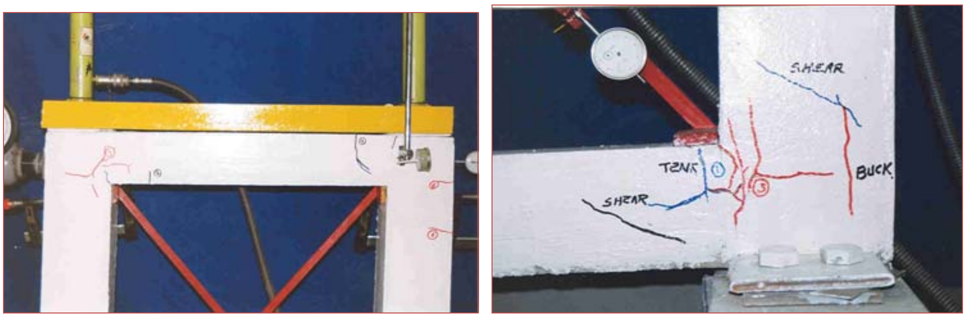

Figure 1. The pushover test of frame F1-P

Load Capacity, Stiffness and Toughness

Over 3.5 fold increase in the lateral load capacity was achieved for the X-braced model frames tested in that study. Test results show that the load capacity of an existing ductile frame can be increased to the desired level by directly adding a bracing system to the frame, without the need for prior strengthening of the existing frame. This point is further substantiated when it is noted that the load corresponding to the appearance of the first plastic hinge in the ductile RC beam (10kN for the unbraced frame) increased by 90 kN when X-bracing was employed. Cross-bracing also appears to increase the initial stiffness of the RC frame. The increased stiffness due to bracing remains true at higher loads up to failure. The increased stiffness, together with the increased capacity, substantially increase the toughness of the braced frame compared to the unbraced frame. Toughness of the test frames, determined as the area under the pushover force-displacement curves shows a five-fold increase for the X-braced frame. This indicates the ability of the X-braced frame to absorb large energies.

Ductility, Overstrength and Performance Factor

Ductility, overstrength and performance factor parameters were determined for the four test model frames and are given in Table 1. The parameters given in this Table are presented in Figure 2, in which V_s, V_y and V_e are forces corresponding to the first yield, structural yield and the elastic response, respectively and $R_\mu = V_e/V_y$, $R_s = V_y/V_s$ and $R = R_\mu R_s$. It should be noted that the performance factor parameters listed in this Table are specific to the model frames tested and do not represent those of the full size frames. The Table indicates that when a ductile frame is braced, in return for the increase in strength, stiffness and toughness, ductility, overstrength and the performance factors are reduced.

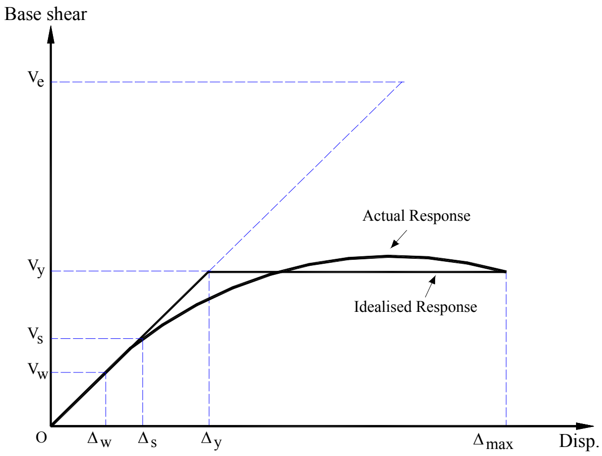

Figure 2. Pushover curve parameters

Table 1: Seismic response parameters of the test frames

Frame	Δ_y (mm)	Δ_{max} (mm)	μ	V_s (kN)	V_y (kN)	V_e (kN)	R_μ	R_s	R
F1-P	2.78	10.0	3.0	9.5	22.0	79.1	3.60	2.31	8.3
F2-P	2.65	10.0	3.8	10.0	21.0	79.5	3.77	2.10	7.9
FB1	6.41	10.0	1.6	60.0	74.0	115.4	1.56	1.23	1.9
FB2	6.45	10.0	1.5	59.5	75.0	116.2	1.55	1.26	1.9

The test results lead us to conclude that X-bracing is more suitable for a strength-based design. However, the relatively small post-yield capacity and the somewhat brittle failure mode of the X-braced frame make this system unfavourable for a ductile design.

2.2. Cyclic Tests

In another experimental study, cyclic tests were carried out on half-scale RC unit frames braced with X-bracing. Details of the test set-up and results are reported elsewhere [18]. Unit frames where selected from the third floor of a three-bayed, four-storey frame of a residential building. Two lateral load resisting systems, namely; an RC moment frame and an X-braced RC frame, were considered for the study. The gravity and earthquake forces acting on these unit frames were determined in accordance with the Iranian seismic code [20] using the seismic force reduction factor for moment frames with moderate ductility. The size of the test specimens was determined based on the available laboratory space and the equipment limits. A 2/5 scaled model, measuring 1.76 m by 1.36 m, was found to be satisfactory. The forces acting on the panels were also scaled down resulting in a lateral load of 22kN and two vertical loads of 35kN for the moment frame and the same lateral load of 22kN and two vertical laods of 38.5kN for the braced frames.

One moment resisting RC frame model, namely F1 and two braced RC frame models, namely FX1 and FX2, were designed using the above gravity and lateral loads. The moment frame was designed according to ACI 318-02 [21] and its detailing was done in accordance with the ACI special provisions for seismic design. Reinforcement details for this frame are shown, on the left hand side, in Figure 3. AISC-LRFD [22] was used to design the brace members and their welded connections to the guest plates. Reinforcement details for the braced frames are also shown on the right hand side of Figure 2. A double-angle brace cross-section, consisting of two 25×25×3.2mm angles, giving a cross-sectional area of 300 mm^2, was chosen for the frame FX1 and a C 30×3.5 mm channel with a cross-sectional area of around 500mm^2 was selected for the frame FX2 (Figure 3). The difference in the brace member cross-section, therefore, made the FX2 frame somewhat stronger than the FX1 frame.

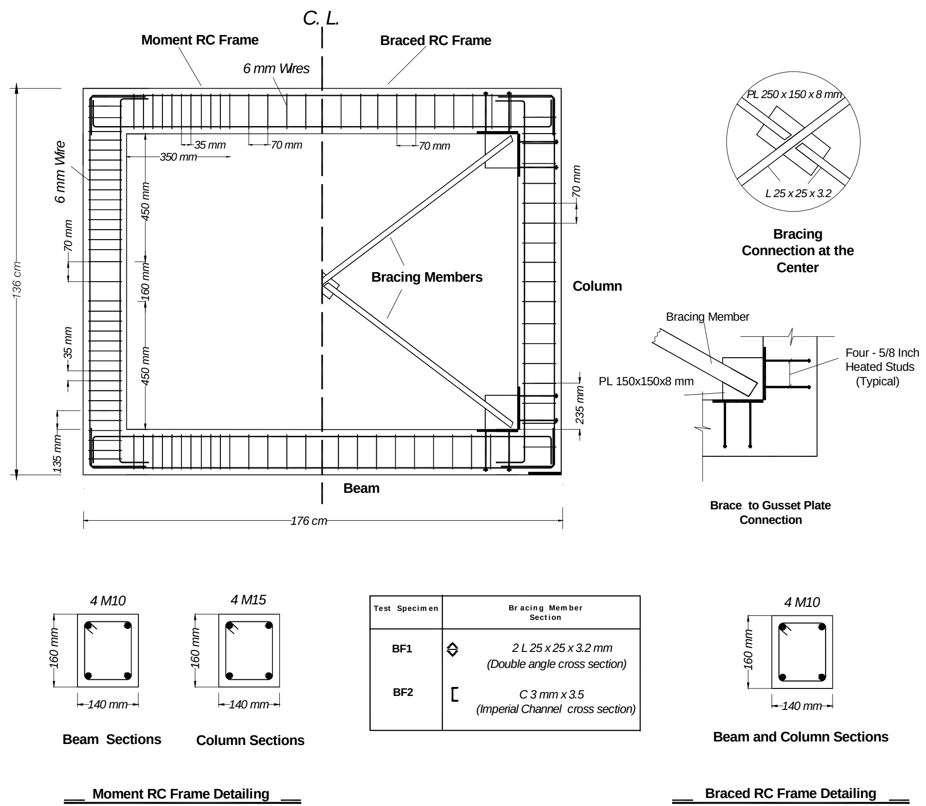

Figure 3. Detailing of the moment RC frame (F1) and the braced RC frames (FX1 & FX2)

The model frames were subjected to gravity loads using two hydraulic jacks. For the cyclic test, the actuator was first pulled to a displacement, d_1, of 5 mm then pushed to the same displacement. The value of d_1 was increased in the following cycles by an increment of 5 mm. The behaviour of the test models was monitored by using electrical and mechanical instrumentations including: Load cells attached to the hydraulic jacks and the actuator to measure applied loads, Linear Voltage Differential Transformers (LVDTs) to measure the lateral deformations and electronic strain gauges to monitor local strains in the reinforcement bars as well as steel bracing elements.

Figure 4. Test set-up and pattern of cracking in the moment frame (F1)

Hysteretic Response and Load Capacity

Figure 4 shows details of crack patterns in frame F1. The hysteretic lateral load-drift curves for the three frames F1, FX1 and FX2 are also shown in Figure 5. For the moment frame F1, at a load of 37.5kN, yielding of the lower bars of the lower beam initiated the plastic response. Failure occurred by plastic hinging at the ends of the upper and lower beams at a load of 55kN. At a drift of 1.9%, corresponding to a lateral load of 105kN, yielding of the double-angle bracing member of the braced frame FX1 initiated the plastic response. A significant drop in the lateral load capacity was observed at a load of 140kN (drift of 4.0%). This was noted to be due to the buckling of brace members. Following this, the lateral load capacity was mainly provided by the RC frame, which failed when plastic hinges were formed at the ends of the lower and upper beams. In the frame FX2, the yielding occurred at a load of about 140kN. The lateral capacity of this frame was not however affected because the bracing members were still acting in the elastic range. Testing was continued to a load of 200kN, which was the loading capacity of the actuator and subsequently the test was terminated. A summary of the yield loads and the maximum sustainable loads and their corresponding displacement ratios for the three tested frames are presented in Table 2.

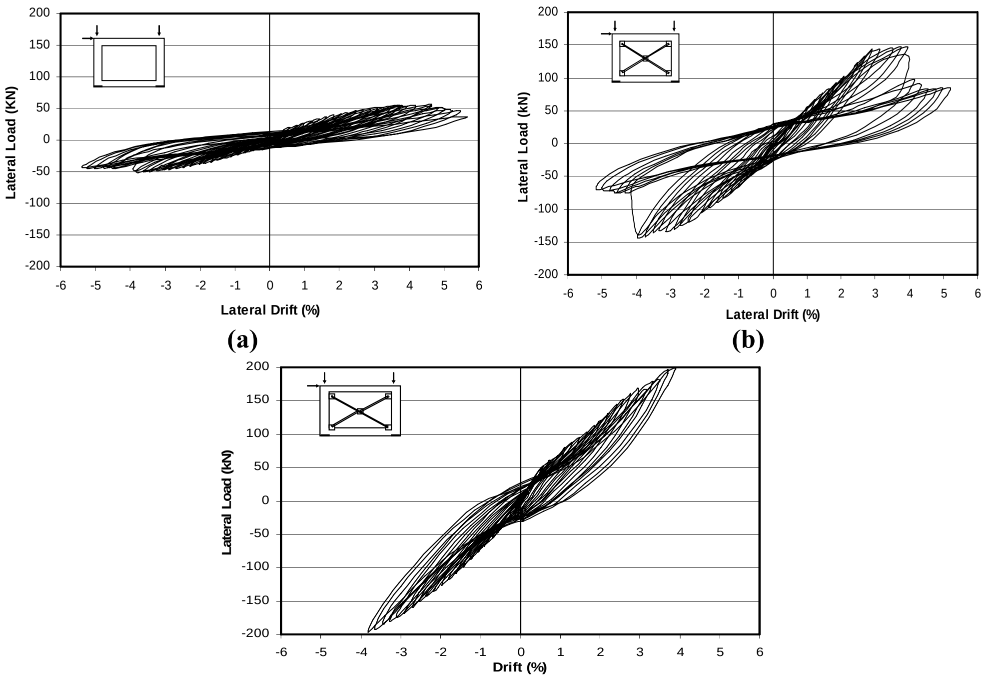

Figure 5. Lateral load-drift hysteresis of frames (a) F1, (b) FX1 and (c) FX2

Table 2: The yield and ultimate strength capacities and their corresponding displacements

Frame	Yield strength (kN)	yield displacement (%)	Ultimate strength (kN)	displacement at ultimate strength (%)
F1	37.5	1.5	55	4.6
FX1	105	1.9	140	4.0
FX2	140	2.8	200	3.9

Stiffness Degradation

The lateral stiffness was calculated as the slope of the line joining the peak of positive and negative loads at a given cycle. The lateral stiffness is an index of the response of the frame from one cycle to the following cycle. Figure 6 illustrates a plot of the lateral stiffness for the three tested frames. Before buckling of the compressive brace, the diagram shows that the lateral stiffness of the frame FX1 was more than double that of the frame F1 and that the rate of stiffness degradation for both systems was almost equal. However, after buckling of the compressive brace, the lateral stiffness of the frame FX1 dropped and became comparable to that of the moment frame (Figure 6). Also, the FX2 frame, having more robust bracing members compared to the frame FX1, shows higher hysteretic stiffness compared to the later. However, both frames show a similar rate of stiffness degradation.

Energy Dissipation Capacity (Toughness)

The energy dissipated by the three tested frames during the cyclic load testing was calculated as the area enclosed by each hysteretic loop. Figure 7 shows a plot of the energy dissipated during a load cycle versus the lateral drift. Also the energy dissipated by each test frame after a number of selected cycles is presented in Table 3. It is observed that at low drift levels, the energy dissipated by the frames FX1 and FX2 was comparable with that of the frame F1. At higher levels of drift, it is clear that the energy dissipated by the braced frames is much higher than that by the moment frame. This proves that the overall seismic performance of the braced frames regarding capacity, stiffness and toughness is expected to be superior to that of the moment frame. This was also deduced from the results of the pushover tests presented earlier.

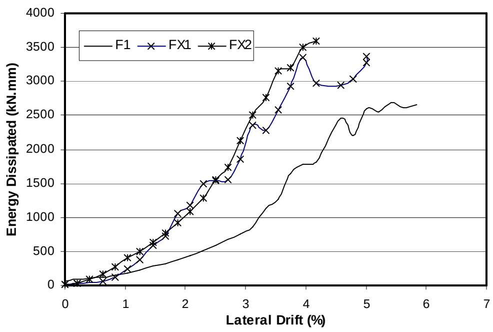

Figure 6. Degradation of the lateral stiffness of test frames

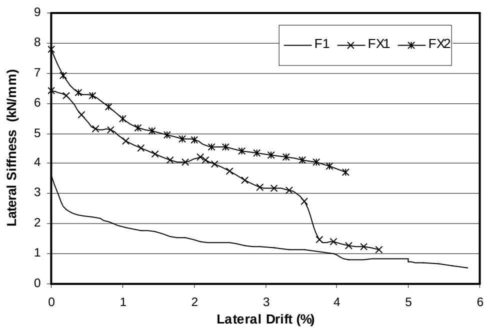

Figure 7. Variation of energy dissipation with the applied displacement

Table 3: Energy dissipation capacity of the test frames

Frame	Cumulative energy dissipated (kN.mm)				
	Cycle 5	Cycle 10	Cycle 15	Cycle 20	Cycle 25
F1	600	2229	5619	13256	25474
FX1	451	4367	13163	27276	32875
FX2	570	3807	11540	26714	-

Ductility

In these tests, ductility is measured both as the ratio of the displacement pertaining to the maximum force Δ_{max}, to the displacement at yield Δ_y and as the ratio of the maximum displacement $\Delta_{available}$ to the displacement at yield point Δ_y of the model frames. These are calculated and shown in Table 4. As it was expected, the addition of X-bracing system somewhat reduces the ductility of a ductile frame, but the reduction in ductility does not affect the energy dissipation capacity of the frames.

Table 4: The ductility of the test frames

Frame	Yield displacement (Δ_y) (mm)	displacement at ultimate strength (Δ_{max}) (mm)	Maximum available displacement ($\Delta_{available}$) (mm)	Ductility corresponding to Δ_{max}	Ductility corresponding to $\Delta_{available}$
F1	18.0	55.4	68.0	3.1	3.8
FX1	22.5	47.5	62.5	2.1	2.8
FX2	33.0	45.6	-	1.4	-

2.3. Seismic Behaviour Factor

In forced-based seismic design procedures, behaviour factor, *R* is a force reduction factor used to reduce the linear elastic response spectra to the inelastic response spectra. The behaviour factor, *R*, therefore accounts for the inherent ductility and overstrength of a structure and the difference in the level of stresses considered in its design. In another study carried out by Maheri and Akbari [14], the seismic behaviour factor (*R*) was evaluated for steel X-braced RC buildings. The *R* factor components including ductility reduction factor and overstrength factor were extracted from inelastic pushover analyses of brace-frame systems of different heights and conFigureurations. In that study 4-storey, 8-storey and 12-storey frames were considered. These are typical numbers of storeys used by some other investigators to cover low-rise to medium-rise framed buildings. All frames were three-bay wide with the central bay braced in the braced dual systems. DRAIN-2DX program was utilised to carry out nonlinear pushover analysis of each system. Inelastic pushover analysis of the multi-storey systems under investigation was carried out at horizontal load steps equal to 2% of the design capacity. A constant gravity load equal to total dead load plus 20% live load was also applied to each frame.

The effects of some parameters influencing the value of *R* factor, including the height of the frame, share of bracing system from the applied load and the type of bracing system were investigated. Of the three variable parameters investigated, the number of storeys appears to be the predominant variable. The other variables, including the type of bracing system and the share of bracing from the applied load, have more localised influences and therefore do not warrant a similar generalisation. The significant effect of the number of storeys on *R* factor of steel-braced RC frames, stems from the fact that shorter braced frames exhibit larger ductility than taller frames, therefore they possess higher ductility 'capacity'. It was therefore found to be prudent to calculate the *R* factors for the frames under consideration using specific ductility 'demands' of $\mu = 2$, $\mu = 3$, $\mu = 4$ and $\mu = 5$. Based on the results obtained, tentative *R* values for steel-braced intermediate ductility, moment resisting RC frame dual systems were presented as shown in Table 5. The proposed *R* factors are given for different ductility demands that constitute the generally accepted range of 'intermediate ductility' response.

Table 5: Tentative values of *R* factor for steel-braced, RC frame dual systems

Ductility Demand	$\mu = 2$	$\mu = 3$	$\mu = 4$	$\mu = 5$
R	5.0	7.0	9.0	12.0

3. CONNECTION OVERSTRENGTH

An important consideration in the design of internally-braced RC frames with direct brace-frame connections is the level of interaction between the strength capacities of the RC frame and the bracing system. In this paper, results of experimental and numerical investigations aimed at investigating the causes and evaluating the level of this interaction are also discussed. Results of the three half-scale RC frames representing a moment frame (F1) with moderate ductility, and two braced frames (FX1 and FX2) already tested under cyclic loading are used for this purpose. These results are also used as basis for developing and calibrating numerical models of full-scale frames. Using the numerical models, a parametric investigation is carried out to determine the role of the main variable parameters affecting the level of capacity interaction between the RC frame and the bracing system.

3.1. Experimental Brace-Frame Capacity Interaction

To investigate the level of interaction in the tested model frames, the corresponding forces in the bracing systems alone were evaluated by considering the relevant test displacements on the diagonals. A simple bilinear model for steel, which accounts for cyclic effects, was assumed and used to represent the force-deflection envelop curve of bracing system alone. The envelop curve of the calculated force-drift relationship for the FX1 bracing system alone (marked as No. 2 in the Figure) is plotted in Figure 8. Also plotted in this Figure, for comparison, are the experimental envelop of the force-drift relationship of the moment frame alone, F1, (marked as No. 1 in the Figure) and the experimental envelop of the force-drift curves of the FX1 braced frame. To be able to gain an insight into the level of capacity interaction between different elements, the envelop curves of the bracing system alone (2) and the moment RC frame (1) are added together to obtain the sum strength capacity of the two elements as also are presented in Figure 4 ((1) + (2)). By comparing the sum strength capacity of the two constituent elements with the actual strength capacity of the braced frame, it is evident that the actual braced frame exhibits a larger capacity than the sum of the capacities of the two elements. This means that by adding a bracing system to an RC frame, the capacity of the RC frame is increased beyond the capacity of the bracing system. The capacity interaction for the frame FX1 is measured, as the minimum of all the evaluated values, as 8.5 percent. It should be noted that the dimensions and reinforcement details and therefore the flexural capacities of the RC frames in F1 and FX1 models are the same. This enables us to make a viable capacity interaction comparison as discussed above. Considering the experimental results, it is evident that the capacity interaction is an overstrength which can be attributed mainly to the effects of brace-frame connections in reducing the effective lengths of the RC beams and columns, hence increasing the stiffness and strength of the frame.

3.2. Numerical Evaluation Of Overstrength

To investigate the level of connection overstrength in full-scale X-braced RC frames, nonlinear pushover numerical analyses of the moment frame, braced frames and the bracing systems were carried out. The OpenSEES (Open System for Earthquake Engineering Simulation) program was utilised to numerically model the frames. Details of the numerical models and the numerical analyses are given elsewhere [19]. The numerical models were calibrated and their accuracy ascertained by comparing the results of the nonlinear cyclic analysis of the moment frame F1 and the braced frame FX1 with the results obtained from their respective cyclic tests.

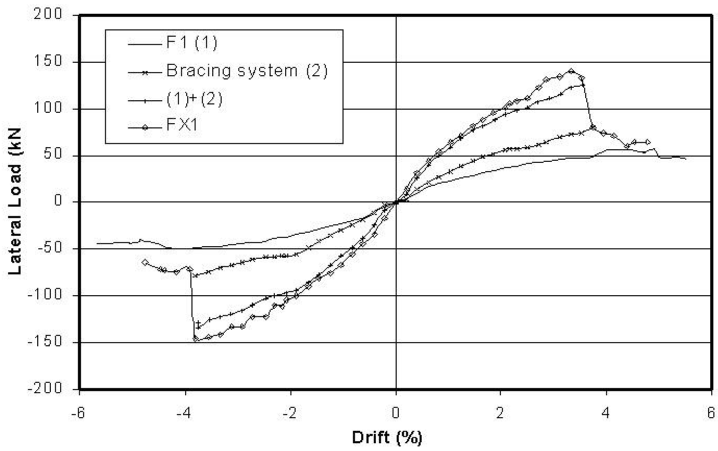

Figure 8. Capacity interaction caused by connection overstrength

After calibrating the numerical models, a series of nonlinear pushover analyses were conducted on full scale 2-D frames of different heights and widths with different bracing conFigureurations. These included frames, 4, 8 and 12 storeys high and 3, 6 and 9 bays wide. The number of braced bays in each frame was also made a function of the number of bays such that the three, six and nine-bay frames had, respectively, one, two and three bays braced. All frames consisted of 3m high and 5m wide unit frames. Another variable parameter in this investigation is the apportioned share of bracing system from the applied loading. Load shares of 30%, 50%, 80% and 100% for bracing system are considered. As it was mentioned earlier, the main factor contributing to the interaction is the effect of connections on reducing the effective lengths of beams and columns. Therefore, considering the nature of this interaction, a representing parameter can be introduced as the ratio of the effective stiffness of the RC frame with brace-frame connections (K_r) to the stiffness of the RC frame without the brace-frame connections (K_i) and designated as ρ. Considering that the connections reduce the effective lengths of RC beams and columns, the effective stiffness of the frame with brace-frame connections corresponds to the stiffness of a reduced frame as shown in Figure 9. For simplicity and conservatively, the reduced frame is assumed to have beams and columns of lengths equal to the distances between the centroids of the four gusset plates as seen in Figure 9. Also, for practical purposes, the parameter ρ is calculated as the ratio of the linear stiffness of the reduced RC frame of a central floor (K_r) and the linear stiffness of the initial RC frame of the same floor (K_i), also shown in Figure 9.

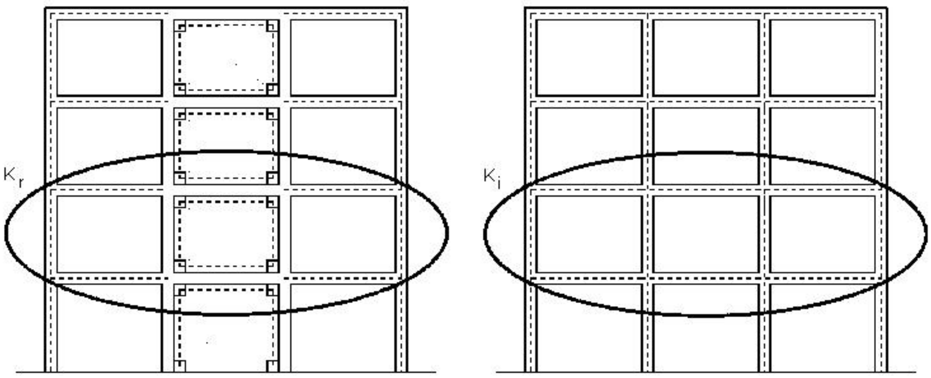

Figure 9. Reduced frame for calculation of connection overstrength

The stiffness ratio, ρ, as described above was calculated for all the frames analysed. The overstrength factors, R, previously determined for these frames with different problem variables were plotted against the stiffness ratio for different frame geometries considered. To condense the results of the 9 relations thus obtained, the linear relation for the 4-storey, 3-bay frame is considered as the base overstrength, R_b, and the effects of the two main variable parameters including the number of braced bays (number of bays in the frame) and the number of storeys are considered respectively as correction factors α and β. Therefore;

$$R = \alpha\beta R_b\ (\%) \tag{1}$$

where, $R_b = 32\rho - 27$

In order that quantitative relations can be drawn between the factors α and β and the stiffness ratio ρ, the former parameters are plotted against the latter in Figure 10.a and Figure 10.b, respectively. Noting the near linear variation of α against ρ the following relations can be presented for this correction factor;

$$\begin{aligned} \alpha &= 0.16m + 0.84, \text{ for } 0.0 < \rho \leq 1.0 \\ \alpha &= 0.09m + 0.91, \text{ for } 1.0 < \rho \leq 1.25 \\ \alpha &= 0.06m + 0.94, \text{ for } 1.25 < \rho \leq 1.40 \end{aligned} \tag{2}$$

Also, as the variation of β with ρ is small, this correction factor can be presented independent of the stiffness ratio in the following form;

$$\beta = 0.0425n + 0.84 \tag{3}$$

In equations *(2)* and *(3)*, m and n are the number of braced bays and the number of storeys, respectively.

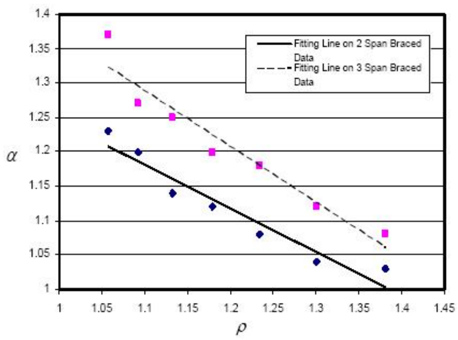

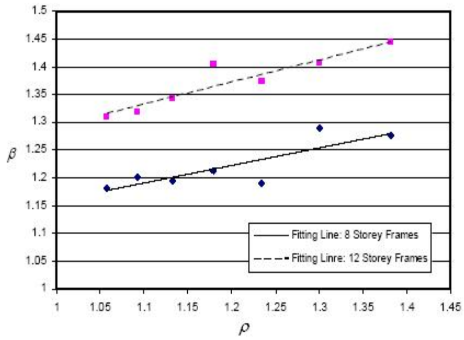

Figure 10. Variation of parameters α and β with respect to stiffness ratio ρ

4. FORCE-RELEASE DEVICES

4.1. Knee Bracing

Knee bracing is used in steel construction to increase the ductility and to increase the seismic performance of the frames. Parallel to the work carried out on the pushover tests of model frames F1-P, F2-P, FB1 and FB2 described in section 2.1, two identical RC frames braced with knee-bracing system were also constructed. The RC frames of these models were identical to the unbraced and X-braced frames and the brace dimensions were also identical to the bracing system of the X-braced frames; the only difference being the four knee elements used at the ends of the diagonal bracing. Details of the bracing system and test set-up and the test results are given elsewhere [13]. The object of the tests was to investigate the role of knee bracing in increasing the ductility of the dual system while maintaining the strength and stiffness requirements. Tests similar to that described in 2.1 were conducted on these frames (Figure 11). The ultimate capacities of the knee-braced frames were found to be 2.5 times that of the unbraced frame. In Figure 12 a comparison is made between the three unbraced, X-braced and knee-braced frames regarding their stiffness and toughness. It is evident that the knee bracing has enabled the frame to possess considerable capacity and stiffness with good capacity to absorb energy. By extracting the ductility ratio from the pushover curves of knee-braced frames as around $\mu = 2.2$, it becomes evident that knee-bracing has also substantially increased the frames ductility compared to the ductility of the X-braced frames ($\mu = 1.5$).

Figure 11. Test set-up for the knee Braced RC frame

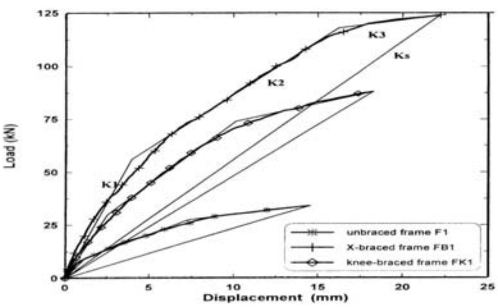

Figure 12. Comparative pushover curves for the knee-braced frame

4.2. Compression Release Tool

In this section another force release tool is presented and its performance is evaluated. This novel tool, named a 'compression release tool' (CRT) when installed in a brace member, releases its compressive force. The proposed CRT is shown in Figure 13. It is composed of two steel plates separated by a gap. The two plates are to be attached together with a maximum of four bars. A cylindrical steel pipe (cylinder) is attached to one of the plates. A steel rod (piston) is attached to the second plate. The cylinder is padded with rubber material. A typical brace member can be divided into two pieces; each is to be welded to one of the CRT steel plates. When this member is subjected to a compressive displacement, the piston will slide inside the cylinder and thus the member will not have any compressive stresses. When it is subjected to a tensile displacement, the bars will transfer the tensile force between the two brace pieces. The bars should be chosen such that the sum of their yield resistances is less than the yield resistance of the brace member. Following a strong earthquake, the brace member is expected to be easily retrofitted by replacing the bars.

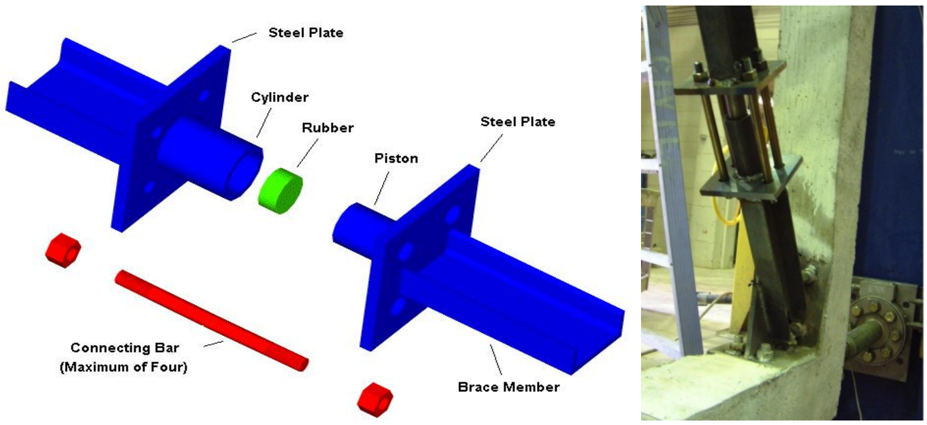

Figure 13. Schematic detail of the CRT

Parallel to the experimental work carried out on the X-braced model frames, constructed for cyclic loading as described above, an experimental study was also conducted to evaluate the effectiveness of the CRT. Two, similar half scale RC frames were constructed and the CRT installed. The CRT can be installed anywhere along the brace member. For the tested specimens, it was decided to install the CRT at the location shown in Figure 13. The size of the steel plates in the CRT was chosen to be 120×120×10mm. The expected axial deformation in the brace members were calculated and based on that it was decided that a 135 mm gap between the steel plates of the CRT is required. To create this gap, the length of the cylinder and the piston were chosen to be 135mm. The inner diameter and wall thickness of the cylinder were chosen to be 40 mm and 5 mm, respectively. The piston was chosen to be 35mm steel rod. The bars connecting the steel plates were different in specimen FXS1 than those in specimen FXS2. They were two-12.7mm and two-16mm steel bars in specimens FXS1 and FXS2, respectively. Tensile load tests on the steel rods revealed that their yield stress is 350 MPa. A photo of an installed CRT is shown in Figure 13. Details of the test specimens and test set-up and results are given by Ghaffarzadeh and Maheri [17].

The frames with CRT (FXS1 and FXS2) were tested under cyclic loading the same way as the moment frames (F1 and F2) and the X-braced frames (FX1 and FX2). The seismic parameters evaluated from the test results include; stiffness degradation, energy dissipation capacity (toughness) and ductility. A discussion of the test results is given as follows:

The lateral load-deformation response for specimen FXS1 indicates the formation of first plastic hinge at a drift level of 1.2%. This was due to the yielding of the two-12.7mm steel bars joining the steel plates of the CRT. This happened at the lateral load of 75kN. The frame failed at the drift of 4.8% corresponding to lateral load of 182kN due to tensile failure of the two-12.7 mm bars. The behaviour of specimen FXS2 was similar to that of specimen FXS1. Yielding of two-16 mm steel bars in the CRT occurred at a drift of 2.5% (lateral load of 140kN). By increasing drift, cracks became visible. Strains in the top reinforcement of the top beam indicate that steel yielded at a drift of 3.4%. The test was terminated because of localized concrete failure in the vicinity of the supports.

Stiffness Degradation

The initial stiffness of specimens FX1 and FX2 was higher than that of the specimens FXS1 and FXS2. This is a direct result from the lower elastic stiffness of bracing members equipped with CRT. The steeper degradation in the lateral stiffness observed in specimens FX1 and FX2 however indicates that using the CRT minimized the cracking in the RC frame and kept the lateral stiffness of the frame almost constant.

Energy Dissipation Capacity (Toughness)

The cumulative energy dissipated by the frames after 5, 10, 15, 20 and 25 cycles were also calculated. It was noted that, at lower displacements, the energy dissipated by the braced frames with the CRT (specimens FXS1 and FXS2) is somewhat less than that of braced frames without the CRT (specimens FX1 and FX2). With increasing displacements and as the bars in CRT yield, the energy dissipated by the frames with CRT is increased to levels higher than those of the frames without the CRT. This indicates that the installation of the CRT did not, by and large, affect the energy dissipation capacity of the braced frames.

Ductility

The available ductility of the four specimens is given in Table 7. It can be observed in this Table that the overall behaviour of the specimen with CRT (specimen FXS1) is more ductile in comparison with specimen FX1 without CRT. The sudden drop in load-drift response curve of specimen FX1 after buckling of compression brace indicates a brittle behaviour. However, in specimen FXS1, in which buckling is inhibited and failure happens by yielding of steel bars of CRT, the behaviour is evidently more ductile (almost two folds). This shows the effectiveness of the CRT in increasing the ductility of the braced frame. By comparing the results of the stronger braced frames without CRT (specimen FX2) and with CRT (specimen FXS2), the favourable effect of the CRT on the ductility of the frame can also be noted.

Table 7: Ductility and performance factor parameters of the CRT test specimens

Test Specimen	Δ_y (mm)	Δ_{max} (mm)	μ	V_s (kN)	V_y (kN)	V_e (kN)	R_μ	R_s	R
FX1	22.5	47.5	2.11	105	112	284	2.53	1.06	2.68
FX2	33.0	---	---	150	168	352	2.09	1.12	2.34
FXS1	17.5	71.5	4.08	75	118	296	2.51	1.57	3.94
FXS2	35.0	---	---	134	160	324	2.03	1.19	2.42

5. CONCLUSIONS

The results of the experimental and numerical investigations presented in this paper lead us to the following conclusions;

1. Internal bracing of RC frames with direct brace-frame connections is not only suitable for seismic retrofitting of existing building but it can also be used as a viable alternative to shear walls as shear resisting elements for the newly constructed buildings.
2. X-bracing is more suitable for a strength-based design. However, the relatively small post-yield capacity and the somewhat brittle failure mode of the X-braced frame make this system less favourable for a ductile design.
3. The proposed CRT can be effectively used in steel bracing systems to eliminate buckling failure. Its use will also result in an adequate energy dissipation capacity for the brace-frame system.
4. The inclusion of CRT can also greatly enhance the ductility of the braced frame. The desired level of ductility can be achieved by appropriate design of the CRT bars.
5. To increase the ductility and maintain the strength and stiffness capacities of the braced frames, Knee bracing of the frame or using CRT on the brace members is recommended. Such systems can be successfully utilised to design for both the damage-level and collapse-level earthquakes for which the damage level may be considered as the yield capacity of the knee elements.
6. The overstrength in a braced RC frame is due to the stiffening effects of connections. This overstrength is termed the capacity interaction or connection overstrength. It is significant and needs to be considered in design.
7. Presentation of the connection overstrength in the form of a frame stiffness ratio, ρ, enable us to use the results and formulations presented here for other types of concentric and eccentric bracing systems.

REFERENCES

1. Bush TD, Jones EA, Jirsa JO., "Behavior of RC Frame Strengthened Using

Structural-Steel Bracing”, *J. Structural Eng., ASCE,* 1991, 117(4), 1115-1126.
2. Badoux M, Jirsa JO., “Steel bracing of RC frames for seismic retrofitting”, *J. Structural Eng., ASCE,* 1990, 116(1), 55-74.
3. Higashi Y, Endo T, Shimizu Y., “Experimental studies on retrofitting of reinforced concrete structural members”, *Proceedings of the Second Seminar on Repair and Retrofit of Structures*, Ann Arbor, MI: National Science Foundation; 1981, 126-155.
4. Nateghi-Alahi F. "Seismic strengthening of eight-storey RC apartment building using steel braces". *Engineering Structures*, 1995; 17(6): 455-61.
5. Usami, H. Azuchi T. Kamiya Y. Ban H. "Seismic strengthening of existing reinforced concrete buildings in Shizuoka prefecture, Japan", Proc. 9th World Conf. on Earthquake Engineering, Japan, Vol. VII, 1988, 421-426.
6. Ohishi H. Takahashi M. Yamazaki Y. "A seismic strengthening design and practice of an existing reinforced concrete school building in Shizuoka city", Proc. 9th World Conf. on Earthquake Engineering, Japan, Vol. VII, 1988, 415-420.
7. Hjelmstad KD. Foutch DA. Del Valle E. Downs RE. "Forced vibration studies of an RC building retrofit with steel bracing" Proc. 9th World Conf. on Earthquake Engineering, Japan, Vol. VII, 1988, 469-474.
8. Tagawa Y. Aoki H. Huang T. Masuda H. "Experimental study of new seismic strengthening method for existing RC structure", 10th World Conf. on Earthquake Engineering, Rotterdam, 1992, 5193-5198.
9. Maheri MR, Sahebi A., “Use of steel bracing in reinforced concrete frames”, *Engineering Structures,* 1997, 19(12), 1018-1024.
10. Tasnimi A. Masoomi A. "Evaluation of response reinforced concrete frames strengthened with steel bracing", Proc. 3rd Int. Conf. on Seism. and Earthq. Engng. Iran, 1999, (in Persian)
11. Abou-Elfath H. Ghobarah A. "Behaviour of reinforced concrete frames rehabilitated with concentric steel bracing", *Canadian J. Civ. Eng.,* 2000, 27, 433-444.
12. Ghobarah A. Abou-Elfath H. "Rehabilitation of a reinforced concrete frames using eccentric steel bracing", *Engineering Structures*, 2001, 23, 745-755.
13. Maheri MR, Kousari R, Razazan M, "Pushover tests on steel X-braced and knee-braced RC frames", *Engineering Structures*, 2003, 25, 1697-1705.
14. Maheri MR, Akbari, R., "Seismic behaviour factor, R, for steel X-braced and knee-braced RC buildings", *Engineering Structures*, 2003, 25(12), 1505-1513.
15. Maheri MR, Hadjipour, A., "Experimental investigation and design of steel brace connection to RC frame", *Engineering Structures*, 2003, 25, 1707-1714.
16. Youssef M.A., Ghaffarzadeh, H. and Nehdi, M. "Seismic performance of RC frames with concentric internal steel bracing", Accepted for publication in *Engineering Structures*.
17. Ghaffarzadeh, H., Maheri, MR, "Mechanical compression release device in steel bracing system for retrofitting RC frames" *Earthquake Engineering and Engineering Vibration*, 2006, 5(1).
18. Ghaffarzadeh, H. Maheri, MR, "Cyclic tests on the internally braced RC

frames", *J. Seismology and Earthquake Engineering*, 2006, 8(3).
19. Maheri, MR, Ghaffarzadeh, H., "Connection overstrength in steel-braced RC frames", *Engineering Structures*, 2008, 30.
20. "Iranian code of practice for seismic resistance design of buildings", Standard No. 2800, 3rd ed. 2005.
21. "ACI Committee 318. Building code requirements for reinforced concrete (ACI 318-02)", American Concrete Institute, Detroit, MI, 2002.
22. "*AISC Manual of steel construction: load and resistance factor design*", 3rd ed. Chicago (IL): American Institute of Steel Construction, 2001.

CD08-KN06

SUSTAINABLE DEVELOPMENT IN CEMENT AND CONCRETE

A.A. Ramezanianpour
Concrete Technology and Durability Research Center of Amirkabir University

ABSTRACT

Cement is the key ingredient in making concrete. Concrete is the second consumed materials after water in the world. When a material becomes as integral to the structure as concrete, it is important to analyze its environmental impacts to conclude if the material is as sustainable as it is prevalent.
In this paper the role of cement and concrete in sustainable development is discussed. The use of bio-fuels and alternative raw materials can reduce the CO_2 emission in cement production. Supplementary cementing materials are new widely used for making durable concretes and reducing the CO_2 emission. Exploiting the thermal mass of concrete to create energy-optimized solutions for heating and cooling residential and office buildings is discussed. Finally the production of recycled aggregate concrete from old concrete structures can have a major environmental impact in the future programs for sustainable development.

Keywords: sustainable development, concrete, cement, durability, CO_2 emission

1. INTRODUCTION

It is impossible to walk through cities without seeing concrete in some form. Whether it is in the latest high rise being constructed, new side walks being cured, in roads connecting the city, in dams, bridges, marine structures, industrial plants, etc. concrete is inescapable. When a material becomes as integral to the structure as concrete, it is important to analyze its environmental impacts to conclude if the material is as sustainable as it is prevalent. If the material does not satisfy the credential of sustainability it should be further developed, especially in present society when environmentally detrimental processes are currently subject to scrutiny.
It is often debated whether concrete can or should be considered to be a sustainable option due to its particular properties and characteristics. Concrete is made of several different elements. In its simplest form this includes cement, water, and aggregate. Cement requires substantial amounts of energy to produce and releases large amounts of carbon dioxide. However, it can also be replaced in part by supplementary cementing materials.
Concrete has a long service life; buildings made of concrete can usually be expected to last hundreds of years with proper maintenance. Sine the structural lifetime is so long, potential waste if another type of building material was used is reduced. As well, once a building requires demolition, its material can be used for subsequent buildings. Truly, when a structure reaches the end of its useful life, its

concrete component can be completely recycled into the aggregates to be used in other concrete mixtures. In spite of the amount of initial energy required to produce concrete, the material has the potential to be efficient over its estimated life expectancy. A list of credentials that should addressed when examining the sustainability of a material is provided:

- Energy required to produce the material
- CO_2 emissions resulting from the material's manufacture
- Toxicity of the material
- Transportation of the material during its manufacturing and delivery
- Degree of pollution resulting from the material at the end of its useful life
- Maintenance required and the materials required for maintenance
- Lifetime of the material and its potential for reuse if the building is demolished

It is important to address all of these factors in deciding if a material can be viewed wholly as a sustainable material. These factors can be separated into two main components, embodied energy is low, but the operational energy is high then a material cannot be deemed sustainable. An ideal solution would be a material with a low embodied energy which results in high operational energy savings. If these two factors can be satisfied then a material, when used with sustainability in mind, is well on its way to reducing its environmental impact.

2. EMBODIEND ENERGY

Embodied energy is the amount of energy required to produce a material. This includes the energy required for the raw material extraction; the energy required to process and manufacture the material; and transportation for all stages of production. It is impossible to assign a value to the embodied energy of concrete on a whole because mix designs vary widely which subsequently changing the embodied energy. Table 1 provides a summary of different elements found in concrete and the approximated values of the relative embodied energy.

Table 1: Embodied energy for cement and concrete

Source	Material	Embodied Energy (GJ/tonne)
The New Ecological Home	Poured on site concrete Cement	1.0–1.6 7–8
Ecohouse 2: A Design Guide	Cement Natural aggregates	4.3–7.8
Cement Association of Canada	Clinker	3.0–6.0

Although there is variation in the values a general idea about the embodied energy of cement can be established. From the table it can be estimated that 7 GJ of energy is required to produce one tonne of cement. The mix used to produce concrete can evidently have a large effect on the amount of embodied energy required. In general, however, the magnitude of this parameter can be understood as well as the importance of attempting to minimize it. The process required to manufacture cement is fairly consistent regardless of the plant type. Conversely, the transportation component and the individual plant part efficiencies can differ and thus have room for improvement. Therefore, the embodied energy can be assumed to be a realistic estimation of the actual embodied energy.

Accordingly, the result of a large embodied energy quantity is a significant production of carbon dioxide. Both of these components of concrete are of concern because they are unsustainable. It must be concluded then that the manufacturing process of cement must be developed further to increase the sustainability of cement and thereby increase the sustainability of the concrete itself. There are two obvious ways in which to reduce the impact that concrete has on the environment. The first is to increase the efficiency during production, and the second is to reduce the amount of cement in the concrete mix. In combination, these two ideas could become a powerful means to creating a versatile material that is practical, beneficial and sustainable in our society.

3. CONCRETE PRODUCTION

To thoroughly assess sustainability and the implications of embodied energy, it is important to have a sufficient comprehension of the processes involved. Possessing this understanding gives depth to the concept of embodied energy, which aids in finding opportunities for improvement, as well as a concept of the environmental impacts. Cement has been marked as a possible threat to the sustainability of concrete. By delving into the nature of cement, this threat can be realized and addressed. The missions resulting from the calcination process cannot be reduced, and thus the CO_2 emissions must be reduced by other means. Improvements to kiln efficiencies; alternate fuel methods; and reduction in the cement quality requirement though intelligent mix design, can all work to aid the reduction of embodied energy and CO_2 emissions.

4. REDUCING ENERGY & EMISSIONS

To reduce the energy-intensity and pollution levels, change must occur on all levels of the concrete process. In Germany, effort was made to decrease the negative environmental effects of the industry by improving the manufacturing process. This was achieved by installing new plants for the purpose of ensuring that the kiln production operation was smoother and energy requirements were decreased. Besides, the existing kilns were optimized in a way that required minimum fan power. A waste heat recovery process was devised to utilize remaining energy losses of the new cement kilns. Finally direct electrical power requirements were decreased by improving the efficiency of the grinding system. Once the manufacturing process was optimized a greater amount of waste fuels was substituted for fossil fuels and alternatives to the cement composition via inclusion of blended cements were derived. Finally, it was admitted that greater research and development was required in the field of “process technologies, use of secondary materials, properties and application of blended cements”.

Table 2 shows the estimated global cement consumption and CO_2 emission in the year 2020.

Table 2: Estimates of global cement consumption and CO_2 emission attributable to clinker production in the year 2020, million tonnes.

Options	No.1 Business as usual	No.2 Challenging option	No.3 Formidable option
Cement Consumption/ production	3,500	2,800	2,100
Complementary Cementing Materials	700	840	1,050
Portland Clinker Requirement	2,800	1,960	1,050
CO_2 Emissions (0.9 T/T clinker)	2,520	1,760	945
%CO_2 increased from the 1990 level	270	190	0

- Cement consumption goes up by about 50% of the 2005 level and the use of CCM increased to 20% of the total cementing material.
- Cement consumption goes down by 20% of the BAU level, and CCM increased to 30% of the total cementing material.
- Cement consumption goes down by 40% of the B.A.U. level, and the use of CCM is increased to 50% of the total cementing material (see Table 3).

Table 3: Projects for CO_2 emission in cement industry

Joint Projects	Individual Companies
The cement sustainability initiative intends to create joint projects to:	As part of commitment to good practice and innovation in sustainable development, companies agree to:
Climate Protection	
Develop a Carbon Dioxide (CO_2) protocol for the cement industry. (project already delivered) Work with WBCSD/World resources Institute (WRI) and other organization to investigate public policy and market mechanisms for reducing CO_2 emissions.	Use the tools set out in the CO_2 protocol to define and make public their baseline emissions. Develop a climate change mitigation strategy, and publish targets and progress by 2006. Report annually on CO_2 emissions in line with the protocol.
Fuels and Raw Materials	
Develop a set of guidelines for the responsible use of conventional and alternative fuels and raw materials in cement kilns.	Apply the guidelines developed for fuel and raw material use.
Emissions Reduction	
Develop an industry protocol for measurement, monitoring and reporting of emissions, and find solutions to more readily assess emissions of substance such as dioxins and volatile organic compounds.	Apply the protocol for measurement, monitoring and reporting of emissions. Make emissions data publicly available and accessible to stakeholders by 2006. Set emissions targets on relevant materials and report publicly on progress.

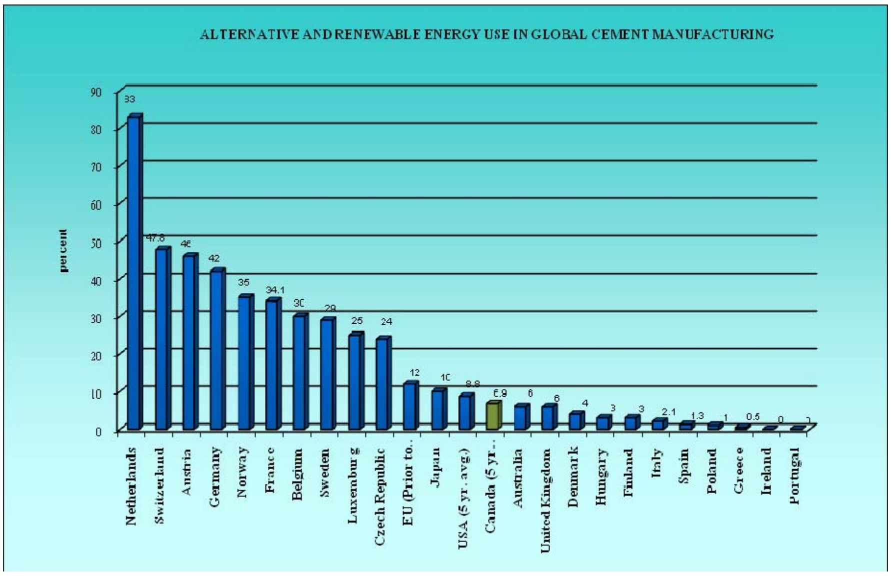

Figure 1. Word AF use (all types) in cement plants

5. SUPPLEMENTARY CEMENTING MATERIALS & SUSTAINABILITY

When concrete is the material of choice one can look forward to having endless options and opportunities in its composition. There are many types of cement, admixtures, aggregate, and supplementary cementing materials that can be incorporated in different quantities. By incorporating a higher quantity of supplementary cementing materials the amount of cement can be reduced, lowering the emissions and energy with a mix.

Supplementary cementing materials have proven to be economical environmental alternatives to typical concrete mixes. Fly ash and silica fume in particular have allowed for significant reductions in CO_2 emissions in cement production. This was possible because of the decreased amount of clinker used to produce the cement and concretes as well as decreasing the requirement of fuel for clinker burning. CO_2 emissions could also be decreased with the increase in the efficiency of clinker in concrete strength development. This can be done by including mineral admixtures to allow for a decrease in the water requirement with fly ash use and strength development by using silica fume. By incorporating 7.5 percent of silica fume to cement during the grinding process, an increase in efficiency of 25% resulted in the clinker.

Another factor that can be manipulated using mix design is the durability. Increased durability decreases maintenance as well as increases lifetime. Longevity can be increased with a reduction in the heat of hydration; reduced porosity. Most widely perhaps, fly ash has been accepted as a great supplement to 100 percent cement use. It improves the most critical cement characteristics such as workability, impermeability and durability. However, regardless of fly ash's positive affect on cement production there have been barriers associated with its use. However, new technologies have been developed as well as newer cement formulations which overcome these previous barriers. Other alternatives have been used such as superplasticizers for water reduction, and silica fume or rice husk ash for porosity minimization and lengthening.

Rice husk ash (RHA) is a byproduct of burning rice husks. In 1982 about 406.6 million tonnes of paddy was produced on a global basis, which represents about 81 million tonnes of husk or 16 million tonnes of ash if an ash content of 20% is assumed. The available ash for cement is approx 4.5 million tonnes. The husk are incinerated and an ash that is predominantly silica is residual. RHA is highly pozzolanic due to its extremely high surface area (50,000 to 100,000 m2/kg). when 5% to 15% RHA is incorporated by mass higher compressive strengths, decreased permeability, resistance to sulfate and acid attack, and resistance to chloride penetration can be expected. By adding in RHA the durability and recycled content on the mix can be increased.

Natural pozzolans are also viewed as effective substitutes for cement. However, it has been observed that the substitution rate, a less workable mortar was produced. Thus, a decrease in compressive strength was witnessed. Yet, as the level of fineness is increased, the comparable strength increases as well. This is most apparent when natural pozzolan substitutions are high. Therefore, using natural pozzolans proves to be an optimal substitute for cement as it provides equivalent strength and reduces the per unit emissions of greenhouse gases.

6. DURABILITY

The durability of a product can have one of the most significant influences on the environment. The less durable a product, the shorter the service life is. This results in new purchases or repairs which is a wasteful practice especially when the industry is as energy intense as cement production. Therefore the longer the service life is the better earth’s natural resources are conserved. The challenge then is to produce concrete that is highly durable, and a high-performance building material for future structure.

The major causes of reinforced concrete deterioration in structures are “corrosion of the reinforcing steel, exposure to cycles of freezing and thawing, alkali-silica reaction and sulfate attack”. The mechanism of concrete expansion and cracking is highly dependent on a high degree of water saturation. Therefore it is evident that water-tightness of concrete is a crucial step to ensure minimal damage. Thus this suggests that the soundness of concrete is closely related to its durability.

Early cracking in concrete is usually a function of either thermal contraction and/or drying shrinkage. The construction industry is driven by economics and thus the mentality of the faster it is done the more profit earned encourages cements with high-early strength, or rather, concrete with high levels of Portland cement to be used. These concretes have low cracking resistances as a result of an increase in “the shrinkage, and elastic modulus on one hand, and a reduction in the creep coefficient on the other hand”. As such, this explains the high level of vulnerability to cracking of high-early-strength concretes to that of moderate or low-strength concrete mixtures.

Early cracking is commonly minimized by incorporation excessive steel reinforcement. However this solution simply replaces a small number of wide cracks with a numerous number of invisible and often unmeasurable micro-cracks. This does not in any sense constitute as a sufficient solution for durability.

If concrete is properly consolidated and cured it will remain watertight unless the pores and cracks within it form interconnected pathways to the surface surrendering the concrete to further deterioration. Evidently, however, the drive of economics does not allow for this. As such, when thermal cracking and durability are of primary concern, it has been shown that supplementary cementing materials (SCM) should be incorporated into the mix design as it will prove to be most cost-effective. The reasoning for this is the property of concrete mixes that contain SCM to have stronger transition zones and are thus less prone to microcracking. Ultimately, by incorporating byproducts such as fly ash or slag into mix design, the durability of concrete is augmented through prolonged watertightness.

The most readily available mineral additive for cement is limestone. In Europe, more limestone is used in Portland-based cements than all other mineral additions combined, notably in the European CEM II L class (24.6% of all European cement manufactured in 2003) and to a lesser extent in the M class, and as minor addition of up to 5% in almost all other Portland cements. It has been shown that much of the alumina from calcium carbo-aluminate hydrates, which can result in a significant decrease in porosity [16]. Both the European cement standard, EN 197-1, and ASTM C150 allow up to 5% limestone [18]. Limestone added in excess of this amount, although constituting essentially a "filler", can also act as an accelerator for alite hydration, so that, with suitable grinding techniques, Cement strength up to 28 days are often not much reduced even at limestone contents as high as 20%. In addition to this, Limestone additions can improve concrete consistency by reducing cement water demand, and provided that a low w/c concrete mix design is used, high limestone replacement as some pure Portland cements [19].

7. RECYCLED AGGREGATE

When concrete structures reach the end of their useful lives, disposal is not the only available next step. Concrete can be crushed and used as recycled aggregate. Much research has gone into determining whether the properties of used aggregates are sufficient for reuse in concrete. It has been found that due to the suctioning behavior of recycled aggregates, water addition is a problem of major concern. The difficulty arises in determining the appropriate proportions of water to aggregate as it is required in higher quantities when using recycled aggregate to that of dense aggregate. Although the elastic modulus continued to increase for the first few days, it stabilized at approximately 7 days. In conclusion, processed building rubble is an adequate source for recycled aggregate that can produce concrete of sufficient strength and durability. The recycled material can be available at good quality without an unacceptable level of harmful impurities. Specifically, the quality should be assessed based on porosity which directly affects the performance of concrete.

In consideration of the environmental performance of materials, one needs to consider effects taking place during the entire life cycle of the material.

It has been found that cement-based materials can permanently absorb CO_2 from the atmosphere. This process is termed carbonation and occurs during the normal service life of a concrete structure and also after demolition. On a geological time frame, the cement in hardened concrete will bind approximately the same amount of CO_2 as was originally liberated by the calcination of its raw materials (mainly limestone) in the cement kiln.

However, the impact that concrete carbonation has in the assessment of overall CO_2 emissions from cement manufacture is generally overlooked, due to the difficulty in estimating its rate. Depending on the concrete composition, the type of concrete structure, and the environment to which the concrete is exposed, total carbonation will take place over years therefore it is necessary to analyze the factors affecting the rate of carbonation. This is difficult to do in a precise manner, and the environmental benefit of this effect is still open to debate. However, a recent Nordic study point to that concrete recycling, in which the concrete is crushed, unexpectedly may lead to significant CO_2 uptake. The significance of these results is still controversial and is under discussion.

The Nordic study points to an opportunity to improve the environmental performance of concrete over its life cycle by enhancing carbonation when this has no negative durability effects. Most effectively, promoting concrete recycling and adapting recycling practices for optimal CO_2 uptake would have a positive environmental benefit.

8. OPERATIONAL ENERGY

As important as it is to reduce the embodied energy and emissions, it is just as important that when implementing a material that the energy requirements during its useful life are not increased as a byproduct of material selection. Concrete offers solutions to reduce the operational energy of structures such as buildings, dams, and roads.

BUILDINGS

Concrete can aid in lowering the operational costs of a building because it posses thermal mass. Thermal mass is material property that stores and slowly releases energy. Materials that have significant thermal mass possess the following qualities:

- High specific heat
- High density
- Low (but not extremely low) thermal conductivity

Concrete is an example of material with high thermal mass. Thermal masses absorb and store energy when their temperatures are below air temperature. The stores energy is later slowly released when the air temperature drops below the temperature of the mass. The main advantages of thermal masses are:

1. There are fewer spikes in the heating and cooling requirements, since mass slows the response time and moderates indoor temperature fluctuations.

2. A massive building uses less energy than a similar low mass building due to the reduced heat transfer through the massive elements.
3. Thermal mass can shift energy demand to off-peak time periods when utility rates are lower. Since power plants are designed to provide power at peak loads, shifting the peak load can reduce the number of power plants required.

Thermal masses can also be used to passively heat a building. This works especially well because solar gain increases during the winter, due to the low angle of inclination of the sun vertical walls are exposed to more solar energy. “Buildings with exterior concrete walls, also called mass walls, utilize less energy to heat and cool than similarly insulated buildings with wood or steel frame walls”. During the day, while the temperature is warmer and the sun is shining, the walls store solar energy. When the temperature drops the thermal energy radiates to warm the house and reduce heating loads. Concern may arise that this effect will occur as well in the summer and heat the house when heat is unwanted. Walls can be sheltered from solar radiation during the summer using overhangs. If the wall temperature can be kept below the interior temperature, the thermal mass will absorb energy from the air, cooling the space. Reducing the amount of addition energy required to heat/cool a building.

Concrete’s thermal mass also makes it possible to involve developments such as radiant heating. This development is a method of heating through radiant heat as opposed to convection heating. Where convective heating warms air and circulates the warm air through the building radiant heat warms materials, and the materials radiate the heat into the space. This method works well when using materials with significant thermal mass because they comfortably release the thermal energy into a room, as well as stores any excess. Radiant heating still uses energy to warm the water, but this energy is significantly less than the energy required, and wasted through convective heating. When heating a building through a typical HVAC the system, the warm air always rises to ceiling of the room, where it is lost, or wasted most people do not benefit from heat that is half a meter above their head. Radiant heating heats habitable space first and foremost, reducing the heating load.

Other developments that can aid in reducing the operational energy include implementing insulating concrete forms (ICFs). This product combines the form work and the insulation for a wall assembly into one, creating less waste and a more consistent air barrier with fewer thermal breaks. By creating a concrete wall sandwiched between insulation a thermally efficient wall is created. The resistance of insulation in addition to the thermal mass of concrete creates a wall where temperature changes are gradual due to the thermal mass, and they are small because of the insulation and building envelope continuity. By eliminating wood or metal studs thermal breaks are reduced, these points where thermal energy is generally lost are eliminated. The elimination of these materials reduces the strain on non-renewable source, like timber, and high energy materials such as steel. This further reduces the environmental impact of a new construction.

DAMS

Pozzolans are known scientifically to be both an environmental beneficial substitute in cement production as well as an economically feasible solution. Since the 1980's, roller-compacted concrete dams (RCC) have been known to be one of the most rapid and economical method for construction of medium-height dams. By 1992, ninety-six RCC dams were built in over seventeen countries. 85% of these dams included pozzolans in the mix design. In fact, high paste content RCC most commonly uses 250 kg/m^3 of concrete with 70-80% pozzolan addition. Of the 85% of dams which incorporated pozzolans in the mix design, fly ash was incorporated in 90%. This quantity hints at the capability pozzolans have in cement/concrete production and the effect it can have on the environment when waste products become commodities.

ROADS

The use of recycled concrete aggregate (RCA) in highway infrastructure has the potential to reduce wastes and costs while producing the type of durable new roads required. Recycled concrete aggregate is produced from "Portland cement concrete pavements, bridge structures and decks, sidewalks, curbs, and gutters that have been removed from serviced, had their steel removed and have been crushed to a desired gradation". Various tests have proven that with the right conditions RCA has the potential to produce materials of significant strength and durability with a higher load carrying capacity.

There are numerous resource conservation benefits that result with the implementation of RCA. Firstly, waste disposal quantities are reduced. In most cities where a lack of landfill space is a real problem, waste reduction is a large benefit. Similarly, the use of these waste materials diminishes the cost of energy typically required for hauling virgin aggregate from quarries. Similarly to fly ash, RCA has bared the stigma associated with waste materials being substandard material. It has been realized that for RCA use to become more extensively used the process control needs to be improved to prevent mix workability issues. This includes watering stockpiles and testing the moisture content of the aggregates regularly. RCA has been used as coarse aggregate in hot-mix asphalt and as dense-graded aggregate.

9. CONCLUSION

Concrete is taking leaps and bounds when it comes to sustainable development. The management of CO_2 emissions along with voiced concern regarding the negative environmental impact of cement production proves that the minds of the industry are in right place. Research involving supplementary cementing materials has continuously proven the benefits of incorporating what is often a waste product from industries into concrete mix design. This can be noted through the increase of durability and strength resulting particularly in greater sustainable practices but also economical ones. Developments in the cement production process suggest that the interest to make improvements is being realized. New innovative methods are also being created to reduce the quantity of cement in a mix which is proof of a new perspective on the role the concrete industry can play in sustainability.

In addition to the developments occurring directly with the production of cement and concrete the application of these materials is also being redefined. Many limitations once binding concrete from becoming sustainable are fading as its use is incorporated into newer areas. Buildings can be built to use concrete’s thermal mass to help reducing energy requirements. The construction of dams is being optimized to use concrete to save energy during construction, and the lifetime of concrete is expanding with its reuse in aggregate form in roads. In combination, concrete has become multipurpose. As a result, although the initial energy production level is high, concrete can become more efficient.

The environmental and economic benefits of development in the direction of sustainability are inescapable. The continual search for opportunities to make this material, which has become such and integral part of our cities all over the world, a more sustainable option, proves that the minds of the masses are in the right place.

REFRENCES

1. 2006 sustainability report. Cement association of Canada. 2006. 10 Apr.2008.
2. The cement sustainability initiative, our agenda for action. World business council for sustainable development. 2002. 10 Apr.2008.
3. Chiras, D. The new ecological home. Vermont: Chelsea green company, 2004.
4. Hoeing, V. and Schneider, M. (2001) German cement industry's voluntary efforts on the issue of climate change- A success story. In V.M. Malhotra (Ed.), third Canmet/ACI international. Sustainable development of cement and concrete. (pp.15). Farmington Hills, Michigan: American concrete institute.
5. Horton, R. (2001). Factor ten emission reductions: the key to sustainable development and economic prosperity for the cement and concrete industry. In V.M. Malhotra (Ed.), third Canmet/ACI international. Sustainable development of cement and concrete. (pp.1). Farmington Hills, Michigan: American concrete institute.
6. Meinhold, U., Mellmann, and G., Maultzsch, M.(2001). Performance of high-grade concrete with full substitution of aggregates by recycled concrete. In V.M. Malhotra (Ed.), third Canmet/ACI international. Sustainable development of cement and concrete. (pp.85). Farmington Hills, Michigan: American concrete institute.
7. Neuwald, Adam D. supplementary cementitious materials. National precast concrete association.
8. Popovic, K. (2001). Reducing CO_2 emission into the atmosphere-achievements and experience of creation cement industry. In V.M. Malhotra (Ed.), third Canmet/ACI international. Sustainable development of cement and concrete. Farmington Hills, Michigan: American concrete institute.
9. "Radiant Heating". Cement association of Canada. 10 Apr. 2008.
10. Rice Husk ash cements: their development and applications. United nations industrial development organization. Vienna. 1985.
11. Roaf, S, M Fuentes, and Thomas. Ecohouse 2: a design guide. England: Architectural P, 2003.

12. South, W. and Hinczak, I (2001). New Zealand Pozzolans-An ancient to a modern dilemma. In V.M. Malhotra (Ed.), third Canmet/ACI international. Sustainable development of cement and concrete. (pp.97). Farmington Hills, Michigan: American concrete institute.
13. Uchikawa, H. (2000). Sustainable development of the cement and concrete industry. In Odd E. Gyorv. And Koji Sakai (Ed.), concrete technology for a sustainable development in the 21st century. (pp.177). New York: E & FN spon.
14. United States Department of transportation. (2005). Recycled concrete: A valuable transportation resource. Federal highway administration. Retrieved April 2008.

CD01

Materials

THEORETICAL AND NUMERICAL STUDY OF THE BAR PLACED IN CONCRETE UNDER AXIAL TENSION LOAD AND DESIGN OF EXPERIMENTAL MODEL

A.M. Goltabar[1], R. Shamstabar Kami[2], S.M. Rezvani Divkolaee[3]
[1]Assistant Professor, Civil Engineering Department, Babol Noshirvani University of Technology, Iran
[2]M.S. Student, Civil Engineering Department, Babol Noshirvani University of Technology, Iran
[3]M.S. Student, Civil Engineering Department, Babol Noshirvani University of Technology, Iran

ABSTRACT
For considering the design considerations and development of retrofitting of structures, exact identification of materials' behavior and their interaction, is an important subject. In concrete structures that include a high percentage of existent and under construction structures, for calculation of anchorage length of bars and investigation of sufficiency of anchorage length of bars, the state of stress distribution in bar and joint surface with concrete and their effective parameters are important. One of the important parameters in modeling the joint surface between bar and concrete is equivalent spring constant between two materials. Most researchers suggest experimental test to obtain actual value of stiffness between two materials. In this study, for obtaining the exact values of stiffness, formulation on the base of equilibrium of elements and investigation of governing differential equations and experimental method were used. In experimental tests, slips and strains, pertinent to applying load were measured by strain gauges and displacement transducers that were installed between 4 stations over concrete and bar surface with an acceptable accuracy.

Keywords: concrete, bar, axial tension, friction, experimental model, displacement

1. INTRODUCTION
Interaction of bar and concrete is one of the important parts of reinforcement design, because limited length of bar has a main effect on the behavior of reinforcement. So, each code according to formulation and experience, presented some value. For better design of reinforcement element and controlling of codes value, interaction of bar and concrete should be attended. For determination of distribution of stress between bar and concrete, there are two methods: theory method and experimental method.

2. DEVELOPMENT OF THEORETICAL AND NUMERICAL METHOD
Axial stiffness between concrete and bar (k_A) is obtained from the following formulation and by using experimental results. Figure (1) shows internal force between concrete and bar. Equilibrium principle on element (1) shows the following result:

$$F_0 - F_1 = \Delta F_1 \tag{1}$$

That F1 and ΔF1 are axial forces in the bar section between element 1 and 2 and friction force of element (1), respectively. In other words, we have:

$$F_i - F_{i+1} = \Delta F_i \tag{2}$$

Also from the Equilibrium principle, we have:

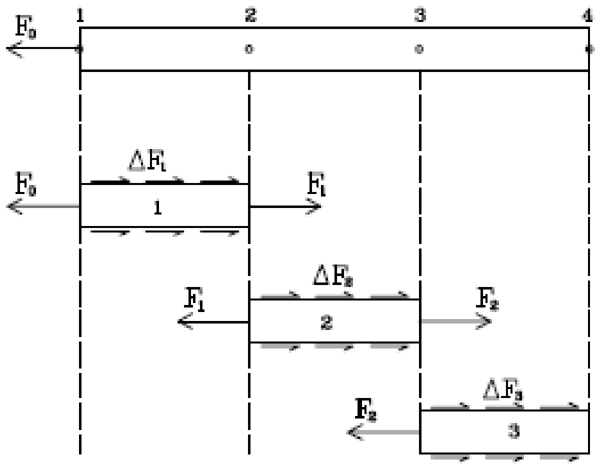

Figure 1. Internal force between concrete and bar

$$F_0 = \Delta F_1 + \Delta F_2 + \Delta F_3 \tag{3}$$

The force of element (i) is always bigger than element (i+1), then: $F_i > F_{i+1}$
Relation between friction force and friction stress is shown in the following form:

$$\Delta F_1 = P.L_1.\tau_1 \tag{4}$$

That P and L_1 are perimeter of bar and length of one small element of bar, respectively. It should be mentioned that variation of friction force between element (1) and (2) is supposed to be equal. Shear stress in element (1) is:

$$\tau_1 = \frac{\Delta F_1}{P.L_1} = \frac{F_0 - F_1}{P.L_1} \tag{5}$$

For element i we can write:

$$\Delta F_i = F_{i-1} - F_i \tag{6}$$

$$\Delta F_i = P.L_1.\tau_i \tag{7}$$

$$\tau_i = \frac{F_{i-1} - F_i}{P.L_1} \tag{8}$$

On the other hand F_1 can be defined in the following form:

$$F_1 = \sigma_1.A_P = E_P.\varepsilon_1.A_P \tag{9}$$

Where σ_1, A_p and ε_1 are normal stress of bar, cross section of bar and normal strain of bar, respectively. If strain is equal along the length of the element (1), we can define it according to displacements of two points.

$$\varepsilon_1 = \frac{u_2 - u_1}{L_1} \tag{10}$$

Where u_1 and u_2 are measured displacements of points in the laboratory. Then F_1 is equal to:

$$F_1 = E_P A_P \left(\frac{u_2 - u_1}{L_1} \right) \tag{11}$$

Friction force of different elements can be stated as follows:

$$\Delta F_1 = F_0 - E_P A_P \left(\frac{u_2 - u_1}{L_1} \right)$$
$$\Delta F_2 = F_1 - F_2 = \frac{E_p A_p}{L_1}((U_1 - U_2) - (U_2 - U_3)) = \frac{E_P A_P}{L_1}\left(u_1 - 2u_2 + u_3\right) \tag{12}$$
$$\Delta F_3 = \frac{E_P A_P}{L_1}\left(u_2 - 2u_3 + u_4\right)$$

Due to earthquake, force is dynamic and since behavior of this case is different from that of the static case, dynamic case should be taken into consideration. Dynamic stiffness between concrete and bar, damping and part of concrete mass are dynamic parameters that are obtained by dynamic equilibriums and experimental results. In time domain, we have:

$$\left[K_d(t)\right]\left\{x(t)\right\}=\left\{f(t)\right\} \tag{13}$$

In one degree freedom and in frequency form, dynamic stiffness is obtained from the following form:

$$K_d(\omega)=-\omega^2 M+K+i\omega c \tag{14}$$

If M is included mass of bar (M_P) and added mass of concrete (M_{add}), we have:

$$K_d(\omega)=-\omega^2\left(M_P+M_{add}\right)+K_A+i\omega C \tag{15}$$

In the right section of Eq.(15), M_{add} and in the left section, dynamic stiffness in frequency form are unknown. Dynamic stiffness in frequency form is defined according to the following form:

$$k_d(\omega)=\frac{F(\omega)}{x(\omega)} \tag{16}$$

It should be mentioned here that excitation of both the system and displacement function are harmonic (sinuous form), but the displacement function has a different phase. Excitation of system function is given in the following form:

$$f(t)=F_0\sin\omega t \tag{17}$$

If force (f(t)) is supposed in dynamic equation of one degree freedom , we have:

$$\begin{gathered} m\ddot{x}+c\dot{x}+kx=F_0\sin\omega t \\ \ddot{x}+\frac{c}{m}\dot{x}+\frac{k}{m}x=\frac{F_0}{m}\sin\omega t \\ \ddot{x}+2\zeta\omega_n\dot{x}+\omega^2 x=\frac{F_0}{m}\sin\omega t \end{gathered} \tag{18}$$

As a result:

$$x(t)=e^{-\zeta\omega_n t}\left[C\cos\omega_d t+D\sin\omega_d t\right]+ \\ \frac{F_0}{K}\frac{1}{\left[\left[1-\left(\frac{\omega}{\omega_n}\right)^2\right]^2+\left(2\zeta\frac{\omega}{\omega_n}\right)^2\right]^{1/2}}\left\{\left[1-\left(\frac{\omega}{\omega_n}\right)^2\right]\sin\omega t-2\zeta\frac{\omega}{\omega_n}\cos\omega t\right\} \tag{19}$$

After some time the displacement function of points will become constant and it has been shown in the form given below:

$$u(t) = u_0 \sin(\omega t - \phi) \tag{20}$$

That has a different phase ϕ than the excitation force wave.
In the laboratory, F_0can be measured. Maximum amplitude of displacement in axial direction can be recorded by sensors. System excitation frequency and displacement vibration frequency are equal, but have a different phase that is due to system damping.

In order to obtain dynamic stiffness in frequency form, we should calculate $F(\omega)$ and $x(\omega)$, that are Fourier conversion of dynamic force and dynamic displacement function, respectively.

$$F(\omega) = \frac{1}{2\pi}\int_{-\infty}^{\infty} f(t)e^{-i\omega t}dt = \frac{1}{2\pi\left(1-e^{-i\omega T}\right)}\int_0^T f(t)e^{-i\omega t}dt \tag{21}$$

$$X(\omega) = \frac{1}{2\pi}\int_{-\infty}^{\infty} u(t)e^{-i\omega t}dt = \frac{1}{2\pi\left(1-e^{-i\omega T}\right)}\int_0^T u(t)e^{-i\omega t}dt \tag{22}$$

Value of $K_d(\omega)$ is equal to:

$$K_d(\omega) = \frac{\int_0^T f(t)e^{-i\omega t}dt = R_a}{\int_0^T u(t)e^{-i\omega t}dt = R_b} \tag{23}$$

As a result:

$$K_d(\omega) = \frac{F_0}{u_0}(\cos\phi + i\sin\phi) \tag{24}$$

Where:

$$\phi = \tan^{-1}\frac{2\rho\left(\frac{\omega}{\omega_n}\right)}{1-\left(\frac{\omega}{\omega_n}\right)^2} \tag{25}$$

3. DESIGN OF EXPERIMENTAL MODEL

The actual form of the bond stress-slip model can be assessed by evaluating the results of pullout test specimens. $250 \times 450 \times 800\ mm$. The pullout specimen was therefore cast to investigate the validity of the mechanics-based relationships derived in the previous section. Fig (1) shows the schematic form of spacemen. Section A-A in Figure 1 shows the built-up reinforcing steel bar used in the pullout specimen.

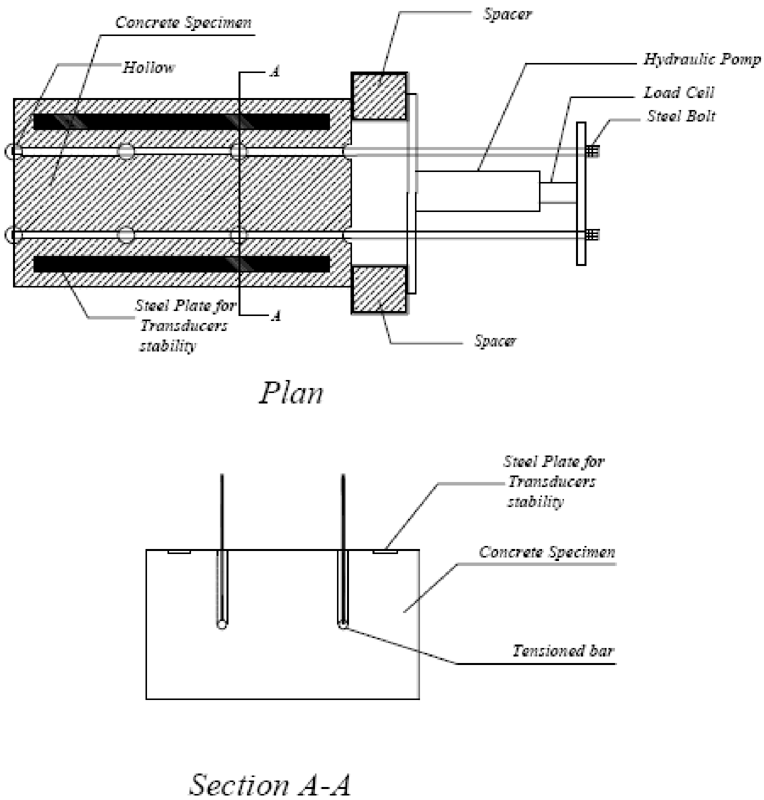

Figure 1. The test set up for pullout specimen

The concrete had a target concrete compressive strength of 25 Mpa to represent the range of strengths commonly encountered in structures. Type 2 Portland cement was used, without admixtures, to obtain a water-cement ratio (*w/c*) of 0.64. The maximum aggregate size was 9.5 mm. The pullout specimen would be tested when the concrete was 44 days old and had a strength of 24 Mpa.
The static yield strength (*fys)* of bars was 350 Mpa and the ultimate strength *fu* was 400 Mpa. The same reinforcing bar was used for both bars.
For loading, the Hydraulic pump has been used. Since the front surface of concrete should be unloaded, force entered into two plates and put spacers at the edges of plates. Because the pump is in the center of the plates, the loads of bars are the same (Figure 2).

Figure 2. Loading of pullout specimen

Specimens were cast with the reinforcing bar secured horizontally by the left and right forms. Blocks on the top form bore against the outside of the side forms to ensure proper bar alignment.

Lateral view of the experimental model is shown in Figure (3). Figure (4) shows top view of spacemen.

Figure 3. Lateral view of pullout specimen

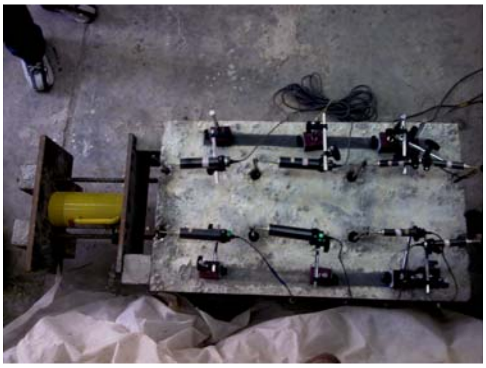

Figure 4. Top view of pullout specimen

There are four transducers for measuring of bar displacement at four points of each of the bars. For stability of transducers, two plates are put on the surface of concrete and the transducers' magnet is activated. Figure(5) shows one transducer on the spacemen.

Transducer number 1 was installed closest to the loaded end of the bar whereas strain gauge number 4 was closest to the unloaded end. A digital data logger and a personal computer where used to record the 8 slip values and the relative tension load (P). The loading rate for loads less than P_{max} ranged from approximately 0.66 to 0.70 Kn /second (150 to 160 lb/second) and, after P_{max} occurred, from –1.90 to –8.69 Kn/second (–430 to –1950 lb/second). The slip rate during the loading stage was calculated by examining the very small end slips that occur at the maximum load level. After those models of various cases are prepared, results are presented in a feature paper.

Figure 5. View of one transducer

4. CONCLUSION

Interaction between bar and concrete is a main point of focus in the concrete design. We can use theory relation for specifying stiffness between bar and concrete. This stiffness has static and dynamic share. Properties of dynamic stiffness can be obtained by using the formulation and experimental results. Also these relations can be compared by the experimental results. For this purpose, the experimental model should be realistic.

REFERENCES

1. L. Vandewalle and F. Mortelmans, ” The bond stress between a reinforcement bar and concrete: is it theoretically predictable?” , Materials and Structures Journal, Volume 21, Number 3 / May, 1988, 1988,21,179-181.
2. Z. Achillides, K. Pilakoutas, “FE modeling of bond interaction of FRP bars to concrete”, Structural Concrete Journal, Volume 7, January 2006, 7-16.
3. Feldman, L. R.,(2006) “Bond of Plain Steel Reinforcement in Concrete,” PhD thesis, Department of Civil and Environmental Engineering, The University of Western Ontario, London, ON, Canada, 272 pp.
4. Feldman, L. R., and Bartlett, F. M.,(2005) “Bond Strength Variability in Pullout Specimens with Plain Reinforcement,” ACI Structural Journal, V. 102, No. 6, Nov.-Dec. pp. 860-867.
5. Baldwin, M. I., and Clark, L. A.,(1995) “The Assessment of Reinforcing Bars with Inadequate Anchorage,” Magazine of Concrete Research, V. 47, No. 171, June, pp. 95-102.
6. Ghorbani, Mohsen, “Study of static and dynamic properties of buried pipeline due to harmonic vibration and earthquake”, Master's thesis, Mazandaran University, 2008.

CD01-002

EFFECTS OF WOOD-PULP FIBERS ON THE MECHANICAL PROPERTIES OF CEMENT COMPOSITES

A.A. Khalilitabas[1], M. Khorrami[2], J. Sobhani[3]
[1]A.A. Khalili is M.Sc. in Material Engineering University of Sistan & Baluchestan, Islamic Azad University, Zahedan-Iran
[2]Building and Housing Research Center, Tehran, Iran
[3]Assistant professor in the Building and Housing Research Center, Tehran, Iran

ABSTRACT
The application of pulp fiber in cement paste has been under consideration to improve the bearing capacities of the cement composites. Cement composites made by various types of fibers have distinct properties regarding the stability and resistance in dissimilar environmental conditions and applied loads. This behavior depends on four main factors: a) fiber type, b) mixture percentage c) fabrication manner, and d) additives. In this work, to distinguish the flexural behavior of fabricated composites with wood-pulp cellules fibers, the experimental samples designed and tested. The samples made with these fibers were compared with the no-fibrous control samples for their flexural strength and modulus of elasticity. Moreover, to characterize the microstructure properties SEM micrographs were analyzed. The results showed that the application of fibers had suitable effects on the improvement of the flexural strength related to the amount of used fibers.

Keywords: cement board, Pulp fiber, flexural strength, Modulus of elasticity, SEM micrograph

1. INTRODUCTION
All over the world, the production of the cement boards, are based on eckhatch procedure. The history for this method, back to about 100 years ago, in which was derived from paper production technology. Following this procedure, water, fibers and cement should be mixed at first and then, using a special process, this matrix converted to cement composite boards (CCB). To fabricate CCB, the cement matrix positioned on the driving belt, water-drained, and after placing the layers on each others, CCB will be formed. In original procedure, asbestos fibers were used which had good consistency with cement paste, physical and chemical properties, durability and mass-productivity specifications. The growth in production of CCB leads to increase in use and application of Asbestos material, in which, in 1985 the outmost production rate was recorded. Unfortunately clinical researches show harmful effects of this material on the humanity health [1]. Consequently, application and fabrication of the asbestos-based products were inhibited in the majority parts of construction industries. Despite this, the need for CCB motivates the researchers to find an effective solution. This solution should cover the

industrial demands production of CCB with an alternative material. The efforts were initiated in 1980's [10-2]. The solution was the mixed application of various types of cellulose, polymer, and suitable additives. The world master producers of CCB were the leaders of these research efforts. Also, several countries were looking for an appropriate and suitable materials and production techniques for their local applications. By the way, cellules and polymer based fibers (in particular Poly Vinyl Alcohol (PVA) fibers and other new products) were globally accepted as an effective material to be used. It is obvious that what is the researchers are seeking for is the economically optimized mixing proportion for production of the standard CCB. In this regard, the local fibers and domestic material and methods are recommended. For that reason, some factories in Thailand, Turkey, and Belgium succeeded to produce CCB with in access and localized materials, however, some other countries are preferred to import materials for this means. In Iran, there are many economical problems in technology transfer and on the other hand because of the dependency of the Iranian factories to PVA, these factories continue to use the asbestos in their products, despite the restricting regulations. In the recent years, with some growths in demands, 40 million tons of CCB and about 4500 km sewage and water pipes were produced with asbestos materials. Beside, the lack of intense restricting rules and regulations encouraged the continuation of the asbestos products in Iran. The first regulation concerned this issue was back to 2001 when the superior council for protecting of the living environment, puts some restrictions on the application of the asbestos materials. This states that after July 2001, the newly established factories are forbidden to use the asbestos in their products and the factories that were previously using the asbestos as a raw material have been ordered to modify their production procedure to replace the asbestos with other allowable material to completely eliminate the applications in the next 7 years.

The current study was started in early 2007 after this rules encouraged the researches seeking appropriate fibers to be replaced with asbestos materials. These fibers should be met all of the advantageous of asbestos and on the other hand these fibers should not affect the human heath. The pulp fiber produced in paper production factories were considered here with some surface treatments. These fibers were used in reinforcing the cement composite boards. After surface treatment process, their mechanical and physical properties regarding the flexural strength and young modulus were investigated. Samples were made with various fiber contents and then using SEM micrographs the micro-structural properties were studied.

2. TESTS AND METHODS

Cement: Type 2 cement supplied by Tehran Cement Factory was used in this study. Standard laboratorial tests (based on Iranian National Standard No. 398) were executed to determine the properties of this cement, which passed the requirements.

Fibers: The major part of the fibers of this study was prepared from the agricultural wastes. These fibers are usually used for paper production in which this paper it was named as wood-pulp. The used dimensions were wide-spread of length and thickness where would be discussed later.

Water: Tap water was used ke samplesto ma.

3. MIX DESIGN AND SAMPLE PREPARATION

The amount of wood-pulp was the major parameter of this study. These fibers were in used in the range of 0 to 14% of cement weight.

Table 1: Mix designs and naming codes

Sample	Cement (g)	Water (gr)	Fiber (gr)	Comments
Control	150	450	--	Non-fiber sample
P2	150	450	3.0	2% Cellulous-fiber
P4	150	450	6	4% Cellulous-fiber
P6	150	450	9.0	6% Cellulous-fiber
P8	150	450	12.0	8% Cellulous-fiber
P10	150	450	15.0	10% Cellulous-fiber
P12	150	450	18.0	12% Cellulous-fiber
P14	150	450	21.0	14% Cellulous-fiber

Composite cements were designed and made with a w/c ratio=3. At first fibers were mixed in rotary mixer with 15 mm horizontal blades for 5 min to be separated. This initial preparation was for untwisting the fibers to be well-dispersed in the cement mortar. Cement, water and fibers were mixed for another 5 minutes. After preparing the materials and mixing process, the prepared mixtures were poured into 8×18×15 cm molds. Excess water was drained with a 0.9 bar suction pump (Figure 1) while applying a 10 kg weight on the samples. Then the samples were dried for 1 hour and cured in a steam cabinet with 100% RH for 14 days. After curing, the samples de-molded and dried for 6 hours in 75˚C to prepare for mechanical tests.

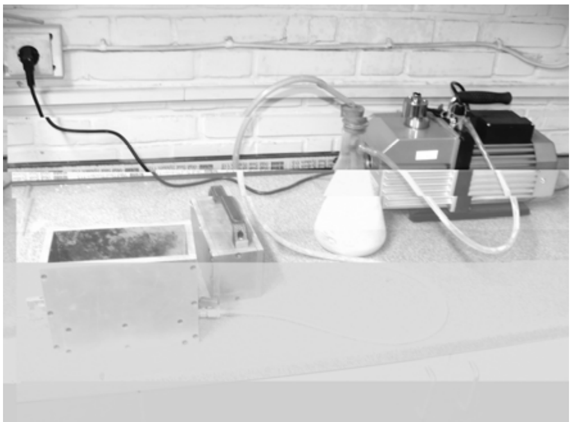

Figure 1. Set up for preparing the samples

4. TESTS
4.1. Tests for fibers
4.1.1. Freeness test
One of the important characteristics of the fiber in cement matrix is the Canadian Standard Freeness (CSF) that was designed for measuring the drainage properties of the wood-paste. The results of CSF test depend on many variables such as: the amount of fine particles and small pieces of available wood, fibrillation degree, flexibility of fibers, and the finesse modulus. The procedure for this test is as follows:

1- Specific volume of wood-paste poured into the cylinders to be drained. Accompanying liquid was brought in the conical case with two orifices one in the bottom and the other located on the side surface of the case.

2- Drained volume of liquid was measured and reported as degree of freeness after some modifications on the values of temperature coefficient and paste density.

3- In this research, the cured fibers were examined for freeness test according CSF.

4- Average measured value for CSF was 500 which were very close to results of other researches.

4.1.2. Morphological tests for fibers
Prepared fibers were poured into the test tubes and de-fibered. After fully separation, length and diameter of fibers as well the diameters of cellulose pores were measured with projectina optical microscope with 30 tries.

Table 2: Morphological characteristics of fibers

Morphological characteristics	Average
Length	mm
Demeter	30.853 micron
Inside cellulose wall	4.102 micron
Pore cellules wall	22.648 micron

5. EXPERIMENTAL CURVES
In this research, the strength of samples was tested in flexural loads. The flexural samples were flat rectangular and tested with a 3-point load system according to the EN12467:2004.

Figure 2 shows the load-deflection curve for CCB with and without fibers. As it can be seen in Figure 2, the application of fibers in CCB increased the flexural bearing capacity (FBC). The maximum observed value in control sample of FBC was 54.42 N, while this enhancement for 4, 6, 8% fiber added samples were 109.75, 238.35, and 289.62, respectively. These values showed that the addition of fibers in cement paste notably increased the FBC. The effect of thickness was not evaluated in this curve, therefore, could not properly reflect the capabilities. Because the more fibers added, the more thickness of CCB appeared and so, the increase of thickness cold be affect the ultimate FBC. To eliminate this deficiency, the following relations were utilized in evaluation of the FBC of CCB:

$$\sigma = M / W \quad \text{(Eq. 1)}$$

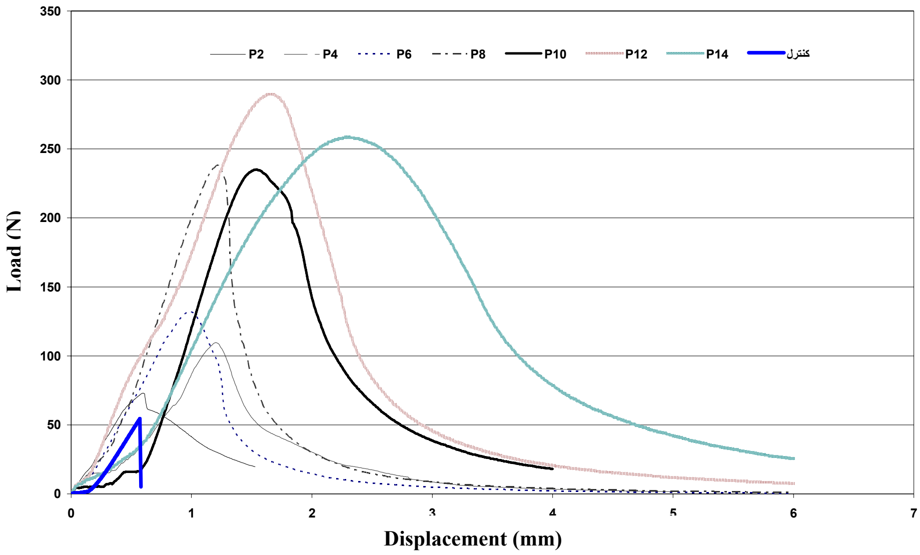

Figure 2. Load-deflection curve of CCB reinforced with cellulous fibers in comparison to the control samples

Where σ is available stress (MPa), M is flexural moment, W is the flexural capacity of the section.

$$M = PL / 4 \quad \text{(Eq. 2)}$$

P is applied concentrated load (N) and *L* is the length of sample.

$$W = BH^2 / 6 \quad \text{(Eq. 3)}$$

Where *B* is width (mm) and H is height (mm) of sample.

$$E = \sigma / \varepsilon \quad \text{(Eq. 4)}$$

Where E is modulus of elasticity (MPa) and ε is strain.

By replacing the values of *M* and *W* in Eq. (1), the stress will be attained as follows:

$$\sigma = \frac{3PL}{2BH^2} \quad \text{(Eq. 5)}$$

Deflection can be calculated by assuming the linear region as:

$$\delta = \frac{PL^3}{48EI} \quad \text{(Eq. 6)}$$

Where *I* is the moment of inertia and δ is the deflection (mm).

By increasing the load *P*, the value of δ could be measured in real time. If the linear region was assumed, it would be computed as:

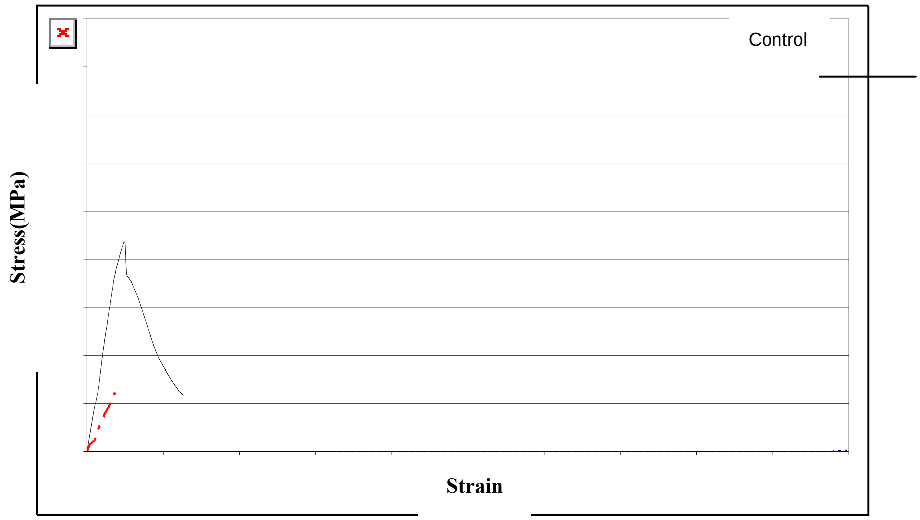

Figure 3. Stress-strain curve of cement composites reinforced by pulp or plant fibers in comparison to the reference sample

$$E = \frac{PL^3}{48\delta I} \quad \text{(Eq. 7)}$$

Where

$$I = \frac{1}{12} BH^3 \quad \text{(Eq. 8)}$$

Using the Eq. 7, the value of ε can be gained:

(Eq. 9)

Based on these relations, flexural strength of CCB samples were evaluated as shown in Figure 3.

For more analysis, the stress-strain curves are plotted in Figure 3. As it can be seen, application of fiber upgrades the maximum yielding stress. Moreover, by increasing the fibers, the area under the stress-strain curve has been increased that is related to the energy absorption properties of boards.

6. FLEXURAL STRENGTH

Figure 4 demonstrates the results of flexural strength of samples. The results proved that the addition of fibers resulted in improvement of flexural strength of CCB. Obviously, the rate of enhancement depends on the type and amount of added fibers and various percentages of fiber replacements affect the mechanism of failure in CCB. Assessment of stress-strain curves of CCB guided us to classify the CCB based on the type and amount of fiber replacements into three groups:

Group 1: Samples with 0-6% fiber replacement
Group 2: Samples with 8-10% fiber replacement
Group 3: Samples with 12-14% fiber replacement
In group 1, as depicted in Figure 4, the flexural strength enhanced slightly with and increase in the fiber amount, whereas the minor enhancement, the failure mechanism of the samples was totally different which varied from brittle to ductile.

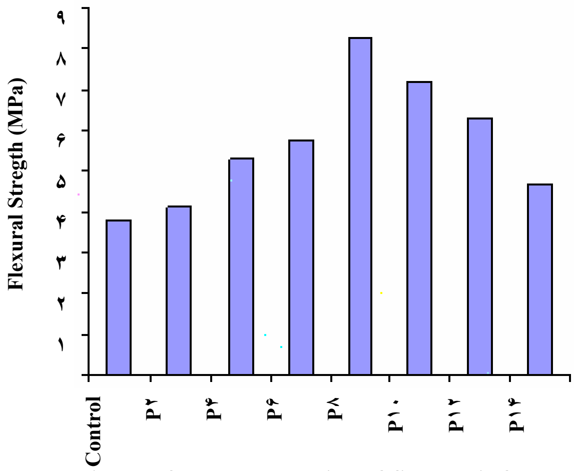

Figure 4. The maximum flexural capacity of fiber-reinforced cement composite boards in comparison to the non-fibrous reference samples

The samples where placed in group 2, have the most flexural capacities in contrast to the reference samples. In some samples in this group, the enhancement reached up to two folds. Moreover, the flexible failure mode was observed for all of samples in this class. In this situation, well-dispersion of fibers with good bond formation between cement paste led to good development of flexural strength of these samples.
In group 3, with increasing the fibers, the more decrease in flexural strength was observed that it is expected to continues up to 14% fiber addition. Assessment of failure mechanism showed that the ductility of samples in this group is higher than other groups. It should be noted that the higher amount of fiber in this group lead to for an unfavorable appearance due to high concentration of fibers at the outer surface of CCB. Moreover, after breaking the samples under load, the balled-shape fibers are visible in some parts of matrix that leads to missed-dispersion of fibers inside the matrix eventually leads to decreasing the flexural strength of this group.
To verify the behaviour and effects of paper-pulp fibers, SEM photographs were analyzed and showed in Figures. 5 and 6. The microstructure of paper-pulp fibers represents the rough surface with good fibrillation. Well ionfibrilizat of fibers forms the numerous fibrils around the outer surface that could help the friction bond strength with cement matrix. On the other hand, the high aspect ratio (10.23) and smaller diameter (30.85 μm) assist in friction strength. The matter will be more important at the interfacial zone of fiber-cement paste and increasing the effective

bond between them. In these pictures very tiny particles associated with the fibers are gibleinegl. Therefore at the sites of cement paste that these materials stanceexi can be interpreted as defects that decrease the strength. Consequently, the existence of these particles in lower amounts could restrict the weak regions inside the cement paste. But other important factor influencing the cement composite with fibers is the fibers orientation in the cement paste. Figure 6 shows the distribution and performance of fiber in cement paste. It is considerable that the fibers are dispersed uniformly throughout the samples. Moreover, the existence of cement particles around the fibers demonstrates the establishment of well interaction between fibers and cement paste. This shows a good bond development between fiber and cement paste.

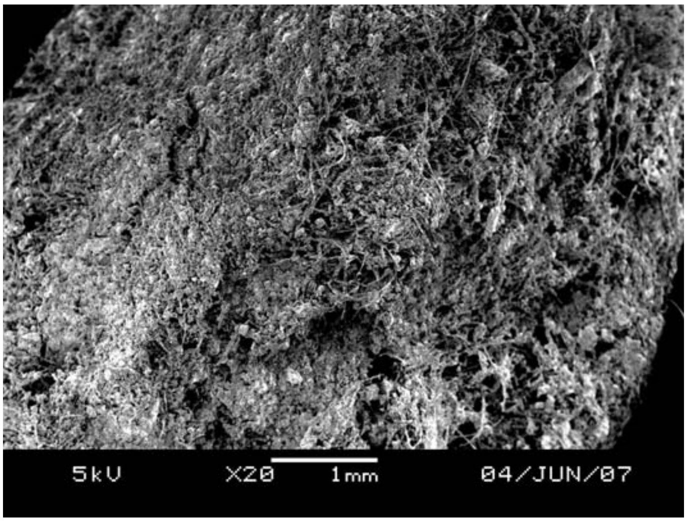

Figure 5. SEM Micrograph of cement paste with Kraft fiber

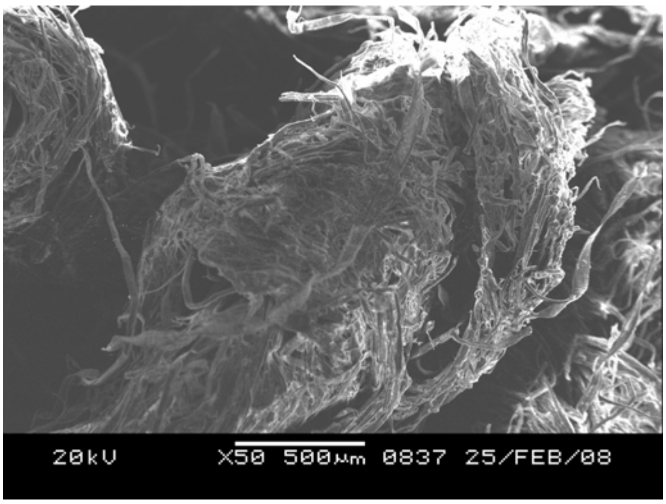

Figure 6. SEM Micrograph of Kraft fiber

7. MODULUS OF ELASTICITY

The modulus of elasticity (ME) is computed for ascending branch of stress-strain curves and the values are depicted in Figure 7. As it can be seen, the modulus of elasticity in all of the samples is lower than reference sample and with increasing the amount of fiber, it will be reduced. Many factors are involved in this property. If the cement composite is considered as a two-phase material (fiber and cement) then ME of the fibers can be effective in overall modulus of elasticity of cement composite so that the more or lesser ME of fibers the more or lesser ME of cement composites will be gained.

It should be noted that the amount of fiber in reinforcing the cement composite is very determinative. To verify this phenomena, the following relation that proposed by Allen [11]which was used to compare with the results of experimental modulus of elasticity of cement composites.

$$E_c = E_m(1-V_f) + E_f V_f \qquad \text{(Eq. 10)}$$

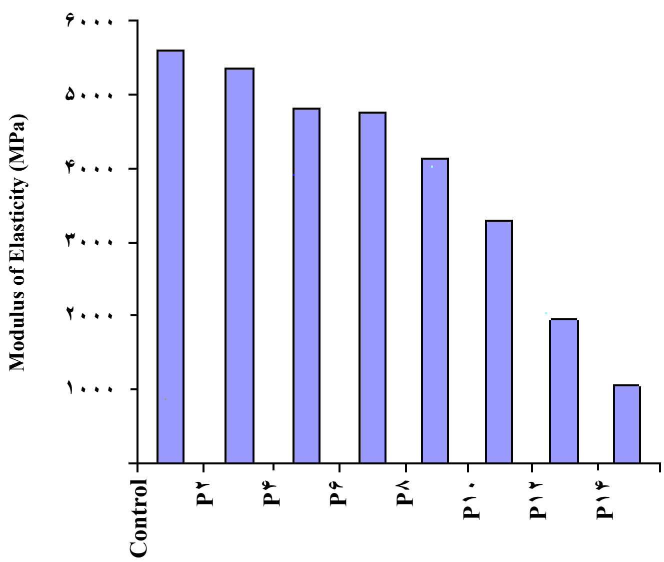

Figure 7. Modulus of elasticity of cement composite boards with and without fibers

Where E_c, E_m, E_f, are the composite, cement matrix and fibers modulus of elasticity respectively and V_f is the volumetric percentage of fiber in the composite.

Experimental results of modulus of elasticity are:

Cement modulus of elasticity = 8.788 GPa

Average modulus of elasticity of pulp= 85.36 GPa

Using the composite component's ME yields great values for in calculated ME for composite material while the experimental observation do not agree with these findings. So it is supposed that the Allen formula is proper when the composite is considered in an ideal condition. Researchers showed [11,5-6] that with application of fiber in cement paste resulted in increase of voids in cement matrix and consequently the micro defects extended. Then generally the modulus of elasticity of cement composite with fiber would we more less that the samples without fibers. Allen [11] proposed a formula regarding this concern as follows:

$$E_m = E_{mo}(1-p) \qquad \text{(Eq. 11)}$$

Where E_{mo} is cement matrix ME without fiber, p is the amount of voids in the composite in percent. Moreover, Allen [11] showed that p is as a part of fiber in percent and could be calculated as follows:

$$p = 0.0522 + 3.7407\ V_f \qquad \text{(Eq. 12)}$$

It seems that the Eqs.11 and 12 is very reliable and could reflect the experimental observations.

On the other hand, in the mixing procedure of cellules fiber and cement paste with water, some bubbles and spumes would appear on the surface of mortar which could be lead to increase the thickness of the samples with fibers. Thus the results obtained from laboratorial study could be comparable and reliable. The reason for producing the bubbles or spumes is the application of alkaline stuffs in chemical process for production of the pulp. When these chemicals components are contacted with oil used to lubrication of the molds, these bubbles or spumes are formed. As a result, though ME of fiber is greater than the cement paste, but because of these process (bubbles or spumes formation) resulted in increment of porosity of composite leads to decrease in reduction of composite ME. Increase in fiber amount would cause to extending the porosity and finally expansion of samples based on Eq.12 then, in all samples with fiber ME would be reduced by increase in fiber amount.

8. CONCLUSION

From the results obtained in the effect of wood-pulp fibers in mechanical properties of cement composites, the following conclusions can be drawn:

1- Cellulose-fibers extracted from the brief-preparation of pulp has good consistency with cement paste and could be dispersed inside the cement matrix and finally have well bonding with cement paste.

2- By increasing the fiber amount up to 8% of cement, the flexural strength of cement boards would be increase and in the range of 8 to 10% this is constant or has very low decreases. With addition of fiber more than 12%, the flexural strength development would have descendent slop.

3- The main reason for decrease of strength of cement composites, are: a) thickening of the samples because of porosity and b) miss dispersion or non-uniform distribution of fiber in cement paste in which fibers want to be like clew and twisting or miss dispersion inside the matrix.

4- Existence of fibrils could aid in binding and uniformity of fibers with cement paste and eventually leads to enhancing the flexural strength.

5- Modulus of elasticity of composites got more affection from the bonding and continuity of the fibers with cement paste than its components like cement or fibers; does the more bonding strength the more modulus of elasticity would be exist.

REFERENCES

1. WHO meeting: "Occupational Exposure Limit for Asbestos", Oxford, United Kingdom, 10-11 April 1989.
2. R.S.P. Coutts, "A review of Australian research into natural fibre cement composites", Cement & Concrete Composites 27 (2005) 518-526.
3. Coutts RSP. Flax fibres as a reinforcement in cement mortars. Int J Cem Compos 1983;5(4):257-262.
4. Bentur A., Midness S., Fiber Reinforced cementitious composites, Elsevier, 1990.
5. Coutts R. S. P., "A review of Australian research into natural fiber cement composites", Cem. Comcr. Comp, 27(2005) 518-526.
6. Bentur A, Akers SAS. The microstructure and ageing of cellulose fiber reinforced cement composites cured in a normal environment. lnt J Cem Compos 1989;11:999109.
7. Aziz, M.A., Paramasivam, P. & Lee, S. L., Concrete reinforced with natural fibers. In concrete Technology and Design, Vol. 2: New Reinforced Concretes, ed.R.N. Swamy. Surrey University Press, 1984, pp.107-40.
8. Kaufmann J.; Winnefeld F. and Hesselbarth D., "Effect of the addition of ultrafine cement and short fiber reinforcement on shrinkage, rheological and mechanical properties of Portland cement pastes", Cem. Concr. Comp., 26(2004) 541-549.
9. Mohr B. J.; Nanko H. and Kurtis K. E., "Aligned kraft pulp sheets for reinforcing mortar", Cem. Concr. Comp., 27(2005) 554-564.
10. Andonian, R., Mai, Y.W. & Cotterell, B., Strength and fracture properties of cellulose fiber reinforced cement composites. Int. J. Cem. Comp, 1(1979) 151-8.
11. Allen H.G., "Tensile properties of seven asbestos cements", Composites, 2(2)(1971) 98-103.

CD01-003

APPLICATION OF SMA IN CONCRETE STRUCTURES

A.R. Khaloo[1], P. Piran Aghl[2], I. Eshghi[3]
[1]Professor of Structural Eng, Sharif University of Technology, Tehran, Iran
[2]MS student in earthquake Eng, Sharif University of Technology, Tehran, Iran
[3]MS in earthquake Eng, Sharif University of Technology, Tehran, Iran

ABSTRACT
Shape memory alloys (SMAs) are increasingly becoming a topic of research in the area of 'smart materials'. SMAs are a novel functional material, which can exhibit large strains under loading–unloading process without residual deformation. They have the ability to remember a predetermined shape even after severe deformation. This article first presents an overview of the characteristics of SMAs associated with the temperature-induced and stress-induced reversible hysteretic phase transformation between austenite and martensite. The recent experimental studies and numerical simulations, which have been led to demonstrate the powerful role played by SMAs, are also presented in this article. Currently, research efforts have been extended to using SMA as sensors, actuators, passive energy dissipaters and dampers for shape control and vibration control of civil structures. This article then presents a review of applications of the SMA materials for passive and active controls of concrete structures.

Keywords: shape memory alloys, shape memory effect, superelastic effect, structural control, smart material

1. INTRODUCTION
Smart systems for civil structures are described as systems that can automatically adjust structural characteristics in response to external disturbances and/or unexpected severe loading toward structural safety, extension of the structure's lifetime, and serviceability [1].
In 1965, shape memory alloys (Nitinol) as a smart material derived from Nickel and Titanium were first patented by Buehler and Wiley [2] in Naval Ordnance Laboratory. Since then, tremendous effort has been infused to the utilization and study of this smart material.
In recent years, the two major properties of SMAs have attracted the attention of many researches for application to smart structural systems. One is the Superelasticity or pseudoelastic effect (PE), which is the ability of a shape memory alloy to accommodate large strains due to stress-induced phase change at a constant, sufficiently high temperature and to recover its initial shape upon unloading. The other is the superthermal effect or shape memory effect (SME), which is the ability to deform an initially austenitic SMA by cooling under constant stress and then to recover the austenitic shape by heating. The magnitude of the

temperature-induced strains depends on the applied stress.
Although SMAs have been known for decades, they have not been used in the concrete structures until rather recently. SMAs can be passive or active components in civil structures to reduce damage caused by environmental impacts or earthquakes.
This paper is divided into three main parts. The first part focuses on the basic characteristics of SMA (Section 2). The second part contains recent research on the damping properties of SMAs (Section 3). The third part presents the Application of SMAs for passive and active concrete structure control (Section 4).

2. BASICS ABOUT SHAPE MEMORY ALLOYS

SMAs are found in two main phases: the high temperature phase, which is called austenite, and the low temperature phase, which is called martensite. SMAs could be transformed from austenite to martensite either by reducing the temperature or by applying a mechanical stress. On the other hand, martensite transforms into austenite by either increasing the alloy's temperature or removing the applied stress.
SMAs have four transformation temperatures: (a) the austenite start temperature (T_{As}), where the austenite starts to develop in the alloy; (b) the austenite finish temperature (T_{Af}), where the development of austenite in the alloy is 100% complete; (c) the martensite start temperature (T_{Ms}), where the development of martensite starts; and (d) the martensite finish temperature (T_{Mf}), where the development of martensite is 100% complete.
There are three groups of shape memory effects [3]. All of them have one common speciality, namely at least one shape (macroscopic state) of the material is recoverable.
In the case of one-way effect the material gets a permanent deformation by applying mechanical load in a relative cool temperature ($T < T_{Af}$). However, this deformation can disappear by heating above T_{Af} and it remains unchanged during the cooling to the start temperature (Figure 1.a).
When the start temperature is above T_{Af}, mechanical load can cause deformation, but it disappears during unload. It seems like an elastic behavior, but the deformation can be unusually great. This effect is the PE, which does not concern only shape memory properties (Figure 1.b).
The third effect is the two-way effect that requires only thermal load to change between two stable shapes. One of the shapes is stable above T_{Af} and the other one is stable below a different temperature $T_{Mf} < T_{Af}$. It has to be mentioned that this effect can be produced only after a special treatment (Figure 1.c).

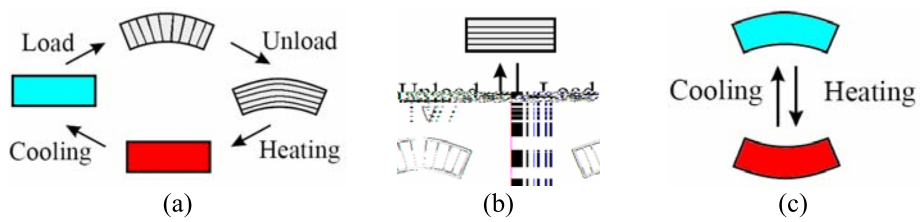

Figure 1. Shape memory phenomena: one-way effect (a), pseudoelasticity (PE) (b), and two-way effect (c) [4]

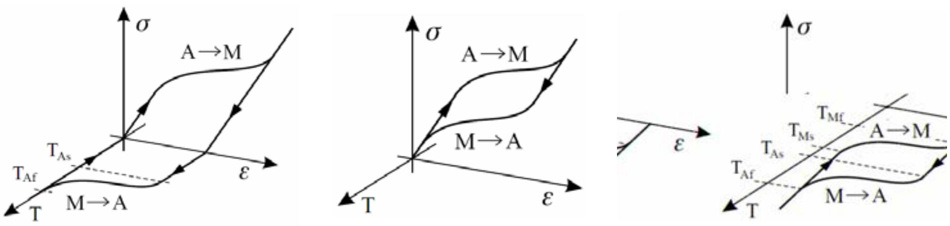

(a) (b) (c)

Figure 2. Shape memory phenomena in stress-strain-temperature space: one-way effect (a), pseudoelasticity (PE) (b), and two-way effect (c) [4]

Behind these effects, there is a crystallographic transformation, namely the martensitic phase transition. As it can be seen from the phenomena, the phase transitions can be induced by mechanical and thermal load. Figure 2 shows the effects in a stress-strain-temperature space. The forward (austenite to martensite, A→M) and backward (martensite to austenite, M→A) transitions and their temperatures are also illustrated.

3. RESEARCH ON THE DAMPING PROPERTIES OF SMAS

The high damping capacity is known as one of the important functional properties of shape memory alloys. Damping, in a technical context, stands for the conversion of mechanical energy to thermal energy and therefore for the ability to reduce movements or vibrations of a structure.

Using SMAs for passive structure control relies on the SMA's damping capacity, which represents its ability to dissipate vibration energy of structures subject to dynamic loading. As reviewed in the last section, the damping capacity comes from two mechanisms: martensite variations reorientation which exhibit the SME, and stress-induced martensitic transformation of the austenite phase which exhibit the PE.

The energy dissipation of the widely-used Nitinol superelastic SMA wires was investigated [5-8]. Dolce and Cardone [9] investigated the superelastic Nitinol wires subjected to tension loading. They observed the dependence of the damping capacity on temperature, loading frequency and the number of loading cycles. It is found that the mechanical behavior of the wires is stable within a useful range for seismic application. In addition, they suggested that the austenite wires should be pretensioned for larger effectiveness of energy dissipation.

A superelastic SMA wire demonstrates the damping capacity not only under tension loading, but also under cyclic bending. In 2000, Ip presented his effort to predict the energy dissipation in SMA wire under pure bending loading. His numerical results showed that the energy dissipated by the superelastic SMA wire is highly sensitive to its diameter; in detail, the thicker the SMA wire, the more energy was dissipated.

Recently, as large cross-section-area SMAs become available, studies on the properties of SMA bars or rods have attracted more attentions. As discovered by Liu et al [10], the damping capacity of a martensite Nitinol bar under tension–compression cycles increases with increasing strain amplitude, but decreases with loading cycles and then reaches a stable minimum value.

Dolce and Cardone [9] compared the martensite damping and austenite damping of Nitinol bars subjected to torsion. They found that the damping capacity of the martensite Nitinol bar is quite a bit larger than that of the austenite Nitinol bar, although the prior cannot remain at its highest value as the residual strain accumulates. They also noticed that the martensite bar's mechanical behavior is independent of loading frequency and that of the austenite bar slightly depends on the frequency. This implies that both martensite and austenite Nitinol bars can work in a wide frequency range and have a good potential for seismic protection.

4. APPLICATION OF SMAS IN CONCRETE STRUCTURE CONTROL

The vibration suppression of concrete structures to external dynamic loading can be pursued by using active control and passive control. In the active control mode, an external power source controls actuators to apply forces to the object structures. For a passive control system, no external power source is required and the impact forces are developed in response to the motion of the structures.

4.1. Smas for Passive Structural Control

The passive structural control using SMAs takes advantage of the SMA's damping property to reduce the response and consequent plastic deformation of the structures subjected to severe loadings. Indeed, martensite or austenite SMA elements as energy dissipation devices absorb vibration energy based on the hysteretic stress–strain relationship.

4.1.1. Sma Braces for Frame Structures

The SMA wire braces are installed diagonally in the frame structures. As the frame structures deform under excitation, SMA braces dissipate energy through stress-induced martensite transformation (in the superelastic SMA case) or martensite reorientation (in the martensite SMA case).

Several different scale prototypes of the devices were designed, implemented and tested. They showed that the proposed devices have characteristics of great versatility, simplicity of functioning mechanism, self-centering capability, high stiffness for small displacements and good energy dissipation capability. The combined steel–SMA type braces were also adopted by Tamai and Kitagawa [11] in their seismic resistance devices as shown in Figure 3. Cardone et al [12] proposed a design for bracings of multi-storey reinforced concrete (RC) frames with a martensitic Ni-Ti adapter as the damping element.

4.1.2. Sma Restrainers for Bridges

Bridge restrainers are elements that are commonly used to connect two adjacent bridge spans or frames and prevent them from experiencing large relative displacements during earthquakes. Superelastic SMAs can be used as damper elements or potential seismic restrainers for bridges.

As shown in Figure 4, DesRoches and Delemont [13] reported their full-scale tests of 25.4 mm diameter superelastic SMA restrainer bars used for seismic retrofit of simply support bridges and their simulation analysis on a multi-span simply supported bridge. The results have shown that the SMA restrainer more effectively reduced relative hinge displacement at the abutment and it provided a large elastic deformation range in comparison with conventional steel restrainer cables. In addition, the SMA restrainer extremely limits the response of bridge decks to near-field ground motion. The increased stiffness of the SMA restrainers at large strains provides additional restraint to limit the relative openings in a bridge.

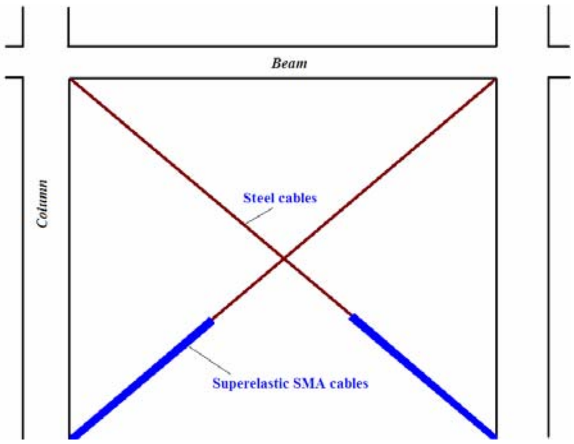

Figure 3. Schematic of the SMA braces for a frame structure

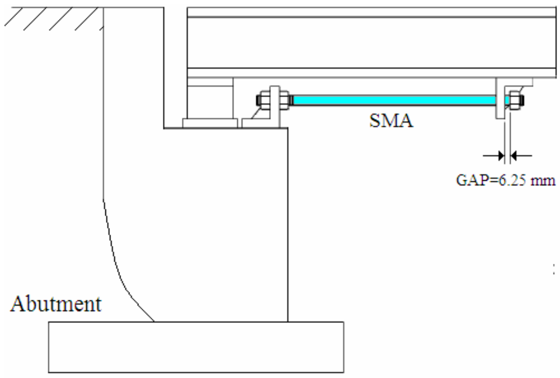

Figure 4. Schematic of the setup of SMA restrainer for a simple-supported bridge

Moreover, Rita Johnson et al [14] conducted a large scale testing program to determine the effects of SMA restrainer cables on the seismic performance of in-span hinges of a representative multiple-frame concrete box girder bridge subjected to earthquake excitations. The SMA cable restrainer which was used in this study is shown in Figure 5. The results of the experimental testing have revealed that the SMA restrainers not only served as effective bridge retrofits, but also result in superior performance relative to equivalent traditional steel restrainer systems. Additionally, results of utilizing the analytical model revealed that using SMA restrainer cables reduced the peak hinge openings by nearly 50% for some cases.

4.1.3. Sma Connectors

Connectors or connections in various structures are prone to damage during an earthquake event. SMA connectors have been designed to provide damping and tolerate relatively large deformations. Tamai and Kitagawa [11] proposed an exposed type column base with SMA anchorage for seismic resistance. The SMA anchorages are made of the Nitinol SMA rods in 20–30 mm diameter and steel bars, as shown in Figure 6.

Figure 5. SMA cable restrainer with the effective length of 1.16 m used as a retrofitting device

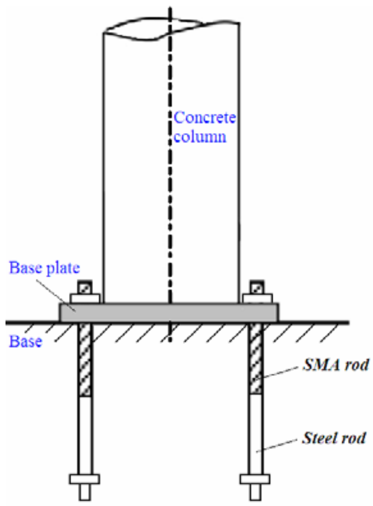

Figure 6. Schematic of SMA bar anchorage for a column

The results obtained from the pulsating tension loading tests and numerical simulation of the SMA rods, have shown that the SMA wires were very effective in dissipating energy and reducing the building's vibration under severe seismic ground motion. Furthermore, the SMA anchorages can recover their original shape after cyclic loadings and therefore their resisting performance remains the same to prevent plastic deformation and damage in the structural columns. Additionally, it is possible to design a column base with SMA anchorage that does not require repair after a severe earthquake, when the maximum rotation responses of the base plate are less than 0.025 rad [15].

4.1.4. Shape Restoration Using Superelastic Smas

In the literature, there is a specific type of application of superelastic SMA wires for structural control purpose different from the aforementioned examples. This application uses the shape restoration property of superelastic SMA wires. For example, Song and Otero [16] developed a more efficient way to use superelastic SMA wires to achieve a larger restoration force in the form of a stranded cable. Figure 7 shows a concrete beam (24 in. × 4 in. × 6 in.) reinforced with fourteen 1/8 in.-diameter superelastic stranded cables via the method of post-tensioning to achieve a 2% pre-strain. Each cable has seven strands and each strand has seven superelastic wires. Special clamps were made to hold the superelastic strands/cables without slippage. After a load of 11,000 lbs and the appearance of a large crack (Figure 7.a), the crack on this beam was closed (Figure 7.b) under the elastic restoration force of the superelastic SMA cables upon removing the load. Two quarter-scale RC column with SMA longitudinal reinforcement in the plastic hinge area were tested on the shaketable by Saiidi and Wang [17]. The exploratory study showed that the residual displacements in the SMA-reinforced columns were very small. Furthermore, Khaloo and Eshghi [18] studied numerically the response of RC columns using smart rebars under static lateral loading. It is found that by using SMA rebars in RC columns, these materials tend to return to the previous state (zero strain), so they reduce the permanent deformations and also in turn create forces known as recovery forces in the structure which lead into closing of concrete cracks in tensile zone and reduction of the eccentricity created in the concrete columns which is the result of permanent deformations.

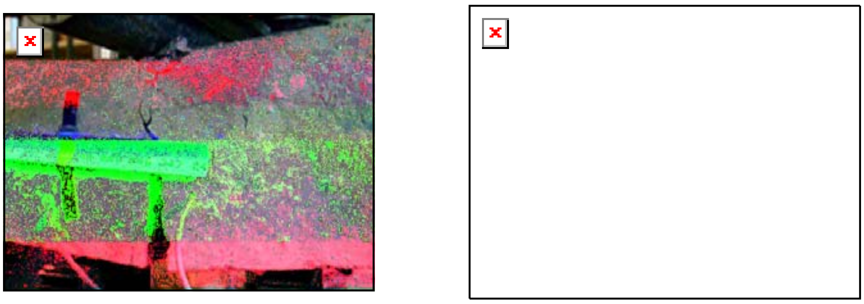

(a) (b)

Figure 7. A large crack during a loading test (a), and the crack closes after the loading test (b)

4.2. Smas for Active Structural Control

The SMA has the capability of recovering a previously formed shape via heat energy, which is referred to as an active property tuning when incorporated into a structural system.

4.2.1. Sma Wires in Concrete

The behavior of a simple concrete beam driven by heated SMA wires using electrical currents was investigated by Li et al [19]. Figure 8 shows the loading apparatus. Prior to the test, a certain pre-tension was imposed on the SMA wires, which were fixed firmly at the two ends of the specimen by the special clamps. Specimens were first loaded at the midspan to a certain deformation until the concrete was cracked. Subsequently, the SMA wires were heated using a constant electrical current of 14 A in order to drive the concrete beam. The test results indicate that recovery forces of the SMA wires can reduce mid-span deformations and compressive strains of the specimens effectively. Furthermore, the heated SMA wires can make cracks close and perform the task of emergency damage repair in civil structures. The load capacity after actuating of the SMA wires increases although the concrete is already cracked. Moreover, the specimen embedded with more SMA wires proves much better than the specimen does with fewer SMA wires.

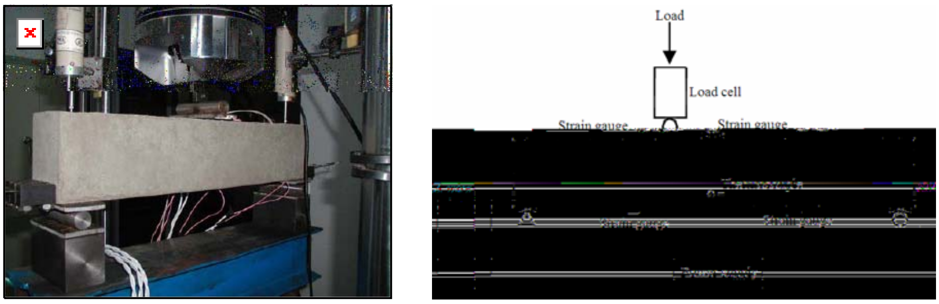

(a) (b)

Figure 8. Set-up of the loading apparatus (a), and Instrumentation sketch (b) for concrete beam with embedded SMA wires

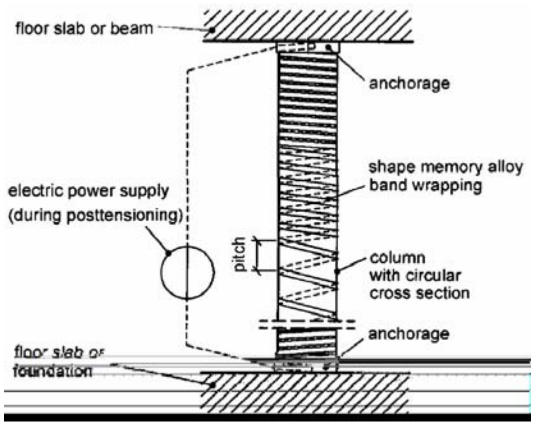

Figure 9. Active Confinement of a concrete column with a prestressed shape memory alloy wrapping for retrofitting purposes [20]

4.2.2. Active Confinement of Concrete Members with Sma

Another application of using SMAs in concrete structures is in the confinement of reinforced concrete members. The increase in load bearing capacity and also ductility by wrapping columns with bands or sheets of steel or FRP is well known. In addition,

it is well known that the strength of confined concrete is a function of the load. Utilizing the shape memory effect for tensioning the wrapping can enhance the effect of confinement. Krstulovic-Opara et al [21] carried out tests on SMA confined concrete members. They performed compression tests of the model scale with confined concrete cylinders. The specimens were jacketed with thin continuous Ni-Ti wires. Stressing of the jacket was done by putting the whole specimen in an oven. The comparison between several variants of stressed and unstressed jacketing showed that the use of SMA spirals alone effectively introduced high levels of active confinement.
Concrete columns could be easily helically wrapped by continuous SMA bands. The pitch of the helix can be fitted to the aimed confinement. Figure 9 shows the setup for the tensioning by resistance heating. Obviously, this technology is suitable in particular for retrofitting, in cases where there is only limited space for mounting, e.g. in cellars of buildings or in case of double columns. The strength values under confinement can theoretical enable very high loads at very high strains. However, only compression strains of several percent are acceptable in columns in order to prevent damage to the concrete or disadvantages to the whole structural system of a building. The load bearing capacity for small strains was hence of interest for the performed calculation. The calculations showed a lower axial strain for the active SMA confined column compared to the steel or CFRP confined column at the same load. On the other hand, a higher axial load can be applied at a given ultimate strain.

5. CONCLUSIONS

This paper presents a review of the basic properties of Nitinol SMA and their applications in passive and active control of concrete structures. The SME enables martensite Nitinol materials to be used as actuators and also enables their applications in active controls of concrete structures. Structural self-rehabilitation using reinforced martensite SMAs is an example of active structural control. Both martensite and superelastic SMAs show strong hysteretic effects in their stress–strain curves for loading–unloading cycles and dissipate energy during these cycles. This provides the basis for developing passive structural damping devices using both martensite and superelastic SMAs. We have seen a trend to combine the advantages of martensite and austenite SMAs to achieve optimal performance in structural control.

REFERENCES

1. Otani S, Hiraishi H and Midorikawa M, Development of Smart Systems for building structures, Proceedings of SPIE 2000, 3988, pp 2-9.
2. Buehler WJ and Wiley RC, US patent 3,174,851, nickel-based alloys, 1965.
3. Perkins J, Shape Memory Effects in Alloys, Plenum Press, New York, 1975.
4. Árpád Peth″o, Constitutive modeling of shape memory alloys based on a finite strain description, Periodica poly technical ser. Mech. Eng. 2000, Vol. 44, No. 1, pp. 115-126.
5. DOLCE M and CARDONE D, Mechanical behavior of shape memory alloys for seismic application 1: Martensite and Austenite NiTi bars subjected to torsion, International Journal of Mechanical Sciences 2001, Vol. 43, pp 2631-56.

6. Piedboeuf MC and Gauvin R, Damping behavior of shape memory alloys: strain amplitude, frequency and temperature effects, Journal of Sound and Vibration 1998, 214(5), pp 885-901.
7. IP KH, Energy dissipation in shape memory alloy wire under cyclic bending, Smart Materials and Structures 2000, Vol. 9, pp 653-9.
8. GRANDHI F and WOLONS D, Characterization of the pseudoelastic damping behavior of shape memory alloy wires using complex modulus, Smart Materials and structures 1999, Vol. 8, pp 49-56.
9. Dolce M and Cardone D, Mechanical behavior of shape memory alloys for seismic applications 2: Austenitic NiTi wires subjected to tension, International Journal of Mechanical Sciences 2001, Vol. 43, pp 2656-77.
10. Liu Y, Xie Z and Humbeeck JV, Cyclic deformation of NiTi shape memory alloys, Materials Science and Engineering 1999, A273–275, pp 673-8.
11. Tamai H and Kitagawa Y, Pseudoelastic behavior of shape memory alloy wires and its application to seismic resistance member for building, Computational Materials Science 2002, Vol. 25, pp 218–27.
12. Cardone D, Dolce M, Ponzo FC and Coelho E, Experimental behavior of R/C frames retrofitted with dissipating and re-centring braces, Journal of Earthquake Engineering 2004, 8 (3), pp 361-396.
13. Desroches R and Delemont M, Seismic retrofit of simply supported bridges using shape memory alloys, Engineering Structures 2002, Vol. 24, pp 325-32.
14. Johnson R, Padgett J E, Maragakis M E, Desroches R and Saiidi M S, Large scale testing of nitinol shape memory alloy devices for retrofitting of bridges, Smart Mater. Struct. 2008, Vol. 17, 035018 (10pp).
15. Tamai H, Kitagawa Y and Fukuta T, Application of SMA rods to exposed-type column bases in smart structural systems, 13th World Conference on Earthquake Engineering Vancouver, B.C., Canada 2004, August 1-6, Paper No. 1884.
16. Otero K, Intelligent reinforced concrete structures using shape memory alloys, M.S. thesis, Advisor: Dr. G. Song, University of Houston; 2004.
17. Saiidi M S and Wang H, Exploratory Study of Seismic Response of Concrete Columns with Shape Memory Alloys Reinforcement, ACI Structural Journal, 2006, May 1, pp 436-43.
18. Eshghi I, Cyclic behavior of reinforced concrete columns using smart rebar, M.S. thesis, Advisor: Prof. A R Khaloo, Sharif University of Technology; 2007.
19. Li H, Liu Z and OU J, Behavior of a simple concrete beam driven by shape memory alloy wires, Smart Mater. Struct. 2006, Vol. 15, pp 1039-1046.
20. JANKE L, CZADERSKI C, MOTAVALLI M and RUTH J, Applications of shape memory alloys in civil engineering structures - Overview, limits and new ideas, Materials and Structures 2005, Vol. 38, June, pp 578-592.
21. Krstulovic-Opara N and Thiedeman PD, Active confinement of concrete members with self-stressing composites, ACI Materials Journal 2000, 97 (3), pp 297-308.

CD01-004

EFFECT OF SILICA FUME ON HYDRATION HEAT AND STRENGTH DEVELOPMENT OF HIGH STRENGTH CONCRETE

[1]M. Nili, A. Ehsani[2]
[1]Ass. Professor, Civil Eng. Dept. Faculty of Eng. Bu Ali Sina University, Hamedan, I.R.Iran
[2]Msc Student, Civil Eng. Dept. Bu Ali Sina University, Hamadan, I.R.Iran

ABSTRACT

Recently, silica fume became a vital ingredient for producing concrete in aggressive hot climate of Iran. In mass structures heat generation due to hydration of cement and strength properties are two important parameters which affect service life of structures. In the early age the temperature in the body of mass concrete is high and tensile strength is low. This special condition may lead to occurrence of thermal cracks. In the present study, concrete specimens with water cement ratio 0.3, were made and 0, 10 and 15 percent Portland cement replaced with silica fume. Temperature rise of the specimens was monitored just after casting in a semi adiabatic box. Temperature rise was recorded for 7 days. Furthermore, compressive strength of the cubic specimens from 1 day after casting to 91 days was measured. The results declared that hydration heat regime is affected by silica fume percent. The mixes with both 10 and 15% silica fume, had peak temperature about 6ºC lower than the specimens without silica fume. Furthermore, peak temperature of the specimens without silica fume occurred 23 hours after casting, while it became about 31 hours for silica fume specimens. The slope of cooling zone of hydration regime in the specimens with 10% silica fume is very mild compare with the others. On the other hand, 10% silica fume enhanced compressive strength more effectively. These results demonstrated that hydration heat and strength development of mass concrete are affected by silica fume content and higher replacement of this pozzolan material may adversely affect service life of structures.

Keywords: silica fume, hydration heat, high strength concrete, strength development

1. INTRODUCTIONS

Strength development of high strength concrete in the body of large mass concrete structures is effectively influenced by temperature rising due to hydration heat. Normally, cement content of high strength concrete is high , therefore temperature in the body of mass structures increase more rapidly and may adversely affect properties of concrete at early or later ages [1]. In addition, the characteristics of heat development such as peak temperature, the time at which peak occur , slope gradient in heating or cooling zone and the remaining time at peak can be responsible for concrete properties in body of large mass concrete[2]. However, nowadays the consulting have no especial considering to a fact that reality of concrete properties in the center of structure is completely different with that named as standard specimens [3].

2. MATERIALS AND TESTING PROGRAM

Crushed stone, with 19 mm maximum nominal size, in two ranges of 5-10 and 10-19 with relative density at saturated surface dry of 2.61 were used. Fineness modulus of sand and relative density were 3.24 and of 2.56 respectively. Absorption value is 3.09 and 2 for fine and coarse aggregate. The cement used was Portland cement Type 2, with a specific gravity of 3.11 and 3750 cm^2/gr surface area. A commercial carboxylic type placticizer, (Gelenium 110M), was used to maintain workability of fresh concrete. Silica fume, made by Semnan Ferro Alley factory, was used at 0%, 5% and 10% (by weight) as partial replacement of cement. The characteristics of silica fume are given in Table 1. Mix proportions of the concrete are given in Table 2. Water-cementitious material *(w/cm)* ratio is 0.3. A pan mixer was used and the mixing procedures are as follows. First, sand and cement were placed and 50% mixing water and half admixture were added and mixed for 1 minute. The remaining water and admixture and coarse aggregate were together added and mixed 2 minutes.

Table 1. Chemical composition of silica fume

Composition	Percent
Al_2O_3	0.5-1.7
SiO_2	85-95
Fe_2O_3	0.4-2
C	0.6-1.5
CaO	2-2.3
MgO	0.1-0.9

Table 2. Mix proportions of the Concrete

	Mixture		
Material	**SF0.D**	**SF10.D**	**SF15.D**
Cement	500	450	425
Water	150	150	150
Fine agg.	845	845	845
Coarse agg.* (5-10 mm)	387	387	387
Coarse agg. (10-19mm)	528	528	528
Micro silica	0	50	75
Super plasticizer	7.5	7.5	7.5
Water/Cementitious material	0.3	0.3	0.3
Slump	150	150	150

*Aggregate in saturated surface dry condition

3. EXPERIMENT RESULTS

3.1. Compressive Strength

Strength development of the concrete mixtures versus age is shown in Figure 1. As it is shown from the early to later ages, compressive strength of the specimens with 10% silica fume is highest compare with two other specimens. However, as silica fume content increased to 15% rate of strength development in the early age was slow but, in the later ages of 28 and 90 days compressive strength of SF15 became higher than SF0. This may be attributed to the fact that in the early age, production of cement hydration, $Ca(OH)_2$, is not enough for activation of 15% silica fume. However, 10% silica fume may be an optimum value for cement replacement in the predetermined water cement ratio.

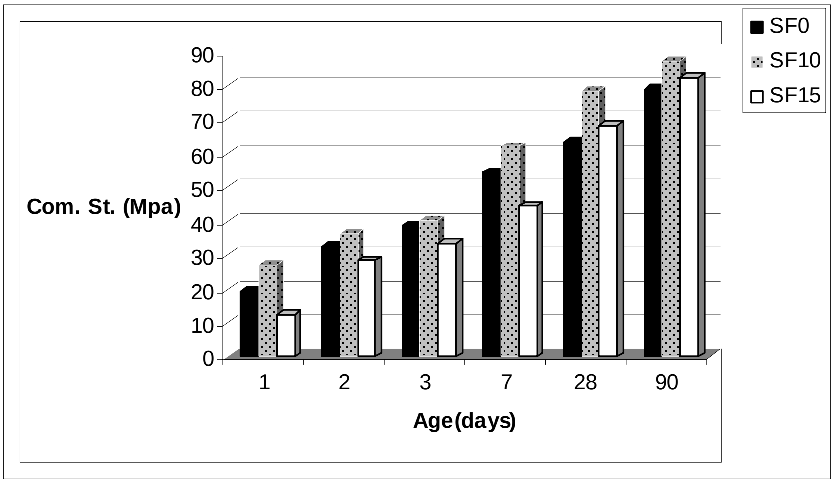

Figure 1. Strength development of the concrete mixtures

3.2. Hydration Heat Development

Temperature rising of the specimens after casting was monitored and is demonstrated in Figure 2. It is shown that regime of hydration heat in silica fume specimens is different compare with the specimens without silica fume. Temperature rising curve during early age hydration can be divided in 4 following pattern:

1: slope of heating zone
2: peak temperature value
3: time of peak temperature
4: cooling zone slope

For the silica fume specimens SF10 and SF15, slope of heat zone decreased compare with SF0. Furthermore peak temperature diminished about 8 to 10°C for 15% and 10% cement replacement. Occurrence of peak temperature postponed for silica fume specimens. An interesting result is that a mild slope is seen in cooling zone for silica fume specimens (Tables 3 and 4). This mild slope is desirable for lower thermal gradient.

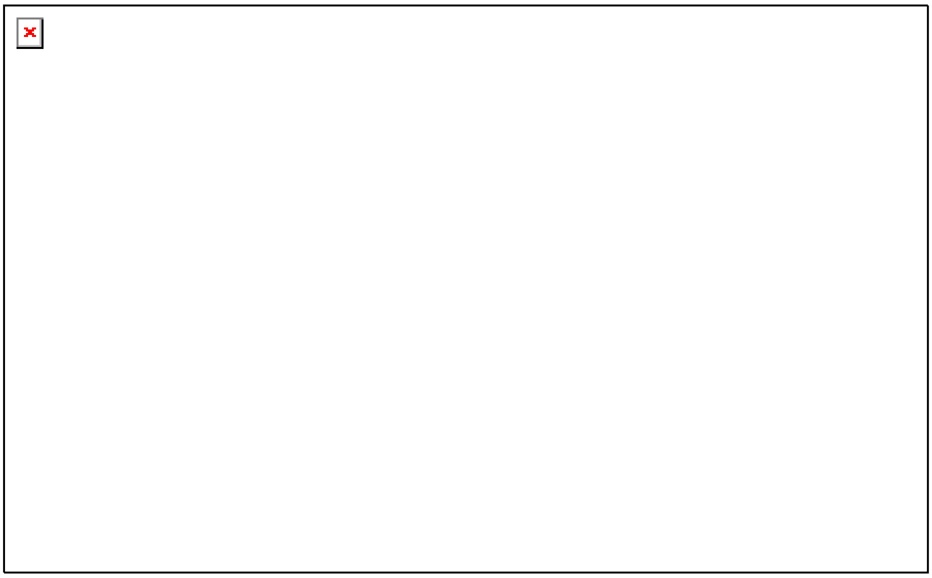

Figure 2. Temperature rising during hydration process

Table 3. Peak temperature, heating and cooling slope of the hydration heat curves

Mixture	Peak temperature. (°C)	95% peak temperature. (°C)	angle of tangent in temperature increasing (degree)	angle of tangent in temperature decreasing (degree)	slope of tangent (G_1)	slope of tangent (G_2)
SF0.D	49.3	46.80	68	38	2.48	0.78
SF10.D	40.0	38.00	58	23	1.60	0.42
SF15.D	40.5	38.50	48	29	1.11	0.55

Table 4: Net peak temperature and time of peak temperature for the mixtures

Mixture	Initial Temperature		Occurrence of Peak Temperature				Maximum net temperature rise. (°C)
	Concrete Temp. (°C)	Ambient Temp. (°C)	Concrete Temp. (°C)	Ambient Temp. (°C)	Time after casting (min)	Time after casting (hr)	
SF0.D	24.2	21.1	49.3	20.5	1374	23	25.1
SF10.D	20.7	19.6	40.0	20.7	1873	31	19.3
SF15.D	19.8	21.0	40.5	19.5	1930	32	20.7

4. CONCLUSIONS

From the present study the following conclusions can be drawn:

- 10% silica fume enhanced compressive strength of the concrete with 0.3 water cement ratio from early to later ages.
- Increasing silica fume content in the specimens did not lead to higher strength.
- Curve of temperature rising versus age was changed as cement was replaced with silica fume as follows:
- Peak temperature decreased about 5°C,
- peak temperature postponed ,
- Slope of heating and cooling zone became mild; this may lead to a desirable low thermal gradient in mass concrete.

REFERENCES

1. Sioulas, B., Sanjayan, J. G., 2000, "*Hydration Temperatures in Large High-Strength Concrete Columns Incorporating Slag*", Cement and Concrete Research, 2000, Vol. 30, pp. 1791-1799.
2. Khan, A. A., Cook, W. D., Mitchell, D., 1995, "*Early age Compressive Stress-Strain Properties of Low-Medium, and High-Strength Concretes*", 1995, ACI Material Journal, November-December 1993, Vol. 92, NO.6, pp.617-624.
3. Cook, W. D., Miao, B., Aitcin, P., Mitchell, D., 1992, "*Thermal Stresses in Large-Strength Concrete Columns*", ACI Material Journal, January-February 1992, Vol. 89, NO.1, pp.61-67.
4. Carlson, R. W., Donald, L. H., Polivka, M., 1979, "Causes *and Control of Cracking in Unreinforced Mass Concrete*", ACI Journal, July 1979, pp. 821-837.

CD01-005

DETERMINATION OF FLEXURAL STRENGTH OF STEEL FIBER REINFORCED CONCRETE WITH DIFFERENT FIBER PERCENTAGE BY MEANS OF 3-POINT BENDING TEST

M. Hajisotude[1], M.Jalal[2], M.M.Raouffard[3]
[1]Assistant professor, Power and Water University of Technology, Tehran, Iran
[2]M.Sc. Student, Dept of civil Engg. School of Engg. Razi University, Kermanshah, Iran
[3]B.Sc. civil engineer, Power and Water University of Technology, Tehran, Iran

ABSTRACT

Nowadays, many buildings and infrastructures are made of concrete and therefore, strength of concrete structural members ensures longer useful life and serviceability of the structure. Beams are one of the most important structural members that must have sufficient load bearing and ductility. Since brittle behavior and low ductility are two noticeable drawbacks of concrete members, they should be reinforced by materials with higher ductility and tensile strength such as steel fibers which can significantly improve these two characteristics of bending members. With this respect, use of industrial steel fiber deposits, percentage of fibers and optimized amount of fibers are critical factors which affect the flexural strength of beams and cost-effectiveness of the projects.

In this paper, experimental results of 3-point bending tests carried out on fiber reinforced concrete beams with different percentage of fibers are presented and compared and also its cost-effectiveness has been considered.

Keywords: concrete, steel fiber deposits, beam, ductility, flexural strength

1. INTRODUCTION

Applications of fiber reinforced concrete have been explained in different literature among which Keivani has mentioned the following items:

Floors cover:

It has been proved that using fibers can reduce the thickness of slabs and covers up to 1.2 times. With this respect, McCarran airport in Las Vegas in 1976 for airplane parking lot surface as wide as 52700m^2 was covered by steel fiber reinforced concrete of 15 cm thickness, while the required thickness was estimated as 37.5cm.

Rehabilitation of dams and hydraulic facilities:

In this application, the concrete resistance against impact and abrasion and cavitation is considered. According to ICOLD report, in order to prevent erosion and deterioration of stilling basins of Mayfield and Alder dams and also spillway of Little Goosc dam, fiber reinforced concrete as 38 to 45cm thick was used for cavitation prevention.

Instable slopes and trenches covering with sprayed concrete:

A kind of this application was used in a refinery in Sweden in an area of 4500m^2.

Explosion and impact resistant structures:
In such cases, the foundations of heavy machinery are of interest to be made of fiber reinforced concrete. With this regard, impact and crack resistance properties of concrete are outstanding.
Concerning flexural strength, studies have shown that fiber reinforced concrete behavior is significantly affected by shape, length to thickness ratio and material of fibers. The fibers can also be prepared from factories or from two resources such as industrial deposits each of which has significances and drawbacks. The common result is that in both cases, the flexural strength of concrete would be improved effectively. In this study, since the economic aspect of the projects was to be taken in to account as an important factor, effect of steel fibers from industrial deposits was investigated in concrete.

2. FLEXURAL TEST (PRISMATIC BEAM WITH THREE-POINT LOADING)

Since based on the studies done before, the most significant effect of steel fibers in concrete has been turned out to be ductility and energy absorption improvement especially in flexural behavior, this part of the research was of great importance. Because the previous studies were based on different standards (Keivani, based on Japan standard and most of other literature based on ASTM), referring to the standards was inevitable.
In this study, in order to maintain the best comparability and recurrence of the tests, direct reference to ASTM was necessary. The results of the tests performed will be presented in the following. All of the tests carried out were corresponding to ASTM C 1018 94b.

2.1. Specimens Preparation

The moulds used were of dimensions 10×10×50cm. at the first step, the moulds were cleaned and greased. The concrete ingredients was prepared according to determined mix design and mixed in the mixer and in order to make specimens with different percent of fibers, in each step, specified percentage of fibers was added to the mixture. after placing the concrete in the mould, vibration was applied to the moulds for a while so that enough compaction of concrete is reached. As a result of presence of fibers in the concrete, fiber reinforced specimens need more vibration time compared to plain concrete specimen to cause the air come out of the concrete. On the other hand, more vibration time causes segregation and bleeding. So, desirable duration of vibration was gradually obtained by some vibration trials.
The moulds were opened after 48 hours and specimens were kept in water basin (Figure 1) for 28 days in the laboratory conditions so that full curing was maintained. During this period, the temperature of about $20^{\circ C}$ and curing conditions were tried to be kept constant.

Figure 1. specimens in water basin in laboratory temperature.

2.2. Test Apparatus

The conditions of test apparatus should be prepared according to ASTM C 1018. The apparatus used is illustrated in Figure 2. it is a kind of STRASSEN TEST, model 205. its final load capacity is 100kN.

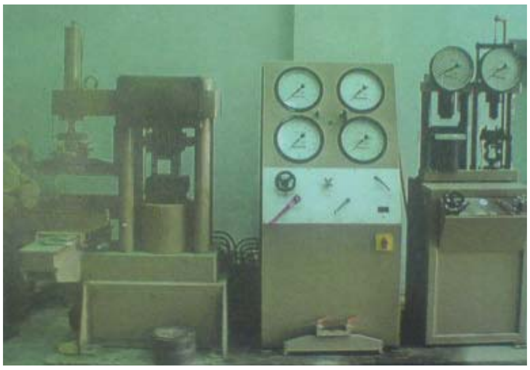

Figure 2. Loading apparatus and measurement gauges

In order that the apparatus thoroughly meet the ASTM C 1018 provisions, some tools were installed. As shown in Figure 3, adjustable supports for load applicator of 30cm distance from the bottom were adjusted.

The load was applied by upper jaw in the middle of the span. The specimens were placed on the supports in order that 10cm of two ends of each specimen locate out of the supports edges. (Standard suggests span of at least 350mm but, loading span should be three times as the cross section dimensions i.e. 300mm).

Displacements were measured and recorded at three points (two support points and at the middle of span).the displacement was calculated by subtracting the average displacement measured at two supports from displacement in the middle of the span.

After some tests, it was observed that the displacements in the supports after the first contact were nearly negligible and could be taken equal to zero. Loading was applied at the minimum rate (about 0.04 mm/min).

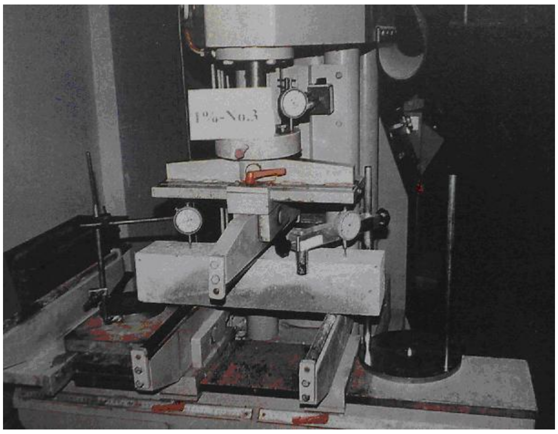

Figure 3. Test apparatus with installed tools for three-point loading

2.3. Tests

After preparation of the specimens for test implementation as mentioned above, three-point loading was applied by the apparatus with instrumentations shown in Figure 3. The measurements were repeated at appropriate time increments and for displacement of 0.02mm. During the test, regular reading of displacement and force gauges and also minimum rate of loading were maintained.

In most of the specimens, large displacements and failure occurred rapidly after formation of the first crack (Figure 4). It would make the measurement a little difficult especially at the time near to the critical point.

Before implementation of the tests, the weights of the specimens were determined and dimensions were carefully measured. The average of parallel dimensions was selected as the dimension of prismatic beam base. The lengths of the specimens were also measured. After start of loading, measurements were recorded at each 0.02mm displacement. Failure was finally completed by splitting of the specimen (Figure 4).

At the failure time of the specimens containing 0 to 3% of fibers, it was observed that two parts of the specimen were completely separated. But concerning the specimens containing 5% of fibers, the connection and bonding between two parts of the specimen was still maintained. Visual inspection of specimens after failure (Figure 5) showed that regarding the fibers, most of them did not fail due to lack of tensile strength but as a result of low bonding between concrete and fibers, they were pulled out of the concrete.

From one hand according to ASTM, the ratio of fiber length to the smallest dimension of the mould is limited and On the other hand, the ratio of length to thickness of fibers is of great importance. With this respect, the more the length of fibers, the better bonding and involvement between fibers and concrete, and tensile failure of fibers is more probable. But long fibers can not be mixed easily in the concrete and especially their distribution in the mould would not be uniform. It can affect the results of flexural tests.

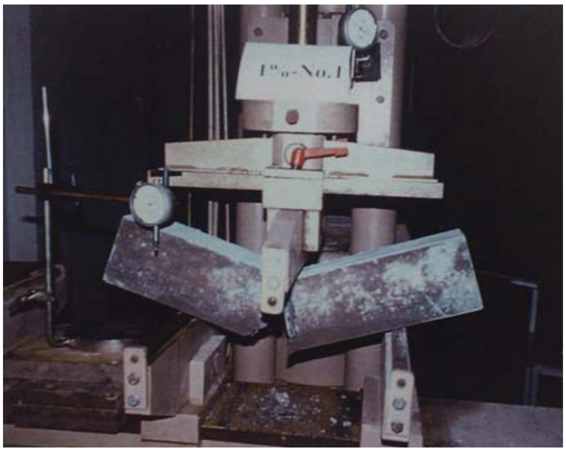

Figure 4. Failure mode of prismatic specimens

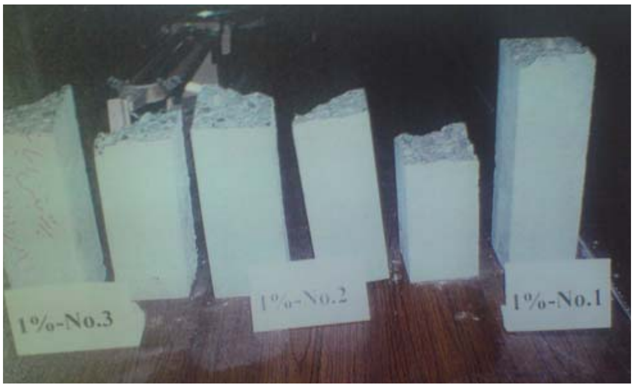

Figure 5. prismatic specimens with 1% of fibers

Figure 6. prismatic specimens after failure

According to this limitation, length of 2.5-3 cm was chosen for fibers. Considering the cross section dimensions of the mould (10*10), this length could cause a little nonuniformity especially in low percentage of fibers. But in higher percentages, visual inspection of cross section revealed uniform distribution of fibers in the specimen cross section (Figure 6).

Figure 7. specimens with 5% of fibers after failure

Figure 7 shows the specimens with 5% of fibers after failure. It is illustrative that despite of full failure for the three specimens, the bonding between two parts of the specimens has yet been maintained via the fibers. If distribution of fibers in the failure location is considered, it will seem desirably uniform. Figures.8 and 9 show illustrative views of fibers distribution in failure surface of the specimens. In short, these observations show that the fibers have been pulled out of concrete and did not split due to excessive tensile stress. Also appropriate distribution of fibers can obviously be seen in the Figures. At the end corner of specimen (where bonding is yet present), it can be considered that the connection and bonding is conserved via just a few number of fibers and in spite of complete failure of concrete, the strength and bonding of the remained fibers is sufficient to carry the weight of specimen (Figure 7). These observations may be actually efficient in selection of length, thickness and particularly shape of fibers.

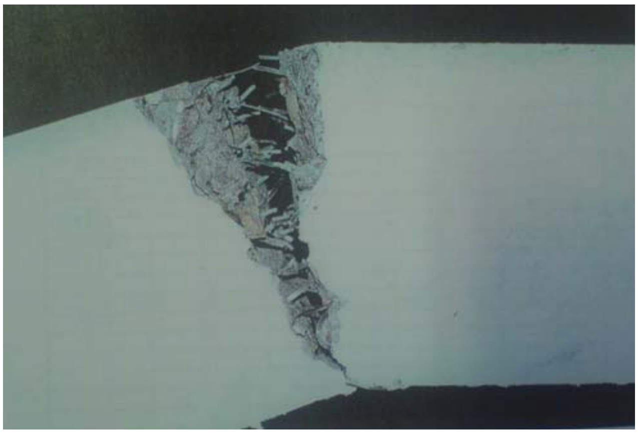

Figure 8. horizontal view of the failed specimen with 5% of fibers

2.4. Results and Discussion

After implementation of each test, the displacements in the middle of the span (mm) with respect to the corresponding force (kN) prepared in a table. Table.1 is an example of such tables. In the first column of the table, the values recorded at the time of test are presented. Displacement values for each 0.02mm are presented for which the corresponding forces are also presented in the next column. Such tables were prepared for all of the tests.

Table 1: values of force-deflection for specimen with 5% of fibers

primary values		final values for curve plotting	
Deflection (mm)	**Force (kN)**	**Deflection (mm)**	**Force (kN)**
0	0	0	0
0.02	0.2	0.13	3.4
0.04	0.4	0.15	3.8
0.06	0.8	0.17	4.2
0.08	1	0.19	4.7
0.1	1.2	0.21	5.1
0.12	1.2	0.23	5.7
0.14	1.4	0.25	6
0.16	1.6	0.27	6.6
0.18	1.8	0.29	7.2
0.2	2	0.31	7.6
0.22	2.2	0.33	8.2
0.24	2.4	0.35	8.4
0.26	2.8	0.37	9
0.28	3.1	0.39	9.4
0.3	3.4	0.41	10
0.32	3.8	0.43	10.5
0.34	4.2	0.45	10.9
0.36	4.7	0.47	11.6
0.38	5.1	0.49	12.2
0.4	5.7	0.51	12.6
0.42	6	0.53	13.1
0.44	6.6	0.55	13.5
0.46	7.2	0.57	14
0.48	7.6	0.59	5
0.5	8.2	0.61	5
0.52	8.4	0.63	5
0.54	9	0.65	5
0.56	9.4		
0.58	10.5		
0.6	10.9		
0.62	11.6		
0.64	12.2		
0.66	12.6		
0.68	13.1		
0.7	13.5		
0.72	14		
0.74	5		
0.76	5		
0.78	5		
0.8	5		
0.82	5		

Figure 9. Vertical view of the failed specimen with 5% of fibers

In all of the tests, displacements increased and recorded as nearly small amounts and approximately proportional to the forces before the maximum strength point. it should be noticed that each reading step included three displacement readings and one force reading. Displacements were measured at the supports and at the middle of the span and absolute amount of displacements at the middle of the span were calculated relative to the supports displacement. In practice, it was observed that displacement values at the supports were stopped after start of the tests. Also the displacement values need to be corrected at the beginning of the test as follows.

At the beginning of the test, loading jaw can not thoroughly be attached on the specimen surface. This is due to the fact that if it is attached, some bending may be created in the specimen before the displacement gauge is adjusted to zero. However, it should be noticed that specimens without smooth surfaces produce even more errors in measurements which can be removed by ignoring the earlier part of the displacements (strains).

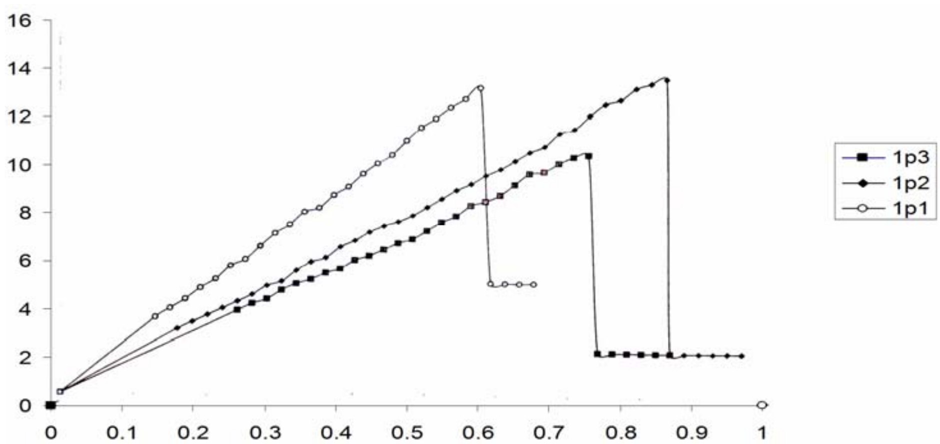

Figure 10. load-deflection curves of three specimens with 1% of fibers

Table 2: characteristics of prismatic specimens

specimen characteristics	fiber percent	length	cross section	weight	density	ave. density	ultimate strength	ave. ultimate strength	ultimate deflection	ave. ultimate deflection	first crack strength	ave. first crack strength
No.	weight percent	mm	mm²	gr	gr/cm³	gr/cm³	kN	kN	mm	mm	kN	kN
1	0	500					6.4		0.49		6.2	
2	0	500	10330.6	11701	2.27	2.34	11.8	7.8	0.41	0.44	11.5	7.57
3	0	500	10449	12645	2.42		5.2		0.42		5	
1	1	500	10149	11861	2.34		14		0.57		13.5	
2	1	500	10449.8	12645	2.42	2.38	14.4	13.13	0.82	0.7	14.2	12.87
3	1	500	10223.7	12201	2.39		11		0.72		10.9	
1	2	500	10214.6	11698	2.29		12.8		0.37		12.4	
2	2	500	10358.1			2.29	11	12	0.52	0.48	10.4	11.6
3	2	500	9832.44	11275	2.29		12.2		0.55		12	
1	3	500	10282.9	12643	2.46		13.1		1.01		13	
2	3	500	10220.9	12464	2.44	2.44	13.6	13.23	0.83	0.86	13.2	12.93
3	3	500	10070	12140	2.41		13		0.74		12.6	
1	5	500	10256.5	12440	2.43		13.3		0.77		13.1	
2	5	500	10140.5	12424	2.45	2.43	13	13.5	0.82	0.82	12.8	13.3
3	5	500	10320	12464	2.42		14.2		0.87		14	

In order to remove the errors, the values in the first two columns were used to plot the force versus preliminary deflections and after determination of the earlier linear part of the test results curve and its extension to displacement axis, the amount of primary displacement of loading determined and removed from the results.

Values of applied load and the corrected displacements were prepared in the next two columns of the Table.

The tables prepared in such a way after plotting the preliminary curve and

correcting the primary readings, were used to plot the final load-deflection curve.
Load-deflection curve of three specimens with equal percentage of fibers were plotted together for comparison. For example Figure 10 shows load-deflection curves of three specimens with 1% of fibers.
From the tables and curves prepared and corrected, all of the critical information has been obtained and presented in Table 2.
Table 2 presents all of the specimens characteristics in different tests. Specimens number and fibers percentage are presented in the first and second columns, respectively. Cross section area and weight of the specimens are given in next three columns. It can be concluded from the table that the more the fibers in the concrete, the lower the slump would be.

3. CONCLUSION

Considering the curves obtained from various tests, the following results can be concluded:

- The results of tests implemented on specimens with equal percent of fibers are in good agreement so as the average of three tests can be taken as the representative of that fiber percentage.
- Although the first correction may cause a little difference in the tests results but, first contact error and support corrections are much more effective than the remained error.
- Deformation is very slow until near point to the failure but after appearance of the first crack, it increases and with a sudden large deformation, specimen fails and the force decreases.
- Final flexural strength of steel fiber reinforced concrete in the beam test with three-point loading increases significantly. For example in 3% of fibers, the strength increase up to 70%
- Amount of maximum deflection increases by increase of fibers percent and in 3% of fibers, it approaches 95%.

REFERENCES

1. Concrete and Aggregates. 1988. Annual Book of ASTM Standards, Part 04.02, ASTM. Philadelphia, PA, 751 pp.
2. Concrete International; “state of art report on fiber reinforced concrete” reported by ACI committee 544, ACI Journal nov.1973- copyright by concrete international / may 1982.
3. ACI Committee 440. 1996. *State-of-the-Art Report on Fiber Reinforced Plastic (FRY) for Concrete Structures (ACI 440R)*, ACI Manual of Concrete Practice, Part 5, American Concrete Institute, Detroit. Ml, 68 pp.
4. ACI Committee 544. 1982. *State-of-the-Art Report on Fiber Reinforced Concrete (AC’I 544. IR-82i.* Concrete International. May. Vol. 4, No. 5, pp. 9-30.
5. Hasani.A. 2000. Effect of steel fibers in controlling of tensile cracks in concrete, building research center.
6. Keivani.A.1992. principles and technology of still fiber reinforced concrete, Rudaki publication.

CD01-006

A STUDY ON BONDING STRENGTH OF POLYMERIC FIBERS TO CEMENTITIOUS MATRIX

H.R. Pakravan[1], M. Jamshidi[2], M. Latifi[3]
[1]M.Sc. student, Textile Engineering Department, Amirkabir University, Tehran, Iran
[2]Assistant Professor, Concrete Department, Building and Housing Research Center (BHRC), Tehran, Iran
[3]Professor, Textile Engineering Department ATMT Research & Excellence (CENMIT) Centers, Amirkabir University, Tehran, Iran

ABSTRACT

Cementitious materials are brittle in nature. Due to this behavior, short, randomly and distributed fibers are mostly being used to reinforce cementitious materials. Added fibers enhance tensile strength and flexural toughness and reduce crack creation and propagation in cement matrix. The major effect of fibers is to act as bridging at crack tips to resist crack propagation. Fiber bonding to cement paste is an important factor that affects performance of the fiber reinforced cementitious composite (FRCC). Bonding energy (adhesion) between these materials is composed of interfacial interactions (chemical bonding) and mechanical interactions (interlocking). The adhesion of fiber to cementitious materials can be evaluated by pull-out test. This test is the newest method and one of the most commonly used practical methods to evaluate performance of fibers in FRCCs.

This article presents the bonding strength results of commercial polymeric fibers to cement matrix. To investigate adhesion of polypropylene (PP), nylon66 (N66) and acrylic (PAN) fibers to cement matrix a single fiber pull-out test setup is designed and fabricated. The specimens were prepared at the water-cement ratio of 0.4 and they were tested at 7, 14 and 28 days of curing. Fiber's surface after pull-out test was also studied by microscopic analysis. Some interesting results were obtained from the pull-out test of different fibers. On the basis of results, it was found that fiber should be selected for FRCC reinforcement due to their mechanical interactions and physical/chemical/mechanical behavior in cement matrix instead of their chemical interactions.

Keywords: adhesion, pull-out test, interfacial interactions, polymeric fibers

1. INTRODUCTION

The application of fibers to reinforce cementitious materials is an ancient subject. At first, asbestos fibers were used in industrial process to produce fiber reinforced cement sheets. Because of their great fiber strength and durability, high physical and chemical resistance, none-combustibility and resistance to weathering attack and cost effectiveness, they were used as building material during the last century with various forms and styles to suit different needs. Despite of these properties, they can cause a major health hazard to human's safety [1]. Hereafter, various types of synthetic fibers were produced and used as asbestos substitutes.

The performance of FRCC depends on many factors, such as fiber material properties (fiber strength, stiffness, and Poisson's ratio), fiber geometry (fiber surface and cross section), fiber volume content, matrix properties (matrix strength, stiffness, Poisson's ratio), and interface properties (adhesion, frictional and mechanical bond) [2].

Bonding depends on the structure of the fiber-matrix interface. Fiber bonding to the cementitious matrix is an important and effective parameter on fiber reinforced cement composites. Also, the performance of fiber reinforced composites is strongly related to the debonding/pull-out behavior of the fibers. For this purpose, the relationship between the pull-out load and the displacement of a fiber, when it is pulled out from the cement matrix, serves as an important parameter in the design of cement composite materials.

Many researchers have been done on the evaluation of bonding between fibers and cement matrix [3-5, and 6]. Some methods and equipments were adapted for pull-out test to evaluate fiber/cement bond strength in the present work.

Fiber pull-out behavior contributes to the energy absorption ability of fibers in FRCCs. Fiber to cement bonding allows stress transfer between them. Regarding to the importance of this behavior in composite materials, fiber/cement interface has been studied in this research.

The aim of the present work is to characterize the bonding mechanisms of polymeric fibers to cement matrices. To determine the bond strengths of polymeric fibers to cement matrix, pull-out test was employed. The test setup was basically similar to the numerous techniques that have been developed by previous researchers. Besides the testing setup, it is also important to understand the way that pull-out specimens are prepared. A new technique for preparing specimens for pull-out test was suggested in this work. Fiber pull-out specimens were prepared with single filaments of PP, N66 and PAN fibers. The surface of the used fibers after pull-out test was evaluated by optical microscope (OM). The effect of fiber types on the pull-out results of fiber/cement matrix at different ages of curing was also studied.

2. MATERIALS AND EXPERIMENTS

Cement used in this study was ordinary Portland cement type II. The type of used synthetic fibers and their properties are given in Table 1. Figures. 1-3 show the optical microscopic images of the longitudinal and cross-sectional surface of the fibers.

Table 1: Properties of fibers

Fiber type	Diameter (μm)	Density (gram/cm^3)	Tensile strength (MPa)
PP	25	0.91	326
N66	26	1.14	1122
PAN	40	1.19	344

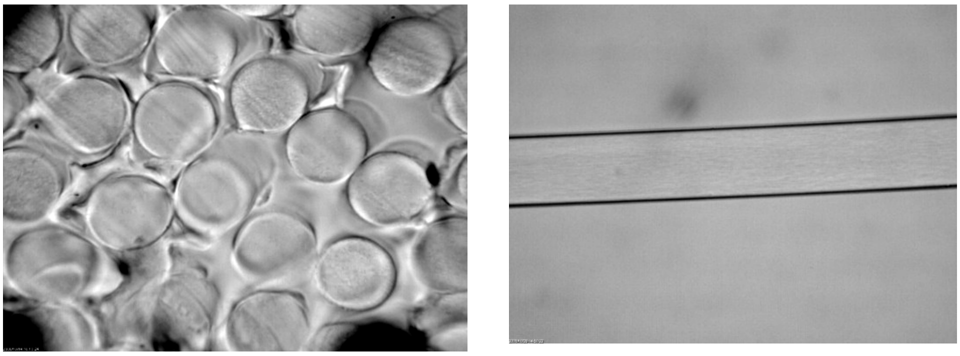

(a) (b)

Figure 1. Microscopic images of N66 fibers: a) Cross-sectional, b) Longitudinal view of fiber surface

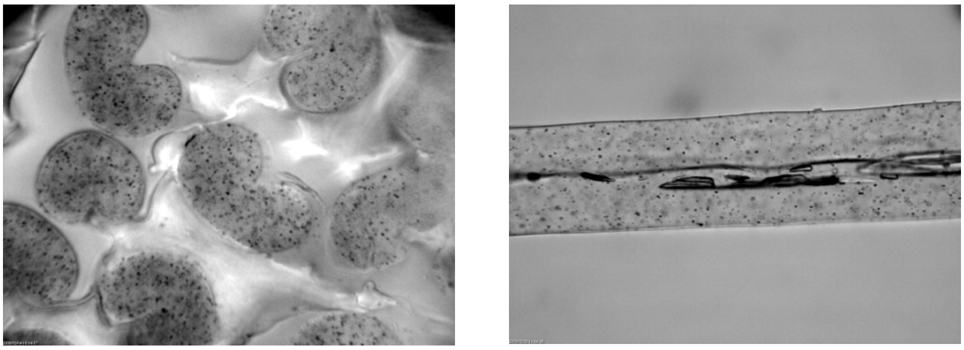

(a) (b)

Figure 1. Microscopic images of PAN fibers:a) Cross-sectional, b) Longitudinal view of fiber surface

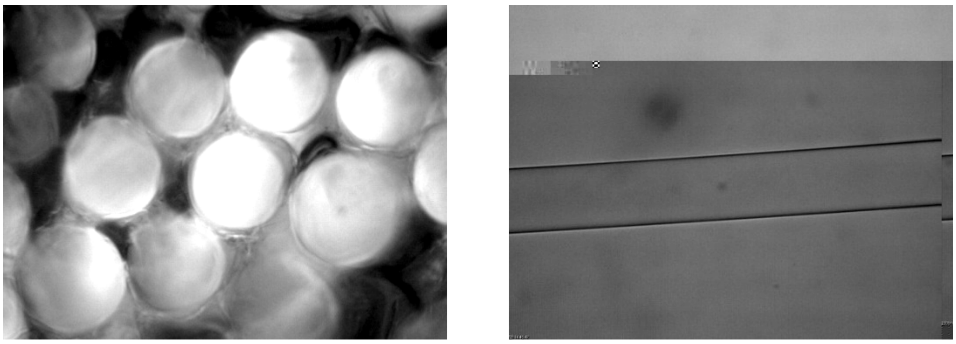

(a) (b)

Figure 1. Microscopic images of PP fibers: a) Cross-sectional, b) Longitudinal view of fiber surface

2.1. Specimen Preparation

Specimens for pull-out test were prepared by the equipment that has been designed and made for this research, as shown in Figure 4. The specimens were prepared with a matrix made by 0.5 of water to cement ratio. After demolding, specimens were subjected to cure in the condition of 23 ± 2°C and 100 ± 5% of relative humidity. Pull-out tests were carried out on specimens after 7, 14 and 28 days of curing. The embedded length for all series was 10mm long. Figure 5 shows the pull-out specimen before test.

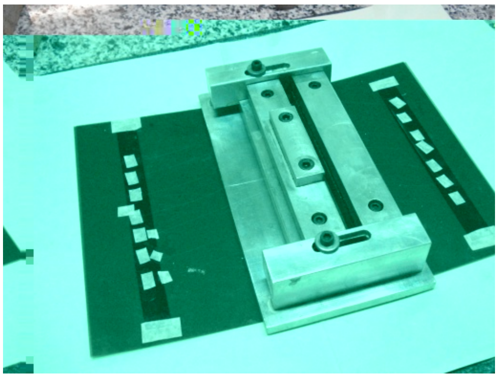

Figure 4. The equipment of pull-out sample preparation.

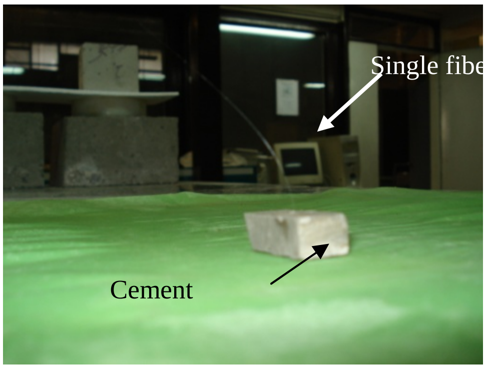

Figure 5. pull-out specimen after cutting

2.2. Pull-Out Test

To investigate the bonding characteristics, single fiber pull-out test was performed. The pull-out tests were carried out by an Instron testing machine (Tinius olsen) at the crosshead rate of 0.02 mm/s as shown if Figure 6. The schematic representation of the test set-up can be seen in Figure 7. The free length of single fiber was 10mm. Load–displacement data of pull-out process were obtained and plotted by computer.

Figure 6. single fiber pull-out test setup system

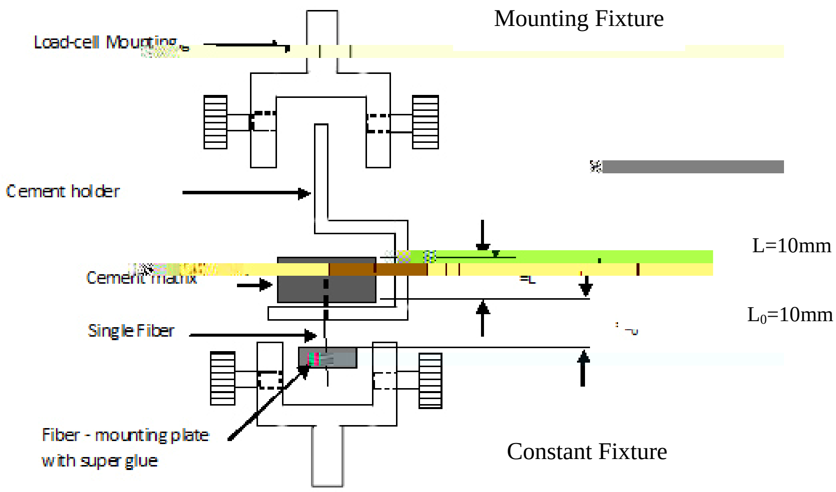

Figure 7. Schematic setup of single fiber pull-out test.

3. RESULTS AND DISCUSSION

3.1. Pull-Out Test Results

The pull-out behaviors of all series are illustrated by the load-extension curves in Figures. 8-10. In all series, it was observed that pull-out force is increased by increasing in fiber displacement to a maximum force. Thereafter, it decreases to zero level because of fiber slippage, pulling out or failure.

The analysis of N66 fibers load-displacement curves shows that there is no significant difference between pull-out load at 7 and 14 days. It can be said that the cement microstructure is not significantly changed during curing period from 7 to 14 days. The bonding strength in 28 days is remarkably higher than 7 and 14 days.

After complete debonding of specimens, N66 fiber begins to slip-out, so pull-out force is decreased.

Increasing the cement curing age of specimens containing PP fiber from 7 to 28 has a positive effect on pull-out load, as shown in Figure 9. Pull-out curves for PP specimens demonstrate that there is no significant difference between 7 and 14 days specimens. Pull-out curve at 28 days indicates that mechanical bonding between PP fiber and cement matrix is maximum. The pull-out curves show that the fiber/matrix bond strength gets close to fiber tensile strength.

In case of PAN fibers, increasing in curing period from 7 to 14 days has no significant effect on pull-out load. At 28 days of curing time, fiber failure happens during pull-out process because of higher bonding strength to cement matrix, as shown in Figure 10.

In all series, increasing curing ages from 7 to 28 days, improves bonding strength. In general, improvement in cement hydration results in decreasing of the porosity of hardened paste. The cement maturity has direct effects on the fiber/matrix bond properties.

In the transition zone more nucleation sites and open space are available in the around of the fiber surface. Based on this microstructure, CH layer in contact with the fibers grows much faster than the cement bulk. As reported by Chan [7], the transition zone is considerably weaker than the cement bulk due to large CH crystals and higher porosity. In other word, longer cement age and consequently the increase of hydration degree results in a decrease in the porosity and finally stronger fiber/cement interface.

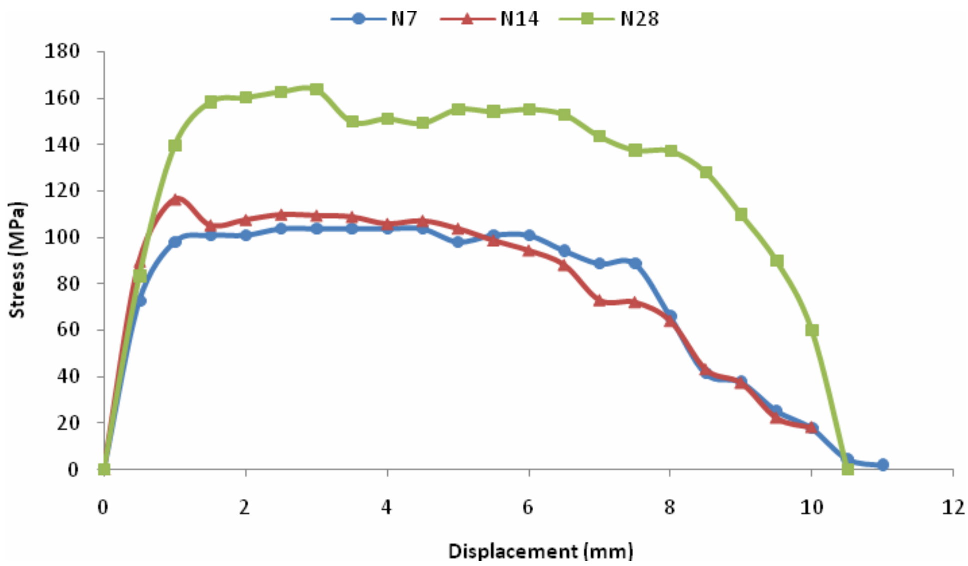

Figure 8. Pull-out behavior of N66 fiber at different cement ages

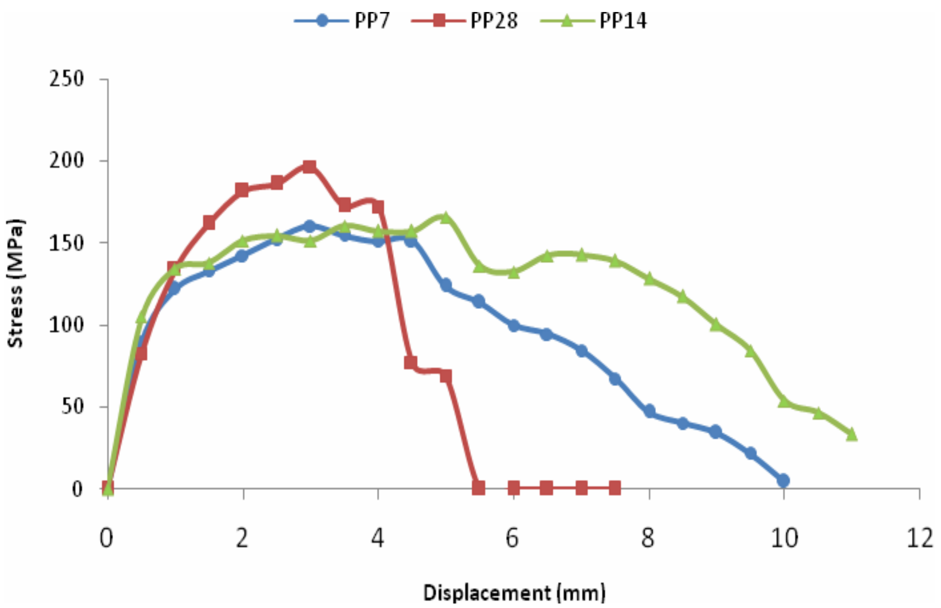

Figure 9. Pull-out behavior of PP fiber at different cement ages

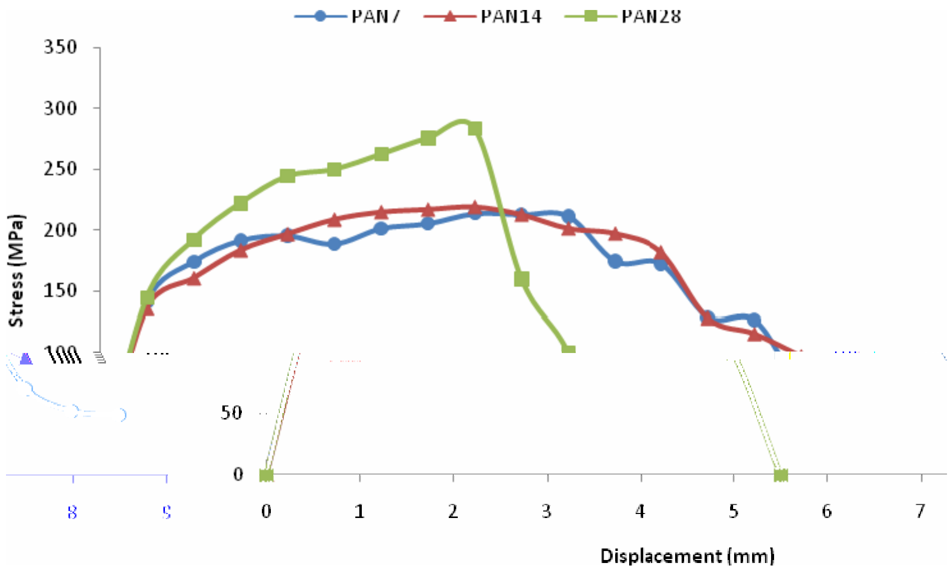

Figure 10. Pull-out behavior of PAN fiber at different cement ages

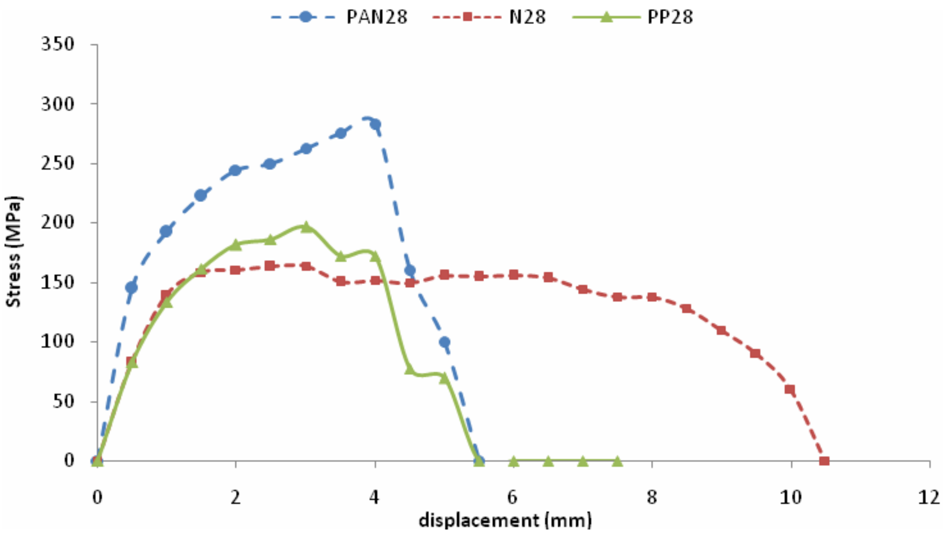

Figure 11. Pull-out curves of tested fiber at 28 days cement curing

Figure 11 shows pull-out curves of different fibers at 28 days of curing. It can be seen that PAN fibers showed higher pull-out strength in comparison to PP and N66 fibers. Figure 12 shows longitudinal image of pulled-out PAN fiber. It is evident that some cement particles are present on fiber surface. Due to the none-round shape of these fibers, during pull-out process, mechanical bonding can be performed because of interlocking effect to cement matrix. The special shape of cross-section indicates higher specific surface than round shape fibers. In other word, PAN fibers have much contacting surface to cement matrix which leads to increasing frictional resistance during pull-out. In the case of other fibers (PP and N66), the smooth surface and round shape of fibers causes less friction. However, in specimens containing PP, due to hydrophobic properties of PP and bleeding of cement paste, water is collected on the surface of the fiber. Therefore, calcium hydroxide (CH) coarse crystals are produced at the PP/cement interface. These crystals are enough big and coarse to deform PP surface. So, during pull-out, PP fibers interlock to these crystals.

3.2. Microscopic Analysis

The surfaces of pulled-out fibers were analyzed using optical microscopy. Figure 12 shows the chemical adhesion between cement bulk and PAN fibers. Due to the affinity between PAN fiber and cement paste which are both hydrophilic, chemical adhesion can be produced. These observations and the image of pulled-out PAN fibers indicate that PAN fibers have both chemical and mechanical bonding to cement paste.

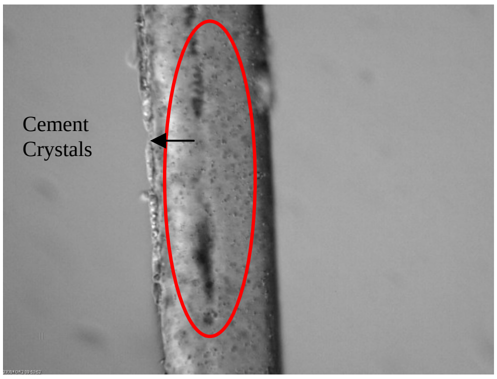

Figure 12. PAN fibers after pull-out process

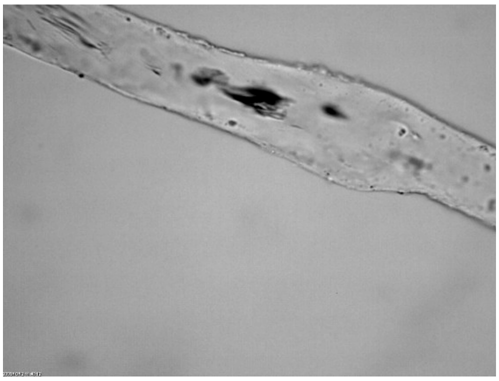

Figure 13. PP fibers after pull-out process

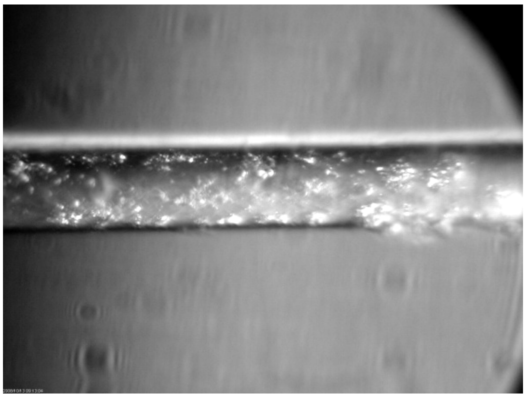

Figure 14. N66 fibers after pull-out process

Study on the pulled-out PP fibers from the cement matrix with optical microscope (OM) reveals the mechanical bonding of PP fiber to cement paste due to fiber deformation and elongation (Figure 13). Deformed points at fiber surface resist to

fiber pull-out and thus, pull-out load are increased. Generally, the force and energy of fiber pull-out are increased with the presence of interlocking points between fibers and cement matrix, but this increase is limited by fiber tensile strength. In general, the friction bonding is changed with fiber deformation at fiber embedded length.
As shown in Figure14, the evaluation of N66 pulled-out fibers shows that cement particles attach to fiber surface. Based on this observation, it's found that N66 fibers have chemical bonding to cement matrix. Microscopic analysis also demonstrates that surface of N66 fibers have not been deformed.

4. DISCUSSION

Regarding to the pull-out behavior of fibers, it is resulted that N66 fiber has lower bonding strength to cement matrix compared to PP fibers. Microscopic analysis demonstrates that PP fiber has no chemical bonding to cement matrix while the presence of cement hydrates particles on the surface of N66 fibers is observed. Based on the observation, it is found that mechanical bonding is more effective than chemical bonding in fiber/cement matrixes.
PAN fibers have both mechanical and chemical bonding to cement matrix, due to their hydrophilic nature and cross section shape. Thus, the bonding strength for this fiber is higher than other studied fibers (Figure 11).
It should be noted that mechanical bonding in fiber/cement interface has an important role to enhance the mechanical performance of cement composite materials.

5. CONCLUSION

- The new pull-out sample preparation method was introduced in this research on the basis of single filament pull-out test.
- Increasing cement curing period from 7 to 28 improved bonding strength for all fibers. In general, the increase in the degree of hydration resulted in the decrease of hardened cement paste porosity.
- The imaging of all fibers surface showed that N66 and PAN fibers had chemical adhesion to cement matrix. The observation of propylene fiber surface confirmed its deformations.
- PAN fibers showed to have better bonding behavior to cement matrix because of mechanical and chemical adhesion. N66 fibers had weaker bonding action with cement paste in comparison to PAN and PP fibers.
- In spite of the lake of chemical adhesion between cement paste and PP fibers, high pull-out force was registered due to the mechanical interlocking.

REFERENCES

1. Pye, A. M., "*A Review of Asbestos Substitute Materials in Industrial APPlications*", Journal of Hazardous Materials, **1979**, Vol. 3, 125-147.
2. Kim, D. j., Naaman, A., El-Tawil E., S., "*Comparative Flexural Behavior of Four Fiber Reinforced Cementitious Composites*", Cement & Concrete Composites, Article in press, **2008**.

3. Peled, A., Zaguri, E., Marom, G., "*Bonding Characteristics of Multifilament Polymer Yarns and Cement Matrices*", Composites: Part A, **2008**, Vol. 39, 930-939.
4. Bentur, A., "*Role of Interfaces in Controlling Durability of Fiber-Reinforced Cements*", Journal of Materials in Civil Engineering, **2000**, Vol.12, No. 1, 21725.
5. Leung, C. K. Y., Ybanez, N., "*Pull-out of Inclined Flexible Fiber in Cementitious Composite*", Journal of Engineering Mechanics, **1997**, Vol. 123, No. 3.
6. Najm, H., Naaman, A.F., Chu, T. J., Robertson, R. E., "*Effects of Poly vinyl alcohol on Fiber Cement Interfaces. Part I: Bond Stress-Slip Response*", Advance Cement Base Materials, **1994,** Vol.1, 115-121.
7. Chan, Y. W., Li, V. C., "*Age Effect on the Characteristics of Fiber/Cement Interfacial Properties*", Journal of Materials Science, **1997**, Vol. 32, 5287-5292.

CD01-007

PREVENTION OF DELETERIOUS ASR BY ASSESSING AGGREGATES AND SPECIFIC CONCRETE MIXTURES

Katrin Seyfarth, Colin Giebson, Jochen Stark
F.A. Finger-Institute for Building Materials Science, Department of Civil Engineering, Bauhaus-University Weimar, Coudraystrasse 11, D-99423, Germany

ABSTRACT
Alkali-silica reaction (ASR) is a major world-wide durability problem and concretes exposed to external alkalis are particularly endangered. In Germany, concrete pavements have a long tradition but the experiences over the last years showed, that the currently standardized test methods are not able to consider externally supplied alkalis from deicers sufficiently. Especially alkali acetate and formate based deicers as used for airfields turned out to be extremely deleterious.
For this reason, an ASR performance-test that was developed at the Finger-Institute (FIB) is used for some years now to assess specific concrete job mixtures regarding their ASR potential under consideration of externally supplied alkalis. The lab-field correlation of this performance-test was assessed by testing two reproduced pavement concretes that showed ASR-distress in the field after 8-12 years in service. It has been shown that the performance-test was able to assess the tested concretes correctly. Contrary, the mortar-bar test could not predict the field performance of the aggregates correctly in all cases.

Keywords: alkali-silica reaction, performance-test, deicer, pavement concrete

1. INTRODUCTION
According to the European standard EN 206-1, sufficient concrete and unit durability is guaranteed when the recommended requirements are met. For the most durability problems ample long-term experience exists and appropriate recommendations are provided. However, ASR occurred with increasing frequency to pavement concretes for highways and airfields in Germany [1, 2, 3] but also in the USA [4, 5] in the past few years despite of following standards and additional recommendations. This shows that the currently standardized ways and test procedures to characterize the reactivity of aggregates and to evaluate the durability of concrete were insufficient to avoid ASR-damage. Especially the deleterious influence of alkali-containing deicers is not well integrated in present ASR-test procedures.
Pavement concretes are one of the most stressed concrete types known. Placing must be done under the given weather conditions, curing is difficult and in central Europe, pavements are exposed to changing temperature and moisture conditions, freeze-thaw cycles as well as deicers. Moreover, permanent dynamic traffic loads create stresses and pre-damages (e.g. micro cracks) that support the progress of

deterioration processes by the ingress of water and deicer. Especially the heavy vehicle traffic plays an important role and increases year by year. All these factors support a possible ASR more or less, depending on how well the concrete mixture is optimized from the very beginning regarding ASR.
A typical ASR-distress on a pavement concrete containing slow/late reacting aggregates occurs after 10-12 years in service. Repair often means complete replacement of the damaged concrete, long before the designed service life of about 30 years is reached. The current situation with increasing numbers of ASR-damages on pavements shows clearly the necessity of an ASR performance-test for pavement concretes that will be exposed to external alkalis.

2. MATERIALS AND METHODS

2.1. Materials

Two damaged German highway pavement concretes were examined by thin section analysis and it was found, that ASR was the main reason for the distress (Figure 1, Figure 2). In concrete 1, the gravel and rhyolite aggregates were affected by ASR. The concrete contained 360 kg/m³ of ordinary portland cement with an Na_2O_{eq} of about 0.95 wt.-% and a w/c of 0.44. The concrete was air-entrained with 4.5-5.0 % air. The damage occurred after 12 years in service. In concrete 2, the used granodiorite aggregates were clearly affected by ASR and first damage occurred after 8 years in service.

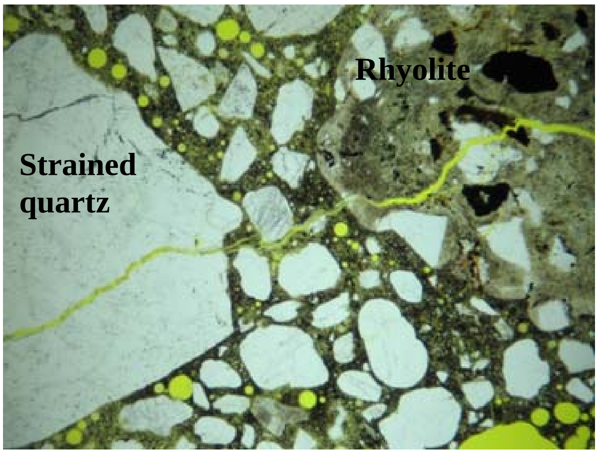

Figure 1. Highway pavement concrete 1, 14 years old, cracks running through aggregate grains, partially filled with ASR gel (Image: Ernst Freyburg, Doreen Erfurt)

The objective was to examine, if the FIB cyclic climate storage as ASR performance-test assesses the ASR potential correctly for these specific concrete mixtures compared to the field experience. Therefore, concrete 1 was reproduced in the laboratory exactly as possible, by using all the coarse and fine aggregates from the original deposits and a comparable portland cement with a Na_2O_{eq} of 0.90 wt.-%. For concrete 2, the granodiorite aggregates from the original deposit were used in a typical mixture that meets all the current requirements for pavement

concretes in Germany [6, 7].
It must be noted of course, that the geological situation in the deposits may have changed more or less over the time, so that the reactivity of the new batches might deviate from the material used 15 years ago. To evaluate this influence, the coarse rhyolite aggregates from the cores of concrete 1 were extracted for a mortar-bar test by means of shock-wave crushing [8]. For concrete 2, the available material was not enough to perform the mortar-bar test.

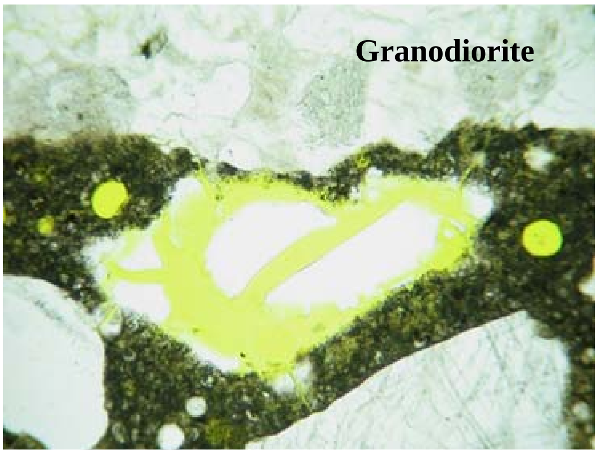

Figure 2. Highway pavement concrete 2, 9 years old, pore with ASR gel next to a granodiorite grain (Image: Ernst Freyburg, Doreen Erfurt)

2.2. Mortar-Bar Test

Prior to the performance-test, new batches from the deposits as well as the extracted coarse rhyolite aggregates from the core of concrete 1 were tested with a mortar-bar test according to the German alkali-guideline [**Error! Bookmark not defined.**]. The aggregate is crushed and sieved to obtain 450 g of the grain size fraction 0.5-1 mm and 1-2 mm respectively. Both grain size fractions are mixed and 450 g of innocuous quartz sand (0.1-0.5 mm) is added. The mortar bars (4×4×16 cm) are prepared according to DIN EN 196-1 using a high-alkali portland cement (Na_2O_{eq} = 1.3±0.1 wt.-%) and a w/c ratio of 0.50. NaOH is added to the mixing water to gain a total Na_2O_{eq} of 2.5 wt.-% in order to boost alkalis and pH. After 1 day curing at 20°C and > 95 % RH, the mortar bars were demolded and initial length and mass were measured. Afterwards, the bars were stored at 70°C above water until the 28th day. The expansion limit for this mortar-bar test is 1.5 mm/m after 28 days.
According to the German alkali-guideline, the tested aggregates are considered as suitable for pavement concretes without any further testing, if they pass the mortar-bar test. If the aggregates fail the test, further testing (e.g. concrete prism test) can be done.

2.3. ASR Performance-Test

Since 2001, an alternating climate test method (cyclic climate storage) is used at the FIB for accelerated simulation of Central European climatic conditions, in order to assess the durability of specific concretes for outdoor structures [9-12].

Both concrete mixtures were prepared without added alkalis (unboosted) and were air-entrained with 4.5-5.0 % air. Concrete prisms (100×100×400 mm) were cast from each mixture with embedded stainless steel studs for the expansion measurements. After 24 hours, the prisms were demolded, wrapped airtight in polyethylene foil and stored for 5 days at 20°C. Subsequently, a flexible foamed rubber tape was glued around the upper edges of the prisms to form a railing that will keep the NaCl solution. At the 7th day after casting, the cyclic climate storage was started. Three prisms of every mixture were applied with the NaCl solution (0.6 mol/l) and three more prisms with distilled water for control (Figure 3). In a special walk-in climate simulation chamber (Feutron, Type 3705/04, Figure 3) the concrete prisms were stored under defined cyclic alternating temperature and moisture conditions. One cycle lasts 21 days and consists of 4 days drying at 60°C (< 10 % RH), 14 days fog at 45°C (100 % RH) and 3 days of freeze-thaw-cycling between +20 and –20°C (Figure 4).

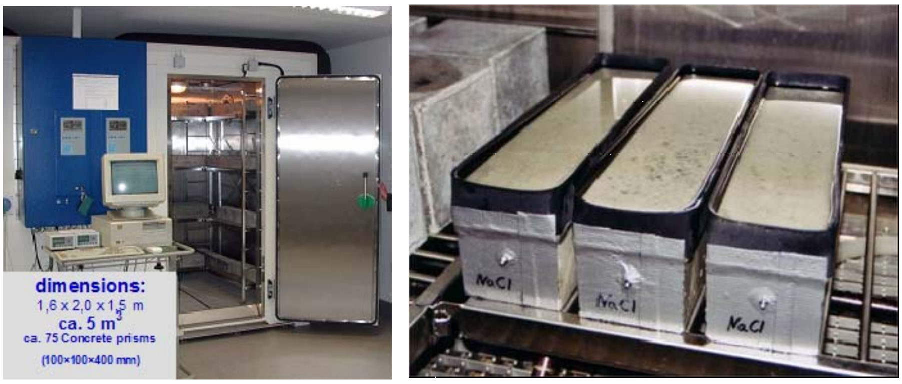

Figure 3. Climate simulation chamber and concrete prisms with NaCl solution (0.6 mol/l)

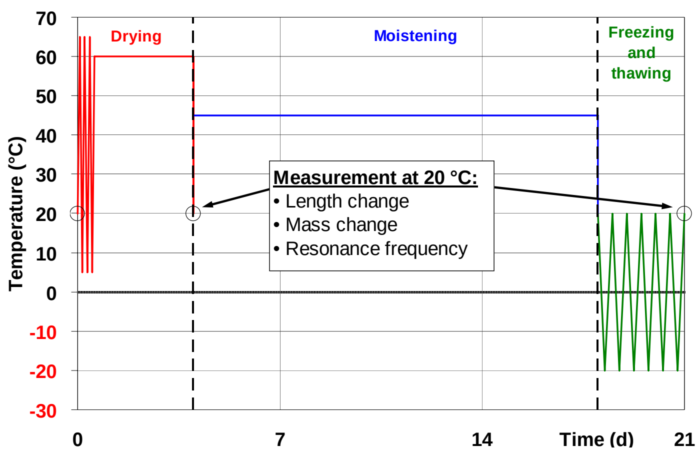

Figure 4. Scheme for one cycle of the cyclic climate storage

At the end of the first drying phase, initial length and weight are measured and 400 g of test solution (deicer or water respectively) is applied on every prism for the first time and remains on the prisms until the end of the cycle. After the cycle is completed, the test solution is removed to measure length change and weight of the prisms and is placed back again when the readings were taken. All measurements are done at 20°C. During the second drying phase, the test solution evaporates completely, leaving behind minor solid residues from the deicer as well as leached substances from the concrete, e.g. alkalis. At the end of the second drying phase new test solution is applied. In this way the cyclic climate storage continued until 9 cycles (7 month) were completed. For pavement concretes exposed to deicers it was found that 8 cycles (6 month) are usually sufficient to assess the potential regarding a deleterious ASR for a typical service life of 20-30 years. The expansion limits after 8 cycles were defined with 0.5 mm/m for application of deicer solutions (higher moisture impact) and with 0.4 mm/m for application of water only.

3. RESULTS

The mortar-bar test results show that the new batches of the rhyolite as well as the extracted rhyolite from the core are clearly reactive. The new batches (8-16 mm, 16-22 mm) show a slightly higher expansion than the original material from the cores. Gravel 2-8 mm and sand 0-2 mm are from the same deposit and are clearly reactive. All the granodiorite aggregates (2-8 mm, 8-16 mm, 16-22 mm) stayed below the limit and are non-reactive (Figure 5).

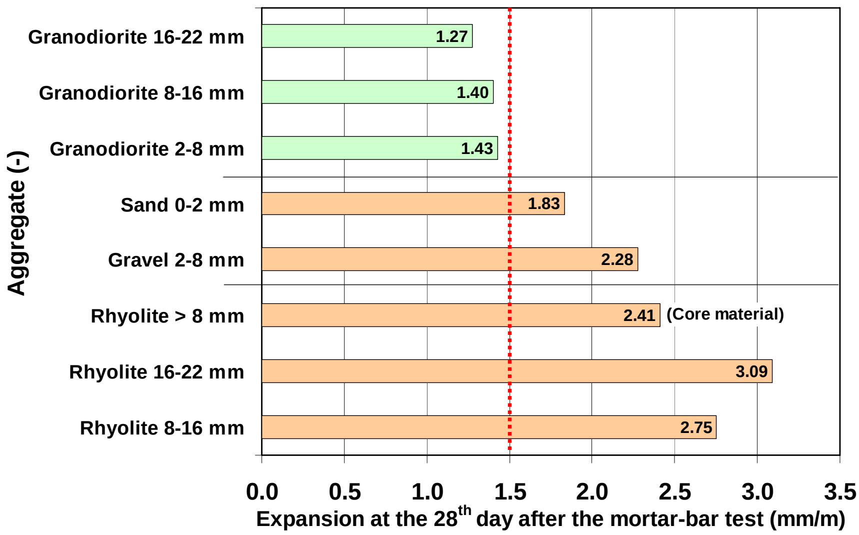

Figure 5. Mortar-bar test results of the used aggregates

For the reproduced concrete 1 with the gravel and the rhyolite, the cyclic climate storage shows that the expansion exceeds the limit of 0.5 mm/m after 7 cycles if exposed to NaCl solution but not if exposed to water only (Figure 6).

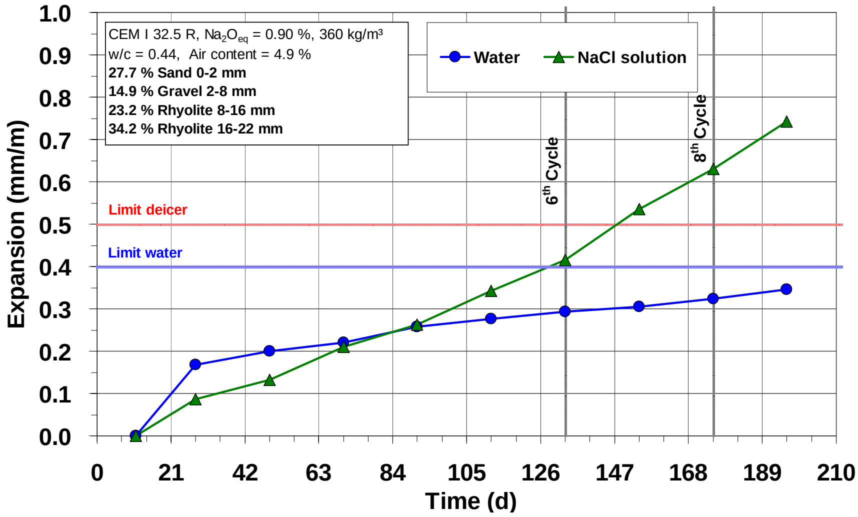

Figure 6. Cyclic climate storage for the reproduced pavement concrete 1

Concrete 2, the typical pavement mixture with the granodiorite aggregates, shows deleterious expansion after 8 cycles if exposed to NaCl solution, but no critical expansion occurred if exposed to water (Figure 7). A subsequent thin section analysis provided clear evidence for an ASR (cracks, ASR-gel), triggered by the granodiorite (Figure 8, Figure 9).

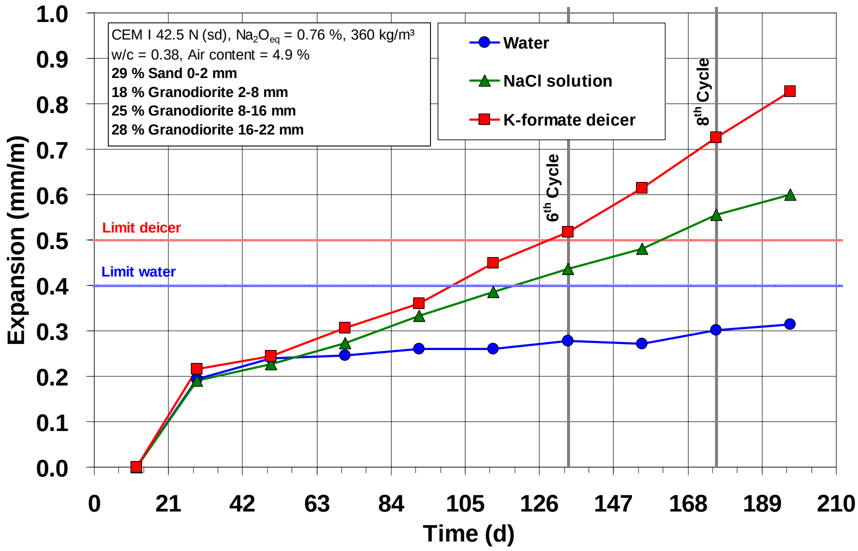

Figure 7. Cyclic climate storage for the pavement concrete 2

If non-reactive aggregates are being used, no deleterious expansion occurs, no matter if alkali-containing deicer solutions or water is applied. As an example, Figure 10 shows the expansion of a pavement concrete with a non-reactive andesite exposed to different deicer solutions.

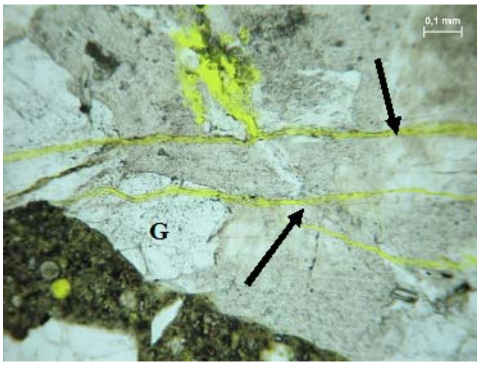

Figure 8. Concrete 2 after the cyclic climate storage, granodiorite grain (G) with micro cracks (Image: Ernst Freyburg, Doreen Erfurt)

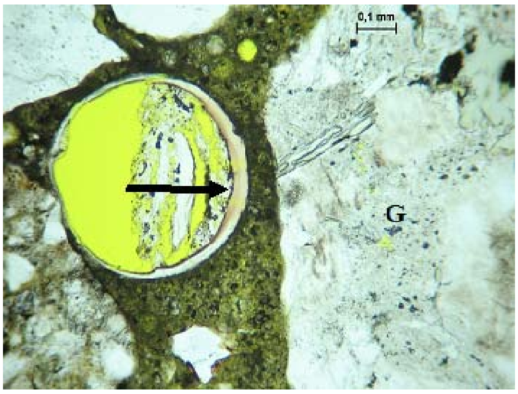

Figure 9. Concrete 2 after the cyclic climate storage, pore with ASR gel next to a granodiorite (G) grain (Image: Ernst Freyburg, Doreen Erfurt)

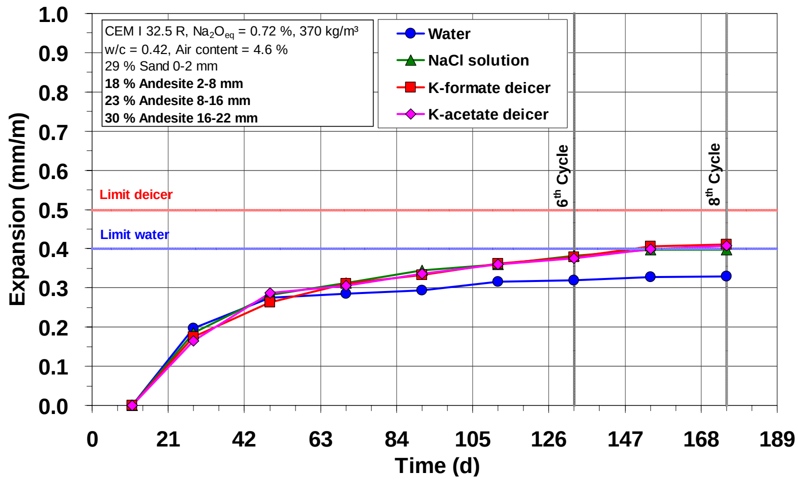

Figure 10. Cyclic climate storage for a pavement concrete with a non-reactive andesite

4. DISCUSSION

Since 2004, more than 130 concretes, mostly job mixtures, with different cements and aggregates were tested with the cyclic climate storage. The objective in this study was to verify, if the ASR potential of two concrete job mixtures can be assessed correctly with the cyclic climate storage compared to field performance, where both concretes showed ASR-distress after 8-12 years in service.

For concrete 1, already the mortar-bar test results showed that the gravel and the rhyolite aggregates are reactive and that the new batches and the material in the cores are comparable. The cyclic climate storage showed correspondingly that after 7 cycles and exposed to NaCl deicer solution a deleterious ASR occurred. This result corresponds well to the field performance, where ASR-distress with that specific concrete mixture occurred after 12 years in service.

For concrete 2, the granodiorite is non-reactive according to the mortar-bar test and a portland cement with $Na_2O_{eq} \leq 0.80$ wt.-% was used. Finally, concrete 2 meets all the requirements of the current regulations for pavement concretes [**Error! Bookmark not defined.**, **Error! Bookmark not defined.**], but deleterious expansion occurred in the cyclic climate storage after 8 cycles exposed to the NaCl deicer solution. Concrete 2 was assessed correctly with the cyclic climate storage compared to field performance, because in the field ASR-distress occurred after 8 years in service. For the original highway concrete with the granodiorite, a portland cement with Na_2O_{eq} of 0.9-1.0 wt.-% was used according to the former regulations ($Na_2O_{eq} \leq 1.0$ wt.-%). But also by following the new regulations for pavement concretes (passed mortar-bar test and $Na_2O_{eq} \leq 0.80$wt.-%), ASR-distress must be expected when using that specific granodiorite. Hence, the mortar-bar test was not able to assess the granodiorite correctly. The mortar-bar test has been available in Germany since 2005 and was introduced in the German alkali-guideline in 2007. Since the mortar-bar test is used for assessing the aggregates for pavements, the risk of ASR should have become lower for pavements build after 2005. But the risk is not eliminated completely, because the mortar-bar test does not asses every aggregate correctly.

It must be noted generally, that the mortar-bar test provides in many cases an acceptable correlation with the performance-test for highway pavement concretes, i.e. under exposure of NaCl deicer solution. But the presented results demonstrate that there are exceptions, as also reported in other studies [13]. The situation is much more serious for airfield pavement concretes, where deicers based on alkali acetates and formates are used instead of NaCl. Concrete 2 (Figure 7) and a concrete with non-reactive andesite aggregates (Figure 10) were also tested with such airfield deicer solutions. Compared to NaCl, this resulted in a much faster and higher expansion for concrete 2 with the supposed non-reactive granodiorite according to the mortar-bar test. Meanwhile, a modified ASTM C 1260 mortar-bar test is recommended from the FAA [**Error! Bookmark not defined.**, 14], which might provide better predictions for airfield concretes as was also found for the tested granodiorite and andesite (Figure 11), but further research is needed with this test.

It was found in a recent study that the solubility of portlandite increases in presence of alkali acetates and formates due to the formation of strong calcium acetate and calcium formate complexes respectively (Figure 12). Thus, more and more OH^- ions will be released gradually which results in an increase of the pH and consequently in an accelerated attack of reactive aggregates [15]. This also means that the mortar-bar test alone is not sufficient to assess the suitability of aggregates for use in airfield concrete pavements, because the mechanism of ASR in presence of alkali acetates and formates is considerably different from the mechanism in presence of NaOH or NaCl. The risk of an underestimation of the aggregate reactivity based on a mortar-bar test is much higher in this case, why a performance-test is highly recommended. Even low-alkali cements are not a reliable countermeasure in this specific case to prevent a deleterious ASR permanently (Figure 13).

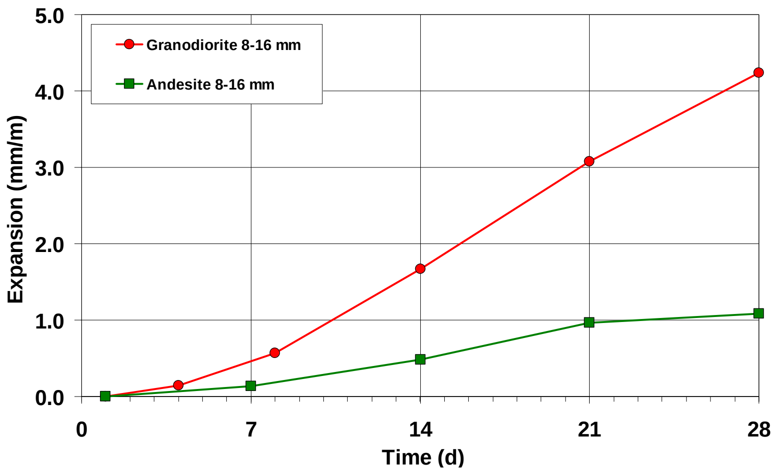

Figure 11. Modified FAA-test, mortar-bars submerged in K-formate deicer solution at 80°C

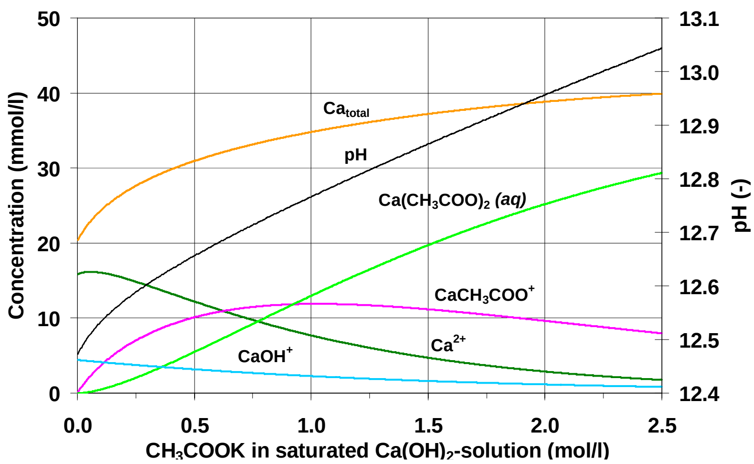

Figure 12. Species distribution in a saturated solution of $Ca(OH)_2$ with addition of CH_3COOK,

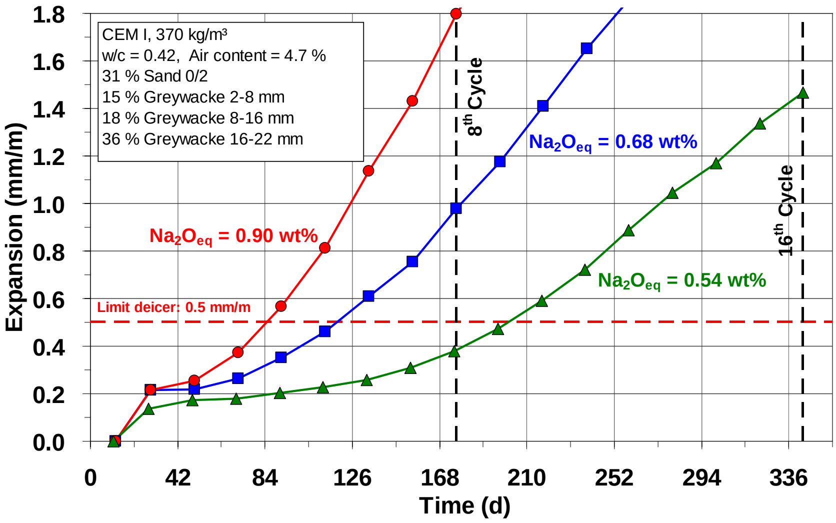

Figure 13. Cyclic climate storage for three tested airfield pavement concretes with a reactive greywacke and different cement Na_2O_{eq} exposed to K-acetate deicer solution

5. CONCLUSIONS

In concrete with reactive aggregates ASR is initiated and accelerated highly, if exposed to alkali-containing deicers. The FIB cyclic climate storage is used as performance-test, considering the influence of external alkalis on ASR. In this study, the cyclic climate storage was compared to field performance. It has been shown that two reproduced highway pavement concretes were assessed correctly regarding their ASR potential. Both concretes and aggregates respectively showed ASR-distress in the field after 8-12 years in service. After 7-8 cycles (5-6 month), the concretes failed the cyclic climate storage if exposed to NaCl deicer solution, in one case despite of following all the current requirements for pavement concretes.

Mortar-bar tests are suitable for a first short-term assessment of the reactivity of aggregates, but some aggregates may be classified incorrectly, especially for the use in concrete pavements. Airfield concrete pavements, exposed to alkali acetate and formate based deicers are particularly endangered. Because of the different mechanism, mortar-bar tests will not be reliable enough in that specific case. Even low-alkali cements are not a reliable method to avoid deleterious ASR if reactive aggregates are used and the concrete will be exposed to alkali-containing deicers, especially based on acetates and formates.

REFERENCES

1. Stark, J. u. a.: Alkali-Kieselsäure-Reaktion. Schriftenreihe des F.A. Finger-Instituts für Baustoffkunde, Bauhaus-Universität Weimar, 2008.
2. Stark, J.; Freyburg, E.; Seyfarth, K.; Giebson, C.: AKR-Prüfverfahren zur Beurteilung von Gesteinskörnungen und projektspezifischen Betonen. beton – Die Fachzeitschrift für Bau+Technik, Verlag Bau+Technik GmbH, Nr. 12/2006 (56. Jahrgang), S. 574-581.
3. Stark, J.; Freyburg, E.; Seyfarth, K.; Giebson, C.: Latest Insights and

Advances in Understanding the ASR and State-Of-The-Art ASR-Test Methods in Germany. International Journal for Restoration of Buildings and Monuments (IJRBM); Aedificatio Verlag GmbH Freiburg, Vol. 12, No. 5/6 (2006), 371-386

4. Rangaraju, P.R., Olek, J.: Potential for acceleration of ASR in the presence of pavement deicing chemicals. IPRF Research Report (2007).
5. Ahlstrom, G.M., Mullarky, J., Faridazar, F.: The United States Federal Highway Administration's efforts to eliminate alkali-silica reaction in concrete transportation structures. In: Broekmans, M.A.T.M. and Wigum, B.J. (editors): Proceedings of the 13th ICAAR, Trondheim, Norway (2008), 454-463.
6. DAfStB-Richtlinie, Vorbeugende Maßnahmen gegen schädigende Alkalireaktion im Beton (Alkali-Richtlinie), Ausgabe 2007-02 (Alkali-Guideline).
7. Bundesministerium für Verkehr, Bau- und Stadtentwicklung: Allgemeines Rundschreiben Straßenbau Nr. 12/2006, Sachgebiet 06.1: Straßenbaustoffe; Anforderungen, Eigenschaften/Sachgebiet 06.2: Straßenbaustoffe; Qualitätssicherung.
8. Linß, E., Müller, A.: Schallimpulszerkleinerung - ein neues Verfahren zur selektiven Zerkleinerung von Beton, Bauhaus-Universität Weimar, Professur Aufbereitung von Baustoffen und Wiederverwertung, 2003.
9. Stark, J., Seyfarth, K.: Assessment of specific pavement concrete mixtures by using an ASR performance-test. In: Broekmans, M.A.T.M. and Wigum, B.J. (editors): Proceedings of the 13th ICAAR, Trondheim, Norway (2008): 320-329.
10. Stark, J., Seyfarth, K., Giebson, C.: Beurteilung der Alkali-Reaktivität von Gesteinskörnungen und AKR-Performance-Prüfung Beton. 16. Internationale Baustofftagung (ibausil), Tagungsbericht Band 2, Weimar (2006): 399-426.
11. Stark, J., Seyfarth, K.: Performance testing method for durability of concrete using climate simulation. Proceedings of the 7th CANMET/ACI International Conference on Durability of Concrete, Montreal, Canada (2006), 305-326.
12. Stark, J., Giebson, C.: Assessing the durability of concrete regarding ASR. Proceedings of the 7th CANMET/ACI International Conference on Durability of Concrete, Montreal, Canada (2006): 225-238.
13. Thomas, M., Fournier, B., Folliard, K., Ideker, J., Shehata, M.: Test methods for evaluating preventive measures for controlling expansion due to alkali-silica reaction in concrete. Cement and Concrete Research 36 (2006), 1842-1856.
14. Federal Aviation Administration (FAA) Engineering News Brief No. 70: Accelerated alkali-silica reactivity in portland cement concrete pavements exposed to runway deicing chemicals. 2005.
15. Stark, J., Giebson, C.: Influence of acetate and formate based deicers on ASR in airfield concrete pavements. In: Broekmans, M.A.T.M. and Wigum, B.J. (editors): Proceedings of the 13th ICAAR, Trondheim, Norway (2008), 686-695.

CD01-008

PERFORMANCE OF NOVEL COVENTRY BINDER AS CEMENT REPLACEMENT

H. Sadeghi Pouya, E. Ganjian
Department of the Built Environment, Faculty of Engineering & Computing, Sir John Laing Building, Coventry University, Coventry, UK

ABSTRACT

Global warming due to emission of green house gasses is one of the main challenges in the twenty first century. The industrial activities have a major impact on global warming due to emission of a large quantity of green house gasses by industries particularly cement manufactures. Production of one ton of Portland cement produce approximately one ton of carbon dioxide. In addition a large quantity of good quality natural limestone is used in production of cement which leads to significant reduction in natural resources. A novel cementitious material (Coventry Binder) was developed at Department of Civil Engineering, Coventry University using 100% industrial wastes (i.e. Basic Oxygen Slag, Plasterboard gypsum waste and cement by pass dust). This paper presents the result of investigation on performance of the novel binder as cement replacement. Paste, mortar and concrete samples were prepared with various proportions of Coventry binder, Portland cement and run of station ash. The compressive strength and density of samples were measure at 3, 7, 28 and 90 days. It was found that paste mixes containing 5 % and 10 % of Coventry Binder in binary system Coventry Binder-OPC gained higher strength at 28 days than OPC samples. Increasing Coventry Binder content in paste mixes results in a considerable decrease of compressive strength.

Keywords: pozzolanic materials, plasterboard gypsum waste; sustainability, basic oxygen slag, Coventry binder, run of station ash, compressive strength

1. INTRODUCTION

In the 21st century one of the most significant and important problems is Global Warming. It can be observed that rapid changes in weather is happening around the world i.e. hurricanes, typhoons, floods, and droughts which cause several damage such as forests fire and agricultural problems. These weather phenomena are the effect of increases in carbon dioxide in the atmosphere, referred to as “Greenhouse gasses”. In the Earth’s atmosphere there are many chemical components, some of which have a natural origin e.g. water vapour, carbon dioxide, methane and nitrous dioxide. Some of these components are artificial i.e., man-made gases used in aerosols [1]. The air pollution started with the Industrial Revolution in the late 18th century. Then the whole world started developing. The manual labour began to be replaced by machinery and all these machines were working using steam power which was getting by coal combustion. This was the main source of CO_2 emission which was released into the atmosphere [2]. Nowadays this problem still exists and even arises as a result of the human convenient and comfortable lifestyle and also because the developing countries i.e. India, China, Eastern Europe are contributing. The Economic policy of each country is close related to Greenhouse gas emissions. Especially developing countries and big countries like the USA have a huge demand for production energy by industry, transportation and in construction industrial processes, such as the production of cement [3]. These economic fields cause the major pollution. It is a major problem to deal with because the impacts of pollutants emitted in one country have a direct impact on citizens from other countries. Industrial processes have a major influence on carbon dioxide emissions and global warming. It is therefore imperative in construction industries to find alternative materials with low environmental impact to help in reducing this negative and dangerous phenomenon [4]. By producing 1 ton of cement, one ton of CO_2 and other gasses are emitted. Concrete is the most popular construction material in the world [5]; however, concrete only exists with cement so novel and modern cementitious materials must be developed to replace the ordinary Portland cement. Most importantly, these new materials must be environmental friendly and also help to utilise various industrial wastes in order to minimise the consumption of the natural sources such as limestone [5]. Development of such a material will also help to reduce the landfills. The majority of waste materials from construction and demolition are currently landfilled [6]. Recycling and reusing waste materials can be an effective solution for escalating problem of landfills [4]. The Civil Engineering Department at Coventry University has been developing a novel binder which is entirely made from waste materials [7]. The developed novel binder was successfully used for construction of road-base, sub-bases and soil stabilisation. The aim of this research is to evaluate the performance of the novel binder which is referred to as ‘Coventry Binder’ as cement replacement. Comparison will also be made for strength of mixes containing the novel binder with mixes made with other pozzolanic materials including BOS and run of station ash (ROSA).W

2. EXPERIMENTAL PROGRAMME

2.1. Materials

Plasterboard Gypsum (PG) used for this project was collected from demolition and reconstruction activities. Gypsum is major component of modern buildings so waste from construction contains up to 30% of gypsum drywall scraps by weight [7]. Plasterboard waste was crushed by grinders and sieved through a 600 micron sieve. The powder was then stored in a sealed bucket [8]. Basic Oxygen Slag (BOS) is a non-metallic by-product of steel produtcion. The slag was grounded by using a laboratory ball mill and after that sieved through a 600 micron sieve. By Pass Dust (BPD) is obtained from kiln bypass in cement industry. By pass dust is the waste highly alkaline materials of Portland cement manufacture. It is generated during the calcining process in the kiln [9]. Run of station ash (ROSA) is an unclassified ash collected from chimney stack of power stations. This is pozzolanic in nature and reacts with calcium hydroxide and alkalis to form calcium silicate/aluminate hydrates which are cementitious compounds. Coventry Binder is a blended mixture of 15 percent Plasterboard Gypsum (PG), 80 percent Basic Oxygen Slag (BOS) and 5 percent By Pass Dust (BPD). Coarse and fine aggregates used in mortar and concrete mixes were of natural source and complied with BS 812.

2.2. Mix Proportions

A large number of paste samples were made during this investigation. The word "paste" which will be using in this paper means a mixture of resembling cementitious powder and water without aggregate. The proportions of pastes used in investigation were design in order to optimize the mixture ingredients to achieve the highest compressive strength. The pastes mixes were prepared in five groups. The mix proportions of mixes are shown in Tables 1 to 4.

Table 1: Mix proportions for Coventry Binder-OPC paste mixtures (Group 1)

Coventry Binder [%]	OPC [%]	W/B
5	95	0.3
10	90	0.3
20	80	0.3
40	60	0.3
60	40	0.3
80	20	0.3

Table 2: Mix proportions for PG-BOS-OPC paste mixtures (Group 2)

PG[%]	BOS [%]	OPC [%]	W/B
10	85	5	0.3
15	80	5	0.3
20	75	5	0.3
30	65	5	0.3
50	45	5	0.3

Table 3: Mix proportions for Coventry Binder-ROSA-OPC paste mixtures (Group 3)

Coventry Binder [%]	ROSA [%]	OPC [%]	W/B
80	10	10	0.3
70	20	10	0.3
60	30	10	0.3
50	40	10	0.3
40	50	10	0.3

Table 4: Mix proportions for BOS-OPC paste mixtures (Group 4)

BOS [%]	OPC [%]	W/B
90	10	0.3
80	20	0.3
60	40	0.3
40	60	0.3
20	80	0.3

The mix in group 5 was made with 100 percent ordinary Portland cement (OPC) and 30 percent of water. This group was used as control mix to be compares with strength samples in groups 1 to 4. Mortar and concrete mixes were also made to investigate the performance and binding properties of Coventry binder with aggregates (Tables 5 and 6).

Table 5: Mix Proportions for mortar mixture

Coventry Binder [kg/m³]	OPC [kg/m³]	Coarse agg. [kg/m³]	Fine agg. [kg/m³]	Water [kg/m³]
266	114	0	1905	171

Table 6: Mix proportion for concrete mixture

Coventry Binder [kg/m³]	OPC [kg/m³]	Coarse agg. [kg/m³]	Fine agg. [kg/m³]	Water [kg/m³]
210	**90**	**1200**	**800**	**135**

2.3. Experimental Method

The mixing for pastes and mortar was carried out in a mechanical mixer having a 2 litre capacity. Mixing and casting procedure was as follows:

- Dry mixing of PG, BOS, BPD, ROSA and OPC (depending on which ingredients are applicable for each mix) for 1 minute.
- Half of the mixing water was added during next one minute of mixing.
- Mixing was continued for next minute at medium speed.
- The mixer was stopped and mixture was scraped off the sides of the bowl.
- The rest of the mixing water was added and mixing was carried out for a further one minute at medium speed.
- The mixture was poured in two layers in 50mm cube moulds.
- Each layer was fully compacted using a vibrating table.

Mortar and concrete mixes were also prepared using the similar procedure with only difference that aggregates were mixed with one third of required water prior to adding the dry mixed binder. 50 mm and 100 mm moulds were used for casting mortar and concrete samples respectively. All samples were demoulded after 24 hours and stored in containers in constant temperature 20±2 °C and 98 % RH humidity. The compressive strength of paste samples was measured at 3, 7, 28 and 90 days and compressive strength of mortar and concrete samples was measured at

3, 7 and 28 days. The Lloyd computerised crushing machine was used for compressive strength test of paste and mortar samples.

3. RESULTS AND DISCUSSION

3.1. OPC-Coventry Binder Paste Mixes (Group 1)

The results of compressive strength (Figure 1) showed that an increase in substitution of OPC with Coventry Binder had no significant beneficial effect on early and long term compressive strength. However, the mix incorporating 5 percent and 10 percent Coventry Binder achieved a higher compressive strength than paste mix made with 100 percent OPC at 28 days. This therefore indicates that the mix with 5% Coventry Binder and 95% Ordinary Portland cement is the optimum mixture in this combination. Pozzolanic reaction of part of slag present in Coventry Binder with calcium hydroxide of cement may be a reason for higher strength of the mix containing 5% Coventry Binder. In other mixes Coventry Binders appeared to act as filler and therefore the strength decreased due to less cement used in the mix.

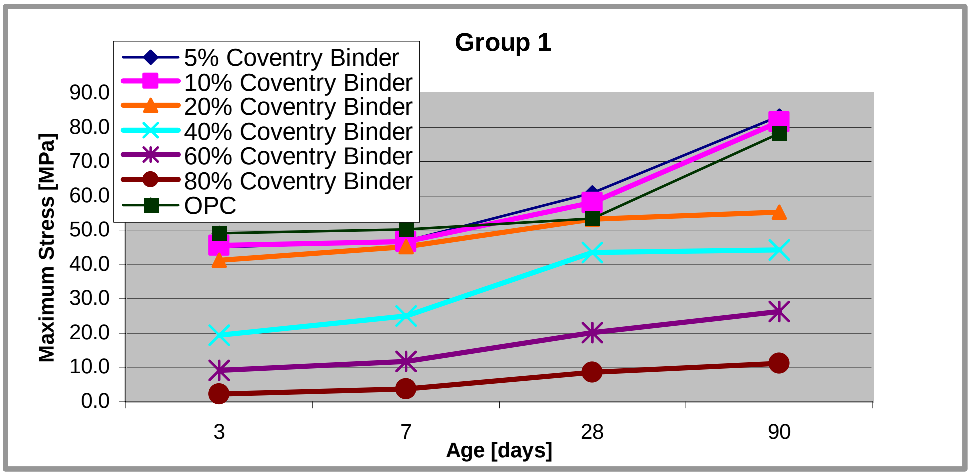

Figure 1. Compressive strength development of Coventry Binder-OPC paste mixes (W/B ratio 0.3)

3.2. PG-BOS-OPC Paste Mixes (Group 2)

Figure 2 shows the compressive strength development of paste mixes made with 5% OPC and various BOS/PG contents. It was observed that in the ternary system increasing the Plasterboard Gypsum content in the mix resulted in decrease in long term compressive strength of pastes in this group. However, substitutions of PG with BOS led to higher strength gain. It can be also observed that all mixes achieved 90-day compressive strength of about 5.0 MPa. It was found that the compressive strength of PG-BOS-OPC mixes were the lowest compared to other mixes studied.

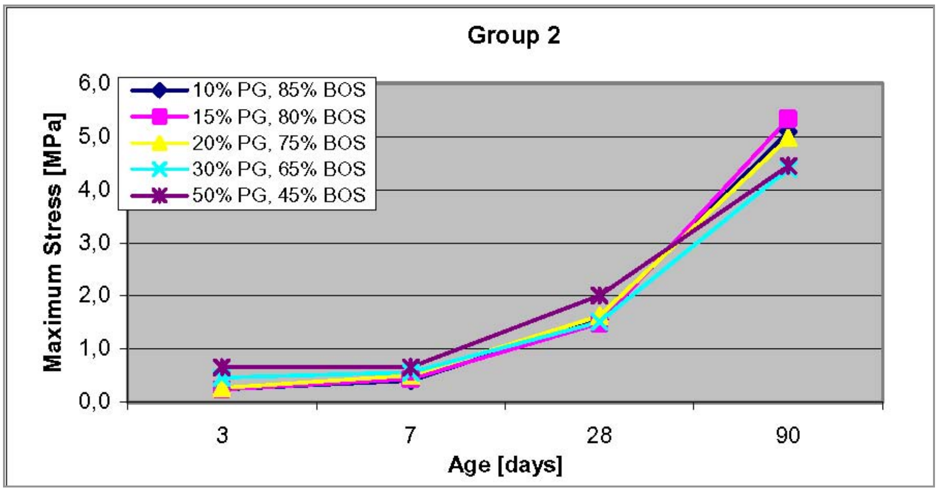

Figure 2. Compressive strength development for PG – BOS mixes (5% OPC content)

3.3. Coventry Binder-Rosa-OPC Paste Mixes (Group 3)

The strength development of paste mixes using various proportions of Coventry Binder and ROSA with constant 10% OPC and water to binder ratio 0.3 are shown in Figure 3. Results indicate that the mix containing 40% Coventry Binder and 50% ROSA achieved the highest strength at 7 and 28 days. Paste mixes containing 40, 50 and 60% Coventry Binder with subsequent amount of ROSA showed similar compressive strength 34.5 MPa at 90 days. This indicates that up to 60% of the binder can be replaced with novel Coventry Binder without significant effect on long term compressive strength of the mix.

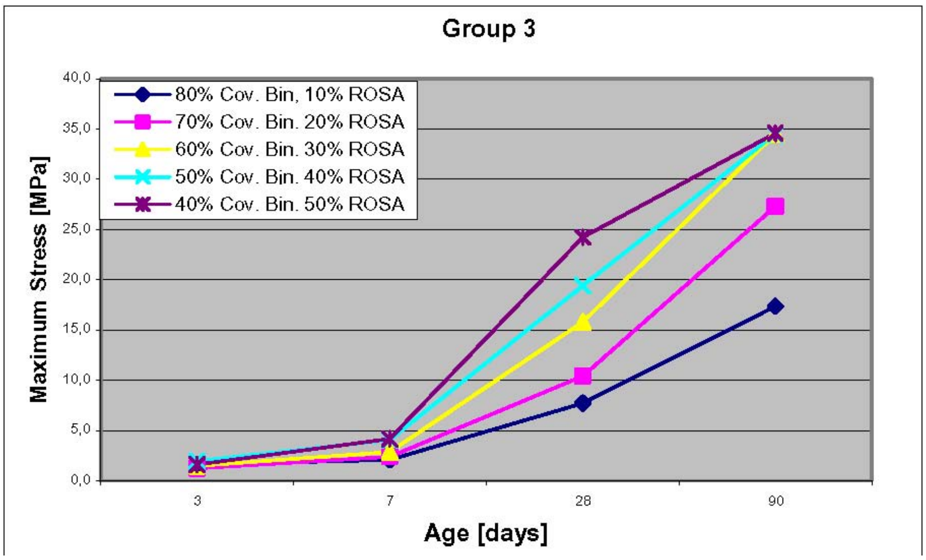

Figure 3. Compressive strength development for Coventry Binder-ROSA mixes (10% OPC content)

Further investigation is needed to evaluate the strength of ternary mixes containing the lesser percentage of Coventry Binder with greater amount of ROSA.

3.4. BOS-OPC Paste Mixes (Group 4)

It was found that replacing of Ordinary Portland Cement with Basic Oxygen Slag does not has beneficial effect on early and long term compressive strength (Figure 4). However, the mix incorporating 40 percent BOS achieved the highest compressive strength at 3 days and mix containing 20 percent BOS achieved the highest long term strength at 28 and 90 days.

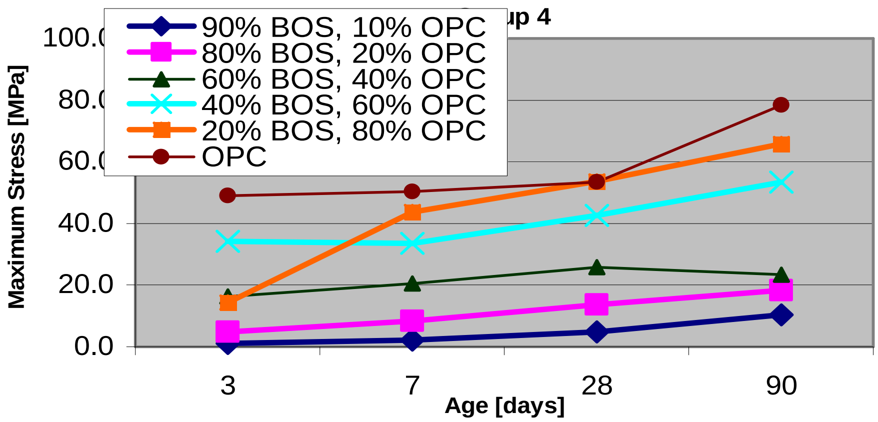

Figure 4. Compressive strength development for BOS-OPC mixes with constant W/B ratio

Therefore it can be observed that the paste mix with 20% BOS and 80% OPC is the optimum mixture in this combination.

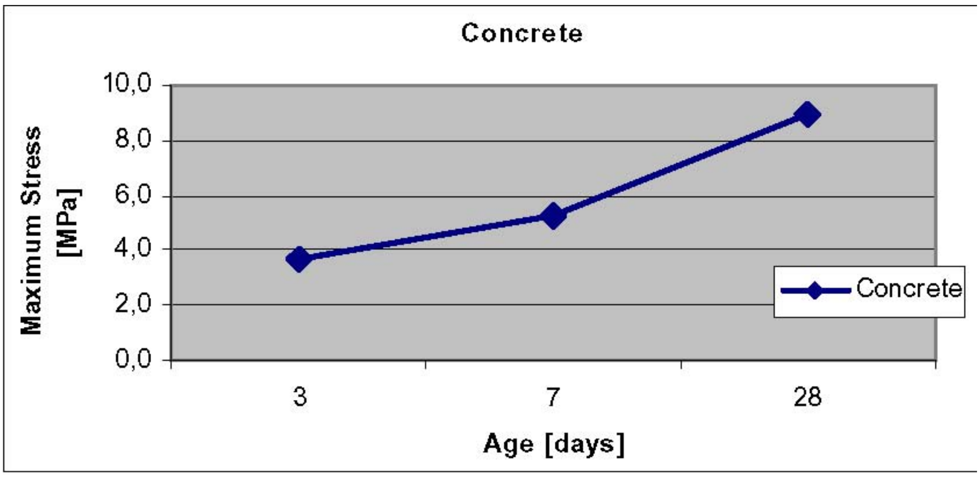

Figure 5. Compressive strength development of concrete made with Coventry Binder

3.5. Coventry Binder-OPC Concrete Mix

Figure 5 shows the strength development of concrete mix containing 210 kg/m^3 Coventry Binder and 90 kg/m^3 OPC. It also contains coarse and fine aggregate. It was found that the long term strength at 28 days is equal 8.9 MPa. The result showed that it the strength was lower that the lowest class of concrete C12/15 with 20 MPa cube strenght (Figure 5) [10]. This indicates that although the paste mixes containing Coventry binder achieved comparable strength with OPC samples, the weak binding of the novel binder with aggregates resulted in low compressive strength ion concrete samples.

3.6. Coventry Binder-OPC Mortar Mix

Mortar mix samples contained 266 kg/m^3 Coventry Binder and 114 kg/m^3 ordinary Portland cement. It was observed that after 3 and 7 days compressive strength was low, however after 28 days age compressive strength was 3.8 MPa (Figure 6). This showed that the long term strength for mortar containing Coventry Binder was comparable to standard class mortar M2.5 and M5 [11].

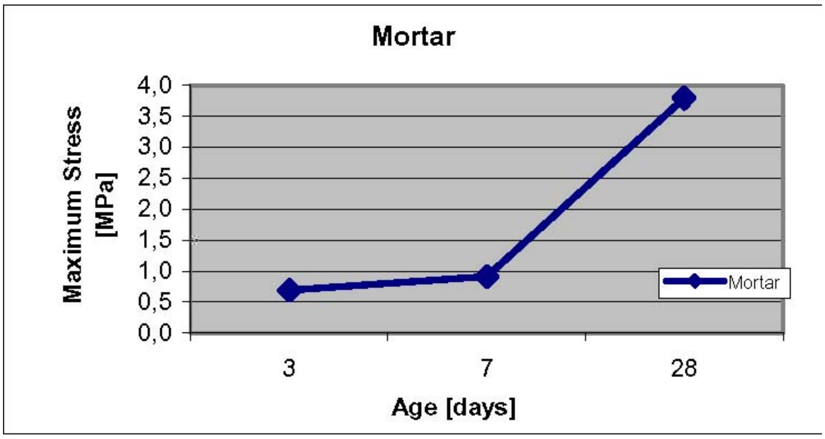

Figure 6. The compressive strength development of mortar mixture contains Coventry Binder

4. CONCLUSIONS

Base on results of this research the following conclusions can be drawn:

- Replacing ordinary Portland cement with Coventry Binder does not have a beneficial effect on early and long term compressive strengths.
- Paste mixes containing 5% and 10% of Coventry Binder in binary system Coventry Binder-OPC gained higher strength at 28 days than ordinary Portland cement paste mixes. Paste mixes containing 20% of Coventry Binder achieved nearly similar compressive strength at 28 days compared to mixes made with 100% OPC.
- In the ternary system PG-BOS-OPC, increasing the amount of Plasterboard Gypsum content in the paste mixes results in a reduction in long term compressive strength. 60% of Coventry Binder can be used as a cement

replacement in ternary system Coventry Binder-ROSA-OPC.

- Replacing ordinary Portland cement with Basic Oxygen Slag does not have a beneficial effect on early and long term compressive strengths. The paste mixes in binary system BOS-OPC containing 20% BOS gained slightly lower compressive strength at 28 days than the OPC samples.
- Paste mixes containing 20% Coventry Binder have a higher compressive strength at 3 days compared to paste mixes containing 20% of Basic Oxygen Slag. Paste mixes containing 40% Coventry Binder showed lower compressive strength than mixes made with 40% BOS at 3 and 7 days; however, the 28-day strength was similar.
- Replacement of high level cement with Coventry Binder resulted in considerably lower strength than ordinary concrete mixes. This is due to relatively weaker binding of the novel binder to coarse aggregates particularly at early ages. However, the long term strength of mortar mixes containing Coventry Binder was comparable to standard mortar class M2.5 and M5.

REFERENCES

1. Owen D.A. Hanley N. (2004). The Economics of Climate Change. 1st edn., Routledge, London.
2. Sakai. K. (2007), Contributions of the concrete industry toward sustainable development. In: Chun Y.-M., Claisse P., Naik T.R., Ganjian E., Sustainable Construction Materials and Technologies. Taylor & Francis, 1-10.
3. Kolstad Ch. D. (2000). Environmental Economics, Oxford University Press, New Yor.
4. Kishore R. (2007) Influence of recycled aggregate on flexural behaviour of reinforced concrete beams. In: Sustainable Construction Materials and Technologies, – Supplementary Papers. Coventry, 36-44.
5. Naik. T.R. (2007), Sustainability of the cement and concrete industries. In: Chun Y.-M., Claisse P., Naik T.R., Ganjian E. Sustainable Construction Materials and Technologies. Taylor & Francis, 19-25.
6. Kraus R.N., Naik T.R., Chun Y.-M. (2007), Use of industrial by-products in sustainable construction practices. In : Sustainable Construction Materials and Technologies – Proceedings of Special Sessions. Coventry, 187-196.
7. Drywallrecycling (2007). Gypsum drywall recycling, http://www.gypsumrecycling.com/ [18 July 2007].
8. Ganjian E., Claisse P., Sadeghi Pouya H. (2007). The Use of Plasterboard and Gypsum Waste in Road Bases, sub-bases and Stabilised Sub-grades, Project code: PBD5-022, Coventry University, Coventry.
9. ASCE Research Library (2002), Use of Cement Bypass Dust as Filler in Asphalt Concrete Mixtures. http://scitation.aip.org/ [12 August 2007]
10. British Standard (2002). BS 8500-2:2002 Concrete-Complementary British Standard to BS EN 206-1 -Part 2: Specification for constituent materials and concrete.
11. British Standard (2005). BS 5628-1:2005 Code of practice for the use of masonry-Part 1: Structural use of unreinforced masonry.

CD01-009

COMPERING THE EFECT OF USING THE COPPER BLAST FURNACE SLAG AND TAFTAN POZZOLAN ON CONCRETE PROPERTIES

M.R. Sohrabi[1], H. Mohsenian[2]
[1]University of Sistan and Baluchestan, Zahedan, Iran
[2]Islamic Azad University of Zahedan, Iran

ABSTRACT
Today large number of researches are carried out on concrete properties due to it's widely use as an important construction material. The most part of concrete is cement which its cost decrease leads to producing of economical concrete. Using the industrial sweepings such as copper blast furnace slag which have pozzolan properties can make the cement economical. By using these materials not only production costs of cement will be reduced but also saving costs of sweepings will be eliminated and natural environment will be protected. In this research copper blast furnace slag milled to mesh325 which in this mesh maximum diameter of grains are 45 micron. 455 cubic specimens with size of 15×15×15 and cylindrical specimens with size of 30×15 have been made. Compressive and tensile experiments carried out and the results showed the positive effect of Taftan pozzolan and copper slag on concrete properties.

Keywords: copper blast furnace slag, compressive and tensile strength of concrete

1. INTRODUCTION
Concrete is a construction material composed of cement as well as sand and aggregate. Today the usage of pozzolans either natural or artificial has been increased. One of these artificial pozzolans is the slag of metal melt furnace such as iron, copper, etc. several researches on iron slag have been carried out in and out of Iran.
Although acceptable studies have been conducted by Prof. Barzin Mobasher at Arizona State University in America; there are no earlier ones in Iran. Slag is a byproduct of metal smelting which float to the top during the smelting process because of its low density. It includes the compounds presenting in ores as well as the materials adding for lowering down the melting point of gangue. Copper ores usually include acid gangue which mainly have silica. These are the industrial waste materials which are removed from melting tank. Up to 300 thousand tons slags are produced each year during the production of copper. Slag was prepared from two kinds of copper furnace: Reverb -from Sarcheshmeh copper Complex- and flash furnace. There is about 1% copper in the slag of converter furnace which transferred to reverb one to obtain. Then it is exposed to the weather and cooled down after exiting the furnace. But in the Flash furnace at the copper factory of

Khatun abad in Rafsanjan, the slag is cooled down by water after exiting. given such a high cooling rate makes the slag not to be crystallized and results in amorphous solid.

Therefore the substituting this kind of slag in the constituent of cement instead of reverb copper slag or pozzolan works very well. In the experiment conducted by Shargh Kan Micronize in Birjand both the slags were distinguished to be completely amorphous and enduring against the mill. Because the subject was comparing the effect of using copper slag and Taftan pozzolan on concrete properties so the grains diameter had to be similar to pozzolan in size. Therefore the slag was milled and the grains diameter decreased less than 45 micron. Because of being amorphous and high hardness (6 to 7 Mohs) this was a slow process. Unexpectedly, reverb kind was milled easier.

2. CHEMICAL ANALYSIS OF REVERB SLAG

As the slag will be a constituent of cement, its elements and components should be examined. Therefore chemical analysis was performed by Khash Cement Factory. The following table 1 demonstrates the chemical analysis of reverb slag:

SiO_2	CaO	Al_2O_3	Fe_2O_3	SO_3	MgO	Cl	K_2O	Na_2O
35.8	6	8.1	46.84	0.72	0.3	0.09	1.44	0.7

Activate module can be calculated by the following formula.

$$\frac{CaO + MgO + Al_2O_3}{SiO_2} \geq 1 \qquad (0.3+6+8.1)/35.8=0.4\leq 1$$

Based on this formula the activation module is less than one and it is expected that it does not have appropriate properties. On the other hand according to ASTMC 618-92A the summation of this three oxides (Fe_2O_3, CaO, SiO_2) exceeds the percentile requirement of pozzolanic activity. This number compares various pozzolans for their degree of reactivity as compared to class F flyash. In this research for the study of compressive and tensile strength samples with different gravity percentages (5, 10, 15, 20, 25, 30) and ages (7, 28 days, 3 months, 6 months, and 1 year) were made and studied within 3 months. Study on 6months and 1 year samples continues.

3. INITIAL AND FINAL SETTING TIMES OF THE CEMENT PASTE

In the present study, the cement of Qaen (type two), the slag of Khatoon abad and Sarcheshmeh Copper Complex and the pozzolan of Taftan were used. The time of the cement paste experiment only carried out on 20% of the pozzolan and the copper slag replacement of cement.

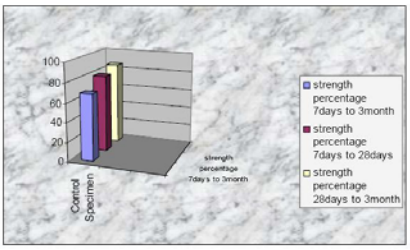

Chart 1. Ratio of Strength Relative to That Other Ages

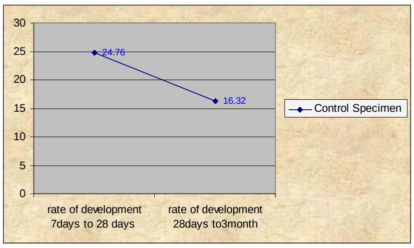

Chart 2. Compressive Strength Rate of Growth for The Witnes Specimen

In this experiment the following results using ASTM C150-200 were obtained: (here the Vicat method has been used) (a cubic specimen 5×5×5 in dimension for compressive strength and a cylindrical specimen 30×15 in dimension for tensile strength). Based on this table, the flash copper slag and the pozzolan behave the same way and have the same final and initial paste, in comparison with the other samples, the reverb copper slag has a more initial set but its final set is closer to the cement one. In higher temperature of Sistan and Baluchestan using of this cement compound is advised because it reduces the volume variety to a minimum and will prevent the likely crack due to the volume changes.

4. STUDY OF THE SAMPLES' COMPRESSIVE STRENGTH WITH THE CONTROL SPECIMEN

Analysis and study of the samples have a considerable importance and should be investigated. Samples with different gravity percentages (5 to 30%) used as cement replacement were made. Study on 6 months and 1 year ones continue. Control Specimen got 68% and 86% of the three months strength after 7 and 28 days respectively. At the end of three month rate of development became 16.32.

Analysis of the Flash Samples:

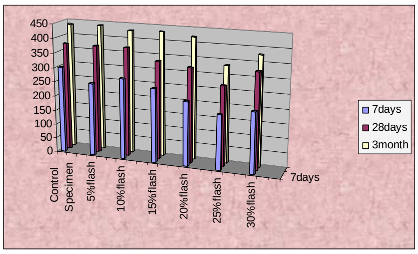

Chart 3. Compressive Strength of the Copper Slag Concrete

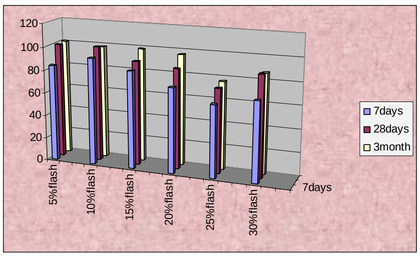

Chart 4. Compressive Strength of Flash Copper Slag concrete

The 5% flash sample considered to be the most samples because its three months strength is 58% superior to the three months sample. And 28 days sample is approximately equal to the control specimen.

The 28 days strength of the 10% flash sample is about 37% superior to the control specimen and the three months sample exceeds in early strength (400) by as much as 428 which is the appropriate percentage.

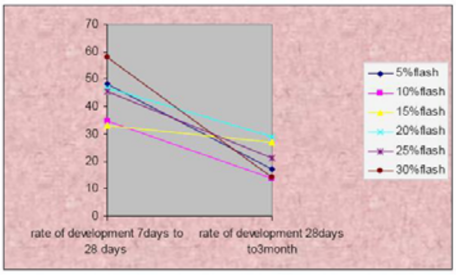

Chart 5. Compressive Strength of Growth for Flash Copper Slag

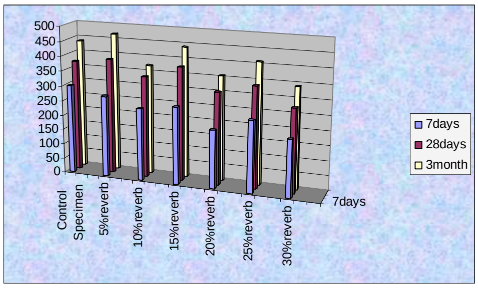

Chart 6. Compertive Results for Reverb Concrete

The strength of the 15% flash sample is about 431 which corresponds to the three months control specimen and it is superior to the specific strength. The 28days sample has the 99% of the control specimen strength. And the rate of compressive strength development during 3 months has increased in comparison to the 28 days sample. Therefore this sample has an appropriate compressive strength. The 3 months sample of the 20% flash has the 96% of the control specimen and compressive strength is superior to the specific one. Note that 28% of the control specimen strength took place during the 28 days period. The 20% flash sample is also appropriate one.

The compressive strength of the 25% flash sample is not appropriate because it has the 73% and the 76% of the control specimen strength during 28 day and 3 month period respectively. This sample has 83% of the specific strength during 3 months which is a very small amount.

The 30% flash sample has a better function than the 55% because it has 88% and 86% of the control specimen strength during 28 day and 3month period respectively. Note that 69% of the control specimen strength took place during the 7 day period. The rate of development for 3month sample is about 14%.

4.1. Analysis of Reverb Sample's Compressive Strength

In this study two dosages of 5% and 15% samples considered to be ideal. At the 28^{th} and 90^{th} day, 5% sample exceeds in strength by as much as 4% and 7% respectively over the control specimen. The strength of 15% sample during the 28 day and 3 month period is respectively 2% and 1% superior to the control sample.

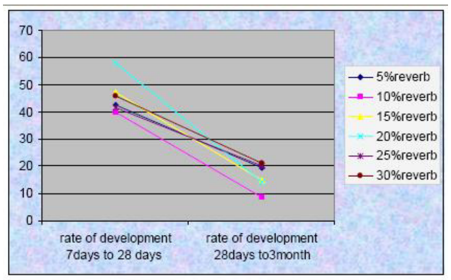

Chart 7. Compressive Strength Rate of Growth Reverb Copper Slag Concrete

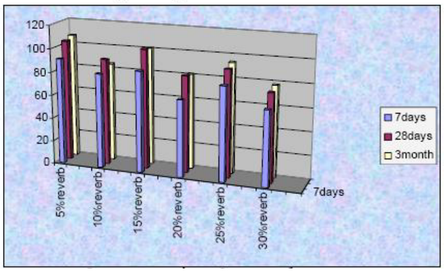

Chart 8. Compressive Strength Rate of Growth for The Witness And Reverb Copper Slag Concrete

Rate of development in 3 month period for 5% sample is about 19.36, reflecting a high rate of development in comparison to the other samples during the 3month period. The strength of the 3 months sample is superior to the control sample as much as 16%. The 20% reverb sample has 83% and 81% of the control specimen strength in 28 day and 3 month period respectively which is not an appropriate sample. But at the 3rd month, 25% reverb sample exceeds in strength by as much as 10% over the control sample and it has 94% of the control sample strength.
At the end of the 3rd month, rate of development for the 15% and 20% samples is 14% but this number for the 25% dosage is about 20%.
Because the 30% sample has 75% and 78% of the control sample strength at 28 day and 3 month period respectively, it is not considered to be an ideal sample. Its rate rate of development is 21%.

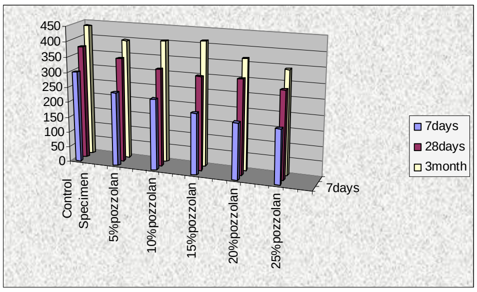

Chart 9. Compressive Strength Rate of Growth for The Witness and pozzolan concrete

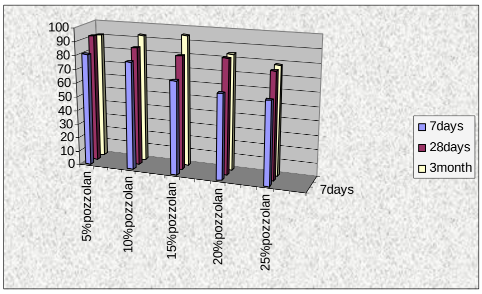

Chart 10. Compressive Strength of the Pozzolan concrete

4.2. Analysis of Pozzolan's Compressive Strength

The best sample for pozzolans was 5% one but it had 92% of strength during the 3 month period. Rate of development for this sample was 14 to 33% while the 15% sample had a high rate of development.
The reverb and flash copper slags behave well than the pozzolans. The 5% flash samples at ages of 7, 28, and 30 days were superior to the 5% pozzolan sample as much as 3-10%. In comparison to the pozzolan sample the compressive strength of

the 10% flash sample was superior as much as 11-19%.

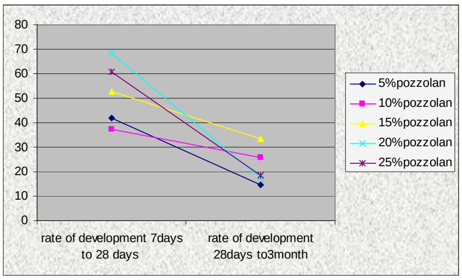

Chart 11. Compressive Strength Rate of Growth for Pozzolan concrete

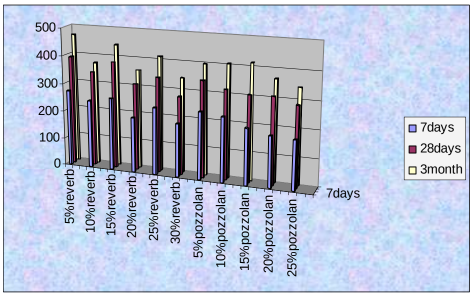

Chart 12. Compertive Results for The Pozzolan and The Flash Slag Concrete

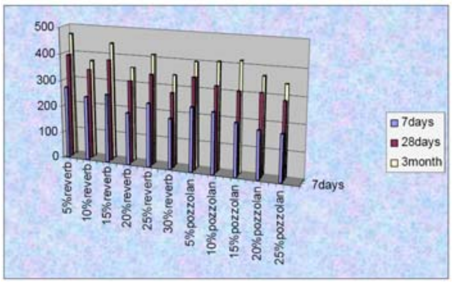

Chart 13. Compertive Results for The Pozzolan and The Reverb Slag Concrete

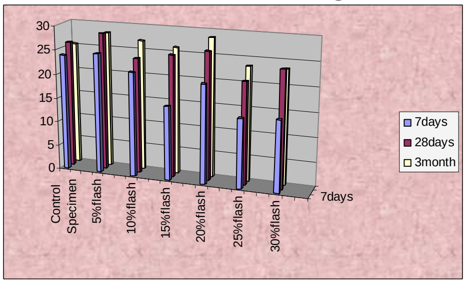

Chart 14. Tensile Strength of The Flash slag Concrete Speciems

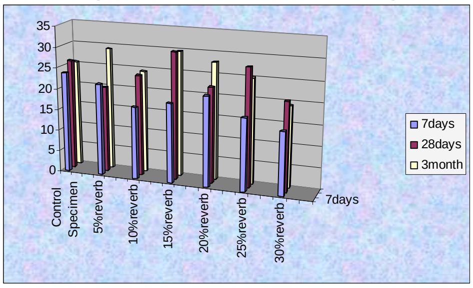

Chart 15. Tensile Strength of The Reverb slag Concrete Speciems

The 15% flash sample exceeds in strength as much as 4.5-26% over the 15% pozzolan sample.
The strength of the 20% flash sample is superior to the pozzolan sample as much as 20%.
The 25% flash sample at age of 7 days was superior to the pozzolan one at age of 7 days over 5% but at the ages of 28, 30 days it was lower than the similar pozzolan sample as much as 3-5%.
The 5-25% reverb samples at the ages of 7,28,and 30 days were superior to the 5-25% pozzolan samples as much as 4-34%.

4.3. The study of tensile VS. Bending Strength

For calculating tensile and flexural strength, cylindrical specimens (15×30 in dimension) were made and the Brazilian method was adopted for calculating the tensile strength but the coefficient made in this method was different from the experimental coefficient.

In experimental method, strength can be calculated from the following formula: (N/mm^2)

(cf= compressive strength of cylindrical specimen)

Experiment on the cylindrical specimens for calculating tensile strength showed this results:

The coefficient for samples at ages of 7, 28 and 90 days became 1057, 1.5 and 1.375 respectively (Kg/Cm^2).

For calculating flexural strength the following experimental formula is used:

Which in comparison to the tensile strength formula is 18% superior. According to the calculated coefficient, the flexural strength is higher than the tensile one.

The tensile strength showed increase with the addition of copper slag. The positive rate of development for three dosages of 5,10 and 20% of reverb samples stand in contrast with the 15, 25 and 30% samples i.e. the increase in ages of samples will decrease the tensile strength.

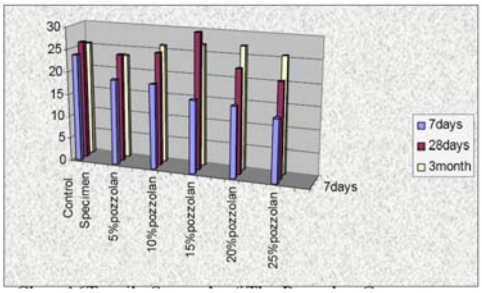

Chart 16. Tensile Strength of The Pozzolan Concrete Speciems

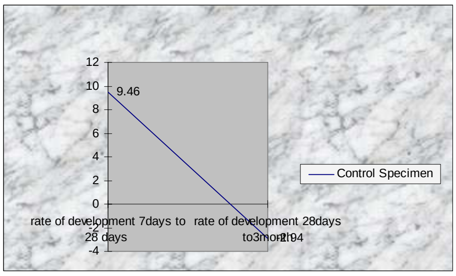

Chart 17. Tensile Strength Rate of Growth for The Witnes Specimen

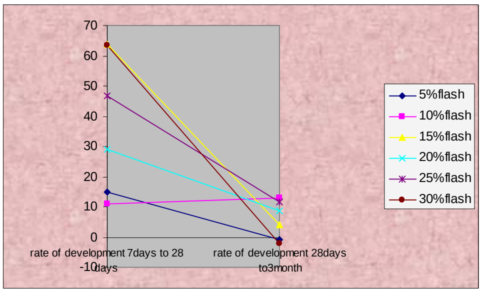

Chart 18. Tensile Strength Rate of Growth Flash Copper Slag Concrete

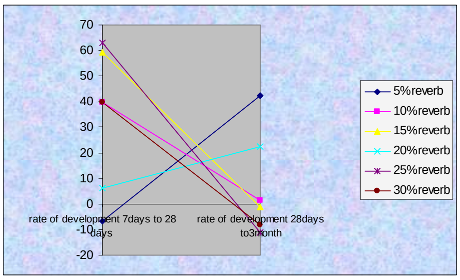

Chart 19. Tensile Strength Rate of Growth Reverb Copper Slag Concrete

For the 10-25% flash samples, the tensile strength is positive as compared to the 5 and 30% samples reflecting negative one.

The increase in percentage and ages of pozzolan translates into an increase in the rate of development. Forexample three dosages of 10,15,and 15% pozzolan samples have a rate of development between 4-22% but 5 and 15% sample have a negative rate of development.

5. CONCLUSION

The studies carried out on the copper slag resulted in an improvement in the concrete properties such as tensile strength as well as compressive one.

The flash samples had a high tensile and compressive strength than the reverb ones. However the reverb samples were better than pozzolan ones. Therefore the flash samples (for 5%slag) considered to be optimum and ideal.

The 10 -20% flash copper slag had a compressive strength as much as the specific one; so the following benefits can be derived from the usage of them in concrete:

1. Using the potential of the artificial pozzolans in development projects
2. Lowering the cost of the concrete production
3. Optimizing the concrete's quality
4. Increasing the concrete efficiency and the quality of concrete productions
5. Increasing the age of concrete constructions against erosion factors
6. Eliminating the materials added in the concrete compound resulted in lowering the cost of the concrete
7. Making a change in development
8. Eliminating slag in copper smelting operation
9. Lowering the use of energy in the concrete production
10. Protecting the environment from the copper wastes
11. Using in the concrete constructions such as damming, silos, water reservoirs, etc.

REFERENCES

1. Concrete Admixtures And Polzzolanas By: Dr. A.A. Ramezanianpour, T. Parhizkar, Dr. A. Taheri Building & Housing Research Center Ministry of Housing & Urban Development Islamic Republic of Iran, 1995.
2. Effect of Copper Slag on The Hydration of Blended Cementitious Mixtures: Proceedings, Asce, Materials Engineering Conference, Materials for the New Millenium, ed. K. Chong, pp. B. Mobasher M. ASCE, and R. Devaguptapu, A.M. Arino 1677-86, 1996.
3. STM C 618-92a, "Standard specification for Flyash and raw or calcined natural pozzolan for use as a mineral admixture in portland cement concrete", 1992.
4. Concrete Construction Handbook Joseph J.Waddel, Joseph A. Dobrowolski, Third edition, Mc Graw hill.
5. Metallurgy of Copper Dr.Hekmat Razavizadeh & Ramse Vaghar

CD01-010

بررسی آزمایشگاهی تأثیر پوزولان خاش بر افزایش مقاومت بتن RCC در سنین بالا

وحید خلیلی خرّم[1]، حمیدرضا وثوقی فر[2]، عباس منصوری[3]
۱. دانشجوی کارشناسی ارشد سازه‌های هیدرولیکی، دانشگاه آزاد واحد تهران جنوب
۲. استادیار دانشکده مهندسی عمران، دانشگاه آزاد اسلامی‌واحد تهران جنوب
۳. استادیار دانشکده مهندسی عمران، دانشگاه آزاد اسلامی‌واحد تهران جنوب

چکیده

در دهه اخیر، بتن غلتکی (Roller Compacted Concrete) بعنوان یک مصالح جدید یا بـه عبـارت بهتـر روش اجرای جدید، در کارهای مختلف بخصوص در صنعت سد سازی پیشرفت فراوانی داشـته و در حـال حاضـر مـورد توجه دست اندرکاران‌این صنعت و موسسات تحقیقاتی و دانشگاهی می‌باشد.

امروزه استفاده از مواد پوزولانی به عنوان مصالحی دارای خاصیت سیمانی و جایگزین شونده در قسمتی از سیمان پرتلند مخلوط‌های بتنی مورد توجه زیادی می‌باشد. علت‌این امر بهبود اکثر خواص بـتن و قیمـت کمتـر بـویژه در پروژه‌های سدسازی می‌باشد.

دراین مقاله با توجه به اینکه پوزولان طبیعی تفتان نزدیکترین منبع به محل اجرای پروژه سـد زیـردان و کارخانـه سیمان خاش می‌باشد تاثیرآن در افزایش مقاومت بتن متراکم غلتکی (RCC) در سـنین بـالا مـورد بررسـی قـرار گرفته است.

نتایج‌این تحقیق تاکیدی بر عملکرد پوزولان خاش در افزایش مقاومت از ۲۸ روز به ۹۰ یـا ۱۸۰ روز بـوده و ایـن موضوع زمانی کارکرد دارد که بخواهیم با ثابت نگاهداشتن سنین مقاومت مشخصه، از مقدارسـیمان کاسـته و بـه انتظار مقاومت دراز مدت پوزولان بنشینیم.

کلیدواژه‌ها: پوزولان، بتن غلتکی، پوزولان خاش، سد بتنی غلتکی

۱- مقدمه

پوزولان ماده‌ای است که در مجاورت با آب آهک خواص سیمانی از خـود نـشان مـی‌دهـد. پـوزولان بـر اسـاس استاندارد ASTM-C618 چنین تعریف می‌شود:«پوزولان ماده‌ای است سیلیـسی یـا سیلیـسی آلومینـاتی کـه بـه خودی خود ارزش چسبندگی ندارد، اما به شکل ذرات بسیار ریز در مجاورت رطوبت با درجات حرارت معمـولی بـا هیدروکسید کلسیم واکنش شیمیایی داشته و ترکیباتی را بـه وجـود مـی‌آورد کـه خاصـیت سـیمانی و چـسبندگی می‌آورد»[7]. پوزولان ماده‌ای ظبیعی یا مصنوعی است که حاوی سیلیس فعـال مـی‌باشـد. لازم اسـت کـه مـاده پوزولان به شکل پودر شده باشد، زیرا فقط دراین صورت سیلیس می‌توانـد در حـضور آب بـا آهـک (کـه بـر اثـر هیدراتاسیون سیمان پرتلندایجاد می‌گردد) سیلیکاتهای کلسیم پایدار را که دارای خواص چـسبندگی انـد، تـشکیل

دهد. همچنین سیلیس مواد پوزولانی باید غیر کریستاله باشد، زیرا قابلیت‌ایجاد واکنش سیلیس متبلور بسیار کم است[8].

سیمان پرتلند پوزولانی سیمانی است که از مخلوط سیمان و پوزولان در کارخانه تهیه می‌شود. اغلب مواد پوزولانی از سیمان پرتلندی است که جایگزین آن می‌شوند ارزانترند. ولی امتیاز آنها در هیدراتاسیون کند و در نتیجه روند افزایش حرارت کم نهفته است. در بتن حجیم‌این امر اهمیت زیادی دارد و به همین دلیل دراین نوع بتن‌ها غالبا سیمان پرتلند پوزولانی با جایگزینی بخشی از سیمان پرتلند با مواد پوزولانی مصرف می‌شود. سیمانهای پرتلند پوزولانی در برابر حمله سولفاتها و بعضی از عوامل مخرب مقاومت خوبی از خود نشان می‌دهند.این امر به دلیل واکنش پوزولانی است که مقدار کمتری آهک به جای می‌گذارد تا به خارج راه یابد و نیز نفوذپذیری بتن را کاهش می‌دهد[6]. لیکن مقاومت در برابر یخ زدن وآب شدن تا سنین بالاتر که واکنش عمده پوزولان تخلخل خمیر سیمان را کاهش داده است،نمی‌تواندایجاد شود[9].

عملکرد پوزولان در جلوگیری از انبساط مضر قلیایی، منفکّ از واکنش زایی آن – که نتیجه قهری آن افزایش مقاومت است – نخواهد بود. پوزولان با تشکیل ژلهایی که ظرفیت نگهداری قلیایی‌ها را افزایش داده و نیز باعث ایجاد ریز ساختاری متراکم تر در مخلوط بتن می‌شود، مانع انبساط مضر قلیایی می‌گردد. در واقع واکنشِ به نسبت زود هنگام سیمان و پوزولان است که مجالی برای واکنش سنگدانه‌های فعال با قلیایی‌های سیمان باقی نمی‌گذارد. این فعل و انفعالات، همانهایی است که باعث افزایش مقاومت بتن توسط پوزولان می‌شود[4].

از علل اصلی استفاده از مواد پوزولانی در سد سازی ملاحظات اقتصادی و دوام است. ولی استفاده ازاین مواد موجب تغییر خواص بتن میگردد. اغلب خاکسترهای بادی با کلسیم کم و پوزولانهای طبیعی باعث کاهش مقاومت‌های سنین ۲۸ روز و افزایش مقاومت نهایی خواهند شد. در مقایسه با بتن بدون پوزولان، بتن‌های سرباره‌ای یا دارای خاکستر بادی با کلسیم کم، معمولا مقاومت‌های کمتری را در سنین یک و سه روزه نشان داده، ولی در عوض کسب مقاومت پس از هفت روز عمل آوری قابل توجه خواهد بود. پوزولانهای فعال مانند خاکستر پوسته برنج و میکروسیلیس قادرند بتن‌های پر مقاومتی در سنین کم و زیادایجاد کنند.این وضعیت به خصوص با کاربرد مواد افزودنی کاهنده آب به منظور کاهش آب مصرفی شدت می‌یابد[8].

اگرچه پوزولان خاش به عنوان یک پوزولان طبیعی در سالهای اخیر مورد بررسی‌های تحقیقاتی و آزمایشگاهی قرار گرفته، اما تا کنون در پروژه ای مورد استفاده گسترده قرار نگرفته است. سد جگین و سد زیردان تقریباً اولین مصرف کنندگان عمده این پوزولان هستند. از آنجا که طراحان سدهای جگین و زیردان – که اولین سدهای مخزنی ایران از نوع RCC هستند – کاربرد پوزولان خاش را در بتن ریزیها پیش بینی کرده اند، قطعاً بر عملکرد این پوزولان واقف بوده اند. باتوجه به‌اینکه درحال حاضر در پروژه سد زیردان پوزولان خاش در حال استفاده است و تا کنون چند هزار متر مکعب بتن ریزی با استفاده از آن انجام شده است. دراین مقاله سعی شده است که به نقش افزایش مقاومت دراز مدت بتنهای RCC در دراز مدت اشاره شود.

۲- روش تحقیق

- سد زیردان

به منظور تامین آب شرب شهرهای چابهار و کنارک و آب موردنیاز برای توسعه کشاورزی دشت‌های پیرسهراب،

کهیر و لاش از طریق مهار آب‌های سطحی و همچنین بهره برداری از آب‌های زیرزمینی دشت‌های سه گانه فوق الذکر، شرکت سهامی‌آب منطقه ای سیستان و بلوچستان در مهرماه سال ۶۲ قرارداد مطالعاتی بـا گـروه همکـاری مهندسین مشاور پژوهاب – آبفن- کاراب منعقد گردید. پس از مطالعات اولیـه طـرح زیـردان بـه عنـوان یکـی از طرح‌های به صورت دو منظوره تامین آب شرب و کشاورزی در اولویت قرار گرفت. متعاقبـاً در اواخـر سـال ۱۳۸۰ اجرای سد مخزنی زیردان که از نوع بتنی وزنی RCC است به پیمانکار واگذار گردید.

- سیمان

سیمان مورد استفاده در بتن غلتکی و سایر اجزای بدنه سد و سازه‌های وابسته، از نوع سیمان پرتلند پوزولانی نـوع IP می‌باشد. مشخصات این سیمان مطابق استاندارد سیمانهای آمیخته (ASTM C595) نوع IP و میزان پوزولان حداقل ۲۵ و حداکثر ۳۵ درصد وزنی محصول می‌باشد.

با توجه به روند افزایش مقاومت ۳، ۷ و ۲۸ روزه سیمان IP، قادر خواهیم بود با برازش منحنی لگـاریتمی، معادلـه مقاومت – زمان را برای این نوع سیمان بدست آوریم (شکل ۱). بر اساس این معادله، مقاومـت ۷، ۲۸، ۹۰ و ۱۸۰ روزه و به دنبال آن ضرایب رشد مقاومت قابل محاسبه است (جداول ۱ و ۲).

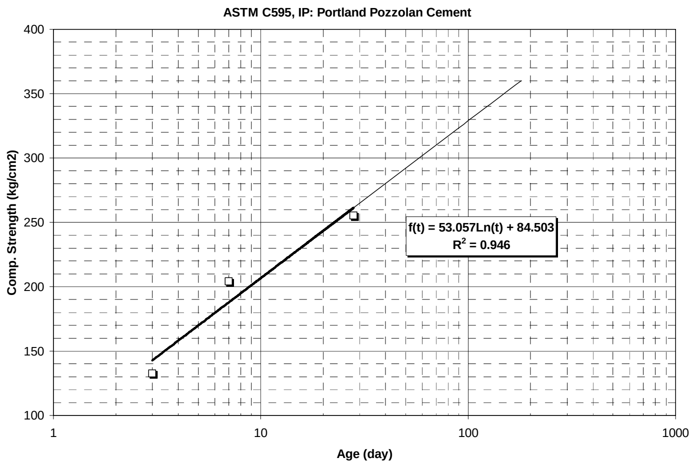

شکل ۱- برازش منحنی لگاریتمی‌بر نتایج ۳، ۷ و ۲۸ روزه سیمان IP

جدول ۱: مقاومتهای محاسبه شده با برازش منحنی لگاریتمی‌بر نتایج ۳، ۷ و ۲۸ روزه سیمان IP

سن (روز)	7	28	90	180
مقاومت فشاری (kg/cm2)	188	261	323	360

جدول ۲: ضرایب رشد محاسبه شده با برازش منحنی لگاریتمی‌بر نتایج ۳، ۷ و ۲۸ روزه سیمان IP

روز/روز	28/7	90/7	180/7	90/28	180/90
کسب شده	1.39	1.72	1.92	1.24	1.11

- پوزولان
سنگهای پوزولانی در اکثر نقاط ایران یافت می‌شوند؛ ولی در حال حاضر می‌توان به دیاتمیت ممقان آذرشهر، پامیس سبلان، توف‌های آتشفشانی تراس جاجرود، زئولیت میانه، توف آتشفشانی بستان آباد و تفتان و پامیس تفتان اشاره کرد. با توجه به اینکه پوزولان طبیعی تفتان نزدیکترین منبع به محل اجرای پروژه زیردان و کارخانه سیمان خاش می‌باشد در ادامه، مشخصات این پوزولان در جدول ۳ به تفصیل بیشتری آورده شده است.

جدول ۳: مشخصات پوزولان تفتان با الزامات استاندارد ASTM C618

ترکیبات شیمیایی	پوزولان تفتان	ASTM C618
SiO_2	۵۶–۵۹	
Al_2O_3	۱۷–۱۹	
Fe_2O_3	۵	
CaO	۵–۷	
MgO	۱/۲–۲	
Na_2O	۳/۵	
K_2O	۱/۳–۲	
L.O.I	۲–۵	حداکثر ۱۰ درصد
SO_3	۱,۷–۳	حداکثر ۴ درصد
$SiO_2+Al_2O_3+Fe_2O_3$	۷۸–۸۳	حداقل ۷۰ درصد

- تستهای آزمایشگاهی
فعالیتهای انجام شده در این آزمایشها، در واقع بخش اول آزمایشهای شناسایی مصالح و بتن غلتکی سد مخزنی زیردان بوده لذا مصالح سنگی استفاده شده در این آزمایشها همان مصالح محلی زیردان بوده و نیز از سیمان تیپ دو پوزولانی ویژه و پوزولان پودر شده تفتان، محصولات کارخانه سیمان خاش استفاده شده است.

در این مطالعات برای هر طرح بتن غلتکی سد زیردان، تعداد ۶ نمونه استوانه ای ۳۰*۱۵ تهیه شده است که پس از گذشت ۷ , ۲۸ و ۹۰ روز نگهداری در شرایط استاندارد آزمایشگاهی به منظور تعیین مقاومت فشاری زیر جک بتن شکن قرار گرفتند. میانگین مقاومت هر دو نمونه بعنوان نتیجه مورد بررسی قرار گرفت.

جدول ۴ مواد متشکله طرحهای اختلاط و نتایج آزمایش را نشان می‌دهد. در این طرحها از سیمان پوزولانی خاش (حاوی ۱۵٪ پوزولان) با افزودن مقداری گَرد پوزولان استفاده شده است.

- مقاومت فشاری ملات سیمان
برای آگاهی از میزان تأثیر پوزولان خاش بر افزایش مقاومت، یک سری آزمایش مقاومت فشاری ملات برای سیمان حاوی ۲۰، ۳۰، ۴۰ و ۵۰ درصد پوزولان مطابق ASTM C349 انجام گرفت. تعدادی از نمونه‌های ساخته شده و همچنین روش آزمایش در شکل ۲ ارائه شده است. همچنین نتایج اخذ شده درشکل ۳ ارائه شده است.

جدول ۴: مواد متشکله و نتایج آزمایشهای طرح اختلاط بتن غلتکی

شماره طرح اختلاط	مواد متشکله (kg/m3)				زمان ویبی (ثانیه)	مقاومت فشاری (kg/cm2)			وزن مخصوص (Kg/m3)
	سنگدانه	سیمان	پوزولان	آب		۷ روزه	۲۸ روزه	۹۰ روزه	
۱	۲۰۶۰	۱۳۶	۵۴	۱۲۰	۳۰	۳۵,۳	۳۳,۰	۳۵,۳	۲۳۵۰
۲	۲۰۴۰	۱۳۶	۵۴	۱۴۰	۲۰	۵۲,۶	۴۴,۴	۱۱۸,۲	۲۳۱۰
۳	۲۰۴۰	۱۵۳	۶۲	۱۴۰	۲۵	۳۹,۷	۷۷,۱	۱۵۳,۰	۲۴۳۰
۵	۱۹۸۰	۲۰۴	۳۶	۱۵۰	۲۰	۹۵,۳	۱۴۷,۷	۲۶۶,۶	۲۳۷۰
۶	۲۰۶۰	۱۶۲	۲۸	۱۲۰	۲۳	۷۳,۰	۱۲۴,۵	۱۵۵,۲	۲۳۱۰
۷	۲۰۶۰	۱۳۶	۵۴	۱۲۰	۲۸	۵۱,۱	۷۱,۲	۱۲۷,۳	۲۳۴۰

جدول ۵: ضرایب رشد طرحهای اختلاط بتن غلتکی

شماره طرح	نسبت پوزولان به مصالح سیمانی	ضریب رشد 28	ضریب رشد 90	کسب شده 28/7	کسب شده 90/7	کسب شده 90/28
1	39.2	0.17	0.19	0.93	1.00	1.07
2	39.2	0.23	0.62	0.84	2.25	2.66
3	39.5	0.36	0.71	1.94	3.85	1.98
5	27.8	0.62	1.11	1.55	2.80	1.81
6	27.5	0.66	0.82	1.71	2.13	1.25
7	39.2	0.37	0.67	1.39	2.49	1.79
	میانگین	0.40	0.69	1.39	2.42	1.76

شکل ۲- نمونه‌های منشوری برای تعیین مقاومت فشاری ملات سیمان

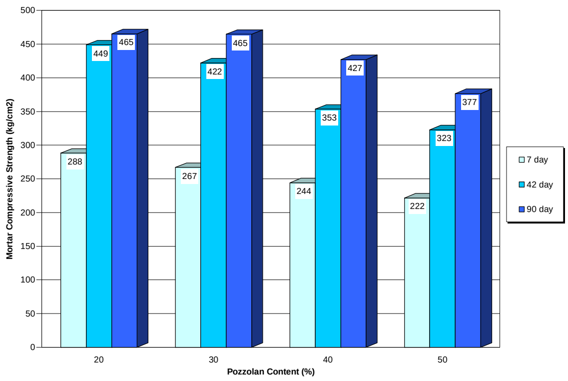

شکل ۳- نتایج مقاومت فشاری نمونه‌های ملات سیمان حاوی مقادیر مختلف پوزولان

در شکل ۴ منحنی‌های رشد لگاریتمی‌برای مقاومت فشاری ملاتهای حاوی ۲۰، ۳۰، ۴۰ و ۵۰ درصد پوزولان با زمان رسم شده است.

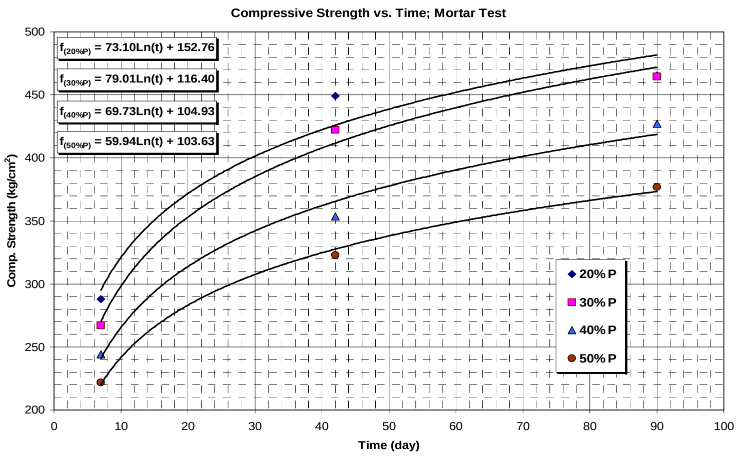

شکل ۴- برازش منحنیهای لگاریتمی‌بر نتایج ۷، ۴۲ و ۹۰ روزه

بر اساس معادلات حاصله از شکل ۴، می‌توان مقاومت فشاری ملات سیمان را بازای مقادیر مختلف پوزولان در سنین ۷، ۲۸، ۹۰ و ۱۸۰ روزه بدست آورد (جدول ۵).

جدول ۵: مقاومتهای محاسبه شده با برازش منحنیهای لگاریتمی‌بر نتایج ۷، ۴۲ و ۹۰ روزه

زمان(روز)	7	28	90	180
f(20%P)	295	396	482	532
f(30%P)	270	380	472	527
f(40%P)	241	337	419	467
f(50%P)	220	303	373	415

با توجه به جدول ۵ ضرایب رشد مقاومت به شرح جدول ۶ بدست آورده می‌شود. میانگین خطی ضرایب رشد در سطر پایینی جدول ۶ محاسبه شده است.

جدول ۶: ضرایب رشد محاسبه شده با برازش منحنیهای لگاریتمی‌بر نتایج ۷، ۴۲ و ۹۰ روزه

میزان پوزولان (%)	28/7	90/7	180/7	90/28	180/90
20	1.344	1.633	1.805	1.215	1.105
30	1.405	1.747	1.950	1.243	1.116
40	1.402	1.740	1.941	1.241	1.115
50	1.377	1.695	1.884	1.231	1.111
میانگین	1.38	1.70	1.89	1.23	1.11

اگر این ضرایب رشد را بر روی نموداری مانند شکل ۵، شامل منحنی‌های درجه سه با ضریب رگرسیون ۱ پیاده شوند، مشاهده می‌شود که بیشترین ضریب رشد در نسبت وزنی ۳۳٫۸ درصد پوزولان حاصل می‌شود؛ یعنی با

فرضِ داشتن مخلوطهای با مقاومت ۷ روزه یکسان، مخلوط حاوی ۳۳٫۸ درصد پوزولان بیشترین افزایش مقاومت را در سنین بالاتر خواهد داشت. بازای مقدار پوزولان بهینه، ضرایب رشد ماکزیمم ۲۸ به ۷، ۹۰ به ۷ و ۱۸۰ بـه ۷ روزه به ترتیب عبارت خواهند بود از ۱٫۴۱، ۱٫۷۵ و ۱٫۹۶

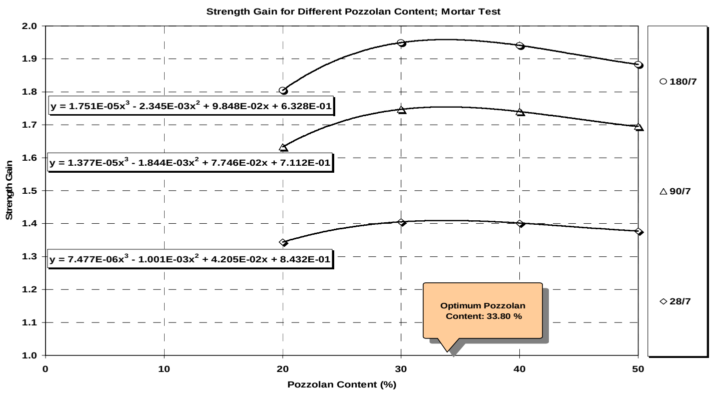

شکل ۵- تعیین درصد پوزولان بهینه با برازش منحنیهای درجه ۳ بر ضرایب رشد

- آزمایشهای مقدماتی طرحهای اختلاط بتن غلتکی

در این مرحله برای هر مخلوط علاوه بر نمونه‌های ۷ و ۲۸ روزه، نمونه‌های ۹۰ روزه نیز ساخته شد تـا بـر اسـاس آنها روند رشد مقاومت دانسته شود. در شکل ۶ مقاومتهای ۹۰ روزه در مقابل مقاومتهـای ۲۸ روزه – بـه تفکیـک برای مخلوطهای حاوی ۲۵ درصد و ۳۵ درصد پوزولان – رسم شده اند. همانگونه که می‌بینید منحنی‌هـای رشـد مقاومت از همبستگی خوبی برخوردارند.

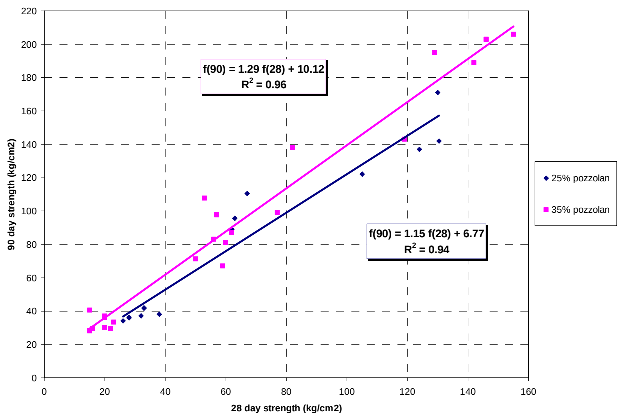

شکل ۶- رابطه بین مقاومت ۹۰ روزه مخلوطهای بتن غلتکی با مقاومت فشاری ۲۸ روزه آنها

بالاتر بودن خط مربوط به پوزولان ۳۵ درصد نسبت به پوزولان ۲۵ درصد در شکل ۶ به معنای آنست کـه بـرای دو مخلوط با مقاومت ۲۸ روزه یکسان، پوزولان ۳۵ درصد باعث افزایش مقاومت بیشتری در سن ۹۰ روزه نـسبت

به پوزولان ۲۵ درصد خواهد شد؛ یعنی مقدار پوزولان فعال، عددی بیش از ۲۵ درصـد مـی‌باشـد. شـکل ۶، رونـد کسب مقاومت ۲۸ تا ۹۰ روزه را بصورت تابعی از مقاومت ۲۸ روزه نشان می‌دهد.

- آزمایشات تکمیلی طرحهای اختلاط بتن غلتکی

در این مرحله مجموعاً ۱۶ طرح اختلاط بتن غلتکی کار شده است. نتایج ۷، ۲۸، ۹۰ و ۱۸۰ روزه همـه طرحهـا در جدول ۷ ارائه گردیده است. مقادیر محاسبه شده در سطر آخر جدول ۷، میانگین ضرایب رشد طرحهای حـاوی ۲۵ و ۳۰ درصد پوزولان است. مقدار متوسط ضریب رشد ۹۰ بـه ۲۸ روزه بـرای طرحهـای حـاوی ۲۵ تـا ۳۰ درصـد پوزولان برابر۱٫۱۹ و ۱۸۰ به ۹۰ روزه برابر ۱٫۱۰ است.

در شکل ۷ منحنیهای آب به سیمان و مقاومت فشاری ۷، ۲۸، ۹۰ و ۱۸۰ روزه، بـرای طرحهـای حـاوی ۲۵ و ۳۰ درصد پوزولان رسم شده است. همانطور که دیده می‌شود در سنین بالاتر، ضرایب رگرسیون منحنیها بیـشتر شـده که این نشان از عملکرد پوزولان در دراز مدت و جبرانِ ضعفهای احتمالی موجود در ریز ساختار بتن غلتکی دارد.

جدول ۷: نتایج طرحهای بتن غلتکی و ضرایب رشد مربوطه

نام طرح	نسبت آب به مصالح سیمانی	زمان ویبی	مقاومت فشاری(kg/cm2)				مقاومت کسب شده				
	وزنی	ثانیه	7	28	90	180	28/7	90/7	180/7	90/28	180/90
R170-20-02	0.70	14	116.8	154.5	173.7	193.2	1.32	1.49	1.65	1.12	1.11
R170-20-03	0.69	30	111.8	156.5	176.0	197.1	1.40	1.57	1.76	1.12	1.12
R190-20-01	0.60	30	128.1	173.9	208.0	230.5	1.36	1.62	1.80	1.20	1.11
R190-20-02	0.63	25	146.0	186.3	212.9	224.5	1.28	1.46	1.54	1.14	1.05
R150-20-01	0.84	20	90.7	124.5	143.7	155.7	1.37	1.59	1.72	1.15	1.08
R150-20-02	0.76	28	93.1	125.1	145.9	158.5	1.34	1.57	1.70	1.17	1.09
R150-20-03	0.76	26	99.1	140.1	152.1	174.2	1.41	1.53	1.76	1.09	1.15
R208-47-01	0.67	10	91.4	125.7	150.4	189.9	1.38	1.64	2.08	1.20	1.26
R210-38-01	0.61	12	126.0	171.0	178.6	202.9	1.36	1.42	1.61	1.04	1.14
R150-20-04	0.83	16	105.3	115.2	150.2	161.2	1.09	1.43	1.53	1.30	1.07
R195-47-01	0.61	15	114.1	115.8	163.9	167.5	1.02	1.44	1.47	1.41	1.02
R195-43-01	0.67	15	84.3	105.7	168.6	175.3	1.25	2.00	2.08	1.60	1.04
R170-20-04	0.74	25	109.6	118.4	162.6	186.9	1.08	1.48	1.71	1.37	1.15
R200-30-01	0.56	∞	174.7	208.3	259.6	275.8	1.19	1.49	1.58	1.25	1.06
میانگین							1.29	1.52	1.67	1.19	1.10

۴- بحث

این تحقیق جهت صحه گذاردن بر عملکرد پوزولان خاش در افزایش مقاومت از ۲۸ روز به ۹۰ یا ۱۸۰ روز بوده و این موضوع زمانی کارکرد دارد که بخواهیم با ثابت نگاهداشتن سنین مقاومت مشخصه، از مقدارسـیمان کاسـته و به انتظار مقاومت دراز مدت پوزولان بنشینیم. یک مقایسه انجام گرفته در خصوص مقاومت فشاری و هزینه تولید بتن دلالت براین موضوع دارد که افزودن پوزولانها به سیمان منجـر بـه اقتـصادی شـدن طـرح و اثـرات زیـست محیطی در ارتباط با روشهای تولید سیمان دارد[18].

این بحث متفاوت از آنست که بخواهیم سنین مقاومت مشخصه را افزایش دهیم چرا که در صورت افزایش سنین مقاومت مشخصه در سنین تعیین شده باید به مقاومت مورد نظر دست پیدا کنیم و در این میان دیگر جـایی بـرای حدس و گمان باقی نخواهد ماند.

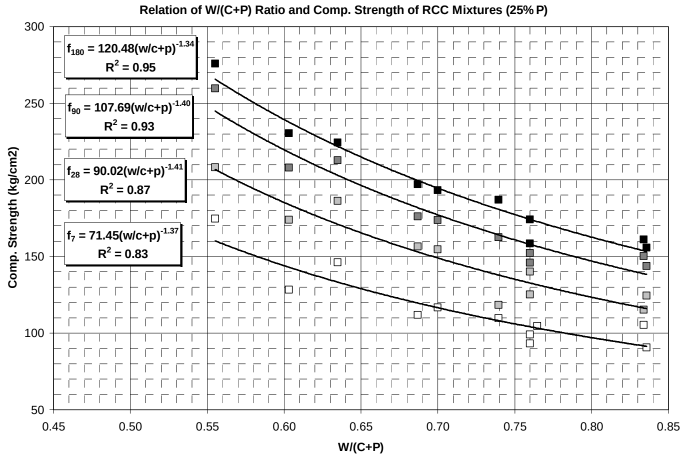

شکل ۷- روابط آب به سیمان و مقاومت فشاری ۷، ۲۸، ۹۰ و ۱۸۰ روزه طرحهای بتن غلتکی

همچنین با تغییر مقاومت مشخصه بتنهای RCC قادر خواهیم بود مقدار سیمان مصرفی در هر متر مکعب را کاهش داده و از پتانسیل افزایش مقاومت پوزولان در دراز مدت بهره مند شویم. در مقایسه با بتن بدون پوزولان، بتن‌های سرباره‌ای یا دارای خاکستر بادی با کلسیم کم، معمولا مقاومت‌های کمتری را در سنین یک و سه روزه نشان داده، ولی در عوض کسب مقاومت پس از هفت روز عمل آوری قابل توجه خواهد بود.[15]مخلوط‌های بتن غلتکی ساخته شده همراه با خاکستر بادی نیز نشان دهنده رشد مقاومتی مناسبی در سنین مختلف جز در سنین ۳ و ۷ روزه از خود نشان داده اند[17]. که‌این موضوع درتحقیق به عمل آمده به وضوح قابل مشاهده بود.

با توجه به‌اینکه استفاده از پوزولان برای کنترل واکنشهای مضر قلیاییِ مصالح منطقه سد زیردان لازم است، اما کاربرد پوزولان بعنوان جایگزین (Replacement) سیمان و برای کاستن از حرارت هیدراسیون و کنترل مسائل حرارتی است و این در صورتی محقق می‌شود که به اثر افزایشی پوزولان بر مقاومتِ دراز مدت آن تکیه کنیم

با توجه به مطالب فوق می‌توان مطالب را به صورت زیر خلاصه نمود:

۱) یکی ازمهمترین خاصیت‌های موجود در بتن پوزولانی افزایش مقاومت دراز مدت آنها است.
۲) کاهش حرارت هیدراسیون می‌تواند احتمال پیدایش ترکهای حرارتی در بتن ریزی قطعات حجیم را کاهش دهد.
۳) یکی از خرابی‌های عمده در سدها، واکنش قلیایی سنگدانه‌هاست. با کاربرد پوزولانها می‌توان تا حدود زیادی واکنش مذکور را تحت کنترل درآورد.
۴) مزیت اقتصادی استفاده از پوزولان، در اکثر موارد قیمت کمتر آن در مقایسه با سیمان است.
۵) درصد بهینه پوزولانها بایستی با توجه به امکانات کارگاه و ملاحظات فنی تعیین گردد. البته با توجه به شرایط گرم آب وهوایی مناطق جنوب‌ایران و رواداریهای زیاد کارگاهی، استفاده از پوزولان با عیار بالا توصیه می‌شود.
۶) استفاده از پوزولانها در بتن هم اقتصادی و هم منجر به اصلاح خصوصیات بتن تازه و سخت شده می‌شود [16] که در آزمایشات انجام گرفته نیز بهبود و رشد خصوصیات بتن غلتکی از جمله

درکارپذیری، مقاومت فشاری، مقاومت سایشی و مسایل حرارتی و جمع شدگی مشاهده شد.

تشکر وقدردانی

بدینوسیله ازمهندس محسن جعفربیگلو و تکنسینهای آزمایشگاه بتن شرکت جهان کوثر (پیمانکار سد زیردان) که در کلیه مراحل ساخت مخلوطهای بتن و انجام آزمایشها، صمیمانه همکاری فراوانی را مبذول داشته اند سپاسگزاری و قدردانی می‌شود.

مراجع

۱- گزارش فنی مهندسین مشاور آبفن و پژوهاب ۱۳۷۷.

۲- دکتر علی اکبر رمضانیانپورومهندس محمدرضا اخلاصی-بررسی ومقایسه مقاومت به سایش بتن‌های مختلف،مجموعه مقالات پنجمین کنفرانس بین المللی عمران-۱۳۷۹-ایران.

۳- دکتر علی اکبر رمضانیانپورومهندس منصور پیدایش،بتن ونقش سیمانهای پوزولانی،نشریه ۲۷۴ مرکز تحقیقات ساختمان ومسکن.

4- ASTM C595 ” Standard Specification for Blended Hydraulic Cements”.

5- Roller–Compacted Concrete on Dams Workshop –IRCOLD – (Tehran–IRAN)– June 21 -2007.

6- V.M.Malhotra,"Supplementary cementing materials for concrete",CANMET,Canada.

7- ASTM C618 ” Standard Specification for Coal Fly Ash and Raw or Calcined Natural Pozzolan for Use as a Mineral Admixture in Concrete”

8- ICOLD Bulletin:State-of-the-art if RCC dams,Version 4.0,September, 2000.

9- Valenta 0. 10th international conference on large dams, Montreal, (1970)103-117.

10- Ghassemi H, MSc. Thesis, University of Tehran, (2002), 215p.

11- Dasmeh A., Fakher A. Shekarchi M. and Gharavi, International Journal of Hydropower and Dam, 7, (2000) 60-63.

12- Dasmeh A., Fakher A., and Shekarchi M., Seventh CANMENT/ACI international conference on fly ash, silica fume, slag and natural pozzolan in concrete, (2001) 341-356.

13- Ayers M.E. and Khan M.S. The need for rational curing standards. Concrete Technology, SP 144-29, (1996) 605-622.

14- Shekarchi M., Debicki G., Clastres P., and Billard Y. 6th CANMET, ACI International Conference on Fly Ash, Silica Fume, Slag and Natural Pozzolan in Concrete, Bangkok, Thailand, (1998) 975-996.

15- V.G.Papadakis,S.Tsimas,"Supplementary cementing materials in concrete".2002 elsevier Science.

16- per-wei Gao,"The characteristics of air voids and frost resistance of RCC with fly ash and expansive agent" 2005 Elsevier science.

17- C.D. Atis, U.K. Svin, O. Karahan, "Strengh properties of roller compacted concrete contaning a non-standard high calcium fly ash"2003 Elsevier Science.

18- Ilker Bekir Topcu, Cenk Karakurt, Mustafa Sarıdemir," Predicting the strength development of cements produced with differentpozzolans by neural network and fuzzy logic"2008 Elsevier science.

CD02

Concrete Structures Analysis and Design

CD02-001

PUSHOVER ANALYSIS OF ASYMMETRIC ORDINARY MOMENT R.C FRAMES DESIGNED ACCORDING TO THE IRANIAN CODES

T. Mahdi[1] and H. A. Darehshiri[2]
[1]Assistance professor, Building and Housing Research Centre, Tehran, Iran
[2]Lecturer, Azad University, Ardekan, Iran

ABSTRACT
In this paper, the nonlinear seismic behavior of three ordinary moment-resisting concrete space frames with unsymmetrical plan in three, four and five stories are evaluated using pushover analysis. The three buildings were originally designed according to existing Iranian codes. Seismic loads are calculated and distributed over the height of the frame using both rectangular and triangular forms. It has been found that the obtained capacity curves have been affected greatly by the forms of loading. Results have been also produced in form of story drifts to establish the performance level of these buildings. The results show that all of the frames in both directions are within the life safety performance level.

Keywords: pushover, concrete frame, Seismic assessment, irregularity, design codes

1. INTRODUCTION

Experience shows that buildings with irregularities are prone to earthquake damage, as observed in many earthquakes in the past. Despite structural regularity is quite easy to obtain through a careful design; it is very common that, in the reality, different irregularities can occur, changing the seismic performance of the building. However, current codes fail to provide acceptable definition of an irregular structure. Moreover, most of the seismic codes fall short of providing sufficient specifications for designing irregular buildings. As an example, the ASCE/SEI 7-05 standard [1] defines five types of horizontal structural irregularities. One type of irregularity is reentrant corner irregularity, and this irregularity is considered to exist where both plan projections of the structure beyond a reentrant corner are greater than 15% of the plan dimension of the structure in the given direction. In the ASCE/SEI 7-05 standard [1], additional provisions are given to increase the design forces for connections of diaphragms to vertical elements and to collectors and for connections of collectors to the vertical elements. Although such provisions are not adequate to take care of all the stresses concentrated at different points of the buildings, the Iranian Code of Practice [2] has not provided similar provisions. Furthermore, the Iranian Code of Practice for Seismic Resistant [2] has given more relaxed regulations for such irregularity by specification projections of more than 25% of the plan dimension in the given direction. Accordingly, there is an apparent need to develop a more accurate analysis procedure to provide information on the seismic response of irregular structures. In this paper, an introductory investigation on the effect of such irregularities on the total behavior of the buildings is carried out.

In this paper; and as shown in Figure 1, reinforced concrete frames having plan projections between 33 to 50% are examined. These buildings have been designed according to the current Iranian codes of practice [2, 3]. However, and to examine the validity of these practices and evaluate the real strength of these structures, a performance based design need to be carried out. To meet this requirement, static pushover analysis is used to investigate the effect of such irregularities on the total behavior of the buildings.

The recent advents of performance based design show that an inelastic procedure commonly referred to as the pushover analysis is a viable method to assess damage vulnerability of buildings [4, 5]. This procedure is a static, nonlinear one in which the magnitude of the structural loading is incrementally increased in accordance with certain predefined patterns. With the increase in the magnitude of the loading, weak links and failure modes of the structure are found. The loading is monotonic with the effects of the cyclic behavior and load reversals being estimated by using a modified monotonic force-deformation criteria and with damping approximations. The present pushover analysis has been carried out using the "SAP2000" software [6]. The method used by this software is based on procedure C given in ATC-40 [7].

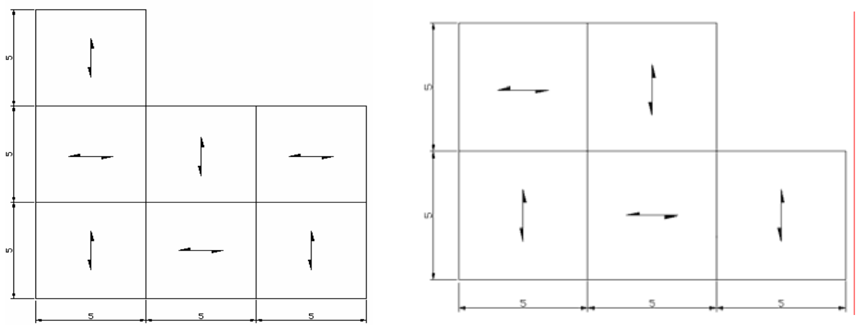

(a) (b)

Figure 1. Plan view of the building structure (a) a 3-story building (b) 4 and 5- story buildings

In most studies, the method was applied to symmetrical structures. Assuming the floors act as rigid diaphragms, the state of damage of the building can be inferred from applying a two dimensional pushover analysis on the building. The advantages and the limitations of this analysis for damage assessment are described by Lawson et al. [8]. Usually, the presence of an asymmetry in a given structure makes the pushover analysis rather complicated, since floor displacements of the building will consist of both translational and rotational components. The lateral load resisting elements located at different positions in plan will experience different deformations. Torsional effect can be particularly damaging to elements located at or near the flexible edge of the building where the translational and

rotational components of the floor displacement are additive.
In the last few years several proposals have been put forward to extend traditional pushover analysis to the assessment of three-dimensional models. Among the early ones is that of Moghadam and Tso [9, 10]. It has been based on the study of the non-linear static behavior of the critical frames only, identified by means of LDP analyses performed on three-dimensional models. Other attempts to extend and verify 3D pushover algorithms can be found in references [11-13]. Furthermore, Fajfar et al. [14-16] extended the N2 method to three-dimensional structures. On the other hand, Chopra and Goel [17] have presented an extension of the MPA (Modal Pushover Analysis) procedure for asymmetric-plan structures.

2. SAMPLE STRUCTURES

In this paper, the nonlinear seismic behavior of three ordinary moment-resisting concrete space frames with unsymmetrical plan in three, four and five stories are evaluated. The plan configurations of these space frames contain reentrant corners. To compare the nonlinear response of structures differently involved in the inelastic range of behavior, each building was designed according to the rules proposed by the Iranian Code of Practice [2], for low ductility structures. However in all these cases, the masses of the floors are less than 5% from the corresponding centers of rigidity of the floors in both perpendicular directions.
Using the Iranian Code of Practice for Seismic Resistant [2], the design was performed with reference to the importance category II, assuming peak ground acceleration equal to 0.25 *g* and parameters shaping a soil profile II spectrum. According to the code provisions the strength level of the structures was defined by assuming an R-factor equal to 5.00 for the low ductility (LD) buildings, and consistently with the supposed importance category, an importance factor equal to 1.0 was assumed.
The floors were considered to be subjected to dead loads equal to 620 kg/m^2 (due to self weight, finishes and permanent partitions) and to live loads equal to 200 kg/m^2. Moreover, claddings weighting 500 kg/m were considered to be present along the external perimeter of buildings and parapets weighting 200 kg/m were considered to be present along the external perimeter of the roof. Design lateral forces are given in Table-1.

Table 1: Design lateral forces

Buildings	Loads (ton)
3-story	52.1
4-story	51.7
5-story	65.1

The three gravity (vertical) loads used in this paper are as follows:

$$GR_1 = 1.1\ (Q_D + Q_L) \tag{1}$$

$$GR_2 = 0.9\ Q_D \tag{2}$$

$$GR_3 = Q_D + 0.2\ Q_L \tag{3}$$

In Equations (1-3), Q_D is the total dead loads and Q_L is the total live loads.
For lateral seismic loads, the analysis was performed by assuming two types of lateral loads distributions. First by assuming a triangular distributions similar to that obtained by the equivalent static analysis method, and second by assuming rectangular distributions proportional to the weight of the floor. Combining these loads with the three vertical loads defined in Equations 1 to 3, buildings were tested under the effect of twenty four different combinations. These are as follows:

(a) PX1 and –PX1 triangular distributions of lateral forces + GR_1
(b) PX2 and –PX2 triangular distributions of lateral forces + GR2
(c) PX3 and –PX3 triangular distributions of lateral forces + GR3
(d) PY1 and –PY1 triangular distributions of lateral forces + GR1
(e) PY2 and –PY2 triangular distributions of lateral forces + GR2
(f) PY3 and –PY3 triangular distributions of lateral forces + GR3
(g) FX1 and –FX1 rectangular distributions of lateral forces + GR1
(h) FX2 and –FX2 rectangular distributions of lateral forces + GR2
(i) FX3 and –FX3 rectangular distributions of lateral forces + GR3
(j) FY1 and –FY1 rectangular distributions of lateral forces + GR1
(k) FY2 and –FY2 rectangular distributions of lateral forces + GR2
(l) FY3 and –FY3 rectangular distributions of lateral forces + GR3

Each of the Frames considered has uniform storey height of 3m. The strength of the beams and columns in the frame are allocated following the "strong column-weak beam" capacity design procedure. All members of the frame have been designed according to the Iranian Concrete Code of Practice [3]. All columns have square cross-section of 300*300 mm. at the upper two stories and 350*350 mm. at the third storey and 400*400 mm for the first and second stories. The required different strength levels in columns were also obtained by varying the amount of reinforcement. All the beams have rectangular cross-section 0f 200*300 mm. Table 2 contains detail of column and beam cross-sections and reinforcements. All members were detailed considering a normal weight concrete with compressive strength of 250 kg/cm^2 and steel having yield strength equal to 4000 kg/cm^2.

Table 2: Columns and beams cross-sections

Buildings		**3-storey**	**4-storey**	**5-storey**
Columns (dimensions in cm.)	First Floor	B= 35 8 Φ20	B= 40 12 Φ 20	B= 40 16 Φ 20
	Second Floor	B= 30 8 Φ 20	B= 35 8 Φ 20	B= 40 12 Φ 20
	Third Floor	B= 30 8 Φ 20	B= 30 8 Φ 20	B= 35 8 Φ 20
	Fourth Floor	-	B= 30 8 Φ 20	B= 30 8 Φ 20
	Fifth Floor	-	-	B= 30 8 Φ 20
Beams (dimensions in cm.)	All	b= 20 h=30	b=20 h=30	b=20 h=30

3. RESULTS

3.1. Global Yield Criteria

Since the yield point is not clear in the plot of base shear versus top displacement, an idealized elasto-plastic system was assumed to find the approximated yield point in the global response of the structure. Yield displacement is based on the idealized elasto-plastic system with reduced stiffness which is evaluated as the secant stiffness at 75% of the ultimate strength.

A sample of the displacements corresponding to the yield points for different vertical and lateral loads for the 5-story is given in Table 3. Same calculations are repeated for pushover curves in the negative direction and the results are similar to those given in Table 3.

Table 3: Displacements (cm.) corresponding to the yield points for different loads

Loads	F_x	P_x	F_y	P_y
GR1	17	17	18	18
GR2	17	17	18	18
GR3	17	17	18	18

3.2. Performance Curves

To obtain the capacity curve, seismic loads are calculated and distributed over the height of the frame using both rectangular and triangular forms. Some examples of the resulting capacity curves for the three buildings are shown in Figure (2). All curves show similar features. They are linear initially but start to deviate from linearity when inelastic actions start to take place. With the increase of displacements, the capacity curves become linear, but with much smaller slopes that sometimes approaching flat shapes. Furthermore, it can be concluded that the curves obtained for all the three gravity loads are approximately similar to each other while they are more sensitive to the type of lateral loads, as shown in Figure (3).

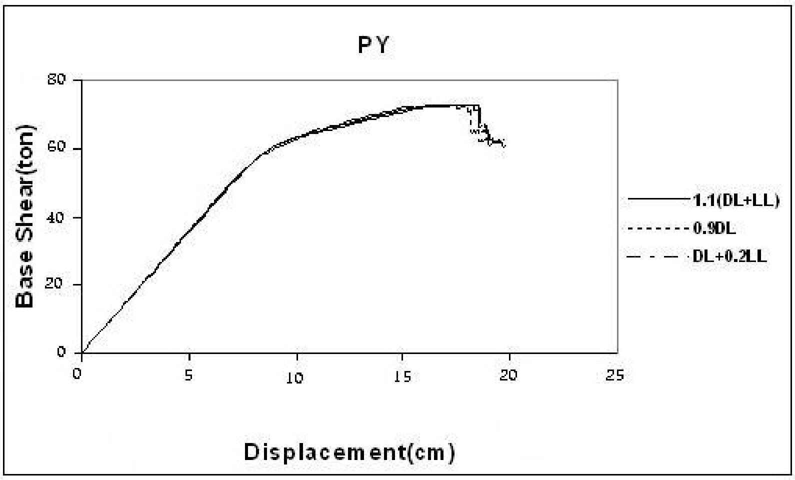

(a)

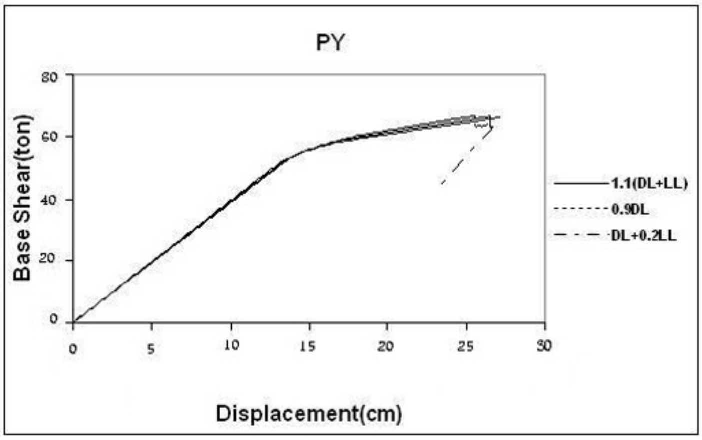

(b)

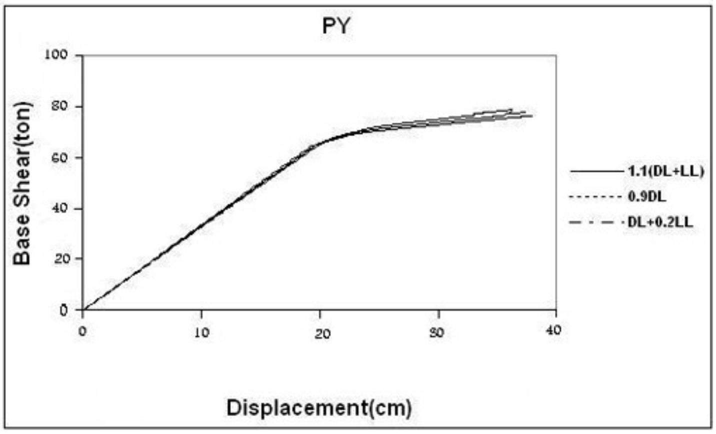

(c)

Figure 2. The performance curves for (a) 3-story building (b) 4-story building (c) 5-story building

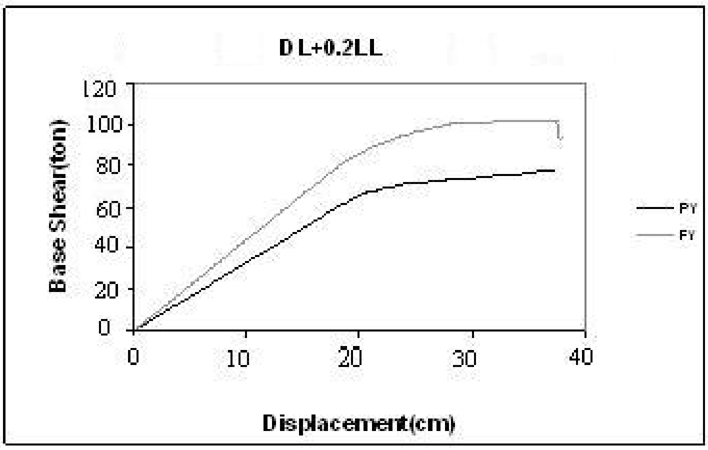

Figure 3. The performance curves for 5-story building for GR3

3.3. The Performance Point

The performance point for a given set of values is defined by the intersection of the capacity curve and the single demand spectrum curve. Results for the 5-Story buildings are given in Tables 4 and 5.

Table 4: Performance points for the 5-story buildings for a fixed gravity load and different lateral loads in the (x) and (-x) directions

Lateral Loads	Displacements at the Performance Point (cm)	Forces at the Performance Point (ton)	Lateral Loads	Displacements at the Performance Point (cm)	Forces at the Performance Point (ton)
PX_1	19.73	69.29	$-PX_1$	-19.87	-69.27
PX_2	19.34	68.23	$-PX_2$	-19.46	-68.26
PX_3	19.53	68.84	$-PX_3$	-19.67	-68.80
FX_1	17.73	84.57	$-FX_1$	-17.87	-84.54
FX_2	17.32	83.78	$-FX_2$	-17.44	-83.83
FX_3	17.33	83.50	$-FX_3$	-17.67	-84.20

Table 5: Performance points for the 5-story buildings for a fixed gravity load and different lateral loads in the (y) and (-y) directions

Lateral Loads	Displacements at the Performance Point (cm)	Forces at the Performance Point (ton)	Lateral Loads	Displacements at the Performance Point (cm)	Forces at the Performance Point (ton)
PY_1	20.97	66.98	$-PY_1$	-21.03	-66.98
PY_2	20.58	66.89	$-PY_2$	-20.62	-66.13
PY_3	20.77	67.00	$-PY_3$	-20.83	-66.97
FY_1	18.77	81.23	$-FY_1$	-18.83	-81.24
FY_2	18.37	81.27	$-FY_2$	-18.37	-81.27
FY_3	18.57	81.25	$-FY_3$	-18.63	-81.25

3.4. Maximum Displacement

Considering the maximum roof displacement of the buildings, the results obtained denote that all of the frames in both directions are within the life safety performance level.

3.5. Inter-Story Drift

On the structure level, the inter-story drift ratio (ID) is one of the simplest and most commonly used damage indicators. Similar comparisons are carried out on the prediction of the maximum inter-storey drift ratios. Samples of the results are presented in Figure (4). In this figure, inter-storey drift ratios are compared to the limit values subscribed by FEMA 356 [18] for the life safety and immediate occupancy performance levels.

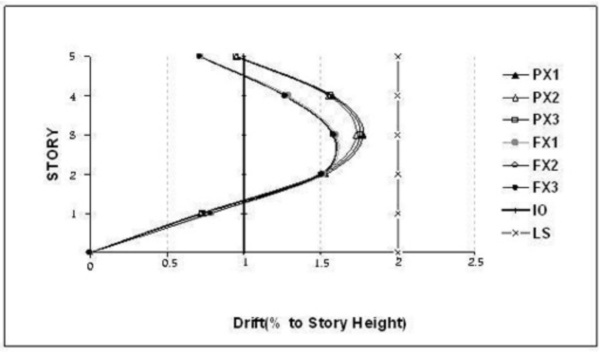

(a)

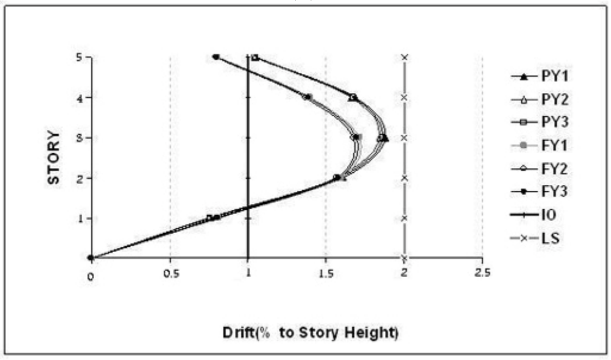

(b)

Figure 4. Performance of 5-story RC frame based on maximum inter-storey drifts ratios X-direction (b) Y-direction

3.5. Plastic Hinge Formation

The damage state of the structure at the peak base shear for the 3-story building is given in Figure 5. For more details on the formation of plastic hinges at different performance level is given in Reference [19].

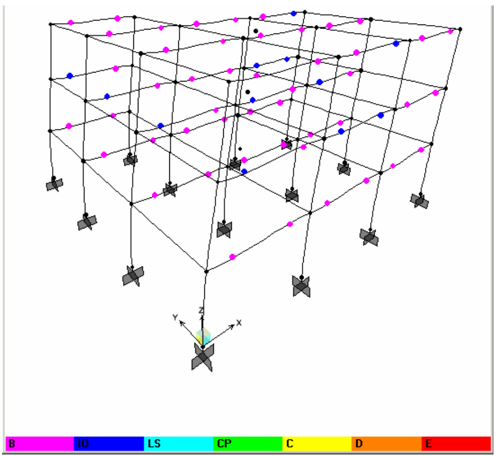

Figure 5. Plastic hinges in the 3-story building under PX_1

4. SUMMARY AND CONCLUSIONS

Since current codes fall short of providing simplified analytical tools for irregular structures, it is necessary to use an analytical procedure that can describe the seismic response of such buildings. The present paper utilizes the pushover analysis; a procedure based on "the capacity curve" concept, to investigate irregular buildings. The results obtained show that:

(a) Performance curves obtained for all the three gravity loads, for a given lateral load, are approximately the same while they show more sensitivity to the type of lateral loads.
(b) Irregularities similar to that investigated in the present paper have little influence on the total behavior of the building.
(c) The results obtained denote that all of the frames in both directions are within the life safety performance level. It can be concluded that using Iranian codes to design irregular reinforced concrete frames of three to five stories is acceptable for providing life safety performance level.
(d) Comparing the formation of plastic hinges in the three buildings, the 5-story building has shown better performance than the other two.

However, given the preliminary nature of this study, additional work considering different 3D buildings need to be carried out before any definitive conclusions and recommendations might be made.

REFERENCES

1. ASCE, Minimum Design Loads for Buildings and Other Structures, ASCE Standard ASCE/SEI 7-05, American Society of Civil Engineers, Reston, Virginia, 2006.
2. BHRC, Iranian Code of Practice for Seismic Resistant Design of Buildings, BHRC publication No. S347, Tehran, 1999.
3. MPO, The Iranian Concrete Code of Practice, MPO publication No. 130, Fourth printing, Tehran, 2004, (in Persian).
4. ATC, Guidelines and Commentary for Seismic Rehabilitation of Buildings, Applied Technology Council, Report No. ATC-33.03; Redwood City, California, 1995.
5. SEAOC, Vision 2000 - A Framework for Performance Based Design, Volumes I, II, III., Structural Engineers Association of California, Vision 2000 Committee, Sacramento, California, 1995.
6. Wilson, E. L., Three Dimensional Static and Dynamic Analysis of Structures, Computers and Structures Inc., Berkeley, California, 2000.
7. ATC, Seismic Evaluation and Retrofit of Concrete Buildings, Volume 1, ATC-40, Report, Applied Technology Council, Redwood City, California, 1996.
8. Lawson, R.S, Vance, V., and Krawinkler, H., Nonlinear Static Pushover Analysis Why, When and How? Proc. of the 5th U.S. National Conf. on Earthquake Engineering, Chicago, Illinois, Vol.1, pp. 283-292, 1994.
9. Moghadam, A. S. and Tso, W. K., Damage Assessment of Eccentric

Multistory Buildings using 3-D Pushover Analysis, Proc. of the 11th World Conf. on Earthquake Engineering, Mexico, paper 997 , 1996.

10. Moghadam A. S., Tso K., Pushover Analysis for Asymmetric and Set-Back Multi-Storey Buildings, Proc. of the 12th World Conference on Earthquake Engineering, Auckland, New Zealand, paper 1093, 2000.
11. Kilar, V. and Fafjar, P., Simple Push-Over Analysis of Asymmetric Building, Earthquake Engineering and Structural Dynamics, 26, pp. 233-249, 1997.
12. Faella, G. and Kilar, V., Asymmetric Multistory R/C Frame Structures: Push-Over Versus Nonlinear Dynamic Analysis, Proc. of the 11th European Conf. on Earthquake Engineering, 1998.
13. Ayala A. G., Tavera E. A., A New Approach for the Evaluation of the Seismic Performance of Asymmetric Buildings, Proc. of the 7th National Conference on Earthquake Engineering, Boston, 2002.
14. Fajfar P., Structural Analysis in Earthquake Engineering-A Breakthrough of Simplified Nonlinear Methods, Proc. of the 12th European Conf. on Earthquake Engineering, London, UK., Keynote paper, 2002.
15. Fajfar, P., Marusic, D. and Perus, I., Torsional Effects in the Pushover-Based Seismic Analysis of Buildings, Journal of Earthquake Engineering, 2005, Vol. 9, No. 6, pp. 831-854.
16. Fajfar P., Dolsek M., Marusic D., Stratan A., Pre- and Post-Test Mathematical Modelling of a Plan-Asymmetric Reinforced Concrete Frame Building, Earthquake Engineering and Structural Dynamics, 2006, Vol. 35, No. 11,pp. 1359-1379.
17. Chopra A. K., Goel R. K. A Modal Pushover Analysis Procedure to Estimate Seismic Demands for Unsymmetric-Plan Buildings, Earthquake Engineering and Structural Dynamics, 2004, Vol. 33, No.8, pp 903-927.
18. ASCE, Prestandard and Commentary for the Seismic Rehabilitation of Buildings - FEMA356, American Society of Civil Engineers, Reston, Virginia, 2000.
19. Darehshiri, H. A., (2007), "Seismic Evaluation of Ordinary Reinforced Concrete Buildings with Unsymmetrical Plan Based on Iran's Design Codes", M. Sc. Thesis, University of Yazd, Iran (in Persian).

CD02-002

DESIGN OF MASONRY INFILLED REINFORCED CONCRETE FRAMES IN DIFFERENT SEISMIC CODES

T. Mahdi[1] and M. Khorramiazar[2]
[1]Assistant Professor, Building and Housing Research Centre, Tehran, Iran
[2]Expert, Building and Housing Research Centre, Tehran, Iran

ABSTRACT

Masonry infilled reinforced concrete frames are among the most widely used types of buildings in Iran. In the past, masonry infill walls have often been treated as nonstructural elements in buildings, and their effects are not included in the analysis and design procedure. Furthermore, the interaction between infill and frame is usually ignored in the design procedure. Past experience has shown that infill walls have significant positive or negative effects on the global behavior of buildings and, therefore, should be addressed appropriately. This paper reviews and compares analysis and design provisions of this system in various seismic design codes and identifies the most important issues that are related to it. Stiffness, strength, natural period, response reduction factor, irregularities, and effect of openings are among the items discussed in this paper.

Keywords: infill, concrete frame, seismic design, design codes, masonry

1. INTRODUCTION

Unreinforced masonry (URM) infill panels are widely used throughout the world, including seismically active regions. They are usually used as interior partitions and external walls in concrete frames, but they are treated as nonstructural elements and not included in the analysis and design procedure. Such a simplified design approach does not predict the level at which the damage in the infill panel occurs, on the other hand it does not consider the global and local effects of having these stiff and brittle elements coupled with the primary lateral load-resisting system [1]. However, and contrary to common practice, field experience and experimental investigations [1-4] show that infill walls, if effectively confined by the frame, are remarkable in increasing the initial stiffness, strength and energy dissipation of RC (reinforced concrete) frames, especially if the structural system itself has little engineered earthquake resistance.

Typically, MI (masonry infill) walls are made of brittle materials that lose capacity in a rapid manner. Accordingly, the combined effect of brittleness and high stiffness has a negative implication on the seismic performance of the bounding frames. In particular, loss of integrity of the infills in the ground storey may produce a soft storey and trigger global collapse [5]. Furthermore, if infills are non-uniformly distributed in planes or in elevation, inelastic deformation demands will concentrate in the part of the building which has more sparse infills (i.e., to the

"flexible" side of a building asymmetrically infilled in plan, or to the "weak" or "soft" storey of the infilled frame) [5]. Generally, improper arrangement of infill walls causes a significant increase in the demand forces on the diaphragm and collector elements (adjacent beams and columns) that results in brittle shear failures, short column phenomena, and torsional response to the translational horizontal components of the seismic action. In such cases, both the frame and the floor system should be adequately designed for such increase in the demand forces.
From the structural point of view, the structural response of infilled frames depends on numerous parameters. Overall geometry of infills, dimensions of concrete members, the variability of mechanical properties of infill and concrete members, reinforcement conFigure urations, the relative frame to infill stiffness, location and dimension of openings, distribution of MI walls throughout the story and construction details are some of these important parameters. Although, a large amount of research related to infilled frame structures has been conducted, some uncertainties still remain. One important source of uncertainty is the type of interaction between the infill and the frame. The interaction between the frame and the infill panel sometimes changes the structural response significantly.
This paper reviews and compares analysis and design provisions related to infilled RC frames in seismic design codes. In designing RC frames, in general, infills can be grouped into two categories: isolated infills and shear infills. However, few seismic codes specify recommendations on isolated infills. When ductile RC frames are designed to withstand large displacements without collapse, masonry infills should be isolated from the confining frame by sufficient gaps at the top and on both sides. The isolation (gaps) between the infill and the frame must be greater than any possible deformation expected by the frame, thus prohibiting any infill/frame interaction. These infills are not considered as structural elements. In this manner, MI walls do not affect the frame performance and frame displacements are not restrained. Another advantage of the isolated MI is that the walls remain undamaged, thereby reducing post-earthquake repair costs. In the following sections, some of the important issues discussed in the seismic codes are reviewed.

2. INATURAL PERIOD

Natural periods of vibration of buildings depend upon their mass and lateral stiffness. Presence of non-isolated MI walls in buildings increases both the mass and stiffness of buildings. Consequently, the natural period of an MI-RC frame is normally lower than that of the corresponding bare frame.
All seismic codes rely heavily on empirical formulae for the natural period for estimating design seismic force. However, few codes specify formulae for MI-RC frames. The comparison of these formulae for different structural systems is given in Table 1. Beside empirical formulae, most seismic standards recommend the use of Rayleigh formula for natural period [6, 10], or other general dynamic methods.
According to Crowley and Pinho [11], the use of uncracked section in the computation of elastic natural periods of RC structures is inadequate because it would lead to an underestimation of the displacement demands. Cracking of critical

elements such as beams generally occurs under gravity loading alone, and even in those cases where cracking is not found to have occurred before the design seismic level of excitation, it will occur early on in the response to excitation and thereafter the stiffness will reduce rapidly. As a result, many seismic codes like IS 2800 provides provisions for calculations of natural periods based on effective stiffnesses [6]. Others like NEHRP 2003 [9] and EC8 [10] have based their equations on the measured periods of buildings during earthquakes where at least a limited amount of cracking of the MI-RC frame occurred. On the other hand, the optional use of T = 0.1N, given by NEHRP 2003 [9] and many other codes, has been found inadequate for MI-RC frames [12]. More details about this subject can be found in Reference [13].

Table 1: Natural period in different codes

Structural type	IS 2800 [6]	UBC 97[7]	ASCE-06 [8] & NEHRP 2003 [9]	EC8 [10]
Steel moment-resisting frames	$0.08(H)^{0.75}$	$0.0853(h_n)^{0.75}$	$0.0724(h_n)^{0.8}$	$0.085(H)^{0.75}$
RC moment-resisting frames	$0.07(H)^{0.75}$	$0.0731(h_n)^{0.75}$	$0.0466(h_n)^{0.9}$	$0.075(H)^{0.75}$
For structures with MI walls	Steel moment frames: $0.8*.08(H)^{0.75}$ Concrete moment frames: $0.8*0.7(H)^{0.75}$	$0.0743(h_n)^{0.75}/\sqrt{A_c}$ (see note no.1)	-	$0.075(H)^{0.75}/\sqrt{A_c}$ (see note no.2)

1- $A_c = \sum A_e\left[0.2 + (D_e / h_n)^2\right]$

A_c is the combined effective area, in m^2, of the MI shear walls in the first story of the structure.

A_e is the minimum cross-sectional area in any horizontal plane in the first story of the building, in m^2. De is the length, in m, of the wall e in the first story in the direction parallel to the applied forces. h_n is the cross-sectional depth in m above the base to Level n. D_e/h_n should not exceed 0.9.

2- $A_c = \sum\left[A_i(0.2 + (l_{wi} / h))^2\right]$

A_c is the total effective area, in m^2, of the MI shear walls in the first story of the structure.

A_i is the effective cross-sectional area of the wall i in the first story of the building, in m^2. Lwi is the length, in m, of the wall i in the first story in the considered direction, and h is the cross-sectional depth in m. l_{wi}/h should not exceed 0.9.

3. RESPONSE REDUCTION FACTOR

The response reduced factor (R) is an empirical factor intended to account for damping, overstrength, and the ductility inherent in the structural system at displacements great enough to surpass initial yield and approach the ultimate load displacement of the structural system [9]. The (R) values, contained in most seismic codes are largely based on engineering judgment of the performance of the various materials and systems in past earthquakes [9]. Furthermore, it is difficult to compare (R) values given in different codes since they use different design philosophies and safety and load factors. Therefore, (R) values need to be compared for different building systems within a particular code only. (R) value for MI-RC frames is generally less than that for bare frames, thus most codes require MI-RC frames to be designed for higher force levels than the corresponding bare frames (about 1.15 to 3.0 times). Comparison of the response reduction factors for different structural systems is given in Table 2.

Table 2: Response reduction factor in different codes

Lateral Resisting System	Allowable Stress		Ultimate Strength		EC8 [10]
	IS 2800 [6]	UBC 94 [14]	UBC97 [7]	New American Codes [8,9 & 15]	
CSMF[1]	10	12	8.5	8	$4.5\alpha_u/\alpha_1$
CIMF[2]	7	8	5.5	5	$3\alpha_u/\alpha_1$
COMF[3]	4	5	3.5	3	-
CSMF[1] + MI Walls	10	8	5.5	SMW[4] 5.5 IMW[5] 4	2[8]
CIMF[2] + MI Walls	7[7]	7	4.2	IMW[5] 3.5 OMW[6] 3	2[8]
COMF[3] + MI Walls	-	6	4.2	-	-

1. CSMF = Concrete Special Moment Resisting Frame
2. CIMF = Concrete Intermediate Moment Resisting Frame
3. COMF = Concrete Ordinary Moment Resisting Frame
4. SMW = Special Masonry Shear Wall
5. IMW = Intermediate Masonry Shear Wall
6. OMW = Ordinary Masonry Shear Wall
7. This reduction factor is for buildings without infill. For infilled frames, natural period is calculated according to table 1
8. This is for RC frames with MI in contact with the frame

4. LATERAL LOAD SHARING BETWEEN INFILL AND FRAME

The RC frame and MI walls must resist the prescribed lateral seismic force in accordance with their relative rigidities considering fully the interaction of the walls and the RC frames as a single system. This analysis must be made in accordance with the principles of structural mechanics considering the relative rigidities of the elements and torsion in the system. Deformations imposed upon members of the RC frame by their interaction with the MI walls must be considered in this analysis [9]. According to most codes, the frame alone is required to be designed to independently resist full vertical loads and at least 25% of the design seismic forces [6, 9, and 13]. MI walls, which are normally very stiff initially, attract most of the lateral forces, but may fail prematurely because of the brittle behavior. In such cases, RC frames must have sufficient backup strength to avoid the collapse of the structure. Accordingly, EC8 [10] puts more strict regulations by requiring that RC frames need to resist at least 50-65% of the total lateral loads in addition to the full vertical loads.

5. PLAN IRREGULARITIES

A building may have a symmetrical geometric shape without re-entrant corners or wings but still be classified as irregular in plan because of distribution of mass (i.e., asymmetric placement of MI walls) or vertical, seismic-force-resisting elements [9]. According to EC8 [10], slight plan irregularities may be taken into account by doubling the accidental eccentricity. In case of severe plan irregularities, due to excessive unsymmetrical placement of MI walls, three-dimensional analysis is required considering stiffness distribution related to the uncertain position of MI walls.

6. VERTICAL IRREGULARITIES

Vertical irregularities are introduced into MI-RC frames due to reduction or absence of MI walls in a particular story compared to adjacent stories, e.g., buildings with parking space in the first story and MI walls on upper stories. In general, this gives rise to mass, stiffness, and strength irregularities along the height of buildings. Vertical irregularities in the bottom stories make the beams and columns of those stories more susceptible to damage or failure [9]. Open ground story buildings have consistently shown poor performance during past earthquakes across the world.

According to IS: 1893 [16], all the columns of the soft/weak storey should be designed for 2.5 times the seismic demand. On the other hand, EC8 [10] recommends an increase in the resistance of columns of soft stories by a factor η that is given by:

$$\eta = 1 + \frac{\Delta V_{RW}}{\sum V_{ED}} \leq q \quad \text{(Units: } \Delta V_{RW}, \sum V_{ED} \text{ in N)} \tag{1}$$

where q is the response reduction factor given in Table-2, ΔV_{RW} is the total reduction in lateral resistance of MI walls in a story compared to the story above, and $\sum V_{ED}$ is the sum of seismic shear forces acting on all structural vertical elements of the story concerned. The design forces are not required to be increased if the factor η is less than 1.1.

7. STRENGTH OF MASONRY INFILL

In designing infill panels, simple analytical tools that encompass the wide variety of possible failure mechanisms of infilled frames should be developed to assist in the design and performance evaluation of these structures. Although strength of MI walls does not have any direct implications on the ultimate strength of ductile RC frames; in some cases, failure modes of MI walls control the failure modes of non ductile RC frames. Many formulae had been developed in the past [17-19], however, these have only been reflected recently in seismic design codes. In cases where the infill component controls the stiffness, FEMA 306 [20] and NZSEE [21] specify four inplane modes of failures, namely, sliding shear failure, compression failure, diagonal tension failure of panel and general shear failure of panel. On the other hand, panel strength in FEMA 356 [22] is given by the shear sliding (bed-joint) strength only with no enhancement for axial stress.

8. STIFFNESS OF MASONRY INFILL

The stiffness of any structure generally affects both forces and displacements. For calculation of design seismic force, the use of a lower estimate of the stiffness leads to unconservative results. On the other hand, controlling the drift requirements under seismic loads, it is unconservative to make a higher estimate of stiffness. Hence, some standards have suggested the use of two different analytical models for buildings:

a. the model to be used for calculation of design seismic force should include all stiffness contributions, including those of nonstructural members.
b. the model to be used for drift calculation should include all possible contributions to flexibility and should not include stiffness contributions of members that cannot be relied upon to provide stiffness at large displacements, such as MI walls.

For example, to calculate forces in the structure, NEHRP 2003 [9] has suggested the use of the natural periods given in Table-1. However, to prevent the use of a flexible frame, an upper bound on the value of natural period that can be used to calculate the design force has been specified. On the other hand, most seismic codes including NEHRP 2003 [9] put lower bound on the overall seismic design force. For determining the story drift limits, NEHRP 2003 has permitted the use of computed natural periods without using the upper limit [9].

MI walls are laterally much stiffer than RC frames, and therefore, the initial stiffness of the MI-RC frames largely depends upon the stiffness of MI walls. Accordingly, it is quite important to have a reliable method to estimate the stiffness of the infill. For global building analysis purposes, the compression struts representing infill stiffness of solid infill panels may be placed concentrically across the diagonals of the frame, effectively forming a concentrically braced frame system. This model has been adopted by many seismic codes [10, 20-22] and is based on the work of Mainstone [23]. In this model, however, the forces imposed on columns and beams of the frame by the infill are not represented. To account for these effects, compression struts may be placed eccentrically within the frames [21-22]. If the analytical models incorporate eccentrically located compression struts as shown in Figure (1), the results should yield infill effects on columns directly. Diagonally concentric equivalent struts may also be used to incorporate infill panel stiffnesses into analytical models for perforated infill panels (e.g., infills with window openings). Analysis of local effects, however, must consider various possible stress fields that can potentially develop within the infill. As an alternative to the approach described above, FEMA 356 [22] suggests the use of multiple compression struts, as have been proposed by Hamburger [24].

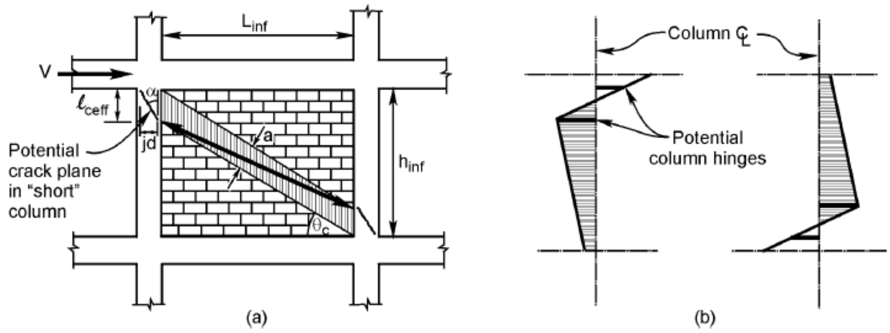

Figure 1. Modeling the adverse effect of an infill panel on the performance of the perimeter frame showing (a) the placement of the strut, and (b) the moment pattern on the columns

9. EFFECT OF OPENINGS IN MASONRY INFILL ON STRENGTH

Presence of openings in MI walls changes the actual behavior of RC frames because of reduction in lateral strength and stiffness. Such infills pose the hazard of out-of-plane collapse. Hence, it is best to avoid situations that lead to infill panels of large width or height [16]. Unfortunately, there is little information on the effects of openings on the strength and stiffness of MI-RC frames in seismic codes [13].

The effect of opening in the infill wall is to reduce the lateral stiffness and strength of the frame. This can be represented by a diagonal strut of reduced width. The reduction factor is defined as ratio of reduced strut width to strut-width corresponding to fully infilled frame. Using IS: 1893 [16], equation for the reduction factor ρ_w is given as:

$$\rho_w = 1 - 2.5A_r,\ \rho_w \geq 0 \tag{2}$$

where, A_r is the opening area ratio, which is the ratio of face area of opening to the face area of infill. On the other hand, NZSEE [21] specifies different reduction factor $\lambda_{opening}$ based on the width of opening measured across a horizontal plane $L_{opening}$ and given by Equation (3):

$$\lambda_{opening} = 1 - \frac{1.5L_{opening}}{L_{\inf}}, \lambda_{opening} \geq 0 \tag{3}$$

According to EC 8 [10], large openings are required to be framed with RC elements across the full length and thickness of walls. Vertical RC elements of at least 150 mm dimension are required at both sides of any opening larger than 1.5 m^2 area .Longitudinal steel in the element shall not be less than 300 mm^2 or 1% of the cross-sectional area of the element. Shear reinforcement in the form of stirrups of at least 5 mm diameter is required with a minimum spacing of 150 mm [10].

10. OUT-OF-PLANE STRENGTH OF MASONRY INFILLS

During earthquakes, MI walls are subjected to high in-plane shear forces because of their high initial stiffness. Tension cracks are formed along the loaded diagonal in MI walls, which causes reduction in their lateral strength. In addition, connection between the RC frame and MI wall is generally weak and MI wall may get separated from RC frames during the in-plane or out-of-plane ground motion, and thus become susceptible for collapse in the out-of-plane direction. However, such an out-of-plane collapse is not common for walls of low slenderness value and for well-confined masonry infill walls. From the above statements, it is clear that isolated infill walls are more susceptible to collapse than shear infill walls in the out-of-plane direction.

Different seismic codes require that nonbearing wall panels that are attached to or enclose the structure be designed to resist the inertial forces and to accommodate movements of the structure resulting from lateral forces [6, 9] or temperature change [9]. This is particularly important for systems composed of brittle materials or materials with low flexural strength [9]. Once masonry walls crack, continued shaking can easily cause collapse in the heavy infill blocks and pose a serious life safety threat to building inhabitants. Furthermore, panel support systems often lack redundancy and failure of a single connection can have catastrophic consequences. In recognition of this, different codes require fasteners to be designed for approximately 4 times the required panel force and that the connecting member be ductile [6, 9]. This is intended to ensure that the energy absorption takes place in the connecting member and not at the connection itself and that the more brittle fasteners remain essentially elastic under seismic loading [9].

The out of plane strength of MI walls has been given by many seismic codes [20-22]. On the other hand, EC8 [10] suggests several preventive measures to avoid brittle failure, premature disintegration, and out-of-plane failure of masonry infill walls during earthquakes, especially for slender walls (ratio of the smaller in length or height to thickness greater than 15). The measures includes providing light wire meshes adequately anchored on masonry infill walls and on RC frames, wall ties fixed to columns and cast into bedding planes of masonry, and concrete posts and belts across the panels and through the full thickness of the masonry infill. On the other hand, FEMA 356 [22] suggests that MI panels not in tight contact with perimeter frame members should be restrained for out-of-plane forces. This may be accomplished by installing steel angles or plates on each side of the infills, and welding or bolting the angles or plates to the perimeter frame members.

11. LOCAL EFFECTS DUE TO MASONRY INFILLS

Presence of infills modifies and magnifies the shear demands on the frame members by shortening the distance between in-span plastic hinges (Figure 1). The shear demand will be a maximum when flexural plastic hinges form at each end of this so-called "short column". EC8 [10] requirements for local effects are as follows:

1) Because of the particular vulnerability of the infill walls of ground floors, a seismically induced irregularity is to be expected there and appropriate measures should be taken. If a more precise method is not used, the entire length of the columns of the ground floor should be considered as the critical length and confined accordingly.
2) If the height of the infills is smaller than the clear length of the adjacent columns, as shown in Figure (2), the following measures should be taken:
   a) The entire length of the columns (L_{ceffi}) is considered as critical region and should be reinforced with the amount and pattern of stirrups required for critical regions;
   b) The consequences of the decrease of the shear span ratio of those columns should be appropriately covered. In this calculation the clear length of the column L_{cl} should be taken equal to the length of the column not in contact with the infills.
   c) The transverse reinforcement to resist this shear force should be placed along the length of the column not in contact with the infills and extend along a length h_c (dimension of the column cross-section in the plane of the infill) into the column part in contact with the infills.
   d) If L_{ceffi}, the length of the column not in contact with the infills is less than 1.5 h_c, the shear force should be resisted by diagonal reinforcement.
3) Where the infills extend to the entire clear length of the adjacent columns, and there are masonry walls on only one side of the column (e.g. corner columns), the entire length of the column should be considered as a critical region and be reinforced with the amount and pattern of stirrups required for critical regions.

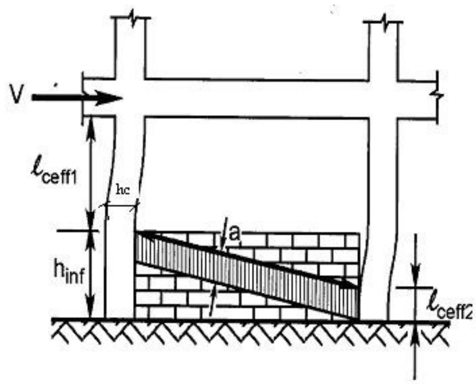

Figure 2. The effect of partial infills on frame performance

4) The length, of columns L_{cl} over which the diagonal strut force of the infill is applied, should be verified in shear for the smaller of the following two shear forces:
   a) The horizontal component of the strut force of the infill, assumed to be equal to the horizontal shear strength of the panel, as estimated on the basis of the shear strength of bed joints; or
   b) The shear force computed in accordance with Equation (4), depending on the ductility class.

$$V = \gamma_{Rd}\left(\left(M_{Rd,c1} + M_{Rd,c2}\right)/\, L_{cl}\right) \tag{4}$$

where L_{c1} is the contact length (L_{ceff} or L_{ceff1}), and γ_{Rd} is an overstrength factor.

SUMMARY AND CONCLUSIONS

In the present paper, design provisions for MI-RC in different seismic codes are reviewed. Taking the current practices into consideration, these provisions provide a good base for design and construct masonry infill panels. However, major issues in various seismic codes need further attention. These issues can be summarized as follows:

Natural Period: Empirical estimation of natural period addresses very simple and regular MI-RC frames. Because of practical reasons, most RC buildings become irregular when masonry infill walls are added in RC frames. Therefore, most of the empirical equations may not estimate the natural periods of such buildings with sufficient accuracy.

Weak and Soft Stories: Design of weak/soft-story frame members is done in different seismic codes based on empirical or semi-empirical relations. Very limited literature is available in support of these relations. Hence there is an urgent need for more research in this area.

Strength and stiffness of MI-RC frame: In calculating the strength and the stiffness of MI-RC frames, many simplified assumptions are used. Neglecting the effect of nonstructural components and the presence of openings in masonry infill walls are some examples of such simplifications. The current 'state-of-the-art' method used to account for infill panels is to model an equivalent strut to represent the stiffness of the panels. It has been reported that this model give good results within the linear range. However, using these models beyond the mortar cracking or failure of the infill walls needs further studies. Furthermore, results from experimental and finite element investigations suggest a strong interaction between in-plane and out-of-plane capacities of the infill walls. Neglecting this interaction may lead to unconservative seismic risk evaluation. Accordingly, reflecting these issues in the new editions of seismic codes is of high priority.

Response Reduction Factor: There is no consensus in various seismic codes on values of response reduction factor, which reflects that more research is needed on reliable estimation of strength and ductility of such buildings.

Irregularities: Sesmic codes address the problems associated with plan and vertical irregularities in MI-RC frames in different ways. However, in case of severe irregularities in plan due to the unsymmetrical arrangement of the infills, spatial models need to be specified for the analysis of the structure, including, if necessary, a sensitivity analysis regarding the position and the stiffness of the infills.

Local effect: Local effects that occurred due to the frame-infill-interaction need to be taken into account. Efficient strengthening methods of nonductile columns need to be specified in seismic codes in order to avoid irreparable damage and catastrophic failure of the structure.

REFERENCES

1. Hashemi, A. and Mosalam, K. M., Shake-table experiment on reinforced concrete structure containing masonry infill wall, Earthquake Engineering and Structural Dynamics, 2006, Vol.35, pp. 1827-1852.
2. Fardis M.N., Design provisions for masonry-infilled RC frames, 12th World Conference on Earthquake Engineering, Auckland, NZ, 2000, Paper No. 2553.
3. Negro P., and Verzeletti, G., Effect of Infills on the Global Behaviour of R/C Frames: Energy Considerations from Pseudodynamic Tests, Earthquake Engineering and Structural Dynamics, 1996, Vol. 25, pp. 753-773.
4. Bertero, V.V., and Brokken, S., Infills in Seismic Resistant Building, Journal of Structural Engineering, ASCE, 1983, Vol. 109, No. 6, pp. 1337-1361.
5. Fardis, M. N., Seismic Design Issues for Masonry-Infilled RC Frames, 1st European Conference on Earthquake Engineering and Seismology, Geneva, Switzerland, Paper No. 313, 2006.
6. Building & Housing Research Center, Iranian Code of Practice for Seismic Resistant Design of Buildings, Standard No.2800, BHRC-PN 374, Tehran, 1999.
7. International Conference of Building Officials (ICBO), Uniform Building Code-Structural Engineering Design provisions, Vol.2, Whittier, California, 1997.
8. American Society of Civil Engineers (ASCE), Minimum Design Loads for Buildings and Other Structures, ASCE/SEI 7-05, Reston, Virginia, 2006.
9. BSSC, NEHRP Recommended Provisions for Seismic Regulations for New Buildings and Other Structures (FEMA 450), Building Seismic Safety Council, National Institute of Building Sciences, Washington, D.C., 2004.
10. CEN, Eurocode 8 - Design of Structures for Earthquake Resistance - Part 1: General rules, UNI EN 1998-1:2005, Brussels, 2004.
11. Crowley, H. and Pinho, R., Simplified Equations for Estimating the Period of Vibration of Existing Buildings", 1st European Conference on Earthquake Engineering and Seismology, Geneva, Switzerland, Paper No. 1122, 2006.
12. Jain, S. K., Saraf, V. K. and Mehrotra, B., Experimental Evaluation of Fundamental Period of Reinforced Concrete Framed Buildings with Brick Infills, Journal of Structural Engineering, 1997, Vol. 23, No. 4, pp. 189-196.
13. Kaushik, H. B., Rai, D. C. and Jain, S. K., Code Approaches to Seismic Design of masonry-Infilled Reinforced Concrete Frames: A State-of-the-Art Review, Earthquake Spectra, 2006, Vol. 22, No. 4, pp. 961-983.

14. International Conference of Building Officials (ICBO), Uniform Building Code-Structural Engineering Design Provisions, Volume 2, Whittier, California, 1994.
15. US Army Corps of Engineers, Seismic Design for Buildings, Washington, UFC 3-310-04, Department of Defence, USA, 2007.
16. Jain, S. K. and Murty, C. V. R., Proposed Draft Provisions and Commentary on Indian Seismic Codes IS 1893 (Part 1), Document No.: IITK-GSDDMA-EQ05-V4.0 and IITK-GSDMA-EQ15-V3.0, Indian Institute of Technology, Kanpur, India.
17. Stafford-Smith B and Carter C., A Method of Analysis for Infilled Frames, Proceedings of the Institution of Civil Engineers, 1969, Vol. 44, pp. 31-48.
18. Saneinejad A, and Hobbs B., Inelastic Design of Infilled Frames, Journal of Structural Engineering, ASCE, 1995, Vol. 121, No. 4, pp. 634-650.
19. Paulay, T. and Priestley, M. J. N., Seismic Design of Reinforced Concrete and Masonry Buildings, John Wiley & Sons, NY, 1992.
20. ATC, Evaluation of Earthquake Damaged Concrete and Masonry Wall Buildings-FEMA306, Applied Technology Council, Redwood City, California, 1998.
21. NZSEE, Assessment and Improvement of the Structural Performance of Buildings in Earthquakes, New Zealand Society for Earthquake Engineering, 2006.
22. ASCE, Prestandard and Commentary for the Seismic Rehabilitation of Buildings-FEMA356, American Society of Civil Engineers, Reston, Virginia, 2000.
23. Mainstone, R. J., On the Stiffness and Strength of Infilled Frames, Current Paper CP 2/72, Building Research Station, Garston, United Kingdom, 1971.
24. Hamburger, R. O., Methodology for Seismic Capacity Evaluation of Steel-Frame Buildings with Infill Unreinforced Masonry, Proceedings of 1993 National Earthquake Conference, Central U.S. Earthquake Consortium, 1993, Memphis, Tennessee, Vol. II, pp. 173-191.

CD02-003

MODELING OF NONLINEAR BEHAVIOR OF RC SHEAR WALLS UNDER COMBINED AXIAL, SHEAR AND FLEXURAL LOADING

B. Ghiassi[1], M. Soltani[2], A. A. Tasnimi[3]
[1]M.Sc. Student, School of Engineering, Tarbiat Modares University, Tehran, Iran
[2]Assistant Professor, School of Engineering Tarbiat Modares University, Tehran, Iran
[3]Professor, School of Engineering, Tarbiat Modares University, Tehran, Iran

ABSTRACT

Predicting the behavior of RC shear walls under bending moment without existence of interaction of any other kind of loadings like shear or axial load is simple and can be conducted with good accuracy. But what is a great concern, is predicting their behavior under the interaction of shear, axial and flexural loadings. In this research, there is an effort to investigate the behavior of RC shear walls under this condition of loading with a novel approach. A general but simple macro model is proposed that can include flexural and shear behavior of the wall by considering the effects of pull put and slippage of reinforcing bars as well as concrete tension softening, stiffening and confinement. This simple model is applicable to different wall shapes with different reinforcement ratios and its prediction has good agreement with experimental results. The predicted behavior of the walls is compared with some available experimental results to show the accuracy of the proposed method.

Keywords: RC shear wall, behavior, nonlinear analysis, P-M-V interaction, modeling

1. INTRODUCTION

Reinforced concrete walls are very effective in resistance of lateral loads imposed by earthquakes. They provide high strength and stiffness and if truly designed, can also provide good ductility for structures.

So many analytical and experimental researches have been carried out to study the seismic behavior of RC walls and RC frame-wall systems. The response of these elements is complex and their overall behavior is influenced by a combination of flexural, shear, and axial deformations. Prediction of the exact inelastic response of RC walls requires accurate analytical material models that consider the important characteristics and behavioral response features such as concrete tension-stiffening, nonlinear shear behavior and effects of loading condition, confinement, transverse reinforcement, and reinforcing bars slippage on strength, stiffness and deformation capacity.

Analytical modeling of the inelastic behavior of RC wall systems can be accomplished either by using microscopic finite element models or macroscopic models. Various analytical models have been proposed for predicting the inelastic behavior response of RC walls through a microscopic or macroscopic approach. Although microscopic finite element models can provide a refined and detailed definition of the local response, their efficiency, practicality, and reliability are questionable due to complexities involved in developing the model and interpreting the results. Macroscopic models, on the other hand, are practical and efficient, although their application is restricted, based on the simplifying assumptions upon which the model is based[1].

A common macro modeling approach is using a beam-column element model. This model consists of an elastic flexural element with a nonlinear rotational spring at each end to account for the inelastic behavior of critical regions (**Error! Reference source not found.**). To model the RC walls more realistically, improvements, such as multiple spring representation [2], varying inelastic zones [3], and specific inelastic shear behavior [4] have been introduced into simple beam column models. However, inelastic response of structural walls subjected to horizontal loads is dominated by large tensile strains and fixed end rotation due to bond slip effects, associated with shifting of the neutral axis. This feature cannot directly be modeled by a beam-column model, which assumes that rotations occur around points on the centroidal axis of the wall and this method disregards the important features of the experimentally observed behavior, including the variation of the neutral axis of the wall cross section, rocking and reinforcing bars slippage [1].

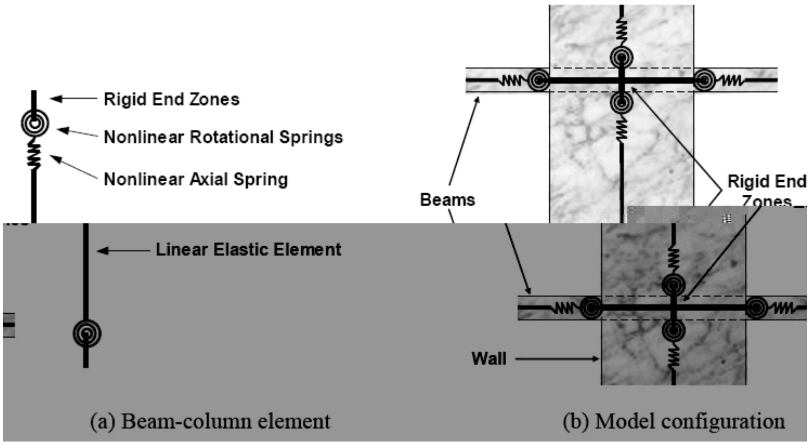

Figure 1. Beam-column element model[1]

Kabeyasawa et al. [5] proposed a new macroscopic three-vertical-line element model (TVLEM) to account for the features that beam-column model cannot capture. In this model, the wall was idealized as three vertical line elements with rigid beams at the top and bottom levels (Figure 1). In this model, shear stiffness degradation was incorporated, but was assumed to be independent of the axial load and bending moment.

This method is improved by different authors such as Vulcano et el. [6], [7], Kabeyasawa [8] and Colotti [9].

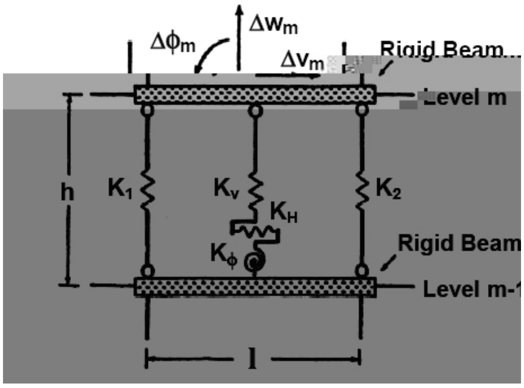

Figure 1. Three-vertical-line element model (TVLEM)[1]

In this paper a novel macro model is proposed that can include flexural and shear behavior of the wall by considering the effects of reinforcing bars pull put and slippage, concrete tension softening and stiffening and confinement. This simple model is applicable to different wall shapes and reinforcement ratios and shows good agreement with experimental results.

2. ANALYTICAL MODEL

The adopted method for nonlinear analysis of RC walls in this paper can take into account the effects of flexural and shear behavior. Flexural behavior is computed by considering a macro fiber model for the wall with including the effects of confinement and reinforcing bars pull-out. Shear behavior is predicted according to a nonlinear analysis of RC elements under in-plane stresses through a fixed smeared crack analysis approach.

In this method, as is shown in Figure 3, the force-displacement curve of the flexural behavior, reinforcement pull out and shear behavior of the wall is computed separately and will be combined to obtain the total nonlinear behavior of the wall. The total behavior of the wall is computed by adding the displacements caused by each of the three behavioral modes that have been mentioned above for any shear value (Figure). If one of the behavioral modes has lower strength than the others, it will be the controlling behavior (e.g. Shear behavior in Figure).

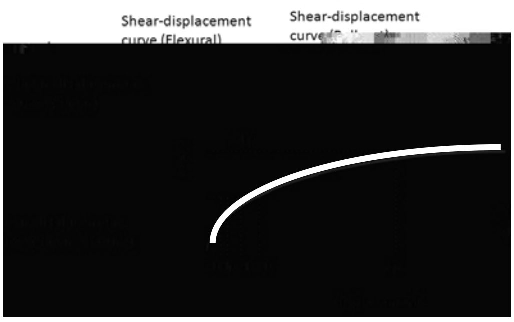

Figure 2. Adopted method for computing the behavior of RC walls

3. FLEXURAL MODELING

3.1. Moment Curvature Analysis

Adopted method here for flexural analysis of RC wall resembles a macro fiber model. In this model, the wall is divided into a series of uniaxial elements (**Error! Reference source not found.**) and then by considering the appropriate material uniaxial nonlinear models, the moment-curvature analysis of the wall will be done with considering the effects of confinement and reinforcing bars pull out from the foundation. Each fiber in the model can have different material properties and steel ratio. Maekawa's [10] material models are used for modeling the uniaxial behavior of the concrete and reinforcing bars.

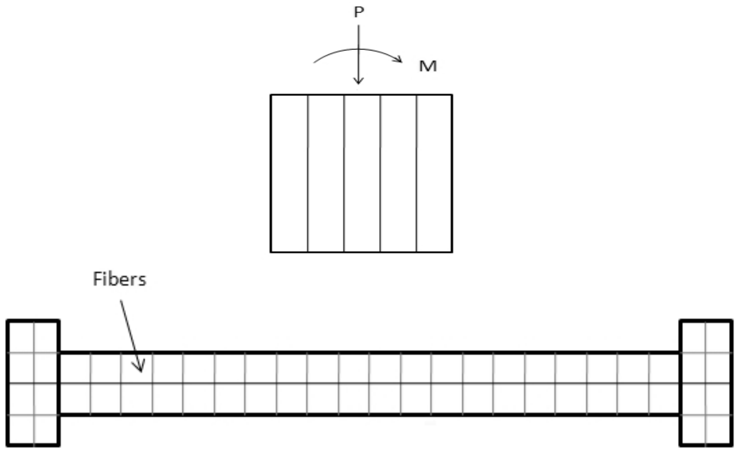

Figure 4. RC wall geometry and fibers definition

Knowing the applied axial force on the wall, the moment curvature analysis is done by assuming a linear strain distribution across the section and calculating the stresses in each fiber (**Error! Reference source not found.**) and controlling if Eq.(1) is satisfied. If this equation is satisfied, the moment and curvature in the section can be computed according to Eq.(2) and Eq.(3) in that step, and if it is not, then the assumed strain distribution should be corrected in an iterative procedure. This procedure is repeated in several steps until the failure of the steels or crushing of the concrete occurs.

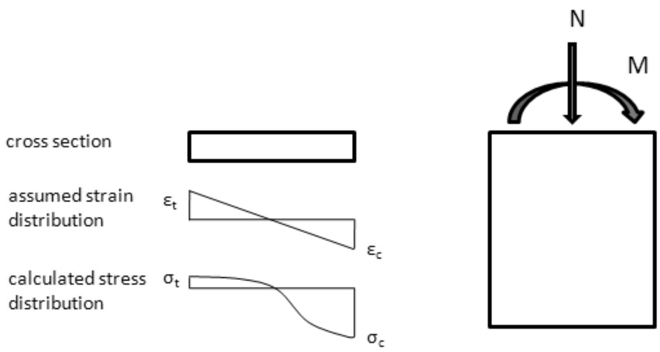

Figure 5. Assumed strain distribution in the section

$$\sum \sigma_i A_i = N \tag{1}$$

$$\sum \sigma_i A_i y_i = M \tag{2}$$

$$\kappa = \frac{\varepsilon_t + \varepsilon_c}{l} \tag{3}$$

where, σ_i is the stress in each fiber, A_i is the area of each fiber, N is the constant axial force applied to the wall, y_i is the fiber distance to the neutral axis of the section, κ is the curvature of the section, ε_t is the first layer strain, ε_c is the last layer strain and l is the length of the section.

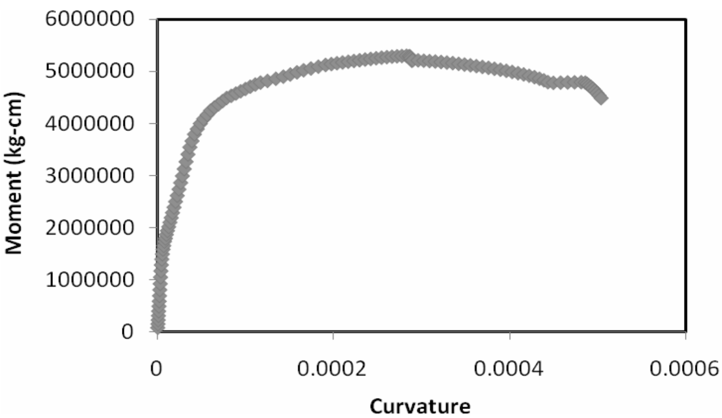

Figure 6. Moment-curvature behavior of a RC wall

3.2. Shear Displacement Curve Due to Flexural Behavior

By using the Eq. (4) the shear corresponding to the moment of the wall can be computed in each step and the curvature is convertible to the wall base rotation, θ, by using the Eq. (5). The top displacement of the wall can also be calculated by using Eq. (6).

$$V = \frac{M}{h} \tag{4}$$

$$\theta = \int_0^h \frac{\kappa . x}{h} dx \tag{5}$$

$$\delta = \theta \frac{l}{h} \tag{6}$$

where h is the wall height. So by computing the shear and the corresponding displacement in each step, the shear displacement curve of the wall due to flexural behavior is attained.

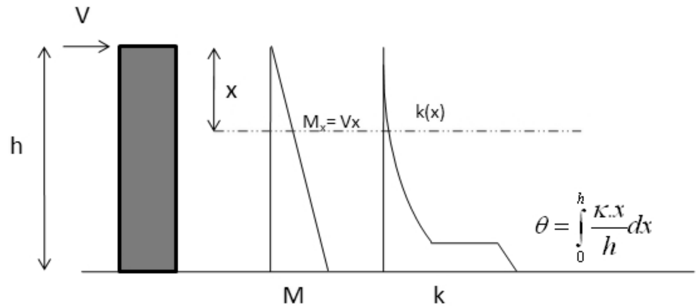

Figure 7. Determination of the wall rotation Figure

4. REINFORCMENT PULL OUT

In reinforced concrete members, local discontinuities, such as pulling out of reinforcing bars from the thicker element and sinking the thinner element to the thicker one, tend to take place as a result of abrupt changes in the section stiffness at the joint planes connecting two components of different thickness [11]. This phenomenon has an important effect on the displacements of the wall that should be considered in the analytical methods to obtain good results in comparison to experimental results. Here, the Maekawa's pull out model [11] is used to consider this important effect. This model describes a relation between steel strain and loaded end slip or relative displacement of steel bar to concrete and is applicable to both elastic and plastic stress states. This model is capable of giving a unique strain-slip relation for a bar that has a long embedded length and that has slip at the free-end prevented (Eq. (7)).

$$\begin{cases} s = \varepsilon_s (2 + 3500\varepsilon_s) \quad for \quad \varepsilon < \varepsilon_y \\ s = s_y \quad for \quad \varepsilon_y < \varepsilon < \varepsilon_{sh} \\ s = s_y + 0.047(f_u - f_y)(\varepsilon_s - \varepsilon_{sh}) \end{cases} \tag{7}$$

where ε_s is the bar strain, s_y is the normalized slip when bar strain is equal to yield strain, f_u is the tensile strength of steel bar, f_y is yield strength of the bar and s is normalized slip that is related to bar diameter and concrete compressive strength as follows:

$$s = \frac{Slip}{D} (\frac{f'c}{200})^{0.67} \tag{8}$$

where D is the bar diameter, $f'c$ is the concrete compressive strength and s is normalized slip as defined in Eq. (8). Using this model, the moment rotation curve of the wall due to slipping can be computed (**Error! Reference source not found.**).

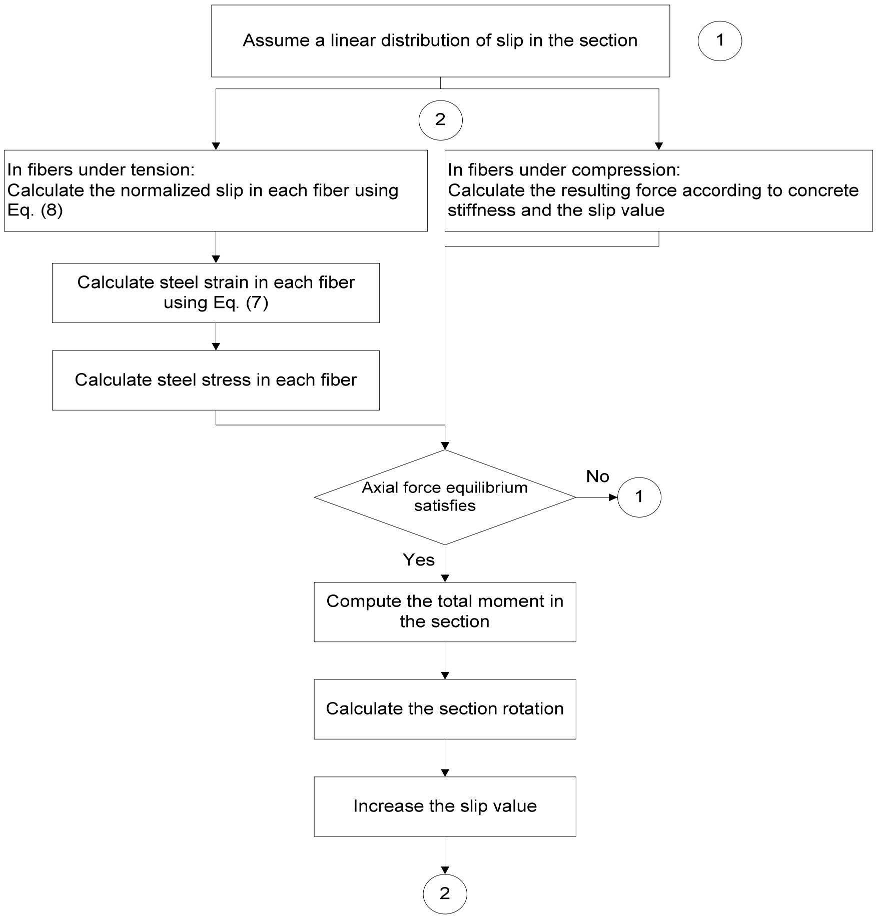

Figure 8. Slip calculation flowchart

5. SHEAR MODELING

Nonlinear analysis of the wall in shear is done through a fixed smeared crack approach by considering the wall as a RC element.

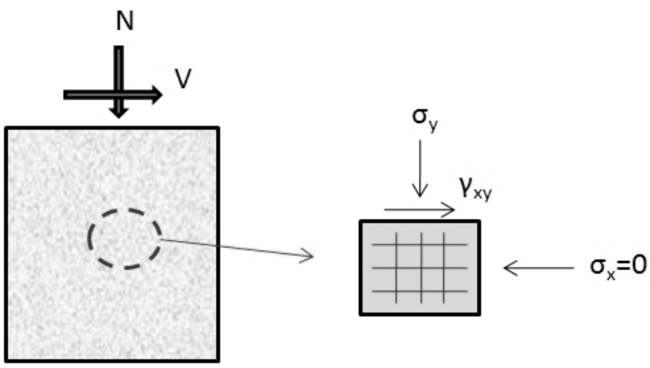

Figure 9. Shear modeling of RC walls

In the smeared crack approaches the cracks and reinforcing bars are idealized as being smeared over the element. The cracks, once generated, are not modeled directly but their effects will be considered by changing the material constitutive models. Generally, the smeared crack approach is conducted by two methods. Rotating crack approach and fixed crack approach. The rotating crack approach assumes that the crack direction coincides with the principal direction of average strain. Accordingly, it can be changed or rotated following the stress condition (**Error! Reference source not found.**), and because the shear stress vanishes on the continually updated principle planes, no shear model is needed in this method. In the step-by-step computation, one crack is considered and the previous ones are erased. So the rotating crack approach does not explicitly account for shear slip and shear stress transfer due to aggregate interlock. In the fixed crack approach the crack direction once generated will not change during the analysis until the direction changes more than a specific value. So there will be shear stress in the assumed crack direction and the shear transfer due to aggregate interlock will be considered. In this paper the fixed smeared crack approach is used to model the shear behavior of RC wall in an iterative procedure as shown in.

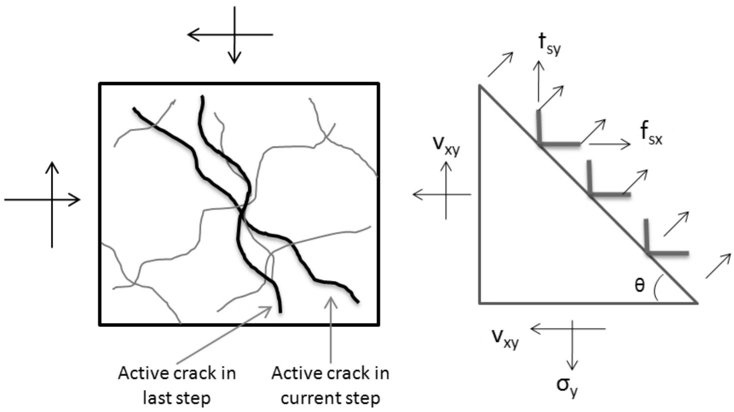

Figure 10. Rotating smeared crack approach

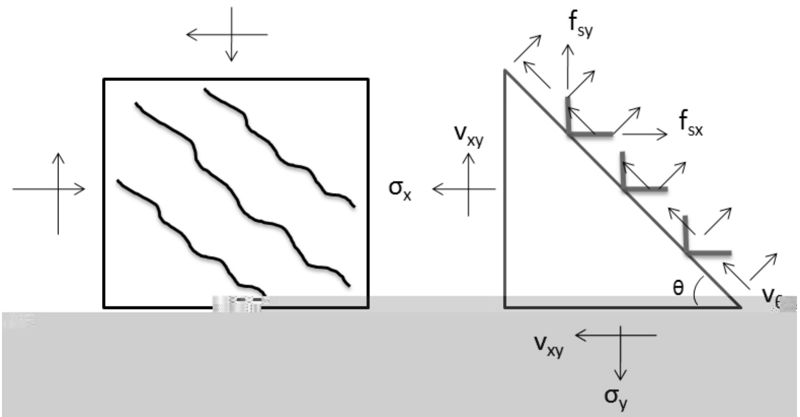

Figure 11. Fixed smeared crack approach

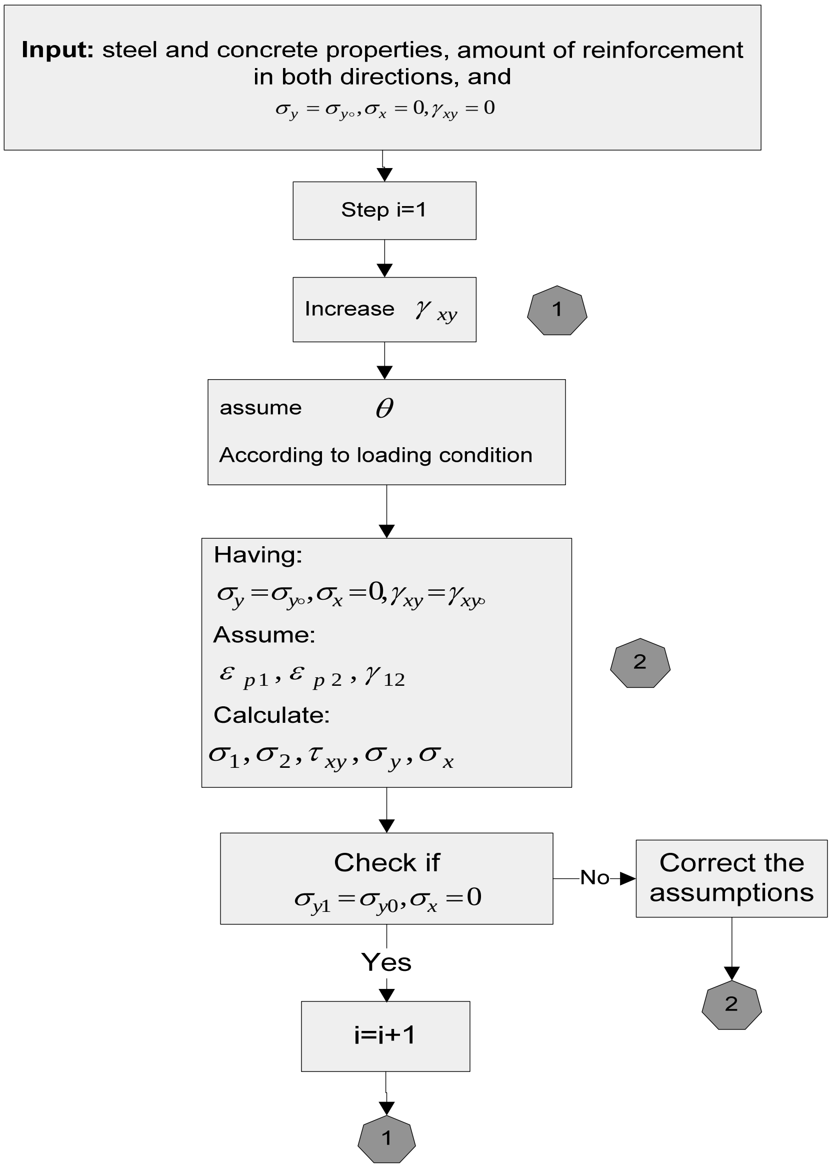

Figure 12. Fixed smeared crack approach flow chart for analysis of RC element

6. VERIFICATION

To control the accuracy of the adopted method, the analysis results are compared with the experimental behavior of some RC walls. The experimental data for the first example are taken from (Lanker and Mang[12]). The wall shape and reinforcement arrangement are shown in. This wall is analyzed with the adopted method and the results are compared in Figure 13.

The second RC wall is taken from Oesterle et al. [13]. This wall is also analyzed with the adopted method and the results are compared in Figure 15.

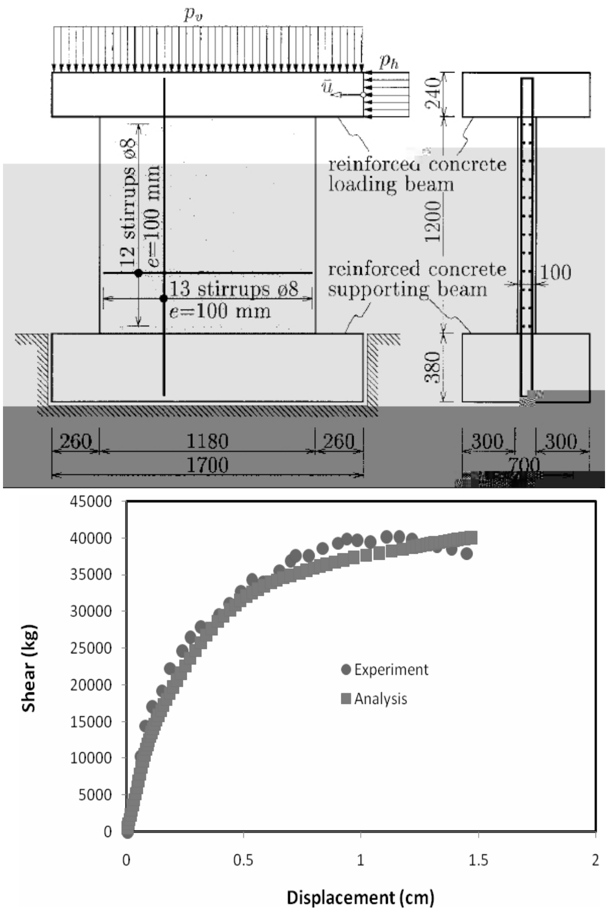

Figure 13. Experimental and analytical behavior of the first wall

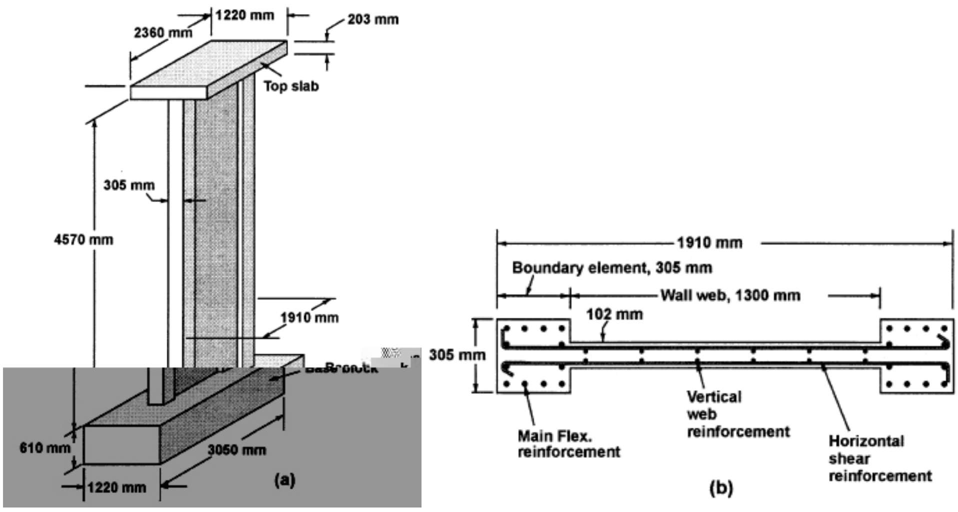

Figure 14. Geometry and reinforcement arrangement of the second wall[14]

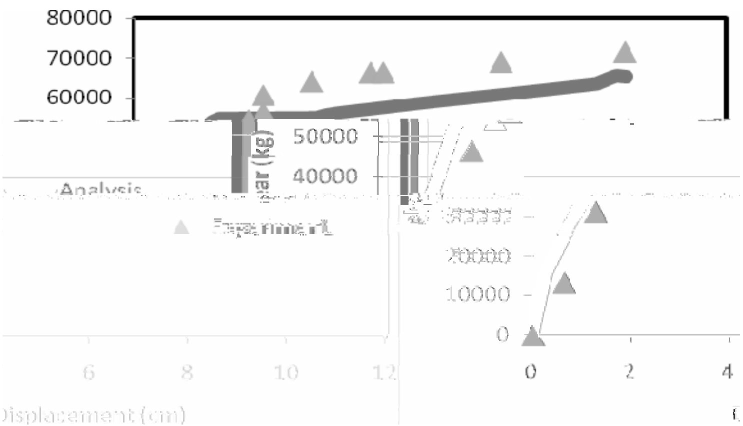

Figure 15. Experimental and analytical results of the second wall

7. CONCLUSION

In this paper a general macro modeling method is proposed that can include flexural and shear behavior of the wall by considering the effects of reinforcing bars pull put and slippage, concrete tension softening, stiffening and confinement. This method can be used to predict the nonlinear response of RC walls by considering all important characteristics and behavioral response features, and is applicable to different wall shapes and the amount of reinforcement. To study the accuracy of the proposed method, the results are compared with some experimental results and their good agreement is shown.

REFERENCES

1. Orakal, K., L.M. Massone, and W. Wallace, *Analytical Modeling of Reinforced Concrete walls for Predicting Flexural and Coupled-Shear-Flexural Responses*. 2006, Pacific Earthquake Engineering Research Center.
2. Takayanagi, T. and W.C. Schnobrich, Computed behavior of reinforced concrete coupled shear walls. 1976, University of Illinois.
3. Keshavarzian, M. and W.C. Schnobrich, Computed nonlinear response of reinforced concrete wall-frame structures. 1984, University of Illinois.
4. Aristazabal-Ochoa, J.D., *Cracking and shear effects of structural walls.* ASCE Journal of Structural Engineering, 1983. **109**(5): p. 1267-1275.
5. Kabeyasawa, T., et al., *analysis of full-scale seven-story concrete test structure.* Journal of Faculty of Engineering, The University of Tokyo, 1983. **37**(2): p. 731-478.
6. Vulcano, A. and V.V. Bertero. Nonlinear analysis of RC structural walls in 8th European Conference on EQ Engineering 1986. Lisbon, Portugal.
7. Vulcano, A., V.V. Bertero, and V. Colotti. Analytical modeling of RC structural walls. in 9th World Conference on Earthquake Engineering. 1988. Tokyo-Kyoto, Japan.
8. Kabeyasawa, T. Design of RC Shear Walls in Hybrid Wall System. 1997.
9. Colotti, V., *Shear behavior of RC structural walls.* ASCE Journal of Structural

Engineering, 1993. **119**(3): p. 728-746.
10. Maekawa, K., A. Pimanmas, and H. Okamura, *Nonlinear Mechanics of Reinforced Concrete*. 2003: Spon Press.
11. Okamura, H. and K. Maekawa, Nonlinear Analysis and Constitutive Models of Reinforced Concrete. 1991.
12. Lancker, R. and H.A. Mang, *Adaptive FE Analysis pf RC Shells, II:Applications.* Journal of Engineering Mechanics, 2001. **127**(12): p. 1213-1222.
13. Oesterle, R.G., et al., *Eartquake-Resistant Structural walls-Tests of Isolated Walls*. 1976, National Science Foundation, Constructuion Technology Laboratories, Portlan Cement Association: Skokie.
14. Palermo, D. and F.J. Vecchio, Compression Field Modeling of Reinforced Concrete Subjected to Reversed Loading: Verification. ACI Structural Journal, 2004. **101**(2): p. 155-164.

CD02-004

SEISMIC EVALUATION OF IRREGULAR REINFORCED CONCRETE STRUCTURES

M.Ghadimi[1], A.Jalali[2]
[1]MS Student of Structural Eng Civil Eng Faculty, Tabriz University, Iran
[2]Pro. Assistance of Civil Eng Faculty, Tabriz University, Iran

ABSTRACT
Seismic evaluation of the behavior of irregular structures is one of the most important steps in the retrofitting process of such structures. Irregularity can be in the elevation or in the plan of a structure. Irregularity in plan shape which is due to the difference between the position of the center of stiffness and the mass center of a structure caused by architectural requirements is usually inevitable. In this study the analytical and experimental models of project CM-4 Structural Retrofit Strategies, part of the Mid-America Earthquake Center Core Research Program under the Thrust Area Consequence Minimization. tested at full scale at the European Laboratory for Structural Assessment (ELSA) of the Joint Research Center (JRC), Ispra, Italy are modeled in the general purpose ABAQUS. The analytical results of the models generated in ABAQUS compare favorably with the experimental and analytical results of the project.
Having verified the reliability the accuracy of the adopted analysis methods the seismic behavior of an irregular reinforced concrete building designed according to the Iranian Code of Practice for Seismic Resistant Design of Buildings, Standard No. 2800 has been investigated using the model. The investigated parameters include the capacity of the building, the maximum displacement, the relative displacement of the stories and the dynamic characteristics of the building.

Keywords: seismic evaluation; irregular structures; maximum displacement; relative displacement

1. INTRODUCTION
One of the most important factors in design of each structure against lateral loads or in retrofitting an existing buildings is the better understanding of the behavior and response of it against such loads. In fact, having enough information about the behavior of an structure can result in more accurate, safer, and more economical design of it. Seismic evaluation of an structure is greatly influenced by its geometry, regularity, and irregularity. Different aspects of response and behavior of regular structures can be predicted to some extent, but in case of irregular ones it is otherwise. Thus according to different building codes much attention should be paid to the design of such structures for which the results of nonlinear and dynamic analyses are used to determine the validity of a design. Given the observations noted above, seismic evaluation of irregular structures is essential.In this study

having verified the capability of an analytical model to simulate the nonlinear behavior of an irregular structure investigated experimentally, the provisions of the Iranian seismic code concerning design of irregular structures are also checked through the nonlinear static and dynamic analyses of an irregular RC building designed according to the mentioned provisions.

2. GENERAL DESCRIPTION OF THE TEST BUILDING

2.1. Geometry of the Test Model

The structure is a simplification of an actual three-story building which is a representative of older construction in Southern Europe without earthquake design provisions. It is also similar to pre-seismic code construction in many other parts of the world. The test building has been designed for gravity loads alone, using the concrete design code applied in Greece between 1954 and 1995. Total dead loads and 30% of live loads are used for the gravity loads in the analysis. An overview of the test building and the plan of a typical repetitive floor are presented in Figure1. Infill walls and stairs are omitted in the model. Dimensions of the building are represented in Figure 2 and details of member dimensions and reinforcement are represented in Figure 3. Slabs are omitted in the analytical model and their contribution to beam stiffness and strength is reflected by effective width of the T-section. For the modeling of beams, a reinforced concrete T-section is utilized and the effective flange width is assumed to be the beam width plus 7% of the clear span of the beam on either side of the web (Fardis, 1994).

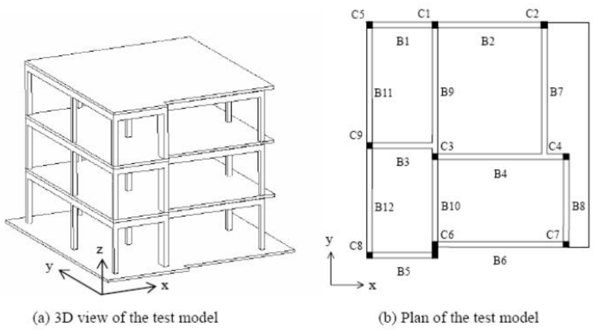

Figure 1. Overview of the Test Model and Plan

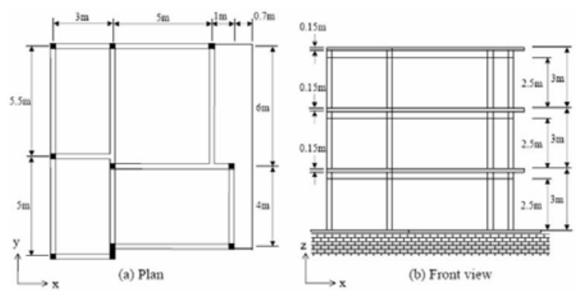

Figure 2. Geometry of the Test Model

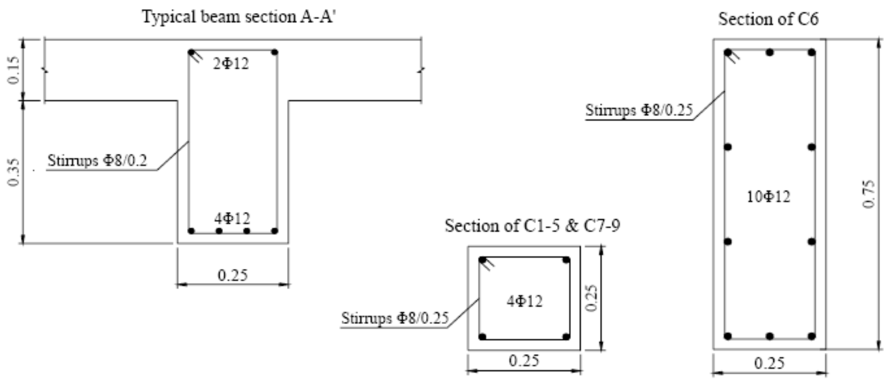

Figure 3. Member Dimensions and Reinforcement

The plan of the test structure in Figure 1(b) shows that beams adjacent to C6 are not in alignment, thus gaps between center lines of beams (B5 and B6) and the column (C6) should be considered in the modeling of the beam column connection at C6. As shown in Figure 4, rigid elements are utilized to connect center lines of beams and columns in order to model the force transfer between members and torsion due to gaps between center lines of members.

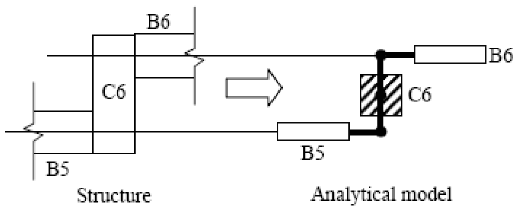

Figure 4. Rigid Arms for Modeling of C6 (Plan)

2.2. Assumed Material Properties And Modeling Assumptions

Assumed material properties and assumptions for the analytical modeling of the test structure are summarized in Table 1.

2.3. Static Pushover Analysis

Nonlinear static pushover analyses are performed in order to estimate overall capacity and basic characteristics of the test structure such as peak base shears and weak directions. The 1st mode shape is utilized in calculating the base shear and distribution of the lateral forces on the structure. It should be noted that according to FEMA356 in case of irregular structures lateral load should be applied in both directions with 100% load in one direction and 30% in the orthogonal direction. Distributions of equivalent lateral load on the plan and pushover curves of the test structure are represented in Figure 5 and Figure 6, respectively.

Using the assumptions summarized in Table **1** nonlinear static pushover analysis of the test structure is performed in ABAQUS and the curve obtained is compared with the one of ELSA model in Figure **7**.

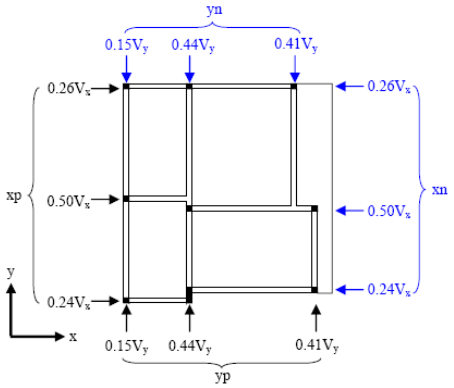

Figure 5. Distribution of Equivalent Lateral Load on the Plan

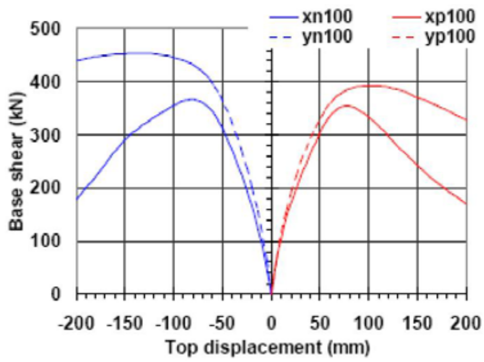

Figure 6. Static Pushover Curves

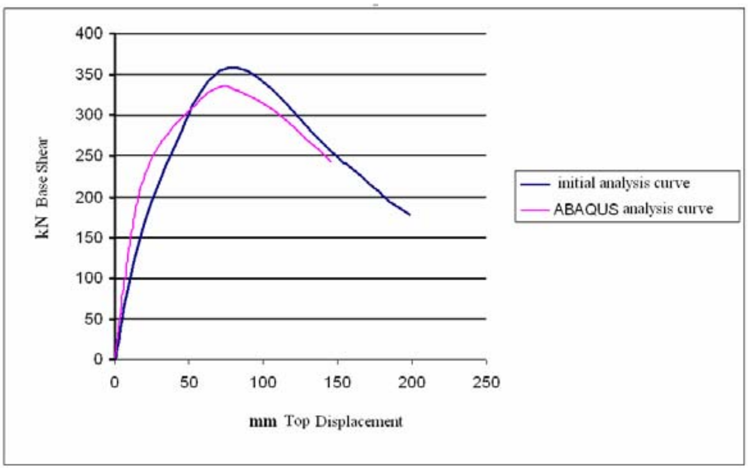

Figure 7. Base Shear-Top Displacement Response of the Test Structure

Dynamic time history analysis using ground motion accelerations, as recommended mostly by building codes, has been used to investigate the seismic behavior of the test structure. Failure prevention was considered as an important criterion for selection of a record to obtain more controllable results and a stream of good response data in the real test. After observation and comparison of analysis results Montenegro 1979 (Herceg Novi) was selected. Two orthogonal components of the selected semi-artificial record, Montenegro 1979 (Herceg Novi) with peak ground acceleration (PGA) intensity of 1g are presented in Figure 8.

Table 1: Assumed Material Properties and Assumptions for the Analytical Modeling Both of ELSA Model & Main Model

Items in analytical modeling		Assumptions	
		Analytical Modeling in ZeusNL	Analytical Modeling in ABAQUS
Material	Reinforcement steel	(FeB32K from Italian market) Yield strength fy=459 MPa (Φ 12) fy=377 MPa (Φ20) Post-yield stiffness to pre-yield stiffness ratio E2/E1=0.0032 (Φ12) E2/E1=0.0056 (Φ20) Young's modulus E1=206000 MPa	Yield strength fy=400 MPa Post-yield stiffness to pre-yield stiffness ratio E2/E1=0.0056 Young's modulus E1=206000 MPa
	Concrete	Compressive strength f'c=25 MPa Confinement factor K=1.01, from Mander et al. (1988)	Compressive strength f'c=25 MPa Confinement factor K=1.1, from Mander et al. (1988)
	Stress-strain relationship	Reinforcement steel Bilinear Elasto-plastic model Concrete Model of Martinez-Rueda and Elnashai (1997) based on Mander et al. (1988)	Reinforcement steel Bilinear Elasto-plastic model Concrete Model of Martinez-Rueda and Elnashai (1997) based on Mander et al. (1988)
	Self weight of RC member	25000 kg/m3	25000 kg/m3
	Gravity loads	DL+0.3LL	DL+0.2LL
	Seismic dead load for mass calculation	DL+0.3LL	DL+0.2LL
	Mass distribution	Distributed at beam column connections	Distributed at beam column connections
	P-delta effect	Considered	Considered
	Viscous damping	No (Only hysteretic damping was considered.	Rayleigh damping has been used
Structural Modeling	Analysis program	ZeusNL (V.1.5)	ABAQUS 6.3
	Element model	Distributed plasticity model	Distributed plasticity model
	Centerline dimensions	Yes	Yes
	Rigid offset at beam column connection	Yes (both at beam ends and column ends)	No
	M-M-N interaction	Yes	-
	Effective flange width of T-beams	Web width plus 7% of the clear span of the beam on either side of the web	-

2.3. NONLINEAR DYNAMIC ANALYSIS

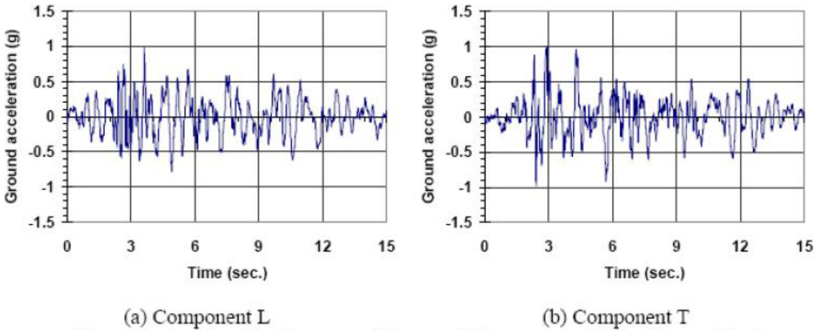

Figure 8. Acceleration Response History of Montenegro 1979 - Herceg Novi

After scaling down their PGA to 0.12g, 0.14g and 0.16g, they were applied to the building in eight different sets of directions as shown in Figure 9. Each combination of directions is defined as D1-D8, respectively.

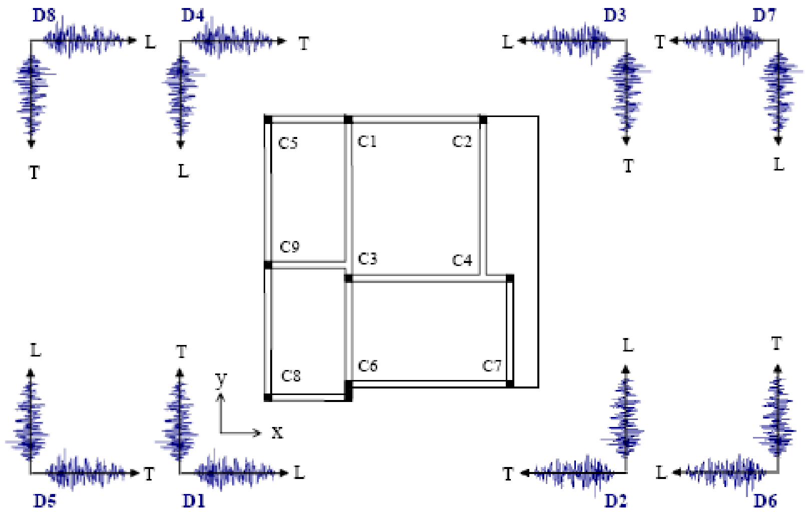

Figure 9. Combinations of Directions to Apply Ground Motions

Montenegro 1979 (Herceg Novi) record at 0.15g PGA in the direction D1 had been selected as an appropriate earthquake scenario for the test. Using the same record at 0.15g PGA in the direction D1 nonlinear dynamic analysis of the test structure is performed in ABAQUS and the curve obtained is compared with the one of ELSA model in Figure 10 and Figure 11. Which verifies the accuracy of the adopted analysis methods.

Having verified the reliability of the analytical model generated and analyzed in ABAQUS, the seismic behavior of an irregular reinforced concrete building designed according to the Iranian Code of Practice for Seismic Resistant Design of Buildings, Standard No. 2800, has been investigated using the model, so that the possible deficiencies of the mentioned code becomes evident. (The designed model is called the main model at the rest of the paper)

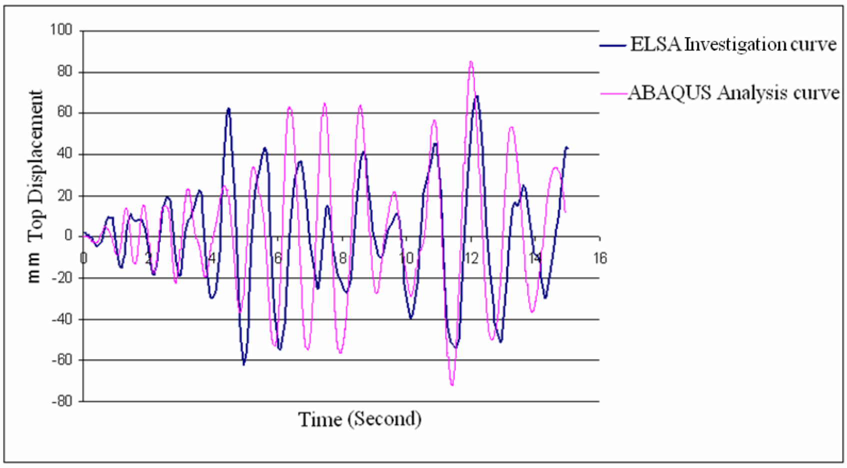

Figure 10. Comparison of the Top Displacement Histories of ELSA Investigation and the Model Generated in ABAQUS (X direction)

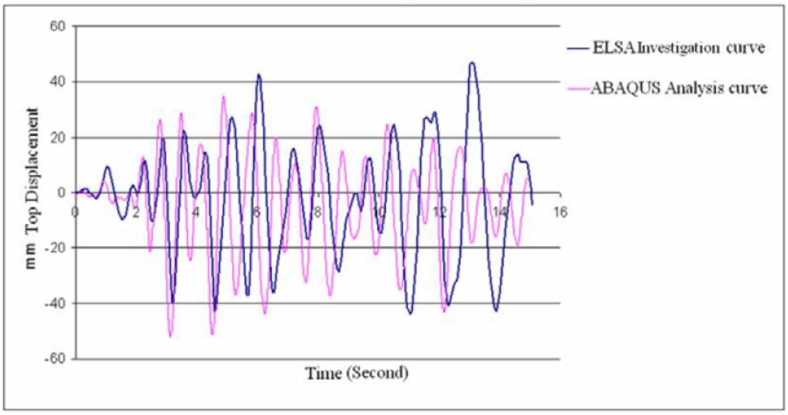

Figure 11. Comparison of the Top Displacement Histories of ELSA Investigation and the Model Generated in ABAQUS (Y direction)

3. DESIGN OF AN IRREGULAR RC BUILDING

The type of irregularity of the building should be selected in such a way that covers most of the existing or under construction buildings. As observed in most of the structures, due to architectural and urban planning provisions, irregularity is usually in plan shapes. Thus a building with irregular plan shape and simple enough to be simulated in ABAQUS has been selected (Figure 12). The structure of the model has been designed according to the Iranian Code of Practice for Seismic Resistant Design of Buildings, Standard No. 2800, and ACI 318-99 in ETABS.V.8.2.7.

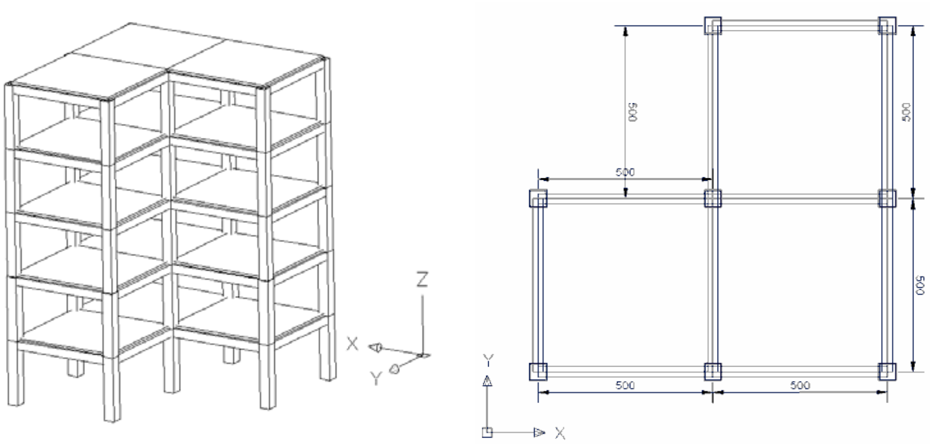

a) 3D View of the Model **b) Plan of the Model**

Figure 12. Overview of the Model and Plan

3.1. Simulation of the Main Model in Abaqus

Assumed material properties and assumptions for the analytical modeling of the main model are summarized in Table 2. A model proposed by Mander et al. (1988) is adopted for stress-strain relationships of confined concrete and evaluating the confining effect K (Figure 13).

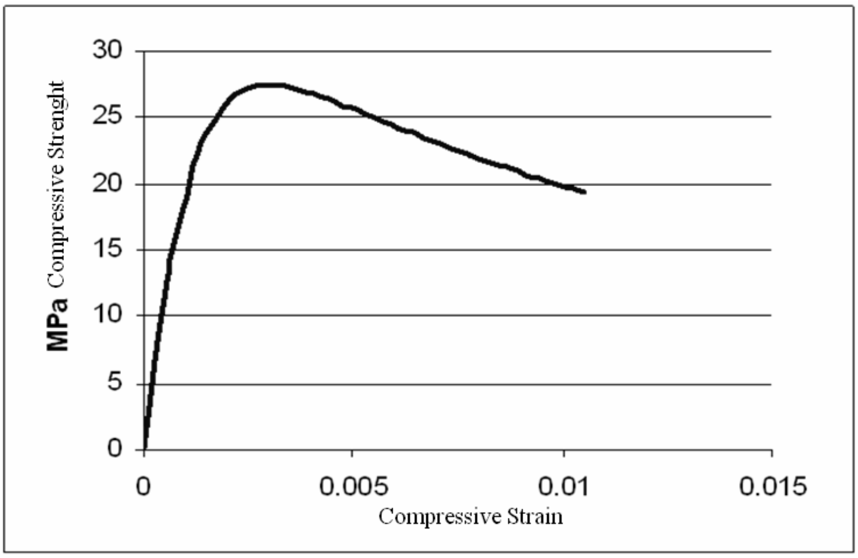

Figure 13. Stress-Strain Relationship of Confined Concrete

3.2. Modal Analysis

In order to understand the overall response of the structure, periods and mode shapes are obtained using 3D modeling in ABAQUS. Three main mode shapes and corresponding frequencies are presented in Figure 14.

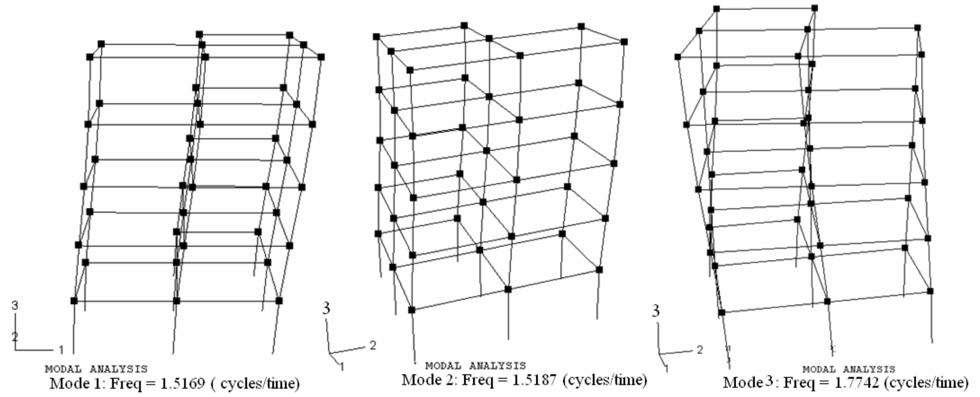

Figure 14. Three Main Mode Shapes

3.3. Nonlinear Static Analysis

As mentioned in previous sections nonlinear static pushover analyses are performed in order to estimate overall capacity and basic characteristics of a structure such as peak base shears and weak directions, and according to FEMA356 in case of irregular structures lateral load should be applied in both directions with 100% load in one direction and 30% in the orthogonal direction. Thus in this phase of the study the model has been subjected to lateral load first in one direction(X) and then in both directions (100% load in one direction and 30% in the orthogonal direction) (Figure 15), and the results are presented in Figure 16.

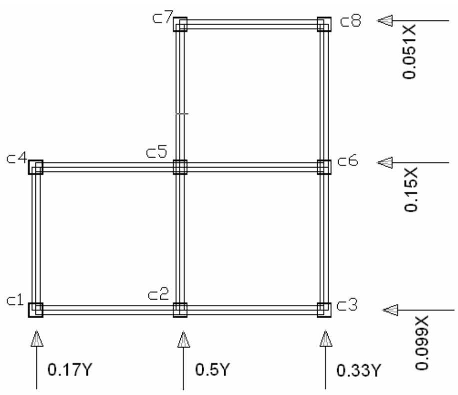

Figure 15. Distribution of Equivalent Lateral Load on the Plan

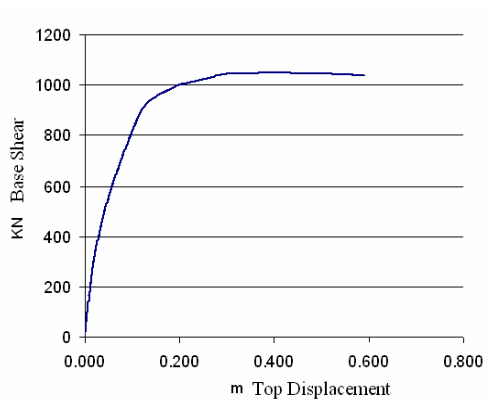

Figure 16. Base Shear Versus top Displacement of the Model

3.4. Nonlinear Dynamic Analysis

Time-history dynamic analysis using ground motion accelerograms has been recommended mostly by building codes. According to the Iranian Code of Practice for Seismic Resistant Design of Buildings, Standard No. 2800 ground motion effects can be applied either by acceleration spectrum or time history. In this study, according to the code, three scaled accelerograms have been used. (Table 3 and

Table 4). The results of the nonlinear dynamic analysis subjected to Montenegro 1979 (semi artificial) ground motion, are indicated in Figure 17, Figure 18, and Figure 19.

Table 3

PGA (y)	PGA (x)	Earthquake
1g	1g	Montenegro1979 (semi artificial)
0.933g	0.878g	Tabas
0.312g	0.214g	El-Centro

Table 4

Max PGA after Scaled	Scale factor	Max PGA	Items	Earthquake
0.35g	0.35	1g	PGA (X)	Montenegro1979 (semi artificial)
0.35g	0.35	1g	PGA (Y)	
0.457g	0.52	0.878g	PGA (X)	Tabas
0.5151g	0.552	0.933g	PGA (Y)	
0.3868g	1.801	0.214g	PGA (X)	El-Centro
0.435g	1.249	0.312g	PGA (Y)	

4. CONCLUSIONS

Since the building has been designed according to the Iranian Standard No. 2800, its provisions and the observations of similar building codes can be used to evaluate the results of the analyses

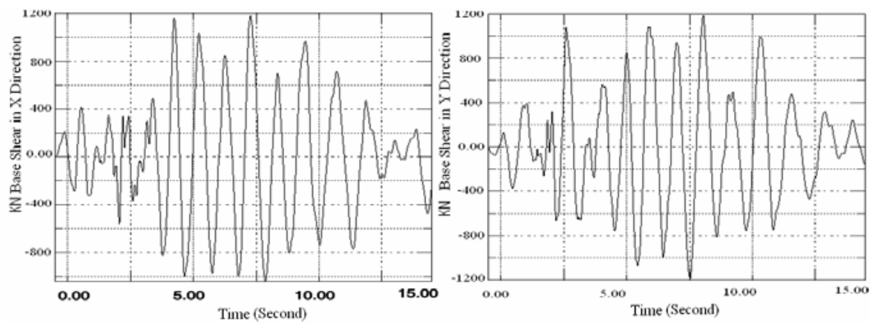

Figure 17. Base Shear-Time Response of the Model in Both Directions (X, Y)

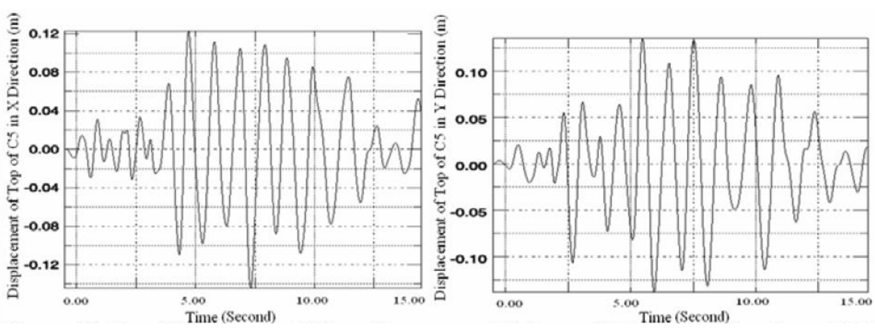

Figure 18. Top Displacement-Time Response of Column C5 in Both Directions (X, Y)

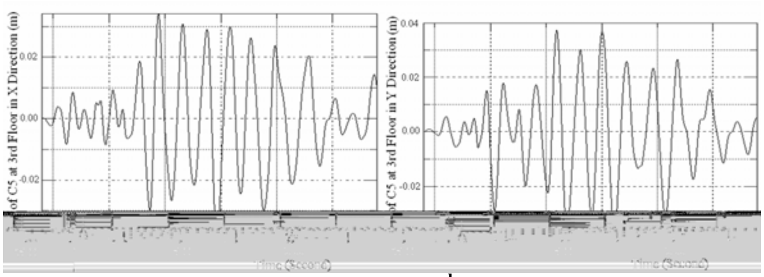

Figure 19. Drift -Time Response of C5 at 3rd Floor in Both Directions (X, Y)

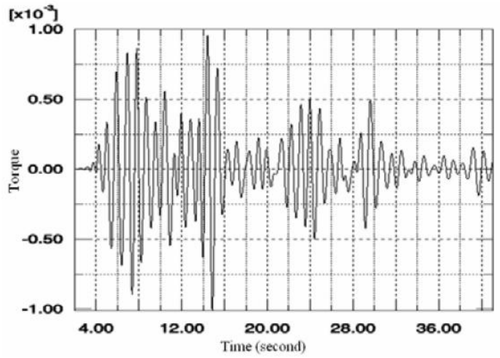

Figure 20. Torque at the Top of Column C5, Subjected to El-Centro Ground Motion.

4.1. The Conclusions of the Nonlinear Static Analysis

1. according to the capacity curve obtained through static pushover analysis the maximum inelastic displacement of the structures with a period of about 0.7 second, 2.5%, determined by FEME and Iranian seismic design code, is observed in the main model and softening of the model begins at the displacement of about 40cm.
2. The displacement of about 40cm is observed in the obtained capacity curve. In this region the amount of the force does not change considerably, and the structure withstands the applied load at the large displacement caused by yield and failure of the longitudinal reinforcement of the members until the collapse of the building. Comparing the results with the results of the model tested by ELSA, it can be concluded that the structure designed according to the Iranian seismic code is much more ductile and can absorb much more energy.
3. As mentioned before, according to the provisions of seismic codes, irregular structures should be loaded in both directions which, as observed in the ELSA model, accounts for the reduction in the ductility of the structure (Figure). While the results obtained by the analysis of the main model (designed by the authors) prove the fact that in the provisions of the Iranian seismic code this phenomenon has been taken into account and no reduction in the ductility of the model due to bidirectional loading has been observed.

4.2. The Conclusions of the Nonlinear Dynamic Analysis

1. The relative lateral displacement of stories of the structure subjected to El Centro

and Tabas accelerograms has not exceeded the maximum amount defined in the Iranian seismic code, except for the lateral displacement of the third story resulted from Montenegro accelerogram which was about 4cm and 1.33% of the allowable relative displacement in the code.
2. The amount of the torsion is considerable and as illustrated in Figure 14 the torsional mode shape is the third mode shape with a period of 0.536 sec which is about the period of the first mode shape (0.659 sec). as was expected, column C5 is subjected to the maximum amount of torsion.

4.3. Final Conclusion

Considering all the results stated above it can be concluded that the provisions of the Iranian Code of Practice for Seismic Resistant Design of Buildings, Standard No. 2800 are appropriate for seismic design of the irregular reinforced concrete structures having 5 stories or being 18 meters in height.

REFERENCE

1. Shah, H, C. Zsutty, T.C and Padilla, L. “The Purpose and Effect of Earthquake” Internal Study Report No.1, the John A.Blume Earthquake Engineering Center, Stanford Univ, 1977.
2. Reitherman, R.K... “Frank Lloyd Wright’s Imperial Hotel: A Seismic Re-evaluation”. Proc. Seventh World Conference on Earthquake Engineering, Istanbul 1980.
3. Dowrick, D.J., Earthquake Resistant Design, John Wiley & Sons, London, 1977.
4. Naito, T., “Earquake-Proof Construction,” Bull. Seism. Soc. Am.17 .No.2, June 1977.
5. Degenkolb, H.,”Seismic Design: Structural Concept,” Summer Seismic Institute for Architectural Faculty, AIA Research Corp., Washington, 1977.
6. Dewell, H.and Willis, B., “Earthquake Damage to Building,” Bull. Seism. Soc. Am.15 .No.4, Dec 1925.
7. Iranian Code of Practice for Seismic Resistant Design of Buildings, Standard No. 2800.
8. S.-H. Jeong & A. S. Elnashai.,” Analytical Assessment of an Irregular RC Frame for Full-Scale 3D PsD Testing-Part I”. Journal of Earthquake Engineering, Vol. 9, No. 1 (2005) 95-128-Imperial College Press.
9. S.-H. Jeong & A. S. Elnashai.,” Analytical Assessment of an Irregular RC Frame for Full-Scale 3D PsD Testing-Part II”. Journal of Earthquake Engineering, Vol. 9, No. 2 (2005) 265.
10. Mander, J. B., Priestley, M. J. N. and Park, R. [1988] “Theoretical stress-strain model for Confined concrete,” ASCE Journal of Structural Engineering 114(8), 1804-1826.
11. ABAQUS USER MANUAL Ver. 6.5.1
12. Shah, S.P., Swartz, S.E., and Ouyang, C., Fracture Mechanics of Concrete Applications of Fracture Mechanics to Concrete, Rock, and Other Quasi-Brittle Materials, John Wiley & Sons, 1995.

CD02-005

NONLINEAR ANALYSIS OF REINFORCED CONCRETE FRAMES INCLUDING MODELING OF JOINT AND BEAM-COLUMN ELEMENTS

S.SH. Hashemi[1], A.A. Tasnimi[2], M. Soltani[3]
[1]PhD Student, Dept. of Civil Engg., Tarbiat Modares University, Tehran, Iran.
[2]Associate professor, Dept. of Civil Engg., Tarbiat Modares University, Tehran, Iran.
[3]Assistant professor, Dept. of Civil Engg., Tarbiat Modares University, Tehran, Iran.

ABSTRACT

In this paper a new method for nonlinear analysis of two dimensional reinforced concrete frames is proposed. In numerical modeling each frame is divided into two types of joint and beam-column elements. The effect of bond-slip has been considered in the formulation of beam-column element by removing perfect bond assumption from fiber method. Joint elements are formulated upon major behaviors including Pull-out of embedded longitudinal bars, shear and flexural deformation of joint panel and shear slip in interface section between joint and neighboring element. Four types of joint elements have been generated according to their position in the frame. Each element type has been modeled based on the major behaviors of that through the combination of one or more defined mechanisms and sub-elements. The reliability of the method has been assessed through the comparison of numerical and experimental results for a one bay two storey frame and a good agreement between experimental and analytical results is observed.

Keywords: nonlinear analysis, RC frames, bond-slip, joint element

1. INTRODUCTION

Much effort has been devoted in the last forty years to the development of models of nonlinear analysis of reinforced concrete frame (*RCF*). These researches can be classified into three categories: behavior of steel and concrete materials, interaction between bars and concrete and finally, numerical method for nonlinear analysis. In the field of material behavior, numerous models have been proposed, among which the Kent-Park model [1] is the most popular model for the stress-strain relationship of concrete and that of Giuffre-Menegotto-Pinto (GMP) [2,3] model for steel bars. In the field of interaction between concrete and bars, Eligehausen et al. [4] proposed a model for bond stress-slip between bars and concrete. Also other researchers such as Muguruma et al., Hawkins et al., Mirza et al. and Mehlhorn et al. proposed their models for bond stress-slip relationship [5]. Other researchers complemented and modified the previous models according to their experimental works and proposed their models [6]. In the beginning two-component model was proposed by Clough et al. [7] for the numerical analysis of *RCF*. After that several concentrated plasticity constitutive models have been proposed to date. Such models include stiffness degrading in flexure, pinching in shear, and fix-end rotations due to bar's Pull-out. Then a more accurate description of the inelastic behavior of reinforced concrete members became possible with distributed nonlinearity models. The most promising model for the nonlinear analysis of reinforced concrete elements is, presently, fiber section model. In this model the element is subdivided into longitudinal steel and concrete fibers. The constitutive relation of the section is derived by integration of the response of the fibers, which follows the uni-axial stress-stain relationship of materials. The fiber model, basically, adopts the perfect bond assumption [8]. Limkatanyu & Spacone [9] have suggested a method based on fiber section for modeling beam or column reinforced concrete element, but instead of the perfect bond assumption, they have considered bond-slip effect. Meanwhile, microscopic modeling of *RCF* and their elements with and without bar-concrete interaction in finite element domain has been proposed, but because of its cost the researchers prefer to suggest the simpler methods.

Moreover a variety of beam-column joint models have been proposed by researchers. Some of the earliest works to simulate the inelastic response of *RCF* were based on the calibration of the Plastic-Hinge formation within beam-column elements to introduce the inelastic action of the joint [10]. Another generation of joint models is decoupling the inelastic response of the beams, columns, and joints to facilitate model calibration. One such model is the zero-length rotational spring element that has been used in order to connect beam to column elements and thereby represent the shear distortion of the joint [11]. More recently, researchers have begun using continuum type elements to represent the response of reinforced concrete joints. This type of formulation greatly increases the computational effort of the analysis but offers the potential for high resolution, accurate, and objective modeling of the joint region. One of these models is proposed by Lows et al. [12].

The major sources of deformation in reinforced concrete frame (*RCF*) are flexural rotation in beams and columns, shear deformation of joints including shear sliding and bar-concrete interaction such as bar's slip. In this study the behavior of frame elements arises from a combination of these deformation mechanisms. In order to achieve this goal two types of elements have been modeled, one is beam-column element which hereafter is called "*BCE*" and the other is joint element that is called "*JE*". *BCE* has been generated based on fiber method but the effect of bar-concrete interaction is imposed into equilibrium equations. Also *JE* is made up of a few mechanisms and sub-elements.

2. BEAM-COLUMN ELEMENT

The free body diagram of an infinitesimal segment *dx* of *BCE* is shown in Figure 1. In formulation only the bond stress tangential to the bars is considered and the bar's dowel effect is neglected. Each *BCE* is a combination of one 2-node concrete frame element and *n* number of 2-node bars with bond interfaces. *n* is the number of longitudinal bars in cross section of *BCE*. This element has been proposed by Limkatanyu and Spacone [9]. Slippage has been allowed to occur because the nodal degrees of freedom of the concrete element and the bars are different. Based on the small deformation assumption, all of the equilibrium conditions have been considered. Considering axial equilibriums in the concrete element and steel bars and also vertical and moment equilibriums in the segment *dx* lead to matrix form of equations which is shown in Equation 1.

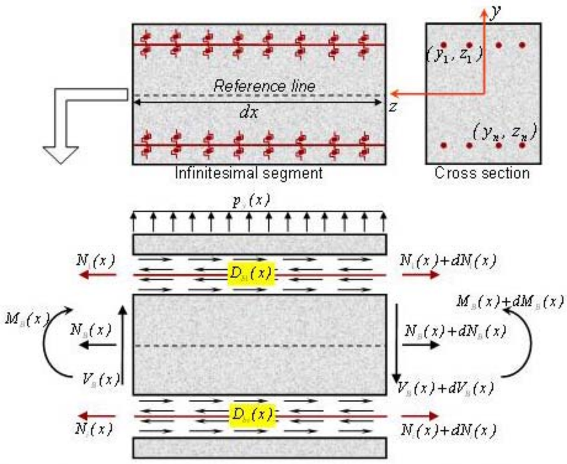

Figure 1. Free body diagram of infinitesimal segment of *BCE* and its components

$$\boldsymbol{\partial}_{\mathbf{B}}^{\mathbf{T}}\mathbf{D}_{\mathbf{B}}(\mathbf{x})-\boldsymbol{\partial}_{\mathbf{b}}^{\mathbf{T}}\mathbf{D}_{\mathbf{b}}(\mathbf{x})-\mathbf{P}(\mathbf{x})=\mathbf{0} \tag{1}$$

Where: $\mathbf{D}_{\mathbf{B}}(\mathbf{x})=\{\overline{\mathbf{D}}(\mathbf{x}):\overline{\overline{\mathbf{D}}}(\mathbf{x})\}^{\mathrm{T}}$ is *BCE* section forces. $\overline{\mathbf{D}}(\mathbf{x})=\{N_B(x)M_B(x)\}^T$ is concrete element section forces. $\overline{\overline{\mathbf{D}}}(\mathbf{x})=\{N_1(x)....N_n(x)\}^T$ is bar axial forces. $\mathbf{D}_{\mathbf{b}}(\mathbf{x})=\{D_{b1}(x)...D_{bn}(x)\}^T$ is bond section forces. $\mathbf{P}(\mathbf{x})=\{0\ \ p_y(x)\ \ 0....0\}^T$ is *BCE* force vector. $\boldsymbol{\partial}_{\mathbf{B}},\boldsymbol{\partial}_{\mathbf{b}}$ are differential operators and are defined in the following forms:

$$\boldsymbol{\partial}_{\mathbf{B}}=\begin{bmatrix}\overline{\boldsymbol{\partial}}_{\mathbf{B}} & \mathbf{0}\\ \mathbf{0} & \overline{\overline{\boldsymbol{\partial}}}_{\mathbf{B}}\end{bmatrix},\quad \overline{\boldsymbol{\partial}}_{\mathbf{B}}=\begin{bmatrix}\frac{d}{dx} & 0\\ 0 & \frac{d^2}{dx^2}\end{bmatrix}$$

$$\overline{\overline{\boldsymbol{\partial}}}_{\mathbf{B}}=\begin{bmatrix}\frac{d}{dx} & 0 & \ldots & 0\\ 0 & \frac{d}{dx} & \ldots & 0\\ \ldots & \ldots & \ldots & \ldots\\ 0 & 0 & \ldots & \frac{d}{dx}\end{bmatrix}_{n*n},\quad \boldsymbol{\partial}_{\mathbf{b}}=\begin{bmatrix}-1 & y_1\frac{d}{dx} & 1 & \ldots & 0\\ \ldots & \ldots & \ldots & \ldots & \ldots\\ -1 & y_n\frac{d}{dx} & 0 & \ldots & 1\end{bmatrix}_{n*(2+n)} \tag{2}$$

y_n is the distance of bar *n* from section reference axis (Figure 1). The *BCE* section deformation vector conjugate of $\mathbf{D}_{\mathbf{B}}(\mathbf{x})$ is $\mathrm{d}_{\mathrm{B}}(\mathrm{x})=\{\overline{\mathrm{d}}(\mathrm{x}):\overline{\overline{\mathrm{d}}}(\mathrm{x})\}^{\mathrm{T}}$. In which

$\bar{\text{d}}(\text{x}) = \{\varepsilon_B(\text{x})\ \kappa_B(\text{x})\}^T$ contains concrete element section deformations and $\bar{\bar{\text{d}}}(\text{x}) = \{\varepsilon_1(\text{x})....\varepsilon_n(\text{x})\}^T$ contains the axial strain of the bars. Displacement vector in the cross section of *BCE* is defined as $\mathbf{u(x)} = \{\bar{\mathbf{u}}\mathbf{(x)} : \bar{\bar{\mathbf{u}}}\mathbf{(x)}\}^{\mathbf{T}}$. In which $\bar{\mathbf{u}}\mathbf{(x)} = \{u_{1B}(x)\ u_{2B}(x)\}^T$ contains concrete element axial and transversal displacements, respectively, and $\bar{\bar{\mathbf{u}}}\mathbf{(x)} = \{u_1(x)...u_n(x)\}^T$ contains the axial displacements of the bars. From small deformation assumption, the element deformations are related to the element displacements through the following relation:

$$\mathbf{d_B(x)} = \partial_{\mathbf{B}}\mathbf{u(x)} \tag{3}$$

The bond slips of bars are determined by the following relation between the bar and concrete element displacements:

$$u_{bi}(x) = u_i(x) - u_{1B}(x) + y_i \frac{du_{2B}(x)}{dx} \tag{4}$$

Where $u_{bi}(x)$ is the bond slip between bar i and surrounding concrete. By introducing the bond deformation vector as $\mathbf{d_b(x)} = \{u_{b1}(x)...u_{bn}(x)\}^T$, Equation 4 can be written in the following matrix form:

$$\mathbf{d_b(x)} = \partial_{\mathbf{b}}\mathbf{u(x)} \tag{5}$$

The weak form of displacement based finite element formulation is determined through the principle of stationary potential energy. The *BCE* nodal displacement (**U**) which is shown in Figure 2 serve as primary element unknowns and the section displacement **u(x)** are related to it through displacement shape function matrix. The relation between nodal displacements and internal deformations can be written through transformation matrix.

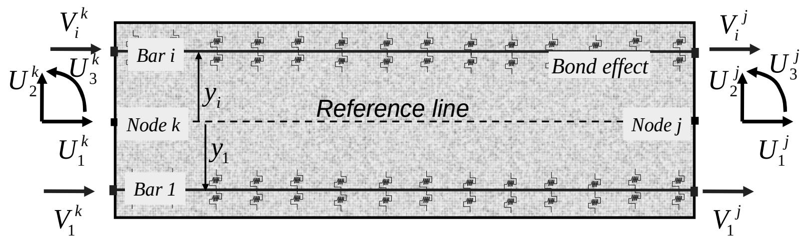

$$U_{1=Dof\ number}^{k=Node\ number} = concrete\ element\ nodal\ displacements$$

$$V_{i=Bar\ number}^{k=Node\ number} = Bar's\ nodal\ displacements$$

Figure 2. Reinforced concrete beam-column element

The nonlinear behavior of *BCE* derives from the nonlinear relation between the section forces and the section deformations through section and bond stiffness matrices ($\mathbf{k_B(x), k_b(x)}$). Section stiffness matrix included axial and bending stiffness of concrete element (*EA(x)* and *EI(x)*) also axial stiffness of the bars ($E_nA_n(x)$). Bond stiffness matrix is diagonal and included slope of bond force-slip relationship of each bar ($k_{bn}(x)$). By using the fiber section method, section stiffness matrix is derived. In this method, the stress-strain relationships of steel and concrete are needed. The bond stiffness matrix is derived through the bond stress-slip relation and perimeter of each bar. These relationships are selected according to Table 1.

Table1. Selected models for material behavior

Concrete stress-strain for compressive region	Park –Kent model [1] and later extended by Scott et al. [13]
Concrete stress-strain for tensile region	Gilbert & Warner model [14]
Steel stress-strain	Giuffre-Menegoto-Pinto model [3]
Bond stress-bond slip	Eligehausen et al. model [4]
Shear stress-shear slip	Walraven model [15]
Shear stress-shear deformation	Anderson et al. model [16]

3. JOINT ELEMENT

In order to model the response of such *JE*, two sub-elements and two significant mechanisms have been considered. The sub-elements are: a concrete and a reinforced concrete deep beam. In which the effects of shear and flexural deformations has been considered based on Timoshenko beam theory. The mentioned mechanisms are: Pull-out of beam or column longitudinal bars embedded in the joint (Pull-out failure), and shear-transfer at the *BCE*-joint interfaces (shear slip). The number of degrees of freedom in each side of *JE* is compatible with the degrees of freedom in the ends of *BCE*s that are in the neighboring of the *JE*. Thus, it will be possible to assemble the global matrix and vectors of *RCF*. In numerical modeling, depending on the position of *JE* in the *RCF*, four types of *JE* can be defined through the combination of sub-elements and mentioned mechanisms. So, firstly, the sub-elements and the mechanisms have been described.

4. REINFORCED CONCRETE SUB-ELEMENT

Reinforced concrete sub-element hereafter is called "*RCSE*". In a similar way to which described for *BCE*, the infinitesimal segment of *RCSE* has free body diagram similar to Figure 1. In this sub-element the effect of shear deformation has been considered based on Timoshenko beam theory. Also slippage has been allowed to occur. Considering axial equilibriums in the concrete part and steel bars, also vertical and moment equilibriums in the segment *dx*, lead to the matrix form of equations which is presented in Equation 1. The definitions in this equation are valid but $\overline{\mathbf{D}}\mathbf{(x)}$ has been rewritten as $\overline{\mathbf{D}}\mathbf{(x)} = \{N_B(x)\, V_B(x)\, M_B(x)\}^T$ and $\overline{\partial}_\mathbf{B}$ and $\partial_\mathbf{b}$

have been rewritten as Equation 6.

$$\bar{\partial}_{\mathbf{B}} = \begin{bmatrix} \frac{d}{dx} & 0 & 0 \\ 0 & \frac{d}{dx} & -1 \\ 0 & 0 & \frac{d}{dx} \end{bmatrix} , \quad \partial_{\mathbf{b}} = \begin{bmatrix} -1 & 0 & y_1 & 1 & 0 & \dots & 0 \\ -1 & 0 & y_2 & 0 & 1 & \dots & 0 \\ \dots & \dots & \dots & \dots & \dots & \dots & \dots \\ -1 & 0 & y_n & 0 & 0 & \dots & 1 \end{bmatrix}_{n*(3+n)} \tag{6}$$

The *RCSE* section deformation vector conjugate of $\mathbf{D_B(x)}$ is $\mathbf{d_B(x)} = \{\bar{\mathbf{d}}\mathbf{(x)} : \bar{\bar{\mathbf{d}}}\mathbf{(x)}\}^{\mathrm{T}}$. In which $\bar{\mathbf{d}}\mathbf{(x)} = \{\varepsilon_B(x)\ \ \gamma_B(x)\ \ \kappa_B(x)\}^T$ contains axial, shear and bending deformations of section of concrete element, respectively. $\bar{\bar{\mathbf{d}}}\mathbf{(x)}$ has similar definition to that of *BCE*. The following displacements are defined at the sub-element level: $\mathbf{u(x)} = \{\bar{\mathbf{u}}\mathbf{(x)} : \bar{\bar{\mathbf{u}}}\mathbf{(x)}\}^{\mathrm{T}}$ is displacement vector along the *RCSE,* in which $\bar{\mathbf{u}}\mathbf{(x)} = \{u_{1B}(x)\ \ u_{2B}(x)\ \ u_{3B}(x)\}^T$ contains axial, transversal and rotational displacements of concrete element, respectively. $\bar{\bar{\mathbf{u}}}\mathbf{(x)}$ has similar definition to that of *BCE*. From small deformation assumption, the element deformations are related to the element displacements through the Equation 3. The bond slips of bars are determined by the following relation between the bar and concrete element displacements:

$$u_{bi}(x) = u_i(x) - u_{1B}(x) + y_i\, u_{3B}(x) \tag{7}$$

By introducing the bond deformation vector as $\mathbf{d_b(x)}$, Equation 7 can be written as Equation 5. The weak form of displacement based finite element formulation is determined through the principle of stationary potential energy. *RCSE* nodal displacement vector is similar to that of *BCE* (Figure 3-a). The section displacement vector is related to nodal displacement vector through the matrix of shape functions. Then the section deformations and bond slips could be determined through Equations 3 and 5.

The nonlinear behavior of *RCSE* derives from nonlinear relation between the section forces and the section deformations through section and bond stiffness matrices. The section stiffness matrix included axial, shear, and bending stiffness of concrete element (*EA(x), GA(x)* and *EI(x)*), also axial stiffness of the bars ($E_nA_n(x)$). The bond stiffness matrix and method for calculation of these matrices are similar to which described for *BCE*. The section shear stiffness derives from shear stress-shear deformation relationship which is selected according to Table 1.

External load vector of this sub-element derives from the external distributed loads along that, which is shown in Figure 3-a as $p_{y1}(x)$ and $p_{y2}(x)$, by using the shape function matrix. The distributed loads derive from the internal loads in the *JE* side sections, which are parallel to that sub-element, based on stress value in concrete and steel fibers of the mentioned side sections. The external load vector will be updated in each load step of nonlinear analysis.

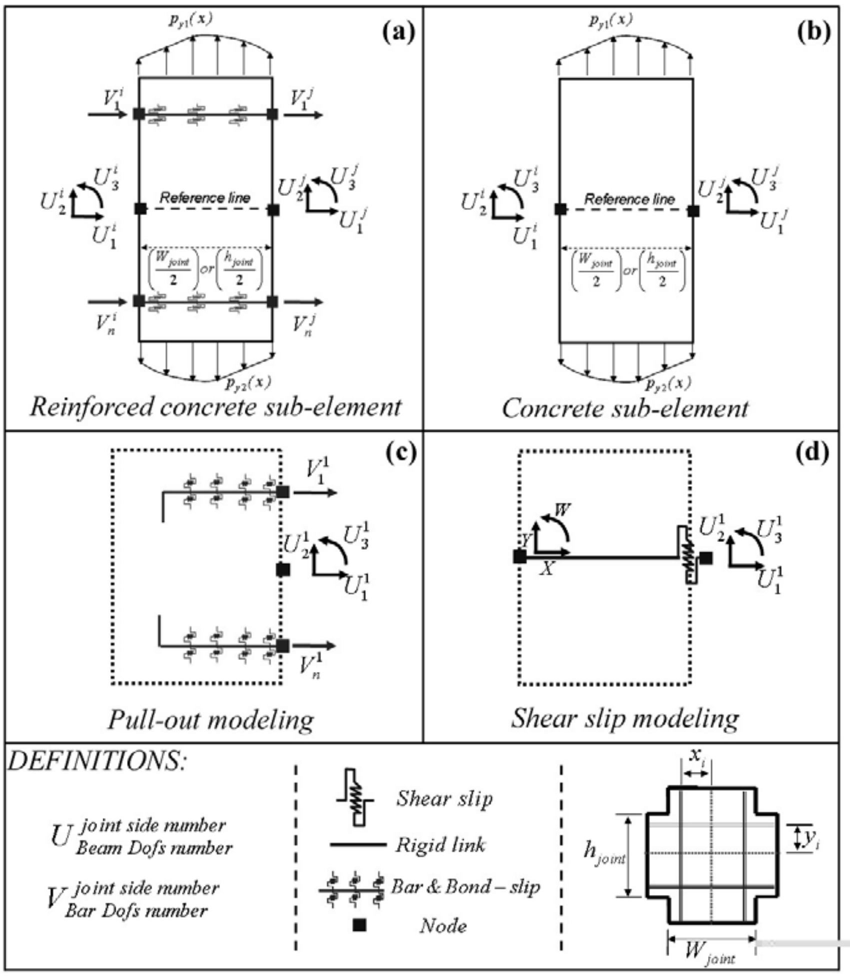

Figure 3. Joint element parts and definitions

5. CONCRETE SUB-ELEMENT

Concrete sub-element hereafter is called "*CSE*" and is not reinforced. That is a regular 2-node concrete frame element with three degrees of freedom in each of two ends (Figure 3-b). The formulation of *CSE* derives frÿm Timoshenko beam theory, fiber method, and material behavior similar to concrete part in *RCSE*. Also, external load which affects on this sub-element is similar to that of *RCSE*.

6. PULL-OUT MECHANISM

According to Figure 3-c, simulation of stiffness and strength loss associated with bond strength deterioration for longitudinal reinforcement embedded in the joint is considered. If nodal displacement vector related to Pull-out behavior is defined as $U = \begin{bmatrix} U_1^1 & U_2^1 & U_3^1 & V_1^1 & . & . & V_n^1 \end{bmatrix}^T$, the slippage of the bars can be defined as below:

$$\mathbf{slip} = \begin{bmatrix} s_1^1 \\ s_2^1 \\ . \\ s_n^1 \end{bmatrix} = \begin{bmatrix} -1 & 0 & y_1 & 1 & 0 & . & 0 \\ -1 & 0 & y_2 & 0 & 1 & . & 0 \\ . & . & . & . & . & . & . \\ -1 & 0 & y_n & 0 & 0 & . & 1 \end{bmatrix} \mathbf{U} = \mathbf{A_{slip}U} \tag{8}$$

In which, y_n is the distance of bar n from reference line. The relationship between Pull-out force and slip for embedded bar number n in the section 1 can be defined as $f_n^1 = k_{slip\ n}^1 \times s_n^1$. In which f_n^1 is Pull-out force and $k^1{}_{slip\ n}$ is slip stiffness of Pull-out behavior. This equation derives from the bond stress-slip relationship related to Pull-out behavior which is selected according to Table 1, embedded length of the bar, conditions of end of the bar and perimeter of the bar section. Because Pull-out force is summation of bond stress on around surface of each embedded bar. The relationship between Pull-out force and slip of all bars in the section 1 can be written in the following matrix form:

$$\mathbf{f_{slip}} = \mathbf{k_{slip}^1} \times \mathbf{slip} \tag{9}$$

Where $\mathbf{k^1_{slip}}$ is a diagonal matrix which includes $k^1{}_{slip\ n}$ and $\mathbf{f_{slip}}$ is Pull-out force vector according to **slip** vector.

The nodal force vector can be expressed in the following form:

$$\mathbf{F} = \mathbf{A_{slip}^T f_{slip}} = \mathbf{A_{slip}^T k_{slip}^1 slip} = \mathbf{A_{slip}^T k_{slip}^1 A_{slip} U} = \mathbf{K_{slip} U} \tag{10}$$

From Equation 10, Pull-out stiffness matrix related to section 1 can be written as $\mathbf{A_{slip}^T k_{slip}^1 A_{slip}}$. The Pull-out stiffness matrix will be imposed into stiffness matrix of *JE*. Also, in order to calculate resisting force vector related to Pull-out behavior and impose it into the resisting force vector of *JE*, it can be written as $\mathbf{A_{slip}^T f_{slip}}$.

7. SHEAR SLIP

According to Figure 3-d, in this method an interface shear component has been considered to represent shear slip and reduction sliding shear. According to degrees of freedom in shear direction in the specified side of *JE*, shear slip can be defined as below:

$$\Delta_{shear\,slip} = U_2^1 - Y = \begin{bmatrix} -1 & 1 \end{bmatrix} \begin{bmatrix} Y \\ U_2^1 \end{bmatrix} = \mathbf{A_{shear\,slip}} \begin{bmatrix} Y \\ U_2^1 \end{bmatrix} \tag{11}$$

If shear force-shear slip relation in the side of *JE* can be defined as $f_{shear\,slip} = k_{shear\,slip}\,\Delta_{shear\,slip}$, the stiffness matrix related to this mechanism and specified degrees of freedom can be written as $\mathbf{A}^{\mathbf{T}}_{\mathbf{shear\,slip}} k_{shear\,slip} \mathbf{A}_{\mathbf{shear\,slip}}$. Also, in order to calculate resisting force vector and impose it into the resisting force vector of *JE*, it can be written as $\mathbf{A}^{\mathbf{T}}_{\mathbf{shear\,slip}} f_{shear\,slip}$. Shear force-shear slip relation is generable by help of shear stress-shear slip relationship according to Table 1 and integration of shear stress over the side surface of the *JE*.

8. TYPE OF JOINT ELEMENTS

Table 2. Types of joint elements in a two dimensional *RCF*

Joint element type	**2*Concrete sub-element**	**Pull-out mechanism 3*Reinforced concrete sub-element 1*Concrete sub-element**	**4*Reinforced concrete sub-element**

♦ Number of sub-elements which is used in assembling.

9. NONLINEAR ANALYSIS AND NUMERICAL VALIDATION

In order to analyze *RCF* based on the proposed method, a computer program has been developed. The solution of equilibrium equations is typically accomplished by an iterative method through a convergence check. In this research the Newton-Raphson method is used as nonlinear solution algorithms [17]. Also the Gauss-Lobatto method is used for numerical integration in which the number of integration points is equal to five. For demonstrating the ability and reliability of the proposed method, verification for a one bay two storey *RCF* is presented. This frame is loaded laterally at the level of second storey and was tested by Vecchio and Emara [18]. The geometry of the specimen and the details of the cross sections are shown in Figure 4. Two 700kN of axial loads was imposed on the column before applying lateral load. Required information for numerical modeling such as bar and concrete material specifications are used as reported in [18]. In numerical modeling, beams and columns will be divided into enough number of *BCE*s. Because, the formulation is displacement based and the response is depend on element size and it is needed the length of *BCE* be enough short. As a simple suggestion, the length of *BCE* can be selected equal or smaller than average crack spacing in beam or column. In these cases convergence will be achieved in the numerical results. The equation which is given by CEB-FIP [19] is adapted for calculation of average crack spacing. Average crack spacing has been calculated as 112 and 90 mm for beams and columns, respectively. So, in numerical modeling first storey columns, second storey columns and the beams are divided into 20, 17 and 28 *BCE*s, respectively. Numerical analysis is carried out utilizing two approaches. In one approach the bond between bars and concrete is assumed to be perfect and in the other one, the effects of bond-slip such as Pull-out of bars in the joint and slip in *BCE*s are considered. Figure 5-a shows the analytical and experimental load-displacement responses. Results show that by perfect bond assumption the estimation of stiffness and capacity is higher than experimental values, but for the case with bond-slip effects, the proposed method has good precision for estimating both cases of stiffness and capacity in numerical analysis.

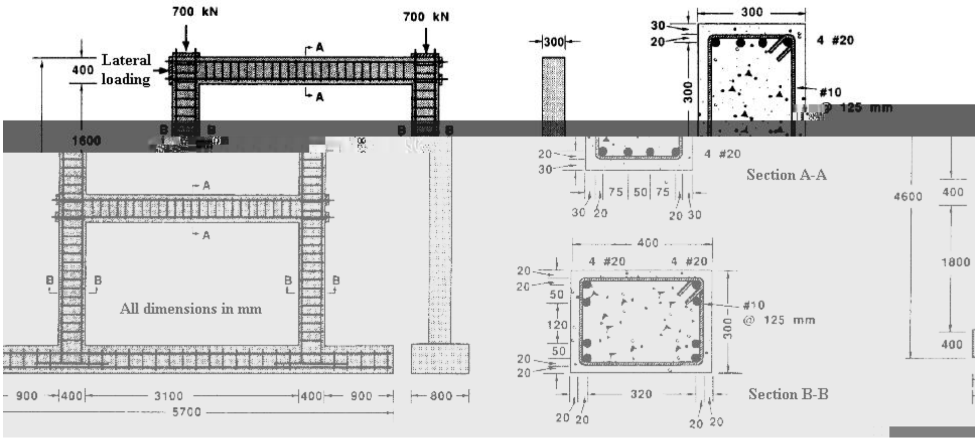

Figure 4. Geometry and details of the tested frame

In order to show the capability of the proposed method in considering Pull-out effect, four analyses with a variety of embedded length of the longitudinal bars of the columns in the footing is carried out. The results are shown in Figure 5-b in which, the case with 300 mm embedded length is the existing value of the model and the others are assumed. The results for two cases with 300 and 1000 mm length are approximately similar. It can be concluded for the existing model because of the sufficiency of embedded length, the Pull-out of the bars in the base is very insignificant.

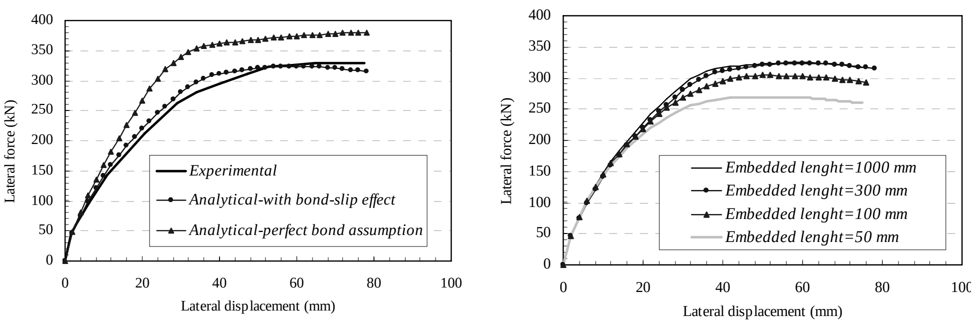

(a) (b)

Figure 5. Load-displacement response of the tested frame (a): comparing bond-slip effect; (b): comparing Pull-out effect

10. CONCLUSION

In this paper a new method for nonlinear analysis of two dimensional *RCF* is proposed. Each *RCF* is divided into two types of joint (*JE*) and beam-column

(*BCE*) elements. The effect of bond-slip has been considered in the formulation of *BCE*. Formulation of the *BCE* is based on the displacement method and displacement shape functions have been used in order to express the internal displacements in term of nodal displacement. *JE*s are formulated upon major behaviors including Pull-out of embedded longitudinal bars, shear and flexural deformation of *JE* and shear slip in interface section between joint and neighboring element. Four types of *JE*s have been generated according to their position in the frame based on major behaviors of them through the combination of one or more defined mechanisms and sub-elements.

In order to utilize the nonlinear analysis based on the proposed method, a computer program is developed and reliability of the method has been assessed through the comparison of numerical with experimental results for a one bay two storey *RCF*. The comparison shows a good agreement between experimental and analytical results. The proposed method can be used as an efficient numerical method for nonlinear analysis of *RCF* because of its capability for modeling of *JE,* with the consideration of bond-Slip effect, Pull-out of bars in the joints, shear slip and shear deformation.

REFERENCES

1. Park, R., Kent, D.C. and Sampton, R.A., Reinforced concrete members with cyclic loading, Journal of the structural division, ASCE, 1972, 98(7): 1341-1360.
2. Giuffre, A. and Pinto, P.E., Il Comportamento del cemento armato per sollecitazzioni cicliche di forte intensita, Giornale del genio civile, Maggio, 1970.
3. Menegoto, M. and Pinto, P., Method of analysis for cyclically loaded RC plane frames including changes in geometry and non-elastic behavior of elements under combined normal force and bending, Symp. Resistance and ultimate deformability of structures acted on by well defined repeated loads, IABSE reports, 1973, Vol. 13, Lisbon.
4. Eligehausen, R., Popov, E. and Bertero, V., Local bond stress-slip relationship of deformed bars under generalized excitations, Report No. UCB/EERC-83/23, Earthquake engineering center, University of California, Berkeley, 1983.
5. Okamura, H. and Maekava, K., Nonlinear analysis and constitutive model of reinforced concrete, Tokyo: Gihodo-shuppan, 1991.
6. Gan, Y., Bond stress and slip modeling in nonlinear finite element analysis of reinforced concrete structures, A thesis submitted for degree of master of applied science graduate, Department of Civil Engineering, University of Toronto, 2000.
7. Clough, R.W., Benuska, K.L. and Wilson, E.L., Inelastic earthquake response of tall buildings, Proceeding of third world conference on earthquake engineering, New Zealand, 1965, 2(2): 68-89.
8. Spacone, E., Filippou, F.C. and Taucer, F.F., Fibre beam-column model for nonlinear analysis of R/C frames: part I. formulation, Earthquake engineering and structural dynamics, 1996, 25: 711-725.

9. Limkatanyu, S. and Spacone, E., Reinforced concrete frame element with bond interfaces. Part I: displacement-based, force-based, and mixed formulations, Journal of structural engineering, ASCE, 2002, 128(3): 346-355.
10. Otani, S., Inelastic Analysis of RC Frame Structures, Journal of the structural division, ASCE, 1974, 100 (ST7): 1433-1449.
11. Alath, S. and Kunnath, S.K., Modeling inelastic shear deformation in RC beam-column Joints, Engineering mechanics: Proceedings of 10th conference: University of Colorado at Boulder, Boulder, Colorado, 1995, May 21-24, Vol. 2. New York, ASCE, 822-825.
12. Lowes, L.N., Mitra, N. and Altoontash, A., A beam-column joint model for simulating the earthquake response of reinforced concrete frames, Report No. 2003/10, Pacific Earthquake Engineering Research Center (PEER), 2004.
13. Scott, B.D., Park, R. and Priestley, M.J.N., Stress-strain behavior of concrete confined by overlapping hoops at low and high strain rates. Journal of the American Concrete Institute, 1982, 79(1): 13-27.
14. Gilbert, R. and Warner, R., Tension stiffening in reinforced concrete slabs. Journal of the structural division, ASCE, 1978, 104(ST12): 1885-1900.
15. Walraven, J.C., Fundamental analysis of aggregate interlock. Journal of the structural division, ASCE, 1981, 107 (ST11): 2245-2270.
16. Anderson, M., Lehman, D. and Stanton, J., A cyclic shear stress-strain model for joints without transverse reinforcement, engineering structures, 2008, 30: 941-954.
17. Bathe, K.J., Finite element procedures, Prentice Hall international, New Jersey, USA, 1996.
18. Vecchio, F.J. and Emara, M.B., Shear deformations in reinforced concrete frames, ACI Structural Journal, 1992, 89(1): 46-56.
19. Comite Euro International du Beton, CEB-FIP Model Code for Concrete Structures, Paris, 1978.

CD02-006

THE ANALYSIS OF FLEXIBLE CONCRETE FOUNDATIONS ON COARSE ALLUVIUM OF TEHRAN

A. Saeedi-Azizkandi[1], A. Fakher[2]
[1]Postgraduate Student, Civil Engineering Department, University of Tehran, Iran
[2]Associate Professor of Geotechnical Engineering, Civil Engineering Dept., University of Tehran, Iran

ABSTRACT
Regarding the increasing expansion of construction in Tehran, the design and construction of raft or grid concrete foundations are very common for tall buildings. Winckler springs are often used by professionals to model soils in the design of flexible concrete foundation. However, it presents a substantial problem because the Winckler springs are not coupled. Such a subgrade reaction theory is too simplified, i.e. it considers a fixed constant value for the stiffness of Winckler springs which leads to an incorrect design. Continuum mechanics theory and numerical simulation tools are available to be used for soil modeling but they are time consuming and most engineers prefer to use Winckler springs to model the soil. In the presented research, a computer program was firstly developed based on finite elements method. It could model a flexible foundation on springs but the springs are coupled by considering stress distribution within soil mass. The used method is very similar to Winckler springs model and tries to modify it. The method is employed for different geological formations in Tehran to show the effects of the properties of coarse alluvium of Tehran on the analysis of concrete foundations.

Keyword: tehran coarse grain alluvium, concrete foundation, stress distribution, deformation

1. INTRODUCTION
Importance of mat foundations:
In recent years, methods of analysis and structure construction have undergone many changes but the use of mat and grid foundations for tall buildings goes back to many years and such concrete foundations have shown their proven role in the transfer of construction forces to the ground.
A number of mat concrete foundation analysis methods, such as strips method, equivalent slab method, beam on flexible foundation or elasticity methods (Backer, 1957), have been used. Despite this, with advances in the methods of finite elements, the analysis of a slab on flexible foundation is the most used and spring is used for soil simulation [1, 2, and 3].
Mat concrete foundations can be assumed as a flexural beam or slab. Only this beam/slab relies on the ground at various points. Since the soil has less stiffness than concrete, ground response could be the most important variable in the design

of flexible concrete foundations and consequently plays an important role for analysis of concrete foundations. Therefore, the soil response is discussed for various geological formations of Tehran soil in this paper.

2. GEOLOGY OF TEHRAN DEPOSITS [4,13]:

Ribben (1966) was a European geologist who worked for the Geological Survey of Iran (GSI) in the mid-20th century. His classification of Tehran alluvia is still widely used by local geologists and engineers. Ribben (1966) divided the Tehran coarse-gained alluvia in two four categories, identified as A, B, C and D, where A is the oldest and D the youngest. Some simple profiles, produced by Fakher et al to schematically show the sequence of Tehran alluvia formation, are presented in Figure 1 and specifications of these alluvia are presented in Table 1 using conventional terminology.

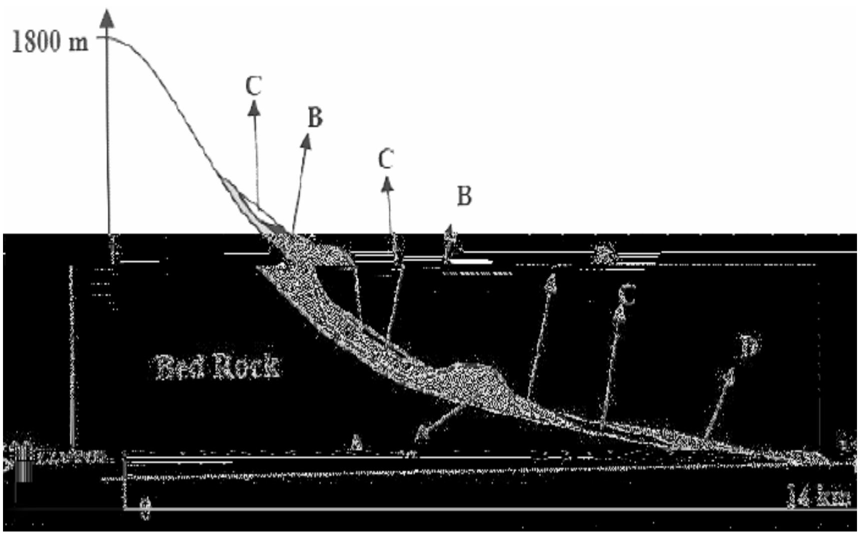

Figure 1. Formation of B, C and D alluvium after folding of A alluvium caused by erosion and sedimentation

3. CONVENSIONAL ANALYSIS OF FLEXIBLE MAT FOUNDATIONS [5]

One of the most common methods of designing foundation is the model of beam/slab on elastic subgrade and the displacement of each point is obtained through the following equations:

If we consider a strip footing with the width of B and unlimited length, the differential equation of deformation of this beam is according to Equation 1:

$$M = E_F . I_F . \frac{d^2 z}{dx^2} \quad (1)$$

M is internal bending moment of each section, and E_F and I_F are elasticity coefficient and moment of inertia of beam section respectively. On the other side, Equation 2 is valid for any beam:

$$\frac{d^2M}{dx^2} = Q \tag{2}$$

Q is soil reaction toward the lower surface of foundation. Winckler, 1967 presented soil reaction theory and in fact it depends on the soil elastic module. Soil Reaction theory is simplified elastic theory. (Q=K.Z) in which q is the pressure under the foundation, Z is elastic settlement, and K is the subgrade reaction coefficient.

Table 1.Comparison of Tehran alluvia based on Ribben classification [4]

Factor	A	B	C	D
Age	5Ma	700ka	50ka	10ka
Litho logy	Homogeneous conglomerate	Heterogeneous conglomerate	Alluvial fan	Recent alluvial
Cementation	Cemented and hard	Variable, but usually weak cement	Cementation less than A and non-hard	non-cemented
Grain size	Clay to 100-250 mm	Very variable up to several meters	Clay to 100-200 mm	Clay to several meters
Dip layer(deg)	0-90	0-15	0	0
Thickness(m)	Maximum1200	Maximum 60	Maximum 60	<10
Sedimentary environment	Fluvial	Fluvioglacial and periglacial	Fluvial	Fluvial
Other name (local name)	Hezardareh alluvial formation	North Tehran heterogeneous alluvial formation	Tehran alluvial formation	Recent alluvial
Location of observation in Tehran	North area	North area	North and central area	Recent and old riverbed

The main difference of E and K is that E is among properties of materials but K depends on dimensions and shape of foundation. To calculate subgrade reaction coefficient we have various field methods but Vesic presented an Equation 3 to find the subgrade reaction coefficient which is [6]:

$$K - 0.65\sqrt[12]{\frac{E_S . B^4}{E_F . I_F}} . \frac{E_S}{B.(1-V_S^2)} \approx \frac{E_S}{B.(1-V_S^2)} \tag{3}$$

In which Es and 5s are respectively elasticity module and soil Poisson coefficient. Subgrade reaction coefficient is a useful method in designing concrete pavements

of roads and airports. Maximum tensile stress is made in the lower surface of concrete slab upon influence of load on a concrete pavement. To change these roles, we use analysis of slab on the elastic subgrade and for this analysis we need to make the subgrade reaction coefficient clear.
According to Equations 1 and 2, we have:

$$-Z.K.B = E_F.I_F.\frac{d^4z}{dx^4} \tag{4}$$

By solving the said equation we will have:

$$Z = e^{-\alpha x}.(A_1.\cos(\beta x) + A_2.\sin(\beta x)) \tag{5}$$

In which A_1 and A_2 are fixed amounts which are calculated according to boundary conditions and loading. In above relation, β coefficient is gained from Equation 6. Based on recommendation of commission 436 of US Concrete Institute, if the distances between columns in a strip are less than 1.75/ β, the foundation is rigid otherwise the foundation will be assumed to be flexible.

$$\beta = \sqrt[4]{\frac{B.K}{4.E_F.I_F}} \tag{6}$$

4. MAIN ASSUMPTIONS OF CONVENSIONAL ANALYSIS

To use soil reaction theory, the substantial assumptions of this theory should be considered in full. The assumptions used in the soil reaction theory (Winckler model [7]) are:

a) The relationship between load (Q) and deflection (Z) is regarded as linear. It means Q is proportionally related to Z.
b) Kv (soil reaction coefficient in vertical direction) is regarded as fixed at all points of contact of foundation with soil. In fact in Winckler model, soil is considered as a series of elastic and independent (uncoupled) springs but it is not an accurate assumption. Not considering the reciprocal influence of springs on each other means that the spring will change its shape due to application of force to each spring and other springs will not be influenced by this force. In another words, soil in Winckler model has not been regarded as a continuum environment. Although due to connection between the constituting particles, soil is a continuum environment. Therefore in order to obtain the correct answer, springs must be related and connected to each other. In this way if a spring changes its form, some of this deformation will transfer to the adjacent springs.

To solve the problem of uncoupled springs, one can model the soil as a continuum body in a finite elements program. But due to the great number of elements, foundation analysis will be very time consuming. Another option is to consider stress distribution in soil in Winckler springs module.
In this paper the second option has been used to analyze concrete foundation.

5. METHOD OF ANALYSIS USED IN THE PRESENTED RESEARCH

In the presented research, a computer program was developed. It uses finite elements method to solve governing Equations. The soil is modeled as spring but stress distribution within soil mass is considered so the springs are couples. The following steps are undertaken to do the analysis.

Step 1:

Concrete foundation is modeled using 4-node flexural plate elements. Each node has 3 degrees of freedom and the stiffness of foundation is presented by Kr [8].
To verify the accuracy of foundation stiffness matrix, the displacement of a rectangular slab (Figure 2) under a uniform load of q is calculated in Table 2. The results are compared with the result of an analytical solution [9] and it shows the results are in a close agreement.

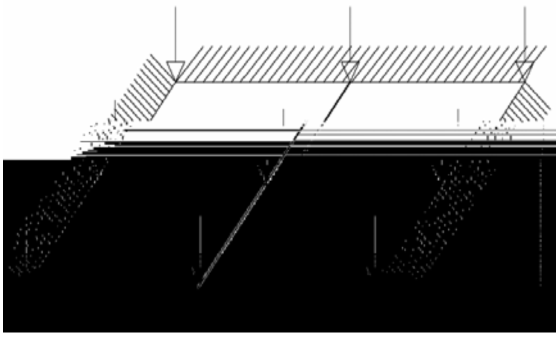

Figure 2. Square slab with fully fixed boundaries

Table 2. Displacement in the center-point slab

Number of element	**٤**	**٨**	**١٦**	**٦٤**	**٨١**	**١٢١**	**analytical solution**
Displacement	0/00148	0/00144	0/00140	0/00130	0/00128	0/00126	0/00126
Coefficient	qa^4/D	qa^4/D	qa^4/D	qa^4/D	qa^4/D	qa^4/D	qa^4/D

Step 2:

Stiffness of Winckler springs is obtained by the use of Vesic relation [6]. To assemble the stiffness matrix of foundation and subgrade, it is enough to add the stiffness of springs to the stiffness related to vertical displacement of each node (the elements on the main diameter of Kr matrix).

Step 3:

Displacement of each node is obtained according to [F] = [K].[Δ]. In this step, the distribution of stress within soil mass has not been considered so far and foundation analysis is done using the conventional analyses of foundation on elastic subgrade.

Step 4:
Based on the displacements gained from Step 2 and stiffness of springs calculated in Step 2, we can obtain the forces applied to soil. Now using Equation 7, we can find the displacement of j node due to applying of F force on the ith node [10].

$$W_j = \frac{F_i.(1-\nu_s^2)}{\pi.R.E_S} \qquad (7)$$

In which R is the distance of points i and j. Therefore displacement of each node is gained through Equation 8.

$$\Delta'_i = \Delta_i + \sum_{j=1} \Delta_{ji} \qquad (8)$$

In which Δ'_i, Δ_i and Δ_{ji} are respectively new displacements of node i, (by considering stress distribution), displacement of node i from Step 3 (without considering stress distribution), and displacement from real forces on various nodes on ith node.

Step 5:
The displacements obtained in Step 4 and Step 3 are compared to each other. If the precision is not enough, new stiffness of springs will be obtained according to the displacement and the forces applied to soil in Step 4, and the program will be implemented again from Step 3. These Steps are repeated until the displacements gained in Steps 3 and 4 have a slight difference.

6. VERIFICATION OF DEVELOPED PROGRAM

A number of examples have been used to assess the validity of the program. One example is presented here. A rectangular mat foundation in 2 m dimensions and thickness of 20 cm is considered on an elastic half–space (E= 40 MPa and 5=0.3). A concentrated force is applied equivalent to the unit to the middle of the edge of foundation (Point C in Figure 3). The results of used method and also the results of mathematical analysis are shown in Table 3 for comparison. The result of "fixed springs" in Table 3 are related to conventional method but the results of "variable spring" are derived when the stiffness of springs were varied according to Step 4, as described above. The comparison shows that the results of Variable spring and Mathematical solution are in a close agreement but the results of fixed spring are different.

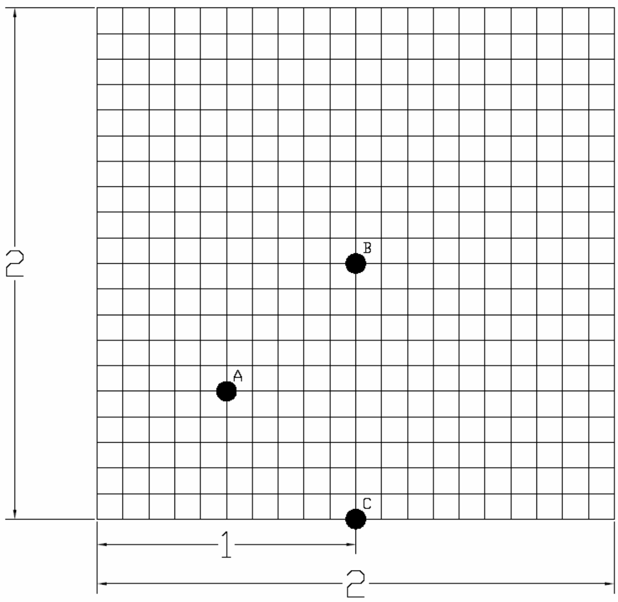

Figure 3. Elements of a square foundation

Table 3.The results of the used method and mathematical analysis.

Difference in percentage of pressure applied below the foundation with regard to mathematical solution	Pressure under the foundation	Difference in percentage of moment in Y direction toward the mathematical solution	Moment in Y direction	Moment difference percentage in X direction toward mathematical solution	Moment in X direction	
	0.306		-0.07		0.05	Mathematical solution [11,12]
%7	0.2845	%1	-0.069	%2	0.049	Variable spring
%70	0.5202	-%56	-0.109	%28	0.036	Fixed spring

7. INFLUENCE OF SOIL STIFFNESS IN FOUNDATION ANALYSIS

Regarding the increasing expansion of construction in Tehran and the type of coarse-grained soil in Tehran, it is highly important to determine the engineering parameters of this soil (the stiffness of spring) for mat concrete foundations analysis. According to the published data from local tests, the stiffness of Tehran soils are summarized in Tables 4&5 for formations of A and C [4, 13]. It should be noted that no accurate data is available for B formation because the size of aggregates are large and consequently large scale in-situ tests should be done to find stiffness of springs.

Table 4: Engineering variables of formations A and C [13]

Source	Amini (1994)		SES (1995)		Pahlavan (2002)		
Location	Generally		North of Koy Nasr Hill	Milad Tower	North of Koy Nasr Hill	End of Koy Nasr	Teachers' Training University
Type of formation	A	C	A	A	A	A	C
KS (MN/m)	280	25-250	170-350		770 1330	770 1330	170 290
E (Mpa)	17	15-150	125	125	168-288	154 288	36 62
V	-	-	0.35	0.38		0.28	

Table 5: Engineering variables of formations A and C [13]

Source	**Asghari (2002)**			**Cheshomi (2006)**		
Location	**End of Koy Nasr**	**North of Koy Nasr Hill**	**Resalat Tunnel**	**End of Koy Nasr**	**Emam Ali Highway**	**Emam Ali Highway**
Type of formation	A	A	A	A	A	C
KS (MN/m3)	900-940	510-1100	225-425	650-760	800-1000	160-260
E (Mpa)	195-204	111-238	49-92	141-165	166-217	39-67
5		0.28		0.29	0.31	0.28

The values presented by Amini (1996) have been recommended based on the conducted studies on Lines 1 and 2 of Tehran Subway and presented as general suggestions. The values presented by Soil Mechanical Engineering Services Company (SES, 1996) have been presented based on drilling several boreholes, sampling and conducting field and laboratory tests. The values presented by Pahlavan (2002) have been recommended based on field tests (plate loading, shear wave and Menard type pressure meter testing). Values presented by Asghari (2002) have been proposed based on plate bearing and large direct shear test. Values presented by Cheshomi (2006) have been recommended based on the direct shearing experiments and plate bearing and seismic inside well loading.

According to the above mentioned researches, the elasticity module of formations A and C are assumed to be 140 MPa and 70 MPa respectively in this study. Poisson ratio of 0.3 is used for both the types of formation.The soil is considered as linear elastic springs

A number of examples have been used to study the effect of subgrade stiffness on the analysis of mat foundation. One example is presented in Table 7. A foundation measuring 5×5 meter with the thickness of 500 mm, under uniform load of 15 ton/m2 is divided into 64 elements and the results of the analysis are shown in Table 7 for both the types of formations A and C.

Table 6: Characteristics foundation

	Foundation
Young module (MPa)	2500
Poisson's ratio	0.2
Bulk module (MPa)	13900
Shear module (MPa)	10400

Table7: Result of investigation on coarse grain alluvium

Type of formation	Es	5s	Displacement (fixed spring) (m)	Displacement (variable spring) (m)	Percent Difference
A	140	0.3	5.16E-3	9.92E-3	92%
C	70	0.3	1.05E-2	1.98E-2	85%

8. CONCLUSIONS

According to the presented study, the following conclusions could be proposed:

- When fixed stiffness Winckler springs are used and stress distribution within the soil mass is neglected in the analysis of flexible mat foundations, the obtained moments have a great difference with the mathematical solution. Therefore, the design of concrete mat foundations is not reliable when fixed stiffness Winckler springs is used.
- Based on comparisons with mathematical solutions, the presented program (used coupled spring method) has appropriate accuracy. In addition to Tehran soil, the method presented for analysis of concrete foundations is usable for all types of soils.
- The influence of considering stress distribution within soil mass (coupled springs) in Formation A is more than Formation C. Therefore, the use of fixed stiffness Winckler springs (conventional method used by professional engineers) is highly recommended for extensive usage in Formation A in Tehran for the design of concrete mat foundations.

REFRENCES

1. Ulrich, E. J., (1988), “Geotechnical Consideration in Mat Foundation Design,” Soil Structure Interaction, ASCE, Illinois Section, Chicago, pp1-33.
2. Ulrich, E. J., (1991), “Sub grade Reaction in Mat Foundation Design,” Concrete International, American Concrete Institute, pp 41-50.
3. Ulrich, E. J., (1995), “Design and Performance of Mat Foundations,” State-of-the-Art Review, Detroit Michigan, American Concrete Institute.
4. Fakher, A. Cheshomi, A., and Khamechian, M. (2007), The addition of geotechnical properties to a geological classification of coarse grain alluvium in a pediment zone. The Quarterly Journal of Engineering Geology and Hydrogeology, 40 (2) 163-174.

5. Braja M. Das., (1941), “Principles of foundation engineering,” Second Edition, PWS-KENT Publishing Company, BOSTON.
6. Vesic AS. Beams on elastic subgrade and the Winckler’s hypothesis. 5th International Conference on Soil Mechanics and Foundation Engineering, Paris 1961; 1:845-50.
7. Winckler, E. (1867) “Die lehre von Elastizitat und Festigkeit (On elasticity and fixity)”, Prague, 182p.
8. Akin, J. E., (1988), “Finite Element Analysis for Undergraduate,” Academic Press, London.
9. Timoshenko, S.P. and Woinowsky-Krieger, S. Theory of Plates and Shells. New York, Mc Grow -Hill Book Co., 1959.
10. Tsytovich, N. A., (1963), “Mekhanika Gruntov (Soil Mechanics),” 4th Ed, Stroiizdat, Moscow.
11. Poulos, H. G. and Davis, E. H., (1974), “Elastic Solution for Soil and Rock Mechanics,” Wiley, New York.
12. Gorbunov-Possadov, M. I. and Serebrjanyi, R. V., (1961), “Design of structure on elastic foundations,” Proc. 5th Int. Conf. Soil Mech. Found. Eng., pp 643-648.
13. Cheshomi, Akbar ,Study of Mechanical Properties of Tehran Coarse Grained Alluvium Based on Combination of Geology and Mechanical Tests, A thesis presented for the degree of Philosophy in Geology, Tarbiat Modares University, 2006.

CD02-007

3D AND THREE PHASE'S MICROMECHANICAL CONSTITUTIVE MODEL FOR THE UNIAXIAL COMPRESSION TEST OF CONCRETE

I. Rasoolan[1] S.A.Sadrnejad[2], A.R.Bagheri[3]
[1]Ph.D Candidate of Civil Eng, Civil Eng. Faculty, K.N.T University, Tehran, Iran
[2]Prof.of Civil Eng, Civil Eng. Faculty, K.N.T University
[3]Associate Prof. of Civil Eng., Civil Eng. Faculty, K.N.T University

ABSTRACT

The mechanical behavior of concrete materials is strongly influenced by its microstructure. The macroscopic properties of concrete materials such as strength and stiffness are dependent on the properties of micromechanics. The advance of composite mechanics and advanced computing technologies has made possible the micromechanical analysis of concrete materials. At first the status of micromechanical modeling with special emphasis on the advantage and disadvantage of each model is presented.

The current paper focuses on the geometrical description and numerical simulation of normal-weight concrete at the mesoscale. In the first part the numerical representation of concrete at the mesoscale is introduced. The internal structure of concrete is considered at the micro level, and is treated as a three phase material comprised of aggregate particle, matrix, and the aggregate- matrix interfaces the generation of the mesoscale geometry, the finite element discretisation and the applied material laws with micro plane theory are described.

The main objective of this paper is to investigate the macroscopic behavior and progressive failure of concrete materials under static loading, as influenced by the properties of its constituents at the meso level.

Keywords: three phases, concrete, itz, finite element, micromechanical

1. INTRODUCTION

Concrete is one of the most popular construction materials, and people have been using it for a long time. Many models, theories and numerical techniques have been developed to represent its mechanical behavior, including a large variety of constitutive models, damage models and other novel developments such as the micro plane model. However, progressively more elaborated constitutive relations have also required a large number of parameters, sometimes difficult to obtain and with no clear physical meaning.

In the 1980s, the meso mechanical approach, sometimes known as numerical concrete, was proposed by Roelfstra et al., and was then followed by others [1]. It consisted of discretizing the first level of material (meso structure) and assigning to each material component its individual geometry and properties. There is no doubt that the complexity of the nonlinear behavior of concrete may be largely associated to its heterogeneity and components. Therefore, it seems reasonable that considering explicitly each material component (geometry and mechanical properties) will allow us to consider a simpler constitutive assumption in exchange for an increasing size of the global problem. After the pioneering work of Roelfstra, different methodologies for considering the meso structure have been proposed such as lattice models, particle models, continuum meso models, DEM models [2] and FEM models [3].

2. CONCRETE WITH THREE PHASES

Concrete is an artificial heterogeneous composite material which consists of aggregates which are bonded together by cement paste. In numerical simulations of concrete structures a homogenous material is usually assumed at the macroscale. Specific constitutive models allow simulating the fracture process at this macroscopic scale [4]. For different experimental setups other parameters are obtained, which implies, that the predictive capacity of the numerical model is restricted to a specific experiment**.** The underlying material structure, e.g. the distribution of the aggregates or the aggregate shape, is normally disregarded by these models.[5]

The influence of the material structure on the macroscopic material behavior can be analyzed using mesoscale models. In literature, concrete at the mesoscale is separated into three main components: the homogenous mortar matrix, the aggregates with a diameter greater than 2.0 mm and the interfacial zone between them. The mortar matrix is mainly composed of cement paste and aggregates with a diameter less than 2.0 mm. Porosities within the matrix are disregarded at this length scale. The interfacial transition zone (ITZ) is about 20 − 100 µm deep [6]. The experimental bond strength of the ITZ was about 33% to 67% of the tensile strength of the matrix [7].

3. CONTINUUM DAMAGE MECHANICS

Continuum damage mechanics is a constitutive theory that describes the progressive loss of material integrity due to the propagation and coalescence of micro cracks, micro voids, and similar defects. These changes in the microstructure lead to a degradation of material stiffness observed on the macro scale. The basic premise of continuum damage mechanics is that micro structural defects (micro cracks, micro voids) in a material can be represented by a set of continuous damage variables. An illustration of this concept is given in Figure 1. The value of the damage variable D at a certain point of the continuum is a measure of the number and size of defects in a small volume at this point.

It is assumed in the sequel that the development of damage does not introduce anisotropy into the material behavior and that a single, scalar damage variable suffices to describe the local damage state. In the more general, anisotropic case, a set of damage variables (or a tensor) must be used (Krajcinovic et al., 1981[8]; Lemaitre, 1996[9] Fichant et al., 1995[10]. The damage variable D is defined as $0 \leq D \leq 1$, where $D = 0$ represents the initial, undamaged material and $D = 1$

represents a state of complete loss of integrity. Strictly speaking, the initial material always contains some defects, but it is assumed that these are accounted for in the virgin material properties, so that the initial damage can be set at zero.
After a certain amount of loading, three regions can generally be distinguished in the material domain W as shown in Figure (1). No damage may have developed at all in a part Ω_O.The damage variable still has its initial value D = 0 in this region and the material properties are those of the virgin material. In a second region Ω_d, some development of damage has occurred, but the damage is not yet critical (0<D< 1). The limiting value *D* = *1* has been reached in the third region Ω_C, i.e., the mechanical integrity and strength have been completely lost in this region. The completely damaged region Ω_C is the continuum damage representation of a crack. It is important to realize that the local, complete loss of strength in Ω_C W implies that stresses are identically zero for arbitrary deformation fields.

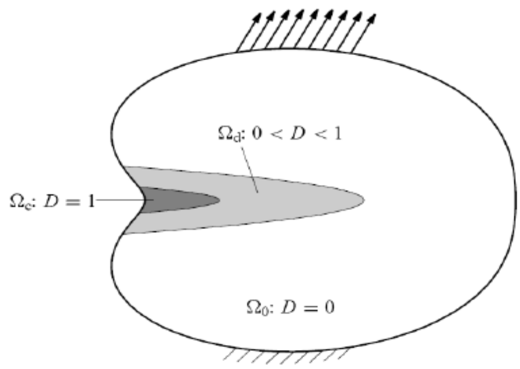

Figure 1. Damage distribution in a continuum [9]

4. LOCAL ISOTROPIC DAMAGE MODEL

Isotropic damage models are based on the simplifying assumption that the stiffness degradation is isotropic, i.e., stiffness moduli corresponding to different directions decrease proportionally, independently of the direction of loading. Since an isotropic elastic material is characterized by two independent elastic constants; a general isotropic damage model should deal with two damage variables. The simplified model with a single variable uses an additional assumption that the Poisson ratio is not affected by damage. The stress-strain law is written in the form:

$$\sigma = (1-\omega)D^e : \varepsilon \tag{1}$$

Where σ is the column matrix of stress components, ε is the column matrix of engineering strain components, D^e is the elastic material stiffness matrix, and ω is the damage variable. The growth of the damage variable must be described by a suitable evolution equation w, a tensor with multiple components. We define a scalar measure of strain called the *equivalent strain*, $\tilde{\varepsilon}$ and evaluate the internal variable κ _ that drives the damage evolution as the maximum value of $\tilde{\varepsilon}$ ever reached in the previous history of the material. Under monotonic loading, κ coincides with $\tilde{\varepsilon}$, but during unloading κ remains constant while $\tilde{\varepsilon}$ decreases. The choice of a specific expression for the equivalent strain directly affects the shape of the elastic domain in the strain space. For instance, one could define the equivalent strain as the scaled energy norm:

$$\tilde{\varepsilon} = \sqrt{\frac{\varepsilon^T D^e \varepsilon}{E}} \tag{2}$$

Scaling by Young's modulus E is introduced in order to obtain a strain-like quantity that is equal to the longitudinal strain in the special case of uniaxial loading. The multiaxial formulation is then a natural extension of the uniaxial one, and the function g that links κ to ω is the same as for the uniaxial model. For the energy-based equivalent strain, the elastic domain is ellipsoidal and symmetric with respect to the origin and the evolution of damage under tensile loading is the same as under compressive loading. For quasi brittle materials such as concrete, damage evolves much faster under tension than under compression. To take that into account, Mazars [11] proposed a definition of equivalent strain in the form

$$\tilde{\varepsilon} = \sqrt{\sum_{i=1}^{3} \langle \varepsilon_I \rangle^2} \tag{3}$$

where ε_I , I = 1; 2; 3, are the principal strains, and the brackets $\langle . \rangle$ denote the "positive part" operator, given by $\langle X \rangle$ = max(0; x), i.e., $\langle X \rangle$ = x for x positive and $\langle X \rangle$ = 0 for x negative.

5. MICRO PLANE FORMULATION WITH KINEMATICS' CONSTRAINT

The orientation of a micro plane is characterized by the unit normal n of components n_i (indices i and j refer to the components in Cartesian coordinate's xi). In the formulation with a kinematics constraint, which makes it possible to describe softening behavior of plane concrete in a stable manner, the strain vector ε_N on the micro plane (Figure 2) is the projection of the macroscopic strain tensor ε_{ij} so the components of this vector are:

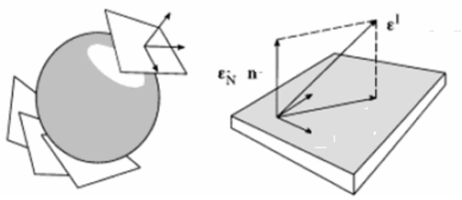

Figure 2. Micro plane and component.[17]

$$\varepsilon_{Ni\ i} = \varepsilon_{ij} n_j \tag{4}$$

The normal strain on the micro plane is $\varepsilon_N = n_i \varepsilon_{Ni}$, that is:

$$\varepsilon_N = N_{ij}\varepsilon_{ij}\,; \quad N_{ij} = n_i n_j \tag{5}$$

where repeated indices imply summation over I=1, 2, 3. The mean normal strain, called the volumetric strain ε_V and the deviatoric strain ε_D on the microplane can also be introduced which are defined as follows:

$$\varepsilon_V = \varepsilon_{KK}/3\ ;\ \varepsilon_D = \varepsilon_N - \varepsilon_V \tag{6}$$

This separation of ε*V* and ε *D* is useful when the effect of the hydrostatic pressure for a number of cohesive frictional materials, such as concrete, needs to be captured. To characterize the shear strains on the micro plane (Figure 2), we need to define two coordinate directions M and L, given by two orthogonal units coordinate vectors m and l of components m_i and l_i lying on the micro plane. To minimize directional bias of m and l among micro planes, one of the unit vectors m and l tangential to the plane is considered to be horizontal (parallel to x - y plane). The magnitude of the shear strain components on the micro plane in the direction of m and l are as $\varepsilon_M = m_i(\varepsilon_{ij} n_j)$ and $\varepsilon_L = l_i(\varepsilon_{ij} n_j)$. Because of the symmetry of tensor ε_{ij} , the shear strain components may be written as follows:

$$\varepsilon_M = M_{ij}\varepsilon_{ij}, \varepsilon_L = L_{ij}\,\varepsilon_{ij}\, j \tag{7}$$

in which the following symmetry tensors were introduced:

$$M_{IJ} = (m_i n_j + m_j n_i)/2 \quad L_{IJ} = (l_i n_j + l_j n_i)/2 \tag{8}$$

Once the strain components on each micro plane are obtained, the stress components are updated through micro plane constitutive laws, which can be expressed in algebraic or differential forms. In the kinematics constraint micro plane models, the stress components on the micro planes are equal to the projections of the macroscopic stress tensor $\sigma\, ij$ only in some particular cases, when the micro plane constitutive laws are specifically prescribed in a manner such that this condition can be satisfied. This happens for example in the case of elastic laws at the micro plane level, defined with elastic constants chosen so that the overall macroscopic behavior is the usual elastic behavior. In general, the stress components determined independently on the various micro planes will not be related to one another in such a manner that they can be considered as projections of a macroscopic stress tensor. Thus the static equivalence or equilibrium between the micro level stress components and macro level stress tensor must be enforced by other means. This can be accomplished [12a, b, c] by application of the principle of virtual work, yielding

$$\sigma_{ij} = \sigma_V \delta_{ij} + \frac{3}{2\pi} \int_\Omega [\sigma_D \left(N_{ij} - \frac{\delta_{ij}}{3} \right) + \sigma_L L_{ij} + \sigma_M M_{ij}] d\Omega \tag{9}$$

Where Ω is the surface of a unit hemisphere, σ_V σ_D are the volumetric and deviatoric part of normal stress component and σ_L and σ_M are as shear stress components on the micro planes respectively. Equation (9) is based on the equality of the virtual work inside a unit sphere and on its surface. The integration in equation (9) is performed numerically by Gaussian integration using a finite number of integration points on the surface of the hemisphere. Such an integration technique corresponds to considering a finite number of micro planes, one for each integration point. An approximate formula consisting of 26 integration points is proposed in this study. In Table 1, direction cosines and weights of the integration points and in Figure 2, their positions on the surface of the unit sphere are shown. Based on the formulation, macroscopic constitutive matrix in the proposed model is obtained as follows:

$$D_{ijkl} = {}^{3}\!/_{4\pi} \int_\Omega \left(\frac{E}{1+\nu}\right) \left[(N_{ij} - \delta_{ij}/3)(N_{kl} - \delta_{kl}/3) + M_{ij} M_{kL} + L_{ij} L_{kl} \right] d\Omega + \frac{E}{1-2\nu} \frac{\delta_{kl}}{3} \delta_{ij} \tag{10}$$

In which *E* and *v* are as elastic modulus and Poisson's coefficient.[12,a,b,c,d,e,f,g,h,i]

6. ANISOTROPY DAMAGE FUNCTION FORMULATION FOR THREE PHASES

Total deviatoric part of constitutive matrices is computed from superposition of its counterparts on the micro planes that such counterparts in turn, are calculated based on the damages occurred on each plane depending on its specific loading conditions. This damage is evaluated according to the five separate damage functions; each of them belongs to the particular loading states. These five loading conditions are as follows: (hydrostatic compression, hydrostatic extension, pure shear, shear + compression, shear + extension) that for three phases (aggregate, matrix and ITZ) are shown in Table (3). The stress-strain diagrams of both aggregate and cement paste are almost linear, except at very high relative stress levels as shown in Figure (3). The stress-strain relationship of concrete, however, has a curved shape, due to the fact that aggregate and cement paste, having different stiffness characteristics, are connected in one bearing system. In concrete types where the stiffness of the matrix is close to the stiffness of the aggregate, the stress-strain relationship of concrete will also be close to linear.

Table 1: Definition of micro planes

Direction cosines of integration points			Weights
l	**m**	**n**	
$\sqrt{1/3}$	$\sqrt{1/3}$	$\sqrt{1/3}$	27/840
$\sqrt{1/3}$	$-\sqrt{1/3}$	$\sqrt{1/3}$	27/840
$-\sqrt{1/3}$	$\sqrt{1/3}$	$\sqrt{1/3}$	27/840
$-\sqrt{1/3}$	$-\sqrt{1/3}$	$\sqrt{1/3}$	27/840
$\sqrt{1/2}$	$\sqrt{1/2}$	0.0	$32/840$
$-\sqrt{1/2}$	$\sqrt{1/2}$	0.0	$32/840$
$\sqrt{1/2}$	0.0	$\sqrt{1/2}$	$32/840$
$-\sqrt{1/2}$	0.0	$\sqrt{1/2}$	$32/840$
0.0	$-\sqrt{1/2}$	$\sqrt{1/2}$	$32/840$
0.0	$\sqrt{1/2}$	$\sqrt{1/2}$	$32/840$
1.0	0.0	0.0	$40/840$
0.0	1.0	0.0	$40/840$
0.0	0.0	1.0	$40/840$

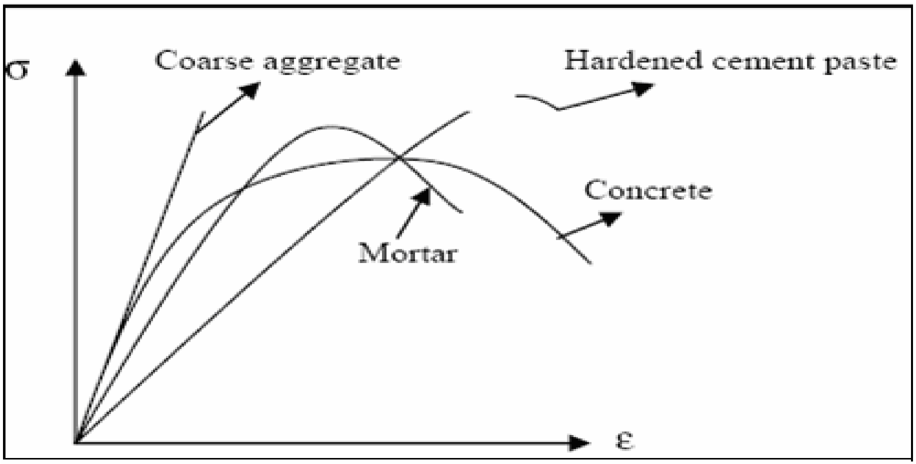

Figure 3. Diagram of concrete and its components.[15]

Table 2: Damage functions for three phases

Load Phases	**Matrix**	**Aggregate**	**ITZ**
hydrostatic compression	$\omega_{HC}=\begin{cases}0 & \varepsilon_{eq\prec i}\\ 1-\left(\frac{h}{\varepsilon_{eq}}\right)^{n} & \varepsilon_{eq}\succ i\end{cases}$	$\omega_{HC}=0$	$\omega_{HC}=\begin{cases}0 & \varepsilon_{eq}\prec p\\ 1-\frac{p}{\varepsilon_{eq}}\exp\left(-\frac{\varepsilon_{eq}-p}{q-p}\right) & p\le\varepsilon_{eq}\prec q\end{cases}$
hydrostatic extension	$\omega_{HT}=\begin{cases}0 & \varepsilon_{eq\prec d}\\ 1-\left(\frac{d}{\varepsilon_{eq}}\right)^{n} & d\le\varepsilon_{eq}\prec e\\ 1 & \varepsilon_{eq\succ f}\end{cases}$	$\omega_{HT}=\begin{cases}0 & \varepsilon_{eq}\le a\\ 1 & \varepsilon_{eq}\succ a\end{cases}$	$\omega_{TH}=\begin{cases}0 & \varepsilon_{eq}\prec k\\ 1-\frac{k}{\varepsilon_{eq}}\exp\left(-\frac{\varepsilon_{eq}-k}{l-k}\right) & k\le\varepsilon_{eq}\prec l\end{cases}$
pure shear	$\omega_{HS}=(\omega_C+\omega_T)$	$\omega_{HS}=(\omega_C+\omega_T)$	$\omega_{HS}=(\omega_C+\omega_T)$
shear + compression	$\omega_{C}=\begin{cases}0 & \varepsilon_{eq\prec x}\\ 1-\left(\frac{z}{\varepsilon_{eq}}\right)^{n} & \varepsilon_{eq}\succ y\end{cases}$	$\omega_{C}=\begin{cases}0 & \varepsilon_{eq}\le c\\ 1 & \varepsilon_{eq}\succ c\end{cases}$	$\omega_{C}=\begin{cases}0 & \varepsilon_{eq}\prec s\\ 1-\frac{s}{\varepsilon_{eq}}\exp\left(-\frac{\varepsilon_{eq}-s}{t-s}\right) & s\le\varepsilon_{eq}\prec t\end{cases}$
shear + extension	$\omega_{T}=\begin{cases}0 & \varepsilon_{eq\prec j}\\ 1-\left(\frac{g}{\varepsilon_{eq}}\right)^{n} & \varepsilon_{eq}\succ j\end{cases}$	$\omega_{T}=\begin{cases}0 & \varepsilon_{eq}\le b\\ 1 & \varepsilon_{eq}\succ b\end{cases}$	$\omega_{T}=\begin{cases}0 & \varepsilon_{eq}\prec m\\ 1-\frac{m}{\varepsilon_{eq}}\exp\left(-\frac{\varepsilon_{eq}-m}{n-m}\right) & m\le\varepsilon_{eq}\prec n\end{cases}$

On each micro plane at each step of loading, there exists one specific loading situation that may be in one of the five mentioned basic loading conditions. For every five moods, a specific damage function according to the authoritative laboratory test results available in the literature is assigned. Then, for each state of on plane loading, one of the five introduced damage functions will be computed with respect to the history of micro-stress and strain components. These five damage functions are as below parameters a - k in the above relations are computed according to laboratory results obtained for each specific concrete. In equation (9), ε_{eq} is as average strain and in the other relations is as the magnitude of projected deviatoric strain vector on each microplane.

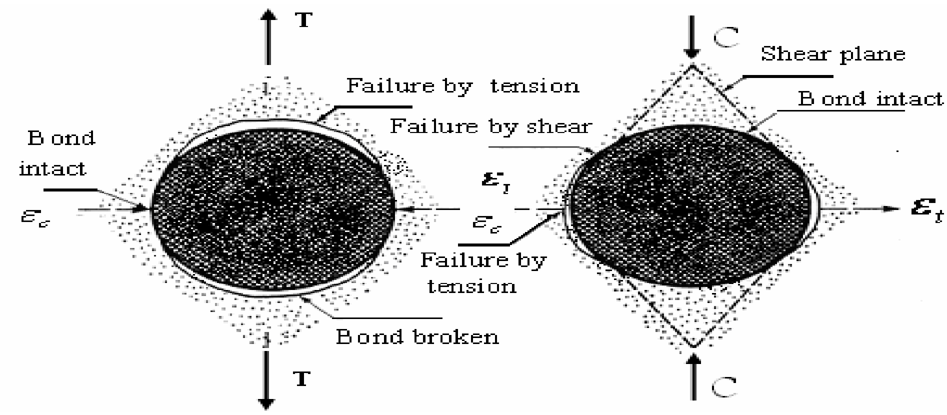

Figure 4. Local stresses around an aggregate particle [16]

7. FAILURE MECHANISM

Figure 4 describes the stress situation around an aggregate particle. The usual failure sequence, independent of the character of loading, is the exceeding of: Tensile bond strength; Shear bond strength; Tensile and shear strength of the cement matrix and Tensile strength of the aggregate particles. The difference in the area of the failure surface results in differences in compressive and tensile properties of both mortar and concrete.

8. GEOMETRICAL MODEL

With have a grading curve, therefore we can use simple methods instead of complex numeral and randomness or x ray methods to find effective diameter and use it to determine two arrangements with maximum and minimum aggregate volume as a repeatable basically element .As a result we can use this element to model the behavior of sample concrete in meso scale and three phases. In the mesoscale model, to simplify the problem, the shape of the coarse aggregate is assumed to be circular and the ITZ zone is modeled as a thin boundary layer around the aggregate. ITZ is a zone in the vicinity of a coarse aggregate, which is formed between bulk cement paste and the aggregate. Its formation is due to the water filled pores near the aggregate and the wall effect. According to static experimental and numerical results, it is well known that ITZ plays a very important role in a concrete mix and it is considered to be the weak link in a concrete composite.

For distribution of aggregates a cubic element fill of isometric spheres on two arrangements could be considered: **a):** regular lap b**):** regular compact

For modeling, two composites as shown in Figures (5, 6) are considered under a loading state of simple uniaxial compression. Due to symmetry, only a quarter of each composite needs to be analyzed and its finite element idealization is shown in the same Figureso it has a thin thickness and the usual continuum elements used in a conventional finite element analysis can not model this reign with real thickness satisfactorily, such an element would cause computational difficulties as its thickness decreases , then t=0.1 cm is employed for its thickness.

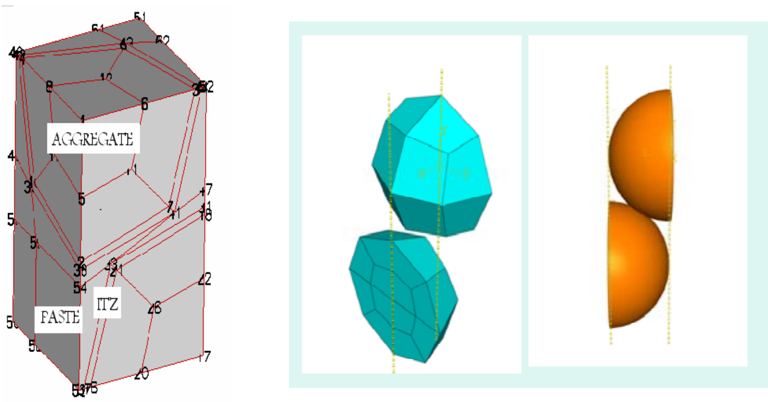

Figure 5. Arrangement a-meshing with three phases

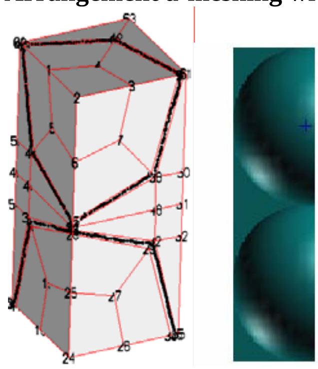

Figure 6. Arrangement b-meshing with three phases

9. MODEL PARAMETERS

In this formulation, we consider just three basic material parameters for every phase's elasticity and Poisson's coefficients and fracture energy that is based on extensive experimental data from literature for mortar and concrete according to table No .3 are given. [13, 14]

Table 3. Model parameters for three phases

Material parameter	aggregate	mortar matrix	ITZ
Young's Modulus(E)-(MPa)	60,000	30,000	10,000
Poisson's Ratio (α)-	0.2	0.23	0.2
Tensile damage threshold	4e-4	2e-4	1e-4
Compressive damage threshold	4e-3	2e-3	1e-3
Compressive strength- (MPa)	80	50	13
Tensile strength- (MPa)	16	3.4	2

10. NUMERICAL EXAMPLE

In this example the proposed micro-plane isotropic damage model is implemented in the finite element code. To establish the validity of the proposed 3d and three phases concrete model, correlation studies of analytical results with experimental evidence from the stress-strain response of concrete specimens under different loading conditions are presented in the following.

11. UNIAXIAL COMPRESSION (UC) TEST

As can be seen in Figure 7, there is a good agreement between the results that were fulfilled by the proposed model and experimental evidences. Experimental observations were experienced by Kupfer and his co-workers in 1969[.] Obviously, there exists an excellent coincidence between the analytical and laboratory data.

12. CONCLUSION

A new damage formulation has been employed into the micro-plane model. This damage formulation has been built on the basis of five fundamental force conditions that can essentially occur on each micro-plane for three phases. Consequently, any arbitrary change of six strain/stress components and change of the characteristics of component (aggregate, matrix, ITZ), normal concrete, high strength concrete led to a combination of five introduced on plane conditions. Therefore, the proposed model is capable of predicting the concrete behavior with any change. The five damage evolutions are functions of equivalent strain that were formulated for any of the five stated conditions. The equivalent strain for the first two conditions are defined as limitation in volumetric strain and for the others is the superimposed projections of deviatoric strain tensor on the corresponding micro-plane. The proposed model has excellent features such as pre failure strain distribution inside material which led to the final failure mechanism, however the basis of its formulation is simple, logical and has some physical insights that make it convenient to perceive.

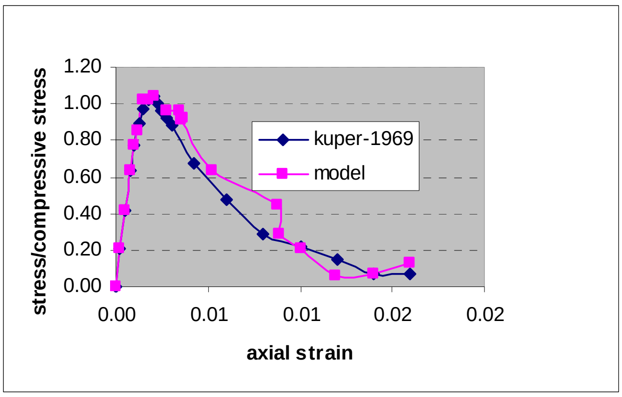

Figure 7. Uniaxial compression test of concrete obtained with proposed micro plane damage model

REFRENCE

1. Roelfstra, P. E., Sadouki, H. and Wittmann, F. H. "b´eton numerique" Material Structure 1985, no.8, pp327-335.
2. Illiu, G.Van Mier, J. G. M., "3D lattice type fracture model for concrete" Eng. Frac. Mech, No.70, 2003.
3. Lopez and Caballeroa and Carol, “3D meso structural analysis of concrete specimens under uniaxial tension. Fracture mechanics of concrete structure", Ia-FraMcos, 2004.
4. Jir´asek and Z.P. Baˇzant. Inelastic Analysis of Structures, Wiley, 2002.
5. Ghavamian and I. Carol. Benchmarking of concrete cracking constitutive laws: Meca project. In N. Bi´cani´c, R. de Borst, H. Mang, and G. Meschke, editors, Computational Modeling of Concrete Structures, EURO-C 2003, pages 179-187, 2003.
6. Mehta, p.k, Monterio.p.j.m,"concrete, structure, properties and materials", Prentice Hall, 1993.
7. T.T.C. Hsu and F.O. Slate. "Tensile bond between aggregate and cement paste or mortar."Journal of the American Concrete Institute, 60:465-486, 1963.
8. Krajcinovic, D., Fonseka, G.U., The continuous damage theory of brittle materials. Part I: General theory. J. Appl. Mech., 1981, 809-815.
9. Lemaitre, J.,' A Course on Damage Mechanics' 2nd edition, 1996, Springer, Berlin.
10. Fichant, S., Pijaudier-Cabot, G., La Borderie, C., 1995. Continuum damage modelling with crack induced anisotropy. Computational Plasticity, Fundamentals and Applications. Proc. 4th Int. Conf., Pineridge Press, Swansea, U.K., 1045–1056.
11. Mazars, J. "A description of micro and macro scale damage of concrete structures.", J. Engrg. Fracture Mech., 25, pp. 729-737, 1986.
12. J., Ozbolt, Z.P., Bazant, "Numerical smeared fracture analysis: Nonlocal micro crack interaction approach”, International Journal of Solids and Structures, 39(6), pp-635-661-1996.
13. Bazant, Z. P., Caner, F. C., Carol, I., Adley, M.D., Akers, S.A. "Micro plane model M4 for concrete: I. Formulation with work-conjugate deviatoric stress". ASCE, J. Eng. Mech. 126(9), 944- 953, 2000.
14. Bažant Z. P., Giovanni, D. L., 2004." Nonlocal micro-planes model with strain-softening yield limits". Intl. J. Solids and Structures, 41: 7209-7240.
15. Bezant .Z. P. and. Part. P. C, "Microplane model for brittle plastic material", I. theory & II. Verification, Journal Engineering Mechanic. 114, 1988, 1672-1702.
16. I. Carol, P. Prat and Z. P. Bazant, "New explicit microplane model for concrete: theoretical aspects and numerical Implementation", Int. J. Solids Struct., 29, 1992, 1173-1191.
17. Carol.I, Bazant. Z. P. and P. Prat, "Geometric damage tensor based on microplane model", J. Engng Mech., 117, 1991, 2429-2448.
18. Bazant Z.P. and Oh B. H., "Microplane model for progressive fracture of concrete and rock', J. Engng. Mech., 111, 1985, 559-582.
19. Bazant Z.P., Xiang .Y, P. C., Prat, " Microplane model for concrete. I. Stress strain boundaries and finite strain", Journal of Engineering Mechanics, ASCE 122(3), 1996, 245-254.

20. Bazant, Z.P., P.G. Gambarova. "Crack shear in concrete: Crack band micro plane model." J. Struct. Eng., ASCE, 110, 1984, pp.2015-2036.
21. Zhou, X.Q, Hoa.h, "Mesoscale modelling of concrete tensile failure mechanism at high strain rates "Computers and Structures 86 (2008) 2013-2026.
22. Inna Mikhailovna Gitman, "Representative Volumes and Multi-scale Modelling of Quasi-brittle Materials"Proefschrift, 2006, Master in Applied Mathematics, Perm State Technical University geboren te Kaluga, Rusland.
23. Mehta, P.K., and Montrerio, "Concrete Structure, Properties and Materials", Prentice-Hall Inc., NewGersy, 2nd Ed-1993, 390 pp.
24. The European Union-Brite EuRam III,"Fatigue of normal weight concrete and lightweight concrete"EuroLight Concrete Document BE96-3942/R34, June 2000 0381, Project BE96-3942.
25. Ellen Kuhl and Ekkehard Ramm,"On the linearization of the microplane model", Mechanics of Cohesive-Frictional Material 3, 1998, 343-364.

CD02-008

MODELING CONCRETE BEHAVIOR UNDER REVERSED CYCLIC LOADING

H. Dabbagh[1], F. Aslani[2]
[1]Assistant Professor, Department of Civil Engineering, University of Kurdistan, Sanandaj, Iran
[2]M.Sc Student, Department of Civil Engineering, University of Kurdistan, Sanandaj, Iran

ABSTRACT

The computational simulating and analysis of reinforced concrete structures nonlinear behavior is subjected to reversed cyclic loading dependent on the modeling of nonlinear constitutive laws of materials. Nonlinear behavior of structural concrete includes cracking, crushing, tension stiffening, compression softening and bond slip where reversed cyclic loadings introduces further complexities, such as stiffness degradation in concrete and the Bauschinger effect in reinforcing steel. In this paper the reliability of presented constitutive models for concrete subjected to reversed cyclic loading that considers transition curve between compression and tension by using crack closing model is investigated. In the analysis of reinforced concrete structures, a number of diverse approaches have been used for material modeling. These include plasticity-based procedures, fracture mechanics procedures, and various nonlinear elastic models where this simulation is related to constitutive models based on elasticity approach. For these aims, by reviewing the results of experimental tests on concrete specimens under cyclic loading in both compression and tension, and by reviewing suggested constitutive models by various researchers especially important simple models, the accordance of these constitutive models with experimental results are investigated.

Keywords: constitutive models, reinforced concrete structures, nonlinear behavior, reversed cyclic loading, crack closing model

1. INTRODUCTION

Although experimental programs in laboratories for identifying nonlinear behavior of reinforced concrete (RC) structures give real results but they are limited to the knowledge of particular cases under restricted structural dimensions, sizes, shapes, loading and boundary conditions but the computational simulation approach has no limit to its application. A significant research effort to characterize the monotonic and cyclic behavior of concrete has been devoted to this task and these research efforts have increased even more with recent development of computational methods applicable to RC structures. A large variety of concrete models have been produced in the last years. These models can be categorized according to three approaches: models which are based on theory of elasticity, models which are based on theory of plasticity and models based on fracture mechanics (CEB [1]).

Also, some combinational models based on plasticity and fracture mechanics theory have been developed. Although it has been proved that the models derived from theory of plasticity and fracture mechanics theory can accurately simulate the observed behavior of concrete, its application in the engineering practice is reduced. This is motivated by the great amount of parameters that are usually needed and the difficulty to obtain them through conventional laboratory tests. In the context of this study, only simplified models which are essentially mathematical formulations derived from the generalization of test results for concrete under various loading histories are treated.

Many of these models have been documented in the literature, like Sinha et al. [2], Karsan and Jirsa [3], Yankelevsky and Reinhardt [4], Mander, Priestley and Park [5], Chang and Mander [6], Bahn and Hsu [7], Elmorsi et al. [8], Palermo and Vecchio [9], Mansour and Hsu [10]and Sima et al. [11] among others. Most of them refer only to the compressive cyclic behavior of concrete and only a few consider the cyclic tension response. Also, some other researchers have considered tension behavior of concrete under cyclic and monotonic loading. Several expressions have been documented in the literature to represent the softening branch, including straight lines (Baˇzant and Oh [12]), polylinear curves (Hillerborg et al. [13]), exponential curves (Gopalaratman and Shah [14]) and Sima et al. [11]), polynomial curves (Lin and Scordelis [15]) and their combinations.

Sinha et al. [2] were the first researchers to describe qualitatively and quantitatively the stress-strain response of concrete under cyclic loading. The experiment was under taken on a series of 48 tests that were performed on concrete cylinders with compressive strength from 20 to 28 MPa and subjected to cyclic axial compressive loading in order to determine the main factors governing the cyclic response of concrete. Karsan and Jirsa [3] later demonstrated that unloading and reloading are not unique and are dependent on the previous load history. They developed an experimental program consisting of 46 short rectangular columns of plain concrete under cyclically varying axial loads to investigate further the findings of Sinha et al. [2]. They concluded that there exists an envelope curve that can be represented by monotonic response of similar concrete properties. They considered the residual plastic strain as the principal parameter to determine the unloading curve equation and proposed an empirical formula to correlate the residual plastic strain with the point on the envelope from which unloading starts. When reloading starts from zero stress to meet the envelope curve, it is found that the reloading curve becomes rather flat in most of its range and maybe represented by a simple straight line (Sinha et al. [2]) or a second-order parabola (Karsan and Jirsa [3]).

Bahn and Hsu [7] developed a parametric study and an experimental investigation on the behavior of concrete under random cyclic compressive loading. They studied a set of parameters in a semiempirical way that controls the overall shape of cyclic stress-strain curve. This was carried out by combining the theoretical simulation and a series of experimental results. A power type equation was proposed for the unloading curve and a linear relationship for the reloading curve. Palermo and Vecchio [9] proposed a constitutive model for concrete consistent with a compression field approach. The concrete cyclic model presented by the authors considers concrete in both compression and tension. The unloading and reloading curves are linked to the envelope curves, which are represented by the monotonic response curves. Unloading is modeled using a Ramberg–Osgood formulation, considering boundary conditions at the onset of unloading and at a zero stress. Reloading is modeled as a linear curve with degrading reloading stiffness. Mansour and Hsu [10] developed an extension of the Softened Membrane Model (Hsu and Zhu [16]) subjected to reversal cyclic shear stresses. This work includes a cyclic uniaxial constitutive relationship for concrete that takes into account a "softening" of the concrete compressive strength caused by a constant tensile strain in the orthogonal direction. The unloading and reloading curves were formed by a set of pieced linear curves. Sima et al. [11] developed a constitutive model for concrete subjected to cyclic loadings in both compression and tension. Particular emphasis has been paid to the description of the strength and stiffness degradation produced by the load cycling in tension and compression, the shape of unloading and reloading curves and the transition between opening and closing of cracks. Two independent damage parameters in compression and in tension have been introduced to model the concrete degradation due to increasing loads. However, some authors (Okamura and Maekawa [17], Hordijk [18]) have provided an accurate approximation of the complete unloading–reloading cycle in tension.

In this paper, firstly the proposed monotonic stress–strain curves (envelope curves) in literature for concrete were compared with each other and experimental result tests in monotonic compression and tension loading. As a result of these comparisons, the suitable envelope curves were selected for cyclic constitutive models. Secondly, the developed constitutive models for concrete under cyclic compression loading in literature were compared with each other and experimental result tests in cyclic compression and tension loading. As a result of these comparisons, the simple and reliable models that have more consistency with experimental result tests are selected for simulation of RC structures.

2. THE COMPUTATIONAL SIMULATION OF NONLINEAR BEHAVIOR OF CONCRETE UNDER REVERSED CYCLIC

2.1. Envelope Curve in Compression Loading

The monotonic curve adopted as envelope should verify some desirable characteristics: the slope at the origin should be equal to the initial modulus of deformation, it should describe correctly the ascending and the descending post peak (softening) branch and it should permit us to adjust the post peak behavior to experimental results.

In this paper, the most important monotonic compression stress–strain curves relationships of concrete are summarized in Table1.

2.2. Envelope Curve in Tension Loading

In the pre-peak branch, a linear elastic relationship represents well the behavior in tension and most researchers have used this approach. The post-peak behavior is in some cases modeled as an abrupt fall to zero stress (perfect-brittle material). However, this simplification in the post-peak behavior does not agree with the experimental results and can produce incoherent results when it is applied in a computational model. In this paper, the most important monotonic tension stress–strain curves relationships of concrete are summarized in Table2.

2.3. Unloading and Reloading Curves for Cyclic Compressive Constitutive Models

When a concrete specimen is monotonically loaded up to a certain strain level and then unloaded to a zero stress level in a typical cyclic test, the unloading curve is concave from the unloading point and characterized by high stiffness at the beginning. The stiffness gradually decreases and becomes very flat at low stress levels and the residual plastic strains are considerably reduced. When reloading is performed from zero stress up to the envelope curve, it has been observed that the curve is rather flat in almost all of its length. The aim of modeling the shape of the unloading and reloading curves is to capture the damage accumulation and the energy dissipation of the material due to cyclic loading. Several types of curves have been used to reproduce the unloading curve also, like the Ramberg–Osgood equation used by Palermo and Vecchio [9] or Chang and Mander [6], the power type used by Bahn and Hsu [6] or the multilinear curve. In turn, reloading can be accurately modeled by a linear curve as is done by most researchers (Palermo and Vecchio [9], Bahn and Hsu [7], among others). The most important cyclic compression constitutive models (include: unloading curve, reloading curve, plastic strain point, common point and etc.) of concrete are summarized in Table3. Based on cyclic compression constitutive models in Table 3, two constitutive models consist of Bahn and Hsu [7], Elmorsi et al. [8] are selected, also, Sinha et al. [2] experimental results are selected to control the accuracy and ability of these cyclic constitutive models (Figures1 and 2). The drawings of these constitutive models have been performed by using MATLAB programming software.

2.4. Unloading and Reloading Curves for Cyclic Tensile Constitutive Models

The response of concrete under cyclic tension has been studied in detail by Reinhardt [20] and Reinhardt et al. [21]. More than 100 tests were performed on plain concrete under cyclic tension and numerical expressions for the softening branch and the unloading and reloading curves were derived. It was observed (like in the case of plain concrete under cyclic compression loadings) that the reloading curve does not return to the envelope curve at the previous maximum unloading strain and further straining is needed for taking up the envelope curve again. This phenomenon is less important than in compression. The energy dissipated in a tension cycle without incursions in the compression zone can be neglected when it is compared with the energy dissipated in a complete compression cycle**.** The most important cyclic tension constitutive models (include: envelope curve, unloading curve, reloading curve, plastic strain point, common point etc.) of concrete are summarized in Table 4. Based on cyclic tension constitutive models in Table 4 two constitutive models consisting of Foster and Marti [22] (used by Petersson [23] envelope curve) and Sima et al. [11] are selected, additionally, Reinhardt [20] experimental results are selected to control the accuracy and ability of these cyclic constitutive models

(Figures 3 and 4). The drawings of these cyclic tension constitutive models have been performed by using MATLAB programming software.

2.5. Transition Curves

A series of tests attempting to characterize the effect of damage in tensions when the specimen is loaded in compression were developed by Ramtani et al. [29]. These test results have shown that completely closing the cracks requires a certain amount of compression. Once the crack is closed, the stiffness of the concrete is not affected by accumulated damage in tension. The transition curve from tension to compression, once the damage in tension is produced, closing the cracked zones is assumed to be linear which is in agreement with the experimental results. The Elmorsi et al. [8] and Sima et al. [11] (using Legeron et al. [30] transition curve) transition curves are compared with Reinhardt [20] experimental result test (Figures 5 and 6). The drawings of these cyclic tension constitutive models have been performed by using MATLAB programming software.

Table 1: The Monotonic Compression Stress-Strain Curves Relationships of Concrete

Envelope Curve	Envelope Curve relationships
Modified Hognestad[24]	$\sigma_c = f_c'\left[1-0.15\left(\frac{\varepsilon_c-\varepsilon_c'}{\varepsilon_u-\varepsilon_c'}\right)\right] \quad \varepsilon_c' \le \varepsilon_c \le \varepsilon_u \quad \sigma_c = f_c'\left[\frac{2\varepsilon_c}{\varepsilon_c'}-\left(\frac{\varepsilon_c}{\varepsilon_c'}\right)^2\right] \quad \varepsilon_c \le \varepsilon_c'$
Young and Smith [25]	$\sigma_c = E_c\varepsilon\,\varepsilon^{(1-\frac{\varepsilon}{\varepsilon_c'})}$
Saenz [26]	$\sigma_c = \frac{E_c\varepsilon}{1+\left(\frac{E_c}{E_p}-2\right)\left(\frac{\varepsilon}{\varepsilon_c'}\right)+\left(\frac{\varepsilon}{\varepsilon_c'}\right)^2}; E_p = \frac{f_c'}{\varepsilon_c'}$
Collins and Mitchell [27]	$\frac{\sigma_c}{f_c'} = \frac{n}{n-1+\left(\frac{\varepsilon_c}{\varepsilon_c'}\right)^{nk}}\left(\frac{\varepsilon_c}{\varepsilon_c'}\right); if \quad \varepsilon_c/\varepsilon_c' < 1 \quad k=1$ $;if \quad \varepsilon_c/\varepsilon_c' > 1 \quad k = 0.67+\frac{f_c'}{62}\ Mpa$ $n = 0.8+\frac{f_c'}{17}, \varepsilon_c' = \frac{f_c'}{E_c}\frac{n}{n-1}, E_c = 3320\sqrt{f_c'}+6900$
Mazars and Pijaudier-Cabot[28]	$\left\{\begin{array}{ll}\sigma = \varepsilon E_c & \varepsilon \le \varepsilon_0 \\ \sigma = \left[\varepsilon_0(1-A)+A\varepsilon e^{\left(\frac{\varepsilon_0-\varepsilon}{\varepsilon_c'}\right)}\right]E_c & \varepsilon > \varepsilon_0\end{array}\right\} A = \frac{f_c'-\varepsilon_0 E_c}{E_c\left(\varepsilon_c' e^{\frac{\varepsilon_0}{\varepsilon_c'}-1}-\varepsilon_0\right)}$

Description:

ε_c' *: the equivalent strain at peak stress* f_c' *: the peak compressive stress*

ε_0 *: the strain at the elastic limit* E_c *: the initial modulus of concrete*

Table 2: The Monotonic Tension Stress-Strain Curves Relationships for Concrete

Envelope Curve	Envelope Curve relationships	Envelope Curve Shape
Heillerborg et al. [13]	**Polylinear curve: Bilinear stress-strain model** $\alpha_1 = 0; \quad \alpha_2 = \alpha_3 = \dfrac{2E_c G_f}{l_{ch} f_t^2}$	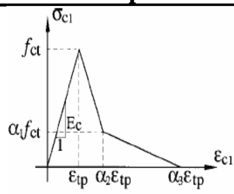
Petersson [23]	**Polylinear curve: The linear softening law** $\alpha_1 = 1/3; \quad \alpha_2 = \dfrac{2}{9}\alpha_3 + \alpha_1; \quad \alpha_3 = \dfrac{18}{5}\dfrac{E_c G_f}{l_{ch} f_{ct}^2}$	
Yankelevsky and Reinhardt [31]	$Ascending\ Branch : \sigma = k_t\delta - (k_t\delta_t - f_t)\left(\dfrac{\delta}{\delta_t}\right)^A \quad \delta \le \delta_t$ $A = \dfrac{k_t\delta_t}{k_t\delta_t - f_t}$ $Descending\ Branch : \sigma = f_t\left\{B - C\dfrac{\delta}{\delta_t} + D\ S_1\ exp[E(1 - S_2)]\right\} \quad \delta \ge \delta_t;$ $F(1 - 3E) = C/D; \ S_1 = \left(\dfrac{\delta}{\delta_t}\right)^F \ S_2 = S_1^3;$ $B = 0.09722; C = 0.0028319; D = 0.90597; E = 0.33247; F = -1.2$	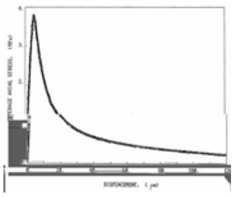
Izumo, shin, Maekawa and Okamura [32]	$\sigma_{cb} = f_t\left(\dfrac{2\varepsilon_{ct}}{\varepsilon}\right)^{0.4}$	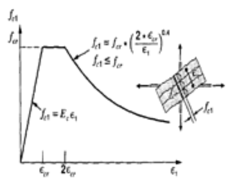
Sima et al. [11]	$\sigma = E_0\varepsilon_{ct}e^{\alpha\left(1 - \frac{\varepsilon}{\varepsilon_{ct}}\right)}, \alpha = \left(\dfrac{G_f E_0}{l^* f_{ct}^2} - \dfrac{1}{2}\right)^{-1} \ge 0$	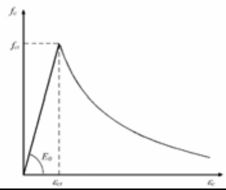

Description:

l_{ch} *: the characteristic length*, G_f *: the fracture energy*, f_t *: the peak tension stress* ε_{tu} *: the cracking strain*

E_c *: the initial mod ulus of concrete*, *w : crack width* ε_{ct} *: the equivalent strain at peak stress*,

3. DISCUSSION ON RESULTS

The concrete cyclic models consider concrete in compression and concrete in tension. The unloading and reloading rules are linked to backbone curves, which are represented by the monotonic response curves. The backbone curves are adjusted for compressive softening and confinement in the compression regime, and for tension stiffening and tension softening in the tensile region. In Figures 1-2, comparison of the Sinha et al. [2] experimental test with two cyclic compression constitutive models consisting of Bahn and Hsu [7] and Elmorsi et al. [8] are shown. As result of this comparison, Bahn and Hsu [7] constitutive model has a suitable result but plastic strain points that was used in these models relatively is not suitable, also, Elmorsi et al. [8] model is a simple model that can be improved by considering suitable unloading and reloading curves. In Figures 3-4, the comparison of Reinhardt [20] experimental test with two cyclic tensions constitutive models consisting of Foster and Marti [22] and Sima et al. [11] are shown. As a result of this comparison Sima et al. [11] Foster and Marti [22] and constitutive models have suitable outcome but these models can improve their ability by using compatible plastic strain points. In Figures 5-6, the comparison of Reinhardt [20] experimental test with two transition curves consisting of Elmorsi et al. [8] and Sima et al. [11] are shown. As a result of this comparison Sima et al. [11] (using Legeron et al. [30] transition curve) model has shown a suitable result but these models can improve their ability by using compatible plastic strain points. In addition, Elmorsi et al. [8] has a relative suitable ability to simulating transition curve.

Table 3: The Cyclic Compression Constitutive Models of Concrete

Model	Plastic Strain, Common and Reloading Points	Unloading and Reloading Curves
Karsan and Jirsa[3]	$\varepsilon_p = \varepsilon_c^{'}(1.76-\beta)\left(0.160\left(\frac{\varepsilon_{new}}{\varepsilon_c^{'}}\right)^2 + 0.133\left(\frac{\varepsilon_{new}}{\varepsilon_c^{'}}\right)\right)$ *where* $0.63 \le \beta \le 0.76$ $\sigma_{new} = f_c^{'}\beta\frac{(\varepsilon_{new}/\varepsilon_c^{'})}{0.315+0.77\beta}e^{\left[1-(\varepsilon_{new}/\varepsilon_c^{'})/0.135+0.77\beta\right]}$ *where* $\beta = 0.76$	$Unloading \quad Branch: \varepsilon_p = \varepsilon_c^{'}\left[0.145\left(\frac{\varepsilon_{un}}{\varepsilon_c^{'}}\right)^2 + 0.13\left(\frac{\varepsilon_{un}}{\varepsilon_c^{'}}\right)\right]$ $Reloading \quad Branch: \varepsilon_p = \varepsilon_c^{'}\left[0.093\left(\frac{\varepsilon_{re}}{\varepsilon_c^{'}}\right)^2 + 0.091\left(\frac{\varepsilon_{re}}{\varepsilon_c^{'}}\right)\right]$
Elmorsi et al.[8]	$E_{un}/E_c = 1-0.3(\frac{\varepsilon_{un}^c}{\varepsilon_{co}}-1) \ge 0.25 \quad for\ \varepsilon_{un}^c/\varepsilon_{co} > 1$ $E_{un}/E_c = 1 \quad for\ \varepsilon_{un}^c/\varepsilon_{co} \le 1$	*Unloading and Reloading Branch modeled by a linear response*
Bahn and Hsu[7]	$\varepsilon_p = \varepsilon_c^{'} c_p\left(\frac{\varepsilon_{un}}{\varepsilon_c^{'}}\right)^{n_p}$ *where* $c_p = 0.3, n_p = 2$ $c_u = 0.95, n_u = 1+\sqrt{\left(\frac{\varepsilon_p}{\varepsilon_c^{'}}\right)}, \sigma_p$: *partial unloading stress*	*Unloading Branch* $\sigma_c = \left(\sigma_p + c_u(\sigma_{un}-\sigma_p)\left(\frac{\varepsilon_c-\varepsilon_p}{\varepsilon_{un}-\varepsilon_p}\right)^{n_u}\right)$ *Reloading Branch* $\sigma_c = \sigma_{ppu} + c_r(\sigma_{re}-\sigma_{ppu})\left(\frac{\varepsilon-\varepsilon_p}{\varepsilon_{re}-\varepsilon_p}\right)^{n_r};$ $c_r = 1, n_r = 1, \sigma_{ppu}$: *patial unloading stress at the corresponding partial unloading strain*
Palermo and Vecchio[9]	$\varepsilon_p = \varepsilon_c^{'}\left[0.166\left(\frac{\varepsilon_{un}}{\varepsilon_c^{'}}\right)^2 + 0.132\left(\frac{\varepsilon_{un}}{\varepsilon_c^{'}}\right)\right]$ $N = \frac{(E_{c2}-E_{c3})(\varepsilon_p-\varepsilon_{un})}{f_{un}+E_{c2}(\varepsilon_p-\varepsilon_{un})} \quad \Delta\varepsilon = \varepsilon-\varepsilon_{un}$	*Unloading Branch* $f_c(\Delta\varepsilon) = f_{un} + E_{c2}(\Delta\varepsilon) + \left[\frac{(E_{c3}-E_{c2})\Delta\varepsilon^N}{N(\varepsilon_p-\varepsilon_{un})^{N-1}}\right]$ *Reloading Branch modeled by a linear response*
Sima et al.[11]	δ_{un} : *is the compressive damage* δ^- *at unloading point* $R = E_{pl}/E_0 \quad r = \varepsilon_{un}/\varepsilon_p$	*Unloading Branch* $\sigma = D^1 e^{D^2\left(1-\frac{\varepsilon-\varepsilon_o}{\varepsilon_{un}-\varepsilon_p}\right)} E_0(\varepsilon-\varepsilon_p)$ $D^1 = \frac{r(1-\delta_{un})}{(r-1)} \quad ; \quad D^2 = Ln\left[\frac{R(1-\delta_{un})(r-1)}{r}\right]$

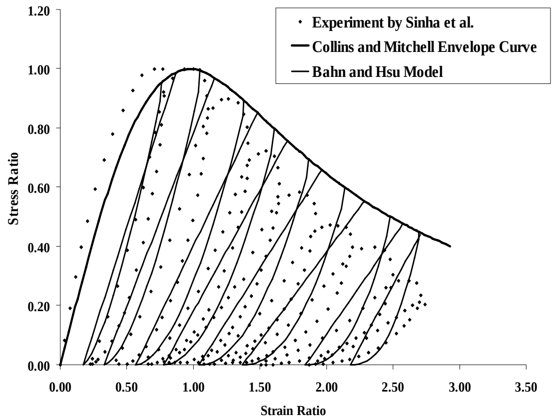

Figure 1. Comparison between Sinha et al. [2] experimental test with Bahn and Hsu [7] constitutive model

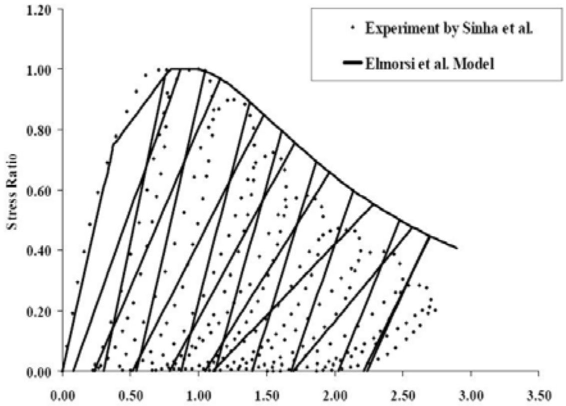

Figure 2. Comparison between Sinha et al. [2] experimental test with Elmorsi et al. [8] constitutive model

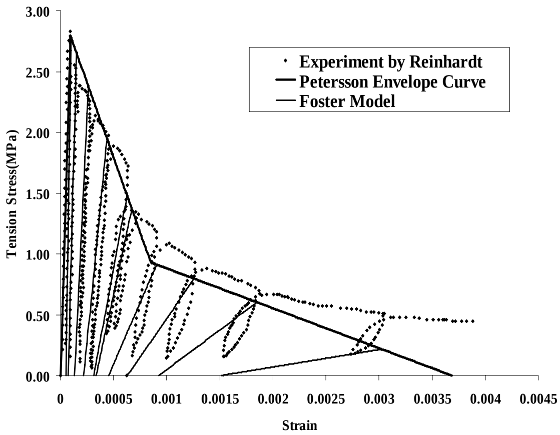

Figure 3. Comparison between Reinhardt [20] experimental test with Foster and Marti [22] constitutive model

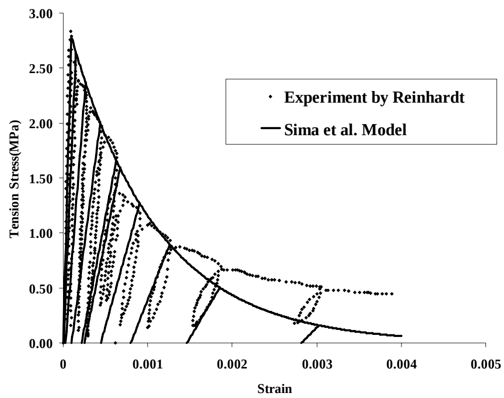

Figure 4. Comparison between Reinhardt [20] experimental test with Sima et al.[11] constitutive model

Table 4. The Unloading and Reloading Curves of Cyclic tension Constitutive Models of Concrete

Model	Unloading and Reloading Curves
Yankelevsky and Reinhardt [33]	$\sigma_0 = 0; \sigma_{z1} = -3 f_t; \sigma_{z2} = -f_t; \sigma_{z3} = -0.75 f_t; \sigma_{z4} = -0.5 f_t; \sigma_{z5} = -0.125 f_t$ $\sigma_F = -0.5 f_t; S_F = \frac{4S_E + 3S_2}{7}\ ; \sigma_G = -f_t; S_G = 0.8 S_F + 0.6 S_2$ $\sigma_D = D_1(S_D - D_3); S_D = \frac{D_1 D_3 - D_2 S_B}{D_1 - D_2}; D_1 = \frac{f_t}{D_3 - S_2}; D_2 = -\frac{\sigma_6 S_B}{S_B + \frac{S_2 \sigma_6}{f_t}}; D_3 = \frac{f_t S_C + \sigma_C S_2}{f_t + \sigma_C}$ $\sigma_c = C_2(S_C - C_3); S_C = \frac{C_1 S_B - C_2 C_1}{C_1 - C_2}; C_1 = \frac{0.75 f_t}{S_B - S_3}; C_2 = \frac{\sigma_A}{S_A - C_3}; C_3 = \frac{3(f_t S_A - \sigma_A S_2)}{3 f_t + \sigma_A}$ $\sigma_B = 0; S_B = \frac{f_t S_A + \sigma_A S_2}{\sigma_A + f_t}\quad \sigma_E = -0.125 f_t; S_E = \frac{8S_B}{3} - \frac{5S_A}{6}$
Okumura and Maekawa [17]	$Loading: \sigma_{cb} = f_t\left(\frac{\varepsilon_{tu}}{\varepsilon}\right)^c \le R_f f_t \quad \varepsilon \ge \varepsilon_{max} \quad \alpha = slop + \left(\frac{\sigma_{0cb}}{E_{b0}(\varepsilon - \varepsilon_p)} - slop\right)\left(\frac{\varepsilon - \varepsilon_p}{\varepsilon_0 - \varepsilon_p}\right)^{PN}$ $E_{b0} = \frac{\sigma_{t\,max} - \sigma_{b0}}{\Delta\varepsilon_{t\,max}}\quad Unloading\ Branch: \sigma_{cb} = E_{b0}(\varepsilon - \varepsilon_p)\alpha + \sigma_{b0} \le R_f f_t \quad \varepsilon < \varepsilon_{t\,max}$ $Reloading\ Branch:$ $\sigma_{cb} = \left(\sigma_{t\,max} - ((\sigma_{t\,max} - \sigma_{b0}) - \sigma_{0cb})\frac{\varepsilon_{t\,max} - \varepsilon}{\varepsilon_{t\,max} - \varepsilon_0}\right) + \sigma_{b0} \le R_f f_t \quad \varepsilon < \varepsilon_{t\,max}$
Foster and Marti[22]	A straight line is used for the unloading branch in tension. The same curve is considered for the reloading branch when there is no incursion in compression during a cycle. The plastic strain point in unloading or reloading is located at half length of unloading strain point.
Palermo and Vecchio[9]	$\Delta\varepsilon = \varepsilon_{1c} - \varepsilon \quad \varepsilon_c^p = 146\ \varepsilon_{1c}^2 + 0.523\ \varepsilon_{1c}$ $f_c(\Delta\varepsilon) = f_{1c} - E_{c5}(\Delta\varepsilon) + \left[\frac{(E_{c5} - E_{c6})\Delta\varepsilon^N}{N(\varepsilon_{1c} - \varepsilon_c^p)^{N-1}}\right]$ $N = \frac{(E_{c5} - E_{c6})(\varepsilon_{1c} - \varepsilon_c^p)}{E_{c5}(\varepsilon_{1c} - \varepsilon_c^p) - f_{1c}}\quad E_{c6} = 0.071 E_c(0.001/\varepsilon_{1c}) \quad \varepsilon_{1c} \le 0.001$ $E_{c6} = 0.0053 E_c(0.001/\varepsilon_{1c}) \quad \varepsilon_{1c} > 0.001$
Sima et al.[11]	A straight line is used for the unloading branch in tension. The same curve is considered for the reloading branch when there is no incursion in compression during a cycle. Based on experimental data from Reinhardt [13], the following criterion is proposed to account for the stiffness deterioration: $\frac{E_{new}}{E_0} = \left(\frac{\varepsilon}{\varepsilon_{ct}}\right)^{-1.05}$

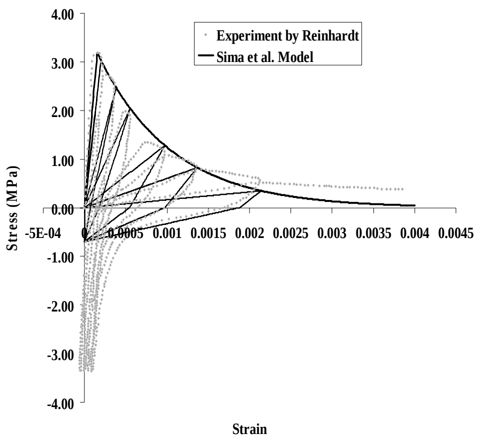

Figure 6. Comparison between Reinhardt [20] experimental tests with Sima et al. [11] constitutive model

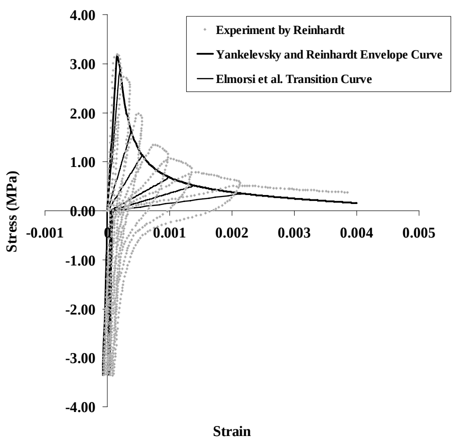

Figure 5. Comparison between Reinhardt [20] experimental tests with Elmorsi et al. [8] constitutive model

4. COUNCLUSION

From the comparison of monotonic compression and tension stress–strain curves of concrete, cyclic compressive and tensile constitutive models of concrete and transition curves, the following conclusions were drawn.

1. Experimental results have shown that the monotonic compression and tension curves of concrete present a linear response until approximately a half of the compressive and tensile strengths. Due to that, a first linear relation is considered until the elastic limit is reached. A nonlinear type equation is considered for the envelope stress-strain curve of concrete beyond the elastic limit. As result of above comparisons, Collins and Mitchell [28] envelope curve in compression and Sima et al. [11] envelope curve in tension have good agreement with experimental data.
2. Unloading response is assumed nonlinear, in the case of full loading, terminates

at the plastic offset strain. Models for the compressive and tensile plastic offset strains have been formulated as a function of the maximum unloading strain in the history of loading. Reloading is modeled as linear with a degrading reloading stiffness. The reloading response does not return to the backbone curve at the previous unloading strain, and further straining is required to intersect the backbone curve. The degrading reloading stiffness is a function of the strain recovered during unloading and is bounded by the maximum unloading strain and the plastic offset strain. Based on the comparisons, Bahn and Hsu [7] cyclic compression constitutive model and Sima et al. [11] and Foster and Marti [22] cyclic tension constitutive models have shown suitable ability to simulation of nonlinear behavior of concrete.

3. Legeron et al. [30] transition curve has shown suitable ability with the usage of Sima et al. [11] envelope curve and unloading curve.

REFERENCES

1. Comite Euro-International du Beton.R.C. Elements under cyclic loading-State of the Art Report, London: Thomas Telford, 1996.
2. Sinha BP, Gerstle KH, Tulin LG. Stress-Strain Relations for Concrete Under Cyclic Loading, ACI Structural Journal, 1964, Vol.61, No.2, pp.195-211.
3. Karsan ID, Jirsa JO. Behavior of concrete under compressive loadings, ASCE Journal of Structural Engineering, 1969, Vol.95, No. ST12, pp.2543-2563.
4. Yankelevsky DZ, Reinhardt HW. Model for Cyclic Compressive Behavior of Concrete, ASCE Journal of Structural Engineering, 1987a, Vol.113, No.2, pp.228-240.
5. Mander JB, Priestley NJN, Park R. Theoretical Stress-Strain Model for Confined Concrete, ASCE Journal of Structural Engineering, 1988, Vol.114, No.8, pp.1804-1826.
6. Chang GA, Mander JB. Seismic energy based fatigue damage analysis of bridge columns: Part I—Evaluation of seismic capacity, Technical report NCEER-94-0006. Buffalo (NY): State University of New York at Buffalo, 1994.
7. Bahn BY, and Hsu TTC. Stress-strain behavior of concrete under cyclic loading, ACI Material Journal, 1998, Vol. 95, No.2, pp.178-193.
8. Elmorsi M, Kianoush MR, Tso WK. Nonlinear analysis of cyclically loaded reinforced concrete structures, ACI Structural Journal, 1998,Vol.95, No.6, pp.725-739.
9. Palermo D, and Vecchio FJ. Compression field modeling of reinforced concrete subjected to reversed loading: Formulation, ACI Structural Journal, 2003, Vol.100, No.5, pp.616-625.
10. Mansour M, and Hsu TTC. Behavior of reinforced concrete elements under cyclic shear II: Theoretical model, ASCE Journal of Structural Engineering, 2005, Vol.131, No.1, pp.54-65.
11. Sima JF, Roca P, Molins C. Cyclic Constitutive Model for Concrete, Journal Engineering Structures, 2008, No.30, pp.695-706.
12. Bazant ZP, Oh BH. Crack Band Theory for Fracture of Concrete, Rilem,

Material and Structures, 1983, Vol.16, No.94, pp.155-177.
13. Hillerborg A, Modeer M, and Petersson PE. Analysis of Crack Formation and Crack Growth in Concrete by means of Fracture Mechanics and Finite Element, Cement and Concrete Research, 1976, Vol.6, pp.773-782.
14. Gopalaratnam VS, Shah SP. Softening Response of Plain Concrete in Direct Tension, ACI Journal, Proc., 1985, Vol.82, No.3, pp.310-323.
15. Lin CS, Scordelis A, Non Linear Analysis of RC Shells of General Forms , ASCE Journal of Structural Engineering, 1975, Vol.101, No.ST3, pp. 523-538.
16. Hsu TTC, Zhu and RRH. Softened membrane model for reinforced concrete elements in shear, ACI Structural Journal, 2002, Vol.99, No.4, pp.460-469.
17. Okamura H, Maekawa K. Nonlinear Analysis and Constitutive Models of Reinforced Concrete, Japan: Giho-do Press, University of Tokyo, 1991.
18. Hordijk DA. Local Approach to Fatigue of Concrete, Delft University of Technology, 1991.
19. Heilmann HG, Hilsdorf H, Finsterwalder K. Strength and Deformation of Concrete under Tensile Stress, Bulletin No.203, Deutscher Ausschuss fur Stahlbeton, 1969, pp.94.
20. Reinhardt HW, Fracture Mechanics of an Elastic Softening Material like Concrete, Heron, 1984, Vol.29, No.2, pp.1-42.
21. Reinhardt HW, Cornelissen HAW, Hordijk DA. Tensile Test and Failure Analysis of Concrete, Journal Engineering Structures, 1986, Vol.112, No.11, pp. 2462-2477.
22. Foster JS, Marti P. Cracked Membrane Model: Finite Element Implementation, ASCE Journal of Structural Engineering, 2003, Vol.129, No.9, pp.1155-1163.
23. Petersson PE. .Crack Growth and Development of Fracture Zone in Plain Concrete and Similar Materials, Rep. No.TVBM-1006, Lund Institute of Technology, Lund, Sweden, 1981.
24. Hognestad EA. A Study of Combined Bending and Axial Load in Reinforced Concrete Members, Bulletin No.399.Urbana (IL, USA): University of Illinois Engineering Experiment Station, 1951.
25. Smith G.M, Young and L.E. Ultimate Theory in Flexure by Exponential Function, Journal of the American Concrete Institute, 1955, Vol.52, No.3, pp. 349-359.
26. Saenz LP, 1964, “Equation for the Stress-Strain Curve of Concrete (Discussion), Journal of American Concrete Institute, 1964, Vol.61, No.9, pp.1229-1235.
27. Collins MP, Mitchell D. Prestressed Concrete Structures,” Prentice-Hall, New Jersey, 1991.
28. Mazars J, Pijaudier-Cabot G. Continuum Damage Theory. Application to Concrete, ASCE Journal of Mechanical Enginerring, 1989, Vol.115, No.2, pp.345-365.
29. Ramtani S, Berthaud Y, Mazars J. Orthotropic Behavior of Concrete with Directional Aspects:Modeling and Experiments. Nuclear Engng Design, 1992, Vol.133, pp.97-111.
30. Legeron F, Paultre P, Mazars J. Damage Mechanics of Nonlinear Seismic

Behavior of Concrete Structures, Journal of Structures Engineering, 2006, Vol.131, No.6, pp.946-955.

31. Yankelevsky DZ, and Reinhardt HW. Response of Plain Concrete to Cyclic Tension, ACI Material Journal, Vol.84, No.5, 1987b, pp.365-373.
32. Izumo J, Shin H, Maekawa K, Okamura and H. An Analytical Model for RC Panels Subjected to In-plane Stresses, Concrete Shea in Earthquake, Elsevier Appl. Sci., 1992, pp.206-215.
33. Yankelevsky DZ, Renhardt HW, Uniaxial Behavior of Concrete in Cyclic Tension, ASCE Journal of Structural Engineering, Vol.115, No.1, 1989, pp.166-182.

CD02-009

SEISMIC BEHAVIOR OF SHORT COLUMNS IN RC STRUCTURES

A. Kheyroddin[1], A. kargaran[2]
[1]Associate professor, School of Civil Engg. Semnan University, Semnan, Iran
[2]M.Sc. of Earthquake Engineering and Instructor of Islamic Azad University-Semnan Branch, Semnan, Iran

ABSTRACT
Civil engineering structures as well as office or apartment building are affected by earthquakes. A common cause of failure seems to be shear stress. The earthquake forces developed at different floor levels in a building need to be brought down along the height to the ground by the shortest path. Short column phenomenan is one of the effective causes of buildings failure in past earthquakes. This destructive phenomenon is due to column heighf difference in a story level that is predominantly because of localing building on sloppy ground. These buildings have unequal height columns along the slope, which causes ill effects like twisting and damage in shorter columns. In some buildings, few or no walls are provided at the first story (pilot). In the structures with difference in story level, major problems is due to discontinuity of floor diaphragm that causes significant changes in period, stiffness distribution of earthquake force and seismic loading of structures . In this research, at first, seismic behavior of short column phenomenon is determined, then, nonlinear behavior of reinforced concrete short columns in 4, 8 and 10 story structures with story level difference is investigated. Short columns and mentioned structures are analysed under the earthquake record of Elcentro with different peak ground acceleration with IDARC software which is nonlinear dynamic analysis program. In this investigation, the results of maximum response, base shear, global damage index and displacement time history and effect of short column in structural failure is evaluated.

Keywords: building with different floor, reinforced concrete, short column, damage index, nonlinear dynamic analysis

1. INTRODUCTION
In dublex structures, story floors with level difference relative to each other are made in two or more different height levels. The effective length of column in interface of these structures are divided in smaller sizes, that each of them act as a short column. In structures, the important difficultes are of lake connection diaphragm. Diaphragms play important role in transfering the lateral forces between resistant parts against earthquake as each disorder or separationin diaphragm floor cause stress concentration in their junction with vertical parts.Their most important role are transferring of intertial force of earthquake to

columns that regarding to stiffness difference of columns, more parts of these forces reach to short columns of floor that in the case of lack of suitable designing, severly damage, when earthquake occurs.(Figure 2).The important point in this structure is the height difference between two parts of dublex structure, that causes out standing changes in period and stiffness and distribution of earthquake force and loading of seismic of structure According to studies and researches ,it has been recognized that shearing force in column (short columns) that connects two dublex structures increase 1.5 to 2.5 relative to shear force in two same column in ordinary structures [1].

Figure 1. Short columns mentioned dublex reinforced concrete [16]

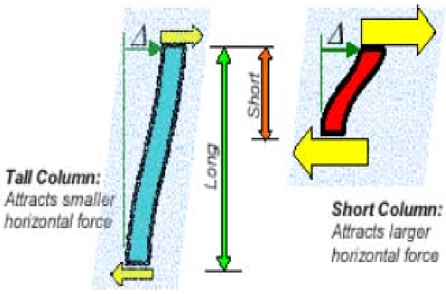

Figure 2. Compare short column and height column [16]

With respect to this subject, many researchers investigated in this field, we can refer to Moretti and Tassios [2,3] that test 8 specimens of RC short columns under fixed axial load and cyclic static displacement they measured steel and concrete strain results of seismic designing with low sheer ratio and seismic behavior of short column. They have measured and surveyed and suggested one truss model for stimulating of short columns of failure mechanism and with distribution of forces in columns. Also experiment studies on nonlinear behavior of different specimens of short column with decreasing or increasing of stirrup of a when reinforced with CFRP and GFRP panles (Carbon alyaf), under the effects of latorp cyclic displacement and wind force fixed. According to loading changes, and ductility by researchers such as Colomb etal [4] Promis al [5], Galal al [6], Ghobarah and Galal [7], Ye al [8] and Galal and Ghobarah [9] has been done. Bakhshi and Tabeshpor [10] analyse nonlinear dynamic, the effect of middle plate and phenomenon of short column with the help of IDARC. Soft ware and with tabes earthquake with maximum acceleration of 0.35g. Abbasnia and barghi [11] surveying many kind of destruction of columns effect cyclic period parameters that physically have effects on kind of destruction have recognized and using experimental information and loading results on some specimen, introduced new models for predicting of column. Kheyroddin and Mirnezami [1] by analyzing three 5, 10 and 15 story metal building seismic parameters such as period changes. Displacement and also formation of short column and factor of destruct have surveyed and suggested. Method for static loading equivalent dublex buildings. Surveying nonlinear behavior of more than 30 model of steel dublex structure in 6 different detail and comparing them in different condition including change, Kheyroddin and Mirnezami [12] suggested dublex floor level difference, effects if bending connects strengh thening of web and flange hardening bond foil. The most confining and stiffness plate suitable method and detail of frames with floor level which have phenomenon of short column

2. RESEARCH SIGNIFICANCE AND METHOD

In this research, seismic behavior of short column in 3 dublex structures have been surveyed that have height level difference 1.6 meter. Plan of all 3 investigated supposed to be equal and have variable height and include 4,8 and 10 story structures. Dimension of structures plan are 19.8 ×14.8 which have five 4.95 meter bay in X direction and four 3.1 meter bay and one 2.4 meter bay in Y direction. Because this plan is practical, dimensions and bay are real and structures have been recognized symmetric .Lateral load resisting system in all structures according to Iranian Code of Practice for Seismic Resistant Design of Buildings [13] in respect of ductility have been used medium concrete flexural frame and for gravitational loading subject of national regulation. Since dublex structures is measured (counted) on irregular height, seismic loading has been done of equivalent static and spectra dynamic. Column and beam dimensions in 4 stories structures in 1 st 2nd and 2 last floors are 45*45,40*40 and 35*35 cm respectively and beams dimensions 30*40 cm in both 2 floors have been brigade. In 8 story structures, columns at two 1 st floor 40*40cm and 2 last floor 35*35 cm and for beams 45*50, 45*45, 35*40 and 30*35cm brigade respectively. In 10 storey structures, like 8 storey structures expect in 2 first floor, Column dimension is 55*55 and beams dimension is 50*55.

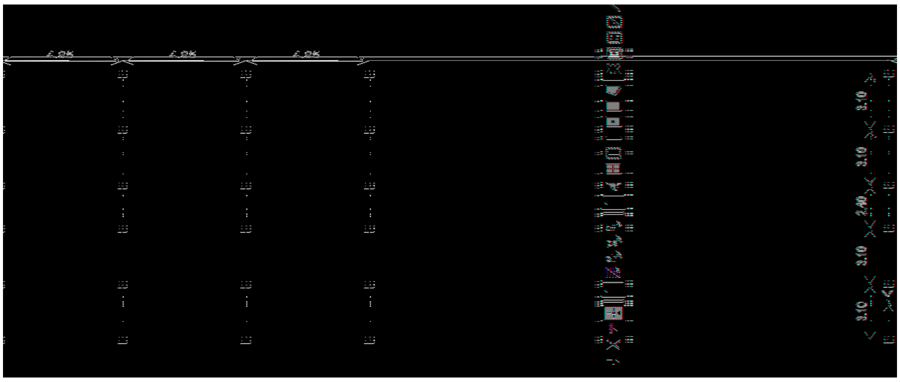

Figure 3. Plan of structures [16]

Damages on structural elements occurs. One progressive process. That causes its failure. This trend include damage stage in small scales, arising gathering damage in medium scales includes increasing of crack and their expending and damage at large scale that structure collapse. To survey actual behavior of structure when earthquake accrue, it is necessary that structure analyse under one nonlinear, analyse. For this IDARC v6.0 [14] nonlinear program has been used that been used for nonlinear analyses of reinforced concrete structures and has the capability to make histertis cycle frame geometrician characteristicsintersectiong reinforced concrete and its damage index is park-ang-wen. One of capabilities IDARC nonlinear software is modeling and indicating the structure behavior at one time step during earthquake to structures. In this research at first damage rate in short column on external frame of 4,8 and 10 storys structures under 0.3g,0.5g and 0.7g PGAs are surveyed and compared then choosing three elements of external frame of structures which include the last short column .medium and first column the following results are surveyd and compared:

- Time history of displacement answer of last short column, medium and first column.
- Time history of shear force in medium and first short column.
- Damage index at the top, down of medium and first short column.

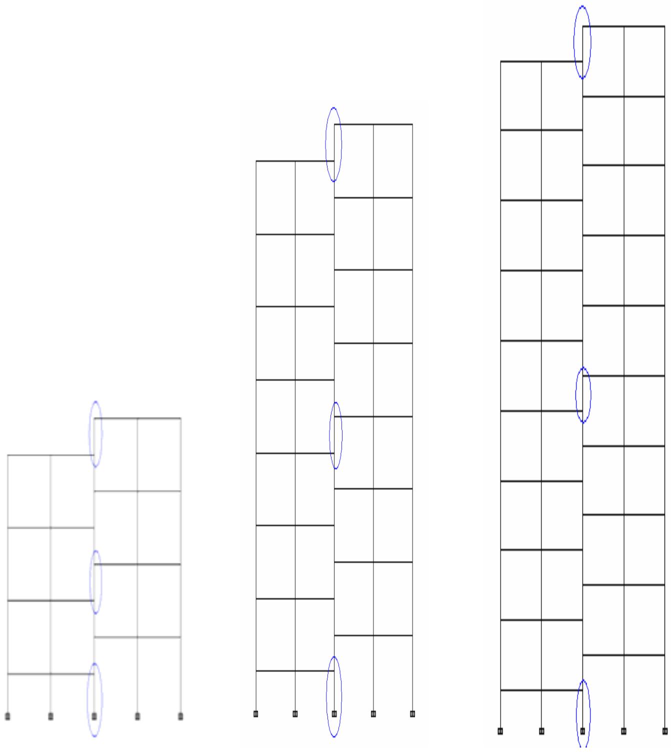

Figure 4. location short columns end, between, first in out frame of structure [16]

Because Elsentor1940 earthquake known as international earthquake by researchers and has been many in designing and rehabilitation of structures all over the world and approximately has complete. Frequency content, intensity time and frequency contain.In this research it has been used for dynamic analysis. Elsentro earthquake in 1940 with maximum speed 0.319g and duration of its story shaking is 30 seconds and have relative long and irregular vibration that one features of earthquake with medium depth and rock bed [15].

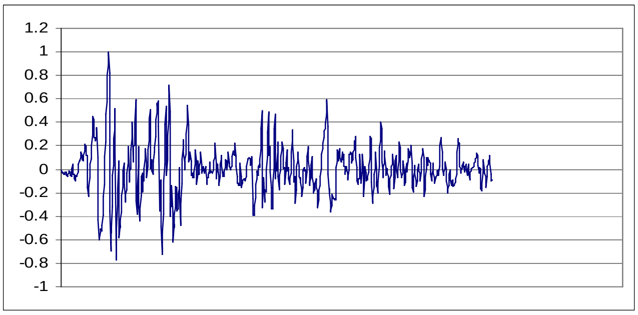

Figure 5. Record of Elsentro Earthquake [16]

2.1. Results of short column behavior under Elsentro Earthquake

Surveying of damage rate of short column in structures stories survey and comparison of from diagram indicates that in all structures increase of PGA the average damage rate in short column indifferent storey increase, Except in 8 floor structure in 0.3g damage in last short column has the most amount, this is because of frequency content in of Elsentro earthquake. Seismic Degree Damage of short column in floor building in all structures increase of structures height especially in upper storys damage index of short column has been increased. In 8 and 10 story structures, failure in short column by 4 and 6 storys are 0 and without failure (Figures 6 and 7).

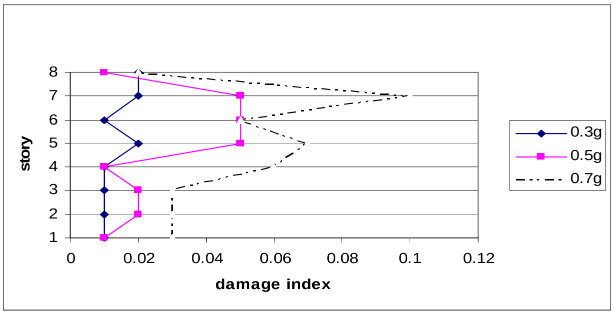

Figure 6. Damage index of short columns in storys of 4 story structure

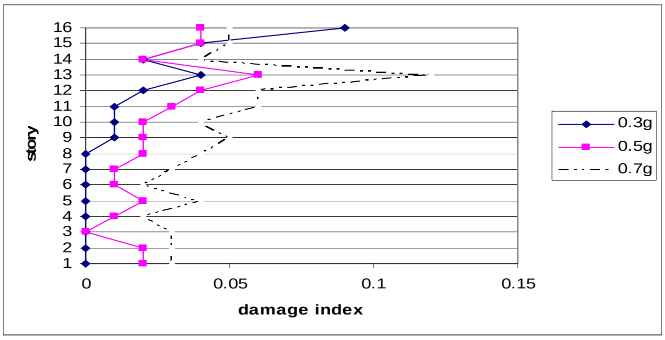

Figure 7. Damage index of short columns in storys of 8 story structure

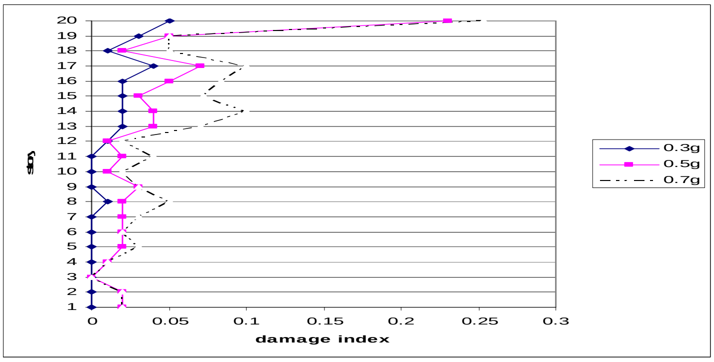

Figure 8. Damage index of short columns in storys of 10 story structure

2.2. Surveying Increasing of Figures Percent of Short Column in Different PGA

Since increasing PGA failure in short column has increased, comparing diagrams of Figures 9 indicates that average failure of short column in 0.7g, 0.5g relative to 0.3g in 1 storey structures has the most and in 8 storey structures has the lowest failure in short column.

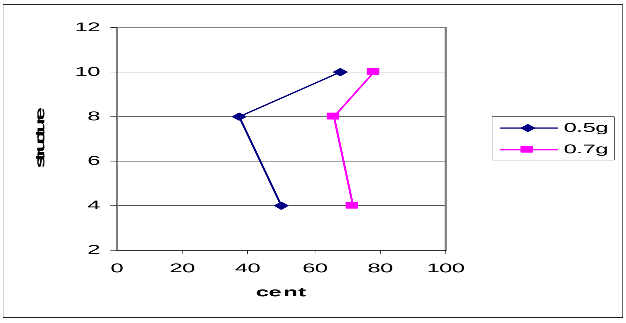

Figure 9. Damage percent average increase of short columns in 0.7g and 0.5g to compare 0.3g in structures

2.3. Investigation of Short Column Influence in Structural Failure

Investigation of short column share in structures failure comparing diagrams of Figures 10 deducts that short column of short column of 4 storey in 0.3 g and 0.7 have more influence in total structures for example in 0.3g in 4,8 and 10 structures 21, 19 and 12 percent if total structures failure related to short column failure in other word in 0.3g and 0.7g increasing the structures height short column from total structures failure will be decreased and in 0.5g short of short column failure in 10 story structures is more.

Figure 10. Short columns influence in structural failure

2.4. Investigation History of Last Medium and First Short Column Displacement in 4 Story Structure

By surveying compression of following answer history conclude that for average displacement history of last short column in 4, 8 and 10 story structures is more than first short column in all structures by increasing PGA. Time history of short column displacement increase except in 3 cases that its 8 and 10 story structures is approximately 25 to 30 percent and also in 4 story structures the first short column in 0.3g and 0.5g has the more displacement history then 0.7g.

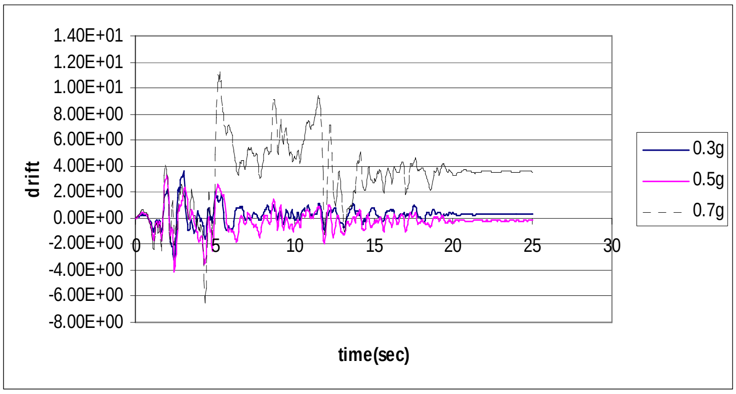

Figure 11. Displacement answer history of first short column at 4 story structure

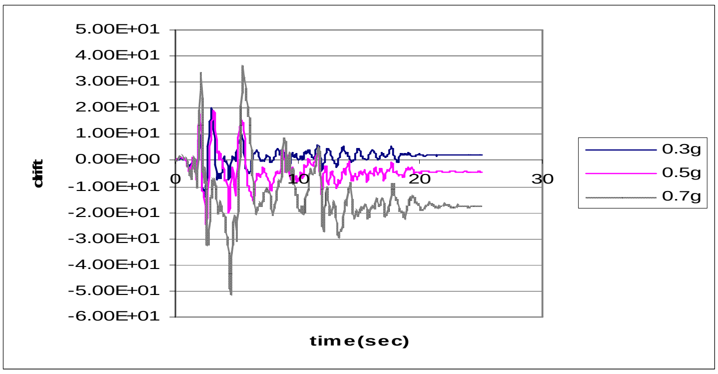

Figure 12. Displacement answer history of first short column at 4 story structure

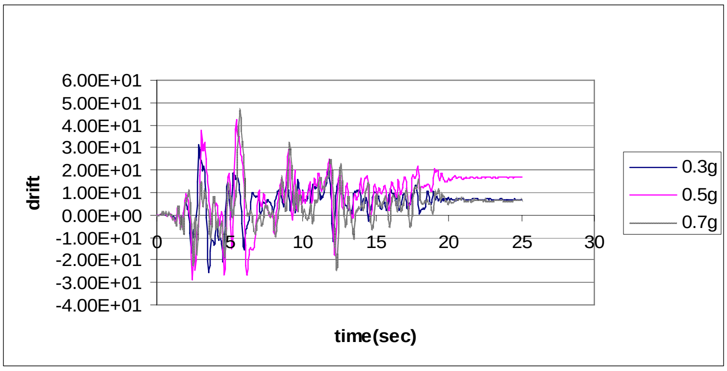

Figure 13. Displacement answer history of first short column at 4 story structure

Paying attention to following Figures it can be concluded that displacement time history of first and medium short column in 4 story structures and last short column in 10 story. Structures is high relative to other structures. For example displacement history of last short column in 10 story structures increasing is 26 and 56 percent more than 4 and 8 story structures.

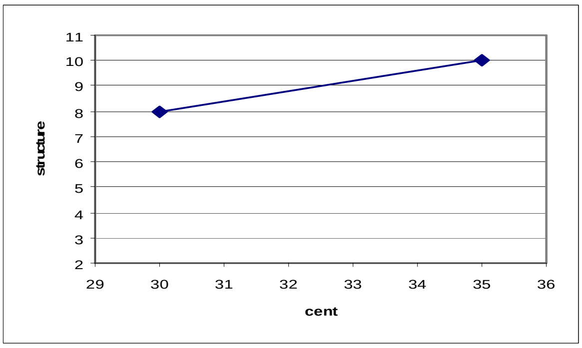

Figure 14. Displacement answer history increase of first short column at 4 story structure relation 8 and10 story structures

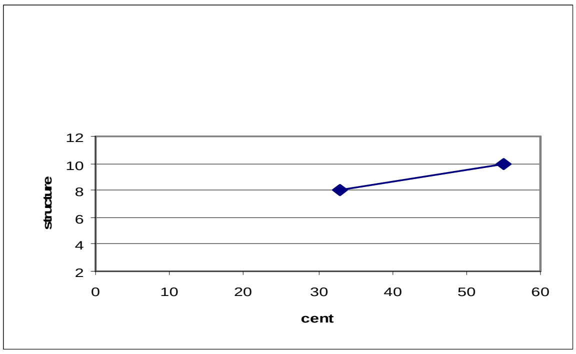

Figure 15. Displacement answer history increase of mid short column at 4 story structure relation 8 and10 story structures

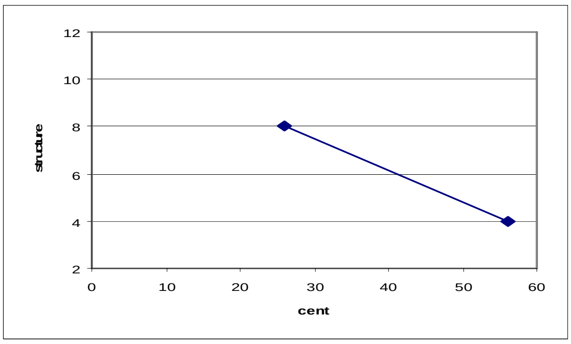

Figure 16. Displacement answer history increase of last short column at 10 story structure relation 4 and 8 story structures

2.5. Investigation of Shear Force History of Last, Medium and First Short Column in 4 Story Structure

Structures by Surveying and comparing of diagrams related to history of shearing it can be concluded that the average of shear force history in first short column in4 story structures and medium short column in 8 story structures and last short column in 10 story structures has the most mount than other column also by this conclusion we can find the exceptional cases in 4story column and last short column in 8 story structures and last short column in 10 story structure in .5 g relative to 0.7g.

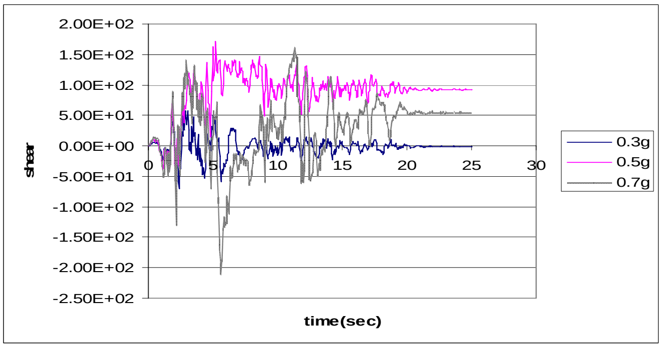

Figure 17. Shear force answer history of first short column at 4 story structure

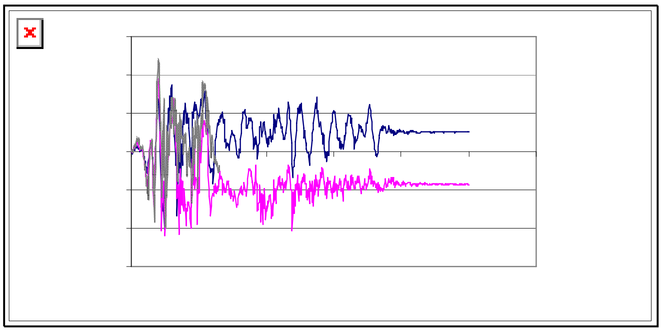

Figure 18. shear force answer history of mid short column at 4 story structure

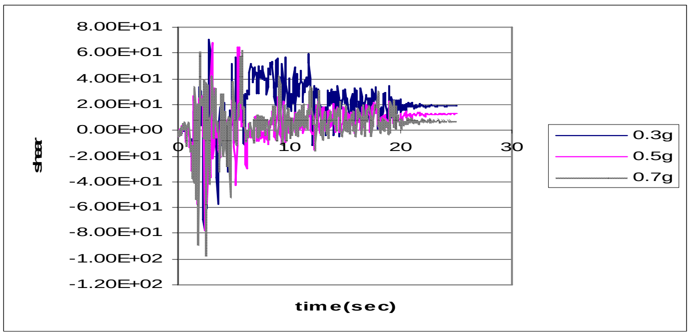

Figure 19. Shear force answer history of last short column at 4 story structure

Pay attention following Figures it can be concluded that shear force time history in first short column in 4 story structures and medium short column in 8 story column and last short column in 10 story structures has the most among than other structure. For example in 1 story structures ,the average shear force response in last short column is about 52 and 80 percent more than 4 and 8 story structure. The important point is that in last and medium short column in 0.5 g is more than 0.7 g that this amount is about 35 to 50 percent.

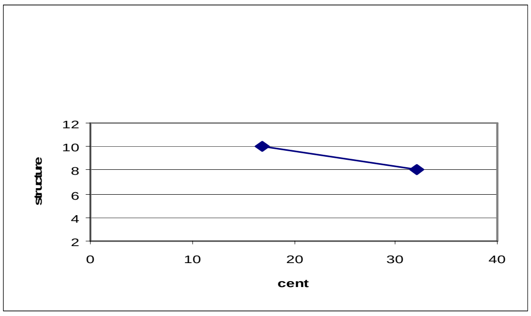

Figure 20. Shear force answer history increase of first short column at 4 story structure relation 8 and10 story structures

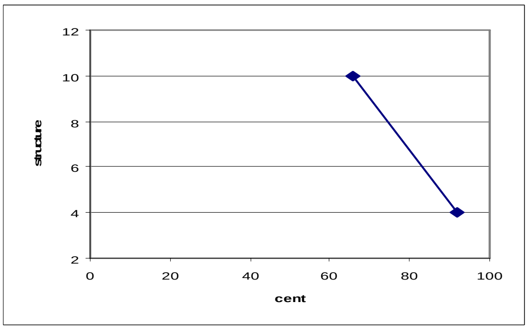

Figure 21. Shear force answer history increase of mid short column at 8 story structure relation 4and10 story structures

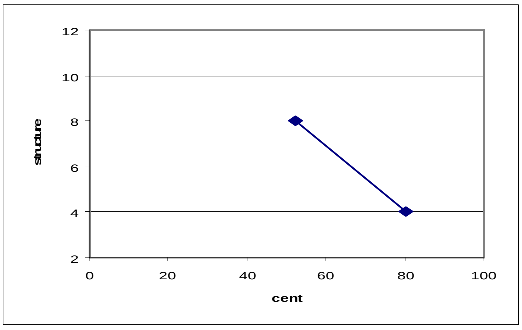

Figure 22. Shear force answer history increase of last short column at 10 story structure relation 4 and 8 story structures

2.6. Damage Index in Upand Down of Last, Medium and First Story Structures Of Structures

comparing Damage index of following Figures concluded that the most damages in 8 and 10 story structures is related to last story structures, especially in its part Because the existence of force flagelliform And lack of suitable distribution of earthquake force in height.In medium short column by increasing of height and story of structures Damage at up and down of column has decreased. as in 0.3 g and 0.5g medium short column has the least Damage and even without Damage and failure rate in its up and down .In approximately equal.In first short column up and down part of 4 story structures in all PGA. Failure has been made but in 8 and 10 story tructures failure in up and down part, failure is seem only at up for PGA as in 8 and 10 story structures in 0.3g and 0.5 of first short column in up and down part is lacke failure the first short column in 8 and 10 story structures in down part.

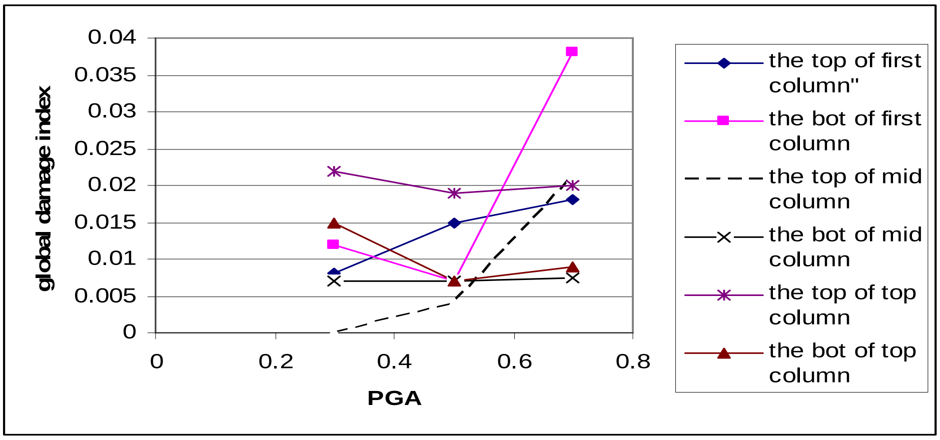

Figure 23. Damage index at up and down of 4 story structure short column

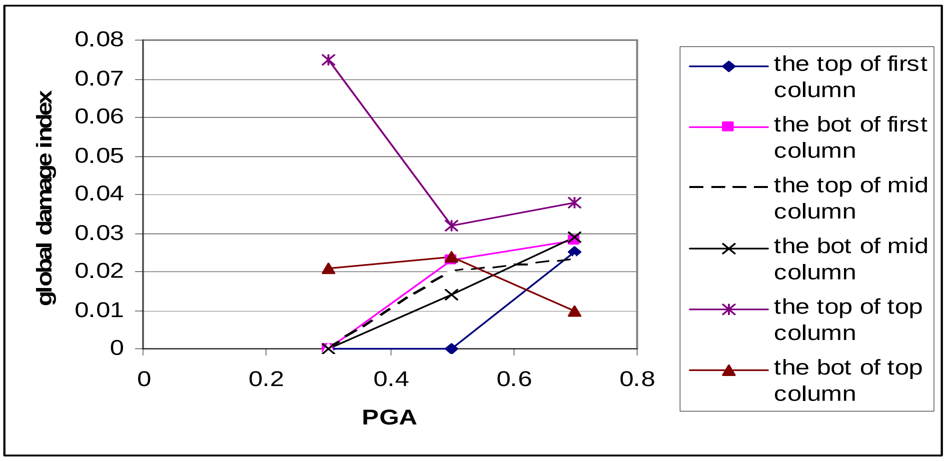

Figure 24. Damage index at up and down of 8 story structure short column

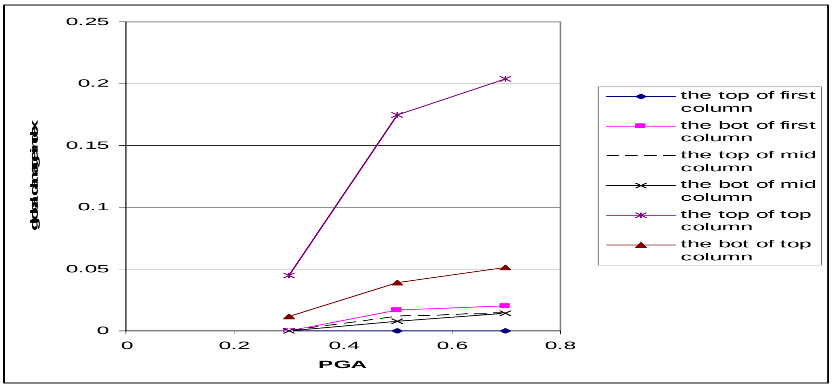

Figure 25. Damage index at up and down of 10 story structure short column

3. CONCLUSION

1. Damagerat in short column in different story increase by height and PGA increase except in8 story structures that 0.3g of last short column tolerat the damage 0.5 and 0.7 g.
2. Short column4 story structures in 0.3 g and 0.7g and short columns of 10 story structures in 0.5 has the most share in total structures failure.
3. The average history of first and medium short column displacement response in 4 story structures and last short column in 10 story structures has the most amount that other structures.
4. The average history of first short column shearing 4 story structures and medium short column in 8 story structures and last short columnin 10 story structureshas the most amount relative other structures in 8 and 10 story structures The shearing force of last and medium short column in0.5 g in more than 0.7g .
5. The part of last short column and down part of first short column in 8 and 10 story structures has more damage and expriment damage at up and down of medium short column in all structures has the least amount and is experimentally equal and is less than 1 st and last column totally under Elsentro earthquake to upper part of short column in 4 story structure more damage is inserted.

REFRENCES

1. Kheyroddin, A., and Mirnezami, A. R.(2002). "Seismic behavior steel buildings with different floor." *Proc., 3rd National conf. on Code of Practice for Seismic Resistant Design of Buildings*., Tehran, Iran.
2. Moretti, M., and Tassios TP. (2007). "Behaviour of short columns subjected to cyclic shear displacements: Experimental results." *Engineering Structures*, 29; 2018-2029.
3. Moretti, M., and Tassios TP. (2006). "Behaviour and ductility of reinforced concrete short columns using global truss model." *ACI Structural Journal*.; 103:319-327.
4. Colomb, F., Tobbi, H., Ferrier, E., and Hamelin, P.(2008) "Seismic retrofit of reinforced concrete short columns by CFRP materials." *Composite*

Structures:82: 475-487.

5. Promis, G., Ferrier, E., and Hamelin, P.(2008) "Effect of external FRP retrofitting on reinforced concrete short columns for seismic strengthening." *Composite Structures*: In Press.
6. Galal, K., Arafa, A., and Ghobarah, A. (2005) "Retrofit of RC square short columns." *Engineering Structures*.; 27:801-813.
7. Ghobarah, A., and Galal, K.(2004) "Seismic rehabilitation of short rectangular RC columns." *Journal of Earthquake Engineering*.; 8:45-68.
8. Lieping, Ye., Qingrui, Yue., shuhong, Zhao., and Quanwang, Li.(2002). "Shear strength of reinforced concrete columns strengthened with carbon Fiber Reinforced plastic sheet." *Journal of Structural Engineering*.;128: 1527-1534.
9. Galal, K., Ghobarah, A.(2003). "Flexural and shear hysteretic behaviour of reinforced concrete columns with variable axial load." *Engineering Structures*.;25:1353-1367.
10. Bakhshi, A., and Tabeshpor, M. R.(2006). "Evaluation of short column fracture calculation in earthquake." Research Bulletin of Seismology and Earthquake Engineering., Vol. 8, No. 1, spring.
11. Barghi, M., and Abasnia, R.(2006). "Augury of RC columns destruction type in cyclic lateral load." Proc,. 7th Int. Conf. on Civil Eng,. Tehran, Iran.
12. Kheyroddin, A., and Mirnezami, A. R.(2004). "Nonlinear behavior of frame connections in building with different floor." Proc,. 1th National Congress on Civil Eng,. Tehran, Iran.
13. "Iranian Code of Practice for Seismic Resistant Design of Buildings." (1384) Standard No. 2800- 05,. Building and Housing Research Center,. BHRC – PN S 253.
14. Valles, RE., Reinhorn, AM., Kunnath, SK., Li, G., and Madan, A. (1996). IDARC 2D: A Program for the Inelastic Damage Analysis of Buildings, state University of New York at Buffalo.
15. Moghaddam, H. (1384) "Earthquake Engineering." PP. 935.
16. Kargaran, A. (2008). Nonlinear seismic performance of short column in RC structures. M.Sc. Thesis, on Earthquake Eng., Department of Civil Engineering, Islamic Azad University, Shahr-kord, Iran, PP.135.
17. Kheyroddin, A., Ghodrati Amiri, G. R., and kargaran, A.(2007). "Effect of resistant system on seismic behavior of short column in RC structures with different floor." Proc., National Conf. on Seismic Retrofitting, Kerman, Iran.
18. Baji, H., and Hashemi, J. (2005). "Advance methods in modeling, analyzing and designing of structures using practical projects with Sap2000, Etabs, Safe. PP. 868.

NONLINEAR ANALYSIS OF REINFORCED CONCRETE ELEMENTS

V. Broujerdian[1], Mohammad T. Kazemi[2]
[1]Ph.D. Candidate, Department of Civil Engg., Sharif University of Tech., Tehran, Iran
[2]Associate Professor, Department of Civil Engg., Sharif University of Tech., Tehran, Iran

ABSTRACT
Introducing a new constitutive model a smeared rotating crack model was developed having the capability of predicting the entire load-deformation response of reinforced concrete elements. The important features of the model are considering the effect of reinforcement ratio on average stress-strain relationships of cracked concrete and considering the gradual reduction of average stiffness of steel bars embedded in concrete. The model applied to predict the response of available test panels and showed a good correlation. Using the simplified version of the model a new expression for shear capacity of reinforced concrete beams without stirrups was derived. The proposed relation captures the dependence of shear strength on size, shear span-to-depth ratio, longitudinal reinforcement ratio, maximum aggregate size, and concrete strength. The model agrees well with fracture mechanics concepts. The proposed relation was calibrated by least-square fitting of the existing experimental beam test database and showed a good agreement.

Keywords: reinforced concrete, shear strength, membrane elements, beams, size effect

1. INTRODUCTION
Shear behavior of reinforced concrete has been of interest to many researchers for several decades. Although several theories and design procedures for structural concrete subjected to shear have been proposed [1,2], ACI Code [3] has not modified its old formulas, yet. Of the many different theories and expressions about shear strength of RC beams that have been developed up to now, only a few consider the size effect. Among them the procedures based on modified compression field theory, MCFT, have gained some acceptance. This theory is the product of much experimental and analytical research conducted at the University of Toronto toward formulating the response of reinforced concrete elements subjected to the in-plane forces [4]. Since the development of MCFT several approaches based on it with different degrees of complexity has evolved. The simplest approach is the general shear design method [5] adopted in the AASHTO [6] and Canadian Code [7], and the most complicated are ones using MCFT in a finite element approach [8].

In the first part of this study, the MCFT is revised in a fundamental level. The literature shows that for panels containing less than 0.1% reinforcement in one direction or panels that were uniaxially reinforced the accuracy of MCFT deteriorates. This deficiency of MCFT arises from its simple constitutive models. Presented in this paper is a set of stress-strain relations for normal strength concrete and mild steel bars embedded in concrete having two salient features: 1) considering the effect of reinforcement ratio on average stress-strain relationships of cracked concrete; and 2) considering the gradual reduction of average stiffness of steel bars embedded in concrete. Incorporating equilibrium, compatibility, and the constitutive laws into a nonlinear analysis procedure, a new smeared rotating crack model was developed having the capability of predicting the entire load-deformation response of reinforced concrete elements. Corroboration study using experimental data from test panels showed that the model has a good accuracy in predicting the behavior of reinforced concrete panels throughout the loading history.

In the second part of the study, using simplified concepts of MCFT and the proposed model a new relation for predicting the shear behavior of reinforced concrete beams was obtained. MCFT based equations for shear take a simple account of crack opening and aggregate interlock across the dominant shear crack, which results in size effect on shear capacity of concrete members. According to simplified expressions derived from MCFT, shear strength for very large sizes is inversely proportional to the beam size [9,10]. However, the limit solution of shear failure load for very large sizes, obtained based on fracture mechanics, reports an exponent of –1/2 for beam size [11-13]. In this study, considering more refined assumptions about the opening of the dominant shear crack of the beam, new expressions for shear strength of RC beams were developed that display size effect in accordance with fracture mechanics for large sizes, asymptotically. The derived equations were compared to the other equations and were applied to existing database of ACI-445F [14] and resulted in a relatively low coefficient of variation.

2. NONLINEAR ANALYSIS OF MEMBRANE ELEMENTS

2.1. Average Stress-Strain Relationship of Steel

The basic information needed for analyzing of a reinforced concrete membrane element is stress-strain relations describing the average characteristics of materials subjected to loading. As the approach of this paper is based on smeared crack concept and average stresses and strains are used, the bond slipping along the bars and shear sliding along cracks are implicitly included and we only need average constitutive laws for steel and concrete.

Steel reinforcement is generally assumed transmit axial force only and hence a uniaxial stress-strain relation is adopted. MCFT uses the usual bilinear uniaxial stress-strain relationship shown in Figure 1(a) for modeling the average behavior of steel bars embedded in concrete [4,15,16]. However, because of disturbed stress field in the cracked reinforced concrete the behavior of an embedded steel bar in concrete is different from that of a bare bar. After the occurrence of the first yielding of reinforcement at a crack location, the average stress-strain curve of steel bars embedded in concrete shows a gradual reduction in stiffness and it continues until its complete yielding. Therefore, in the present study, a trilinear piecewise stress-strain relationship is adopted [Figure 1(b)]. The initial part of the proposed curve is a straight line with a slope of E_s, the modulus of elasticity of steel, up to $0.8 f_{yield}$. Then it changes to a slope of $E_s / 20$ and reaches the peak at f_{yield} where remains constant until failure. The details of this curve have been obtained based on an extensive data fitting on the test panel results introduced later in this paper. To maintain the simplicity of the model it is assumed that the average stress-strain relation of steel is independent of concrete specifications. The model allows for elastic unloading [Figure 1(b)].

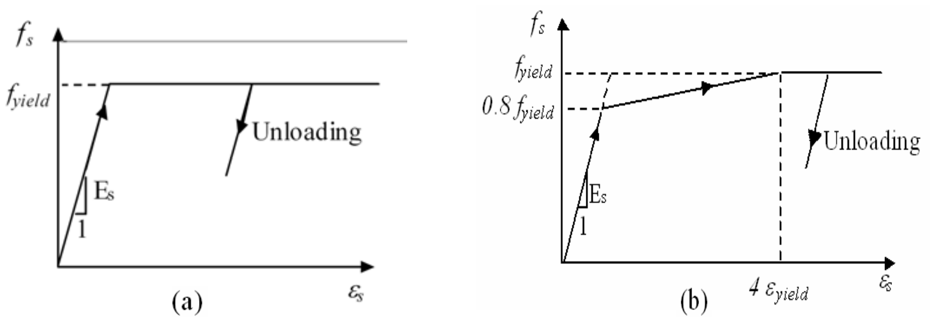

Figure 1. Constitutive relation for reinforcement: (a) bare steel bar; (b) proposed relation for steel bar embedded in concrete.

2.2. Average Compressive Stress-Strain Relationship of Concret

It is often recognized that cracked concrete in compression subjected to transverse tensile strains has lower strength and stiffness than uniaxially compressed concrete. This phenomenon called compression softening is usually quantified by incorporating a softening coefficient into a basic stress-strain curve [4,15,17]. Our suggested basic compressive stress-strain curve consists of Hognestad curve [18] for ascending portion and another second-degree parabola for descending portion. This part is specified by ε_f which is the strain when the stress has fallen to zero (Figure 2). This strain derived based on Kent and Park [19] research is:

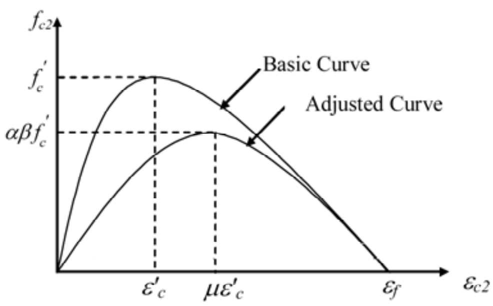

Figure 2. The proposed stress-strain relation-ship for cracked concrete in compression

$$\varepsilon_f = \frac{(f_c' + 7)\varepsilon_c' - 0.042}{f_c' - 7} \tag{1}$$

where f_c' is the concrete uniaxial compressive strength in MPa and ε_c' is the strain in concrete cylinder at the peak stress f_c' (ε_c' is a negative quantity). The suggested curve for falling branch reflects the phenomenon that a low strength concrete has a low-slope descending portion. It must be noted that the proposed model is calibrated for reinforced concrete specimens $890\ mm$ square × $70\ mm$ thick. To use this model in a FEM program with different mesh sizes, appropriate size effect factors must be incorporated into the constitutive laws.

Studying the available panel test results, a definite effect of reinforcement ratio on average stress-strain relationship of cracked concrete in compression was recognized. To capture this phenomenon two modification factors of α and μ are introduced as follow for adjusting the values of f_c' and ε_c', respectively:

$$f_c'' = \alpha f_c', \ \alpha = 1 + 0.03(100\rho_x)^2 (100\rho_y)^2 \tag{2}$$

$$\varepsilon_c'' = \mu \varepsilon_c', \ \mu = 1 + 0.04(100\rho_x)^2 (100\rho_y)^2 \tag{3}$$

where ρ_x and ρ_y are the reinforcement ratios of the orthogonally reinforced concrete panel in x and y directions, respectively. For describing the softening effect, the basic compression curve, defined above, is modified in term of the peak stress attainable. By adopting the modification factor introduced by Vecchio and Collins [4]:

$$\beta = \frac{1}{0.8 - 0.34\varepsilon_{c1} / \varepsilon_c'} \leq 1 \tag{4}$$

the suggested compression curve will be obtained as (Figure 2):

$$f_{c2} = \beta f_c'' \left[\left(\frac{\varepsilon_{c2} - \varepsilon_c''}{\varepsilon_c''} \right)^2 - 1 \right] \quad \frac{\varepsilon_{c2}}{\varepsilon_c''} \leq 1 \tag{5a}$$

$$f_{c2} = \beta f_c'' \left[\left(\frac{\varepsilon_{c2} - \varepsilon_c''}{\varepsilon_f - \varepsilon_c''} \right)^2 - 1 \right] \quad \frac{\varepsilon_{c2}}{\varepsilon_c''} > 1 \tag{5b}$$

where f_{c2} and ε_{c2} are the average principal compressive stress and strain in the cracked concrete, respectively and ε_{c1} is the co-existing principal tensile strain.

2.3. Average Tensile Stress-Strain Relationship of Concrete

The stiffening effect of post-cracking tensile stresses in the concrete between cracks has been recognized for quite some time. Neglecting this contribution of concrete called tension stiffening can cause a significant overestimation of post-cracking deformation in reinforced concrete structures [20]. The gradual reduction in stiffness due to progressive cracking is referred to as strain softening. These phenomena have been quantified by some constitutive laws obtained from reinforced concrete panel tests [4,16,21-23].

The tensile tests on reinforced concrete panels have revealed that there are three rather distinct areas in the average tensile stress-strain response of cracked concrete [24]: a) a linearly ascending portion before cracking; b) a fluctuating portion, called crack formation phase, where must cracks form; and c) a descending portion with a stable crack pattern, regarding this behavior, the conceptual model proposed for average tensile stress-strain relationship of cracked concrete is shown in Figure 3. According to this Figure, the proposed model can be expressed as:

$$f_{c1} = E_c \varepsilon_{c1} \quad \varepsilon_{c1} < \varepsilon_{cr} \tag{6a}$$

$$f_{c1} = f_{cr} \quad \varepsilon_{cr} < \varepsilon_{c1} < \varepsilon'_{cr} \tag{6b}$$

$$f_{c1} = \frac{f_{cr}}{1 + \sqrt{k\varepsilon_{c1}} - \sqrt{k\varepsilon'_{cr}}} \quad \varepsilon'_{cr} < \varepsilon_{c1} \tag{6c}$$

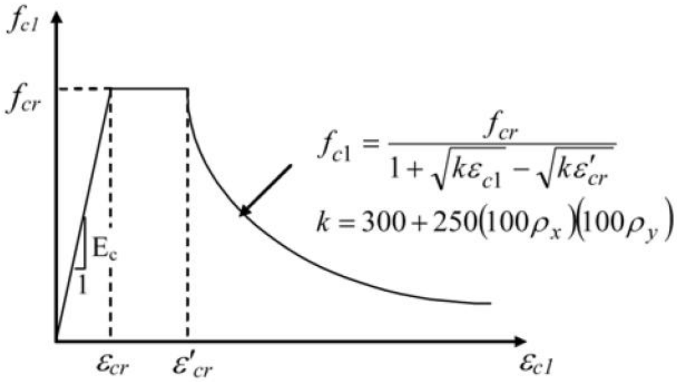

Figure 3. The proposed stress-strain relationship for cracked concrete in tension.

The parameters of the model are described as follows. f_{c1} is the average principal tensile stress in the cracked concrete. E_c is the elastic modulus of the concrete in tension which can be taken as $2f'_c/\varepsilon'_c$. f_{cr} is the first cracking strength of concrete in a reinforced panel. Examining the available panel test results showed that in addition to f'_c the reinforcement ratio has also an influence on f_{cr} and the following relation in MPa units was obtained:

$$f_{cr} = 0.3\alpha'\sqrt{f_c' + 8} \tag{7}$$

where α' was interestingly obtained equal to α defined in Eq. (2). The ε_{cr} in Eq. (6) is the average tensile strain at which the concrete begins cracking and ε_{cr}' is the corresponding value at the end of crack formation phase. A survey of aforementioned database revealed that ε_{cr}' has a direct relationship with the reinforcement ratio of the concrete panel. Examining different formulas and best fitting of the database with them the following relation was obtained:

$$\varepsilon_{cr}' = \eta\varepsilon_{cr}\ ,\ \eta = 1 + 6(100\rho_x)(100\rho_y) \tag{8}$$

To account for the dependence of post-cracking tensile response of concrete on the reinforcement ratio, as already described, some alternative relations were examined and finally the best relation with the use of data fitting was obtained as:

$$k = 300 + 250(100\rho_x)(100\rho_y) \tag{9}$$

2.4. Validation of the Proposed Model

The problem at hand is to determine the load-deformation response of an orthogonally reinforced concrete membrane element subjected to monotonically increasing in-plane stresses shown in Figure 4. The proposed constitutive laws along with the equilibrium and compatibility equations form a system of nonlinear equations needing a numerical method to solve.

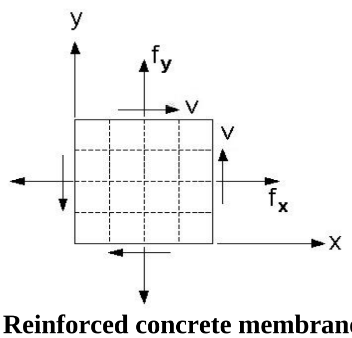

Figure 4. Reinforced concrete membrane element.

As an example of the theoretical model's application to the analysis of reinforced concrete elements, an analysis was made of Panel PV20 tested at university of Toronto by Vecchio and Collins [4]. This specimen was tested in pure shear. For this panel the compressice strength of the concrete was 19.6 MPa. The predicted response for this element based on MCFT [4] and DSFM [16] and the experimental curve is summarized in Figure 5. Note that for this panel the proposed model provides excellent correlations with experimental results.

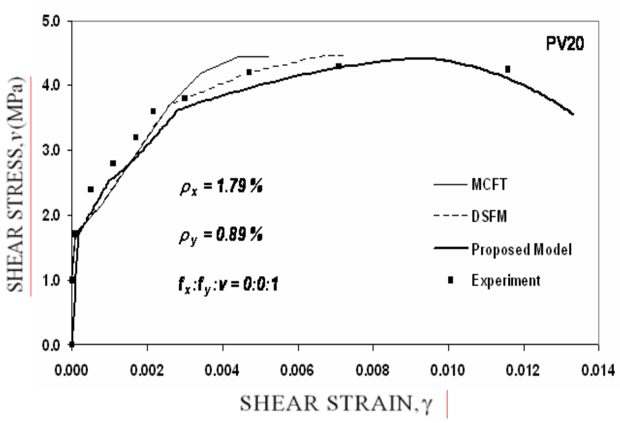

Figure 5. Comparison of experimental and predicted responses for Panel PV20.

3. A SIMPLIFIED MODEL FOR SHEAR CAPACITY PREDICTION OF BEAMS

3.1. Size Effect in Shear According to Simplified Mcft

Simplified-MCFT explanation for size effect in shear is that the shear strength of beams not containing stirrups is a function of the shear crack width. Crack widths, in turn, increase nearly both with the tensile strain in the reinforcement and with the spacing between the cracks [10]. Larger members have more widely spaced cracks and therefore are expected to fail at lower shear stress. To maintain beam action up to the failure, nearly all of the shear force V_c must be transmitted by the shear stress across the main diagonal cracks. For most of the concretes, cracking will occur along the interface between the aggregates and the cement paste. The resulted rough cracks are capable to transfer shear by aggregate interlock. Decreasing the aggregate size reduces this capacity. In the development of the MCFT, Vecchio and Collins [4] suggested that for cracks transmitting only shear stress, the limiting stress would be:

$$v_{ci} = \frac{0.18\sqrt{f_c'}}{0.31 + 24w/(d_a + 16)} \tag{10}$$

where w is the crack width (crack opening displacement) in *mm* and d_a is the maximum aggregate size in *mm*. Using the parameters identified by the MCFT, Collins and Kuchma [9] proposed the following relation for the shear capacity of members without shear reinforcement:

$$v_c = \frac{V_c}{bd} = \frac{245}{1275 + 35(0.9d)/(d_a + 16)}\sqrt{f_c'} \tag{11}$$

with f_c' not to be taken greater than $70\,MPa$. This equation represents a strong stress singularity with power of –1 around the crack tip that yields a size effect on shear strength with power of -1 for very large sizes. This very strong stress singularity and size effect is objectionable based on fracture mechanics. Exponent –1/2 is the strongest size effect possible [12].

3.2. A Simplified Model for Size Effect in Shear

The failed part of a beam, subjected to two concentrated loads, with shear span a, containing the dominant shear crack, is shown in Figure 6. The function that defines crack opening along its length is a complex function. This complexity is the result of many factors such as the effect of the shear stresses transmitted across the crack, the presence of longitudinal bars crossing the crack, and the size effect on the crack shape. The current procedures based on MCFT, approximate the crack opening profile by a constant value that is the average crack opening [5,9,10]. In the present study, we use a linear function for the crack opening that satisfies the essential boundaries of the crack; zero opening at the crack tip and maximum opening at the bottom. Thus, we introduce the following relation:

$$w(y) = \frac{y}{d} w_{\max} \tag{12}$$

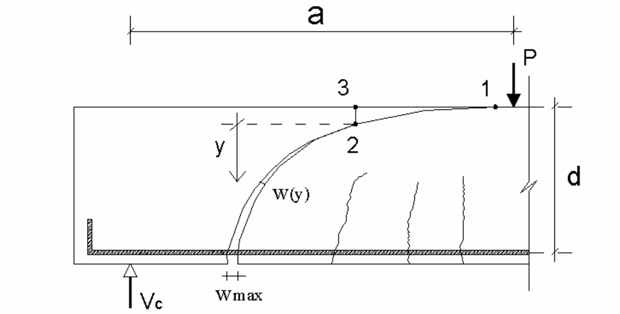

Figure 6. Left part of a beam containing the dominant shear crack

where y is the distance from the crack tip and $w_{\max}$ is the crack opening at the level of tensile bars. On the other hand, $w_{\max}$ can be considered as a function of the beam geometry and material properties calculated from the following relation [13]:

$$w_{\max} = k \frac{(a/d)v_c}{\rho E_s} d \tag{13}$$

where k is a constant factor and E_s is the modulus of elasticity of longitudinal reinforcement. Combining Eqs. (10), (12), and (13), we obtain a relation for the shear transfer capacity of crack surface as a function of y:

$$v_{ci}(y) = \frac{0.18\sqrt{f_c'}}{0.31 + \dfrac{0.24kv_c}{d_s\sqrt{f_c'}} y} \tag{14}$$

Where

$$d_s = \frac{\rho E_s (d_a + 16)}{100(a/d)\sqrt{f_c'}} \tag{15}$$

As seen from Eq. (15), d_s is a function of the beam geometry and the materials properties. On the other hand, Eq. (14) shows that d_s has the dimension of length. Thus, we name d_s the depth scale.

To calculate the shear capacity of the beam, we consider it at the moment prior to unstable crack growth. From shear-compression interaction behavior of the concrete we know that increasing the compression stress above a certain value causes decreasing in the shear capacity of the concrete. Thus, the compression zone above the crack tip, which is subjected to high compression stresses, has a small shear capacity. Therefore, we ignore the shear contribution of this area and only rely on aggregate interlock capacity across the crack [13]. For calculating shear capacity of the beam, V_c, it is sufficient to integrate the vertical component of v_{ci} over the whole crack length:

$$v_c = \frac{V_c}{bd} = \frac{1}{d}\int_{crack} v_{ci}(y)\sin\alpha dl \tag{16}$$

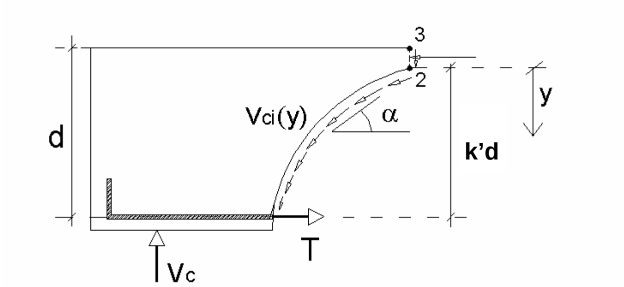

Figure 7. Free-body-diagram of the left part of the beam at shear failure.

where α is the crack inclination angle at the position y (Figure 7) and dl is crack length element. Using geometrical relation and substituting Eq. (14) into Eq. (16), the integral is calculated easily and we obtain:

$$\frac{v_c}{v_0} = \frac{4v_0 d_0}{v_c d}\ln\left(1 + \frac{v_c d}{4v_0 d_0}\right) \tag{17}$$

where k' is a constant factor (Figure 7) and

$$d_0 = Ad_s \ , \ v_0 = B\sqrt{f_c'} \tag{18}$$

Two constants A and B are related to k and k' by $A = 0.556 / kk'^2$ and $B = 0.581k'$ and determined empirically from data fitting. Checking limit states of Eq. (17) shows that it yields a size independent relation for shear capacity of very small beams, in accordance with plastic solution, and for very large sizes the shear strength converges to linear elastic fracture mechanics solution, i.e. a size effect with power of –1/2. Hence, the asymptotic behavior of Eq. (17) is in agreement with theoretical expectations.

Employing Eq. (17) for design is complicated, as it needs iteration or a computer. Thus, it is appropriate to simplify this equation. The limits of Eq. (17) for the both very small and very large sizes, obtained from l'Hopital rule [15], yield the same results. As an approximation, we can use the asymptotic function to estimate v_c / v_0 for the full size range. It is interesting that we can do similar simplification twice [13] and we obtain:

$$v_c = \beta \sqrt{f_c'} \ , \ \beta = \frac{B}{\sqrt{1 + d / Ad_s}} \tag{19}$$

This relation has the same general form of the relation obtained from fracture mechanics and verified by various test results [11, 26]. Best fitting of the ACI-445F database contained 398 data [14] by this equation, yields $A = 1.33$ and $B = 0.50$ and the coefficient of variation is cov = 19.2 %.

To provide additional safety margin, the curve of a design formula must be passed near the lower border of a scatter band. This is usually obtained as a 5% cut-off according to the least-square method. Thus the value of B is reduced to 0.35 [13]. Figure 8 represents the mean and lowered fitting of ACI-445F database by the proposed equation, and compare it with ACI's simple formula [3], shown with dashed line. As seen in this Figure the ACI formula may continue to be used safely within a certain range, and beyond that it is unsafe.

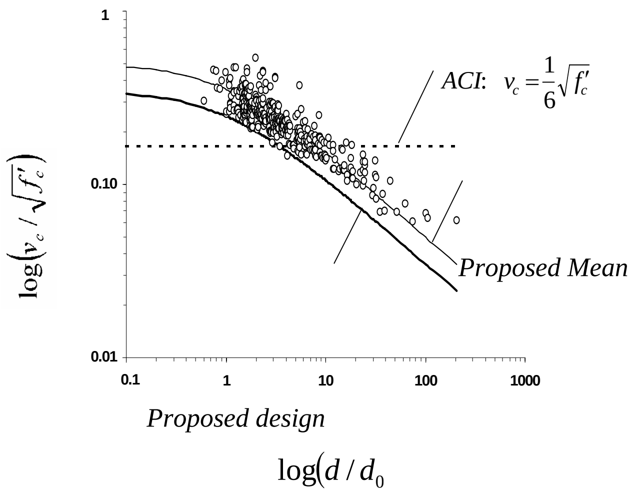

Figure 8. Comparison to ACI-445F database of proposed equation and ACI [3] simple shear formula

4. CONCLUSIONS

An orthotropic concrete constitutive model was developed that takes into account the interaction of reinforcement ratio on concrete behavior. Compression softening and tension stiffening were also considered in the model. Incorporating equilibrium, compatibility, and the constitutive laws into a nonlinear analysis procedure, a new smeared rotating crack model was developed having the capability of predicting the entire load-deformation response of reinforced concrete elements. Corroboration study using experimental data from test panels showed that the model has a good accuracy in predicting the behavior of reinforced concrete panels throughout the loading history. Using the simplified version of the model and incorporating MCFT concept a new expression for shear capacity of reinforced concrete beams without stirrups was obtained. Limit states of this expression agrees well with the limit solutions of shear failure load for very small and very large sizes; based on plastic and fracture mechanics solutions, respectively. The proposed relation was calibrated by optimum fitting of ACI-445F databank, which resulted in low coefficient of variation. Finally, applying a safety factor, it proposed as shear strength design formula.

REFERENCES

1. ASCE-ACI Committee 445, "Recent Approaches to Shear Design of Structural Concrete," *ASCE Journal of Structural Engineering*, V. 124, No. 12, Dec. 1998, pp. 1375-1417.
2. CEB, "Concrete Tension and Size Effect," Contributions from CEB Task Group 2.7. Comite Euro-International du Beton, Lausanne, Switzerland, 1997.
3. ACI Code, "Building Code Requirements for Structural Concrete (ACI 318-05) and Commentary (ACI 318R-05)," American Concrete Institute, Farmington Hills, MI, 2005.
4. Vecchio, F. J., and Collins, M. P., "The Modified Compression-Field Theory for Reinforced Concrete Elements Subjected to Shear," *ACI Journal*, V. 83, No. 2, Mar.-Apr. 1986, pp. 219-231. [5] Collins, M.P., Mitchel, D., Adebar, P., and Vecchio, F.J., "A General Shear Design Method," *ACI Structural Journal*, Vol. 93, No. 1, Jan.-Feb. 1996, pp. 36-45.
5. AASHTO, "LRFD Bridge Design Specifications and Commentary," 3rd ed., American Association of State Highway and Transportation Officials, Washington, D.C, 2004.
6. CSA, "Design of Concrete Structures. Standard CSA A23.3-94," Canadian Standards Association, Rexdale, Ontario, 2005.
7. Vecchio, F. J., "Nonlinear Finite Element Analysis of Reinforced Concrete Membranes." *ACI Structural Journal*, Vol. 86, No. 1, Jan.-Feb. 1989, pp. 26-35.
8. Collins, M. P. and Kuchma, D., "How Safe Are Our Large, Lightly Reinforced, Concrete Beams, Slabs, and Footings?" *ACI Structural Journal*, Vol. 96, No. 4, 1999, pp. 482-490.
9. Lubell, A., Sherwood, T., Bentz, E., and Collins, M. P., "Safe Shear Design of Large, Wide Beams," *ACI Concrete International*, Vol. 26, No. 8, Aug. 2004, pp. 67-78.

10. Bazant, Z. P., and Kazemi, M. T., "Size Effect on Diagonal Shear Failure of Beams without Stirrups," *ACI Structural Journal*, V. 88, No. 3, May-June 1991, pp. 268-276.
11. Bazant, Z. P., and Yu, Q., "Designing against Size Effect on Shear Strength of Reinforced Concrete Beams without Stirrups: I. Formulation," *ASCE Journal of Structural Engineering*, Vol. 131**,** No. 12, Dec. 2005, pp. 1877-1885.
12. Kazemi, M.T., and Broujerdian, V., "Reinforced Concrete Beams without Stirrups Considering Shear-Friction and Fracture Mechanics," *Canadian Journal of Civil Engineering*, Vol. 33, No. 2, Feb. 2006, pp. 161-168.
13. Reineck, K.-H., Kuchma, D.A., Kim, K.S., and Marx, S., "Shear Database for Reinforced Concrete Members without Shear Reinforcement," *ACI Structural Journal*, Vol. 100, No. 2, Mar.-Apr. 2003, pp. 240-249.
14. Vecchio, F. J., Collins, M. P., Aspiotis, J., "High-Strength Concrete Elements Subjected to Shear," *ACI Structural Journal*, V. 91, No. 4, Jul.-Aug. 1994, pp. 423-433.
15. Vecchio, F. J., "Disturbed Stress Field Model for Reinforced Concrete: Formulation," *ASCE Journal of Structural Engineering*, V. 126, No. 8, Aug. 2000, pp. 1070-1077.
16. Belarbi, A., and Hsu, T. T. C., "Constitutive Laws of Softened Concrete in Biaxial Tension-Compression." *ACI Structural Journal*, V. 92, No. 5, Sep.-Oct. 1995, pp. 562-573.
17. Park, R., and Paulay, T., "Reinforced Concrete Structures," John Wiley & Sons, Inc., New York, N.Y., 1975, 769 pp.
18. Kent, D. C., and Park, R., "Flexural Members with Confined Concrete." *ASCE Journal of Structural Engineering*, V. 97, No. 7, Jul. 1971, pp. 1969-1990.
19. Hsu, T. T. C., and Zhang, L. X., "Tension Stiffening in Reinforced Concrete Membrane Elements," *ACI Structural Journal*, V. 93, No. 1, Jan.-Feb. 1996, pp. 108-115.
20. ACI Committee 224, "Cracking of Concrete Members in Direct Tension," *ACI Journal*, V. 83, No. 1, Jan.-Feb. 1986, pp. 3-13.
21. Carreira, D. J., and Chu, K. H. "Stress-Strain Relationship for Reinforced Concrete in Tension," *ACI Journal*, V. 83, No. 1, Jan.-Feb. 1986, pp. 21-28.
22. Belarbi, A., and Hsu, T. T. C., "Constitutive Laws of Concrete in Tension and Reinforcing Bars Stiffened by Concrete," *ACI Structural Journal*, V. 91, No. 4, Jul.-Aug. 1994, pp. 465-474.
23. Wollrab, E., Kulkarni, S. M., Ouyang, C., and Shah, S. P., "Response of Reinforced Concrete Panels under Uniaxial Tension," *ACI Struc. Journal*, V. 93, No. 6, 1996, pp .648-657.
24. Thomas, G.B., and Finney, R.L., "Calculus and Analytic Geometry," Addison-Wesley, U.S.A., 1984.
25. Kazemi, M. T., and Broujerdian, V., discussion of "Repeating a Classic Set of Experiments on Size Effect in Shear of Members without Stirrups," by Bentz, E. C., and Buckley, S., *ACI Structural Journal*, Vol. 103, No. 5, Sep.-Oct. 2006, pp. 754-755.

CD02-011

FINITE ELEMENT MODELING AND INVESTIGATION OF THE EFFECTS OF MASONRY INFILLS ON THE BEHAVIOR OF REINFORCED CONCRETE (RC) FRAMES

M.R. Noorfard[1], M. S. Marefat[2],
[1] M.Sc Student, School of Civil Eng., University College of Eng., University of Tehran
[2] Professor, School of Civil Eng., University College of Engineering, University of Tehran

ABSTRACT
In this study, a finite element model for masonry-infill of RC frames has been introduced. The micro model incorporates the bricks, bed and head joints, surrounding RC frame and the interface between frame and masonry infill. The results of the analysis have been validated by experimental data reported in the literature. A parametric study has been conducted and the effects of strength, stiffness, aspect ratio of infill panels and the effect of relative stiffness of frame to masonry panel on lateral response of the structure have been investigated. It was found that infill panels increase stiffness and ultimate strength of the frames significantly, and by increasing stiffness and strength of infill, stronger failure mechanisms are activated, and failure of masonry panels shift to failure of concrete frame. It was also observed that aspect ratio plays an important role in determining failure mechanisms not only in the infill but also in the frame.

Keywords: masonry infill, RC frame, finite element modeling, lateral response, failure mechanism.

1. INTRODUCTION
Masonry walls are widely used as infill in steel and concrete structural frames throughout the world. They are usually treated as non-structural elements, and their interaction with the bounding frame is often ignored in design. But experiences of various earthquakes and also recent researches show that masonry infills have very essential effects on the behavior of the structures. Because of high initial stiffness, infills can concentrate a greater part of the earthquake force to the infilled panels. Generally, the behavior of infilled frame is completely different from that of the bare frame because of the interaction between frame and infill [1, 2].
To identify and predict the behavior of infilled frame, several experimental tests have been carried out and a number of different analytical models have been developed. Equivalent diagonal strut is one of the most applicable methods to model infill panels that was presented by Polyakov [3] for the first time. Stafford smith [4] showed that width of the equivalent strut depends on the contact length of the frame and infill. After that Mainstone [5] proposed methods to estimate equivalent strut element characteristics. Saneinejad [6] proposed equations to evaluate the ultimate strength of infill panels. Liauw [7] developed plastic analysis

methods to predict the in-plane limit loads of steel infilled frame. Sophisticated finite element models have also been developed to analyse infilled structures. Mehrabi [8] used interface element for modeling mortar joints.

In this research the effects of masonry infills on the behavior of the reinforced concrete frames has been investigated by finite element modeling in ANSYS. The recorded results of Mehrabi's experimental tests [1] have been used to validate the analyses.

2. FAILURE MECHANISMS OF MASONRY INFILL IN RC FRAMES

The main failure mechanisms in masonry infill panels are diagonal cracking, diagonal-sliding cracking, bed joint sliding and corner crushing. Shear failure of the beam and column and short column phenomenon, which will happen if infill panel is not extended to the upper beam of the frame, are the most important failure mechanisms in the frame [1, 2, 5]. Figure 1 shows different failure mechanisms of masonry infills in RC frames.

The behavior of infilled frames under lateral load depends on different parameters such as panel aspect ratio, stiffness and strength of the infill and frame, material properties, vertical loads and presence of gap between frame and infill [2, 5]. In this study a two dimensional finite element model has been introduced to study the response of infilled frames under monotonically increasing lateral load.

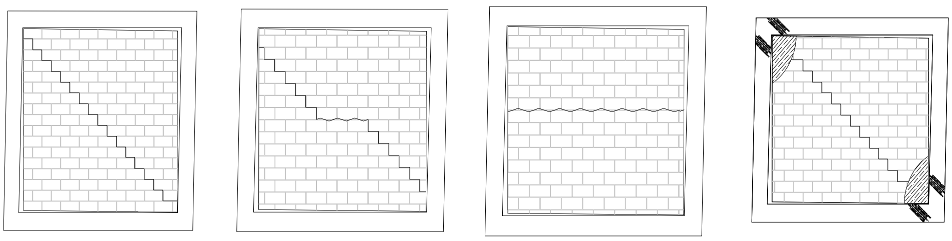

a. diagonal cracking **b. diagonal-sliding cracking** **c. bed joint sliding** **d. corner crushing and shear failure in frame components**

Figure 1. Possible failure mechanisms of masonry infills in RC frames

3. EXPERIMENTAL TESTS OF MEHRABI

In 1994, Mehrabi [1] carried out some experimental tests on reinforced concrete infilled frames and investigated different parameters such as monotonic and cyclic loading and different combinations of weak and strong frame and infills. Three specimens of these tests have been used to validate our numerical model. The specimens are 5 and 7, which were masonry-infilled RC frames and Specimen 1, which was a bare frame. Specimens 1 and 5 had weak flexural concrete frame and that of Specimen 7 was strong. The details of weak and strong frames are shown in Figure 2.

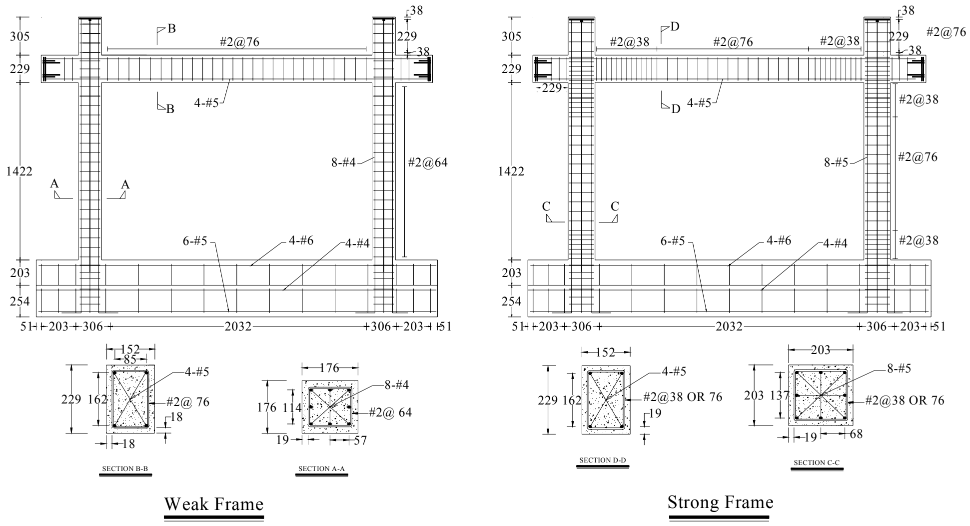

Figure 2. Weak and strong frame of the tests [1]

Masonry infills of the specimens consisted of 19.2×9.2×9.2 cm solid masonry blocks with head and bed joints of a thickness of 10 mm. Also, infill panels had the height/length ratio of about 1/1.5 and they have completely filled the surrounding frame. These specimens were subjected to a constant vertical compressive load of 294 KN. For the infilled specimens the vertical load was distributed between the column and the beam. For the bare frame specimen the vertical load was applied completely to the columns. Characteristics of the specimens have been summarized in Table 1.

Table 1: Specifications of different specimens [1]

Specimens number	Type of Load	Frame Concrete			Three-Masonry Prisms			Compressive Strength (MPa)	
		Secant modulus (MPa)	Compressive strength (MPa)	Strain at peak stress	Secant modulus (MPa)	Compressive strength (MPa)	Strain at peak stress	Brick	Mortar
1	Monotonic	21930	30.9	0.0018	-	-	-	-	-
5	Cyclic	18070	20.9	0.0026	8.95	13.86	0.0023	15.59	13.38
7	Cyclic	18620	33.4	0.003	9.08	13.59	0.0026	15.59	15.52

4. THE PROPSED NONLINEAR FINITE ELEMENT MODEL

To evaluate both global and local behavior of masonry infill, a numerical micro model considering all bricks and mortars of head and bed joints as well as reinforced concrete frame components has been used. To model bricks, 4-node 2-D plane element (PLAN42 [9]) has been used in both elastic and plastic cases. The plastic case was applied to represent the crushing of bricks at the corner of masonry infill panel. For other parts of infill panels, the bricks have been represented by elastic plane element. It helps to decrease the computation time. To model bricks, cracking has also been disregarded. The head and bed joints of the mortar have been represented by 2-node nonlinear spring COMBIN39 [9] that is a unidirectional element with nonlinear generalized force-deflection capability. The shear performance of the mortar joints have been represented by inclined spring element with response along shear resistance surface of mortars. The tension and compression behavior of mortar joints have also been represented by straight spring element with response along normal to mortar surfaces.

The concrete frame has been represented by 4-node 2-D plane element (PLAN42) and an elastic-perfect plastic formulation (Drucker–Prager) has been adopted [9]. This Drucker–Prager model is a constitutive model for the behavior of brittle material such as concrete. Reinforcing bars have been also modeled with 2-node elastic-hardening plastic bar element LINK8 [9]. They were connected to the 4-node concrete element at the two external nodes. The contact surfaces of infill panel and bounding frame have been represented by TARGE169 and CONTA172 [9]. These elements are surface to surface contact elements which have sufficient parameters for modeling every kind of contact surfaces. A schematic representation of an infilled frame model consisting of all element types has been shown in Figure 3.

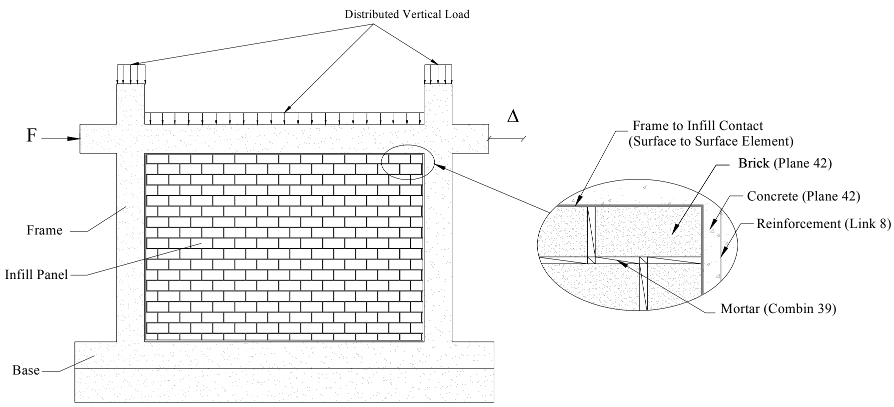

Figure 3. Infilled frame model

According to the results of material tests [1], parameters of the analyses have been estimated. The value of E modulus for mortars and bricks has been estimated based on that of the three-course masonry prisms tests and the equation existent in literature [10]. Mentioned equation depends on the ratio of brick to mortar thickness. Shear behavior of mortar joints has been evaluated based on the E modulus and mohr-coulomb formulation with parameters C (cohesion) and μ (friction coefficient) that has been obtained from direct shear tests.

The nonlinear behavior of concrete of the frame has been defined by the Drucker-Prager model and parameter C (cohesion) and Ø (friction angle). In the plane stress case, Drucker-Prager's constitutive law reduces to a single continuous yield surface, whose equation reads:

$$\sqrt{\frac{1}{3}(\sigma_x^2+\sigma_y^2-\sigma_x\sigma_y)\tau_{xy}^2}+\alpha(\sigma_x+\sigma_y)-k\le 0 \qquad (1)$$

Parameters *k* and α are related to C and Ø of the considered material:

$$\alpha=\frac{2\sin\varphi}{\sqrt{3}(3-\sin\varphi)}\,; \qquad k=\frac{6c\cos\varphi}{\sqrt{3}(3-\sin\varphi)}. \qquad (2)$$

These parameters determine the yield stresses in uniaxial tension and compression σ t and σ c:

$$\sigma_t=\frac{k}{\frac{1}{\sqrt{3}}+\alpha}\,; \qquad \sigma_c=\frac{k}{\frac{1}{\sqrt{3}}-\alpha}. \qquad (3)$$

The complete set of analysis parameters have been described in Table 2. The specifications of the concrete frame reinforcing bars such as yield and ultimate stress that have been obtained from tension test results [1] have been shown in Table 3.

Table 2: Specifications of numerical models

Specimens number	Bricks		Mortar Joints				Frame Concrete		
	E Modulus (MPa)	Compressive Strength (MPa)	E Modulus (MPa)	Compressive strength (MPa)	*C* (MPa)	*μ*	E Modulus (MPa)	Drucker–Prager parameter *C* (MPa)	Drucker–Prager parameter Ø
1	-	-	-	-	-	-	21930	4.26	60
5	11000	15.59	3500	13.38	0.4	0.9	18070	2.71	61
7	11000	15.59	3500	15.52	0.4	0.9	18620	4.44	61

Table 3: Specifications of numerical models

Reinforcing Bars				
Bar Size	Diameter (mm)	E Modulus (MPa)	Yield Stress (MPa)	Ultimate stress (MPa)
No.2	6.35	2.1E5	370	450
No.4	12.7	2.1E5	410	660
No.5	15.9	2.1E5	410	660

Specimens number	Contact surfaces of frame & infill	
	Normal penalty stiffness (MPa/mm)	Friction coefficient *μ*
5	190	0.5
7	190	0.5

According to the experimental specimens, infilled frames have been modeled on the 315×90×46 cm reinforced concrete base. The lateral and vertical loading have been applied to the model in the case of displacement and force control, respectively. To prevent the occurrence of tension in the concrete beam, the lateral displacement of the first and last nodes of it has been constrained. Also, the weight of different components of frame and infill panel has been ignored in modeling.

5. COMPARISON OF GLOBAL AND LOCAL BEHAVIOR WITH TESTS

Lateral displacement at the mid-height node of the top beam in the frame is compared to the test results. Also, the local behavior has been evaluated by considering the crack paths that have occurred in different places, sliding in the bed joints, crushing in the corners of the infill panel and the occurrence of the shear failure in the concrete frame component. Figure 4 shows the lateral load-lateral displacement curves obtained from the numerical models and tests for specimens 1, 5 and 7.

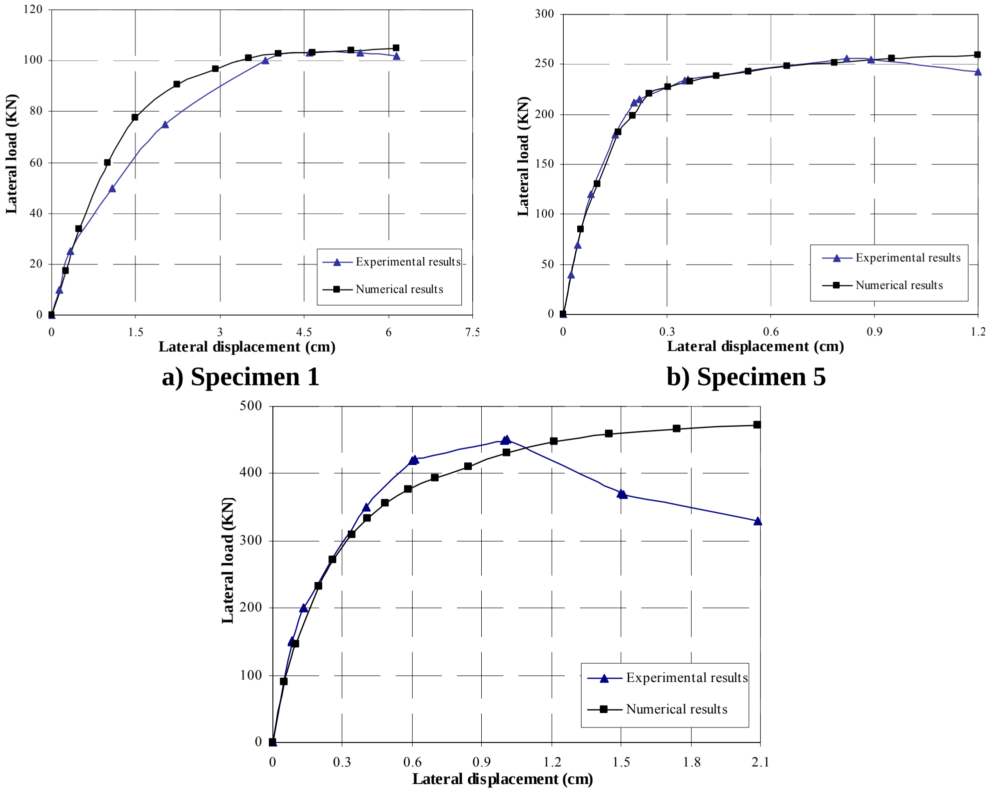

c) Specimen 7

Figure 4. Numerical and experimental lateral load-lateral displacement

The Figures show that the model has been relatively successful in predicting the global behavior over small deformation range and to some extent the large deformation response. It should be noted that the experimental curves of specimens

5 and 7 are envelopes of hysteresis curves of cyclic tests.

The deformed shapes obtained from numerical analysis for specimens 5 and 7 have been presented in Figure 5. The numerical results indicate that the prevailing mechanism at the ultimate strength of specimen 5 is shear failure in the column of concrete frame. In this model, the first important event in the process of increasing lateral load is creation of crack and tearing at the common border of the frame and infill panel and in the tension corners of the infill panel. As loading continues, the cracks form in the bed joints of mortar at the mid height of the masonry panel and propagate in the direction of compression diameter. Increasing of the lateral load, eventually leads to shear failure at the upper end of the windward column. All of these agree with experimental evidence.

The simulated model of Specimen 7 indicates that after creation of crack and tearing at the common border of the frame and infill panel, the diagonal-sliding cracks appear. The prevailing mechanism at the ultimate strength for mentioned specimen is crushing at the compressive corner of the infill panel. It should be noted that no shear failure is observed in the components of the RC frame. All of these also agree with experimental evidence.

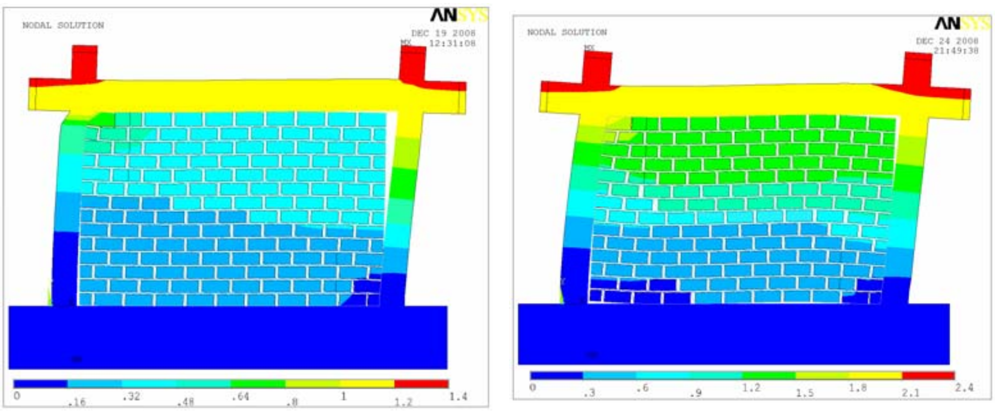

a) Specimen 5 **b) Specimen 7**

Figure 5. Deformed shapes obtained from numerical analysis

By comparing the results of the proposed model with the similar recorded experimental results and confirming the validation of the analysis, parametric studies will be carried out. Numerical models of the experimental specimens 5 and 7, have been named *WF-SI* (Weak frame and strong infill panel) and *SF-SI* (Strong frame and strong infill panel), respectively.

6. PARAMETRIC STUDY OF MASONRY-INFILLED RC FRAMES

In the parametric study, the effect of strength of frame and infill, dimensions and aspect ratios of panels have been investigated.

6.1. Strength of Frame and Infill

Different combinations of weak and strong frame and infill have been analyzed.

Specifications of the infilled frames with strong masonry infills have already been mentioned in the preceding sections. Specifications of the weak masonry infills [11] are presented in Table 4.

Table 4: Specifications of weak masonry infill for numerical modeling

Bricks		Mortar Joints			
E Modulus (MPa)	**Compressive Strength (MPa)**	**E Modulus (MPa)**	**Compressive strength (MPa)**	***C* (MPa)**	***μ***
5000	13.5	1700	4	0.25	0.75

Various models such as *SF-SI*, *WF-SI*, *SF-WI* (Strong frame and weak infill panel) and *WF-WI* (Weak frame and weak infill panel) have been analyzed. Comparison between infilled frame and the respective bare frame is presented in Figure 6. It is seen that both stiffness and strength of the infilled frame are significantly higher than those of the bare frame, but the maximum lateral displacement of infilled frame is less than that of bare frame. The maximum lateral resistance of *SF-SI* is 38% higher than that of *SF-WI*. Also, the Figureshows that lateral strength of *SF-SI* and *SF-WI* is 82% and 42% higher than that of *WF-SI* and *WF-WI*, respectively. This indicates activation of stronger failure mechanisms when strong frame and infill is used.

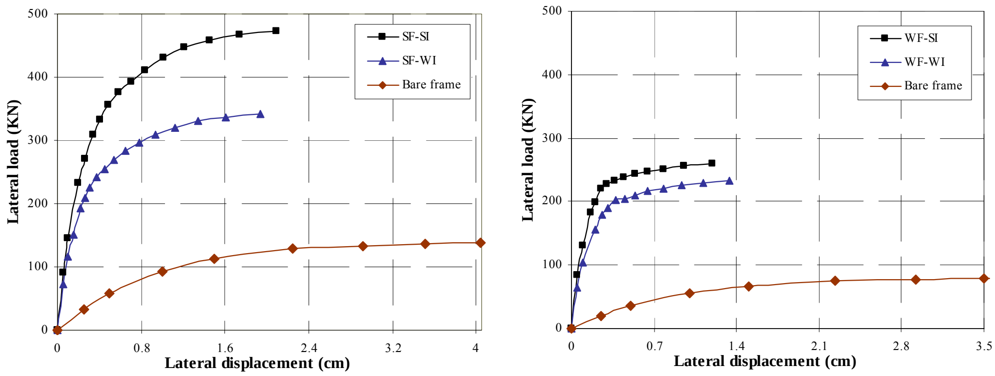

Figure 6. Lateral load-lateral displacement of weak and strong frame and infill

The numerical results for *SF-WI* indicate that after occurrence of diagonal-sliding cracks, large slips occur along the bed joints at the ultimate strength. Shear failure in the windward column is the prevailing mechanism at the ultimate strength for *WF-WI*. The deformed shapes obtained from numerical analysis for *SF-WI* and *WF-WI* have been presented in Figure 7.

6.2. The Effect of Aspect Ratio

In order to investigate the mentioned parameter, three height/length ratios 1/1, 1/1.5 and 1/2 for panels, which have been named *AR-1/1*, *AR-1/1.5* and *AR-1/2*, respectively, have been analyzed. The model *SF-SI* of preceding section is compared to model *AR-1/1.5* in this study. The models in these aspect ratios have similar height and different length. Comparison of the models has been presented in Figure 8. The results show that lateral strength of *AR-1/2* is 26% and 9% higher than that of *AR-1/1* and *AR-1/1.5*, respectively.

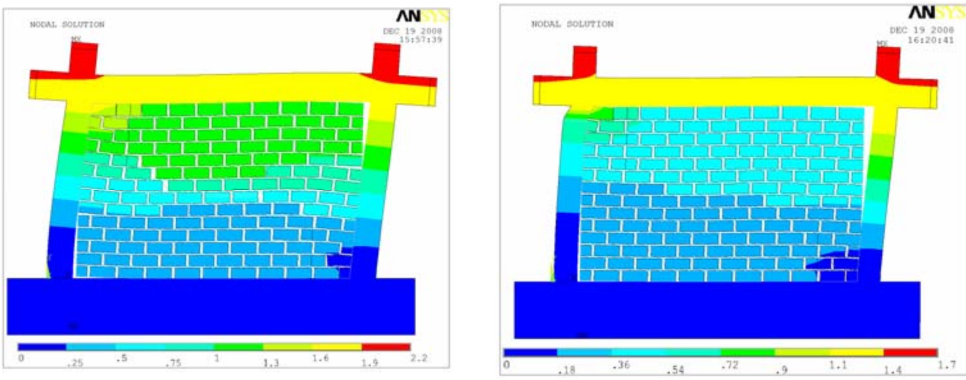

a) SF-WI **b) WF-WI**

Figure 7. Deformed shapes obtained from numerical analysis for *SF-WI* and *WF-WI*

The numerical results for *AR-1/1* indicate that after occurrence of diagonal cracks, the maximum lateral resistance is reached when crushing occur at the corners of the infill panel. For *AR-1/2* the numerical results indicate that after occurrence of diagonal-sliding cracks and corner crushing in the infill panel, shear failure in the column of RC frame is the prevailing mechanism at the ultimate strength. These results show that different panel aspect ratios can activate different failure mechanisms in masonry infilled RC frames. The deformed shapes obtained from numerical analysis for *AR-1/1*and *AR-1/2* have been presented in Figure 7.

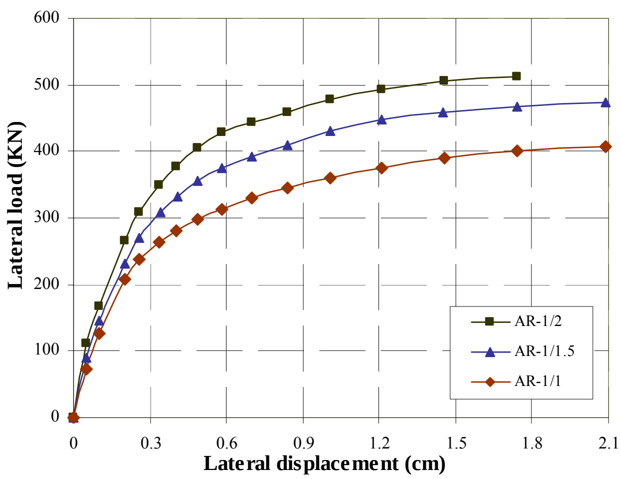

Figure 8. Lateral load-lateral displacement for numerical modeling of different aspect ratios

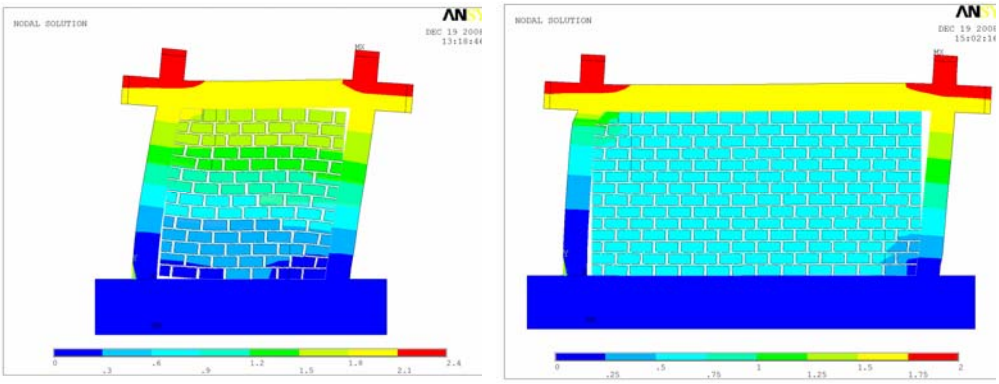

a) AR-1/1 b) AR-1/2

Figure 9. Deformed shapes obtained from numerical analysis for AR-1/1 and AR-1/2

The values of the initial stiffness, secant stiffness, ultimate strength, ductility and damping for different types of mentioned infilled frame and their bare frames are summarized in Table 4.

Table 5: Stiffness, strength, ductility and damping for all analyzed models

	Weak Frame			**Strong Frame**			***AR-1/1***	***AR-1/2***
	Bare frame	***WF-SI***	***WF-WI***	**Bare frame**	***SF-SI***	***SF-WI***		
Initial stiffness (KN/cm)	78.4	1698	1286	131.2	1800	1470	1446	2218
Secant stiffness* (KN/cm)	65.18	1231.7	878.5	101.36	1239.3	880.9	1023.1	1491.4
Ultimate strength (KN)	80.3	259.2	233.2	145.9	470.5	341.3	407.6	512.3
Ductility	6.67	5.45	5.83	7.56	8.04	7.43	9.09	6.71
Damping (%)	19.16	19.37	19.71	27.3	27.96	27.56	27.21	28.1

* From the idealized force-displacement curve [12].

As can be observed from Table 5, infill panels can improve the performance of RC frames. The strong frame and strong infill panels have a better performance than other combinations of strong and weak frame and infill in terms of load resistance and energy dissipation capability.

7. CONCLUSIONS

In this study, a numerical micro-model has been introduced to investigate the behavior of masonry infills in RC frames. The model incorporates the effects of bricks, bed and head joints of mortar and takes into account nonlinear characteristics such as cracking, sliding of mortar joints and crushing of masonry

infills and shear failure in the frame components. Validation of the analyses was done by appropriate test results.
The effects of several parameters such as strength of both frame and infills and panel aspect ratio were investigated. The study shows that stiffness and strength of the infilled frame is significantly higher than that of a bare frame. The maximum lateral resistance of a strong frame and strong infill is significantly higher than that of weak frame and infill. It was found that masonry infills can increase energy-dissipation capacity of RC frames when are used with strong frames. Also using masonry infills with weak frames can lead to occurrence of brittle shear failure at the columns of RC frames. The results of parametric studies indicate that changing the aspect ratios of panels can not only change the ultimate strength of the infilled frames, but can also activate different failure mechanisms. For a panel with height/length ratio of 1/2, addition of infill panels can lead to brittle shear failure at the columns, whereas it does not occur in aspect ratios of 1/1 and 1/1.5.

REFERENCES

1. A.B. Mehrabi, P.B. Shing, M.P. Schuller & J.L. Noland, "Experimental Evaluation of Masonry Infilled RC Frames", Journal of Structural Engineering, 1996, Vol. 122, No.3, March, 228-237.
2. H.A. Moghaddam, "Seismic Design of Masonry Buildings", Scientific Publications Institute of Sharif University, 2001, Iran, Tehran.
3. Polyakov, S.V., "On the interaction between masonry filler walls and enclosing frame when loaded in the plane of the wall", Translations in Earthquake Engineering, Earthquake Engineering Research Institute, Oakland, California, 1960, pp.36-42.
4. Stafford Smith, B. "Behaviour of the square infilled frames." J. Struct. Div., ASCE 1966, Vol. 92, No.1, January, 381-403.
5. FEMA 306, Evaluation of earthquake damaged concrete and masonry wall buildings, Applied Technology Council (ATC-43 Project); 1998.
6. Saneinejad A. and Hobbs B., "Inelastic design of infilled frames", Journal of Structural Engineering, 1995, Vol. 121, No. 4, April, 634-650.
7. A.B. Mehrabi, P.B. Shing, " Finite element modeling of masonry-infilled RC frame", Journal of Structural Engineering, 1997, Vol. 123, No.5, May.
8. J.L. Dawe, C.K. Seah, AND Y. LIU, "A computer model for predicting infilled frame behavior", NRC, Can. J. Civ. Eng. 28: 133-148, Canada, 2001.
9. ANSYS. Release 11.0, Ansys manual set 2007.
10. A. Gabor, E. Ferrier, E. Jacquelin, P. Hamelin, "Analysis and modelling of the in-plane shear behavior of hollow brick masonry panels", ELSEVIER, Construction and Building Materials, 20 (2006) 308-321.
11. A.A. Tasnimi, "Behavior of brick walls recommended by standard 2800", BHRC Publication, 2004, No. R-404.
12. FEMA 356 "Prestandard and commentary for the seismic rehabilitation of buildings", November 2000.

REINFORCED CONCRETE SLABS DESIGN BASED UPON CONCRETE CODE OF IRAN (CCI) AND BRITISH STANDARD (BS) PROVISIONS

O. Azadegan[1], M.A. Kazerooni[2] and M.J. Fadaee[3]
[1&2]Graduate Students
[3]Associate Professor
Civil Engineering Department, Shahid Bahonar University of Kerman, Kerman, Iran

ABSTRACT

One of the common methods for analyzing and designing two-way reinforced concrete slabs is the Moment Coefficients Method. In this paper, the Moment Coefficients Method for designing two-way slabs stated in the Concrete Code of Iran (CCI) is considered and compared with the same method stated in the British Standard (BS). For this purpose, the provisions recommended in the above mentioned codes are compared first, and then the differences are discussed.

The effect of different provisions on determining the amount of the required steel for the slabs having different edge conditions is considered through a numerical study. In the end, the cases in which the use of a specific code gives conservative or economic results are concluded.

Keywords: two-way slab, concrete code of Iran (CCI), British standard (BS), moment coefficient method, safety factors

1. INTRODUCTION

Analysis of plates and shells to attain internal actions for designing structural elements is one of the fields that scientists and engineers have been working on for years. These attempts have led to some exact and approximate solutions.

One of the approximate solutions which is used to analyse rectangular plates under uniform normal loads is the Moment Coefficients Method. This method is mostly used to analyze reinforced concrete slabs and helps one to find internal bending moments and shear forces by applying some coefficients. The amounts of these coefficients depends on slab supports conditions and the slab spans ratios.

Moment Coefficients Method is a very restricted method but as it's rather simple to use, it has been mostly applied in analysis and design of concrete slabs. Each concrete design code has its own provisions for using Moment Coefficients Method.

In this paper, the manner of using this method in CCI[1] and BS[2] codes is studied and compared to clarify which code leads to a more economical or conservative design.

2. ANALISING SLABS BY MOMENT COEFFICIENTS METHOD

The Moment Coefficients Method defines some coefficients to attain internal bending moments and shear forces. The amounts of these coefficients mainly depend on the ratio of the slab dimensions and the slab supports conditions. The larger the amount of the ratio of long span to short span the stiffer the short span becomes, and so it absorbs more energy.
The moments would be calculated by the following relation:

$$M = C \times w \times l^2 \tag{1}$$

in which, M is the maximum positive or negative internal moment of middle strip of the slab per unit length, C is the moment coefficient given by the code, w is uniformly distributed load and l is the span length.
Based upon the code provisions, M is the maximum bending moment at the middle and is reduced linearly to one-third of this value at the sides as indicated in Figure 1. Figure 1.a is plotted based on CCI and Figure 1.b is plotted based on BS provisions.

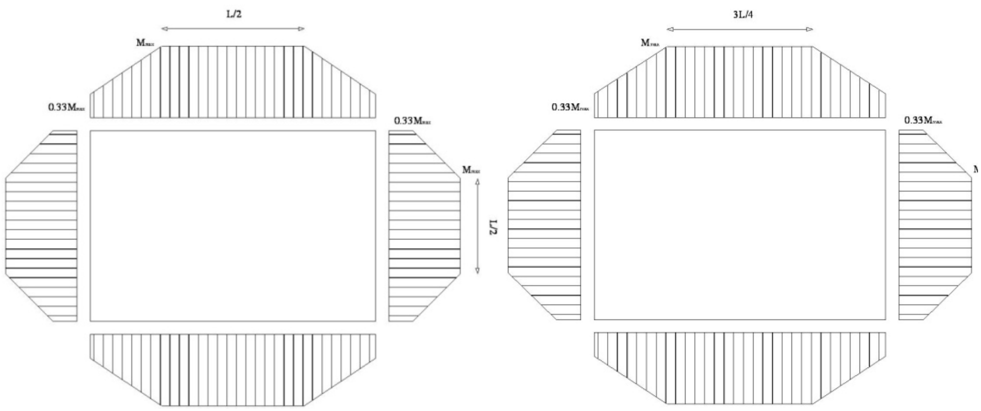

a b

Figure 1. Schematic view of bending moment diagram

3. PARTIAL SAFETY FACTORS

The partial safety factors which are used in both codes to attain ultimate loads are defined as follows:
In CCI code:
Ultimate dead load, "D" = 1.25 times service dead load, "d"
Ultimate live load, "L" = 1.5 times service dead load, "l"
In BS code:
Ultimate dead load, "D" = 1.4 times service dead load, "d"
Ultimate live load, "L" = 1.6 times service dead load, "l"
Cited relations indicate that the ultimate loads in BS code are more conservative than the ultimate loads in CCI code.

4. COMPARING THE MOMENT COEFFICIENTS

To study the differences between the two codes, the differences of coefficients are studied first. In Figure 2 the ratio of CCI coefficients of negative moments to BS coefficients of negative moments are plotted versus the ratio of slab spans. The curves are related to the case of 4 continuous edges.

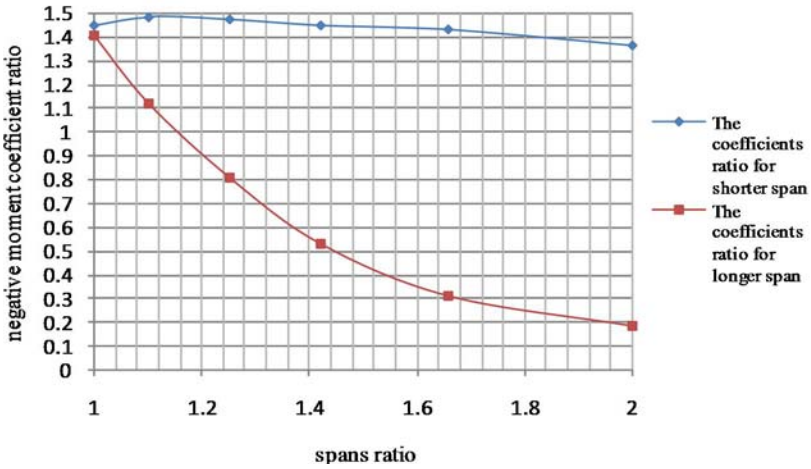

Figure 2. Comparing coefficients of CCI and BS codes

It can be seen that the value of coefficients for shorter span in CCI code is always more than in BS. But, for longer span CCI code decreases the coefficients values noticeably.

For comparing effects of loads partial safety factors, dead load is assumed constant when the live load is varying (for dead load=5.75 kN/m^2 and live load varying from 1 to 7 kN/m^2) and the ratio of ultimate load in CCI on ultimate load in BS is plotted in Figure 3.

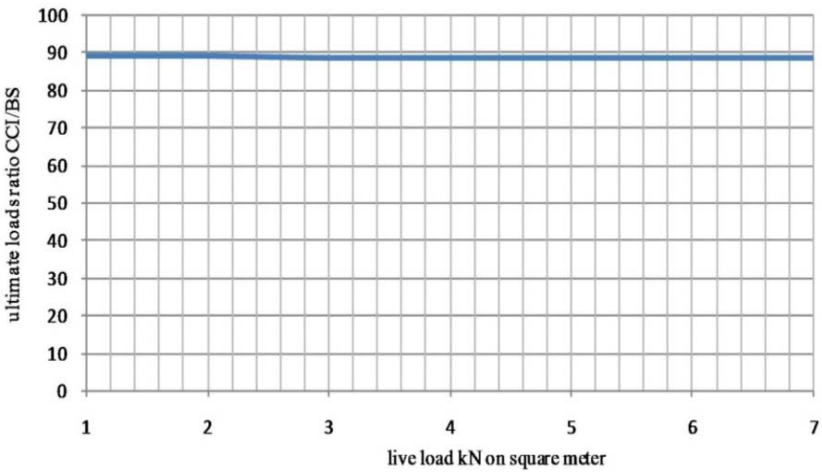

Figure 3. Effect of live load on ultimate loads

As the variation of the cited ratio due to change of live load is negligible, the numerical study would be just done for a constant value of live load. The amount of long span to short span ratio would be changed to clarify its effect on designing results.

5. NUMERICAL STUDY

A two-way slab having 150mm thickness is given in (Figure 4). The applied live load is supposed to be $2kN/m^2$ and the dead load is taken as equal to $2kN/m^2$ (the slab weight is not taken into account). This slab is designed having constant shorter span by the value of 4m when the longer span is 1.0, 1.1, 1.25, 1.42, 1.66 and 2.0 times the shorter span length, respectively.

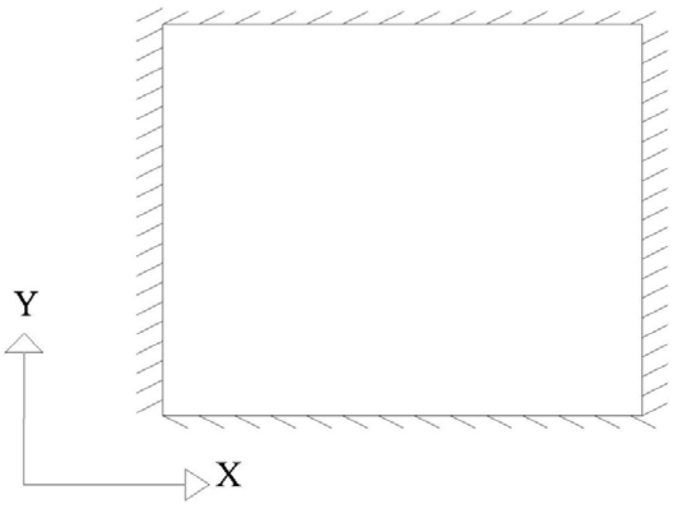

Figure 4. Slab view

For a numerical study, both CCI and BS provisions are used and the analysis results are summarized in Table 1. Then the slab is designed upon both codes. Design results are given in Table 2 and compared in Table 3. This example would be solved by other supports condition.

The values given in Table1 are the amounts of flexural moments calculated by using Table 15-8-2-4 of CCI and Table 3.14 of BS which give moment coefficients values for analysis. Table 1 indicates that the CCI results, when the spans ratio gets close to 2.0, are almost identical to that of one-way slab. On the other hand, based upon BS provisions, the moment coefficients for shorter span do not change when the spans ratio varies.

As the spans ratio gets closer to 2.0, BS presents a more economical design. Moreover, when the ratio gets closer to 1.0, BS would lead to a more conservative design.

In the following tables, M^- is the ultimate negative moment on slabs edges calculated by moment coefficients and given for both codes; M^+ is the ultimate positive moment at the middle of spans and given for both codes; and A_s is the amount of flexural steel rebar area used in each case. The total A_s given in Tables 3 and 6 would define the summation of whole rebar value which is used in slabs and is calculated by following relation:

$$\text{Total } A_s = (2A_{s\,(\text{for } M^- \text{ on La})} + A_{s\,(\text{for } M^+ \text{ on La})})\, L_A + (2A_{s\,(\text{for } M^- \text{ on LB})} + A_{s\,(\text{for } M^+ \text{ on LB})})\, L_B$$

In which L_A is the length of shorter span and L_B is the length of longer one.

Table 1: Analysis results

Spans ratio	CCI M^- Parallel to Y dir (kN.m/m)	CCI M^+ Parallel to Y dir (kN.m/m)	CCI M^- Parallel to X dir (kN.m/m)	CCI M^+ Parallel to X dir (kN.m/m)	BS M^- Parallel to Y dir (kN.m/m)	BS M^+ Parallel to Y dir (kN.m/m)	BS M^- Parallel to X dir (kN.m/m)	BS M^+ Parallel to X dir (kN.m/m)
1.0	7.335	3.366	7.335	3.366	5.679	4.397	5.862	4.397
1.1	8.965	4.162	7.100	3.226	6.778	5.130	7.094	5.320
1.25	10.595	4.958	6.622	3.252	8.061	6.137	9.160	6.870
1.42	12.062	5.802	5.587	2.785	9.343	7.090	11.821	8.866
1.66	13.203	6.694	4.492	2.193	10.415	7.804	16.154	12.116
2.0	14.018	7.423	3.912	1.688	11.542	8.794	23.450	17.587

Table 2: Rebar design results

Spans ratio	CCI M^- Parallel to Y dir (A_s mm^2)	CCI M^+ Parallel to Y dir (A_s mm^2)	CCI M^- Parallel to X dir (A_s mm^2)	CCI M^+ Parallel to X dir (A_s mm^2)	BS M^- Parallel to Y dir (A_s mm^2)	BS M^+ Parallel to Y dir (A_s mm^2)	BS M^- Parallel to X dir (A_s mm^2)	BS M^+ Parallel to X dir (A_s mm^2)
1.0	177.331	80.522	177.331	80.522	122.484	94.533	126.491	94.533
1.1	217.701	99.772	171.547	77.141	146.581	110.483	153.513	114.640
1.25	258.442	119.104	159.783	77.761	174.862	132.508	199.248	148.595
1.42	295.436	139.693	134.450	66.514	203.326	153.433	258.852	192.706
1.66	324.427	161.555	107.768	52.312	227.256	169.191	357.723	265.508
2.0	345.254	179.501	93.717	40.205	252.556	191.104	529.619	390.926

Table 3: Design comparison

Spans ratio	CCI/BS Total A_s
1.0	0.643
1.1	0.730
1.25	0.825
1.42	0.927
1.66	1.079
2.0	1.250

To attain more reliable conclusions, the boundary conditions of the slab are changed. In the new conditions, only the longer spans are continuous.
The analysis results are summarized in Table 4. The designing results and comparisons' ratios are given in Tables 5 and 6, respectively.
The same as previous example, by using CCI provisions, obtained amounts show that the results would be close to the condition of one-way slab, when the spans ratio gets closer to 2.0. On the other hand, BS presents constant amount for shorter edge of span which means that shorter edge absorbs a greater amount of energy.
As the spans ratio gets close to 2.0, BS presents a more economical design. However, when the ratio gets closer to 1.0, BS would lead to a more conservative design.
Figure 5, indicates that the values of used steel amount ratio obey a uniform conFigure uration when spans ratio increases.

Table 4: Analysis results

Spans ratio	CCI M^- Parallel to Y dir (kN.m/m)	CCI M^+ Parallel to Y dir (kN.m/m)	CCI M^- Parallel to X dir (kN.m/m)	CCI M^+ Parallel to X dir (kN.m/m)	BS M^- Parallel to Y dir (kN.m/m)	BS M^+ Parallel to Y dir (kN.m/m)	BS M^- Parallel to X dir (kN.m/m)	BS M^+ Parallel to X dir (kN.m/m)
1.0	12.225	4.641	0.000	3.366	8.427	6.229	0.000	6.229
1.1	13.040	5.111	0.000	3.029	9.160	6.962	0.000	7.537
1.25	13.692	5.792	0.000	2.817	10.168	7.603	0.000	9.733
1.42	14.018	6.473	0.000	2.224	11.175	8.427	0.000	12.560
1.66	14.344	7.087	0.000	1.877	11.816	8.885	0.000	17.164
2.0	14.670	7.701	0.000	1.228	12.824	9.710	0.000	24.915

Table 5: Rebar design results

Spans ratio	CCI M^- Parallel to Y dir (A_s mm^2)	CCI M^+ Parallel to Y dir (A_s mm^2)	CCI M^- Parallel to X dir (A_s mm^2)	CCI M^+ Parallel to X dir (A_s mm^2)	BS M^- Parallel to Y dir (A_s mm^2)	BS M^+ Parallel to Y dir (A_s mm^2)	BS M^- Parallel to X dir (A_s mm^2)	BS M^+ Parallel to X dir (A_s mm^2)
1.0	299.565	111.396	0.000	80.522	182.976	134.516	0.000	134.516
1.1	320.273	122.830	0.000	72.387	199.248	150.610	0.000	163.285
1.25	336.911	139.448	0.000	67.297	221.722	164.741	0.000	212.003
1.42	345.254	156.128	0.000	53.047	244.312	182.976	0.000	275.548
1.66	353.613	171.221	0.000	44.718	258.750	193.139	0.000	381.093
2.0	361.989	186.364	0.000	29.214	281.535	211.492	0.000	565.041

Table 6: Design comparison

Spans ratio	CCI/BS (Total steel reinforcement)
1.0	0.710
1.1	0.765
1.25	0.836
1.42	0.895
1.66	1.026
2.0	1.175

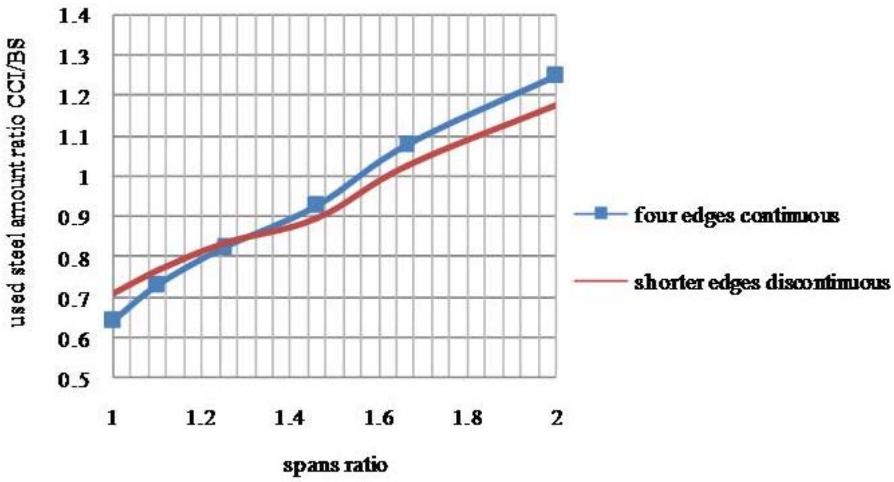

Figure 5: Variation of used steel amount ratio

By the spans ratio of about 1.6, it seems that the ratio of CCI/BS total steel reinforcement would be more than one and indicated that BS provisions lead to a more economical design.

6. CONCLUSION

In this paper, the Moment Coefficients Method for designing two-way slabs stated in the Concrete Code of Iran (CCI) is considered and compared with the same method stated in the British Standard (BS).

As the numerical study shows, by changing the value of spans ratio in a two-way slab, the codes give a different result for the amount of steel flexural rebar. For the spans ratio about 1.5-1.6 the codes lead to almost the same amount of steel rebar. For spans ratio more or less than 1.5-1.6 the difference in steel amount increases as it is plotted in Figure 5.

Obtained amounts show that by using CCI provisions, the results would be close to the results of one-way slab, when the spans ratio gets close to 2.0. On the other hand, BS presents constant amount for shorter edge of slab which means that

shorter edge absorbs a greater amount of energy.
As the spans ratio gets close to 2.0, BS presents a more economical design. However, when the ratio gets closer to 1.0, BS would lead to a more conservative design.
The maximum average variation occurs in span ratio of 1.0, for which CCI gives steel amount about 67 percent of the steel amount of BS. Therefore, it is very important to clarify the fundamental differences between two codes, to show which design is really safer or more economical.
To define which code gives better provisions for slabs design the constructions and economical conditions must be considered. As CCI provisions give more economical results for spans ratio between 1.0 and 1.6, and more compatible with construction and economical conditions of Iran, would be more reliable to use.

REFERENCES

1. British Concrete Standard, BS 8110-1: 1997, ISBN 0 580 26208 1.
2. Iranian Concrete Institude, concrete code of Iran (CCI), ISBN 978 964 179 021 1.

CD02-013

CLOSED-FORM SOLUTION OF SEMI-SPHERE CONCRETE SHELL UNDER LATERAL LOAD

V. Shokraneh[1], M.S.Marefat[2]
[1]M.Sc. Student, School of Civil Engineering, University of Tehran, Tehran, Iran
[2]Professor, School of Civil Engineering, University of Tehran, Tehran, Iran

ABSTRACT

Closed-form solution is one of the exact and reliable approaches in analysis of structures. Here, a semi-sphere shell under lateral load (equal to earthquake load), based on theory of shells and plates, has been studied. Internal forces are present in closed-form. In this study, materials are assumed to be isotropic, homogenous and elastic and the shell acts as a membrane. The outcome of this analysis can be used in studying the behavior of revolutionary shells under lateral load.

Keywords: shells of revolution, membrane, earthquake, closed-form solution, dome

1. INTRODUCTION

In this article, the behavior of a spherical shell under lateral load is studied. Emphasis is placed on dome structures. Domes have positive Gaussian curvature. These types of shells are used to cover the roofs of sports halls and large liquid tanks. The containment shield structures of nuclear power plants also have dome-like roofs. Various pressure vessels are either completely composed of a single rotational shell or have shells of rotation as their end caps.

Firstly, the governing membrane equations of shells of revolution will be derived. Then, we shall apply the analysis of a semi sphere membrane shell under seismic equivalent load.

2. GEOMETRICAL DESCRIPTION

We can define two principal radii of curvature at any point on the middle surface of a shell with non-zero Gaussian curvature. Figure 1 shows two principal sections containing the normal shell at point P. These sections create two plane curves with two local principal radii of curvature, r_1 and r_2 , as shown in Figure 1. One of these sections is called meridional curve while the projection of another section on a plane perpendicular to the axis of revolution creates the parallel circles on the shell surface.

The middle surface of a shell of revolution with non-zero positive Gaussian quadrature can be described rather like the earth. Thus, through any point we may take two sections, one perpendicular to the axis of revolution, and the other containing the axis. The first cuts the shell in a parallel curve (circle of latitude) and the other in a meridian (plane of longitude). At any point, the radius of curvature of the meridian is called r_1 , and the radius of parallel circle, r, is the projected value of another principle radius of curvature which has been denoted by r_2.[2]

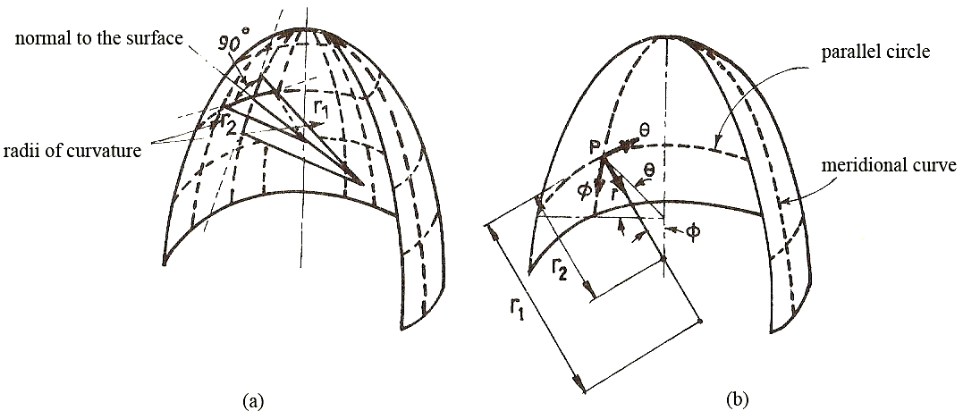

Figure 1. A parial perspective view of a surface of revolution showing the principal sectins at a point P, the principal radii of curvature, the meridians and the parallel circles

Parallel circles form the perimeter of the base of a cone, the apex of which is the center of curvature for r_2. Due to rotational symmetry, the center of curvature of r_2 always lies on the axis of revolution. However, the center of curvature of r_1 does not have to lie on the axis.

The angle between the normal to the surface at P with the axis of revolution has been denoted by φ. We have also denoted the horizontal angular position of P, from some arbitrary origin, by the angle θ. The direction of the axis of revolution is assumed to coincide with the z axis. [2]

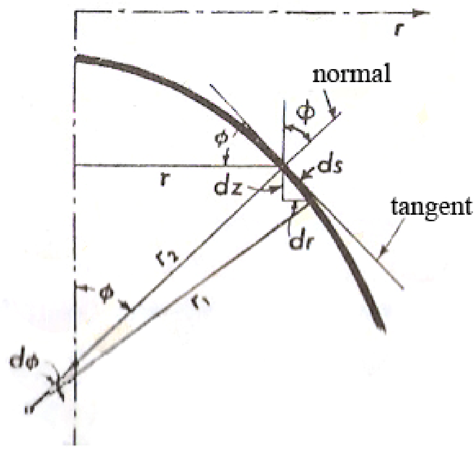

Figure 2. A meridional section of rotational showing the geometrical parameters of shell surface

Referring to Figure 2, the radius of parallel circle, r, at point P can be written as

$$r = r_2\ Sin(\varphi)$$

Also referring again to Figure 2, the following relations exist among the shell geometrical parameters.[2]

$$ds = r_1\ d\varphi$$

$$dr = ds\ Cos(\varphi) \tag{1}$$

$$dz = ds\ Sin(\varphi)$$

$$\frac{dr}{d\varphi} = r_1\ Cos(\varphi) \tag{2}$$

$$\frac{dz}{d\varphi} = r_1\ Sin(\varphi) \tag{3}$$

Combining the above relations, we obtain the following inter-relation between the surface parameters r_1, r_2, and φ.

$$\frac{1}{r}\frac{dr}{d\varphi} = \frac{r_1}{r_2}\ Cot(\varphi) \tag{4}$$

3. GOVERNING MEMBRANE EQUATION

To derive the membrane equilibrium equations for shells of revolution, we consider the free body diagram of an element of the shell in Figure 3. The element shown in Figure 3 is taken out from the shell by two pairs of infinitesimally adjacent sections. The first pair of sections is meridians while the second pair contains the normal at the corner points. Since these two intersections are principal sections, they are mutually orthogonal to each other.

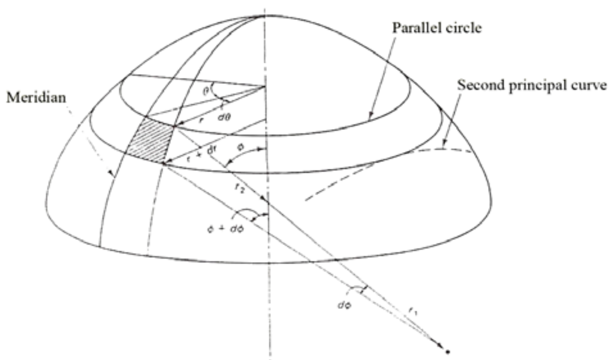

Figure 3. An infinitesimal element of a rotational surface

The free body diagram of Figure 4 shows the internal membrane forces, $N_\phi, N_\theta, N_{\phi\theta}$ and their differential variations, N_ϕ designates the meridional force, N_θ the hoop force, and $N_{\phi\theta}$ the membrane shear force; the quantities P_r, P_ϕ, P_θ represent the intensity of external distributed applied loading, in the r, ϕ, θ directions, respectively. [3]

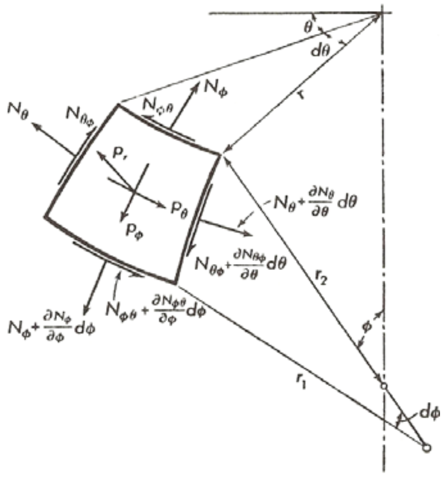

Figure 4. Free body diagram of a rotational shell element

We write the equations of equilibrium in the r, ϕ, θ directions. Because of the double curvature, the membrane forces have projections in all three directions and thus contribute to all three equilibrium equations. Figure 5, shows the contributions of N_ϕ and N_θ in various directions. [3]

The equilibrium equation in the meridional direction is ;

$$\frac{\partial N_{\phi\theta}}{\partial \theta} r_1 d\theta\, d\phi + \frac{\partial (r N_\phi)}{\partial \phi} d\theta\, d\phi - N_\theta\, r_1 d\theta\, d\phi\, \mathrm{Cos}\,\phi + P_\phi\, r\, r_1 d\theta\, d\phi = 0 \quad (5)$$

If we divide both sides of this equation by $d\theta\, d\phi$ we obtain;[3]

$$\frac{\partial (r N_\phi)}{\partial \phi} + r_1 \frac{\partial N_{\phi\theta}}{\partial \theta} - r_1\, N_\theta\, \mathrm{Cos}\,\phi + P_\phi\, r\, r_1 = 0 \quad (6)$$

We derive the equilibrium equation in the hoop direction in a similar fashion;[3]

$$\frac{\partial (r N_{\phi\theta})}{\partial \phi} + r_1 \frac{\partial N_\theta}{\partial \theta} + r_1\, N_{\theta\phi}\, \mathrm{Cos}\,\phi + P_\theta\, r\, r_1 = 0 \quad (7)$$

The third equilibrium equation is obtained by projecting all the forces in the direction normal to the shell, i.e., in the r direction. By doing so, we obtain;[3]

$$N_\theta\, r_1 \,Sin\,\phi + N_\phi\, r - P_r\, r\, r_1 = 0$$

Which, upon division by $(r\ r_1)$ yields:[3]

$$\frac{N_\phi}{r_1} + \frac{N_\theta}{r_2} = P_r \qquad (8)$$

Equations 6, 7 and 8 constitute the governing equilibrium equations of the membrane theory for shells of revolution. These relations yield $N_\phi, N_\theta, N_{\phi\theta}$, i.e. the membrane force field in the shell.

Note that the meridional and hoop forces N_ϕ, N_θ appear in all three equations. This indicates that a doubly curved shell is a complex and efficient structure; all three forces $N_\phi, N_\theta, N_{\phi\theta}$ contribute to carrying the load in any direction. The spatial interaction of internal forces, manifested in their presence in all equilibrium equations, is indicative of an efficient and profound behavior of doubly curved shells. This spatial collaboration is very rare in framed structures.

4. SHELLS OF REVOLUTION WITH NONAXISYMMETRIC LOADING

Shells structures can be subjected to loadings which are not axisymmetric. Examples of nonaxisymmetric loadings are: wind forces, earthquake effects, soil pressure on buried pipes, and temperature gradients in composite and/or metallic shells.

To perform a membrane analysis of rotationally symmetric shells under arbitrary loading, we must use all three coupled simultaneous partial differential equations (6,7,8). If we eliminate N_θ from these equations, we obtain the following relations:[1]

$$r_2 \frac{\partial N_\phi}{\partial \phi} Sin\,\phi + (r_1 + r_2)\, N_\phi\, Cos\,\phi + r_1 \frac{\partial N_{\phi\theta}}{\partial \theta} = -\, r_1\, r_2 (P_\phi\, Sin\,\phi - P_r\, Cos\,\phi) \qquad (9a)$$

$$r_2 \frac{\partial N_{\phi\theta}}{\partial \phi} Sin\,\phi + 2 r_1\, N_{\phi\theta}\, Cos\,\phi - r_2 \frac{\partial N_\phi}{\partial \theta} = -\, r_1\, r_2 \left(P_\theta\, Sin\,\phi + \frac{\partial P_r}{\partial \theta}\right) \qquad (9b)$$

For a distributed loading we can expand the loading functions, P_r, P_ϕ, P_θ , in terms of Fourier series. These expansions have the following forms:[1]

$$P_\phi = \sum_0^\infty P_{\phi n}\, Cos\, n\theta + \sum_1^\infty q_{\phi n}\, Sin\, n\theta$$

$$P_\theta = \sum_1^\infty P_{\theta n}\, Sin\, n\theta + \sum_0^\infty q_{\theta n}\, Cos\, n\theta \qquad (10)$$

$$P_r = \sum_0^\infty P_{rn}\, Cos\, n\theta + \sum_1^\infty q_{rn}\, Sin\, n\theta$$

For known loadings, the so-called "Fourier coefficients" $P_{\theta n}, P_{\phi n}, q_{\phi n}, \ldots$ can be determined using Fourier series analysis.
Equations (9) have solutions which are separable in θ and ϕ. For each value of n there are two different solutions: One in which P_ϕ, N_ϕ, N_θ are functions of ϕ multiplied by $\cos n\theta$, while $P_\theta, N_{\phi\theta}$ are functions of ϕ multiplied by $\sin n\theta$; and the other, in which $\cos n\theta$ and $\sin n\theta$ are interchanged. Both solutions are found in the same way and for the first we write ;[1]

$$\begin{aligned} P_\phi &= P_{\phi n} \operatorname{Cos} n\theta \\ P_\theta &= P_{\theta n} \operatorname{Sin} n\theta \\ P_r &= P_{rn} \operatorname{Cos} n\theta \end{aligned} \tag{11}$$

$$\begin{aligned} N_\phi &= N_{\phi n} \operatorname{Cos} n\theta \\ N_\theta &= N_{\theta n} \operatorname{Sin} n\theta \\ N_{\phi\theta} &= N_{\phi\theta n} \operatorname{Cos} n\theta \end{aligned} \tag{12}$$

Where $N_{\phi n}, N_{\theta n}, N_{\phi\theta n}$ are, in general, functions of ϕ. Substituting these expressions into (13) and canceling the common factor of $\cos n\theta$ in (9a), $\sin n\theta$ in (9b) we find:

$$\frac{\partial N_{\phi n}}{\partial \phi} + \left(1 + \frac{r_1}{r_2}\right) N_{\phi n} \operatorname{Cot}\phi + n \frac{N_{\phi\theta n}}{\operatorname{Sin}\phi} \frac{r_1}{r_2} = r_1\left(-P_{\phi n} + P_{rn} \operatorname{Cot}\phi\right) \tag{13a}$$

$$\frac{\partial N_{\phi\theta n}}{\partial \phi} + 2\frac{r_1}{r_2} N_{\phi\theta n} \operatorname{Cot}\phi + n \frac{N_{\phi n}}{\operatorname{Sin}\phi} = r_1\left(-P_{\theta n} + \frac{n}{\operatorname{Sin}\phi} P_{rn}\right) \tag{13b}$$

These ordinary differential equations can be solved analytically on numerically. Since equations (9) are linear we may superimpose any of these solutions to obtain other solutions; typical shell analyses and designs are based on just one or two terms.

4.1. Stresses in Domes under Seismic Load

For a simple model of earthquake force, acting on the shells of revolution, we assume the following distribution,

$$\begin{aligned} P_r &= -P \operatorname{Cos}\theta \operatorname{Sin}\phi \\ P_\phi &= -P \operatorname{Cos}\theta \operatorname{Cos}\phi \\ P_\theta &= +P \operatorname{Sin}\theta \end{aligned} \tag{14}$$

For a hemispherical dome of radius **a** subjected to this load, equations (13) become:

$$\frac{\partial N_{\phi n}}{\partial \phi} + 2\, N_{\phi n}\, \mathrm{Cot}\,\phi + n\frac{N_{\phi\theta n}}{Sin\,\phi} = a\left(-P_{\phi n} + P_{rn}\,\mathrm{Cot}\,\phi\right) \tag{15a}$$

$$\frac{\partial N_{\phi\theta n}}{\partial \phi} + 2\, N_{\phi\theta n}\, \mathrm{Cot}\,\phi + n\frac{N_{\phi n}}{Sin\,\phi} = a\left(-P_{\theta n} + \frac{n}{Sin\,\phi}P_{rn}\right) \tag{15b}$$

In terms of the new variables:

$$\begin{aligned} U &= N_{\phi n} + N_{\phi\theta n} \\ V &= N_{\phi n} \quad N_{\phi\theta n} \end{aligned} \tag{16}$$

The equations become:

$$\begin{aligned} &\frac{\partial U}{\partial \phi} + \left(2\,\mathrm{Cot}\,\phi + \frac{n}{Sin\,\phi}\right)U = a\left(-P_{\theta n} - P_{\phi n} + \frac{n + \mathrm{Cos}\,\phi}{Sin\,\phi}P_{rn}\right) \\ &\frac{\partial V}{\partial \phi} + \left(2\,\mathrm{Cot}\,\phi - \frac{n}{Sin\,\phi}\right)V - a\left(P_{\theta n} - P_{\phi n} - \frac{n - \mathrm{Cos}\,\phi}{Sin\,\phi}P_{rn}\right) \end{aligned} \tag{17}$$

Each of these first order differential equations has the form:

$$\frac{\partial U}{\partial \phi} + p(\phi).U + q(\phi) = 0 \tag{18}$$

The general solution to this equation is;

$$U = \left[C \quad \int q e^{\int p d\phi}\, d\phi\right] . e^{-\int p d\phi} \tag{19}$$

With the help of relations (16) and (18) we find:

$$U = \left[A - 2Pa\left(-\mathrm{Cos}\,\phi + \frac{\mathrm{Cos}^2\phi}{2}\right)\right]\frac{1 + \mathrm{Cos}\,\phi}{\mathrm{Sin}^3\phi} \tag{20}$$

$$V = \left[B + 2Pa\left(-\mathrm{Cos}\,\phi - \frac{\mathrm{Cos}^2\phi}{2}\right)\right]\frac{1 - \mathrm{Cos}\,\phi}{\mathrm{Sin}^3\phi}$$

Returning to the relations (16) and multiplying the resulting expressions, for the actual field variables $N_{\phi n}, N_{\phi\theta n}$, by $\cos\theta$ and $\sin\theta$, respectively, we obtain:

$$N_{\phi} = \frac{\mathrm{Cos}\,\theta}{\mathrm{Sin}^3\phi}\left[\frac{A+B}{2} + \frac{A-B}{2}\mathrm{Cos}\,\phi + Pa\mathrm{Cos}^2\phi\right] \tag{21}$$

$$N_{\phi\theta} = \frac{\mathrm{Sin}\,\theta}{\mathrm{Sin}^3\phi}\left[\frac{A-B}{2} + \frac{A+B}{2}\mathrm{Cos}\,\phi + 2Pa\,\mathrm{Cos}\,\phi - Pa\mathrm{Cos}^3\phi\right]$$

The integration constants A and B can be determined by imposing the physical condition that N_ϕ and $N_{\phi\theta}$ must be finite at $\phi = 0$. Hence after some algebraic manipulations, we obtain the following final solution to the problem;

$$N_\phi = \frac{Pa(1-\cos\phi)}{\sin\phi(1+\cos\phi)}\cos\theta$$

$$N_{\phi\theta} = \frac{-Pa(1-\cos\phi)(\cos\phi+2)}{\sin\phi(1+\cos\phi)}\sin\theta$$

$$N_\theta = \frac{-Pa(1-\cos\phi)(2+2\cos\phi+\cos^2\phi)}{\sin\phi(1+\cos\phi)}\cos\theta$$

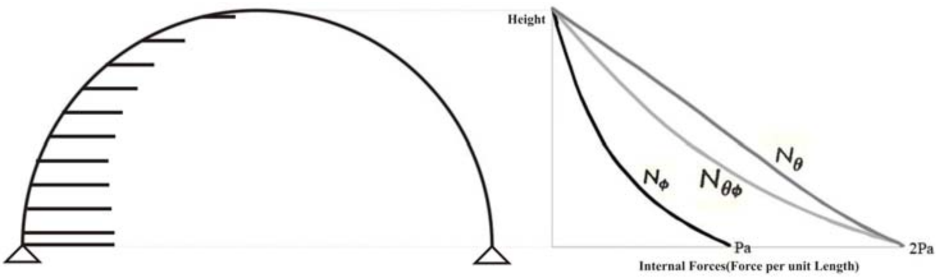

Figure 6. Variation of internal membrane forces in a hemispherical dome subjected to seismic load

5. CONCLUSION

In this study, a closed form solution for a hemisphere membrane shell of revolution under lateral seismic load is presented. The results are sketched in Figure 6. The curves indicate that all three forces, i.e., hoop, meridional, and shear components reach their maximum at the support, vary non-linearly over the height, and reduce to zero at apex. The outcome of this work can be used for analysis of dome structures under seismic inertial load.

REFERENCES

1. Farshad, M, Shell Structures (in Farsi), Shiraz university Publications, Vol. I, 78-110.
2. Flugge, W, Stresses in shells, Springer Verlag , Berlin 1973.
3. Rahimian, M, Theory of Elasticity (in Farsi), Tehran university Publications 2003.
4. Szilard, R, Theory and Analysis of Plates, Classical and Numerical 1974 Methods, Prentice-Hall, New Jersey 1974.
5. Timoshenko, S.P. and Woinowsky-Krieger, S Theory of Plates and Shells, Mc Graw Hill book co, 1959.

OPTIMUM DESIGN OF 2-D REINFORCED CONCRETE FRAMES USING A GENETIC ALGORITHM

M. Izadi Niaki[1], M. R. Maheri[2]
[1]M.Sc. Student, Dept. of Civil Engineering, Shiraz University, Shiraz, Iran.
[2]Professor, School of Engineering, Shiraz University, Shiraz, Iran.

ABSTRACT
Construction of concrete structures involves at least three different materials: concrete, steel and formwork. A large number of parameters, therefore, have to be dealt with in proportioning a reinforced concrete element, including width, depth, number and diameter of rebar. Consequently, together with experience, trial and adjustment are necessary in the choice of concrete sections. A trial section has to be chosen for each critical location in a structural system. The trial section has to be analyzed to determine if its nominal resisting strength is adequate to carry out the applied factored loads. Since more than one trial is often necessary to arrive at the required section, this process is time consuming. Also, the final design of a practiced designer is different from that of a beginner and it is never known whether the result is an optimum design.
The objective of this research is to design optimally reinforced concrete frames that satisfy the limitations and specifications of the American Concrete Institute (ACI) Building Code and Commentary using a Genetic Algorithm (GA). The GA used in this study has an adaptive penalty function. New options are added to the GA, including tournament selection with specified conditions or repairing operator that acts on beams and columns to accelerate convergence of the program. Design results show that the algorithm presented here compares advantageously with classic methods or other GA algorithms used previously for optimum design of concrete frames.

Keywords: concrete frame, genetic algorithm, optimization, design, reinforced concrete

1. INTRODUCTION
In the design of RC frames in proportioning a reinforced concrete element, members' width and depth and the number and diameter of bars have to be dealt with. Consequently, trial and adjustment are necessary in the choice of concrete sections.
The objective of this paper is to design optimally reinforced concrete frames that comply with the limitations and specifications of the American Concrete Institute (ACI) Building Code and Commentary using a Genetic Algorithm (GA). The optimization of the reinforced concrete members is more challenging than the optimization of members made of isotropic materials, such as steel. The problem

has been considered by several researchers. Krishnamoorty and Mosi (1981) presented cost optimization of two-dimensional frames with rectangular cross-sections using sequential unconstrained minimization technique (SUMT). They considered nonlinear constitutive relationships but had no actual design code. Their cost function includes only the material costs of concrete, steel reinforcement and formwork. Moharrami and Grierson (1993) carried out minimum cost design of RC building frames subjected to vertical and lateral loading, based on the ACI code ("Building" 1989) using the Optimality Criteria approach. The columns had rectangular cross-sections and the beams were considered rectangular, L or T shapes. Their design variables were the width, depth and longitudinal steel reinforcement of the beams and columns. Their cost function included the material costs of the concrete, reinforcement and the formwork. Fadaee and Grierson (1996) presented minimum cost design of three-dimensional RC frames with members subjected to biaxial moments and shear forces based on the ACI code ("Building" 1995). Beams and columns were assumed to have rectangular sections. The cost function included the material costs of concrete, steel and the formwork. Later, Camp, Pezeshk and Hanson (2003) discussed optimum flexural design of two-dimensional reinforced concrete frames using a genetic algorithm (GA). The frames were subjected to vertical and lateral loads and their beams and columns had rectangular sections. They applied a modified version of GA to achieve a low-cost design according to the ACI code ("Building" 1999). The design variables used were depth and width of the sections and the number and diameter of the reinforcement bars. Their cost function included the material costs of the concrete, reinforcement and the formwork. Lee and Ahn (2003) also minimized the cost of two-dimensional reinforced concrete frames subjected to gravity and lateral loading based on the ACI code ("Building" 1999) and the UBC (1997) using GA. Beams and columns had rectangular sections and their design variables were depth and width of the sections and area of the reinforcement. Their cost function included the material costs of the concrete, reinforcement and the formwork. Chan and Wang (2006) also carried out optimum nonlinear stiffness design of two-dimensional tall reinforced concrete buildings under service loads. Beams and columns had rectangular sections and area of the reinforcement was assumed as constant. The cost function also included only the concrete cost.

2. FORMULATION OF THE COST FUNCTION

The first step in an optimization is determination of the objective function. In this research, this function includes costs of the concrete, steel and formwork for beams and columns, where formwork cost includes labor cost. Beams and columns have rectangular sections. The design variables are depth and width of the sections and number and diameter of the reinforcement bars, hence the reinforcement topology can be determined.

Description of the cost function for beams is as follows,

Minimize F :

$$F = C_c l_b b_b h_b + C_s (l_{bl} A_{sbl} + l_{bm} A_{sbm} + l_{br} A_{sbr}) + C_f l_b (2h_b + b_b) \qquad (1)$$

Subjected to $c_{1b} \le 0$ $c_{2b} \le 0$ ... $c_{nb} \le 0$

Where, C_c is cost of the concrete per cubic foot; C_s is cost of the steel per cubic foot; C_f is cost of the formwork per square foot (including labor); l_b is length of the beam; b_b is width of the beam and h_b is height of the beam. In this research, beams are subdivided into three segments: the left segment, the middle segment and the right segment. According to this subdivision, l_{bl} is length of the left segment of beam; also A_{sbl} is area of the reinforcement for the left segment. Similarly l_{bm}, l_{br}, A_{sbm} and A_{sbr} are length of the middle segment, length of the right segment, area of the reinforcement for the middle segment and area of the reinforcement for the right segment, respectively. c_{1b}, $c_{2b}, \ldots c_{nb}$ are beams constraint functions according to specifications and limitations of the ACI-318-05 code and commentary (ACI-318R-05).

Description of the cost function for columns is as follows,

Minimize F:

$$F = C_c l_c b_c h_c + C_s l_c A_{sc} + 2C_f l_c (h_c + b_c) \qquad (2)$$

Subjected to $c_{1c} \le 0$ $c_{2c} \le 0$ ... $c_{nc} \le 0$

Where, l_c is length of the column; b_c is width of the column; h_c is height of the column and A_{sc} is area of the reinforcement. c_{1c}, $c_{2c}, \ldots c_{nc}$ are columns constraint functions according to specifications and limitations of the ACI-318-05 code and commentary (ACI-318R-05).

3. PENALTY FUNCTION

All engineering optimization problems have constraints to satisfy, whereas GA is basically introduced for unconstrained optimization. To overcome this problem and optimize engineering problems with GA, we can apply penalty functions which are proposed for constrained problems to convert them into unconstrained problems. Several different ideas have been proposed to improve penalty function methods for engineering constrained optimization problems. In this research, the method introduced by Bean and Hadj-Alouane (1992) is employed. Their penalty function is revised, based on the feasibility or infeasibility of the best penalized solution during recent generations. Their penalty function allows either an increase or a decrease in the imposed penalty during evolution as shown below. This involves the selection of two constants, β1 and β2 (β1>β2>1), to adaptively update the penalty function multiplier, and the evaluation of the feasibility of the best solution over successive intervals of *Nf* generations. As the search progresses, in every *Nf* generation the penalty function multiplier is updated, based on whether the best solution was feasible during that interval. Specifically, the penalty function is,

$$f_p(X,k) = f(X) + \sum_{i=1}^{m} \lambda_k d_i^k \tag{3}$$

$$\lambda_{k+1} \begin{cases} \lambda_k \beta_1 & \text{If previous } N_f \text{ generations have infeasible best solution} \\ \lambda_k / \beta_2 & \text{If previous } N_f \text{ generations have feasible best solution} \\ \lambda_k & \text{Otherwise} \end{cases}$$

$$\beta_1 > \beta_2 > 1$$

It is recommended that $\beta_1 = 5$ and $\beta_2 = 3$.
The total cost function can then be determined as,

$$F_T = F + \sum_{i=1}^{m} \lambda_k d_i^k \tag{4}$$

After analyzing each frame, the feasibility of the frame can be assessed. If the solution is infeasible, it is penalized; otherwise the penalty term in the cost function is set at zero.

4. FRAME ELEMENTS SPECIFICATIONS

4.1. Beams

Flexural moment varies along a beam in a frame. At supports, the negative moments govern, whereas, in the middle of the beam it is the positive moment that governs. For this reason, beams are subdivided into three segments, left, middle and right as shown in Figure 1,

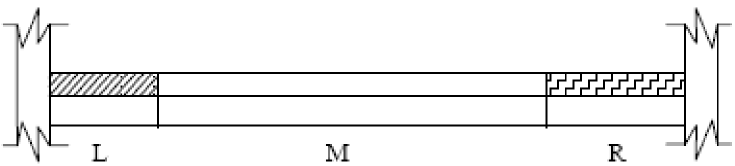

Figure 1. Beams subdivision along their lengths.

Each segment can be designed according to its maximum moment, thereby individual longitudinal reinforcement for each segment can be found. Notice that width and depth of the section are constant along the beam.
Beams are assumed to have rectangular sections and the longitudinal reinforcements of the beams are arranged in only one layer for tensile and compression steel. Number and size of the bars in different rows are not the same but all bars in a row are of the same size. Beams section specifications are shown

in Figure 2,

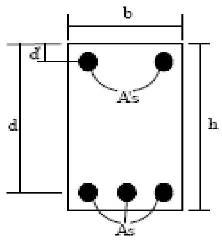

Figure 2. Beams section specifications.

Moreover, shear reinforcement will be calculated for beams. Indeed, at first, beams dimensions and longitudinal reinforcements will be produced by GA and then the shear reinforcement will be calculated for the given specifications. GA does not produce shear reinforcement; it produces only section dimensions and number and size of the longitudinal bars. Therefore, for each beam there exist fourteen variables, two for width and depth of the section for the whole beam and four for number and size of the longitudinal bars in each segment.

4.2. Columns

Columns are considered to have a uniform section along their height. In other words, their section dimensions and number and size of the longitudinal bars are constant along their length. Similar to beams, columns have rectangular sections and their longitudinal reinforcements are arranged in only one layer for tensile and compression steel. But unlike beams, number and size of the bars in different rows are of the same size. According to the ACI, minimum number of longitudinal bars in columns is assumed to be four, two for each row.

Production of section dimensions, number of longitudinal bars and their sizes and finally calculation of shear reinforcement is the same as that of the beams. Consequently four variables participate in columns design, two for width and height of the section and two for number and size of the longitudinal bars.

5. REINFORCED CONCRETE FRAMES AND RELATED CONSTRAINTS

All engineering structures have to be resistant under the applied loads. They must carry loads safely, not deform excessively. ACI-318-05 code, used in this research, outlines relations needed for design of concrete structures. These relations form constraints which are applied to beams, columns and concrete frame.

5.1. Beams Constraints

1. Moment constraint: As mentioned before, flexural moment varies along the beams. Accordingly, this constraint is calculated for the left, the middle and the right segment of beams.
2. Maximum spacing for crack control: According to the Portland Cement Association (PCA) notes on ACI, the spacing of reinforcement (Grade 60 bars) closest to a surface in tension shall not exceed that given in tables 9A-1 and

9A-2 of the PCA notes on ACI.

3. Maximum deflection constraint: According to the ACI code, computed deflection of a beam, not supporting or attached to nonstructural elements likely to be damaged by large deflections, shall not exceed $l/360$.
4. Minimum width constraint: Minimum clear spacing between parallel bars in a layer shall be d_b, but not less than 1 inch.
5. In this research, widths of the beams are restricted to widths of their associated columns.
6. Another restriction applied to the beams is that their widths are limited to their depths.
7. Maximum depth constraint: "It is also common practice in design of reinforced concrete beams to fix the maximum ratio of the depth to the width of the beam. Typically, h_max /*b* varies from 2 to 3", [3]. In this research this ratio is set at 2.5.
8. Minimum shear reinforcement constraint: Shear reinforcement designed for specified section characteristics shall not be less than minimum shear reinforcement specified by ACI-318-05. The constraint m8 defined for this case is calculated for the left and the right support shear forces separately.
9. Maximum shear reinforcement constraint: Shear reinforcement must satisfy the relation below,

$$V_s \leq 4V_c \tag{5}$$

5.2. Columns Constraints

1. Minimum longitudinal reinforcement ratio constraint: Longitudinal reinforcement ratio of the columns shall not be less than 0.01.
2. Maximum longitudinal reinforcement ratio constraint: Longitudinal reinforcement ratio of the columns shall not be greater than 0.08.
3. Minimum width constraint: In tied reinforced compression members, clear distance between longitudinal bars shall be not less than $1.5d_b$ nor less than 1.5 inches.
4. Constraint related to column interaction diagram: Columns in structural systems are rarely subjected to pure axial force; rather a combination of axial force and flexural moment is exerted to columns. This matter affects columns strength, and interaction of axial force and flexural moment has essential role in calculation of columns capacity. For design purpose, column load-moment strength interaction is used. If the factored axial force and bending moment lies inside the design strength diagram, the capacity of the column is satisfactory.
5. Since the frame under study is a two-dimensional frame, widths of the columns are limited to their depth.
6. Minimum shear reinforcement constraint: Shear forces are not the major criterion in columns design. Indeed columns are designed for axial force and bending moments, then they are checked for shear forces. Similar to beams,

shear reinforcement of the column shall not be less than the minimum permitted shear reinforcement specified by ACI-318-05.

7. Maximum shear reinforcement constraint: Shear reinforcement must satisfy the relation below,

$$V_s \leq 4V_c \tag{6}$$

5.3. Frame Constraints

Besides beams and columns constraints, stability of the frame is considered as a whole frame constraint. If the frame is not stable laterally, the related constraint is applied to the frame.

6. GENETIC ALGORITHM

The genetic algorithm used in this research has an adaptive penalty function that has been already explained. The crossover operator has the probability of 0.8, and three types of operators; one-point, two-point and uniform operators have been used. To determine which type of crossover is used, a two-bit binary string is produced. The string "00" refers to one-point crossover, the strings "01" and "10" refer to two-point crossover and finally the string "11" refers to a uniform crossover. One- and two-point crossovers are the least disruptive to the population, while uniform crossover is the most disruptive operator. The mutation rate varies between 0.008 and 0.02. If previous generation has feasible best solution, the rate is 0.008, otherwise the rate is 0.02. Selection operator is a binary tournament selection with specific conditions.
Sometimes in design procedure, the designer comes across sections that violate constraints, but minor changes in section depth, section width, number of bars or diameter of bars makes it a convenient section. This problem has been dealt with adding a new operator to GA called repairing.

7. DESIGN EXAMPLES

7.1. Uniaxial Short-Tied Columns

The first example is a problem presented by Zielinski et al. (1995). The aim is to design three uniaxial short-tied columns, each column is subjected to a factored axial force, P_f, and a factored bending moment, M_f. Loadings and material properties for each column is listed in Table 1.

Table 1: Design properties for short-tied columns [3]

Design example	d' (in.)	f_y (psi)	f'_c (psi)	P_f (lb)	M_f (ft-lb)
1	2.56	58,015	3,626	553,030	326,740
2	2.76	58,015	4,351	400,160	266,997
3	2.95	58,015	4,351	449,618	414,510

Values for the column dimensions in inches range from $7 \le b \le 30$ and $7 \le h \le 30$. Camp, Pezeshk and Hanson (2003) designed this problem according to ACI-318-99, using a modified version of GA. In this research the designed columns have been checked by drawing their exact interaction diagrams. These diagrams show that the columns have acceptable design and their axial forces and bending moments lie inside the design diagrams. Comparison between the exact interaction diagrams and the interaction diagrams drawn in this research, shows that the latter has good accuracy. Figure 3 shows both diagrams and the point related to loading for the first column.

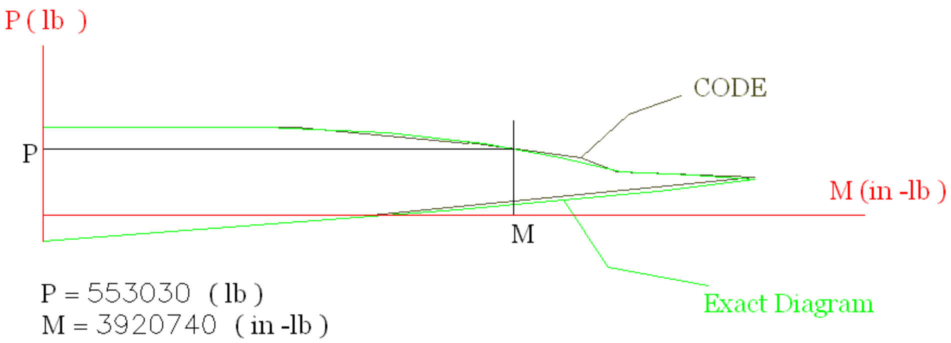

Figure 3. First column interaction diagrams and its point of loading.

Table 2 lists the design results. It should be noted that the costs in the table are for 1 foot height of columns. Columns "Result (Ave)", "Result (Min)" and "Result (Max)" show decrease or increase percents in cost for average, minimum and maximum results attained in this research versus result attained by Camp, Pezeshk and Hanson (2003), respectively. All costs are in terms of US dollar.

Table 2: Design results for uniaxial short-tied columns

column 1	Population size	Number of Generations	Ave-Cost ($)	Min-Cost ($)	Max-Cost ($)	Min-Size (in)	As (in2)	Time (sec)	Result (Ave)	Result (Min)	Result (Max)
Camp , Pezeshk, Hanson	–	–	–	34.31	–	8.5 * 29.5	4	–	–	–	–
This research	200	50	39.81	39.38	41.12	13 * 30	4	36 - 37	16.03%	14.78%	19.85%
column 2	Population size	Number of Generations	Ave-Cost ($)	Min-Cost ($)	Max-Cost ($)	Min-Size (in)	As (in2)	Time (sec)	Result (Ave)	Result (Min)	Result (Max)
Camp , Pezeshk, Hanson	–	–	–	32.18	–	12 * 25	3.14	–	–	–	–
This research	200	50	30.98	30.34	31.68	9.5 * 28.5	2.66	36 - 37	-3.73%	-5.72%	-1.55%
column 3	Population size	Number of Generations	Ave-Cost ($)	Min-Cost ($)	Max-Cost ($)	Min-Size (in)	As (in2)	Time (sec)	Result (Ave)	Result (Min)	Result (Max)
Camp , Pezeshk, Hanson	–	–	–	38.01	–	12 * 29.5	4	–	–	–	–
This research	200	50	39.07	38.04	39.65	13 * 30	3.6	36 - 37	2.79%	0.08%	4.31%

7.2. Two-Bay Six-Story Frame

Figure 4 shows a two-bay six-story reinforced concrete frame designed by Rajeev and Krishnamoorthy (1998) based on Indian Standard Code of Practice for Reinforced Concrete (IS 1978) design code. The frame was also designed by Camp, Pezeshk and Hanson (2003) based on the ACI-318-99 code using a modified version of GA.

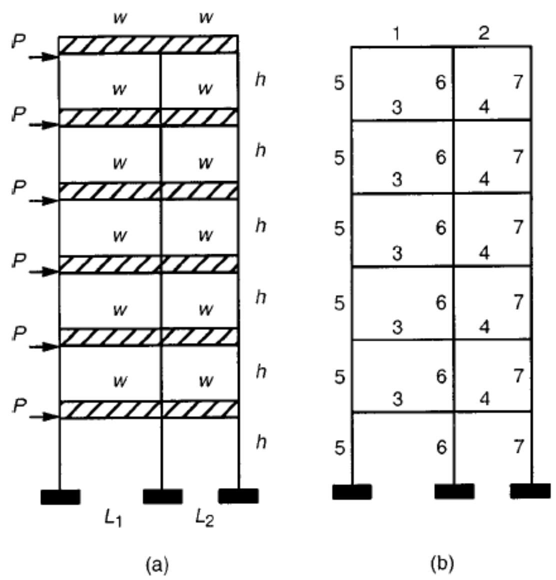

Figure 4. Two-bay six-story frame: (a) geometry and loading; and (b) beam and column group numbering [3].

The dimensions of the frame are: $h = 4m(13.12\,ft)$, $L_1 = 6m(19.69\,ft)$, and $L_2 = 4m\ (13.12\,ft)$. A factored uniformly distributed vertical load of $w = 30KN/m(2056lb/ft)$ is applied to every beam in the frame. In addition, a lateral load of $P = 10KN(2248lb)$ is applied to each story. The cost of concrete, steel and formwork is estimated as $US\$735/m^2(US\$20.81/ft^3)$, $US\$7.1/kg$ $(US\$1578/ft^3)$, and $US\$54/m^2(US\$5.02/ft^2)$, respectively (Rajeev and Krishnamoorthy 1998). The unit weight of concrete and steel is approximately $145(lbs/ft^3)$ and $490(lbs/ft^3)$. The strength of concrete, $f_c^{'} = 3000\ (psi)$, and the yield strength of steel, $f_y = 60000(psi)$.

Rajeev and Krishnamoorthy (1998) did not consider the shear capacity of the beam sections, while Camp, Pezeshk and Hanson (2003) designed the frame with and without shear capacity of the beam. Table 3 shows design results attained by Camp, Pezeshk and Hanson (2003) when the moment and shear capacities of the beams and the load-moment interaction in the columns with moment magnification due to frame stability and column slenderness have been considered, but they did not design shear reinforcements. Also longitudinal reinforcement was considered constant along the beam.

Table 3: Design results considering column slenderness for two-bay six-story frame attained by Camp, Pezeshk and Hanson (2003) [3]

	Beam Group Number				Column Group Number		
RC-GA	1	2	3	4	1	2	3
b (in.)	10	8	9	9	7	8	7
h (in.)	22	19	18	19	8	22	12
$A_{s\ bottom}$ (in.^{2})	4 #4	1 #5	4 #4	1 #6	4 #6	4 #6	6 #4
$A_{s\ top}$ (in.^{2})	1 #9	3 #6	3 #7	2 #5			
Cost	$25,471						

In this research, there are not any groupings for beams and columns. Each beam and column has its particular section, defined in the previous sections. The moment and shear capacities of the beams and columns have been considered and longitudinal and shear reinforcements have been designed for each element. Figure 5 shows numbering of the frame elements.

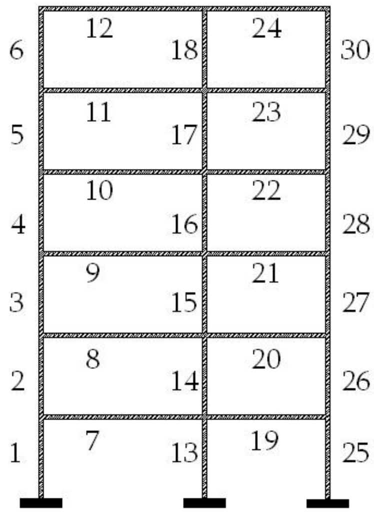

Figure 5. Numbering of the frame elements.

This frame has 240 variables, 168 variables for beams and 72 variables for columns. Design time for 200 generations with a population size of 150 is about 80 min. The best solution has the cost of US$30910. Table 4 lists section dimensions, longitudinal reinforcements designed for some elements of the best solution.
In this table:

- b: Width of the section, in.
- h: Height of the section, in.
- $nb\_b\_(l/m/r)$: Number of bottom bars in the left/mid/right segment.
- $nb\_u\_(l/m/r)$: Number of upper bars in the left/mid/right segment.
- $n\_bar\_b\_(l/m/r)$: Bottom bars size for the left/mid/right segment.
- $n\_bar\_u\_(l/m/r)$: Upper bars size for the left/mid/right segment.

Table 4: Section dimensions, longitudinal reinforcements designed for some elements of the best solution.

No	b (in)	h (in)	nb_b_l	nb_b_m	nb_b_r	nb_u_l	nb_u_m	nb_u_r	n_bar_b_l	n_bar_b_m	n_bar_b_r	n_bar_u_l	n_bar_u_m	n_bar_u_r
1	16	18	4	4	4	4	4	4	7	7	7	7	7	7
7	12	22	3	4	2	3	2	2	6	6	6	6	10	8
10	9	22	2	3	2	2	3	3	7	6	4	5	5	6
15	10	16	2	2	2	2	2	2	6	6	6	6	6	6
24	9	16	3	3	2	3	4	4	5	5	5	5	4	4
30	9	10	2	2	2	2	2	2	4	4	4	4	4	4

Table 5 lists shear reinforcements designed for some elements of the best solution.

Table 5. Shear reinforcements designed for some elements of the best solution.

No	Av_s_l	Av_s_r	Av_s_min_l	Av_s_min_r	x_.5vc_l	x_.5vc_r	x_vc_l	x_vc_r
1	0.0133	0.0133	0.0133	0.0133	78.72	78.72	0	0
7	0.01	0.0165	0.01	0.01	37.2376	136.6009	0	186.2017
10	0.0089	0.0169	0.0075	0.0075	60.6602	137.5829	22.3205	176.1657
15	0.0083	0.0083	0.0083	0.0083	78.72	78.72	0	0
24	0.015	0.0075	0.0075	0.0075	63.6099	119.03	36.2199	147.06
30	0.0075	0.0075	0.0075	0.0075	78.72	78.72	0	0

In this table:

- $Av\_s\_(l/r)$: Shear reinforcement area in unit length for the left/right half of the elements, in^2/in.
- $Av\_s\_\min\_(l/r)$: Minimum permitted shear reinforcement area in unit length for the left/right half of the elements, in^2/in.
- $x\_.5vc\_(l/r)$: Distance between point with shear force of $.5vc$ (vc is shear resistance provided by concrete) and point with shear force of zero for the left/right half of the elements, in.
- $x\_vc\_(l/r)$: Distance between point with shear force of vc (vc is shear resistance provided by concrete) and point with shear force of zero for the left/right half of the elements, in.

In this research, design time has been assumed as a determining parameter, here the selection operator with specified conditions and now the operator repairing has been used to accelerate convergence of the program. In fact, the selection used in this research causes fewer violated constraints to get in a population as the generation number grows, and then these selected populations are repaired by using the repairing operator. As a result, design time for the two-bay six-story frame with 240 variables is about 80 min., whereas the program used by Camp, Pezeshk and Hanson (2003) need 13 hours to design the same frame with only 36 variables.

8. CONCLUSIONS

In this research, optimal design of reinforced concrete frames regarding cost was considered within the limitations and specifications of the ACI code. To design these frames a GA based optimization program was introduced. This program is shown to be applicable and effective especially for problems with large numbers of constraints. Tournament selection with specified conditions and a new repairing operator was used to decrease the design time. The design time in this research is much shorter than the design time needed for the GA implemented by Camp, Pezeshk and Hanson (2003). Design time for the modified version of GA implemented by the latter researchers was about 9.75 times the design time needed for the GA introduced in this research, while the frame variables used in this research are about 6.67 times the variables used for the frame designed by Camp, Pezeshk and Hanson (2003).

9. UNIT CONVERSIONS

1 in. =25.4 mm, 1 kip=4,450 N, 1 k in. =113 N mm, 1 ksi=6.9 MPa

REFERENCES

1. American Concrete Institute. "Building Code Requirements for Structural Concrete and Commentary–ACI-318r-05". (2005). Farming Hills, MI., USA.
2. Ashlock, D. "Evolutionary Computation for Modeling and Optimization", Springer, New York. (2006).
3. Camp, C., Pezeshk, S., "Flexural Design of Reinforced Concrete Frames Using Genetic Algorithm", Journal of Structural Engineering, (2003), Vol. 129, No.1, pp.105-115.
4. Chan, C., Wang, S.M., "Nonlinear Stiffness Design Optimization of Tall Reinforced Concrete Buildings under Service Loads", Journal of Structural Engineering, (2006). Vol. 132, No. 6, pp. 978-990.
5. De Jong, K. Fogel, L. Schwefel, H. “Handbook of Evolutionary Computation“. Oxford University Press. LONDON, (1997).
6. Lee, C.J, Ahn. “Flexural Design of Reinforced Concrete Frames by Genetic Algorithm“. Journal of Structural Engineering, (2003). Vol. 129, No. 6, pp. 762-774.
7. Moharrami, H. Grierson, D.E., "Computer-Automated Design of Reinforced Concrete Frames". Journal of Structural Engineering, (1993). Vol. 119, No. 7, pp. 2036-2058.
8. Sarma, K.C., Adeli, H., "Cost Optimization of Concrete Structures". Journal of Structural Engineering, (1998), Vol. 124, No. 5, pp. 570-578.

CD02-015

A DIRECT APPROACH FOR DUCTILITY COMPUTATION OF FLEXURAL RC MEMBERS

H. Akbarzadeh Bengar[1], A.A. Maghsoudi[2]
[1]Academic staff, Civil Engineering Department, Shomal University, Amol, Iran
[2]Associate Professor, Civil Engineering Department, Kerman University, Kerman, Iran

ABSTRACT
In seismic areas, ductility is an important factor in design of concrete members under flexure; it is due to the increase in capacity of plastic displacement. As a result, the inertial forces imposed on the structures can be decreased. The effective factors on ductility are; concrete compression strength f'_c, the percentage of tension and compression steel, ρ and ρ', the amount of stirrups confinement for concrete ρ_c, the stirrups spacing, brittle effect of concrete strength, yield stress of longitudinal bars f_y and the effect of width to the depth of the section b/h. Perhaps the most simple and general definition for section ductility of members is defined, as the ratio of curvatures at ultimate load to curvatures at yield load ($\mu=\phi_u/\phi_y$).In this paper, a proposed method was considered to calculate the flexural curvature ductility ratio of reinforced concrete (RC) sections. Based on the proposed method, computer software was produced to calculate the curvature ductility in confined RC beams. The method is based on actual characteristics of a concrete flexural section by considering almost all effective ductility parameters such as available experimental concrete compression diagrams. By the developed software, the ductility factor of 250 beams under efficient circumstances were investigated completely. The nonlinear multiple regression analyses was also performed for these 250 beams and a direct equation is introduced to determine the ductility factor. Based on the obtained experimental results a comparison was made between the proposed direct method and experimental results, and it was shown that a good agreement is available.

Keywords: ductility, flexural member, RC, nonlinear multiple regression

1. INTRODUCTION
In seismic areas, ductility is an important factor in design of concrete members under flexure; it is due to the increase in capacity of plastic displacement. As a result, the inertial forces imposed on the structures can be decreased [1-2]. The effective factors on ductility are; concrete compression strength f'_c, the percentage of tension and compression steel, ρ and ρ', the amount of stirrups confinement for concrete ρ_c, the stirrups spacing, brittle effect of concrete strength, yield stress of longitudinal bars f_y and the effect of width to the depth of the section b/h [3-10].

Beams ductility can be presented based on behaviour of members section or the entire members' behaviour. Prevalent criterion of beams ductility calculation according to entire members' behaviour are the ratio of ultimate displacement to yield displacement ($\mu=\Delta_u/\Delta_y$), ratio of ultimate rotation to yield rotation ($\mu=\theta_u/\theta_y$) and the value of structure absorbed energy. Perhaps the most simple and general definition for section ductility of members is defined, ratio of curvatures at ultimate load to curvatures at yield load ($\mu=\phi_u/\phi_y$). The entire members' behaviour reveals the actual behaviour of the structure but calculation of member section behaviour is simpler. However, the experimental results show that the difference between curvature and displacement value of ductility are quite small [6, 8] and hence, the curvature ductility is used generally to investigate the member behaviour.
The effect of concrete confinement with ties on flexure ductility was studied by many researchers [4, 9, 11-14]. But in this research, ductility is calculated based on the actual characteristics of a RC flexural section (Experimental strain-stress curves for confined and unconfined concrete) and act as a separator proposed curves, which divide the zone into; effective confined concrete core, unconfined concrete core and unconfined concrete cover. The method is also based on actual characteristics of a RC flexural section by considering almost all effective ductility parameters such as available experimental concrete compression diagrams.
The calculations of the accurate values of curvature ductility of members are usually complicated particularly in confined concrete beams and therefore, by the use of simplified formula can be much easier [15]. Lee and Pan presented an algorithm and simplified formulas for estimating the relationship between only the tension reinforcement and ductility of reinforced concrete beams. They considered the effects of concrete confinement and spilling of the concrete cover. Calculating of ductility based on Lee and Pan's method is time consuming and difficult.
Based on a proposed method in this research, computer software was produced to calculate the curvature ductility in confined beams. By the developed software, the ductility factor of 250 RC beams under efficient circumstances which are mentioned above were investigated completely. The nonlinear multiple regression analysing was also performed for these 250 RC beams data and a direct equation is introduced to determine the ductility factor.
To investigate the performance and accuracy of the proposed equation, fifteen HSC beams were cast and tested under bending and also the available results of nine HSC beams were selected from research by Tsong et al. [16].

2. CURVATURE DUCTILITY CALCULATION BASED ON PROPOSED METHOD

Perhaps the most simple and general definition for section ductility of members is defined as ratio of curvature at ultimate load to curvature at yield load ($\mu=\phi_u/\phi_y$) shown in Figure 1 where M_y, corresponds to the moment at the beginning of the yielding flat plateau in the moment-curvature curve and M_u, is the moment when the ultimate load was reached during testing.

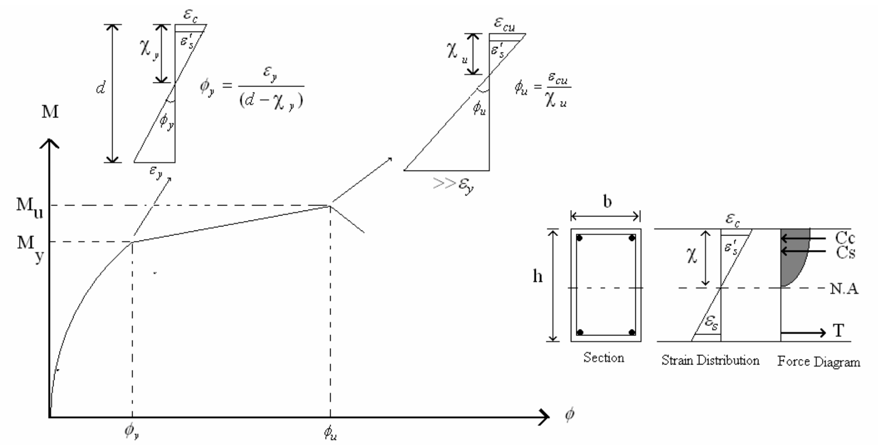

Figure 1. Moment-curvature curve and strain distribution

3. EFFECTIVE CONFINED CONCRETE CORE

3.1. Separator Curves at Transverse Level

There have been many attempts to describe the separator curves of confined concrete. Sheikh and Uzumeri, Sheikh and Yeh and Hwang and Yun made analytical and experimental studies on the mechanism of concrete confinement by considering the various parameters [9, 13-14]. They introduced the concept of the effectively confined concrete area. Fafities and Shah and Woods et al. experimentally investigated the confinement effects of HSC columns [4, 17]. Effective confined concrete area that causes an increase in both member strength and ductility is less than core nominal area which is placed centre to centre of two adjacent transverse bars [13]. Effective confined area of concrete is calculated according to parameters, such as shape of transverse and distance between longitudinal bars. At the section of transverse level with regard to the distance between the longitudinal bars, some of compressive concrete core area is unconfined when it is under bending. The unconfined concrete in core area is hatched and is shown in Figure 2. Longitudinal bars confined concrete effectively in its vicinity. It is assumed that unconfined concrete stress for hatched area out of inside concrete core is uniform.

In this research, a confinement model is proposed to divide concrete inside tie into effective confined concrete core and unconfined concrete core. Therefore, the compression concrete zone of rectangular section under bending is divided by the separator proposed curves.

The relation for separator curves of confined and unconfined concrete areas is as:

$$Y = aX^{n} \tag{1}$$

where, terms *a* and *n* are the experimental constants.

It is possible to obtain the values of *a* and *n* by considering the coordinate of the stirrup corner (point M) in Figure 2, and the separator curves which is lying

between a triangular and elliptical shape, in which the values of A (the hatched area) and θ are respectively equal to $C^2/5.5$ and 45° as Sheikh and Uzumeri suggested [13].
Hence;

$$a = \frac{1}{1.75}\left(\frac{2}{C}\right)^{0.75} \quad \text{and } n=1.75 \tag{2}$$

Having the values of *a* and *n*, and substituting in Eq. 1, the following equation is obtained:

$$Y = \frac{1}{1.75}\left(\frac{2}{C}\right)^{0.75} X^{1.75} \quad \text{or } Y = \frac{1}{1.75}\left(\frac{2}{C}\right)^{0.75}\left|X\right|^{1.75} \tag{3}$$

where $C > 0, -\frac{C}{2} \le X \le \frac{C}{2}$

Now, the Eq. 4 can be written by considering the known values of *a* and *n* and the coordinate of point M.

$$h = \frac{1}{1.75} \times \left(\frac{2}{C}\right)^{0.75} \times \left(\frac{C}{2}\right)^{1.75} \Rightarrow h = \frac{C}{3.5} \tag{4}$$

3.2. Separator Proposed Curves at Midway Between Ties (i.e., critical section)

It is clear that, confinement of concrete is improved if transverse (stirrup) reinforced layers are placed relatively close together along the longitudinal axis of the beam. There will be some critical spacing of transverse reinforcement layers above which the section midway between the transverse sets will be ineffectively confined, and therefore, it seems the available equation will be inappropriate.
The concrete confinement between the stirrups sets (ie, the spacing between two adjacent stirrups) is affecting on buckled place between stirrups sets. The minimum effective confinement lies between two stirrups. This is clearly illustrated in Figure 3. The maximum value of Y is located at a section midway between stirrups sets. Here, such a section is called a critical section. A suggested value of $0.25S \tan\theta$ is reported by Sheikh and Uzumeri [13], where θ is 45°. Hence, for analysing purpose, the critical section can be calculated by considering of actual effective concrete confinement area at transverse level which is equal to area that 0.25S at sides of width and height of the section.
Now, Figure 4, illustrates a proposed critical section along the beam's length and it is possible to define the equations for the proposed separator curves in such a section, for both confined concrete and unconfined effective concrete core.
To obtain, the distance *O′* from axis *X* and *Y*, the following operations are treated;

$$MG = d' + d''' - d'', \quad d''' = 0.25\,S, \quad MG = d' + 0.25\,S - d''$$

$$C_1 = b - 2MG, \quad H_1 = \frac{C_1}{3.5}$$

$$C_2 = h - 2MG \ , \quad H_2 = \frac{C_2}{3.5}, \quad C_3 = C_2, \quad H_3 = H_2 \tag{5}$$

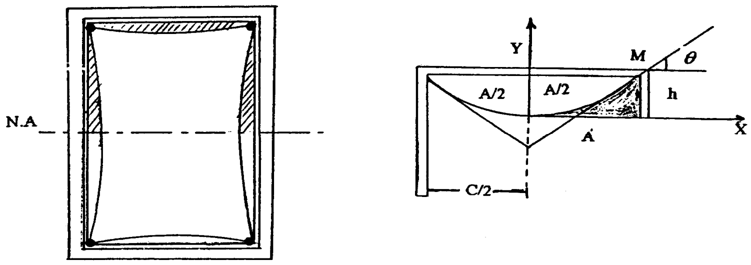

Figure 2. Unconfined concrete in core and separator curve

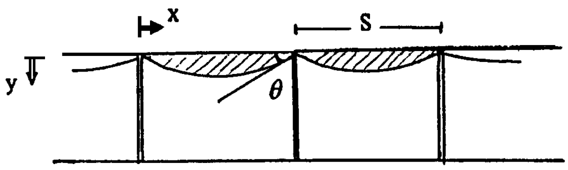

Figure 3. Unconfined concrete midway between the transverse sets

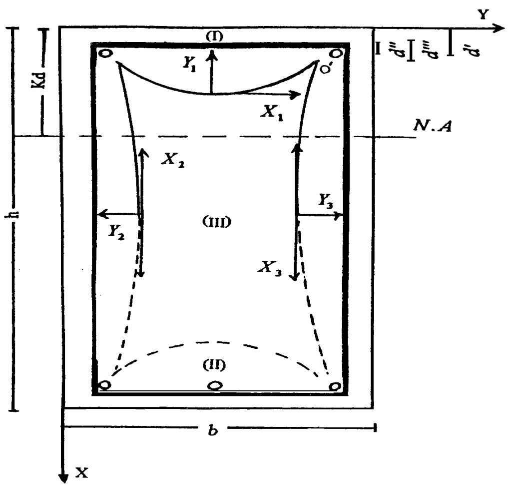

Figure 4. Proposed critical section midway between the transverse sets

C_1, H_1, C_2, H_2, C_3 and H_3 are the base and height of the separator curves 1, 2 and 3 respectively. Therefore, based on Eq. 3, it is possible to derive the separator curves 1, 2 and 3 for each local coordinate curve (Figure 4).
The equation for separator curve 1:

$$Y_1 = \frac{1}{1.75}\left(\frac{2}{C_1}\right)^{0.75}\left|X_1\right|^{1.75} \quad , \quad Y = MG + H_1 - Y_1 \quad , \quad X = \frac{b}{2} + X_1 \tag{6}$$

The equation for separator curve 2:

$$Y_2 = \frac{1}{1.75}\left(\frac{2}{C_2}\right)^{0.75}\left|X_2\right|^{1.75} \quad , \quad Y = MG + H_2 - Y_2 \quad , \quad X = \frac{b}{2} + X_2 \qquad (7)$$

The equation for separator curve 3:

$$Y_3 = \frac{1}{1.75}\left(\frac{2}{C_3}\right)^{0.75}\left|X_3\right|^{1.75} \quad , \quad Y = MG + H_3 - Y_3 \quad , \quad X = \frac{b}{2} + X_3 \qquad (8)$$

3.3. Flowchart to Determine the Moment-Curvature

By using separator curves; experimental stress-strain data of confined, unconfined concrete; and bars stress-strain relationship; a computer program was developed to calculate the moment-curvature curves for confined reinforced concrete beams (i.e., for both high strength and normal strength concrete (HSC and NSC)), and therefore, the curvature ductility is obtained based on moment-curvature curve. The proposed algorithm is demonstrated by the flowchart shown in Figure 5.

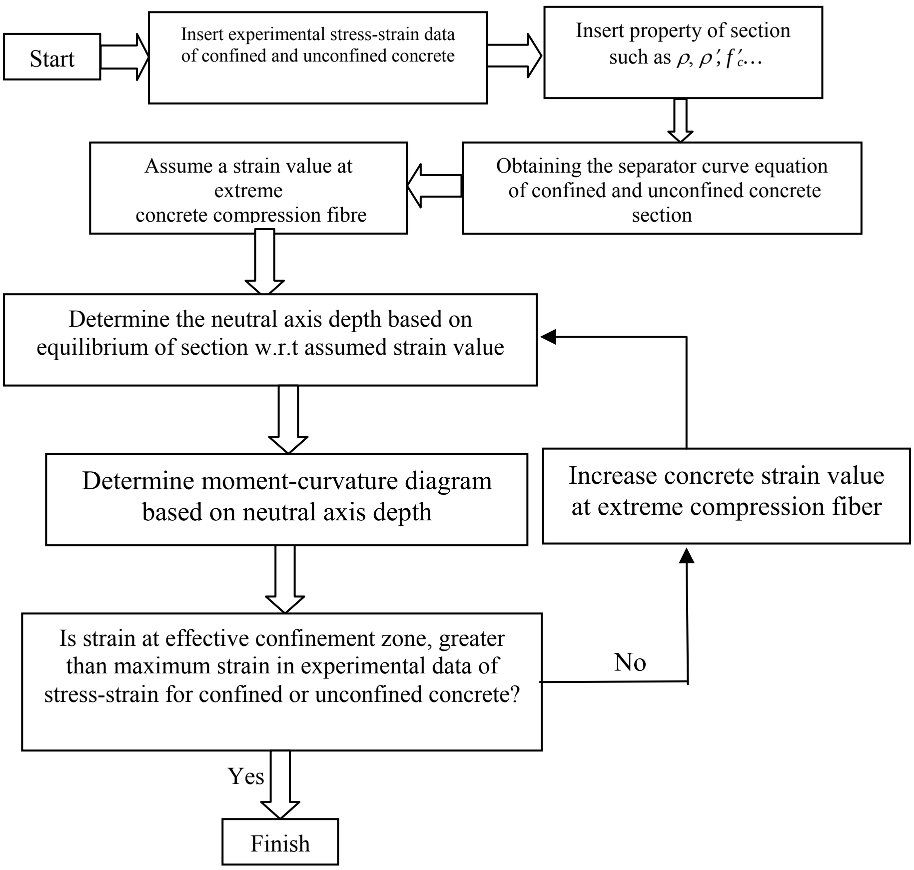

Figure 5. Flowchart to obtain moment-curvature diagram

By use of computer software which is based on proposed method, 250 beams with various assumed properties (shown in Table 1) were studied to determine the curvature ductility (μ_ϕ).
The electrical strain gauges were fixed on the surfaces of concrete cylindrical specimens and tested under compression and the stress-strain diagrams under the load were plotted. Two diagrams of total are shown in Figure 6. Behaviour of Steel was applied perfectly, where equation for steel was given in reference [18].

Table 1: Selected beams results studied by computer software

f'_c	ρ	ρ'	ρ_c	s/d	μ_ϕ	f'_c	ρ	ρ'	ρ_c	s/d	μ_ϕ
79.3	0.0440	0.0293	0.01338	0.25	15.2	41.3	0.0261	0.0087	0.01633	0.50	12.7
79.3	0.0440	0.0293	0.01338	0.50	16.8	41.3	0.0261	-	0.01633	0.25	8.0
79.3	0.0440	0.0293	0.00735	0.50	11.0	41.3	0.0261	-	-	-	2.6
79.3	0.0440	0.0147	0.00735	0.25	7.0	41.3	0.0174	0.0087	-	-	5.7
79.3	0.0440	0.0147	0.00735	0.50	8.0	26.6	0.0061	0.0061	0.01633	0.50	15.9
79.3	0.0440	-	0.00735	0.50	5.4	26.6	0.0061	-	0.01633	0.25	12.7
79.3	0.0147	-	-	-	7.0	26.6	0.0122	-	-	-	3.8

f_y=420 MPa and b/h=0.65

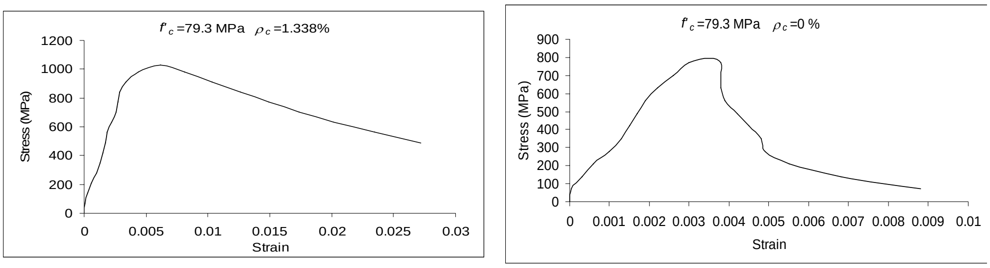

Figure 6. Experimental concrete stress-strain diagram

4. ANALYZING THE DATA BY NONLINEAR REGRESSION METHOD

Any regression analysis should be preceded by a great deal of thought devoted to what variables should be included in the analysis, how these variables might influence the dependent variable, the correlation among the independent variables and ease of using a predictive model based on the selected independent variables. Therefore the first step in the regression analysis should be the development of the form of the predictive model based on a rational analysis of the problem. Regression analysis can then be used to develop the parameters of the model, test the importance of the variables included and develop confidence intervals for the predictions. A nonlinear model is defined as an equation that is nonlinear in the coefficients or a combination of linear and nonlinear in the coefficients. For example Gaussians, ratios of polynomials and power functions are all nonlinear. In matrix form, nonlinear models are given by the formula:

$$y = f(x, \beta) + \varepsilon \tag{9}$$

Where y is an n-by-1 vector of observations, f is a function of β and X, β is a m-by-1 vector of unknown parameters, x is the n-by-m matrix made up of n observations on each of m independent variables and ε is an n-by-1 vector of errors.

Nonlinear models are more difficult to fit than linear models because the coefficients cannot be estimated using simple matrix techniques. Instead, an iterative approach is required that follows these steps: a) Start with an initial estimate for each coefficient. For some nonlinear models, a heuristic approach is provided that produces reasonable starting values. For other models, random values on the interval [0,1] are provided. b) Produce the fitted curve for the current set of coefficients. The fitted response value $\hat{y}$ is given by:

$$\hat{y} = f(x,b) \tag{10}$$

and involves the calculation of the Jacobian of f(x,b), which is defined as a matrix of partial derivatives taken with respect to the coefficients. c) Adjust the coefficients and determine whether the fit improves. The direction and magnitude of the adjustment depend on the fitting method [19]. Many methods can be used to solve these problems such as Gauss-Newton. This method is potentially faster than the other methods, but it assumes that the residuals are close to zero.

The magnitude of ductility is dependent upon the different variables such as; concrete compression strength f'_c, the percentage of tension and compression steel, ρ and ρ', the amount of stirrups confinement for concrete ρ_c, the stirrups spacing, brittle effect of concrete strength, yield stress of longitudinal bars f_y, and the effect of ratio of width to the height of the section, *b/h*. Here, a constant longitudinal yield stress value of 420 MPa is assumed.

Table 2: Details of testing program of tested beams [5-6] and Comparison of experimental and direct proposed equation results

Beam No.	f'_c (MPa)	d (mm)	d' (mm)	A_s	ρ (%)	ρ/ρ_b	A'_s	ρ' (%)	$\mu_{(exp)}$	$\mu_{(eq.11)}$	Error (%)
BC1	56.31	254	42	2Φ14	0.61	$\rho_{min=0.13}$	2Φ14	0.61	11.84	11.15	6.19
B1	69.50	254	-	2Φ14	0.61	$\rho_{min=0.13}$	-	-	10.25	10.46	2.00
BC2	63.48	250	47	2Φ20	1.25	0.24	2Φ14	0.61	6.84	8.96	23.66
B2	70.50	250	-	2Φ20	1.25	0.24	-	-	5.38	7.88	31.72
BC3	63.21	251	42	4Φ18	2.03	0.36	2Φ14+1Φ18	1.01	5.75	7.56	23.94
B3	70.80	251	-	4Φ18	2.03	0.36	-	-	4.52	5.50	17.82
BC4	71.45	250	47	4Φ20	2.51	0.43	2Φ14+1Φ20	1.24	5.60	7.40	24.32
B4	72.80	250	-	2Φ20	2.51	0.43	-	-	2.82	4.37	35.47
BC5	65.54	259	42	4Φ22	3.05	0.52	2Φ14+1Φ25	1.60	5.31	6.71	20.86
B5	71.50	259	-	4Φ22	3.05	0.52	-	-	-	3.04	-
BC6	73.77	256	40	4Φ28	4.81	0.79	2Φ14	0.61	3.20	1.21	62.50
B6	71.00	256	-	4Φ28	4.81	0.79	-	-	1.03	1	3.00
BC10	73.42	256	40	4Φ28	4.81	0.79	2Φ20	1.23	3.29	2.76	19.20
BC11	72.98	256	40	4Φ28	4.81	0.79	2Φ28	2.41	4.33	5.78	25.09
BC12	74.35	256	40	4Φ28	4.81	0.79	3Φ28	3.61	6.50	8.99	27.69
									Average error		21.12

ρ_c =0 and f_y=400

Table 3: Details of testing program of tested beams [16] and Comparison of experimental and direct proposed equation results

Beam No.	f'_c (MPa)	A_s	ρ(%)	A'_s	ρ'(%)	Stirrups Spacing (cm)	Stirrups ρ_c (%)	$\mu_{(exp)}$	$\mu_{(eq.11)}$	Error (%)
C-1	61.80	2#6	3.39	2#4	1.51	4	5.47	25.63	35.05	26.87
C-2	60.80	2#6	3.39	2#4	1.51	8	2.73	15.00	19.54	23.23
C-3	61.80	2#6	3.39	2#4	1.51	16	1.37	11.13	14.03	20.67
C-4	63.80	2#6	3.39	2#5	2.36	4	5.47	41.82	37.37	11.91
C-5	61.80	2#6	3.39	2#5	2.36	8	2.73	17.84	21.35	16.44
C-6	63.80	2#6	3.39	2#5	2.36	16	1.37	11.17	16.35	31.68
C-7	62.80	2#6	3.39	2#6	3.39	4	5.47	46.60	39.99	16.5
C-8	61.80	2#6	3.39	2#6	3.39	8	2.73	25.00	24.49	2.08
C-9	63.80	2#6	3.39	2#6	3.39	16	1.37	24.8	19.03	30.32
C-1	61.80	2#6	3.39	2#4	1.51	4	5.47	25.63	35.05	26.87
								Average error		19.96

The computer software, based on proposed method was testified for 250 RC beams of mentioned variables. Nonlinear regression method is used to analyze these 250 beams data. The analysis results provide the following direct equation to determine the ductility factor:

$$\mu = 1027.48\rho_c^{1.24} + 2.33\left(\frac{b}{h}\right)^{2.13} + 3.04\left(\frac{s}{d}\right)^{0.68} - 76.92\rho^{0.49} + 276.00\rho'^{1.02} + 2447.55\left(\frac{f'_c}{E_c}\right)^{0.93} + 8.39 \quad (11)$$

R-square and average errors of the proposed equation are 0.91 and 13 percent respectively.

5. COMPARISON OF EXPERIMENTAL AND DIRECT PROPOSED EQUATION

To evaluate the accuracy of proposed direct Eq. 11, the experimental results of tests reported by Akbarzadeh and Maghsoudi, and Tsong et al. [5-6, 16] are investigated. Table 2 and 3 present the detailed testing programs. Curvature ductility is defined as the ratio of curvatures at ultimate load to curvatures at yield load ($\mu=\phi_u/\phi_y$). The experimental yielding curvature, ϕ_y, corresponds to the curvature at the beginning of the yielding flat plateau in the moment-curvature curve. The experimental ultimate curvature, ϕ_u, is the curvature when the ultimate load was reached during testing. For the tested beams, experimental curvature ductilities and the obtained ductility amount of these beams based on proposed equation are compared and shown in Table 2 and 3. The average error for experimental and proposed direct Eq. (11) is 20 percent, which indicates that a good agreement is available.

6. CONCLUSIONS

In seismic areas, flexural ductility is an important factor in design of concrete members. The calculation of the accurate values of ductility of a member is usually complicated and therefore a direct and accurate approach to obtain such value is necessarily required particularly in seismic regions. The proposed direct Eq. (11) for calculating the curvature ductility satisfies this requirement with an average error as low as 20 %.

REFERENCES

1. Englekirk, R.E., Seismic Design of Reinforced and Precast Concrete Buildings. John Wiley and Sons, 2003.
2. Maghsoudi, A. A., Design for Ductility of Structures, Shaheed Bahonar University Publications, Kerman, Iran, 1996.
3. Hadi, M.N.S. and Elbasha, N., Effects of tensile reinforcement ratio and compressive strength on the behaviour of over-reinforced helically confined HSC beams, Construction and Building Materials, 2007, 21, 2, 269-276.
4. Woods, J.M., Kiousis, P.D., Ehsani, M.R, Saadatmanesh, Ehsani and Fritz W., Bending ductility of rectangular high strength concrete columns, Engineering Structures, 2007, 29, 8, 1783-1790.
5. Akbarzadeh, H. and Maghsoudi, A.A., Ductility of HSC members under bending", Iranian Journal of Science & Technology, Transaction B, Engineering, 2007, 31, B1.
6. Maghsoudi, A.A. and Akbarzadeh, H., Flexural ductility of HSC members, Journal of Mechanic Engineering and Structure, 2006, 24, 2.
7. Rashid, M.A. and Mansur, M.A., Reinforced High-Strength Concrete beams in flexure ACI Structural Journal, 2005, 102, 3, 462-471.
8. Maghsoudi, A. A. and Akbarzadeh, H. Effect of ρ′ on ductility of HSC members under bending, Proseding of the Seventh International Symposium on Utilization of High-Strength/High Performance Concrete, ACI, Washington, D.C., USA, 2005.
9. Hwang, S. and Yun, H., Effects of transverse reinforcement on flexural behaviour of high-strength concrete columns, Engineering Structures, 2004, 26, 1, 1-12.
10. Ashour, A.A., Effect of compressive strength and tensile reinforcement ratio on flexural behaviour of high-strength concrete beams, Engng. Structural Journal, 2000, 413-423.
11. Ziara, M. M., Haldane, D. and Kuttab, A. S., Flexural behaviour of beams with confinement, ACI Structural Journal, 1995, 92, 1.
12. Chung, H.S., Yang, K.H., Lee, Y.H. and Eun H.C., Stress-strain curve of laterally confined concrete, Journal of Engineering Structures, 2002, 24, 1153-1163.
13. Sheikh, S.A. and Uzumeri, S.M., Analytical model for concrete confinement in tied columns, Journal of Structural Division, ASCE, 1982,108, 12, 2703-2722.
14. Sheikh, S.A. and Yeh, Y.Y., Tied concrete columns under axial load and flexural, Journal of Structural Engineering, ASCE, 1990, 116,10, 2780-2800.
15. Lee, T.K and Pan, A.D. E., Estimating the relationship between tension reinforcement and ductility of reinforced concrete beam sections, Engineering Structures, 2003, 25, 8, 1057-1067

16. Tsong, Y., Yen, L. H. and Jaw, W. T., Amelioration of stirrup and compression reinforcement on the ductility of reinforced high-strength concrete beam, Proceeding of the Structures Congress, San Francisco, CA, 1989.
17. Fafitis, A. and Shah, S. P., Predictions of ultimate behaviour of confined columns subjected to large deformations, ACI Structural Journal, 1985, 423-433.
18. Wang, P. I. and Shah, S. P., High strength concrete in ultimate strength design, Journal of The Structural Division, ASCE, 1978, 104, 11, 1761-1773.
19. Seber, G. and Wild, C. J., Nonlinear Regression, John Wiley and Sons, 2003.

CD02-016

NONLINEAR FINITE ELEMENT ANALYSIS OF FLANGED RC SHEAR WALLS BASED ON MULTI-LAYER SHELL ELEMENT

A. Mortezaei[1], A. Kheyroddin[2], G. Ghodrati Amiri[3]
[1]Lecturer, Civil Engineering Dept., Islamic Azad university- Semnan branch, Semnan, Iran
[2]Associate Professor, Faculty of Civil Engineering, Semnan University, Semnan, Iran
[3]Professor, Center of Excellence for Fundamental Studies in Structural Engineering, College of Civil Engineering, Iran University of Science and Technology, Iran

ABSTRACT
Nonlinear simulations for structures under earthquakes have been widely focused on in recent years. However, precise modeling for the nonlinear behavior of reinforced concrete shear walls, which are the major lateral-force-resistant structural member in high-rise R.C. buildings, still has many items to be investigated. In this paper, based on the principles of composite material mechanics, a multi-layer shell element model is proposed to simulate the in-plane bending and the coupled in-plane bending-shear nonlinear behaviors of RC shear wall. The multi-layer shell element is made up of many layers with different layers of thickness, and different material models (concrete or rebar) are assigned to various layers so that the structural performance of the shear wall can be directly connected with the material constitutive law. Besides the traditional elasto-plastic-fracture constitutive model for concrete, which is efficient but does not give satisfying performance for concrete under complicated stress condition, a novel concrete constitutive model, referred as microplane model, which is originally proposed by Bazant et al., is developed to provide a better simulation for concrete in shear wall under complicated stress conditions and stress histories. Three flanged shear walls under static push-over load were analyzed with the proposed shear wall model for demonstration. The simulation results show that the multi-layer shell elements can correctly simulate the in-plane bending failure for tall flanged walls and the coupled in-plane bending-shear failure for short flanged walls. In addition, with microplane concrete constitutive law, the behavior and the damage accumulation of flanged shear wall can be appropriately modeled, which is very important for the performance-based design of structures under disaster loads.

Keywords: flanged shear wall, nonlinear analysis, microplane, multi-layer shell element

1. INTRODUCTION
Nonlinear simulations for structures under earthquakes have been widely focused on in recent years. However, precise modeling for the nonlinear behavior of reinforced concrete (RC) flanged shear walls, which are the major lateral-force-resistant structural member in medium-rise and high-rise buildings, still has not

been successfully solved. As the cross section of the flanged shear wall member is much bigger than that of the beam and column member, its deformation behavior under the lateral load is more complicated and the research has focused on the nonlinear analysis model for flanged shear wall. In this paper, based on the principles of composite material mechanics, a multi-layer shell element model is proposed to simulate the coupled in-plane/out-plane bending or the coupled in-plane bending-shear nonlinear behaviors of RC flanged shear wall. At the element level, the model uses the shell element that is made up of multiple layers with different thickness and different material models (concrete or rebar) are assigned to various layers. Since the model relates the nonlinear behaviors of the shear wall element to the constitutive relations of concrete and steel directly, it has many advantages in the description of the actual complicated nonlinear behaviors. In the nonlinear analysis for the concrete structures, the constitutive relation of the concrete has great effect on the analysis results.

Although the traditional elasto-plastic-fracture constitutive model for concrete is efficient, it does not give satisfying performance for concrete under complicated stress condition. So at the material constitution level, a novel concrete constitutive model, referred to as microplane model, which is originally proposed by Bazant et al. [1, 2, 3 and 4], is developed to provide a better simulation for concrete in shear wall under complicated stress conditions and stress histories. In order to validate the capacity of the proposed shear wall model, three flanged shear walls with different nonlinear behaviors under given load cases were taken as examples. Pushover analysis and static cyclic loading analysis was carried out on these shear walls with the proposed shear wall model to illustrate the capacity of the proposed model.

2. MULTI-LAYER SHELL ELEMENT

The proposed multi-layer shell element is based on the principles of composite material mechanics and it can simulate the coupled in-plane/out-plane bending and the coupled in-plane bending-shear nonlinear behaviors of RC shear wall. Basic principles of multi-layer shell element are illustrated in Figure 1. The shell element is made up of many layers with different thickness. And different material properties are assigned to various layers. This means that the rebars are smeared into one layer or more. During the finite element calculation, the axial strain can be obtained in one element. Then according to the assumption that plane remains plane, the strains and the curvatures of the other layers can be calculated. And then the corresponding stress will be calculated through the constitutive relations of the material assigned to the layer. From the above principles, it is seen that the structural performance of the shear wall can be directly connected with the material constitutive law.

The constitutive model of the rebars is set as the perfect elasto-plastic model. Because the rebars in different directions are smeared into one layer, so if the ratios of the amounts of the distributing rebars to the concrete in the longitudinal direction and transverse direction are the same, the rebar layer can be set as isotropic. But if the ratios in the two directions are different, the rebar layer should be set as orthotropic with two principal axes. And in different principal axis, the stiffness is set differently according to the ratio of the amount of rebars to concrete, in order to simulate longitudinal rebars and transverse rebars respectively.

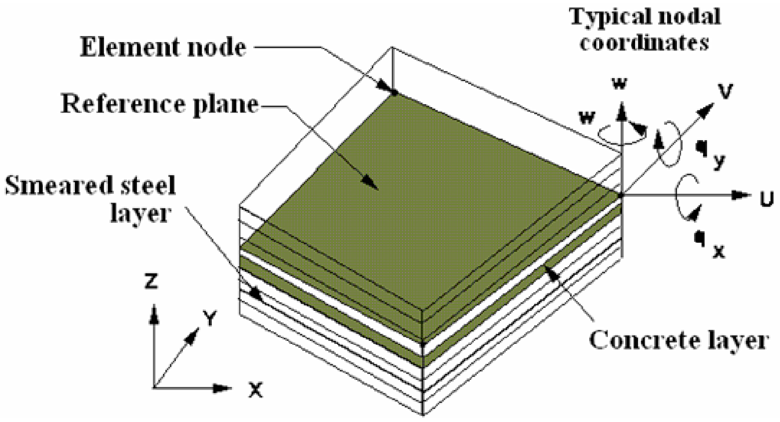

Figure 1. Multi-layer shell element

3. NONLINEAR FINITE ELEMENT PROGRAM

The NONLACS2 (NONLinear Analysis of Concrete and Steel Structures) program utilizes the basic structure of the NONLACS program [5] with the same finite element formulation and differs from the previous programs in terms of its versatility, to analyze both normal and high-strength concrete systems, to eliminate the element size effect (mesh size dependency) using both fracture mechanics and strength-based approaches, to utilize different models for concrete in compression and tension, and to determine the ultimate concrete tensile and compressive strain, ε_{tu} and ε_{cu}, respectively. The program can be used to predict the nonlinear behavior of any plain, reinforced or prestressed concrete, steel, or composite concrete-steel structure that is composed of thin plate members with plane stress conditions. This includes beams, slabs (plates), shells, folded plates, box girders, shear walls, or any combination of these structural elements. Time-dependent effects such as creep and shrinkage can also be considered.

3.1. Concrete Properties

As shown in Figure 2(a), the ascending branch of the concrete uniaxial stress-strain curve up to the peak compressive strength is represented by the Saenz equation [6]:

$$\sigma = \frac{E_0\,\varepsilon}{1 + \left(\frac{E_0}{E_{sc}} - 2\right)\left(\frac{\varepsilon}{\varepsilon_{max}}\right) + \left(\frac{\varepsilon}{\varepsilon_{max}}\right)^2} \tag{1}$$

where E_0 is the initial modulus of elasticity of the concrete, E_{sc} is the secant modulus of the concrete at the peak stress, σ is the stress, ε is the strain, and ε_{max} is the strain at peak stress. The descending or the strain-softening branch is idealized by the Smith and Young model [7]:

$$\sigma = \sigma_c \left(\frac{\varepsilon}{\varepsilon_{max}} \right) \exp \left(1 - \varepsilon / \varepsilon_{max}\right) \tag{2}$$

where σ_c is the compressive strength of the concrete. For uniaxially loaded concrete, σ_c is equal to f'_c. For high-strength concrete, the compressive stress-strain response is modeled using a modified form of the Popovics' equation [5].

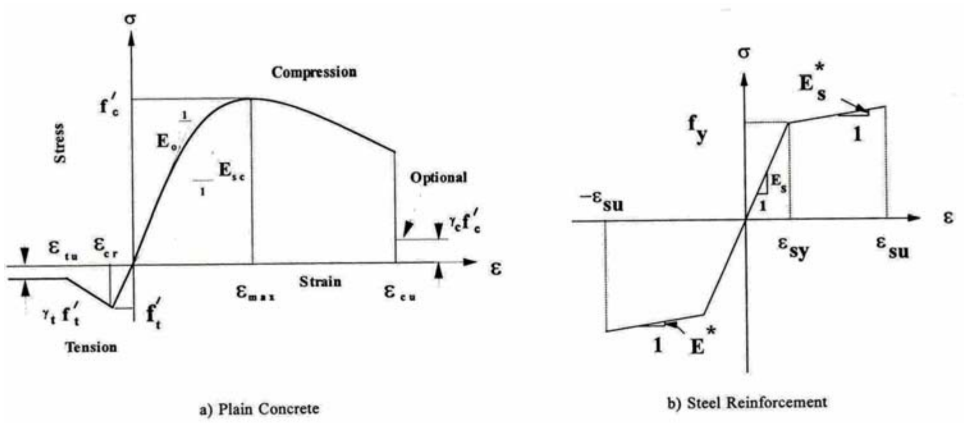

Figure 2. Uniaxial stress-strain curves

For analysis of most plane stress problems, concrete is assumed to behave as a stress-induced orthotropic material. In this study, the orthotropic constitutive relationship developed by Darwin and Pecknold [8] is used for modelling the concrete using the smeared cracking idealization. The constitutive matrix, D, is given by:

$$D = \frac{1}{(1-\nu^2)} \begin{bmatrix} E_1 & \nu\sqrt{E_1 E_2} & 0 \\ \nu\sqrt{E_1 E_2} & E_2 & 0 \\ 0 & 0 & \frac{1}{4}(E_1 + E_2 - 2\nu\sqrt{E_1 E_2}) \end{bmatrix} \tag{3}$$

in which, E_1 and E_2 are the tangent moduli in the directions of the material orthotropy, and ν is the Poisson's ratio. The orthotropic material directions coincide with the principal stress directions for the uncracked concrete and these directions are parallel and normal to the cracks for the cracked concrete. The concept of the" equivalent uniaxial strain" developed by Darwin and Pecknold [8] is utilized to relate the increments of stress and strain in the principal directions. Therefore, stress-strain curves, similar to the uniaxial stress-strain curves, can be used to formulate the required stress-strain curves in each principal direction.

The strength of concrete, σ_c, and the values of E_1, E_2 and ν are functions of the level of stress, and the various stress combinations. The concrete strength, when subjected to biaxial stresses is determined using the failure envelope developed by Kupfer et al. [9]. The values of E_1 and E_2 for a given stress ratio ($\alpha=\sigma_1/\sigma_2$) are found as the slopes of the σ_1-ε_1 and σ_2-ε_2 curves, respectively. For the descending branches of both compression and tension stress-strain curves, E_i is set equal to a very small number, 0.0001, to avoid computational problems associated with negative or zero values for E_i. The concrete is considered to be crushed, when the equivalent compressive strain in the principal directions exceeds the ultimate compressive strain of the concrete, ε_{cu}. Two models are used for determination of the concrete ultimate compressive strain, ε_{cu}, for high and normal-strength concretes [10] and confined concretes [11]. For elimination of the numerical difficulties after crushing ($\varepsilon>\varepsilon_{cu}$) and cracking of the concrete ($\varepsilon>\varepsilon_{cu}$), a small amount of compressive and tensile strength as a fraction of concrete strength, $\gamma_c f'_c$ and $\gamma_t f'_t$, is assigned (optional) at a high level of stress [Figure 2(a)], where parameters γ_c and γ_t define the remaining compressive and tensile strength factors, respectively.

Cracking of the concrete is idealized using the smeared cracking model, and is assumed to occur when the principal tensile stress at a point (usually a Gauss integration point) exceeds the tensile strength of the concrete. The stiffness across the crack is assumed to be zero and the principal directions are not allowed to rotate. The aggregate interlock at the cracks and the dowel action between the reinforcing steel and the concrete are considered using the shear retention factor, β. In reality, the concrete is able to resist tension between the cracks in the direction normal to the crack; this tension-stiffening phenomenon is implemented in the algorithm by assuming the ascending and the descending branches of the tensile stress-strain curve to terminate at ε_{cr} and ε_{tu}, respectively.

4. DEMONSTRATION CASES

In order to validate the capacity of the proposed shear wall model, three flanged shear walls were selected as the demonstration models. Pushover analysis and static cyclic loading analysis was carried out on these shear walls with the proposed shear wall model. For the shear wall, the lengths in two directions in the wall plane are both much larger than the thickness of the wall. This is much different from the beam and column members, and it will lead to bending deformations as well as shear deformations which can not usually be neglected at the same time when the wall is under lateral load in plane. These shear deformations in the wall plane have an important effect on the failure type of the wall and this complicated behavior causes the nonlinear analysis of the shear wall to become much more difficult than the beam element directly. Since, the shear span ratio of the wall is a main factor which affects the shear deformation behavior, case 1 and case 2 will simulate the coupled in-plane bending-shear nonlinear behaviors of RC flanged shear wall with different shear span ratios respectively. And case 3 simulates the out-plane bending behaviors of RC flanged shear wall. Figure 3 shows the finite element model in case 1, and the finite element model for case 2 and case 3 are similar to case 1.

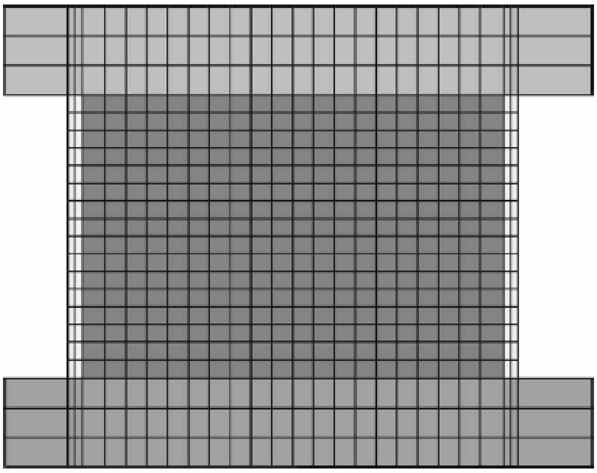

Figure 3. Finite element model in case 1

4.1. Shear Wall Case 1

The shear span ratio of the shear wall in this case is 2. For pushover analysis, the in-plane lateral load increased by step is only applied at the top of the wall. Besides, static cyclic loading process is also analyzed. In both the two analyses, the vertical load with the axial force ratio of 0.2 is applied in advance at the top of the wall. The load-displacement curve for pushover is plotted in Figure 4. From Figure 4, it can be seen that the utmost loading capacity of the shear wall is about 170kN with the displacement of about 7mm. At this time, quite a lot of concrete elements at the bottom had cracked and most tensile rebars had yielded. After that, as the crack expanded, the compressive area was getting smaller and smaller, which caused the loading capacity to drop. It can be concluded that the failure type of the wall in this case is mainly in-plane bending failure and shear deformation doesn't play an important part in the response of the shear wall.

Displacement of the shear wall along the height at different stages in pushover is shown in Figure 5, indicating that the shape of lateral displacement is of bending type. So, the deformation behavior of shear wall structure is clearly illustrated here.

Load-Displacement curve for cyclic loading is plotted in Figure 6 and the pinch effect is shown in it. This reflects the actual response characteristics of the flanged shear wall under cyclic load clearly. Besides, exterior envelope of the load-displacement curve has entered the softening part, which indicates that the microplane model can simulate the damage accumulation of flanged shear wall during the cyclic loading process precisely. This is very important for the performance-based design of structures under disaster loads.

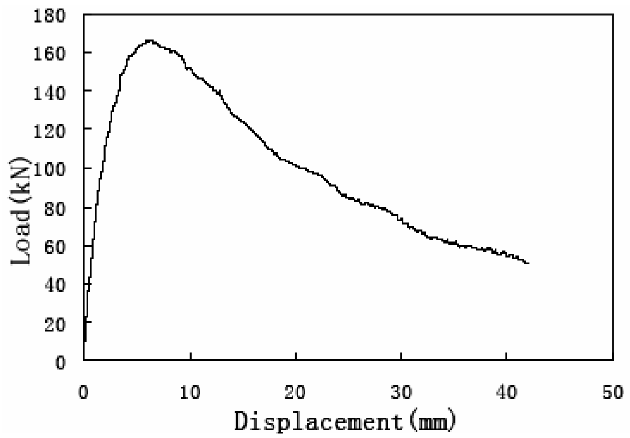

Figure 4. Load-Displacement curve for pushover

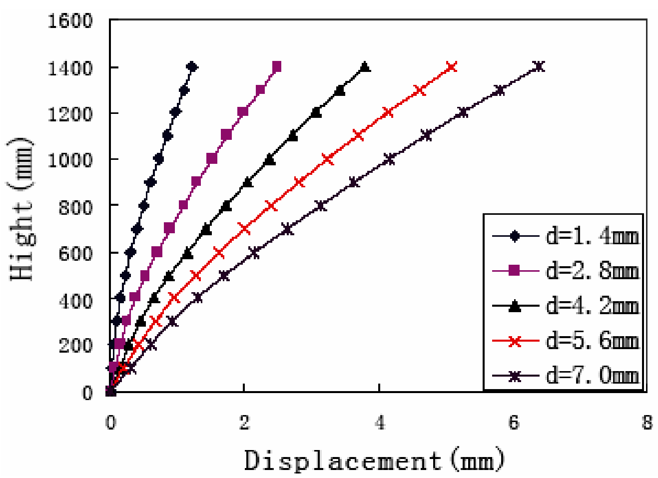

Figure 5. Displacement along the height at different stages in pushover

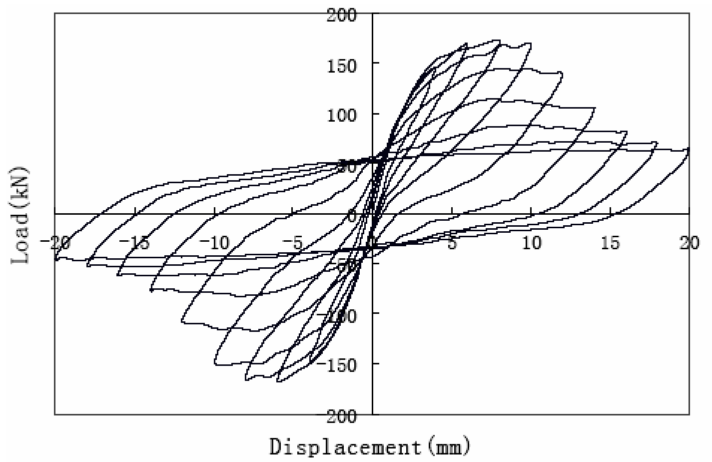

Figure 6. Load-Displacement curve for cyclic loading

4.2. Shear Wall Case 2

The shear span ratio of the shear wall in this case is 1, therefore this wall belongs to the type of short wall and the in-plane shear failure always occurs in this type of walls. The load-displacement curve is shown in Figure 7 and the curve of the same relation in case 1 is also shown in Figure 7 for a comparison. It can be seen that the stiffness and the loading capacity of the wall in case 2 are much larger than that in case 1 because the shear span ratio has affected the response characteristic of the shear wall under the lateral load. In the state of maximum loading capacity, a compressive column had formed in the diagonal direction of the wall. After that, the concrete of the diagonal compressive column was crushed and quitted the loading gradually, which caused the loading capacity of the wall to drop. But this process is more brittle than the descending process in case 1. This can be proved by comparing the descending part of the two curves in Figure 7.

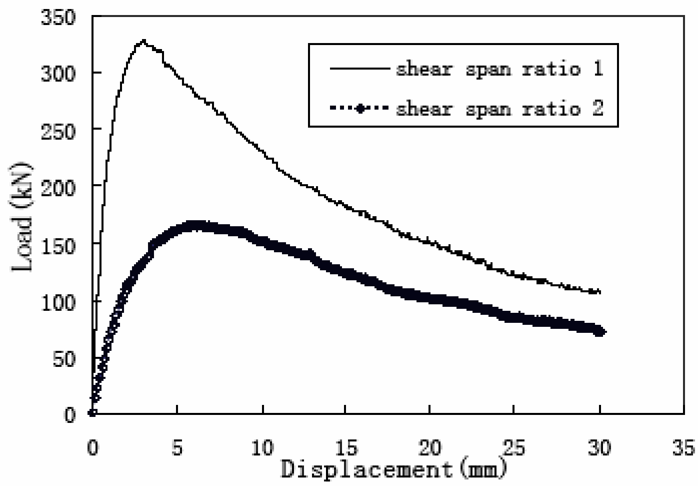

Figure 7. Load-Displacement curve for pushover

This is a typical in-plane shear failure process of shear wall. Obviously, shear deformation plays an important part in the response of the shear wall in this case and the shear failure process has much more brittleness than the bending failure process.

In Figure 8, the pinch effect can still be seen in the load-displacement curve for cyclic loading. And similarly to Figure 6, exterior envelope of the load-displacement curve has entered the softening part because of the damage accumulation of shear wall during the cyclic loading process. But the exterior envelope of the load-displacement curve in case 2 is steeper than case 1 because the shear failure process has much more brittleness than the bending failure process.

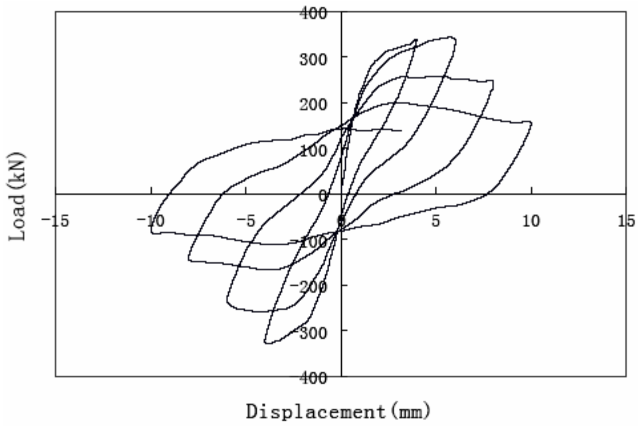

Figure 8. Load-Displacement curve for cyclic loading

4.3. Shear Wall Case 3

In the actual shear wall structures, the flanged shear walls are laid in both longitudinal and transverse directions. When the lateral load is applied to structure in one direction, the response of the wall with the plane in the same direction will present the coupled in-plane bending-shear nonlinear behavior just as in the above case 1 and case 2. But the wall with the plane perpendicular to the loading direction will bend out of the loading plane and present the out-plane bending behavior. This must be considered in the finite element analysis for shear wall structures.

In case 3, the geometric model is the same as in case 1. To study the out-plane bending behavior of flanged shear wall, the out-plane lateral load increased by step is applied at the top of the wall, and the vertical load with different axial force ratios is applied in advance at the top of the wall.

Figure 9 shows the relation between the lateral load and the lateral displacement at the top of the wall under different axial forces studied. Because the thickness of the shear wall is much smaller than the height, the out-plane bending behavior of the shear wall is very similar to the bending behavior of the 1-D beam element. This can be proved from Figure 9.

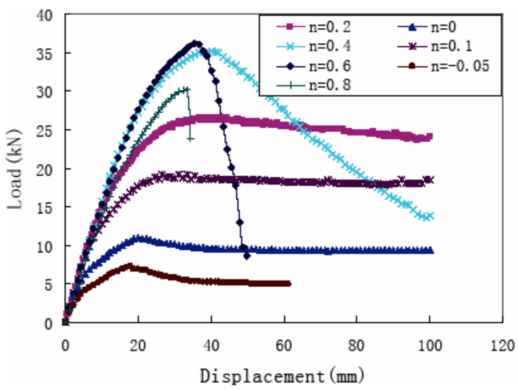

Figure 9. Load-Displacement curves under different axial force ratios in case 3

5. CONCLUSION

The proposed multi-layer shell element model based on the principles of composite material mechanics relates the nonlinear behaviors of the shear wall element to the constitutive relations of concrete and steel directly, and therefore it has many advantages in the description of the actual complicated nonlinear behaviors. And at the material constitution level, a novel concrete constitutive model, referred to as micro-plane model is introduced to provide a better simulation for concrete in flanged shear wall under complicated stress conditions and stress histories. The simulation results show that the multi-layer shell element model can correctly simulate the coupled in-plane/out-plane bending failure for tall flanged walls and the coupled in-plane bending-shear failure for short flanged walls. And with micro-plane concrete constitutive law, the cycle behavior and the damage accumulation of flanged shear wall can be precisely modeled, which is very important for the performance-based design of structures under earthquake loads.

REFERENCES

1. Bazant, Z., Caner, F., Carol, I., Adley, M. and Akres, S., "Microplane model M4 for concrete. I: formulation with work-conjugate deviatoric stress", Journal of Engineering Mechanics, 2000, 126(9), pp 944-953.
2. Bazant, Z., Xiang, Y. and Prat, P., "Microplane model for concrete. I: stress-strain boundaries and finite strain", Journal of Engineering Mechanics, 1996, 122(3), pp 245-254.
3. Bazant, Z. and Prat, P., "Microplane model for brittle-plastic material. I: theory", Journal of Engineering Mechanics, 1988, 114(10), pp 1672-1688.
4. Bazant, Z. and OH, B., "Microplane model for progressive fracture of concrete and rock", Journal of Engineering Mechanics, 1985, 111(4), pp 559-582.
5. Kheyroddin, A., (1996), "Nonlinear Finite Element Analysis of Flexure-Dominant Reinforced Concrete Structures", Ph.D. Thesis, Department of Civil Engineering and Applied Mechanics, McGill University, Montreal, Canada, 290p.
6. Saenz, L.P., “Equation for the Stress-Strain Curve of Concrete in Uniaxial and Biaxial Compression of Concrete”, ACI Journal, 1965, 61(9), pp 1229-1235.
7. Smith, G.M., and Young, L. E., “Ultimate Theory in Flexure by Exponential Function”, ACI Journal, 1955, 52(3), pp 349-359.
8. Darwin, D. and Pecknold, D.A., “Nonlinear Biaxial Stress-Strain Law for Concrete”, ASCE Journal of the Engineering Mechanics Division, 1977, 103(EM4), pp 229-241.
9. Kupfer, H.B., Gerstle, K.H. and Rusch, H., “Behavior of Concrete Under Biaxial Stresses” ACI Journal, 1969, 66(8), pp 656-666.
10. Pastor, J.A. (1986). “High-Strength Concrete Beams”, Ph.D. Thesis, Cornell University, New York, Ithaca.
11. Scott, B.D., PARK, R. and PRIESTLY, M.J.N., "Stress-Strain Behavior of Concrete Confined by Overlapping Hoops at Low and High Strain Rates", ACI Journal, 1982, 79(1), pp 13-27.

CD02-017

THEORETICAL AND EXPERIMENTAL STUDY OF UNBOUNDED POST-TENSIONED CONTINUOUS SLAB DECKS CONSISTING OF HIGH STRENGTH SCC

A.A. Maghsoudi[1], M. Torkamanzadeh[2]
[1]Associate. Prof., Civil Engineering. Dept., Kerman University, Kerman, Iran
[2]M.Sc Student, Civil Engineering. Dept., Kerman University, Kerman, Iran

ABSTRACT

Self-Consolidating Concrete, SCC is the new generation type of concrete which is not needed to be compacted by vibrator and it will be compacted by its own weight. Since SCC is a new innovation, therefore, understanding the implementation of this type of concrete on the ultimate unbounded tendon stress of post-tensioned self-consolidating concrete of bridge slabs decks (PSCCSD) is critical. For this purpose, the theoretical and experimental investigation of continuous tow span PSCCSD consisting of high strength concrete was performed. The slabs deck (L=7.5 m, b=1 m, h=0.2 m) were simulated by this concrete and the percentage of tensile and compressive steel reinforcement are in accordance with the provision of the ACI-08 for prestressed conventional (vibrating) concrete structures. During the test, the strains on concrete, steel strands and ordinary bar and deflections were measured at different locations along each span. Based on the experimental measurements, the values of experimental ultimate unbounded tendon stress f_{ps} for two tested post-tensioned SCC, continuous slabs were measured. The theoretical early and up to date works, as well as the codes recommendations for predictions of internal unbounded tendon stress at ultimate (for conventional concrete used in prestressed structures) are reviewed and their relations are used to compare with the only available experimental results of post-tensioned continuous SCC slabs of this study. It was found that the experimental results are higher than the theoretical as well as the codes prediction values suggestion for f_{ps}. However, among the theoretical values suggested by different selected codes of this study, the ACI-08 values are close to the experimental values of this study.

Keywords: post-tensioned, continuous slab decks, SCC, Ultimate unbounded stress

1. INTRODUCTION

The development of SCC started in Japan (Tokyo University) in the mid 80's with the aim of reducing durability problems in complicated and heavily reinforced concrete structures due to lack of skilled workers and poor communication between designers and construction engineers [1]. Even though conventional (vibrating) concrete previously (and still today) in some applications was cast without any

compaction, this new concrete was deliberately designed to be able to fill every corner of the form and encapsulate all reinforcement with maintained stability only under the influence of gravitational forces.
The amount of pressure on Iranian transportation infrastructure continues to increase as our growing population demands new roads and older roadways need to be replaced. Only a portion of the necessary funds are available for building new bridges and replacing deficient ones. Therefore, research in bridge design is crucial. High quality structures need to be designed and built with increasing efficiency to allow them to serve society better for a longer period of time, while leaving finances for other undertakings. This research document focuses on one specific type of bridge system; post-tensioned self consolidating concrete slabs made continuous over tow spans through the use of continuity diaphragms. This type of bridge system was selected because it has many advantages (see Figure 1).

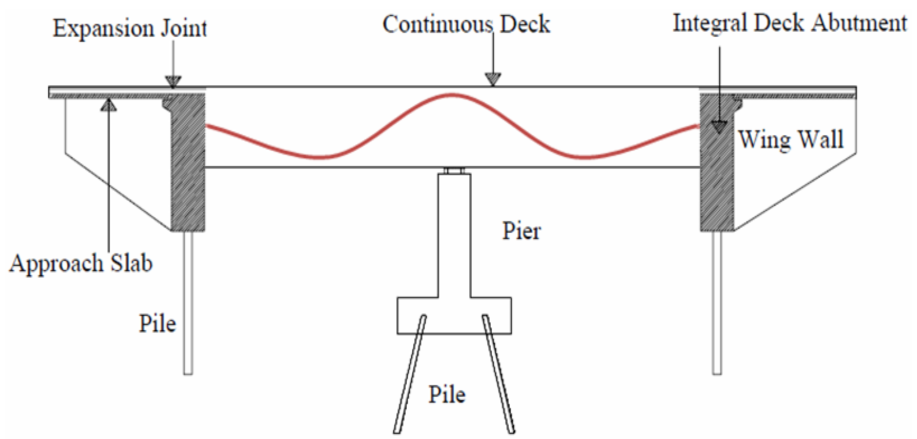

Figure 1. Post-tensioned concrete slabs made continuous

A continuous bridge is one in which two or more simple spans are connected end-to-end with continuity diaphragms. To understand the moments that develop in a continuity diaphragm, consider a simply supported system. The ends of the girder are able to rotate freely throughout the service life of the bridge from the effects of creep, shrinkage, prestress loss, live loads, temperature gradients, and other loading conditions. In a continuous system, no further end rotation is allowed after the continuity diaphragm is poured and the ends of the slabs are fixed. Restraint moments must then develop in the continuity slabs to oppose those moments that would rotate the end of the slab if it were unrestrained.
A continuous bridge has several advantages over a series of simple span structures. First, there is a reduction in mid-span bending moments and deflections. This is economical because the deck cross-section can be reduced, or fewer prestressing strands can be used in cases where the member size is fixed [2]. Secondly, making a bridge continuous will improve serviceability by eliminating joints in the deck. The removal of joints will improve the riding surface of the bridge, and durability will be increased because the water and salts from the deck will not drain onto the

substructure. Many people consider this the most important advantage [3]. In addition, the exclusion of joints in a design will reduce the initial cost of the bridge and also reduce bridge maintenance. Third, a bridge that has been made continuous will redistribute moments if the load capacity is exceeded for a particular girder in the system [2]. To determine the change in force in an unbounded post-tensioned tendon due to load on a structure, the entire structure needs to be analyzed rather than individual sections. The change in tendon strain due to applied loads should be calculated by the structure displacements. To calculate the strain in unbounded tendon the displacements of anchorage are required. The calculation of unbounded tendon strain generally requires an iterative procedure. The procedure becomes more complicated when nonlinearities due to cracking, material stress-strain relations, eccentricity changes with applied loads, and joint opening in segmental construction etc., are included in the analysis. Time dependent effects due to creep and shrinkage of concrete and relaxation of prestressed reinforcements, and the effect due to temperature gradient across the section depth are important in the analysis to predict accurate deflections, strains and stresses in concrete structures at the serviceability limit state. In addition, the contribution of the uncracked concrete to the stiffness of the structure, which is known as the tension stiffening effect, should be considered.

The studies mentioned above were useful only to find the tendon stress at the ultimate limit state. To determine the strain in unbounded tendons due to the entire loading range up to ultimate, the structural analysis has to be performed to find displacements for the given loads. This becomes difficult as the unbounded tendon stresses are not known a priori, thus iterative methods are generally required. Simplified methods are also available to determine the behavior of concrete structures with internal unbounded tendons due to service loads considering cracking. Most of these methods are however limited to beams with symmetrical loads and tendon profiles.

1.1. Theoretical Early and up to Date Work for Predictions of Internal Unbounded Tendon Stress at Ultimate

Baker [4] was among the first to propose an equation to calculate the unbounded prestressing tendon strain, ε_{ps} at ultimate Eq. (1):

$$\varepsilon_{ps} = \varepsilon_{pe} k \left(\Delta \varepsilon_{ps}\right) \tag{1}$$

Where ε_{pe}= strain due to effective prestress which is the stress in the tendon after the effects of self weight, short and long term losses; $\Delta\varepsilon_{ps}$= change in strain calculated for an identical but bonded tendon due to load in excess of the dead load leading to ultimate failure of the structure; k = reduction factor representing the effect of absence of bond between the concrete and tendon. He suggested a value of k equal to 0.1 be used in design to be on the safe side. This value was found to be very conservative [5], especially for beams with smaller span-to-depth ratios.

The ultimate tendon stress, f_{ps} has been calculated by assuming linear material stress strain relation for unbounded prestressing steel**,** which is usually the case in practice according to many researchers, because the steel stresses generally remain within the elastic range Eq. (2):

$$f_{ps} = E_{ps}\varepsilon_{ps} \tag{2}$$

Where E_{ps}= modulus of elasticity of prestressing steel. Several other investigators [6, 7] modified the value of *k* based on experimental results by relating *k* to the neutral axis depth of the critical section at ultimate. However the determination of the neutral axis depth needs iteration as f_{ps} and neutral axis depth are interdependent.

The effect of nonprestressed steel and the continuity of the concrete member have not been addressed in the above work. Therefore, more experimental studies were done to determine these effects on the value of f_{ps}, at ultimate, using simple and continuous members**.**

To calculate the stress in the prestressing steel at nominal strength, the following equation was adopted in the latest version of the ACI-Code [8] Eq. (3):

$$f_{ps} - f_{se} + 70 + \frac{f_c'}{100\rho_p} \tag{3}$$

Where $\rho_p$the prestressing is steel ratio; f_c' is the concrete compressive strength, in psi; and f_{se} is the effective stress of the prestressing steel, in MPa. Eq. (1) was derived by Mattock et al. [2] Based on evaluation of experimental data of unbounded members tested before 1971. Using the test results of post-tensioned unbounded slabs, supported with an analytical truss model, Mojtahedi and Gamble [9] concluded that increasing the span-to-depth ratio of unbounded members reduces the stress increase in the prestressing steel. Based on their findings, the ACI Building Code, in its 1983 version, limited the use of Eq. (3) to members with span-to-depth ratios of 35.

Two major drawbacks of the ACI Building Code equations are: 1) they neglect the effect of bonded tension reinforcement; and, more importantly, 2) they do not consider the effect of multispan systems or loading pattern in continuous members, which has a major influence on the stress in unbounded tendons. In 1976, Tam and Pannell [10] accounted for the effect of bonded tension reinforcement using the following Eq. (4).

$$f_{ps} = f_{se} + E_{ps}\varepsilon_{cu}\psi\left(\frac{d_p - c}{L}\right) \tag{4}$$

In which the neutral axis depth *c* is extrapolated in accordance with Tam and

Pannell's approach as follows Eq. (5).

$$c = \frac{\left(f_{pe} + 10.5E_{ps}\varepsilon_{cu}\, d_p/L\right)A_{ps} + A_s f_y - A_s^{'} f_y^{'} - 0.85 f_c^{'}(b - b_w)h_f}{0.85\beta_1 f_c^{'} b_w + 10.5 E_{ps}\varepsilon_{cu} A_{ps}/L} \tag{5}$$

where A_s and $A_s^{'}$ are the area of bonded tension and compression steel, respectively; E_{ps} is the modulus of elasticity of the prestressing steel; ε_{cu} is the ultimate concrete compression strain; L is the span length; and ψ is the ratio of the equivalent plastic hinge length L_p to the neutral axis depth c. For rectangular sections or flanged sections with rectangular section behavior, b_w = b. Based on their own test results of simply supported members loaded with single concentrated load at midspan, Tam and Pannell [10] recommended the use of a value of ψ = L_p/c = 10.5. Using a value of $E_{ps} = 2 \times 10^5\ MPa$, ε_{cu} = 0.003 and ψ = 10.5 leads to a value of $E_{ps}\varepsilon_{cu}\ \psi =\ 6000\ MPa$. Note that Eq. (4) does not take into account the effect of continuous members. In 1991, based on the results of analytical studies [11, 12] and test data of internally unbounded members, Harajli and Kanj [13] proposed the following lower bound design equation taking into consideration the effect of bonded tension reinforcement, member span-to-depth ratio and loading pattern in continuous members Eq. (6):

$$f_{ps} = f_{pe} + \gamma_o f_{pu}\left[1 - \frac{A_{ps} f_{pe} + A_s f_y}{b d_p f_c^{'}}\right] \tag{6}$$

In which the term $(A_{ps} f_{pe} + A_s f_y)/b d_p f_c^{'}$ need not be taken greater than 0.23, and γ_o is a combined member span-to depth ratio and continuity coefficient given as Eq. (7):

$$\gamma_o = \frac{n_o}{n}\left[0.12 + \frac{2.5}{L/d_p}\right] \tag{7}$$

where n_o is the number of loaded spans required to form a collapse mechanism, and n is the total number of spans between anchorages. In principle, the value of n_o is equal to unity for evaluating the stress at the section of maximum positive moment, and n_o = 2 for evaluating the stress at the section of maximum negative moment at an interior support. In its 1998 version, however, the same code introduced a totally new equation that was also adopted by the AASHTO Guide Specification [14] Eq. 8, 9

$$f_{ps} = f_{pe} + 6200\left[\frac{d_p - c}{l_e}\right] \le f_{py} \text{ and } \quad l_e = \left[\frac{l_i}{1 + N_s/2}\right] \tag{8}$$

$$c = \frac{A_{ps}f_{py} + A_s f_y - A_s' f_y' - 0.85\beta_1 f_c'(b - b_w)h_f}{0.85\beta_1 f_c' b_w} \tag{9}$$

For rectangular section behavior, b_w = b; *le* and l_i are the effective tendon length and length of tendon between anchorages, respectively; and N_s = number of support hinges required to form a mechanism crossed by the tendon. In its 2005 version of AASHTO LRFD [15] introduced a total Eq. (10):

$$f_{ps} = f_{pe} + 6300\left(\frac{d_p - c}{l_e}\right) \le f_y \text{ and } l_e = \left(\frac{2l_i}{2 + N_s}\right) \tag{10}$$

In 1991, Naaman and Alkhairi [16] proposed the following expression Eq. (11):

$$f_{ps} - f_{pe} + \Omega_u E_{ps} \varepsilon_{cu}\left[\frac{d_p}{c} - 1\right]\frac{L_1}{L_2} \le 0.94 f_{PY} \tag{11}$$

Where Ω_u is a bond reduction factor, expressed as Ω_u = $k/$ (L/d_p), and L_1/L_2 is the ratio of the length of loaded span(s) in continuous members to the total length of tendon between anchorages (see Figure 2).

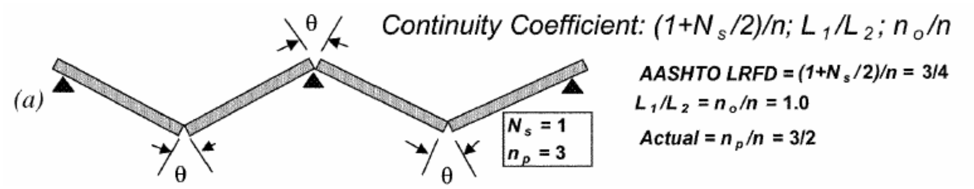

Figure 2: Loading patterns with associated collapse mechanisms and corresponding values of continuity coefficient Canadian code (A23.3-M94, 1994)

The equation given in the Canadian code [17], Eq. (12) to predict unbounded tendon stress at ultimate accounts indirectly for nonprestressed steel area, f_c' , and span-to-depth ratio. This equation was derived assuming formations of plastic hinges at ultimate limit state (Loov, 1987):

$$f_{ps} = f_{pe} + 8000\left(\frac{d_p - c}{l_e}\right) \le f_y \tag{12}$$

British code (BS 8110, 1997)

The equation given in the British Code [18], Eq. (13)

$$f_{pb} = f_{pe} + \frac{7000}{l/d}\left(1 - 1.17\frac{f_{pu}A_{ps}}{f_{cu}bd}\right) \quad and \quad x = 2.47\left[\left(\frac{f_{pu}A_{ps}}{f_{cu}bd}\right)\left(\frac{f_{pb}}{f_{pu}}\right)d\right] \qquad (13)$$

where, b: width or effective width of the section or flange in the compression zone, f_{pe}: design effective prestress in the tendons after all losses, f_{cu}: characteristic strength of concrete, f_{pu} : specified tensile strength of prestressing steel, A_{ps}: area of prestressing tendons in the tension zone, f_{pb}: design tensile stress in the tendons, *d:* effective depth to the centroid of the steel area, *x:* depth of the neutral axis.

1.2. Analysis of Initial Effects Due to Prestress and Self-Weight

Initial analysis of the effects due to prestress and self-weight are considered in two parts. In the first part, the effective tendon forces are applied to the member as an external load effect. Section strains at any location along the member are determined from section equilibrium. In the second part, the self-weight is applied to the structure, also as a load effect with strains again determined at discrete sections. Initial strain from the analysis of the tendon forces alone are considered in the equilibrium calculations (see Figure 3).

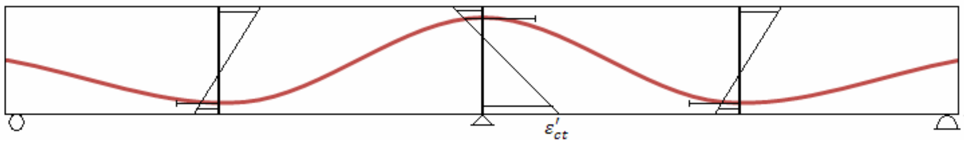

Figure 3. Initial strains at three sections along continues slab with prestress forces acting alone

1.3. Application of External Loads to the Member

The first application of external loads occurs in the analysis with the application of the cracking load. It is assumed that the member first cracks at the maximum moment section when the tensile capacity of concrete is exceeded. The corresponding cracking moment defines the magnitude of the bending moment distribution and hence the load level. Initially the structure is assumed to remain uncracked with the cracking load applied to attain a snapshot of the beam behavior just prior to cracking is obtained (Figure 4). It is reminded that in all above reports the conventional (vibrated) concrete were used to find the ultimate unbounded tendon stress, f_{ps}, and therefore argent research is needed to find out the value of f_{ps} while using SCC (non vibrating concrete) in post-tensioned concrete structures. Although, the use of SCC in simple post-tensioned concrete slab is reported but no work was observed for this type of concrete while using in continuous post-tensioned deck slabs constructions.

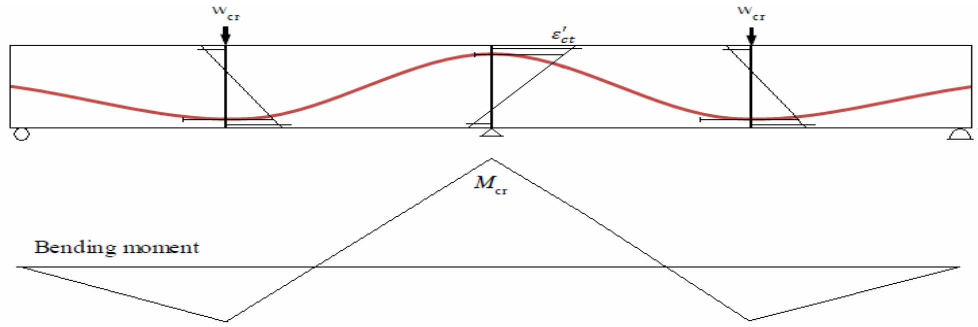

Figure 4. Application of first cracking load to the uncracked slab

1.4. Experimental Program

Two continuous unbounded post-tensioned self-consolidating concrete slab tests, PSCC slab1 and PSCC slab2 were conducted. As yet there is no any standard for SCC used in prestressed concrete, the post-tensioned slabs were designed according to ACI 318-08 [8] for conventional (vibrating) concrete. The tendons used were strand, supplied by Bridon Ltd. The overall dimensions of the continuous slabs were identical with an overall length of 7500 mm, each span length of 3500 mm, a width of 1000 mm, and a depth of 200 mm. PSCC slab1 and PSCC slab2 had four longitudinal parabolic tendons with a nominal diameter of 11.11 mm and area of 74.54mm^2 (see latter in Figure 6). Each tendon was supported on seven steel chairs to maintain the variable designed eccentricity of the tendons. At the mid-span and central support of the slabs the height of eccentricity was 30 mm. The heights of the chairs were interpolated considering the tendon curvature as a second degree parabola. Each tendon passes through the dead and live anchorages that were identical and supplied by CCL Ltd. The general layout of the unbounded post-tensioned one-way SCC slabs is shown in Figure 5. The post-tensioning was carried out by the first author by elongating the strands, to a specific load, from the live anchor using a hydraulic jack after the SCC gained a minimum strength of $50\,MPa$. The live end was locked using wedges with the load transferred to the concrete. The non-jacked end of the strand was prelocked using wedges at the dead anchor. Bursting reinforcement was designed, according to ACI 318-08 [8], to resist tensile bursting forces around individual anchorages. Seven transverse, 8 mm diameter, ordinary reinforcement steel bars having a nominal yield stress of $420\ MPa$ were positioned at each end of the slab adjacent to the dead and live anchorages. The bars were tied using ten 12 mm diameter closed links. The results of fresh and hardened SCC used are presented in Table 1. However, further details of the tested specimens are given in reference [19].

Table 1: Fresh and hardened concrete characteristics specimens

Specimen	Fresh and hardened concrete characteristics specimens							
	Average compressive cube strength at transfer, f_{ci} (Mpa)	Average compressive cube strength at 28 days, f_{cu} (Mpa)	L- box		J- ring		V- funnel	Slump flow
			h_1/h_2	t (sec)	h_2-h_1 (mm)	D (mm)	t (sec)	D (mm)
SCC slab1	59.0	67.1	0.36	0.83	76	68	7.01	68
SCC slab2	61.0	68.0	0.37	0.89	77	74	6.85	74

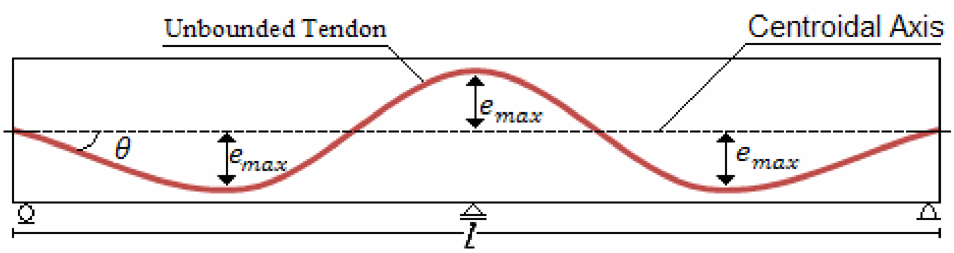

Figure 5: General layout of the unbounded post-tensioned slabs

1.5. Material Properties

Tensile tests were carried out to determine the material properties of the ordinary bars and the tendon. The nominal ultimate tensile strength of the tendon, was 2005*MPa*, corresponding to a nominal breaking load of 150*kN*. The nominal yield load was specified as 110*kN*. The strain gauges were fixed onto the strands and the reinforcement bars (by the first author) before concrete casting. Four displacement transducers LVDTs were used to measure the deflection at the mid span of the slabs and under load. A data logger system was used to record the load and strain at regular intervals during the slabs test. The strains in the tendons were recorded during the post-tensioning process.

1.6. Test Set Up and Experimental and Theoretical Comparison

The loading arrangements are shown in Figure 6 for testing the two spans post-tensioned slabs. A 1400kN pushing capacity jack applied the load, which was measured and controlled by different load cells. The slabs were loaded at tow locations using spreader plates 1000×30×30*mm*, as shown in Figure 6. A data logger system was used to record the applied load, the strains in the tendons and concrete surface, and the vertical deflections. The load-tendon strains are plotted and shown in Figure 7. Also the values of experimental ultimate unbounded tendon stress, f_{ps} for two tested post-tensioned SCC slabs are measured and compared with the theoretical values suggested by different researchers (Table 2).

Figure 6. Test setup

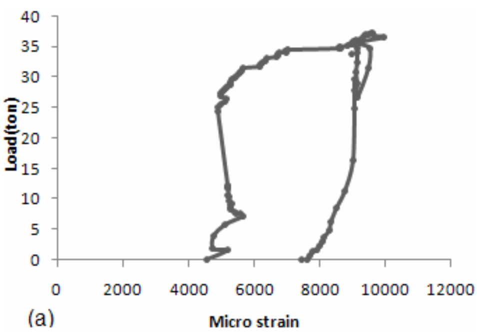

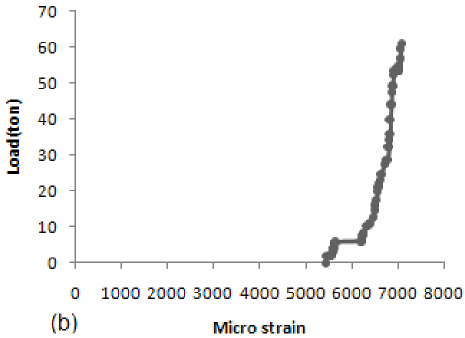

Figure 7(a) load-tendon strain curve for slab1 **(b) load-tendon strain curve for slab2**

Table 1: Experimental and theoretical comparison of ultimate unbounded stress, f_{ps}

Specimens	Experimental		Theoretical (f_{ps} (*MPa*))						
	ε_{ps}	$f_{\sigma 2}$ (*MPa*)	Tam and Panell	Harajli and Kanj	ACI	Aashto	Aashto lrfd	Canadian	BS
SCC Slab 1	0.009961	1788.65	1247.21	1564.91	1594.37	1218.37	1308.15	1358.46	1417.36
SCC Slab 2	0.007079	1599.08	1247.21	1556.76	1594.37	1218.37	1308.15	1358.46	1417.36

2. CONCLUSIONS

The values of experimental ultimate unbounded tendon stress, f_{ps} for two tested post-tensioned SCC (none vibrating), continuous slabs were measured and compared with the available theoretical values suggested by different codes and researchers for conventional (vibrating) concretes. Although no vibrating is used in SCC, but for two tested specimens the obtained results are indicated that the

experimental values of f_{ps} are higher than the five codes suggested value and close to the ACI-08 value.
Also, the obtained experimental values of f_{ps} are higher than the two theoretical values suggested by Tam and Panell, and Harajli and Kanj, and close to the value suggested by Haragli and Kanj. However, comparing the theoretical and five selected codes value, it was found that the theoretical suggested value by Haragli and Kanj are close to the code value provided by ACI-08.
It was also found that, no change in f_{ps} values are obtained for either of the slabs tested while compared to the theoretical and codes values, except for the values obtained by Haragli and Kanj which are similar to the experimental values and are different for either of the slabs. This is because in this method, the amount of ordinary tensile and compression reinforcement used are taken into consideration.

REFERENCES

1. Okamura. H., “Self Compacting High Performance Concrete,” Concrete International, V.19.No.7, July, 1997, PP.50-54.
2. Mattock, A.H., Kaar, P. H. (1960). “Continuous Precast-Prestressed Concrete Bridges. Development Department Bulletin D43.” Portland Cement Association, Research and Development Laboratories, Vol. 2, No. 5.Stokie, Illinois.
3. Freyermuth, C.L. (1969). “Design of Continuous Highway Bridges with Precast, Prestressed Concrete Girders.” Journal of the Prestressed Concrete Institute, Vol. 14, No 2.
4. Baker L. (1949), "A Plastic Theory of Design for Ordinary Reinforced and Prestressed Concrete including Moment Redistribution in Continuous Members", Magazine of Concrete Research (London), Vol. 1, No. Z, June 1949, pp. 57-66.
5. Panuell, F. N. (1969), "The Ultimate Moment of Resistance of Unbounded Prestressed Concrete Beams", Magazine of Concrete Research, V. 21, No. 66, March, 1969, pp. 43-54.
6. Janney, J. Ry Ho~estad, E. & McHenry, D. (1956), "Ultimate Flexural Strength of Prestressed and Conventionally Resourced Concrete Beams", Journal of the ACI, Proceedings, Vo1.52, No.6, Feb., 1956, pp. 601-620.
7. Gifford, F.W. (1954), "The Design of Simply Supported Prestressed Concrete Beams for Ultimate Loads", Proceedings of the Institution of Civil Engineers (London), Part III, Vo1.3, No.1, Apr., 1954, pp. 125-243.
8. ACI Committee 318, “Building Code Requirements for Structural Concrete (ACI 318-08) and Commentary (318R-08),” American Concrete Institute, Farmington Hills, Mich., 2008, 471 pp.
9. Mojtahedi, S., and Gamble, W.,”Ultimate Steel Stress in Unbounded Prestressed Concrete,” Journal of the Structural Division, ASCE, V. 104, No. ST7, July 1978, pp. 1159-1165.
10. Tam, A., and Pannell, F., “The Ultimate Moment of Resistance of Unbounded Partially Prestressed Reinforced Concrete Beams,” Magazine of Concrete Research, V. 28, No. 97, Dec. 1976, pp. 203-208.

11. Harajli, M. H., and Hijazi, S. A., “Evaluation of the Ultimate Steel Stress in Partially Prestressed Concrete Members,” PCI Journal, V. 36, No. 1, 1991, pp. 62-82.
12. Harajli, M. H., “Effect of Span-Depth Ratio on the Ultimate Steel Stress in Unbounded Prestressed Concrete Members,” ACI Structural Journal, V. 87, No. 3, May-June 1990, pp. 305-312.
13. Harajli, M., and Kanj, M., “Ultimate Flexural Strength of Concrete Members Prestressed with Unbounded Tendons,” ACI Structural Journal, V. 88, No. 6, Nov.-Dec. 1991, pp. 663-673.
14. Aashto, “Guide Specifications for Design and Construction of Segmental Concrete Bridges,” 2nd Edition, American Association of State Highway and Transportation Officials, Washington, D.C., 1999.
15. Aashto, “LRFD Bridge Design Specifications,” American Association of State Highway and Transportation Officials, 16. Washington, D.C., 2005.
16. Naaman, A.E., and Alkhairi, F.M., “Stress at Ultimate in Unbounded Post-Tensioned Tendons: Part 2-Proposed Methodology,” ACI Structural Journal, V. 88, No. 6, Nov.-Dec. 1991, pp. 683-692.
17. CSA Standard A23.3-M94**,** "Design of Concrete Structures", Canadian Standard Association, Toronto, Ontario, Canada, 1994,220 pp**.**
18. BS 8110 (1997), "Structural Use of Concrete”, Part 1, British Standards Institution, London, UK, 1997.

CD02-018

THE FINITE ELEMENT ANALYSIS OF RC JOINTS STRENGTHENED WITH EXTERNAL FRP COMPOSITES

M. Kazem Sharbatdar[1], Mostafa Fakharifar[2]
[1]Assistant Professor, Faculty of Civil Engineering, Semnan University, Semnan, Iran
[2]M.Sc Student, Faculty of Civil Engineering, Semnan University, Semnan, Iran

ABSTRACT
Externally bonded fiber-reinforced-polymer (FRP) sheets have been successfully used for strengthening of damaged or deficient reinforced concrete members. Despite of a lot of research conducted and tests on application of these new sheets during the last decade, further research is still required to consolidate recent developments and expand the scope of application of FRPs for structural applications. Nonlinear finite element analysis combined with laboratory testing constitutes an efficient approach for pursuing this objective.
The objective of this paper is exploring and illustrating the contribution of a refined three-dimensional (3D) constitutive FE model for investigating the nonlinear response of concrete joint, reinforced with steel rebars and strengthened with external FRP sheets. The analyses were carried out by using finite element software having different capacities. Different parameters such as application of FRP sheets with different patterns, different loading conditions and different strengthened areas have been considered to show the results. Several results regarding increasing ultimate values in the strengthened model in comparison with the reference specimen, ductility of the strengthened model, and evaluation of ductile against non-ductile joint have been presented in this paper.

Keywords: FE model, nonlinear analysis, RC joint members, FRP sheets, strengthening

1. INTRODUCTION
Existing reinforced concrete (RC) structures that were designed according to pre-1970's codes often have inadequate reinforcement detailing, which not only results in deficient lateral load resistance, but also in insufficient energy dissipation, rapid strength deterioration and improper hinging mechanisms during earthquakes, leading to excessive drifts and ultimately to structural collapse. Non-ductile detailing is generally manifested through deficient joint shear resistance, deficient column shear capacity, deficient column's main reinforcement lap splices, deficient anchorage of beam positive reinforcement at the beam-column joint, and deficient beam shear resistance. In particular, recent earthquakes have demonstrated that RC beam-column joints that have been constructed based on pre-1970's design codes may initiate and cause total collapse of structures. For instance, Figure 1-a [1] shows a RC structure that collapsed during the 1999 Kocaeli Earthquake in Turkey

in which joints failures appear to be the major contributor to such collapse, while Figure 1-b shows a close-up of a non-ductile failure of a beam-column joint during the same earthquake. Beam-column joint deficiencies combined with the weak column/strong beam glitch contradict failure hierarchy of the design capacity concept. A failure in the beam is usually less critical than that in the column, and the latter is less critical than a failure in the joint. Hinging in the joint, being at the point of intersection of the beam and column, allows excessive rotations both in the beam and column in conjunction with a loss of load carrying capacity of the column. Such dangerous failure mechanism is unacceptable and must be prevented in design.

(a) **(b)**

Figure 1. Damages to moment resisting frames during the Kocaeli 1999 earthquake: (a) joint induced structural collapse; (b) beam-column joint failure [1]

There is a perceived void in the current literature for studies that focus on the behavior of reinforced concrete beam–column joints under cyclic loading. In fact, most reported research in the literature is mainly on cyclic behavior of connections [3] in newly designed steel structures and also concrete connections retrofitted by traditional rehabilitation techniques [2]. Moreover; most of the recent researches involved in finite element modeling of RC connections; are concerned with exterior beam-column joints.

This study intends to investigate the effect of various combinations of FRP wrapping patterns on the performance of interior reinforced concrete beam–column joints, i.e. ductility, under combined axial and lateral cyclic loads. A three-dimensional finite element analysis model of FRP wrapped beam–column joints, which exhibit material and geometric nonlinearities that are due to large displacements, confinement effect, and concrete nonlinear behavior, are developed. The FEA model is validated through leveraging an experimental study on a FRP-wrapped beam–column joint.

2. EXPERIMENTAL TEST ON INTERIOR RC BEAM-COLUMN JOINTS

There are abundant experimental tests regarding RC beam-column joints, and most of them have been carried out on exterior beam-column joints. In addition; limited researches have been investigated on finite element modeling of interior beam-column joints. A. Mukherjee et al [5] have performed a fully detailed, comprehensive experimental test on interior RC beam-column joints strengthened with FRP laminates. The test scheme and specimen which have been investigated in the test are firstly introduced. Eventually, the FE model calibrated regarding the experimental study is presented and results are analyzed.

2.1. Specimens Details

Two different types of RC joints have been cast for experimental verification [5]. One set of joints has adequate steel reinforcements with proper detailing of reinforcements at the critical sections (Figure 2). In the other set of specimens the beam reinforcements have deficient bond lengths at the junctions with the columns (Figure 3). When the beam was transversely loaded the first set was characterized by a long plastic zone (ductile) while the second set failed in reinforcement pull out and exhibited sudden failure (non-ductile).

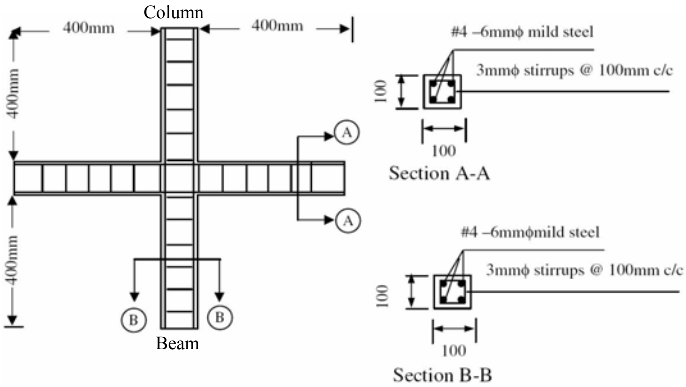

Figure 2. Specimen with ductile joint reinforcement [5]

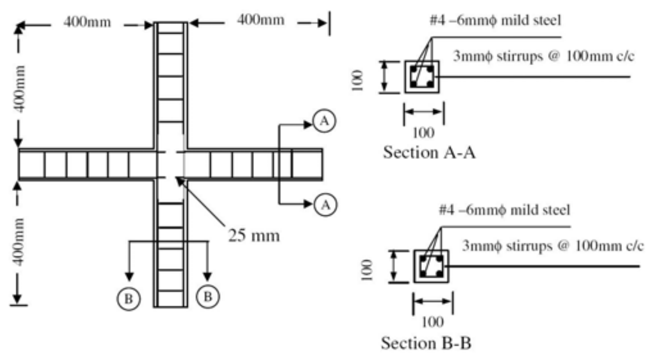

Figure 3. Specimen with non-ductile joint reinforcement [5]

The specimens in Figures (2) and (3) were strengthened using carbon and glass FRP materials. Prior to the application of the FRP, the concrete substrate was smoothed by grinding. Figures (4) and (5) present schematic arrangement for two typical systems; L-overlays and precured carbon plates which were utilized respectively, in the aforementioned experiment. In Type A; GFRP/CFRP sheets have been applied in L shape to upgrade the joints. These sheets have been applied in several layers. FRP has been applied on the top and bottom surface of concrete surfaces, so the fibers were along the axes of the members (Figure 4a). Then, FRP wraps were provided over the inner layers (Figure 4b), the direction of fibers in wraps was perpendicular to the axis of the members. Figure 5a shows glass fiber sheets (80mm wide and 250mm long) on either side of the joint. Only one layer is provided on one side. Two layers of FRP have been provided on the other side to evaluate its efficacy.

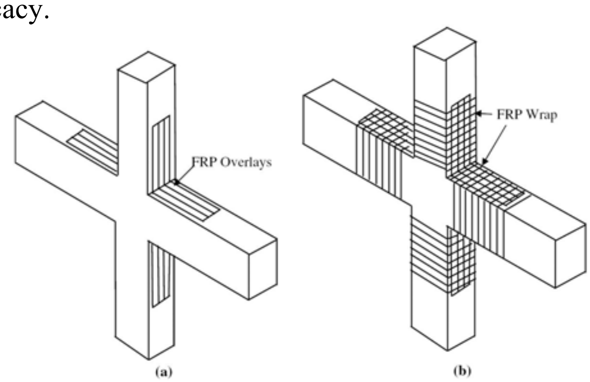

Figure 4. Type a strengthening system-use of composite overlays [5]

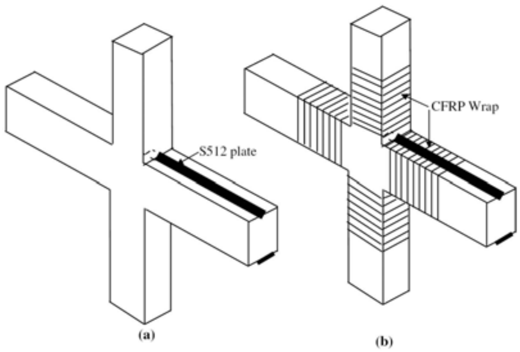

Figure 5. Type B strengthening system-use of precured carbon plate [5]

Both the column and the beam are then wrapped by unidirectional glass fibers with 100mm lap length. Same conFigure uration is repeated using carbon fiber sheet using 1 and 2 layers of overlays and single wrap with 100mm overlap. Both adequate and deficient joints were reinforced using this conFigure uration.

Furthermore, procured carbon plate (25mm wide and 1.2mm thick) have been used in the beams in Type B to improve bending stiffness. To achieve a good bond between the plate and the concrete, a groove (25mm wide and 25mm deep) has been created inside the joint. The plates have been inserted into the joint as shown in Figure 5, and then the groove has been filled by injecting epoxy resin, and the plates have been inserted in the groove as shown in step 1 of Figure 5. The beams and columns have then been wrapped using a single wrap of carbon sheet.

2.2. Test Program

The experimental setup which has been utilized by A. Mukherjee et al [5] is shown in Figure 6. The column was fixed at its ends on a loading frame. It was subjected to a constant axial load of 100KN which is 50% of ultimate load carrying capacity of the column. Cyclic load was applied using a hydraulic actuator with load cycle based on increasing displacement control. Three cycles were repeated at each level of displacement. Vertical deflection of the tip of the beam was recorded directly by the linear variable displacement transducer (LVDT). The compressive strength of concrete used in this experiment has been 30N/mm^2 and also properties of other material used are shown in Table (1). The same values have also been used for FE modeling of aforementioned specimens. Totally, 12 specimens at two categories of ductile and non-ductile reinforcement, including as-built and strengthened specimens with different patterns have been tested in this experimental research by [5].

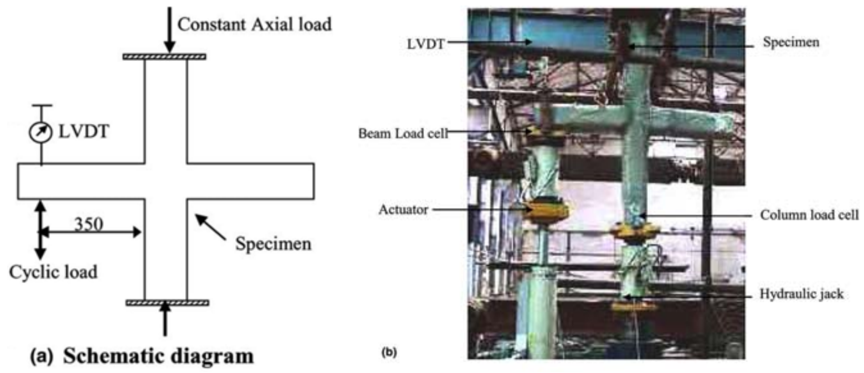

Figure 6. Experimental setup [5]

The elaborate test matrixes for adequate and deficient specimens which have been investigated through this experiment are presented in Tables (2) and (3) respectively.

Table 1: Properties of materials [5]

Material	Effective thickness (mm)	Ultimate strength (MPa)	Tensile modulus (GPa)	Ultimate strain
Glass-G (fiber)	0.36	2250	70	0.0239
Carbon-C (fiber)	0.11	3500	230	0.0117
Carbon plate-CP (composite)	1.2	2800	165	0.017
Mild steel longitudinal reinforcement	6 mm dia	275	198	0.045
Mild steel transverse reinforcement	3 mm dia	555.13	193	0.043

Table 2: Test matrix for ductile specimen [5]

S. no	Specimen name	Details
1	D-1	-
2	G1L-D	Type A with single L of GFRP at top and bottom
3	G2L-D	Type A with two L of GFRP at top and bottom
4	C1L-D	Type A with single L of CFRP at top and bottom
5	C2L-D	Type A with two L of CFRP at top and bottom
6	CP1-D	Type B with CFRP plate at top and bottom

Table 3: Test matrix for non-ductile specimen [5]

S. no	Specimen name	Details
1	ND-1	-
2	G1L-ND	Type A with single L of GFRP at top and bottom
3	G2L-ND	Type A with two L of GFRP at top and bottom
4	C1L-ND	Type A with single L of CFRP at top and bottom
5	C2L-ND	Type A with two L of CFRP at top and bottom
6	CP1-ND	Type B with CFRP plate at top and bottom

3. FINITE ELEMENT MODELING OF INTERIOR RC BEAM-COLUMN JOINTS

All specimens which have been investigated in the experimental study conducted by Mukherjee [5] are modeled in this section by using non-linear finite element ANSYS *ver 11*.

3.1. Material Models

The constitutive relationships employed to describe the mechanical behavior of materials as well as the interaction between steel bars and concrete are basically those proposed in CEB-FIP Model Code 1990 [4], with some slight modifications. In compression, the behavior of the concrete is that proposed by the same code and, in tension, a linear elastic behavior is assumed up to the strength of concrete in tension (f_{ct}). For the sake of comparison, a second model that indirectly incorporates the tension-stiffening effect [6] is also implemented. In such a model, the progressive loss of rigidity after cracking is quantified indirectly through an adaptation of the tension behavior introducing a softening branch, which is calibrated using the α and ε_m parameters. Both the curves are illustrated in Figure 7. The aforementioned parameters are usually set at $0.5\leq\alpha\leq0.7$ and ε_m= 0.0020. In this case, fracture mechanics could be used to establish these values, based on energy criteria [8].

The perfect plasticity model of the behavior of the longitudinal reinforcement bars and also the interaction between reinforcement bars and concrete are shown in

Figures (8) and (9), respectively. The parameters shown in Figure 9 depend on the bond conditions and confinement of concrete, as established in CEB-FIP Model Code 1990 [4].

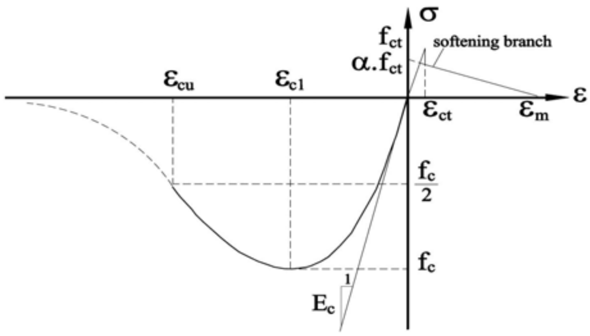

Figure 7. Stress-strain relationship for concrete [6]

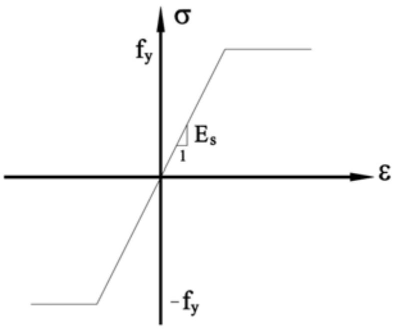

Figure 8. Stress-strain relationship for steel [6]

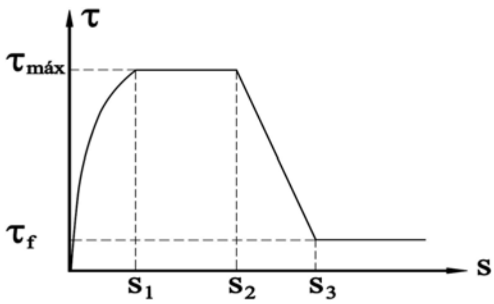

Figure 9. Bond stress-slip relationship [4]

Solid 65, Solid46 and Link8 are the element used in ANSYS to develop these FE models. The Solid65 and Link8 elements were used to model the concrete and reinforcement, and also layered solid elements, Solid46, were used to model the FRP composites.

3.2. Bond Model

The correct simulation of the bond between concrete and reinforcement bars plays a significant role in the proper modeling of beam-column connections. When the bond forces tend to zero it is apparent that the majority of the shear force will be transferred across the joint core by a diagonal compression strut mechanism and hence severe diagonal tension cracking is less likely if bond deterioration occurs at an early stage of loading [9]. A complex interaction between flexural response of the adjacent beam element and the joint shear transfer mechanism occurs also due to the stress penetration into the panel zone from the beam bars, combined with a fixed-end rotation in the beam due to progressive bond degradation and pull out mechanism. The discrete bond model implemented in ANSYS consists of a one-dimensional (1D) finite element with a realistic bond-slip relationship as shown in Figure 10. Additional information on the discrete bond model can be found in [7].

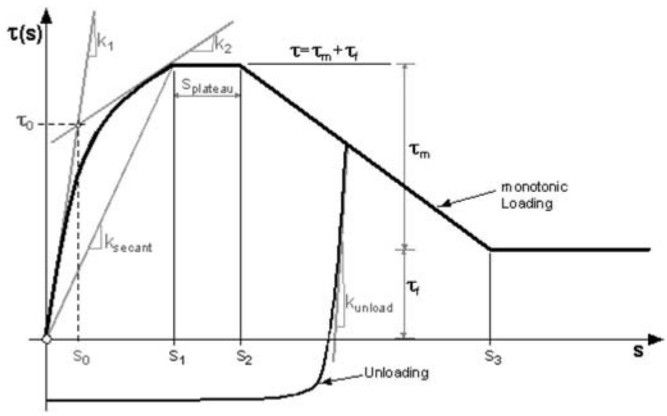

Figure 10. Bond-slip relationship for deformed bars [7]

For plain round bars with a diameter of 12 mm, the total bond strength was approximately $\tau_m + \tau_f$ = 1 MPa (τ_m = mechanical bond; τ_f = frictional bond) for a slip of s_1 = 0.03 mm [10]. During cycling, the bond degradation valid for deformed bars is principally due to the shear failure of concrete between the ribs of the bar. In the case of smooth bars, it is reasonable to assume that friction is the only source of bond mechanism at the steel-concrete interface and that it is scarcely influenced by the cycling.

3.3. Analytical Modeling of Specimens

Two different finite element models for each of the specimen in two different categories of ductile and non-ductile were analyzed. Albeit, neither of the experimental specimen had been investigated for monotonic loading, but in order to acquire the ductility and load-displacement curves for specimens; all the FE models in this analyses went under monotonic loading for non-linear analysis. A relatively fine discretization was employed for monotonic loading as Figure 11a. On the other hand, for saving computation time, cyclic analyses were carried out using a relatively coarse discretization shown in Figure 11b. The FE model of steel bars is shown in Figure 11c.

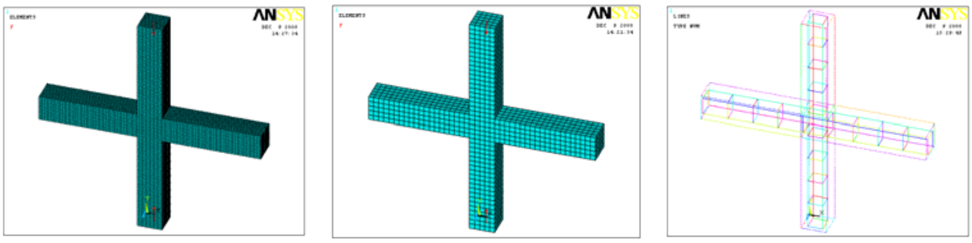

(a) (b) (c)

Figure 11. Finite Element model of Ductile specimen: a) fine 3D FE mesh used for monotonic loading; b) coarse 3D FE mesh used for cyclic loading; c) steel bars FE model

The experimental control specimen of ductile category (D-1) was firstly modeled and then went under both monotonic and cyclic loading to asses and validate the accuracy of FE model. Figure 12 compares the applied force versus free tip of the beam drift curves for monotonic loading of the fine and coarse models with the envelope curve from the cyclic experiments for ductile specimen. It can be seen that the numerical results agree reasonably well with the experimental results. The coarse model, however, slightly overestimated the peak resistance and exhibited slightly more brittle response. For both models the failure mode was diagonal shear failure of the joint. This point confirms the accuracy of FE model; therefore FE model is extended to acquire further results.

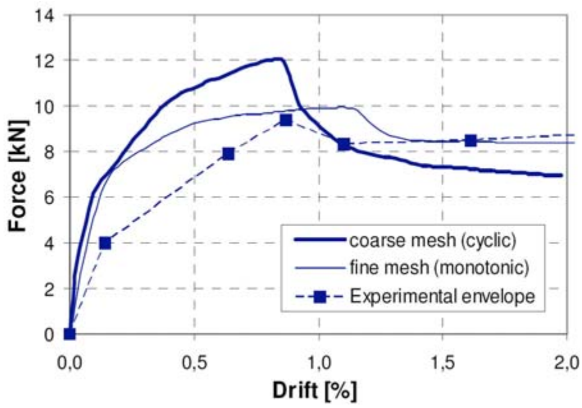

Figure 12. Comparison of the model response for the coarse and fine meshes with experimental results for ductile specimen

Non-linear finite element analyses for the entire models including ductile and non-ductile; has been implemented by utilization of the two different patterns of strengthening Type A & B.

The usage of two different types of strengthening which has been performed for both ductile and non-ductile FE models is illustrated in Figure 13.

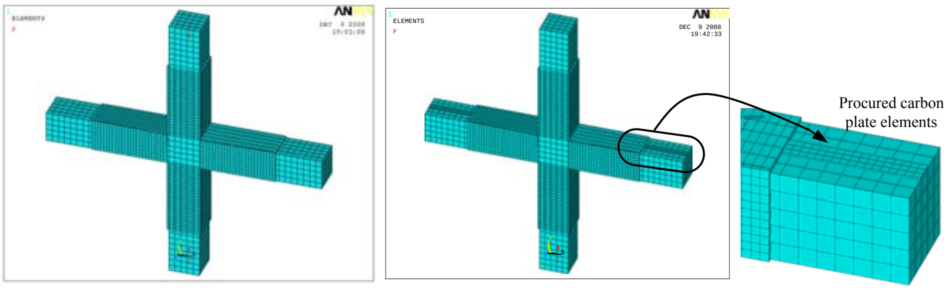

(a) (b)

Figure 13. Finite element model of strengthened joint: a) Strengthening Type A; b) Strengthening Type B

3.4. Results for FE Models with Ductile Joint Reinforcement

The displacement levels of the first few cycles do not generate any nonlinear deformation in the model. The onset of stiffness degradation is identified by simultaneous appearance of tension cracks at the root of the cantilever beam. The analyses show that at this point the steel started to yield and it was not capable of taking any further load. The additional load from this point was carried out by the FRP. At this point, linearity of the ascending and the descending paths is lost. This phenomenon is yield point.

The post yield behavior is signified by monotonic degradation of stiffness. Ability of the structure to survive an earthquake depends to a large extent, on its ability to dissipate the input energy. Forms of energy dissipation include kinetic energy, viscous damping and hysteretic damping, etc. An estimate of the hysteretic damping can be found by the area enclosed in the load–displacement hysteresis loops. Yield points for ductile specimen are provided in Table (4). Columns 2 & 3 of Table (4) summarize the percentage increase in the yield load. The CP1-D exhibited the highest increase in the yield load followed by the C2L-D, G2L-D, C1L-D and G1L-D specimens. It may be noted that the forces at the tensile face of the beam are shared by the steel and FRP in proportion of their relative stiffnesses. The stiffness of carbon is considerably higher than that of glass. Therefore, for the same tip load, the tensile force in steel is lower in the carbon reinforced FE model than in the glass reinforced models. As a result, the steel in the carbon reinforced models yield at higher tip loads. The CP1-D models are anchored at the joint through a groove. Therefore, they exhibit higher stiffness than other sheet models. The models with two-layer reinforcement had higher yield loads than the models with one layer reinforcements. Due to FRP reinforcements the displacement at yield increased to a much lesser extent than the load (Comparison of column 2 (or 3) with 4 (or 5), Table 4). Another interesting point is that the glass reinforced models had much higher displacement at yield than the carbon reinforced models. This is due to the higher stiffness of carbon than glass. There is satisfactory agreement between FE model and experimental test results. The initial stiffness and the ultimate displacements are also summarized in Table (5).

It is worthwhile to mention that almost all the values of increase and promotion for

FE models are higher in comparison with experimental results. This is due to the reduction of degrees of freedom in analytical finite element model in comparison with the real specimen. FE models are inherently stiffer than real specimens. Figure 14 reveals the ratio of ductility for strengthened specimen versus control specimen. Apparently ductility for all strengthened FE ductile models has increased between 25 to 78%. The joint shear crack, which ultimately caused the model to fail, was similar to the shear cracks observed in the experiments.

Table 4: Yield points of ductile specimens

Specimen	Yield load		Deflection at yield load	
	% increase		% increase	
	experiment	FE model	experiment	FE model
Control-D	-	-	-	-
G1L-D	21.32	23.48	-10.00	-9.25
G2L-D	48.42	51.12	58.95	61.25
C2L-D	57.89	59.60	-3.16	-3.62
CP1-D	116.18	112.10	161.84	158.31

Table 5: Ultimate points in ductile specimens

Specimen	Initial stiffness		Ultimate deflection	
	% increase		% increase	
	experiment	FE model	experiment	FE model
Control-D	-	-	-	-
G1L-D	17.14	18.25	14.65	15.22
G2L-D	75.00	73.28	29.21	31.25
C2L-D	140.94	138.25	42.83	44.21
CP1-D	41.37	45.95	20.63	19.75

Unfortunately, a direct comparison of the sequence of cracking (flexural to shear) was not possible since monotonic loading of the test specimens was not performed. The finite element

model for monotonic loading (fine mesh) was also used to investigate: 1) the influence of the bond strength (Figure 15a) and 2) the influence of the normal column force (Figure 15b). Figure 15 shows the influence of the ultimate bond strength ($\tau_m + \tau_f$) on the response of the joint. It can be seen that with higher bond strength the resistance is higher and the failure more brittle. Figure 15b shows the influence of the axial column force on the applied force versus free tip of beam drift curve. It can be seen that with higher compressive force the joint shear (thus overall subassembly) resistance increases.

The time that analyses finished and elements turned to fail, pondering through strain distribution in the control model revealed that the beam has failed at the joint through the formation of a hinge. The hinge has formed between the two shear links of the beam. It seems concrete has spalled in such a fashion that two semicircular surfaces have been created. The FRP reinforced models, on the other hand, did not have the semicircular failure planes. The failure planes were approximately vertical. It could be concluded that the difference in the failure mode is due to the presence of the FRP wraps.

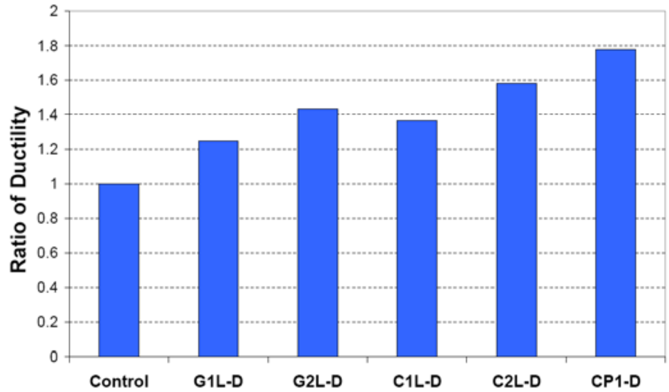

Figure 14. Ductility for Strengthened ductile models

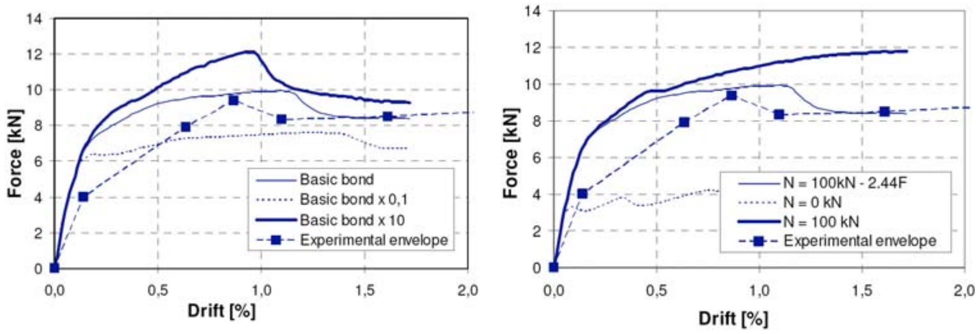

(a) **(b)**

Figure 15. Comparison of numerical and experimental results for monotonic loading: a) effect of variation of bond strength; b) effect of variation of axial load

3.5. Results for FE Models with Non-Ductile Joint Reinforcement

Non-linear analyses show that to some extent the extracted results from non-ductile FE models are close to ductile FE model. However due to the presence of continuous steel bars in the joint area, ductile model have a higher load bearing capacity, stiffness and energy dissipation capability. In Tables (6) & (7) the yield and ultimate points for non-ductile models are given. The G2L-ND exhibited the highest increase in the yield load followed by the C2L-ND, CP1-ND and C1L-ND. The models with two-layer reinforcement had higher yield loads than the models with one layer. Due to FRP usage the displacement at yield increased to a much lesser extent than the load (Comparison of column 2 (or 3) with 4 (or 5), Table 6).

Table 6: Yield points of non-ductile specimens

Specimen	Yield load % increase		Deflection at yield load % increase	
	experiment	FE model	experiment	FE model
Control-ND	-	-	-	-
G2L-ND	103.75	42.56	15.24	16.32
C1L-ND	12.60	13.25	-18.29	-19.23
C2L-ND	79.36	36.45	4.27	5.34
CP1-ND	68.36	-45.25	78.05	81.21

Table 7: Ultimate points in non-ductile specimens

Specimen	Initial stiffness % increase		Ultimate deflection % increase	
	experiment	FE model	experiment	FE model
Control-ND	-	-	-	-
G1L-ND	41.46	42.56	20.45	22.36
G2L-ND	9.52	13.25	55.11	58.12
C2L-ND	32.49	36.45	41.37	39.96
CP1-ND	-41.17	-45.25	16.08	17.91

The load-displacement envelopes for ductile and non-ductile FE models are plotted in Figures (16-17). The envelopes let us compare the relative performance of the models. All the FRP reinforced models have higher peak loads than the control model. For ductile joints the CP1 model has the highest peak load followed by the C2L, G2L and G1L. For non-ductile joints the G2L-ND model has the largest envelope area followed by the C2L-ND, CP1-ND and C1L-ND. Comparing these Figures reveal the superior performance of ductile joints.

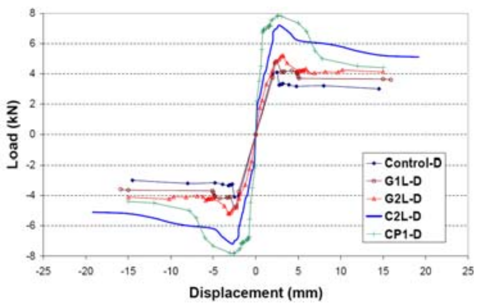

Figure 16. Load-Deflection envelope for ductile models

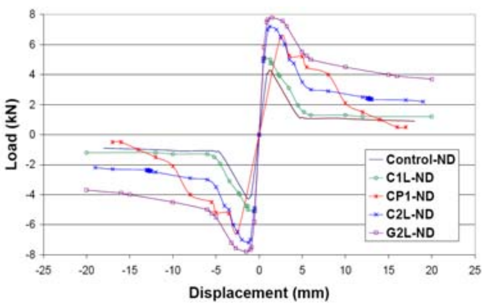

Figure 17. Load-Deflection envelope for non-ductile model s

Ductility promotion for non-ductile joints is approximately between 16 to 51% (Figure 18).

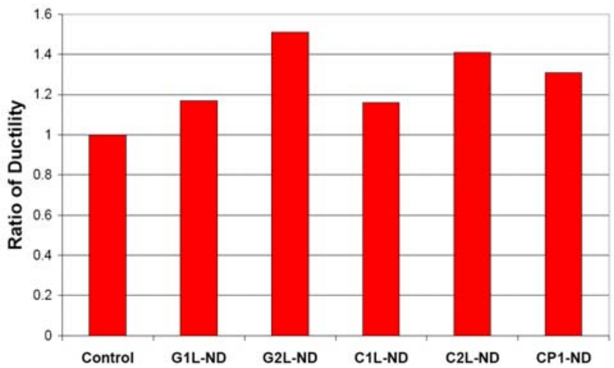

Figure 18. Ductility for Strengthened non-ductile models

4. CONCLUSION

With application of FE models (validated based on experiment) for two different types of RC joints including ductile and non-ductile reinforcement details the promotional effect of both glass and carbon composite has been investigated. These two composites could be efficiently used for seismic retrofitting of RC joints regardless of reinforcement details. Obviously due to presence of continuous steel bars in the joint area for ductile joints, they exhibit a more superior, ductile behavior rather than non-ductile joints. The main cause of superior performance of the FRP reinforced joints is the continuous confinement provided by the FRP wraps which impede the creation of hinge through the spalling of concrete. FE models confirm the advantage of carbon reinforcements over glass reinforcement in case of ductile joints. But for non-ductile joints, glass reinforcing is preferable. Utilization of FRP sheets have a promotional efficiency regarding to yield load, performance and initial stiffness of joints. Commonly CFRP strengthened joints reveal stiffer behavior than GFRP strengthened joints regardless of reinforcing details.

REFRENCES

1. Saatcioglu M., and Ghobarah A., 'The August 17, 1999, Kocaeli Earthquake – Damage to Structures', Canadian Journal of Civil Engineering 28(4), 2001, 715-737.
2. Alcocer S, Jirsa Jo. Strength of reinforced concrete frame connections rehabilitated by jacketing. Struct J, ACI 1993;90(3):249-61.
3. Anderson JC, Duan J, Xiao Y, Maranian P. Cyclic testing of moment connections Upgraded with weld overlays. J Struct Eng ASCE 2002;128(4):509-16.
4. Comite´ Euro-International du Be´ton CEB-FIP Model Code 1990: Final draft, CEB Bulletin D'Information, 1990. p. 203-5.
5. Mukherjee Abhijit, Joshi Mangesh. FRPC reinforced concrete beam-column joints under cyclic excitation. J Composite Structures 2004; 70: 187-99.
6. Figure ueiras Ja. Ultimate load analysis of anisotropic and reinforced concrete plates and shells, PhD thesis. Swansea, University College of Swansea, 1983.
7. Ozbolt, J., Lettow, S. and KOZAR, I., 2002. Discrete Bond Element for 3D

Finite Element Analysis of Reinforced Concrete Structures.
8. Ranjbaran A. Dena: finite element program for the non-linear stress analysis of two-dimensional, metallic and reinforced concrete, structures. Comput Struct 1994;51(2):191-211.
9. Lettow, S. Ein Verbundelement für nichtlineare Finite Elemente Analysen - Anwendung auf Übergreifungsstöße. Dissertation, Institut für Werkstoffe, Universität Stuttgart, 2006.
10. Fabrocino G. and Cosenza E., 2002. Experimental behaviour of smooth bars anchorages in existing RC Buildings. 2002 “Concrete struct in the 21st Century”: w-463.

CD02-019

3D FINITE ELEMENT MODELLING OF BOND-SLIP BETWEEN REBAR AND CONCRETE IN PULL-OUT TEST

J. Shafaie[1], A. Hosseini[2], M. S. Marefat[3]
[1]MSc. Student, School of Civil Engineering, University of Tehran, Tehran, Iran
[2]Assistant Professor, School of Civil Engineering, University of Tehran, Tehran, Iran
[3]Professor, School of Civil Engineering, University of Tehran, Tehran, Iran

ABSTRACT
A reinforced concrete material is a composite material made up of two components with unequal mechanical behaviour and physical features. In general, the external load is already applied to concrete and the reinforcing bars receive its part of the load only from the surrounding concrete by bond. In composite structures, the bond between different components of reinforced concrete member has a primordial role and its negligence conducted to poor structural response. Therefore, for modeling of reinforced concrete structures one needs a simple and realistic bond-slip model. There are various finite element models for bond-slip relationship between reinforcement and concrete. In this paper, modeling of the transition region between steel and concrete as a cohesion layer in the finite element program (Ansys) is discussed. A 3D finite element model to represent this layer has been introduced. The layer involves modeling the ribs and effects of slip and bond stress of the bar. The accuracy of the models is assessed by comparison of the finite element numerical response with experimental data from pullout test.

Keywords: pull-out test, finite element, bond-slip relationship

1. INTRODUCTION
A reinforced concrete (RC) structure is a composite structure made up of two materials with different characteristics, namely, concrete and steel. In general, the external load is already applied to concrete and the reinforcing bars receive its part of the load only from the surrounding concrete by bond. “Bond stress” is the name assigned to the shear stress at the bar-concrete interface which, by transferring load between the bar and the surrounding concrete, modifies the steel stresses. This bond, when efficiently developed, enables the two materials to form a composite structure. In composite structures, the bond between different components of reinforced concrete member has a primordial role and its negligence is conducted to poor structural response. These complex phenomena have led engineers in the past to rely heavily on empirical formulas for the design of concrete structures, which were derived from numerous experiments. For these reasons, the incorporation of bond is carried out considerably in recent works. The properties of this interaction depend on several factors, such as friction, mechanical interaction and chemical adhesion [1, 2].

In the past, a number of experimental investigations have been carried out in order to clarify and understand the behaviour of deformed bars pulled out from a concrete block under monotonic and cyclic loading conditions. These experimental results are well documented in the specific literature [9]. Based only on the experimental results it is difficult to filter out the influences of material and geometrical parameters on the bond behaviour. Therefore, to better understand the bond behaviour, a reliable bond model (simulation of the transmission of forces in the bond zone, see Figure 1a) that can be employed in a three-dimensional finite element, an analysis is needed. The numerical modelling of the bond behaviour is principally possible at two different levels: (1) detailed modelling (see Figure 1b) in which the geometry of the bar and the concrete is modelled by three-dimensional elements and (2) phenomenological modelling (see Figure 1c) based on a smeared or discrete formulation of the bar-concrete interface [3].

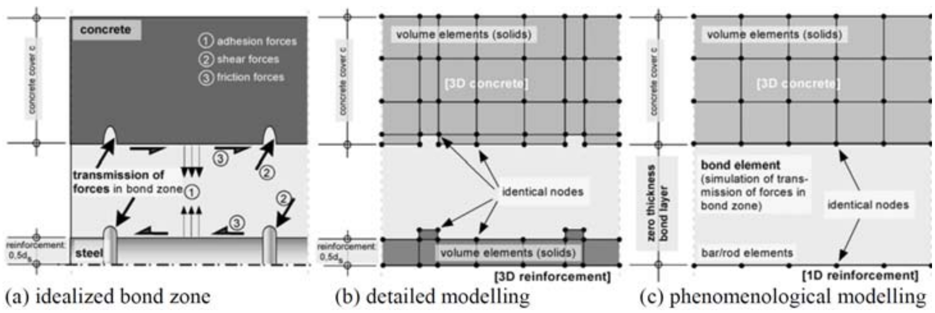

Figure 1. Schematic simulation of the idealized bond zone [3]

In the phenomenological modelling of bond the concrete and the reinforcement are discretised by two- or three-dimensional finite elements. The link between the bar and the concrete can be realized by a discontinuous approach where bond is defined by discrete, zero-thickness elements (springs) whose behaviour is controlled by the bond stress-slip relationship. This approach is able to realistically predict the bond behaviour for different geometries and for different boundary conditions only if a realistic constitutive model for the surrounding concrete is used. However, the model is not able to automatically predict the bond behaviour of a given bar geometry. Consequently, the influence of these parameters must be stored in advance in the basic parameters of the bond model. Thus one has the possibility to realistically simulate the behavior of reinforced concrete structures with relatively low effort in modelling and computing time. By the use of detailed modelling, such as both modelling of the ribs of the reinforcement and the concrete lugs (see Figure 1b) between the ribs of the reinforcement a quite fine finite element mesh has to be generated. This leads again to a high effort in modelling work and also to a really long computing time in particular while carrying out a finite element analysis on complex reinforced concrete structures [3, 4].

2. REINFORCEMENT FINITE ELEMENT MODELS

In finite element modelling of reinforced concrete structures, there are three different alternative representations of reinforcement: smeared, embedded and discrete reinforcement models. The first one is rarely used and therefore it depends on the nature of used structure. The discrete and embedded representations are formulated and introduced in the developed program [4, 5].

2.1. Discrete Reinforcement Representation

The discrete modelling of steel reinforcement is the first approach used in finite element analysis of reinforced concrete structures [10]. The discrete representation of reinforcement uses one dimensional truss elements and it is the only way for accounting for bond slip and dowel action effects, Figure 2.

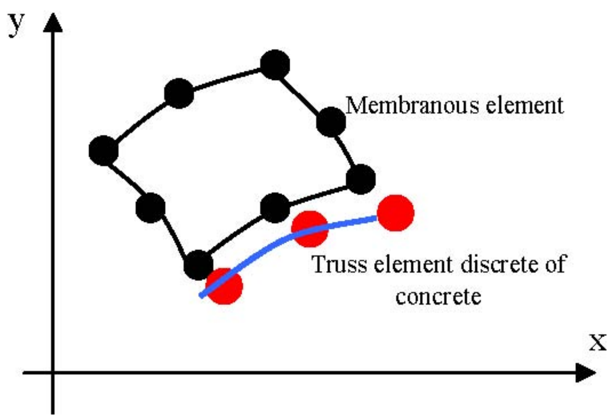

Figure 2. Discrete representation of steel bars [4]

A significant advantage of discrete representation is that it can account for possible displacement of the reinforcement with respect to the surrounding concrete. The bond effects are usually related with this representation and the bond-link or cohesive models can be used to connect the steel and concrete nodes in order to consider this effect. The main disadvantage is that the finite element mesh patterns are only restricted by the location of reinforcement and consequently the increase of the number of concrete elements and the degrees of freedom. In this way, Lagrange or Serindipity isoparametric concrete elements are used and a line three node truss elements is used to represent the steel and the compatibility between concrete and steel must be guaranteed [4].

2.2. Embedded Reinforcement Representation

In this representation, the reinforcement bar is considered as an axial member incorporated in the concrete element such that its displacements are consistent with membranous concrete elements and bond loss can be considered, Figure 3.

In this scope, many works have presented different formulations for this model. Embedded models allow for an independent choice of concrete mesh. So, the same number of nodes and degrees of freedom are used for both concrete and steel. The disadvantage of this procedure is that additional degrees of freedom increase the computational and numerical treatment [4].

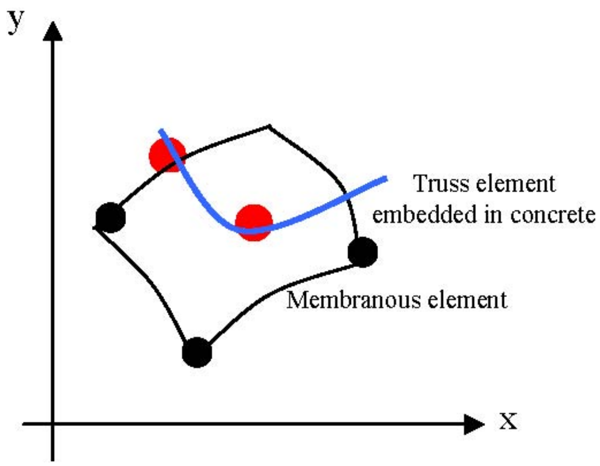

Figure 3. Embedded representation steel bars [4]

3. FINITE ELEMENT MODELS FOR BOND

Two different elements have been typically proposed to include the bond-slip effect in the finite element analysis of RC structures. One is bond link element and the other is bond zone element as also known as contact element.

These elements are associated with the discrete reinforcement model, which has the advantage of representing different material properties more precisely. Afterwards other bond conditions at different nodes can be easily represented [5].

To describe the bond behaviour between concrete and steel, the vertical and horizontal relative displacement between concrete and steel in the local coordinates can be considered. The same type of isoparametric elements and it has, at the unloaded stage, no physical dimension in the transverse direction. It uses linear, quadratic or cubic interpolation functions corresponding to the number of nodes per element. In linear analysis, the vertical relative displacements are too small compared to the horizontal displacement [4].

3.1. Analysis With Bond Link Element

Bond-link element consists of two orthogonal springs which connect and transmit shear and normal forces between a reinforcing bar node and an adjacent concrete node (Figure 4). Since the link has no physical dimensions, the two connected nodes originally occupy the same location in the finite element of undeformed structure [5].

The bond element is a two-node finite element. The element displacement field is a slip which is defined as a relative movement between the reinforcing bar and concrete in the direction parallel to the axis of the reinforcing bar.

The bond effect is assumed as an interaction between reinforcing bars and surrounding concrete. When the change of stresses in concrete and steel occurs, the effect of bond begins and becomes more pronounced at the end anchorages of reinforcing bars and in the vicinity of cracks.

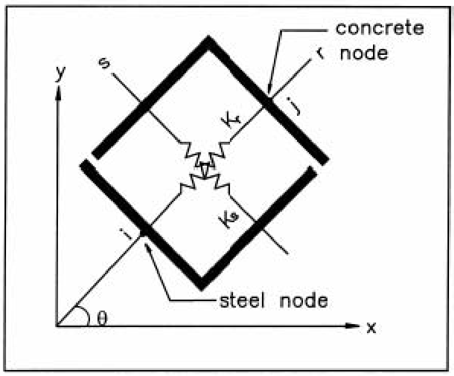

Figure 4. Bond-link model [4]

3.2. Analysis With Contact Element

The behaviour of the concrete-steel interface must be described from stress-strain laws. Many constitutive relationships are presented in the literature. In this element, the contact surface between the steel bar and the concrete in the immediate vicinity of the steel bar is modeled by a bond stress-slip law which considers the special properties of the bond zone. The most important differences are that contact element has the dimension along the steel-concrete interface (it does not have physical dimension in other two directions) and it provides a continuous contact surface between - steel bar and concrete [5].

3.3. Analysis Without Bond

In this case, the stiffness matrices of the steel elements are computed in local axis at the nodes of non bond. The concrete element stiffness matrices are calculated in the global axis and they are transformed steel local axes at common nodes. In y-direction, concrete and steel have the same degree of freedom but have different degree of freedom in x-direction at common nodes [4].

4. LOCAL BOND SLIP RELATIONSHIP

4.1. Differential Equation Governing The Slip

In Figure 5 a steel reinforcement embedded in a concrete mass is shown. Over a small piece of the bar, dx, the change in the relative displacement of the steel to concrete , dΔ, is equal to change in steel deformation, δs, minus the change in concrete deformation, δc. That is [7]:

$$d\Delta = \delta s - \delta c \tag{6}$$

The magnitudes of differential deformation for the reinforcement and concrete, if we assume an elastic state, are given in equation 7 and 8 respectively ac follows:

$$\delta_s = (\sigma_s / E_s)dx \tag{7}$$

$$\delta_c = (\sigma_c / E_c)dx \tag{8}$$

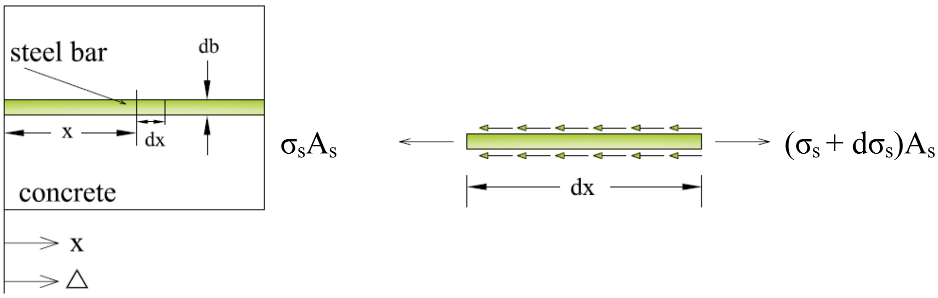

Figure 5. Bond consideration for steel reinforcement in concrete.

where the sub-scripts "s" and "c" refer to steel and concrete respectively. The terms used in equation 1 are general (independent of the type of reinforcement) and apply to local level (vary with location and stage of the test) [7].

In practice, the value of δc is negligible relative to δs because the concrete section is usually much larger than the steel section and the normal stress in concrete is much lower. Therefore, the second term in equation 6 is neglected and whole differential slip at local level is attributed to the steel deformation. It follows that equation 6 reduce to [7]:

$$d\Delta \sim \delta s \tag{9}$$

Substituting from equation 7 into equation 9 and re-arranging, we can write:

$$\frac{d\Delta}{dx} = \frac{\sigma_s}{E_s} \tag{10}$$

If we differentiate both sides of the above equation with respect to dx, the following equation will be obtained:

$$\frac{d^2\Delta}{d^2x} = \left(\frac{1}{E_s}\right)\frac{d\sigma_s}{dx} \tag{11}$$

On the other hand, the bond stress and steel stress (over segment dx) are inter-related from the condition of equilibrium that states (Figure 5):

$$(\sigma_s + d\sigma_s)A_s = \sigma_s A_s + \tau \times dx \times \pi \times d_b$$

Simplifying:

$$\frac{d\sigma_s}{dx} = \tau \times (\frac{\pi d_b}{A_s}) \quad (12)$$

If we substitute from equation 12 into equation 11, the following equation will be attained:

$$\frac{d^2\Delta}{d^2x} = \tau(s(x)) \times (\frac{\pi d_b}{A_s E_s}) \quad (13)$$

Where d_b is the diameter, A_s is the cross sectional area, E_s is the Young's modulus of the reinforcing bars and s(x) is the slip between concrete and steel abscissa x [7]. Equation 13 is known as the fundamental differential equation for the bond between a steel reinforcement and concrete. This equation has been drawn in the same form as shown above or in other forms (but with the same concept) by various authors.
It is assumed that the bond characteristics of reinforcing bar are analytically described by a local relationship of bond $\tau=\tau(s)$, in which τ is the shear stress acting on the contact surface between bars and concrete and s is the slip; that is the relative displacement between those of the steel bar and concrete.

4.2. Analytical Expressions for Bond-Slip Relationship

The experimental evidence indicates that the load transfer between reinforcement and concrete is mainly accomplished through bearing of the reinforcing bar lugs on the surrounding concrete and through friction at large slip values (Figure 1a). The adhesion is negligible. This behavior can be described using so-called bond stress-slip relationships.
The simple bi-linear bond stress-slip model is selected and the parameters of the model are derived from the experiment data corresponding to material features of each specimen. The bond stress-slip relationship which is used in the model and the corresponding components are shown in Figure 6.

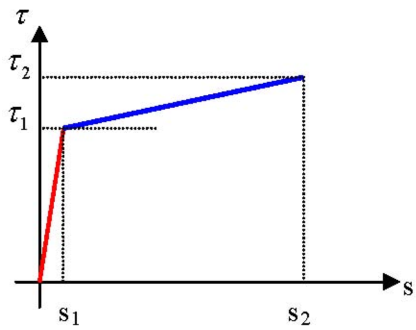

Figure 6. Bi-linear bond stress-slip [4].

$$\tau_1(s) = E_{b1}s \qquad s \leq s_1 \quad (14)$$

$$\tau_2(s) = \tau_1 + E_{b2}(s - s_1) \qquad s_1 \leq s \leq s_2 \tag{15}$$

s_1= 2 mm, s_2= 10.5 mm, τ_f = 10.55 MPa and τ_1 = 13.50 MPa

5. NUMERICAL EXAMPLES

5.1. Finite Element Modeling of Pullout Test

To study the bond behavior of steel reinforcement in a concrete matrix, we use pull-out tests of a steel bar (Ø12mm) with ribs (see Figure 1) which was performed by Eligehausen (2003) [9].

To investigate the performance of the cohesion layer, numerical investigations on pullout specimens have been carried out. The specimen is an anchor of a reinforcing bar d_b=12 mm in a well confined cylinder of concrete of 150mm height and 60mm diameter which corresponds to anchorage length of 5 bar diameters (embedment length lE=5 db =60 mm).

For the numerical investigations the finite element software (Ansys) has been used and a detailed FE model in 3D mode with and without bond-slip effect as cohesion layer to simulate bond have been employed. Since rib of reinforcement are being simulated, the mesh size close to the rib in steel bar, concrete and cohesion layer should be small enough to accurately describe the deformation and stress gradients. However, for the remaining regions coarse mesh can be used in order to reduce the computational costs. The results of these numerical investigations are compared with the results of the experimental investigations [8]. The test specimen used in the finite element model is shown in Figure 7.

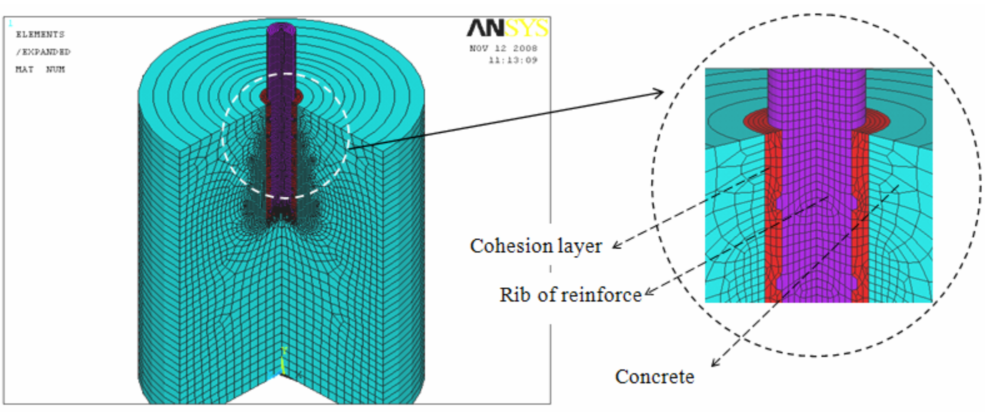

Figure 7. Finite element model

Table 1 shows the summary of the basic material variable used in the experimental and numerical investigations.

Table 1: Summary of the material parameters

Material properties	Values (kg/cm^2)
Concrete compressive strength	300
Concrete tensile strength	30
Concrete E modulus	273664
Concrete Poisson's coefficient	0.2
Steel E modulus	2100000
Steel yield stress	3000
Steel Poisson's coefficient	0.3

A displacement control load being applied to the end of the reinforcement in pull-out test Figure 8.

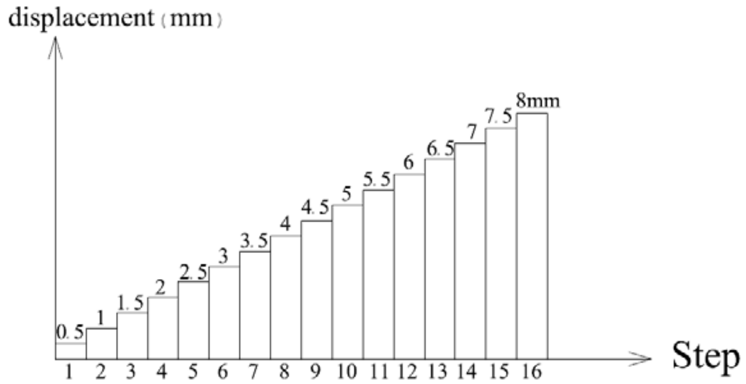

Figure 8. Displacement control load applied to the end of the reinforcement

In this paper, the concrete and the reinforcement bar was modeled by eight-node Serendipity axisymmetric elements (Plane 82, Axisymmetric) with 2×2 Gauss integration points.

5To display the bond slip effect between concrete and steel, two distinct models are selected, such as: (1) full perfect, (2) bi-linear model. These models are introduced in finite element program (Ansys) and the collected results are analysed and discussed in the next section.

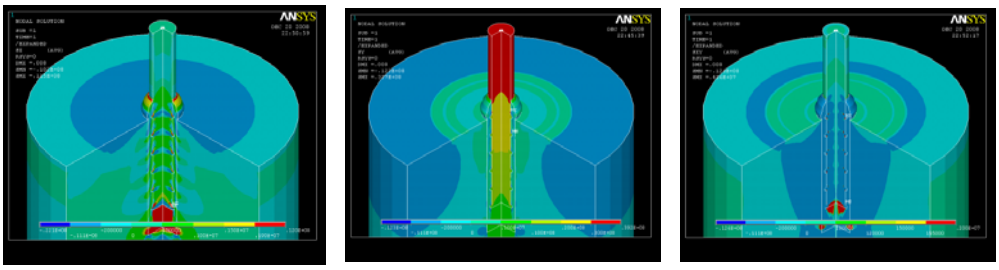

(a) (b) (c)

Figure 9. Stress distribution in reinforced concrete with bi-linear law of bond, (a) σ_{xx}, (b) σ_{yy} and (c) τ_{xy}.

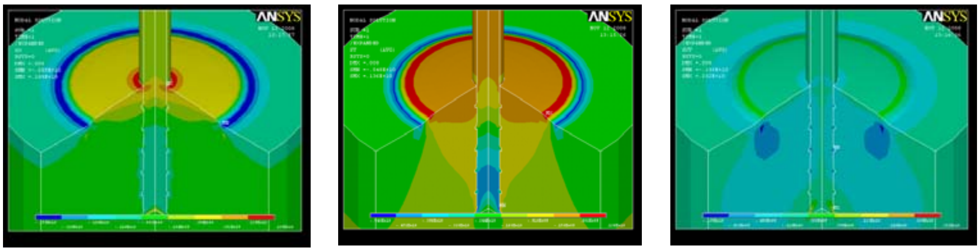

(a) (b) (c)

Figure 10. Stress distribution in reinforced concrete for perfect bond, (a) σ_{xx}, (b) σ_{yy} and (c) τ_{xy}.

The bond stress-slip relation obtained in the finite element calculation when the three dimensional modelling of the reinforcement is used are substantially corresponding to the curves of the experimental investigations.

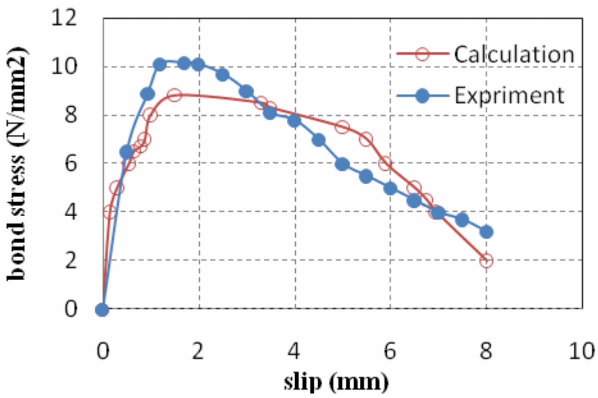

Figure 11. Comparison bond stress-slip graph in 3D finite analysis and experiment

According to the normal and shear stress curves (Figures 9-10), it is possible to appreciate how the connection influences the transmission of the efforts from steel bar towards the concrete and vice versa.

6. CONCLUSION

In this paper the methods of modeling of reinforcing bars and bond-slip models between steel rebar and concrete in the finite element program is described. Then one analytical expression of bond-slip relationship is selected and the pull-out test with slip and without slip modeled by finite element software (Ansys) in 3d mode and then the obtained results are presented and compared with experimental data from pullout test. It was found that stress distribution in the steel bar and concrete of pull-out tests may principally be influenced by the properties of the interface.

1. In the improvement of finite element models of composite material, it is necessary to use not only the constitutive laws of concrete and steel but also one of the interface.
2. The stress distribution in the steel bar of pull-out tests may principally be

influenced by the properties of the interface.
3. The finite element studies of pullout tests with a short embedment length (local bond conditions) show relatively good agreement between experimental and numerical results.
4. The cohesion layer is able to predict transfer of bond stresses from reinforcement into concrete realistically.
5. The proposed approach predicts the stress field in the concrete and along the steel bars (local behaviour)

REFERENCES

1. Kwak, H, G. and Kim, S, P., Bond–slip behavior under monotonic uniaxial loads, 2001, Engineering Structures Vol. 23, pp 298-309.
2. Khalfallah, S., Tension Stiffening Bond Modelling Of Cracked Flexural Reinforced Concrete Beams, 2008, Journal of Civil Engineering and Management, pp. 131-137.
3. Lettow, S., Eligehausen, R., The Simulation of Bond between Concrete and Reinforcement in Nonlinear Three-dimensional Finite Element Analysis, 2003, IWB, University of Stuttgart, Stuttgart, Germany.
4. Khalfallah, S. and Ouchenane, M., A Numerical Simulation of Bond for Pull-Out Tests: The Direct Problem, 2007, Asian Journal of Civil Engineering (Building and Housing) Vol. 8, No. 5, Pages 491-505.
5. Youai, G., Bond Stress and Slip Modeling in Nonlinear Finite Element Analysis of Reinforced Concrete Structures, 2000, MSc thesis, Department of Civil Engineering, The University of Toronto, Canada.
6. Ožbolt, J., Lettow, S. and I. Kožar., Discrete Bond Element For 3d Finite Element Analysis Of Reinforced Concrete Structures, 2002.
7. Marefat, M, S., The Mechanics of Bond for Helical Devices Anchored in Concrete, PhD thesis, 1993, Department of Civil and Environment engineering, The University of Waterloo, Ontario, Canada, PP. 1-20.
8. Lettow, S., Mayer, U. and Eligehausen, R., experimental investigations on the bond behaviour of ribbed reinforcing bars, 2003, Universität Stuttgart: Institut für Werkstoffe im Bauwesen.
9. Fib-Bulletin No. 102000. Bond of reinforcement in concrete-state of the art report, Lausanne.
10. Ngo D., Scordelis A.C., Finite element analysis of reinforced concrete beams, 1967, ACI Journal, No. 14, PP. 152-163.

CD02-020

A NONLINEAR DYNAMIC BASED REDUNDANCY INDEX FOR REINFORCED CONCRETE FRAMES

A.A.Fallah[1], A.Sarvghad Moghadam[2], A. Massumi[3]
[1]Ph.D. Candidate, Science and Research Branch Islamic Azad University, Tehran, Iran
[2]Associate Professor, Civil Engng. Dept., International Institute of Earthquake Engineering and Seismology, Tehran, Iran
[3]Assistant Professor of Structural Engineering, Graduate School of Engineering, Tarbiat Moallem University of Tehran (Kharazmi), Tehran, Iran

ABSTRACT

In almost all codes of practice for seismic resistant design of buildings, a behavior factor is used to reduce design base shear. The behavior factor is affected by several parameters such as ductility, overstrength and redundancy reduction factors. There are two common approaches to assess the effects of redundancy on the strength of a structural system, which are as follows: Static Pushover Analysis and Incremental Dynamic Analysis. The two indices: redundancy strength coefficient and redundancy variation coefficient have been introduced to measure these effects. Simplified methods are developed and presented to calculate these parameters. In this paper the redundancy strength and the redundancy variation parameters are evaluated for the reinforced concrete plane frames with different number of stories, bays and ductility capacities. The investigations indicate that these two parameters are mainly the results of redundancy reduction factors.

Keywords: redundancy, behavior factor, ductility, concrete frames, redundancy strength index, redundancy variation index

1. INTRODUCTION

Although behavior factor (R) has been an important subject in structural engineering studies in recent years but most important studies in this field get back to the last two decade. Among the researchers in this field, Freeman is the one who calculated behavior factor with using the capacity spectrum method. According to this method, to compute the quantity of R by an analytical method, it can be formulated as follows:

$$R = R_A \times R_B \times R_C \times \ldots \times R_N \qquad (1)$$

Where Rx are parameters such as arrangement of frames, type of structural system, composition of loads, degree of uncertainty, damping, characteristics of nonlinear behavior in structure, characteristics of materials, ratio of building dimensions, failure mechanism and other effective parameters. The range of effective factors in determining R is such that it would almost be impossible to find two buildings with identical behavior factors. In other words, each building has its own unique features. Therefore, instead of adding all effective factors, as mentioned in the behavior factor relation, usually only the factors having more determinant role in the behavior factor are studied. In this paper, two main coefficients namely the structural capacity and the force resulting from earthquake are primarily considered, and the factors that help increase the capacity and reduce the seismic forces are determined in the following steps.

In 1991, separate researches on behavior factor, also known as Uang plasticity coefficient method were accomplished by Uang [1]. In 1997, Pandey and Barai [2] studied the structural sensitivity response to uncertainty. They assumed that for every structure subjected to a given loading, the general uncertainty is proportional to the reverse structural sensitivity response; thus, the structural response sensitivity reduces with increasing uncertainty.

In 1999, Bertero and Bertero studied uncertainty in the seismic resistant design. In this study, they explained the main concepts of seismic uncertainty and defined the probabilistic effect of uncertainty on structural failure.

In 2003, Wen, and Song [3], studied the reliability of structural behavior under earthquakes. They believed that when more elements are involved in resistance against lateral load, the probability for collapse of all elements, at the some time, is lower than the case when le elements with equal resistance are involved.

In 2004, Hosain and Tsopelas tried to determine structural uncertainty in reinforced concrete buildings. In that, they studied r_s (uncertainty resistance coefficient) and r_v (uncertainty variation coefficient) and their relation with the component's plastic rotation ductility factor (μ_θ). The effects of number of stories and bays, the length of bays and story height were studied as well. They then studied the effect of uncertainty on behavior factor (R_R). Here, the effect of number of stories and bays, bays' length, story height and also the effect of gravity loads on uncertainty coefficient are studied. Even the effect of number of frames present at each lateral load direction has been considered, and finally, the procedure to compute uncertainty coefficient using uncertainty resistance and uncertainty change coefficients were studied.

2. REDUNDANCY

The redundancy concept has been considered by engineers, especially after Kobe, Northridge and Turkey earthquakes, during which many buildings with low redundancy degree were damaged. Therefore, the redundancy topic was introduced seriously, and the degree of redundancy in structural systems was considered for seismic design.

There is some information about the useful effects of redundancy in structural resistance, but the efficient methods measurement methods are not available as yet. The effects of three parameters are usually considered to measure redundancy degree, which include:

1. Static redundancy degree of system
2. The ratio of probability in system failure to parts failure
3. Involvement of additional capacity which was not necessary for design

Some researchers studied the effects of redundancy degree with deterministic method; that is, use of nonlinear static analyses. There are few studies in which probabilistic method is applied to determine the effects of redundancy degree using structural reliability.

Seismic redundancy degree (n) for a structural system is actually the number of critical areas (plastic hinges) in a structural system which continue to yield until the structure exceeds the allowable limit leading to emergency disasters like plastic displacement or complete collapse. In engineering problems of earthquake, it is assumed that if all critical points (plastic hinges) yield simultaneously, the structure would fail under earthquake shaking. The redundancy degree is defined using the parallel and serial structural system reliability theory, determining the probability of failure in serial systems by weakest connection model and setting the probability of failure in parallel systems through secure decay model [4].

In 1999, Bertero et al studied the effect of redundancy and redistribution of internal forces in seismic design and stated that a part of behavior factor is originated from redundancy degree and can not be determined independent from overstrength and ductility. They also assumed that when the structure can not withstand gravity loads under the effect of earthquake forces, it would collapse. About structural resistance against displacement due to increasing lateral load, the resistance in the first yielding point is considered, and the maximum resistance is predicted using the reliability of displacement capacity.

A structure takes advantage of the positive effects of redundancy degree when:

a) Change coefficient in “structural demand” reduces in comparison to change coefficient in "structural capacities"
b) Addition resistance increase
c) Curvature capacity increases in plastic hinges
d) A minimum rotation capacity is ensured in all elements of structural system

According to much uncertainty in structural capacity and demand, one of the methods in studying the redundancy of structural systems under seismic loads, is to use the reliability concept. In one kind of structural system without change in materials and conFigure uration, the redundancy degree factor can only influence the reliability on structural stability against earthquake induced lateral loads and the structure behavior factor, seriously. It should be considered that the redundancy degree is different in similar frames. If the size of an element, its reinforcement and implementation details change, the failure mechanism may naturally change, but even for two completely similar frames, redundancy degree will be different for various lateral load models [5].

Behavior factor used in codes, which reduces the level of elastic forces in the design process and in its primary formulation, is defined in terms of ductility coefficient ($R\mu$) and the additional resistance coefficient (Rs)[6]. Ductility coefficient is computed considering nonlinear response of structural system. The relationships for computing functional ductility coefficient is formulated by some researchers by involving the natural period of structure and its ductility capacity, which are commonly based on nonlinear response change of a multi-story building relative to nonlinear response of a system with single degree of freedom [7].

The overstrength capacity show the actual lateral resistance in comparison to modeling resistance overstrength may be divided into two general parts. The first part is related to the overstrength resistance modeling until the first hinge yields in a structure and the second part is related to formation of the first hinge until a mechanism for total failure of a structure is developed [8].
In ATC-19, the formulation of behavior factor (R) is introduced [8]. This coefficient includes an additional factor (R_R) used to account for the effect of redundancy degree in a structure. These effects include probability effects and others related to structural systems geometry either in a plan or at a point in height. Therefore, behavior factor (R) is equal to:

$$R=R_{\mu}.R_S.R_R \tag{2}$$

Some effective parameters in redundancy and structural systems reliability are the ratio of demand to the capacity of structural systems, the kind of failure mechanism formed, building high, the number of stories, the length and the number of bays. This study computes the probabilistic and deterministic effects of redundancy through obtaining two redundancy resistance index (r_s) and redundancy variation index (r_v). These two indexes are used in measuring the resistance reduction coefficient from R_R redundancy for structural frames with two-dimensional reinforced concrete.

3. REDUNDANCY INDEXES

Redundancy resistance index r_s represent the ability of a structural system in redistributing forces while failure and the capability of a structure in transferring the forces of elements yielded to the elements with higher resistance. This index is a function of static redundancy, ductility, strain hardening and the average resistance of elements in a structural system. Second index having probability nature is an r_v redundancy variations index. This index measures the probability effect of elements resistance on structural system resistance. It is also a function of static redundancy in a structural system, and on the other hand is a function of statistical nature in ductility and structural elements resistance. Following variables are used in computing above indexes:

- Base shear in the beginning of yielding system.
- Ultimate base shear.
- The number of local failure or the number of plastic hinges caused during ultimate failure of structure.
- The access of elements curvature to ultimate curvature.

4. REDUNDANCY RESISTANCE INDEX

Redundancy resistance index r_s are defined as the ratio of average ultimate resistance ($\overline{S}_u$) to yielding resistance ($\overline{S}_y$). In which $\overline{S}_y$ is the average system resistance non redundant system.

$$r_s = \frac{\overline{S}_u}{\overline{S}_{nr}} = \frac{\overline{S}_u}{\overline{S}_y} \tag{3}$$

So that in this equation, both parameters $\overline{S}_u$ and $\overline{S}_y$ can be defined with respect to nonlinear static analysis curve (Figure 1) [9].

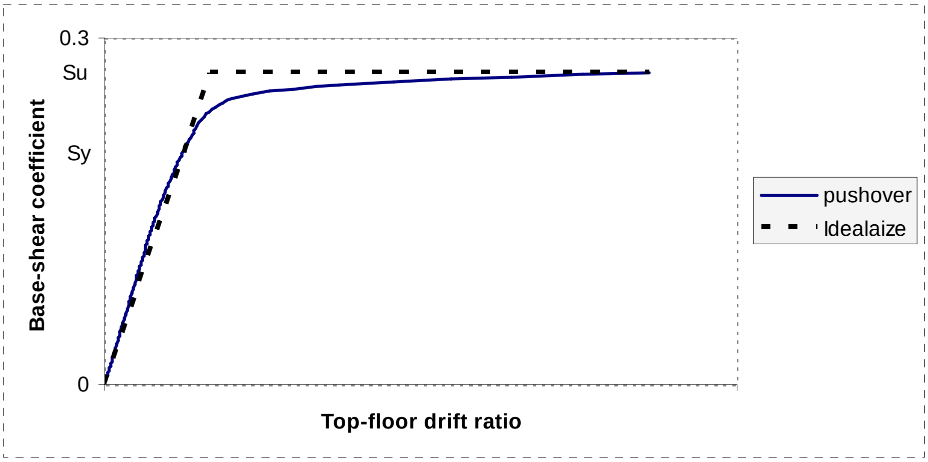

Figure 1. Base-shear versus top-floor drift curve

In a method suggested for this paper in studying the effects of redundancy using nonlinear dynamic analysis with increased acceleration, the base shear during failure and yielding is considered. In previous studies, this method is applied for studying the effects of overstrength [10]. In this study, the system failure standards that will be considered in nonlinear static and dynamic analyses with increased acceleration are as follows:

- Limitations related to storey drift which according to code [11] for buildings which period lower than 0.7 second are limited to 2.5% and for structures with period more than 0.7 second are limited to 2%.
- The index of structure stability which in a structure with high ductility is limited to 0.125 and in a structure with low ductility is limited to 0.25.
- The formation of failure mechanism in a structure and collapsing structure.
- The access of structure failure index to a number one according to park-Ang criterion [12].

In pushover static analyses performed in this study, it is assumed that lateral loads with reverse triangular distribution are inserted into a structure which is proportional to Iran 2800 standard earthquake force. In nonlinear dynamic analysis with increased acceleration, the maximum acceleration of any record is coordinated to a primary number (here it is considered to be 0.02g) and in one stage in increased to 0.02g and the structure is analyzed in every step until when one of the four above-mentioned criteria's is occurred. In this stage, the analysis is stopped and base shear is used during yielding and maximum base shear is used for measuring rs redundancy resistance index.

5. REDUNDANCY VARIATION INDEX

The relation between resistance of a structural system and the resistance of its composing elements is obtained using plastic analysis of structure. In this relation, the selection of failure mechanism is important because it can result in non-actual estimates from redundancy variation index. For simplify computations, one sway mechanism according to Figure (2) is considered. This mechanism is based on the "strong column" and "weak beam" assumption which column resistance is at least 20% more than the resistance of beams.

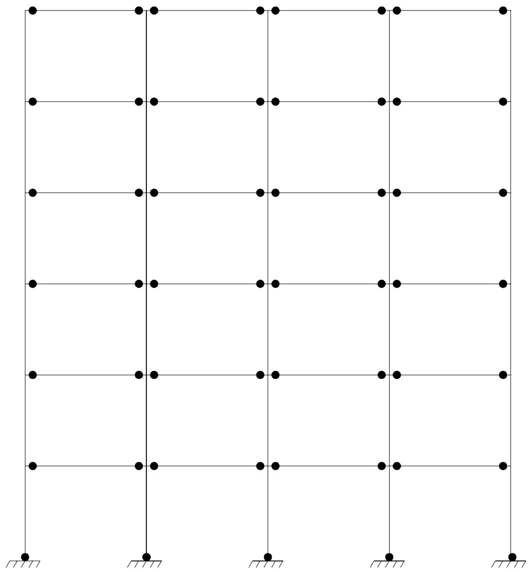

Figure 2.Sway type failure mode of a generic plane frame

The frame strength (base shear strength) for any failure mode could be represented by the following expression:

$$S = \sum_{i=1}^{n} C_i . M_i \tag{4}$$

Where S= frame strength (base shear); n= number of plastic hinges in the frame resulting from the particular failure mode or collapse mechanism considered; M_i=yield moment of the structural element where plastic hinge "i" is formed; and C_i=coefficient with units radians length that is a function of the plastic rotation and geometry of the structure. Eq. (4) is of the form of the strength equation of a parallel system type.

The mean value of the frame strength can be derived from the fallowing expression:

$$\overline{S} = \sum_{i=1}^{n} C_i . \overline{M}_i \tag{5}$$

Where Mi = mean value of the strength of the structural element where plastic hinge "i" is formed.
Accordingly the standard deviation of the frame strength σ_f can be obtained from:

$$\sigma_f = \sqrt{\sum_{i=1}^{n} \sum_{j=1}^{n} C_i C_j \rho_{ij} \sigma_{Mi} \sigma_{Mj}} \tag{6}$$

Where ρ_{ij} = correlation coefficient between the strengths Mi and Mj and σ_{Mi} = standard deviation of the yield moment Mi. also ρ_{ij} = 1 for i=j. To further simplify the deviation, a regular multistory multi-bay frame with the following properties is considered.
1. The frame is composed of elements with identical normally distributed strengths:

$$\overline{M}_i = \overline{M}_j = \overline{M}_e \tag{7}$$

$$\sigma_{Mi} = \sigma_{Mj} = \sigma_e \tag{8}$$

2. The correlation coefficient between the strength of any two pairs of elements is the same.

$$\rho_{ij} = \rho_e \tag{9}$$

3. The bays of the frame have identical spans and the stories identical high which result in:

$$C_i = C_j = C \tag{10}$$

Eq.(5) and (6) now become:

$$\overline{S} = n.c.\overline{M}_e \tag{11}$$

$$\sigma_f = C\sigma_e \sqrt{n + n(n-1)\rho_e} \tag{12}$$

The following relationship between the coefficient of variation (COV) of the frame strength υ_f and the COV of the element strength v_e is calculated by dividing Eq. (12) to Eq. (11):

$$v_f = \frac{\sigma_f}{\overline{S}} = \frac{\sigma_e}{\overline{M}_e}\sqrt{\frac{1+(n-1)\rho_e}{n}} = v_e\sqrt{\frac{1+(n-1)\rho_e}{n}} \tag{13}$$

The redundancy variation index r_v is defined as the ratio between υ_f and v_e:

$$r_v = \frac{v_f}{v_e} = \sqrt{\frac{1+(n-1)\rho_e}{n}} \tag{14}$$

For a parallel system with unequally correlated elements, ρ_e could be substituted with the average correlation coefficient $\overline{\rho}$ defined as:

$$\overline{\rho} = \frac{1}{n(n-1)}\sum_{\substack{i,j=1\\ i\neq j}}^{n}\rho_{ij} \tag{15}$$

Therefore, Eq. (14) Can be modified using the average correlation coefficient of the strengths of the plastic hinges as fallows:

$$r_v = \sqrt{\frac{1+(n-1)\overline{\rho}}{n}} \tag{16}$$

Hence the redundancy variation index r_v is a function of the number of plastic hinges "n" and their average correlation coefficient between their strengths, and represents a measure of the probabilistic effects of redundancy on the system strength, its values range between 0 and 1.

For a building structure where a single plastic hinge causes collapse (n=1), r_v =1 and the structure under consideration in non redundant. The other extreme value r_v=0 indicates an infinitely redundant structural system and is reached either when an infinite number of plastic hinges are required to cause collapse (practically "n" attains large values) or when element strengths in a structure are uncorrelated (the average correlation coefficient in Eq.(16) is zero).

Using Eq.(16) r_v can be estimated from a pushover or dynamic analysis and for a particular value of the average correlation coefficient of the structural member strength.

6. REDUNDANCY FACTOR "R_R"

The overall effects of redundancy on the structural strength may be completely described by the ratio of the ultimate strength of a structural system to the ultimate strength of non-redundant structure. Thus:

$$R_R = \frac{S_u}{S_{nr}} \tag{17}$$

Where S_u = structural system strength which includes all the effects of redundancy; and S_{nr} =the same strength but for non-redundant structural system. Assuming that the strength of a structure is distributed normally, the characteristic or design strength of a structural system, its standard deviation, the coefficient k is formed. Therefore, both Su and S_{nr} may be written as follows:

$$S_u = \overline{S}_u - k\sigma_f \tag{18}$$

$$S_{nr} = \overline{S}_{nr} - k\sigma_{nr} \tag{19}$$

Where σ_f = standard deviation of the frame strength; σ_f =standard deviation of the non-redundant frame strength; $\overline{S}_u$ = average of the ultimate frame strength and $\overline{S}_{nr}$ = average of the non-redundant frame strength.

An expression for σ_f could be obtained as follows:

$$r_v = \frac{\sigma_f}{v_e} \frac{1}{r_s \overline{S}_{nr}} \Rightarrow \sigma_f = r_v r_s v_e \overline{S}_{nr} \tag{20}$$

By virtue of $\overline{S}_u = r_s . \overline{S}_{nr}$; Eq. (19) results into:

$$S_u = r_s \overline{S}_{nr} - k r_v r_s v_e \overline{S}_{nr} = r_s (1 - k r_v v_e) \overline{S}_{nr} \tag{21}$$

Where r_v=redundancy variation index; r_s =redundancy strength index and v_e=COV of the strength of the structural system elements.

Using Eq. (19) and (21), Eq.(17) becomes:

$$R_R = \frac{r_s (1 - k r_v v_e) \overline{S}_{nr}}{\overline{S}_{nr} - k\sigma_{nr}} = r_s \left(\frac{1 - k v_e r_v}{1 - k v_{nr}} \right) \tag{22}$$

Where v_{nr} is the COV (coefficient of variation) for non-redundant frame strength. A non-redundant frame structure could be modeled as a parallel system consisting of ideal elastic-brittle elements. Such a system behaves like a series system, where failure of one element results in the system collapse, and that the safety index of the system is equal to that of the element. For a non-redundant system, (n=1) $v_{nr}=v_e$. Therefore, the redundancy factor (R_R) can be expressed as follows:

$$R_R = r_s \left(\frac{1 - k v_e r_v}{1 - k v_e} \right) \tag{23}$$

7. CASE STUDY ABOUT THE EFFECTS OF REDUNDANCY ON TWO-DIMENSIONAL CONCRETE FRAMES

In order to compute redundancy indices, 16 frame samples from 2 bay to 5 bay and with two, four, six and ten stories were designated. SAP2000 software [13] and the IDARC software [14] are used for nonlinear dynamic and nonlinear static analyses. For nonlinear static analysis, 16 frame samples with high ductility and 16 frame samples with low ductility are selected (Figure 3).

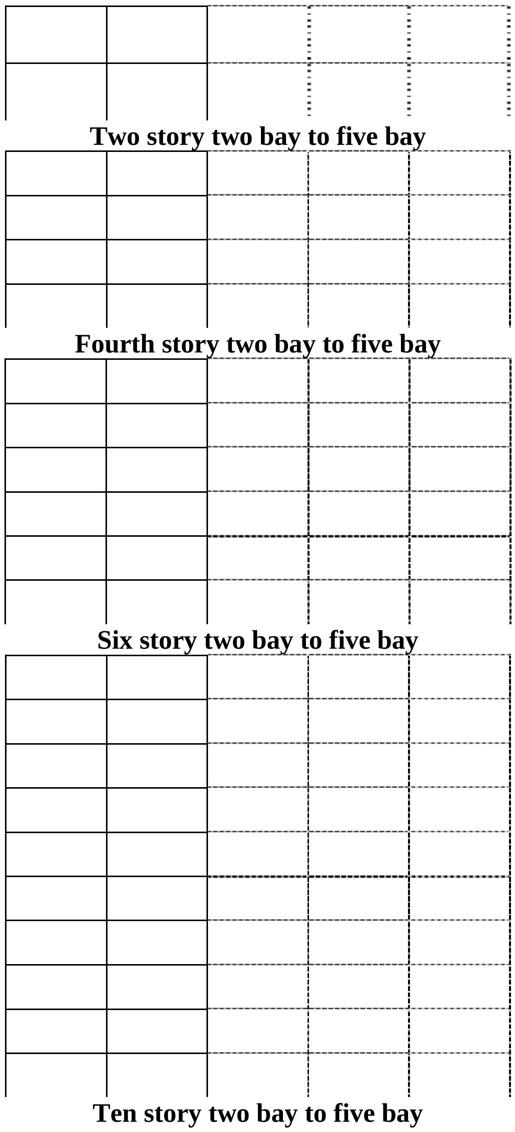

Figure 3. Reinforced concrete frames with two story two bay to ten story five bay

The lateral load pattern applied to the structure is reverse triangular, which is

approximately in accordance with lateral force criteria of the earthquake standard 2800 of Iran. Four different cases of design and analysis are considered for comparison. In the first case, the bay length is 4 meters and the story height is 3 meters and in the second case, the story height is increased from 3 to 4 meters. In the third case, the bay length is increase to 5 meters and finally in the forth case, the gravity loading intensity is increased to 30%. Therefore, in static nonlinear analysis, one hundred twenty eight frames are designed with SAP2000and then analyzed by the IDARC. Response curves are computed in terms of displacement at the top of structure (Δtar) with respect to base shear divided by structure weight (C_b). Two values, base shear coefficient during yielding and also maximum base shear coefficient are important over curve. The r_s index is obtained by dividing maximum base shear coefficient to the base shear coefficient when yielding.
Using maximum number of plastic hinges formed in nonlinear static analysis, one can obtain r_v index. As a result of having these two indices, resistance reduction coefficient can be obtained from redundancy according to relations in the third part.
In order to carry out nonlinear dynamic analysis with increased acceleration by the IDARC software, begins to analyze with a primary PGA value in any stage, and it continues the operation with 0.02g increase relative to the previous measure, until one of the failure conditions is reached. In this case, the value of base shear coefficient is applied for computing r_s and also for computing r_v index. The number of plastic hinges formed while failure is used to compute 16 frames with high ductility and 16 frames with low ductility. Eight seismic records are applied, equally, for both linear and nonlinear static analysis methods, for 4 different cases. Finally, 1024 frames were analyzed with different cases and the values of base shear coefficient while forming the first plastic hinge. Maximum base shear coefficient and the number of plastic hinges when failing are used as parameters required for computing r_s, r_v and R_R indices. It is necessary to note that the average values obtained from eight records is the basis for computing above indices.

8. CONCLUSION

Comparing the responses obtained from Static Pushover Analysis method (SPO) with Incremental Dynamic Analysis (IDA), it is concluded that in most conditions, R_R coefficients obtained from static method are larger than dynamic method, but this difference is maximally 10%. According to result from Figure(4), we can conclude that the results obtained from nonlinear static method are in good agreement with results obtained by nonlinear time history method and may be used as a reliable method.
Finally, it should be emphasized that these results are only for frames modeled in this study and might not hold true for all other structural models.

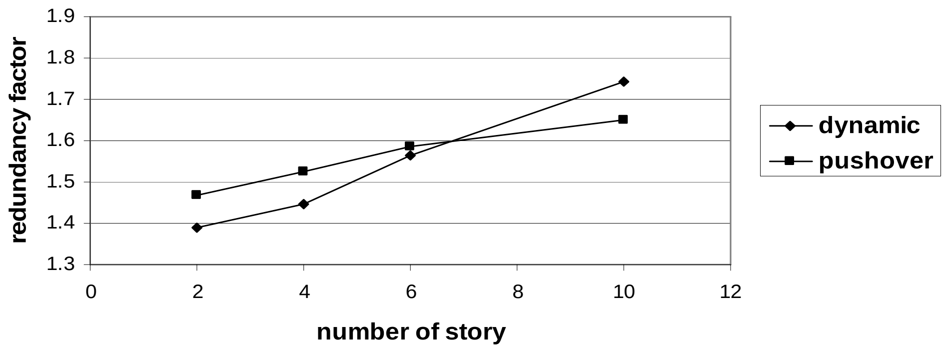

Figure 4. Average of redundancy modification factor with number f story

REFRENCES

1. Uang, C.M., "Establishing R and C_d Factors for Building Seismic Provisions," Journal of Structural Engineering, 1991, Vol. 117, No.1, PP.19-28.
2. Pandy, P.C. and Barai, S.V., "Structural Sensivity as a Measure of Redundancy" Journal of Structural Engineering, 1997, Vol. 123, No.3, PP.360-364.
3. Wen, Y.k, and Song S.H., "Structural Reliability/Redundancy under Earthquakes, " Journal of Structural Engineering, 2003, Vol12, No1, PP 56-66.
4. Bertero, R.D. and Bertero, V., "Redundancy in Earthquake-Resistant Design,"Journal of structural Engineering, 1999, Vol. 125, PP.81-88.
5. Husain, M., and Tsoplas, P., "Meusures of Structural Redundancy in Reinforced Concrete Buildings. II: Redundancy Response Modification Factor R_R," Journal of Structural Engineering, 2004, Vol 130, No.11, PP.1659-1666.
6. Tasnimi, A.A. and Mahmoudi, M. (1998), “Prediction of Overstrength of Reinforced Concrete Moment Resisting Frames, Using Non-Linear Inelastic Analysis.” Proceeding of the 11th European Conference on Earthquake Engineering, Balkema, Rotterdam, CD.
7. Mahmoodi Sahebi, M., and Tasnimi, A.A., 1377 " the effect of alternation period and additional resistance on seismic demand for reinforced concrete bending frames" thesis in the course of structure engineering doctorate, Tehran, technical and engineering college of Tarbiat Modares university.
8. Massumi, A., Tasnimi, A.A. and Saatcioglu, M. (2004), Prediction of Seismic Overstrength of Concrete Moment Resisting Frames Using Incremental Static and Dynamic Analyses, Proceedings of 13th World Conference on Earthquake Engineering, Vancouver, BC, Canada, CD.
9. ATC, 1995, Structural Response Modification Factors, ATC-19, Applied Technology Council, Redwood City, California.
10. Husain, M., and Tsopelas, P., "Measures of Structural Redundancy in Reinforced Concrete Buildings. I: Redundancy Indices," Journal of Structural Engineering, 2004, Vol. 130, No.11, PP.1651-1658.
11. Massumi, A., (2004), “Estimation of Response Modification Factors for RC-MRF Structures, Emphasizing on the Effect of Overstrength and Redundancy”,

PhD Thesis of Structural Engineering, Dept. of Civil Engineering, Tarbiat Modarres University.

12. Iranian Building & Housing Research Center, (1997), Iranian Building Code, Series Standard 2800, Code of Practice for Seismic Resistant Design of Building, Three Revised Edition.
13. Park, Y. J., and Ang, A. H. S. “Mechanistic seismic damage model for reinforced concrete.” J. Struct. Eng., 1985, Vol. 111(4), PP. 722-739.
14. Habibullah, A. and Wilson, E.“SAP2000 Version 9.02: A Computer Program for Integrated Finite Element Analysis and Design of Structures,”University of California, Berkely.
15. Valles, R.E., Reinhorn, A.M., Kunnath, S.K., C. and Madan, A. 1999 “IDARC2D Version 5.0: A Computer Program for Inelastic Damage Analysis of Building.” Technical Report NCEER-96-0010, State University of New York at Buffalo.

CD02-021

EVALUATION OF REDUCTION FACTOR FOR REINFORCED CONCRETE BUILDINGS RETROFITTED WITH CFRP JACKETS

G.R. Ghodrati Amiri[1], B. Radman[2] and R. Mirza Hessabi[3]
[1]Professor, School of Civil Engineering, Iran University of Science and Technology, Tehran, Iran
[2]M.Sc., School of Civil Engineering, Shomal University, Amol, Iran
[3]M.Sc., School of Civil Engineering, Iran University of Science and Technology, Tehran, Iran

ABSTRACT
Reduction factor shows the efficiency of lateral load resistance systems in dissipation of seismic energy through inelastic behavior. This parameter is broadly used in guidelines to determine elastic resistance of the structure. Since these seismic guidelines mainly put their emphasis on common lateral load resistance systems, it may not be appropriate to use the published reduction factor values in designing composite or strengthened lateral load resistant systems. The main objective of this research is to examine the quantitative impacts of confined concrete columns with CFRP jackets on reduction factor. Therefore, three models of 4, 7 and 10-story buildings, in a veryhigh seismic zone were selected. Pushover analyses were performed by means of the software SAP 2000 for three-dimensional models. Finally, the reduction factor of reinforced concrete (RC) buildings that were retrofitted with CFRP jackets was found to be 9.9. This result indicates an enhancement in the seismic resistance and specially, in ductility of the buildings.

Keywords: concrete buildings, reduction factor, confinement, carbon fiber reinforced polymer (cfrp) jackets, pushover analysis

1. INTRODUCTION
Reduction factor shows the efficiency of lateral load resistance system in dissipation of seismic energy through inelastic behavior. This parameter is broadly used in guidelines to determine elastic resistance of the structure. By taking many parameters and effects into consideration, depending on type of the lateral load resistant system, different seismic design guidelines reduce the calculated values for earthquake loads. These parameters and effects are namely structural system ductility, structural indeterminacy degree, structural overstrength and dissipation of seismic energy. For the first time, in the first decade of the twentieth century, following obtained experiences and study results from real earthquakes, researchers proposed the vertical seismic shear force to be a ratio of total weight of the building. In the following years, it was found that for higher buildings, the stiffness reduces and the period of vibration increases as the height increases. As a result, earthquake imposes lower accelerations to higher buildings. With finding out this

phenomenon, further development of structural dynamics knowledge and better understanding of structures behavior, it was understood that reduction factor is related to the number of building stories.

Accurate determination of the reduction factor of a building would improve exactness of the calculation of its seismic resistance, evidently. This factor depends on various parameters such as type of the lateral load resistant system, fundamental vibration period of the building, force-deformation model for materials, ductility capacity, overstrength factor and design safety factors.

In the present study, firstly, different definitions were explained and then possible effects of abovementioned parameters on reduction factor were investigated. Since seismic retrofitting of buildings is a new concept in Iran, quantitative effects of confinement of RC sections with CFRP jackets on reduction factor of RC buildings were subsequently studied, Three models of 4, 7 and 10-story buildings, in a very high seismic zone were selected. Pushover analyses were performed by means of the software SAP 2000 for three-dimensional models.

2. MODELING APPROACH

Some of the most important force-deformation models are bilinear, trilinear and those with reduction of stiffness and resistance in each cycle. The force-deformation relationship should be based on experimental documents or those, which are stated in [1-3]. For a pushover analysis, it is possible to utilize the general force-deformation relationship that is illustrated in Figure 1 or any other proper curves, which describe the performance under constant increase of displacement. For nonlinear dynamic methods, force-deformation relationships should describe the performance under both constant increases of displacement or under numbers of displacement cycles.

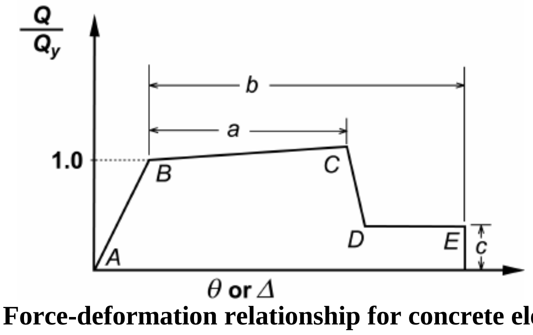

Figure 1. Force-deformation relationship for concrete elements [3]

3. DUCTILITY FACTOR

The most significant parameter in determining reduction factor of a structure is the ductility factor. Ductility factor is shown with (μ) and is calculated from below equation:

$$\mu = \frac{\Delta_u}{\Delta_y} \tag{1}$$

where, μ is the ductility factor defined as the ratio between the maximum displacement (Δ_u) and the yield displacement (Δ_y). Higher values of ductility factors would mean higher ductility capacities and therefore, higher reduction factors.
Several studies have been conducted for determination of reduction factors. Most of these studies propose that for a specified earthquake record, the reduction factor depends on ductility and fundamental period of vibration of the building [4-6]. Consequently, with a high precision, reduction factor could be expressed in terms of ductility as stated in Eq. (2):

$$R_\mu = R_\mu(T, \mu) \qquad (2)$$

An excellent overview has been presented by Miranda and Bertero (1994). In this paper, a bilinear spectrum was used for the reduction factor R_μ [6]:

$$R_\mu = (\mu - 1)\frac{T}{T_C} + 1 \qquad , \qquad T < T_C \qquad (3)$$

$$R_\mu = \mu \qquad , \qquad T \geq T_C \qquad (4)$$

where, μ is the ductility factor as defined above, ${}_cT$ is characteristic period of the ground motion and T is the fundamental period of structures.
Fundamental period of structures (T) is a major factor in calculation of reduction factor and could be assessed using various experimental methods or by means of computers. Increase of this parameter would increase reduction factor. The fundamental period of a non-retrofitted reinforced concrete building without shear walls could be computed from the below experimental relationship [7]:

$$T = 0.8 \times 0.07 H^{3/4} = 0.056 H^{3/4} \qquad (5)$$

where, H is the building height in meters.

4. OVERSTRENGTH FACTOR

In most of design guidelines, structures are designed so that none of their elements exceed the elastic state. However, since some plastic hinges form after exceeding this limitation, it does not always result in the collapse of the structure. By forming plastic hinges, general stiffness of the structure would decrease but still, it can resist higher loads. This procedure will continue until the formation of plastic hinges cause an instability mechanism and stiffness of the structure become zero. In the case that structure loses its ductility capacity simultaneously, it would collapse. As a result, in mentioned guidelines, the extra resistance of elements after the formation of plastic hinges is neglected. This resistance capacity is defined as the overstrength factor (R_S) and is calculated as ratio of the yield base shear to the design base shear by:

$$R_S = \frac{V_y}{V_w} \tag{6}$$

where V_y is the yield base shear, V_w is the design base shear.

5. DESIGN SAFETY FACTOR

There are many reasons for considering a safety margin in designing a structure and this margin is usually applied through safety factors (*Y*). However, these factors do not enter directly in seismic design procedures and it is not common to employ safety factors in seismic design guidelines. Nevertheless, in seismic guidelines this safety factor is implied through the reduction factors.

ACI-318 proposes to increase earthquake loads by multiplying them in 1.87. This design code also allows designers to multiply 0.75 in any load combinations, which include seismic loads [8]. Hence, the safety factor of moment resistant concrete frames is given by:

$$Y = 0.75 \times 1.87 = 1.403 \tag{7}$$

6. CALCULATION OF REDUCTION FACTOR

By considering important parameters, reduction factor of a structure, could be determined by [9]:

$$R_w = Y \times R_\mu \times R_S \tag{8}$$

where, R_μ is the period-dependent ductility factor, R_S is the period-dependent over strength factor and *Y* is the safety factor.

7. MODELING AND ANALYSIS

SAP2000 Nonlinear Version 8 has been utilized for analysis and design procedures [10]. This program is capable of performing static and dynamic analyses of structures in three dimensions. This program is compatible with most of the design guidelines.

A Three-dimensional model of each structure was created in SAP2000 to carry out nonlinear static analysis. In addition, a P-Δ analysis has been performed for every model. The ACI 318-99 guideline was employed for design purposes, since this guideline is supported by the SAP2000 program.

8. INTRODUCING MODELS

Three symmetrical moment resistance RC frame buildings are considered in this study. Three structures of 4, 7 and 10-story buildings are modeled in three dimensions with height to width ratio of about 1 to 2. These structures are considered according to Iranian Seismic Design Code (Standard 2800-05) [7] as residential buildings with a medium importance factor (*I*=1.0). Based on this code, structures are assumed located in a very high seismic zone with a design ground acceleration of 0.35g and the soil type is assumed class *II*. For all of the three models, span lengths equal to 4 *m* in both directions. The 4-story model consists of a three- bay frame, 7-story consists of four bays and the 10-story consists of five bays (Figure 2). Typical floor-to-floor height is 3.2 m.

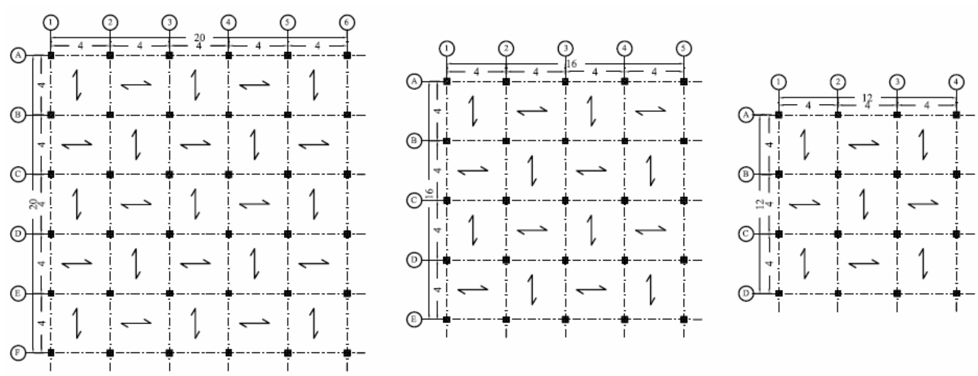

Figure 2. Plan view of 4, 7 and 10 story buildings

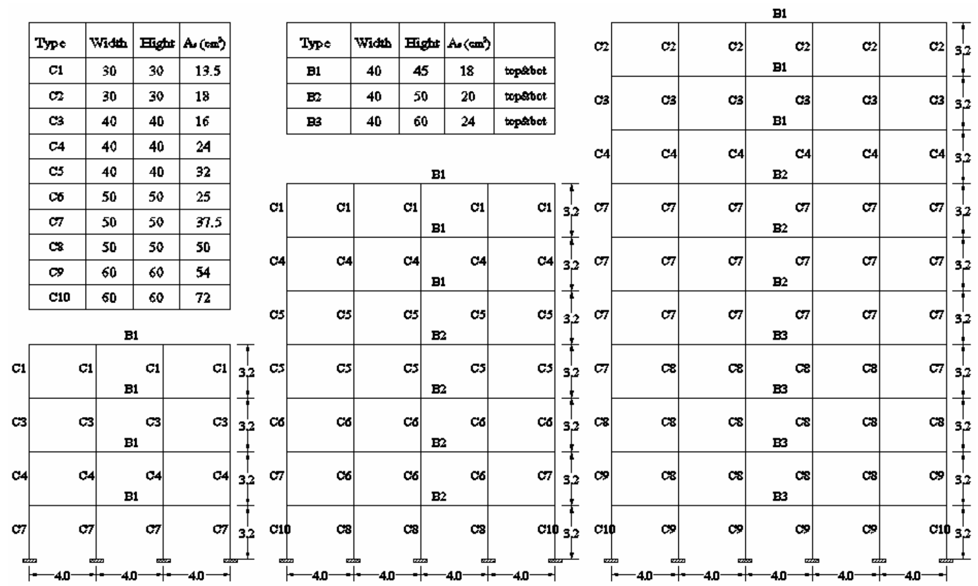

Type	Width	Hight	As (cm²)
C1	30	30	13.5
C2	30	30	18
C3	40	40	16
C4	40	40	24
C5	40	40	32
C6	50	50	25
C7	50	50	37.5
C8	50	50	50
C9	60	60	54
C10	60	60	72

Type	Width	Hight	As (cm²)	
B1	40	45	18	top&bot
B2	40	50	20	top&bot
B3	40	60	24	top&bot

Figure 3. Frame properties of 4, 7 and 10-story models

Beam and column dimensions and the amount of longitudinal reinforcement were specified as could be seen in Figure 3. Table 1 presents the final FRP jacket thicknesses for all columns.

Concrete properties are assumed to be 210 kg/cm^2 for the compressive strength, 218800 kg/cm^2 for modulus of elasticity and 0.2 for Poisson ratio. The strength of both longitudinal and transverse reinforcements is chosen to be 3000 kg/cm^2 with modulus of elasticity of 2.1×10^6 *kg/cm²*. The CFRP tensile strength and modulus of elasticity (E_{frp}) are 42400 kg/cm^2 and 2.32×10^6 kg/cm^2, respectively. The rupture strain of employed CFRP fibers is 0.18 and their thickness is 0.1375 *mm/layer*.

Table 1: Initial and final thicknesses of the FRP jackets for all columns.

Member group	Member sizes (mm)		Longitudinal reinforcement	FRP thickness (mm)	
	Width	Depth		Initial	Final
C1	30	30	13.5	0.000	0.412
C2	30	30	18.0	0.000	0.678
C3	40	40	16.0	0.000	0.678
C4	40	40	24.0	0.000	0.963
C5	40	40	32.0	0.000	0.963
C6	50	50	25.0	0.000	1.513
C7	50	50	37.5	0.000	1.788
C8	50	50	50.0	0.000	1.788
C9	60	60	54.0	0.000	1.513
C10	60	60	72.0	0.000	1.788

The dead and participating live loads on the stories are 650 kg/m^2 and 200 kg/m^2, respectively. Dead loads, which are exerted by internal partitioning walls, are also participated in abovementioned value of dead loads. Loads that are related to peripheral walls and parapets are assumed to be 700 *kg/m* and 250 *kg/m.* Lateral loads were determined by means of an equivalent static method and are applied in directions as stated in Iranian Seismic Design Code (Standard 2800-05) [7].

9. APPLIED MODEL FOR FRP CONFINED CONCRETE

In the last few years, many studies have been conducted on the stress–strain behavior of FRP-confined concrete and various models have been proposed [11]. However, the stress–strain model for FRP confined rectangular sections, that has been proposed by Teng and Lam appears to be a suitable model for our study as it is simple and it captures the main characteristics of the stress–strain behavior of FRP-confined concrete [12].

Based on this model, the compressive strength and axial rupture strain of FRP-confined concrete in rectangular sections are calculated as described by the following equations [13]:

$$\frac{f'_{cc}}{f'_{co}} = 1 + 3.3k_{S1}\frac{f_1}{f'_{co}} \tag{9}$$

$$\frac{\varepsilon_{cc}}{\varepsilon_{co}} = 1.75 + 12k_{S2}\left(\frac{f_1}{f'_{co}}\right)\left(\frac{\varepsilon_{h,rup}}{\varepsilon_{co}}\right)^{0.45} \tag{10}$$

where, f_1 is the equivalent confining pressure, defined as follows:

$$f_1 = \frac{2E_{frp}\varepsilon_{h,rup}t}{\sqrt{D^2 + B^2}} \tag{11}$$

where E_{frp} is the elastic modulus of the FRP, B and D are dimensions of the rectangular cross-section ($D \geq B$), $\varepsilon_{h,rup}$ is the FRP hoop rupture strain and t is the thickness of FRP fibers.

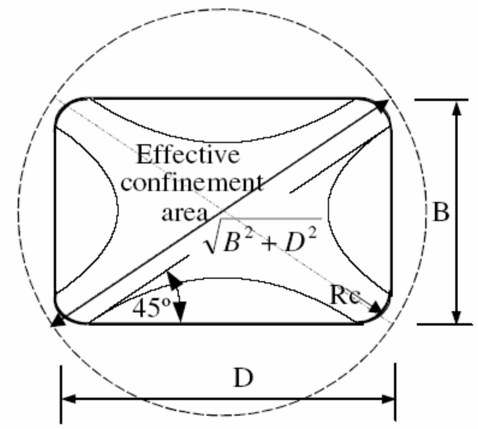

Figure 4. Confinement action in rectangular columns [13]

According to Figure 4, Teng and Lam proposed the following model for determination of the total area of concrete enclosed by the FRP jacket:

$$\frac{A_e}{A_C} = \frac{1 - \left[\left(\dfrac{\frac{B}{D}(D-2R_C)^2 + \frac{D}{B}(B-2R_C)^2}{3A_g}\right)\right] - \rho_{SC}}{1 - \rho_{SC}} \tag{12}$$

where, ρ_{SC} is the cross-sectional area ratio of longitudinal steel and R_C is radius of the rounded corners. These researchers suggested Equations (13) and (14) for the shape factor for strength (k_{S1}) and the shape factor for strain (k_{S2}):

$$k_{S1} = \left(\frac{B}{D}\right)^2 \frac{A_e}{A_C} \tag{13}$$

$$k_{S2} = \left(\frac{D}{B}\right)^{0.5} \frac{A_e}{A_C} \tag{14}$$

where most of the parameters are the same as previous equations and A_e is the area of the effectively confined concrete and A_C is the total area of concrete enclosed by the FRP jacket.

10. PUSHOVER ANALYSIS

As mentioned before, the models were analyzed using SAP2000 [10], which is a general-purpose structural analysis program for static and dynamic analyses of structures. For nonlinear analysis of initial models, axial force–moment hinges and pure moment hinges are assigned to the ends of beams and columns, respectively. Rupture strains and rotations of plastic hinges could be evaluated using the stated nonlinear static criteria in [1-3].

The moment-rotation relationships of plastic hinges are similar to the moment-rotation relationship of moment hinges except that they are compatible with the moment-axial load interaction curves. The moment-axial load interaction curves of columns Figures could be determined using principal theories. Effect of FRP confinement on increase of strength and ductility of the columns could be concerned in interaction curves. Figure 6 shows an example of the moment-axial load interaction curves for a rectangular column with dimensions of 40×40 *cm*.

For performing a pushover analysis, two kinds of load distributions are utilized in this study:

a) Distribution type *I*; distribution is proportional to the lateral loads that have been calculated from a linear spectral dynamic analysis.
b) Distribution type *II*; distribution is uniform where the lateral loads are proportional to the weight of each story.

For better clarifying the results, which are presented in Table 2, Figure 7 shows the base shear-top displacement relationship for the non-retrofitted frame (labeled as ‘‘initial’’) and the retrofitted frame (labeled as ‘‘final’’). It is evident from Figures and tables that confinement of reinforced concrete columns with FRP fibers would increase their strength and ductility by 19 and 38 percents respectively. Therefore, this method could be considered as a major way for enhancing seismic performance of concrete structures.

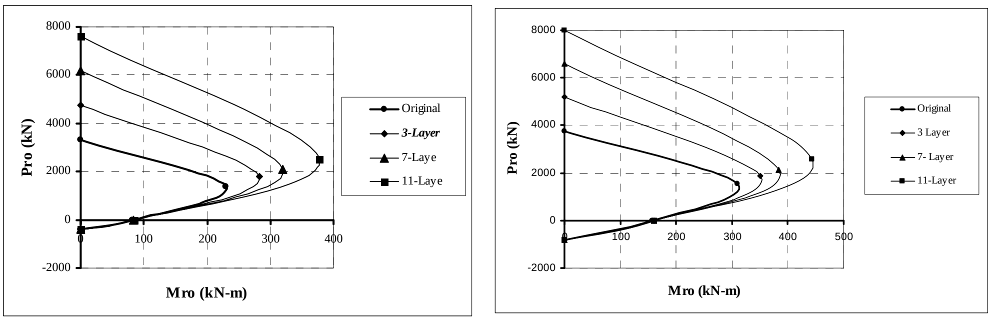

(a) (b)

Figure 6. The moment-axial load interaction curves for a rectangular FRP-confined columns with dimensions of 40×40 cm for (a) ρ_l=1% and (b) ρ_l=2%

In Table (2) effective parameters such as ductility factor (R_μ), overstrength factor (R_S) and safety factor (Y) were obtained for evaluating the reduction factor. Using these values and by means of Eq. (8) the reduction factor of RC buildings could be calculated.

Table 2: Different parameters of reduction factor for models

Model	Design	Yield		Ultimate		μ	R_μ	R_s	Y	R_w
	V_w, ton	V_y, ton	Δ_y, cm	V_u, ton	Δ_u, cm					
4S-O-1*	66.7	198.9	7.9	217.4	13.2	1.7	1.7	3.0	1.4	7.0
4S-R-1	66.7	214.4	8.4	247.2	19.2	2.3	2.3	3.2	1.4	10.3
4S-O-2	66.7	212.3	6.7	235.9	10.4	1.6	1.6	3.2	1.4	7.0
4S-R-2	66.7	233.3	7.3	271.1	15.7	2.2	2.2	3.5	1.4	10.6
7S-O-1	168.7	480.2	19.0	529.0	28.8	1.5	1.5	2.8	1.4	6.1
7S-R-1	168.7	533.7	18.3	629.9	42.7	2.3	2.3	3.2	1.4	10.3
7S-O-2	168.7	582.3	14.0	640.9	19.1	1.4	1.4	3.5	1.4	6.6
7S-R-2	168.7	728.1	17.5	842.5	32.9	1.9	1.9	4.3	1.4	11.4
10S-O-1	334.1	1080.0	30.0	1173.2	43.3	1.4	1.4	3.2	1.4	6.5
10S-R-1	334.1	1161.1	32.0	1334.3	67.0	2.1	2.1	3.5	1.4	10.2
10S-O-2	334.1	1217.1	24.0	1301.1	32.5	1.4	1.4	3.6	1.4	6.9
10S-R-2	334.1	1318.8	26.0	1549.8	43.1	1.7	1.7	3.9	1.4	9.2

***Note: Model identification is "number of story – non retrofit (O) / retrofit (R) – lateral load type."**

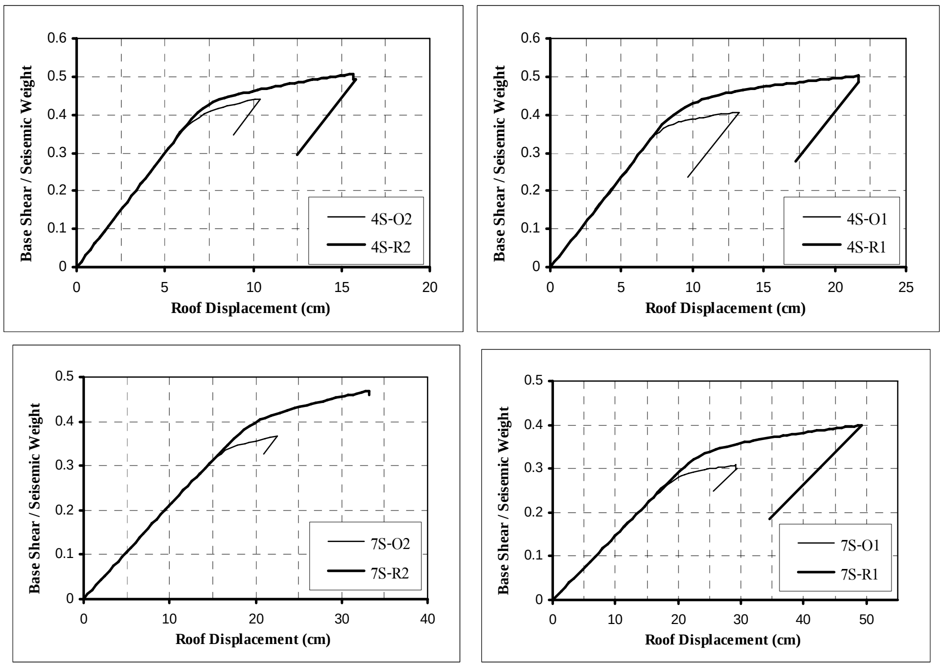

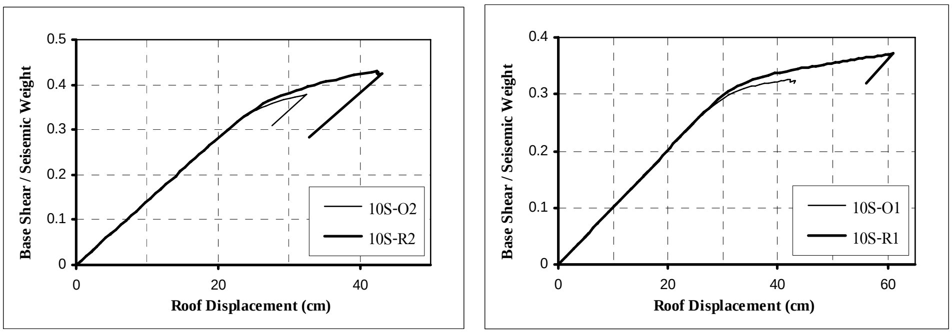

Figure 7. Comparison of capacity curves of a 4-story frame, 7-story frame and 10-story buildings

In Table 3, reduction factor values for each of the models under both lateral load distributions are represented. As it is apparent, average of reduction factor value for non-retrofitted reinforced concrete buildings is 6.7 and is 9.9 for retrofitted RC buildings.

Table 3: The reduction factor for non-retrofitted and retrofitted models

Story	Non-retrofitted		Retrofitted	
	Lateral Load Type *I*	Lateral Load Type *II*	Lateral Load Type *I*	Lateral Load Type *II*
4	7.1	7.0	10.3	10.6
7	6.1	6.5	10.1	9.7
10	6.5	6.9	9.3	9.2
Average	6.7		9.9	

11. CONCLUSIONS

The results derived from the nonlinear static analyses of initial models, which were desi In Table 3, reduction factor values for each of the models under both lateral load distributions are represented. As it is apparent, average of reduction factor value for non-retrofitted reinforced concrete buildings is 6.7 and is 9.9 for retrofitted RC buildings.

based on [7], are stated as below:

1. Confinement of reinforced concrete columns would increase their strength and ductility by 19 and 38 percents, respectively.
2. Reduction factor of a non-retrofitted reinforced concrete building without shear walls is evaluated to be 6.7 but with confinement of columns with CFRP jacket, this factor would increase to 9.9.
3. Application of CFRP fibers for confinement of reinforced concrete columns would increase their resistance, ductility and capacity of seismic energy dissipation. Moreover, it would move the failure point from columns to beams.

REFERENCES

1. IIEES, International Institute of Earthquake Engineering & Seismology, (2002), "Guideline for seismic retrofitting current buildings" (In Persian).
2. ATC-40, (1996), "Seismic evaluation and retrofit of concrete buildings", Applied Technology Council.
3. FEMA-356, (2000), "Prestandard and commentary for the Seismic rehabilitation of buildings", Federal Emergency Management Agency.
4. Nassar, A., Osteraas, J. and Krawinkler, H. (1992), "Seismic design based on strength and ductility demands", Proceding of the Earthquake Engineering Tenth World Confrence, Balkema, Roterdam, pp.5861-5866.
5. Miranda, E. and Bertero, V.V., (1994), "Evaluation of strength reduction factors for earthquake resistant design", Earthquake Spectra, Vol.10, 357-379.
6. Fajfer, P., Eeri, M., (2000), "A Nonlinear Analysis Metod for Performance Based Seismic Design", Erthquake Spectra, Vol.16, No.3, pp.573-592.
7. Iranian Code of Practice for Seismic Resistant Design of Buildings [2005], Standard No. 2800, Third Revision, Building & Housing Research Center, Iran (In Persian).
8. ACI-318, (1999), "Building code requirements for structural concrete and commentary. American Concrete Institute", Fifth Printing, Farmington Hills, Michigan, USA.
9. Uang, C. and Maarouf, A., (1994), "Deflection amplification factor for seismic design provision", Journal Structural Engineering, pp. 2423-2436.
10. Computer & Structures Inc., (2005), "SAP 2000, analysis program", Berkeley, California.
11. Berthet, J.F., Ferrier, E. and Hamelin, P., (2005) "Compressive behavior of concrete externally confined by composite jackets", Construction and Building Materials.
12. Lam, L. and Teng, J.G., (2003), "Design-oriented stress-strain model for FRP confined concrete in rectangular columns", J Reinf Plast Compos.
13. Zou, X.K., Teng, J.G., De Lorenzis, L. and Xia, S.H., (2007), "Optimal performance based design of FRP jackets for seismic retrofit of reinforced concrete frames", Composites, Part B.

CD02-022

CONCRETE SHEARE WALLS STRENGTHENING STRUCTURAL ELEMENTS FOR SEISMIC REHABILITATION OF MASONRY BUILDINGS

A. Moslehi Tabar[1], M. Ansari[2]
[1]Assistant Professor, Dept. of Civil Engineering, Tafresh University, Tafresh, Iran
[2]M.Sc Student, School of Civil Engineering, University of Tehran, Tehran, Iran

ABSTRACT

This paper aims at investigating the behavior of masonry buildings strengthened with concrete shear walls. To this end, a masonry wall with openings extracted from an individual two-storey masonry building is modeled using ANSYS finite element software. A number of nonlinear static analyses were conducted on the model. The nonlinear behavior of the existing model was compared with that of the model enhanced with concrete shear wall. The results obtained from the numerical analyses confirm that the load-carrying capacity of the unreinforced masonry buildings degrades due to the global failure of the wall. Whereas, the masonry buildings strengthened with concrete shear wall may achieve their target displacement. Moreover, the results reveal that the wall load-carrying capacity may be upgraded, if the added shear wall is connected to both the diaphragm and adjacent masonry wall.

Keywords: rehabilitation, masonry building, concrete shear wall, push-over analysis

1. INTRODUCTION

The masonry buildings have extensively been constructed in Iran for low-rise buildings, because of their cost-effectiveness. Most of them have been designed regardless of the effect of earthquake induced loads. In other words, these kinds of buildings are non-engineered structures which may be susceptible to a significant risk during an earthquake.

Among the points of weakness associated with the masonry buildings, the lack of appropriate tying system, improper masonry elements, large openings, etc. are note worthy.

Since many of the important buildings such as schools are structured with unreinforced masonry buildings, it is necessary to rehabilitate those using proper solutions.

One of the methods used for seismic rehabilitation of masonry buildings is known as simple rehabilitation method [1]. In this method, the building weaknesses are retrofitted one by one. Another method is coating a reinforced concrete layer on the masonry walls. By using this method, the lateral load-carrying capacity of structure is enhanced. In the above-mentioned methods providing integrity for the

diaphragm is mandatory.
Among the other methods used for rehabilitation of masonry buildings, the use of an external lateral resisting system is noteworthy. In this method, the lateral load-carrying capacity of the structure is mainly provided with the added lateral resisting elements.
Another method that can be used is structure of an exposed lateral seismic load-carrying system. For this purpose, a concrete shear wall, well known as an effective lateral resisting system, can be used. Providing appropriate integrity among the added shear walls, the existing masonry walls and the diaphragm is a key concern in this method. The mobilization of induced actions among these elements is another concern.

2. CASE STUDY

In this study, an existing two-storey masonry building with an area of 829 m^2 is investigated (see Figure 1).

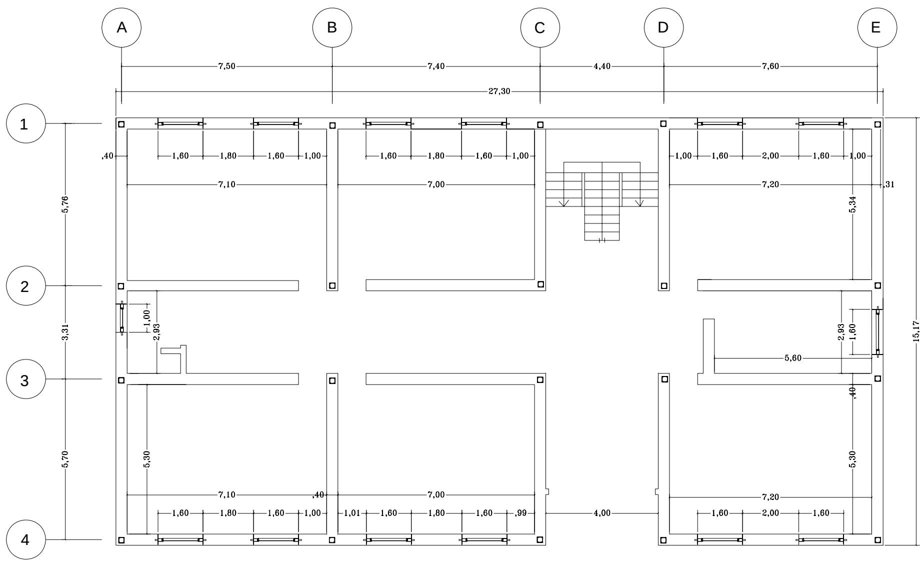

Figure 1. Typical floor plan

In order to assess the structural system of the building, a set of destructive and non-destructive inspection program was prescribed. This inspection program indicated that the building possesses unreinforced masonry system, having some rawbacks, including:

a. Inappropriate tying system
b. Improper bricking
c. Lack of diaphragm integrity

The above drawbacks cause the building to be a seismic vulnerable structural system. Several methods were investigated for seismic rehabilitation of the building [2]. The methods were compared with each other regarding the technical and economical aspects. Among them, the method of adding concrete shear wall was assessed as the best solution. According to the initial studies, four L-shape shear walls were provided as shown in Figure 2.

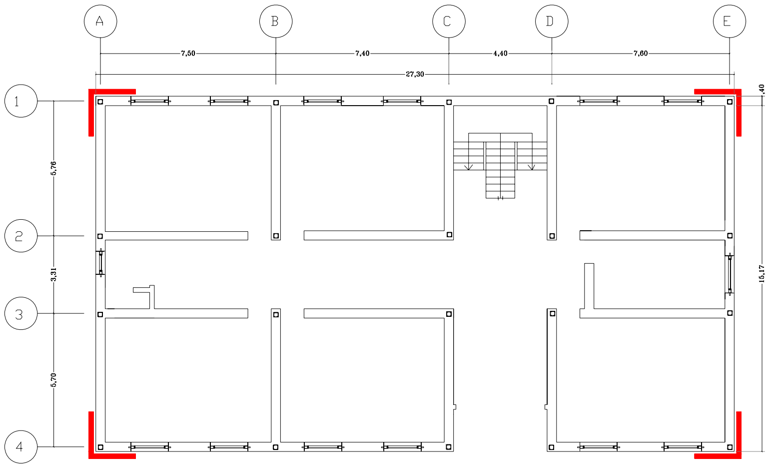

Figure 2. Concrete shear walls position

In order to study the effect of adding concrete shear wall on lateral behavior of the masonry building, the nonlinear behavior of one of the perimeter axis (Axe1) was evaluated using ANSYS finite element software. The lateral behavior of this axis was studied in its existing situation as well as in presence of concrete shear walls. Since the number of shear walls is limited, the diaphragm rigidity should be provided. The diaphragm rigidity conditions may be satisfied using such details as shown in Figure 3.

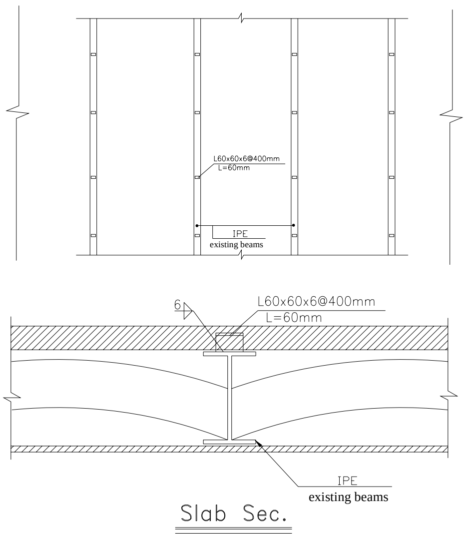

Figure 3. Details for providing diaphragm rigidity

Since the gross mass of the masonry buildings has mainly arisen from the masonry walls, two details were utilized to connect the concrete shear walls to the building: Firstly, connecting the shear walls to both the diaphragm and masonry walls of the building; secondly, connecting the shear walls to the diaphragm, only. In essence, in first detailing, the lateral force is transmitted to the shear walls through the diaphragm while both the diaphragm and masonry walls contribute to the transition of lateral forces to the shear walls. The proposed details for connection of the concrete shear walls to the diaphragms and to the adjacent masonry walls are illustrated in Figures 4 and 5, respectively. Also the details shown in Figure 6 were proposed for transferring the lateral forces from shear wall to the earth.

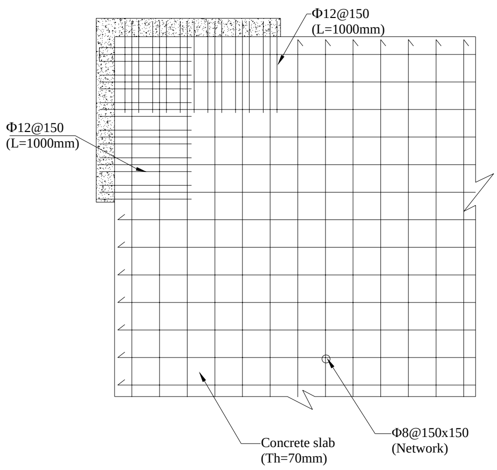

Figure 4. Shear wall-to-diaphragm connection

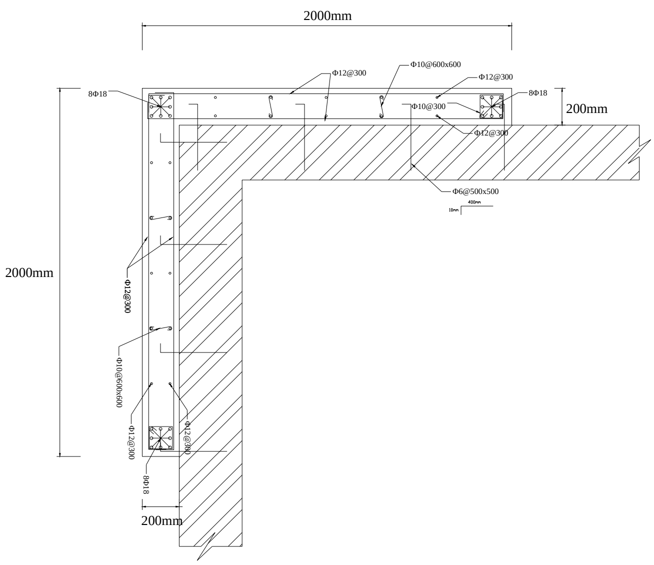

Figure 5. Proposed details to connect concrete shear wall to masonry one

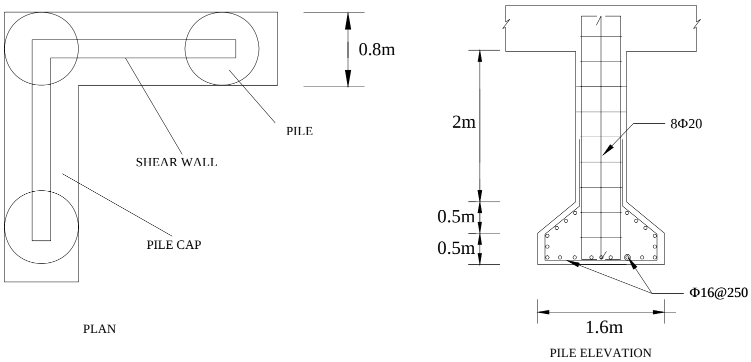

Figure 6. Proposed details for shear wall foundation

3. FAILURE MECHANISM AND MATERIAL MODELS FOR UNREINFORCED MASONRY STRUCTURES

Masonry wall is a composite structure that consists of brick and mortar. The geometry, axial loading and material properties, play an essential role in the response of the wall and in the mechanism of failure. Figure 7 shows different in-plane failure modes for masonry walls.

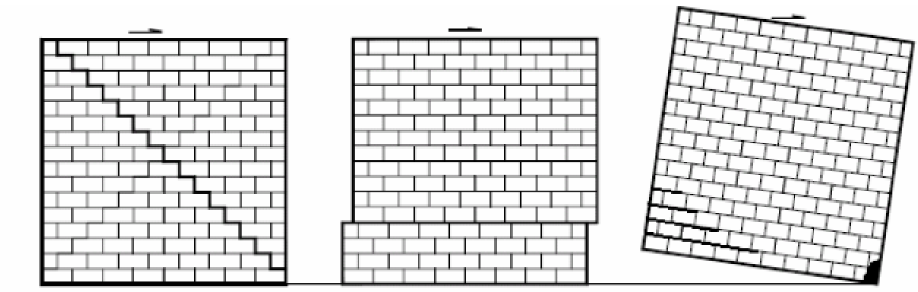

a) Shear failure [5]. b) Sliding failure [5] c) Rocking failure [5]

Figure 7. In-plane failure mechanisms in masonry walls

Several researchers have proposed failure criteria for masonry material. Page [7] suggested a microscopic finite element model for masonry, considering elastic elements for bricks and link elements for joints. Although this model could present global nonlinear behavior of masonry walls and crack distribution, it failed to express the failure in bricks and the effect of multi axial stresses on the response. Ganz [8] also presented a failure criterion for masonry under biaxial compressive stresses, neglecting the tensile strength.

William and Warkne [9] developed a constitutive model for tri-axial behavior of brittle materials like concrete. The model considers multi axial stresses of brittle material and takes into account cracking, crushing and sliding phenomena by reflecting their effects on the stiffness matrix [4, 9].

The general form of William and Warkne's theory has been used here. The above model as has been developed in ANSYS, has also been recommended by [3] for masonry material. In another study, Kumar and Bhandari adopted a similar model for masonry arches [10].

4. MODELING

As previously mentioned, to study the behavior of masonry building strengthened with concrete shear wall, a typical perimeter axis (Axe 1) is employed. Nonlinear static analysis was carried out using ANSYS finite element software. Nonlinear material was assigned to the masonry and concrete elements. To this end, William-Warkne failure criterion was employed for materials. The element SOLID65 was used to model masonry and concrete walls. This element has capability to idealize brittle materials for cracking and crushing phenomenon. The element SHELL63 was applied for the modeling of horizontal and vertical ties. Figure 8 shows a scheme of the model.

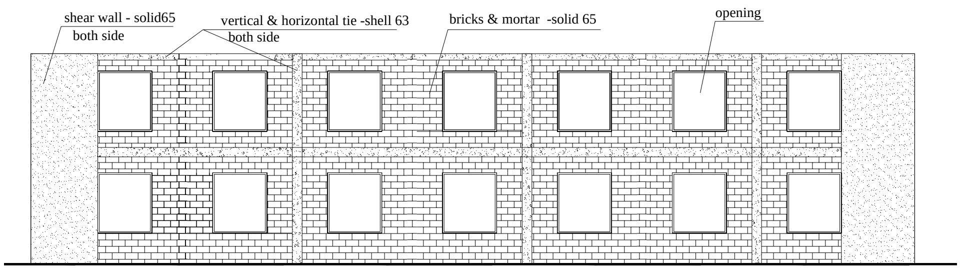

Figure 8. A scheme of the model

The mechanical properties of the brick and mortar employed in the building were obtained according to the test results. The test results are summarized in Table 1.

Table 1. Specifications of the existing masonry walls

f_{cb}	f'_{cb}	V_t	V_s
MPa	MPa	MPa	MPa
10	1.2	0.18	0.095

In the above table:

f_{cb} : *compressive strength of bricks*

f'_{cb} : *compressive strength of masonry walls*

V_t : *allowable tension stress*

V_s : *allowable shear stress*

5. ANALYSIS PROCEDURE

In order to identify the nonlinear behavior of the building, a nonlinear static analysis, well known as Push-over analysis, was conducted on the model. Since the height to length ratio of the wall is low, the first deformation pattern which is well adapted to the first mode of vibration was applied to the model. For this purpose a prescribed displacement was applied to top of the building.

The target displacement was obtained according to FEMA 356. In the following, the target displacement is calculated for the model with and without strengthening elements:

a. Existing masonry wall:

$$T = \frac{2\pi}{\sqrt{k/m}} = \frac{2\pi}{\sqrt{30000/16}} = 0.145\sec$$

$$\delta_t = C_0 C_1 C_2 C_3 S_a \frac{T^2}{4\pi^2} g = 1.2x1x1.1x1x(0.3x2.5)x\frac{0.145^2}{4\pi^2} x9.81 = 0.005m$$

b. Strengthened masonry wall:

$$T = \frac{2\pi}{\sqrt{k/m}} = \frac{2\pi}{\sqrt{50000/16}} = 0.112\sec$$

$$\delta_t = C_0 C_1 C_2 C_3 S_a \frac{T^2}{4\pi^2} g = 1.2x1x1.1x1x(0.3x2.5)x\frac{0.112^2}{4\pi^2} x9.81 = 0.003m$$

The parameters k and m denote the wall stiffness and the wall mass, respectively. The wall stiffness was estimated from the initial linear analysis.

6. ANALYSIS RESULTS

The crack pattern shown in Figure 9 illustrates that under a 5-mm target displacement, a major failure had taken place in the existing masonry wall. While in the strengthened masonry wall, the minor cracks are localized round the openings under its target displacement (Figure 10).

The in-plane shearing stress contour shown in Figure 11 indicates that the applied acts are localized mostly within the concrete shear walls, and the shearing stress is nearly uniform within the masonry elements. The maximum shearing stress applied to the masonry element in the strengthened wall is, approximately, half of that in the existing wall.

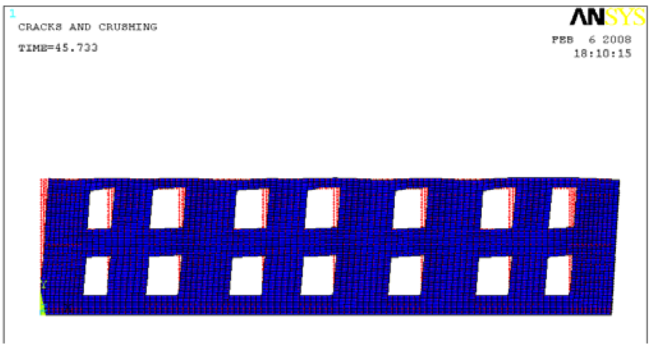

Figure 9. Crack pattern in the existing masonry wall

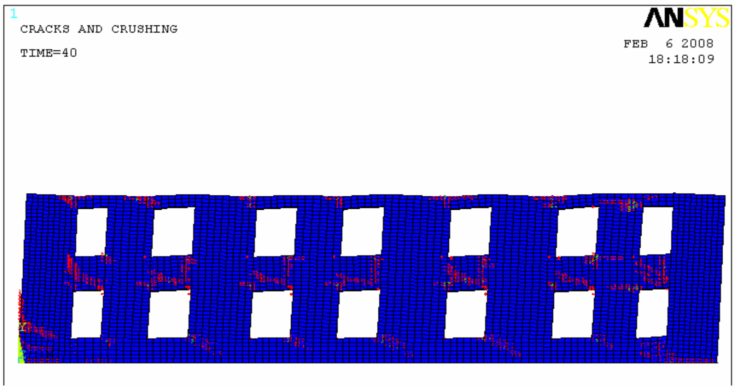

Figure 10. Crack pattern in the strengthened masonry wall

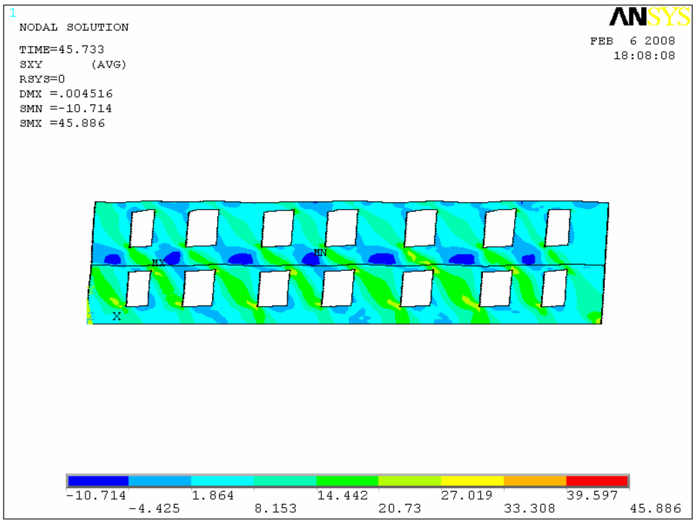

Figure 11. In-plane shearing stress contour in the existing masonry wall

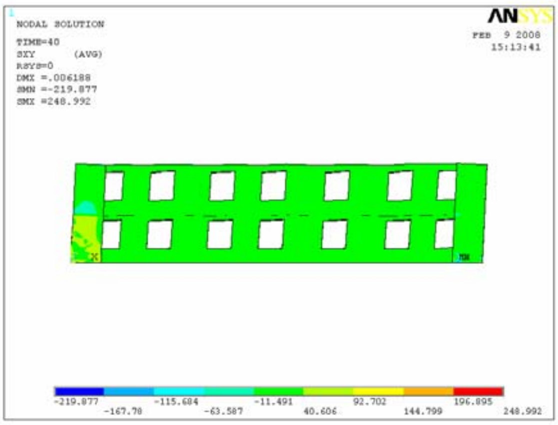

Figure 12. In-plane shearing stress contour in the strengthened masonry wall

In Figure 13, the base shear is depicted versus the top displacement for all the models. As observed, the strengthened masonry models show more stiffness and strength in comparison with the existing model. Furthermore, as previously noted, the added shear walls are more efficient if connected to both the diaphragms and masonry walls. In essence, as the added shear walls are attached to the diaphragms only, a significant promotion is not achieved. This is due to the considerable mass of the walls in the masonry buildings. In case of connecting shear walls to both the diaphragms and masonry walls, the lateral strength and initial stiffness is increased by 50% and 100%, respectively.

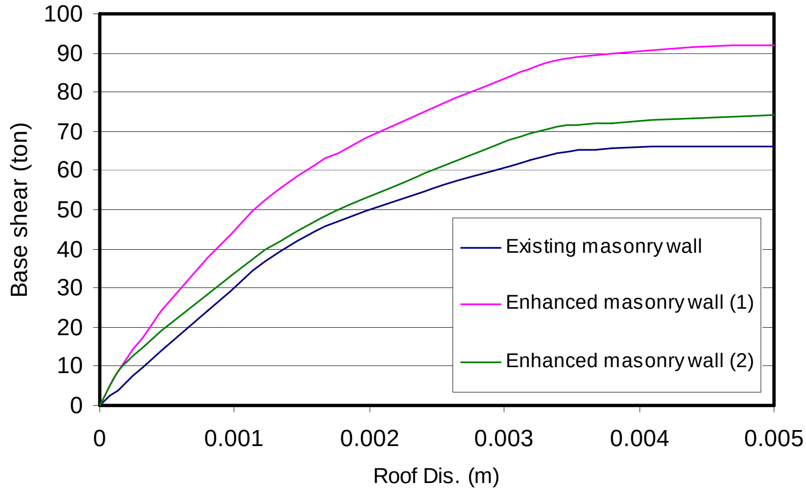

(1) Shear wall connected to both diaphragm and adjacent masonry wall
(2) Shear wall connected to diaphragm only

Figure 13. Base shear versus roof displacement

7. CONCLUSION

This paper dealt with one of the efficient methods for seismic rehabilitation of masonry buildings. Through the nonlinear analyses performed using ANSYS finite element software, it was confirmed that the lateral behavior of masonry buildings may be promoted by providing concrete shear walls. According to the numerical results, the added concrete shear walls become much more efficient if connected to both the diaphragms and adjacent masonry walls. The analysis results indicate the load-carrying capacity of the existing masonry walls is thoroughly deteriorated due to the major cracks. While, in the strengthened masonry walls the cracks are minor and localized round the openings. In addition, the concrete shear walls and masonry ones can contribute to the lateral forces, resulting in reduction of shear demand on the masonry walls. Also, in case of connecting shear walls to both the diaphragms and masonry walls the lateral strength and initial stiffness is increased by 50% and 100%, respectively.

REFERENCES

1. FEMA 356 Seismic rehabilitation prestandard, Federal Emergency

Management Agency.; 2002.
2. Moslehi Tabar A, Ansari M, Seismic Rehabilitation of School Buildings, Report No. S-87-12, Permayon Advanced Strengthening Co., Tehran, 2008 (in Persian).
3. Gambarotta L. Lagomarsino S. Damage models for the seismic response of brick masonry shear walls. PartII: The continuum model and its applications. Earthquake Engineering and Structural Dynamic 1997; 26:441-462.
4. ANSYS. Release 5.4, ANSYS Manual Set, 1996, ANSYS Inc., Southpoint, 275 Technology Drive,Canonsburg, PA 15317, USA.
5. ElGawady M. Seismic in-plane behavior of URM walls upgraded with composites. A Thesis for theDegree of PHD, EPFL, Laussane, Switzerland, 2004.
6. Laursen PT, Lngham JM. Structural testing of large-scale post-tensioned concrete masonry walls. Journal of Structural Engineering ASCE; Oct 2004:1497-1505.
7. Ali S. Page A. Finite element model for masonry subjected to concentrated loads. Journal of Structural Engineering. ACSE 1988; 114(8):1761-1784.
8. Ganz HR, Thürlimann B. Versuche an Mauerwerksscheiben mit Normalkraft und Querkraft (Test of masonry walls under axial and shear forces). IBK Bericht Nr. 7502-4. Institut für Baustatik und Konstruktion. ETH Zürich, 1984.
9. William KJ, Warkne EP. Constitutive model for the tri-axial behaviour of concrete, Proceeding of the International Association for Bridge and Structural Engineering 1995, 19, ISMES, Bergamo, Italy, 1995.
10. Kumar P, Bhandari NM. Non-linear finite element analysis of masonry arches for prediction of collapse load. Structural Engineering International 3/2005:166-174.

CD02-023

F.E MODELING OF NORMAL AND SELF-CONSOLIDATING RC BEAMS AND EXPERIMENTAL BENDING BEHAVIOR OF SCC BEAMS

A.A. Maghsoudi[1], E. Hosseini Mehrab [2]
[1]Associate Professor, Civil Engineering Dept., Kerman University, Iran
[2]M.Sc. Student, Civil Engineering Dept., Kerman University, Iran

ABSTRACT
Development of a new generation of concrete, self-consolidating concrete, SCC is a very desirable achievement in the RC structures for overcoming problems associated with many problems such as congestions of steal reinforcement. This non-vibrating concrete is not affected by the skill of workers, and shape and amount of reinforcing bar arrangement of a structure. Due to high-fluidity and resisting power of reinforcing of SCC, it can be pumped longer distances. In this research, the finite element, F.E modeling of four normal concrete (vibrating concrete), NC and SCC beams in bending is performed and the results are compared together. For the experimental phase, the results of available tested beams of dimensions 20 cm width, 30 cm height and 300 cm length are used. For modeling longitudinal steel bars and concrete, the 2-node and 8-node 3-D elements, are used respectively. The 8-node element has ability to consider cracking in tension and concrete crushing in compression. The deflection, cracking, yield and ultimate loads, as well as beams ductility are compared numerically and experimentally. The comparison of results obtained by two methods indicates that a satisfactory agreement is achieved.

Keywords: self-consolidating and normal concrete, bending behavior, finite element modeling

1. INTRODUCTION
Concrete structural components require the understanding of the responses of those components to a variety of loading. There are a number of methods for modeling the concrete structures through both analytical and numerical approaches. Finite element analysis (FEA) is a numerical one widely applied to the concrete structures based on the use of the nonlinear behavior of materials. FEA provides a tool that can simulate and predict the responses of reinforced concrete members. The use of FEA has increased because of progressing knowledge and capability of computer package and hardware. Any attempts for engineering analyses can be done conveniently and fast using such versatile FEA packages.
Self-consolidating concrete (non vibrating concrete), SCC is a new type of concrete that is able to flow and compact under its own weight and completely fill the formwork even in the presence of dense reinforcement, whilst maintaining

homogeneity and without the need for any additional compaction. This has generated tremendous interest since the initial development in Japan by Okamura [1] in the 1980s in order to reach durable concrete structures. Since that time, Japanese contractors have used SCC in different applications. In contrast with Japan, research in Europe, America and Iran started only recently [2, 3]. The advantages of SCC over normal concrete (vibrating concrete), is that NC offers many benefits to the construction practice; the elimination of the compaction work results in reduced costs of placement, equipment needed on construction, time and improved quality control [4]. Therefore, a comparison of these two types of concrete, i.e. NC and SCC in bending can be interesting, especially for practical engineers.

2. MATERIALS PROPERTIES MODELING

2.1. Reinforced Concrete

An eight-node solid element, solid65, was used to model the concrete. The solid element has eight nodes with three degrees of freedom at each node-translation in the nodal x, y, and z directions. The element is capable of plastic information, cracking in three orthogonal directions, and crushing [5]. The geometry and node locations for this element type are shown in Figure 1.

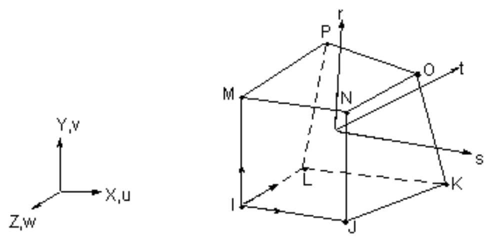

Figure 1. Solid65-3-D reinforced concrete solid [6]

2.1.1. Concrete Mechanical Properties

2.1.1.1. Self-Consolidating Concrete

Development of a model for the behaviour of concrete is a challenging task. Concrete is known as a quasi-brittle material and has a different behaviour in compression and tension. In this research, the graph of nonlinear-isotropic stress-strain of SCC is obtained by the first author from results of compression test of concrete specimens in the laboratory with the help of embedded sensor (Figure 2).

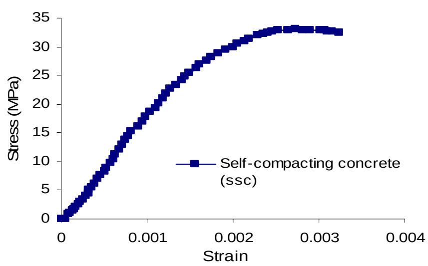

Figure 2. Self-consolidating concrete stress-strain diagram

2.1.1.2. Normal Concrete

For NC, Saenz-Smith relationship has been used to introduce stress-strain diagram, science convergence plays the main role. Therefore, ascending branch of stress-strain curve of Saenz relationship [7] and for descending branch, Smith and Young relationship [8] have been used (Figure 3).

$$f_c = \frac{E_0 \varepsilon_c}{1 + \left(\frac{E_0}{E_{sc}} - 2\right)\left(\frac{\varepsilon_c}{\varepsilon_c'}\right) + \left(\frac{\varepsilon_c}{\varepsilon_c'}\right)^2} \tag{1}$$

$$f_c = f_c'\left(\frac{\varepsilon_c}{\varepsilon_c'}\right)\exp\left(1 - \frac{\varepsilon_c}{\varepsilon_c'}\right) \tag{2}$$

$$E_{sc} = f'_c / \varepsilon'_c, \text{ (MPa)}$$

Eq.s (1,2), represent the relations between f'_c, ε'_c, E_0 and E_{sc}, which can be found from stress-strain curve and in this paper, the ascending and descending branches of curve have been acquired of equations (1) and (2), respectively.

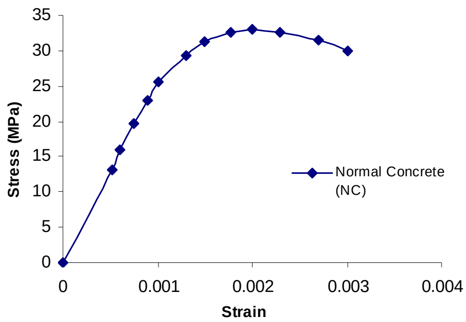

Figure 3: Normal concrete stress-strain diagram

2.1.2. Steel Reinforcement

A link8 element was used to model the steel reinforcement. Two nodes are required for this element. Each node has three degrees of freedom, translations in the nodal x, y, and z directions. The element is also capable of carrying plastic deformation. The geometry and node locations for this element type are shown in Figure 4.

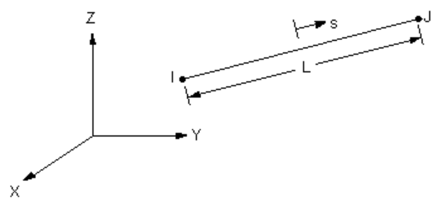

Figure 4. Link8 3-D spar [6]

Here, the stress-strain curve for steel reinforcement used in SCC beams was obtained from steel bars tested in tension. The curve has an initial linear elastic portion, a yield plateau (yield point beyond which the strain increases with little or no increase in stress), a strain-hardening range in which stress again increases with strain and finally a range in which the stress drops off until fracture occurs which has been shown in Figure 5. The following relationships used in this study are those obtained by testing the bars in tension and the stress-strain curve for steel reinforcement has the following characteristics:

1: elastic portion; $\varepsilon_s < \varepsilon_y \Rightarrow f_s = E_s\, \varepsilon_s$ (3)

2: yield plateau; $\varepsilon_y \le \varepsilon_s \le \varepsilon_{sh} \Rightarrow f_s = f_y$ (4)

3: strain hardening;

$$\varepsilon_{sh} < \varepsilon_s \le \varepsilon_u \quad f_s = f_y + \left(f_u - f_y\right)\left[2\frac{\varepsilon_s - \varepsilon_{sh}}{\varepsilon_u - \varepsilon_{sh}} - \left(\frac{\varepsilon_s - \varepsilon_{sh}}{\varepsilon_u - \varepsilon_{sh}}\right)^2\right] \tag{5}$$

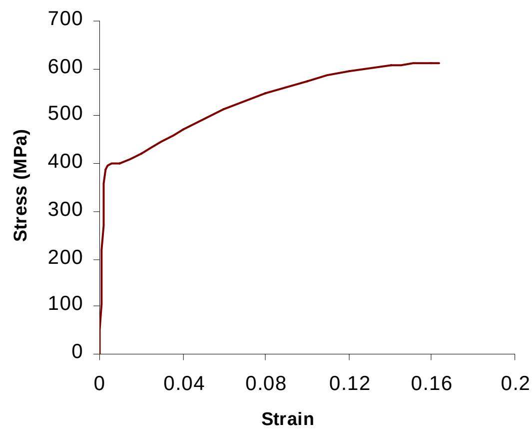

Figure 5. Stress-strain diagram of tested tensile steel

Material properties for the steel reinforcement (ε_y, ε_{sh}, ε_u, f_y, f_u) and concrete (f'_c, ε'_c) are obtained (Figures 2, 3, 5).

3. FINITE ELEMENT MODELING

As an initial step, a FEA requires meshing of the model. In other words, an important step in FE modelling is the selection of the mesh density. A convergence of results for steel reinforcement and concrete is obtained when an adequate number of elements are used in the model; this is practically achieved when an increase in the mesh density has a negligible effect on results. The ANSYS software has been performed and the results are shown in Figures 6, 7.

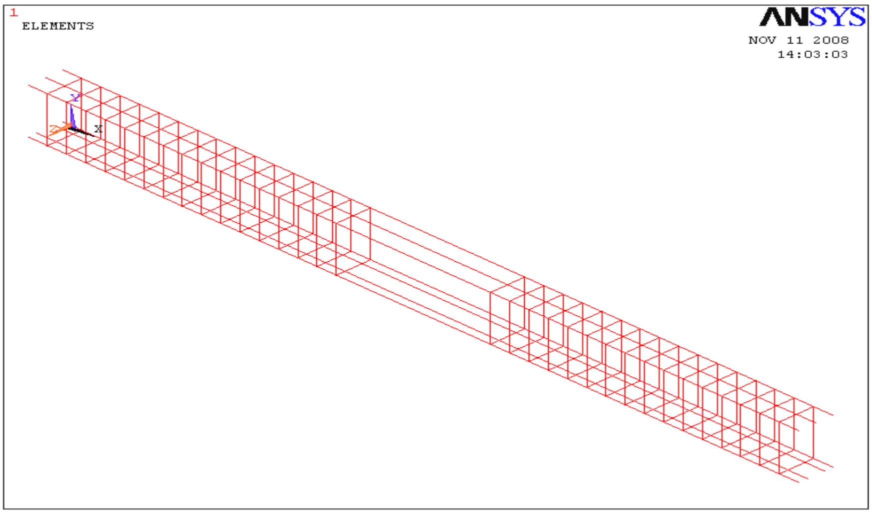

Figure 6. Finite element model of steel

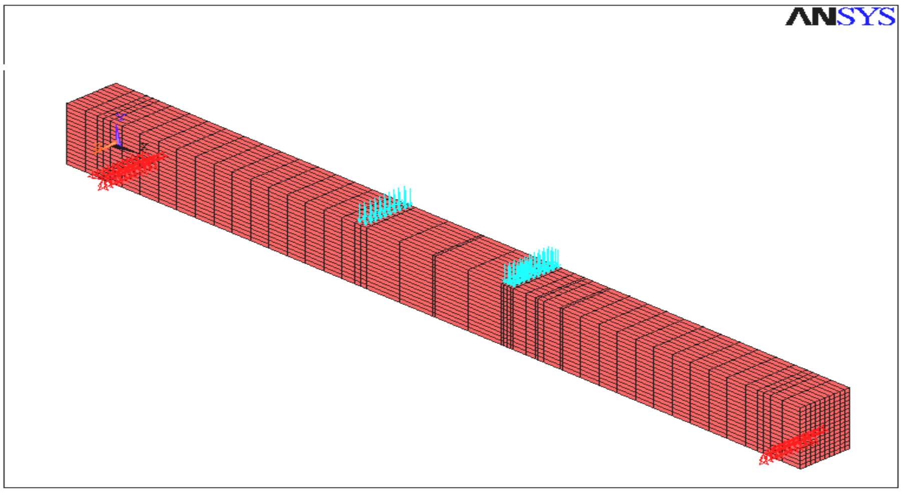

Figure 7. Finite element model of concrete

4. BEAMS PROPERTIES

Four simply supported reinforced SCC beams (SCCB1-SCCB4) with 300*200 dimension and 3000mm length were tested [9] under two point loading (statistical increasing) with a constant moment region (Figure 8). All beams were designed for the shear span to depth ratio of 3.5. The clear cover for the tested beams was maintained at a minimum of 25mm. Different types of electrical and mechanical strain gauges were attached on the steel bars and concrete surface by the first author. Also, the LVDTs were placed at different locations of beams. During the test, the readings of these sensors were recorded by the data logger.

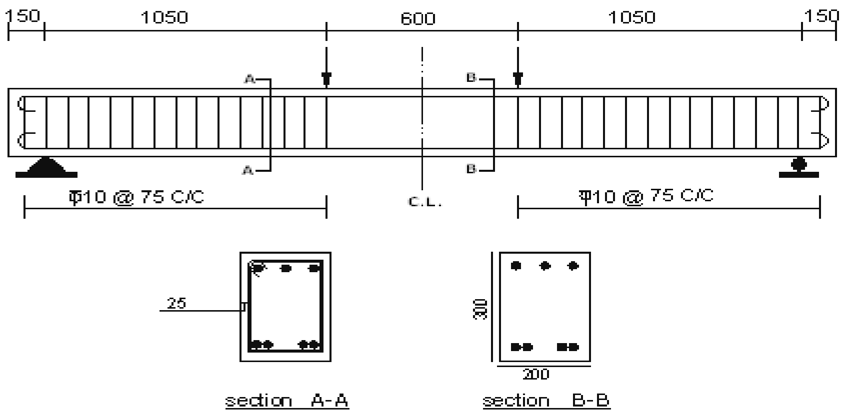

Figure 8. Details of tested beams

The beams details are presented in Table 1. The typical test set up for the tested SCC beams is shown in Figure 9.

Table 1: Details of testing program of tested beams [9]

Beam No.	f'_c (MPa)	d (mm)	d′ (mm)	A_s	ρ/ρ_b	A'_s	(KN/m^3) γ_C
SCCB1	33.0	256	42.9	2Φ18+1Φ16+1Φ14	0.511	2Φ14+1Φ18	22.80
SCCB2	31.5	255	43.5	4Φ20	0.746	2Φ14+1Φ20	23.03
SCCB3	35.0	254	45.4	4Φ22	0.91	2Φ14+1Φ25	22.60
SCCB4	25.0	*251*	42.0	4Φ28	1.48	2Φ14	22.30

Figure 9. Typical test set up for loading arrangement [9]

The SCC mix was designed by the first author and the range of fresh properties is summarized in Table 2. It was found that the SCC was consolidated exceptionally well under its own weight for four specimens.

Table 2: Test results of fresh concrete

L-box		V-funnel	J-ring		Slump flow
h_1/h_2	t (sec)	t (sec)	h_2-h_1 (mm)	D (mm)	D (mm)
0.83	0.40	7.5	13	75	76

5. COMPARISON OF RESULTS

The comparison of stress-strain diagrams of SCC and NC are shown in Figure 10.

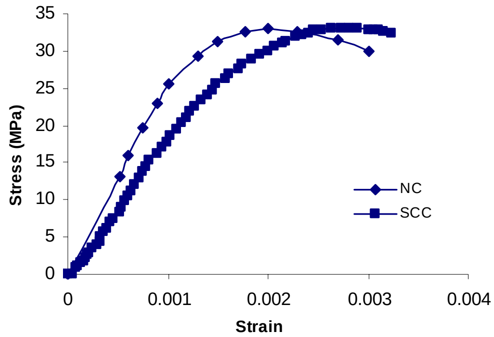

Figure 10. SCC and NC concrete stress-strain diagram

The numerical and experimental deflections are compared for two types of concrete and the results are shown in Figures 11, 12.

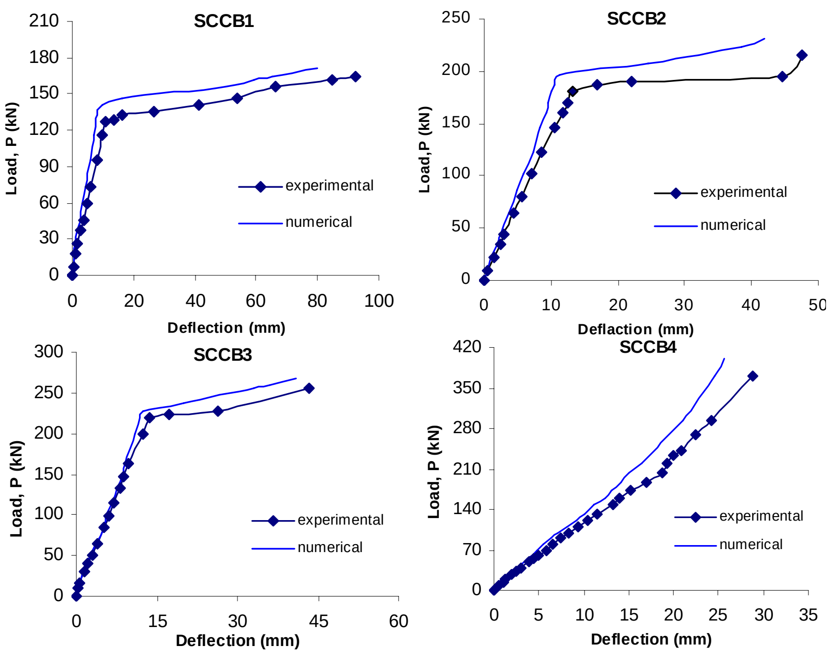

Figure 11. Load-deflection curves of experimental and numerical SCC beams

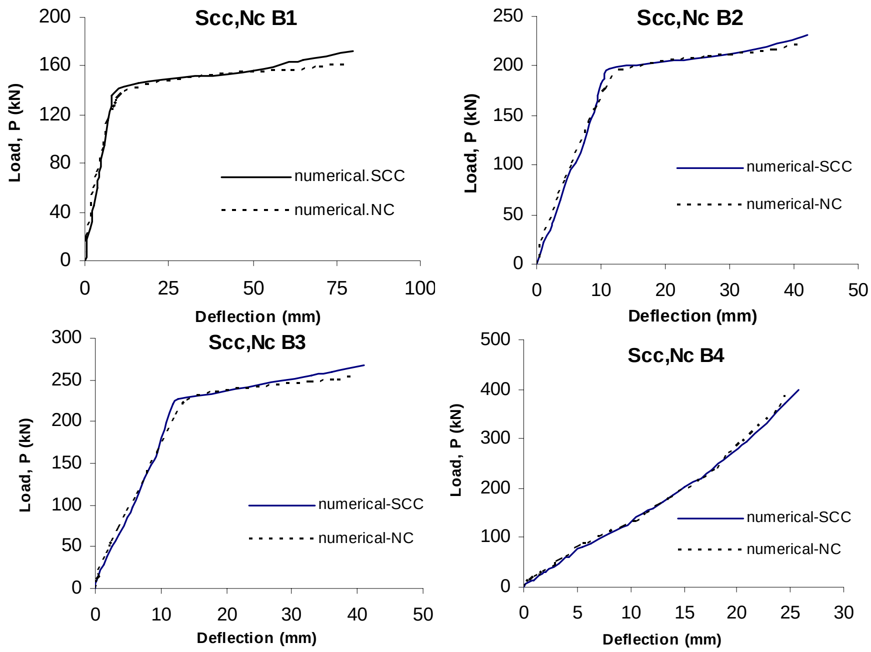

Figure 12. Load-deflection curves of F.E model of SCC and NC beams

The comparison results of deflections, ductility, cracking, yielding and ultimate loadings and F.E modeling of SCC and NC beams including the percentages of errors are presented in Tables 3-5.

Table 3: Comparison of deflections and ductility between experimental and numerical results of SCC beams

Beam No	Experimental results		Numerical Results		μ_{exp}-SCC	μ_{num}-SCC	Error for Δy (%)	Error for Δu (%)	Error for μd (%)
	Δy (mm)	Δu (mm)	Δy (mm)	Δu (mm)					
SCCB1	10.73	92.2	9.5	80	8.6	8.42	10.85	12.87	2.1
SCCB2	12.48	47.58	11.3	42	3.82	3.71	10.25	9.7	3.0
SCCB3	12.4	43.43	11.6	39	3.5	3.38	5.1	8.2	3.4
SCCB4	28.79	28.79	25.8	25.8	1	1	10.4	10.4	-

Table 4: Comparison of cracking, yielding and ultimate loads between F.E model of SCC and NC beams

Beam No.	F.E model of SCC beam			F.E model of NC beam			Error (%)		
	P_{cr} (KN)	P_y (KN)	P_u (KN)	P_{cr} (KN)	P_y (KN)	P_u (KN)	P_{cr}	P_y	P_u
B1	18.5	140	172	19.3	136.3	163	-4.3	3	5.2
B2	11	190	231	11.4	176	218	-3.6	7.3	5.6
B3	17	219	268	17.5	210	252	-2.9	4.1	6
B4	20	400	400	20.7	385	385	-3.5	4	4

Table 5: Comparison of deflections and ductility between F.E model of SCC and NC beams

Beam No	F.E model of SCC beam		F.E model of NC beam		μ num SCC	μ num NC	Error for μd (%)
	Δy (mm)	Δu (mm)	Δy (mm)	Δu (mm)			
B1	9.5	80	9.8	78.2	8.42	8	5
B2	11.3	42	11.7	40.8	3.71	3.48	7
B3	11.6	39	12.3	37.5	3.38	3.05	9.7
B4	25.8	25.8	24.2	24.2	1	1	-

6. CONCLUSIONS

The following conclusions can be drawn:

Comparison of numerical and experimental results of yield deflection (Δy), with a percentage error range of 5.1 to 10.8 is an indication of satisfactory results of F.E modelling.

Except beam SCC4 which is reinforced with a high amount of steel reinforcement, all other three tested SCC beams achieved an experimental minimum ductility index, μ_{dexp} value of 3.5. In other words this an acceptable minimum value for reinforcement of NC beams suggested in seismic regions. It is therefore, concluded that, if reinforced SCC beams are well designed in bending, it can impose sufficient ductility at ultimate loads.

In a comparison of numerical modelling of SCC and NC it was concluded that, the cracking loads in SCC beams are slightly lower than the NC beams. However, the ultimate and yielding loads of SCC beams are slightly higher than the NC beams.

The SCC beams are shown to be more ductile than the NC beams both experimentally as well as numerically.

REFERENCES

1. Okamura, H., “Self-Compacting High-Performance Concrete”, Concrete International. (July 1997), Vol.19, no. 7, pp. 50-54.
2. Skarendahl, A and Petersson, State of the Art Report of Rilem Technical Committee174-Scc, Self Compacting Concrete, O. (2001), Report No.23.
3. Maghsoudi. A. A and Arabpour Dahooei. Effect of Nanscale Materials in Engineering Properties of Performance Self Compacting Concrete, F. (2005), *7th International Conf. In Civil Eng., University of Tarbiat Modares, Tehran-Iran.*
4. Holchemacher, Klaus & Yvette klug, “A database for the Evaluation of Hardened Properties of SCC”, (2002), LACER NO.7, pp.123-134.
5. K.J., William, E.D., Warnke, “Constitutive Model for the Triaxial Behaviour of Concrete”, Proceedings of the International Association for Bridge and Structural Engineering, (1975), 19, p.174, ISMES, Bergamo, Italy.
6. ANSYS, ANSYS User’s Manual, Version 9.
7. Saenz, L.P., “Equation for the Stress-Strain Curve of Concrete in Uniaxial and

Biaxial Compression of Concrete", ACI Journal, (1965), V. 61, No. 9, pp. 1229-1235.

8. Smith, G.M., and Yaung, L.E. "Ultimate Theory in Flexure by Exponential Function", J. of Am. Concr. Inst., (1955), V. 52, No. 3, pp. 349-359.
9. Diba, S. M., "Behavior of Beams with Self-Compacting Concrete Under Flexure", A Thesis Submitted for Master of Science in Civil Engineering, Iran University of Science and Technology, (March 2007), Civil Eng., Dept., Iran, Tehran.

CD02-024

SEISMIC FINITE ELEMENT ANALYSIS OF IRREGULAR REINFORCED CONCRETE BUILDINGS IN ELEVATION

A. Mortezaei[1], S.M. Zahrai[2]
[1]Lecturer, Civil Engineering Dept., Islamic Azad university- Semnan branch, Semnan, Iran
[2]Associate Professor, Center of Excellence for Engineering and Management of Infrastructures, School of Civil Engineering, the University of Tehran, Tehran, Iran

ABSTRACT

Near field ground motions are different from ordinary ground motions in that they often contain strong coherent dynamic long period pulses and permanent ground displacements. The dynamic motions are dominated by a large long period pulse of motion that occurs on the horizontal component perpendicular to the strike of the fault, caused by rupture directivity effects. This paper addresses multistorey reinforced concrete buildings, irregular in elevation under near field earthquakes. Two twelve-story buildings with two and four large setbacks in the upper floors respectively, as well as a third one, regular in elevation, have been designed to the provisions of ACI 318-2005 for the high (DCH) and medium (DCM) ductility classes, and the same peak ground acceleration (PGA) and material characteristics. All buildings have been subjected to inelastic dynamic time-history analysis for selected input motions. The assessment of the seismic performance is based on both global and local criteria. It is concluded that irregular buildings demonstrate poor seismic performance in terms of ductility and energy dissipation capacity during severe seismic events. As expected, DCM buildings are found to be stronger and less ductile than the corresponding DCH ones.

Keywords: reinforced concrete buildings; irregularity in elevation; near field; setbacks; seismic performance; time-history analysis

1. INTRODUCTION

Recent major earthquakes (Northridge 1994, Kobe 1995, Chi -chi 1999 and Bam 2003, etc.) have shown that many near-fault ground motions possess prominent acceleration pulses. Some of the prominent ground acceleration pulses are related to the large ground velocity pulses, others are caused by mechanisms that are totally different from those causing the velocity pulses or fling steps. Near fault ground motions, which have caused severe damages in recent disastrous earthquakes, are characterized by a short-duration impulsive motion that will transmit large energy into the structures at the beginning of the earthquake.

The paper addresses multistorey reinforced concrete (RC) frame buildings with setbacks, i.e. a reduction of the length of the building along its height (irregularity in elevation). It focuses on buildings with large setbacks in the upper floors.

Irregular conFigure urations either in plan or in elevation were often recognized as one of the main causes of failure during past earthquakes. Focusing on buildings with setbacks, observed damage after strong earthquakes indicates an inferior performance of this type of structure [1]. Experimental [2, 3] as well as analytical [4] studies involving frames with setbacks designed and detailed to modern codes such as the ACI 318-2005 [5] showed a quite satisfactory seismic performance of this type of structure. Nevertheless, the seismic behavior of reinforced concrete multistorey buildings with setbacks under the near field earthquake has not yet been studied.

The present paper focuses on the seismic performance of multistorey RC frame buildings with setbacks in the upper stories, designed to the provisions of the ACI 318-2005. In order to examine the influence of the design ductility class on the seismic behavior of the buildings, all frames were designed for both the high (DCH) and the medium (DCM) ductility classes. Buildings designed for the low (L) ductility class with low dissipation capacity and low ductility have not been examined here since they are only recommended for low seismicity areas.

2. DESIGN CONSIDERATION

Six twelve story reinforced concrete (R.C.) frame buildings were designed according to the requirements of ACI 318-2005[8], three of them (FRH, FRH-1 and FRH-2) for the high (DCH) ductility class and the rest (FRM, FRM-1 and FRM-2) for the medium (DCM) ductility class, with the same materials and the same peak ground acceleration. The geometry of the typical plane frames of all buildings are shown in Figure 1. Two of them (FRH and FRM) correspond to buildings regular in elevation, without any setbacks, as shown in Figure 1. The other four frames have the same conFigure uration in the lower eight stories and large setbacks (about 40% of the length of the lower storey) in the upper ones, two of them (FRH-1 and FRM-1) in the upper two, and the rest (FRH-2 and FRM-2) in the upper four stories.

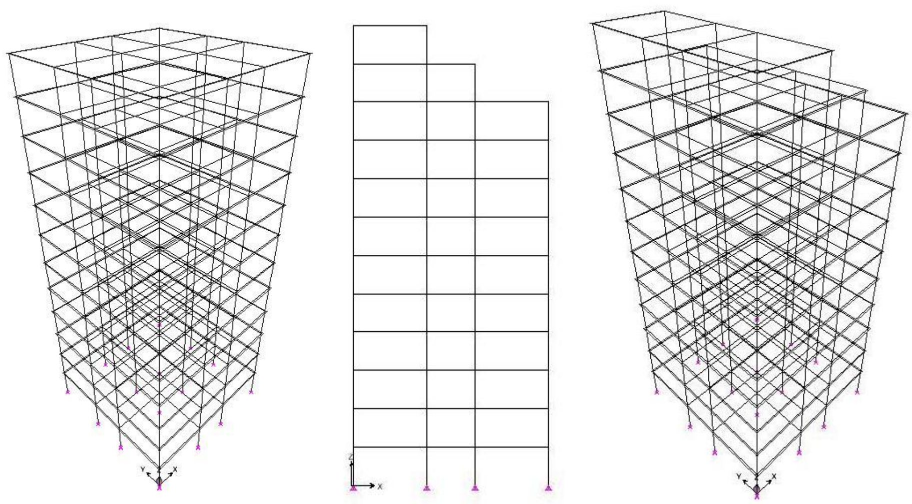

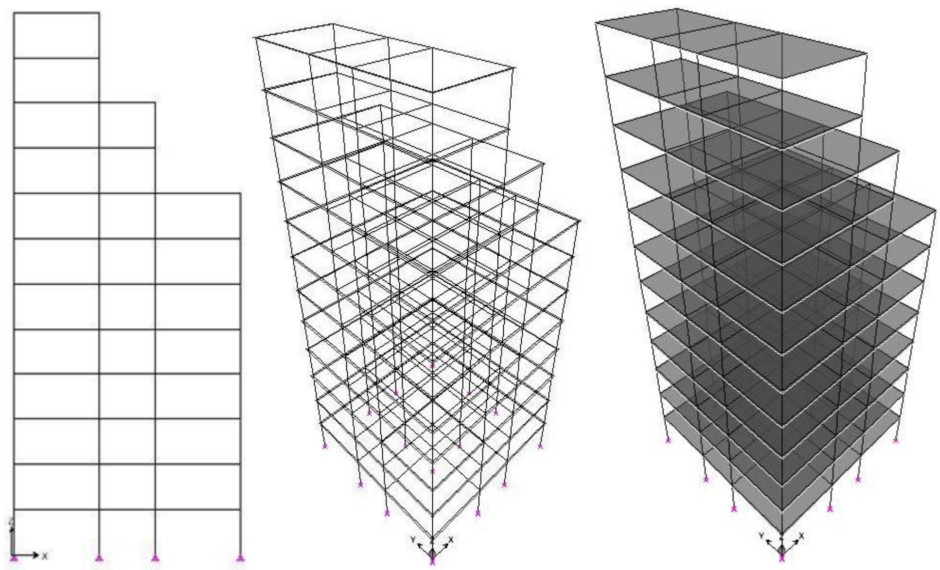

Figure 1. Geometry of the typical plane frames of all buildings

Irregular frames FRH-1, FRH-2, FRM-1 and FRM-2 were designed with the aid of modal response spectrum analysis, whereas in the cases of the regular FRH and FRM frames the (static) 'lateral force method of analysis' was used. The first 4 modes of vibration were considered in the multimodal analysis of all irregular frames, with total contributing masses of more than 90% in all cases. The natural periods of the frames were found to be 1.21 s, 1.12 s and 1.10 s for FRH, FRH-1 and FRH-2 respectively, and 1.21 s, 1.12 s and 1.07 s for FRM, FRM-1 and FRM-2 respectively. The, strange at first sight, fact that stiffer frames have longer natural periods than the less stiff ones can be attributed to the reduction of mass (because of the setbacks) at a rate greater than the one of stiffness.

The results of a detailed estimation of the required steel quantities and concrete volume show that FRM and FRM-1 have exactly the same cross-section dimensions with FRH and FRH-1 respectively, while the only difference between FRM-2 and FRH-2 concerns the cross-section dimensions of the interior columns of the lower four stories, which results in a 4% increase of required concrete volume in FRM-2 in comparison with FRH-2.

DCH structures generally require less longitudinal and more transverse reinforcement than the corresponding DCM ones. This is a very significant effect of the ductility class, the clear trend being that the percentage of longitudinal steel decreases, while that of the transverse reinforcement increases with increasing ductility class. The difference is more pronounced in irregular structures. On the other hand, ductility class seems not to affect significantly the total amount of the required reinforcement. Based on the foregoing comparisons, it appears that from the economical point of view both ductility classes for medium and high seismicity areas are essentially equivalent.

3. ASSESSMENT OF SEISMIC PERFORMANCE- PROCEDURE

All frames have been subjected to both inelastic dynamic time-history analysis and inelastic static pushover analysis. Inelastic dynamic time-history analysis of the structures was carried out with the aid of the IDARC computer code [6], including several new features and elements, as well as capability for seismic reliability analysis. The dynamic input has been given as a ground acceleration time-history which was applied uniformly at all the points of the base of the structure; only one (horizontal) component of the ground motion has been considered while dynamic soil–structure interaction was neglected. *P–Δ* effects were considered.

Inelastic static pushover analysis was carried out with the aid of the well-known ETABS000 computer code [7]. Two vertical distributions of the lateral loads were applied: a ‘uniform’ pattern, based on lateral forces proportional to mass regardless of elevation, and a ‘modal’ pattern, proportional to the story lateral forces given by the multimodal analysis. In each case, the ‘target displacement’ was defined as the seismic demand derived from the elastic response spectrum.

The possibility of failure in each member, as well as in each story of the structures, was checked by applying appropriate global, as well as local, failure criteria. Global failure was assumed to coincide with story failure; a dual criterion based on a limiting interstorey drift of 2% and the simultaneous development of a sidesway collapse mechanism involving all vertical members was adopted for assessing storey failure; regardless of mechanism formation, a structure was assumed to have collapsed if the interstorey drift at any location exceeded a limiting value of 3% [8].

The input motions used in this study were two horizontal components of the records from the earthquakes of Naghan (1978), Tabas (1980), Manjil (1986) and Bam (2003), which are among the ones that caused the most serious damage, including collapses and casualties, during the past forty years. All these records are characterized by the fact that they come from surface earthquakes with small epicentral distances (representing the typical destructive earthquakes in Iran). The time–acceleration diagrams are plotted in Figure 2.

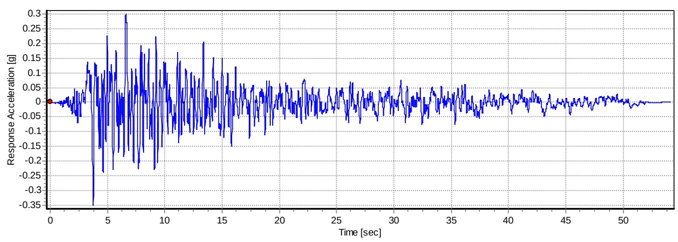

(a)

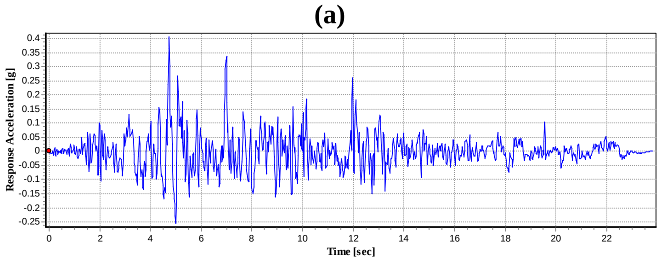

(b)

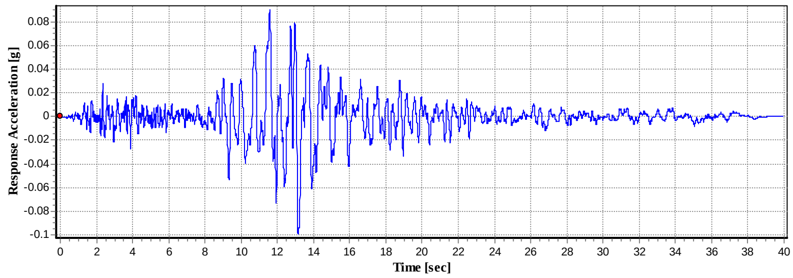

(c)

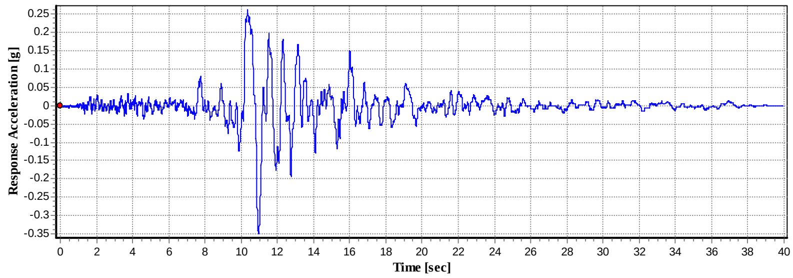

(d)

Figure 2. Time histories of input accelerograms. (a) Naghan; (b) Tabas; (c) Manjil (d) Bam

4. ASSESSMENT OF SEISMIC PERFORMANCE -RESULTS

Figure 3 summarizes the interstorey drift ratios for the DCH frame structures of Figure 1 for the 'design' and the 'collapse prevention' earthquake. These results represent the mean values of the drift ratios resulting from any of the eight input motions (every earthquake with two directions) used in the inelastic dynamic time-history analysis. It is permitted to consider mean values if the response is obtained from at least seven records.

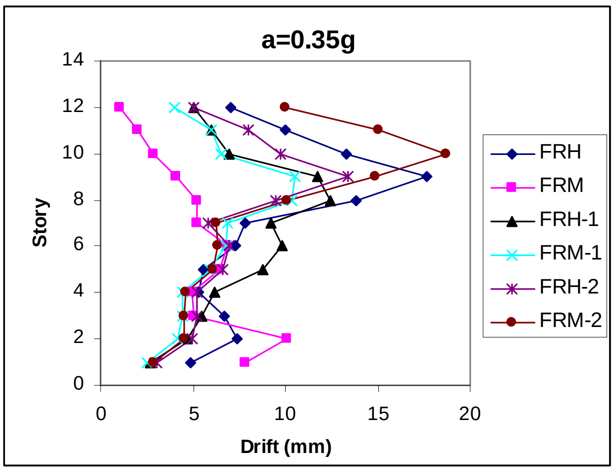

(a)

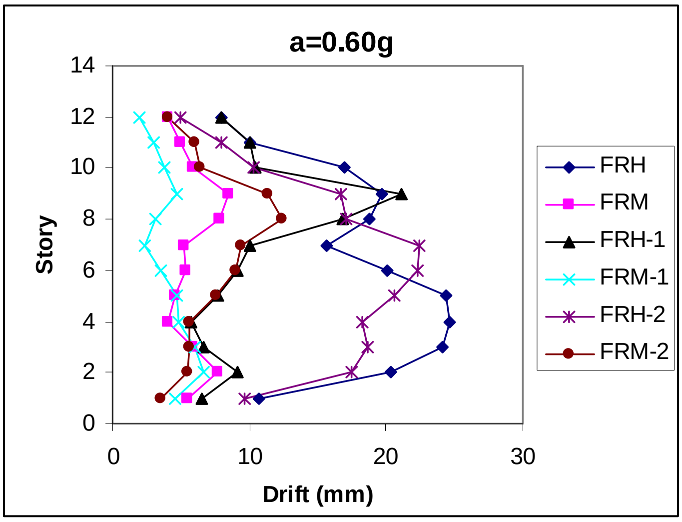

(b)

Figure 3. Interstorey drift ratios for DCH structures resulting from time-history analysis. (a) a_g=0.35*g*; (b) a_g=0.60*g*

As can be seen in Figure 3, interstorey drifts of the irregular frames are quite low, not exceeding 0.40% for the design earthquake and 1.0% for the collapse prevention one, which are well below the adopted failure values (2%–3%). These values can be considered as very satisfactory, particularly for pure frame multistorey structures. Comparing with the regular frames, the interstorey drifts of the irregular frames seem to be similar or even lower, mainly because of the lower natural periods. Exceptions to this trend are the interstorey drifts of FRH-2 and FRM-2 in the upper two stories where the stiffness has been drastically decreased. On the other hand, interstorey drift ratio values of both ductility levels seem to be similar enough, with the values of DCM frames being lower than the corresponding of the DCH ones at the lower stories and higher at the upper ones.

5. CONCLUSIONS

The following remarks that resulted from the analysis of two-dimensional 12-story plane frames strictly apply only in the case of medium-to-high-rise buildings, irregular in elevation but regular in plan, similar to those studied in this paper. For other structures, in particular those with irregularities in plan and for low-rise or very tall buildings, further studies have to be carried out to check the validity of the remarks made herein.

The seismic performance of the studied multistorey reinforced concrete frame buildings with setbacks in the upper stories, designed for the high (DCH) and the medium (DCM) ductility level, can be considered satisfactory, not inferior and in some cases even superior to that of the regular ones, even for motions twice as strong as the design earthquake.

Interstorey drift ratios of irregular frames were found to remain quite low even in the case of the ‘collapse prevention’ earthquake with an intensity double that of the ‘design’ one. This fact, combined with the limited plastic hinge formation in columns, exclude the possibility of formation of a collapse mechanism.

Most of the input energy of the irregular frames is dissipated in beams where plastic hinges form. Plastic hinges in columns do appear in the case of an earthquake with twice the design intensity, but the ductility requirements seem to be much lower than the available values.

Irregular structures seem to be stronger. On the other hand, all DCM frame structures seem to be, as expected, stronger and less ductile than the corresponding DCH ones.

As far as the effect of ductility class is concerned, buildings of both ductility classes seem to perform equally satisfactorily during the design earthquake. However, a potential weakness in the shear capacity of DCH beams (mainly those of the regular structure) has been detected.

From the economical point of view, differences between DCH and DCM design seem to be very small, even negligible, and no clear trends were detected, other than that the percentage of longitudinal bars in the total reinforcement decreases while that of the transverse reinforcement increases with increasing ductility class.

REFERENCES

1. Penelis GG, Sarigiannis D, Stavrakakis E, Stylianidis KC. A statistical evaluation of damage to buildings in the Thessaloniki, Greece earthquake of June 20, 1978. In: Proceedings of the 9th world conference on earthquake engineering, VII. 1989. p. 187-92.
2. B.M. Shahrooz and J.P. Moehle, Seismic response and design of setback buildings, *Journal of Structural Engineering, ASCE* 116 (5) (1990), pp. 1423-1439.
3. S.I. Wood, Seismic response of R/C frames with irregular profiles, *Journal of Structural Engineering, ASCE* 118 (2) (1992), pp. 545-566.
4. Kappos AJ, Scott SG. Seismic assessment of a R/C building with setbacks using nonlinear static and dynamic analysis procedures. In: Proceedings of the 6th conference on seismic design practice into the next century. 1998. p. 107-13.
5. Building Code Requirements for Structural Concrete: ACI 318-2005.
6. IDARC 2D Version 6.1, Feb. 2006, USER’S GUIDE.
7. ETABS2000: Integrated finite element analysis and design of structures. In: Computers and structures; 2000.
8. A.J. Kappos, Analytical prediction of the collapse earthquake for r/c buildings: Suggested methodology, *Earthquake Engineering & Structural Dynamics* 20 (2) (1991), pp. 167-176.

CD02-025

NUMERICAL STUDY OF THE DIAPHRAGM BEHAVIOR OF THE COMPOSITE FLOOR SYSTEMS SUBJECTED TO LATERAL LOAD

S.M. Zahrai[1], L. Sarkissian [2]
[1]Associate Professor, Center of Excellence for Engineering and Management of Infrastructures, Dept. of Civil Engrg., University of Tehran, Enghelab Avenue, Tehran, Iran
[2]M.Sc of Earthquake Engrg, University of Tehran, Iran

ABSTRACT

The influence of the in-plane flexibility of composite floor systems on the seismic response of the structures may become significant, particularly when considerable floor slab cracking and yielding are expected. As in recent years the use of composite floor systems is increasing, in this study the lateral in-plane behavior of composite floor diaphragms in steel structures is investigated through numerical simulations. The structures considered in the study were two models of the prototype buildings, where the elastic and inelastic response of the diaphragms under lateral load is analyzed using 3-D finite element models and FEM linear and nonlinear structural analysis. It was found that under the seismic load specified in the code, the criterion of diaphragm rigidity is too small, so the composite floor systems can be assumed as rigid body, however under lateral loads with higher amplitudes, by developing the cracks in the concrete slabs, nonlinear behavior and stiffness degradation of the diaphragms might occur. The results showed that for both single story structures the ultimate strength of the diaphragms was very high about 20 to 33 times of the seismic load specified in Iran's seismic code, however the ultimate strength of the second diaphragm was considerable showing an increment about 50~60 percent compared to the ultimate strength of the first diaphragm. The comparisons between the numerical and previously obtained experimental results showed that FEM overestimates the diaphragm response in terms of stiffness and deformability; however conservatively estimates the diaphragms strength.

Keywords: composite floor system, numerical simulation, finite element method, nonlinear analysis, diaphragm, seismic load, crack pattern, ultimate strength, in-plane stiffness

1. INTRODUCTION

The contribution of the floor systems in transferring the lateral loads (seismic actions, wind pressures, etc.) to the vertical structural elements and subsequently to the foundation of the building structures is well known and indisputable. The floor systems in building structures, are usually designed to carry the gravity loads to the vertical structural elements, however they should be also designed to resist the lateral forces and be able to transfer them to the resisting systems by a diaphragm action. If the floor elements act together in resisting the horizontal action and have the same deflection and show high in-plane lateral stiffness, the floor performance is known as rigid diaphragm behavior. In current design practice of building structures the floors sub assemble, according to the specifications of many building codes are usually considered as a rigid diaphragm. Even this assumption is often used to reduce the degrees of freedom of the structure and simplifies seismic response analysis of many types of buildings, however for some classes of structural systems, the effect of diaphragm deformability cannot be disregarded, especially in the case of rectangular buildings with large aspect ratios where considerable inelastic floor slab behavior is expected [6]. Since the diaphragm behavior is one of the most important factors in the seismic response of the structures, researchers have conducted studies on this subject, but the studies have not a long precedent and they are mostly performed in the last two decades.

An extended numerical parametric study was carried out to study the diaphragm behavior of RC floor systems (slabs and beams). The results show that the influence of aspect ratio on the criterion of the diaphragms rigidity (Δ_d / Δ_s) is considerable, although there is no clear correlation between these two structural characteristics [10]. The seismic behavior of wood diaphragms in unreinforced masonry buildings has been studied through the tests on three test specimens, using different rehabilitation methods. The results indicate that FEMA 273 tended to overpredict the stiffness and significantly underpredict yield displacement and ultimate deformation levels, while FEMA 356 tended to underpredict stiffness and overpredict yield displacement [7]. The studies on the low rise steel buildings with metal roof deck have shown that the lateral period is influenced by the diaphragm in-plane flexibility and the forces in the resistant elements can be amplified due to dynamics of the flexible diaphragm, also the shaking table results have indicated that the diaphragm in-plane deformations are twice of the values obtained from static analysis [11].

The diaphragm behavior of different types of floor systems usually differs substantially and depends on the details of the floor system, so as the use of composite floors is increasing, due to their low weight and economic benefits, in this paper the behavior of composite floor systems (CFS) (steel beams with upper concrete slab) in typical steel structures under lateral load with the influence of the gravity load, and also the in-plane characteristics of the diaphragm such as the deformability, stiffness, ultimate strength, yield point and crack pattern was investigated.

2. ANALYTICAL MODELS OF THE FLOOR DIAPHRAGMS WITH LINEAR BEHAVIOR

2.1. Design and Description of Prototype Buildings

The structures considered in this study are 3-D single-story typical steel buildings consisting of composite floor and X bracings, common in many countries. The 10.8m×7.2m×3m prototype buildings considered in the study are illustrated in

Figure 1. The girders and floor joists are *I* shapes supported on box columns braced by X bracings having box sections. The overall geometry of the structures presented in Figure 1 is the same and the main difference is the direction of the floor joists.

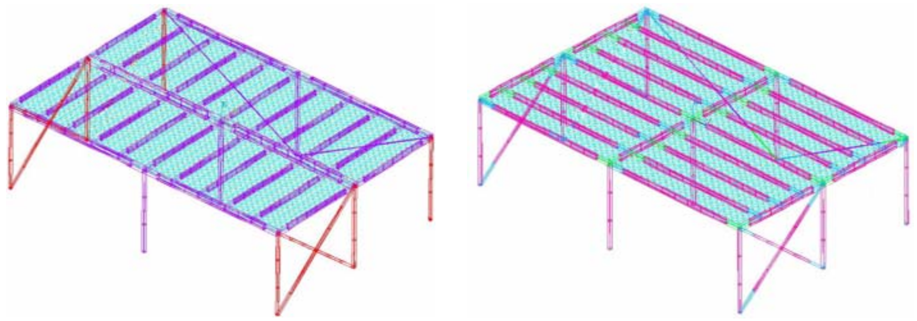

(a) (b)

Figure 1. The steel buildings prototype: (a) The floor joists parallel to the lateral load. (b) The floor joists perpendicular to the lateral load.

The composite floors were designed with the AISC code specifications and composite structures design handbook [12]. Thickness of the floor slab was obtained as 8cm and the spacing between the floor joists in the structures shown in Figure 1, were set to 108cm and 90cm respectively.
The seismic design of the structure was performed according to the seismic code of Iran [2], where the specified seismic lateral load for the structure, V, is given by:

$$V = CW, \quad C = \frac{ABI}{R} \tag{1}$$

Where C is the seismic shear force coefficient, A is zonal acceleration, B is the seismic response factor, I is the importance factor, R is the force modification factor and W is the seismic weight of the structure.
For these administrative building structures in Tehran we have:
A=0.35, B=2.5, R=6, I =1
So we have C=0.146 and the total seismic load calculated for both of the structures, obtained from Eq.(1) is 54.1 kN.

2.2. Linear Analysis

The linear analysis of the structures was performed using SAP2000 computer program. For each structure two finite element models were developed, in the first models the floors were modeled by SHELL element having four nodes in each element to consider in-plane flexibility of the diaphragm. The beams, columns and bracings were modeled by FRAME element and the connection between these elements was modeled by the coincident nodes. The scaled structures with flexible diaphragm were analyzed under lateral load specified in the seismic code [2], with the influence of gravity load. The FEM model and deformed shape of the structure with flexible diaphragm is presented in Figure 2(a) and (b). Due to flexibility of the diaphragm the displacement of mid point of the diaphragm is more than the side points as shown in Figure 2(b). In the second models rigid diaphragm hypothesis was used and the floors were modeled by rigid diaphragms. Figure 2(c) and (d) shows the FEM model and deformed shape of the structure with rigid diaphragm. In this model the displacements of all points of the diaphragm are the same as shown in Figure 2 (d).

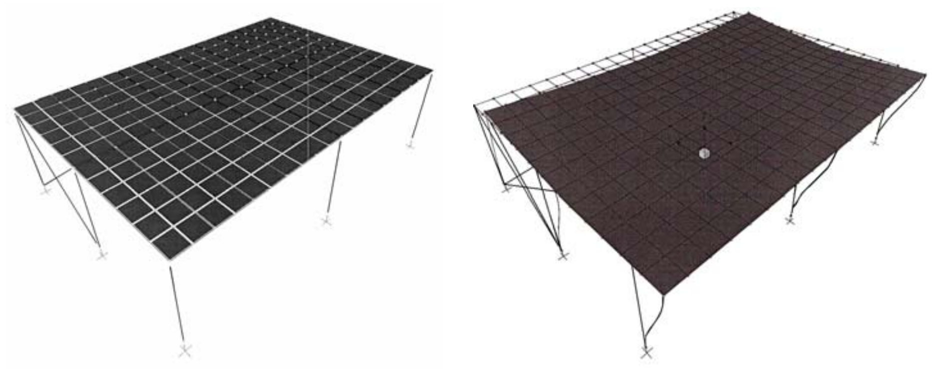

(a) (b)

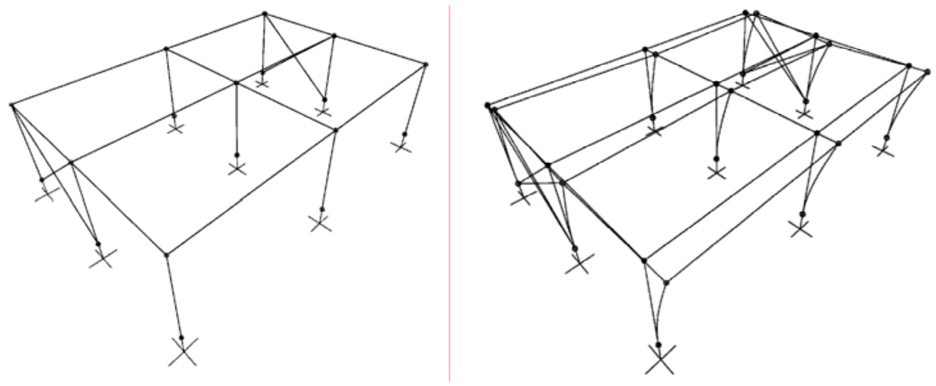

(c) (d)

Figure 2. (a) Meshing of the FE Model with Flexible Diaphragm. (b) Deformed Shape. (c) Model of Structure with Rigid Diaphragm. (d) Deformed Shape

2.3. Results of Linear Analysis

The results of analysis of the FEM models for both structures and also the results of the rotating tests are presented in Table1. In this table RD1 and RD2 are the FE models with rigid diaphragm and FD1 and FD2 are the FE models with flexible diaphragm. Also E1 and E2 are the specimens tested under lateral and gravity loads.

Table 1: Results Obtained from Three Models for the Structures

Bracing force(kg)		$\frac{\Delta_d}{\Delta_s}$	*Diaph. net disp. (mm)*	*Story drift (mm)*	*Diaph. mid disp. (mm)*	*Lateral load (kg)*	*Model*	
Tensile	*Compressive*							
429.5	*433.1*	–	*0*	*0.30498*	*0.30498*	*1380*	*RD1*	*Sample1-Joists parallel to the lateral load*
433.3	*426.4*	*0.07*	*0.2089*	*0.29835*	*0.31924*	*1380*	*FD1*	
519	*429*	*0.082*	*0.026*	*0.319*	*0.345*	*1380*	*E1*	
429.5	*433.1*	–	*0*	*0.30498*	*0.30498*	*1380*	*RD2*	*Sample2-Joists perpendicular to the lateral load*
432.8	*426.8*	*0.068*	*0.02046*	*0.29869*	*0.31915*	*1380*	*FD2*	
440.8	*483.1*	*0.063*	*0.020*	*0.32*	*0.34*	*1380*	*E2*	

The results show that both of the composite floor diaphragms were rather rigid under the lateral load specified in the seismic code. The difference between the calculated tensile and compressive bracing forces were obtained using Table1 where for the first specimen were about 17% and 1% respectively, while in the second specimen were 3% and 10.5%.
The net displacement of the diaphragm is the relative displacement of the mid frame to the side frames, which is given by:

$$\Delta_d = \Delta_m - \Delta_s \tag{2}$$

Where Δ_d is the diaphragm displacement, Δ_m is the displacement of the mid frame and Δ_s is the displacement of the side frames or the story drift. The proportion of $\frac{\Delta_d}{\Delta_s}$ is a criterion to evaluate diaphragms rigidity in some building codes, for example with respect to the specification of Iran's seismic code[2], if $\frac{\Delta_d}{\Delta_s} \leq 0.5$, the diaphragm can be assumed rigid. As in these structures proportion of $\frac{\Delta_d}{\Delta_s}$ was small (0.063 to 0.083), these composite floors under lateral load behave as rigid diaphragms. One of the effective parameters in the diaphragm behavior of floor systems is aspect ratio of the floor plan, so that for high plan aspect ratios, in-plane flexibility of the diaphragms increases significantly, but there is no clear relation between aspect ratio and $\frac{\Delta_d}{\Delta_s}$ [3]. Therefore in these structures with low aspect ratio[1] (L/D=1.5), the behavior of floor system as a rigid diaphragm, is somehow expectable.

3. ANALYTICAL MODELS FOR THE FLOOR DIAPHRAGMS WITH NONLINEAR BEHAVIOR

3.1. Description of Prototype Buildings

In some cases floor diaphragm may undergo lateral loads more than the seismic lateral load of a single story building specified in the building codes. For example the seismic lateral force on a floor diaphragm in lower stories of a multistory building is much more than the seismic lateral load of a single story building with a similar plan. So in the second part of the study, the nonlinear behavior of diaphragms of composite floor systems is studied. In order to ascertain nonlinear behavior of composite diaphragms and study the nonlinear characteristics of diaphragms (such as in-plane deformations, stiffness, ultimate strength, etc.) the stiffness of lateral load resisting system of the structures were increased by doubling the number of X bracings. It was to give priority to the failure of diaphragms compared to the failure of structures. Structures considered in this part of study and meshing of the FEM models are presented in Figure 3. Connections of the columns to the foundation are rigid connections, while the connection of beams and braces to the columns are hinge connections.

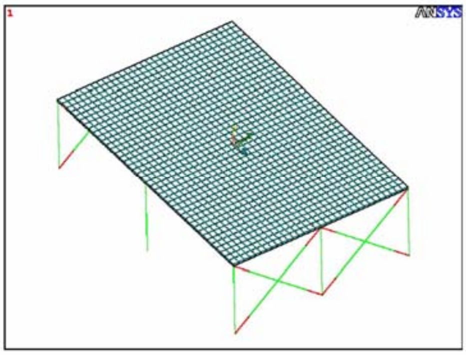

Figure 3. Meshing of the FEM Models

3.2. Theoretical Nonlinear Analysis

The seismic load was simulated by lateral cyclic load applied at the roof level distributed on the floor thickness and the pattern of the amplitudes of lateral cyclic load was the same as the previously conducted experiments. The nonlinear analysis of the structures was performed using ANSYS [8]. The elements used in modeling the structures are described as follows.

3.2.1. Used Elements [1]

-SOLID65:

In this study the concrete slab of composite floor system is modeled by SOLID65 element and the temperature reinforcement is considered by the volume ratio. The connectivity between the concrete and the steel beams is modeled by common joints within a distance same as the spacing of the shear keys.

-BEAM24: BEAM24 is a uniaxial element of arbitrary cross-section (open or single- celled closed section) with tension-compression, bending and St.Venant torsional capabilities. The element has plastic, creep, and swelling capabilities in the axial direction as well as a user-defined cross section.
In this study BEAM24 element were used to mesh the steel elements of the structural steelwork, such as girders, joists of the composite floors, columns and bracings.
-BEAM44: BEAM44 is a uniaxial element with tension, compression, torsion and bending capabilities. This element allows a different unsymmetrical geometry at each end and permits the end nodes to be offset from the centroidal axis of the beam.
Since in this element the properties of each end of beam (such as stiffness) may differ, in this study BEAM44 element were used to develop hinge connections of beams and bracings to the columns, so that all steel elements were meshed by BEAM24 element, except the end elements of the beams and braces which were meshed by BEAM44 element, then by releasing the moment of the node located at the connections, hinge connections were created.
The application of BEAM24 and BEAM44 elements in developing the FEM model is presented in Figure 4.

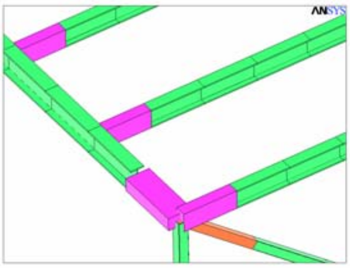

Figure 4. Application of the Beam Elements in Modeling the Structures

3.2.2. Loading
3.2.2.1. Gravity Load
The gravity load includes dead and live loads and a load related to scaling and simulation requirements. Because as the scale factor is 0.5 the materials used in the scaled structure must be twice of the prototype ones, so to cover the lack of weight, Q_{ρ} a load equal to the weight of concrete slab is considered in total gravity load. The total gravity load applied on the diaphragms is given by:

$$Q_{tot} = Q_{DL} + Q_{LL} + Q_{\rho} = 372 \text{ kg/m}^2 = 3650 \text{ Pa} \tag{3}$$

The total gravity load was applied on SOLID65 element as uniform pressure of 3650 Pa with *Load key=6*.
Also the weight of structural elements was included using base acceleration of g=9.8 m/s² upward which is equivalent to acceleration of structural elements

downward [1].

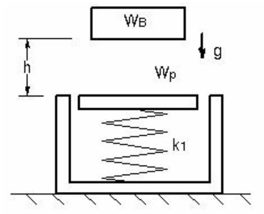

(a)

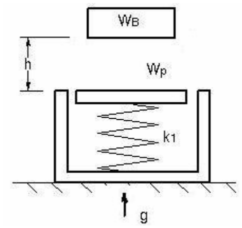

(b)

Figure 5. Applying the Structures Weight in the Software: (a) Downward Acceleration of the Structure. (b) Upward Acceleration of the Base

3.2.2.2. Lateral Load

The lateral load was applied as uniform compressive pressure on the elements located at the edge of the floor slab. Since lateral cyclic load was applied in reverse directions, in the southern edge elements *Load key=2* and in the northern edge elements *Load key=4* were used. Amplitudes of lateral cyclic load in each cycle (which are the same as the previously conducted tests) [9] for both structures are shown in Figure 6. The end points of the curves are the failure points of diaphragms of the structures.

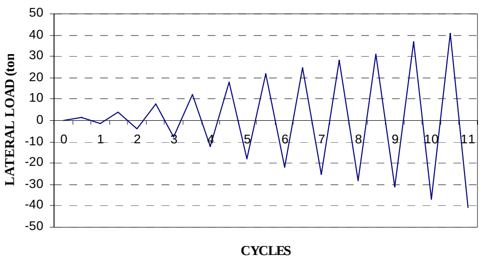

(a)

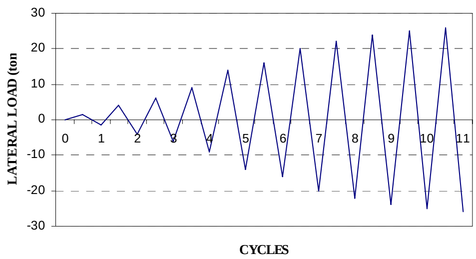

(b)

Figure 6. Amplitudes of Lateral Load. (a) First model. (b) Second model

3.3. Results of Nonlinear Analysis

3.3.1. Ultimate Strength

After loading and unloading in each cycle, the lateral loads of the next cycle were applied with larger amplitude as shown in Figure 7. The composite diaphragms concrete failed when the solutions of nonlinear analysis were not converging, because despite the time steps were too small and decreased automatically, and also the number of iterations were too large, after a large number of iterations the nonlinear analysis diverged. The criterion of concrete failure is the criterion of William and Warnke, which represents a surface of failure, using the properties of the concrete, such as uniaxial tensile and compressive stresses and the coefficients of shear transfer in open and close cracks [8]. The displacement solution of side frame (story drift) is presented in Figure 7. The end points of the graphs shown in Figure 7 relates to the divergence of solutions. According to Figure 11 the ultimate strength of the diaphragms are 27 tons and 40.8 tons, respectively. The results show that the ultimate strength of the second diaphragm is greater than the first one with a factor of 1.511.

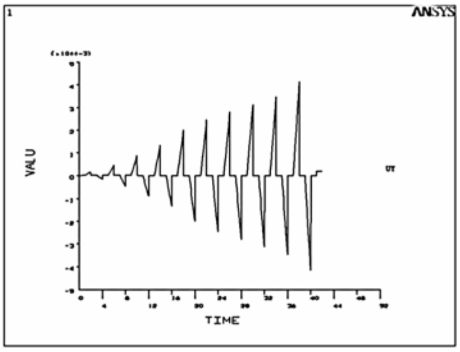

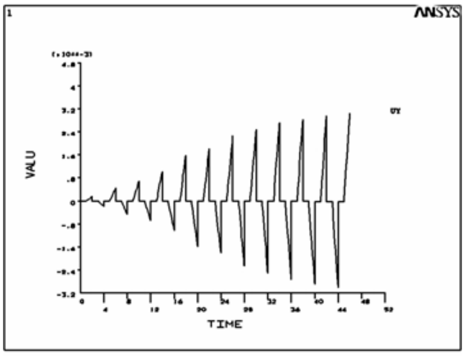

(a) (b)

Figure 7. Solutions of Nonlinear Analysis. (a) First model. (b) Second model

3.3.2. Crack Pattern

In both diaphragms some cracks developed under the gravity load which were the same in both models, however cracking under the gravity load were nominal and the main cracks developed under the lateral load. In the first model the first cracks appeared when the lateral load was about 6 tons, then by increasing the lateral load, most of the cracks developed parallel to the joists or the direction of lateral load, but under the loads about the ultimate strength (26 tons), a few cracks developed near the braced frames, which inclined about 45º to the joists. In the second model the first cracks appeared when the lateral load was about 31 tons, then by increasing the lateral load, most of the cracks developed near the braced frames, which inclined about 45º to the joists. Crack patterns of the diaphragms of two models are illustrated in Figure 12 [8].

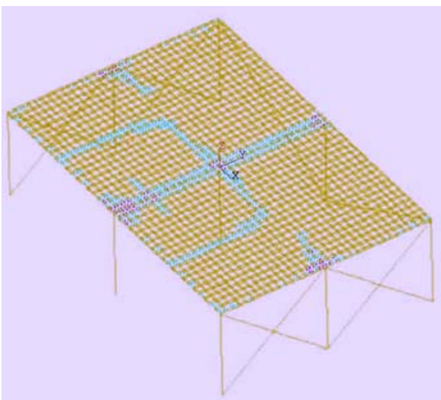

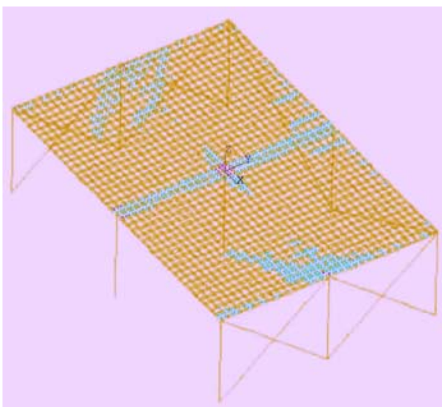

(a) (b)

Figure 8. Crack Patterns of Concrete Slabs of the Diaphragms. (a) First model. (b) Second model

Performance of diaphragms is generally controlled by a combination of shear and flexural actions. In this study, performance of the composite diaphragms can be perceived from the crack patterns of the diaphragms, so that if the diaphragms are considered as beams on the braced frames as their support, in the first model the crack pattern indicates that the flexural action is dominate, but in the second model the crack pattern shows that the shear action is dominant.

3.3.3. Diaphragms' Deformation and Stiffness

Deformed shapes of the diaphragms were extracted using a path through axis 2-2 (shown in Figure 4). For example deformed shape of the diaphragm of the first model under lateral load of 6 tons is illustrated in Figure 9. The horizontal axis is calibrated as diaphragm width, which is 5.4 m, and the vertical axis presents displacement of all points of the diaphragm. Net displacement of the diaphragm can be found from deformed shapes of diaphragm, which is difference of mid and side frames of the diaphragm.

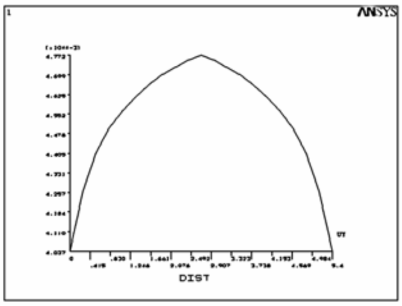

Figure 9. Deformed shape of the first diaphragm

The analytically obtained load-displacement curves of the diaphragms are shown in Figure 10. The horizontal axis is the net displacement of the diaphragms and the vertical axis is total lateral load applied on the diaphragm [12].

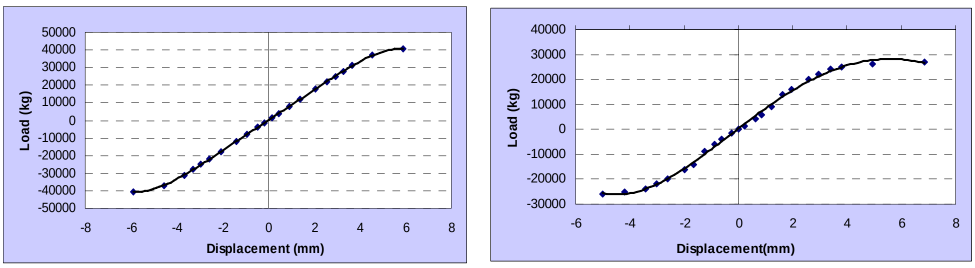

(a) (b)

Figure 10: Load-displacement curves of the diaphragms.(a)First model.(b)Second model

In order to compare in-plane flexibility of the diaphragms, the displacement of two diaphragms versus lateral load is traced in one coordinate system (Figure 11a)). As shown in Figure 11(a) the displacement of the diaphragms under lateral loads less than 20 tons is almost the same, but under lateral loads more than 20 tons the displacement of the first diaphragm compared to the second one increases significantly. For example under ultimate load of the first diaphragm, the displacement of the first diaphragm is about 2.2 times of the second one. The comparison was made in the joint region, since the ultimate strength of the diaphragms was not the same.

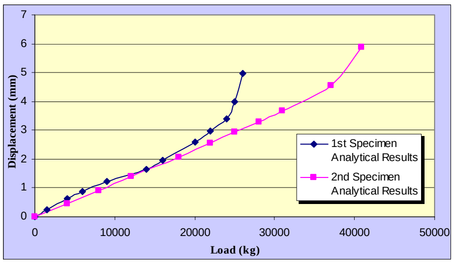

(a)

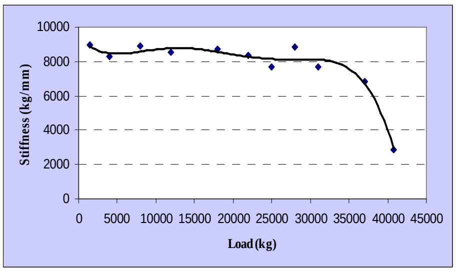

(b)

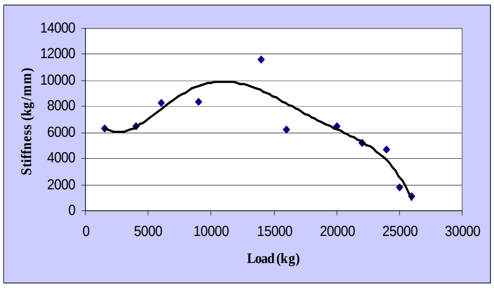

(c)

Figure 11. (a) The displacement of two diaphragms. (b) and (c)Variation of the diaphragms stiffness of First and Second model.

One of the most important characteristics of the diaphragms which affect their behavior is their in-plane lateral stiffness. As the stiffness is the load required for unit displacement in a specific point, slope of the load-displacement curves (shown in Figure 10) represents the in-plane stiffness of the diaphragms. Variation of stiffness of two diaphragms versus lateral load is presented in Figure 11(b) and (c). As shown, in the first model the diaphragm stiffness is rather constant until lateral load is 18 tons (about 60% of the ultimate strength), then decreases about 70% until failure. However in the second model the diaphragm stiffness is constant until 34 tons (about 85% of the ultimate strength), then decreases about 50% until failure [8].

3.3.5. Stress Contours of Diaphragms

Since the structures have low plan aspect ratios, the distribution of shearing stress in the diaphragms is more important. The contours of shearing stress (S_{XY}) in the diaphragms are presented in Figure 12. Due to the symmetry of the models, the absolute values of shearing stress in two sides of the axis of symmetry are the same, but have different signs. As shown in Figure 18 in both diaphragms the maximum shearing stress is observed near the braced frames. Maximum of the shearing stress for the first diaphragm is about 2.04 MPa ($0.452\sqrt{f'c}$), and for the second diaphragm is about 2.730 MPa ($0.618\sqrt{f'c}$), which shows an increase about 36% comparing to the first one.

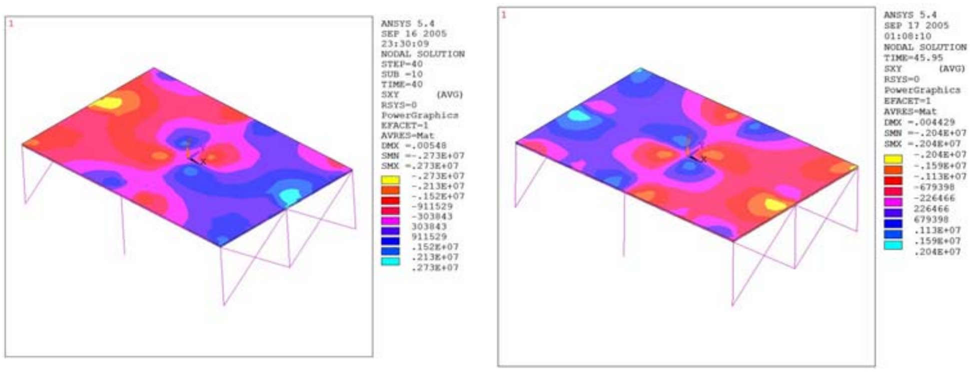

(a) (b)

Figure 12. Contours of Shearing Stress in the Diaphragms. (a) First Model. (b) Second Model

3.4. Analysis of Results

The results of nonlinear structural analysis by ANSYS are compared with the results previously obtained from quasi-static cyclic lateral loading test as follows.

The ultimate strengths of the diaphragms, obtained from nonlinear FEM analysis were 27 tons and 40.8 tons respectively, while the ultimate strengths obtained from the tests were 29 tons and 47 tons, which show errors about 7% and 13% comparing to the values obtained from the tests. The difference between the results can be described as follows; ANSYS computer program can predict failure of the concrete using the criterion of William and Warnke [1], which represents a surface of failure, by means of properties of the concrete. However after failure of the concrete, some other structural elements, such as the columns, braces and the joists, and also the interlocking of the temperature reinforcement with the concrete and the joists, resist the lateral load until overall failure of the structure; so the ultimate strength of both diaphragms obtained from the tests are slightly higher than the analytical ones.

The crack pattern of both diaphragms, obtained from numerical analysis using ANSYS illustrated in Figure 8, are in good agreement with the crack pattern of concrete observed in the previous tests ([4] and [9]). As shown in the diaphragm of the first specimen most cracks are parallel to the direction of lateral load, but in the diaphragm of the second specimen most cracks inclined about 45º to the joists, showing that the test results confirm the results of FEM nonlinear analysis.

According to the results obtained in the previous experiments ([4] and [9]), it is obvious that for both diaphragms the finite element method generally underpredicts the diaphragms displacements under lateral load and overpredicts the diaphragms stiffness compared to the ones obtained from tests. The difference between the results of two methods can be described as follows; in FEM analysis of diaphragms, size of the elements affect the displacement values of the response, and if the discretisation mesh is not fine enough the stresses of the lateral resisting elements may be determined with a good approximation, but the response displacements may be determined with some errors [3]. In modeling of the structures, with respect to the hardware abilities, the diaphragms were meshed by 11.25 cm x 13.5 cm elements as shown in Figure 3, so by using finer elements in meshing of the diaphragms, the analytical displacement responses of the diaphragms may be closer to the experimental ones. Also concrete is not a homogeneous material and has rather complicated behavior, so modeling the concrete by simplified material models may result in inaccurate results in the nonlinear analysis of concrete elements.

The results analysis show that if two individual diaphragms are designed under gravity load with the same conditions, the diaphragm with joists perpendicular to the lateral load, exhibits a better performance under lateral loads, so it is recommended that in a building with low plan aspect ratio, composite floor systems are so constructed that the direction of the joists in the vicinity of braced frames or shear walls, is perpendicular to the direction that the main lateral load resisting elements act, or the joists are set in a staggered manner all over the plan. If a building has a high plan aspect ratio, directing the joists in the long direction would lead to better performance of the composite diaphragm, however in some cases directing the joists to be perpendicular to the lateral load would be with some penalties, because if the joists are in the long direction of the diaphragm, they are less efficient under gravity load and it would be more costly.

4. CONCLUSIONS

In this paper the behavior of composite diaphragms was studied in two parts, in the first part the diaphragms were subjected to the lateral seismic load specified in the seismic code and distribution of the lateral load among the resistant elements was studied using FEM analysis with rigid diaphragm and flexible diaphragm hypothesizes and verified with the results of the tests on the half scale specimens. The results show that under the seismic load specified in Iran's seismic code [2], the criterion of diaphragm rigidity (Δ_d / Δ_s) is too low and the diaphragms can be assumed rigid. Also the forces of bracings calculated from the methods have errors less than 17%, which indicates that using the rigid floor diaphragm model provides adequate results for the stresses of the laterally resisting vertical structural elements and the story drift. The models considered in the first part after increasing the stiffness of the side braced frames, were subjected to the quasi-static reverse cyclic lateral load up to failure. The results show that the second diaphragm (where the joists direction was perpendicular to the lateral load direction) has higher lateral in-plane stiffness and there were no significant stiffness degradation until 85% of the ultimate load, but the first diaphragm (where the joists direction was parallel to the lateral load direction) had lower stiffness and the stiffness degradation started at a load of 48% of the ultimate load. The ultimate strength of the second diaphragm was considerable showing an increment about 50~60 percent compared to the ultimate strength of the first diaphragm, also for both of the single story structures the ultimate strength of the diaphragms was very high and was about 20 and 33 times of the seismic load specified in Iran's seismic code, respectively. The comparisons between the numerical and experimental results previously obtained by the authors showed that FEM overestimates the diaphragm response in terms of stiffness and deformability; however FEM conservatively estimates the diaphragms strength. Generally it seems that one of the most important parameters in the diaphragm behavior of the composite floor systems is the direction of the joists relative to the lateral load and it is recommended that the composite floor systems are so constructed that the joists direction is perpendicular to the direction toward which the main lateral load resisting elements act.

5. ACKNOWLEDGMENTS

The writers acknowledge the financial support provided by building and housing research center of Iran (BHRC) who founded this research. The supports provided by Center of Excellence of Infrastructural Engineering at the University of Tehran where this research was conducted, is also appreciated. The authors wish to express their appreciation to eng.K.Khalili Jahromi and also the technical staff of the structural engineering laboratory of BHRC, for their most useful collaboration in this project.

REFERENCES

1. ANSYS 5.4 Help (1992). “Analysis Guide and Theory Manual”.
2. B.H.R.C. (2005). “Iranian Code of Practice for Seismic Resistant Design of Buildings”, Standard No.2800, Tehran, Iran.
3. Doudoumis N. and Athanatopoulou A.M. (1998). “Modeling the Floor Diaphragm Action of Multi-Story Buildings with 2-D Finite Element Models”, Proceedings, Seismic Design Practice into the Next Century, Rotterdam, 1998.
4. Khalili Jahromi K., Zahrai S.M., Sarkissian L., Moslehitabar A., Koosha F. (2008). “Experimental and Analytical Case Study of Diaphragm Performance in composite Slabs under Lateral Load”, BHRC Publication No.R-483.
5. Ministry of Housing and Urban Development (2004). “Iranian National Building Code, Part 6: Loads”.
6. Naeim, F. (1989). “The Seismic Design Hand Book”, Van Nostrand Reinhold, New York, pp.210-237.
7. Peralta D.F., Bracci J.M., Hueste M.B.D. (2004). “Seismic Behavior of Wood Diaphragms in Pre-1950 Unreinforced Masonry Buildings.” J.Struct. Eng. 130(10), 1487-1496.
8. Sarkissian L. (2005), “Study of the behavior of the composite floor systems under lateral load” , M.Sc. Thesis, University of Tehran.
9. Sarkissian L., Khalili Jahromi K., Zahrai S.M. (2006). “Impact of Joists

Direction on the Diaphragm Behavior of Composite Floor Systems" JSEE, 2006, Vol.8, No.1, pp29-38.
10. Syrmakezis C., Chronopoulos M., (1990) "A Parametric Analysis of R.C. Diaphragms" Eerthquake Resistant Construction and Design, Balkema, Rotterdam.
11. Tremblay R., Berair T. and Filiatrault A., "Experimental Bihaviour of Low-Rise Steel Buildings with Flexible Roof Diaphragms." 12 WCEE (2000).
12. Viest I.M., Joseph P. Colaco, Leon R.T. (1997). "Composite Construction Design for Buildings." Mc Graw-Hill.

CD02-026

INFLUENCE OF CENTRAL VERTICAL BAR ON THE BEHAVIOUR OF HIGH STRENGTH CONCRETE TRANSFER BEAM-COLUMN JOINTS

Motamed, Jubin & al-Hussaini, Abbas
School of Architecture and the Built Environment
University of Westminster, London, UK

ABSTRACT

Beam column joint (BCJ) specimens tested under monotonic loading were compared with joint shear failure predicted according to EC8-NA [1] and ACI352 [2].
Inadequacy of these design codes for accurate estimations of the shear stresses at BCJ are identified. A design rule for the prediction of BCJ failure for high strength concrete (HSC) is given. The proposed method offer better accuracy when the results are compared with design rules from the above codes and research results.
Finite element numerical models for BCJ specimens were compared with the experimental ones. Furthermore parametric investigations of the influence of Central Vertical Bar, CVB, on the shear capacity of HSC- BCJ were conducted.
Strut and tie model for BCJ with CVB was developed to guide the designers towards using the proposed design rule to calculate the amount of shear CVB and stirrups required in order to resist the excessive joint shear.

Keywords: high strength concrete, transfer beam column joint, central vertical bar

1. INTRODUCTION

The shear design of beam-column joint (BCJ) is normally assessed in seismic countries where ACI [2], AIJ [3&4], IKU [5], AETL [6] and EEFIT [7] reports following earthquakes have identified BCJ as critical part of the reinforced concrete frame structure. The joint shear design for BCJ has been the subject of numerous research projects in the past three decades. This paper investigates the shear behaviour of external beam column joints of HSC column and transfer beam (see Figure 1) exposed to monotonic loading.
Many tall reinforced concrete frames are built with transfer beams to provide clear spaces in their entrance halls. With the advantages of HSC, such buildings usually have HSC columns. The external BCJ (see Figure 1) made of transfer beam and HSC column has unique shear behaviour, which has not been investigated fully by other researchers.
The authors' investigations on 12 beams [8,9], Figure 2, indicated that:

- When the shear span to depth ratio a/d = 3 then HSC beams shear resistance may be less than that of NSC beams (Figure 3a).
- When adding CHB in the beams then shear resistance of HSC beams

significantly improves and become greater than that of NSC.

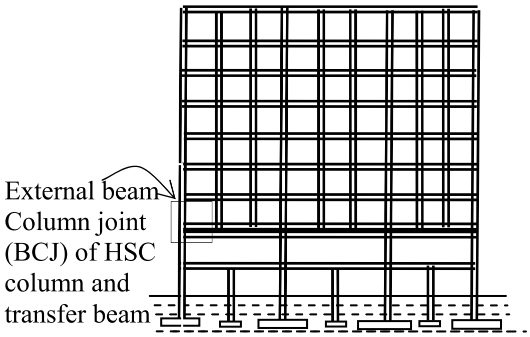

Figure 2. A multi storey RC frame with transfer beams of 3≥ hb /hc≥2.5

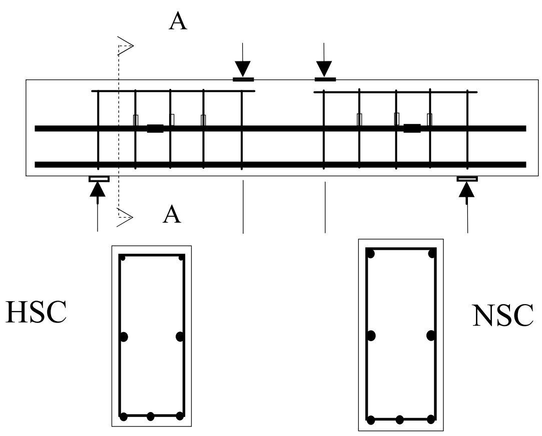

SectionA-A

Figure 2. Tweleve HSC and NSC beams tested by the authors

The reasons for such behaviour are due to (i) the stabilising arching affect in the beam as the result on the presence of CHB (Figure 3b) (ii) the double-strut action produced by the presence of central bar in addition to the main reinforcement (Figure 3c).

The ratio of beam depth to column depth is defined as the aspect ratio (h_b/h_c) has significant influence of BCJ behaviour (Figure 3a). Taylor's [10] demonstrated that shear behaviour of short beam is analogous to the behaviour of BCJ when aspect ratio ≤ 2. Similarly Motamed [8&9] has shown that the shear resistance in HSC beams with CHB produces stabilising arching affect, due to the dowel action as well as double strut action, is comparable to short beams shear behaviour, hence HSC beam with CHB will behave similar to BCJ with central vertical bar (CVB). Therefore, since the short beam behaviour is analogues to the behaviour of BCJ thus, it can be assumed that $h_b/h_c \approx a/b$ (Figure 3a). Similarly, BCJ shear resistance with vertical central bars in the column with aspect ratio $3 \geq h_b/h_c \geq 2$ is analogous to HSC beam, $3 \geq a/d \geq 2$ with CHB (Figure 3b).

Following review of the EC8-NA [1] and ACI352 [2] design methods and the past experimental research on BCJ, an empirical design equation for the joint shear is introduced which is proportional to the joint concrete strength, the shear resisting contribution of the dowel action from the vertical central bars and the confinement stirrups.
The proposed design rule for joint shear allows for prediction of quantity of the vertical central bar in the column as shear reinforcement in high strength concrete BCJ with large aspect ratio.

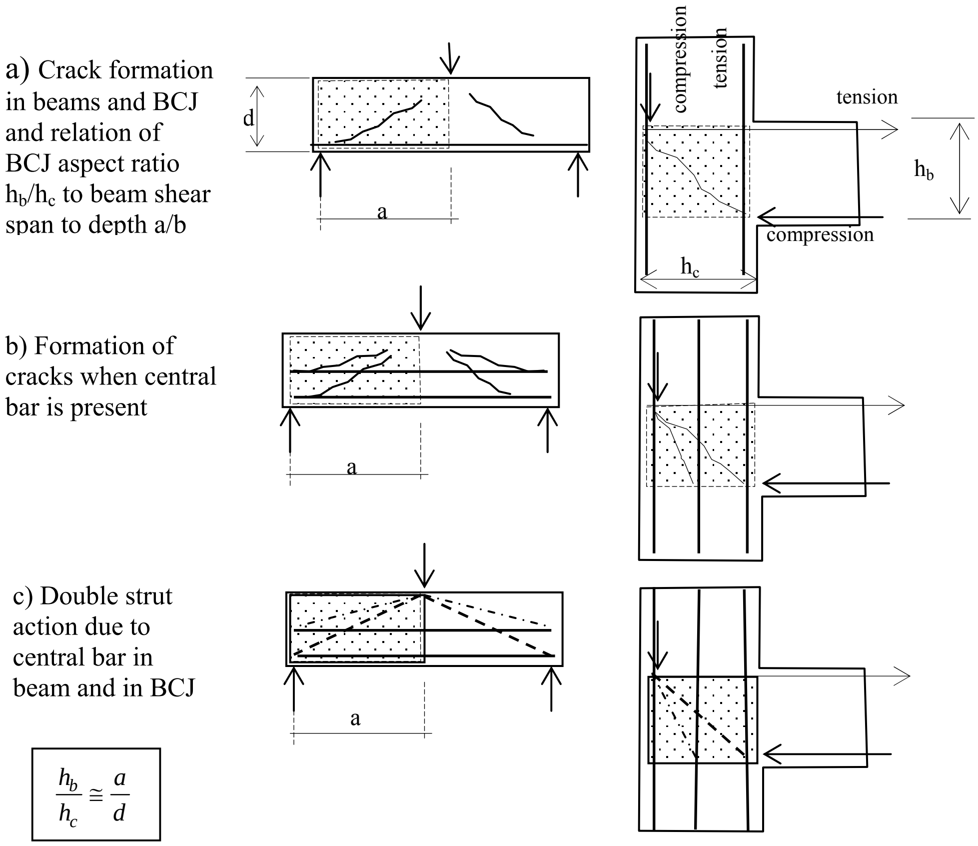

Figure 3. Cracks formation and strut and tie action in short beams and BCJ

2. CALCULATION OF JOINT SHEAR FORCE

A brief review is that $V_{u,joint}=T_n-V_{col}$ (Figure 4) , where $V_{u,joint}$ is the joint shear, V_{col} is the horizontal shear force across the column and T_n is tension force in the tension reinforcement of the beam which is given by $T_n = M_n/z$, where M_n is the beam moment at the column face and z is the flexural lever arm. The theoretical joint shear force is dependent on the assumptions used to calculate M_n and z. M_n is taken as $M_n= P (L + d')$ as shown in Figure 4, where L is the distance from the load P to the face of the column and d' is the distance from the face of the column to the centroid of the of column reinforcement as shown in the Figure.

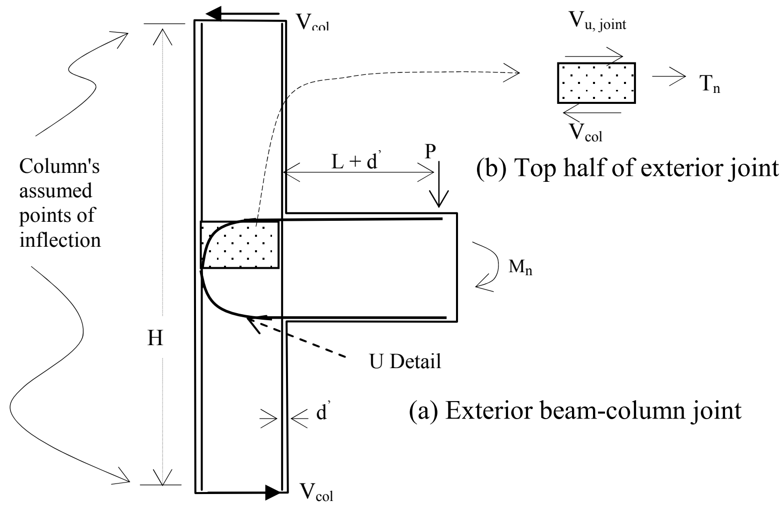

Figure 4. Forces acting on external beam column joints

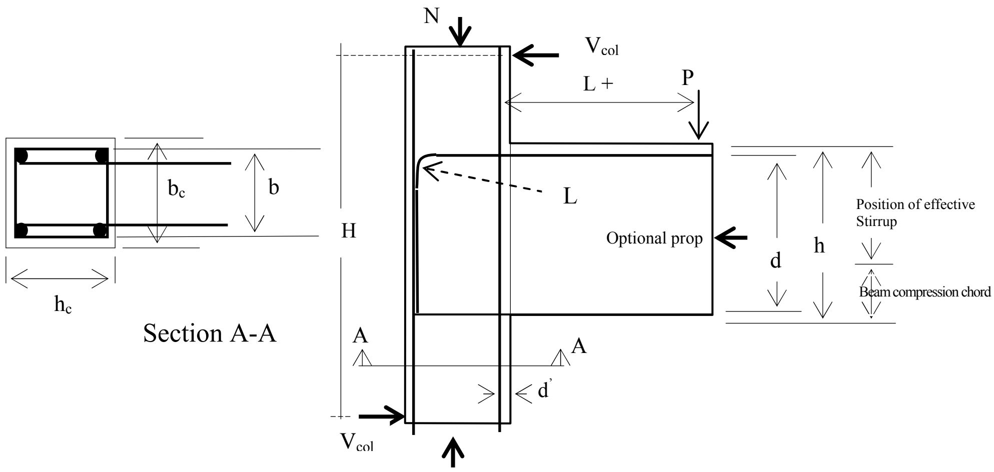

Figure 5: Typical elevation of external beam-column joint specimens used in the tests listed in Table 1

The tensile force in the beam reinforcement is calculated by section analysis assuming that plane section remains plane. The rectangular-parabolic stress block defined in EC2 [11] is used for the concrete.

The stress is assumed to reach a maximum value of $0.8f_{cu}$ at a compressive strain of 0.002. The width of the compressive stress block is taken as the beam width in the analysis of the beam-column joints. An elasto-plastic stress-strain response is assumed for the reinforcement with an elastic modulus of 200 GPa. No material factors of safety are applied.

2. ANALYSIS OF THE AVAILABLE TEST DATA

There is a general lack of agreement among researchers over the influence of variables such as concrete strength, column loading, joint aspect ratio, joint stirrups, beam thrust, beam reinforcement and column vertical bars on the joint shear behaviour of the external BCJ. Furthermore numerous tests on BCJ under cyclic loading simulating earthquakes behaviour have been performed; however, these researches have a number of shortcomings such as lack of detail investigation of the influence of shear stress at BCJ due to incremental strain development in the reinforcement.

In order to investigate these factors, available data from tested BCJ specimens were statically used to develop the parametrical values for the proposed equation of concrete contribution to joint shear at BCJ.

A finite element model, Figure 8, has been developed for typical specimens and loaded with incremental monotonic loading condition. FE model was used to study the above influences as well as to compared its results with those of the test results and with the predications of the proposed design equation.

Research on monotonically-loaded, external beam-column joints were carried out in the UK, by Ortiz [12], Taylor [14], Scott [15], Scott Hamill [16], Parker & Bullman [17], Wilson [20] and Vollum [19]; similarly in Germany by Kordina [13]. Test data from these experiments are shown in Table 1.

The relationship between shear index and stirrups index, Figure 6, show that there is a linear increase of shear in the joint as the amount of stirrups increases. However this occurs after all the concrete contribution to resist the joint shear has been taken into account. Neither of the above two equations make provision for this behaviour even though both design methods specify minimum stirrup requirements. Furthermore neither of the two equations predicts the degree of dependency of joint shear strength on joint aspect ratio, Figure 7.

A shear analysis is carried out to develop a relationship between concrete strength and the joint shear strength for the specimens shown in table 2. These analyses show that the joint shear strength has a closer relationship to $(f_c')^{2/3}$ of EC8-NA rather than $(f_c')^{1/2}$ of ACI/ ASCE Committee 352. This is because the variance of shear index of specimens without stirrups is 0.29 (0.54-0.25=0.29) for EC8 and 0.43 (0.94-0.51=0.43) for ACI, Figure 6.

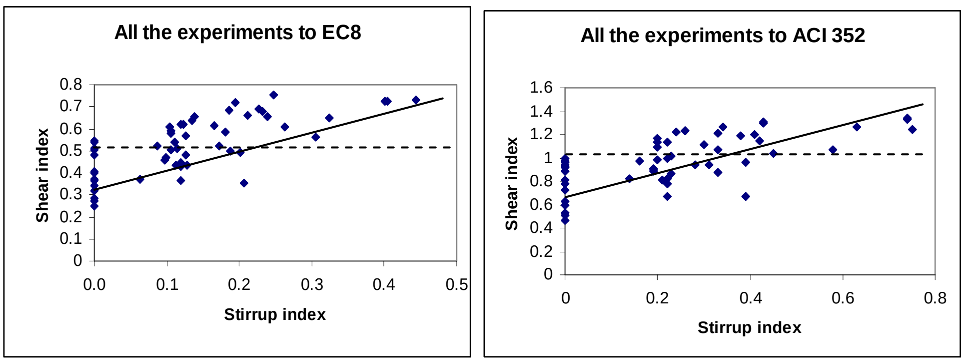

Figure 6. Relationships between Joint Shear index and Stirrup index according to EC8-NA and ACI 352

Table 1: Specimens geometry and beam reinforcement for beam-column joints; HSC joints are shown bold in shade

Researcher	Identity	H_c mm	L mm	h_c mm	d_c mm	b_c mm	h_b mm	d_b mm	b_b mm	ρ_b
Ortiz[12]	BCJ1	2000	1050	300	267	200	400	367	200	0.011
	BCJ2	2000	1100	300	267	200	400	367	200	0.011
	BCJ3	2000	1100	300	267	200	400	367	200	0.011
	BCJ4	2000	1100	300	267	200	400	367	200	0.011
	BCJ5	2000	1100	300	267	200	400	367	200	0.011
	BCJ6	2000	1100	300	267	200	400	367	200	0.011
	BCJ7	2000	1100	300	267	200	400	367	200	0.011
Kordia[13]	RE2	3000	1000	200	167	200	400	365	200	0.009
	RE3	3000	1000	200	167	200	400	265	200	0.018
	RE4	3000	1000	200	167	200	400	265	200	0.012
	RE6	3000	1000	200	167	200	400	265	200	0.012
	RE7	3000	975	230	217	230	350	315	230	0.013
	RE8	3000	975	230	217	230	350	315	230	0.013
	RE9	3000	975	230	217	230	350	315	230	0.013
	RE10	3000	975	230	217	230	350	355	230	0.012
Taylor [14]	P1/41/24	1290	470	140	110	140	200	170	100	0.024
	P2/41/24	1290	470	140	110	140	200	170	100	0.024
	P2/41/24A	1290	470	140	110	140	200	170	100	0.024
	A3/41/24	1290	470	140	110	140	200	170	100	0.024
	D3/41/24	1290	470	140	110	140	200	170	100	0.024
	B3/41/24	1290	470	140	110	140	200	170	100	0.024
	C3/41/24BY	1290	470	140	110	140	200	170	100	0.024
	C3/41/13Y	1290	470	140	110	140	200	173	100	0.024
	C3/41/24Y	1290	470	140	110	140	200	170	100	0.024
Scott [15]	CIAL	1700	750	150	117	150	210	179	110	0.011
	C4	1700	750	150	117	150	210	177	110	0.021
	C4A	1700	750	150	117	150	210	177	110	0.021
	C4AL	1700	750	150	117	150	210	177	110	0.021
	C7	1700	750	150	117	150	300	267	110	0.014
	C3L	1700	750	150	117	150	210	177	110	0.021
	C6	1700	750	150	117	150	210	177	110	0.021
	C6L	1700	750	150	117	150	210	177	110	0.021
	C9	1700	750	150	117	150	300	267	110	0.014
Scott& Hamil [16]	C4ALN0	1700	750	150	117	150	210	177	110	0.021
	C4ALN1	1700	750	150	117	150	210	177	110	0.021
	C4ALN3	1700	750	150	117	150	210	177	110	0.021
	C4ALN5	1700	750	150	117	150	210	177	110	0.021
	C4ALH0	1700	750	150	117	150	210	177	110	0.021
	C6LN0	1700	750	150	117	150	210	177	110	0.021
	C6LN1	1700	750	150	117	150	210	177	110	0.021
	C6LN3	1700	750	150	117	150	210	177	110	0.021
	C6LN5	1700	750	150	117	150	210	177	110	0.021
	C6LH0	1700	750	150	117	150	210	177	110	0.021
	C6LH1	1700	750	150	117	150	210	177	110	0.021
	C6LH3	1700	750	150	117	150	210	177	110	0.021
Parker & Bullman [17]	4b	2000	850	300	245	300	500	445	250	0.009
	4c	2000	850	300	245	300	500	445	250	0.009
	4d	2000	850	300	245	300	500	445	250	0.009
	4e	2000	850	300	245	300	500	445	250	0.009
	4f	2000	850	300	245	300	500	445	250	0.009
	5b	2000	850	300	245	300	500	445	250	0.009
	5f	2000	850	300	245	300	500	445	250	0.014
Sarsam[18]	EX2	1536	1422	204	172	157	305	272	152	0.010
Vollum [19]	EBCJ6	2000	450	200	167	200	300	257	200	0.008
	EBCJ8	2000	450	200	167	200	300	257	200	0.012
Wilson[20]	J1	3000	850	300	269	154	300	257	154	0.017

Table 2: Table for Shear indices: $V_j/b_ch_cf_c^{2/3}$ (average value=0.525) and $V_j/b_ch_c\sqrt{f_c}$ and Stirrup indices: $A_{sje}fy/b_ch_cf_c^{2/3}$ and $A_{sje}fy/b_ch_c\sqrt{f_c}$. Shaded and bold specimens are in HSC

Researcher	Identity	Bar Detail	Fc MPa	f_{yb} (MPa)	P (kN)	$A_{sje}f_y/b_ch_c\sqrt{f_c}$ √MPa	$V_j/b_ch_c\sqrt{f_c}$ √MPa	$A_{sje}f_y/b_ch_cf_c^{2/3}$ MPa2/3	$V_j/b_ch_cf_c^{2/3}$ MPa2/3
Ortiz	BCJ1	L Bar	34	720	118	0	0.92	0.0	0.51
	BCJ2	L Bar	38	720	125	0.16	0.97	0.1	0.52
	BCJ3	L Bar	33	720	118	0	0.99	0.0	0.55
	BCJ4	L Bar	34	720	130	0.33	1.07	0.2	0.59
	BCJ5	L Bar	38	720	115	0	0.89	0.0	0.48
	BCJ6	L Bar	35	720	115	0	0.93	0.0	0.51
	BCJ7	L Bar	35	720	170	0.74	1.33	0.4	0.73
Kordia	RE2	L Bar	25	420	67	0	0.94	0.0	0.54
	RE3	L Bar	40	420	80	0.26	1.23	0.1	0.66
	RE4	L Bar	32	420	51	0.19	0.91	0.1	0.50
	RE6	L Bar	32	463	66	0.38	1.19	0.2	0.66
	RE7	L Bar	26	448	117	0.43	1.31	0.2	0.75
	RE8	L Bar	28	464	105	0.42	1.15	0.2	0.65
	RE9	U Bar	28	454	110	0.41	1.2	0.2	0.68
	RE10	U Bar	24	459	100	0.45	1.04	0.3	0.61
Taylor	P1/41/24	L Bar	33	500	35	0.3	1.11	0.2	0.61
	P2/41/24	L Bar	29	500	35	0.33	1.21	0.2	0.68
	P2/41/24	L Bar	47	500	47	0.26	1.23	0.1	0.64
	A3/41/2	L Bar	27	500	35	0.34	1.26	0.2	0.72
	D3/41/2	L Bar	53	500	50	0.24	1.22	0.1	0.62
	B3/41/2	L Bar	22	500	30	0.75	1.24	0.4	0.73
	C3/41/2	U Bar	32	500	29	0.31	0.94	0.2	0.52
	C3/41/1	U Bar	28	500	27	0.33	0.88	0.2	0.50
	C3/41/2	U Bar	60	500	45	0.23	1.02	0.1	0.51
Scott	CIAL	L Bar	33	540	22	0.23	0.87	0.1	0.48
	C4	L Bar	41	540	30	0.2	1.09	0.1	0.58
	C4A	L Bar	44	540	32	0.2	1.13	0.1	0.59
	C4AL	L Bar	36	540	28	0.22	1.14	0.1	0.62
	C7	L Bar	35	540	32	0.22	0.78	0.1	0.43
	C3L	U Bar	35	540	22	0.22	0.82	0.1	0.45
	C6	U Bar	40	540	22	0.21	0.81	0.1	0.43
	C6L	U Bar	46	540	26	0.19	0.9	0.1	0.47
	C9	U Bar	36	540	28	0.22	0.67	0.1	0.36
Scott& Hamill	C4ALN	L Bar	42	522	27	0	0.96	0.0	0.51
	C4ALN	L Bar	46	522	34	0.2	1.17	0.1	0.61
	C4ALN	L Bar	42	522	35	0.43	1.3	0.2	0.69
	C4ALN	L Bar	50	522	40	0.63	1.26	0.3	0.65
	C4ALH	L Bar	104	522	43	0	0.89	0.0	0.40
	C6LN0	U Bar	51	522	24	0	0.78	0.0	0.40
	C6LN1	U Bar	51	522	25	0.19	0.89	0.1	0.46
	C6LN3	U Bar	49	522	29	0.39	0.96	0.2	0.50
	C6LN5	U Bar	37	522	34	0.74	1.34	0.4	0.73
	C6LH0	U Bar	101	522	36	0	0.81	0.0	0.37
	C6LH1	U Bar	102	522	37	0.14	0.82	0.1	0.37
	C6LH3	U Bar	97	522	41	0.28	0.94	0.1	0.43
Parker & Bullman	4b	L Bar	39	570	138	0	0.46	0.0	0.25
	4c	L Bar	37	570	170	0	0.59	0.0	0.32
	4d	L Bar	39	570	150	0	0.51	0.0	0.27
	4e	L Bar	40	570	160	0	0.53	0.0	0.28
	4f	L Bar	38	570	183	0	0.63	0.0	0.34
	5b	L Bar	43	485	236	0.39	0.67	0.2	0.35
	5f	L Bar	43	515	322	0.58	1.07	0.3	0.56
Sarsam	EX2	L Bar	52	500	37	0	0.72	0.0	0.37
Vollum	EBCJ6	U Bar	26	540	100	0.22	0.99	0.1	0.57
	EBCJ8	U Bar	33	540	120	0.2	0.98	0.1	0.54
Wilson	J1	L Bar	32	520	76	0	0.97	0.0	0.54

The dotted lines in the graphs represent the empirical values 0.525 and 1.058 of equations (1) and (2) respectively. The results of the specimens below the dotted lines indicate over estimation of the joint shear. Ignoring the minimum reinforcement requirements; the numbers of joint failures which are within the safe prediction of EC8-NA [1] are 28 out of 56 tests i.e. 50% of total specimens. Whereas for ACI 352, the numbers of safe prediction of joint failures are 23 out of 56 test i.e. 41%. (These are shown above the horizontal dotted line, Figure 6).

A linear relationship between shear index and stirrup index can be plotted when the shear indices are above 0.35 and 0.7 for EC8-NA and ACI 352 respectively. From the graph, Figure 6, it can be noted that the upper limit of stirrup index for EC8 ≤ 0.4 and for ACI ≤ 0.75

From table 2 it can be concluded that for EC8-NA [1], the mean values for shear index in BCJ for L-reinforcement, Figure 5, is 0.54 and for U-reinforcement, Figure 4, is 0.49.

3. PROPOSED DESIGN EQUATION FOR EXTERNAL BEAM COLUMN

Both design codes ACI 352[2] and EC8-NA [1] specify minimum shear stirrup requirements, however, they do not give provision for the joint strength to be increased by the stirrups.

The design recommendations of these codes fail to predict the observed dependence of joint shear strength on the joint aspect ratio, as well as the influence of HSC and detailing of the anchorage on the behaviour of BCJ. Also they do not provide any recommendation if the amount of stirrups is not adequate in order to provide sufficient shear strength at BCJ when the shear forces are high.

As noted above the HSC beams may be weaker in shear than NSC beams when span depth ratio is 3, it can also be deduced that HSC-BCJ will be weaker than NSC-BCJ when the joint aspect ratio exceed 2.5.

Past research work by Motamed [7] on 12 beams demonstrated that for the design of HSC beams with a/d=3, CHB produced superior shear capacity due to the development of dowel action which in turn enhanced the stabilising arching affect in the beams.

Using Baumann's [21] dowel cracking expression, the dowel force causing cracking is:

$$V_{du} = D_{cr} = 1.64\, h_c d_b\, f_{cu}^{1/3} (n)^{1/4} \quad \text{(for n number of bar in the beam)} \qquad (3)$$

$$V_{du} = D_{cr} = 1.95\, h_c d_b\, f_{cu}^{1/3} \quad \text{(for n = 2 i.e. bar at mid-depth, BCJ with CVB)} \qquad (4)$$

Where d_b= diameter of the dowel bars and n is number of bars,
V_{du} = dowel force, f_{cu}= cube crushing strength of concrete of 150 mm cubes in N/mm^2.

The stabilising arching effect in the beam with a/d = 3 makes the beam perform like a short beam 2≤a/d≤3 and is analogous to BCJ shear (Figure 3a).

BCJ with central vertical bar in column, the dowel shear resistance is

$$V_{jd} = V_c + 1.95\ h_c\ d_b\ f_{cu}^{1/3} \tag{5}$$

$V_c = \gamma(f_c)^{2/3}\ b_e.h_c$ is joint shear resistance due to concrete (6)

$$V_{jd} = \gamma(f_c)^{2/3}\ b_e.h_c + 1.95\ h_c\ d_b\ f_{cu}^{1/3} \tag{7}$$

Where γ = 0.54 or 0.49 for L-type, or U-type detail connections shown in Figures 4 and 5.

Proposed design rule is based on refining EC8-NA [1] design rule by using γ factor for beam detailing and including the dowel action from the central bar within the depth of the column.

The proposed method for designing shear stirrups in BCJ adopted from Fip Recommendation [22] for short beams is:

$$F_{nw} \approx \left(\frac{2 \times \frac{5}{8} \times h_b / h_c - 1}{3 - N_n / F_n} \right) .K.F_n \tag{8}$$

where K= 2/3 for all perimeter BCJ or K = 1 for corner BCJ, described in para 2 of page 5, F_{nw} is the yield force in the beam reinforcement or $F_{nw} = \sum A_{st} f_y$, A_{st} is total area and f_y is the yield stress of stirrups, F_n is the shear force $V_{u,joint}$ at BCJ (Figure 4), N_n is the axial force acting on the column, if any. The value 5/8 is portion of depth of beam where the stirrups are effective.

As the angles Θ_1 and Θ_2 between the struts and ties decrease, Figure 7, the aspect ratio increases, it is therefore desirable to introduce vertical central bar when $f_{cu} \geq 60$MPa and $\Theta_1 \leq \tan^{-1}0.5$.

Looking at equation (8), when $h_b/h_c \leq 1.25$ no joint stirrups would be required, this is checked with Wilson's experimental results which has h_b/h_c=1, table 2. Without stirrups the shear index is 0.54, which is the same as the predicted Figure to design proposal rule of equation (7) when no central vertical reinforcement, dowel bars, are used because $\Theta_1 \leq \tan^{-1}0.5$.

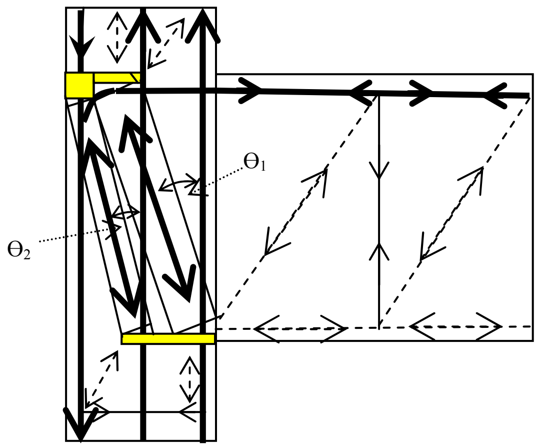

Figure 7. Strut and tie model for BCJ with central vertical reinforcement

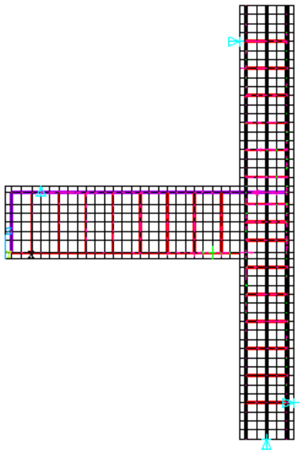

Figure 8. FEM parametric model of Ortiz BCJ4 with central vertical bar

The reason $(f_c)^{2/3}$ $b_e.h_c$ was taken for concrete contribution in the proposed rule is the result of the comparison with $(f_c)^{1/2}$ $b_e.h_c$. The accuracy of EC8-NA for predictions compared to experiments was 50% as compared to ACI352 [2] which was 41%, Figure 6.

VC joint shear from the concrete compression strut action is $Vc=0.54fc^{2/3}b_eh_c$ for L detailing shown in Figure 5, and $Vc = 0.49\ fc^{2/3}b_eh_c$ for U detailing shown in Figure 4.

4. CONCLUSION

1. A design method has been developed, based on statistical data of published 56 test results of BCJ, to calculate the shear resistance in HSC and NSC beam-column joint.
2. The proposed equation is a function of aspect ratio and the magnitude of shear force in BCJ and lower-bound theorem of plasticity maintained.
3. The results given by the proposed design equation are 79% of the total actual experimental data while the results produced from EC8 provided only 21% of the actual experimental results (assuming the experimental results is equal 1).

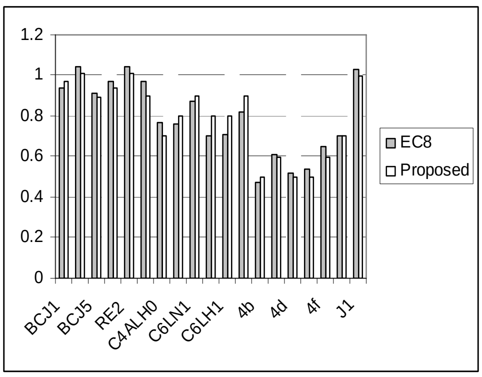

Figure 9. Design rule for all specimens without shear reinforcement

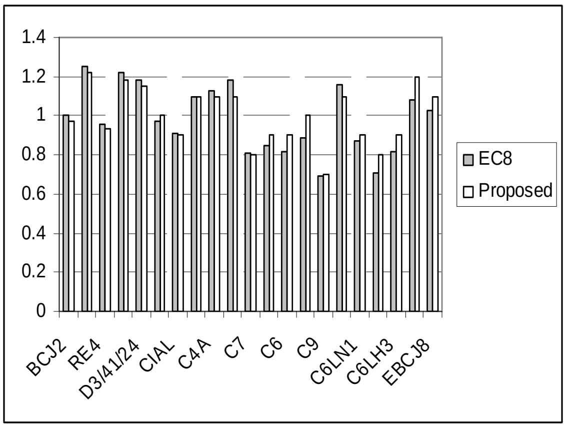

Figure 10. Design rule for all specimens with minimum shear reinforcement

REFERENCES

1. Eurocode 8: Design provisions for earthquake resistance of structures, London, British Standard Institution, 1995.
2. ACI-ASCE Committee 352, 'Recommendations for Design of Beam-Column Joints in Monolithic Reinforced Concrete Structures'. ACI Journal Proceedings: Part 3, Detroit, American Concrete Institute 1998.
3. Reports on the damage investigation of the 1985 Mexico Earthquake (1988), Architectural Institute of Japan.
4. Reports on the damage investigation of the 1990 Mexico Philippine Earthquake (1992), Architectural Institute of Japan.
5. Hirosawa, M AND Ishibashi, K, "Investigation on Structural Damage of the Public Multiple Dwelling Houses", Annual Report of the Institute of Kogakuin University, Vol.1, 1995.
6. Reports on the damage investigation of the 1995 Hyogo-Ken Nambu Earthquake, Araigumi Engineering and Technical Laboratory, 1995.
7. Motamed. J, 'The Bam earthquake of 26 December 2003, Iran', Published report on Institution of Structural Engineer www.istructe.org/eefit/files/bam .pdf. April 2004.
8. Motamed. J, 'Shear in normal strength and high strength reinforced concrete beams with stirrups and horizontal web bars'. University of Westminster, MSc Dissertation, 1997.
9. Al-Hussaini A, Motamed J. 'HSC beams with combination of links and horizontal web steel as alternative shear reinforcement'. 6th International Symposium on Utilization of High Strength/High Performance Concrete, Leipzig, June 2002, p 611-629.
10. Taylor, H.P.J. 'The Behaviour of In Situ Concrete Beam column Joints', Cement and Concrete Association, May 1974, Technical Report no. 42492, 33p.
11. Eurocode 2: Design of concrete structures, Part 1-1, General rules and rules for buildings, BS EN 1992-1-1:2004, British Standards Institution, London, Dec 2004.
12. Reys de Ortiz. I. 'Strut-and-tie modeling of reinforced concrete short beams

and beam column joints'. PhD thesis, 1993, University of Westminster.

13. Kordina K. Bewehrungsfuhrung in Ecken und Rahmenendknoten, Deutscher Ausschuss fu¨r Stahlbeton, Heft 354, 1984.
14. Taylor, H.P.J. 'The Behaviour of In Situ Concrete Beam column Joints', Cement and Concrete Association, May 1974, Technical Report no. 42492, 33p.
15. Scott RH. The effects of detailing on RC beam column connection behaviour. The Structural Engineer 1992; 70(18):318-24.
16. Scott RH, Hamill SJ. Connection zone strain in reinforced concrete beam column connections, In: Proceedings of the 11th International Conference on Experimental Mechanics, Oxford, UK, 1998. pp. 65-69.
17. Parker DE, Bullman PJM. Shear strength within reinforced concrete beam column joints. The Structural Engineer 1997;75(4):53-70.
18. Sarsam KF, Phillips ME. The shear design of insitu reinforced beam-column joints subjected to monotonic loading. Magazine of Concrete Research 1985; 37(130):16-28.
19. Vollum, R.L, Newman, J. B. 'The design of external, reinforced concrete beam-column joints'. The Structural Engineer, Volume 77/Nos 23 & 24, 7 December 1999.
20. Wilson, I. D.: 'SIFCON joints in precast concrete structures', 8th BCA Annual Conf. on Higher Education and the Concrete Industry, Southampton, July 1998, p 227.
21. Baumann. T., Rusch.H, 'Versuche zum Studium derVerdubelungswirkung der Biegezugbewehrung eines Stahlbetonbalkens, Heft 210, Berlin, Deutscher Ausschuss fur Stahlbeton, 1970.
22. FIP Recommendations, Practical Design of Structural Concrete, Fip Commission 3, Practical design, September 1996, Publ. SETO, London, September 1999, (distributed by *fib* Lausanne)

CD02-027

THE EFFECT OF STEEL MESH RATIO AND AXIAL LOAD ON THE BEHAVIOR OF STRENGTHENED BRICK WALLS WITH RC OVERLAY

Tavahhodi, S.M.[1], Tasnimi, A.A.[2], Yaghoubifar, A.[3]
[1]Msc student, Dept of civil Engg.Tarbiat Modares Univercity, Tehran, Iran
[2]Professor, School of Engg. Tarbiat Modares Univercity, Tehran, Iran
[3]Phd student, Dept of civil Engg.Tarbiat Modares Univercity, Tehran, Iran

ABSTRACT

Concrete is one of the most important materials used in many types of construction. This material is widely used in seismic rehabilitation of buildings, particularly in strengthening of masonry buildings. The latter covers a wide range of historical to conventional brick buildings which are the most vulnerable in the earthquake prone areas. One of the most available, economical and simple conventional techniques used in strengthening of brick buildings is 3 to 5 mm thick concrete overlay (shotcrete) with steel mesh on the brick wall surfaces. This method of strengthening improves the seismic behavior and lateral and in-plane strength of brick walls which depends on the thickness, strength of concrete and the amount of reinforcement. In this paper, the effect of shotcrete on strength and stiffness of brick walls has been investigated utilizing micro-modeling through ABAQUS software based on discrete elements method. Results of numerical and an experimental analysis of the in-plane shear behavior of strengthened brick walls are compared and discussed. The main variables considered in this investigation are the compressive axial load applied on the wall as well as the reinforcement ratio.

Keywords: RC overlay, strengthening, brick walls, discrete element

1. INTRODUCTION

Shotcrete has grown into an important and widely used construction technique, especially in strengthening of masonry structures. The masonry brick wall is a composite material which has no similar directional properties due to its mortar joints as a plane of weakness. In many researches carried out, two different approaches based on macro and micro models have been used. Its numerical representation shall be based on micro-modeling for its individual components (brick and mortar) or macro-modeling for a masonry element (composite unit).

In such a case if the material is regarded as an anisotropic homogeneous continuum, then the interaction between the components can be ignored in modeling and analysis. Depending on the desired level of accuracy and the simplicity, the detailed micro-modeling or simplified micro-modeling may be used. In detailed micro-modeling the units and mortar in the joints are represented by continuum elements whereas the unit-mortar interface is represented by discontinuous elements. In this approach the material properties like modulus of elasticity, Poisson's ratio, inelastic properties of the bricks and mortar are taken into account. In micro-model approach it is possible to characterize separately mortar, blocks and their interfaces, adopting suitable constitutive laws for each component, which take into account their different mechanical behavior. The micro model is probably the best tool available to analyze and understand the real behavior of masonry, particularly concerning its local response but requires an intensive computational effort. The macro-models constitute an effective method to analysis the global response of masonry structures. In such an approach, masonry is regarded as an equivalent material, where mortar and blocks are jointed together, and appropriate relations are established between averaged masonry strains and averaged masonry stresses. Lourenco (1996) has proposed a non- linear constitutive model for in-plane loaded walls based on the plasticity theory. Therefore macro-modeling can be used to reduce time consuming and establishing a relation between average masonry strains and average masonry stresses. Finally either use of micro-modeling or macro-modeling of masonry brick buildings or components requires a description of the material obtained experimentally. In the present study, the micro-model is used to obtain the actual behavior of walls by assuming that brick, mortars and their interface as three separate elements.

2. EXPERIMENTAL WORKS

A series of experiments have been studied by second and third authors on six walls in two groups in order to study the effects of reinforced concrete overlay on the behavior with the following specifications:

Group-1: Samples tested in this group, used for studying the rocking mode of failure, had 1800 mm length, 1200 mm height and 200mm thick, under 39.22 KN gravity force. Lateral load was applied in cyclic manner on the wall. The walls are named as bellow:

No Shotcrete Brick Wall 1-"NSW1"
Single side Shotcrete Brick Wall 1- "SSW1"
Double side Shotcrete Brick Wall 1-"DSW1"

Group-2: Samples tested in this group, used for studying the shear sliding mode of failure, had 1800 mm length, 800 mm height and 200mm thick, under 39.22 KN gravity force. Lateral load was also applied in cyclic manner on the wall. The walls are named as bellow:

No Shotcrete Brick Wall 2-"NSW2"
Single side Shotcrete Brick Wall 2- "SSW2"
Double side Shotcrete Brick Wall 2-"DSW2"

With these descriptions and considering the experimental results, numerical modeling was carried out utilizing the software ABAQUS.

(a) None strengthened (b) Single side strengthen((c) Double side strengthened

Figure 1. Samples of Tested brick walls

3. NUMERICAL MODELING OF MASONRY SAMPLES

Defining a reliable interface element is a primary step for the simplified micro-modeling approach. For the interface element two kinds of stiffness as normal stiffness and tangent stiffness are considered, which are given respectively by equation 1.

$$k_n = \frac{E_b E_m}{t_m(E_b - E_m)} \quad , \quad k_s = \frac{G_b G_m}{t_m(G_b - G_m)} \tag{1}$$

Where t_m is the actual thickness of the joint, E_b and E_m are the modulus of elasticity, G_b and G_m are the shear modulus, for brick and mortar respectively. It is assumed that the mortar shear behavior in two horizontal directions is approximately the same. These directions are defined as *n* and *s* directions. Shear strength is depended on cohesive parameters, internal frictional angle and applied normal stress. For high vertical stress, shear failure occurs through brick crushing. The elastic domain is bounded by a composite yield surface that includes tension, shear and compression failure. Nonlinear behavior of the masonry units in compression involves parabolic hardening and then parabolic-exponential softening in both directions with different fracture energies. Compressive strength is obtained from brick and mortar prism experiment. It has been recommended to use concrete propositional values for fracture energy in compression [1]. The micro modeling utilized in this research considers the brick, mortar and interface elements and analysis was carried out through ABAQUS computer program. For modeling of masonry units, nonlinear tension behavior of them, involves an exponential softening curve distinctively for both directions, with mode of fracture energies G_{fx}^{I} and G_{fy}^{I}. Based on descriptions in reference [3], an average value of the bond mode I fracture energy equal to 0.012 Nmm/mm^2 was adopted. In simplified micro-modeling, it is important how to define the interface element. According to the reference [2] the approximate amount of mode II fracture energy is suggested equal to 0.1c. Cohesive type elements, used for interface elements, and they are composed of two faces separated by a thickness. The relative motion of the bottom and top faces measured along the thickness direction represents opening or closing of the interface. Stretching and shearing of the mid-surface of the element are associated with membrane strains in the cohesive element [4]. The available traction-separation model in ABAQUS assumes initially linear elastic behavior followed by the initiation and evolution of damage. When surfaces are in contact they usually transmit shear as well as normal forces across their interface. There is generally a relationship between these two force components. The relationship, known as the friction between the contacting bodies, is usually expressed in terms of the stresses at the interface of the bodies. The friction model applied here is the classical isotropic Coulomb friction model. The model defines the critical shear stress, τ_{crit}, at which sliding of the surfaces starts as a fraction of the contact pressure, *p*, between the surfaces ($\tau_{crit} = \mu p$). μ is known as the coefficient of friction. In the default model the coefficient of friction is defined as a function of the equivalent slip rate and contact pressure [4].

4. NUMERICAL MODELING OF TESTED BRICK WALLS

A non-strengthened (NSW1), a single side strengthened (SSW1), and double side strengthened (DSW1) brick wall samples were selected from a group of experimentally tested specimens [5]. All samples have 1800 mm length, 1200 mm height and a thickness of 200mm. Mortar average thickness was 1 cm. These walls were subjected to a 4 ton distributed gravity load and a cyclic lateral load at their upper level.

a)Wall NSW1

This wall is a non-strengthened brick wall. For the numerical analysis of this wall the fracture energies for mode I, II and III were selected from reference [4]. The upper and lower beams are assumed to be rigid in order to minimize the time of analysis. The gravity load is applied in a linear increscent procedure within first 5 seconds and remains constant to 20th second. Lateral displacement of the wall increases linearly from 5th second to 20th second. The wall analysis results for lateral displacement and Von-Mises average stresses are given in Figure1. Good agreement is obtained in comparison with numerical results. The predominant failure mode for this wall was rocking.

b) Wall SSW1

Standard tests on concrete overlay and rebar steel mesh and material properties are necessary for numerical modeling of either single or double side strengthened brick wall. Compression and tension behavior and damage functions curves (both in compression and tension) of concrete layer are defined using proper behavior models. Brick and interface properties are described as above and rebar mesh specifications are given in Table 2. The reinforced concrete elements in ABAQUS program was carried out using 3D concrete element and embedding rebar mesh surface element. The location of rebar element is assumed to be placed at mid surface of concrete element and tied to concrete element via a contact element. Also complete compatibility is assumed for reinforced concrete overlay and brick wall connection. The analysis of the model is carried out for 4 ton gravity load and the relevant results are compared with that of experimental work. Figure 3 show deformations for two loading states A and B for wall SSW1 corresponding to its concrete and brick faces. For both analytical and experimental results the failure rocking mode is observed. It is evident that the specimen SSW1 was twisted due to unbalanced distribution of stiffness in its section. In order to study the accuracy of the numerical modeling, experimental and numerical shear-displacement curves for this wall is compared and illustrated in Figure 3-e, which indicate good correlation.

Table 1: Engineering Properties of Non-strengthened Brick Wall NSW1

	Brick	Cohesive Element	Contact Element
Density (kg/mm^3)	2.10x10^{-9}	2.36x10^{-9}	
Elastic	E~1020 N/mm^2 ν=0.15	N/mm^3 $K_{nn} = 82$ $K_{ss} = 36$ $K_{tt} = 36$	
Damage		$f_n = 0.027$ $f_s = 0.140$ $f_t = 0.140$	
Tangential Contact			$tg\varphi = 0.53$
Normal Contact			Hard Contact

a) Deformed shape at failure state [5]

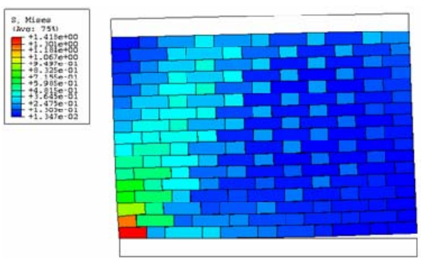

b) Stress distribution under lateral displacement and gravity load

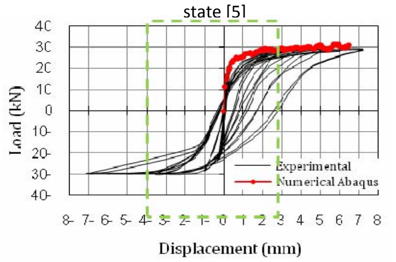

Shear-Displacement Relationship

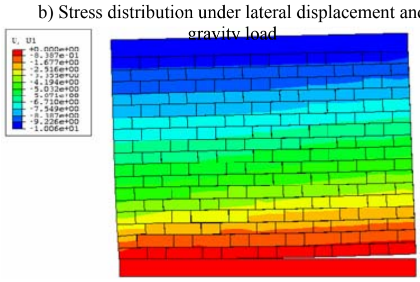

c) Horizontal displacement under Lateral displacement and gravity load

Figure 2. Comparison of Experimental and Analytical Results for Wall NSW1

Table 2: Engineering properties of reinforced concrete overlay

	Density (ton/mm^3)	Elastic Properties	Damage Plasticity
Concrete overlay properties	ρ=2.4x10^{-9}	E=2600 N/mm^2 ν=0.20	Dilation Angle=25 Eccentricity=0.1 f_{b0}/f_{bc}=1.16 K=0.67 Viscosity Parameter=0
Rebar properties	ρ=7.85x10^{-9}	E=210000 N/mm^2 ν=0.20	Yield Stress=640 Plastic Strain=0

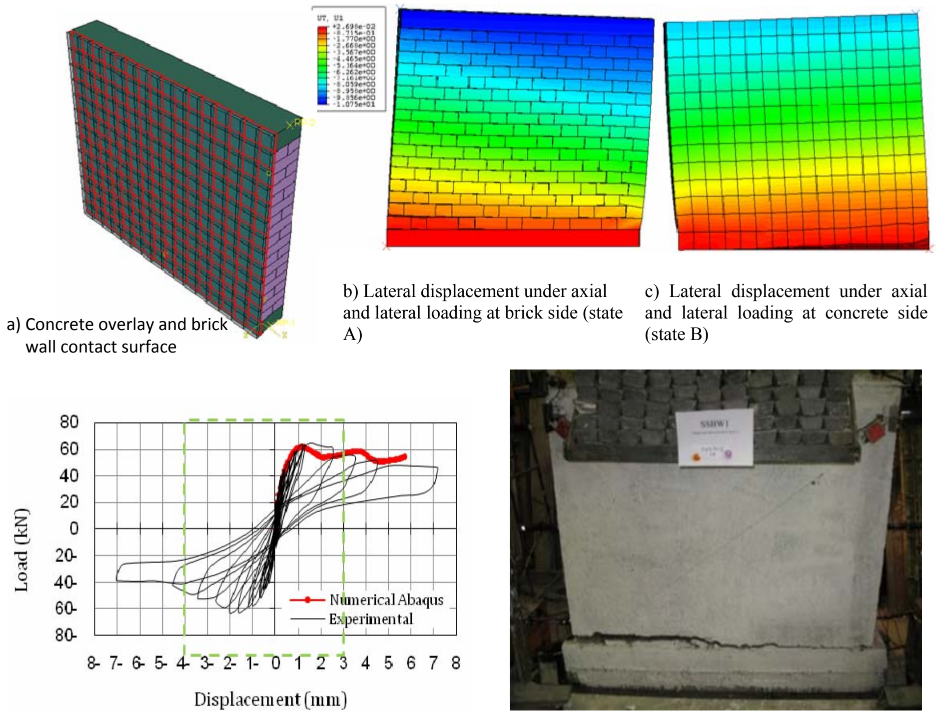

a) Concrete overlay and brick wall contact surface

b) Lateral displacement under axial and lateral loading at brick side (state A)

c) Lateral displacement under axial and lateral loading at concrete side (state B)

e) Shear-Displacement Relationship

d) Deformed shape at failure state [5]

Figure 3. Comparison of Experimental and Analytical Results for Wall SSW1

c) Wall DSW1

The modeling of double side strengthened wall (DSW1) in ABAQUS is almost similar to that of SSW1. The material properties are also the same. Numerical modeling is represented in Figure 4-a. In order to study the accuracy of the numerical modeling, experimental and numerical shear-displacement curves are prepared and compared in Figure 4-b. From this figure it is evident that stiffness of both result are the same in elastic state and good agreement is obtained for plastic state. Due to numerical instability the maximum deformation of 6mm was imposed during the numerical analysis.

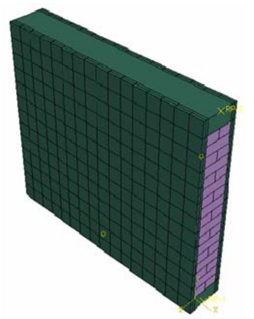

a) Concrete overlay and brick wall contact surfaces

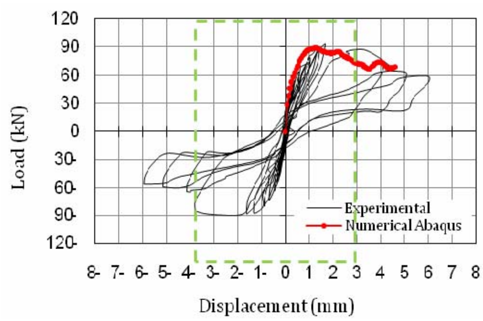

b) Shear-Displacement Relationship

Figure 4. Comparison of Experimental and Analytical Results for Wall DSW1

5. PARAMETRIC STUDYING

The verification and calibration of the modeling of strengthened wall specimens, yields the non-linear numerical analysis as a tool to obtain the effect of some design parameters, such as amount of shear reinforcement and magnitude of axial compression load on the capacity of such specimens. So in this section these effects are discussed and concluded.

6. EFFECT OF REINFORCEMENT

In this study the amount of reinforcement throughout the wall surface is considered as a variable. For this purpose two cases were considered. In the first case, for single fixed spacing the wall is modeled with different rebar size. In the second case, for a specific rebar size, the effect of various spacing is studied. It is found that an increase in the quantity of reinforcement (through amount of rebar or change of spacing) has a direct influence on load carrying capacity. This is clearly illustrated in the numerical modeling results shown in Figures 5. From this figure we can conclude that the maximum shear strength increases with the increase of reinforcement rebar or reducing the spacing. The interesting point is that the initial stiffness does not much vary for both cases.

7. EFFECT OF AXIAL COMPRESSION STRESSES

The influence of axial compression stress on masonry shear strength is illustrated in Figure 6. These figures show the Load-Displacement envelops of the two masonry walls (SSW1 and DSW1) that had the same dimensions and reinforcement details, but were subjected to varying levels of axial compression stress. This figure shows that for higher rebar diameter the bearing capacity of the wall increases and for lower diameter, as the higher load applied the lower capacity results.

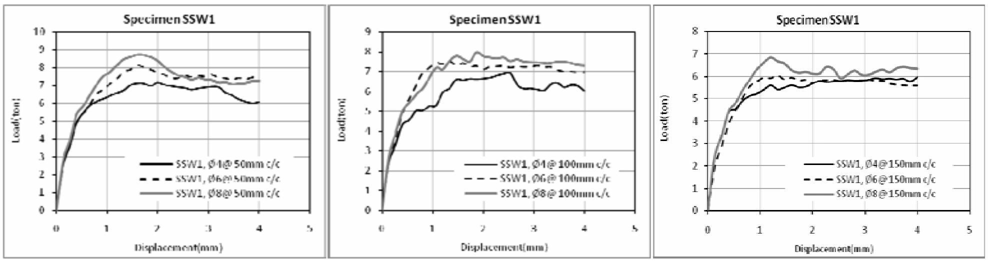

a) Effect of shear reinforcement on the strength of masonry wall (SSW1)

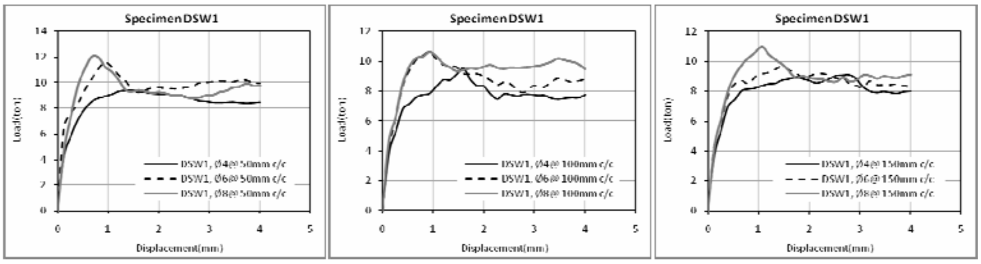

b) Effect of shear reinforcement on the strength of masonry wall (DSW1)

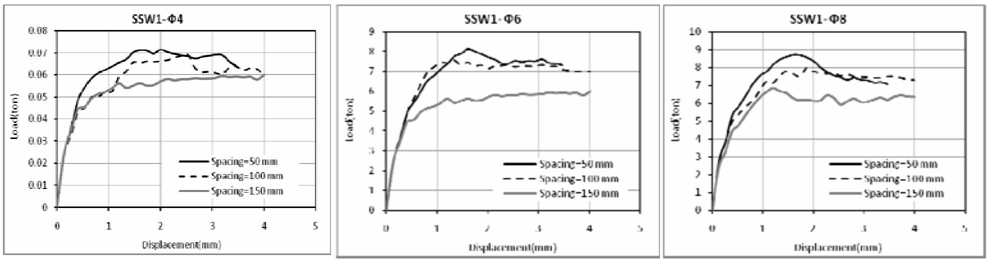

c) Spacing effect of shear reinforcement on the strength of masonry wall (SSW1)

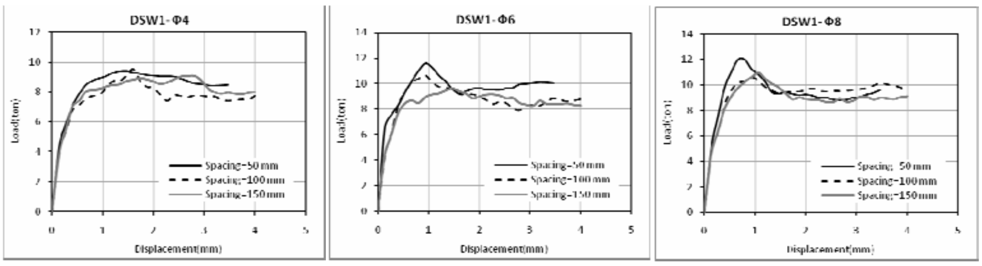

d) Effect of shear reinforcement with various spacing on masonry shear strength of DSW1

Figure 5. Comparison of Experimental and Analytical Results for Wall DSW1

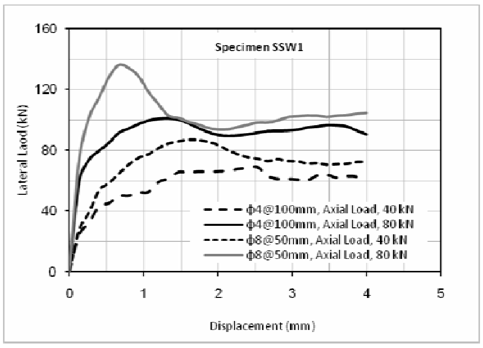

a) Effect of axial compression load on masonry shear strength for wall SSW1

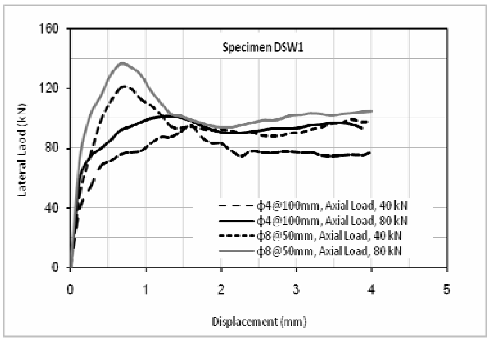

b) Effect of axial compression load on masonry shear strength for wall DSW1

Figure 6. Comparison of Experimental and Analytical Results for Wall DSW1

8. CONCLUSIONS

According to the obtained results from the calibrated non-linear numerical analysis it is concluded that shear capacity of the strengthened brick walls is due to the contribution of brick wall, reinforced concrete overlay and steel rebar. Also initial diagonal cracks did not widen significantly under increasing lateral displacements, but instead new sets of diagonal cracks formed and gradually spread over the wall diagonals, accompanied by higher energy dissipation and more ductile behavior.

The applied axial compression load has a significant influence on the in-plane shear performance of masonry shear walls, mainly because it suppressed the tensile field in a material inherently weak in tension.

REFERENCES

1. Lourenco P.B.; "Analysis of Masonry Structures with Interface Elements Theory and Applications"; report no. 03-21-22-0-01; June 1994.
2. Lourenço P.B. A User/Programmer Guide for the Micro-Modeling of Masonry Structures; Delft University of Technology; Faculty of Civil Engineering; report no. 03-21-1-31-35, November 1996.
3. Lourenco P.B.; "Computational Strategies for Masonry Structures"; Delft University Press, February 1996.
4. Abaqus Theory Manual, version 6.3, Hibbitt Karlson & Sorensen, Inc 2002.
5. Yaghoubifar A.; "Experimental and Analytical Investigation on the Behavior of Strengthened Brick Walls"; Msc Thesis; Superviser Proff. A.A. Tasnimi.

CD02-028

COMPARISON OF DIFFERENT CURING EFFECTS ON CONCRETE STRENGTH

M. Naderi[1], R. Sheibani[2], and M. A. Shayanfar[3]
[1]Associate. Prof., Imam Khomeini International University, Head of Civil. Eng. Dept., Takestan Azad University, Iran
[2]P. G. Student, Civil Eng. Dept. Takestan Azad University, Iran
[3]School of Civil Engineering, Iran University of Science and Technology, Tehran, Iran

ABSTRACT
The purpose of this investigation was to conduct a laboratory test program on how much different curing conditions affect the attainable strength of concrete. To achieve this purpose, a laboratory test program was conducted. The laboratory program consisted of casting 150 mm by 150 mm concrete cubes using eight different mix designs and subjecting them to six different curing conditions. In order to investigate the influence of curing conditions, on the compressive strength of concrete cubes, for each mix design three cubes were chosen for every curing regime. The curing regimes employed were: immersion in drinking water; covering with wet hessian and polythene sheet; keeping under dry laboratory conditions; keeping in open air; curing compound and steam curing. Except for steam curing system, the specimens of which were tested at the age of three days, for all other curing conditions, the compression tests were performed at the age of 28 days. It has been found that the curing system greatly influences the concrete strength. While the highest gain in compressive strength was recorded for cubes covered with wet Hessian and polythene sheet, the lowest gain in compressive strength was recorded for the specimens cure using steam curing.

Keywords: concrete, compressive strength, curing systems

1. INTRODUCTION
Concrete is a mix of cementitious (binding) solids [e.g., cement (calcium silicates, calcium aluminates, and calcium alumino-ferrites) and sometimes fly ash (aluminates and silica) and micro-silica], aggregate (sand and stones), and water. The cementitious solids of concrete, upon mixing with water, react in highly exothermic, temperature-dependent hydration reactions (the higher the temperature, the faster the hydration reactions) producing a firm, hard mass. There are four major stages in the hydration reactions: 1) surface reactions produce a ‘‘gel’’ on cementitious particles and release heat, lasting about 30 min, 2) hydration is slowed for several hours because diffusion of water into the cement particle is inhibited by the gel, 3) vigorous hydration and heat development occur for up to 20 h as water reaches un-hydrated cement inside the gel coating (stiffening of the concrete occurs during this stage), and 4) hydration continues to decline for years [1-3].

To ensure that hydration continues, especially at the surface, the concrete must be cured. Curing means water at the surface of the concrete is retained to allow the concrete to hydrate to a point where it has a strong, durable structure. If curing is inadequate, the water evaporates and hydration stops, resulting in a low-strength concrete. If adequate moisture isn't maintained in the curing environment, the concrete won't develop maximum compressive strength, and cracking may occur. Durability of the concrete may also be reduced due to inadequate hydration of the cementitious material.

Ambient atmospheric conditions can adversely influence the thermal and moisture structure of freshly poured concrete. If concrete becomes too warm or temperature gradients too large during the first several days after the concrete is poured or if there is insufficient water in the concrete, the concrete may crack or may not develop its maximum potential strength, reducing its long-term durability [4-7] .Surface drying may even affect the underlying concrete, as water will be drawn from the lower levels into the dry surface concrete. Any significant internal drying also will slow or stop hydration and the structure may not gain adequate strength.

For hydration to continue, the relative humidity inside the concrete has to be maintained at a minimum of 80%. If the relative humidity of the ambient air is that high, there will be little movement of water between the concrete and the ambient air and no active curing is needed to ensure continuation of hydration. Prevention of the loss of water from the concrete is of importance not only because the loss adversely affects the development of strength, but also because it leads to plastic shrinkage, increased permeability and reduced resistance to abrasion.

Continuous curing for a specified time, starting as soon as the surface of the concrete is no longer liable to damage is desirable. Such conditions can be achieved by continuous spraying or pounding or by covering the concrete with wet burlap. Probably the best method for curing concrete, although sometimes the least practical, is to flood the surface continuously with water for the first week after placement. But, if concrete dries between soakings, this alternate wetting and drying may actually damage the concrete. When water curing, the sprinkler should be going continuously for at least one week. On inclined or vertical surfaces, soaking hoses can be used. If w/c is low, continuous wet curing is highly desirable.

Another method of curing is called water barrier method. The techniques used include covering the surface of the concrete with overlapping polyethylene sheeting. White sheeting is preferable because it has the advantage of reflecting of solar radiation in hot weather [8].

Method of spraying curing compounds, which form a membrane may be used as well. It is obvious that the membrane must be continuous and undamaged. The timing of curing is also critical. The curing spray should be applied after bleeding has stopped. The most common way to cure new concrete is through a liquid membrane-forming curing compound also known as "cure and seal". These materials are usually sprayed or rolled on the surface. When dry, they form a thin film, which restricts moisture evaporation from the surface.

Timing is most important when using a curing compound. These products must be applied as soon as final finishing is complete. Otherwise, they could mar the concrete's surface. Also, the ready mix concrete supplier should be checked for recommendations on what to do when cold/freezing temperatures are anticipated. The next most important thing is the application rate. In this regard the manufacturer's recommendations should be followed completely.

The optimum time is the instant when the free water on the surface of the concrete has disappeared so that water shine is no longer visible [9].

Most penetrating sealers are made from derivatives of silicone called silanes or siloxanes designed to penetrate concrete pores. Once there, they react with the alkaline materials and moisture present to form silicone, making concrete water-repellent. While penetrating sealers usually cost more, they should last longer. Another reason for penetrating sealers popularity is that, when properly applied, they don't change the concrete's appearance. The major concern is that there can be no other membrane cure or sealer on the concrete when applying and the concrete must be at least 28 days old.

Internal concrete temperature is the most important factor affecting early compressive strength of concrete. Because of this, external heat is usually applied to produce high early compressive strengths concrete products after 12 to 18 hours of curing. Temperature is critical to meeting the dual concerns of higher early strength or reduced curing time. These methods are called accelerated curing methods. High early concrete strengths are most efficiently produced by increasing the internal temperature of the concrete while maintaining high moisture content in the curing environment. Heating reduces the relative humidity of the air surrounding the concrete. Thus, moisture must be added to the heated air to maintain the same relative humidity of the air.

Three heating methods are commonly used to accelerate curing: 1) Discharging steam or hot air directly into the curing environment puts the heating medium directly in contact with the concrete. 2) Enclosing steam or hot water in pipes heats the concrete by convection and radiation. 3) Attaching electrical resistance wires to the forms and covering them with insulation heats the product by heating the forms.

Circulating steam around the products is one of the most widely used accelerated curing methods, primarily due to the ease of producing and transporting steam to the concrete member. It’s an efficient method that increases the temperature and maintains a 100% relative humidity around the concrete products. Steam can be produced in high or low-pressure boilers, then piped to the casting bed, or generated by smaller steam packs located close to the products. An advantage of steam is that it contains relatively large quantities of heat per pound of steam at a relatively low temperature. This provides both an effective and economical method of transferring heat from the boilers to the concrete products. Heating air and discharging it directly into the curing environment can also increase internal temperature. There are two problems with this type of system. First, exhaust gases of unvented fossil fuel heaters contain carbon dioxide that combines with calcium hydroxide, a byproduct of cement hydration, forming weak calcium carbonates instead of strong calcium silicate hydrates. This produces a white powder on the concrete’s surface. Second, reduced moisture in the air allows surface drying of the concrete. If heated air is used to accelerate curing, the products should be covered to prevent moisture loss or misted with water to increase the relative humidity of the surrounding air and prevent premature drying.

The accelerated curing cycle can be divided into three periods of preset, rising temperature, and maximum temperature. Little or no cement hydration occurs during preset. Initial set ends the preset period. Heat shouldn't normally be applied until after initial set has occurred. Duration of the preset period is affected by admixture type and dosage, cement type, presence of pozzolans or ground granulated blast furnace slag, initial concrete temperature, and air temperature in the curing environment.

Advantages of proper curing includes: a less permeable, more water-tight concrete; reduced permeability means the concrete will be more resistant to freezing, salt scaling and attack by chemicals; prevents formation of plastic shrinkage cracks caused by rapid surface drying; increases abrasion resistance as the surface concrete will have a higher strength and significant reduction in scaling problems.

Curing should begin immediately after the finishing operation. Minimal delay is especially important in hot and/or dry weather to avoid rapid evaporation from the concrete surface. The benefits of curing concrete are significant, as can be the problems if curing is not performed as detailed above.

In order to investigate the influence of curing conditions, on the compressive strength of concrete cubes, for each mix design, three cubes were chosen for every curing regime. The curing regimes employed were: immersion in drinking water; covering with wet hessian and polythene sheet; keeping under dry laboratory conditions; keeping in open air; curing compound and steam curing. Except for steam curing system, the specimens of which were tested at the age of three days, for all other curing conditions, the compression tests were performed at the age of 28 days.

2. EXPERIMENTATION

2.1. Materials and Specimens

Concrete used in during these experiments, was made from ordinary Portland cement (binder), natural zone 2 sand (fine aggregate), basalt aggregate with maximum size of 20mm (coarse aggregate) mixed with sufficient drinking water and required additives where necessary. The mix proportions of eight different mixes used in this investigation are listed in Table 1.

Table 1: Mix designs.

No.	Cement (Kg/m^3)	Water (Kg/m^3)	Fine aggregate (Kg/m^3)	Coarse aggregate (Kg/m^3)	Super Plasticizer (Kg/m^3)	Silica Fume (Kg/m^3)
1	250	205	1227	661	0	0
2	360	205	1050	730	0	0
3	435	205	962	740	0	0
4	512	205	895	730	0	0
5	603	205	820	715	0	0
6	574	195	651	937	0	0
7	556	130	685	937	7.85	0
8	513	130	685	1080	7.85	43

In order to see the effect of different curing regimes on the compressive strengths of concrete, 150 mm cubes were prepared using mix designs shown in Tables 1. All of the cubes were covered with damp hessian and left to cure in the moulds for 24 hours. They were then removed from the moulds and labeled. Depending on the curing method chosen, the cubes were kept in water tank, covered with wet hessian and polythene sheet, covered with chemical curing agent, left under dry laboratory conditions, left in open air, or moved to accelerated steam curing chamber.

Except for the cubes cured under steam which were tested at the age of three days, the compressive strength of the specimens cured under other curing regimes were measured at the age of 28 days in accordance with BS1881: Part 116 [10].The steam curing systems was performed as specified in ASTM C 267 and 579. The temperature cycle used in this system of curing is shown in Figure 1.

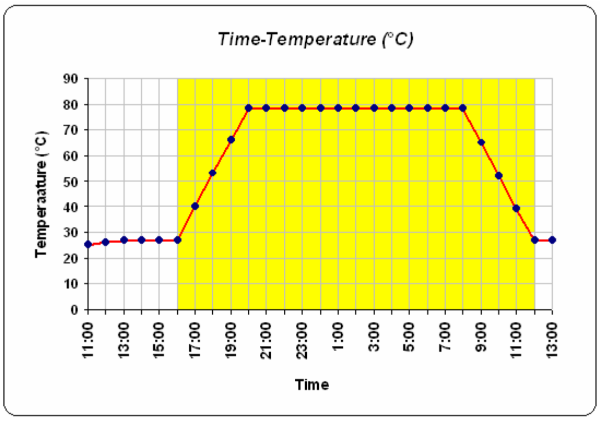

Figure 1. Duration and the temperature employed for the accelerated curing.

3. RESULTS AND DISCUSSION

The results of measured compressive strengths of cubes made using eight different concrete mixes and cured by immersion in water tank are shown in Figure 2.

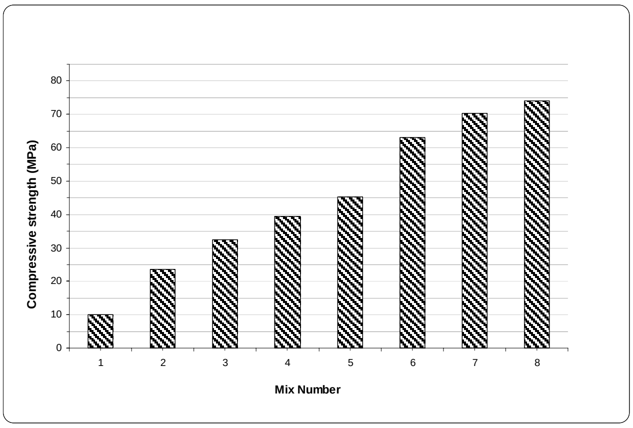

Figure 2. Compressive strengths of eight different mixtures cured by immersion

As it can be seen from this figure, the compressive strengths recorded for eight different concrete mixes range from 10 to about 75 MPa.
As is shown in Figure 3, the compressive strengths of the cubes made out of eight different concrete mixes, cured by wet hessian and polythene sheet coverage, are shown in Figure 3. This figure shows that, under this system of curing the cubes compressive strengths are seen to be between about 12 to 80 MPa. If these values are compared with their relative values recorded for the water immersion curing systems, it can be seen that covering the concrete cubes with wet hessian and polythene sheet tend to increase the cubes compressive strengths. It should be noted that although this increase is not very significant but it reflects the importance of the covering systems and their influence on the strength attained.

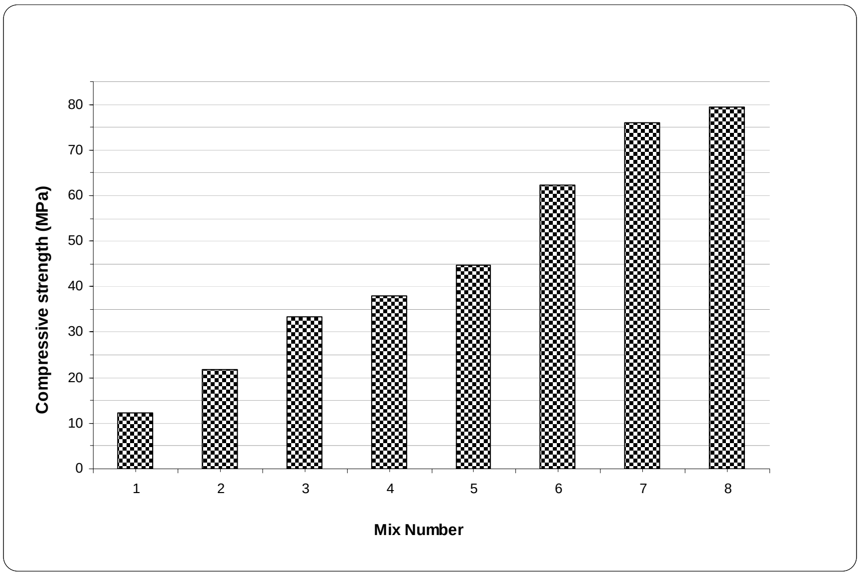

Figure 3. Compressive strengths of eight different mixtures, cured under wet hessian and polythene sheet

The results of the cubes compressive strengths cured using curing compound are shown in Figure 4. It can be seen from this figure that the measured compressive strengths of the cubes cured under this system of curing, has gained strengths from about 10 to about 64 MPa. Comparison of these results with those obtained for the other two curing regimes tends to show that the use of curing compound as curing agent produces lowest compressive strengths among the three curing systems.
Examination of the results shown in figure 5, which belongs to the concrete cubes cured by steam curing, tends to suggest that this curing method has produced the lowest compressive strengths among the four curing regimes discussed so far. Because while the lowest compressive strength recorded for this system appears to be about 6 MPa, the highest value recorded is about 57 MPa.

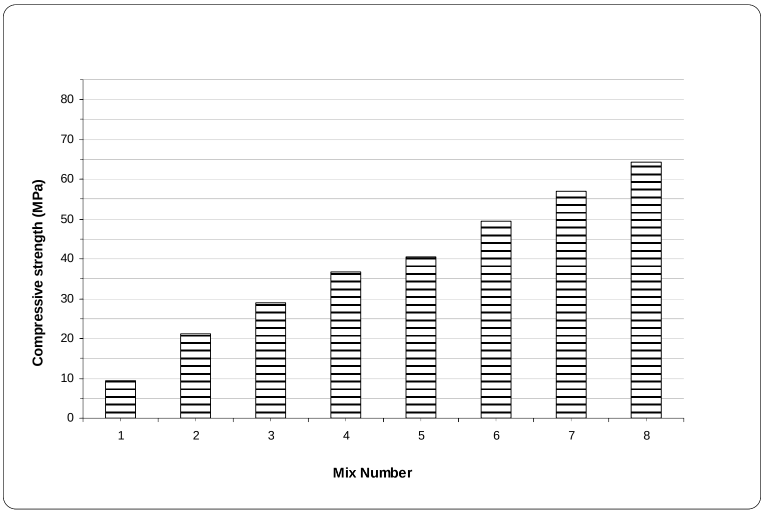

Figure 4. Compressive strengths of eight different concrete mixtures, cured using curing compound.

It should be noted compared with 28 days used for other curing systems, the age of testing used for this system of curing was three days. The results of this series of experiments tends to show that this curing system can be used where early concrete strength is of paramount importance.

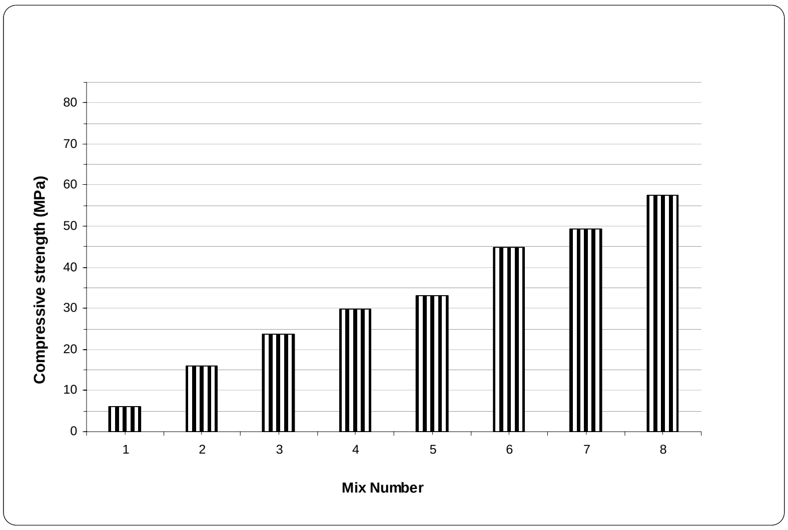

Figure 5. Compressive strengths of eight different concrete mixtures, cured by live steam

The compressive strengths of the cubes left under dry laboratory conditions, are shown in Figure 6. Examination of Figure 6 shows that if the concrete cubes are left under dry laboratory condition, compared with the other curing systems discussed so far, their compressive strengths would tend to decrease. This decrease appears to be more for weaker concrete mixes.

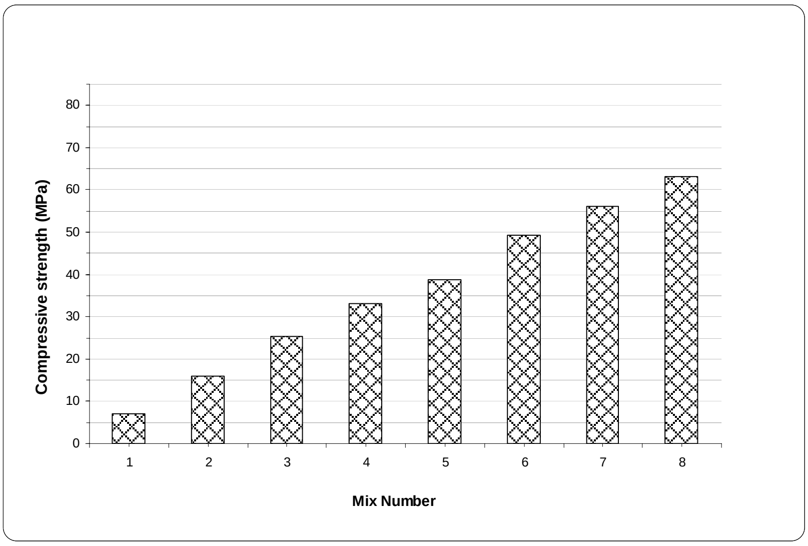

Figure 6. Compressive strengths of different concrete mixtures, left under dry laboratory conditions

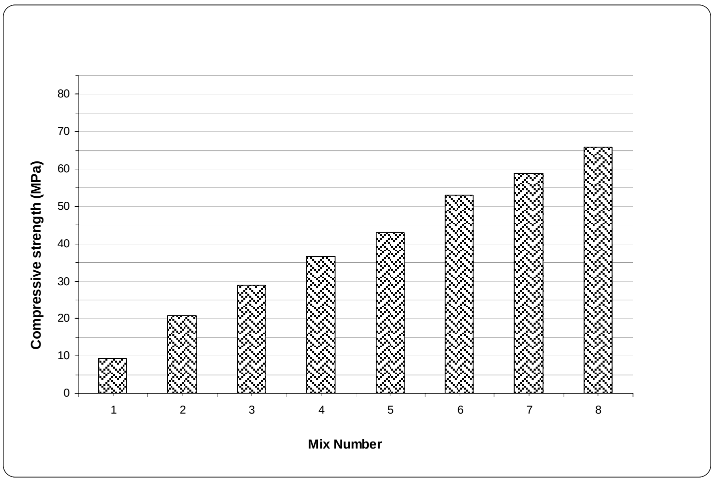

Figure 7. Compressive strengths of eight different concrete mixtures, left in open air

Figure 7 shows the compressive strengths of the cubes kept in open air after their removal from the mold. Examination of these results tends to indicate that compared with normal wet curing, leaving the concrete cubes in open air affects their compressive strengths. The compressive strengths of the cubes kept in open air for 27 days, appears to rage from about 8 MPa, to about 66 MPa. Comparison of these values with the respective values of the cubes kept under dry laboratory

conditions, tends to show an increase for the attainable compressive strengths of the cubes kept in open air. It should be noted that during the conduction of these experiments the temperature of the open air never reached below about 10 degree C. Comparison of the respective results shown in figure 8 tends to suggest that, among the curing systems employed covering of the concrete cubes with wet hessian and polythene sheet appears to have the highest positive effect on the attainable concrete compressive strength. It can also be seen from this figure that, compared with the results obtained from other curing regimes, steam curing tends to produce the lowest cube compressive strengths for the employed mix designs. Figure 8 also shows that compared with wet coverage, the immersion method of curing, tends to produce lower compressive strength.
The collective results of all the cubes cured, using six different curing regimes are depicted in Figure 8.

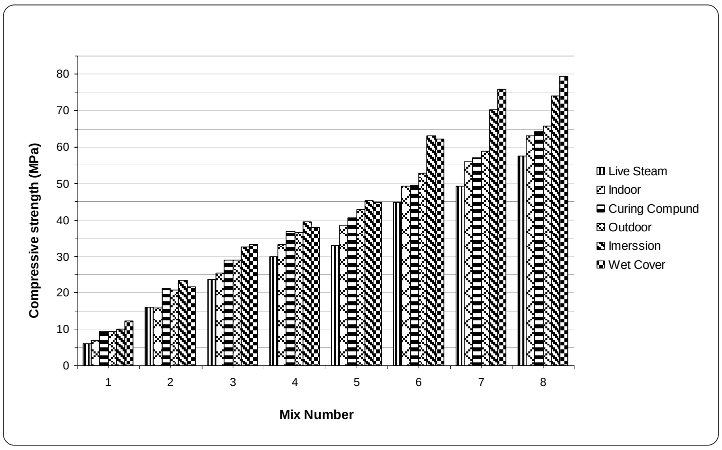

Figure 8. Compressive strengths of eight different concrete mixtures cured under different curing systems

4. CONCLUSIONS

From the results presented and discussed in this paper following conclusions can be made:

1) Different curing systems have different effects on the compressive strength of concrete.
2) Among the curing systems employed in this research, covering with wet hessian and polythene sheet produced the highest concrete compressive strength.
3) In comparison with covering with wet hessian and polythene sheet, the immersion curing system, produced lower compressive strength.
4) Steam curing produced the lowest compressive strength among the curing systems examined.
5) Compared with wet curing systems, leaving the cubes in open air and dry laboratory conditions after 24 hours of casting, tends to produce lower compressive strength.

REFERENCES

1. MATHER, B. (1990). "How to make concrete that will be immune to the effects of freezing and thawing." ACI SP-122, Paul Klieger Symposium on Performance of Concrete. D. Whiting, ed., American Concrete Institute, Detroit, MI, 1-18.
2. Accelerated Curing of Concrete at Atmospheric Pressure-State of the Art, ACI 517.2R-87 (Revised 1992), American Concrete Institute, 1980.
3. [3] Time of Setting of Concrete Mixtures by Penetration Resistance, ASTM C 403, ASTM, 1995.
4. Fitz Gibbon, M.E., 1976: Large pours for reinforced concrete structures. Concrete, **10** (3), 41.
5. FITZ GIBBON, M.E., 1976: Large pours-2, heat generation and control. Concrete, **10** (12), 33-35.
6. Gopalan, M.K., and Haqua, M. N., 1987: Effect of curing regime on the properties of fly-ash concrete. Amer. Concr. Inst. Mater. J., **84** (1), 14-19.
7. Neville, A. M., 1996: Properties of Concrete. John Wiley and Sons, 844 pp.
8. Mccall W. Calvin, "Energy Consumption for Curing Precast Prestressed Concrete," Concrete International, November 1982.
9. Pfeifer, Donald, W. and Marusin, Stella, "Energy Efficient Accelerated Curing of Concrete", Prestressed Concrete Institute, 1981.
10. BS 1881: Part 116, Method for determination of compressive strength of concrete cubes, British Standards Institution, London, 1983.

CD02-029

AN INVESTIGATION ON THE BEHAVOIR OF ONE-LAYER AND TWO-LAYER 3D PANELS IN SHEAR AND FLEXTURAL TEST

H. Afshin, E. Sheykh Milani, B. Ferdowsi
Sahand University of Technology, Civil Engineering Faculty, New Sahand Town, Iran

ABSTRACT
The 3D panels are a new system of construction. This system is used as wall and ceiling in buildings. The structural behavior of 3D panels is dependent on the strength and rigidity of connector elements. In this article flexural and shear tests have been conducted on six 3D panels. The results have been compared with results of finite element software, ANSYS. The details and results of the test program are described, and the observed behaviour patterns are discussed.

Kewords: 3D panels, shear test, flexural test, sandwich panel

1. INTRODUCTION
Precast concrete sandwich panels (PCSP) have two concrete faces and one polystyrene layer between concrete faces. The concrete faces are connected to each other with shear connectors. The arrangment and spacing of shear connectors in PCSP vary depending on several factors, such as desired composite action, applied load, span of the panel and type of shear connectors used. There aro no specific rules for arranging the connectors. The complex behaviour of PCSP due to its material nonlinearity, the uncertain role of the shear connectors and the interaction between various components has led researchers to rely on experimental investigations backed by simple analytical studies. The lack of information on the behaviour of this important type of concstruction is due to the high cost of full scale testing and the extreme difficulty of fabrication of small-scale models.

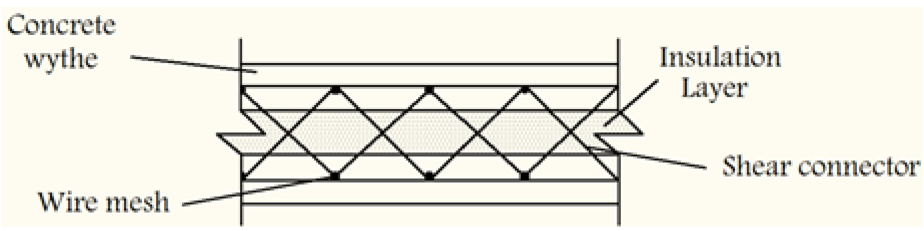

Figure 1. 3D panel

2. EXPERIMENTAL STUDIES
2.1. Characteristics of Panels
The diameter of longitudinal bars and shear connectors is 3 mm. The dimensions are shown in Figure 2. Characteristics of panels are given in Table 1.

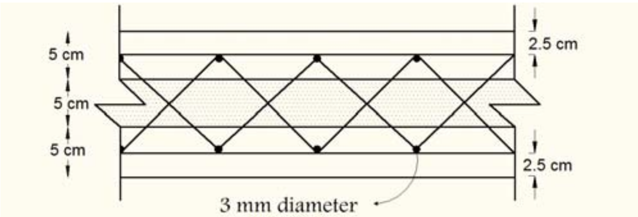

Figure 2. 3D panel

Table 1: Characteristics of panels

No.	**Dimension (m)**	**Compressive strength 10×10×10 (kg/cm^2)**		f'_c	
1	0.15×1×3	284	Top.	227.2	Top.
		305	Bot.	244	Bot.
2	0.15×1×3	318	Top.	254.4	Top.
		298	Bot.	238.4	Bot.
3	0.15×1×3	315		252	
4	0.15×1×3	303		242.4	
5	0.15×1×3	313	Top.	250.4	Top.
		300	Bot.	240	Bot.
6	0.15×1×3	315		244.8	

2.2. Flextural Test

The panels were tested using four-point test according to ASTM D3043 [1] and the data was transferred to the computer. Etch test was carried on until the complete failure of the panel. Cracking pattern was similar in all panels at this stage. The test set up for flexural test is shown in Figure 3.

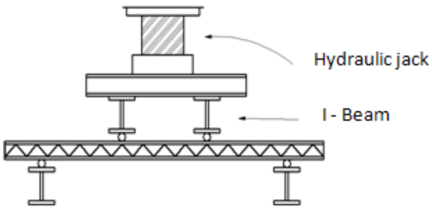

Figure 3. Flexural test set up

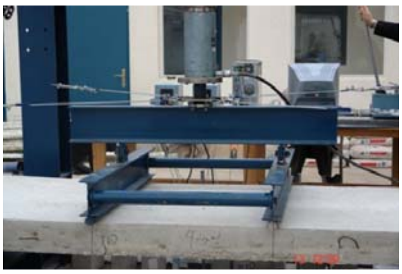

Figure 4. Cracking pattern in one layer panel in flexure

Figure 5. Cracking pattern in two layer panel in flexure

2.3. Shear Test

The shear test set up is shown in Figure 6. The load is near one of the supports in order to simulate pure shear conditions.

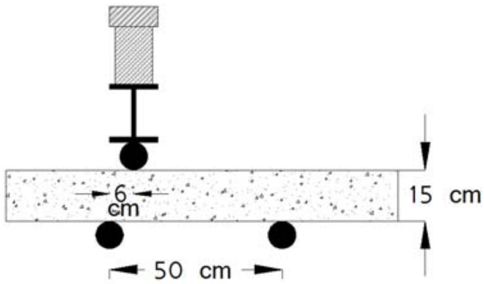

Figure 6. Shear test set up

Cracking pattern for two-layer panels is shown in Figure 7.

Figure 7. Cracking pattern for two-layer panel in shear test

3. RESULTS AND DISCUSSIONS

3.1. Flextural Test Results

Flexural test results are shown in the following Figure. The load bearing capacity of one-layer panel is more than two-layer panel but the ductility of two-layer panel is more.

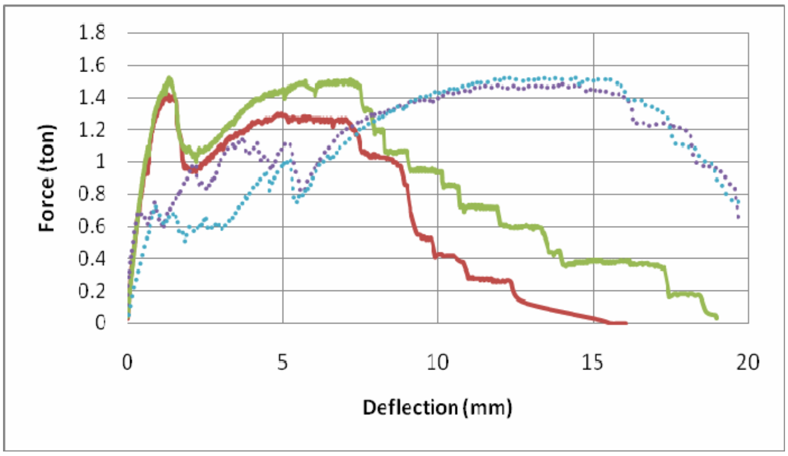

Figure 8. Load-Defection curve for panels in flexure

3.2. Shear Test Results

In shear test, one-layer 3D panels fail at 14 ton and have brittle behavior but two-layer panels have a ductile behavior although their load bearing capacity is about 5 tons. Figure 9 shows the behavior of one-layer and two-layer 3D panels in Shear test.

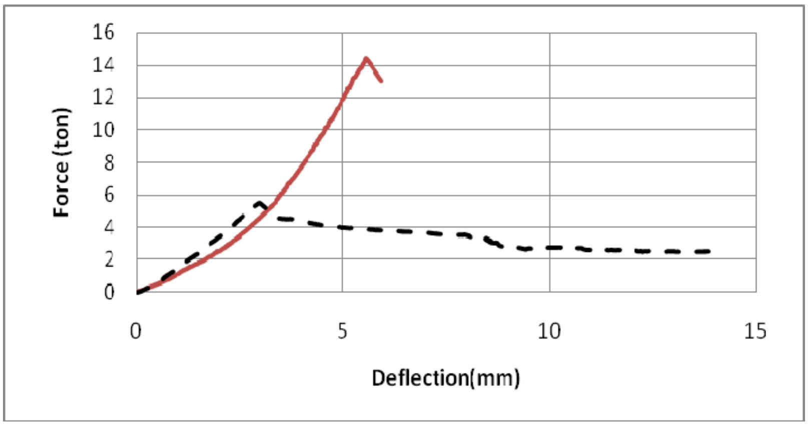

Figure 9. Load-Defection curve for panels in shear

4. THEORETICAL STUDIES

4.1. Finite Element Modelling

Solid 65 and link8 elements are used to model concrete and bars in ANSYS respectively. Translations at Z direction are restrained at both supports but at X direction only one support is restrained. The following Figures show the finite element model.

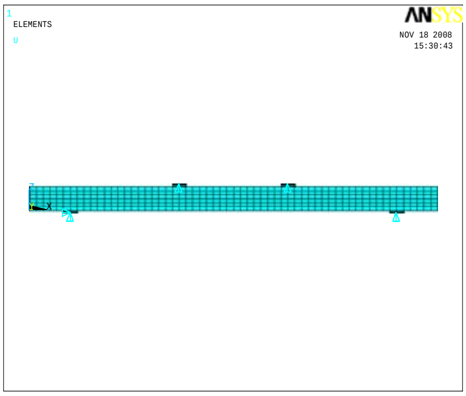

Figure 10. Model for one-layer panel in flexure

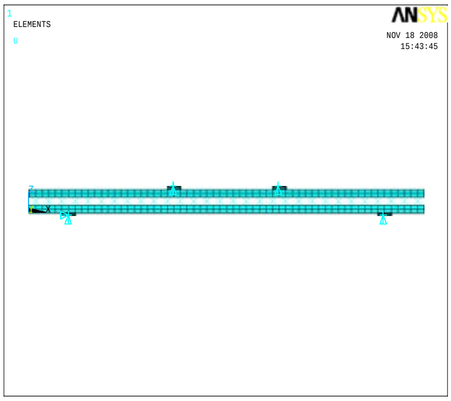

Figure 11. Model for two-layer panel in flexure

5. COMPARISON OF THEORITICAL AND EXPERIMENTAL STUDIES

Experimental and theoretical results have been compared in Figure 12 and 13 for one-layer and two-layer panels.

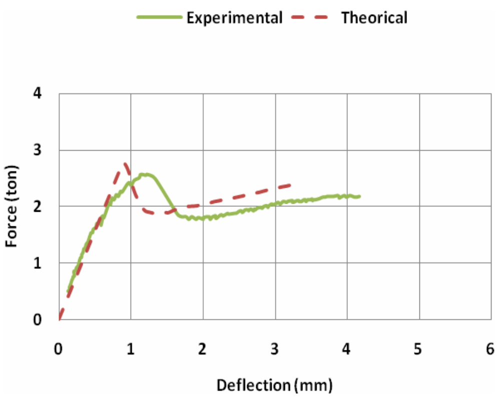

Figure 12. One-layer panels in shear

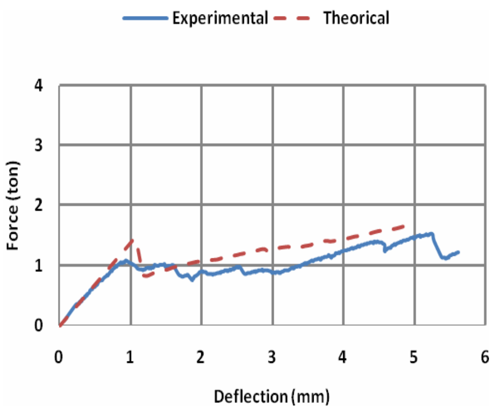

Figure 13. Two-layer panels in shear

6. CONCLUSION

a) The rigidity of one-layer panels is more than that of two-layer panels.
b) In flexure there is no difference in the load capacity of one-layer and two-layer panels although two-layer 3D panels have no concrete in the middle layer.
c) By eliminating concrete from the middle layer and substituting it with bars the ductility of the panel increases.

REFRENCES

1. ASTM international, Standard test method for structural panels in flexure, standard, 2006, D3043-00.
2. Benayoune A. *Precast concrete sandwich panel as a building system*, Ph.D. Thesis, Department of Civil Engineering, University of Putra, Malaysia, 2003.
3. Benayoune, A. et al. *Non-linear finite element modelling of precast concrete sandwich panels under transverse loads.* In: Proceeding of the 2nd Word Engineering Congress, Hilton, Sarawak, Malaysia; 2002. p. 260-64.
4. Bush TD, Stine GL. Flexural behaviour of composite precast concrete sandwich panels with continuous truss connectors. PCI J 1994; 3(2):112-21.
5. Bush TD, Zhiqi Wu. Flexural analysis of prestressed concrete sandwich panels with truss connectors, PCI J 1998; 43(5):76-86.
6. Carol I, Bazant ZP. *New developments in micro-plane and multicrack models for concrete*, In: Wittmann, Aedificatio FH, editors. Int. Proceedings of FRAMCOS2, Germany, 1995.
7. Einea A, Salmon DC, Tadros MK, Culp T. *Partially composite sandwich panel deflection*. ASCE J Struct Eng 1995; 121(4):83-778.
8. Einea A, Salmon DC, Tadros MK, Culp T. A new structurally and thermally efficient precast sandwich panel system. PCI J 1994; 39(4):90-101.
9. Einea A. *Structural and thermal efficiency of precast concrete sandwich panel system*, Ph.D. thesis, Department of Civil Engineering, University of Nebraska-Linkoln, Omaha, NE., 1992.
10. Ellinna SHM. *The behaviour of precast concrete sandwich panel as slab*, B.E. Report, Universiti Putra Malaysia, 2000.
11. PCI committee on pre-cast concrete sandwich wall panels, *State of the Art of Precast/Prestresses Sandwich Wall Panels*, PCI J 1997; 42(2):92-133.

CD02-030

EXPERIMENTAL INVESTIGATION OF THE JACK ARCH SLAB RETROFITTED BY CONCRETE LAYER

Saeed Pourfallah[1], M. R. Maheri[2] and M. A. Najafgholipour[1],
[1]Research student, Department of Civil Engineering, Shiraz University, Iran
[2]Professor, Department of Civil Engineering, Shiraz University, Iran

ABSTRACT

Considering the widespread use of jack arch roofs and the need for seismic retrofitting of this system of flooring in Iran the behaviour of the retrofitted form of these slabs is unknown. The Iranian building codes also do not deal sufficiently with this type of roofing and as a result little control is applied on their method of construction. The retrofitting method of adding a concrete layer (CL) is a method which was first introduced in Romania after the earthquake of 1990. This paper reports on an experimental investigation of this method and comparison with other retrofitting methods. For this purpose, a number of slabs with different methods of retrofitting such as the Romanian method, the method recommended by the Iranian Standard 2800, the two way method and a slab without retrofitting were constructed. Then, the slabs were loaded step by step in out of plane direction and the load-displacement pushover curves for the slabs were obtained. Using these curves, the seismic strength parameters of different slabs are determined and compared.

Keywords: jack arch slabs, retrofitting, concrete layer, masonry, pushover test

1. INTRODUCTION

Jack arch slabs have been extensively used to floor and roof urban and rural buildings in Iran. The jack-arch flooring system is stable under normal static conditions. The brick arches transfer the gravity loads, mainly in compression, to the supporting steel beams. The load is then transferred via the steel beams in flexure and shear to the load-bearing walls. However, reports of slab damage and collapse in recent earthquakes in Eastern Europe and Iran by Razani and Lee (1973) [1]; Maheri (1990) [2]; Maheri (1998) [3] and Maheri (2003) [4], reflect the weakness of the unanchored slab under dynamic loading. To overcome this problem, Moinfar (1968) [5] suggested that the slab beams be joined together at their ends by either transverse beams or by steel tie bars. This form of anchored jack-arch slab has a better seismic response because the relative movements of the slab beams are somewhat prevented. The Iranian seismic code; Standard 2800 [6], has adopted these suggestions and many slabs have recently been constructed using these anchoring methods.

It should be noted that the contemporary jack-arch slab construction in Iran is still considered a non-engineered slab in the Iranian seismic code, and there are no particular design procedures for their engineered design. Simple methods of increasing the seismic performance of the slab in the form of inter-span transverse beams have been proposed and their effectiveness investigated both experimentally and numerically (Maheri and Imanipour [7]). Finally, procedures for engineered design and construction were introduced (Maheri and Rahmani [8] and Maheri [9]). Following the Romanian earthquake of 1990, a number of damaged jack arch slabs were retrofitted by adding a reinforced concrete layer on top of the floor, effectively making the slab to act as a composite slab.

In this paper, a jack arch slab retrofitted with a concrete layer (Romanian method), is experimentally investigated and compared with slabs retrofitted with other methods. For this purpose, four full-scale jack arch slabs were constructed using the conventional material and workmanship. One slab was tested without any retrofitting and the other three slabs were first retrofitted by one of the; concrete layer, two-way slab and the Standard 2800 anchoring methods and then each slab was subjected to out-of-plane pushover loading and the load-displacement curves have been obtained for each slab.

Method for Retrofitting of Jack Arch Slabs

The above different methods of retrofitting jack arch slabs are here further discussed.

2. CONCRETE LAYER (ROMANIAN) METHOD:

In this method, the flooring on the slab is first removed. Then a mesh of reinforcement with maximum bar spacing equal to 100cm, is welded on the slabs beams. Finally, the slab is covered with a layer of concrete having an average thickness of around 5 cm (Figure 1).

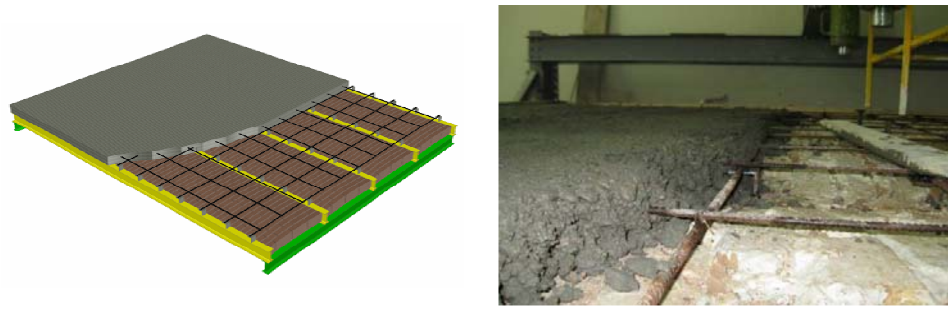

Figure 1. Concrete layer method for retrofitting jack arch slabs

3. TWO WAY METHOD (MAHERI)

In 1995, Maheri presented a new method for retrofitting of jack arch slabs [10]. In this method a series of secondary beams are placed between the primary beams of the slab (Figure 2). By this method the one way jack arch slab is changed to a two way slab. Also, because the masonry arches of the slab are divided in the locations of the secondary beams, these discontinuities reduce the contribution of the masonry arch in resisting the load of the slab and effectively reduce their role to infills. Maheri has introduced this method of construction as an engineered version of the jack arch system and has proposed procedures for its engineered design and construction.

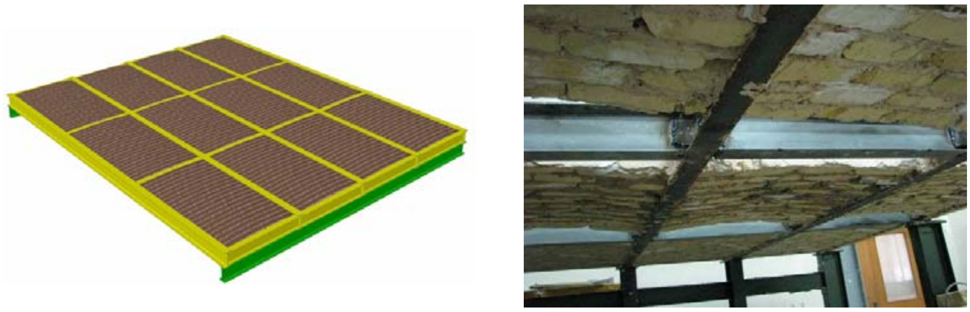

Figure 2. Two way method retrofitting jack arch slabs

4. IRANIAN BUILDING CODE METHOD

This method is recommended by standard 2800. In this method a cross belt is welded on the slab beams (Figure 3).

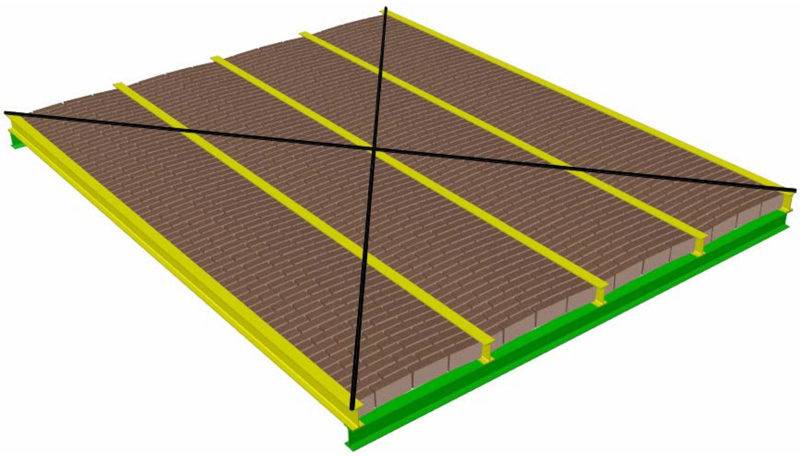

Figure 3. Standard 2800 method for construction jack arch slabs

Test Specimens and Load Setup

All the specimens are made with the same size and materials. Only their retrofitting method is different. The slabs are 3.2 m×4 m in size each having 5 primary beams. The beams are IPE 12 with spacing equal to 80 cm. Traditional clay bricks are used for making the masonry arches. The rise of arch is 5 cm. In turn, out of plane pushover load was applied to each slab. The out of plane load was applied on a line in the middle of the slab to distribute the load in one direction using two hydraulic jacks (Figure 4). In each step a total 5.72kN load is applied to the specimens. The out of plane displacements of the slabs were recorded by 6 mechanical gages in each load step (Figure 5).

Figure 4. Loading setup

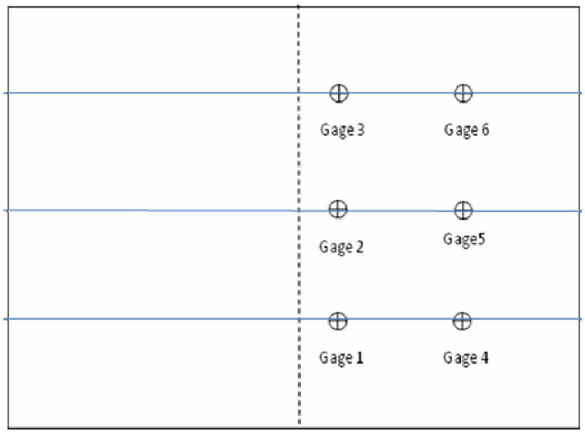

Figure 5. Gage positions

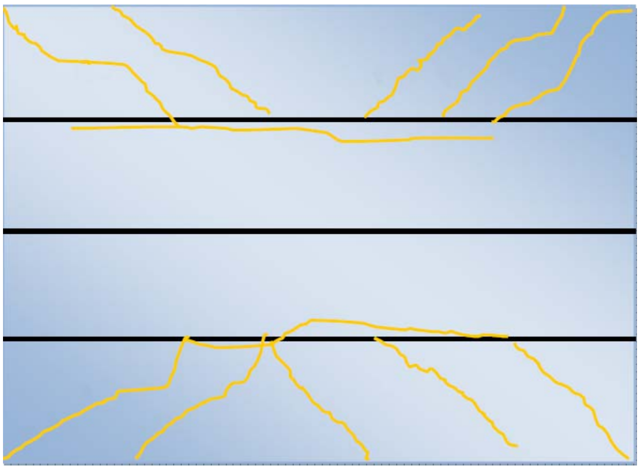

Figure 6. Crack pattern in the traditional jack arch slab

5. TRADITIONAL JACK ARCH SLAB

This specimen is made with the mentioned properties without any retrofitting. The results of the test on this slab can be used as a benchmark. The test was carried out on the slab 28 days after casting of the concrete layer. During the loading of the slab, the first crack occurred diagonally at one corner of the slab at the load of 22.88 kN. Further diagonal cracks developed at other corners and parallel to the corner cracks as shown in Figure 6. The ultimate load which could be sustained by the slab was 62.92 kN. However, the slab retained its integrity and no brittle failure was observed in the brick arches. The load-displacement curve for this slab, using the central gage (gage 2) is presented in Figure 7.

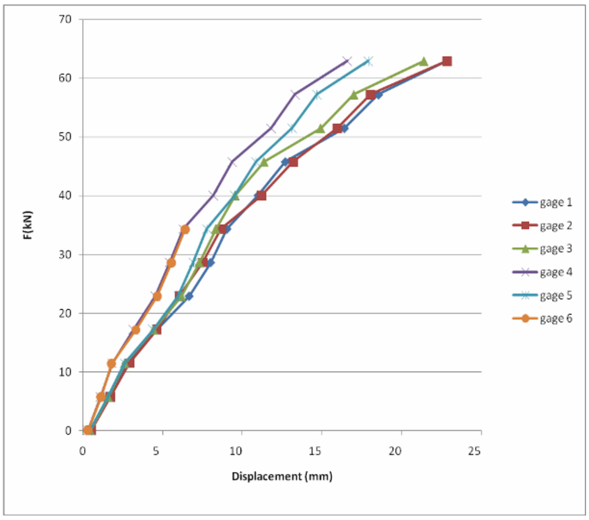

Figure 7. Load-displacement curve for traditional jack arch slab

6. SLAB RETROFITTED BY CONCRETE LAYER:

After making the jack arch slab, the slab was retrofitted as follows:

a) The flooring was first removed and the beams top flanges and masonry arches were cleaned.

b) Slab reinforcement: If the beams of the slab are IPE 16 or more, considering the brick width (10 cm), the top flange of the beams and a minimum 6 cm of the beams web would be in contact with concrete. Therefore, using bars Φ12@50 cm in a direction perpendicular to the beams appeared to be sufficient. However, in many slabs, beams of IPE 14 or less are used and the contact between concrete and beams would not be sufficient. For this reason a connecting method, similar to that used in composite slabs was adopted. In this method, shear keys are used for increasing the concrete-beams contact. 5 cm long, 5×5×5cm angles were welded at 30cm spacing for shear keys. A mesh with bars Φ8@30 cm, corresponding to the minimum steel ratio of ρ_{min}=0.002 was then welded on to the shear keys. The concrete having f'c=30 MPa was used to an average depth of 5cm to cover the reinforcement mesh. After 28 days, the test was carried out in a similar manner to the first slab.

The first cracks occurred at the corners of the slab in a diagonal pattern similar to the non-retrofitted slab, at the load of 143kN (Figure 8). A small number of further diagonal cracks occurred at higher loads (Figure 8). The loading continued until the ultimate strength of the slab (194.5kN). Similar to the first slab, the behavior of this slab was also ductile and no brittle failure or collapse happened in the brick arches. The load-displacement curve is presented in

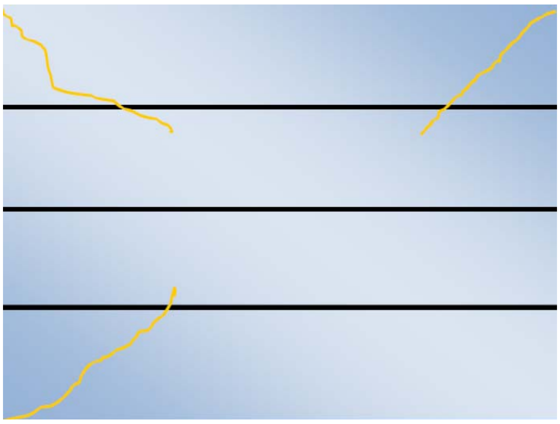

Figure 8. Crack pattern in the Concrete Layer method

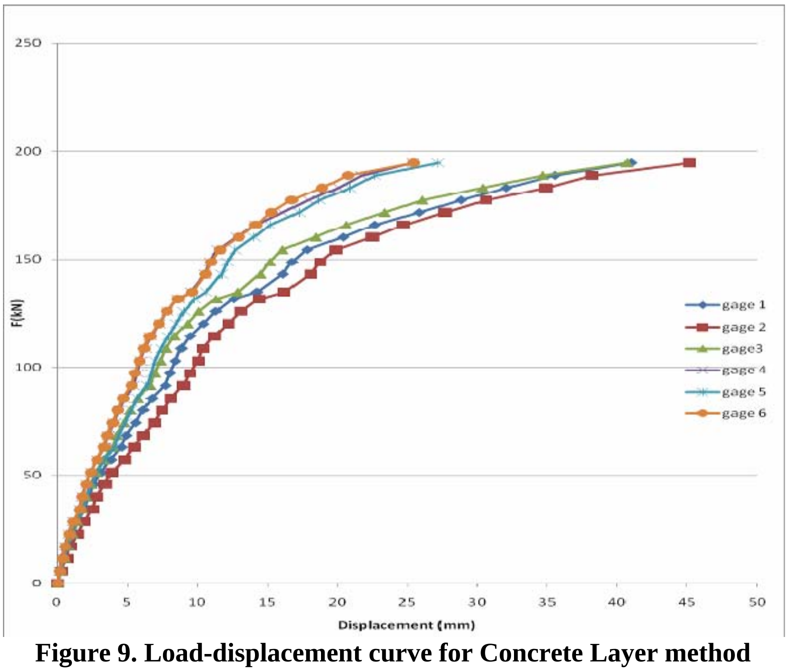

Figure 9. Load-displacement curve for Concrete Layer method

7. SLAB RETROFITTED BY THE TWO WAY METHOD

After construction of the jack arch slab, this method of retrofitting was applied to it. In this method IPE 12 were used for secondary beams and were placed in two rows at 1.33 m distance apart. The test was carried out in a similar way to the other slabs.

The first crack occurred at an outer brick arch at 51.48kN. After this initial crack, the diagonal cracks occurred at the corners at 85.8kN (Figure 10). The test continued until the ultimate strength of the slab (102.96kN). Similar ductile response was noted for this slab, where no spalling or collapse of brick arches happened. The load-displacement curve for this retrofitted slab is presented in Figure 11.

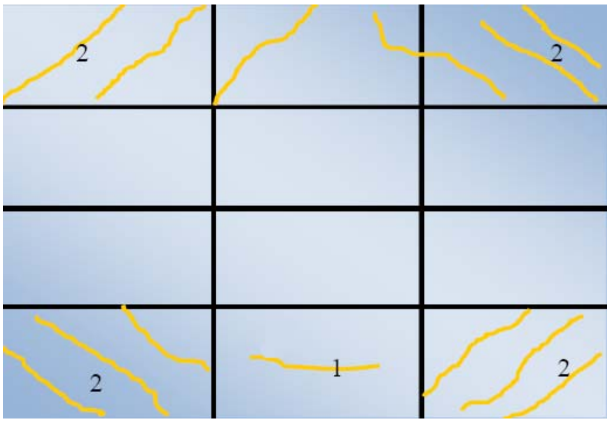

Figure 10. Crack pattern in the two way method

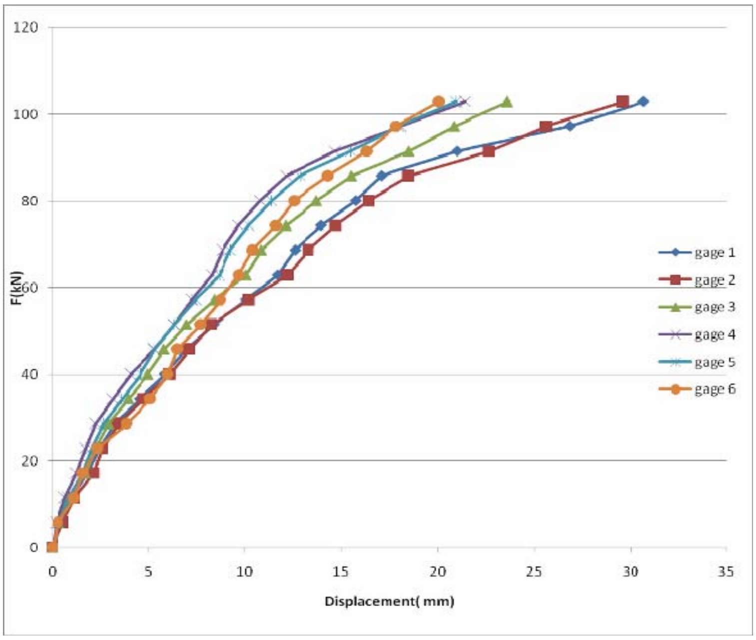

Figure 11. Load-displacement curve for two way method

8. SLAB RETROFITTED BY THE STANDARD 2800 RECOMMENDATIONS

Reinforcing bars Φ14 were used for retrofitting this slab. The cross diagonal bars were welded to top of the flanges of the main beams. After 28 days, the test was carried out in a similar manner to the other slabs.

The first crack occurred at 51.48kN at one corner. At higher loads, his crack followed by some cracks parallel to the primary beams (Figure 12). The test continued until the ultimate strength of the slab at 74.36 kN. Similar to the other slabs, no brittle failure was noted in the brick arches. The load-displacement curve for this retrofitted slab is presented in Figure 13.

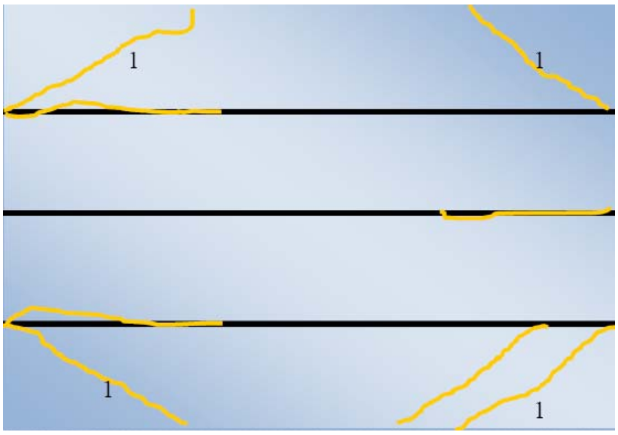

Figure 12. Crack pattern in the standard 2800 method

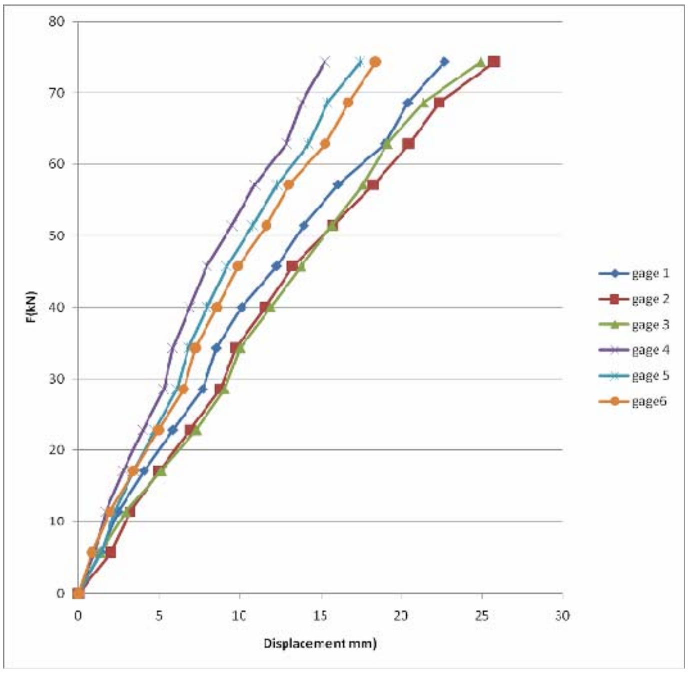

Figure 13. Load-displacement curve for standard 2800 method

9. COMPARSION OF RESULTS

For comparison of the test results, the strength and performance parameters, derived from the load-displacement curves of gage 2 for the four slabs, are presented in Table 1.

Table 1: Comparison of the strength and performance parameters of the slabs

Parameters	Traditional (non-retrofitted)	Concrete layer	Two way	Standard 2800
Ultimate Strength (kN)	63	194	102	36
Ultimate displacement (mm)	22	45	29	25
Toughness (kN.mm)	6690	69000	14000	7900
Ductility	1.7	2.84	2.21	1.46

Ultimate Strength

The concrete layer method increased the ultimate strength of the slab by up to 3 times. This method has the highest effect on increasing the ultimate out of plane strength of the jack arch compared to the other retrofitting methods (Figure 14).

Ultimate displacement

The Ultimate displacement in the slab retrofitted by the concrete layer method was 198% more than the traditional slab (Figure 15).

Ductility ratio

Ductility ratio in the slab retrofitted by concrete layer was 167% more than the traditional slab (Figure .16).

Toughness

The concrete layer increased the toughness of the slab 10 folds compared to the traditional jack arch. This method has the highest effect on the toughness with respect to the other retrofitting methods (Figure17).

Weight of slabs

The increase in the weight of the slab due to retrofitting is not suitable, because it increases the gravity and seismic loads and puts further demands on other elements of the buildings. Adding a concrete layer increased the weight of the slab by 25%. This is a considerable amount of weight increase compared to other retrofitting methods (Figure 18).

Construction cost

In the concrete layer method, the retrofitting costs are divided in two parts. First, cost for retrofitting the slab, which is around 2.6 times the cost of construction of a traditional slab. Second, the costs for retrofitting other element, due to weight increase. This part is a function of the type of structural system and is unique for each building (Figure 19). It seems that the concrete layer method, though effective in considerably increasing the strength and performance parameters of the slab, compared to other methods, it suffers from being more time consuming, technically more difficult to perform and particularly far more costly.

In following Figures, 1, 2, 3 and 4 respectively stand for traditional, standard 2800, two way and Concrete Layer.

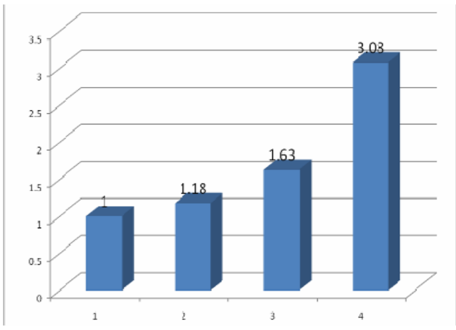

Figure 14. Ultimate strength

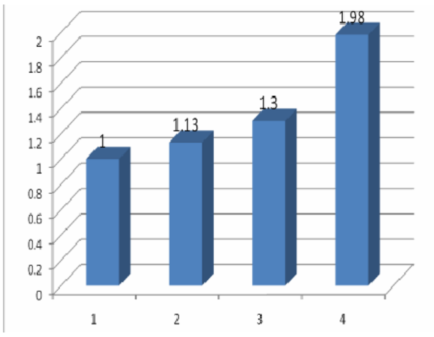

Figure 15. Ultimate displacement

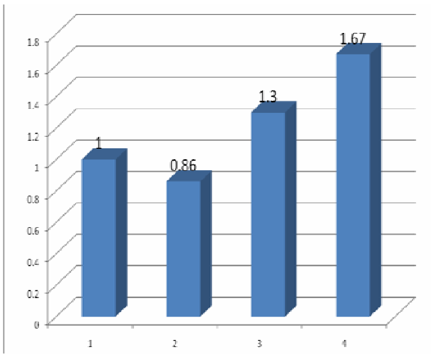

Figure 16. Ductility ratio

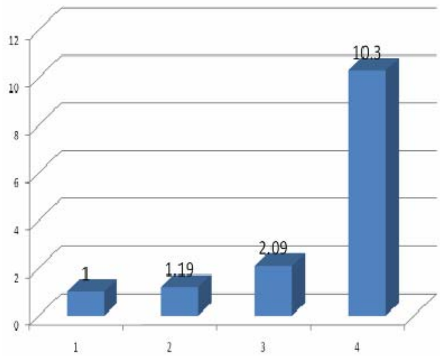

Figure 17. Toughness

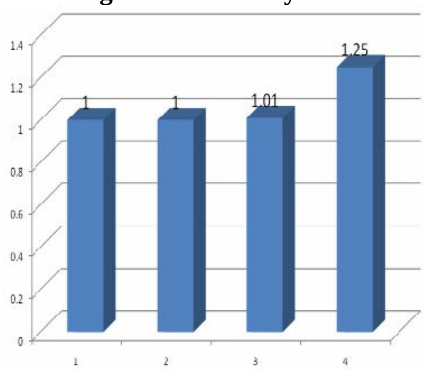

Figure 18. Weight of slabs

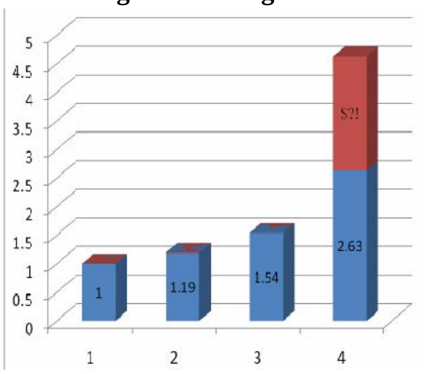

Figure 19. Construction costs

10. CONCLUSIONS

Based on the results of the tests presented in this paper the following conclusions can be drawn regarding the effectiveness of the concrete layer (Romanian) retrofitting method;

1. The method is very effective in increasing the strength and ductility of the jack arch slab and enhancing its seismic performance. However, it is time consuming and particularly suffers from the excess cost, both in terms of retrofitting the slab itself and the secondary costs of strengthening other elements of the building due to the increased weight.
2. To reduce the secondary costs of the method, it is recommended that after the positioning of the concrete layer, the brick arches be removed, in effect, converting the jack arch slab into a composite steel-concrete slab. However, by doing so, the primary costs of the retrofitting will be increased due to the removal of the brick arches and construction of the necessary false ceiling.
3. Considering the cost-ineffectiveness of the method, it is recommended that it be used to retrofit special buildings or buildings in which due to the overstrength of its members, the secondary cost of retrofitting are minimal.

REFERENCES

1. Razani, R, Lee, K.L., The engineering aspect of the Qir earthquake of April 10.1972 in Southern Iran, National Academy of Engineering, Washington DC, 1973.
2. Maheri, M. R, The engineering aspects of Manjil, Iran earthquake of June 1990, Earthquake engineering. Field investigation team (EEFIT) report, Institute of civil engineers, London, UK. Oct 1990.
3. Maheri, M. R, Lessons from Golbaf, Kerman earthquake of 14 March 1990, Pro. 1st.
4. Iran-Japan workshop on recent earthquake in Iran and Japan, Tehran, pp 319-330, 1998.
5. Maheri, M. R, Performance of building roofs in the 2003, Bam, Iran, earthquake, Earthquake Spectra, Vol. 21, No. S1, pp S411-S424, 2005.
6. Moinfar, A. A., Earthquake engineering trend in Iran, Pro. of 3rd World Conf. on Earthquake. Eng., New Zealand, Vol. 3, 1965.
7. Building and Housing Research Center, Iranian Code of Practice for |Seismic Resistant Design of Building Standard No 2800, Tehran, 2005, p. 135.
8. Maheri, M. R, Imanipour, A., Seismic evaluation of proposed two way jack arch slab, Pro. of 3rd Int. Conf. on Seism. and Earthq. Eng., SEE3, Vol. 2, Tehran, Iran, pp. 605-612, 1999.
9. Maheri, M. R, Rahmani, H., Static and seismic design of one way and two way jack arch masonry slabs, J. of Engineering Structures, Vol. 25, No. 13, pp. 1639-1654, 2003.
10. Maheri, M. R, Sesumic Design and Construction of Jack Arch Masonry Slabs, International Institute of Earthquake Engineering and Seismology, Tehran, Iran, 2004.
11. Maheri, M. R, Bahar, O., Analytical studies of the seismic behavior of the I-beam jack arch system, Pro. of 2rd Int. Conf. on Seism. and Earthq. Eng., SEE2, Vol. 1, Tehran, Iran, pp. 819-828, 1995.

CD02-031

تغییرشکل‌ها و آسیب‌های بوجود آمده در برج‌های خنک‌کننده بتنی در اثر نشست غیریکنواخت در حالت غیرخطی

سعید صبوری[1]، مریم ترابی[2]

۱. دانشیار دانشکدهٔ عمران دانشگاه صنعتی خواجه نصیرالدین طوسی، تهران

۲. کارشناس ارشد سازه هیدرولیکی، دانشگاه صنعتی‌خواجه نصیرالدین طوسی، تهران

چکیده

نشست غیر یکنواخت در سازه‌های بزرگ، از اهمیت زیادی برخوردار است. این موضوع در برج‌های خنک‌کننده، به‌دلیل بزرگی ابعاد سازه در هر دو جهت قطر و ارتفاع، اهمیت بیشتری می‌یابد و نشست غیر یکنواخت محتمل‌تر می‌باشد؛ چرا که به دلیل طول زیاد پی، امکان تفاوت جنس خاک زیر پی بیشتر است. همچنین به‌دلیل ارتفاع قابل ملاحظه این نوع سازه‌ها، نیروی باد به عنوان یک بارگذاری عمده محسوب شده که باعث به‌وجود آمدن نیروهای متفاوت در ستون‌ها و در نتیجه نشست غیریکنواخت می‌شود.

در این تحقیق، برج خنک‌کننده شازند اراک توسط نرم‌افزار ABAQUS مدل شده است. در پی و پوسته، از مدل پلاستیسیته آسیب‌دیده بتن و در ستون‌ها، از مدل ترک گسترده استفاده شده است. نشست غیر یکنواخت به صورت مدل ریاضی کسینوسی به پی اعمال شده و دامنه آن برابر نصف نشست یکنواخت تحت وزن می‌باشد. آنالیزها با درنظر گرفتن اثرات غیرخطی مصالح و هندسه صورت گرفته است. نتایج نشان می‌دهد پی تغییرشکل افقی پیدا می‌کند و آسیب کششی زیادی می‌بیند. همچنین ستون‌ها و پوسته تغییرمکان جانبی قابل ملاحظه‌ای نسبت به وزن پیدا می‌کنند، به‌گونه‌ای که ماکزیمم تغییرمکان نسبی ستون‌ها ۰/۱۳ درصد می‌باشد و ماکزیمم تغییرمکان نسبی پوسته، ۰/۰۶۲ درصد می‌باشد که در ۰/۴۴ ارتفاع آن رخ داده است.

کلیدواژه‌ها: برج‌های خنک کننده بتنی، نشست غیریکنواخت، مدل پلاستیسیته آسیب دیده بتن

۱- مقدمه

برجهای خنک‌کننده، سازه‌های عظیمی‌هستند که از پوسته، ستون‌ها و پی تشکیل شده‌اند. با توجه به طول زیاد پی، امکان تفاوت جنس خاک و در نتیجه وقوع نشست غیریکنواخت، بیشتر است. همچنین به دلیل ارتفاع زیاد این نوع سازه‌ها، باد به عنوان یک بارگذاری عمده، باعث ایجاد نیروهای متفاوت در ستون‌ها و در نتیجه نشست غیریکنواخت می‌شود. نشست غیریکنواخت در سازه‌ها به خصوص سازه‌های عظیم، باعث ایجاد نیروهای اضافی شده و به عنوان یک فاکتور بارگذاری عمده باید در نظر گرفته شود.

اولین تحقیق در مورد نشست غیر یکنواخت برجهای خنک کننده، توسط «گولد» در سال ۱۹۷۲ صورت گرفت [۱]. وی فرض کرد که یکی از ستونها به اندازه δ_R نسبت به ستونهای مجاور خود جابجایی نسبی داشته باشد و

میزان این جابجایی به اندازه‌ای باشد که نیروی محوری ستون ناشی از بار مرده در اثر این جابجایی، برابر صفر گردد. وی همچنین فرض می‌کند این نشست، صرفاً موجب تغییر در نیروی پنج ستون مجاور گردد.

بعد از «گولد»، «وندا» به مطالعه و بررسی نشست غیر یکنواخت پرداخت[۲]. وی در آنالیز خود از مدل و فرضیه «گولد» استفاده نمود یعنی فرض نمود فقط یک ستون به میزانی نشست داشته باشد که نیروی فشاری ناشی از بار مرده آن به صفر تقلیل یابد. همچنین این نشست، فقط موجب تغییر در نیروی پنج ستون مجاور گردد. «وندا» بر خلاف «گولد»، پوسته را با استفاده از روش المان محدود و توسط کامپیوتر آنالیز نمود و مشاهده کرد با دور شدن از محل ستون نشست کرده، اثر نشست در ستون‌ها کمتر است.

سپس «کریشنا»[۱] در سال ۱۹۹۲ به بررسی نشست غیر یکنواخت در برجهای خنک کننده پرداخت[۳]. او درآنالیز خود از منطق «گولد» بهره جست و اثر نشست یک ستون را بررسی کرد، یعنی مقدار نشستی را به یکی از ستونها اعمال کرد که در اثر آن، نیروی محوری ستون در اثر بار مرده صفر گردد. وی با استفاده از نرم افزار، برجی مشابه برج «وندا» آنالیز نمود و مشاهده کرد که نیروهای ستون‌ها به مراتب کمتر از نتایج به‌دست آمده توسط «وندا» می‌باشد. علت آن این است که «وندا» در محاسبه نیروی ستون‌ها، صرفاً پنج ستون را وارد محاسبات نموده بود، ولی «کریشنا» ستون‌ها را توسط برنامه آنالیز نمود و به دلیل شکل پذیری ستون‌ها، قسمتی از نشست به پوسته منتقل می‌شود، بنابراین تنش‌های به‌وجود آمده، کمتر است.

سپس «صبوری» در سال ۲۰۰۰، به بررسی نشست غیریکنواخت پرداخت. وی برج نیروگاه اصفهان را تحت مدل ریاضی کسینوسی در محدوده الاستیک آنالیز نمود و به این نتیجه رسید که بیشترین تغییرات نیروها در قسمت پایینی پوسته و در رینگ تحتانی می‌باشد و با افزایش ارتفاع، مقدار نیروها کاهش می‌یابد.

در سال ۲۰۰۴ «اختری» به مطالعه نشست غیریکنواخت پرداخت. وی نیز نشست غیریکنواخت را به صورت مدل ریاضی کسینوسی در نظر گرفت؛ و با استفاده از نرم افزار ANSYS5.4، برج را آنالیز غیر خطی نمود و به این نتیجه رسید که تنش‌ها در کلیه قسمت‌ها به مقدار زیادی نسبت به حالت خطی کاهش می‌یابند ولی مقدار تغییر شکل برج افزایش پیدا می‌کند [۹].

مدل ریاضی نشست غیریکنواخت

در سال ۱۹۷۷،«چسیلسکی»[۲] برای رسیدن به یک الگوی مناسب نشست، نشست غیر یکنواخت ۴ برج را در مدت ۶ سال اندازه گیری کرد [۴]. و برای هر برج، در سالهای مختلف نشست‌های غیر یکنواخت بدست آمده را با سریهای ریاضی تقریب زد و به مدل ریاضی زیررسید:

$$\begin{aligned}\omega = {} & A_0 + A_1\cos\beta + \beta_1\sin\beta + A_2\cos2\beta + \beta_2\sin2\beta + A_3\cos3\beta \\ & + \beta_3\sin3\beta + A_4\cos4\beta + \beta_4\sin4\beta\end{aligned} \tag{1}$$

که در رابطه فوق، ω نشست بر حسب متر، β زاویه مرکزی و A_0 تا A_4 و همچنین B_1 تا B_4 اعداد ثابت می‌باشند. با توجه به اینکه در رابطه (۱) جمله اول صرفاً نشست یکنواخت کلیه ستونها را بدست می‌دهد و جمله

۱-Krishna
۲- Ciesielski

دوم و سوم نشان دهنده انحراف تمام برج به صورت یک جسم صلب می‌باشد و بطبع این نوع نشست‌ها باعث بوجود آمدن تنش در برج نمی‌شوند، لذا با توجه به نوع خاک و ماکزیمم اختلاف نشست که ممکن است در برجهای مذکور بوجود آید، رابطه ساده زیر که جمله چهارم در رابطه (۱) می‌باشد، برای محاسبه نشست غیر یکنواخت ارائه شد:

$$\omega = 0.03\cos 2\beta \qquad (۲)$$

او برج را بر اساس مدل ارائه شده توسط رابطه (۱) آنالیزکرد و چنین نتیجه گرفت که در صورتی که نشست غیر یکنواخت قابل توجهی در برجهای خنک کننده به‌وجود آید، نیروهای داخلی ایجاد شده در سازه این برجها، تا حدی زیاد است که ممکن است باعث خرابی آنها شود.

اندازه گیریهای واقعی انجام شده توسط «چسیلسکی» نشان می‌دهد که فرض نشست صرفاً یکی از ستونها در برجهای خنک کننده به عنوان نشست غیر یکنواخت، نمی‌تواند گویای همه واقعیت باشد، لذا به نظر می‌رسد برای تعیین یک مدل مناسب به طوری که بتواند پاسخگوی هر گونه نشست غیر یکنواخت احتمالی باشد، نیاز به رابطه جامعتری است.

«کالوزا»[۳] و «ماتژا»[۴]، مدل ریاضی بهتری را برای نشست غیر یکنواخت برجهای خنک کننده به صورت زیر ارائه نمودند [۵]:

$$\omega = \Delta U\cos(n\theta) \qquad (۳)$$

که در آن ΔU برابر نصف حداکثر اختلاف نشست اعمال شده پی، θ زاویه مرکزی و n با توجه به تعداد ستونهای برج خنک کننده از ۲ تا نصف تعداد ستونهای برج می‌تواند در نظر گرفته شود. آنها با اعمال رابطه (۳) برای دو مقدار$n=۲$ و $n=۴$ بر روی تعدادی از برجهای خنک کننده که در مقیاس ۱/۱۰۰ ساخته شده بودند، نیروهای داخلی و همچنین تغییرشکلهای سازه برج مذکور را اندازه‌گیری کردند و مشاهده نمودند افزایش نیروهای غشایی محیطی در نواحی رینگهای سخت کننده تحتانی و فوقانی قابل توجه است.

از طرف دیگر «کاتو» و همکارانش، نشست برج خنک کننده را از دیدگاه آمار بررسی نمودند [۶]. ایشان مدل ریاضی $U = U_0 + \sum_{i=1}^{n} U_i.\cos(i\theta - \theta_i)$ را برای نشست غیر یکنواخت قائم برجهای خنک کننده در نظر گرفتند که U_0 مقدار نشست یکنواخت می‌باشد و U_i و θ_i به ترتیب عبارتند از ضریب فوریه و اختلاف فاز برای‌هارمونیک i ام. در این مدل اختلاف فاز θ_i به صورت تصادفی تغییر می‌کند، بنابراین نیازی به محاسبه ندارد. مقدار متوسط نشست U_0 توسط آنالیز کامپیوتری و با مدل کردن خاک زیر برج توسط فنرهایی بدست می‌آید، بنابراین تنها کافیست ضریب فوریه U_i تعیین شود که با روشهای مختلفی قابل حصول می‌باشد. یک روش این است که با داشتن شناخت کافی از خاک منطقه و اندازه گیریهایی که روی سازه می‌شود، ضرایب بدست آیند؛ نظیر کاری که «چسیلسکی» انجام داد. در روش دیگر، با توجه به اطلاعات موجود در زمینه سازه و خاک زیر آن، به تعیین انحراف معیار و میانگین نشست اقدام نموده و با توجه به این دو متغیر، نشست ماکزیمم و نشست مینیمم را بدست آورده و در نتیجه اختلاف نشست حاصل می‌شود.

۱- Kaluza

۲- Mateja

با توجه به اینکه نوع خاک می‌تواند نقش تعیین کننده‌ای در رابطه با حداکثر اختلاف نشست داشته باشد، لذا «صبوری» در سال ۲۰۰۰، با استفاده از مطالعات «کاتو» و منظور نمودن نوع خاک زیر پی، رابطه (۳) را تکمیل نموده و مدل ریاضی زیر را ارائه نمود [۷و۸] :

$$\omega = \frac{k}{(2-k)} U_0 \cos(n\theta) \qquad (۴)$$

که n تعداد ستونهای برج خنک کننده از ۲ تا نصف تعداد ستونهای برج می‌تواند در نظر گرفته شود. $U_{\circ}$ میانگین نشست برج تحت اثر وزن خود و با فرض پایه الاستیک می‌باشد و $KU_{\circ}/(2-K)$، نصف اختلاف نشست حداکثر بین ستون‌ها می‌باشد و ضریب k نیز مقدار ثابتی است که با توجه به جنس خاک می‌توان آن را از منحنی‌ها استخراج نمود. حداقل مقدار k را می‌توان برابر با ۰/۳ برای خاک رسی، و حداکثر آن را برابر با ۰/۶۶ برای خاکهای ماسه ای منظور نمود[۷]. زیرا خاکها با مشخصات مختلف، عملکردهای مختلفی در مسئله نشست دارند؛ با مشاهده جدول (۱) مشخص می‌شود که مقدار نشست کل در خاکهای ماسه ای کمتر از خاکهای رسی می‌باشد اما اختلاف نشست در خاکهای ماسه ای تقریباً برابر با نشست حداکثر است ولی در خاکهای رسی، این اختلاف نشست بسیار کوچکتر از نشست حداکثر می‌باشد [۸]. بنابراین می‌توان چنین نتیجه‌گیری کرد که اثر نشست غیر یکنواخت بر سازه، در خاکهای ماسه‌ای بیشتر از خاکهای رسی است.

جدول ۱: مقایسهٔ نشست در خاک‌های رسی و ماسه ای

رس (به طور معمول تحکیم یافته و یا کمی‌بیش از حد تحکیم یافته)	**ماسه**	**مورد**
ρ_{max} و $\Delta\rho$	$\Delta\rho$، به خصوص تحت اثر بارهای دوره ای و یا دینامیکی	عامل کنترل کننده طراحی پی
بزرگ	کوچک	میزان نشست
آهسته	سریع	آهنگ نشست
به شکل بشقابی	بزرگ در لبه‌های پی،ρبی قائده	الگوی نشست
$\Delta\rho_{max}$ معمولاً خیلی کمتر از ρ_{max}	$\Delta\rho_{max}$ اغلب نزدیک به ρ_{max}	رابطه بین $\Delta\rho_{max}$ و ρ_{max}
نسبتاً کوچک زیرا ρ با قائده بوده و آهسته اتفاق می‌افتد	نسبتاً بزرگ زیرا ρ بی قائده بوده و سریع اتفاق می‌افتد	اثر $\Delta\rho$ مفروض بر روی سازه

مدلسازی بدنه برج

در این تحقیق، برج شازند اراک به ارتفاع ۱۳۰ متر و شعاع متوسط پی۱۸۳/ ۵۳ متر مدل شده است. پی، ستونها و پوسته، به ترتیب با المان‌های حجمی(C3D8 , solid)، تیر (B31, beam) و پوسته‌ای (S4, S3R, shell) مدل شده‌اند. مدل المان بندی شده برج در شکل (۱) نشان داده شده است. المانهای حجمی‌در هر گره، ۳ درجه آزادی انتقالی دارند. المانهای تیر و پوسته‌ای، درهر گره، ۳ درجه آزادی انتقالی و ۳ درجه آزادی دورانی دارند. با توجه به

اینکه ضخامت المان‌های پی نسبت به دو بعد دیگرش قابل ملاحظه است، لذا استفاده از المانهـای پوسـته‌ای در پی، باعث ایجاد خطاهای عددی می‌شود؛ همچنین به دلیل سطح مقطع بزرگ المان‌های پی نسبت به طولـشان و نیز به دلیل عدم وجود دقت کافی در مدل کردن سختی پیچشی خاک، استفاده از المانهـای تیـر در پـی، منطقـی نبوده. استفاده از المان‌های حجمی‌درستونها، باعث می‌شود که نتایج فقط براساس تنش- کرنش حاصل شوند، که این کار از نظر مهندسی قابل قبول نمی‌باشد و بهتر است خروجی‌های نیرو و لنگر را نیز داشته باشیم لـذا المـان-های تیر انتخاب گردیدند. جهت به‌دست آوردن نتایج دقیق، در نزدیکی محل اتصال پوسته به سـتونها، تـا ارتفـاع ۲۲ متر، از مش بندی ریزتری در پوسته استفاده شده است.

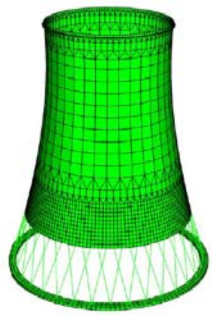

شکل ۱- مدل المان بندی شده برج شازند اراک

برخی از آرماتورهای پی به صورت آرماتورهای منفرد و برخی دیگر، به صورت لایه‌ای فولادی با ضخامت معادل، مدل شده است. آرماتورهای ستون‌ها، به صورت منفرد و آرماتورهای پوسته به صورت لایه‌ای فولادی با ضخامت معادل، مدل شده‌اند.

رفتار فولاد برای مدلسازی آرماتورها به صورت دو خطی با سخت شوندگی سینماتیکی در نظر گرفته شـده اسـت. درجدول (۲) مشخصات فولاد مورد استفاده درآرماتورها آمده است.

جدول ۲: مشخصات فولاد به کار رفته در آرماتورها

f_y (MPa)	E (MPa)	E_s (MPa)	ρ (kg/m^3)
۴۰۰	۲/۱E۵	۲/۱E۳	۷۸۵۰

برای مدل کردن بتن، در پی و پوسته، از مدل پلاستیسیته آسیب دیده بتن؛ و درسـتونها از مـدل تـرک پوشـشی، استفاده شده است. مدل پلاستیسیته آسیب دیده بتن، با نتـایج آزمایـشگاهی مطابقـت بهتـری دارد، زیـرا بازیـابی سختی به هنگام وارد شدن از کشش به فشار را در نظر می‌گیرد. همچنین در این مدل، کاهش سختی بـه هنگـام باربرداری‌ها در نظر گرفته می‌شود که این کاهش با افزایش کرنش پلاستیک، افزایش می‌یابد. مشخصات بتن بـه کار رفته در جدول (۳) آمده است. با توجه به مشخصات زیر، منحنی‌های تنش- کرنش فشاری و کششی بـرآورد شده‌اند [۹].

جدول ۳: مشخصات بتن به کار رفته در مدل

f'_c (MPa)	f'_t (MPa)	$E_\circ$ (MPa)	E_S (MPa)	υ	ρ (kg/m^3)
۲۸	۳/۵	۳۱۵۰۰	۱۵۰۰۰	۰/۲	۲۴۰۰

مدلسازی خاک زیر سازه

برای مدل کردن خاک، از فنرهایی در ۳ جهت استفاده شده است. سختی فنرها که تابعی از شعاع‌های پی و مدول برشی خاک می‌باشد، از روی نمودارهای ارائه شده، محاسبه شده است[۱۰]. مدل ریاضی نشست غیر یکنواخت پی، $\frac{k}{2-k}U_\circ \cos(n\theta)$ می‌باشد که $\frac{k}{2-k}U_\circ$ نصف حداکثر اختلاف نشست پی می‌باشد که با ماسه‌ای بودن خاک، حداکثر اختلاف نشست اعمال شده، همان نشست میانگین پی، $U_\circ$، می‌باشد؛ یعنی $\omega = 0.5U_\circ \cos(n\theta)$ که درآن، $2 \le n \le 18$ (n، شماره مود نشست).

تغییرشکل‌ها و آسیب‌های بوجود آمده

ابتدا سازه برج تحت وزن تحلیل شد، سپس مودهای مختلف نشست به آن اعمال گردید و آنالیزها صورت گرفت. منظور از مود نشست صفر، آنالیز تحت وزن می‌باشد. نتایج تحلیل‌ها در نمودارهای مربوطه آمده است.

۱- پی

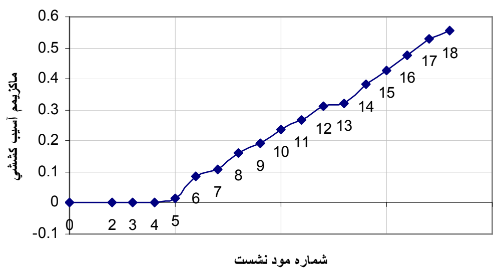

شکل۲- ماکزیمم آسیب کششی پی

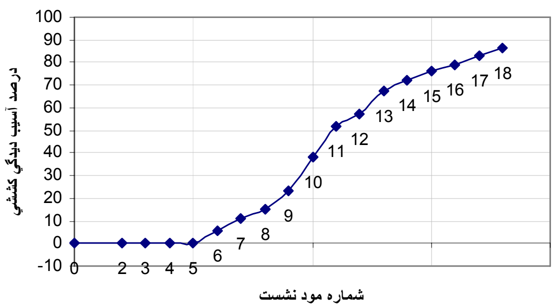

شکل ۳- درصد آسیب دیدگی کششی پی

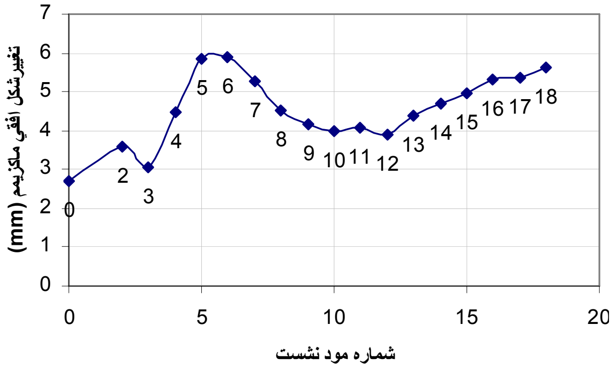

شکل ۴- ماکزیمم تغییرشکل افقی بوجود آمده در پی

در اثر نشست غیر یکنواخت، حداکثر آسیب کششی پی از مقدار صفر در حالت تحت وزن به مقدار۵۶٪ در مود نشست n=۱۸ رسیده است.لازم به ذکر است که در اثر نشست غیر یکنواخت، پی هیچ گونه آسیب فشاری ندیده است و مقدار آن در تمامی‌مودها صفر می‌باشد.

در مود نشست n=۲ و n=۳ و n=۴، پی مانند حالت تحت وزن، اصلاً آسیب کششی ندیده است. و بعد از آن با افزایش شماره مود نشست، درصد آسیب دیدگی کششی افزایش یافته است. به طوری که ماکزیمم آن در مود نشست n=۱۸ رخ داده است. یعنی در اثر نشست غیر یکنواخت، ۸۷٪ پی آسیب کششی دیده است.

نشست غیر یکنواخت باعث شده است که در پی، تغییر شکل افقی بوجود آید. به طوری که در بحرانی ترین حالت که مود نشست n=۶ می‌باشد، مقدار ماکزیمم آن از ۲/۷ mm در حالت تحت وزن به ۵/۸۹ mm رسیده است. یعنی مقدار آن، ۲/۲ برابر شده است. همچنین ماکزیمم تغییر شکل نسبی پی، ۰/۰۰۰۰۵۳ یعنی ۰/۰۰۵۳ درصد می‌باشد. (منظور از تغییرشکل نسبی پی، نسبت تغییرشکل افقی به قطر آن می‌باشد.)

شکل (۵)، شکل تغییریافته پی را در مود نشست n=۱۸ نشان می‌دهد. گفتنی است که فرم تغییریافته پی، برای وضوح بیشتر، مقیاس شده است.

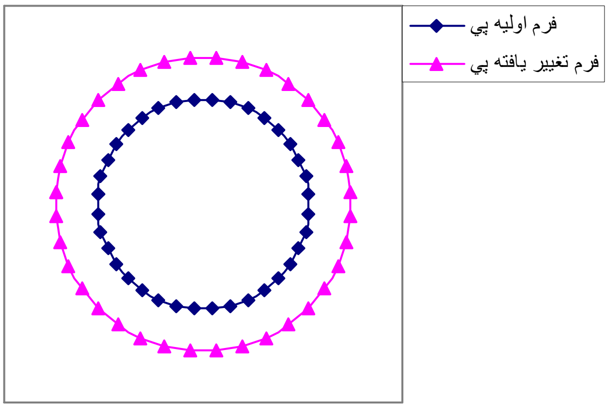

شکل تغییریافته پی نسبت به حالت وزن

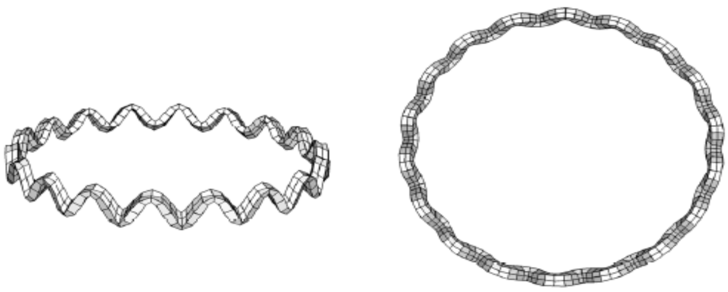

شکل ۵- فرم تغییر یافتهٔ پی در مود نشست n =۱۸

چنانچه کانتور آسیب کششی پی را در مود نشست n= ۱۸ را در نظر بگیریم که میزان آسیب کششی و نیز درصد آسیب دیدگی کششی پی، از بقیه مودها بیشتر است؛ مشاهده می‌گردد که ناحیه آسیب کششی پی از لبه خارجی آن که در امتداد ستون می‌باشد، آغاز شده و به ترتیب در ناحیه اطراف ستون‌ها گسترش یافته است. لازم به ذکر است که نرخ آسیب کششی در اطراف ستون‌هایی که نشستشان با در نظر گرفتن نشست تحت وزن، $-u_{\circ} + 0.5u_{\circ}$ می‌باشد به مراتب بیشتر است از ستون‌هایی که نشست همراه وزنشان $-u_{\circ} - 0.5u_{\circ}$ می‌باشد. یعنی پی اطراف ستون‌هایی که نشست غیریکنواخت باعث شده به سمت بالا جابجایی داشته باشند، بیشتر آسیب کششی دیده‌اند. کانتور آسیب کششی پی در مود نشست n=۱۸ در شکل (۶) نشان داده شده است.

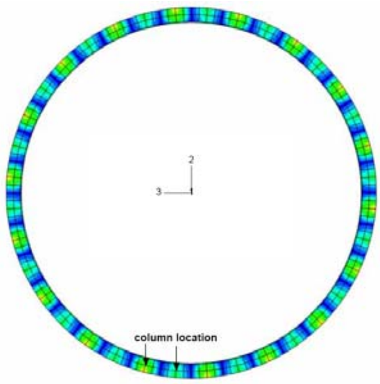

شکل ۶- کانتور آسیب کششی پی در مود نشست n=۱۸

۲- ستون‌ها

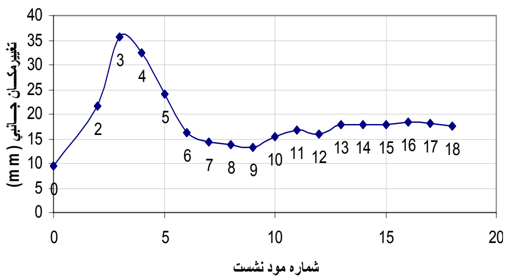

شکل ۷- ماکزیمم تغییرمکان جانبی بوجود آمده در ستون‌ها

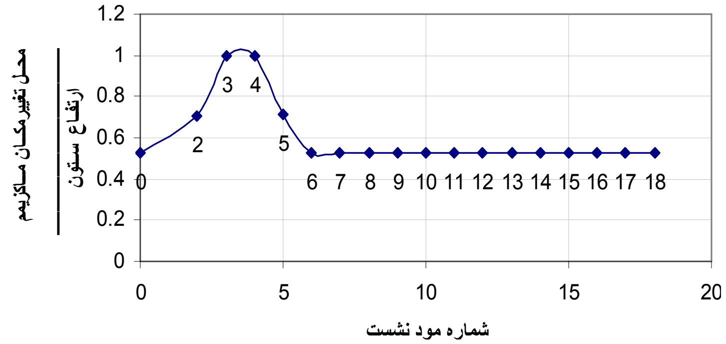

شکل ۸- محل ماکزیمم تغییرمکان جانبی بوجود آمده در ستون‌ها

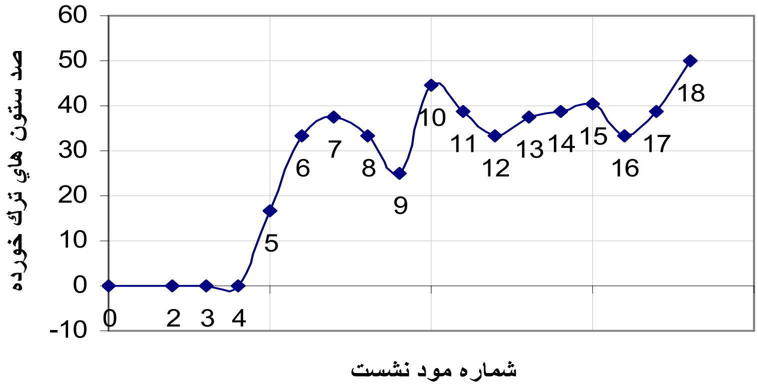

شکل ۹- میزان درصد ستون‌های ترک خورده

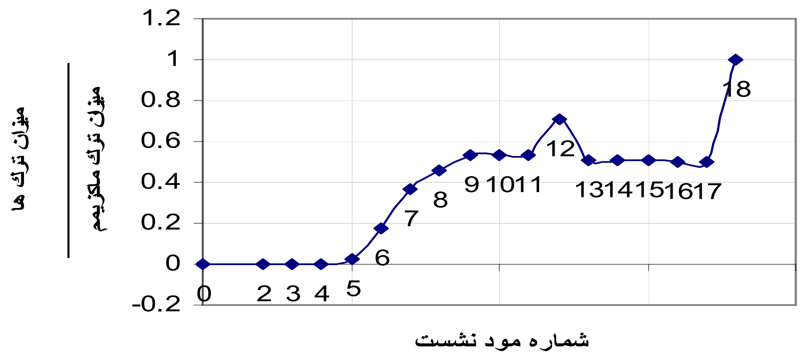

شکل ۱۰- نمودار نرمال شده تعداد ترک‌های بوجود آمده در ستون‌ها

در اثر نشست غیریکنواخت، ماکزیمم تغییر مکان جانبی ستون‌ها از ۹/۵۶ mm در حالت وزن، بـه ۳۵/۶۸ mm در مود نشست n=۳ رسیده است. یعنی مقدار ماکزیمم آن نـسبت بـه وزن، ۳/۷ برابـر شـده اسـت. همچنـین مقـدار ماکزیمم تغییر مکان نسبی آن تحت نشست غیر یکنواخت، ۰/۰۰۱۳ یعنی ۰/۱۳ درصد می‌باشـد. مـاکزیمم تغییـر مکان جانبی و نسبی ستون‌ها که در مود نشست n=۳ بوجود آمده است، در انتهای ستون یعنی محل اتصال ستون

به پوسته رخ داده است.

تحت وزن و مود نشست n=۲ و n=۳ و n=۴، هیچ یک از ستون‌ها ترک نخورده است. اما در مود نشست n=۱۸، ۵۰٪ تعداد ستون‌ها ترک خورده است. چنانچه در هر مود نشست، تعداد ترک‌هایی را که در کل ستون‌ها بوجود می‌آید را نسبت به مقدار ماکزیمم تعداد ترک‌ها، نرمال کنیم به نمودار (۱۰) می‌رسیم که نشان می‌دهد بیشترین تعداد ترک‌های ستون‌ها، در مود نشست n=۱۸ بوجود آمده است.

۳- پوسته

از آنجایی که رینگ تحتانی، محدوده کاملاً مشخصی نیست، لذا منظور از رینگ تحتانی، ناحیه حدودی آن می‌باشد.

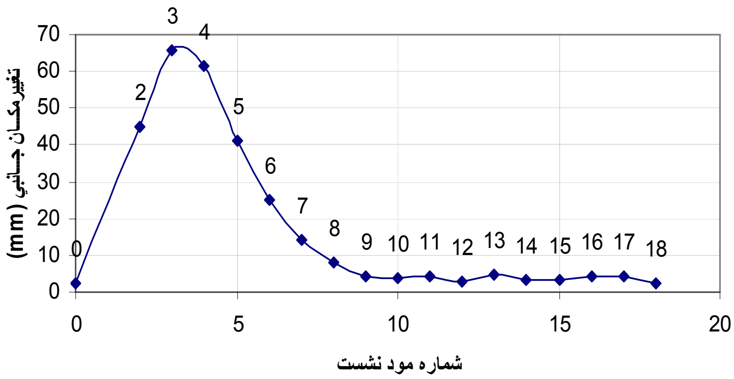

شکل ۱۱- ماکزیمم تغییرمکان جانبی بوجود آمده در پوسته

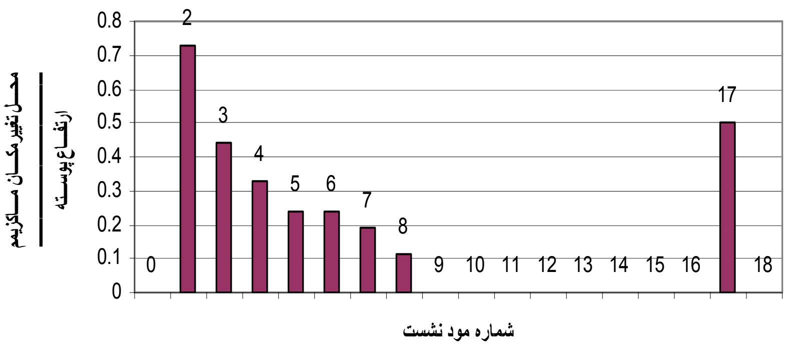

شکل ۱۲- محل ماکزیمم تغییرمکان جانبی بوجود آمده درپوسته

تحت نشست غیریکنواخت، مقدار آسیب دیدگی کششی در کل پوسته، در تمام مودهای نشست به جز مودهای نشست n=۴ و n=۵، برابر صفر بدست آمد یعنی پوسته هیچ‌گونه آسیب کششی ندیده است. در مود نشست n=۴ و n=۵ نیز، آسیب کششی فوق‌العاده ناچیز بدست آمده است. چنانچه ۴ متر اطراف رینگ فوقانی را به عنوان «ناحیه اطراف رینگ فوقانی» در نظر بگیریم، در مود نشست n=۴، ۱۵٪ ناحیه اطراف رینگ فوقانی، دچار آسیب دیدگی کششی شده است اما مقدار آسیب دیدگی ناچیز می‌باشد به گونه‌ای که مقدار ماکزیمم آن، ۴٪ می‌باشد.

همچنین در مود نشست n=۵، ۴/۸٪ ناحیه حدودی رینگ تحتانی دچار آسیب دیدگی کششی شده است و مقدار این آسیب‌دیدگی نیز فوق‌العاده اندک است به گونه‌ای که مقدار ماکزیمم آن، ۱٪ می‌باشد.

لازم به ذکر است که در اثر نشست غیریکنواخت، پوسته در هیچ یک از مودهای نشست، آسیب فشاری ندیده است به گونه‌ای که مقدار آن در تمامی‌مودها برابر صفر بدست آمده است.

ماکزیمم تغییر مکان جانبی پوسته از ۲/۱۵mm در حالت تحت وزن، به ۶۵/۹mm در مود نشست n=۳ رسیده است. یعنی مقدار ماکزیمم آن نسبت به حالت وزن، ۳۰/۷ برابر شده است. همچنین ماکزیمم تغییر مکان نسبی آن ۰/۰۰۰۶۲ یعنی ۰/۰۶۲ درصد می‌باشد. ماکزیمم تغییر مکان جانبی پوسته تحت نشست غیریکنواخت که در مود n=۳ بوجود آمده است، در ارتفاع ۴۷ متری پوسته (یعنی ۰/۴۴ ارتفاع پوسته) رخ داده است. همچنین قابل مشاهده است که در اکثر مودهای نشست، ماکزیمم تغییر مکان جانبی پوسته، در ابتدای ناحیه حدودی رینگ تحتانی (ابتدای پوسته) حاصل شده است.

شکل (۱۳) فرم تغییریافته برج را در مود نشست n=۳ نشان می‌دهد که ماکزیمم تغییرمکان جانبی ستون و پوسته در آن رخ داده است. گفتنی است که شکل مذکور برای وضوح بیشتر، بزرگنمایی شده است.

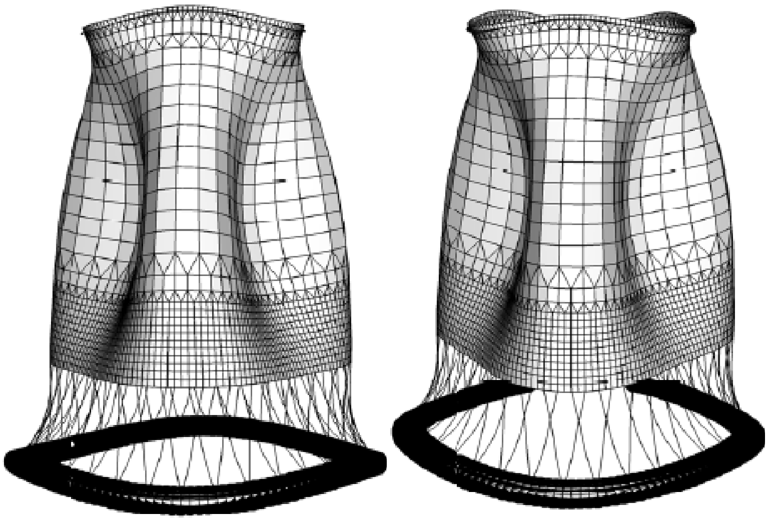

شکل ۱۳- فرم تغییریافته برج در مود نشست n=۳

نتیجه‌گیری

۸۷٪ پی آسیب کششی دیده است به گونه‌ای که مقدار ماکزیمم آسیب کششی آن، ۵۶٪ می‌باشد. همچنین اطراف ستون‌ها، بیشتر آسیب کششی دیده است. اما پی هیچ‌گونه آسیب فشاری ندیده است. ماکزیمم تغییرشکل نسبی پی ۰/۰۰۵۳ درصد می‌باشد که در مود نشست n=۶ رخ داده است لذا این مود برای کنترل تغییرشکل پی در بارگذاری نشست غیریکنواخت، مناسبتر می‌باشد. ماکزیمم تغییر مکان نسبی بوجود آمده در ستون‌ها، ۰/۱۳ درصد می‌باشد. همچنین ۵۰٪ ستون‌ها ترک خورده است. تنها در دو مود نشست، ناحیه اطراف رینگ فوقانی و ناحیه حدودی رینگ تحتانی آسیب کششی ناچیزی دیده است به‌گونه‌ای که مقدار ماکزیمم آن ۴٪ می‌باشد. اما

پوسته هیچ‌گونه آسیب فشاری ندیده است. ماکزیمم تغییرمکان نسبی پوسته، ۰/۰۶۲ درصد می‌باشد کـه در ۰/۴۴ ارتفاع آن رخ داده است. مود نشست n=۳ که در اثر آن، ستون‌ها و پوسته ماکزیمم تغییر مکان نسبی را داشته‌اند، برای کنترل تغییر مکان ستون‌ها و پوسته در بارگذاری نشست غیر یکنواخت، مناسب‌تر است. در مود نشست آخر (n=۱۸)، پی بیشترین آسیب کششی را دیده است و ستون‌ها بیشترین ترک‌ها را خورده‌اند.

مراجع

1. P.L.Gould, "Differential Settlement of Hyperbolic Cooling Towers, Proc. Of ASCE, Journal of Structural Division, Vol. 98, No. ST, oct 1972, PP: 2207-222.
2. L. Wenda , L.Baoqing , L. Rengi"The Effect of unequal Settlement of Foundation on the Stress Resultants of Hyperbolic Cooling Towers & the unequal Settlement Tolerance Limit", Journal of Engineering Structures, Volume 8 , Issue 1 , January 1986, PP:39-45.
3. S.V. Krishna Mohan Rao , T.V.S.R. Appa Rao, "Stress Resultants in Hyperboloid Cooling Tower Shell Subjected to Foundation Settlement", Journal of Computers and Structures , Vol. 52, No. 4, 1994, PP : 813-827.
4. R. Ciesielski, A. Cuminski, M. Zak, "Large Settlement of Hyperboloidal Cooling Towers", Proc. Con. on Large Ground Movement and Structures.UWIST. Cardiff. July 1977, PP : 672-686.
5. R. Kaluza , O. Mateja, "Problems of Influence of Irregular Displacements of Foundation on the State of Stress & Displacements of a Hyperbolic Cooling Tower", High Technical School, Opol , Poland , PP : 47-59.
6. S. Kato , Y. Chiba, "Stochastic Stress Analysis of Cooling Tower Shells due to Differential Settlement", Shells, Membrane & Space Frames, Proc. IASS Symposium, Osaka, 1986, Vol. 1, PP : 121-128.
7. S. Kato, K.J. Han, M.Cheong, "Stress Evaluation of Cooling Towers Subjected to Uneven Settlements With Stochastic Characteristics", Journal of Engineering Structures, Vol. 13, Issue 4, 1991, PP : 329-344.

۸. سعید صبوری، «بررسی نیروهای داخلی ایجاد شده در برجهای خنک کن بتنی در اثـر نشـست نـا مـساوی» مجله بین المللی علوم مهندسی، جلد ۱۲، شماره ۲، صفحه ۱۹۹-۲۱۳، ۱۳۸۰

9. Lee J. , Fenves G.L. , " plastic-damage model for cyclic loading of concrete structures" , journal of engineering mechanics, vol. 124, no. 8, pp: 892-900, 1998.
10. John L. Tassoulas, Eduardo Kausel., "On The Dynamic Stiffness Of Circular Ring Footing on an Elastic Stratum", International journal for numerical and analytical methods in geomechanics, Vol. 8, pp: 411-426, 1984.

۱۱. علی اختری باغان، «بررسی اثر نشست نامتقارن بر روی برج بتنی خنک کننده نیروگاه شـازند»، پایـان نامـه کارشناسی ارشد، دانشگاه صنعتی خواجه نصیر طوسی، ۱۳۸۱.

12. R. Kaluza, J. M. Gigil, "Experimental Analysis of the Imposed Displacements at the Base of a Cooling Tower on its Buckling Stability" Thin- Walled Structures 23, 1995, PP : 367-378.
13. T.W. Lambe, R.V. Whiteman "Soil Mechanics" John Wiley and Sons, New York, 1979.

۱۴. علی کبیر بیک، « نشست غیر یکنواخت افقی و قائم در برجهای خنک کن»، پایـان نامـه کارشناسـی ارشـد، دانشگاه صنعتی خواجه نصیرالدین طوسی، ۱۳۷۶.

۱۵. امیر مسعود معطر خرازی، «بررسی اثر نشست غیر یکنواخـت در بـرج‌هـای خنـک کـن بتنـی»، پایـان نامـه کارشناسی ارشد، دانشگاه صنعتی امیرکبیر،۱۳۷۳.
۱۶. سعید صبوری- علی اختری باغان، «بررسی غیرخطی یـک بـرج خنـک کننـده بتنـی در برابـر اثـر نشـست غیریکنواخت»، اولین کنگره ملی مهندسی عمران، اردیبهشت ۱۳۸۳، دانشگاه شریف.
۱۷. بهنام سعادتی. «بررسی رفتار لرزه‌ای برج‌های خنک‌کننده بتنی با ارتفاع سـتون‌هـای متفـاوت »، پایـان‌نامـه کارشناسی ارشد عمران- گرایش سازه، دانشگاه صنعتی خواجه نصیر طوسی، ۱۳۸۳.
18. W.F. Chen “Plasticity in reinforcement concrete”, MacGraw-Hill Book Company, 1982.
19. U.Wittek, R.Meiswinkel "Non-linear behavior of RC cooling towers and its effects on the structural design", Engineering Structures, vol. 20, No. 10, pp: 890-898, 1998.
20. ABAQUS/Standard User’s Manuals, Version 6.3-1, Hibbitt, Karlsson and Sorensen, Inc., USA, 2002.
21. Lubliner J., Oliver J., oller S., Onate E., “ A plastic-Damage model for concrete” international journal of solids and structures, Vol. 25, pp: 299-329, 1989.
22. Noh SY, Kratzig WB, Meskouris K. “Numerical simulation of serviceability, damage evolution and failure of reinforced concrete shells.” Computers and Structures. 2003, vol. 81, pp: 843-857.

CD02-032

بررسی عددی رفتار تیرهای خمشی بتن مسلح تقویت شده با CFRP به دو روش چسباندن و نزدیک سطحی (NSM)

محمد سعید کریمی[۱]، مهران ناصری[۲]

۱. استادیار و عضو هیات علمی‌دانشگاه سمنان

۲. دانشجوی کارشناسی ارشد دانشگاه سمنان

چکیده

تقویت خمشی تیرهای بتن آرمه به دو روش چسباندن ورقهای FRP به سطوح خارجی اعضاء و استفاده از نوارهای FRP به روش Near -Surface-Mounted (NSM) می‌تواند انجام می‌شود. تقویت خمشی اعضاء بتن آرمه به روش NSM به عنوان یکی از تکنولوژیهای جدید می‌تواند جایگزین تقویت خمشی تیرها با ورقهای FRP که در سطوح خارجی چسبانده شده اند، شود. نظر به اینکه در تقویت با روش NSM نوارهای FRP از سه جهت در بتن محصور می‌شوند، لذا پیوستگی و مسائل خرابی رایج در سیستم تقویت با ورقهای FRP که در سطوح خارجی چسبانده شده اند، کاهش یافته و یا حذف می‌شوند. دراین مقاله، با استفاده از روش‌های عددی، آیین نامه ای ونتایج آزمایشگاهی، رفتار تیرهای خمشی بتن مسلح تقویت شده با ورقها و نوارهای FRP مورد بررسی قرار می‌گیرد. در مدل عددی از مدل آسیب دیدگی پلاستیک بتن برای شبیه سازی رفتار غیر خطی بتن و نرم شوندگی کرنش استفاده می‌گردد. بدین منظور تعداد ۸ تیر بتنی مسلح تقویت شده که به دو روش چسباندن ورقهای FRP و NSM قبلا در آزمایشگاه ساخته و آزمایش شده اند به کمک نرم افزار اجزاء محدود ABAQUS تحلیل و سپس با استفاده از راهنمای طراحی ACI 440-2R-02 ظرفیت نهایی تیرها محاسبه و نتایج با یکدیگر مقایسه شده است. نتایج نشاندهنده افزایش مقاومت تسلیم و نهایی نمونه‌ها و پیش بینی صحیح مدهای شکست خمشی و میزان مقاومت اسمی، اثر انتقال نیرو بین CFRP، چسب و بتن اطراف می‌باشد. همچنین مقایسه ظرفیت نهایی تیرها حاصل از نتایج عددی با روابط پیشنهادی کمیته ACI 440-2R-02 نشان می‌دهد که ظرفیت نهایی مقاطع تقویت شده در این راهنمای طراحی، بیشتر برای مقاطع با درصد آرماتورهایی نزدیک به آرماتور ماکزیمم مناسب می‌باشند.

کلیدواژه‌ها: مقاوم‌سازی خمشی، تیرهای بتن مسلح، مدل آسیب دیدگی پلاستیک بتن، FRP

مقدمه

در حالت سرویس اعضاء خمشی سازه‌های بتن مسلح ممکن است نیاز به تقویت به علت خوردگی آرماتورها و خرابی بتن، اشتباه در محاسبات و یا ساخت، افزایش بارهای بهره‌برداری و یا خرابی‌های پیش بینی نشده سازه داشته باشند. این شرایط مستلزم مقاوم کردن سازه‌ها برای افزایش مقاومت خمشی آنها می‌باشد. یکی از روشهای

شناخته شده جهت تقویت خمشی تیرها، دیوارها و دالها، چسباندن ورقهای FRP به سطح خارجی آنها می‌باشد. از خصوصیات مصالح FRP، مقاومت کششی بالا و وزن کم آنها و مقاومت در برابر خوردگی در محیطهای کلریدی می‌باشد. شکست زود هنگام در اعضاء خمشی تقویت شده با صفحات FRP بکار برده شده در سطوح خارجی تیر (قبل از اینکه مقطع به ظرفیت خمشی نهایی خود برسد) عموماً به علت جدایی پیوستگی میان صفحات FRP و بتن یا پوسته شدن پوشش بتن می‌تواند رخ دهد. Brena et al (2003) [3] جداشدگی میان صفحات طولی CFRP و بتن را در تغییر شکلهایی کمتر از نصف تغییر شکل ظرفیت نمونه‌های کنترلی، گزارش داده است. Nguyen et at (2001) [4] مشاهده نموده است که به علت لایه لایه شدگی و یا پاره شدن زود هنگام پوشش بتن تنها بخش محدودی از صفحات FRP باعث افزایش ظرفیت خمشی تیرها می‌شوند. Grace et at (2002) [5] شکست ترد ناشی از کشش‌برشی و جداشدگی را برای تیرهای مقاوم شده با صفحات FRP شناسایی کرده است. Shin (2003) و Lee [6] شکست تیرهای مقاوم شده با صفحات FRP را تحت بارهای ثابت در باری کمتر از ظرفیت خمشی نهایی مقطع گزارش داده‌اند. علاوه بر مساله شکست ناشی از جداشدگی صفحات FRP، زخمی‌شدن FRP، حرارت و خرابی ناشی از محیط از مشکلات دیگر تقویت به روش چسباندن صفحات FRP در سطح خارجی بتن می‌باشد. لازم به یادآوری است مهار کردن FRP می‌تواند باعث بهبود استحکام و جلوگیری از پوسته‌شدن صفحات FRP چسبانده شده در سطوح خارجی شود. به علت زیانهایی که در روش تقویت ورقهای FRP که در وجه پایین تیر چشبانده شده اند وجود دارد، پیشنهاد می‌شود که مصالح FRP بجای استفاده در سطوح خارجی محافظت نشده، در محیط داخلی بتن استفاده شود. این تکنولوژی به NSM (Near-surface-mounted) اشاره می‌کند. بتن اطراف از تغییر در خصوصیات مکانیکی FRP و خرابی ناشی از گرما محافظت می‌کند. از مزایای دیگر استفاده از تکنولوژی NSM، بهبود پیوستگی و انتقال نیرو در بتن اطراف و قابلیت افزایش مقاومت خمشی منفی در پلها و دالها، می‌باشد. بررسی رفتار سازه قبل و بعد از مقاوم سازی در مواردی از قبیل مقاومت، شکل پذیری و نوع شکست با رفتار سازه تقویت نشده متفاوت است. بنابراین آزمایشهای تجربی و یافتن روشهای عددی و تحلیلی برای پیش بینی رفتار سازه‌های تقویت نشده ضروری بنظر می‌رسد. مدلسازی عددی بر پایه تحلیل اجزاء محدود (FEA) تقریبا می‌تواند رفتار کلی تیر مقاوم شده را به خوبی پیش بینی کند. هرچند از معایب این روش نیاز به اطلاعات مطالعات آزمایشگاهی جهت مدل سازی می‌باشد. از میان روشهای عددی متفاوت بکار گرفته شده می‌توان به روش اجزاء محدود غیر خطی برای شبیه سازی رفتار کلی تیرهای تقویت شده با CFRP ارائه شده توسط Ziraba and Baluch [7] اشاره نمود. این روش قادر است رفتار اعضای تقویت شده دارای هرگونه تاریخچه بارگذاری قبل از تقویت را پیش بینی کند. Arduini et. al در سال 1997 [8] مدل عددی را با استفاده از FEA مطابق با تئوری ترکهای پخشی (Smeared crack) معرفی کرد. از المانهای هشت گره ای دو بعدی برای بتن تیرهای مقاوم شده با صفحات FRP استفاده شد. فرض پیوستگی کامل میان صفحات FRP و بتن در نظر گرفته شد. مانند مدلهای تحلیلی نتایج بدست آمده از حل عددی اندکی سخت تر از نتایج آزمایشگاهی بود. حل عددی نتایج خوبی را در مقایسه با نتایج آزمایشگاهی جهت توسعه ترک نشان داد. دو روش مقاوم سازی NSM و چسباندن ورقهای FRP در شکل ۱و ۲ نشان داده شده است.

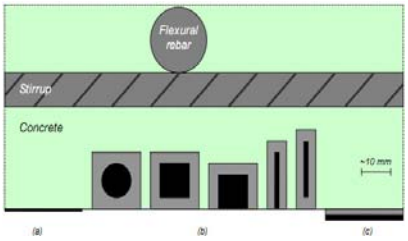

شکل ۱- تکنیکهای مقاوم سازی با FRP a – ورقه b- NSM : میله‌های گرد، مربع شکل و نوار c- صفحه

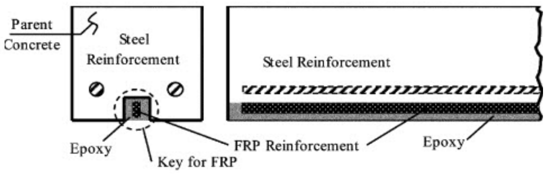

شکل ۲- عضو بتنی تقویت شده با نوار FRP به روش NSM [1]

۱- بررسی مطالعات آزمایشگاهی نمونه‌ها

با توجه به نوع تقویت خمشی تیرهای بتن آرمه، جهت مقایسه با نتایج تحلیلی، دو مطالعه آزمایشگاهی مختلف برای تیرهایی که با ورقهای FRP بصورت چسباندن به سطوح خارجی و نیز برای تیرهایی که به روش نزدیک سطحی (NSM) تقویت شده‌اند انتخاب گردید. مطالعه آزمایشگاهی اول در دانشگاه فردوسی مشهد [2]، مطالعه آزمایشگاهی دوم [1] در دانشگاه Villanova انجام شده است. در مطالعه آزمایشگاهی اول نمونه‌ها دارای ابعادی با عرض مقطع ۱۵۰، ارتفاع۲۰۰ و طول ۲۰۰۰ میلیمتر بوده و در مطالعه آزمایشگاهی دوم از نمونه‌هایی با سه عرض مقطع مختلف ۱۵۲٫۴، ۲۲۹، ۳۰۵ با ارتفاع ۱۹۰ و طول ۲۷۴۳ میلیمتر استفاده شده است. برای جزئیات مشخصات مکانیکی بتن و آرماتور و روند انجام آزمایش به مراجع [1] و [2] رجوع شود. جزئیات نمونه‌های آزمایشگاهی در شکلهای ۳و۴ ارائه شده است. دراین مقاله نمونه‌های B2، B3، B6 و B7 از مطالعه آزمایشگاهی اول و نمونه‌های 6-1Fa&b و 9-1Fa&b از مطالعه آزمایشگاهی دوم جهت بررسی درنظر گرفته شده است.

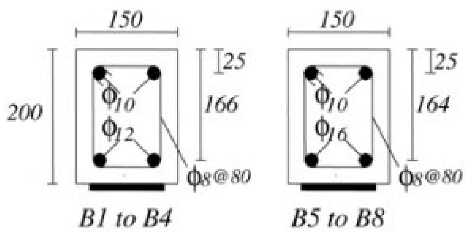

شکل ۳- جزئیات نمونه‌های آزمایشگاهی سری اول [2]

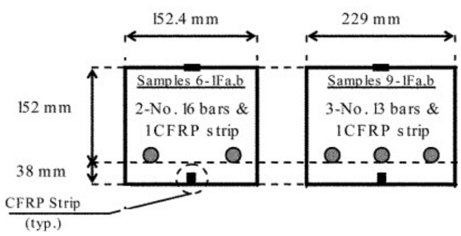

شکل ۴- جزئیات نمونه‌های آزمایشگاهی سری دوم [1]

۲- مدل‌سازی عددی تیرهای تقویت شده در نرم افزار اجزاء محدود ABAQUS

۲-۱ المانهای بکار برده شده جهت مصالح و مش‌بندی آنها

۲-۱-۱ بخش بتنی

تیرهای بتنی بصورت سه بعدی مدل شده اند، در حالی که امکان مدلسازی آنها به صورت دو بعدی نیز وجود دارد. در آنالیزها تیرها بصورت کامل مدل شده اند، لیکن جهت کاهش زمان محاسبات می‌توان از تقارن تیرها نیزاستفاده نمود. جهت مش بندی تیر از المان C3D8R استفاده شده است.

۲-۱-۲ بخش فو لادی

دو روش جهـــت اختـــصاص المـــان آرمـــاتور وجـــود دارد. در روش اول، از المـــان تیـــر و یـــا خرپـــا جهت معرفی آرماتور استفاده و در روش دوم آرماتورها در یک و یـا چنـد لایـه بـصورت میلگردهـایی بـا فاصـله یکنواخت معرفی می‌شوند. لایه‌های آرماتور بصورت لایه‌های پخش شده در حجم المان با ضخامت ثابتی برابر بـا مساحت هر میلیگرد تقسیم بر فاصله میلگردها در نظر گرفته می‌شوند.در این مقاله از المان خرپا با مش بندی سه بعدی خطی T3D2 جهت معرفی آرماتورها استفاده است.

۲-۱-۳ ورقهای و نوارهایCFRP

ورقه‌های CFRP با المانهای shell استاندارد و خطی با نام S4R مدل شده اند. این نوع المان توسط Hibbitt, Karlsson & Sorensen Inc (1997) [9] استفاده شـده و نتـایج مناسـبی از آن گرفتـه شـده اسـت. نوارهـای CFRP نیز بصورت المان خرپا مدل شده اند.

۲-۲ شبیه سازی رفتار مصالح

۲-۲-۱ بتن

از مدل آسیب‌دیدگی پلاستیک برای شبیه سازی رفتار آن اسـتفاده مـی‌شـود.در ایـن مـدل فـرض مـی‌شـود کـه خردشدگی فشاری بتن و ترک خوردگی آن مکانیزمهای اصلی شکست می‌باشند. هر دوی این پدیـده‌هـا ناشـی از شروع و گسترش ترکها می‌باشند. روش خسارت پلاستیسیته باعث کاهش سختی الاستیک هنگامی‌که المان وارد مرحله پلاستیک شده، می‌شود. از این رو المان نمی‌تواند به مقاومت اولیه اش برگـردد کـه ایـن امـر بـه ویـژه در بارگذاری سیکلی بسیار مهم است. پارامترهای اصلی مورد نیاز برای استفاده از این مدل عبارتند از:

الف- منحنی نرم شوندگی بتن که در آن رفتار کششی بتن با تعریف منحنی نرم شدگی کشش- باز شدگی تـرک توضیح داده می‌شود (شکل ۵). در مدل خسارت پلاستیسیته مـی‌تـوان رفتـار پـس گـسیختگی در کـشش را بـا اختصاص کرنش، بازشدگی ترک (تغییر مکان) و شکست انـرژی شـبیه سـازی نمـود. در شـکل ۴، F_{cr} مقاومـت کششی بتن است که شروع و گسترش ترکها را کنترل می‌کند، Gf کل انرژی شکست اسـت کـه توسـط Hillerborg(1974) [10] پیشنهاد شده و بصورت مقدار انرژی لازم برای شروع، گسترش و شکست کامل یک ترک در واحد سطح می‌باشد. انرژی شکست می‌تواند بصورت دیاگرام تنش- تغییر مکان نشان داده شود (شکل ۶). مقـدار انرژی شکست بین 40 N/m برای بتن با مقاومت پایین تا 210 N/m برای بتن با مقاومت بالا متغیر می‌باشد.

ب- منحنی تنش کرنش بتن تحت بارگذاری فشاری تک محوره که در شکل ۷ نشان داده شده است. کـه در آن F'_c مقاومت فشاری بتن و ε کرنش بتن می‌باشد.

۲-۲-۲ فولاد

از مدل الاستیک پلاستیک کامل برای مدل سازی رفتار فولاد استفاده شده است. در این روش فولاد تا رسیدن به تنش تسلیم، الاستیک می‌باشد. دراین نقطه تحت بار ثابت جاری می‌شود. پارامترهای مورد نیاز این مـدل ضـریب کشسانی فولادEs، نسبت پواسون و تنش تسلیم فولاد می‌باشد.

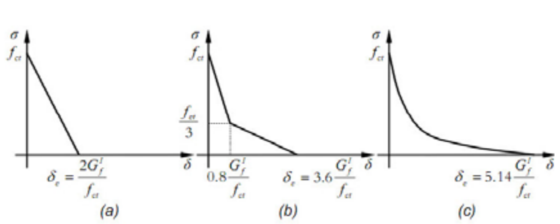

شکل ۵- منحنی نرم شوندگی بتن: a) تقریب خطی b) تقریب دو خطی c) حالت کلی

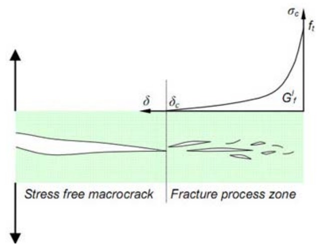

شکل ۶- انرژی شکست در نمودار تنش تغییر مکان

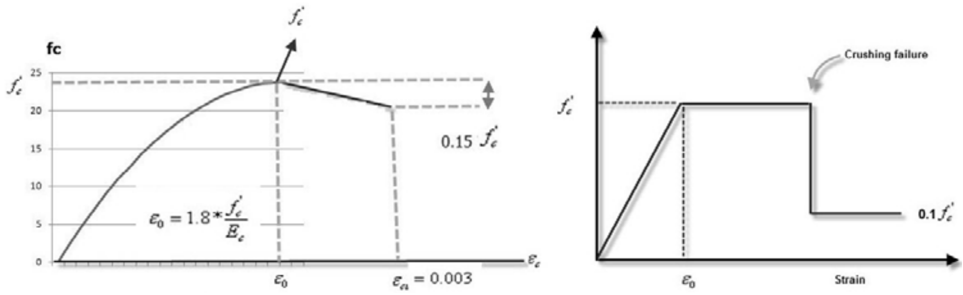

الف **ب**

شکل ۷- منحنی تنش کرنش بتن در فشار تک محوره الف- مدل مرجع [11] ب- منحنی Hognestad

۲-۲-۳ ورق و نوار CFRP

از مدل شکست ترد برای شبیه سازی رفتار ورقها و نوارهای CFRP استفاده می‌شود. دراین روش فرض می‌شود رفتار ورقهای FRP تا رسیدن به کرنش نهایی خطی است. دراین نقطه ترک گسترش می‌یابد و ماده تمامی‌ظرفیت باربری خود را یکباره از دست می‌دهد. پارامترهای مورد نیاز این مدل، ضریب کشسانی پلیمرهای الیافی(E_{FRP})، ضریب پواسون (ν) و کرنش نهایی شکست (ε_u) می‌باشد.

۳- تحلیل عددی

تحلیل عددی دراین مطالعه با استفاده از نر افزار ABAQUS 6.8-1 انجام شده است.دراین شبیه سازی از تماس مقید (Tied Contact) برای چسباندن ورقهای CFRP به سطح تیر و Embeded region برای ادغام نوارهای CFRP به بتن استفاده شده است. از مجموع ۲۷ نمونه آزمایشگاهی مراجع [1] و [2]، چهار نمونه B2-12D-1L15, B7-16D-1L15, B6-16D-1L10, B3-12D-2L15 از مرجع [2]، و چهارنمونه 9-1Fa&b, 6-1Fa&b از مرجع [1]، جهت مدلسازی عددی استفاده شده است.

۴- مقایسه نتایج عددی و نتایج آزمایشگاهی

نمودار بار تغییر مکان وسط دهانه نمونه‌ها برای چهار تیر سری اول و چهار تیر سری دوم به همراه نتایج آزمایشگاهی آن در شکلهای ۸ و ۹ آورده شده است.

۵- مقایسه بین نتایج آنالیز اجزاء محدود با روابط ACI440.2R.02

نسبت بارهای نهایی که براساس روابط ACI440 [12] محاسبه شده در جدول شماره ۱ برای نمونه‌های تقویت شده با ورقهای CFRP ارائه شده است. این نسبتها برای نمونه‌های B2وB3 از یک کمتر است؛ در حالیکه برای نمونه‌های B6 وB7 و بزرگتر از یک است. بار نهایی تحلیلی تیرهای مقاوم شده با نوارهای CFRP به روش NSMبا رابطه ارائه شده در مرجع [1] محاسبه و با نتایج عددی مقایسه شده است (جدول ۲). مقاومت نهایی تیرهای تقویت نشده نیز براساس روابط ACI 318-05 [13] محاسبه و درجداول زیر با عنوانP_{con} آورده شده است.

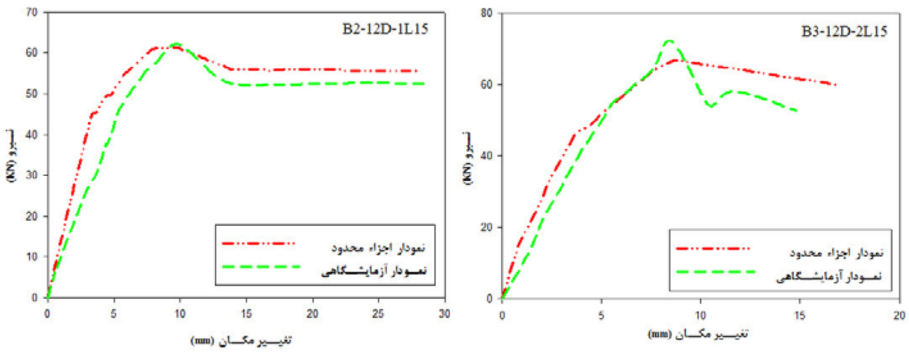

شکل ۸-الف- نمودار بار جابجایی وسط دهانه برای تیرهای مقاوم شده با ورقهای CFRP

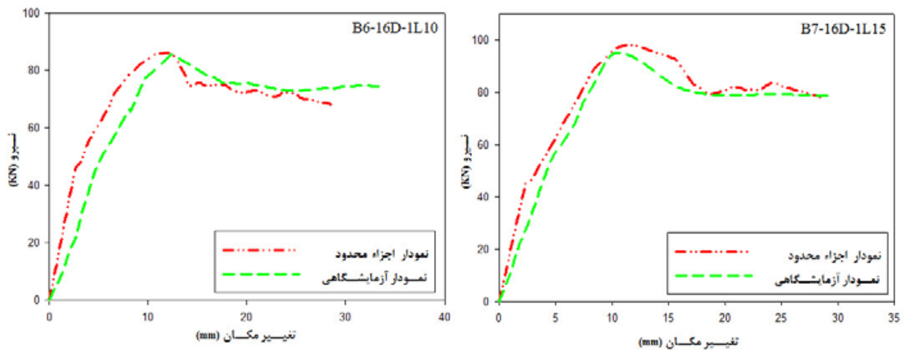

شکل ۸-ب- نمودار بار جابجایی وسط دهانه برای تیرهای مقاوم شده با ورقهای CFRP

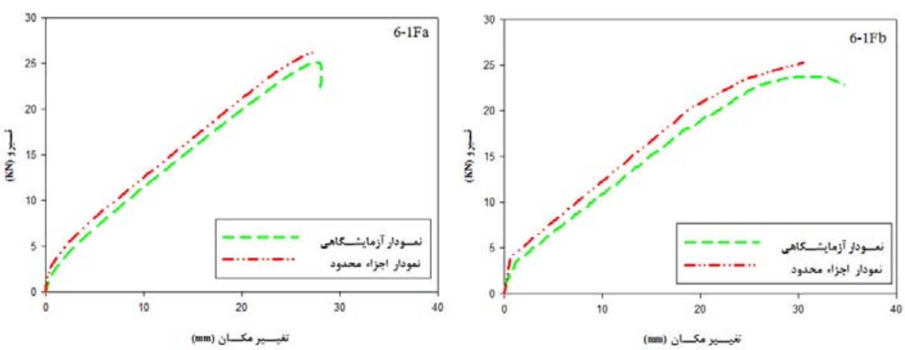

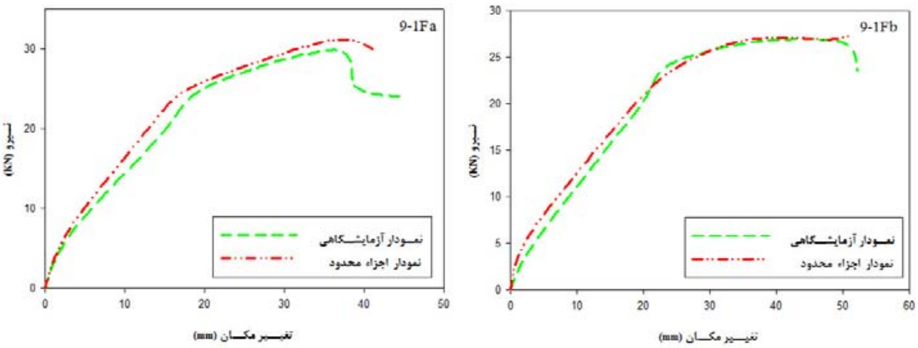

شکل ۹- نمودار بار جابجایی وسط دهانه برای تیرهای مقاوم شده با نوارهای CFRP به روش NSM

جدول ۱: مقایسه بین نتایج اجزاء محدود و روابط محاسبه شده توسط ACI440.2R.02

نام نمونه	ρ	P_{con} (KN)	P_{ACI} (KN)	P_{FEA} (KN)	$\frac{P_{ACI}}{P_{con}}$	$\frac{P_{FEA}}{P_{con}}$	$\frac{P_{FEA}}{P_{ACI}}$
B2-12D-1L15	$0.3\rho_b$	41.25	68.98	61.30	1.67	1.48	0.89
B3-12D-2L15			86.20	67	2.09	1.60	0.78
B6-16D-1L10	$0.6\rho_b$	60.86	83.59	86.37	1.37	1.41	1.03
B7-16D-1L15			88.51	98.42	1.45	1.61	1.11

جدول ۲: مقایسه بین نتایج اجزاء محدود و روابط محاسبه شده در مرجع [1]

نام نمونه	ρ	P_{con} (KN)	P_{Yield} (KN)	P_{FEA} (KN)	$\frac{P_{Yield}}{P_{con}}$	$\frac{P_{FEA}}{P_{con}}$	$\frac{P_{FEA}}{P_{Yield}}$
61-Fa	$0.684\rho_b$	18.9	20.9	27.1	1.1	1.43	1.29
61-Fb			21.3	25.29	1.12	1.33	1.18
91-Fa	$0.47\rho_b$	20.6	25.3	30.1	1.22	1.46	1.18
91-Fb			24.5	27.3	1.18	1.32	1.11

۶- نتیجه گیری

در این تحقیق اثر ورقها و نوارهای FRP در تقویت خمشی تیرهای بتن مسلح با استفاده از تحلیل‌های عددی و مدل آسیب دیدگی پلاستیک بتن بررسی و براساس مقایسه بین مقادیر بدست آمده از تحلیل‌های عددی، آزمایشگاهی و آیین نامه ای نتایج زیر بدست آمد:

- تحلیل عددی انجام شده با استفاده از مدل آسیب دیدگی پلاستیک با استفاده از نرم افزار اجزاء محدود ABAQUS قادر به پیش بینی منحنی بار – تغییر مکان، بار شکست و حالت شکست تیرهای تقویت شده با FRP می‌باشد.
- انرژی شکست بتن موثرترین پارامتر در پیش بینی شکست‌های ناشی از جداشدگی ورقهای CFRP از سطح تیر بدلیل ترک خوردگی کششی می‌باشد.

- نتایج عددی نمونه‌های تقویت شده، مقاومت و سختی بیشتری نسبت به نتایج نمونه‌های آزمایشگاهی، از خود نشان می‌دهند.
- با توجه به مقایسه نتایج بدست آمده با روابط آیین نامه ACI440.2 مشاهده می‌شود روابط طراحی این آیین نامه اثر تقویت کنندگی ورقهای FRP در مقاومت تیرهای خمشی با درصد آرماتور کم را دست بالا برآورد می‌کند. لذا روابط پیشنهادی توسط کمیته ACI440.2، بیشتر برای درصد آرماتورهایی نزدیک به آرماتور ماکزیمم در تیرهای تقویت شده با ورقهای FRP مناسب می‌باشند.

مراجع

1. Yost Joseph Robert, Shawn P. Gross, David W. Dinehart, and Jason J. Mildenberg, 2007, Flexural Behavior of Concrete Beams Strengthened with Near-Surface-Mounted CFRP Strips. *ACI Structural Journal/July-August 2007*.
2. M.R. Esfahani, M.R. Kianoush, A.R. Tajari, 2006 , “Flexural behaviour of reinforced concrete beams strengthened by CFRP sheets”, Engineering Structures, ScienceDirect.
3. Brena, S. F, Bramblett, R. M.; Wood, S. L. and Kreger, M. E., 2003, “Increasing Flexural Capacity of Reinforced Concrete Beams Using Carbon Fiber-Reinforced Polymer Composites,” *ACI Structural Journal, V. 100, No. 1, Jan.-Feb., pp. 36-46*.
4. Nguyen, D, Chan, T.; and Cheong, H., 2001, “Brittle Failure and Bond Development Length of CFRP-Concrete Beams,” *Journal of Composites for Construction, ASCE, V. 5, No. 1, pp. 12-17*.
5. Grace, N, Abdel-Sayed, G.; and Ragheb, W., 2002, “Strengthening of Concrete Beams Using Innovative Ductile Fiber-Reinforced Polymer Fabric,”*ACI Structural Journal, V. 99, No. 5, Sept.-Oct., pp. 692-700*.
6. Shin, Y. S, and Lee, C., 2003, “Flexural Behavior of Reinforced Concrete Beams Strengthened with Carbon Fiber-Reinforced Polymer Laminates at Different Levels of Sustaining Load,” *ACI Structural Journal, V. 100, No. 2, Mar.-Apr., pp. 231-239.*
7. Ziraba Y.N.,Baluch M.H., " Computional model for reinforced conrete beams strengthened by epoxy bonded steel plates" , Finite Element Analysis Des, vol 20, No4,253-271, 1998.
8. Arduini, M., Nanni, A., Parametric Study of Beams with Externally Bonded FRP Reinforcement. ACI Structural Journal, V.94, No. 5, September-October 1997b, pp. 493-501.
9. Hibbitt, Karlsson & Sorensen Inc (1997),ABAQUS Standard user manual, version 5.6, Pub. HKS Ink, Rhode Is, New York.
10. Hillerborg, A.; Modeer, M. and Petersson, P.E. (1976): Analysis of Crack Formation and Crack Growth in Concrete by Means of Fracture Mechanics and Finite Elements. Cement and Concrete Research, vol.6, p. 773-782, 1976.
11. Coronado C., Lopez M.M., ”Sensitivity analysis of concrete beams strengthened with FRP laminates”, Cement &Concrete Composites, Elsevier Science Publishers, Vol.28, 102-114, 2006.
12. ACI Committee 440.2R-02. Guide for the design and construction of externally bonded FRP systems for strengthening concrete structures, 2002.
13. ACI 318-05. Building code requirements for structural concrete (318M-05) and commentary (318RM-05). Farmington Hills (Michigan, USA): American Concrete Institute (ACI); 2005.

CD02-033

بررسی تاثیر دمای اولیه بتن بر میزان جذب آب و جذب آب موبینه آن

هرمز فامیلی[1]، محسن تدین[2]، پویا حاجی تقی تهرانی[3]
۱. استادیار دانشکده عمران دانشگاه علم و صنعت ایران
۲. استادیار دانشکده را ه آهن دانشگاه علم و صنعت ایران
۳. دانشجوی کارشنا سی ارشد دانشگاه علم و صنعت ایران

چکیده

شرایط ساخت بتن تاثیر پذیری آن را از شرایط اقلیمی‌خود به خصوص دما اجتناب ناپذیر نموده است و از آنجا که دما ی محیط همواره تابع زمان و مکان می‌باشد، لذا بررسی آن به عنوان یک پارامتر متغیر در بتن و آثار تغییرات ان حائز اهمیت است.

در این مقاله این آثار بر خصوصیات جذبی بتن که ملاک مهمی‌از دوام بتن می‌باشد مورد بررسی قرار گرفته است. در این راستا نمونه‌هایی با دماهای اولیه ۱۰، ۲۰، ۳۰و ۴۰ درجه سانتیگراد ساخته شد و در شرایط آزمایشگاهی و کارگاهی عمل آوری گردید. مشاهده گشت که در سن ۲۸ روز بتن با دمای اولیه ۲۰°C کمترین میزان جذب اولیه و نهایی را در بین سایر نمونه‌ها دارا بوده و با افزایش دما از ۲۰°C جذب آب نمونه‌ها افزایش می‌یابد.. در جذب موبینه نیز نتایج مشابهی احراز شد و با افزایش دمای اولیه بتن از ۲۰°C آهنگ جذب موبینه آن نیز افزایش یافت.

کلیدواژه‌ها: دمای اولیه، بتن تازه، جذب آب اولیه، جذب اب نهایی، جذب آب موبینه

۱- مقدمه

بتن یکی از مصالح ساختمانی پرمصرف در ساخت پل‌ها، ساختمان‌ها، سکوها، جداول و همینطور در سازه‌های زیرزمینی مثل تونل‌ها و خطوط لوله‌های بتنی می‌باشد. در حالت کلی، بتن یکی از مصالح بسیار بادوام به شمار می‌آید که می‌تواند در شرایط محیطی بسیار سخت مثل شرایط محیطی دریایی، صنعتی و غیره، مقاومت خوبی را از خود به نمایش بگذارد.سنگدا نه، سیمان، آب و بعضا افزودنی‌های مختلف همگی از مواد تشکیل دهنده بتن هستند که میزان، نوع و شرایط آنها همگی در کیفیت بتن تاثیر گذار است ولی آنچه این مصالح اولیه را در کنار یکدیگر همچون جسمی‌همگن قرار می‌دهد واکنش‌هایی است که به تبع حضور سیمان در بتن صورت گرفته و محصولات آن ضمن ایجاد چسبندگی لازم بین مصالح از مقاومت‌هایی بر خوردار است که این مقاومت در بتن‌های متعارف چه از نظر مکانیکی و چه دوامی‌کمتر از مقاومت‌های سنگدانه است. بنابر این محصولات واکنشهای سیمان، به عنوان ضعیف ترین بخش در بتن شناخته می‌شوند و لذا این واکنشها و پارامترهای تاثیر گذار در آنها از اهمیت زیادی برخوردار است که تاکنون مطالعات فراوانی در این زمینه انجام گرفته است.

یکی از این پارامترهای تاثیر گذار دمای بتن می‌باشد. از آنجا که واکنش هیدراسیون سیمان یک واکنش شیمیایی نسبتا کند می‌باشد درجه حرارت بتن در هر مرحله ازعمر آن در روند این واکنش تاثیر گذار بوده و تاثیرات خاصی بر ویژگیهای بتن می‌گذارد این تاثیرات چه در دوره ساخت بتن تازه، چه در دوره عمل آوری و چه در دوره بهره برداری آن در خواص بتن تاثیر گذار است.

به نظر می‌رسد به دلیل تاثیرات زیادی که دمای بتن تازه با توجه به روش ساخت آن از دمای محیط می‌گیرد و همچنین تغییراتی که در دمای محیط در طی فصول، ماهها، روزها و حتی ساعات روز مشاهده می‌گردد، دمای اولیه بتن یک پارامتر بسیار تاثیر پذیر و متغیر نسبت به دمای محیط اطراف آن می‌باشد. ضمن آنکه دما در بتن تازه به سبب واکنش‌های هیدراسیون نیز افزایش می‌یابد که این پدیده به خصوص در مورد بتن‌های حجیم مقادیر قابل ملا حظه ای پیدا می‌کند.

لذا بررسی اثرات دما در بتن تازه بر روی خصوصیات مقاومتی و دوامی‌آن موضوع با اهمیتی است که در این تحقیق سعی شده است این تاثیرات در موردویژگیهای جذبی بتن که پارامتر مهمی‌در دوام آن محسوب می‌شود مورد بررسی قرار گیرد.

۲- کلیات

در حقیقت به استثنای خسارت مکانیکی، کلیه اثرات نامطلوب بر دوام در برگیرنده جابجایی مایعات از میان بتن است. سه نوع سیال وجود دارند که عموماً بر دوام بتن اثر می‌گذارند و می‌توانند به داخل بتن وارد شوند آب (خالص و یا حاوی یونهای مهاجم) دی اکسید کربن و اکسیژن. این مواد می‌توانند به روشهای مختلف در بتن جابجا شوند اما کلیه این جابجاییها عمدتاً به ساختار خمیر هیدراته شده سیمان بستگی دارد. دوام بتن عمدتاً به ساختار خمیر هیدراته شده سیمان و به سهولتی که مایعات و سیالات می‌توانند از آن بگذرند بستگی دارد.

ساختار بتن را می‌توان به دو دسته فیزیکی و شیمیائی تقسیم نمود. ساختار شیمیائی در واقع واکنشهای شیمیائی هیدراسیون است که بین سیمان و آب انجام می‌شود. ساختار فیزیکی یا به عبارت دیگر ریز ساختار شامل منافذ موجود در بتن است. بتن دارای منافذ گوناگون در اندازه‌های متفاوت است.

به طور کلی، خمیر سیمان هیدراته شده شامل سه سیستم مهم است:

۱- سیستم جامد
۲- سیستم منافذ
۳- سیستم محلول در منافذ

سیستم‌های جامد و محلول در منافذ مربوط به ساختار شیمیایی و سیستم منافذ محدود به ساختار فیزیکی بتن می‌باشد. سیستم جامد در واقع محصولات هیدراسیون است که شامل ژل، -H C-S هیدروکسید کلسیم و فازهای آلومینات و فریت است.

سیستم منافذ شامل منافذ ژل است که اندازه آن‌ها بسیار کوچک، در حدود ۴۰ nm و منافذ موئین که نسبتاً بزرگترند و اندازه آنها حدود ۵۰۰ nm – ۲۰۰ است. به علاوه منافذ دیگری نیز وجود دارند که اندازه آن‌ها بزرگتر از منافذ موئین است که در نتیجه تراکم ناقص بتن ایجاد می‌شود.

بخشی یا تمام سیستم منافذ با محلول پر می‌گردد، که این محلول عمدتاً شامل هیدروکسید سدیم NaOH،

هیدروکسید پتاسیم KOH، هیدروکسید کلسیم $Ca(OH)_2$ است.
کل حجم منافذ موئین موسوم به تخلخل است و معمولاً بـرای مقیـاس کیفیـت بـتن از مقـدار تخلخـل اسـتفاده می‌شود. ارتباط بین منافذ موئین نقش تعیین کننده‌ای در نفوذپذیری و دوام دارد. در واقع منافـذی کـه مـستقل و بدون ارتباط به یکدیگر هستند، اثری در نفوذ پذیری ندارند و در شکل (۱) رابطه بین ارتباط منافذ بـر نفوذپـذیری نشان داده شده است.
حجم منافذ موئین تابع نسبت آب به سیمان میباشد. بعبارت دیگر، مقدارآب اولیه خمیر سیمان ودرجه هیدراسیون برحجم وخصوصیات منافذموئین اثرمیگذارد. هرچه نسبت آب به سیمان بیشترباشدحجم منافذ موئین افزایش می‌یابد.

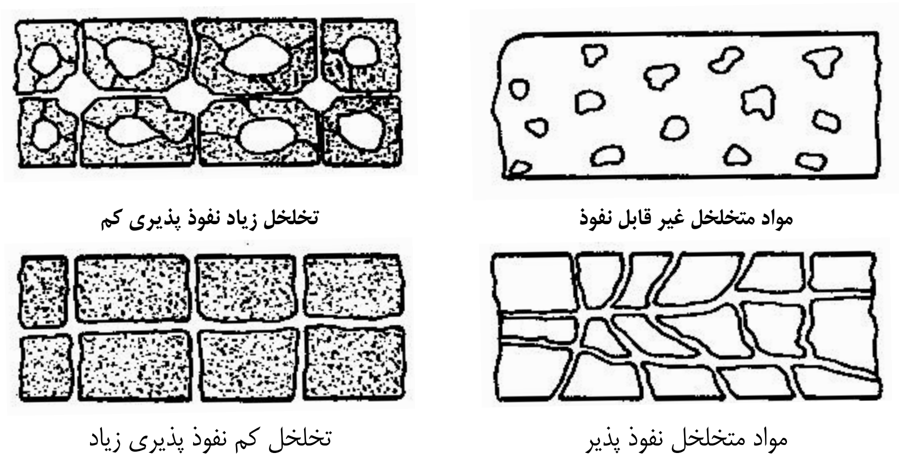

شکل ۱- رابطه بین ارتباط منافذ بر نفوذ پذیری.

رفتار لایه سطحی بتن مهم ترین عامل تعیین کننده شدت آسیب پذیری سازه‌های بتنی است. معمولاً نفوذ پذیری بتن به عنوان معیار سنجش دوام بتن است. نفوذ پذیری کم، نشان دهنده مقاومت زیاد بتن در مقابـل حرکـت آب است. در واقع، بسیاری از پژوهشگران هنوز نفوذ پذیری را مهم ترین خاصیت مربوط به دوام می‌دانند. این فرضیه در مورد بتن‌هایی که به طور دائم غوطه ورند صحت دارد. زیرا در چنین شرایطی بتن اشباع و در معرض ستون یـا ارتفاع آب است. اما در موارد دیگر که سازه در معرض هوا قرار دارد (مانند پل‌ها)، فرآیند نفوذپذیری صادق نیست. در چنین شرایطی سطح خارجی بتن اشباع نبوده و غیر از بخشی از سـازه (کـه در معـرض جـذر و مـد اسـت)، در معرض ستون آب نمی‌باشند، به عبارت دیگر جذب موئین به جای نفوذ پذیری، کنترل کننده عبور آب است.
جذب موئینه عبارتست از آب جذب شدهٔ بتن که از طریق پدیدهٔ موئینگی انجام می‌شود. بـا افـزایش مقـدار منافـذ موئینه بتن، به مقدار جذب موئینه افزوده می‌شود، در جذب موئینه، نیرویی که سبب حرکـت آب مـی‌شـود حاصـل اختلاف فشار بین دو طرف هلالی (ناشی از آب در منافذ بتن) است. بنابراین نیروهای موئینه، در بتن کاملاً اشـباع وجود ندارند و حرکت آب متوقف می‌گردد. اگر r شعاع منفذ موئین باشد معمولاً ارتفاع آب (H) معـادل $\frac{15}{r}$ بـه دست می‌آید.

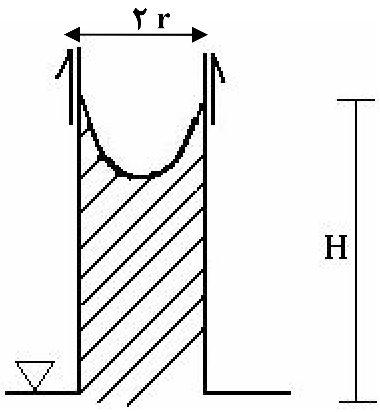

شکل ۲- مکش موئین ناشی ازانرژی سطحی

اگر آب در تماس با بتن غیر اشباع باشد، حتی در غیاب نیروهای خارجی، از طریق فرآیند موئینه جـذب مـی‌شـود. براساس نظریه مک کارتر و همکارانش، بخشی از سازه که بالاتر از سطح زمین در معرض فرآیند خـشک شـدگی ناشی از تابش خورشید و باد قرار دارد. بنابراین لایه سطحی بتن دارای مقداری آب غیر یکنواخـت اسـت و مقـدار رطوبت،کمتر از حد اشباع می‌باشد و گرادیان رطوبت در محدودۀ پوشش بتنی وجود دارد. بنابراین روند حرکـت آب در ناحیه پوشش از نوع جریان غیر اشباع است و شامل نیروهای مکنده موئینه است.

بر همین اساس برای سازه‌هایی که در سطح زمین قرار دارند آزمایش جذب موئینه مطلوب می‌باشد.

نفوذ پذیری تحت تأثیر عوامل متعددی قرار می‌گیرد که از آن جمله مـی‌تـوان بـه نـسبت اب بـه سـیمان، عیـار سیمان، سنگدانه‌ها، درجه هیدراسیون سیمان، رطوبت نمونه اشاره کرد. به نظـر مـی‌رسـد افـزایش دمـا در دوران عمل اوری باعث کاهش کل تخلخل می‌گردد ولی قطر منافذ مویینه را که مرتبط بـا نفوذپـذیری بـتن هـستند را افزایش میدهد. برای بررسی تاثیرات دمای اولیه بتن بر این پدیده آزمایشاتی انجام گرفت که در ادامه به آن اشاره می‌گردد.

۳- فرضیات اولیه آزمایش

در این پژوهش از سیمان پرتلند نوع ۲ استفاده شد. همچنین از ماسه شکسته با حد اکثر انـدازه 4/75 و همچنـین شن نیمه شکسته با حد اکثر اندازه ۱۹ میلیمتر استفاده گردید. آب مصرفی نیز آب شهر تهران بود.

طرح اختلاط مطابق با طرح اختلاط ملی ایران انجام گرفت. نسبت آب به سیمان برابر 0/47 و عیار سـیمان برابـر ۴۰۰ کیلو گرم فرض شد.

در ادامه سعی شد تا دماهای ۱۰، ۲۰، ۳۰ و ۴۰ درجه سانتیگراد در مخلوط بتن تازه ایجاد گردد. دمای هوا در حین ساخت بتن در حدود ۳۲ درجه سانتیگراد بود لذا برای ایجاد دماهای مورد نظر از فرمول پیشنهادی در ACI 306 R استفاده گردید. رابطه (1)

$$T = \frac{\text{۰/۲۲}(c\,T_c + G_d\,T_G + S_d T_s) + T_w\,W_m + T_G\,W_G + T_s\,W_s}{\text{۰/۲۲}(c + G_d + S_d) + W_t} \qquad (۱)$$

که در آن c , G_d , S_d به ترتیب وزن سیمان، شن در حالت خشک و ماسه در حالت خشک و W_t، W_m، W_G، W_S، به ترتیب میزان آب کل، آب مصرفی، رطوبت شن، رطوبت ماسه و T_c، T_G، T_s به ترتیب دماهای سیمان، شن و ماسه است.

و چنانچه در شرایط خاص برای خنک کردن بتن به جای بخشی از آب از یخ استفاده شود آنگاه عبارت $W_m\ T_w$ به عبارت $(W_m - W_i)T_w + W_i(۰/۵T_i - ۸۰)$ تبدیل می‌شود. که در آن W_m و W_i به ترتیب آب مصرفی و جرم یخ و T_W و T_i به ترتیب دمای آب مصرفی و دمای یخ می‌باشد.

از آنجا که ظرفیت گرمایی ویژه آب ۵ برابر ظرفیت گرمایی ویژه مصالح سنگی و سیمان است لذا بهینه ترین روش برای ایجاد دماهای مختلف در بتن تازه تغیر دمای آب می‌باشد. برای این منظور با جایگذاری دماهای مطلوب در رابطه فوق حجم آب و یخ لازم بدست آمد.(برای جبران اتلاف‌های حرارتی ناشی از اختلاف درجه حرارت مخلوط بتن و هوای محیط در حین ساخت، دمای تعادل در این رابطه باید اندکی کمتر از دمای مطلوب ما لحاظ گردد تا نهایتا دمای مطلوب در بتن احراز گردد.) نتایج در جدول ۱ دیده می‌شود.

جدول ۱: مقادیر آب و یخ استفاده شده و دمای آنها در هر مخلوط

کد طرح اختلاط	دمای اسمی در فرمول [°C]	آب مصرفی [lit]	یخ [kg]	دمای آب [°C]	دمای یخ [°C]	دمای شن و ماسه [°C]	دمای سیمان [°C]	دمای بتن [°C]
T=10	T=6	109	130	5	-10	30	30	T=10
T=20	T=18	۲۰۳	۳۶	5	-10	30	30	T=20
T=30	T=29	239	0	28	-	30	30	T=30
T=40	T=40	239	0	40	-	50	30	T=40

۴- آزمایشات انجام شده و نتایج آن

- جذب آب

جذب آب بتن‌ها با الگوبرداری از دستور BS 1881–Part 122 و عمدتاً شبیه به BS 1881 قدیمی‌به صورت درصد وزنی با استفاده از میانگین‌گیری نتایج ۳ آزمونه مکعبی ۱۰۰ میلی‌متری در مورد نمونه‌های ازمایشگاهی و دو عدد مغزه 7/5 میلی متری از نمونه‌های کارگاهی به دست آمد. نحوه‌ی آماده‌سازی آزمونه‌ها برای انجام این آزمایش به این صورت بود که پس از خارج شدن از قالب، ابتدا به مدت ۲۷ روز به داخل حوضچه آب منتقل شدند، سپس از آن خارج و توزین شدند و برای خشک شدن به درون گرمخانه با دمای ۱۱۰ درجه سانتیگراد انتقال یافتند. پس از گذشت حدود ۳ روز و رسیدن آزمونه‌ها به وزن ثابت (m_0)، آزمایش مذکور با غوطه‌ور کردن آنها در آب آغاز گردید. در ادامه با خارج ساختن آزمونه‌های غوطه‌ور شده از آب در زمان‌های ۱، ۲۴ و ۷۲ ساعت، ابتدا آب اضافی آنها توسط پارچه‌ای گرفته شد و سپس، با اندازه‌گیری وزن آنها (m_t) و قرار دادن در رابطه (۱) میزان جذب آب آنها به صورت درصد وزنی به دست آمد که بعد از ۱ روز آهنگ جذب آب نمونه‌ها بسیار اندک است و پس از ۳ روز تغییر خاصی نمی‌کند. همچنین نمونه‌ها کمتر از آبی که هنگام خارج شدن از

حوضچه دارا هستند، جذب آب می‌کنند.در این آزمایش، جذب آب یک ساعته به عنوان جـذب آب اولیـه و جـذب آب سه روزه به عنوان جذب آب نهایی در نظر گرفته شده است.

$$\frac{m_t - m_0}{m_0} \times 100 = \text{جذب آب در زمان } t \qquad (۲)$$

که در آن:

m_t = وزن آزمونه مرطوب در زمان t

m_0 = وزن آزمونه خشک شده در گرمخانه

همچنین میزان درصد آب جذب شـده نمونـه‌هـای آزمایـشگاهی در پایـان ۲۸ روز بعـد از خـروج از حوضـچه در جدول(۴) و نمودار (۳)آورده شده است.

همانطور که از نتایج مشاهده می‌شود نمونه‌ها بـه انـدازه میـزان آب خـود هنگـام خـروج از حوضـچه، جـذب آب نمی‌کنند و میزان اندکی کمتر از آن قادر به جذب آب هستند ؛ ولی روند تغییرات آب جذب شده نمونه‌ها در پایـان ۲۸ روز قرار گیری در حوضچه با تغییرات دما، با روند تغییرات آب جذب شده نمونه‌ها بعد از خشک شدن و غوطـه وری مجدد به مدت ۷۲ ساعت، همسو می‌باشد.

همچنانکه از نتایج مشخص است کمترین میزان جذب آب اولیه و نهایی در سن ۲۸ روز، مربوط به مخلوط T=20 و بیشترین آن مربوط به مخلوط T=40 می‌باشد.

جدول ۲: نتایج جذب آب اولیه (۱ ساعته بر حسب ٪)

سن آزمونه	شرایط عمل آوری	نام طرح و میزان جذب آب اولیه (٪)			
		T=10	T=20	T=30	T=40
۲۸ روزه	آزمایشگاهی	4/23	4/15	4/28	4/37
۲۸روزه	کارگاهی	4/92	4/68	4/98	5/17

جدول ۳: نتایج جذب آب نهایی (۷۲ ساعته بر حسب ٪)

سن آزمونه	شرایط عمل آوری	نام طرح و میزان جذب آب نهایی (٪)			
		T=10	T=20	T=30	T=40
۲۸ روزه	آزمایشگاهی	9/27	9/08	9/41	9/61
۲۸روزه	کارگاهی	9/40	9/16	9/59	9/80

جدول ۴: میزان آب جذب شده نمونه‌ها در پایان سن ۲۸ روز

سن آزمونه	شرایط عمل آوری	نام طرح و میزان جذب آب (٪)			
		T=10	T=20	T=30	T=40
۲۸ روزه	آزمایشگاهی	9/9	9/86	10/15	10/31

علت اختلاف میزان جذب آب با تغییرات دمای اولیه بتن را میتوان اینگونه تفسیر نمود.در بتن منافذ متعددی وجود

دارد که کل این منافذ و فضاهای خالی تخلخل بتن را تشکیل می‌دهند. ولی تنها منافذی قابلیت جـذب آب و بـه طور کلی نفوذ پذیری را دارا هستند که ضمن داشتن قطر مناسب، با یکدیگر ارتباط نیز داشته باشند.آنچه در حجم و شکل این منافذ تاثیرات عمده ای دارد، درجه هیدراسیون سیمان و نحوه توزیع محـصولات آن در بـین اجـزای بتن است.

همانطور که در مورد مقاومت نیز به آن اشاره شد، دمای اولیه بالا (در این آزمایش دماهای بالاتر از نمونه T=20) باعث افزایش سرعت هیدراسیون و تولید سریع محصولات میگردد ولـی ایـن سـرعت بـالای هیدراسـیون باعـث تجمع محصولات حول ذرات هیدراته نشده سیمان گشته و ضمن آنکه سیمان به طور کامل هیدراته نمی‌گـردد، این محصولات فرصت کافی جهت توزیع یکنواخت بین ذرات بتن را نداشته و نهایتا باعث ایجاد بافت ضعیف تر و نفوذ پذیر تر در بتن میگردد.(ضمن آنکه در بتن ممکن است نقاط ضعیف موضعی نیز به وجود آید.)

همچنین در دماهای اولیه پایین نیز (مثل نمونه T=10) درجه پایین هیدراسیون سیمان باعث افـزایش جـذب آب نسبت به دماهای بالا تر (مثل نمونه T=20) است.

اختلاف نفوذ پذیری در نمونه‌های آزمایشگاهی و کارگاهی را میتوان در شرایط مناسب تر عمل آوری نمونـه‌هـای آزمایشگاهی دانست زیرا در معرض آب قرار داشتن این نمونـه‌هـا باعـث ایجـاد هیدراسـیون کامـل تـر و بافـت بهترنسبت به نمونه‌های کارگاهی گشته است.

هر چند این اختلاف، کمتر از آنچه پیش بینی می‌شد واقع گشت که شاید بتوان این پدیده را ناشی از دمای بالای عمل‌آوری و تا ثیر آن در افزایش سرعت تکامل واکنشهای هیدراسیون سیمان درنمونـه‌هـای کارگـاهی در طـول مدت عمل آوری نسبت به نمونه‌های آزمایشگاهی دانست.

همچنین در این آزمایش بعـد از خـروج نمونـه‌هـا در پایـان ۲۸ روز عمـل آوری آزمایـشگاهی، وزن اشـباع آنهـا اندازه‌گیری شد و سپس جهت انجام آزمایش جذب آب در اون قرار گرفتند. ولی بعـد از سـه روز غوطـه ور شـدن مجدد نمونه‌ها در آب و ثابت شدن جذب آب آنها مشاهده شد که نمونه‌ها بـه میـزان آب از دسـت داده، قـادر بـه جذب آب نیستند و حدود ۹۰٪ آب از دست داده را مجددا جذب می‌کنند. نمودار(۳). به نظر می‌رسد کـه ایـن ۱۰٪ آب غیر قابل جذب مجدد، آب موجود در منافذ ریز ژلی و یا منافذ غیر مرتبط موجـود در محـصولات هیدراسـیون می‌باشد که پس از خشک شدن آنها، آب قادر به نفوذ مجدد در آن نمی‌باشد.

همچنین مشاهده شد که روند بین درصد آب جذب شده نمونه‌ها در پایان سن ۲۸ روز، و درصـد جـذب آب آنهـا پس از سه روز یکسان می‌باشد.(نمودار(۳)).

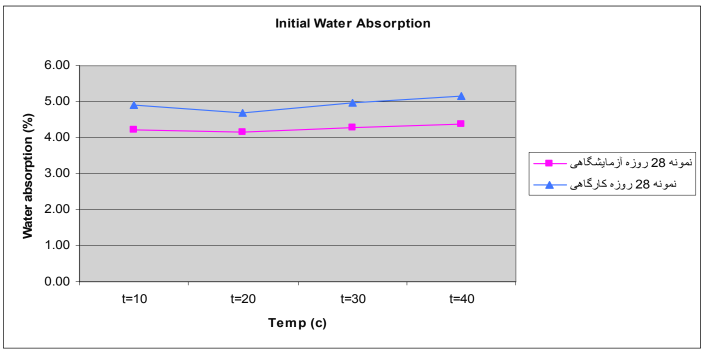

نمودار ۱- تغییرات میزان جذب آب اولیه (۱ ساعته) با تغییرات دما

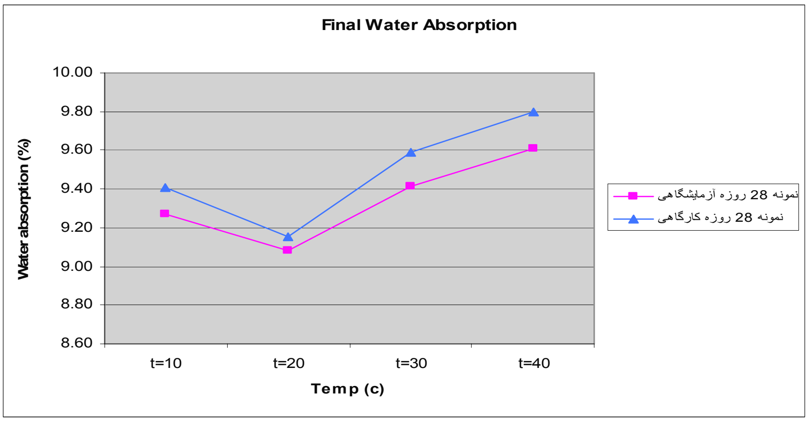

نمودار ۲- تغییرات میزان جذب آب نهایی (۷۲ ساعت) با تغییرات دما

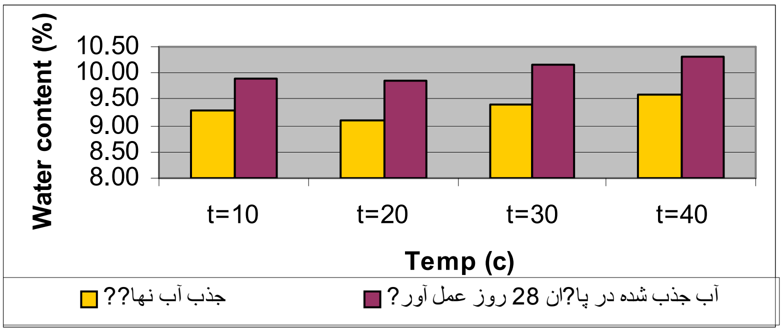

نمودار ۳- نمودار تغییرات میزان آب جذب شده نمونه‌ها در پایان ۲۸ روز عمل‌آوری درحوضچه و جذب اب نهایی نمونه‌ها تغییرات دما

جذب آب مویینه

آزمایش جذب آب مویینه طبق دستور RILEM CPC 11.2, TC 14-CPC انجام گـــردید. این آزمـایش فقـط در مورد نمونه‌های آزمایشگاهی ۱۰×۱۰ و ۲ نمونه از هر مخلوط انجام گرفت.

نحوه عمل‌آوری و خشک شدن نمونه‌ها در گرمخانه مطابق با آزمـایش تعیـین جـذب آب بـود. در ایـن آزمـایش، آزمونه‌های خشک شده در داخل ظرف گونه ای قرار گرفت که کف آن اندکی بالاتر از کف ظرف باشد برای ایـن منظور نمونه‌ها بر روی تخته‌های باریک چوبی قرار داده شد و سپس ظرف تا ارتفاع ۱±۵ میلی‌متر بـالاتر از کـف آزمونه‌ها پر از آب گردید. در تمام مدت آزمایش سطح آب ثابت نگاه داشته شد.

اندازه‌گیری جذب آب مویینه در فواصل زمانی ۳، ۶، ۲۴ و ۷۲ ساعت از زمان قرار دادن آزمونـه‌هـا در آب صـورت گرفت. هنگام توزین، آزمونه‌ها به‌ترتیب از درون آب خارج شد به کمک پارچه آب سطحی آن خشک شد، نمونه‌ها وزن شد و مجددا داخل ظرف قرار گرفت. به این ترتیب با داشتن وزن آزمونـه خـشک شـده در گرمخانـه (m_0) و وزن آزمونه در زمان t (m_t)، میزان جذب آب در واحد سطح یا عمق معادل نفوذ آب از رابطه (۳) محاسبه شد.

$$i_t = \frac{m_t - m_0}{A} \qquad (۳)$$

که در آن:

i_t = میزان آب جذب شده در واحد سطح در زمان t [gr/mm^2]، برابر با عمق معادل نفوذ آب [mm]

m_0 = وزن آزمونه خشک شده در گرمخانه [gr]

m_t = وزن آزمونه در زمان t [gr]

A = سطح مقطع نمونه [mm^2]

با ترسیم نقاط به دست آمده در دستگاه $i - \sqrt{t}$ و برازش یک خط مستقیم از این نقاط، ضریب جذب آب مویینه S (شیب خط برازش شده) و ثابت جذب آب مویینه C (عرض از مبدأ خط برازش شده) به دست آمد. رابطه عمومی‌خط برازش شده به شکل زیر است:

$$i = C + S\sqrt{t} \qquad (۴)$$

که در آن:

i = میزان آب جذب شده در واحد سطح [gr/cm^2] برابر با عمق معادل نفوذ آب [cm]

C = ثابت جذب آب مویینه [cm]

S = ضریب جذب آب مویینه [$cm/hr^{0.5}$]

t = زمان [hr]

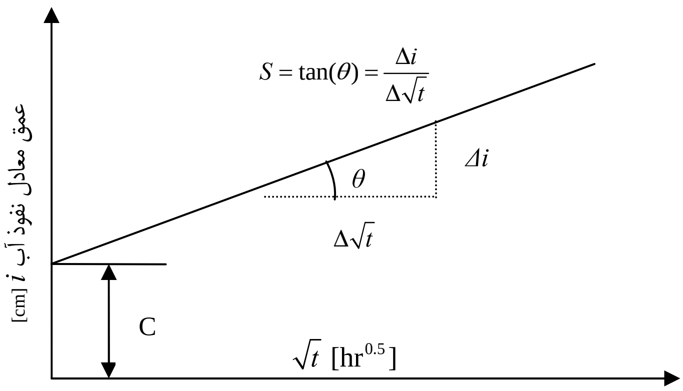

در روش دیگر میتوان خط i-log(t) را نیز رسم نمود. و S,C را با برازش خط در این دستگاه مختصات بدست آورد.

$$i = C + S\log(t) \qquad (۵)$$

S و C از دستگاه مختصاتی انتخاب می‌گردد که خط برازش داده شده در آن دستگاه بیشترین ضریب همبستگی را برای نقاط در آن دستگاه ایجاد کند.

نتایج جذب موئینه آزمونه‌ها درجدول (۵) مشاهده میشود. ضرائب همبستگی(R) بدست آمده بین 0/961 و 0/987 که بطور میانگین 0/976 می‌باشد. ضرائب همبستگی بدست آمده مناسب بوده وبیانگرهمگرائی قابل قبـول نقـاط نمودارi برحسب جذرزمان می‌باشد.

اگر نمودارi برحسب لگاریتم زمان ترسیم شود، ضرائب همبستگی بین مقادیر 0/961 و 0/972 و به طور میـانگین 0/967خواهند بود که در مقایسه با روش جـذر زمـان همبـستگی ضـعیف تـری بـین نقـاط برقـرار خواهـد بـود. (جدول(۶))

بنابر این مقادیر ثابت جذب و ضریب جذب مویینه نمودار جذر زمان مد نظر خواهد بود.

ضریب جذب موئینه (S) در نمونه‌ها با تغییر دمای اولیه بـتن متغیـر بـوده و مقـادیراین ضـرائب از $cm/hr^{0.5}$ 0/134 تا 0/156 تغییر می‌کند.

ثابت جذب موئینه (C) درنمونه‌ها از 0/218 تا0/326متغیر است. ثابت جذب موئینه به نوع بـتن و روش پرداخـت سطح آن وابسته است.

جدول ۵: نتایج آزمایش جذب آب مویینه

نام طـــرح	جذب آب در واحد سطـح برابر با عمق معادل نفوذ آب [cm]				مشخصات خط برازش شده منحنی $i-\sqrt{t}$		
	۳ ساعت	۶ ساعت	۲۴ ساعت	۷۲ ساعت	ثابت جذب مویینه [cm]	ضریب جذب مویینـه [cm/hr0.5]	ضریب همبستـگی R2
T=10	0/43	0/57	0/99	1/40	0/218	0/143	0/987
T=20	0/47	0/62	1/05	1/38	0/291	0/134	0/971
T=30	0/52	0/71	1/22	1/57	0/326	0/154	0/961
T=40	0/48	0/63	1/10	1/54	0/249	0/156	0/986

جدول ۶: مشخصات خط برازش شده i-log(t)

نام طرح	مشخصات خط برازش شده منحنی i– log(t)		
	ثابت جذب مویینه [cm]	ضریب جذب مویینـه [cm/hr0.5]	ضریب همبستـگی R2
T=10	0/013	0/334	0/962
T=20	0/089	0/316	0/971
T=30	0/087	0/366	0/972
T=40	0/025	0/365	0/961

هر چند مقادیر ثابت جذب مویینه به نوعی نشان دهنده پتانسیل جذب آب مویینه بتن هستند. اما باید توجـه نمـود که در بحث جذب آب موئینه بتن، آهنگ جذب آب موئینه نسبت به ثابت جذب موئینه اهمیت بیـشتری دارد و در بررسی نتایج جایگاه مهمتری را به خود اختصاص می‌دهد.

در تجزیه و تحلیل نتایج جذب آب موئینه، روند جذب آب موئینه بتن باید بررسـی شـود. لـذا «ضـریب جـذب آب

مویینه S» از این جهت اهمیت پیدا می‌کند و در این بخش تشریح می‌شود.
تغییرات ضریب جذب مویینه با تغییرات دما در نمودار (۴) نشان داده شده است. همانگونه که مشاهده می‌گردد کمترین ضریب جذب مویینه را نمونه T=20 داراست و پس از آن نمونه‌های T=10، T=30 و T=40 به ترتیب قرار گرفته‌اند.
آزمایش جذب مویینه و آزمایش جذب آب تحت تاثیر عوامل کم و بیش مشابهی هستند بنابراین به همان دلایلی که در مورد آزمایش جذب مطرح گردید (تاثیرات دمای اولیه بتن در درجه هیدراسیون سیمان نسبت به زمان و نحوه توزیع محصولات در بین اجزای بتن) این نتایج حاصل گشته است.

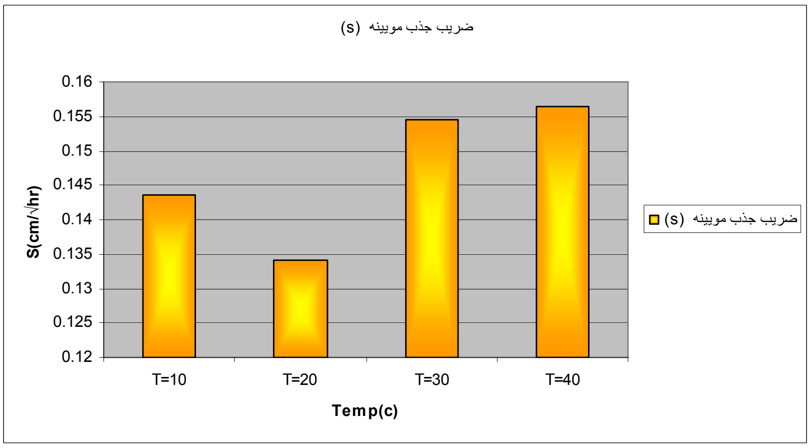

نمودار۴- تغییرات ضریب جذب آب مویینه با تغییرات دما

۵- نتیجه‌گیری

۱- درجه و سرعت هیدراسیون سیمان عواملی تاثیر گذار بر میزان جذب آب بتن می‌باشند. آنچنانکه در این آزمایش، بتن T=20 به دلیل داشتن شرایط بهتر از این لحاظ، نسبت به نمونه‌های دیگر کمترین جذب آب را دارا بود. و نمونه‌ها با دماهای اولیه بالا تر به دلیل داشتن بافت ضعیف تر به دلیل سرعت بالای هیدراسیون، و نمونه‌ها با دمای پایین تر به دلیل درجه هیدراسیون ضعیف تر دارای نفوذ پذیری بیشتری بودند که این روند در هر دو سری نمونه‌های آزمایشگاهی و جداول یکسان بود.
۲- در این آزمایش مشاهده شد که نمونه‌ها حدود ۹۰٪ آبی را که هنگام خروج از حوضچه پس از ۲۸ روز دارا بودند، در پایان آزمایش جذب آب مجددا جذب می‌کنند.
۳- روند بین نتایج میزان آب جذب شده نمونه‌ها در هنگام خروج از حوضچه در پایان ۲۸روز و جذب آب نهایی آنها، در دماهای مختلف، یکسان است.
۴- روند تغییرات ضریب جذب آب مویینه در این آزمایش نشان میدهد که بتن T=20 کمترین آهنگ جذب آب مویینه را داراست و پس از آن نمونه‌های T=10، T=30 و T=40 به ترتیب قرار گرفته اند. همچنین روند نتایج آزمایش جذب آب و جذب آب مویینه در این آزمایش کم و بیش یکسان می‌باشد.
۵- پیشنهاد می‌شود این ازمایشات در سنین بالاتر نیز انجام گیرد تا ادامه این روند در سنین به اندازه کافی بالا

مشاهده گردد.

۶- پیشنهاد میشود اثر همزمان دمای اولیه و عمل‌آوری نیز بر جذب اب ان بررسی گردد.

مراجع

۱- «آیین‌نامه بتن ایران (تجدید نظر اول)»، دفتر تحقیقات و معیارهای فنی، سازمان برنامه و بودجه، شماره نشریه: ۱۲۰،

۲- «آیین‌نامه ملی پایایی بتن در محیط خلیج فارس و دریای عمان (پیشنهادی)»، شماره نشریه: ض ـ ۴۲۸، مرکز تحقیقات ساختمان و مسکن،

۳- کومار مهتا، پ.، مونته‌ئیرو، د، ج، م. (۱۳۸۵) «ریزساختار، خواص و اجزای بتن (تکنولوژی بتن پیشرفته)»، ترجمه: رمضانیانپور، ع، ا.، قدوسی، پ.، و گنجیان، ا.، دانشگاه صنعتی امیرکبیر،

۴- نویل، آ. (۱۳۷۸) "خواص بتن"، ترجمه : فامیلی، ه.، ابوریحان بیرونی،

۵- رمضانیانپور، ع.ا.، پاشائی، ر.، "کربناسیون در سازه‌های بتن مسلح "، مرکز تحقیقات ساختمان و مسکن، ۱۳۷۵، نشریه شماره ک-۲۳۷.

۶- قدوسی، پ.، پرهیزکار، ط.، رمضانیانپور، ع. ا.، و مظفری، ن. (۱۳۸۳) "فن‌آوری بتن در شرایط محیطی خلیج‌فارس؛ جلد دوم: روشها و توصیه‌ها برای افزایش عمر مفید سازه‌های بتنی"، شماره نشریه: ک – ۳۷۰، مرکز تحقیقات ساختمان و مسکن، ص. ۱۶۱.

7- Civil Aviation Directory, Meteorological Office, Bahrain Air port Publication , 1990.

8- Comitte Euro-International Du Beton, "Durable concrete structures", Design Guide, Thomas Telford publications, 1989.

9- Emerson , M ,"Mechanisms of water Absorbsion by Concrete", Transport and Road Research Labratort ;U.K; 1990.

10- Mehta, P.K., "Concrete Structures, properties and Materials", Prentice-Hall Publications, 1986.

11- Novokshchenov, V. , "Detrioration of Reinforced concrete in the Marine Industrial Enviroment of the Persian Gulf-A case stady", Marials and structures, 1995.VOL.28, PP.392-400.

12- Powers,T.C., "Structure and Physical properties of hardened Portland cement paste", Jornal of the American ceramic society,1985.vol.41, pp.1-6.

CD02-034

تاثیر دمای بتن تازه بر مقاومت‌های مکانیکی و الکتریکی آن در سنین مختلف

هرمز فامیلی[1]، محسن تدین[2]، پویا حاجی تقی تهرانی[3]
۱. استادیار دانشکده عمران دانشگاه علم و صنعت ایران
۲. استادیار دانشکده را ه آهن دانشگاه علم و صنعت ایران
۳. دانشجوی کارشنا سی ارشد دانشگاه علم و صنعت ایران

چکیده

از آنجا که عمدتا ساخت بتن در شرایطی در تماس مستقیم با محیط انجام می‌گیرد پیوسته تحت تاثیر شرایط اقلیمی‌خود واقع می‌گردد. دما مهمترین عامل اقلیمی‌است که بیش از هر عامل دیگری بتن را تحت تاثیر قرار می‌دهد. این تاثیرات بر بتن تازه و سخت شده قابل توجه است.

در این مقاله تاثیرات دمای اولیه بتن بر مقاومت‌های فشاری، کششی و همچنین مقاومت ویژه الکتریکی آن مورد بررسی قرار گرفت. در این راستا نمونه‌هایی با دماهای اولیه ۱۰، ۲۰، ۳۰و ۴۰ درجه سانتیگراد ساخته شد و مشاهده گشت که با افزایش دمای اولیه بتن مقاومت فشاری کوتاه مدت آن تا سن ۷روز افزایش می‌یابد ولی مقاومت‌ها دراز مدت آن به خصوص در سن ۹۱ روز کاهش یافته است.

همچنین آزمون کشش برزیلی بر روی این نمونه‌ها انجام شد و مشاهده شد که تا سن ۲۸ روز نمونه‌های با دمای اولیه ۲۰ درجه ساتیگراد بیشترین مقاومت کششی را دارا می‌باشند و با افزایش دمای اولیه مقاومت کاهش می‌یابد. در مورد مقاومت ویژه الکتریکی نیز نتایج مشابهی مشاهده گشت با این تفاوت که تنها در سن ۹۱ روز مقادیر اختلاف مقاومت مقادیر قابل توجهی پیدا کرد و بتن با دمای اولیه ۱۰ درجه سانتیگراد بیشترین مقدار مقاومت ویژه الکتریکی را دارا بود.

کلیدواژه‌ها: دمای اولیه، بتن تازه، مقاومت فشاری، مقاومت کششی، مقاومت ویژه الکتریکی

۱- مقدمه

بتن یکی از مصالح ساختمانی پرمصرف در ساخت پل‌ها، ساختمان‌ها، سکوها، جداول و همینطور در سازه‌های زیرزمینی مثل تونل‌ها و خطوط لوله‌های بتنی می‌باشد. در حالت کلی، بتن یکی از مصالح بسیار بادوام به شمار می‌آید که می‌تواند در شرایط محیطی بسیار سخت مثل شرایط محیطی دریایی، صنعتی و غیره، مقاومت خوبی را از خود به نمایش بگذارد.سنگدا نه، سیمان، آب و بعضا افزودنی‌های مختلف همگی از مواد تشکیل دهنده بتن هستند که میزان، نوع و شرایط آنها همگی در کیفیت بتن تاثیر گذار است ولی آنچه این مصالح اولیه را در کنار یکدیگر همچون جسمی‌همگن قرار می‌دهد واکنش‌هایی است که به تبع حضور سیمان در بتن صورت گرفته و محصولات آن ضمن ایجاد چسبندگی لازم بین مصالح از مقاومت‌هایی بر خوردار است که این مقاومت در

بتن‌های متعارف چه از نظر مکانیکی و چه دوامی‌کمتر از مقاومت‌های سنگدانه است. بنابر این محصولات واکنشهای سیمان، به عنوان ضعیف ترین بخش در بتن شناخته می‌شوند و لذا این واکنشها و پارامترهای تاثیرگذار در آنها از اهمیت زیادی برخوردار است که تاکنون مطالعات فراوانی در این زمینه انجام گرفته است.

یکی از این پارامترهای تاثیر گذار دمای بتن می‌باشد. از آنجا که واکنش هیدراسیون سیمان یک واکنش شیمیایی نسبتا کند می‌باشد درجه حرارت بتن در هر مرحله ازعمر آن در روند این واکنش تاثیر گذار بوده و تاثیرات خاصی بر ویژگیهای بتن می‌گذارد این تاثیرات چه در دوره ساخت بتن تازه، چه در دوره عمل آوری و چه در دوره بهره برداری آن در خواص بتن تاثیر گذار است.

به نظر می‌رسد به دلیل تاثیرات زیادی که دمای بتن تازه با توجه به روش ساخت آن از دمای محیط می‌گیرد و همچنین تغییراتی که در دمای محیط در طی فصول، ماهها، روزها و حتی ساعات روز مشاهده می‌گردد، دمای اولیه بتن یک پارامتر بسیار تاثیر پذیر نسبت به دمای محیط اطراف آن می‌باشد که پیوسته با تغییرات آن در حال تغییر است. ضمن آنکه دما در بتن تازه به سبب واکنش‌های هیدراسیون نیز افزایش می‌یابد که این پدیده به خصوص در مورد بتن‌های حجیم مقادیر قابل ملا حظه ای پیدا می‌کند.

لذا بررسی اثرات دما در بتن تازه بر روی خصوصیات مقاومتی و دوامی‌آن موضوع با اهمیتی است که در این تحقیق سعی شده است این تاثیرات در مورد مقاومت فشاری، کششی و مقاومت ویژه الکتریکی بتن مورد بررسی قرار گیرد.

۲-کلیات

۲-۱- اثرات دما بر روی خواص بتن تازه

عموماً افزایش دما در بتن سبب افت روانی وکاهش بِشتر اسلامپ در بتن تازه می‌گردد و نتیجتاً کارایی کمتری در بتن ایجاد می‌گردد و تخلخل بیشتر و جداشدگی بیشتر بعد از ریختن بتن به قالب ممکن است اتفاق بیافتد، لذا معمولاً در کارگاهها برای جبران این ضعف آب بتن را افزایش می‌دهند که در نتیجه افزایش نسبت آب به سیمان، حجم بیشتر خمیر و تخلخل و نفوذپذیری بیشتر آن، مقاومت بتن کاهش می‌یابد. چنانچه آب و سیمان هر دو افزایش یابند نیز باز بدلیل افزایش حجم خمیر سیمان نسبت به سنگدانه بتن از نظر مقاومت و دوام ضعیف تر می‌گرددو جمع شدگی‌های بتن نیز بیشتر می‌گردد. (ضمن آنکه سیمان بیشتر خود دمای هیدراسیون را از این طریق نیز بالا می‌برد).

در ACI 305 که مربوط به بتن ریزی در هوای گرم است؛ عواقب افزایش دما در بتن تازه را اینگونه برشمرده است:

۱- نیاز به آب بیشتر در بتن
۲- افزایش کاهش اسلامپ
۳- گیرش سریعتر و در نتیجه جابجایی، تراکم، پرداخت سخت‌تر و ریسک بالاتر ایجاد درزهای سرد
۴- استعداد بیشتر در تشکیل ترک‌های پلاستیک ناشی از جمع شدگی.
۵- سختی بیشتر در کنترل هوای محبوس شده در بتن (هنگامی‌که از مواد حباب زا استفاده می‌گردد)

۲-۲- مقاومت بتن

مقاومت بتن در بسیاری از موارد به عنوان با ارزش‌ترین خاصیت آن در نظر گرفته می‌شود. گو اینکه در بسیاری از موارد عملی ممکن است سایر مشخصه‌های آن مانند دوام و نفوذپذیری اهمیت بیشتری داشته باشند.
مقاومت یک تصویر کلی از کیفیت بتن به دست می‌دهد زیرا مقاومت با ساختار خمیر هیدراته شده سیمان رابطه مستقیم دارد. با توجه به ماهیت واکنشهای هیدراسیون سیمان دما عاملی تاثیر گذار بر مقاومت بتن در کنار عوامل دیگری چون درجه تراکم، نسبت آب به سیمان، نوع سیمان، عیار سیمان، سنگدانه‌ها، آب اختلاط، مواد افزودنی، شرایط عمل آوری، شکل و هندسه نمونه، رطوبت نمونه و... می‌باشد.
تاثیر دما در دوران عمل آوری بر مقاومت بتن توسط پژوهشگران زیادی مورد بررسی قرار گرفته و آنچه از نتایج آنها می‌توان استنباط کرد آنست که افزایش دما در دوران عمل آوری بتن چنانچه همراه با حفظ رطوبت باشد، باعث افزایش آهنگ کسب مقاومت آن تا سن ۲۸ روز می‌گردد ولی در سنین بالاتر مقاومت‌های نهایی بتن را کاهش می‌دهد. همچنین از آنجا که درجه هیدراسیون سیمان تابعی از زمان و دماست مقاومت بتن ممکن است بر مبنای بلوغ، که به صورت تابعی از زمان و دمای عمل‌آوری می‌باشد، بررسی گردد.

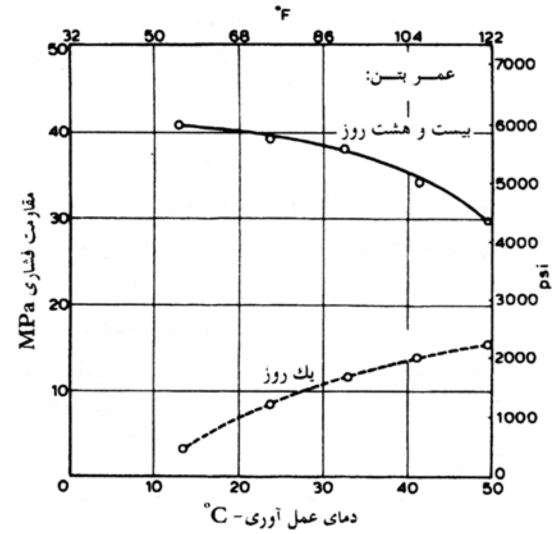

شکل ۱- تاثیر دمای عمل آوری بر مقاومت فشاری در عمرهای ۱ و ۲۸ روز

۲-۳- رفتار بتن تحت فشار تک محوری

منحنی تنش کرنش تا حدود ۳۰٪ مقاومت نهائی (f'_c) رفتار خطی و ارتجاعی نشان می‌دهد و این بدین دلیل است که تحت بارگذاری کوتاه مدت ریز ترکها در ناحیه انتقال ثابت مانده و بر هم نمی‌خوردند. در تنش‌های بالاتر از این نقطه منحنی تا تنشهای حدود $0/75 f'_c$ تا $0/9 f'_c$ انحنای بیشتری پیدا می‌کند و سپس خمیدگی تندی پیدا کرده و سرانجام نزول پیدا کرده تا آنکه نمونه به گسیختگی برسد.

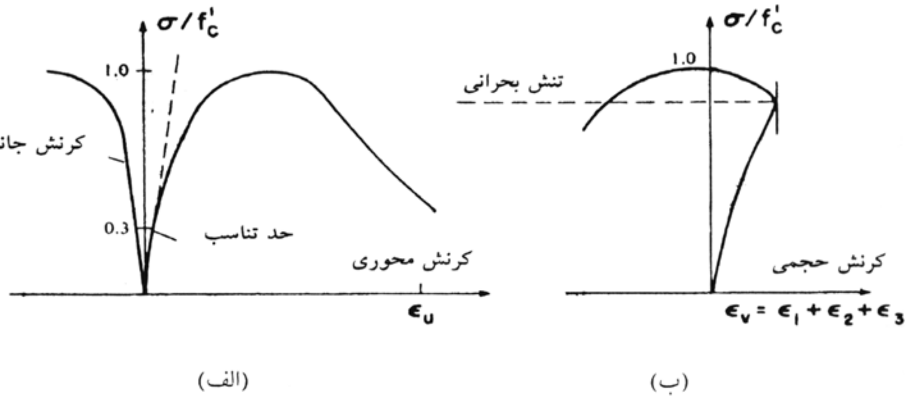

شکل ۲- منحنی معمولی تنشهای فشاری تحت الف-کرنشهای محوری ب) کرنش‌های حجمی

۲-۴- مقاومت کششی بتن

مقاومت فشاری و کشش بتن با یکدیگر در ارتباط مستقیم هستند و معمولاً نسبت مقاومت کششی به فشاری در محدوده 0/07 تا 0/11 است، روابط زیادی برای ارتباط این دو مقاومت مطرح شده است ولی از آنجا که عوامل مختلفی چون روش آزمایش، مشخصات سنگدانه‌ها، کیفیت بتن و نحوه عمل آوری آن و مواد افزودنی هر یک به نحوی در این مقاومت‌ها و تغییرات آنها تاثیر گذار است لذا هیچ رابطه‌ای را نمی‌توان در این مورد تعمیم کلی داد.

وجود حباب هوا نیز افت بیشتری در مقاومت فشاری نسبت به مقاومت کششی آن ایجاد می‌کند. تراکم ناقص نیز افت بیشتری در مقاومت کششی ایجاد می‌کند.

روش مستقیم آزمایش مقاومت کششی بندرت انجام گیرد و این امر بدلیل اعمال تنش‌های ثانویه غیرقابل اجتناب از طرف فک‌های دستگاه این آزمایش است. متداولترین روشهای اندازه‌گیری مقاومت کششی بتن روش دو نیمه شدن (ASTM-C469) و کشش ناشی از خمش سه نقطه‌ای (ASTM-C78) می‌باشد.

-آزمایش دو نیم شدن: در این آزمایش استوانه استاندارد ۳۰×۱۵ سانتیمتر در امتداد قطرش به صورت خوابیده تحت فشار قرار می‌گیرد بار به طور پیوسته و با سرعت ثابتی در محدوده تنش کششی بتن و بین ۷ تا ۱۴ کیلوگرم بر سانتیمتر مربع تا هنگام شکست نمونه بر آن اعمال می‌شود. تنش فشاری سبب ایجاد کششی یکنواخت در راستای عمود بر امتداد قطر قائم می‌شود مقاومت کششی دو نیمه شدن از رابطه

$$T = \frac{2P}{\pi L D} \qquad (۱)$$

بدست می‌آید که در آن T تنش کشش، P بار شکست، L طول نمونه و D قطر نمونه می‌باشد. در مقایسه با نتایج مقاومت کششی حاصل از روش مستقیم، مقاومت کششی حاصل از روش دو نیمه شدن بین ۱۰ تا ۱۵ درصد بیشتر است. شکل(۳).

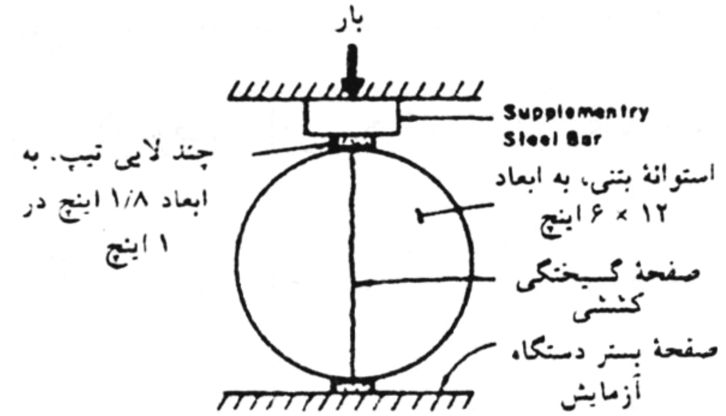

شکل ۳- آزمایش دو نیم شدن – ASTM C496

۲-۵- آزمایش مقاومت الکتریکی بتن

مقاومت الکتریکی بتن پارامتر بسیار مهمی‌است که به شکل غیر مستقیم، شدت فرایند نفوذ پذیری و خوردگی بتن را مورد ارزیابی قرار می‌دهد. در مقایسه با بتن با مقاومت الکتریکی کم، که در آن جریان بـه آسـانی بـین نـواحی آندی و کاتدی عبور می‌کند، در بتن با مقاومت الکتریکی بالا فرایند نفوذ پذیری و خوردگی کند خواهد بود.

مقـاومت الکتریکـی بتن به طور گستــرده برای ارزیابی غیر مستقیم ویژگی‌هـــای بتن همـــانند نفوذ پـذیری آن و میزان خلل و فرج مرتبط با یکدیگر مورد استفاده قرار میگیرد.

این آزمایش باید یر روی بتن اشباع از آب یا اشباع از محلول آب نمک انجام گیـرد و نتیجـه بـتن غیـر اشـباع یـا خشک به مراتب بالاتر از بتن اشباع خواهد بود.

مقاومت الکتریکی بتن تابع پارامترهایی به شرح زیر است:

۱- ساختار فیزیکی بتن: با افزایش تخلخل (به ویژه منافذ بزرگ) از مقاومت الکتریکی کاسته می‌شود.

۲- ساختار شیمیائی بتن: وجود عناصر شیمیائی در منافذ بتن بر مقاومت الکتریکی اثر دارد. مثلاً وجـود کلـر در محلول منافذ باعث کاهش مقاومت الکتریکی می‌گردد. همچنـین در محلـول منافـذ بـتن یـون‌هـایی از قبیـل Al^{3+} , Ca^{2+} و Si^{4+} و K^{-} یافت می‌شوند که نوع و مقدار آنها اثر مهمی‌بر مقدار مقاومت الکتریکـی بتن دارد.

۳- رطوبت: افزایش رطوبت در بتن از مقاومت الکتریکی بتن می‌کاهد.

۴-پلاریزاسیون ذرات : همجهت بودن دو قطبیهای موجود در بتن و جریان، باعث کاهش مقاومت الکتریکی بتن می‌گردد.

۵- درجه هیدراسیون سیمان: در خلال چند ساعت اولیه پس از مخلوط نمودن مقاومـت ویـژه بـتن خیلـی کند افزایش می‌یابد و سپس تا عمر حدود ۱ روز به سرعت زیاد می‌شـود و از آن پـس بـا رونـد کمتـری افـزایش می‌یابد یا ثابت می‌گردد. مگر آنکه بتن خشک شود. خشک شدن مقاومت ویژه را افزایش می‌دهد.

ظرفیت خازنی بتن با عمر آن و افزایش فرکانس کاهش می‌یابد. خمیر سیمان خـالص بـا نـسبت آب بـه سـیمان ۰/۲۳ دارای ظرفیت خازنی خیلی بیشتری از بتن با نسبت آب به سیمان ۰/۴۹ و با عمر یکسان است.

۶- عیار سیمان: هر تغییری در حجم نسبی خمیر سیمان مقاومت الکتریکی بتن را تحت تأثیر قرار مـی‌دهـد. مشاهده شده است که در یک نسبت آب به سیمان ثابت، افزایش عیار سیمان در مخلوط، باعث کـاهش مقاومـت ویژه الکتریکی آن می‌گردد. علت عمده این پدیده به بیشتر شدن الکترولیـت (آب منفـذی) موجـود در بـتن بـرای عبور جریان نسبت داده شده است.

۷- نسبت آب به سیمان: جریان الکتریسته در داخل بتن مرطوب اساساً به وسیله عمـل الکترولیتـی هـدایت می‌شود یعنی به وسیله یونهای موجود در آب قابل تبخیر آن، ولیکن وقتی لوله‌هـای مـویین منقطـع شـده باشـند جریان الکتریکی از میان ژل صورت می‌گیرد. هر افزایش در حجم آب و در تمرکز یونهای موجـود در آب منفـذی مقاومت ویژه خمیر سیمان را کاهش می‌دهد و در مواقع مقاومت ویژه به شدت با افزایش در نسبت آب به سـیمان کاهش می‌یابد.

۸- نوع سیمان و مصالح: نوع سیمان در رسانایی الکتریکی بتن تأثیر گـذار اسـت سـیمان‌هـای پـر آلـومین مقاومت الکتریکی بالاتری در بتن نسبت به سیمانهای پرتلند معمولی ایجاد می‌کنند.
هدایت الکتریکی سنگدانه‌ها نیز در رسانایی بتن تأثیر گذار است هر چه رسـانایی سـنگدانه‌هـا بیـشتر باشـد، بـتن مقاومت الکتریکی کمتری خواهد داشت.

۹- افزودنیها: عموماً افزودنیهای شیمیایی مقاومت ویژه بتن را کاهش نمی‌دهند ولیکن می‌تـوان مـواد مـضاف ویژه‌ای را به منظور تغییر مقاومت ویژه به کار برد. تأثیر افزودنیهای پوزولانی مانند خاکستر بادی و دوده سیلـسی در افزایش مقاومـت الکتریکـی چـشمگیر مـی‌باشـد، مقاومـت الکتریکـی بـتن‌هـای معمـولی حـاوی ۱۰ درصـد میکروسیلس جایگزین شده بیش از ۳ برابر بتن معمولی بدون میکروسیلیس بدست آمده است.

۱۰- دمای نمونه آزمایش: افزایش دمای بتن در هنگام آزمایش، مقاومت الکتریکی را افزایش می‌دهد.

۱۱- تأثیر ولتاژ و فرکانس جریان: مقاومت ویژه بتن با افزایش ولتاژ و فرکانس زیاد می‌شود

در کنار پارامترهای فوق به نظر می‌رسد دمای اولیه بتن نیز از طریق تاثیراتی که بر سـاختار خمیـر هیدراتـه شـده سیمان می‌گذارد بر مقاومت الکتریکی بتن تاثیر گذار باشد.

- مقاومت ویژه الکتریکی

آنچه که در بحث مقاومت الکتریکی بتن حائز اهمیت است مقاومت ویژه الکتریکی بتن می‌باشد زیرا مقاومت ویژه الکتریکی وابسته به جنس ماده می‌باشد و به شکل و ابعاد آن بستگی ندارد. مقاومت ویژه الکتریکـی از رابطـه (۱) قابل محاسبه است.

$$R = P\frac{L}{A} \qquad (۱)$$

R: مقاومت الکتریکی اهمی(Ω)

P: مقاومت ویژه الکتریکی $(\Omega.m)$

L: طول نمونه(m)

A: سطح مقطع نمونه (m^2)

۳- فرضیات اولیه آزمایش

در این پژوهش از سیمان پرتلند نوع ۲ استفاده شد. همچنین از ماسه شکسته با حد اکثر انـدازه 4/75 و همچنـین شن نیمه شکسته با حد اکثر اندازه ۱۹ میلیمتر استفاده گردید. آب مصرفی نیز آب شهر تهران بود.

طرح اختلاط مطابق با طرح اختلاط ملی ایران انجام گرفت. نسبت آب به سیمان برابر 0/47 و عیار سـیمان برابـر ۴۰۰ کیلو گرم فرض شد.

در ادامه سعی شد تا دماهای ۱۰، ۲۰، ۳۰ و ۴۰ درجه سانتیگراد در مخلوط بتن تازه ایجاد گردد. دمای هوا در حین ساخت بتن در حدود ۳۲ درجه سانتیگراد بود لذا برای ایجاد دماهای مورد نظر از فرمول پیشنهادی در ACI 306 R استفاده گردید. رابطه (۲)

$$T = \frac{0/22(c\,T_c + G_d\,T_G + S_d T_s) + T_w\,W_m + T_G\,W_G + T_s\,W_s}{0/22(c + G_d + S_d) + W_t} \qquad (۲)$$

که در آن c , G_d , S_d به ترتیب وزن سیمان، شن در حالت خشک و ماسه در حالت خشک و W_t ، W_m ، W_G ، W_S ، به ترتیب میزان آب کل، آب مصرفی، رطوبت شن، رطوبت ماسه و T_c ، T_G ، T_s بـه ترتیـب دماهای سیمان، شن و ماسه است.

و چنانچه در شرایط خاص برای خنک کـردن بـتن بـه جـای بخـشی از آب از یـخ اسـتفاده شـود آنگـاه عبـارت $W_m\,T_w$ به عبارت $(W_m - W_i)T_w + W_i(۰/۵T_i - ۸۰)$ تبدیل می‌شود. کـه در آن W_m و W_i به ترتیب آب مصرفی و جرم یخ و T_W و T_i به ترتیب دمای آب مصرفی و دمای یخ می‌باشد.

از آنجا که ظرفیت گرمایی ویژه آب ۵ برابر ظرفیت گرمایی ویژه مصالح سنگی و سـیمان اسـت لـذا بهینـه تـرین روش برای ایجاد دماهای مختلف در بتن تازه تغیر دمای آب می‌باشد. بـرای ایـن منظـور بـا جایگـذاری دماهـای مطلوب در رابطه فوق حجم آب و یخ لازم بدست آمد.(برای جبران اتلاف‌هـای حرارتـی ناشـی از اخـتلاف درجـه حرارت مخلوط بتن و هوای محیط در حین ساخت، دمای تعادل در این رابطه باید اندکی کمتر از دمای مطلوب ما لحاظ گردد تا نهایتا دمای مطلوب در بتن احراز گردد.) نتایج در جدول ۱ دیده می‌شود.

جدول ۱: مقادیر آب و یخ استفاده شده و دمای آنها در هر مخلوط

کد طرح اختلاط	دمای اسمی در فرمول [°C]	آب مصرفی [lit]	یخ [kg]	دمای آب [°C]	دمای یخ [°C]	دمای شن و ماسه [°C]	دمای سیمان [°C]	دمای بتن [°C]
T=10	T=6	109	130	5	-10	30	30	T=10
T=20	T=18	۲۰۳	۳۶	5	-10	30	30	T=20
T=30	T=29	239	0	28	-	30	30	T=30
T=40	T=40	239	0	40	-	50	30	T=40

۴- آزمایشات انجام شده

در ابتدا آزمایش تعیین روانی بر بتن تازه مطابق استاندارد ASTMC143 انجام گردید.

در ادامه برای تعیین مقاومت فشاری مخلوط‌های ساخته‌شده، از آزمونه‌های مکعبی ۱۰۰ و ۱۵۰ میلی‌متری نمونه‌های عمل آمده آزمایشگاهی و همچنین مغزه‌های به قطر7/5 میلی متری تهیه شده از نمونه‌های عمل آمده در شرایط کارگاهی براساس استاندارد BS1881 و ASTM C617-94 استفاده گردید.
آزمایش مقاومت کششی مطابق با استاندارد ASTM-C469 به صورت دو نیم کردن و ترکاندن نمونه‌های استوانه ای 30×15 سانتیمتر و مغزه‌های 7/5 میلی متری کارگاهی، در اثر اعمال بار خطی در امتداد طول آزمونه انجام میشود(آزمایش کشش برزیلی). سن آزمایش در مورد هر دو سری از نمونه‌ها ۲۸ روز است

۴-۱- آزمایش تعیین روانی بتن تازه

پس از ساخت هر مخلوط آزمون اسلامپ انجام گردید و مشاهده گشت با افزایش دمای اولیه بتن تازه به دلیل افزایش سرعت هیدراسیون و گیرش سریعتر بتن افت اسلامپ افزایش پیدا می‌کند و بتن سفت تر می‌گردد. به طور تقریبی به ازای افزایش هر ۱۰ درجه سانتیگراد در دمای اولیه بتن، اسلامپ حدود ۲ سانتیمتر کاهش می‌یابد، این پدیده می‌تواند باعث افزایش درصد هوای بتن نیز گردد.

جدول ۲: نتایج آزمون اسلامپ

نام طرح	اسلامپ
T=10	۱۰۰
T=20	۸۰
T=30	۶۰
T=40	۴۵

۴-۲- آزمایش مقاومت فشاری

نتایج مقاومت‌های ۷، ۱۴، ۲۸، ۴۲ و ۹۱ روزه آزمونه‌های مکعبی ۱۵ و۱۰ سانتیمتری آزمایشگاهی و مقاومت‌های ۲۸ روزه نمونه‌های استوانه ای 7/5 سانتیمتری کارگاهی، برای ۴ مخلوط در جدول (۳) و نمودار (۲) و (۳) مشاهده می‌شود. (نتایج آزمونه‌های ۱۰ سانتیمتری با اعمال ضریب 0/97 به ۱۵ تبدیل شدند)

جدول ۳: نتایج مقاومت فشاری(بر حسب مگاپاسکال)

سن آزمونه	شرایط عمل آوری	نام طرح و میزان مقاومت فشاری(mpa)			
		T=10	T=20	T=30	T=40
۷ روزه	آزمایشگاهی	16/6	19/4	21/7	24/5
۱۴روزه	آزمایشگاهی	27/1	29/7	29/3	27/9
۲۸روزه	آزمایشگاهی	33/1	34/6	33/8	31/8
۲۸روزه	کارگاهی	16/9	13/4	13/2	10/1
۴۲روزه	آزمایشگاهی	35/2	36/7	35/7	32/1
۹۱روزه	آزمایشگاهی	40/3	38/7	37/3	33/9

در ارتباط با مقاومت فشاری،در نمونه‌های عمل آوری شده در آزمایشگاه (در داخل حوضچه آب با دمای ۲۲ درج

سانیگراد با افزایش دمای اولیه بتن سرعت هیدراسیون و کسب مقاومت‌های اولیه افزایش می‌یابد ولی به دلیل سرعت بالای تشکیل محصولات هیدراسیون، فرصت کافی برای پخش شدن یکنواخت این محصولات نبوده و تجمع آنها حول ذرات سیمان مانع از هیدراسیون کامل ذرات سیمان گشته و ایجاد تخلخل بیشتر در بتن می‌کند، لذا در مقایسه با دماهای اولیه پایین تر، بتن مقاومت‌های پایین تری در سنین بالا تر خوا هد داشت.

همانگونه که در نمودار (۲) مشاهده میگردد تا سن ۷ روز مقاومت فشاری، T=40 در بین سه طرح دیگر بیشترین مقدار را داراست. در فاصله سنین ۱۴-۷ روز این روند تغییر کرده و بتن T=20 به بیشترین مقاومت در بین سه طرح دیگر دست یافته است. با توجه به تفاوت اندک مقاومت بتن T=20 و T=30 در سن ۱۴ روز می‌توان حدس زد که در همین فاصله زمانی بتن T=30 برای مدتی بیشترین مقاومت را در بین سه طرح دیگر داشته است که پس از مدتی مقاومت T=20 از آن بیشی گرفته است. تا این سن بتن T=10 به دلیل روند بسیار کند هیدراسیون، کمترین مقاومت را در بین سه طرح دیگر داراست.

در سن ۲۸ روز که متداول ترین سن آزما یش مقاومت فشاری است و اکثرا به عنوان مبنایی برای سنجش مقاومت فشاری در نظر گرفته می‌شود، بتن T=20 همچنان بیشترین مقاومت را داراست و پس از آن به ترتیب بتنهای T=30، T=10 و T=40 قرار گرفته اند. از این سن به بعد بتن T=40 کسب مقاومتی چندانی نسبت به سه طرح دیگر نمی‌کند.

بتن T=10 همچنان در حال کسب مقاومت است آنچنانکه در سن ۴۲ روز بتنهای T=10 و T=30 مقادیر مقاومت بسیار نزدیک به هم دارند و نهایتا در سن ۹۱ روز بتن T=10 با 40/3 مگاپاسکال بیشترین مقدار مقاومت و بتن T=40 با مقدار 33/9 مگا پاسکال کمترین مقدار را در بین سه طرح دیگر دارا می‌باشد. همان طور که مشاهده می‌شود در این آزمایش، با سنگدانه، آب و سیمان مصرف شده و شرایط عمل آوری بتن، از دمای ۱۰ تا ۳۰ درجه سانتیگراد به ازای افزایش هر ۱۰ درجه سانتیگراد در بتن تازه، حدود 1/5 مگاپاسکال کاهش مقاومت و از ۳۰ تا ۴۰ درجه سانتیگراد حدود 3/5 مگاپاسکال کاهش مقاومت در سن ۹۱ روز مشاهده می‌گردد و بتن T=40 حدود ۸۰ درصد مقاومت بتن T=10 را در سن ۹۱ روز داراست.

در مورد نمونه‌های کارگاهی تنها توانستیم در سن ۲۸ روز آزمون مقاومت فشاری را انجام دهیم. در این سن بیشترین مقاومت فشاری را جدول T=10 بدست آورد و پس از آن به ترتیب نمونه‌های T=20 و T=30 مقادیر نزدیک به هم داشتند و نمونه T=40 کمترین مقدار مقاومت را دارا بود. علت این اختلاف در میزان مقاومت بین دماهای مختلف در این سن نسبت به نمونه‌های آزمایشگاهی را می‌توان در شرایط عمل آوری این نمونه‌ها جستجو کرد. باید توجه داشت که دمای هوا به هنگام عمل آوری این نمونه‌ها به طور متوسط ۳۳ درجه سانتیگراد در شبانه روز می‌بود. این دمای بالا در زمان عمل آوری باعث افزایش آهنگ کسب مقاومت این نمونه‌ها نسبت به نمونه‌های آزمایشگاهی گشته چنانکه تا سن ۲۸ روز توانسته اند به بخش بیشتری از مقاومت خود دست پیدا کنند. ولی به دلیل رطوبت رسانی کمتر در طول مدت عمل آوری، این نمونه‌ها به مقاومت‌های کمتری نسبت به نمونه‌های عمل آمده در آزمایشگاه دست یافته اند. نمودار(۳)

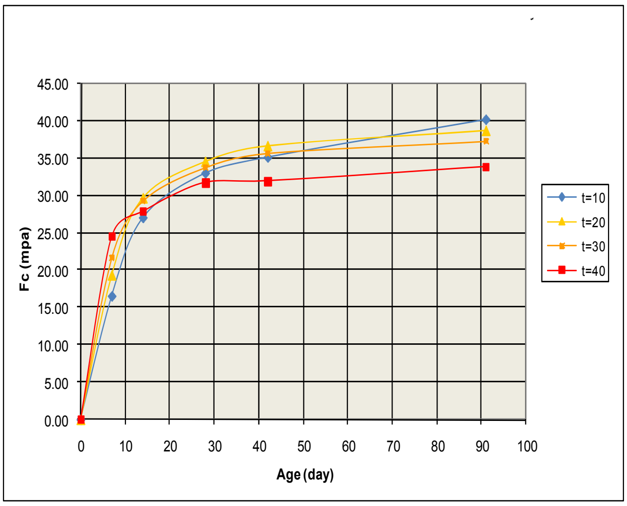

نمودار ۱- تغییرات مقاومت فشاری با افزایش سن نمونه‌ها در دماهای مختلف

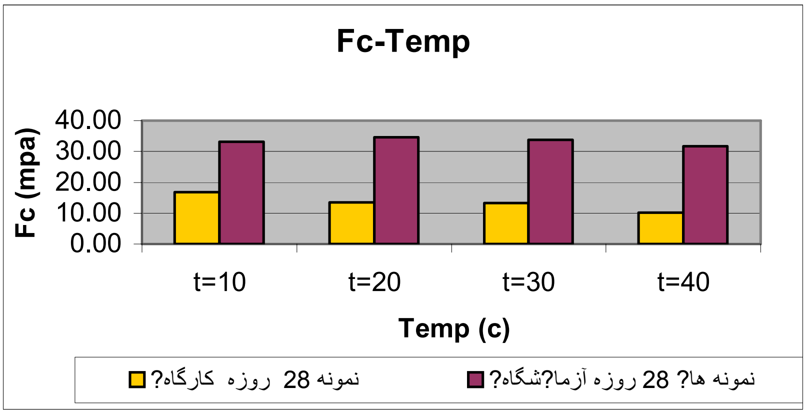

نمودار ۲- تغییرات مقاومت فشاری نمونه‌های آزمایشگاهی و کارگاهی نسبت به دمای اولیه بتن در سن ۲۸ روز

بنا بر این این طور به نظر می‌آید که هر دو عامل دمای اولیه بتن تـازه و دمـا در حـین عمـل آوری پارامترهـای تاثیرگذار در آهنگ و میزان کسب مقاومت‌های نهایی بتن می‌باشند. لذا در سنجش وارزیابی مقاومت بتن در سنین مختلف، این دو عامل و تاثیرات آنها نیز بهتر است مورد توجه قرار گیرد.

۴-۳- نتایج آزمایش مقاومت کششی (کشش برزیلی)

نتـایج مقاومـت کشـشی ۲۸ روزه آزمونـه‌هـای اسـتوانه‌ای ۱۵×30 آزمایـشگاهی و همچـنین مغـزه‌هـای 7/5 سانتیمتری جداول کارگاهی در جدول(۴)و نمودار(۴) مشاهده می‌شود.

جدول ۴: نتایج آزمایش مقاومت کششی برزیلی

سن آزمونه	شرایط عمل آوری	نام طرح و میزان مقاومت کششی(mpa) T=10	T=20	T=30	T=40
۲۸ روزه	آزمایشگاهی	2/64	2/86	2/46	2/40
۲۸روزه	کارگاهی	1/55	2/23	1/47	0/92

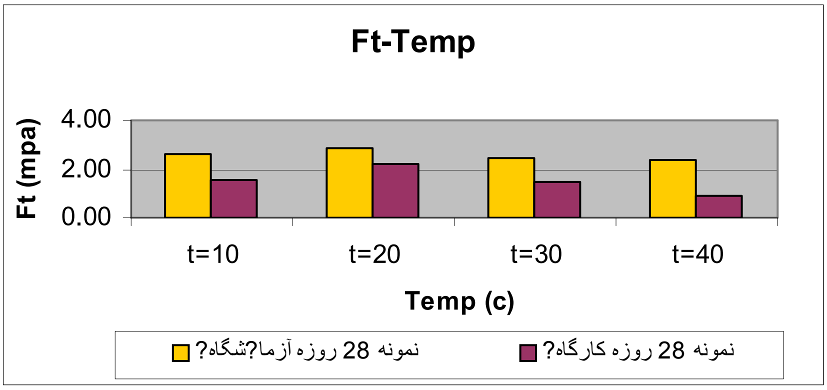

نمودار۳- تغییرات مقاومت کششی نمونه‌های آزمایشگاهی و جداول در دماهای مختلف

مقاومت کششی و فشاری بتن در ارتباط مستقیم با یکدیگرند لذا به همان دلا یلی که در مورد مقاومت فشاری بتن ذکر گردید، در سن ۲۸ روز مقاومت کششی نمونه‌های T=20 بیشترین مقدار و نمونه‌های T=40 کمترین مقدار را دارا بود.

در مورد مقاومت کششی چندین نکته قابل تامل است. اول آنکه آهنگ افزایش مقاومت کششی با افزایش عمر بتن نسبت به مقاومت فشاری آن کندتر است بنابراین نسبت مقاومت کششی به فشاری با افزایش عمر بتن کاهش می‌یابد. همچنین مقاومت کششی در برابر عمل آوری بسیار حساستر است (اثرات جمع شدگی غیر یکنواخت بسیار حادتر روی کشش نسبت به فشار اثر می‌گذارد)

بنابر این می‌توان گفت که علت کاهش مقاومت T=10 نسبت به T=20 در سن ۲۸ روز در هر دو سری نمونه‌ها (به خصوص نمونه‌های کارگاهی) رشد کند تر مقاومت کششی نمونه‌های T=10 نسبت به T=20 در مقایسه با مقاومت فشاری آنها دانست.(در حالیکه مقاومت فشاری ۲۸ روزه نمونه‌های کارگاهی T=10 بیش از T=20 بود.)

تراکم مناسب در بتن تازه هنگام قرار گیری در قالب در بهبود مقاومت کششی بتن بسیار موثر است. از آنجا که نمونه‌های آزمایشگاهی ضمن داشتن شرایط عمل آوری مناسب تر، از تراکم بهتری نیز برخوردار بوده اند، لذا مقاومت کششی بزرگتری نسبت به نمونه‌های کارگاهی دارا می‌باشند.

همچنین در منابع ذکر شده است که به دلیل حساسیت مقاومت کششی در برابر عمل آوری نسبت تنش کششی به فشاری در بتنی که در هوا عمل آمده نسبت به بتنی که در شرایط استاندارد عمل آوری شده کمتر است. ولی در این آزمایش چنین نتیجه ای حاصل نگشت و نسبت مقاومت کششی به فشاری در نمونه‌های عمل آمده در

آزمایشگاه کمتر از این نسبت در نمونه‌های عمل آمده در کارگاه بود. (آزمایشگاهی Ft/Fc > Ft/Fc کارگاهی) می‌توان این احتمال را داد که افزایش دمای اولیه بتن تاثیرات بیشتری در کاهش مقاومت فشاری نمونه‌های کارگاهی نسبت به مقاومت کششی آنها دارد که این امر باعث افزایش نسبت مقاومت کششی به مقاومت فشاری این نمونه‌ها در مقایسه با این نسبت در نمونه‌های آزمایشگاهی می‌گردد.

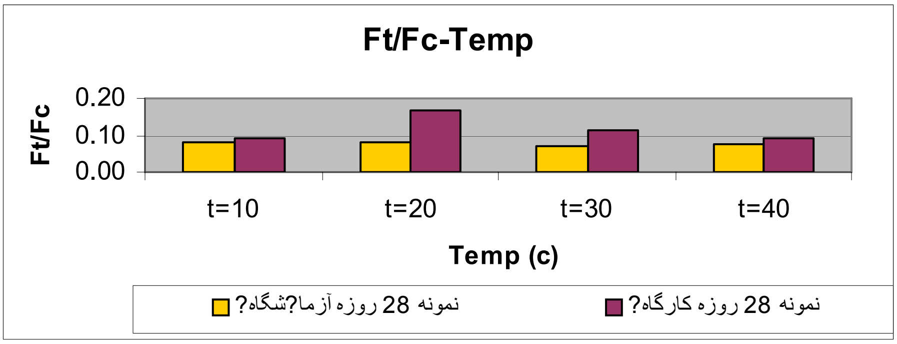

نمودار ۴- نسبت مقاومت کششی به فشاری در نمونه‌های آزمایشگاهی و کارگاهی در دماهای مختلف.

۳-۵-۶- آزمایش تعیین مقاومت ویژه الکتریکی

در این آزمایش از آزمونه‌های مکعبی ۱۰۰و۱۵۰ میلی‌متری با شرایط عمل‌آوری آزمایشگاهی و مغزه‌های ۷۵ میلی متری جداول کارگاهی استفاده شد. تعداد آزمونه‌های ساخته شده در این آزمایش برای هر مخلوط با توجه به ماهیت غیرمخرب بودن آن ۳ عدد بود که در سنین۷، ۱۴، ۲۸، ۴۲ و ۹۱ روز، آزمونه‌ها از آب خارج و پس از انجام آزمایش، تحت آزمایش مقاومت فشاری قرار گرفتند.

برای تعیین مقاومت الکتریکی آزمونه‌های ساخته‌شده، در استانداردهای مختلف دستورالعمل خاصی وجود ندارد. از این رو برای انجام این آزمایش از وسایل و روش خاصی استفاده شد.

برای انجام این آزمایش از یک دستگاه تعیین کننده مقاومت الکتریکی با فرکانس ۱ KHz و ظرفیت نهایی MΩ ۱، به همراه دو صفحه مسی استفاده شد.

این آزمایش در سنین ۲۸، ۴۲ و ۹۱ روز بر روی نمونه‌های ۱۰ و ۱۵ سانتیمتری آزمایشگاهی و در مورد جداول به دلیل محدودیت‌های موجود فقط در سن ۲۸ روز بر روی مغزه‌های 7/5 سانتیمتری انجام گرفت که نتایج این آزمایش در جدول (۴) و نمودارهای (۶و۷) نشان داده شده است.

جدول ۴: نتایج آزمایش مقاومت ویژه الکتریکی

سن آزمونه	شرایط عمل آوری	نام طرح و مقاومت ویژه الکتریکی (W-cm) T=10	T=20	T=30	T=40
۲۸روزه	آزمایشگاهی	۳۰۱۴	۳۰۶۵	۳۰۴۱	۲۸۷۴
۲۸روزه	کارگاهی	۲۶۵۶	۲۷۷۳	۲۷۴۹	۲۳۸۰
۴۲روزه	آزمایشگاهی	۳۱۱۱	۳۳۳۸	۳۱۸۱	۳۰۳۹
۹۱روزه	آزمایشگاهی	۵۵۷۵	۵۳۶۹	۵۳۱۹	۴۵۶۴

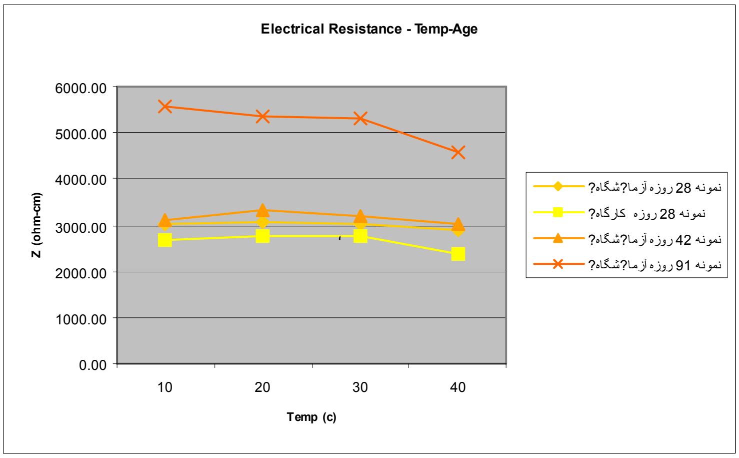

نمودار ۵- تغییرات مقاومت ویژه الکتریکی نسبت به دمای اولیه بتن و زمان.

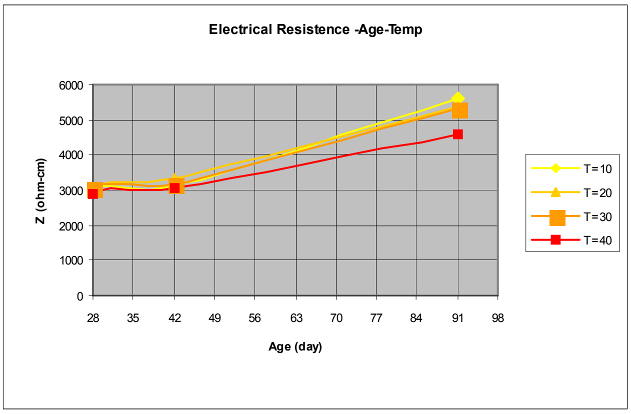

نمودار ۶- تغییرات مقاومت ویژه الکتریکی نسبت به زمان و دمای اولیه بتن.

همانگونه که در جدول (۴) و نمودارهای (۶ و۷) مشاهده می‌گردد در نمونه‌های آزمایشگاهی در سن ۲۸ روز نمونه‌های T=20 دارای بیشترین مقدار و پس از آن به ترتیب نمونه‌های T=30 و T=10 و در نهایت نمونه T=40 دارای کمترین مقدار مقاومت ویژه الکتریکی است. ولی تفاوت بین مقاومت نمونه‌های T=20، T=30 و T=10 در این سن به نسبت چندان زیاد نمی‌باشد.

در مورد نمونه جداول این اختلافات بیشتر بود چنانچه نمونه‌های T=20 و T=30 دارای بیشترین مقدار مقاومت و پس از آن نمونه‌های T=10 به دلیل درجه هیدراسیون ضعیف تر نسبت به دو نمونه قبل قرار داشت و کمترین مقاومت در نمونه T=40 به دلیل بافت ضعیف تر اجزای بتن و نفوذ پذیری زیاد آن قرار داشت.

علت اختلاف بیشتر، بین نتایج نمونه‌های جداول را می‌توان ناشی از تفاوت در شرایط عمل آوری آنها نسبت به نمونه‌های کارگاهی و هیدراسیون سریعتر این نمونه‌ها نسبت به نمونه‌های آزمایشگاهی دانست.

این آزمایش در سن ۴۲ روز بر روی نمونه‌های آزمایشگاهی انجام گردید و باز نمونه T=20 دارای بیشترین مقدار

مقاومت و پس از آن نمونه‌های T=30 و T=10 با مقادیر نزدیک بـه هـم و در نهایـت نمونـه T=40 کمتـرین میزان مقاومت را دارا بود.

در سن ۹۱ روز روند نتایج تغییر کرد و نمونه T=10 دارای بیـشترین مقـدار مقاومـت و پـس از آن نمونـه‌هـای T=20، T=30 وT=40 به ترتیب قرار داشتند. در این سن اختلاف بین مقاومت‌های نمونه‌ها به اندازه کافی بزگ بود به طوریکه اختلاف بین مقاومت نمونه T=10 و T=40 در حدود ۱۰۰۰ اهم–سانتیمتر بود.

به نظر می‌رسد که سرعت کند هیدراسیون و تکامل ساختار نمونه T=10 باعث کسب مقاومـت الکتریکـی واقعـی آن در سن ۹۱ روز گردید.

آنچه به نظر می‌رسد آنست که این آزمایش در مورد بتن‌هایی که در دماهای اولیه متفاوت ساخته شـده انـد، بهتـر است در سنین بالای ۹۰ روز انجام گیرد.

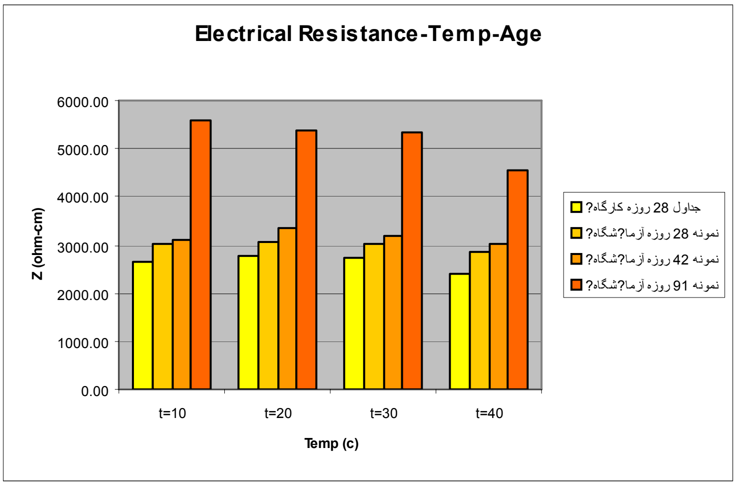

نمودار۷- تغییرات مقاومت ویژه الکتریکی نسبت به تغییرات دمای اولیه بتن در سنین مختلف در نمونه‌های آزمایشگاهی و جداول کارگاهی

۵- نتیجه‌گیری و پیشنهاد

۱- به نظر می‌رسد که روابط ارائه شده مربوط به دمای تعادل بتن، از دقت کافی بر خوردار نمی‌باشند و در عمـل دمای محیط اطراف ساخت بتن و شرایط محیطی ساخت آن، در دمای تعادل آن بسیار تاثیر گذار است. لذا بهتر است عامل دمای محیط در حین ساخت بتن نیز، در این روابط لحاظ شود.

۲- دمای اولیه بتن پارامتر تاثیر گذاری بر روی ویژگیهای بتن تـازه مـی‌باشـد.عمـده ایـن تـاثیرات در تغییـرات اسلامپ بتن مشاهده گشت آنچنانکه به ازای افزیش هر ۱۰ درجه سانتیگراد، اسـلامپ بـه میـزان تقریبـا ۲ سانتیمتر کاهش می‌یابد.

۳- با افزایش دما، مقاومت فشاری در سنین اولیه افزایش می‌یابد ولی با افزایش عمر بتن این روند تغییر می‌یـا بد و بیشترین مقاومت در سنین بالا (۹۱ روز) در پایین ترین دما که در این آزمایش بتن T=10 بود مشاهده گردید. در حالیکه تا سن ۴۲ روز بتن T=10 هنوز نسبت به دو بتن T=20 و T=30 مقاومت کمتری داشـت و این نشاندهنده روند کند تر هیدراسیون این بتن و کسب مقاومت‌های بیشتر در سنین بالا تر آن مـی‌باشـد.

بتن T=40 در سن ۹۱ روز کمترین مقاومت را در بین ۴ طرح دارا بود.

۴- دمای دوران عمل آوری نیز بر سرعت رشد مقاومت تاثیر گذار است آنچنانکه در نمونه‌های کارگاهی در سن ۲۸ روز بتن T=10 بیشترین مقاومت را در بین نمونه‌های دیگر کارگاهی دارا بود در حالیکه در نمونه‌های آزمایشگاهی در این سن نمونه T=20 بیشترین مقدار را دارا بود.

۵- آهنگ کسب مقاومت کششی بتن نیز با تغییرات دما متغیر است. این روند تغییرات در سن ۲۸ روز همانند تغییرات مقاومت فشاری نمونه‌هاست.

۶- در آزمایش مقاومت الکتریکی در سن ۲۸ روز بیشترین مقاومت را نمونه T=20 دارا بود ولی اختلاف بین مقاومت‌ها در این سن نسبت به سنین بالا تر اندک است.در مورد جداول نیز همین روند با مقادیر کمتر مقاومت به دلیل شرایط ضعیف تر عمل آوری، مشاهده گشت.

۷- با ادامه انجام آزمایش مقاومت الکتریکی در سن ۹۱ روز اختلافات بین نتایج به میزان قابل توجهی رسید آنچنانکه نمونه T=10 بیشترین مقاومت را دارا بود و نمونه T=40 با اختلاف ۱۰۰۰اهم-سانتیمتر (۱۰ اهم-متر)، نسبت به T=10 کمترین مقدار مقاومت را احراز نمود. بنا بر این در آزمایش مقاومت الکتریکی نمونه‌های ساخته شده در دماهای اولیه مختلف بهتر است که این آزمایش در سنین به اندازه کافی بالا انجام گیرد. که در این آزمایش این سن ۹۱ روز می‌بود.

مراجع

۱- «آیین‌نامه بتن ایران (تجدید نظر اول)»، دفتر تحقیقات و معیارهای فنی، سازمان برنامه و بودجه، شماره نشریه: ۱۲۰، ص. ۴۳۳.

۲- «آیین‌نامه ملی پایایی بتن در محیط خلیج فارس و دریای عمان (پیشنهادی)»، شماره نشریه: ض — ۴۲۸ ، مرکز تحقیقات ساختمان و مسکن

۳- کومار مهتا، پ.، مونته‌ئیرو، د، ج، م. (۱۳۸۵) «ریزساختار، خواص و اجزای بتن (تکنولوژی بتن پیشرفته)»، ترجمه: رمضانیانپور، ع، ا.، قدوسی، پ.، و گنجیان، ا.، دانشگاه صنعتی امیرکبیر،

۴- نویل، آ. (۱۳۷۸) «خواص بتن»، ترجمه : فامیلی، ه.، ابوریحان بیرونی، ص. ۱۰۰۹.

۵- قدوسی، پرویز، «ارزیابی آسیب دیدگی بتن سبک در مقابل خوردگی آرماتور»، گزارش نهایی طرح پژوهشی دانشگاه علم و صنعت ایران، ۱۳۷۹.

۶- قدوسی، پ، پرهیزگار، ط، رئیس قاسمی، ا.م.، «ارزیابی دوام بتن‌های حفاظت شده با پوشش‌های سطحی بر اساس آزمایش شدت خوردگی به روش پتانسیو استاتیک»، اولین کنفرانس انجمن مهندسان راه و ساختمان ایران، تهران، ۱۳۷۸.

7- ACI 305R-91, Hot Weather Concreting, Reported by ACI committee

8- ACI 306R-88, Cold Weather Concreting , Reported by ACI committee-306.Reapproved1997.

9- ASTM C 143/C 143M – 98. (1998) “Standard Test Method for slump of Hydraulic Cement Concrete”.

10- ASTM C469-92-Standard Test Method for Static Modulus of Elasticity and Poisson’s Ratio of Concrete in Compression.

11- ASTM C78-92 Standard Test Method for Flexural Strength of Concrete (Using

Simple Beam with Third-Point Loading.
12- B.P.Hughrd, A.K.O.Soleit and R.W.Brierley, New technique for determining the electrical resistance of concrete, Mag.concr.Res, 37, No.133, pp.243-8(1985)
13- E.Hammond and T.D.Robson, Comparison of electrical properties of various cement and concretes , The engineer, 199, pp.78-80 (21 Jan 1955); pp.114-15(28 Jan. 1955).
14- F.M.Lea, The Chemistry of Cement and concrete (Arnold, London,1970).
15- G.J.Verbeck and R.A Helmuth, structures and physical properties of concrete paste , proc. 5th int. symp. On the chemistry of cement, Tokyo, Vol.3, pp.1-32(1968).
16- Ghodousi,P., "Effects of corrosion on the Bond and strength of Reinforced concrete Beams", ph.d Thesis, Leeds University, 1992.
17- h.w. ngtonWhitti , J. Mc Carter and M. C. Forde,"The Comduction of Electrisity through Concrete", Magazine of concrete Research ,Vol.33,No.114, Maech 1981.
18- h.w.Whittington , J. Mc Carter and M. C. Forde,"The Comduction of Electricity through Concrete", Magazine of concrete Research ,Vol.33,No.114 ,Maech 1981.
19- W.F.Chen , Plasticity in reinforced Concrete , McGraw-hill Book co., pp.20-21.
20- W.Anton k.Schindler , M.S.E , The Importance of Concrete Temperature Control During Concrete Pavement Construction in Hot Weather Conditions, Department of Civil Engineering, University of Texas at Austin
21- U.S.Army Corps of engineers , Test method for coefficient of linear thermal expansion of concrete, CRD-C 39-81 Hand book of concrete and cement, 2 pp.
22- K.W.Nasser and A.M.Neville, J.ACI, Proc., VOl.64, No.2, pp.97- 103, 1967.

CD03
Construction Technology and Implementation Methods

CD03-001

EFFECT OF CASTING TEMPERATURE ON THE RISK OF CRACKING IN THE MASS CONCRETE COLUMNS CONTAIN SILICA FUME

M. Nili[1], S. Nazari [2], A.M. Salehi[3]
[1]Associate Professor, Bu Ali Sina University, Hamedan, I.R.Iran
[2]Msc Student, [3]Msc, Bu Ali Sina University, Hamedan, I.R.Iran

ABSTRACT
In this paper the effect of different casting temperatures on cracking potential of mass high strength columns were studied. Four mix proportions with 0.3 water-cementing ratio were made and two different casting temperatures, 26ºC and 40ºC were applied to simulate moderate and hot climate conditions. Cement was replaced by silica fume at 0%, %5, %8 and %11. Temperature rising of the mixtures, due to hydration, after casting was monitored till 7 days. Furthermore, compressive strength of the specimens was determined at the ages of 1 to 91 days. Thermal analysis of 4 large columns, 600×600×200 to 1800×1800×2000 mm, was carried out by finite element method [3-7]. In this regard, two demolding time, 24 and 48 hours were selected to clarify the effect of ambient temperature on risk of cracking. The results declare that tensile stress of the 600 mm columns with 24 hours demolding time, irrespective of casting temperature, was higher than tensile strength and will be cracked. However, 48 hours demolding time induced lower tensile stress and diminished risk of cracking. Silica fume has no considerable effect on risk of cracking.

Keywords: mass concrete, casting temperature, risk of cracking, silica fume, demolding time

1. INTRODUCTION
Heat evolution during hydration of cementing materials in high strength mass concrete lead to thermal stress, which in-turn induce thermal cracking in the body of structures[1-2].Therefore, this is a task of researchers to clarify thermal behavior of mass structures made by high strength concrete to develop a convenient design method to control crack potential [5]. Huge foundations, pile, columns of bridges, thick walls and tunnels lining are examples of mass structures which thermal cracks were observed. In large structures, due to low thermal diffusion properties of concrete, heat spreading is very slow [6-8]. In this regard, concrete temperatures in excess of 65ºC have been reported [8]. The high temperature can adversely affect the performance of the concrete. Thermal cracking will occur when thermal stresses exceed the tensile strength of concrete [9]. The geometry of a member, water cement ratio, cement content and type of supplementary cementing materials govern the magnitude of heat lost to the environment and lead to high thermal

gradient [9].
Cement replacement with different pozzolan is known as an important way to diminish temperature rising [8]. Effect of silica fume on hydration heat is influenced from water cementitious material and also superplacticizer content. It was observed that in high water cement ratio, about 0.5, silica fume behave as cement [4]. However, as water cement ratio decrease silica fume have no considerable effect on hydration heat development. On the other hand, at water cement ratio of 0.4 silica fume diminish hydration heat [5]. Slag-blended cements assist in reducing hydration temperatures of concrete with nominal strength of 100, 80, 60 and 40 Mpa [9]. Casting temperature and demolding time are the other important parameters which may affect risk of cracking in silica fume specimens which are studied in the present paper.

2. MATERIALS AND TESTING METHOD

Crushed stone, with 19 mm maximum nominal size, in two ranges of 5-10 and 10-19 with relative density at saturated surface dry of 2.61 were used. Fineness modulus of sand and relative density was 3.4 and 2.6 respectively. Absorption value is 1.9 and 2.1 for fine and coarse aggregate. The cement used was Portland cement Type 2, with a specific gravity of 3.12 and 3750 cm^2/gr surface area. A commercial carboxylic type placticizer, (Gelenium 110M), was used to maintain workability of fresh concrete. Silica fume, made by Semnan Ferro Alley factory, was used at 0%, 5%, 8% and 11% (by weight) as partial replacement of cement. Chemical properties of silica fume are given in Table 1. Mix proportions of the concrete are given in Table 2. Water-cementing material ratio is 0.3.

Table 1. chemical composition of silica fume

Composition	Percent
Al_2O_3	0.5-1.7
SiO_2	85-95
Fe_2O_3	0.4-2
C	0.6-1.5
CaO	2-2.3
MgO	0.1-0.9

For all mixtures a cylindrical (150×300mm) specimen was molded just after casting and was put in a semi adiabatic box for monitoring the hydration temperature rising. Temperature rising was monitored via a Data Logger at 1 minute interval till 6 days. Guardian, 4C-Heat and 4C Temp&Stress soft wares were used for determination of heat properties and thermal analysis. Consequently, risk of cracking in large columns was determined. The columns size was 600, 1000, 1400 and 1800 mm, and height of all columns was 2000 mm. Two climate zones, moderate with air temperature of 20 to 30°C and hot with 30 to 45°C, were chosen. Wind velocity was 5m/sec. Sixteen four analyses were carried out for determination of cracking risk (tensile stress/tensile strength). Furthermore, compressive strength of the cube specimens (100×100×100 mm) accordance to standard condition was also measured at the ages of 1, 2, 3, 7, 14, 28 and 91 days.

Table 2. Mix proportions of the Concrete

Material		SF0D	SF5.D	SF8.D	SF11.D
Cement	(kg/m^3)	540	513	496.8	480.6
Water	(kg/m^3)	164.7	164.7	164.7	164.7
Fine agg.	(kg/m^3)	865	859	856	853
Coarse agg.* (5-10 mm)	..	203	202	202	201
Coarse agg. (10-19mm)	..	626	623	621	619
Micro silica(%)		0	5	8	11
Super plasticizer	..	3.24	7.5	7.5	7.5
Water/Cementitious material		0.3	0.3	0.3	0.3
Slump		150	150	150	150

*Aggregate in saturated surface dry condition

3. TESTING RESULTS

Casting temperatures for moderate (M) and hot climates (H) is given in Table 3. As it is shown, for moderate climate casting temperature is between 26.5 to 28 °C. However, casting temperature for hot climate is between 36 to 41 °C. Casting temperature was adjusted based on trial mixtures and the proposed equation in [1].

Table 3. Casting temperature of the mixtures

	S0 (M)	SF5 (M)	SF8 (M)	SF11 (M)	S0 (H)	SF5 (H)	SF8 (H)	SF11 (H)
Casting Temp.	27.5	27	26.5	28	36	40.5	41	39

After casting, temperature rising was monitored via a semi adiabatic box. Heat development parameters were also calculated from the following equation using 4C-Heat software:

$$Q(M) = Q_{\infty}.\exp(-(\frac{\tau_e}{M}))^{\alpha} \qquad (1)$$

Where,

$Q(M)$ Correspond to heat value at maturity M**,**

Q_{∞} Is final heat value and

τ_e And α are constants.

Using the above parameters and the measured strength properties in predetermined casting and curing and also ambient temperature, temperature regime, peak temperature, stress and risk of cracking were calculated by 4C Temp&Stress

software.

3.1. Moderate Casting Temperature

Peak temperature of different mixtures, due to hydration of cementing materials, is shown in Figure 1. As it is shown, higher peak temperature belonging to the columns with larger size. In the specimens without silica fume peak temperature change between 65 °C to 85°C for 600 and 1800 mm columns size respectively. Silica fume diminished peak temperature not so effectively. Risk of cracking for 24 and 48 hours demolding time are also demonstrated in Figures 2 and 3 when respectively. It is shown that risk of cracking of the specimens was changed in the same manner with peak temperature. Demolding time of 24 hours lead to this fact that only 600 mm column can be conservatively. However, 48 hours demolding time decreased risk of cracking and 1000mm column will also be considered without cracking.

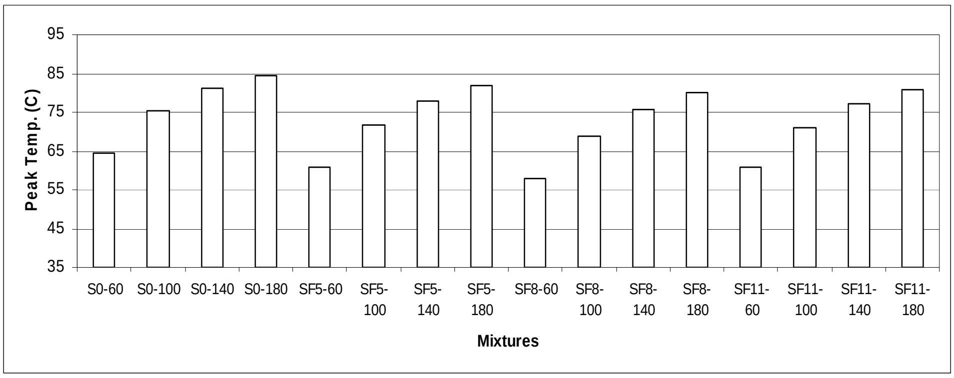

Figure 1. Peak temperature versus concrete mixtures (Moderate)

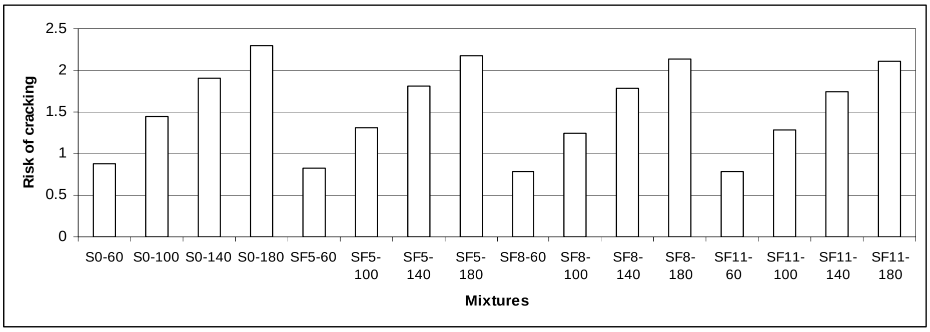

Figure 2. Risk of cracking versus mixtures (Moderate) – remolding time: 24 hours

3.2. High Casting Temperature

Temperature rising, risk of cracking at demolding time of 24 and 48 hours were shown in Figures 4, 5 and 6 when casting temperature was about 40 °C. Due to high casting temperature peak temperature values increased more than moderate one. However, a comparison of risk of cracking in moderate and hot casting temperature declare that , due to lower thermal gradient in hot casting lead to lower risk of cracking. As it is shown, 48 hours demolding was also diminished risk of cracking. Silica fume have no considerable effect on cracking potential, just similar to moderate casting temperature.

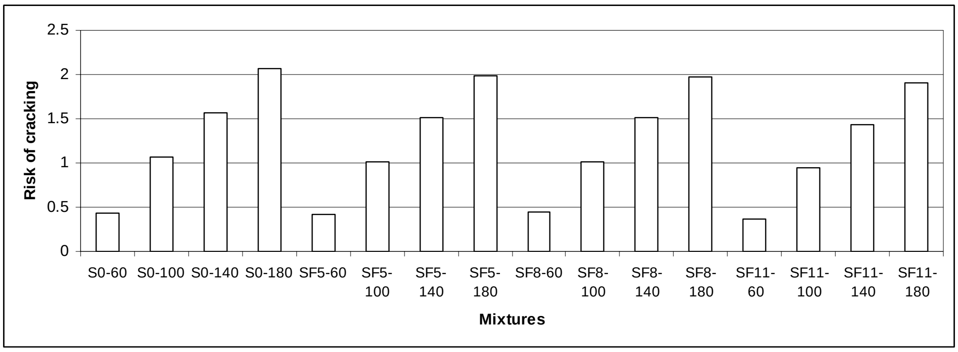

Figure 3. Risk of cracking versus mixtures (Moderate) – remolding time: 48 Hours

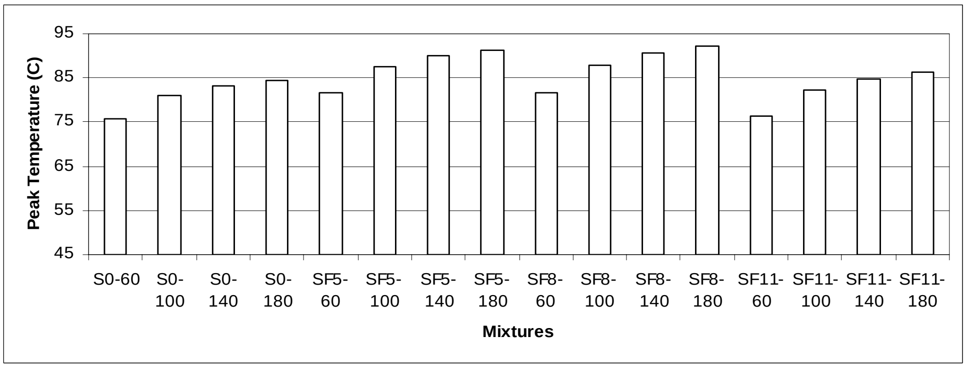

Figure 4. Peak temperature versus concrete mixtures (Hot)

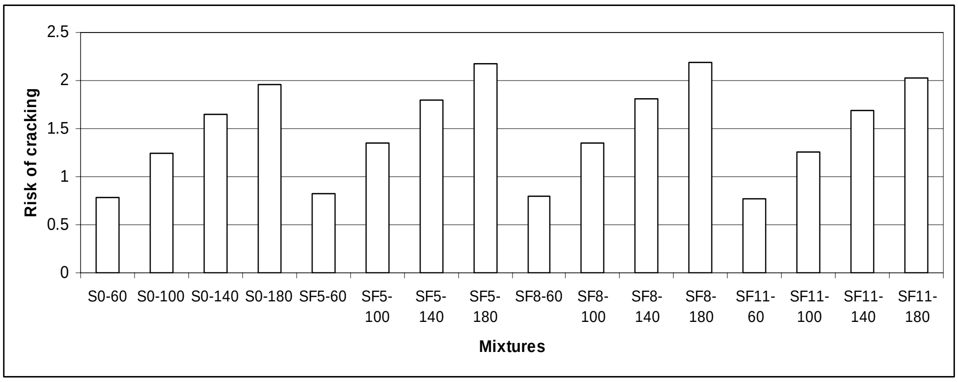

Figure 5. Risk of cracking versus concrete mixtures Remolding time: 24 hours

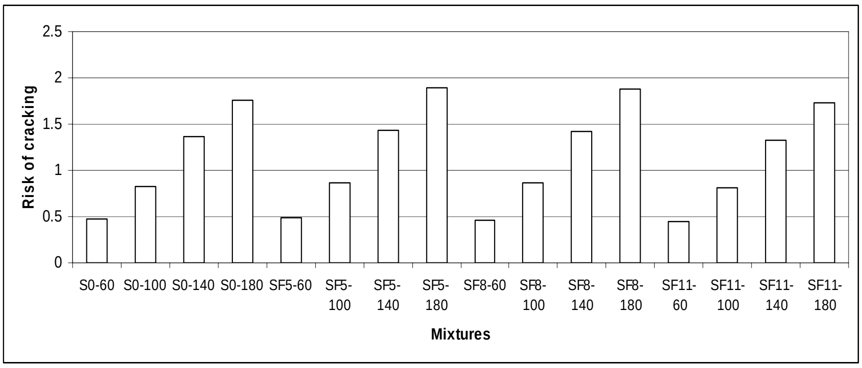

Figure 6. Risk of cracking versus mixtures (Hot) Remolding Time: 48 Hours

4. CONCLUSIONS

From the present study the following conclusions can be drawn:

- Hydration peak temperature is highly affected by size of structures.
- Higher casting temperature led to higher peak temperature.
- Silica fume had no considerable effect on hydration peak temperature of the mixtures.
- High casting temperature (40 °C) led to high peak temperatures however, due to low thermal gradient risk of cracking decreased.
- It was concluded that demolding time of 48 hours in both casting temperatures diminished risk of cracking.

REFERENCES

1. Neville, A.M. “Properties of Concrete”.
2. ACI Committee 207, 1996, “Mass Concrete (ACI 207.1R-96),” American Concrete Institute.
3. DTI Building Technology, March 1998, “4C Temp&Stress Ver. 2.0 for Windows User Manual Building Technology".
4. Kjellsen, K.O., Wallevik, O. H. and Hallgren, M., 1999, “On the compressive strength development of high performance concrete and paste - effect of silica fume,” Materials and Structures, Vol. 32, pp. 63-69.
5. Langan, B. W., Weng, k., Ward, M. A., 2002, “Effect of silica fume and fly ash on heat of hydration of Portland cement,” Cement and Concrete Research, Vol. 32, pp. 1045-1051.
6. Myers, J.J., Shen, J., “The Influence of Surface Area-to-Volume and Accelerated Curing On the Quality Control of High Strength Concrete,” University of Missouri-Rolla.
7. Spang, H., 2000, “4C-Heat Ver. 1.0, User Manual,” Taastrup, 23 March 2000, Building Technology.
8. Cook, D, Buquan, P.C. Aitcin, Mitchell, D. “Thermal stresses in large high-strength Concrete columns” ACI Mater J 89(1) (1992) 61-68 (Jan.-Feb.).
9. Sioulas, B., Sanjayan, J.G, “Hydration Temperatures in Large High-Strength Concrete Columns Incorporating Slag”, “Cement and Concrete Research, Vol. 30, pp. 1791-1799.

CD03-002

EVALUATION OF THE FLUIDITY AND MECHANICAL PROPERTIES OF LIGHT-WEIGHT SELF-COMPACTING CONCRETE CONTAINING EXPANDED POLYSTYRENE (EPS)

M.M. Ranjbar[1], R. Madandoust[1], S.Y. Mousavi[2], S.J. Hashemi[2]
[1]Assistant professor, Department of civil Engineering, Guilan University, Rasht, Iran
[2]MSc. Student, Dept of civil Engg, Faculty of Engg, Guilan University, Rasht, Iran.

ABSTRACT
This paper presents the results of an experimental investigation on the effects of expanded polystyrene polymeric beads on the properties of light-weight self-compacting concrete in fresh and hardened states. Since the aim of this study is to produce structural lightweight self-compacting concrete (with compressive strength above 17 MPa), EPS beads were partially substitute for aggregates by 10, 15, 22.5 and 30 percentages by volume. Fluidity and mechanical properties of self-compacting EPS concrete was compared with ordinary self-compacting concrete with slump flow of about 65cm. The slump flow was kept in allowable range and the effects of EPS were evaluated on the other fluidity parameters such as V-funnel and L-box. The results obtained, showed that with increasing in EPS volume, V-funnel time increased while blocking ratio decreased. At the stage of hardened concrete, compressive strength (at different ages), tensile strength, ultrasonic pulse velocity (UPV) and water absorption were studied.

Keywords: light-weight self-compacting concrete, expanded polystyrene, fluidity, mechanical properties

1. INTRODUCTION
Light-weight concrete with density varying between 1400 to 2100 kg/m^3 in contrast with normal concrete with density about 2400 kg/m^3 has been used for structural purposes for so many years. Light-weight concrete has been center of attention because of its low density leading to the decrease in the area-sectional which results in decreasing the final cost of structure. Light-weight concrete used in this study is made by using porous fine aggregates with a low density. Water absorption is the most significant demerit of many of these light-weight aggregates. From a fresh state point of view, increasing the amount of water in matrix (associated with water absorption of this aggregates) can cause increase in the amount of structure self-weight. Also, this water absorption cause decreasing in slump flow and to solve this problem additional water required. In term of hardened state, as the time passes, the evaporation causes rapid loss of surface bleeding which results rapid drawdown in pore water level. This in turn, makes an increase in pore water pressure, which tends to bring the neighboring solid particles closer which resulted that shrinkage cracking appears [1,2]. Different studies were

shown that because of interesting in properties such as hydrophobia, closed cell nature (prevention from going paste or water in to light-weight structure) and non-absorbent, employing the light-weight expanded polystyrene beads as suitable ultra light-weight aggregates in mortar or concrete for structural and non-structural applications is increasing [3,4]. These properties can overcome disadvantages discussed above.

Self-compacting concrete (SCC) was first produced in Japan in 1980s [5] with problems in consolidation of the normal concrete was to achieve concrete with favorite compaction and high durability. In fact, SCC has a very high fluidity, which removed many of the problems associated with normal concrete such as segregation, bleeding, absorption, permeability and etc. In addition, without any vibration placement in complex or dense reinforced formworks, filled it and covered the space around the bars. Compared to normal concrete, reduction of the harmful effects of sound in urban environments and the industrial process costs are additional advantages [6]. Fillingability, passingability and resistance to segregation are three key properties that SCC must comprise at fresh state [7]. The first two properties are achieved by employing a high-range water reducing. In order to avoid the segregation of coarse aggregates, the plastic viscosity of SCC should be increased. For these purpose, three methods were suggested. The First is using high powder content. Employments of some mineral admixtures such as fly ash, ground blast furnace slag, silica fume, limestone powder or quartzite powder is a possible way for the first method [8,9]. The second is employing a viscosity-modifying agent (VMA). Finally, the last one is a combination of the first and second methods.

Because of self-weight of light-weight aggregates, for compaction of concrete may results in increasing in segregation and bleeding problems. Noticeable problem associating with unsuitable vibration is inefficient dissipation of light-weight aggregates. This condition raises light-weight aggregates to the surface of concrete and forms a weak layer. As the SCC which dose not needs any vibration, it looks like that these problems can be kept at the lower level. But because that SCC must be compacted by its own weight (without any compaction) and the weight of self-compacting light-weight concrete reduces in comparison to SSC, so the balance between compaction and weight of SCC must be established. The major objective of the present study is to provide information about this balance in light-weight self-compacting concrete. To attain this aim and because of the interesting property of EPS as ultra light-weight aggregates, on this study,

2. EXPERIMENTAL PROGRAMME

2.1. Materials

Ordinary Portland cement (opc) meeting the requirements of ASTM C 150 were used for preparation of the self-compacting EPS concrete specimens in all compositions. Commercial dry uncompacted silica fume (SF) was used as a cementations material. The chemical compositions of OPC and SF are given in Table 1.

Table 1: Chemical composition properties of (OPC) and (SF) detail

	Cement	Silica fume
SiO_2	21.46	91.7
Al_2O_3	5.55	1
Fe_2O_3	3.46	0.9
CaO	63.95	1.68
MgO	1.86	1.8
SO_3	1.42	0.87
K_2O	0.54	-
Na_2O	0.26	0.1
LOI	-	2

Table 2: Grading and physical properties of expanded polystyrene

EPS type	Type I	Type II
Sieve size (mm)	*Cumulative passing (%)*	
9.5	100	100
4.75	96	2
2.36	2	0
1.18	2	0
Physical properties		
Mostly beads size(mm)	2.36	4.75
Specific gravity	0.025	0.018

To mix the self-compacting EPS concrete and for curing the specimens, potable water specified by ASTM D 1129 was used. Natural river sand (0-4.75mm) with fines modulus of 2.83 and crushed gravel with 12.5mm were used. The coarse and fine aggregates have specific gravities of 2.71 and 2.6 and mean water absorption of 0.8% and 0.58%, respectively. Sika Viscocrete-1 as a third generation of super-plasticizer and meets the requirements for super-plasticizer according to SIA 162 (1989) was used in all mixtures. This type of modified polycarboxylate based has been used by other researchers as VMA [10]. Solid content, PH and specific gravity of VMA were provided by its manufacturer to 35.7%, 6.5 and 1.08, respectively. Expanded polystyrene equally replaced by fine and coarse aggregates by using two types of commercial EPS with different specific gravity and grading which were used to prepare self-compacting EPS concrete. Type 1 with mostly 2.36 mm beads size and type 2 with mostly 4.75 mm size replaced fine sand and gravel, respectively. As seen, to prevent grading disturbance of coarse and fine aggregates, mostly beads size was selected in the grading range of aggregates, respectively. The EPS beads properties and grading details are presented in table 2.

2.2. Mixture Proportion of Self-Compacting Eps Concrete

The mixing sequences were as follows. Coarse and fine aggregates, EPS and some mixing water (25%) were initially homogenized for 1min in rotary planetary mixer.

Thereafter, binder materials including cement and SF were added. Finally, the remaining water and VMA (according to Table 3) were introduced to the wet mixture, while mixing was going on for 4 minutes. This optimum time is required to disperse VMA and stabilize viscosity. The water/cement ratio and binder content of the mixtures were maintained at 0.53 and 418 kg/m^3 throughout this study, respectively. In order to keep slump flow in allowed ranges, VMA was used in different dosages. The VMA was adjusted between 0.4 to 0.63% by weight of binder content and EPS beads replaced aggregates with 10, 15, 22.5 and 30 percentages by volume to produced structural self-compacting EPS concrete with compressive strength above 17 MPa and density ranging 1700-2100 kg/m^3. Fluidity and mechanical properties of self-compacting EPS concrete was compared with ordinary SCC that designed for slump flow about 65cm. The details of the mixtures including Silica fume which was replaced in 10% of the cement mass -are presented in Table 3.

Table 3: Mixture properties of self-compacting EPS concrete

Mix No.	Cement (Kg/m^3)	SF (Kg/m^3)	Water (Kg/m^3)	Gravel (Kg/m^3)	Sand (Kg/m^3)	% volume of EPS	%VMA of binder
1	380	38	196	822	925	0	0.62
2	380	38	196	689	792	10	0.55
3	380	38	196	623	726	15	0.50
4	380	38	196	524	626	22.5	0.45
5	380	38	196	424	527	30	0.40

The major problem of light-weight concrete is desirable dispersal of aggregates in matrix. As shown in Figure 1, the specimens of self-compacting EPS concrete containing different percentages of EPS beads shows desirable dispersal of EPS up to 22.5% compare to 30% in concrete specimens. Hence, a replacement up to 22.5% volume of EPS seems not to need any innovations. So, the beads can be used the way that already been explained. This should be qualified by more experiments. To assess the effect of workability loss where produced in sites, all of the fresh-state properties were tested 30 min after mixing. Some portion of the concrete mixture was used to fresh properties experiments and the remaining part was poured into the moulds in one layer and without any compaction other their self-weight to assess mechanical properties of self-compacting EPS concrete. After 24 h casting, they were demolded and curing was conducted according ASTM C 511 and then kept in the curing environment until the date of testing.

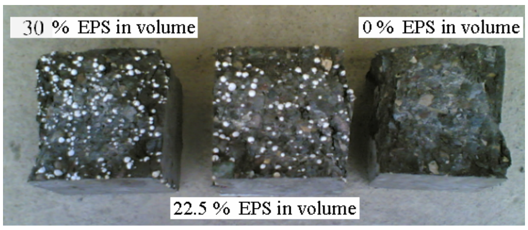

Figure 1. Desirable dispersal of EPS in self-compacting concrete specimens

2.3. Concrete Tests

Mechanical properties of hardened concrete are strongly related to fresh properties. Several experiments were conducted in each mixture to assess the most important features of fresh properties of light-weight self-compacting concrete. (i) Slump flow test is primarily to assess workability, filling ability and consistency of concrete without any obstructions. According to EFNARC, a SCC must have a slump flow ranging between 650-800mm. (ii) V-funnel flow test should be used to assess the ability to achieve smooth flow through narrow spacing without blockage. This test measured variable for describing the cohesion, viscosity and fillingability of SCC. Some researchers believe that V-funnel times represent the flowability and stability or segregation resistance of SCCs through V-shaped funnel test [11,12]. According to EFNARC, a stable and flowable SCC must has a V-funnel flow time varying between 6–12 s. (iii) L-box evaluates fillingability and passingability of SCC and also representative yield stress of the materials. The passing ability, on the other hand, shows the compatibility between the size of the coarsest particles of the concrete and the gap between the reinforcing steel bars in the structure to be cast [10]. According to EFNARC, a SCC must have a blocking ratio varying between 0.8-1. Fluidity is defined either qualitatively as the ease of placement or quantitatively by rheological parameters [9]. As previously expressed, ease of placement can defined by fillingability, passingability that are two of the three key properties of fresh concrete, were evaluated simply by experiments discussed before. From the quantitative view, Plastic viscosity and yield stress are two most common rheological parameters were assessed as Bingham equation. If the viscosity is too low, an increase of shear rate is recommended to avoid segregation. On the other hand, if viscosity is too high, a low shear stress would be necessary [13]. So, for self-compactibility, concrete should have an adequate plastic viscosity together with a low yield stress approaching to the behavior of a Newtonian fluid [9]. The measurement of yield stress and plastic viscosity requires a rheometer, and, where not available, alternative simpler tests such as slump flow, V-funnel times… can be used [9]. Moreover, these experiments are not costly and they can easily be carried out in sites. So, in this study the above tests were conducted to evaluate the fluidity of self-compacted EPS concrete. The water content in a mixture can be classified into free water and the bound water. Free water is the interstitial water existing between fines and aggregates. It disperses and lubricates the solid particles in concrete to create fluidity and plasticity of concrete. Therefore, it is the quantity and quality of free water that determines much of the rheological behavior of fresh concrete [14]. As mentioned above, hydrophobic is one of the main features of EPS beads, so increasing replacement of EPS in concrete can cause an increase the free water in matrix which affects the fluidity of self-compacting EPS concrete. On the other hand, increase in EPS in matrix can change many things such as size, kind and conFigure uration of aggregates, decrease internal friction and, above all, decrease the weight of matrix in ration with the condition without EPS. So, it has been tried to estimate these affects on fresh self-compacting EPS concrete by means of the above experiments and obtain the desirable EPS percentage. For each concrete mixture, the average compressive strength of three 100mm cubes at the age of 7, 28 and 60 days were obtained. Compression test loading was done by a system with the maximum capacity of 3000 KN and a loading rate of 0.25 N/mm^{2}s per specimens. 15×30 cylindrical was taken from the mixture to measure tensile strength. Water absorption tests were conducted on three 100 mm cube specimens according to the ASTM C 642 at 28 days. For the determination of water absorption, because of the temperature suggested by ASTM (100-110°C) EPS beads initially shrink and finally evaporate, saturated surface dry cubes were placed in an oven at 60 °C until a constant mass was achieved [15]. Before measuring compressive strength of the specimens at 28 days, the UPV measurements were conducted to measure the time needed for propagation of a sonic waves according to ASTM C 597.

3. RESULTS AND DISCUSSIONS

3.1. Fresh Concrete Tests Results

The first part of the results was attributed to the fresh properties of self-compacted EPS concrete. In Figure 2 the common effects of density and EPS percentage on slump flow and V-funnel time shows. Since Slump flow is not a suitable factor to exhibit the fresh behavior exactly, so the slump flow was kept in allowed range specified by EFNARC and other parameters effective on fluidity were evaluated. Segregation and bleeding were visually checked during the slump flow test and were not observed in any of the mixtures with the exception of mix No.5 in which segregation of aggregate near the edges of the spread-out concrete was observed. In other words, for light-weight self-compacting concrete with slump flow over than 680 mm, segregation symbols often appears. It can be seen from Figure 2, slump flow values were 640-700mm, while mix No. 5 has lower contents of VMA, The biggest slump flow attributed the maximum percentage of EPS in volume and mix No. 1 has minimum slump flow. Therefore, slump flow increased with the increase in EPS percentages. It was due to decreased in internal friction with an increase in EPS percentages. This, in turn, shows a better flowability in self-compacting EPS concrete in compare to SCC with no EPS. But, this is not enough for evaluating the fluidity of self-compacting EPS concrete, so other experiments must be conducted to assess other parameters such as viscosity, cohesion, segregation, blocking and etc. The time measured via the V-funnel flow was in the range of 6–15 s. As observe in Figure 2, an increase in EPS percentage caused an increase in V-funnel time, while slump flow has target range 60-70 cm. The V-funnel times for all mixtures were within the EFNARC range of SCC, apart from mix No. 5 which exceeded upper limit of V-funnel time. Felekoglu and his colleague [16] reported that the V-funnel time will decrease with increasing in water/powder values or free water content increase. But the results showed in self-compacting EPS concrete increasing in free water content, produced by increase in the hydrophobia EPS beads in matrix will increase V-funnel time. On the other hand, internal friction of matrix was decreased with increasing in the amount of EPS in concrete due to smooth surface of EPS compare to aggregates.

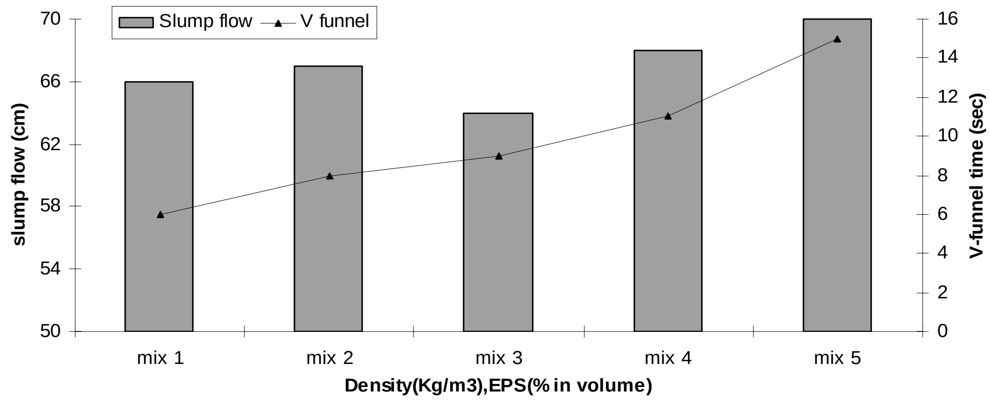

Figure 2. Variation of density with slump flow and V-funnel time

In the other words, limiting the coarse aggregate content by replacing them with EPS will cause the relative distance between coarse aggregates to be increased. Therefore, the frequency of colliding between aggregates decrease and finally, the energy dissipation decrease. So, it seems with an increase in EPS content, the V-funnel time was decreased. But an increase in EPS percentage caused increasing V-funnel time. The reason probably is the lower self-weight of self-compacting EPS concrete compare to SCC. An increase in EPS in matrix decrease self-weight and a decrease flowability of matrix in the funnel lead to a decrease the V-funnel time. So in self-compacting EPS concrete, self-weight is a major parameter to characterize the fresh-state behaviors while in SCC, free water is the major case. In the base of EFNARC range for V-funnel time varying between 6-12 s, mix No.5 is rejecting. The results show that Light-weight self-compacting concrete with density higher than 1900 kg/m^3 satisfies the fresh-state behaviors of concrete related to viscosity, cohesion and segregation and lower amount of density were rejected. In the blocking ratio point of view L-box test was performed in all mixtures. Results of blocking ratio of all the different mixes are presented in Figure 3. Blocking ratio vary between 0.9-0.78 for self-compacting EPS concrete. As the effect of EPS, blocking ratio decreased with the increased in EPS percentages. So, in the base of EFNARC, mix No. 5 is rejecting. Aggregate blocking is more probable in mixtures where blocking ratio is lower than 0.8. But in self-compacting EPS concrete, it did not seem that blocking ratio lower than 0.8 for mix No. 5 are pertinent to aggregates blocking between gaps. When aggregates replaced by EPS with mostly beads size lower than G_{max} the blocking must be solved. Like V-funnel time, probably the lower self- weight of self-compacting EPS concrete compare to SCC is the reason. Fewer Self-weight of self-compacting EPS concrete, decreasing the flowability of the fresh concrete in horizontal section.

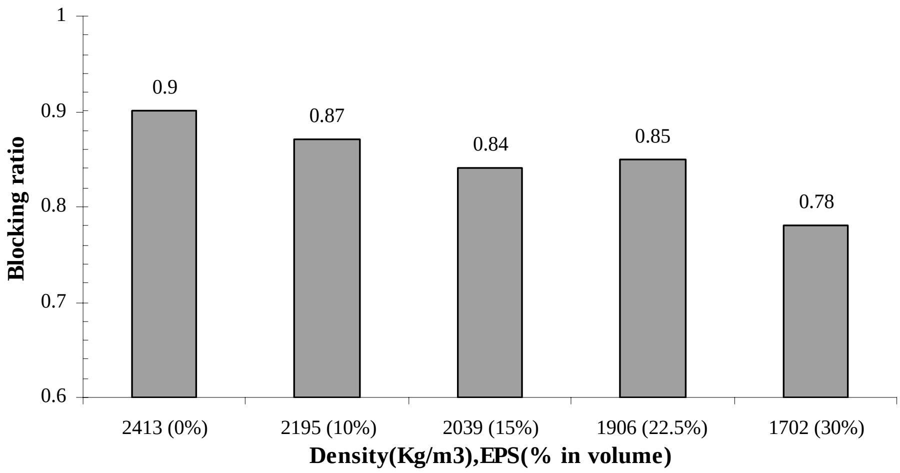

Figure 3. Variation of density with blocking ratio

3.2. Hardened Concrete Tests Results

The second part of results was attributed to the hardened properties of self-compacted EPS concrete. These results are reported in Table 4.

Table 4: Test results of hardened properties of light weight self-compacted concrete

Mix No.	Density (Kg/m^3)	Compressive strength (MPa)			split tensile strength (MPa)	UPV (Km/s)	absorption
		7 days	28 days	60 days			
1	2413	32.5	47.3	53.4	5.37	4.808	5.1
2	2195	26.2	33.2	38.3	4.17	4.545	5.8
3	2039	21.1	25.1	27.5	3.69	4.315	5.5
4	1906	18.7	21.9	22.8	3.14	4.042	6.8
5	1702	14.8	17.1	18.2	2.69	3.724	7.92

3.3. Compressive Strength

Standard cubes were tested for compressive strength after 7, 28 and 60 days of curing. All of the mixtures represented a continuous increase in compressive strength with age. Similar to EPS concrete, the rates of strength development for self-compacting EPS concrete was greater initially and lower as the curing ages increased. The results show that the compressive strength decreases with increasing EPS content at all ages. This is due to lower strength of EPS compared to fine and coarse natural aggregates. On the other hand, bond between EPS and paste or mortar are fragile due to its smooth surface. According to Figure 4, mix No.1 developed highest compressive strength up to 47.3 MPa While mix No. 5 shows lower about 17.1 MPa at the age of 28 days. It can be observed for replacement aggregates by 30% EPS in volume, compressive strength decreased about 64% and replacement aggregates with more than 30% cause to leave structural condition.

Because of this study purpose was produced structural self-compacting EPS concrete; replacements above 30% are not conducted. Mix No.5 had structural strength, but in fresh state, it was rejected. This means that concrete in fresh state is more remarkable than hardened one. Variation of compressive strength with different percentage of EPS by volume or density is represented in Figure 4 and 5, respectively. Density is one of the most important factors in concrete. In self-compacting EPS concrete, with increase in EPS volumes decreasing in density were shown. Also, as shown in Figures 4 and 5, approximately linear relationships were evaluated between EPS volume and density with Compressive strength. This relationship was confirmed by other researcher for light-weight EPS concrete containing SF [15].

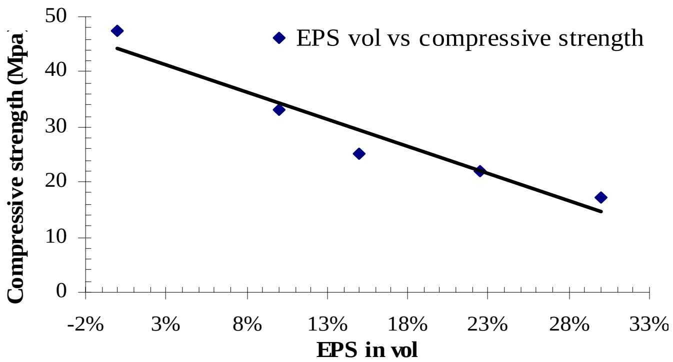

Figure 4. Variation of EPS vol. with compressive strength

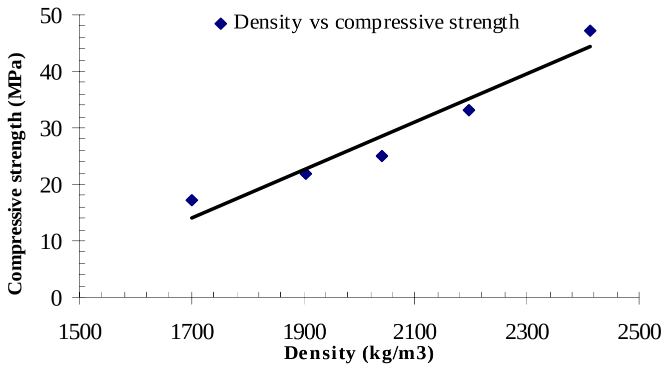

Figure 5. Variation of density with compressive strength

3.4. Tensile Strength

Tensile strength is one of the most important fundamental properties of concrete. In Table 4, the influence of EPS content on splitting tensile strength is presented. With increasing amount of EPS content or decreasing the density, splitting tensile strength also decreased. The relationship between compressive strength and splitting tensile strength for self-compacting EPS concrete is presented in Figure 6. It can be seen that with an increase in compressive strength, the splitting tensile strength increases. Against to SCC in which failure is typically brittle and with separation of concrete in two pieces, in self-compacting EPS concrete failure is more gradual and the samples do not separate. This mode of failure was reported earlier for light-weight EPS concrete by k. Ganesh Babu and colleague [15].

3.5. Ultrasonic Pulse Velocity and Relationship with Compressive Strength

Ultrasonic pulse velocity (UPV) is one of the non-destructive methods for assessing the quality and homogeneity of the in situ concrete. In table 4 UPV values for all mixtures was given. It can be observed from this table, when compared to the control mixture, use of EPS generally decreased the UPV. The variation of compressive strength with UPV is presented in Figure 7.

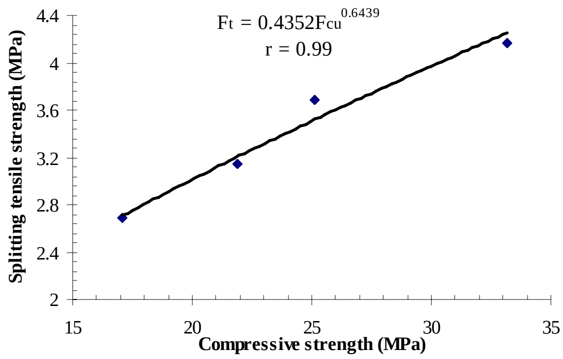

Figure 6. Relationship between splitting tensile strength and compressive strength

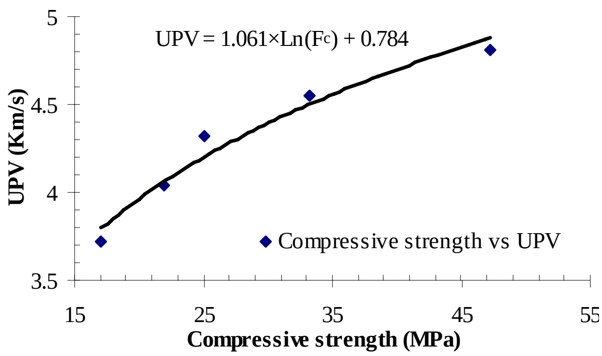

Figure 7. Relationship between UPV and compressive strength

With an increase in compressive strength, UPV was increased. The results of this study were suggested by Eq. (3) for the Relationship between UPV and compressive strength of self-compacting EPS concrete.

$$UPV=1.061\times \mathrm{Ln}(f'_c)+0.784 \tag{3}$$

3.6. Absorption

Water absorption is one of the major parameters of durability of concrete which related to its porosity. Water absorption is a measure of the portion of the total volume of concrete occupied by pores. According to table 4, maximum water absorption was detected with mixture with higher percentages of EPS. This can be expected that the specimens with high percentage of EPS will include to more amounting of free water. By the time when this free water vaporized will lead to an increase in pores which resulted to an increase in the amount of concrete water absorption.

4. CONCLUTION

The behavior of self-compacting EPS concrete was represented in two parts. In the first part, it was shown that light-weight self-compacting concrete with slump flow over than 680 mm, segregation symbols often appears. V-funnel time increased with increasing in the EPS percentages, while slump flow was kept in allowed ranges specified by EFNARC. But L-box was decreased with increasing in EPS volume. This was probably attributed to the lower self- weight of self-compacting EPS concrete compare to SCC.

On the other hand, Light-weight self-compacting concrete with density higher than 1900 kg/m^3 satisfies the fresh-state behaviors of concrete related to viscosity, cohesion and segregation and lower amount of density were rejected. The second part of this study was considered the hardened state of self-compacting concrete. The results show that compressive and tensile strengths and absorption increased with increasing EPS content, while UPV decreased.

REFRENCES

1. Grube H, Rickert J. “Selbstverdichtender Beton-ein weiterer Entwicklungsschritt des 5-Stoff-Systems Beton”, Beton 49, H.4, 1999; p. S.239-44.
2. A. Sivakumar, Manu Santhanam, “A quantitative study on the plastic shrinkage cracking in high strength hybrid fiber reinforced concrete”, Cement & Concrete Composites 29 (2007) 575-581.
3. D. Saradhi Babu, K. Ganesh Babu, T.H. Wee, “Properties of lightweight expanded polystyrene aggregate concretes containing fly ash” Cement and Concrete Research 35,(2005) 1218-1223.
4. R. Sri Ravindrarajah, A.J. Tuck, “Properties of hardened concrete containing treated expanded polystyrene beads”, Cement and Concrete Composites 16 (1994) 273-277.
5. Efnarc. Specification and Guidelines for Self-Compacting Concrete. London: Efnarc Publication; 2002. p. 1-32.
6. Stephan Assie, Gilles Escadeillas, Vincent Waller, “Estimates of self-compacting concrete ‘potential’ durability” Construction and Building Materials 21,(2007)1909-1917.
7. Eva Mnahoncakova, Milena Pavlikova, Stefania Grzeszczyk, Pavla Rovnani ´kova´, Robert Cˇ erny Hydric, “thermal and mechanical properties of self compacting concrete containing different fillers” Construction and Building Materials 22 (2008) 1594-1600.
8. G. Heirmana, L. Vandewalle, D. Van Gemert, V. Boel, K. Audenaert, G. De

Schutter, B. Desmet, J. Vantomme, “Time-dependent deformations of limestone powder type self-compacting concrete” Engineering Structures.

9. Burak Felekoglu, “Utilization of high volumes of limestone quarry wastes in concrete industry (self-compacting concrete case)” Resources, Conservation and Recycling 51 (2007) 770-791.
10. Tayyeb Akram, Shazim Ali Memon, Humayun Obaid, “Production of low cost self compacting concrete using bagasse ash” Construction and Building Materials.
11. Sakata S, Maruyama K, Minami M. “Basic properties and effects of welan gum on self compacting concrete”. In: Bartos PJM, Marrs DL, Cleland DJ. Editors In: Proceeding of RILEM international conference on production methods and workability of concrete. 1996, p. 237-53.
12. Masahiro Ouchi, Sada-Aki Nakamura, Thomas Osterberg, Sven-Erik Hallberg, Myint Lwin, “Applications of self compacting concrete in Japan”, Europe and the united states, 2003 ISHPC.
13. Nielsson I, Wallevik OH. In: Wallevik O, Nielsson I, editors. “Rheologycal evaluation of some empirical test methods”, preliminary results proceedings of the 3rd international RILEM symposium Reykjavik, Iceland. RILEM Publishers PRO 33; 2003. p. 59-68.
14. Sam X. Yao and BEN C. Gerwick, “Development of Self-Compacting Lightweight Concrete For RFP Reinforced Floating Concrete Structures”, Ben C. Gerwick, Inc, 601 Montgomery Street, San Francisco, California, U.S.A.
15. K. Ganesh Babu, D. Saradhi Babu, “Behavior of lightweight expanded polystyrene concrete containing silica fume”. Cement and Concrete Research 33(2003) 755-762.
16. Burak Felekoglu, Selcuk Turkel, Bulent Baradan “Effect of water/cement ratio on the fresh and hardened properties of self-compacting concrete” Building and Environment 42 (2007) 1795-1802.

CD03-003

PRACTICAL APPLICATION OF INNOVATIVE TECHNOLOGY IN FLOOR CONSTRUCTION

A. Fadai, Vienna, Austria

ABSTRACT

The main objective of this paper is to show the benefits of using innovative technology i.e. post-tensioning and concrete core activation for the more widespread practical applications in concrete buildings.

In consideration of the spans up to 20.00 m and heavy superimposed loads structures built using unbonded post-tensioning systems provided many advantages compared to conventionally reinforced concrete structures.

The advantages of using post-tensioning with unbonded tendons, structural behavior, concerning constructive aspects and economy will be illustrated by the presentation of several commercial building and parking structures.

Reductions in concrete and reinforcing steel quantities are two of the advantages that directly impact overall construction costs.

Concrete core activation is a heating and cooling system based on simple physical principles to create a low-cost system. Concrete possesses a large capacity to store heat, and water functions well as a heat conductor.

Keywords: unbonded post-tensioning, free tendon layout, floor construction, fire protection, fire resistance, concrete core activation

1. INTRODUCTION

Slabs supported on columns are defined as flat slabs. For the purpose of this section flat slabs may be of uniform thickness or they may incorporate drops (thickenings over columns). Figure 1 illustrates typical arrangements of slabs in floor construction.

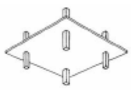

Flat Slab-Economical for spans between 6.0 m and 9.0 m. Loads light to medium.

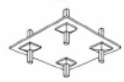

Flat Slab–Economical for spans between 6.0 m and 9.0 m. Loads light to medium.

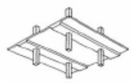

Continuous Band–Effective for large spans, 8.0 m to 12.0 m. Loads light to medium.

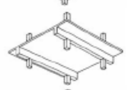

Beam and Slab–One span is excessive, up to 20.0 m and the other does not exceed 8.0 m to 9.0 m. Loads medium to heavy.

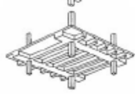

Ribbed One Way–Recommended where spans are predominantly in one direction. Loads medium to heavy.

Figure 1. Typical arrangements of slabs in floor construction

2. UNBONDED MONOSTRAND SYSTEM

The unbonded tendon as the name implies is never bonded to the concrete. The strand is carefully coated with grease which gives a low frictional resistance and contains anti-corrosive additives. Separating the grease from the concrete is an extruded plastic tube (Figure 2).

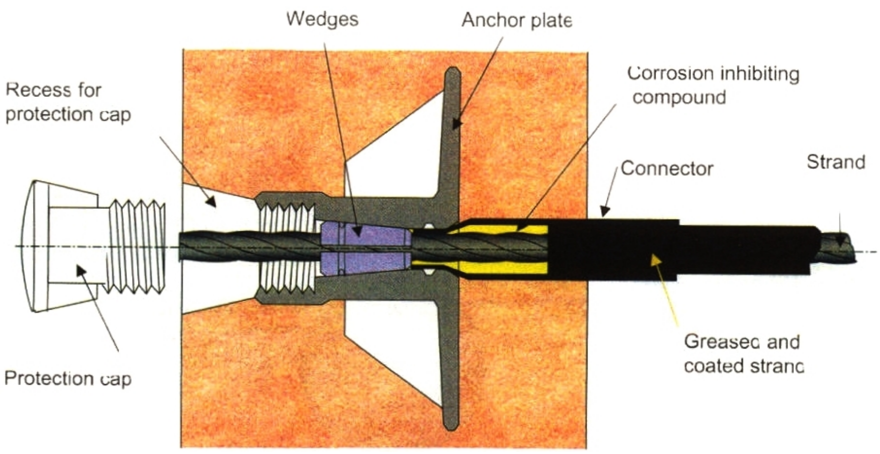

Figure 2. Classical anchorage of monostrand for flat slab [5]

The tendons are individually anchored at each end and stressed one at a time. Strands are stressed and held by wedges fitting neatly inside a single anchor specially designed to retain the bursting forces and distribute the prestressing forces evenly into the concrete (Figure 2).

2. CONSTRUCTION PROCEDURE FOR UNBONDED POST-TENSIONING

In slabs with unbonded post-tensioning, the operations are normally carried out as follows:

1. Erection of slab supporting formwork
2. Fitting of end formwork; placing of stressing anchorages
3. Placing of bottom and edge reinforcement
4. Placing of tendons
5. Placing of top reinforcement and tendons
6. Concreting of the section of the slab
7. Removal of end formwork and forms for the stressing block-outs
8. Stressing of cables according to stressing program
9. Stripping of slab supporting formwork

3. DESIGN OF POST-TENSIONING FLOORS

Flat slabs should be analyzed using a proven method of analysis, such as grillage (in which the plate is idealized as a set of interconnected discrete members), finite element, yield line or equivalent frame. Appropriate geometric and material properties should be employed.

The design of post-tensioning floors differ from that of reinforced concrete in that forces are applied to the structure which have a positive effect on behavior.
Prestress applied eccentrically to the slab produces deflections which are opposite in direction to those produced by self weight and variable loads, so the designer can vary the prestress to balance out any chosen proportion of these loads "load-balancing method" (Figure 3).

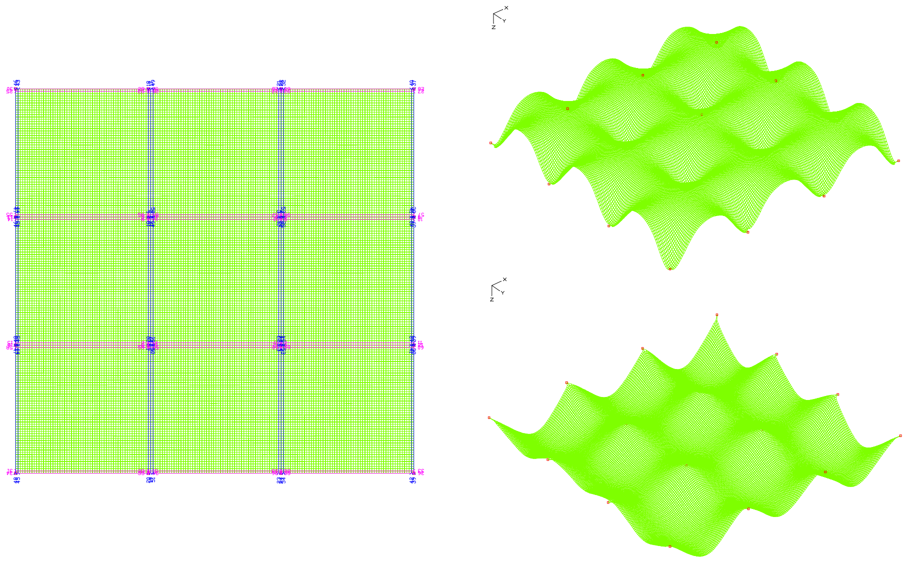

Figure 3. Illustration of transverse effect of prestress

Due to the additional stiffness of the slab achieved by prestressing, the thickness of the slab may be reduced without affecting performance or compliance with standards.
Post-tensioning automatically allows for wider spacing of columns and the introduction of additional stiffening elements increases this facility still further.
The limit states are placed in two categories [1]:
Ultimate **L**imit **S**tates (**ULS**) are those associated with collapse or with other forms of structure failure.
Serviceability **L**imit **S**tates (**SLS**) correspond to states beyond which specified service requirements are no longer met (deformation, cracking of concrete).
For prestressed slabs the control of deflection is a main concern.

4. FREE TENDON LAYOUT

A reversed parabola is the most common gradient as it provides uniform distributed counterbalance. However the tendon layout is not that much of importance for floor slabs as for bridges.
Tests have shown that there is no much difference for tendons that are supported only by two chairs over the support and are placed horizontally for most of the span [1]. This method "free tendon layout" spares chairs and reduces field labor costs and is less prone to field errors [2].

The design should be oriented to maximize site efficiency for the indirect cost (less labor, formwork systems, cycle redundancy, etc) and accounts for almost 60 % of the savings. The use of the free tendon layout concept, with very few control points and less saddles, is mandatory. This also forces the software to be able to model explicitly complex tendon shapes, not just parabolas (Figure 4).

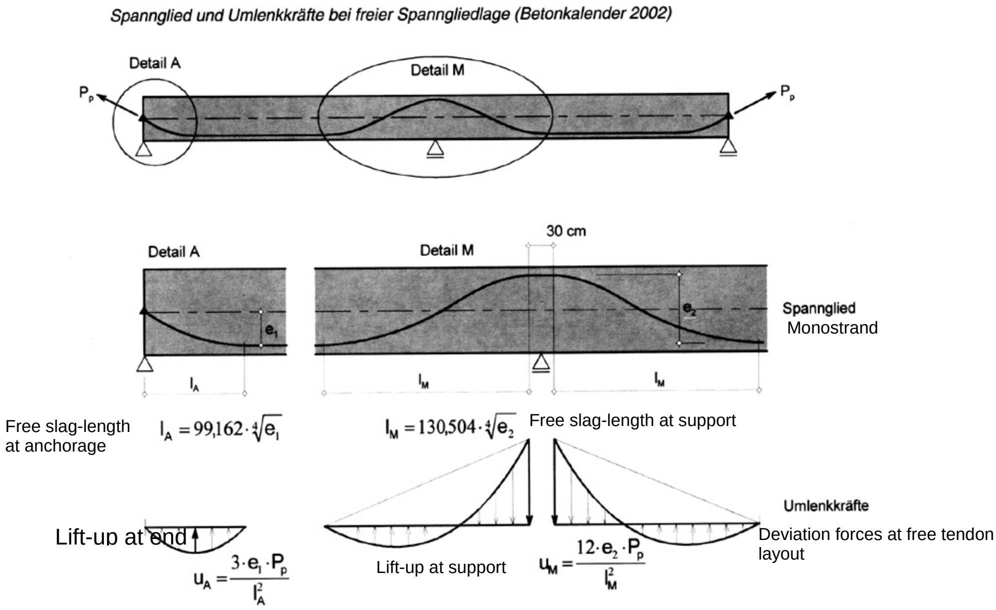

Figure 4. Free tendon layout [3]

There are substantial differences between the North American and the European practice with regard to the amount and the placement of mild reinforcement. The European Code does not permit any section without bottom reinforcement [1]. A further reduction is possible using the so called design concept “reinforced concrete with tendons”. The tendons utilize the permissible deflections. The ultimate limit state and crack control is utilized by mild reinforce only [2].
A defect of tendons is especially in the case of fire not relevant for the bearing capacity [3].

5. FIRE PROTECTION AND RESISTANCE

Research Report “Fire Resistance of Fiber-Reinforced, Reinforced and Prestressed Concrete”, was published by the Austrian Federal Ministry of Transportation, Infrastructure, and Technology in its series of publications on "Road Research" in 2004 [4].
When concrete is exposed to fire temperatures, constraining forces are generated within the reinforced concrete structure and the strength of the composite materials, i.e. concrete and steel, is gradually reduced. Explosive spalling of the inner concrete cover reduces the load-bearing capacity of the structure.
Further investigations within the research program concerned the residual strength

of concrete and steel after a fire, the behavior of monostrands in the event of a fire, and the determination of the load-bearing capacity of a structure.

5.1. Behavior of Monostrands in Case of Fire

In case of fire monostrands are normally better protected (by a second reinforcement layer) than the reinforcing steel. In case of steep temperature gradients the protection layer may spall off more rapidly and the monostrand gets directly exposed to fire.

As a consequence, the corrosion protection is destroyed. If the concrete is not spalling off, the monostrand is durably protected by the concrete; it is heated slowly and the following processes can be observed:

The HDPE-sheath can resist temperatures ranging from 120°C to 140°C for a short duration and can resist temperatures of 100 °C for a longer duration. Higher temperatures will lead to a slow degradation (decompensation).

If for instance the prestressed strand is deflected inside the structure, it exerts lateral forces to the plastic sheathing which may result in perforation of the plastic sheathing even at temperatures of only 75°C (softening point).

The agent for corrosion protection (grease) remains unchanged up to a temperature of 180°C. If temperatures exceed this value, the presently used greases get destroyed. Because of the temperature increase the corrosion protection mass expands causing pressure in the plastic sheathing. Test results show pressures up to 9 bar inside the plastic sheathing, without causing any spalling of the concrete [4].

It can be stated that a long-term durability of monostrands after fire exposure is provided by the used corrosion protection systems up to maximum temperature of approximately 150°C in case of linear prestressing tendon layouts and of approximately 100°C in case of deflected prestressing tendon layouts. Even if the corrosion protection system is destroyed a short-term use of the monostrands is possible under the above described conditions [4].

In order to document the development of strength with continually increasing temperatures on a single test sample and in the full range of possible temperatures, a sample of prestressing steel with Ø9.4 mm (Figure 5) was put into a wire welding machine and exposed to a temperature increase to 950 °C over a length of 220 mm [4].

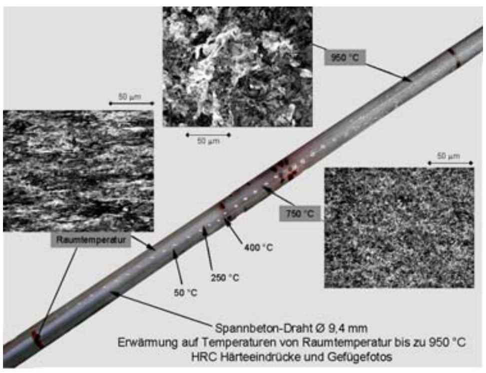

Figure 5. A sample of prestressing steel, temperature increase to 950 °C [4]

5.2. Fire Protection-Concrete Cover

Minimum concrete cover shall be provided in order to ensure an adequate fire resistance.

Reinforced concrete with tendons behaves like reinforced concrete. A defect of tendons is especially in the case of fire not relevant for the bearing capacity.

Nominal cover	2.0 cm
Minimum cover of prestressing steel	3.0 cm

Unbonded post-tensioning und fire resistance class REI 90 [6]
Prestressing steel (monostrand) in second reinforcement layer

Nominal cover	3.5 cm
Minimum cover of prestressing steel	4.5 cm

The values can vary according to the standards of the various countries.

6. PRESTRESSED SLABS–BENEFITS FOR INVESTORS, ARCHITECTS, ENGINEERS AND CONTRACTORS

The application of unbonded post-tensioning systems provides many advantages compared to conventionally reinforced concrete structures.

Prestressing offers:

- Greater resistance to cracking and water seepage
- Slabs may be designed to be waterproof without the need for expensive membranes. This is particularly important in trafficable roof structures
- Increased movement joint spacing, up to 50-60 m

Increased design flexibility:

- Longer spans providing larger column-free areas
- Reduced deflection under maximum design load

Significant savings in material:

- Thinner slabs result in a lighter structure
- Reduces column and foundation loads
- Reduces building height can result in significant cladding savings in high-rise structures
- Less weight to be considered along the height of the building is of an advantage for earthquake design.

Speedier methods of construction:

- Simpler and more rapid fixing of tendons and reinforcing steel, no complex fixing details
- Fast formwork turnaround. Stressing is carried out 3-4 days after concrete is poured, after which, formwork and props may be removed, which also provides earlier access to other trades.

6.1. Concrete Core Activation in Floor Construction

Concrete core activation is a heating and cooling system based on simple physical principles. Concrete possesses a large capacity to store heat, and water functions well as a heat conductor.

The principle or the essence of concrete core activation is not new; by bringing the mass of a building up to a certain temperature, one takes care of the heating or cooling in comparison with the surrounding temperature. It uses the storage capacity of the concrete floor layers; night air and cool earth energy, or low-level heating energy can all be stored in the concrete floor to create a low-cost system [9].

The activated layers absorb the heat from the room in order to cool the room during operating periods. The heat is subsequently released during the time remaining. The complete concrete floor construction is cooled or heated through an integrated piping system, which is evenly woven, before the concrete is casted (Figure 6).

The system is simple to install, from the assembly of the water supply pipes onwards. Pre-fabricated modules are installed to the concrete layer in externally supplied reinforcement casings. The cooling and heating functions are both possible using the same pipe distribution system and this is fully integrated into the ceilings making it completely invisible (Figure 6).

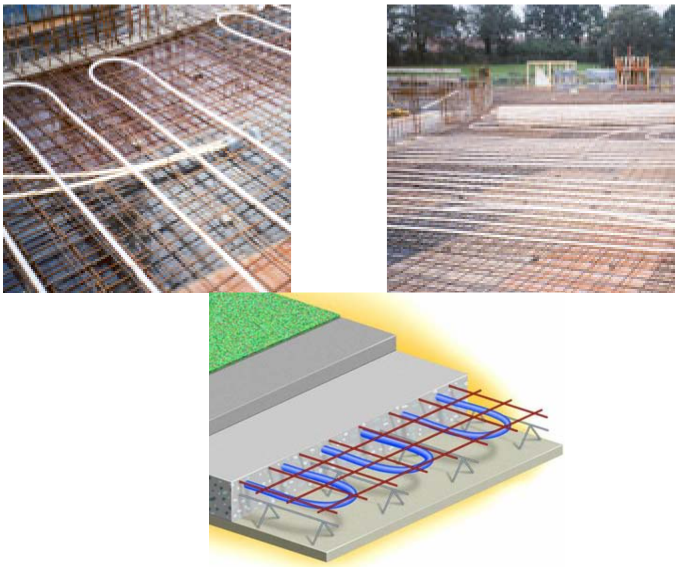

Figure 6. Concrete core activation [8]

If the daytime sees high temperatures, then the system is subjected to its greatest loads. The cooling floor reduces the comfortable temperature range to between 21°C und 26°C. During the night time, the water circulating through the system releases the heat back out through the floor [7].

Water reliably transports the cooling and heating energy, meaning that the temperature is not prone to swings. Water is for heating and cooling, air is just for ventilating - the energy-saving slogan is certainly justified.

The harsh construction site environment, particularly during the structural build phase, as well as the decades of use to which the pipes are subsequently exposed, require a highly durable raw material.
The cross-linking has numerous advantages: it results in a material which is dimensionally stable, non-sensitive to stress cracks and highly durable.
The concrete core activation system takes care of the basic load, and in the case of optimally conFigured buildings, the entire cooling and heating requirements. Under these circumstances radiator installations beneath the windows and false ceilings for ventilation channels become entirely unnecessary [7].

7. COMPLETED STRUCTURES

The benefits of using post-tensioning for the more widespread practical applications in concrete buildings and the advantages of using post-tensioning with unbonded tendons, concerning constructive aspects, economy and structural behavior will be illustrated by the presentation of several commercial building and parking structures.

8. CONCLUSIONS

The unbonded post-tensioning enabled the designer to limit deflections under service load conditions, so the designer could vary the prestress to balance out any chosen proportion of self weight and variable loads. Due to the additional stiffness of beams and slabs achieved by prestressing, the thickness of beams and slabs could be reduced. Post-tensioning allowed also for wider spacing of columns.
Particularly with regard to the low ambient temperature post-tensioning with unbonded tendons offered a special advantage. Stressing procedure could take place without grouting operation.
The concrete core activation system takes care of the basic load, and in the case of optimally conFigured buildings, the entire cooling and heating requirements. Under these circumstances radiator installations beneath the windows and false ceilings for ventilation channels become entirely unnecessary.
Owners, contactors and architects benefited from concrete core activation system and from thinner beams and slabs as well as from a weight reduction in floor constructions. Moreover, post-tensioning allowed earlier stripping of formwork shortening overall construction time. For high durability tendons provided crack-free beams and slabs. In addition, Post-tensioned beams and slabs offered increased seismic resistance.

REFERENCES

1. Eurocode 2 - Design of concrete structures Part 1-1: General rules and rules for buildings, November 2005.
2. Wicke, M.; Maier, K.: Free Tendon Layout. XIII. FIP-Congress Amsterdam, Austrian Concrete Society. Vol. 32, May 1998.
3. Wicke, M.; Maier, K.: Anwendung des Spannbetons, Betonkalender, Vol. 2, Ernst & Sohn Verlag, Berlin, 2002.
4. Austrian Federal Ministry of Transportation, Infrastructure and Technology:

Fire Resistance of Fibre-Reinforced, Reinforced and Prestressed Concrete, Vol. 544, Vienna 2004.
5. International Federation for Structural Concrete (fib): Factory applied corrosion protection of prestressing steel, State-of-art report, Bulletin 11, January 2001.
6. Eurocode 2-Design of concrete structures Part 1-2: Design of concrete structures. General rules – structural fire design, February 2007.
7. Uponor Contec: http://www.uponor.at
8. RAU: http://www.rau.eu
9. Tagungsband Heizen und Kuehlen mit Beton, Vereinigung der Oesterreichischen Zementindustrie, 2009.

CD03-004

EXPERIENCE GAINED DURING DESIGN AND CONSTRUCTION OF THE JEGIN RCC DAM IN IRAN

M.E. Omran[1], A.A .Jalalzadeh[2]
[1]Department of Civil Engineering, University of Kurdistan, Mahab Ghodss Consulting Engineers, Tehran, Iran
[2]Mahab Ghodss Consulting Engineers, Tehran, Iran

ABSTRACT
Construction of the Jegin RCC large dam in Iran has been completed in January 2007. Jegin dam with 78 meter height and 400,000 cube meter in concrete volume is located in a remote area at the South-east of the Country, in a region with very high temperatures and extremely difficult working conditions. Although the original design was already a straight gravity RCC dam type, when performing the definitive construction design some improvements were introduced in order to achieve an "RCC- friendly" design. As a consequence the new design, together with the optimization of the construction processes, enabled the Contactor to place the RCC rapidly and efficiently, which led to a better execution quality, a schedule reduction and lower cost. This paper deals with the original and actual design criteria and construction of RCC works including development of mix design and full scale trails. RCC placement, compaction and quality control procedures and other relevant aspects are also discussed.

1. INTRODUCTION
The Jegin Roller-Compacted Concrete (RCC) dam is the first large RCC dam in Iran; a smaller RCC dam that is essentially the core of a spillway was completed in 2002 on the Karkheh River in southwest Iran. Jahgin is 78 m high, 220 m long at the crest and was contain approximately 400000 m^3 of concrete of which some 270000m^3 was RCC.
The dam is in southern Iran some 350 Km east of Bandar Abbas and some 107 Km north of Jask that is on the coast (see Figure1). The conditions at the Jegin site are very challenging, probably as challenging as at the site of any RCC dam completed to date. There is a total lack of water and throughout the year the temperatures are high, particularly in the summer when they can be in excess of 50° C for significant periods. During 2002 there was no rain at all on the site and the maximum temperature was 54°C. There were also significant floods; the design flood is in excess of 10 730 m^3/sec.
Prior to the start of the trial mix programme, an extensive search was made for sources of supplementary cementitious materials that were reasonably close to the Jegin site, two natural Pozzolans were found together with an air-cooled blast furnace slag and a copper slag.
In addition it was ascertained that a low lime fly ash from India was being

imported into the Country. None of the Iranian materials had ever been used in concrete before let alone in a structure as important as Jegin dam. The sources of the Iranian supplementary cementitious materials together with the two cement suppliers, both of whom added natural pozzolans in their cements, are shown in Figure 1.

2. CONSTRUCTION MATERIALS

2.1. Portland Cements

Two ASTM Type-II Portland cements were investigated during the trial mix programme; the preferred cement from Hormozgan and alternative cement from Kerman (see Figure1).

2.2 Pozzolans

An extensive search was made in southern Iran for suitable pozzolans. The following five possible materials were located;

- a natural Pozzolan from Khash;
- a ground slag from Esfahan (it was originally thought that this was a ground-granulated blast-furnace slag (GGBFS), but it was eventually ascertained that the slag was air cooled rather than granulated);
- an imported low lime fly ash from near Mumbai in India;
- a natural pozzolan from Sirjan;
- a ground copper slag from near Jiroft;

In addition, some fine river sand was also investigated, to see if it could be used as ' fine' in the mixes to reduce the quantity of natural pozzolan which might be required. The location of two cements and various potential pozzolans relative to the Jahgin site are shown in Figure 1.

1. Hormozgan Cement 2.Kerman Cement 3. Khash Pozzolan
4. Sirjan Pozzolan 5. Esfahan GBFS 6. Copper Slag

Figure 1. Location of potential cementitious- materials sources in southern Iran

2.3 Aggregates

The sandstone aggregates were obtained from gravel borrow pit in the reservoir area. Considering the Jegin dam site condition, it has been decided to transport RCC with vacuum chute system. In order to avoid segregation of the aggregate, 75mm maximum size aggregate given in the primary study has been changed by engineer to 38mm. It's to be mention that, the difference in cementitious material requirements for mixture with maximum size aggregate from 38mm to 76mm is less in RCC than in conventional concrete. An aggregate plant was designed to crush the oversize material and four size of aggregate were used; a partially crushed 20 t0 5mm material and two fine aggregates, the first crushed and second uncrushed (5).

3. TRIAL MIX PROGRAMME–STAGE 1

The trial mix programme at Jegin was carried out in two stages. The objective of the first stage was to assess the performance of all the potential cementitious materials to see which could achieve the strengths required at Jegin dam. Three of the five pozzolans were considered to be 'base' materials: the natural pozzolan from Khash; ground slag from Esfahan and, the low-lime fly ash from India.

3.1. Optimum Workability/Water Content

After gradation has been optimized for each of the combinations of the base cement and the base supplementary cementitious materials, the RCC was visually optimized by using a "Standard" set of mixture proportions:-

- 100 + 100 (cement + supplementary cementitious materials) in the case of the natural pozzolan:
- 50 + 150 in the case of the ground slag;
- 120 + 100 in the case of the low-lime fly ash

In all three cases the optimum workability was in the range of a Loaded Ve Be (ASTM C1170) time of circa14 to 18 sec with an acceptable range (for the laboratory tests) of between 10 and 25 sec. The optimum water contents commensurate with these workabilities were:

- 140 Kg/m^3 for the Khash natural pozzolan (for the 100 + 100 mixture proportions);
- 135 Kg/m^3 for the Esfahan ground slag (for the 50 + 150 mixture proportions)- this was later found to be a little low;
- 127 kg/m^3 for the Indian low-lime fly ash (for the 120+100 mixture proportions).

3.2. Mix Proportions

Two RCCs were to be used in the dam body at Jegin:

- RCC1 was to be used near the upstream face of the dam where the dynamic loading was greatest. This was to have a characteristic cylinder compressive strength of 200 kg/cm2 at the design age of 365 days: a target (average) strength of 220 kg/cm2 was defined
- RCC2 for the majority of the dam body; this was to have a characteristic

cylinder compressive strength of 120 kg/cm2 at the design age of 182 days; a target (average) strength of 145kg/cm2 was defined.

Three sets of mix proportions were designed to obtain the requirements of RCC as shown in Table 1. Most of the mix proportions have a total cementitious content of 195 kg/m3. The results of the stage-1 programme showed that there were essentially only two pozzolans which were satisfactory for the RCC Jahgin, both in terms of their strength development and also in terms of practically. These were the natural pozzolan from Khash and the Indian low-lime fly ash. The sirjan natural pozzolan had a very similar performance to the Khash natural pozzolan, but there were potential supply and transportation problems.

Table 1: Chosen mix proportions for the Jegin Stage 1 trail mix programme

Mix No*.	Cement + natural Pozzolan + water	Mix No.	Cement+ground slag+water	Mix No.	Cement + low-lime fly ash + water
HK.Mix1	70 + 125 + 139	HE.Mix1	30 + 165 + 139	HI.Mix1	45 + 150 + 127
HK.Mix2	95 + 100 + 140	HE.Mix2	40 + 155 + 140	HI.Mix2	70 + 125 + 128
HK.Mix3	120 + 75 + 142	HE.Mix3	50 + 145 + 142	HI.Mix3	95 + 100 + 129
HK.Mix4	145 + 50 + 144	HE.Mix4	70 + 125 + 144	HI.Mix4	120 + 75+ 131
HK.Mix5	170 + 25 + 146	HE.Mix5	90 + 105 + 146	HI.Mix5	145 + 50 + 134
HK.Mix6	195+ 0 + 146	HE.Mix6	110+ 85 + 146	HI.Mix6	170+ 25 + 137
HK.Mix7	240 + 0 + 150	HE.Mix7	130+ 65 + 150	HI.Mix7	150+ 30 + 135

*The first letter of the Mix. No. refer to cement (H = Hormozgan) and the second the pozzolan (K = Kash natural pozzolan), E = Esfahan ground slag, I = Indian low-lime fly ash

3.3. Development of Strength with Age of the Stage–I Mixes

3.3.1. Khash Natural Pozzolan

Six mixes were designed containing the Khash natural pozzolan (and Hormozgan Type–II cement), all with a total cementitious content of 195 kg/m^3. The natural pozzolan content varied from 0 Kg/m^3 in HK. Mix6 (the H refers to the cement, Hormozgan type II, and the K to the supplementary cementitious material, Khash natural pozzolan) to 125 Kg/m^3 in KH. Mix 1. The development of strength with age of the HK series is shown in Figure 2. All the mixes are developing strength much in line with expectation and they might be expected to continue to do so.

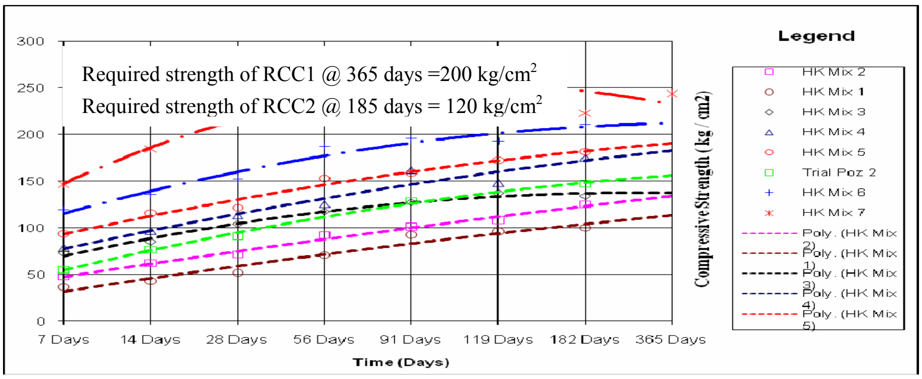

Figure 2. Development of strength with age of the Stage-I HK (Hormozgan cement + khash natural Pozzolan) series of mixes

A comparison was also made between the HK Series and the KK series of mixes (Kerman Type – II cement and Khash natural pozzolan). The strengths of the mixes containing the two different cements are very similar and it was determined that the two cement might be interchangeable.
On the basis of the data, it has been concluded that the Khash natural pozzolan could successfully be used as a cementitious material in the RCC at Jegin Dam.

3.3.2. Indian Low–Lime Fly Ash

Seven mixes have been designed containing the Indian flash. The development of strength with age of the HI series (Hormozgan Type – II cement and Indian fly ash) is shown in Figure 3.

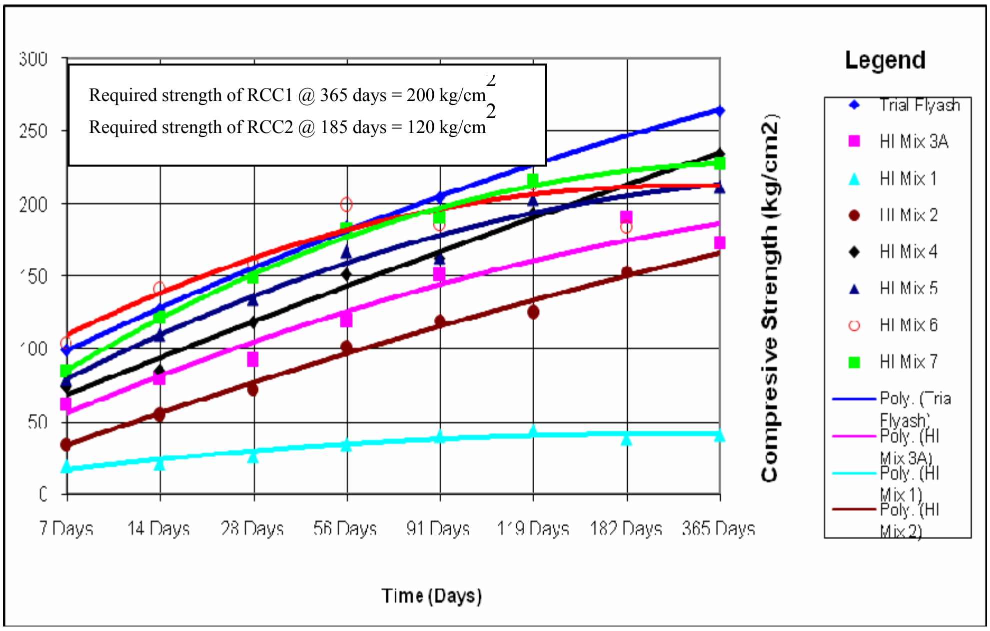

Figure 3. Development of strength with age of the Stage-I HI (Hormozgan cement + Indian low-lime fly ash) series of mixes

The development of strength of HI.Mix2, HI.Mix3 and HI.Mix4 is very similar to the pattern found at Olivenhain dam in the USA (Pauletto & Dunstan 2003), where RCCs with cylinder compressive strengths of 40 kg/cm^2 to 70 kg/cm^2 at an age of 7 days achieved, strengths of 120 to 180 kg/cm^2 at 91 days and 230 to 330 kg/cm^2 at an age of one year.
As with the HK Series, apart from some scattered results with H.Mix4, HI. Mix6 between 91 and 182 days, all the mixes are developing strength in line with expectations.
A comparison was also made between the HI Series and the KI Series of mixes (Kerman Type-II cement and Indian fly ash). As with the KK Series the mixes containing the two different cements are developing strength along similar lines.

The two type – II Portland cement (Hormozgan and Kerman) seem to have similar characteristics when used in association with both the supplementary cementitious materials at Jegin.

It would be possible to design an RCC containing the Indian fly ash (it has very good fresh properties) to achieve the strength requirements at Jegin, but given that the material has to be imported, it was concluded that it would only be sensible to use the material if there was a serious problem with the supply of the Khash natural pozzolan.

3.3.3. Esfahan Ground Slag

Initially it was thought that the Esfahan slag was granulated when discharged from the blast furnace. It is now understood that the material is air cooled. No ground air–cooled blast-furnace slag has been used in an RCC dam to date.

Seven mixes were designed containing the Esfahan GBFS (ground-granulated blast-furnace slag) but unfortunately the performance was found to be very poor. On the basis of the data to date and considering the difficulty to mill the material and the 1450 km it would have to be transported (see Figure 1), it has been concluded that the use of the Esfahan GBFS as a cementitious material in the RCC at Jegin would seem to be unlikely and it is no longer being considered for use in the dam.

3.4. Supplementary Stage 1 Programme

Following the 91 days results of the stage 1 trail mix programme, a supplementary programme was designed so as to have a preliminary look at the RCC1 mix and the leveling concrete, together with some potential retarders. Only Khash natural pozzolan was used as a pozzolan in this Series.

3.4.1. RCC1

Three rcc1 mixes were tried in the supplementary programme: 175+50 (cement + pozzolan), the expected mix; 160 + 65 (a lower-strength mix); and, 190 + 35 (a higher- strength mix). All had a total cementitious content of 225 kg/m^3. The mixes were designed to achieve target strength of 225 kg/cm2 at the age of one year. To achieve such strength with a 100 percent Portland cement RCC, the same cement content of 225 kg/cm^2 would be required (HK. Mix6 and HK.Mix7) and as there would be little strength gain after an age of 56 days.

It is expected that RCC1-3 (190+35) almost achieve the target cylinder compressive strength of 225 kg/cm^2 at the design age of 365 days, and the supplementary Stage 1 programme showed that it was possible to achieve the specified strength even without an admixture, at a rather high cementitious content.

3.4.2. Leveling Concrete

Three leveling concretes were designed for the supplementary programme: 160+120+195 (cement + pozzolan + water) the expected mix; 145+135+195 (a lower-strength mix); and, 175+105+195 (a higher-strength mix). All the mixes had a total cementitious content of 280 kg/m3, and all were designed for a slump of 35 t0 50mm and for a 182 day cylinder compressive strength of about 145kg/cm^2. The total cementitious content is necessary rather high, because of the very high water demand of the Jahgin aggregates.

3.4.3. Retarder

Admixture s from five or six different suppliers tested during the supplementary programme. After a number of preliminary tests, two retarders were chosen for future study: Sitka Retarder and Forsook Conplast R. After an extensive further study Conplast R was chosen for use in the RCC for Jegin.

4. TRIAL MIX PROGRAMME – STAGE 2

4.1. Aggregate

The Stage 2 aggregate was obtained from the same source as the Stage 1 aggregate, but the shape was rather better, this was a function of the development of the new aggregate plant.

4.2. Optimization of Mixture Proportions for Stage 2 Trial Mix Programme

Following the stage-I trial mix programme, it was agreed that the natural pozzolan from khash be used in the RCC for the Jegin. The RCCs containing Khash natural pozzolan will have the properties, both fresh and hardened, required for the dam. It was decided that the following mixes be studied in detail in the Stage-II trial mix programme.

The necessary dosage of retarder to produce an initial set of 15 to 20 hours at different temperature; an RCC2, and RCC1 and a leveling concrete with both the Khash natural pozzolan and the Indian fly ash as detailed in Table 2; Grout Enriched Vibratable RCC for the interface (upstream and downstream faces and against the abutment).

It has been agreed that the khash natural pozzolan should be the preferred option and that the Indian fly ash should be a back up.

Three batches, from each of which eight cylinders were manufactured, were made for each of the mixes in Table 2.

The cylinders are being tested at ages of 7, 14, 28, 56, 91, 182, 365 and 1000 days.

The development of strengths with age of specimens manufactured (in Stage–II trial mixes) with Hormozgan Type–II cement and khash natural pozzolan as well as Indian fly ash are shown in Figures 4 and 5.

4.3. Recommended Mixture Proportions Used in Jegin Dam

Three mixes were required for the main dam at Jegin:

- RCC1 designed for required cylinder compressive strength of 200 kg/m^2 at the design age of a year;
- RCC1 designed for required cylinder compressive strength of 120 kg/m^2 at the design age of a 182 days;

A leveling concrete placed against the foundation as a platform for the RCC having a required cylinder xcompressive strength of 200 kg/cm^2 at the design age of a year.

Table 2: Suggested mixture proportions for the concrete studied in the Stage-II trial mix Programme for Jegin dam

Mix	Cement (kg/m3)	Pozzolan (kg/m3)	Slump (mm)	L. V Be time (s)
Khash natural pozzola				
HK.RCC.1-1	150	75		10 - 15
HK.RCC.1-2	165	60		10 –15
HK.RCC.1-3	180	45		10 - 15
HK.RCC.2-1	90	105		12 - 18
HK.RCC.2-2	105	90		12 - 18
HK.RCC.2-3	120	75		12 - 18
HK.Levelling.1	135	145	10 - 40	
HK.Levelling.2	150	130	10 - 40	
HK.Levelling.3	165	115	10 - 40	
HK.Levelling.4	165	85	10 - 40	
HK.Levelling.5	180	70	10 - 40	
HK.Levelling.6	195	55	10 - 40	
Indian low-lime fly ash				
HI.RCC.1-1	95	125		10 - 15
HI.RCC.1-2	110	110		10 –15
HI.RCC.1-3	125	95		10 - 15
HI.RCC.2-1	70	125		12 - 18
HI.RCC.2-2	85	110		12 - 18
HI.RCC.2-3	100	95		12 - 18

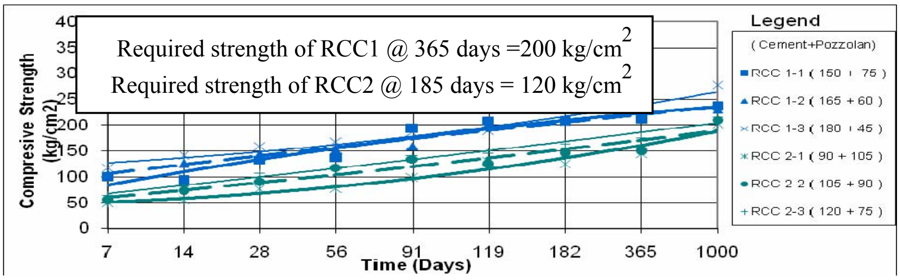

Figure 4. Development of strength with the age of the RCC-1, RCC-2 mixes containing Khash natural pozzolan

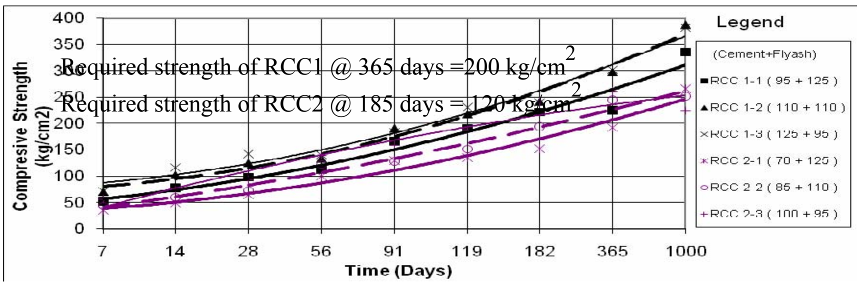

Figure 5. Development of strength with the age of the RCC-1, RCC-2 mixes containing low - lime Fly ash

In order to decide the final mixes used in the dam body, it was of interest to compare the results from the cofferdam RCC with the strengths of RCC2-3 from the Stage-II programme and with HK.Mim3 from the Stage-1 programme (see Table 3). As can be seen in the Table 5, RCC2-3 has higher long term strength than HK.Mix3 (because of water reduction of the retarder). However the strengths of the specimens manufactured from the RCC placed in the coffer dam are significantly higher than those of RCC2-3, by about 15 % at the design age of 182 days.

Table 3. Comparison between the strength of the various RCC mixes having proportion of 120 +75 (Hormozgam Portland cement + Khash natural pozzolan)

	Cylinder compressive strength (kg/cm^2)			
	7 day	**28-day**	**91 day**	**182 day**
Cofferdam	88	129	179	182
Stage-II RCC2-3	64	108	142	164
Stage-I HK.Mx3	73	104	127	145

4.3.1. Optimization of Mixture Proportions Of RCC2

In the stage –II of the trial mix programme, three mixes were tried, RCC2-1 (90+105), RCC2-2 (105+90) and RCC2-3 (120+75), all with Hormozgan Portland cement, khash natural pozzolan and Fosroc Conplast R as a retarder/water reducer, together with a free water content of circa 130kg/$m^{3.}$

The results of compressive testing of three mixes (see Figure 4) have been compared to the results of testing of the HK series from Stage-I of the programme presented in Figure 2. There is a reasonable correlation, so much so that the best-fit relationships did not change significantly at any age. At the design age of 182 days, to achieve the design strength of 145 kg/cm^2, the cement and natural pozzolan contents required were almost exactly those of RCC2-2(and HK.Mix3). Given the significant difference between the strengths achieved in the field and the laboratory with RCC2-3(120+75), it might be expected that there could be a similar difference with RCC2-2 and thus a reasonable margin between the required strength and that achieved during the full-scale placement. It has been agreed that RCC2-2 will be used in the dam itself subject to a satisfactory full-scale trials).

4.3.2. Optimization of Mixture Proportions Of RCC1

None of the three mixes, RCC1-1 (150+75), RCC1-2 (165+60) or RCC1-3 (180+45) tried in Stage-II of the trial mix programme achieved the design strength at an age of 182 days and as there does not seem to be significant increase in strength between the ages of 182 and 365 days, none of the mixes is likely to achieve the design strength at the design age at 365 days.

The strengths of the stage-II RCC1 mixes, all of which had a total cementitious content of 225 kg/m^3, have been plotted in Figure 4. The results are rather scattered (as might be expected with a set of data being the average of three RCC2 mixes. In the Figure it can again be seen that none of the mixes (apart from the all-Portland cement mix) achieved the design strength (225 kg/cm^2) at an age of 182 days. In order to achieve the required strength of RCC1, the total cementitious content will have to be increased.

There is a very reasonable correlation between the Portland cement content of the all cement mixes and their long-term strength (see Figure. 2), e.g. HK.Mix6 (and KK.Mix6) (cement content=195 kg/m^3) with a long-term cylinder compressive strength of circa 200 kg/cm2 and HK.Mix7 (cement content=240 kg/cm^3) with a long-term cylinder compressive strength of circa 245 kg/cm^2. In order to achieve the design strength 0f 225 kg/cm^2, it was decided that the mixture proportions of RCC1 be 160+90+130 (cement + pozzolan + water).

Coincidently this has the same natural pozzolan content as RCC2. Thus in order to change from RCC2 to RCC1, a further 55 kg/m^3 of cement is added to RCC2.

Test results obtained from leveling concrete at Stage –II indicate that a leveling concrete having mixture proportions of 185+105+150 (cement + pozzolan + water) could be used against the foundation.

5. COFFER DAM

5.1. Preliminary Full-Scale Trial

In early March 2003, preliminary full–scale trial was conducted on the site (see Figure 12). The trial showed that an RCC containing Hormozgan Portland cement and Khash natural pozzolan was cohesive, and could be placed in very high air temperatures without segregation or any other major problem.

40 days after completion of the trial, 100-mm diameter cores were extracted from the trial section. In spite of the very early age and the small diameter the cores through the suitably-retarded RCC were very good.

Following the successful cores, placement of RCC started in the cofferdam (see Figure 13), placement of 20000 m3 was used to train all the personal involved with the project, to refine the construction methodology and to further prove the maximum proportions of the concretes used in the dam itself (3).

The final full-scale trial was conducted at the top of coffer dam using the final mixtures proportion for RCC1, RCC2 and GEVR. The extracted 45 days cores are shown in Figures 8 and 9.

Figure 6. Photograph of the initial full Scale trial at Jegin dam

Figure 7. Photograph of RCC placement in coffer dam at Jegin with chute in background

Figure 8. Typical transitions between GEVR and the RCC (24 hrs. joint)

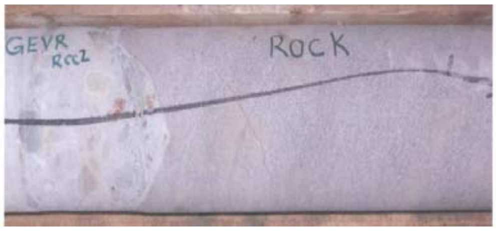

Figure 9. Typical transition between GEVR and the rock abutment

6. DESIGN OF THE DAM

Before construction of main dam and in agreement with all parties involved in Jegin dam, a number of modifications were made to the original design of the dam so as to make construction easier and thus more rapid and of a higher quality.

There were two main changes: first, all the galleries were made either horizontal or vertical. The latter were shafts and were separated in to 'man access' or 'equipment access'. The second main change was to move the bottom outlets to the left abutment, and to construct them within traditional concrete blocks, thus separating them from the RCC placement in the main body of the dam. The bottom outlets discharged on the concrete steps before joining the river downstream of the main stilling basin, see Figure 10.

A further change to the construction procedure was to remove the traditional facing concrete and replace it with GEVR (grout-enriched vibratable RCC). This had been tested successfully in the coffer dam. The dam thus relied on the RCC itself for impermeability (5).

Figure 10. Down-stream and up- stream view of Jegin dam

7. CONSTRUCTION OF DAM

7.1. Concrete Production

The geometry of the dam site and the relatively reduced space to locate the installations were the additional difficulties for the design of the plants. Figure11 shows the final layout of the concrete and cooling plants at right abutment at Jegin dam site. The supply of the aggregate from the main stockpiles was done by 25-tonne dump trucks. Those trucks downloaded on receiving hoppers with a capacity from 4 to 6 hours average production. The hoppers were connected with the batching plant by automatic control systems that could feed the material into the

weighing hoppers.
The concrete plant had a nominal capacity of 2*160m^3 /hour, and consisted in two plants each with two 2.250m3 capacity horizontal twin-shaft bath type mixers. The cooling plant combined with a water chiller plant to cool the mixing water to 4degree centigrade and the flak ice plant with total capacity of 180 tone of ice per day.
The cementitious materials were transported from the cement factories to the site by road, and the natural pozzolan from Khash to the site were deliver by big-bag. In order to have a storage for cementitious materials to supply the production of more than one week, four large 800-tonne silos and eight further small 60 tone silos were erected closed to the concrete plants. A combination of both pneumatic transportation systems and screw conveyors is used to feed the receiving hoppers of each mixer.

7.2. RCC Transportation

The transportation systems selected for the transportation of concrete was a combination of 45 degree inclined steel chute and trucks on the dam. Still chute was built up in such a way that it could be removed as the dam was raised. As shown in the Figure 12, the chute was supported on the excavation on the right abutment. A surge hopper at the top of the chute regulated the flow of concrete out of mixers. The chute ended in a swinging element that moved to change its loading position from one truck to the other. Figure 12 shows a view of the chute that has been used for the transportation of roller compacted concrete in Jegin dam (1).
The chute has worked successfully, and the high-paste concrete in the RCC mix has not shown any segregation. The flexible cover on the top of the steel chute has been working as a protection against solar radiation, and thus avoiding excessive drying of the mix in its way down to the placement.


Figure 11. View of vacuum chute used at Jegin dam and general view of site lay out

7.3. RCC Placement

The RCC was transported from the delivery point of the steel chute to the point of placement on the lift by dump trucks. Dozer type D4 was then used to spread the RCC and single-drum 11 tones vibratory roller were used for compaction (see

Figure 12). However in areas where the access for the larger roller was difficult or closed to the forms, the compaction was done by small double-drum 3.5 tones roller.

A special type of cantilever formwork was used to form the faces of the dam. GEVR (grout-enriched vibrated RCC) was used against the forms instead of the conventional immersion vibrated concrete.

The great advantage of the GEVR is that just a water/cementitious material grout applied onto the surface before the RCC is spread on top of it, and then consolidated by immersion vibrators.

Transverse joints were formed inserting galvanized sheets into the fresh fully compacted RCC that are left in place acting as joint inducers. PVC membranes were inserted in the GEVR in the upstream face of the dam and downstream spillway sections to seal the transverse joints. The surface of compacted RCC was continuously cured by means of low-pressure water jets creating a thin nebula on top of the surface. Due to the extreme high temperatures on site, this was a major activity at Jahgin. Depending on the time elapsed between consecutive layers and weather conditions, different steps of treatments of the horizontal joints were defined. Cleaning of the surfaces was done by brooms and high capacity vacuum trucks.

Figure 12. View of spreading and compaction of RCC in Jegin dam

Conclusions

- A suitable supplementary cementitious material has been found in Iran for use in the RCC dam at Jegin;
- In spite of the Khash natural pozzolan having never been used in concrete before, suitable concretes containing the material have been designed and tested in the laboratory;
- Both the construction methodology and the RCC have been successfully tested at full-scale.
- In spite of the very challenging conditions at the Jegin dam site, a suitable methodology has been developed for the construction of the dam and a very forgiving RCC designed.
- The plant layout and the construction methods have been optimized and

adopted according to the changes incorporated to the design.

- We believe that with these changes and an efficient management of all activities involved, a successful RCC experience have been achieved in our project.

REFERENCES

1. A.G.Ghafuri, M.E.Omran, M.Dunstan, Trial mix programme for Jegin dam– the first major RCC dam in Iran, Proceeding of the 4th international symposium on Roller –compacted concrete, November 2003, Madrid, Spain.
2. M.E.Omren, M. Dunstan, Trial mix programme for the Jegin Roller Compacted Concrete Dam–Iran, Proceeding of Eighth CANMET/ACI, International conference on Fly ash, silica-fume, Slag and natural pozzolans in concrete, May 2004, Los Vegas, U.S.A.
3. M.E.Omran, M.J.Olapour, R.Perovdin, F.Ortaga, Experience gained during design and construction of the Jegin RCC Coffer dam. Proceeding of the 4th international symposium on Roller – compacted concrete, November 2003, Madrid, Spain.
4. J.A.Garcia, F.Villegas, C. Tejada, M. Dunstan, New Victoria dam, Western Australia, Proceeding of the international symposium on Roller–compacted concrete, November 1991, Beijing, China.
5. M.E.Omren, M. Dunstan, Material Investigation and Mix Design Programme for the Jegin RCC Dam in Iran, Proceeding of the fifth international symposium on Roller Compacted Concrete Dams, 2-4 November 2007, Guiyang, China.

CD03-005

APPLICATION OF SELF CONSOLIDATING CONCRETE IN CONSTRUCTION INDUSTRY

A. Monir Abbasi, A.A. Jalal Zadeh
Mahab Ghodss Consultant Engineering, 17 Takharestan St., Dastgerdi Ave., Tehran

ABSTRACT

Self consolidating concrete (SCC) is a novel concrete which uses in many structures in all over on the world. It is a concrete which flows under own weight and completely fills the mold, passes from congested reinforcement without any bleeding or segregation. This type of concrete contains high range water reducing admixture and often viscosity modifying admixture also more fine aggregate compared to conventional concrete. It can reduce labor requirement, increase strength, durability and productivity, eliminate noise and hazard. For these good specifications, SCC uses in improper reach concreting, dense reinforcement elements, thin layer concrete construction and so on. Mahab Ghodss consultant engineering applied SCC in some Dams and tunneling projects. This article presented some executive experience of three projects which some structure of them constructed by SCC successfully. Finally some recommendation for mix design and whole scale construction SCC in site are proposed.

Keywords: self consolidating concrete, concrete, mix proportion, rheological tests

1. INTRODUCTION

Self Consolidating Concrete (SCC) is a concrete that able to flow under its weight and completely fill the formwork, even in the presence of dense reinforcement, without the need of any vibration, while maintaining homogeneity [1].

It was first developed in Japan in 1986 [2]. SCC is used mainly for repair applications and for casting concrete in restricted areas [3]. Though showing good performance, SCC used in Japan, America and Europe and many countries in buildings, bridges, tunneling and other applications [4].

SCC can accelerate placing and reduce labor requirement, increase strength, durability and productivity, eliminate noise and hazard, but little increasing in material cost [3]. Mahab Ghodss consultant engineering as a pioneer in application of novel technology uses SCC in some project such as Karoon III Dam and power plant, Resalat tunnel and Gotvand dam and power plant. In this article specification of these SCC concrete are presented.

2. APPLICATION OF SCC IN KAROON III DAM AND POWER PLANT

Project of Karoon III Dam and power plant sited in 28 Km east of Izeh city. The main objects of this project are:

- Supply 4172 Gw.hr power in year

- Supply agricultural water for 120 Km^2 land
- Flood control of Karoon river

SCC is used in entrance structure of orifice in this dam. This structure located out of reach of cable crane and because the level of around blocks is lower than this block, pumping concrete rate is low and so, it might create cold joint in the structure. Also this structure had congested reinforcement. For whole above reasons, this structure must construct with SCC. Figure 1 shows the plan of this structure.
The cement used was type II. Maximum size of aggregates was 19 mm, sand to total aggregates ratio, water to cement ratio and paste amount were 0.58, 0.42 and about 300 respectively.

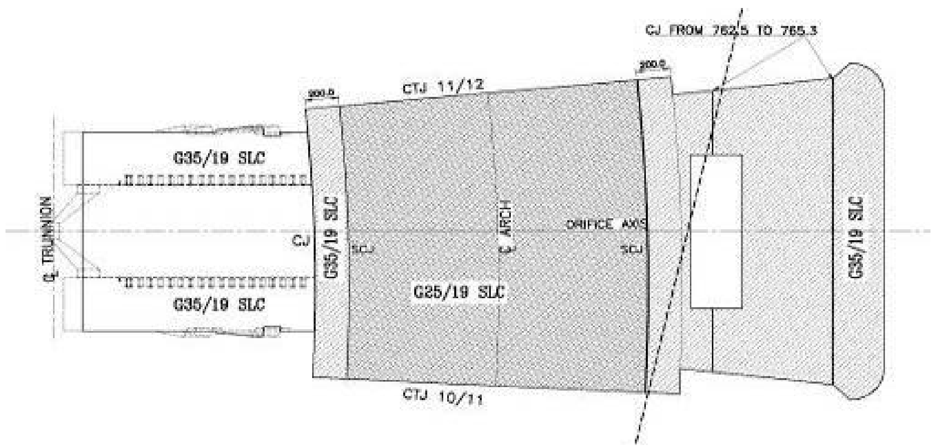

Figure 1. Plan of structure

A high range water reducing admixture which is type A, F according ASTM C494 [5] with density of 1050 also was used. The mixture proportions are presented in Table 1.

Table 1: Mixture proportions

Description	Coarse Agg.	Fine Agg.	Cement	Water	HRWR
Unit	Kg	Kg	Kg	m^3	% by weight of cement
Amount	775	1080	380	0.160	1

For shortening concrete placing area and avoiding large movement of concrete in the forms, temporary construction joints were applied.
V- Funnel and T-50 tests were drawn for fresh concrete according EFNARC [1]. Figure 2 and 3 shows the V-Funnel and T-50 tests apparatus. Compressive strength of 28 days concrete was tested according ASTM C39 [6]. Table 2 shows average of test results. The orifice concreting is shown in Figure 4.

Figure 2. V-Funnel tests apparatus

Figure 3. T-50 tests apparatus

Table 2: Average of test results

Description	T-50	V- Funnel	Compressive strength
Unit	Sec	Sec	Mpa
Amount	3.5	9	35

Figure 4. Orifice concreting

3. APPLICATION OF SCC IN RESALAT TUNNEL

Resalat tunnel is a key project which relating east and west section of Resalat highway. In this project B section of lining was built lastly and it hadn't proper access. Construction of this section with conventional concrete might cause many voids and this structure would be very weak. So we had to create SCC to build this section. Figure 5 shows the section of the tunnel lining.

In situ piles were constructed by SCC because of improper reach, congested reinforcement, and lack of vibration and also long height of concrete shooting. The SCC pile is shown in Figure 6.

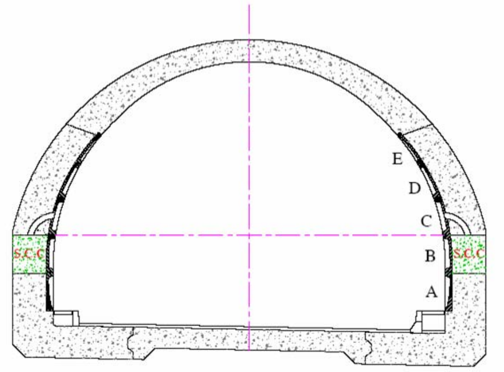

Figure 5. Lining section

Figure 6.The SCC pile

Maximum size of aggregates was 20mm and sand to total aggregates ratio, volume of paste and water to cement ratio were 0.69, about 360lit/m^3 and 0.42 respectively. High range water reducing admixture, viscosity modifying admixture were used for achieving SCC with good rheology. Also for increasing stability of fresh concrete and resistant against segregation and bleeding inert filler was added to mixture.

For compensating shrinkage strain of concrete an expanding admixture also added to SCC mixture. The mixture proportions are shown in Table 3.

Table 3: Mixture proportions

Description	Coarse.Agg Agg.	Fine.Agg Agg.	Cement	Water	Filler	HRWR	VMA	EX.A
Unit	Kg	Kg	Kg	Kg	Kg	Lit	lit	lit
Amount	530	1200	400	167	100	3.6	2.0	2.7

Slump flow and V-Funnel tests were drawn for fresh concrete according EFNARC[1]. The Result of tests is presented in table 4.

Table 4: Test results

Description	Slump flow	V-Funnel
Unit	mm	Sec
Amount	680	9

4. APPLICATION OF SCC IN GOTVAND DAM AND POWER PLANT

Gotvand dam and power plant project located in 25 Km north of shooshtar city. The major objects of this project are:

- Supply 4250 Gw.hr power in year.
- Supply agricultural water
- Flood control of Karoon river

SCC is used in some structure of this project such as around of steel lining, around of penstocks, around of spiral cases, paving of seal beam and etc. In this article concreting around of steel lining is described.

In this structure because of erection of steel pipes and multiplicity of stiffeners, there is no proper reach to molding. In such cases application of conventional concrete may cause poor concrete with many entrapped air and voids. For preventing this disease, SCC is used to concreting the structure.

Maximum size of aggregates was 19mm and sand to total aggregates ratio, volume of paste and water to cement ratio were 0.58, about 310lit/m^3 and 0.43 respectively. A high range water reducing admixture also was used to increase filling ability of concrete. The mixture proportions are shown in Table 5.

Because fine aggregate used in this project had proper grading, additional fillers or mineral additive wasn't required.

The slump flow test [1] and visual inspection were drawn for fresh concrete. The average of slump flow test was 675mm. Slump flow spread is shown in Figure 7.

Figure 7. Slump flow spread

Table 5: Mixture proportions

Description	Coarse Agg.	Fine Agg.	Cement	Water	HRWR
Unit	Kg	Kg	Kg	m^3	% by weight of cement
Amount	796	1082	380	0.164	1

5. SUMMARIZE

According to large scale SCC experience, the following recommendations are proposed:

- SCC used where it is required such as improper reach to formwork, congested reinforced concrete, thin layer concreting and so on.
- For decreasing loss of workability by time, water to cement ratio must select more than 0.4 but for increasing workability, it doesn't require increasing free water and it can accomplish by use of chemical admixtures.
- The sand used in SCC has lower fineness modulus than conventional concrete.
- Total volume of aggregates, maximum size of aggregates, average diameters of aggregates and sand grading are the significance parameters in SCC mix design.
- SCC requires curing much than conventional concrete to prevent plastic shrinkage, loss of strength and cracking.
- SCC is more sensitive to aggregate grading especially fine aggregate, amount of cement and mineral additive of filler and amount of HRWR.
- Application of SCC in construction requires more strength and no leaking formwork than conventional concrete.

ACKNOWLEDGMENTS

The authors would like to acknowledge Mahab Ghodss concrete technology group and Mr.Ghand Ali, Mr.Kiani and Mr.Zafari for their assistance in conducting this article.

REFERENCES

1. Specification and guidelines for self- compacting concrete, EFNARC, 2002, 32.
2. Su N., Hsu K., Chai H., A simple mix design method for self-compacting concrete, cement and concrete research, 2001,31,1799-1807.
3. Ghezal A., Khayat K.H., Optimizing self – consolidating concrete with limestone filler by using statistical factorial design methods, ACI Materials Journal , 2002, 99, May – June, 264-272.
4. Persson B., A comparison between mechanical properties of self-compacting concrete and the corresponding properties of normal concrete, cement and concrete research, 2001,31,193-198.
5. ASTM C 494, Standard specification for chemical admixture for concrete, 1998 Annual Book ASTM Standards, 9.
6. ASTM C39, Standard test method for compressive strength of cylindrical concrete specimens, 1998 Annual Book ASTM Standards, 5.

CD03-006

بررسی خوردگی آرماتور در عرشه تعدادی از پل‌های راه‌آهن واقع در ناحیه کویری ایران

محمد شکرچی زاده[1]، سید رحمان طاهری[2]، محسن تدین[3]، فرهاد پرگر [4]، مصطفی حق طلب [5]
۱. عضو هیئت علمی‌دانشکدهٔ مهندسی عمران، پردیس دانشکده‌های فنی دانشگاه تهران
۲. دانشجوی کارشناسی ارشد مهندسی عمران، پردیس دانشکده‌های فنی دانشگاه تهران
۳. عضو هیئت علمی‌دانشکده فنی، دانشگاه بوعلی سینا همدان
۴. کارشناس ارشد انستیتو مصالح ساختمانی دانشکده فنی دانشگاه تهران
۵. عضو هیئت علمی‌گروه مهندسی عمران، دانشکده فنی دانشگاه ملایر

چکیده

در سال‌های اخیر تعداد زیادی از سازه‌های بتنی در مناطق مختلف کشور در اثر عوامل گوناگون دچار آسیب‌دیدگی و یا خرابی زودرس شده‌اند. خوردگی میلگردها در بتن از جمله رایج ترین این خرابی‌ها در سازه‌های بتن مسلح بوده و یکی از مهمترین مشکلاتی است که امروزه مهندسان عمران در نگهداری سازه‌های بتن مسلح با آن مواجه می‌باشند. در سازه‌های بتنی که چندین سال از ساخت آنها می‌گذرد تعیین میزان و سرعت خوردگی آرماتور یکی از پارامترهای موثر در مقاوم‌سازی سازه می‌باشند.

در این تحقیق به منظور ارزیابی خوردگی آرماتورها در پل‌های راه‌آهن واقع در ناحیه کویری، آزمایش‌های مقاومت فشاری، تعیین عمق کربناتاسیون، پروفیل یون کلر، پتانسیل خوردگی آرماتور و سرعت خوردگی آرماتور بر روی عرشه پل‌ها انجام شد. در نهایت با مقایسه نتایج و ارزیابی ظاهری، دلیل اصلی خوردگی آرماتور تعیین گردید. بر اساس نتایج بدست آمده به نظر می‌رسد در ناحیه کویری ایران مشابه سواحل خلیج فارس خرابی‌های ناشی از نفوذ یون کلر وجود داشته و کیفیت نازل بتن پدیده کربناتاسیون را تسهیل و آسیب‌دیدگی را تشدید می‌کند.

کلیدواژه‌ها: خوردگی آرماتور، نیم پیل، سرعت خوردگی آرماتور،کربناتاسیون، یون کلر

۱– مقدمه

در سال‌های اخیر در مناطق مختلف دنیا، خوردگی میلگردهای فولادی در بتن به عنوان دلیل اصلی خرابی‌های زودرس و در برخی موارد تخریب کلی سازه بتن مسلح شناخته می‌شود [1]. همچنین بررسی سرعت خوردگی آرماتور به منظور مطالعه عملکرد آرماتورها در تعیین طول عمر مفید سازه‌های بتنی مسلح اهمیت دارد.

در این مقاله خوردگی آرماتور در عرشه پل‌های راه‌آهن با عمر تقریبی ۳۰ سال مورد بررسی قرار گرفت. با انجام مشاهدات ظاهری و آزمایش‌های مقاومت فشاری، عمق کربناتاسیون، پروفیل یون کلر، پتانسیل نیم پیل و سرعت خوردگی آرماتور، علت خرابی در هر دسته از پل‌ها تعیین گردید. بر اساس سوابق و شواهد و مقالات منتشر شده، آسیب‌دیدگی‌های ناشی از نفوذ یون کلر در نواحی جنوبی و حاشیه خلیج فارس گزارش شده است. این

در حالی است که در تحقیق حاضر به این نوع آسیب‌دیدگی در ناحیه کویری ایران پرداخته شده است.

۲- خوردگی فولاد در بتن

خوردگی فولاد در بتن عمدتا به‌دلیل نفوذ یون کلر و پدیده کربناتاسیون می‌باشد. اگر میلگردهای فولادی به طور آزاد در شرایط محیطی مرطوب و دارای اکسیژن محصور شده باشند، خورده خواهند شد. هنگامی‌که میلگرد در بتن مدفون می‌گردد، pH زیاد محیط بتن سبب ایجاد یک لایه محافظ اکسید آهن بر روی سطح آرماتور می‌گردد که آن را از خوردگی حفظ می‌کند. لایه اکسید آهن، پوشش متراکم و غیر قابل نفوذی را ایجاد می‌کند که با محدود کردن حرکت کاتیون‌ها و آنیون‌ها در نزدیک سطح فولاد، خوردگی را متوقف می‌کند. این لایه محافظ با کاهش pH محیط(به طور عمده به دلیل کربناتاسیون) و یا حضور یون‌های کلر و سولفات از بین می‌رود [2].

۲-۱- خوردگی ناشی از کربناتاسیون

زمانی که pH محیط اطراف میلگرد از ۱۱/۵ بیشتر باشد لایه محافظ روی میلگرد سالم باقی می‌ماند و میلگرد را از خوردگی حفظ می‌کند. زمانی که pH از این مقدار کمتر می‌شود لایه محافظ ناپایدار می‌شود و حفاظت به عمل آمده از میلگردها از بین می‌رود. کربناتاسیون بتن دلیل اصلی برای کاهش pH در بتن شناخته می‌شود. کربناتاسیون و کاهش pH ناشی از آن به طور معمول از سطح بتن آغاز می‌شود و به شکل جبهه کربناته شده به سمت مرکز بتن پیش می‌رود. سرعت کربناتاسیون به عوامل محیطی (رطوبت، دما و غلظت دی اکسید کربن هوا) و مشخصات بتن(نفوذ پذیری و قلیاییت) بستگی دارد. در یک بتن با کیفیت مناسب، سرعت کربناتاسیون در حدود ۱ میلی متر بر سال می‌باشد [3].

۲-۲- خوردگی ناشی از نفوذ یون کلر

خوردگی ناشی از یون کلر یکی از دلایل اصلی خوردگی در نقاط مختلف دنیا شناخته می‌شود. حضور یون کلر در سازه بتنی، زمانی که اکسیژن و رطوبت لازم در دسترس باشد می‌تواند باعث خوردگی میلگردهای فولادی گردد.

یون کلر به دو روش اصلی وارد بتن می‌شود:

روش اول،کلر موجود در مصالح بتن (سنگدانه‌ها، افزودنی‌ها...).

روش دوم، نفوذ یون کلر از محیط پیرامون به داخل بتن (آب دریا، نمک‌های یخزدا...).

یون کلر در داخل بتن می‌تواند به دو صورت وجود داشته باشد. یونی که با انجام واکنش‌های شیمیایی مقید شود که در نتیجه هیچ تاثیری بر فرآیند خوردگی فولاد در بتن ندارد و یا به صورت آزاد باشد.

روش ارزیابی سازه

بررسی وضعیت یک سازه بتن مسلح اولین گام برای بازسازی و ترمیم آن می‌باشد. برای تعیین علل خرابی‌ها و گستردگی آن، بررسی مقدار خوردگی و ارزیابی وضعیت کنونی سازه ضروری می‌باشد. یک بررسی دقیق شامل دو مرحله است. مرحله اول ارزیابی و مطالعه اولیه سازه بر اساس مشاهدات ظاهری است که باید ماهیت خرابی‌ها

را مشخص نماید و پایه ای برای مطالعات دقیق تر باشد. در حالی که استفاده از آزمایش‌های الکتروشیمیایی در مرحله بعد برای مطالعه وضعیت دقیق میلگردها و برآورد سرعت خوردگی ضروری است.

الف- مشاهدات ظاهری

خرابی‌های ناشی از خوردگی با استفاده از مشاهده ظاهری برنامه ریزی شده قابل تشخیص می‌باشند. طبقه بندی خرابی‌ها برپایه وضعیت ظاهری، محل و علت آن تعریف می‌شود. خرابی‌ها با توجه به گسترش ترک ناشی از خوردگی تعریف شده اند. در پروژه حاضر که شامل بررسی حدود ۳۰ پل راه‌آهن در ناحیه کویری ایران بود مساحتی در حدود ۴۰۰ متر مربع ارزیابی ظاهری شد و محل جداشدگی‌ها مشخص گردید. در این محل‌ها ترک‌های موازی سطح در نواحی که پوشش روی آرماتور از بتن اصلی جدا شده است قابل شناسایی می‌باشند. این خرابی‌ها بیشتر در نواحی که بتن در معرض رطوبت قرار دارد، رویت می‌شوند. متوسط ضخامت پوشش بتنی عرشه پل‌ها در حدود ۳۰-۲۵ میلی‌متر می‌باشد.

ب) آزمایش‌های انجام شده

بر پایه مشاهدات ظاهری، عرشه پل‌ها به دو دسته بدون خوردگی (a) و خوردگی زیاد (b) تقسیم شدند. در ادامه نتایج آزمایش‌های انجام شده ارائه می‌شود.

۳-۱- مقاومت فشاری

برای ارزیابی مشخصات سازه ای مصالح موجود، مغزه‌هایی با قطر ۱۰ سانتی متر از سازه تهیه شده و مورد آزمایش قرار گرفتند. متوسط مقاومت فشاری مغزه‌ها در دو سطح (a) و (b) در جدول (۱) ارائه شده است. این مقادیر متوسط ۳ نمونه آزمایش شده می‌باشد. با توجه به نتایج مقاومت فشاری می‌توان به طور تقریبی نسبت آب به مواد سیمانی در بتن را بین ۰/۵۵ تا ۰/۶ ارزیابی نمود. این میزان نسبت آب به مواد سیمانی برای اجرای ابنیه فنی زیاد به نظر می‌رسد و قطعا ملاحظات دوام و پایایی بتن مورد عنایت قرار نگرفته است.

جدول ۱: نتایج مقاومت فشاری مغزه‌ها

سطح خوردگی	متوسط مقاومت فشاری مغزه‌ها (kg/cm^2)
(a)	۲۱۰
(b)	۱۹۴

۳-۲- عمق کربناتاسیون

کربناتاسیون باعث کاهش pH محیط، انحلال فازهای جامد حاوی کلر مقید در محلول حفره ای، آزاد شدن کلر مقید و ایجاد کلر آزاد می‌شود. کلر آزاد شده می‌تواند وارد قسمت‌های کربناته نشده بتن شود. این پدیده موجب افزایش غلظت کلر آزاد در ضخامت بتن پوششی روی آرماتور شده و ممکن است کلر را در سطح میلگرد به مقدار بحرانی برساند. بنابراین سازه‌های حاوی کلر که کربناتاسیون در آنها رخ داده است نسبت به سازه‌هایی که فقط از یک معضل رنج می‌برند، بیشتر در معرض خوردگی قرار دارند [4، 5].

عمق کربناتاسیون را می‌توان با پاشیدن محلول فنل‌فتالئین بر روی مقطع بتن تـشخیص داد. در منـاطقی کـه تحـت تاثیر کربناتاسیون نبوده، مقدار pH بتن تقریبا" بیشتر از ۸/۵ و فنل‌فتالئین در این مناطق به رنگ ارغوانی در می‌آید.

جدول ۲: نتایج آزمایش تعیین عمق کربناتاسیون

حالت خوردگی	متوسط عمق کربناتاسیون (mm)
(a)	۳۰
(b)	۵۰

متوسط عمق کربناتاسیون سطوح بتن مسلح در جدول شماره (۲) نـشان داده شـده اسـت. مطـابق جـدول (۲) در سطوحی از بتن که خوردگی آرماتور مشاهده شده است(b)، متوسط عمق کربناتاسیون ۵۰ میلیمتر بوده که با توجه به اینکه متوسط ضخامت پوشش بتنی روی آرماتور در پل‌ها ۳۰ میلیمتر می‌باشـد، مـی‌تـوان نتیجـه گرفـت کـه آرماتورهـا در ایـن ناحیـه تحـت تـاثیر پدیـده کربناتاسـیون قـرار گرفتـه انـد. در ناحیـه(a) متوسـط عمـق کربناتاسیون۳۰میلیمتر و مساوی مقدار پوشش بتنی روی آرمـاتور مـی‌باشـد. در ایـن ناحیـه آرماتورهـا در آسـتانه قرارگیری در معرض پدیده کربناتاسیون هستند.

۳-۳- پروفیل یون کلر

برای تعیین مقدار کلر در بتن، از بخش‌های مختلف عرشه پل‌ها نمونه برداری انجام شد. میزان کلر کـل (Total Chloride) موجود، طبق استاندارد ASTM C114 اندازه‌گیری شد. پروفیل‌هـای یـون کلـر سـطوح (a) و (b) در شکل (۱) به طور نمونه نشان داده شده است. همانگونه که دیده می‌شود، مقدار یون کلر در نزدیکی آرماتور (عمق ۳۰میلی‌متر) در سطح (a) کمتر از مقدار کلر آستانه خوردگی (حدود ۰/۰۷) مـی‌باشـد[6] . در نتیجـه در سـطح (a) احتمال خوردگی تحت اثر یون کلر بسیار کم است. در حالیکه در سطح (b) مقدار کلر در نزدیکی آرماتور به مقدار کلر بحرانی نزدیکتر است. بنابراین در این سطح خوردگی تحت اثر یون کلر بسیار محتمل اسـت و بـا توجـه بـه میزان عمق کربناتاسیون و مقدار یون کلر در نزدیکی آرماتور می‌تـوان نتیجـه گیـری نمـود کـه کربناتاسـیون در ترکیب با یون کلر منجر به کاهش مقدار کلر آستانه خوردگی و توسعه وگسترش خرابی‌ها شده است.

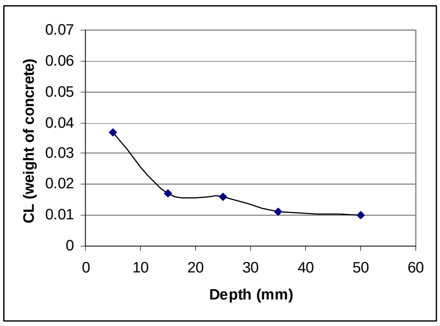

(a) **سطح بدون خوردگی**

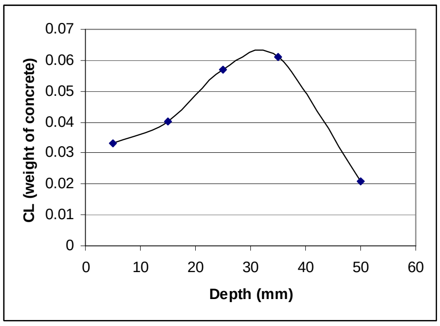

(b) **سطح با خوردگی زیاد**

شکل ۱- پروفیل یون کلر تهیه شده در دو سطح (a) و (b)

بر اساس پروفیل‌های ارائه شده به نظر می‌رسد مقدار کلر اولیه در بتن در حدود ۰/۰۱ تا ۰/۰۲ درصد وزنی بتن بوده و در محدوده مجاز می‌باشد. این در حالی‌است که کلر موجود در بتن تا عمق ۴-۳ سانتیمتر از محیط پیرامون وارد بتن شده است و به نظر می‌رسد منشا آن کلر موجود در شن‌های روان و اتمسفر در منطقه کویری و خصوصا در فصول و مواقعی که با شبنم و رطوبت همراه است می‌باشد. علاوه بر آن افت مقدار کلر در نزدیکی سطح خارجی که مشخصا در شکل (b-۱) ملاحظه می‌شود به دلیل پدیده کربناتاسیون می‌باشد که موجب تجزیه نمک فریدل و کم شدن کلر مقید و آزاد شدن آن و حرکت نمک‌ها به سمت داخل بتن می‌شود.

۳-۴- آزمایش پتانسیل نیم پیل

آزمایش تعیین پتانسیل نیم پیل، آزمایشی غیر مخرب و استاندارد می‌باشد که به طور گسترده در ارزیابی وضعیت خوردگی مورد استفاده قرار می‌گیرد. این آزمایش مطابق با استاندارد ASTM C876 و با استفاده از الکترود Ag/AgCl انجام شده است.

باید توجه داشت که حضور اکسیژن، غلظت کلر و مقاومت الکتریکی بتن تاثیر زیادی بر روی قرائت‌های ناشی از پتانسیل نیم پیل دارند. در این آزمایش معیار بررسی خوردگی طبق الکترود Ag/AgCl آرماتور چنین می‌باشد:

۸۳- mV < پتانسیل: با احتمال بیش از ۹۰ درصد، هیچ خوردگی آرماتور در زمان آزمایش وجود ندارد.

۸۳- mV > پتانسیل > ۲۳۳- mV : فعالیت خوردگی نامشخص است.

۲۳۳- mV > پتانسیل: با احتمال بیش از ۹۰ درصد خوردگی رخ داده است.

در شکل (۲) به عنوان نمونه، نتایج آزمایش پتانسیل خوردگی آرماتور برای دو سطح مذکور ارائه شده است. در شکل (۲) منفی‌ترین پتانسیل نیم پیل در ناحیه با خوردگی زیاد(شکلb-۲)، ۳۲۰- میلی ولت است. در حالیکه در ناحیه بدون خوردگی(a) این مقدار ۱۴۰- میلی ولت می‌باشد. با توجه به توضیحات ارائه شده در قبل، در سطح (b) با احتمال بیش از ۹۰ درصد، خوردگی رخ داده است. در حالیکه در سطح (a) فعالیت خوردگی نامشخص است.

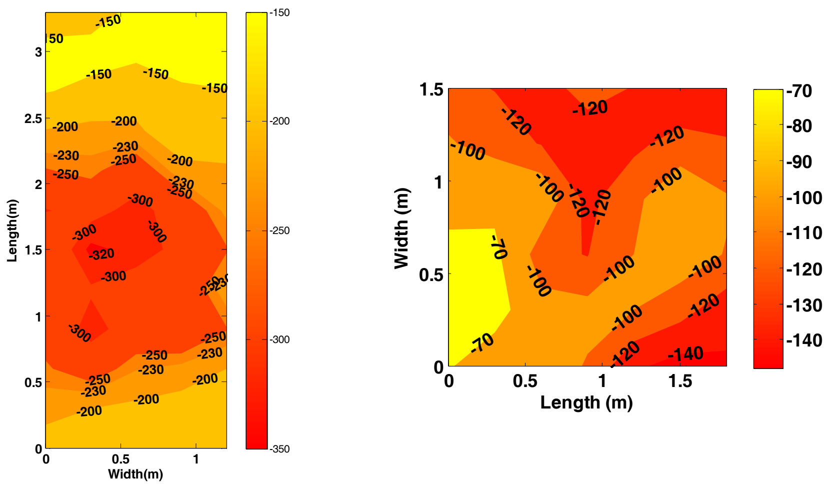

(b) سطح با خوردگی زیاد　　　(a) سطح بدون خوردگی

شکل ۲- نتایج آزمایش پتانسیل خوردگی آرماتور

۳-۵- آزمایش تعیین سرعت خوردگی آرماتور

اندازه‌گیری با دستگاه گالواپالس یک روش پلاریزاسیون سریع برای تعیین میزان خوردگی در سازه‌های بتن مسلح به حساب می‌آید. این روش بخاطر مشکلات اندازه‌گیری‌های نیم پیل در محیط‌های مرطوب و یا نیمه مرطوب بعلت کمبود اکسیژن و همینطور سرعت زیاد آن در بدست آوردن میزان خوردگی آرماتور در بتن، توسعه یافته است. با استفاده از دستگاه گالواپاس، پتانسیل نیم پیل و سرعت خوردگی آرماتور قابل تعیین می‌باشند. محدودیت‌های بحرانی برای طبقه بندی ریسک پذیری میزان خوردگی در جدول (۳) نشان داده شده است [۷].

جدول ۳: تخمین مقدار خوردگی قابل مشاهده از روی قرائت‌های انجام شده با دستگاه گالواپالس

مقدار خوردگی	مقدار اندازه‌گیری شده (µA/cm2)
در حالت مقاوم	<۰/۵
کم	۰/۵ – ۵
متوسط	۵ – ۱۵
زیاد	>۱۵

نتایج آزمایش تعیین سرعت خوردگی آرماتور به طور نمونه در شکل (۳) نشان داده شده است. همانطور که در این شکل دیده می‌شود، نقشه خطوط همتراز سرعت خوردگی در سطوح مورد نظر (a و b) قابل مقایسه با نتایج به دست آمده از پتانسیل نیم پیل (ارائه شده در شکل (۲)) است. حداکثر سرعت خوردگی در سطح (b) بیش از ۱۶ میکرو آمپر بر سانتی متر مربع می‌باشد که طبق جدول (۳) مقدار خوردگی در این سطح زیاد است و آزمایش نیم پیل نیز احتمال خوردگی را بیش از ۹۰درصد نشان می‌دهد. این در حالیست که نتایج سرعت خوردگی در سطح a حداکثر ۲/۵ میکرو آمپر بر سانتیمتر مربع است که نشان دهنده سرعت خوردگی کم می‌باشد. ضمنا مقادیر پتانسیل نیم پیل در محدوده عدم قطعیت قرار دارد.

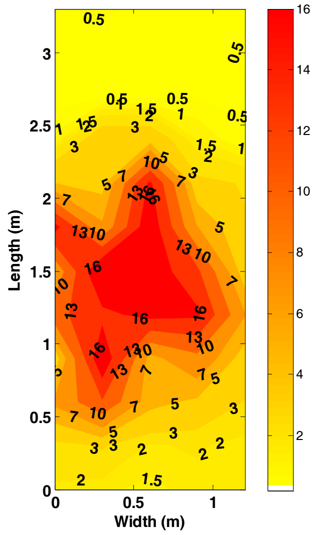

(b) سطح با خوردگی زیاد

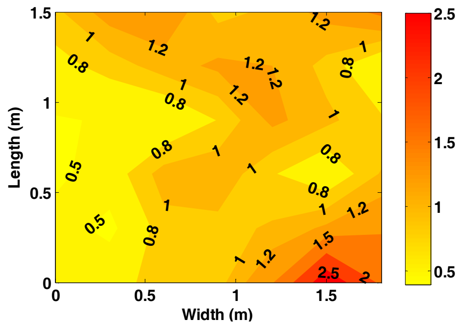

(a) سطح بدون خوردگی

شکل ۳- نتایج آزمایش سرعت خوردگی آرماتور

۴- نتیجه‌گیری

۱ – ارزیابی خرابی سازه‌های بتن مسلح به منظور ترمیم آن، باید در یک نظام منطقی اجرا شود. یـک تـرمیم بـا کیفیت نیازمند شناخت علت وقوع خرابی، مشاهدات کامل آسیب‌ها، مشخصات دقیق محل‌های آسیب دیده است.

۲ – با توجه به نتایج به دست آمده عامل اصـلی وقـوع خـوردگی در بـتن مـسلح عرشـه پـل‌هـا وقـوع پدیـده کربناتاسیون می‌باشد.

۳ – مقدار پتانسیل نیم پیل تنها احتمال خوردگی را نشان می‌دهد و حتی در برخی از حالتها استفاده از این روش با محدودیت‌هایی همراه است. در حالیکه با استفاده از روش سرعت خوردگی می‌توان مقدار خـوردگی را در نواحی خورده نشده و خورده شده و یا حتی نواحی مشکوک به خوردگی تعیین نمود.

۴ – پدیده کربناتاسیون در ترکیب با یون کلر منجر به توسعه وگسترش وسعت خرابی‌ها و خـوردگی آرمـاتور در سازه‌های بتن مسلح می‌شود. همانگونه که دیده شد، در سطوح دارای شدت خرابی زیاد، خوردگی تحت اثـر توام کربناتاسیون و یون کلر رخ داده است. در حالیکه در سطوح دارای شدت خـوردگی کـم خـوردگی تنهـا ناشی از پدیده کربناتاسیون محتمل می‌باشد.

۵ – بر اساس مطالعات انجام شده در قالب این تحقیق مشخص می‌شود که خوردگی ناشی از نفوذ یون کلـر در کشور محدود به سواحل و جزایر خلیج فارس نمی‌شود و در نواحی مرکزی کشور خصوصا در نواحی کویری این نوع خرابی‌ها وجود دارد. بدیهی‌است اجرای سازه‌ها و ابنیه بتنی با کیفیت نـازل و نـسبت آب بـه مـواد سیمانی زیاد موجب بروز پدیده کربناتاسیون و تشدید فرایند خوردگی و آسیب‌دیدگی بتن خواهد شد.

مراجع

1. Vaysburd A.M., Emmons P.H., 2004, Corrosion inhibitors and other protective systems in concrete repair: concepts or misconcepts, Cement and Concrete Composites, Vol. 26, NO. 3, PP. 255-263.
2. Ghods, P., 2006, Literature Review, Depassivation of steel in concrete, Carleton University, Department od Civil and Environmental Engineering.
3. Kurtis K.E., Monteiro P., 1999, "Analysis of Durability of Advanced Cementitious Materials for Rigid Pavement Construction in California", Pavement Research Center-Institute of Transportation Studies- University of California at Berkeley.
4. Bertolini, L., Elsener, B., Pedeferr, P., Polder, R., 2004, Corrosion of steel in concrete, Prevention, Diagnosis, Repair, Wiley-VCH.
5. Broomfield J.P., 1997, Corrosion Of Steel in Concrete, E & FN SPON, London.
6. Shekarchizadeh, M., Pargar, F., 2008, "Investigation of Chloride Threshold Value in an old Concrete Structure", Journal of Faculty of Engineering, University of Tehran, Issue 42. Vol. 6.

۷. پرگر، فرهاد، اردیبهشت ۱۳۸۵، «بررسی پارامترهای موثر بر غلظـت کلـر بحرانـی بـرای شـروع خـوردگی میلگردهای فولادی در بتن»، پایان‌نامه کارشناسی ارشد در رشته مهندسی عمران، دانشکده فنـی دانـشگاه تهران.

CD03-007

بتن ریزی در هوای سرد و اقدامات اصلاحی در جهت کاهش مدت زمان اجرای اسکلت بتنی با سیستم قالب تونلی

سعید اسعدی

چکیده

از آنجائیکه در سیستم قالب تونلی همواره موضوع مدیریت زمان مطرح می‌باشد لذا بتن ریزی در هـوای سـرد از اهمیت خاصی برخوردار بوده و با توجه به سرمای شدید در منطقـه آذربایجـان کـه معمـولا بـتن ریـزی در اکثـر پروژه‌ها متوقف می‌شود، با اجرای تمهیداتی از قبیل ساخت و نـصب هیترهـای برقـی فـن دار در داخـل تونلهـا و پوشش‌های مناسب و استفاده از مشعل و لوله گرمایشی و... امکان بتن ریزی در هوای سرد و بـالابردن مقاومـت بتن میسر می‌گردد.

۱ - تامین ضوابط آیین نامه ای

مطابق مبحث ۹ مقررات ملی ساختمان هوای سرد به وضعیتی اطلاق می‌شود که برای ۳ روز متوالی شـرایط زیـر برقرار باشد.

الف – دمای متوسط هوا در شبانه روز کمتر از ۵ درجه سلسیوس باشد.

ب – دمای هوا برای بیشتر از نصف روز از ۱۰ درجه سلسیوس زیادتر نباشد.

به منظور اطمینان کافی از وضعیت نگهداری بتن در پروژه آذران دمای بـتن در طـول شـبانه روز ۲ بـار در نقـاط مختلف سازه ثبت می‌شود.

برای رساندن دمای بتن به حد مطلوب هنگام اختلاط بتن از آب گرم استفاده شده و مطابق آیین نامـه، از تمـاس

مستقیم آب گرم با سیمان در صورتی که دمای آن بیش از ۴۰ درجه سلسیوس باشد در حین ریختن مصالح در مخلوط کن، کنترل لازم به عمل می‌آید.

انتخاب نسبت آب به سیمان با توجه به روند کسب مقاومت در دمای محیط بوده و کمتر از ۰/۴ می‌باشد.

عمل آوردن بتن تازه حداقل به مدت ۲۴ ساعت و تا رسیدن به مقاومت ۵ مگاپاسکال ادامه می‌یابد.

عمل آوری بتن با استفاده از پوشش (رولهای پشم شیشه که در داخل نایلون قرار داده می‌شود) و گرم کردن داخل تونلها با هیترهای برقی و گازی تا ۱۵ درجه سانتی گراد انجام می‌گیرد.

مزیت استفاده از هیترهای برقی و گازی نسبت به گرم کننده‌ها با مواد سوختی نظیر نفت و گازوئیل به این علت است که از احتمال تبخیر آب و کربناتی شدن سطوح بتنی در اثر احتراق، جلوگیری به عمل آید.

با توجه به اینکه در سیستم قالب تونلی به جهت افزایش سرعت عملیات اجرایی، باز کردن قالب‌ها در مدت زمان کمتری از زمان تعریف شده در مبحث ۹ مقررات ملی انجام می‌شود، لذا از مواد روان کننده که خاصیت تندگیرکننده دارند استفاده و برای مراقبت بتن بعد از قالب برداری از پایه‌های اطمینان در وسط دهانه‌ها استفاده شده و دقت لازم بعمل می‌آید تا همیشه پایه‌های اطمینان در دو طبقه متوالی وجود داشته باشند و تا حد امکان هر دو پایه اطمینان نظیر در دو طبقه، روی هم و در امتدادی واحد قرار گیرند.

بلوک A1 - زمستان ۸۶

بلوک B1 - زمستان ۸۶

۲- تهیه آبگرم بچینگ

برای تهیه آبگرم لازم در بچینگ از تانکر آب و استتار کردن آن و مجهز نمودن به سیستم گرمایش بوسیله مشعل‌های گازی، همراه با نصب ترموستات جهت رسانیدن دمای آب بتن به ۶۰c، استفاده می‌شود.

مشعل گرمایشی جهت حرارت به قسمت پایین تانکر آب بچینگ

بچینگ بتن زمستان ۸۷

جلوگیری از یخ زدن مصالح بچینگ

با اجرای لوله‌کشی در محل دپوی مصالح بچینگ و نصب گرم کن با مشعل گازو ئیلی و عبور دادن هوای گرم از

داخل لوله‌ها، از یخ زدگی مصالح جلوگیری می‌شود.

مشعل گرمایشی

لوله گرمایشی

جهت حفظ حرارت در محل دپوی مصالح بچینگ، سطح مصالح را با رول‌های پشم شیشه (با کاور نایلونی) پوشانیده و بر روی آن چادر برزنتی کشیده می‌شود.

در قسمت پایین با گذاشتن یک خرک و ایجاد اختلاف ارتفاع، با قرار دادن هیترهای برقی فن دار، سطح فوقانی مصالح گرم نگه داشته می‌شود.

پوشش دپوی مصالح بچینگ

۴- تامین گرمایش داخل قالب‌های تونلی

جهت جلوگیری از افت دمای بتن هنگام بتن ریزی حدود ۱۲ ساعت قبل از بتن ریـزی بـا قـرار دادن هیترهـای برقی فن دار در داخل قالب‌های تونلی و استتار آنها در قسمت خروجی با چادر، گرمایش داخل قالب تـونلی تـامین شده و دمای قالب‌ها به ۱۰°C می‌رسد.

هیتر برقی فن‌دار

استتار قسمت خروجی قالب تونلی

۵- عمل آوری و کنترل دمای بتن

به منظور جلوگیری از افت دمای بتن در محل بـتن ریـزی، مقـدار تهیـه بـتن در بچینـگ در هـر مرحلـه، بـه ۲ مترمکعب تقلیل و بدین ترتیب مدت زمان حمل مصرف بتن کاهش می‌یابد.

پوشش روی بتن توسط پشم شیشه و برزنت

پس از اتمام بتن ریزی، گرمایش داخل قالب‌های تونلی تا مدت ۴۸ ساعت بعد از بتن ریزی ادامه یافتـه و سـطح بتن با پشم شیشه پوشانیده و بر روی پشم شیشه نیز همانند پوشش روی مصالح بچینگ، چادر کشیده می‌شود، و

آرماتورهای انتظار ریشه دیوارها با نایلون پوشانده می‌شود. با رعایت موارد فوق الذکر تا دمای ċ ۱۸- نیـز بـتن ریزی انجام گردید. در زمستان سال ۸۶ که متوسط دمای شهر جدید سهند به دمای ċ ۱۵- رسید، کل تعطیلـی پروژه به مدت ۸ روز آن هم بدلیل کولاک شدید بود.

بتن‌ریزی در شب

کاهش مدت زمان اجرای اسکلت بتنی و اقدامات اصلاحی

۱ – اقدامات انجام گرفته جهت کاهش مدت زمان اجرای اسکلت بتنی

در راستای تحقق و نیل به اهداف کیفی تعیین شده از طرف شرکت مادر در سال ۸۷ که کاهش مدت زمان اجرای اسکلت بتنی پروژه آذران به میزان ۵۰ درصد نسبت به سال ۸۶ مد نظر قرار گرفتـه، از همـان ابتـدای سـال ۸۷ برای هر یک از بلوک‌ها، مطابق نمودارهای پیوستی (صـفحات ۵۲ الـی ۶۴) جهـت مقایـسه مـدت زمـان اجـرا، شناسنامه مدت زمان اجرای اسکلت تهیه گردید به طوریکه بیشترین مدت زمان اجرای اسکلت مربـوط بـه بلـوک A1 در مدت ۱۲۸ روز و کمترین مدت اجرا مربوط به بلوک A3 در مدت ۷۳ روز انجام گرفته است.

بیشترین زمان اجرای یک نیم ست در بلوک A1 به مدت ۸ روز و با مطالعه و رفع موانع، در بلوک B3 بـه ۲ روز رسید

بطور خلاصه مواردیکه در سرعت دادن کار اجرا ی اسکلت نقش اساسی داشته اند به شرح زیر می‌باشد:

۱- افزایش سرعت بتن ریزی با اضافه کردن حجم پاکت به میزان ۰/۸ مترمکعب

افزایش حجم پاکت بتن به مقدار ۰/۸ مترمکعب

۲- کوتاه نمودن مسیر حمل بتن و اضافه نمودن تراک میکسر جهت حمل بتن.

۳- افزودن تعداد نفرات پیمانکار

۴- به منظور جابجایی قالب‌های کناری، میانی و Plat formها با توجه به اختلاف محل بست قالب، از سیم بکسل جداگانه مخصوص به همان قالب استفاده می‌شد که باز و بسته کردن مجدد سیم بکسل‌ها باعث کندی عملیات می‌گردید، با تجمیع کل سیم بکسل‌ها در قلاب تاورکرین و تعویض از همان قسمت سرعت جابجایی قالب‌ها افزایش یافت.

تجمیع سیم بکسل‌ها در قلاب تاور جهت جابجایی سریع قالب‌ها

۵- انجام عملیات تمیز کاری و روغن کاری قالب‌ها به هنگام خروج برروی پلت فرم (PLAT FORM) و انتقال به نیم ست دیگر (توضیح اینکه قبلا کار تمیز کاری و روغن کاری قالب‌ها پس از انتقال آنها به سطح زمین صورت می‌گرفت و سپس به نیم ست بعدی انتقال داده می‌شد)


تمیزکاری و روغن کاری قالب‌ها در روی پلت فرم‌ها

۶- تعلیم و آموزش کارگران و استادکاران جهت افزایش بینش آنها به احداث ساختمان با دید صنعتی
۷- تعریف وظیفه و تخصص خاص برای هر نفر (مثلا نصاب باز شو، نصاب قالب‌های کناری و غیره)
۸- افزایش ساعات کاری کارگاه (شروع تایم کاری در تابستان از ساعت ۶ صبح تا ۲۰ شب)
۹- انتخاب پیمانکار جداگانه جهت اجرای کلیه عملیات جوشکاری در دیوارها و سقف‌ها

۲- مطالعه و بررسی در سرعت دادن به عملیات الکتریکی

۱- لوله‌های تولیدی کارخانه یزد پولیکا از نوع PVC طوسی نسوز که قبلا استفاده می‌شد و مقاومت فشاری عمودی کافی نداشت با نوع پلیکای PVC سخت نسوز سفید تولیدی کارخانه ثابت پلی اتیلن تعویض شد که این امر باعث کاهش تعداد لوله‌های شکسته شده در مرحله اجرای مش دوم سقف و بتن ریزی گردید.
۲- تهیه نقشه ثابت SHOP DRAWING
۳- تهیه شابلن و فنر خم متناسب با سایز لوله جهت ایجاد خم لوله‌های برق دیوارها


خم کاری لوله‌ها با استفاده از فنر و شابلن خم

۴- تهیه شابلن جهت ساخت بوشنهای سر لوله‌های برق دیوارها بصورت سری
۵- سوراخ کاری محل ورود لوله‌ها به قوطی‌های کلید و پریز به صورت سری
۶- تهیه پلا ستفوم جهت محل قرارگیری لوله‌های انتظار سقف و دیوار و محل باز شوها با توجه بـه ابعـاد آنهـا و ایجاد سوراخهای لازم در آنها به صورت سری.

استفاده از پلا ستفوم جهت محل قرارگیری لوله‌های انتظار سقف

استفاده از پلا ستفوم جهت محل قرارگیری لوله‌های انتظار دیوار

۷- علامت گذاری لوله‌ها با رنگهای متنوع برای شناسایی محل سیستمهای مختلف از جمله روشنائی پریز بـرق و تلفن و آنتن و درب باز کن برای تسریع در لوله گذاری سقف درکارگاه موقت.
۸- کد گذاری و دسته بندی لوله‌های خم و غلافهای جفت و تکی و قوطی‌های سوراخ شده بـا توجـه بـه تعـداد سایز آنها در نقشه SHOP DRAWING جهت جلو گیری از اشتباه نفرات پیمانکار در مرحله اجرا.
۹- کدگذاری و دسته بندی با توجه به تعداد آنهـا در نقـشه SHOP DRAWING جهـت جلـوگیری از اشـتباه نفرات پیمانکار در مرحله اجرا صورت می‌گیرد.
۱۰- ساخت غلاف فلزی قوطی‌های کلید و پریز از لوله سبک نرده ای به قطر ۱/۴ ۲ اینچ و جوش ۲ عدد میلگرد نمره ۵ بطول ۴۰ سانتی متر و بستن آن با سیم آرماتوربندی به مش دیوارها، جهت قرارگیری محل دقیق قـوطی کلید و پریز و فاصله از دیواره قالب تونلی

غلاف قوطی‌های کلید و پریز

۱۱- حضور مستمر ناظر تاسیسات برقی در زمان بتن ریزی و آموزش یک نفر به عنوان کارگر فنی جهت کنترل و ترمیم لوله‌ها در صورت شکستگی لوله‌ها در حین بتن ریزی

ترمیم شکستگی لوله‌ها در حین بتن ریزی

۳- مطالعه و بررسی در سرعت دادن به عملیات مکانیکی

۱- لوله‌کشی سیستم فاضلاب و ونت (لوله‌های به قطر ۵۰ الی ۶۳ میلیمتری) معمولاً با انجام شیارکنی و برش کاری دیوارهای داخلی و خارجی صورت می‌گرفت که موجب تخریب دیوارها و افزایش نخاله می‌شد. در پروژه آذران یک غلاف از جنس لوله PVC با یک سایز بزرگتر از لوله مورد نظر همزمان با اجرای دیوارها در داخل دیوار قرار داده و بعد از اتمام دیوارچینی غلاف را برداشته و برای استفاده مجدد به طبقه دیگر انتقال می‌یابد که بدین ترتیب از تخریب دیوار جلوگیری می‌شود.

استفاده از غلاف جهت جلوگیری از تخریب دیوارها در هنگام لوله کشی

۲- محل عبور لوله‌های آب شهری به داخل واحدها، مطابق نقشه‌های اجرایی در مشاعات و داخل واحدها به صورت زیرسقفی مشخص و از نظر معماری نیاز به اجرای سقف کاذب دارد. در بلوک‌های تیپ A لوله‌های نمایان به مقدار ۴۰۳۲ مترطول و در تیپ B به مقدار ۱۶۲۰ مترطول می‌باشد. با تغییر نقشه‌های اجرایی و اجرای لوله‌ها بصورت توکار از هزینه مربوط به خرید مصالح و دستمزد اجرای سقف کاذب شامل (خرید مصالح از قرار هر مترطول به مبلغ ۵۰۰۰۰ ریال – رابیتس بندی ۵۰۰۰ ریال – گچ و خاک ۲۵۰۰۰ ریال – دستمزد آهن کشی به مبلغ ۳۰۰۰۰ ریال) جمعاً به ازای هر مترطول به مبلغ ۱۰۰۰۰۰ ریال، به مبلغ کل ۵۶۵/۲۰۰/۰۰۰ ریال صرفه جویی گردید.

۳- اجرای ساپورت لوله‌ها در داکتهای تاسیساتی معمولاً پس از اتمام اسکلت انجام می‌شود. در پروژه آذران عملیات آهن کشی داکتها با استفاده از مصالح پرت حاصل از نبشی کشی دیوارهای خارجی، همزمان با اجرای اسکلت با قرار گرفتن شاخکهای فلزی در داخل بتن اجرا می‌شود.

آهن‌کشی داکتها در حین بتن ریزی

۴- جهت کاهش عملیات آهن کشی در چاهک‌های آسانسور بلوک‌های تیپ A و B، دیوارهای برشی در

طبقات (یک ضلع در بلوک A و سه ضلع در بلوک B) پلیت‌گذاری شده و از حجم عملیات آهن کشی به مقدار ۶۰ درصد در بلوک‌های تیپ B و ۳۰ درصد در بلوک‌های تیپ A کاسته شده است.

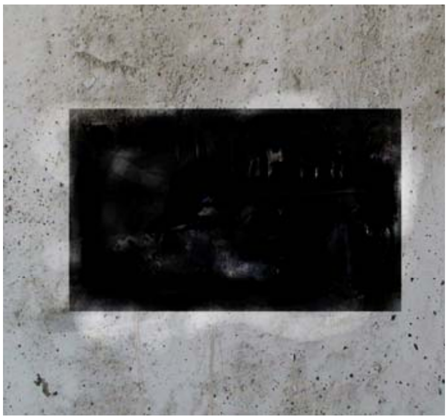

پلیت گذاری دیوار بتنی چاهک‌های آسانسور

۵- نقشه‌های تاسیسات مکانیکی در رابطه با هماهنگی محل اوپنینگ‌ها (داکتهای تاسیساتی) با نقشه‌های معماری و سازه و با در نظر گرفتن طول اتصالات مصالح مصرفی در لوله کشی سیستم فاضلاب سرویس‌ها و رایزرهای آب باران اصلاح شده و در این رابطه نقشه‌های ازبیلت SHOP-DROWING تهیه گردید.

۶- جهت اجرای بازشوهای مربوط به تاسیسات مکانیکی در سقف‌ها در زمان بتن ریزی سقف، نسبت به ساخت قالب‌های فلزی مربوط به محل عبور لوله با دو سایز بیشتر از قطر لوله‌ها به شکل کونیک اقدام گردید.

برای اینکه محل بازشوها در طبقات در امتداد هم قرار بگیرند، مختصات مرکز بازشو در سقف قالب تونلی سوراخ کاری شده و با قرار گیری پین قالب بازشو (میلگرد نمره ۱۶) در سوراخ مذکور و بعد از گیرش اولیه بتن، قالب مذکور برای استفاده در سقف طبقه بعدی برداشته می‌شود.

قالب فلزی محل عبور لوله‌ها از سقف بتنی

CD03-009

بررسی خوردگی آرماتور در عرشه تعدادی از پل‌های راه‌آهن واقع در ناحیه کویری ایران

محمد شکرچی زاده[۱]، سید رحمان طاهری[۲]، محسن تدین[۳]، فرهاد پرگر [۴]، مصطفی حق طلب [۵]

۱. عضو هیئت علمی‌دانشکدهٔ مهندسی عمران، پردیس دانشکده‌های فنی دانشگاه تهران

۲. دانشجوی کارشناسی ارشد مهندسی عمران، پردیس دانشکده‌های فنی دانشگاه تهران

۳. عضو هیئت علمی‌دانشکده فنی، دانشگاه بوعلی سینا همدان

۴. کارشناس ارشد انستیتو مصالح ساختمانی دانشکده فنی دانشگاه تهران

۵. عضو هیئت علمی‌گروه مهندسی عمران، دانشکده فنی دانشگاه ملایر

چکیده

در سال‌های اخیر تعداد زیادی از سازه‌های بتنی در مناطق مختلف کشور در اثر عوامل گوناگون دچار آسیب‌دیدگی و یا خرابی زودرس شده‌اند. خوردگی میلگردها در بتن از جمله رایج ترین این خرابی‌ها در سازه‌های بتن مسلح بوده و یکی از مهمترین مشکلاتی است که امروزه مهندسان عمران در نگهداری سازه‌های بتن مسلح با آن مواجه می‌باشند. در سازه‌های بتنی که چندین سال از ساخت آنها می‌گذرد تعیین میزان و سرعت خوردگی آرماتور یکی از پارامترهای موثر در مقاوم‌سازی سازه می‌باشند.

در این تحقیق به منظور ارزیابی خوردگی آرماتورها در پل‌های راه‌آهن واقع در ناحیه کویری، آزمایش‌های مقاومت فشاری، تعیین عمق کربناتاسیون، پروفیل یون کلر، پتانسیل خوردگی آرماتور و سرعت خوردگی آرماتور بر روی عرشه پل‌ها انجام شد. در نهایت با مقایسه نتایج و ارزیابی ظاهری، دلیل اصلی خوردگی آرماتور تعیین گردید. بر اساس نتایج بدست آمده به نظر می‌رسد در ناحیه کویری ایران مشابه سواحل خلیج فارس خرابی‌های ناشی از نفوذ یون کلر وجود داشته و کیفیت نازل بتن پدیده کربناتاسیون را تسهیل و آسیب‌دیدگی را تشدید می‌کند.

کلیدواژه‌ها: خوردگی آرماتور، نیم پیل، سرعت خوردگی آرماتور،کربناتاسیون، یون کلر

۱- مقدمه

در سال‌های اخیر در مناطق مختلف دنیا، خوردگی میلگردهای فولادی در بتن به عنوان دلیل اصلی خرابی‌های زودرس و در برخی موارد تخریب کلی سازه بتن مسلح شناخته می‌شود [1]. همچنین بررسی سرعت خوردگی آرماتور به منظور مطالعه عملکرد آرماتورها در تعیین طول عمر مفید سازه‌های بتنی مسلح اهمیت دارد.

در این مقاله خوردگی آرماتور در عرشه پل‌های راه‌آهن با عمر تقریبی ۳۰ سال مورد بررسی قرار گرفت. با انجام مشاهدات ظاهری و آزمایش‌های مقاومت فشاری، عمق کربناتاسیون، پروفیل یون کلر، پتانسیل نیم پیل و سرعت خوردگی آرماتور، علت خرابی در هر دسته از پل‌ها تعیین گردید. بر اساس سوابق و شواهد و مقالات منتشر شده، آسیب‌دیدگی‌های ناشی از نفوذ یون کلر در نواحی جنوبی و حاشیه خلیج فارس گزارش شده است. این

در حالی است که در تحقیق حاضر به این نوع آسیب‌دیدگی در ناحیه کویری ایران پرداخته شده است.

۲- خوردگی فولاد در بتن

خوردگی فولاد در بتن عمدتا به‌دلیل نفوذ یون کلر و پدیده کربناتاسیون می‌باشد. اگر میلگردهای فولادی به طور آزاد در شرایط محیطی مرطوب و دارای اکسیژن محصور شده باشند، خورده خواهند شد. هنگامی‌که میلگرد در بتن مدفون می‌گردد، pH زیاد محیط بتن سبب ایجاد یک لایه محافظ اکسید آهن بر روی سطح آرماتور می‌گردد که آن را از خوردگی حفظ می‌کند. لایه اکسید آهن، پوشش متراکم و غیر قابل نفوذی را ایجاد می‌کند که با محدود کردن حرکت کاتیون‌ها و آنیون‌ها در نزدیک سطح فولاد، خوردگی را متوقف می‌کند. این لایه محافظ با کاهش pH محیط(به طور عمده به دلیل کربناتاسیون) و یا حضور یون‌های کلر و سولفات از بین می‌رود [2].

۲-۱- خوردگی ناشی از کربناتاسیون

زمانی که pH محیط اطراف میلگرد از ۱۱/۵ بیشتر باشد لایه محافظ روی میلگرد سالم باقی می‌ماند و میلگرد را از خوردگی حفظ می‌کند. زمانی که pH از این مقدار کمتر می‌شود لایه محافظ ناپایدار می‌شود و حفاظت به عمل آمده از میلگردها از بین می‌رود. کربناتاسیون بتن دلیل اصلی برای کاهش pH در بتن شناخته می‌شود. کربناتاسیون و کاهش pH ناشی از آن به طور معمول از سطح بتن آغاز می‌شود و به شکل جبهه کربناته شده به سمت مرکز بتن پیش می‌رود. سرعت کربناتاسیون به عوامل محیطی (رطوبت، دما و غلظت دی اکسید کربن هوا) و مشخصات بتن(نفوذ پذیری و قلیاییت) بستگی دارد. در یک بتن با کیفیت مناسب، سرعت کربناتاسیون در حدود ۱ میلی متر بر سال می‌باشد [3].

۲-۲- خوردگی ناشی از نفوذ یون کلر

خوردگی ناشی از یون کلر یکی از دلایل اصلی خوردگی در نقاط مختلف دنیا شناخته می‌شود. حضور یون کلر در سازه بتنی، زمانی که اکسیژن و رطوبت لازم در دسترس باشد می‌تواند باعث خوردگی میلگردهای فولادی گردد.
یون کلر به دو روش اصلی وارد بتن می‌شود:
روش اول،کلر موجود در مصالح بتن (سنگدانه‌ها، افزودنی‌ها...).
روش دوم، نفوذ یون کلر از محیط پیرامون به داخل بتن (آب دریا، نمک‌های یخزدا...).
یون کلر در داخل بتن می‌تواند به دو صورت وجود داشته باشد. یونی که با انجام واکنش‌های شیمیایی مقید شود که در نتیجه هیچ تاثیری بر فرآیند خوردگی فولاد در بتن ندارد و یا به صورت آزاد باشد.

روش ارزیابی سازه

بررسی وضعیت یک سازه بتن مسلح اولین گام برای بازسازی و ترمیم آن می‌باشد. برای تعیین علل خرابی‌ها و گستردگی آن، بررسی مقدار خوردگی و ارزیابی وضعیت کنونی سازه ضروری می‌باشد. یک بررسی دقیق شامل دو مرحله است. مرحله اول ارزیابی و مطالعه اولیه سازه بر اساس مشاهدات ظاهری است که باید ماهیت خرابی‌ها

را مشخص نماید و پایه ای برای مطالعات دقیق تر باشد. در حالی که استفاده از آزمایش‌های الکتروشیمیایی در مرحله بعد برای مطالعه وضعیت دقیق میلگردها و برآورد سرعت خوردگی ضروری است.

الف- مشاهدات ظاهری

خرابی‌های ناشی از خوردگی با استفاده از مشاهده ظاهری برنامه ریزی شده قابل تشخیص می‌باشند. طبقه بندی خرابی‌ها برپایه وضعیت ظاهری، محل و علت آن تعریف می‌شود. خرابی‌ها با توجه به گسترش ترک ناشی از خوردگی تعریف شده اند. در پروژه حاضر که شامل بررسی حدود ۳۰ پل راه‌آهن در ناحیه کویری ایران بود مساحتی در حدود ۴۰۰ متر مربع ارزیابی ظاهری شد و محل جداشدگی‌ها مشخص گردید. در این محل‌ها ترک‌های موازی سطح در نواحی که پوشش روی آرماتور از بتن اصلی جدا شده است قابل شناسایی می‌باشند. این خرابی‌ها بیشتر در نواحی که بتن در معرض رطوبت قرار دارد، رویت می‌شوند. متوسط ضخامت پوشش بتنی عرشه پل‌ها در حدود ۳۰-۲۵ میلی‌متر می‌باشد.

ب) آزمایش‌های انجام شده

بر پایه مشاهدات ظاهری، عرشه پل‌ها به دو دسته بدون خوردگی (a) و خوردگی زیاد (b) تقسیم شدند. در ادامه نتایج آزمایش‌های انجام شده ارائه می‌شود.

۳-۱- مقاومت فشاری

برای ارزیابی مشخصات سازه ای مصالح موجود، مغزه‌هایی با قطر ۱۰ سانتی متر از سازه تهیه شده و مورد آزمایش قرار گرفتند. متوسط مقاومت فشاری مغزه‌ها در دو سطح (a) و (b) در جدول (۱) ارائه شده است. این مقادیر متوسط ۳ نمونه آزمایش شده می‌باشد. با توجه به نتایج مقاومت فشاری می‌توان به طور تقریبی نسبت آب به مواد سیمانی در بتن را بین ۰/۵۵ تا ۰/۶ ارزیابی نمود. این میزان نسبت آب به مواد سیمانی برای اجرای ابنیه فنی زیاد به نظر می‌رسد و قطعا ملاحظات دوام و پایایی بتن مورد عنایت قرار نگرفته است.

جدول ۱: نتایج مقاومت فشاری مغزه‌ها

سطح خوردگی	متوسط مقاومت فشاری مغزه‌ها (kg/cm^2)
(a)	۲۱۰
(b)	۱۹۴

۳-۲- عمق کربناتاسیون

کربناتاسیون باعث کاهش pH محیط، انحلال فازهای جامد حاوی کلر مقید در محلول حفره ای، آزاد شدن کلر مقید و ایجاد کلر آزاد می‌شود. کلر آزاد شده می‌تواند وارد قسمت‌های کربناته نشده بتن شود. این پدیده موجب افزایش غلظت کلر آزاد در ضخامت بتن پوششی روی آرماتور شده و ممکن است کلر را در سطح میلگرد به مقدار بحرانی برساند. بنابراین سازه‌های حاوی کلر که کربناتاسیون در آنها رخ داده است نسبت به سازه‌هایی که فقط از یک معضل رنج می‌برند، بیشتر در معرض خوردگی قرار دارند [4، 5].

عمق کربناتاسیون را می‌توان با پاشیدن محلول فنل‌فتالئین بر روی مقطع بتن تـشخیص داد. در منـاطقی کـه تحـت تاثیر کربناتاسیون نبوده، مقدار pH بتن تقریبا" بیشتر از ۸/۵ و فنل‌فتالئین در این مناطق به رنگ ارغوانی در می‌آید.

جدول ۲: نتایج آزمایش تعیین عمق کربناتاسیون

حالت خوردگی	متوسط عمق کربناتاسیون (mm)
(a)	۳۰
(b)	۵۰

متوسط عمق کربناتاسیون سطوح بتن مسلح در جدول شماره (۲) نـشان داده شـده اسـت. مطـابق جـدول (۲) در سطوحی از بتن که خوردگی آرماتور مشاهده شده است(b)، متوسط عمق کربناتاسیون ۵۰ میلیمتر بوده که با توجه به اینکه متوسط ضخامت پوشش بتنی روی آرماتور در پل‌ها ۳۰ میلیمتر می‌باشد، مـی‌تـوان نتیجـه گرفـت کـه آرماتورهـا در ایـن ناحیـه تحـت تـاثیر پدیـده کربناتاسـیون قـرار گرفتـه انـد. در ناحیـه(a) متوسـط عمـق کربناتاسیون۳۰میلیمتر و مساوی مقدار پوشش بتنی روی آرمـاتور مـی‌باشـد. در ایـن ناحیـه آرماتورهـا در آسـتانه قرارگیری در معرض پدیده کربناتاسیون هستند.

۳-۳- پروفیل یون کلر

برای تعیین مقدار کلر در بتن، از بخش‌های مختلف عرشه پل‌ها نمونه برداری انجام شد. میزان کلر کـل (Total Chloride) موجود، طبق استاندارد ASTM C114 اندازه‌گیری شد. پروفیل‌هـای یـون کلـر سـطوح (a) و (b) در شکل (۱) به طور نمونه نشان داده شده است. همانگونه که دیده می‌شود، مقدار یون کلر در نزدیکی آرماتور (عمق ۳۰میلی‌متر) در سطح (a) کمتر از مقدار کلر آستانه خوردگی (حدود ۰/۰۷) مـی‌باشـد[6] . در نتیجـه در سـطح (a) احتمال خوردگی تحت اثر یون کلر بسیار کم است. در حالیکه در سطح (b) مقدار کلر در نزدیکی آرماتور به مقدار کلر بحرانی نزدیکتر است. بنابراین در این سطح خوردگی تحت اثر یون کلر بسیار محتمل اسـت و بـا توجـه بـه میزان عمق کربناتاسیون و مقدار یون کلر در نزدیکی آرماتور می‌تـوان نتیجـه گیـری نمـود کـه کربناتاسـیون در ترکیب با یون کلر منجر به کاهش مقدار کلر آستانه خوردگی و توسعه وگسترش خرابی‌ها شده است.

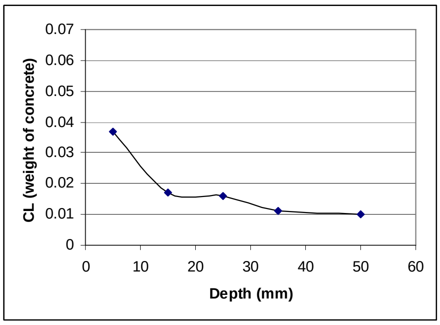

(a) سطح بدون خوردگی

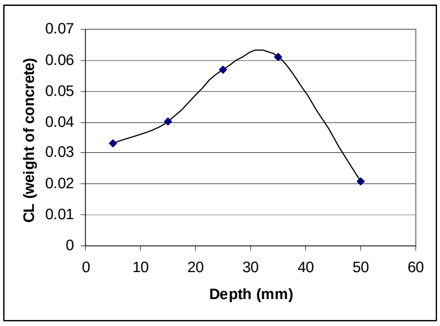

(b) سطح با خوردگی زیاد

شکل ۱- پروفیل یون کلر تهیه شده در دو سطح (a) و (b)

بر اساس پروفیل‌های ارائه شده به نظر می‌رسد مقدار کلر اولیه در بتن در حدود ۰/۰۱ تا ۰/۰۲ درصد وزنی بتن بوده و در محدوده مجاز می‌باشد. این در حالی‌است که کلر موجود در بتن تا عمق ۴-۳ سانتیمتر از محیط پیرامون وارد بتن شده است و به نظر می‌رسد منشا آن کلر موجود در شن‌های روان و اتمسفر در منطقه کویری و خصوصا در فصول و مواقعی که با شبنم و رطوبت همراه است می‌باشد. علاوه بر آن افت مقدار کلر در نزدیکی سطح خارجی که مشخصا در شکل (b-۱) ملاحظه می‌شود به دلیل پدیده کربناتاسیون می‌باشد که موجب تجزیه نمک فریدل و کم شدن کلر مقید و آزاد شدن آن و حرکت نمک‌ها به سمت داخل بتن می‌شود.

۳-۴- آزمایش پتانسیل نیم پیل

آزمایش تعیین پتانسیل نیم پیل، آزمایشی غیر مخرب و استاندارد می‌باشد که به طور گسترده در ارزیابی وضعیت خوردگی مورد استفاده قرار می‌گیرد. این آزمایش مطابق با استاندارد ASTM C876 و با استفاده از الکترود Ag/AgCl انجام شده است.

باید توجه داشت که حضور اکسیژن، غلظت کلر و مقاومت الکتریکی بتن تاثیر زیادی بر روی قرائت‌های ناشی از پتانسیل نیم پیل دارند. در این آزمایش معیار بررسی خوردگی طبق الکترود Ag/AgCl آرماتور چنین می‌باشد:

‎-۸۳ mV < پتانسیل: با احتمال بیش از ۹۰ درصد، هیچ خوردگی آرماتور در زمان آزمایش وجود ندارد.

‎-۸۳ mV > پتانسیل > ‎-۲۳۳ mV : فعالیت خوردگی نامشخص است.

‎-۲۳۳ mV > پتانسیل: با احتمال بیش از ۹۰ درصد خوردگی رخ داده است.

در شکل (۲) به عنوان نمونه، نتایج آزمایش پتانسیل خوردگی آرماتور برای دو سطح مذکور ارائه شده است. در شکل (۲) منفی‌ترین پتانسیل نیم پیل در ناحیه با خوردگی زیاد(شکلb-۲)، ۳۲۰- میلی ولت است. در حالیکه در ناحیه بدون خوردگی(a) این مقدار ۱۴۰- میلی ولت می‌باشد. با توجه به توضیحات ارائه شده در قبل، در سطح (b) با احتمال بیش از ۹۰ درصد، خوردگی رخ داده است. در حالیکه در سطح (a) فعالیت خوردگی نامشخص است.

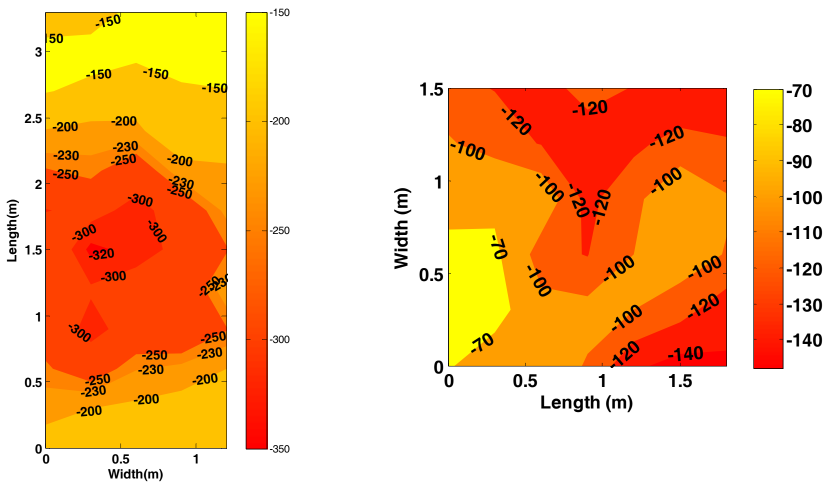

(b سطح با خوردگی زیاد

(a سطح بدون خوردگی

شکل ۲- نتایج آزمایش پتانسیل خوردگی آرماتور

۳-۵- آزمایش تعیین سرعت خوردگی آرماتور

اندازه‌گیری با دستگاه گالواپالس یک روش پلاریزاسیون سریع برای تعیین میزان خوردگی در سازه‌های بتن مسلح به حساب می‌آید. این روش بخاطر مشکلات اندازه‌گیری‌های نیم پیل در محیط‌های مرطوب و یا نیمه مرطوب بعلت کمبود اکسیژن و همینطور سرعت زیاد آن در بدست آوردن میزان خوردگی آرماتور در بتن، توسعه یافته است. با استفاده از دستگاه گالواپاس، پتانسیل نیم پیل و سرعت خوردگی آرماتور قابل تعیین می‌باشند. محدودیت‌های بحرانی برای طبقه بندی ریسک پذیری میزان خوردگی در جدول (۳) نشان داده شده است [۷].

جدول ۳: تخمین مقدار خوردگی قابل مشاهده از روی قرائت‌های انجام شده با دستگاه گالواپالس

مقدار خوردگی	مقدار اندازه‌گیری شده (µA/cm2)
در حالت مقاوم	‎<۰/۵
کم	۰/۵ – ۵
متوسط	۵ – ۱۵
زیاد	‎>۱۵

نتایج آزمایش تعیین سرعت خوردگی آرماتور به طور نمونه در شکل (۳) نشان داده شده است. همانطور که در این شکل دیده می‌شود، نقشه خطوط همتراز سرعت خوردگی در سطوح مورد نظر (a و b) قابل مقایسه با نتایج به دست آمده از پتانسیل نیم پیل (ارائه شده در شکل (۲)) است. حداکثر سرعت خوردگی در سطح (b) بیش از ۱۶ میکرو آمپر بر سانتی متر مربع می‌باشد که طبق جدول (۳) مقدار خوردگی در این سطح زیاد است و آزمایش نیم پیل نیز احتمال خوردگی را بیش از ۹۰درصد نشان می‌دهد. این در حالیست که نتایج سرعت خوردگی در سطح a حداکثر ۲/۵ میکرو آمپر بر سانتیمتر مربع است که نشان دهنده سرعت خوردگی کم می‌باشد. ضمنا مقادیر پتانسیل نیم پیل در محدوده عدم قطعیت قرار دارد.

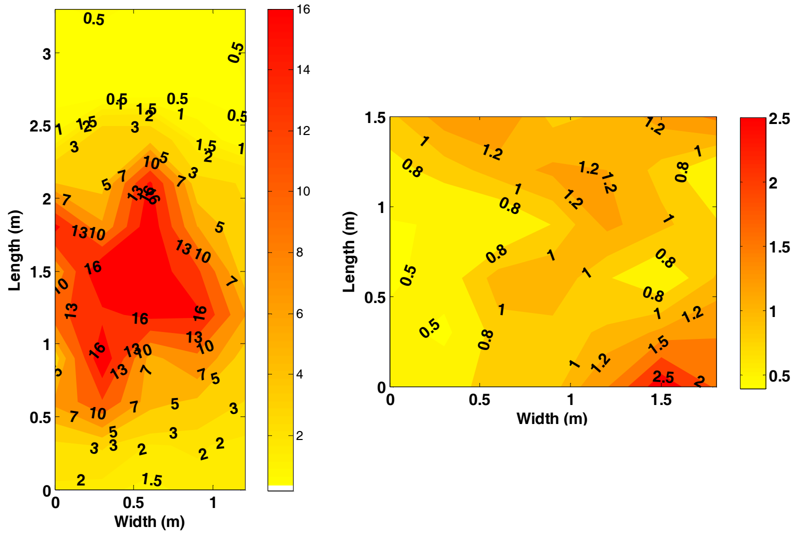

(b) سطح با خوردگی زیاد   (a) سطح بدون خوردگی

شکل ۳- نتایج آزمایش سرعت خوردگی آرماتور

۴- نتیجه‌گیری

۱ – ارزیابی خرابی سازه‌های بتن مسلح به منظور ترمیم آن، باید در یک نظام منطقی اجرا شود. یک ترمیم با کیفیت نیازمند شناخت علت وقوع خرابی، مشاهدات کامل آسیب‌ها، مشخصات دقیق محل‌های آسیب دیده است.

۲ – با توجه به نتایج به دست آمده عامل اصلی وقوع خوردگی در بتن مسلح عرشه پل‌ها وقوع پدیده کربناتاسیون می‌باشد.

۳ – مقدار پتانسیل نیم پیل تنها احتمال خوردگی را نشان می‌دهد و حتی در برخی از حالتها استفاده از این روش با محدودیت‌هایی همراه است. در حالیکه با استفاده از روش سرعت خوردگی می‌توان مقدار خوردگی را در نواحی خورده نشده و خورده شده و یا حتی نواحی مشکوک به خوردگی تعیین نمود.

۴ – پدیده کربناتاسیون در ترکیب با یون کلر منجر به توسعه وگسترش وسعت خرابی‌ها و خوردگی آرماتور در سازه‌های بتن مسلح می‌شود. همانگونه که دیده شد، در سطوح دارای شدت خرابی زیاد، خوردگی تحت اثر توام کربناتاسیون و یون کلر رخ داده است. در حالیکه در سطوح دارای شدت خوردگی کم خوردگی تنها ناشی از پدیده کربناتاسیون محتمل می‌باشد.

۵ – بر اساس مطالعات انجام شده در قالب این تحقیق مشخص می‌شود که خوردگی ناشی از نفوذ یون کلر در کشور محدود به سواحل و جزایر خلیج فارس نمی‌شود و در نواحی مرکزی کشور خصوصا در نواحی کویری این نوع خرابی‌ها وجود دارد. بدیهی‌است اجرای سازه‌ها و ابنیه بتنی با کیفیت نازل و نسبت آب به مواد سیمانی زیاد موجب بروز پدیده کربناتاسیون و تشدید فرایند خوردگی و آسیب‌دیدگی بتن خواهد شد.

مراجع

1. Vaysburd A.M., Emmons P.H., 2004, Corrosion inhibitors and other protective systems in concrete repair: concepts or misconcepts, Cement and Concrete Composites, Vol. 26, NO. 3, PP. 255-263.
2. Ghods, P., 2006, Literature Review, Depassivation of steel in concrete, Carleton University, Department od Civil and Environmental Engineering.
3. Kurtis K.E., Monteiro P., 1999, "Analysis of Durability of Advanced Cementitious Materials for Rigid Pavement Construction in California", Pavement Research Center-Institute of Transportation Studies- University of California at Berkeley.
4. Bertolini, L., Elsener, B., Pedeferr, P., Polder, R., 2004, Corrosion of steel in concrete, Prevention, Diagnosis, Repair, Wiley-VCH.
5. Broomfield J.P., 1997, Corrosion Of Steel in Concrete, E & FN SPON, London.
6. Shekarchizadeh, M., Pargar, F., 2008, "Investigation of Chloride Threshold Value in an old Concrete Structure", Journal of Faculty of Engineering, University of Tehran, Issue 42. Vol. 6.

۷. پرگر، فرهاد، اردیبهشت ۱۳۸۵، «بررسی پارامترهای موثر بر غلظت کلر بحرانی برای شروع خوردگی میلگردهای فولادی در بتن»، پایان‌نامه کارشناسی ارشد در رشته مهندسی عمران، دانشکده فنی دانشگاه تهران.

CD03-010

بتن ریزی در هوای سرد و اقدامات اصلاحی در جهت کاهش مدت زمان اجرای اسکلت بتنی با سیستم قالب تونلی

سعید اسعدی

چکیده

از آنجائیکه در سیستم قالب تونلی همواره موضوع مدیریت زمان مطرح می‌باشد لذا بتن ریزی در هوای سرد از اهمیت خاصی برخوردار بوده و با توجه به سرمای شدید در منطقه آذربایجان که معمولا بتن ریزی در اکثر پروژه‌ها متوقف می‌شود، با اجرای تمهیداتی از قبیل ساخت و نصب هیترهای برقی فن دار در داخل تونلها و پوشش‌های مناسب و استفاده از مشعل و لوله گرمایشی و... امکان بتن ریزی در هوای سرد و بالابردن مقاومت بتن میسر می‌گردد.

۱ - تامین ضوابط آیین نامه ای

مطابق مبحث ۹ مقررات ملی ساختمان هوای سرد به وضعیتی اطلاق می‌شود که برای ۳ روز متوالی شرایط زیر برقرار باشد.

الف – دمای متوسط هوا در شبانه روز کمتر از ۵ درجه سلسیوس باشد.

ب – دمای هوا برای بیشتر از نصف روز از ۱۰ درجه سلسیوس زیادتر نباشد.

به منظور اطمینان کافی از وضعیت نگهداری بتن در پروژه آذران دمای بتن در طول شبانه روز ۲ بار در نقاط مختلف سازه ثبت می‌شود.

برای رساندن دمای بتن به حد مطلوب هنگام اختلاط بتن از آب گرم استفاده شده و مطابق آیین نامه، از تماس

مستقیم آب گرم با سیمان در صورتی که دمای آن بیش از ۴۰ درجه سلسیوس باشد در حین ریختن مصالح در مخلوط کن، کنترل لازم به عمل می‌آید.

انتخاب نسبت آب به سیمان با توجه به روند کسب مقاومت در دمای محیط بوده و کمتر از ۰/۴ می‌باشد.

عمل آوردن بتن تازه حداقل به مدت ۲۴ ساعت و تا رسیدن به مقاومت ۵ مگاپاسکال ادامه می‌یابد.

عمل آوری بتن با استفاده از پوشش (رولهای پشم شیشه که در داخل نایلون قرار داده می‌شود) و گرم کردن داخل تونلها با هیترهای برقی و گازی تا ۱۵ درجه سانتی گراد انجام می‌گیرد.

مزیت استفاده از هیترهای برقی و گازی نسبت به گرم کننده‌ها با مواد سوختی نظیر نفت و گازوئیل به این علت است که از احتمال تبخیر آب و کربناتی شدن سطوح بتنی در اثر احتراق، جلوگیری به عمل آید.

با توجه به اینکه در سیستم قالب تونلی به جهت افزایش سرعت عملیات اجرایی، باز کردن قالب‌ها در مدت زمان کمتری از زمان تعریف شده در مبحث ۹ مقررات ملی انجام می‌شود، لذا از مواد روان کننده که خاصیت تندگیرکننده دارند استفاده و برای مراقبت بتن بعد از قالب برداری از پایه‌های اطمینان در وسط دهانه‌ها استفاده شده و دقت لازم بعمل می‌آید تا همیشه پایه‌های اطمینان در دو طبقه متوالی وجود داشته باشند و تا حد امکان هر دو پایه اطمینان نظیر در دو طبقه، روی هم و در امتدادی واحد قرار گیرند.

بلوک A1 - زمستان ۸۶

بلوک B1 – زمستان ۸۶

۲– تهیه آبگرم بچینگ

برای تهیه آبگرم لازم در بچینگ از تانکر آب و استتار کردن آن و مجهز نمودن بـه سیـستم گـر مـایش بوسـیله مشعل‌های گازی، همراه با نصب ترموستات جهت رسانیدن دمای آب بتن به ۶۰c، استفاده می‌شود.

مشعل گرمایشی جهت حرارت به قسمت پایین تانکر آب بچینگ

بچینگ بتن زمستان ۸۷

جلوگیری از یخ زدن مصالح بچینگ

با اجرای لوله‌کشی در محل دپوی مصالح بچینگ و نصب گرم کن با مشعل گازو ئیلی و عبور دادن هوای گـرم از

داخل لوله‌ها، از یخ زدگی مصالح جلوگیری می‌شود.

مشعل گرمایشی

لوله گرمایشی

جهت حفظ حرارت در محل دپوی مصالح بچینگ، سطح مصالح را با رول‌های پشم شیشه (با کاور نایلونی) پوشانیده و بر روی آن چادر برزنتی کشیده می‌شود.

در قسمت پایین با گذاشتن یک خرک و ایجاد اختلاف ارتفاع، با قرار دادن هیترهای برقی فن دار، سطح فوقانی مصالح گرم نگه داشته می‌شود.

پوشش دپوی مصالح بچینگ

۴- تامین گرمایش داخل قالب‌های تونلی

جهت جلوگیری از افت دمای بتن هنگام بتن ریزی حدود ۱۲ ساعت قبل از بتن ریـزی بـا قـرار دادن هیترهـای برقی فن دار در داخل قالب‌های تونلی و استتار آنها در قسمت خروجی با چادر، گرمایش داخل قالب تـونلی تـامین شده و دمای قالب‌ها به ۱۰°C می‌رسد.

هیتر برقی فن‌دار

استتار قسمت خروجی قالب تونلی

۵- عمل آوری و کنترل دمای بتن

به منظور جلوگیری از افت دمای بتن در محل بـتن ریـزی، مقـدار تهیـه بـتن در بچینـگ در هـر مرحلـه، بـه ۲ مترمکعب تقلیل و بدین ترتیب مدت زمان حمل مصرف بتن کاهش می‌یابد.

پوشش روی بتن توسط پشم شیشه و برزنت

پس از اتمام بتن ریزی، گرمایش داخل قالب‌های تونلی تا مدت ۴۸ ساعت بعد از بتن ریزی ادامه یافتـه و سـطح بتن با پشم شیشه پوشانیده و بر روی پشم شیشه نیز همانند پوشش روی مصالح بچینگ، چادر کشیده می‌شود، و

آرماتورهای انتظار ریشه دیوارها با نایلون پوشانده می‌شود. با رعایت موارد فوق الذکر تا دمای ċ ۱۸- نیز بتن ریزی انجام گردید. در زمستان سال ۸۶ که متوسط دمای شهر جدید سهند به دمای ċ ۱۵- رسید، کل تعطیلی پروژه به مدت ۸ روز آن هم بدلیل کولاک شدید بود.

بتن‌ریزی در شب

کاهش مدت زمان اجرای اسکلت بتنی و اقدامات اصلاحی

۱ – اقدامات انجام گرفته جهت کاهش مدت زمان اجرای اسکلت بتنی

در راستای تحقق و نیل به اهداف کیفی تعیین شده از طرف شرکت مادر در سال ۸۷ که کاهش مدت زمان اجرای اسکلت بتنی پروژه آذران به میزان ۵۰ درصد نسبت به سال ۸۶ مد نظر قرار گرفته، از همان ابتدای سال ۸۷ برای هر یک از بلوک‌ها، مطابق نمودارهای پیوستی (صفحات ۵۲ الی ۶۴) جهت مقایسه مدت زمان اجرا، شناسنامه مدت زمان اجرای اسکلت تهیه گردید به طوریکه بیشترین مدت زمان اجرای اسکلت مربوط به بلوک A1 در مدت ۱۲۸ روز و کمترین مدت اجرا مربوط به بلوک A3 در مدت ۷۳ روز انجام گرفته است.

بیشترین زمان اجرای یک نیم ست در بلوک A1 به مدت ۸ روز و با مطالعه و رفع موانع، در بلوک B3 به ۲ روز رسید

بطور خلاصه مواردیکه در سرعت دادن کار اجرا ی اسکلت نقش اساسی داشته اند به شرح زیر می‌باشد:

۱- افزایش سرعت بتن ریزی با اضافه کردن حجم پاکت به میزان ۰/۸ مترمکعب

افزایش حجم پاکت بتن به مقدار ۰/۸ مترمکعب

۲- کوتاه نمودن مسیر حمل بتن و اضافه نمودن تراک میکسر جهت حمل بتن.

۳- افزودن تعداد نفرات پیمانکار

۴- به منظور جابجایی قالب‌های کناری، میانی و Plat formها با توجه به اختلاف محل بست قالب، از سیم بکسل جداگانه مخصوص به همان قالب استفاده می‌شد که باز و بسته کردن مجدد سیم بکسل‌ها باعث کندی عملیات می‌گردید، با تجمیع کل سیم بکسل‌ها در قلاب تاورکرین و تعویض از همان قسمت سرعت جابجایی قالب‌ها افزایش یافت.

تجمیع سیم بکسل‌ها در قلاب تاور جهت جابجایی سریع قالب‌ها

۵- انجام عملیات تمیز کاری و روغن کاری قالبها به هنگام خروج برروی پلت فرم (PLAT FORM) و انتقال به نیم ست دیگر (توضیح اینکه قبلا کار تمیز کاری و روغن کاری قالب‌ها پس از انتقال آنها به سطح زمین صورت می‌گرفت و سپس به نیم ست بعدی انتقال داده می‌شد)

تمیزکاری و روغن کاری قالب‌ها در روی پلت فرم‌ها

۶- تعلیم و آموزش کارگران و استادکاران جهت افزایش بینش آنها به احداث ساختمان با دید صنعتی

۷- تعریف وظیفه و تخصص خاص برای هر نفر (مثلا نصاب باز شو، نصاب قالب‌های کناری و غیره)

۸- افزایش ساعات کاری کارگاه (شروع تایم کاری در تابستان از ساعت ۶ صبح تا ۲۰ شب)

۹- انتخاب پیمانکار جداگانه جهت اجرای کلیه عملیات جوشکاری در دیوارها و سقف‌ها

۲- مطالعه و بررسی در سرعت دادن به عملیات الکتریکی

۱- لوله‌های تولیدی کارخانه یزد پولیکا از نوع PVC طوسی نسوز که قبلا استفاده می‌شد و مقاومت فشاری عمودی کافی نداشت با نوع پلیکای PVC سخت نسوز سفید تولیدی کارخانه ثابت پلی اتیلن تعویض شد که این امر باعث کاهش تعداد لوله‌های شکسته شده در مرحله اجرای مش دوم سقف و بتن ریزی گردید.

۲- تهیه نقشه ثابت SHOP DRAWING

۳- تهیه شابلن و فنر خم متناسب با سایز لوله جهت ایجاد خم لوله‌های برق دیوارها

خم کاری لوله‌ها با استفاده از فنر و شابلن خم

۴- تهیه شابلن جهت ساخت بوشنهای سر لوله‌های برق دیوارها بصورت سری
۵- سوراخ کاری محل ورود لوله‌ها به قوطی‌های کلید و پریز به صورت سری
۶- تهیه پلا ستفوم جهت محل قرارگیری لوله‌های انتظار سقف و دیوار و محل باز شوها با توجه بـه ابعـاد آنهـا و ایجاد سوراخهای لازم در آنها به صورت سری.

استفاده از پلا ستفوم جهت محل قرارگیری لوله‌های انتظار سقف

استفاده از پلا ستفوم جهت محل قرارگیری لوله‌های انتظار دیوار

۷- علامت گذاری لوله‌ها با رنگهای متنوع برای شناسایی محل سیستمهای مختلف از جمله روشنائی پریز بـرق و تلفن و آنتن و درب باز کن برای تسریع در لوله گذاری سقف درکارگاه موقت.
۸- کد گذاری و دسته بندی لوله‌های خم و غلافهای جفت و تکی و قوطی‌های سوراخ شده بـا توجـه بـه تعـداد سایز آنها در نقشه SHOP DRAWING جهت جلو گیری از اشتباه نفرات پیمانکار در مرحله اجرا.
۹- کدگذاری و دسته بندی با توجه به تعداد آنهـا در نقـشه SHOP DRAWING جهـت جلـوگیری از اشـتباه نفرات پیمانکار در مرحله اجرا صورت می‌گیرد.
۱۰- ساخت غلاف فلزی قوطی‌های کلید و پریز از لوله سبک نرده ای به قطر ۱/۴ ۲ اینچ و جوش ۲ عدد میلگرد نمره ۵ بطول ۴۰ سانتی متر و بستن آن با سیم آرماتوربندی به مش دیوارها، جهت قرارگیری محل دقیق قـوطی کلید و پریز و فاصله از دیواره قالب تونلی

غلاف قوطی‌های کلید و پریز

۱۱- حضور مستمر ناظر تاسیسات برقی در زمان بتن ریزی و آموزش یک نفر به عنوان کارگر فنی جهت کنترل و ترمیم لوله‌ها در صورت شکستگی لوله‌ها در حین بتن ریزی

ترمیم شکستگی لوله‌ها در حین بتن ریزی

۳- مطالعه و بررسی در سرعت دادن به عملیات مکانیکی

۱- لوله‌کشی سیستم فاضلاب و ونت (لوله‌های به قطر ۵۰ الی ۶۳ میلیمتری) معمولاً با انجام شیارکنی و برش کاری دیوارهای داخلی و خارجی صورت می‌گرفت که موجب تخریب دیوارها و افزایش نخاله می‌شد. در پروژه آذران یک غلاف از جنس لوله PVC با یک سایز بزرگتر از لوله مورد نظر همزمان با اجرای دیوارها در داخل دیوار قرار داده و بعد از اتمام دیوارچینی غلاف را برداشته و برای استفاده مجدد به طبقه دیگر انتقال می‌یابد که بدین ترتیب از تخریب دیوار جلوگیری می‌شود.

استفاده از غلاف جهت جلوگیری از تخریب دیوارها در هنگام لوله کشی

۲- محل عبور لوله‌های آب شهری به داخل واحدها، مطابق نقشه‌های اجرایی در مشاعات و داخل واحدها به صورت زیرسقفی مشخص و از نظر معماری نیاز به اجرای سقف کاذب دارد. در بلوک‌های تیپ A لوله‌های نمایان به مقدار ۴۰۳۲ مترطول و در تیپ B به مقدار ۱۶۲۰ مترطول می‌باشد. با تغییر نقشه‌های اجرایی و اجرای لوله‌ها بصورت توکار از هزینه مربوط به خرید مصالح و دستمزد اجرای سقف کاذب شامل (خرید مصالح از قرار هر مترطول به مبلغ ۵۰۰۰۰ ریال – رابیتس بندی ۵۰۰۰ ریال – گچ و خاک ۲۵۰۰۰ ریال – دستمزد آهن کشی به مبلغ ۳۰۰۰۰ ریال) جمعاً به ازای هر مترطول به مبلغ ۱۰۰۰۰۰ ریال، به مبلغ کل ۵۶۵/۲۰۰/۰۰۰ ریال صرفه جویی گردید.

۳- اجرای ساپورت لوله‌ها در داکتهای تاسیساتی معمولاً پس از اتمام اسکلت انجام می‌شود. در پروژه آذران عملیات آهن کشی داکتها با استفاده از مصالح پرت حاصل از نبشی کشی دیوارهای خارجی، همزمان با اجرای اسکلت با قرار گرفتن شاخکهای فلزی در داخل بتن اجرا می‌شود.

آهن‌کشی داکتها در حین بتن ریزی

۴- جهت کاهش عملیات آهن کشی در چاهک‌های آسانسور بلوک‌های تیپ A و B، دیوارهای برشی در

طبقات (یک ضلع در بلوک A و سه ضلع در بلوک B) پلیت‌گذاری شده و از حجم عملیات آهن کشی بـه مقـدار ۶۰ درصد در بلوک‌های تیپ B و ۳۰ درصد در بلوک‌های تیپ A کاسته شده است.

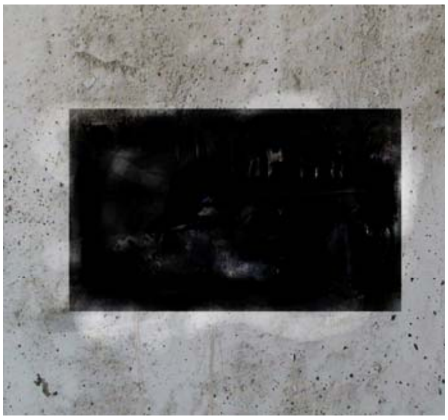

پلیت گذاری دیوار بتنی چاهک‌های آسانسور

۵- نقشه‌های تاسیسات مکانیکی در رابطه با هماهنگی محل اوپنینـگ‌هـا (داکتهـای تاسیـساتی) بـا نقـشه‌هـای معماری و سازه و با در نظر گرفتن طول اتصالات مصالح مصرفی در لوله کشی سیـستم فاضـلاب سـرویس‌هـا و رایزرهای آب باران اصلاح شده و در این رابطه نقشه‌های ازبیلت SHOP-DROWING تهیه گردید.

۶- جهت اجرای بازشوهای مربوط به تاسیسات مکانیکی در سقف‌ها در زمان بتن ریزی سقف، نسبت بـه سـاخت قالب‌های فلزی مربوط به محل عبور لوله با دو سایز بیشتر از قطر لوله‌ها به شکل کونیک اقدام گردید.

برای اینکه محل بازشوها در طبقات در امتداد هم قرار بگیرند، مختصات مرکز بازشو در سقف قالب تونلی سـوراخ کاری شده و با قرار گیری پین قالب بازشو (میلگرد نمره ۱۶) در سوراخ مذکور و بعد از گیـرش اولیـه بـتن، قالـب مذکور برای استفاده در سقف طبقه بعدی برداشته می‌شود.

قالب فلزی محل عبور لوله‌ها از سقف بتنی

CD04

Seismic Evaluation and Rehabilitation

CD04-001

UPGRADING THE DUCTILITY AND SEISMIC BEHAVIOR FACTOR OF ORDINARY RC FRAMES USING FIBER COMPOSITE SHEETS

A. Niroomandi[1], A. Maheri[2]
[1]Seismic Retrofitting Center, Shiraz University, Iran
[2]Faculty of Engineering, University of Bristol, UK

ABSTRACT
The ductility and seismic behavior factor (R) are evaluated for an existing Reinforced Concrete (RC) frame that has been retrofitted with web-bonded Carbon Fiber Reinforced Polymer (CFRP) system. For this purpose, firstly using a nonlinear finite element analysis the flexural stiffness of FRP-retrofitted and original exterior and interior joints of the frame are determined. The obtained stiffness is then implemented into another software package in order to analyze the FRP-retrofitted frame using nonlinear static analyses. Then the *R* factor components including ductility reduction factor and over strength factors are extracted from pushover analyses. The results are compared with the results of the original RC frame and the same frame that has been retrofitted with steel bracings reported by other investigators. The results show that the ductility and the seismic behavior factor of the existing RC frame that has been retrofitted with CFRP sheets are better than the original frame, and upgrade the ductility of the ordinary RC frame to the Intermediate and even Special RC frame.

Keywords: seismic behavior factor (R), nonlinear static analysis, pushover, reinforced concrete frame, web-bonded CFRP-retrofitting, steel bracings

1. INTRODUCTION

Recently, FRP has been utilized for retrofitting or upgrading RC structures. Parvin & Granata [1] indicated that when joints of an RC frame were reinforced with FRP laminates, the moment capacity was increased up to 37 percent. Mahini & Ronagh [2] used a method for strengthening of exterior beam-column joints using web-bonded FRP sheets. They tested the effectiveness of web-bonded CFRP on energy absorption capacity of $1/2.2$ scale RC joints, in order to evaluate the possibility of relocating the plastic hinge location away from the column face. Their experimental studies showed that the FRP repairing/retrofitting system can restore/upgrade the integrity of the joint, keeping/upgrading its strength, stiffness and ductility as well as shifting the plastic hinge from the column facing toward the beam in such a way that the joint remains elastic. The practicality and effectiveness of using web-bonded FRPs on plastic hinge relocation has been also reported by Smith and Shrestha [3]. In another experimental study Balsamo et al. [4] evaluated the seismic behavior of a full-scale RC frame repaired using CFRP laminates. They indicated that the repaired frame had a large displacement capacity without exhibiting any loss of strength, while providing almost the same energy dissipation of the original frame.

In this paper, seismic behavior factors affecting parameters for CFRP-retrofitted ordinary moment-resisting RC frame are evaluated and compared with corresponding original moment resisting and steel-braced RC frames. The *R* factor components including ductility reduction factor and over strength factor are extracted from nonlinear static analyses of the frames. For this purpose, an eight storey three bay existing RC moment resisting frame which was retrofitted by Maheri & Akbari [5] using steel bracing systems is retrofitted again with web-bonded CFRP method in order to compare their ductility and seismic behavior factor.

2. GEOMETRY AND MATERIAL PROPERTIES OF THE RC FRAME

Figure 1 shows the selected frame of this study. The design dead and live loads are assumed to be 2750*kg/m* and 1750*kg/m* respectively. The compressive strength, f'_c and tensile strength, f_t of the concrete are taken as 27.46 MPa and 3.668 MPa, respectively. In addition, the elastic modulus of the concrete E_c is taken as 24.63 GPa and the yield stress of steel reinforcement is assumed to be 412 MPa.

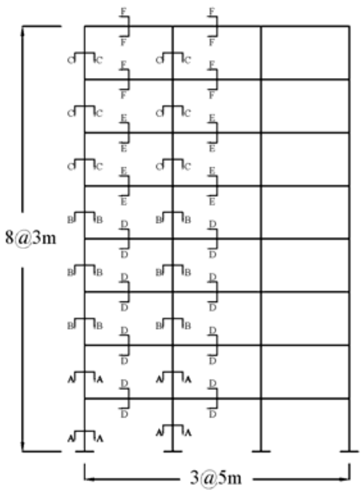

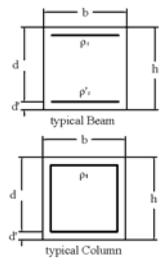

section	b	h	d	ρ_t	ρ_s	ρ'_s
A-A	700	700	650	0.019	—	—
B-B	500	500	450	0.022	—	—
C-C	500	500	450	0.013	—	—
D-D	500	500	450	—	0.012	0.009
E-E	500	500	450	—	0.011	0.0071
F-F	500	500	450	—	0.0071	0.004

Figure 1. Selected moment resisting frame [5]

Design base shears were determined for a Peak Ground Acceleration (PGA) of $0.3g$. The weight of the system is taken as the dead load plus 20 percent of live load as an estimation of the equivalent earthquake load, based on the Iranian earthquake code [6]. Initial *R* factor was assumed to be equal to 6 for this system. The moment resisting frame was designed based on "weak beam-strong column" principle using ACI-95 Code [7] and the steel bracings system was designed using

AISC-LRFD Code [8]. Dimensions and flexural reinforcements of the designed beam and column sections are shown in Figure 1. In this Figure, ρ_t, ρ_s and ρ'_s are the total steel ratio of column, tensile and compressive steel ratio of the beam respectively. All members and joints reinforcements have been designed to achieve the desirable strength and ductility [5].

3. NONLINEAR FINITE ELEMENT ANALYSIS OF RC JOINTS

The models of typical exterior and interior joints are shown in Figure 2. It can be seen that ten different models have been analyzed by finite element method for both original and retrofitted joints.

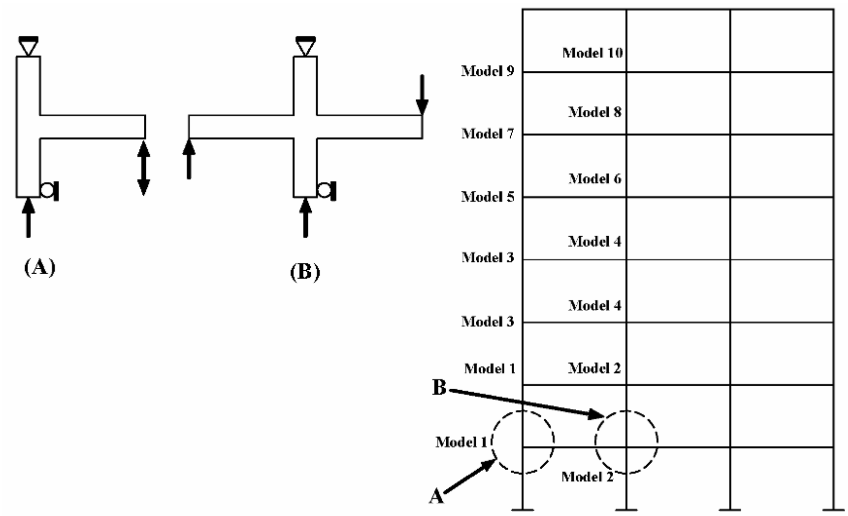

Figure 2. Analytical modeling of exterior and interior joints under lateral loads

The behavior of the RC joint retrofitted with web-bonded CFRP is analyzed using ANSYS software [9]. Both material and geometric nonlinearities are taken into account in the nonlinear finite element analysis by ANSYS. In order to model the characteristics of concrete, ANSYS SOLID65 elements is used. This element is capable of simulating the cracking and crushing of the concrete. Furthermore, to model the longitudinal reinforcement and the FRP composites, LINK8 and SOLID45 elements, are used respectively [1]. The FRP length has been chosen based on the Paulay and Priestly [10] design approach for obtaining the desirable plastic hinge relocation. For verification of the modeling and the analysis for the RC joint, an experimental study conducted on an exterior RC joint by Mahini & Ronagh [2] was selected. Figure 3 shows the “Beam tip load – Displacement” curves extracted from the non-linear FE analysis and the experimental data. Considering satisfactory agreement could be observed between the curves, it is concluded that the presented FE modeling is reliable. The required FRP thickness was obtained using nonlinear finite element analysis according to the desirable plastic hinge relocation. The required FRP thickness in the first level was calculated to be 4.95 mm, decreasing as the height of the frame increases. Other characteristics of CFRP laminates are given in Table 1. Note that the characteristics given in Table 1 satisfy the consistency conditions which are necessary for a non-isotropic material like ANISO in the analysis as described in reference [9] and stated by Kachlakev et al. [11]. The numerical models of retrofitted exterior and interior joints at seventh floor of the selected frame are depicted in Figure 4. Figures 5 and 6 show the failure mechanism of retrofitted exterior and interior joints (Isosurface style of concrete strain) at seventh level of the selected frame before and after retrofitting by web-bonded CFRP sheets. It can be seen that desirable plastic hinge relocation is achieved successfully thanks to CFRP sheets, as it was already obtained from an experimental study by Mahini & Ronagh [2]. Figure 7 shows the failure mechanism of an exterior RC joint tested by Mahini & Ronagh [2] before and after retrofitting by web-bonded FRP sheets.

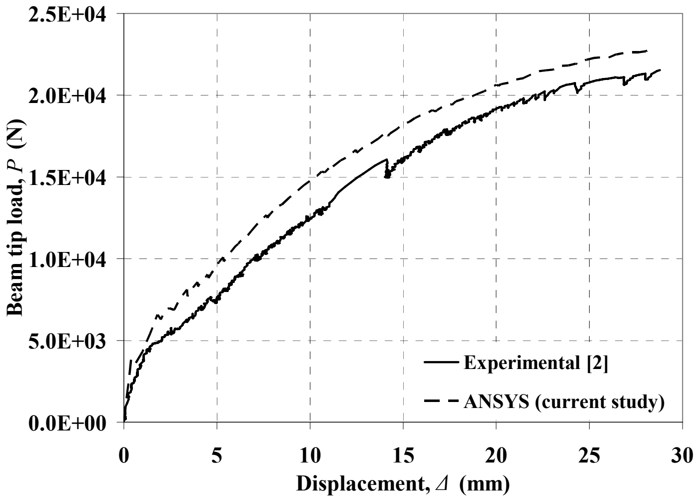

Figure 3. "Beam tip load – Displacement" curve for an exterior RC joint from experiment [2] and calculated from FE analysis

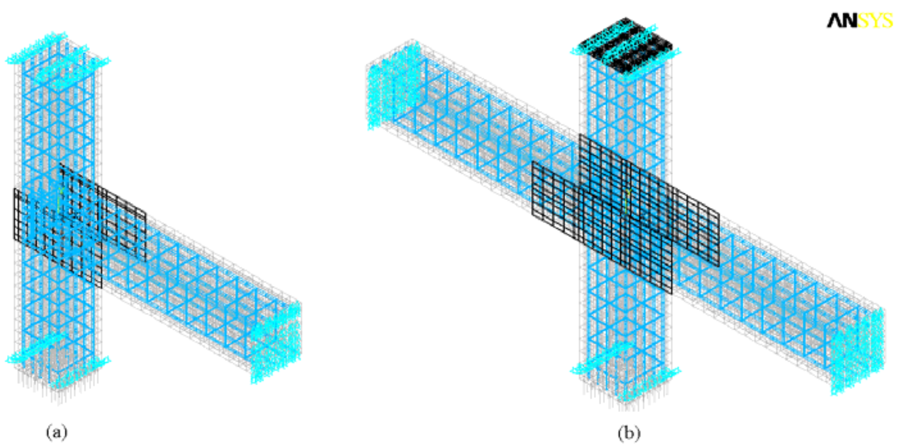

Figure 4. Finite element models of an (a) exterior and (b) interior retrofitted joint

Table 1: Mechanical properties of CFRP sheets used for FE modeling [9]

Modulus of elasticity (MPa)	**In fibers direction**	E_x=240000	**Compressive strength (MPa)**	**In fibers direction**		σ_x=80
	Perpendicular to fibers direction	E_y=18581		**Perpendicular to fibers direction**		σ_y=80
		E_z=18581				σ_z=80
Tensile strength (MPa)	**In fibers direction**	σ'_x=3900	**Shear modulus (MPa)**	G_{xy}=12576	**Poisson's ratio**	υ_{xy}=0.2
	Perpendicular to fibers direction	σ'_y=53.7		G_{xz}=12576		υ_{xz}=0.2
		σ'_z=53.7		G_{yz}=7147		υ_{yz}=0.3

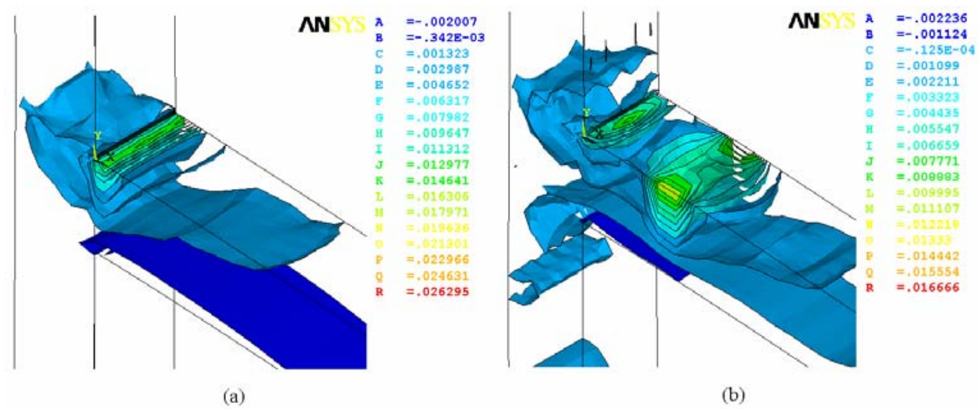

Figure 5. Failure mechanism of an exterior joint (a) before and (b) after retrofitting by web-bonded CFRP sheets

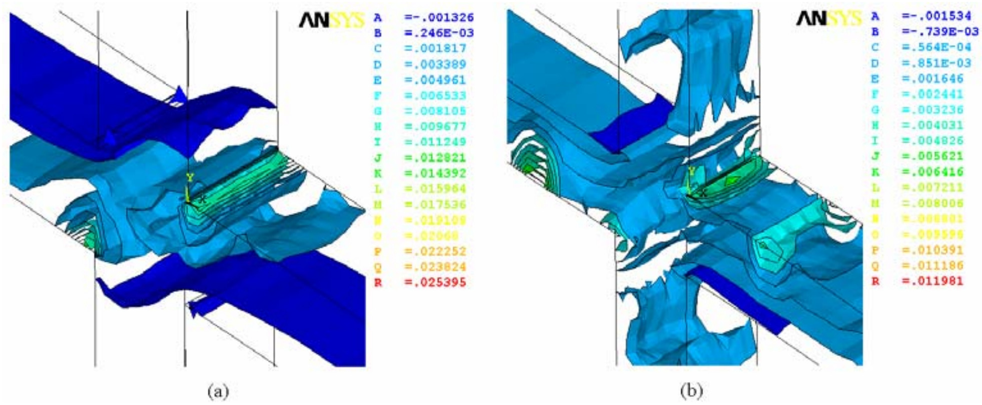

Figure 6. Failure mechanism of an interior joint (a) before and (b) after retrofitting by web-bonded CFRP sheets

Figure 8 shows the "moment-rotation" curves of an exterior original and FRP-retrofitted beam-column joint at seventh level of the selected frame. In this Figure, K_{13} is the difference between the two curves.

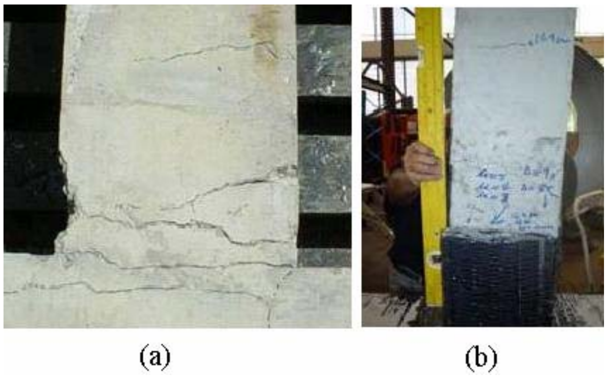

Figure 7. Failure mechanism of an exterior joint (a) before and (b) after retrofitting by web-bonded FRP sheets [2]

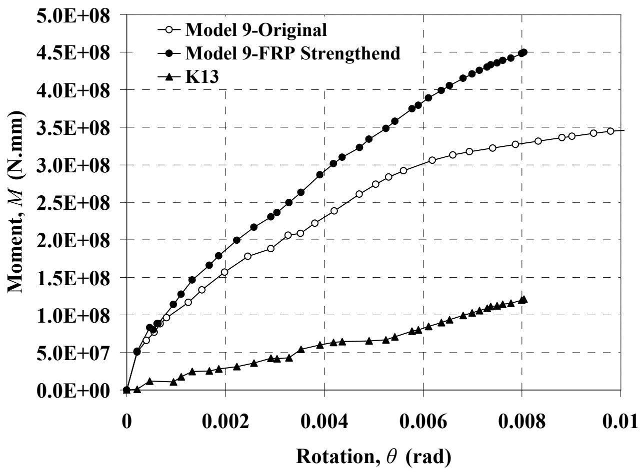

Figure 8. "Moment-rotation" curve of an exterior original and FRP-retrofitted joint

3. NONLINEAR STATIC ANALYSIS OF THE FRAMES

- **Original Frame:** Nonlinear static analysis (pushover) of each system is carried out using SAP 2000 10.1.0 program [12]. For this purpose, a constant gravity load equal to the total dead load plus 20 percent of the live load is applied to each frame, and an inverted triangular distribution over the height is used as the lateral load pattern. $P-\Delta$ effect is also considered in the analysis. Force-deformation criteria for plastic hinging is defined based on ATC-40 [13] and FEMA356 [14] patterns.
- **Retrofitted Frames:** The analytical models of the retrofitted frames with web-bonded CFRP system and steel bracings are shown in Figure 9. This frame has already been retrofitted using steel bracing system (Maheri & Akbari [5]). In order to model the FRP-retrofitted frame, SAP 2000 Non-Linear Link (NLLink) elements are used, which can simulate the equivalent additional stiffness to the beams provided by web-bonded CFRP sheets on the system. These elements are assumed to be located at a distance of 500 mm away from

the column face, corresponding to the FRP length. In Figure 9, K_i is the additional rotational stiffness of each retrofitted beam, which is modeled on the original frame with a NLLink element. The "moment-rotation" curve of original and FRP retrofitted joints are extracted from finite element analysis and the differences are used as the rotational stiffness of retrofitted joints.

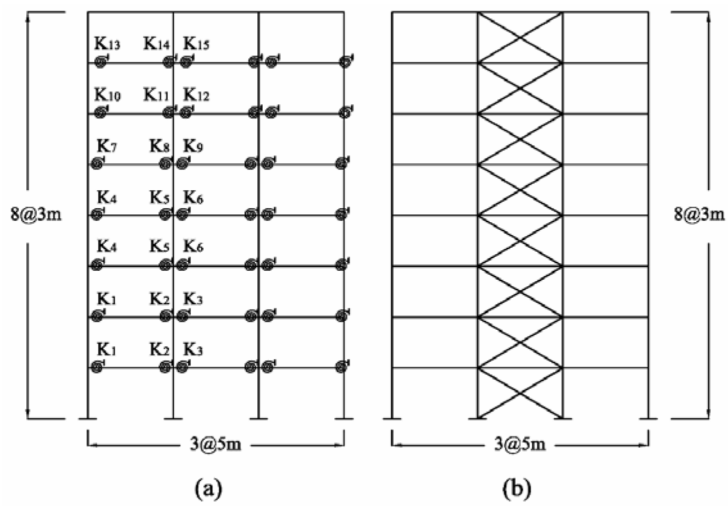

Figure 9. Analytical modeling of the (a) web-bonded CFRP (current study) and (b) steel-braced frame [5]

The base shear versus roof displacement curves of original and retrofitted (both steel-braced and FRP-retrofitted) frames are shown in Figure 10. In this Figure, X-brace retrofitting systems examined by Maheri & Akbari [5] have been designed based on 50% and also 100% of the lateral loading on the RC frames.

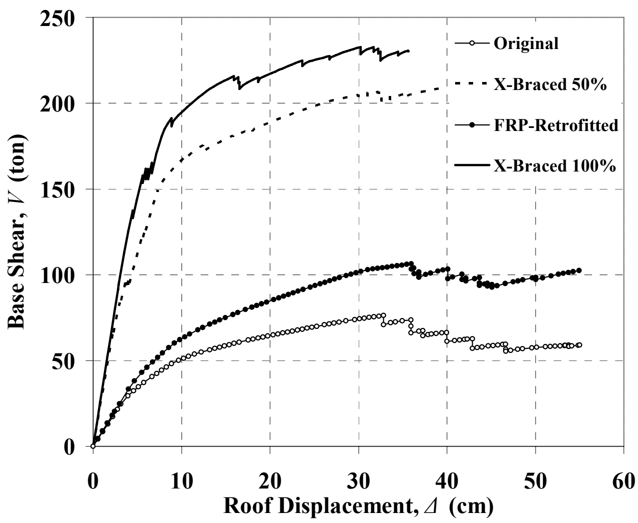

Figure 10. Base shear-roof displacement curves of all frames

4. SEISMIC BEHAVIOR FACTOR AFFECTING PARAMETERS

In forced-based seismic design procedures, seismic behavior factor, R is a force reduction factor used to reduce the linear elastic response spectra to the inelastic response spectra. In other words, seismic behavior factor is the ratio of the strength required to maintain the structure elastic to the inelastic design strength of the structure. The seismic behavior factor, *R*, therefore accounts for the inherent ductility and over strength of a structure as well as the difference in the level of stresses considered in its design. Taking into account the above three components, It is generally expressed in the following,

$$R = R_{\mu}.R_{s}.Y \tag{1}$$

Where, R_{μ} is the ductility-dependent component, also known as the ductility reduction factor, R_s is the over strength factor and *Y* stands for the allowable stress factor. With reference to Figure 11, in which the actual "force-displacement" response curve is idealized by a bilinear "elastic-perfectly plastic" response curve, the seismic behavior factor parameters may be defined as:

$$R_{\mu} = V_e / V_y \, , R_s = V_y / V_s \, , Y = V_s / V_w \tag{2}$$

Where, V_e, V_y, V_s and V_w denote the elastic response strength of the structure, the idealized yield strength, the first significant yield strength and the allowable stress design strength, respectively. For structures designed using an ultimate strength method, the allowable stress factor, *Y*, becomes unity and the seismic behavior factor is therefore reduced to:

$$R = R_{\mu}.R_s = \left(V_e / V_y\right)\!.\!\left(V_y / V_s\right) = \left(V_e / V_s\right) \tag{3}$$

The structure ductility, μ, is defined in terms of the maximum structural drift (Δ_{max}) and the displacement corresponding to the idealized yield strength $\left(\Delta_y\right)$ as:

$$\mu = \frac{\Delta_{max}}{\Delta_y} \tag{4}$$

Many investigators have discussed the two main components of *R* factor presented in Eq. (3). In particular, the ductility dependent component, R_{μ}, has received considerable attention. Ductility reduction factor R_{μ} is a function of both of the characteristics of the structure, including ductility, damping and fundamental period of vibration (T), and the characteristics of earthquake ground motion. Nassar and Krawinkler [15] presented a relation for R_{μ} in the following form:

$$R_{\mu} = [c(\mu - 1) + 1]^{1/c} \tag{5}$$

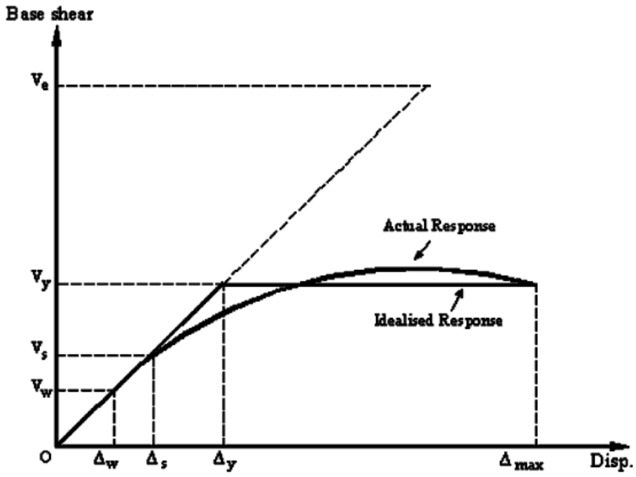

Figure 11. Typical pushover response curve for evaluation of behavior factor, *R* [5]

Where,

$$c(T, \alpha) = \frac{T^a}{1 + T^a} + \frac{b}{T} \tag{6}$$

In Eq. (6), α is the post-yield stiffness given as a percentage of the initial stiffness of the system and a and b are parameters given as functions of α that can be obtained from Table 2 [16].

Table 2: a and b values regarding α [16]

α (%)	a	b
0	1	0.42
2	1	0.37
10	0.8	0.29

5. DETERMINATION OF SEISMIC BEHAVIOR FACTOR

A number of performance parameters may govern the capacity of a structure. In order to carry out a nonlinear static analysis, one or a number of these parameters should be considered for determination of the displacement limit state (Δ_{max}). For the medium-rise ductile building considered in this study, the global drift (maximum roof displacement) is commonly used as a failure criterion. In evaluation of the displacement ductility, μ, the ultimate capacity of each frame is assumed when the global drift has been reached to 1.5% of the system height. This criterion is based on the NEHRP recommendations [17] for RC moment resisting frames. The idealized "force-displacement" (obtained based on the FEMA-356 method) and the capacity curves for the FRP-retrofitted frame are shown in Figure

12. In this Figure, V_y and Δ_y, are yield strength and yield displacement, respectively, and Δ_t and V_t are the target displacement and its corresponding base shear. To calculate the yield displacement, Δ_y, and yield strength, V_y, line segments on the "force–displacement" curve were located using an iterative procedure that approximately balanced the area above and below the curve [14]. The effective lateral stiffness, K_e, shall be also taken as the secant stiffness calculated at a base shear force equal to 60% of the effective yield strength of the structure [14]. After calculation of μ, now R_μ can be obtained from Eq. 5, 6 and Table 2 and R_s is determined from Eq. 2. The seismic behavior factor parameters of all systems have been presented in Table 3. It can be seen that the ductility ratio of FRP-retrofitted frame is improved in comparison with the original frame, and is very similar to the one obtained for the X-Braced frames. The R factor of FRP-retrofitted frame is improved significantly in comparison with the original frame and is also better than X-Braced frames.

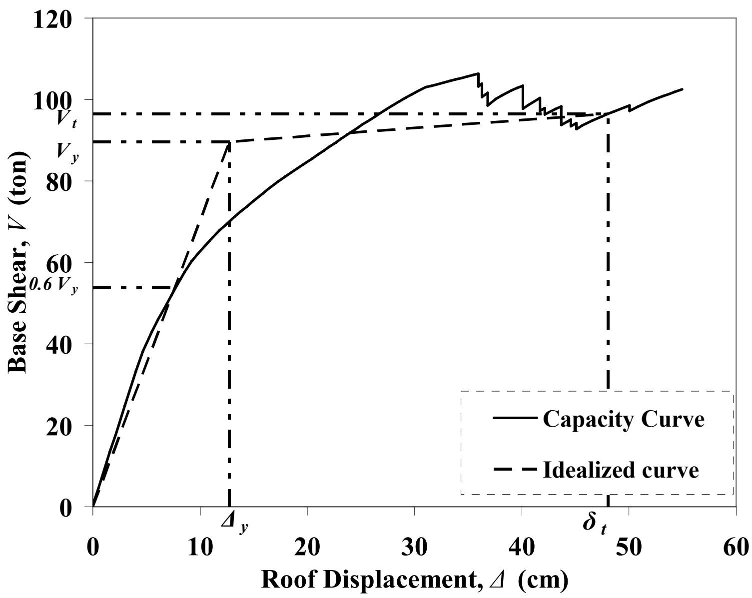

Figure 12. Capacity and Idealized curve of FRP retrofitted frame based on the FEMA356

Table 3: Seismic behavior factor parameters of all systems

Frame	μ	R_μ	R_s	R
Original [5]	2.27	2.4	1.92	4.6
Xbraced-50% [5]	2.7	2.66	2.97	7.9
Xbraced-100% [5]	2.84	2.86	3.33	9.5
FRP Retrofitted	2.83	3.016	3.193	9.63

6. CONCLUSIONS

Conventional retrofitting systems in earthquake-resisting frames have some limitations. For example, conventional steel bracings in RC frames which were considered in this paper for verification of web-bonded CFRP retrofitting are able to dissipate considerable energy by yielding under tension, but they buckle without much energy dissipation in the compression loads [18]. In this paper, an eight-storey frame that was previously strengthened with steel bracings system is selected and retrofitted with web-bonded CFRP. In order to estimate the flexural stiffness of the FRP retrofitting system, nonlinear finite element analysis by ANSYS is employed. The additional flexural stiffness of the FRP joints is implemented into the frame using NLLink elements on the beam end of exterior and interior joints. A systematic evaluation of each system including ductility ratio and seismic behavior factor is made using nonlinear static analysis. Based on the obtained results, it is concluded that the ductility ratio and the seismic behavior factor of the FRP retrofitted RC frame are significantly improved in comparison with the original frame and increased from 4.6 (original frame) to 9.63 (FRP retrofitted frame).

REFERENCES

1. Parvin, A. and Granata, P., Investigation on the Effects of Fiber Composites at Concrete Joints, Journal of Composites part B, 2000, 31, pp 499-509.
2. Mahini, S. S., and Ronagh, H. R., A New Method for Improving Ductility in Existing RC Ordinary Moment Resisting Frames using FRPs, Asian Journal of Civil Engineering (Building and Housing), 2007, Vol. 8, no. 6.
3. Smith, S. T., and Shrestha, R., A Review of FRP Strengthened RC Beam Column Connections, Proceeding of the Third International Conference on FRP Composites in Civil Engineering (CICE 2006), 13-15 December-Miami, Florida, USA, pp 661-664.
4. Balsamo, A., Colombo, A., Manfredi, G., Negro, P., and Prota, A., Seismic Behavior of a Full Scale RC Frame Repaired using CFRP Laminates, Engineering Structures, 2005, 27, pp 769-780.
5. Maheri, M. R., and Akbari, R., Seismic Behavior Factor, R, for Steel X-Braced and Knee-Braced RC Buildings, Engineering Structures, 2003, 25, pp 1505-1513.
6. Iranian Code of Practice for Seismic Resistance Design of Buildings, standard no.2800 2nd. Edition-1999.
7. ACI Committee 318. Building Code Requirements for Reinforced Concrete (ACI 318-95) and Commentary (ACI 318R-95). American Concrete Institute, Detroit, Michigan, 1989.
8. Manual of Steel Construction, Load and Resistance Factor Design, LRFD. 2nd ed. American Institute of Steel Construction, Chicago. III, 1994.
9. ANSYS. ANSYS Manual set., ANSYS,Inc., Canonsburg, PA 15317, USA, 2005.
10. Paulay, T., and Priestley, M.J.N., Seismic Design of Reinforced Concrete and Masonry Buildings, John Wiley & Sons, INC, 1992.

11. Kachlakev, D., Miller, T., Yim, S. & Chansawat, K., Finite Element Modeling of Reinforced Concrete Structures Strengthened with FRP Laminates, Final Report for Oregon Department of Transportation Research Group, Internet File, 2001.
12. SAP2000 Non-linear version 10.1.0. Analysis Reference Manual. Computers and Structures Inc., Berkeley, Calif, 2006.
13. ATC. Seismic Evaluation and Retrofit of Concrete Buildings. ATC-40, Applied Technology Council, Redwood City, 1996.
14. American Society of Civil Engineering (ASCE). Prestandard and Commentary for the Seismic Rehabilitation of Buildings., prepared for the Federal Emergency Management Agency, FEMA 356, 2000.
15. Nassar, A.A., and Krawinkler, H., Seismic Demands for SDOF and MDOF Systems, report No. 95. Stanford, California: The John A. Blume Earthquake Engineering Center, Stanford University, 1991.
16. Miranda, E., Eeri, M., and Bertero, V., Evaluation of Strength Reduction Factors for Earthquake-Resistant Design, Engineering Spectra, Vol 10, No. 2, 1994, PP. 357-379.
17. Federal Emergency Management Agency (FEMA). NEHRP Provisions for the Seismic Rehabilitation of Buildings. Rep FEMA 273 and 274, Washington DC, 1997.
18. Ravi Kumar, G., Satish Kumar, S. R., and Kalyanaraman, V., Behavior of Frames with Non-Buckling Bracings under Earthquake Loading, Journal of Constructional Steel Research, 2007, 63, pp 254-262.

CD04-002

APPLICATION OF EXPANSIVE AGENT (EA) TO PRODUCE POST TENSIONING FORCE IN FRP JACKETS FOR LATERAL RETROFITTING OF RC COLUMNS

A.A.Mortazavi[1], M.Jalal[2], M.M.Khodaparast[3]
1. Associate professor, Power and Water University of Technology, Tehran, Iran
2. M.Sc. Student, Dept of civil Engg. School of Engg Razi University, Kermanshah, Iran
3. B.Sc., Power and Water University of Technology, Tehran, Iran

ABSTRACT
Repair and strengthening of RC structures using FRP materials is one of the new and effective techniques ever used. With this respect, strengthening of structural elements by external lateral confinement can lead to increased strength and ductility. In this way, using an efficient and optimized method for lateral confinement is of great importance.

A novel, economic and simple technique for the repair and strengthening of RC members by means of expansive agent(EA) to produce post tensioning force, has been proven to perform well following experimental work undertaken at the University of Sheffield. The aim of the technique is to ensure the enhancement of the member strength and ductility by localized strengthening.

The above technique is equivalent to increasing the effectiveness of the composite confinement and it becomes possible to strengthen large columns with smaller amounts of composites, which are utilized earlier at much higher strengths. In addition, the level of axial strain achieved at failure is improved significantly. The paper will present details of experimental work with different types of confining material (glass and carbon), amounts of reinforcement and levels of initial pre-stressing.

Keywords: strengthening, expansive agent, post tensioning, FRP jacket

1. INTRODUCTION
Since the 1995 Kobe earthquake in Japan, composites have started being used for the repair and strengthening of columns against seismic actions. The composites are applied as external lateral reinforcement and are often used to prevent shear and anchorage/splicing failures, which can result in the enhancement of the ductility of RC elements.

The Japanese philosophy on earthquake resistant design aims to achieve ductility through low ratios of reinforcement and low steel strengths. This results in very large sections, which as a result require little shear reinforcement. However, during seismic violent load reversals, the shear demand can be higher than estimated, for example as a result of vertical accelerations. In addition, splicing of reinforcement causes additional bursting forces, which are difficult to contain with nominal shear reinforcement. External lateral confinement can address both of the above problems, in addition to providing other benefits.

In Europe and New Zealand, the seismic philosophy for achieving ductility is different, relying more on increasing the non-linear concrete stains through concrete confinement [3]. The advantage of this philosophy is that apart from smaller cross-sections, a significantly higher amount of lateral reinforcement is required. This lateral reinforcement, which is there to confine the concrete, is also beneficial in resisting additional shear and preventing splice and anchorage failures.

The enhancement of concrete ductility by confinement is central to the principles of Eurocode 8. However, researchers dealing with FRP confinement do not always consult the huge wealth of published work, which is derived from the earthquake engineering research. In addition, there is a fundamental difference between mild steel confinement and high strength composite materials.

Mild steel reinforcement attains its yield strength (around 80% of its ultimate strength) at a strain of around 0.002, whilst composites fracture at strains ranging from 0.014–0.02. Unconfined concrete crushes when the lateral strain is at best 0.001. This means, that for low levels of confinement, steel is relatively well utilised (around 50%), whilst composites are at best utilised at 7% of their capacities.

2. MATERIALS

The properties of the fibres and resin used for confinement are shown in tables 1 and 2. Where:

E_{frp} Young's modulus of elasticity

f_{frpu} ε_{frpu} Ultimate tensile strength and elongation of pultruded laminate

T_{GM} Glass transition temperature

V_{f+} Volumetric fibre content

Table 1: Physical and Mechanical properties of Fibre sheets [6]

Fibre	E_{frp} GPa	f_{frpu} MPa	ε_{frpu} %	Thickness mm	Density gr/cm^3	T_{GM} C^o	V_f %	Composition
GFRP AR	65	1700	2.88	0.135	2.6	-	100	Bi-Directional
CFRP 240	240	3900	1.55	0.117	1.7	100-130	100	Uni-Direction

Table 2: Physical and Mechanical properties of Epoxy Plus Structural Adhesive [6]

Epoxy	Colour	Strength MPa	$E_{m\ flexural}$ GPa	Density kg/litre	T_{GK} C^o	Coverage/ Thickness	Manufacturer U.K.
Adhesive	Mid grey	19	9.8	1.535	60	2-4mm	SBD
Primer	Translucent	-	-	1.12	-	4-6 m^2 /l	SBD

The next important material required for pre-stressing is the Expansive Agent (EA). It is supplied as a powder and the colour is grey when mixed with water [7] This material is normally used for concrete demolition and is placed in pre-drilled holes. Figure 1 illustrates the relation between expansion pressure and reaction time for different hole diameters (when used for demolition) over a period of four days. Figure 1 also shows the EA when mixed with water (20% - 23%). In this experimental work the EA was mixed with cement in different proportions.

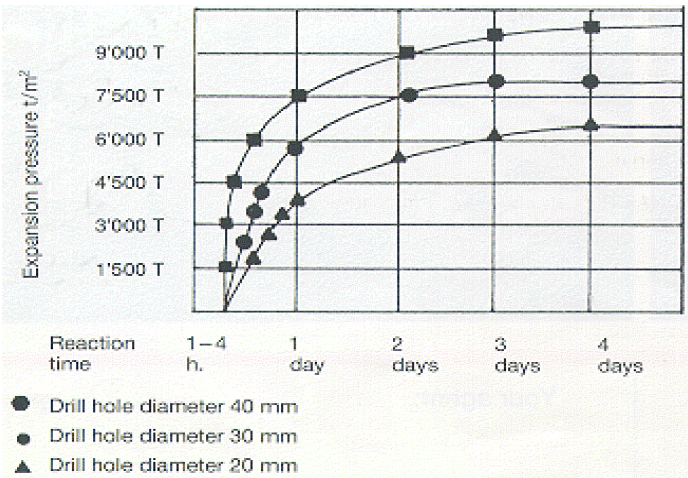

Figure 1. Properties of Expansive Agent (EA)

3. THE EFFECT OF CONFINEMENT STIFFNESS

In order to investigate the effect of confinement stiffness, the EG was confined directly by metal tubes. The tubes were selected to apply different confinement stiffness levels with different materials (steel or copper), thicknesses, diameters as shown in Figure 2 and different EA ratios. The ratio of length (L) to inner diameter (D) of the tubes was set to be around 10. It is obvious that, choosing different thicknesses of confinement materials (t), elastic modulus of the tubes (E) and radius of tubes or jacket (r), can change the confining stiffness (CS) as defined by 2E t / ID.

Figure 2. Metal tubes filled with EG

Thirty six metal tubes were filled and tested with EG levels 5%, 10% and 20% of EA. The EG consisted of Betonamit (EA), 50% cement, the rest of mix ratio completed by sand (was variable) and appropriate water (between 17% to 20% of the weight of mix).

Various methods of sealing the tubes were tried during casting to prevent any leakage due to the high pressure created by the EG. Due to the possibility of welding on the black steel, one end was fixed while the other end remained open until the expansive grout (EG) was poured into the tube. The end was then sealed by fastening a screw. Due to the characteristics of the metals, welding of copper and annealed steel tubes was not a feasible solution. Two solid plugs were therefore fitted with a located pin designed. In addition, a layer of silicon seal was applied to the surfaces of the plugs to prevent any leakages. The pipes were instrumented with 3 strain gauges placed at the mid length and equally spaced along the circumference. Two gauges were used to measure lateral strain and one to measure the axial strain. Since the strain gauge had a length of 15 mm, only two strain gauges, which were fixed one laterally and the other one axially were used for the smaller copper and black steel pipes.

4. EFFECT OF VOLUME OF EG

This sub-phase investigated the effect of 3 different amounts of expansive grout (EG) with the same EA ratio (20%) on steel tube cylinders having the same confining stiffness.

All tubes were instrumented on the outside with three surface strain gauges to measure lateral strain and one strain gauge to measure axial strain.

The first sample (S1) was filled with expansive material without any core in the middle. The second sample (S2) had a concrete core with a diameter of 50 mm placed in the middle. Additional strain gauges were placed at the mid height of the concrete core to monitor lateral and axial strain. The third sample (S3) was similar to S2, but the concrete core had a diameter of 66 mm. Figure 3 shows samples S1, S2, and S3. To avoid any leakage from the top and the bottom of the cylinders, two steel plates (with rubber washers) were used.

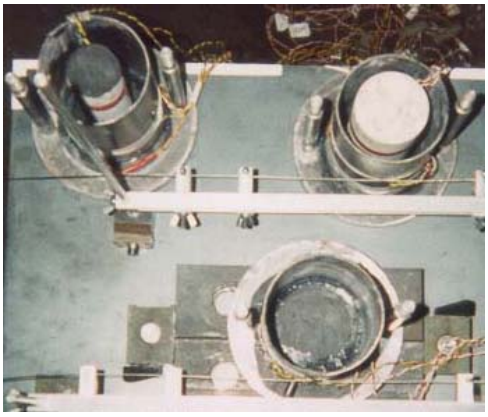

Figure 3. The cylinders filled with different volume of EG

When all samples were ready to be cast, as shown in Figure 5-33, the grout was poured in the 7 mm gap provided. The amount of the expansive grout (EG) that was used determined as a function of the amount of expansive agent (EA). Ratios (in weight) of 10%, 20%, 30% or 40% were used. Whilst filling the EG through the gap, vibrating by a smooth vibrator machine took place. The expansive grout was injected using a silicon gun with plastic pipe attachment with a diameter of five mm.

5. SPECIMEN DETAILS

Since the chemical pre-tension (expansive pressure) is caused by the EA reacting against the confining jacket this means that the magnitude of this pre-tension depends on the degree of stiffness of the jacket and percentage of EA. Experiments were conducted by using these two parameters to quantify the amount of pre-tensioning on the jacket. Following that series of testing, concrete cylinders were confined with pre-tensioned composites.

To vary the stiffness and strength of the confining jacket, one, two and three layers of carbon and glass sheets were used. Different percentages of EA were mixed with cement (10% and 20%) to achieve different confining pressures. Also, different materials for jacketing (Glass and Carbon) were used to achieve different stiffness and strength.

A total of eighteen 100mm x 200mm concrete specimens were prepared without any pre-tensioning, 36 specimens were prepared with different levels of confinement pre-stressing and 15 unconfined specimen were tested under compression to determine the plain concrete strength. The concrete consisted of ASTM Type 1 Portland cement, river sand aggregate with a fineness modulus of 2.5 and gravel river aggregate with a maximum size of 10 mm. The water-cement ratio (w/c) was about 0.52 by mass. The average 28-days compressive strength of the concrete specimens was 31 MPa. Concrete specimens wrapped with one layer of Carbon and two layers of Glass without pre-tensioning force were designated as C0101, C0102, G0201 and G0202, respectively, whereas concrete cylinders with the same characteristics but pre-tensioned with 10% of EA and one layer of jacket were designated as C71101, C71102, G72101 and G72102, and with 20% of EA were designated as C71201, C71202, G72201 and G72202, respectively. Similar designation names were used for two and three layers either for non-pre-tensioned or pre-tensioned samples.

6. PREPARATION OF SPECIMENS

For the wrapping of concrete cylinders without pre-tensioning, after applying the epoxy primer on the concrete surface, epoxy adhesive was applied and Carbon/Glass sheets were wrapped around the concrete cylinder until one wrapping layer was completed (with one third overlap). At the same time a special roller was used to help impregnate the fibre with resin and hardener and give a smooth finish. After curing, the strain gauges were glued directly onto the body of the jacket.

For the pre-tensioned specimens, a gap is needed between the concrete and FRP for the insertion of the EA. For these experiments, the FRP jacket was pre-manufactured with a diameter 14mm larger than the concrete cylinder. After curing, the jacket was placed around the concrete and the ends were capped to seal the expansive agent inside. Strain measurements were taken during the expansion phase of the expansive agent for up to four days. The testing procedure followed was then the same as for the unconfined specimen.

7. TEST PROCEDURE AND OBSERVATIONS

The application of displacement to the specimens was controlled manually. The displacement was applied incrementally with each displacement level being held for a few seconds at each 0.1mm increment. All specimens were tested under centric (axial) loading. Failure was always explosive due to the high strain energy stored by the FRP material and it took place around the middle of the cylinder height as shown in Figure 4.

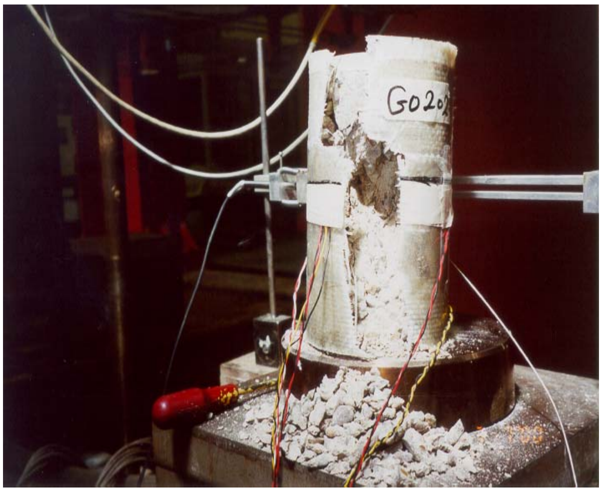

Figure 4. Failure of the specimen confined with FRP jacket.

8. EXPERIMENTAL RESULTS

The stress-strain diagrams for the specimen tested with one layer of either glass or carbon FRP are shown in Figure 5. Each graph shows the results for the unconfined cylinders as well as for the confined with or without pre-stressing. The right hand part of the graph shows the longitudinal strain whilst the left hand part shows the lateral strain. Strain measurements shown are the average values from the strain gauges and DV devices. The results are in general in good agreement between the two types of measurements, even though strain gauges measure local strains and DV devices integrate the strains over the length. The strain gauges also show the pre-strain that was developed by the EA. The longitudinal strain gauges on the pre-tensioned specimen show contradicting trend. Whilst the Carbon wrapped specimen show the strain to remain compressive, in the case of glass the strain eventually becomes tensile. This is partly because the glass wrapping contains longitudinal fibres as well, which restrain the concrete from expanding and lock some strain in the mid-height. It is also partly to do with the wrapping overlap, which creates eccentric deformations on the specimen. Eccentric deformations and initial slip of the jacket may explain the tensile strains in the glass.

9. CONCLUSIONS

This paper has shown experimental results from concrete specimen wrapped with glass and carbon FRP. In this investigation EA was used to produce post tensioning force in FRP jackets. It has shown that post tensioning can be used to enhance the load capacity and behaviour of concrete.

REFERENCES

1. Mortazavi A., “Strengthening, ductility and repair of RC structures by lateral confinement”, MPhil thesis, University of Sheffield, Oct. 1998.
2. Weber & Broutin Ltd., En-Force strength in construction, SBD, 1999, UK.
3. Betonamit, “The non-explosive cracking agent for universal application”, 1998, UK, Re. No. 1504010.
4. Pilakoutas K., “Ductility design of reinforced concrete members”, 16th European Seminar on Earthquake Engineering, Stara L., Czechoslovakia 6-12 Oct. 1991, pp 62-71.
5. Eurocode No 8, "Design provisions for earthquake resistance of structures", Part 1-4, "Strengthening and repair of buildings" (Draft), Commission of the European Communities, Brussels, 1995.

CD04-003

EFFECTS OF FRP WRAPPING ON THE BOND-SLIP BEHAVIOR OF REINFORCING BAR

J. Shafaie[1], A. Hosseini[2], M. S. Marefat[3]
[1]MSc. Student, School of Civil Engineering, University of Tehran, Tehran, Iran
[2]Assistant Professor, School of Civil Engineering, University of Tehran, Tehran, Iran
[3]Professor, School of Civil Engineering, University of Tehran, Tehran, Iran

ABSTRACT
Fiber reinforced polymer (FRP) composites are being successfully used for strengthening of existing reinforced concrete (RC) structures because of their superior properties. Effects of wrapping with FRP on the strength and ductility of concrete members have been extensively investigated but information about effects of external confinement on the bond-slip behavior is very limited. In this paper the effect of external confinement with CFRP strips and internal confinement with transverse stirrup at beam splice test is evaluated and the results of two confinements are compared with one another. The main examined parameters include concrete cover, development/splice length, diameter of the reinforcing bar, concrete compressive strength and the amount of ordinary transverse reinforcement in the splice/development region. Test results indicated that external confinement with CFRP is more effective than internal confinement on bond strength and bond failure ductility.

Keywords: FRP, Strengthening, Beam splice test, Bond-slip relationship

1. INTRODUCTION
In structural concrete construction, the concrete is reinforced to compensate for its relative weakness in tension. The interfacial action between the reinforcement and the surrounding concrete involve many different mechanisms that collectively establish the phenomena of “bond”. The nature of bond can vary extensively with varying loads, various types of reinforcement, and variety of situations [1].
The main parameters that influence the bond strength between steel reinforcing bars and concrete are well documented in the technical literature. Important among these parameters include concrete cover, development/splice length, diameter of the reinforcing bar, concrete compressive strength, and, for conventionally confined concrete, the amount of ordinary transverse reinforcement in the splice/development region [2].
There are two types of bond failure between reinforcing bars and concrete, and the parameters that influence each of them are well documented in literature. If the concrete cover around the reinforcing bar is large or the concrete is well-confined by transverse reinforcement, or both, bond failure occurs by pullout as a result of the shearing-off the concrete keys between the lugs. On the other hand, if the

concrete cover is small, and the concrete is either unconfined or moderately confined, bond failure occurs by splitting of the concrete around the reinforcing bar. The most common parameters that influence the splitting bond strength include concrete strength, bar diameter, cover and spacing of reinforcement, and area of transverse reinforcement [3, 5].

The amount of confinement is an effective factor in bond strength between steel and concrete. ACI code mentioned this parameter in calculating the development length of reinforcing bar (K_{tr}) [4, 9].

Concrete confinement becomes particularly important in areas of seismic risk. Concrete confinement in areas of seismic risk reduces bond deterioration under cyclic loading, enhances the energy absorption and dissipation capabilities and consequently improves the chances of the structure or structural components to survive under earthquake loading [2].

In this paper the effect of external confinement with CFRP strips and internal confinement with transverse stirrup on bond strength and bond-slip behavior of reinforcing bar is evaluated. For this purpose two series of the experimental test results have been used. The experimental tests carried out by Harajli and Hamad (2002) [3] which examine external confinement with CFRP strips on beam splice test and the experimental tests carried out by Harajli, Hamad, and Rteil (2004) [2] which examine internal confinement with transverse stirrup on beam splice test are used and the results of two experimental tests are compared with each other. According to the experimental test result, bond stress-slip graphs are presented and compared together.

1.1. Bond Stresse

The bond stress around the reinforcement will appear if force or stress in the steel bar or concrete varies from one point to the other. According to Figure 1, the amount of bond stress in the infinitesimal length of reinforcing bar that is displayed with μ, according to satisfying equilibrium bond stress (μ) is equal to:

$$\mu = \frac{d_b}{4} \frac{\Delta f_s}{\Delta x} \tag{1}$$

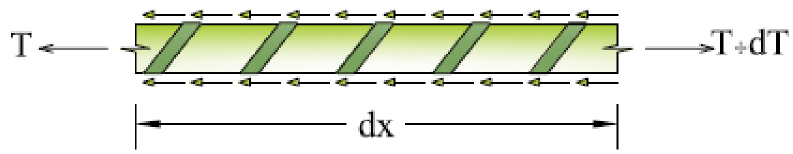

Figure 1. Representation of bond stress on the reinforcement

The nature of bond can vary extensively with varying loads, various types of reinforcement, and variety of situations. Conventionally, two broad types of bond are defined: anchorage/development bond and flexural bond [6, 7].

1.2. Anchorage/Development Bond
Anchorage/development bond refers to the interaction between the reinforcement and concrete when an axial tension or compression force has to be transferred to the concrete [1, 7].

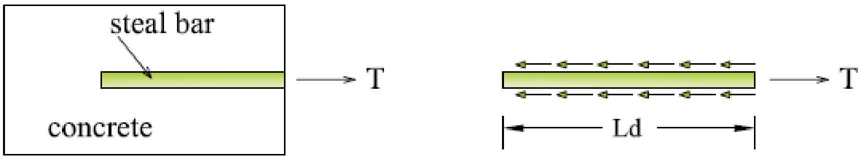

Figure 2. Anchorage/Development bond.

$$\mu_{ave} = \frac{d_b}{4} \frac{f_s}{l_d} \quad (2)$$

1.3. Flexural Bond
Flexural bond refers to a situation where a gradient in bending moment occurs and the force, in the reinforced concrete member, is subjected to change [1, 7].

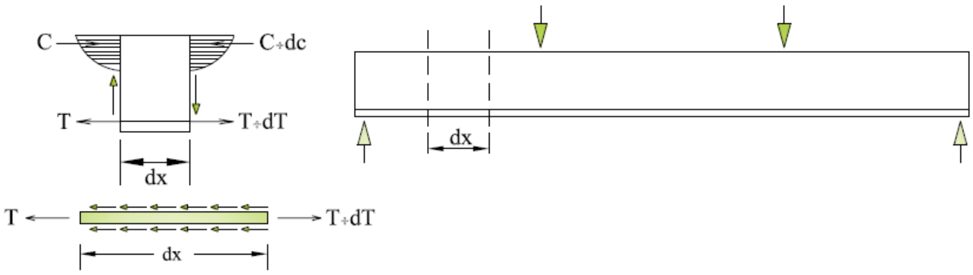

Figure 3. Flexural bond considerations

$$\mu(x) = \frac{V}{\pi d_b z} \quad (3)$$

2. DIFFERENT KINDS OF TESTS TO DETERMINE THE BOND STRENGTH
The bond strength between reinforcement and concrete is usually determined by the following tests [7, 8].

2.1. Pull-Out Test
This test evaluates the bond capacity of various types of bar surfaces relative to specific embedded length. The distribution of tensile stress will be uniform around the reinforcing bar at specific sections and varies along the anchorage length of the bar and a radial distance from the surface of the bar (Figure 2). However, this test does not represent the effective bond behavior in the surface of the bars in flexural members, because stresses vary along the depth of concrete section [6, 7].

2.2. Embedded Rod Test

In these tests, the tensile force is increased gradually and the number of cracks and their spacing and width are recorded. The bond stresses vary along the bar length between cracks. The strain in the steel bar is maximum at the cracked section and decreases toward the middle section between cracks [6, 7].

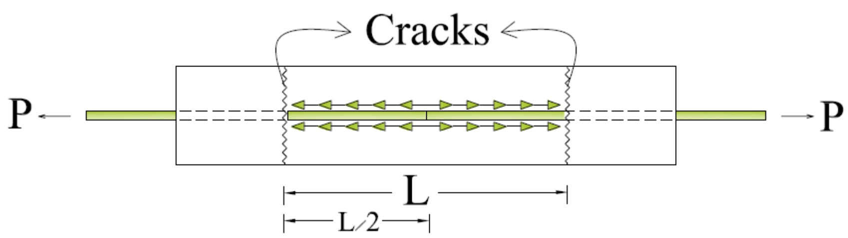

Figure 4. Bond mechanism in an embedded bar.

2.3. Beam Splice Test

Tests on flexural members are also performed to study the bond effectiveness along the surface of the tension bars. In this paper the beam splice test is used for studying the effect of confinement on bond-slip response of the reinforcement in the concrete [6].

3. EXPERIMENTAL PROGRAM

3.1. Properties of Test Specimen and Test Variables

The test specimen consisted of beam specimen with spliced reinforcement at midspan. Dimensions of the specimens and test parameters are presented in Figure 1 and Table 1, respectively. Four different sizes of reinforcement were used (16, 20, 25, and 32 mm). The number of splices and the width of the specimens were calibrated to produce six different ratios of minimum concrete cover-to-bar diameter c/db varying between 0.56 and 2.0. The concrete side cover, bottom cover, and 1/2 the clear distance between the spliced bars were kept identical for each specimen. The splice lengths L_s for all specimens were selected at 5db, small enough to produce local bond conditions. A bond-free length, extending outside the ends of the specimen, was secured using polyvinyl chloride (PVC) tubes for slip measurement. The spliced bars consisted of Grade 60 steel. The clear distance between the bar ribs were 6.5, 6.0, 12.0, and 9.0 mm for the 16, 20, 25, and 32 mm bars, respectively. All specimens were confined with ordinary transverse reinforcement. The transverse reinforcement consisted mainly of two (6 or 10 mm in diameter) stirrups or ties, placed within the splice region at 1/4 the splice length from each splice end producing a spacing of transverse reinforcement in each specimen equal to $L_s/2$ (Figure 1). Each stirrup consisted of two legs for the specimens with two splices or one leg for the specimens with one splice. The area and spacing of transverse reinforcement were selected to produce a practical range of values of the transverse reinforcement parameter A_{tr} /snd_b between 0.011 and 0.12 [2].

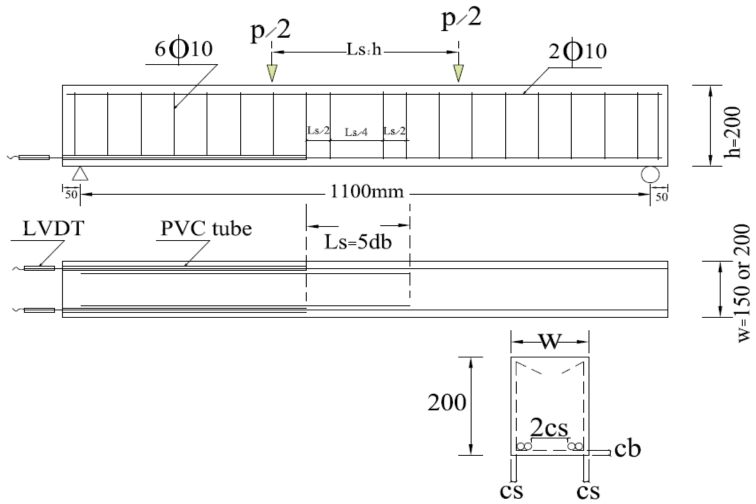

Figure 5. Specimen's dimensions and splice details.

Table 1: Summary of test parameters [2].

Specimen	Bar diameter db, mm	Concrete cover cb=cs, mm	c/db	No. of Splices n	Splice length LS, mm	Atr /n (mm^2)	S (mm)	A_{tr}/ snd_b	Concrete strength fc ′, MPa
B1N	16	21.5	1.34	2	80	28.3	40.0	0.044	40.7
B1W	16	34.0	2.1	2	80	28.3	40.0	0.044	40.7
	16	34.0	2.1	2	80	78.5	40.0	0.12	43.2
B2N	20	17.5	0.88	2	100	28.3	50.0	0.028	42.7
B2W	20	30	1.5	2	100	28.3	50.0	0.028	39.0
	20	30	1.5	2	100	78.5	50.0	0.079	43.2
B3N	25	50	2.0	1	125	28.3	62.5	0.018	42.7
B3W	25	25	1.0	2	125	28.3	62.5	0.018	40.7
B4N	32	43	1.34	1	160	28.3	80.0	0.011	39.0
B4W	32	18	0.56	2	160	28.3	80.0	0.011	39.0

3.2. Specimen Casting and Testing

The concrete mixture was designed to achieve a target concrete compressive strength fc′ of 41 MPa. Portland cement, washed sand, and crushed limestone with 10 mm maximum size aggregate were used to prepare the concrete mixture. The cement: sand: aggregate proportions by weight were 0.32:0.5:1.0 with a water-cement ratio (w/c) of approximately 0.45. Each two specimens were cast together. The concrete strengths were determined using three standard 150 x 300 mm cylinders taken from each batch. Actual concrete strengths are given in Table 1 [2].

3.3. Loading Equipment and Arrangement of Strain Gauges

The specimens were loaded with two symmetrical point loads to produce a constant moment region extending a distance equal to 1/2 the member height h outside the splice zone on either end of the splice. Slip of each splice and deflection of the specimen at midspan were measured using mechanical gages [2, 3].

4. DISCUSSION OF TEST RESULTS

The bond stress u at any load level during load application is calculated using the following bond relation

$$u = \frac{A_b f_s}{\pi d_b l_s} = \frac{f_s d_b}{4 l_s}$$

Where A_b is the area; l_s is the splice length ($5d_b$) of the bar; and f_s is the steel stress, calculated using cracked section analysis corresponding to the level of applied load.

All specimens developed clear bottom splitting or side splitting cracks along the splice length and failed in splitting mode. Splitting cracks were preceded by flexural cracks forming simultaneously at both ends of the splice. Following the formation of the splitting cracks, the load resistance dropped suddenly and diminished gradually with increasing load. Because the load resistance and deflection of the specimens are linearly related to the bond strength and bar slip, the general shape of the load-deflection behavior of the specimens was very similar to the bond stress versus slip response [2].

Table 2. Comparison of test data for different types of concrete confinement [3]

Specimen	$\frac{U_{max}}{\sqrt{f_c'(mpa)}}$ (plain concrete)	(confined concrete) $U_{max}/\sqrt{f_c'(mpa)}$		
		Transverse reinforcement	CFRP (Harajli and Hamad 2002)	
			One CFRP wrap	Two CFRP wraps
B1N	1.09	1.13	1.18	1.08
B1W	1.33	1.34 1.51 (10 mm)	1.52	1.57
B2N	0.82	0.90	0.90	1.09
B2W	1.04	1.10 1.20 (10 mm)	1.28	1.20
B3N	1.17	1.39	1.47	1.27
B3W	0.71	0.91	0.89	0.91
B4N	0.82	0.77	0.91	0.93
B4W	0.52	0.64	0.64	0.66

Figure 6, 7, and 8 show variation of the bond-slip response for the same specimen with an increase in the area of ordinary transverse steel, FRP reinforcement, respectively.

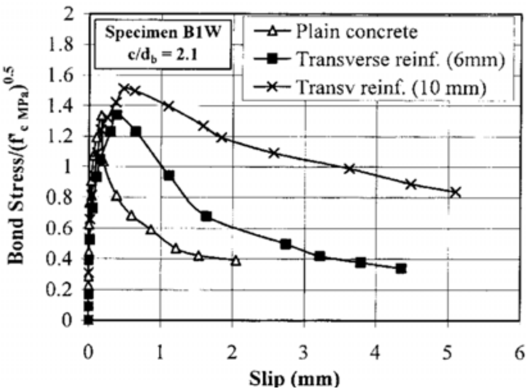

Figure 6. Effect of area of ordinary steel on bond stress-slip response for specimen B1W[2]

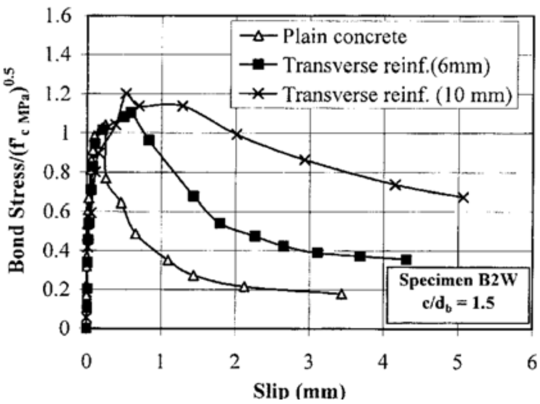

Figure 7. Effect of area of ordinary steel on bond stress-slip response for specimen B2W [2]

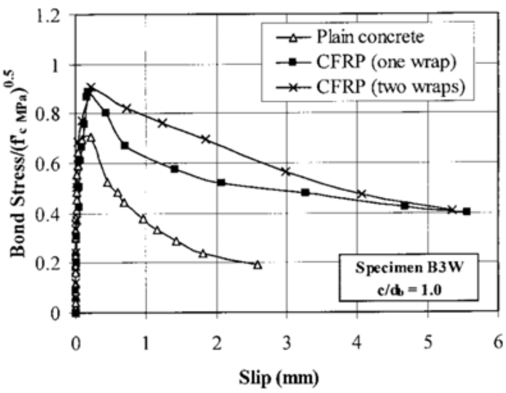

Figure 8. Typical effect of area of FRP sheets on local bond stress-slip response [3]

In the specimens confined with CFRP, flexible sheets were wrapped around the perimeter of the specimens along the full splice length. All specimens (Table 2) were confined with either single or double CFRP wraps. The design thickness of the sheets is equal to 0.13 mm (0.005 in.). The modulus of elasticity, the tensile strength, and strain at break of fibers are equal, respectively, to 230,000 MPa, 3500 MPa, and 1.5%.

Comparing the current bond-slip results for concrete confined with transverse reinforcement with those obtained earlier using other types of confinement as shown in Figure 6 to 8; it is interesting to observe that the shape of the bond stress-slip response tends to be intrinsically similar irrespective of the type and amount of confinement used. The corresponding response can be divided into four distinct stages of behavior as shown schematically in Figure 9 and as described previously by Harajli, Hamad, and Karam (2002) [2, 3]:

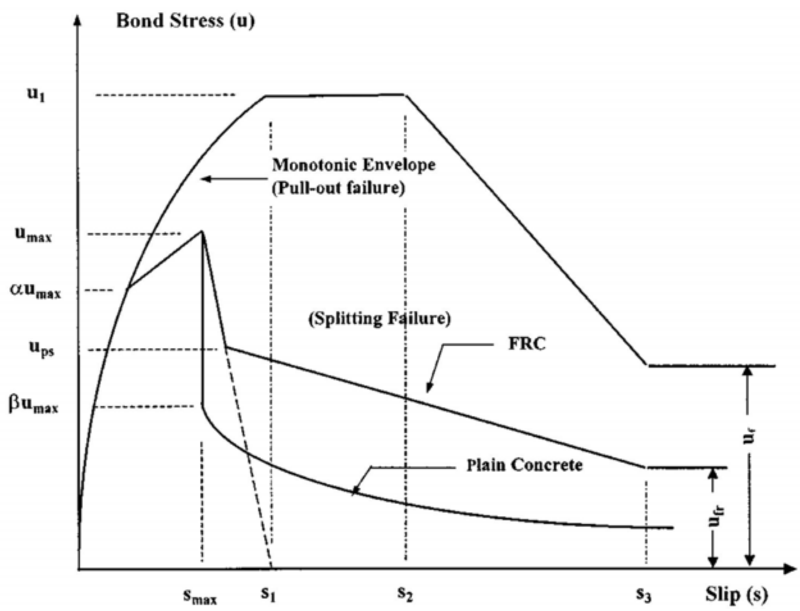

Figure 9. General model of local bond stress-slip behavior of confined concrete [3]

1) Initial stiff bond-slip response associated with adhesion and friction, which coincides perfectly with bars that undergo pullout bond failure in well-confined concrete; 2) soft pre-splitting response associated with the formation of circumferential tensile cracks in the concrete surrounding the steel bar and their gradual propagation toward the surface until the peak bond strength at which splitting occurs is reached; 3) sudden drop in the bond resistance down to a post-splitting bond strength as a result of a state of dynamic equilibrium between the radial component of the bond force and the post-splitting tensile resistance of the concrete matrix (confined or unconfined) surrounding the bar; and 4) gradually deteriorating bond resistance with increasing slip beyond splitting associated with the progressive widening of the splitting cracks until the bond resistance diminishes completely. It is clear from the comparisons made in Figure 2 to 4 that one of the most evident and important contributions of confinement reinforcement

to the local bond behavior is the significant reduction in bond deterioration following bond failure relative to plain unconfined concrete.

5. CONCLUSIONS

This study concentrated on the experimental investigation of confinement on local bond-slip behavior of reinforcing bar embedded in plain concrete at beam splice tests. The influence of two main parameters on bond slip response was evaluated namely, external confinement with FRP sheet and internal confinement with transverse stirrup.

From the test results, the following conclusions can be drawn.

1. The value of the ultimate bond stress is not influenced by the bond length, but increases as concrete compressive strength increases.
2. The bond stress-slip curves are clearly nonlinear, and have a tendency to become parabolic in form.
3. External and internal confinement causes ductility in the bond-slip relationship.
4. The bond strength due to confinement increases in proportion to the modulus of elasticity of FRP.
5. For small development/splice lengths corresponding to local bond conditions, confining the concrete with ordinary transverse steel increases the bond strength only slightly, but leads to considerable improvement in the ductility of bond behavior in the post-splitting stage.
6. For confined concrete, the shape of the local bond stress-slip response consists of four distinct stages of behavior. The corresponding behavior tends to be identical irrespective of the type of confinement used.
7. Because external confinement with FRP is more effective in restricting the width of the splitting cracks than internal confinement with ordinary steel, for the same area of confinement reinforcement per unit length along the splice and taking into account the relative modulus of elasticity of the material, the increase in bond resistance acquired for concrete confined externally with FRP sheets is considerably higher as compared with concrete confined internally with ordinary steel.

REFERENCES

1. Marefat, M, S., The Mechanics of Bond for Helical Devices Anchored in Concrete, PhD thesis, 1993, Department of Civil and Environment engineering, The University of Waterloo, Ontario, Canada, PP. 1-20.
2. Harajli, M. H., Hamad, B. S. and Rteil, A. A., Effect of Confinement on Bond Strength between Steel Bars and Concrete, ACI Structural Journal, 2004, V. 101, No. 5, September-October., pp. 595-603.
3. Harajli, M. H., and Mabsout, M. E., Evaluation of Bond Strength of Steel Bars in Plain and Fiber-Reinforced Concrete, ACI Structural Journal, 2002, V. 99, No. 4, July-Aug., pp. 509-517.
4. ACI Committee 318, Building Code Requirements for Structural Concrete (ACI 318-02) and Commentary (318R-02), 2002, American Concrete Institute, Farmington Hills, MI, USA.

5. Harajli, M. H., Hamad, B. S. and Karam, K., Bond-Slip Response of Rebar Embedded in Plain and FRC, 2002, Journal of Materials in Civil Engineering, ASCE, V. 14, No. 6, Nov.-Dec., pp. 503-511.
6. Hassoun, M. N., Al-Manaseer, A., Structural Concrete Theory and Design, 2005, JOHN WILEY & SONS, Third Edition, PP. 216-230.
7. Mostophinegad, D., Design of Concrete Structures, 1385, Arkan Danesh, Third Edition, Volume 2.
8. Keynia, A, M., Analysis and Design of Concrete Structure, 1373, Jahad Daneshgahi Esfehan, Forth Edition.
9. Iranian Concrete Code, 1382, First edition.

CD04-004

EFFECT OF TIEROD POSITION IN SIESMIC REHABILITATION OF ANCHORED CONCRETE QUAYWALLS

A. Derakhshani[1], M.S. Fayyazi[2], Kh. Bargi[3]
[1]M.Sc. student of Marine Structures, Faculty of Civil Engineering, University of Tehran
[2]M.Sc. student of Structures, Faculty of Civil Engineering, University of Tehran
[3]Professor in Faculty of Civil Engineering, University of Tehran

ABSTRACT

One of the most common marine structures is anchored concrete quaywall. Obviously, anchoring the wall will reduce the penetration depth, maximum bending moment and lateral displacement of wall in both static and dynamic conditions.

In this research, first, effect of tierod position in anchored concrete quaywalls in primary static condition is considered and compared with two methods: "Free Earth Method" and "Finite Difference Method". Also, practical curves of "maximum moment" and "tierod axial force" are given versus r (ratio of tierod depth to wall length) in static condition.

Then, dynamic response of different cases (various tierod depths) is illustrated and compared. Practical history curves of "maximum positive and negative moment", "tierod axial force" and "lateral displacements" are provided via "Finite Difference Method". Analyzing these charts, influence of tierod position on anchored quay walls in seismic condition is investigated about seismic behavior and rehabilitation of the structure. Suitable tierod position results in better serviceability and lower maximum moment in concrete quay wall profile and therefore economical one.

Keywords: anchored quaywall, seismic evaluation and rehabilitation, tierod

1. INTRODUCTION

Flexible walls include "Anchored Sheet pile walls" or" Anchored Bored/ Continuous/ secant pile walls " are used as quaywalls. Weight of such walls is ignored comparing with lateral forces. When their height from the dredge line is more than about 6 meters, it is common to use an anchorage system [3, 5, and 7]. Using anchorage decreases penetration depth, maximum bending moment and lateral displacement in both static and dynamic conditions. In classical methods which the equilibrium equations are used, the deformation is ignored; so, it becomes necessary to utilize the numerical methods. This will help the designer to evaluate the serviceability of the structure in case of an earthquake. To rehabilitate the structure in seismic condition, the effect of tierod position in anchored concrete quaywalls is evaluated. It can improve the serviceability and also results in more economical construction using concrete wall profiles with more suitable sections [4, 8].

2. STATIC ANALYSIS AND DESIGN

2.1. Free Earth Method

"Free Earth Method" is a simple classic method which is primarily used here to analyze and design the anchored quaywall; assumptions and parameters which are used in this method are shown in Figure 1 [3 , 5 , 6 , 7].

But in such methods some facts are ignored. For example:

- Wall moving tendency toward soil.
- Wall and anchor flexibility.
- Real lateral soil pressure distribution.

So, for more accurate analysis, a numerical method is used via FLAC 2D software as will be described later.

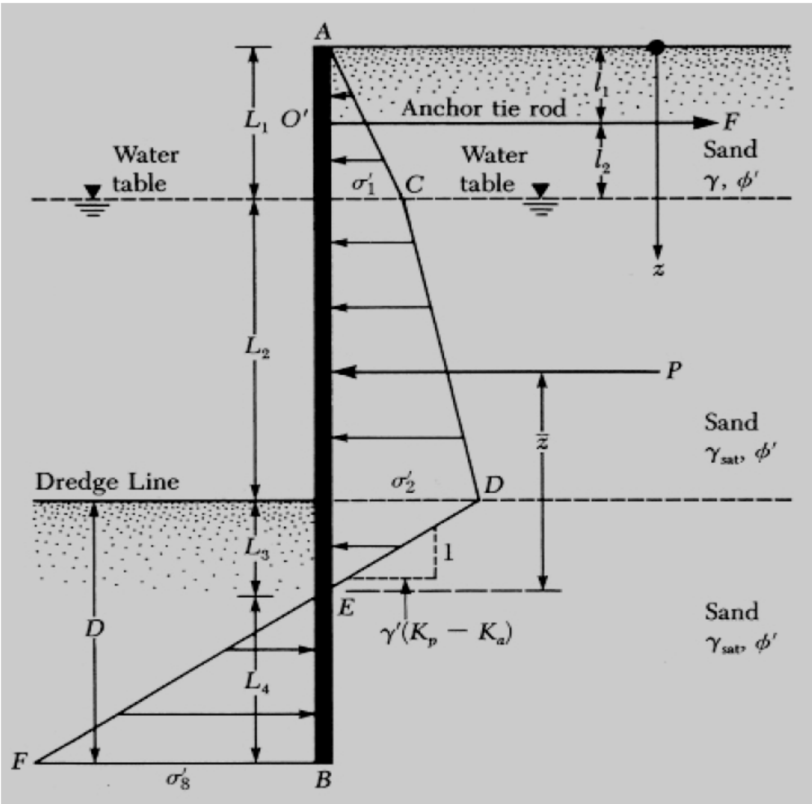

Figure 1. Free Earth Method [7]

2.2. Matlab Programming

Using Matlab software, a program is developed in order to analyze anchored concrete quaywalls utilizing "Free Earth Method" in sand. "Maximum moment" and "tierod axial force" curves are displayed versus tierod depth ratio to concrete wall length.

Soil properties and model parts properties are showed in tables 1 and 2 respectively.

Table 1: Soil properties

	Y (kN/m3)	Ysat (kN/m3)	φ (Degree)	C (kN/m2)
Sand	21	25	38	0

Table 2. Model parts properties

	E(N/m2)	A (m2/m)	P (m/m)	I (m4/m)	L1 (m)	L2(m)
Quaywall	3,20E+10	1,9	4,3	3,67	4	18
wall	3,20E+10	1	2	0,083		
Cable	2,00E+11	0,00277				

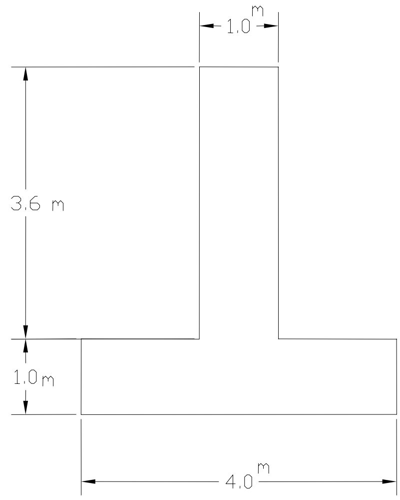

Figure 2. Concrete quaywall profile

As it is determined in Figure 3 and Table 3, with deepening tierod position its axial force increases and vice versa, maximum moment in concrete quaywall profile decreases. ("r" is the ratio of tierod depth to quaywall length).

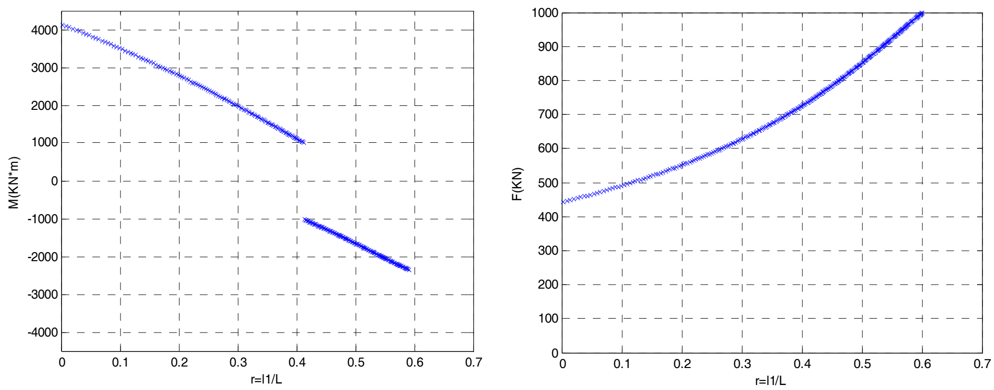

Figure 3. (a) Maximum moment, (b) Tierod axial force

Table 3: Matlab program results for three tierod positions (Free Earth Method)

Sand				
l1 (m)	**R (l1/L)**	**M (KN*m)**	**F (KN)**	**D (m)**
4.09	0.15	3167	518.7	5.59
8.01	0.29	2024	623.7	5.15
12	0.45	-1317	791.7	4.31

3. DYNAMIC ANALYASIS WITH "FINITE DIFFERENCE METHOD"

Evaluating the serviceability of the structure in case of an earthquake needs modeling with a strong, accurate and fast numerical method**.** So, "Finite Difference Method" is used in this research. At first the structure is modeled in static condition by means of "FLAC 2D" software and then the dynamic analysis is done [1, 2].

3.1. "Flac 2d" Software Introduction

This software is a computational one based on explicit "Finite Difference Method" and is equipped with tools which can consider various geotechnical aspects. In this research the effect of tierod position in anchored concrete quaywall is mentioned for economical Seismic rehabilitation; therefore, complicated soil behavior is considered by means of Mohr-Coulomb plastic soil model [1, 2].

3.2. Problem Solution Stages with "Flac 2d" (FDM)

First, general problem environment is created via Finite Difference elements, then Mohr-Coulomb behavior model is selected and material properties are assigned. Before solving problem it is necessary to determine boundary and initial conditions.

Modeling and loading procedure:

- Modeling soil considering initial stress in soil mass.
- Installing main and anchorage walls in soil.
- Positioning tierod between two walls.
- Excavating front of main wall to final dredging level.
- Applying water pressure.
- Solving problem in static condition.

After evaluating wall behavior in static condition, acceleration is applied to the lower model boundary with shape of a sinusoidal wave with maximum amplitude of 0.25g in two seconds duration. The general geometry of model is shown in Figure 4.

Dynamic loading procedure:

- Applying seismic load with ***PGA*** of 0.25g.
- Dynamic analysis of the problem.

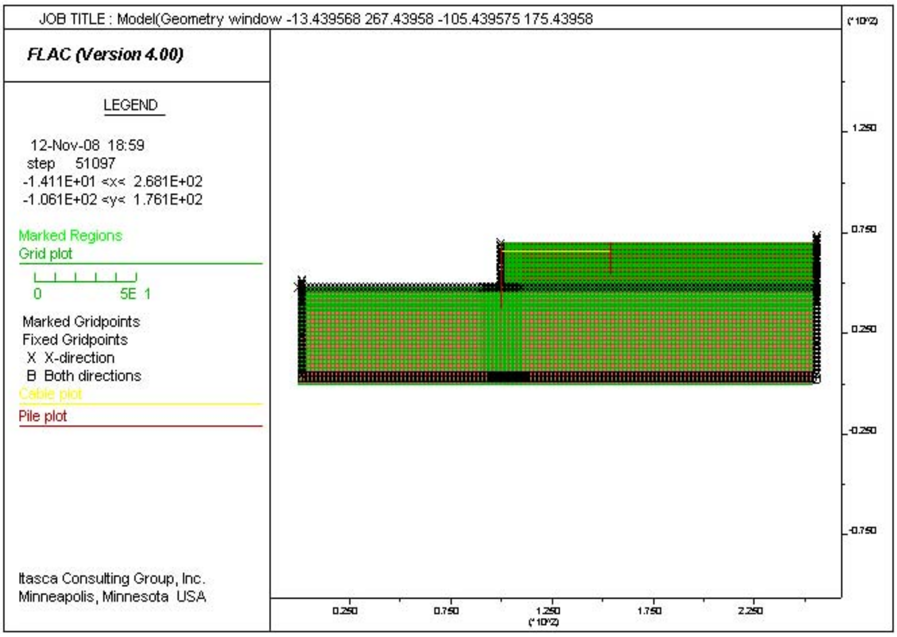

Figure 4. "Finite Difference Method" modeling

4. ANALYSIS RESULTS

In order to find about consistency in primary static analysis results of two methods, Figure 5 is prepared. It is shown that both methods result in similar tierod axial force and maximum quaywall moment based on various tierod positions ("r" is ratio of tierod depth to quaywall length).

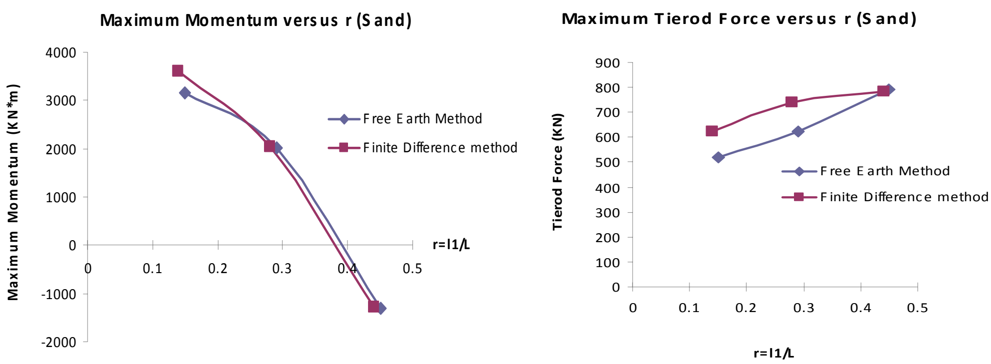

(a) (b)

Figure 5

Results of dynamic analysis are illustrated in Figures 6 to 9 .Lateral displacements are shown in Figure 6.Charts show that lateral displacements in bottom and middle of the quaywall based on different tierod depths are almost similar to each other during time history.

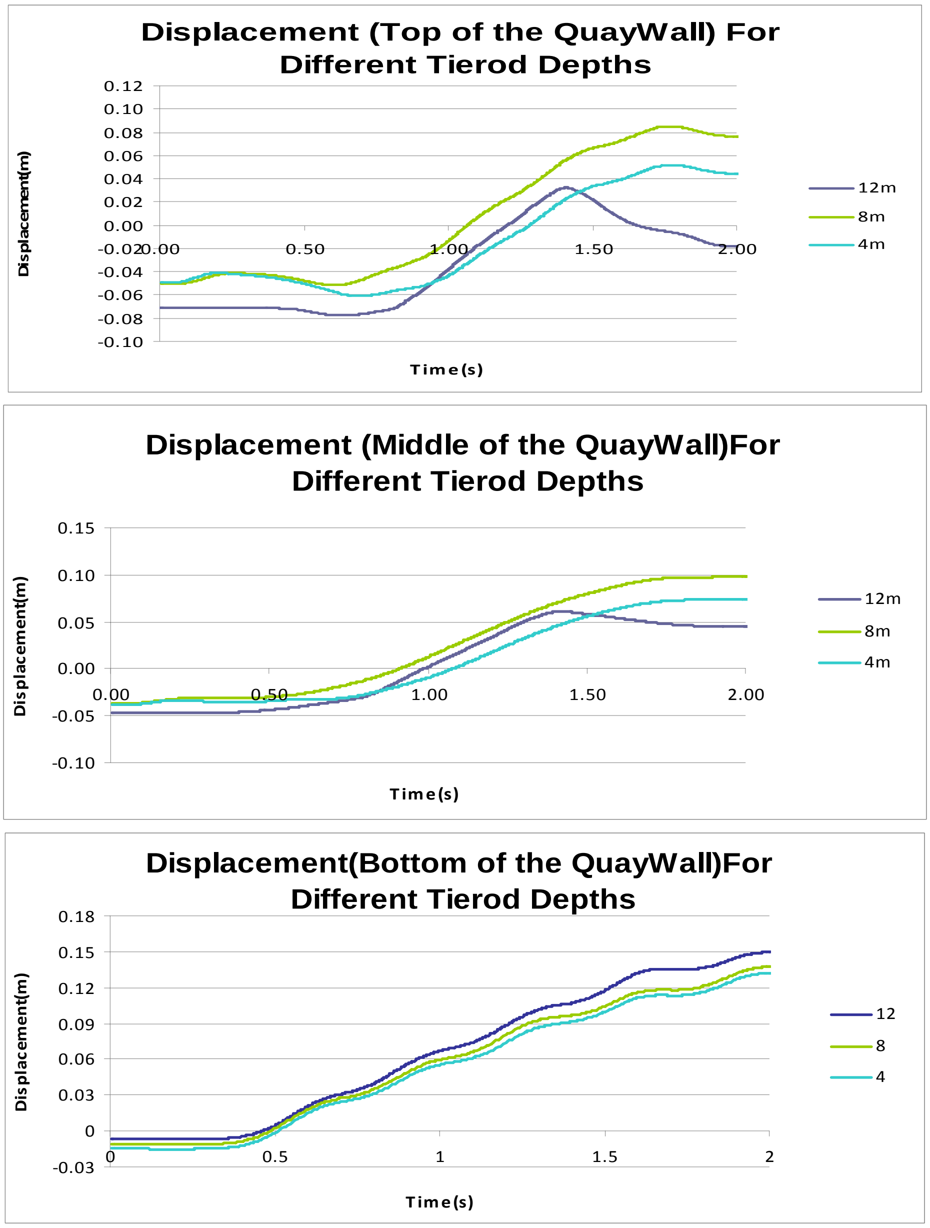

Figure 6

But as the main criteria of serviceability, different displacements of quaywall top that are shown above, have more changes with deepening tierod position, during assigned earthquake. Note that all lateral quaywall top displacements are limited between -0.08m to 0.09m. So, they are not more than allowable displacement of 0.30m due to "OCDI".

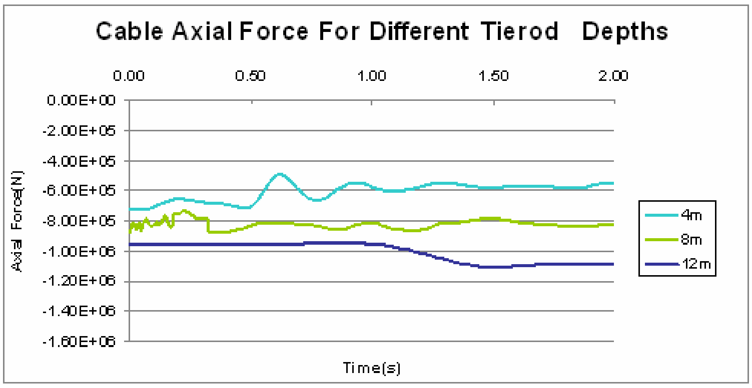

Figure 7. Tierod axial force history

As it has been determined in Figure 7, Tierod axial force increases with deepening tierod position in all history duration.
Similarly, maximum positive moment in quaywall (Figure 8) increases with deepening tierod position in all history duration.
Absolute amount of maximum negative moment in quaywall (Figure 9) in all history duration decreases with deepening tierod position.

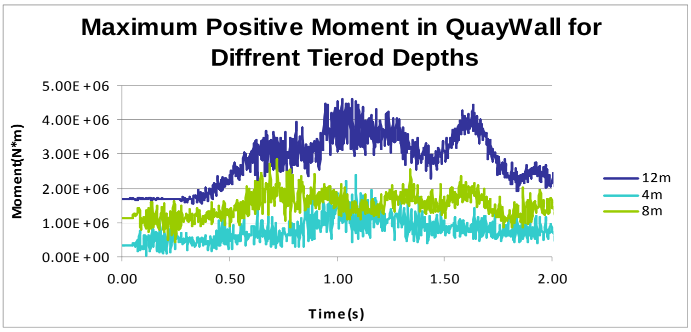

Figure 8.

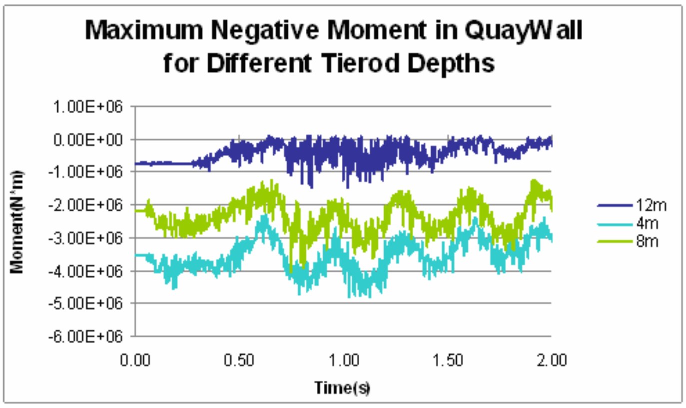

Figure 9. Maximum negative moment in quaywall history

5. CONCLUSIONS

Considering the results which were discussed above, in earthquake duration the absolute amount of both positive and negative maximum moments in anchored concrete quaywall is the least when tierod is in depth of about 8 meters. The tierod axial force in depth of 8 meters is between axial forces in two other depths in all history duration.

It is inferred that an appropriate serviceability is obtained due to various tierod positions and all cases satisfy the horizontal quaywall top displacement limit (based on “OCDI"). Hence, to rehabilitate the structure in seismic condition economically, it is logical to select a tierod position which gives lower maximum moment and axial force (so, economical wall profile and anchorage system) in earthquake duration. It is possible to select a suitable tierod position through curves and analyses of this research.

REFERENCES

1. Kristian Krabbenhoft, Lars Damkilde, Sven Krabbenhoft,"Ultimate limit state design of sheet pile walls by finite elements and nonlinear programming", 2005 www.elsevier.com/locate/compstruc.
2. Itasca consulting group, Inc,”FLAC Manual”, version 4.0, 2002.
3. Technical Standards and Commentaries for Port and Harbor Facilities in Japan,”OCDI, The Overseas Coastal Area Development Institute of Japan", 2002.
4. Arcelor RPS,”Piling Handbook”, 8TH EDITION, 2005.
5. U.S. Department of Transportation /FHWA with permission “USSteel, Steel Sheet Piling Design Manual", 1984, July.
6. Bowles. J. E,"Foundation Analysis and Design", McGraw Hill, 1996.
7. Das. B. M., “Principles of Geotechnical Engineering”, 2nd Ed., PWS-KENT, 1990.
8. Department of the Army U.S. Army Corps of Engineers Washington, DC 20314-1000 “Design of Sheet Pile Walls” 1994,

CD04-005

ACCURACY OF COMMON MACRO-ELEMENT MODELS IN PREDICTING BEHAVIOR OF CONCRETE INFILLS

Sh. Zare
Department of Civil Engineering, Amirkabir University, Tehran, Iran

ABSTRACT

Reinforced concrete infills improve seismic behavior by increasing lateral strength, initial lateral stiffness, and energy dissipation capacity of buildings, so it is important to implement a model which can predict behavior of infilled buildings correctly. Duo to convenience and simplicity in application proposes, modeling of infills with macro element models can be implemented in place of micro element. In this study, two applicable macro-element models namely one-strut and three-strut was implemented for modeling of these infills and accuracy of these models in predicting actual behavior of structure was compared with experimental tests which have been carried out in recent years on concrete and steel frames. The results show that in frames with strong members when the critical mode is failure in infill; three-strut can simulate ultimate strength and initial stiffness better than one-strut model. This paper also indicates that frame weakness can affect dramatically on the concrete infilled frame behavior and interrupt infill performance.

Keywords: concrete infill, macro element model, three-strut model

1. INTRODUCTION

Infilling frame with reinforced concrete wall is one of the strengthening techniques for reinforced medium rise buildings. Reinforced concrete infills improve seismic behavior by increasing lateral strength, initial lateral stiffness, and energy dissipation capacity of reinforced concrete buildings, and limit both structural and nonstructural damages caused by earthquake. Figure 1 shows a schematic view of these infills.

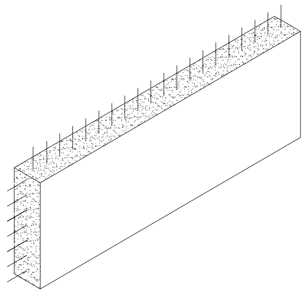

Figure 1. Schematic view of Concrete Infill

The various theoretical models reported in the literature for predicting the seismic behavior of infills can be classified into two categories: (i) micro element-based and (ii) macro element-based models. Theoretical microelement models, such as the finite element model provide a rigorous analytical approach to evaluate the dynamic response of infills. A number of finite element models have been developed and used to predict the in-plane lateral load behavior of these infills [5].Macro element modeling offers an alternative approach in which the entire infill panel is represented as a single strut or multi-strut approach [1, 2]. In this way, only the equivalent global behavior of the infill panel is taken into account in an analysis. Thus, for analysis focusing on overall structure response, macro element models can be implemented in place of micro element models. Application of microelement not only has some complexity in modeling, it is also time consuming. Further more, in this study two applicable methods, namely one-strut and three-strut were implemented for modeling of concrete infills and accuracy of the results was compared with the experimental test which had been carried out previously on concrete infills.

2. DESCRIPTION OF MACRO-ELEMENT MODELS

2.1. One-Strut Model

Firstly, one-strut model based on FEMA 356 was used for modeling of concrete infill. It is very important to identify the modes of failure or other effects which need to be controlled or avoided. Based on experimental tests only two modes, the corner crushing (CC) and sliding shear (SS), are of practical importance, (Comite 1996). In order to determine the governing failure mode, the capacity of the infill panels in first and second failure mode were estimated. Because of high value of shear strength in RC infills, in most cases corner crushing mode is dominant. The FEMA 356 provisions prescribe a strut with an area equal to the thickness of the masonry infill panel times; the strut width is given by Eqn. 1.

$$a = .175(\lambda_1 h_{col})^{-0.4} r_{\inf} \tag{1}$$

$$\lambda_1 = \left[\frac{E_{me} t_{\inf} \sin 2\theta}{4 E_{fe} I_{col} h_{\inf}} \right]^{\frac{1}{4}} \tag{2}$$

h_{col} And r_{inf} are the height and diagonal length of infill panel respectively, E_{me} is expected modulus of elasticity of infill materials, t_{inf} and h_{inf} are thickness and height of infill panel, I_{col} is the moment of inertia of column and E_{fe} is expected modulus of elasticity of frame materials. It is justifiable to assume that the panel properties in the diagonal direction are the properties governing the behavior of the infill panel. Concrete material is modeled using total strain rotating crack model (DIANA 2005) that describes the tensile and compressive behavior using one stress-strain relationship. The concrete in compression is defined using a parabolic stress-strain $(\sigma - \varepsilon)$ relationship as shown in Figure 2 and defined by equations 3 through 6.

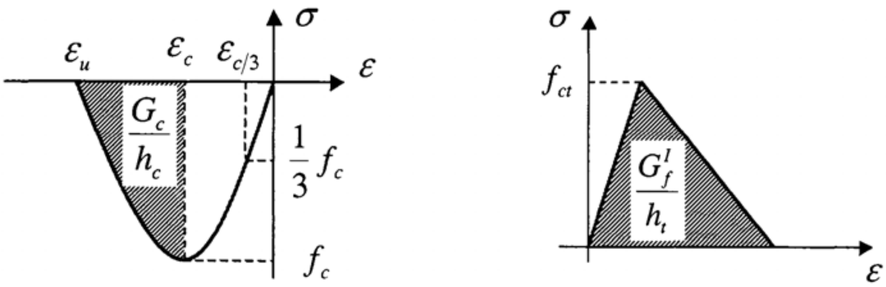

(a) Compressive behavior (b) Tensile behavior

Figure 2. Concrete material model (DIANA 2005)

$$\sigma=\begin{cases} \dfrac{f_c}{3}\dfrac{\varepsilon}{\varepsilon_{c/3}} & if\, 0\geq\varepsilon>\varepsilon_{c/3} \\ \dfrac{f_c}{3}\left(1+4\left(\dfrac{\varepsilon-\varepsilon_{c/3}}{\varepsilon_c-\varepsilon_{c/3}}\right)-2\left(\dfrac{\varepsilon-\varepsilon_{c/3}}{\varepsilon_c-\varepsilon_{c/3}}\right)^2\right) & if\,\varepsilon_{c/3}\geq\varepsilon>\varepsilon_c \\ f_c\left(1-\left(\dfrac{\varepsilon-\varepsilon_c}{\varepsilon_u-\varepsilon_c}\right)^2\right) & if\,\varepsilon_c\geq\varepsilon>\varepsilon_u \\ 0 & if\,\varepsilon\leq\varepsilon_u \end{cases} \tag{3}$$

$$\varepsilon_{c/3}=\frac{1}{3}\frac{f_c}{E_c} \tag{4}$$

$$\varepsilon_c=4\varepsilon_{c/3} \tag{5}$$

$$\varepsilon_u=\varepsilon_c+\frac{3}{2}\frac{G_c}{h_c f_c} \tag{6}$$

Where:

f_c = the maximum compressive strength based on uniaxial concrete compression test result, E_c =the initial modulus of elasticity of concrete in compression estimated in unite of kg/cm^2 as $E=15800\sqrt{f'_c}$, ε_c = the strain at which 1/3 of the compressive strength is reached, ε_c = the strain at which the maximum compressive strength is reached, ε_u = the ultimate strain in compression at which the material has no strength. G_c= the fracture energy in compression determined to be consistent with the assumed value of ε_u per table 1. The tensile behavior of concrete is modeled using elastic with linear softening relationship as shown in Figure 2 where f_{ct} is the tensile strength of concrete as determined in concrete split tension test. The value of G_f is estimated in units of N/m as $G_f = \alpha_d f_{ck}^{0.7}$ where $\alpha_d = 6.75$ and f_{ck} is the characteristic strength in unit of MPa taken as the same as f_{ct} in this study.

2.2. Three-Strut Model

Because concrete infills are strong members, interaction between infill, beam and column are important and need a model to represent characteristics of concrete-infilled frame correctly. Usage of a multi-strut model rather than single strut will better represent the actual stressed area within the infill and also facilitate the modeling of the progressive failure occurring at the corner contact region, not just at the corner points. Use of three-struts for modeling of infills was studied by El-Dakhakhni [2]. Based on research, it is suggested that at least two additional off-diagonal struts located at the points of maximum field moments in the beams and the columns are required to reproduce theses moments as shown in Figure 3.

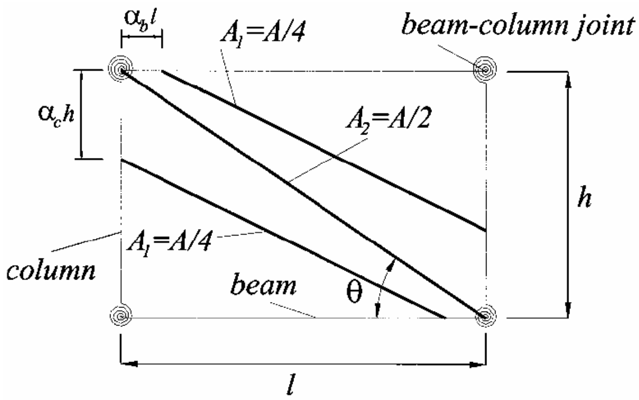

Figure 3. Schematic view of three-strut model [2]

It is suggested that the total diagonal struts area, A, is to be calculated by

$$A = \frac{(1-\alpha_c)\alpha_c ht}{\cos\theta} \tag{7}$$

Concrete material is modeled using total strain rotating crack model as described by equation 3 through 6.

3. MODELLING OF TEST SPECIMENS USING MACRO MODELS

To evaluate accuracy of macro-element models to determine behavior of structures, some experimental study which has been previously conducted including two CICF (concrete-infilled concrete frame) and one CISF (concrete-infilled steel frame) specimens was implemented. Each model has special characteristics which will be discussed shortly. Six CICF specimens were tested at the University of Gazi in Turkey under reversed-cyclic lateral loading by Sinan altin et al. [3]. The specimens are one-bay two story concrete-infilled concrete frames. In this study, only the first and second specimens were considered. The first specimen shows poorly lap spliced columns of nonductile RC frame, while providing RC infill walls. The second specimen is similar to the first specimen but longitudinal reinforcements pass continuously along two stories in boundary elements of infills. These two specimens were considered as representatives of common concrete frames. Figure 4 shows these test specimens in testing.

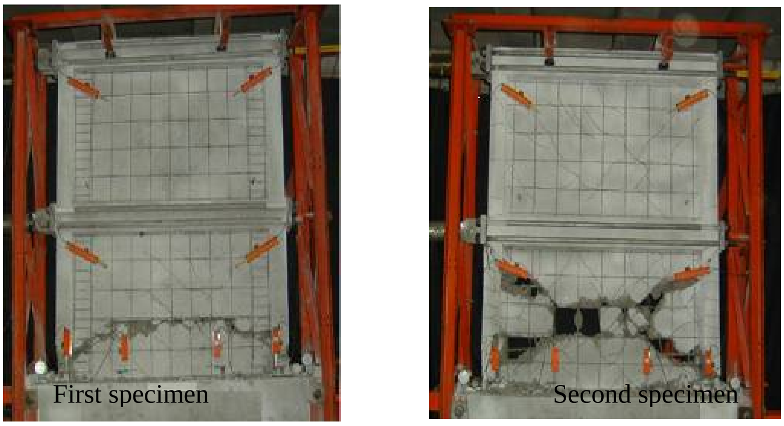

Figure 4. Sinan altin et al test specimens [3]

One CISF specimen was tested in the Building and Housing Research Center in Iran by Moghadam and Mohammadi. This specimen was one-bay one story concrete-infilled steel frame. The details of the test can be found in [5].
The load displacement behavior of test specimens was evaluated by using nonlinear push over analysis. Push over analysis simulated the nonlinear lateral load displacement relationship of the test specimen analytically. Analytical model for a specimen is given in Figure 5 as an example.

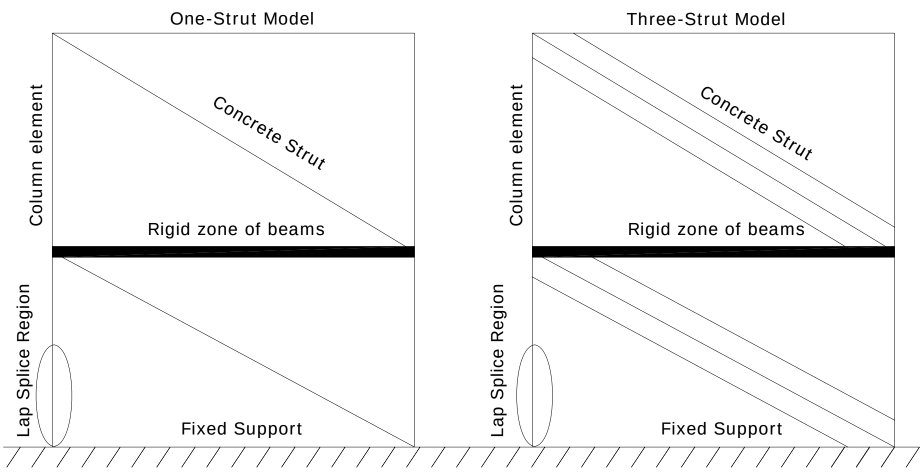

Figure 5. Analytical model of specimen

Columns and beams were modeled based on FEMA 356 provisions. Because there is no special element in the software for modeling lap splices it was modeled as concentrate hinge based on FEMA 356 provisions. Numerical values of the parameters for the concrete compression material model are presented in table 1.

Table 1: Parameters for concrete compression material model

Specimen	f_c (MPa)	$\varepsilon_c/3$	ε_c	ε_u	G_c (KN/mm)	h_c (mm)
CICF	298	.000364	.001456	.015	.138	305
CISF	150	.0003	.0012	.015	.138	305

4. COMPARASION BETWEEN EXPERIMENTAL AND ANALYTICAL RESULTS

In the following, load displacement relationship of each specimen by means of one-strut and three-strut models was obtained and compared with experimental tests. Figure 6 shows load deflection relation of first CICF specimen. It was observed using one-strut and three-strut models; both adequately simulate initial stiffness of concrete-infilled frame. It can be seen that strut model can not predict behavior of infill in ultimate load, as well as in the descending segment of backbone cure. The reason for this is in the following. Because of deficiency in lap slice region in the column, this point acts as a fuse and failure occurred in this region. It means the ultimate load is equal to column tensional-force and does not depend on infills strength, so implementing one-strut or three-strut models caused nearly similar results.

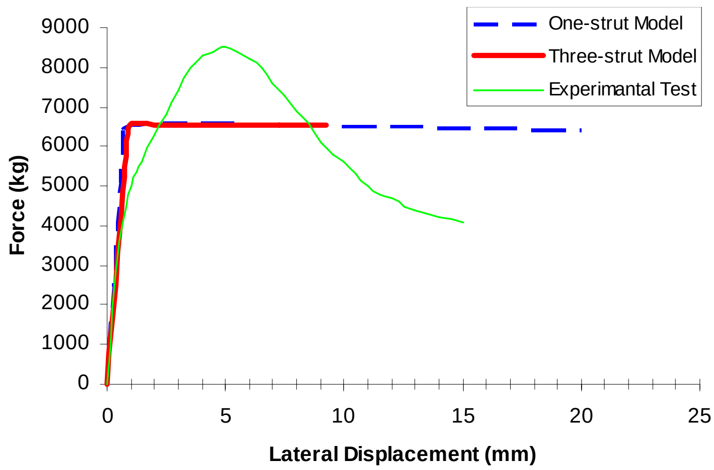

Figure 6. Load-deflection relations for first CICF specimen

Figure 7. Illustrates load-deflection relation of second CICF specimen, it shows that the three-strut model curve has a better coloration with the experimental test. In this case because of continuous longitudinal reinforcement, the column has

higher strength than concrete infills so failure in infills is prior to failure in columns. It means concrete infills act as a fuse and behavior of this element widely affects CICF specimen behavior. The three-strut analytical model adequately simulates the behavior of infilled test specimen until the ultimate load was attained. The displacement corresponding to ultimate load which was predicted by one-strut and three-strut models is the same with experimental tests. But using one-strut model gets a much higher ultimate load than the experimental test and the three-strut model.

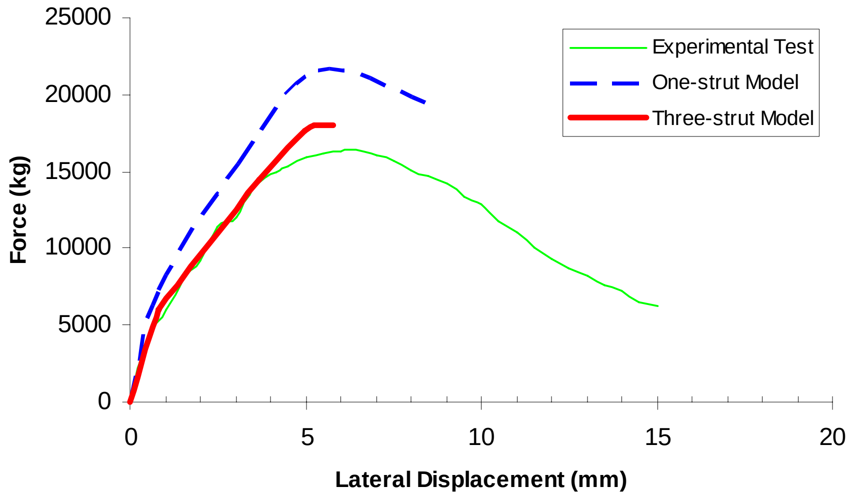

Figure 7. Load-deflection relations for second CICF specimen

From Figures. 6 and 7 it is concluded that concrete infills are strong members and can attract large amount of forces in earthquakes. But their performance depends strongly on perimeter beams and columns. For example, premature failure in poor concrete-frame caused by lap splice can have a dramatic effect on infilled-frame behavior and reduced ultimate load of about 100 percent.

Figure 8. Depicted nonlinear behavior of CISF specimen tested in Iranian Building and Housing Research Center by Moghaddam and Ghazimahale. Due to higher tensional strength of steel columns as compared with concrete ones, corner crushing failure occurred in infill. This fact has been reported based on experimental test which was conducted on steel frame [5]. Furthermore, behavior of infill has a main effect on behavior of CISF. It was observed that one-strut model gives a higher strength than three-strut and use of this model in modeling of this element may be non-conservative. Stiffness of three-strut model has a nearly good correlation with experimental test before ultimate load. One-strut model neither attains a much more ultimate force than the experimental test nor does it give an appropriate stiffness before and after the ultimate load.

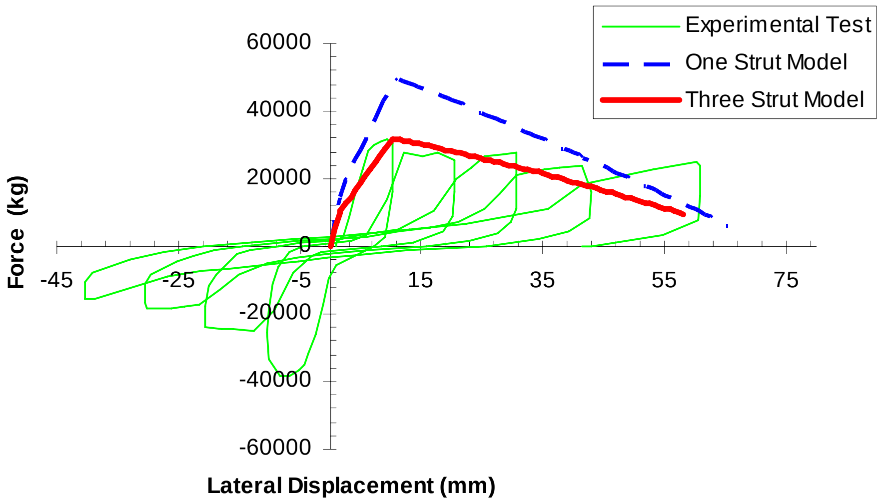

Figure 8. Load-deflection relations for specimen CISF

There were differences between the part of analytical and experimental load displacement curves at which after the ultimate load was reached. One of the main reasons for the difference between the analytical and experimental initial stiffness is the difference in the method of load application. While cyclic loading was applied during experiments, analytically the load was increased monotonously up to failure. This difference in application of loading affected the initial stiffness of analytical and experimental results.

CONCLUSION

- Analytical studies were performed to understand the effect of one-strut and three-strut proposed models on the behavior of concrete-infill in steel and concrete-frames. This paper shows that in frames with strong members when the critical mode is failure in infill; three-strut can simulate ultimate strength and initial stiffness better than one-strut model.
- Three-strut model can appropriately estimate initial stiffness of infill frame and no matter failure mechanism occurs in frame or infill.
- Displacements corresponding to ultimate load which are predicted by one-strut and three-strut models are the same with experimental tests.
- This study shows that one-strut model based on FEMA 356 can estimate stiffness and strength of concrete infill superior than reality.
- Infills impose shear force to adjacent elements. Therefore, using a model to consider this fact is mandatory. Three-strut model can predict possibility of shear failure in beam and columns adjacent to concrete infills.
- Premature failure in poor concrete-frame caused by lap splice, can affect dramatically the infilled-frame behavior.
- Concrete infills are strong members and can attract large amount of forces in earthquakes. Incorrect modeling can disturb hinge propagation in structural elements and cause unreasonable results.

REFERENCES

1. Stafford Smith, B. Carter, C., A method of analysis for infill frames, Proc. Inst. Civ. Eng., 1969, 44, 31-48.
2. Wael W. El-Dakhakhni, Mohamad E., Ahmad A., Three-strut model for concrete masonry-infilled steel frames, Journal of structural enginerring,2003, 129, February.
3. Sinan A., Ozgur A., Mehmet E. K., Strengthening of RC nonductile frames with RC infills: An experimental study, Journal of cement & concrete composites, 2007, Article in press.
4. Musa O. S., Guney O., Ugur E., Rehabilitation of reinforced concrete frames with reinforced concrete infils, ACI structural Journal, 2004, August.
5. H. Moghadam, M. Mohammadi., Improvement of Mechanical Properties of Infill panels, PHD theses, Sharif University, 2007.
6. FEMA-356, Prestandard and Commentary for the Seismic Rehabilitation of Buildings, Building seismic safety council, 2000, Washington (DC)

CD04-006

DETERIORATION EVALUATION OF COOLING TOWER UNIT 28 IN MOBAREKEH STEEL COMPLEX AND PROVIDING ITS REPAIR PROCEDURES

F. Moodi[1], A.A. Ramezanianpour[1], M. Peydayesh[1], A. Nadimi[2], M. Pajouhesh[2], M. Rasouli[2]
[1]Concrete Technology and Durability Research Centre, Amirkabir University of Technology
[2]Mobarekeh Steel Complex

ABSTRACT

It is generally supposed that concrete is one of the best durable materials but, it is a fact that all concrete structures will deteriorate with time, though the rate at which they deteriorate varies considerably, as it is affected by many factors. Deterioration will change the performance and appearance of structure, which may affect its performance under normal working conditions.

Cooling tower unit 28 is one of the concrete structures in the Mobarekeh Steel Complex which was observed with various remarkable deteriorations. This concrete structure was directly subjected to circulation of industrial water and under aggressive sulfates, corrosion reinforcement, lack of timely attention and periodical investigations at regular time intervals were found responsible for serious deteriorations.

In order to have an optimal use of the structure and its stability and to achieve an adequate repair procedure, a thorough and logical investigation of distress causes was carried out. The survey includes information collection and visual sketching of distress locations, several in-situ NDT tests, the determination of various aggressive ions in depth of concrete, and some other laboratory tests on core specimens taken from selected components of the structure. Based on studies carried out, different deterioration mechanisms were determined and then concrete removal methods and appropriate repair procedures were suggested. Finally, durability and the remaining service life of repaired structure is predicted.

Keywords: distress evaluation, concrete, inspection, durability, maintenance strategies

1. INTRODUCTION

Worldwide concrete with Portland cement is the most widely used construction material in buildings and civil engineering structures. There are several reasons such as appropriate resistance to water, easily flexibility on various shapes and dimensions, inexpensive and easy availability of its materials constituents. Over the years, the type and quality of concrete materials and construction methods have varied considerably. In parallel, there has been an increased understanding of the mechanisms underlying the behavior of concrete and its performance in service. It is an unfortunate, but inescapable fact that all concrete structures will deteriorate with time, though the rate at which they deteriorate varies considerably, as it is affected by many factors. Deterioration changes the performance and the appearance of the structure, and as a final consequence it may affect its safety and behavior under normal working conditions on exploitation. Usually in the past, some maintenance actions were taken into consideration when already visible traces of deterioration were observed. Where periodical inspections were not carried out at regular time intervals, serious damages might be already presented at the first inspection [4, 5, 6].

Cooling tower unit 28 is one of the concrete structures in the Mobarekeh Steel Complex which was seriously damaged. This structure is used for cooling and decreasing water temperature circulated in the steel production lines. The concrete was subjected to circulation of industrial water and under aggressive sulfates, corrosion of reinforcement, without periodical inspections at regular time intervals and thus serious deteriorations were presented. Damages owing to corrosion of reinforcement have caused expansion and eventually resulted in cracking, delaminating and spalling of concrete.

In order to have an optimal use of the structure and its stability and achieving an adequate repair procedure, a thorough and logical investigation of distress causes was carried out. The survey includes information collection and visual surveying and sketching of distress locations, several in-situ NDT tests, determination of various aggressive ions in the depth of concrete, and some other laboratory tests on core specimens taken from selected components of the structure. Considerations and visual investigation and inspections of the structure, surface impairments, NDT tests and collecting core samples for laboratory tests are shown in Figure 1. Based on the results of preliminary inspections and in-situ and laboratory tests, various deterioration mechanisms were determined and then concrete removal methods and adequate repair procedures were suggested. At the final stage of this study, durability and the remaining service life of the repaired structure is predicted [1].

2. OBSERVATIONS, VISUAL SURVEYING AND INSPECTIONS

In order to investigate the performance of the cooling tower structure which is in a propagation phase of deterioration, an assessment of the current condition of the structure is necessary. This investigation is also necessary because of several other factors such as current maintenance, rehabilitation, serviceability conditions changes, investigation of structural stability and its function, and a study of current environmental conditions. Current state could include rapid assessment and visual inspection up to complex considerations which are taken into account in long time planning and performance. The main purpose of visual surveying and investigation is the diagnosing of probable causes of any visual deterioration and ensuring that the structure remains in its integration and satisfactory conditions. An instance of visual surveying of distress locations is shown in Figure 2 [1].

The most important deteriorations which were obviously seen in the exposed concrete in cooling tower unit 28 are longitudinal cracking due to corrosion of reinforcement in beams and columns and also severe sulfate and frost attacks (see Figure 3). Nevertheless, the essential distresses which are manifested in this structure is classified as follows:

a) Longitudinal cracking in direction of steel bars in beams and columns (Figure 3).
b) Severe corrosion of reinforcement (Figure 4).
c) Severe removing of cement paste and exposed aggregates (Figure 5).
d) Sulfate and frost attack.
e) Delamination of concrete walls.
f) Leakage and efflorescence (Figure 6).
g) Low concrete cover over reinforcement.
h) Spalling of concrete cover due to corrosion.
i) Disintegration and scaling.

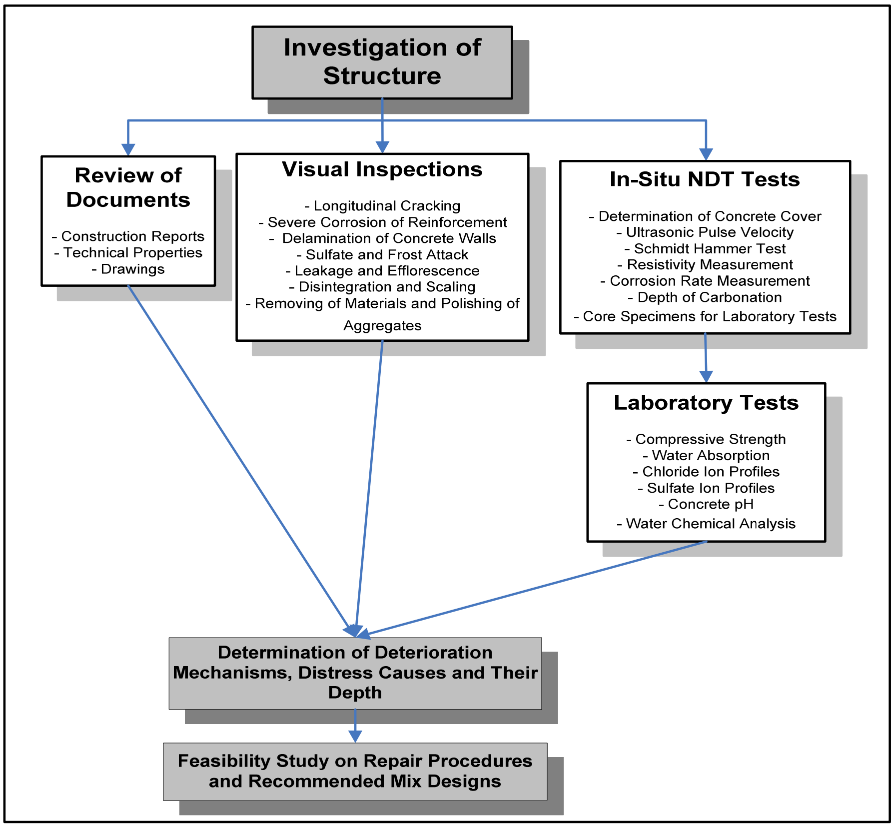

Figure 1. Flowchart of various stages of diagnosing distresses in cooling tower unit 28.

3. IN-SITU TESTS

In the first stage of the inspection and evaluation of the structure and according to visual surveying and inspections, various non destructive tests (NDT) comprising the determination of concrete cover, pulse velocity measurement, concrete strength by Schmidt hammer, resistivity measurement, determination of corrosion rate and depth of carbonation (Figure 7) were carried out. In continuing of the completion of quality and quantity of studies in laboratory, 17 core specimens were taken from selected beams, columns and concrete walls at different levels of the cooling tower [1].

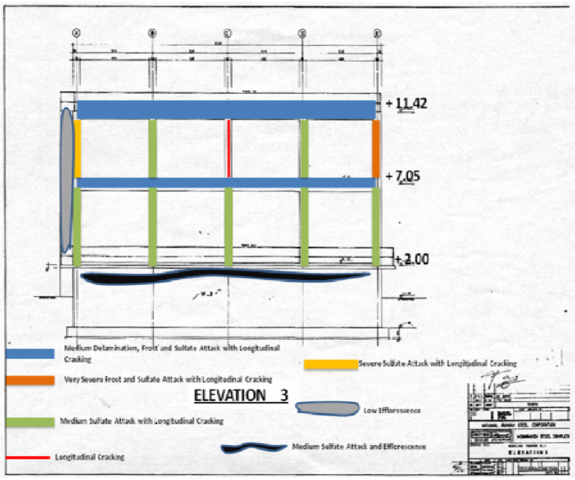

Figure 2. Schematic and sketching of distress locations in the western view of cooling tower unit 28

Figure 3. Longitudinal cracking and sulfate attack

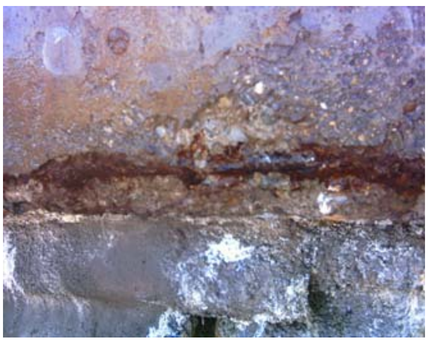

Figure 4. Severe corrosion of reinforcement

Figure 5. Removing of cement paste and exposed aggregates

Figure 6. Leakage and efflorescence

Figure 7. Determination of carbonation depth

4. LABORATORY TESTS

In the laboratory, compressive strength, water absorption, chloride and sulfate ion profiles and concrete pH in different depths of core samples are implemented. During taking of core specimens it was seen that the cover of concrete in all samples taken from concrete walls and some of those taken from beams is separated due to the corrosion of reinforcement.

Water could be considered as one of the most important reasons which cause impairments in concrete and concrete structures. Water is the initial compound of life and decomposes the most natural materials and also causes most of the difficulties for concrete durability. Water also is one of the reasons of decrease in quality in porosity materials and is responsible for the intrusion of aggressive ions into concrete and is one of the resources for chemical processes causing quality reduction.

One sample from circulated water in the cooling tower unit 28 was taken for chemical analysis. Chloride and sulfate ions contents in this sample were less than the allowable limit which is in the Iranian code of practice. Nevertheless, these ion contents in a constant volume of concrete are more than the allowable limit; therefore, the concrete of cooling tower's structure was subjected to aggressive ions. Its intensity depends on concrete quality, concrete cover, and permeability of concrete and on how the structure is maintained during its service life [1].

5. CONCLUSION OF EVALUATION STUDIES AND TECHNICAL RECOMMENDATIONS

Concrete is one of the most widely used construction materials alike other materials with a life time. Concrete deteriorations, due to several causes could considerably affect the technical life time of concrete structures. Therefore, the awareness of deteriorations and their mechanisms, their prevention and/or decreasing the intensity of damages, creating delay in their progress, and considering appropriate requirements afterwards are one of the most important duties of civil engineers who deal with concrete works. On the other hand, the concept of innovative construction materials and also innovative concretes is not only considered as its own materials. But the concept of life time and durability design is also one of the essential parts which must be taken into account .Life time and durability design concepts, along with its deep and wide considerations are surrounded by all material parameters, environmental conditions, construction, conditions, human resources and technological conditions [8, 9, 10].

Nevertheless, all concrete structures are always subjected to deteriorations which is affected by many factors. In addition, considering the concepts of life time and durability design for such structures, maintenance planning during physical service life of the structure is one of the most important factors increasing the life time of concrete structures.

In the evaluation of concrete durability of cooling tower unit 28, attention was given to the knowledge of physical-chemical processes of concrete distresses causes in real structure which have been observed and for diagnosing of these causes, several in-site and laboratory tests were carried out. However, interactions of physical and chemical causes of distresses, which are sometimes complicated, are considered. Regarding the tests results and visual inspection, the conclusion is as follows [1]:

a) Based on considerations and according to concrete Iranian code of practice, the structure of cooling tower unit 28 was subjected to moisture, wet and dry conditions, freezing and thawing, periodic cooling and warming, hence locating in very severe environmental condition.
b) The average compressive strength of concrete specimens shows very high compression strength (average: 44 Mpa on cylindrical specimens) and it is also very dense with low permeability (with 2.25% maximum water absorption).
c) In spite of high compressive strength and low permeability, the structure was always subjected to aggressive harmful ions which was available in water, so that stresses due to wet and dry conditions and periodic cooling-warming caused cracking and ingress of aggressive ions into concrete was intensified.
d) High leakage and penetration of water from inside to the outside of concrete walls of the structure caused an intensive corrosion of reinforcement and sulfatation of concrete. Low cover of concrete in some locations in concrete walls also caused corrosion and concrete delaminations.
e) As some parts of beams and columns in the structures were under 70-90% moisture and other parts were simultaneously subjected to environment and wet-dry condition, corrosion in these elements was developed as cavities. From the point of view of corrosion, increase of concrete water saturation is a useful effect in decreasing the oxygen penetration and on the other hand, it could be harmful because concrete electrical conductivity is considerably enhanced by increasing the degree of saturation. Therefore, it is not surprising that maximum corrosion and cracking in beams and columns occurred in places where there were wet and dry conditions. Getting sulfate of concrete because of aggressive sulfate ion of water and disintegration and exposure of aggregate due to freezing and thawing conditions intensified the concrete surface distresses. Sulfate ion profile in depth of a concrete core is shown in Figure 8.
f) Besides the insensitive factors of deterioration in the structure, one of the most important causes of distress development was the lack of maintenance planning during service life of the structure, lack of periodical inspection and timely prevention of distress development.
g) With chloride ion contents in the depth of concrete cores (Figure 9), corrosion of reinforcement, delamination of concrete cover, sulfatation and frost of concrete surfaces, it could be concluded that the concrete must be removed up to the minimum depth of 100 mm and replaced with a higher strength and low permeable concrete.
h) Also due to the penetration of water from the interior to the exterior, the interior surface of concrete walls must be cleaned and coated with impermeable materials. In addition, the existing joints which have caused leakage of water to the outside must be filled with appropriate resin.

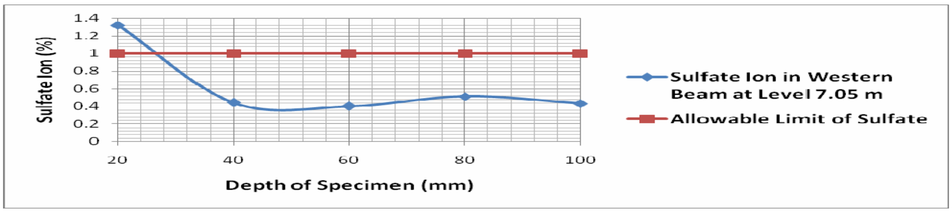

Figure 8. Sulfate ion profile in the depth of a concrete beam at a level of 7.05m.

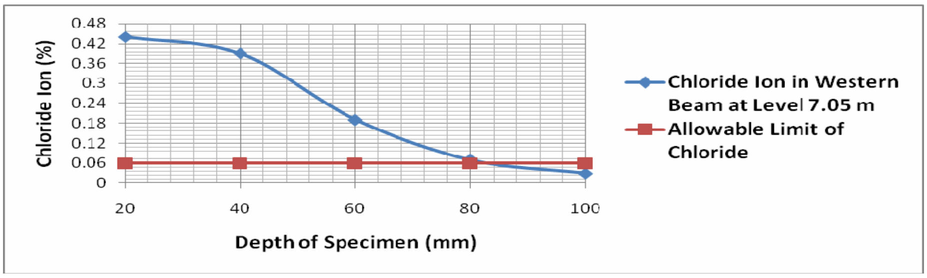

Figure 9. Chloride ion profile in the depth of a concrete beam at a level of 7.05m.

6. MIX DESIGN OF REPAIR MATERIALS

Each repair work has its exclusive conditions and its own requirements in identifying the necessary criteria for repair since in many cases more than one appropriate material for use is available. Concrete repair materials can be formulated to provide a wide variety of properties. Final selection of material or combination of various materials has been implemented by consideration of several factors such as ease of application, cost, skill availability and necessary equipments for their usage. Information about the service life of materials, which were used in previous repair works, plays an essential role in the selection, usage and maintenance of such materials [2, 3].

In selection of repair materials, emphasis is on those which might have higher performance and durability. Therefore, selection of these materials must be on the basis of awareness of their physical and chemical properties, the purpose of their usage and the natural condition of environment in places where they are used.

On the basis of usual inspections, in-site and laboratory tests results in previous sections and knowing the distresses causes such as corrosion of reinforcement, sulfate and frost attacks, with the intension of providing repair mix design and its planning, the following items are carried out [1]:

a) Methods for removal of damaged concrete and surface preparation.
b) Mix design alternatives on the basis of various tests on concrete material constituents.
c) Repair procedures alternatives based on various concrete deteriorations.
d) Prediction of durability and service life of repaired structure.

7. REPAIR PROCEDURES

Concrete is one of the multiple applied construction materials which is used with reasonable cost, having appropriate strength and durability and flexibility on shapes and dimensions. In concrete structure of cooling tower unit 28, some problems such as lack of timely maintenance, environmental conditions, aggressive chemical components on passage of time, were the causes of concrete deteriorations and serious distresses. Therefore, repair of damaged places by replacing with appropriate concrete under various procedures which depend on distress depth, its severity and extent, is necessary [2, 3, 7].

In the repair works of this structure, improvement and provision of concrete appearance acceptance in terms of their color and texture between repair zones and other parts are considered. In addition, repair zones must be permanently bonded with main concrete and also have enough low permeability, without shrinkage and crazing cracking and enough resistance against freezing and thawing. Therefore, repair of this structure needs more attention and necessary design and plan as compared to other buildings in the Mobarekeh Steel Complex. With consideration of impairments of the structure and its severity and extent, the following repair procedures alternatives are recommended [1]:

a) Formwork and pouring of concrete in beams and columns.
b) Patch repair of minor deteriorations.
c) Shout Crete for concrete walls.
d) Repair of cracks by injection.
e) In the result of water penetration from inside to outside, the interior surface of concrete walls must be cleaned and coated with impermeable materials.

8. CONCLUSION

It is generally accepted that in the design of concrete structures, durability properties of materials must be considered along with their other characteristics, such as mechanical properties and costs. In the evaluation of concrete durability and the durability of concrete structures, attention must be paid to the point in which most information about physical-chemical processes causing concrete deteriorations is obtained from actual structure history because the simulation of long term status in laboratory is very difficult. Although in reality, the concrete distress is rarely found due to a unique cause. Usually in advanced stages of material degradation, more than one harmful phenomenon is observed. In general, physical and chemical causes of distresses are so complicated and so intensified together that often the separation of cause and effect is not even feasible.

Permeability is one of the most important concrete parameters affecting durability. Most aggressive materials which are generally soluble in water penetrate through concrete capillary pores. Also, concrete with low porosity is dense and has better quality in terms of durability and strength. Water absorption is due to low water pressure in concrete. Hydration and concrete drying could decrease water pressure in concrete and increase absorption. In some parts of cooling tower unit 28, periodic water absorption and drying caused deposition of water harmful ions in concrete thereby resulting in increasing of sulfate and chloride ion contents in concrete. After absorption of chloride in water by concrete, it contaminates in depth and chloride gradually penetrates in concrete. Ingress of chloride ion continues in concrete where it reaches reinforcing bars and results in the progress of corrosion.

Therefore, it is important that the concrete surface condition should be improved by replacement with high strength concrete up to 100 mm in depth and also by applying impermeable coating materials so that the service life of cooling tower could be considerably enhanced (minimum 30 years). In addition of the concept of structural life time and durability design consideration, maintenance planning, periodic inspection activities and timely prevention of the progress of deterioration during service life of the structure are necessary precaution actions.

ACKNOWLEDGEMENT

A note of appreciation and special thanks to Engineer Shahriari , Deputy of Technology, Dr Ezadi, Director of Research and Development, and Engineer Aghajani ,Director of Technical Support , Mobarekeh Steel Complex for their support and help during this research.

REFERENCES

1. Ramezanianpour A.A., MOODI F. and PEYDAYESH M., Deterioration Evaluation of Cooling Tower Unit 28, Reports No 1,2 and 3, Mobarekeh Steel Complex, 2008.
2. Moodi, F, Development of a Knowledge-Based Expert System for the Repair and Maintenance of Concrete Structures, PhD. Thesis, Newcastle upon Tyne University, Newcastle upon Tyne, 2001, UK.
3. USACE, Engineering and Design: Evaluation and Repair of Concrete Structures, Engineer Manual 1110-2-2002, U.S. Army Corps of Engineers, 1995, USA.
4. Mehta P.K. and Monterio D.J.M., Concrete (Microstructure, Properties, and Materials) (Advanced Concrete Technology), Translated by Ramezanianpour A.A., Ghoddusi P. and Ganjian E., Amirkabir University of Technology Press, 2004, Iran.
5. Mailvaganam N.P., Repair and Protection Concrete Structures, Translated by Ramezanianpour A.A. and PASHAEI R., Norpardazan Press, 2007, Iran.
6. Cordon W.A., Repair of Concrete; Concrete Construction Handbook, 2nd Edition, McGraw-Hill Ltd., 1974, USA.
7. ICRI, Guide for Selecting Application Methods for Repair of Concrete Surfaces, Guideline No. 03731, International Concrete Repair Institute, 1992, USA.
8. Rilem, ‘Draft Recommendation for Damage Classification of Concrete Structures’, Journal of Materials and Structures, No. 27, 1994, pp 362-369.
9. Rilem, Durability Design of Concrete Structures, Technical Report No. 14, Chapman and Hall Ltd., 1996, London.
10. Federation International DU Beton, Assessment; Maintenance and Rehabilitation, Task Group 5.3, Document A: Technical Report on Assessment and Rehabilitation of Concrete Structures, TG 5.3, Fib, 2007, Switzerland.

CD04-007

INVESTIGATION OF A MANAGEMENT FRAMEWORK FOR PERIODIC ASSESSMENT OF CONCRETE STRUCTURES BASED ON INSPECTION AND VISUALIZATION

F. Moodi[1], A.A. Ramezanianpour[1], M. Peydayesh[1], A. Nadimi[2], M. Pajouhesh[2], M. Rasouli[2]
[1]Concrete Technology and Durability Research Centre, Amirkabir University of Technology
[2]Mobarekeh Steel Complex

ABSTRACT

In order to assess old concrete structures and to evaluate possible distresses, determination of their current conditions is necessary. The aim of this assessment is to gather information on important distress, their causes and the severity and extent. This information is only obtained from a thorough and logical inspection, regular reports during service life of structures, and also design and construction details.

Some of the concrete structures in industrial situations are subjected to various distresses due to different activities and lack of timely attention. These impairments cause incompatibility changes on mechanical, physical and chemical concrete properties and usually along with concrete disintegration. Nevertheless, it is realized that, in durability point of view, most concrete structures become deteriorated during their service life, where their severity and extent are affected by various factors. Unfortunately, lack of timely attention and determination of concrete distress causes, especially in places where periodic inspections have not been implemented at regular intervals, often cause concrete structures to become degraded and the estimation of these damages have shown a high cost of repair activities. Therefore, in order to achieve an adequate evaluation and actual cause of impairment and to provide the inspection, maintenance and repair strategies along with acceptable criteria in concrete structures, the present research work was carried out in four stages. It comprises evaluation methods, inspection management, criteria of repair materials and procedures selection, and finally provides a management system for inspection and visualization according to distress mechanisms. For the application of this research, the system results are used by a case study taken from the evaluation of concrete structures in the Mobarekeh Steel Complex.

Keywords: concrete distress, inspection, maintenance strategies

1. INTRODUCTION

Identification of distress cause is the most difficulty and important stage of any repair process. Before deciding on any repair work, the cause of impairment must be diagnosed as clearly as possible. Sometimes the cause is obvious, but as a rule a careful investigation is required. Only afterwards should the method of repair be chosen. A thorough and logical investigation of the current condition of the

structure is the first step of any repair or rehabilitation project.
After a comprehensive evaluation, the scope of both the cause and effect of concrete defect, damage and deterioration must be conducted in order to determine the necessary actions to be taken. The results of the evaluation, together with the user's needs or requirements form the necessary external information to select the repair method. Selection of repair methods depend on the nature of impairment, consideration of durability, constructability and compatibility with the existing structure, environment, availability of materials, cost and whether the repair is a temporary or permanent restoration [4, 12].
In order to assess most of the old concrete structures or those with advanced distresses, the determination of their current conditions are often necessary. The aim of this assessment is to gather information on distress importance, their causes and the severity and extent. This information is only obtained from a thorough and logical inspection, regular reports during service life of structures, and also design and construction details [3, 7].
Some of concrete structures in industrial situations are subjected to various distresses due to different activities and lack of timely attention. These impairments cause incompatibility changes on mechanical, physical and chemical concrete properties, usually along with concrete disintegration. Nevertheless, it is understood that, from a durability point of view, most concrete structures get deteriorated during their service life, where their severity and extent is affected by various factors. Unfortunately, lack of timely attention and determination of concrete distress causes, especially in places where the periodic inspections have not been implemented at regular times, often cause concrete structures to become degraded. The estimate of these damages shows high cost of repair activities. Therefore, in order to achieve an adequate evaluation and actual cause of impairment and to provide the inspection, maintenance and repair strategies along with acceptable criteria in concrete structures, the present research work was carried out in four stages. It comprises evaluation methods, inspection management, criteria of repair materials and procedures selection, and finally providing a management system for inspection and visualization according to distress mechanisms. For the application of this research, the system results are used by a case study taken from the evaluation of concrete structures in the Mobarekeh Steel Complex.

2. RESEARCH OBJECTIVES

The research objectives comprise four stages. In the first stage, repair and maintenance strategies, evaluation methods, rehabilitation of concrete structures, characteristics of deterioration and its consequences, and maintenance and durability recommendations for concrete structures were provided. Information regarding maintenance and durability of concrete is very useful for structural and construction engineers and users who may be conducting research on developing their preliminary strategies [1, 7, 11, 12].
The second stage of this research includes inspection planning; deduct values for various distresses in concrete structures, in-situ evaluation of structure according to

different NDT tests and laboratory tests. It is noted that this information is very useful for field inspectors or engineers who are involved in evaluation, repair and maintenance of concrete structures [1, 4, 6, 7, 10].

In the third stage, appropriate materials in durable mix design, repair material selection for concrete structures, concrete removal and preparation for repair methods, and application procedures and techniques for the repair of concrete were provided. This is valuable information for users and engineers who dealt with material and repair procedures selection and also those who intended to work as supervisors on construction repair sites [1, 8, 9].

In the fourth and final stage of the project, various distresses manifested in concrete structures along with their mechanisms, classification of distresses with deduct values was determined and a set of inspection forms and a potential rating system in different concrete structures were provided. At the end of this stage, the system results are used by a case study taken from the evaluation of concrete structures in the Mobarekeh Steel Complex [1, 11, 12].

3. DISTRESS CATEGORIES IN CONCRETE STRUCTURES

Identifying distresses and determining their causes thereby assisting in the design of durable replacement materials or adequate repair methods are important parts of any concrete repair program. It is important to draw conclusions based on the best observations and information available, in order to effectively rehabilitate a structure. This information may be obtained from visual inspection observations by an engineer or may be taken from pictures and databases. In some cases, it may be taken from in-situ tests (e.g. non-destructive testing (NDT)) or laboratory tests (e.g. petrographic examination) [4, 6, 10].

Concrete structures in the Mobarekeh Steel Complex with extension and various activities and enormous production lines are subjected to different deteriorations. These structures consist of cooling towers (e.g. power station, water distribution, unit 28 and 06), hot strip mill walls, acid washing unit, power tunnels, slab unit and concrete pavements. Distresses category in various concrete structures in the Mobarekeh Steel Complex which generally cover all manifestation of deteriorations are classified into physical and chemical causes (see Figure 1) [1].

4. DETERMINATION OF DETERIORATION MECHANISMS IN CONCRETE STRUCTURES

Deterioration of concrete structures follows well identifiable deterioration mechanisms. These mechanisms represent the interaction between the actual environment and the structure, with its geometry and materials composition. It is also evident that all deterioration mechanisms depend on some aggressive substance penetration from the surrounding environment into the outer layer of concrete (covercrete). The development in time of nearly all types of deterioration mechanisms of concrete structures may be modeled by two phases, the initiation phase and the propagation phase [3].

By visual inspection, in-situ and laboratory tests, and evaluation of concrete structures in the Mobarekeh Steel Complex which have been carried out by the authors, all distresses in these structures presented in Figure 1 are in propagation, progress and development phase. Therefore, it is necessary that immediate attention must be drawn towards repair of these structures to comply with principals and technical properties. Some of deterioration causes are as follows [1]:

- Frost attack
- Sulfate attack
- Corrosion of reinforcement
- Acid attack
- Cracking due to salt expansion in the interior pores
- Surface disintegration
- Thermal stresses
- Scaling and spalling

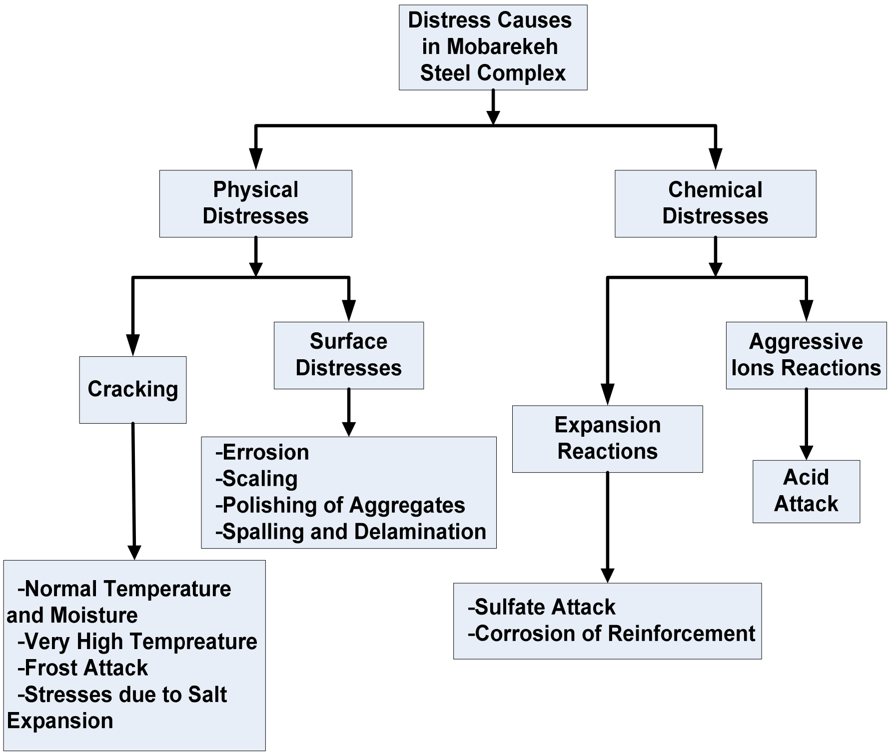

Figure 1. Distresses category in concrete structures in Mobarekeh Steel Complex

5. EVALUATION OF CONCRETE IN A CONCRETE STRUCTURE

A thorough and logical evaluation of the current state of the concrete in a structure is the first step of any repair or rehabilitation work. Therefore, a visual inspection of the exposed concrete is the first step in an in-situ examination of a structure. The purpose of such an examination is to locate and define areas of distress or deterioration. A condition survey will usually include a mapping of the various types of concrete deficiencies that might be found such as cracking, surface problems (disintegration and spalling) and joint deterioration. One objective of an Evaluation Management System (EMS) is to create assessment procedures that will allow the current condition of the structure, and its components to be expressed numerically to take the best recommended action in the repair and maintenance management. The criteria for the evaluation of a concrete structure are shown in Table 1 [4].

Table 1: The Confidence Level (CL) for the Evaluation of Concrete (ECON) structure

Zone	Confidence Level (CL)	Description	Recommended Action
Minor	95-100	Excellent: No noticeable impairments.	Prompt action is not required, but periodic investigation is recommended. In some cases, protection might be needed.
	85-94	Very Good: Barely noticeable impairments. Some ageing or dusting may be visible.	
Mode rate	70 - 84	Good: Clearly noticeable impairments. Only minor defect, damage and deterioration are evident.	Detailed investigation and economic analysis of repair alternatives are recommended. In some cases, appropriate repair and protection methods will be needed.
	50 - 69	Fair: Moderate impairments. Some defect, damage and deterioration are evident, but concrete remains serviceable.	
Major	30 - 49	Poor: Severe impairments in at least some major components of the structure have occurred. Concrete remains serviceable.	Detailed investigation and an engineering evaluation should be made to determine the demand for repair, replacement strengthening and stabilization. Safety evaluation is recommended.
	0 - 29	Very Poor: Very severe and extensive impairments in most components of the structure. General failure or a complete failure of structural components.	

Once the condition of the structure is understood and documented, the next step in the maintenance management process is to initiate action to correct unsatisfactory conditions and to begin planning for future maintenance and repair needs. For this purpose, a quantitative rating system for the condition of concrete in a structure would make possible the determination of which components within a structure most merit repair. The Evaluation Confidence Level (ECL) extends from 0 to 100, with 0 representing *Very Poor* condition and 100 representing *Excellent* condition. The Confidence Level (CL) is divided into *Minor*, *Moderate* and *Major* zones.

The Confidence Level (CL) prescribed here can be applied to Mobarekeh Steel Complex concrete structures in general. The rating system described allows the Confidence Level to be determined by visual inspection using limited equipment such as binocular, covermeter, ruler and carbonation depth. Values in each parts of the survey are properly interpreted as representing the current conditions found at the time the structure was inspected and rated. The rating is related to structural integrity and serviceability of the structure. The Confidence Level system is not intended to replace the detailed investigation needed to fully document structural deficiencies, to identify their causes and to formulate plans for correcting them. An extended investigation comprising detailed investigation and analysis, and engineering evaluation should be made when the Confidence Level is less than 50 [4].

6. DEVELOPMENT OF DEDUCT VALUES FOR VARIOUS DISTRESSES IN CONCRETE STRUCTURES

The Deduct Value is determined by visual inspection and by recording the information needed in the field inspection. The inspection and condition assessment procedure for determining Deduct Values is based on simple visual inspection techniques. If the condition of the structure being inspected is severely damaged i.e. a Confidence Level of below 50, more detailed investigation and engineering evaluation should be made.

Deduct Values for various distress categories are classified in cracking in concrete (Table 2), disintegration and scaling, spalling and delamination. An inspector should be familiar with the types of distress before performing an inspection to determine the Deduct Value. Deduct Values are based on considering previous works carried out and the author's opinion and experience. They involve two considerations [4]:

1) The knowledge and experience of expert engineers in the safety of the structure which has been degraded by various types of distress, and
2) Serviceability of the structure.

Table 2: Deduct values for cracking in concrete structures

Surface Appearance	Type of Crack	Depth of Crack	Deduct Value Width of Crack Very Fine (VFI)<0.25mm	Fine (FI) 0.25–1mm	Medium(ME) 1–2 mm	Wide (WI) > 2 mm
Pattern	21- (PCC) Crazing	SS	5	10	-	-
	22- (PDC) D-Cracking	SS	5	10	-	-
		DE	10	20	30	40
		TH	15	30	40	50
	23- (PMC) Map Cracking	SS	5	10	20	30
		DE	10	20	30	40
		TH	15	30	40	50
Individual	24- (ILC) Longitudinal	SS	5	10	20	30
		DE	10	20	30	40
		TH	20	30	50	70
	25- (ITC) Transverse	SS	2	5	10	15
		DE	5	10	15	30
		TH	10	15	25	40
	26- (IDC) Diagonal	SS	10	20	30	40
		DE	15	30	40	60
		TH	20	40	60	80
	27- (IRC) Random	SS	5	10	20	30
		DE	10	20	30	40
		TH	15	25	40	60

Surface and Shallow (SS) (up to 10 mm), Deep (DE) (10 –20 mm), Through (TH) (> 20 mm)

7. CALCULATION OF THE COMPONENT CONFIDENCE LEVEL (CCL)

Once the distress modes in each component of the structure to be rated are determined, the Component Confidence Level (CCL) can be calculated. By inputting the distress types into management system software, hand calculation of Deduct Values and the Confidence Level (CL) can be avoided. Considering the previous work [4, 5], generating a model for concrete distress simulation and the author’s experience and knowledge, the following formula is used for calculating the Component Confidence Level (CCL).

$$CCL = 100–[1.0(DV_1)+0.4(DV_2)+0.2(DV_3)+0.15(DV_4)+0.1(DV_5)] \quad (1)$$

The Component Confidence Level (CCL) is based on the five largest deduct values (DV), with DV_1 the largest value and other values in descending order to the fifth largest, DV_5. Table 3 shows an example of how the Component Confidence Level (CCL) for a column of cooling tower unit 28 in Mobarekeh Steel Complex has been calculated [1].

Table 3: Example of calculation of the CCL for a column of cooling tower unit 28 in Mobarekeh Steel Complex

Step 1: Inspect component to determine distresses and quantities.		
		
(24) (51) (32)	(43)	(24) (42)
Step 2: Calculate Deduct Values for each distress**.**		
24) ILC-TH-WI = 70 (51) SC-SL = 10 (32) LD-SL = 5	(43) FT-SE = 40	(24) ILC-DE-ME = 30 (42) CA-SE = 4
Step 3: Rank the Deduct Values in descending order to the smallest. Only the five largest are used in the Component Confidence Level (CCL) calculation.		
Distress and Quantity (Step 1)	**Deduct Value (Step 2)**	**Rank (Step 3)**
(24) ILC-TH-WI	70	DV_1
(42) CA-SE	40	DV_3
(43) FT-SE	40	DV_2
(24) ILC-DE-ME	30	DV_4
(51) SC-SL	10	DV_5
(32) LD-SL	5	-
Step 4: Calculate the CCL based on the ranked Deduct Values: $CCL = 100 – [1.0(DV_1) + 0.4(DV_2) + 0.2(DV_3) + 0.15(DV_4) + 0.1(DV_5)]$ $CCL = 100 – [1.0(70) + 0.4(40) + 0.2(40) + 0.15(30) + 0.1(10)] = 0.50$ The CCL is 0.5 which is Very Poor according to Table 1 (Very severe and extensive impairments in most columns of the structure)		

8. INSPECTION AND VISUALIZATION FORMS FOR CONCRETE STRUCTURES

With the purpose of evaluation of current concrete structures application and according to previous sections, deteriorations are classified in five groups and various distresses are coded as shown in Figure 2. If distresses in concrete structures are in propagation phase, the evaluation of current condition of structure is necessary. Evaluation of current state of structure with the other factors such as current maintenance, rehabilitation, change of serviceability condition, consideration of structure stability and study of concrete application in current environment condition must also be paid attention [2, 3].

The purpose of this evaluation is to gather information about distresses severity and extent. This information is only obtained from a thorough and logical inspection and completed inspection forms for concrete structures. In addition, for planning maintenance of structure during its service life, periodic and regular inspections and preventing from distress progress and development which are important for enhancing service life of concrete structures, different inspection forms in a set of 12 sheets are provided [1].

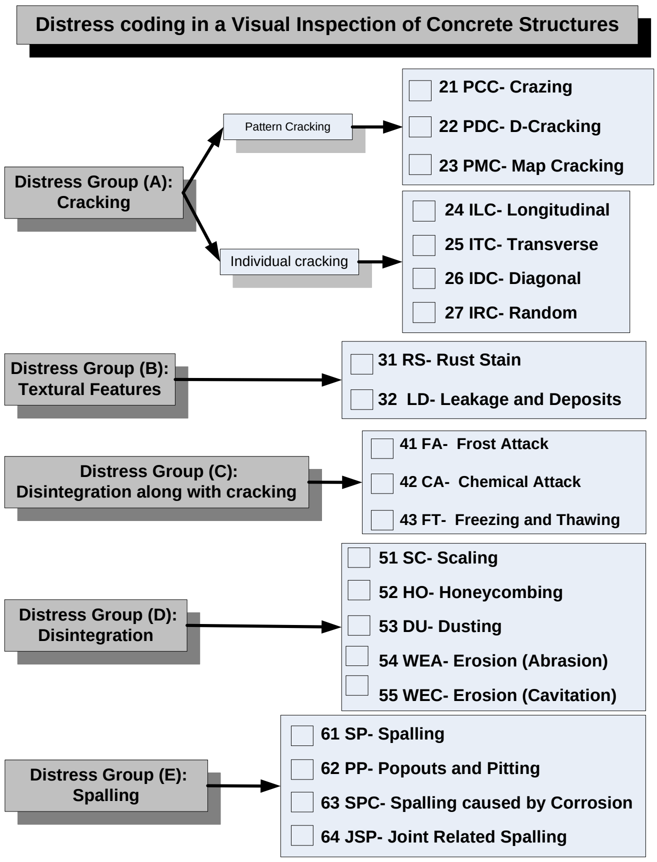

Figure 2. Distress coding in a visual inspection in a concrete structure.

9. CONCLUSION

One objective of an evaluation management system is to create assessment procedures that will allow the current condition of the structure and its components to be expressed numerically so as to assist in choosing the best course of action in the repair and maintenance management. Engineering judgment and experience were needed to develop a set of criteria in order to implement a quantitative rating of the overall state of concrete using the results of the observation of signs of distress and weighting scales based on severity and extent. It is important that the observed conditions be described in unambiguous terms that can be used by the user to enable him to take engineering and management actions for the repair and maintenance of the structure.

Once the current conditions of structure are documented and determined, the next step in the process of repair and maintenance management is applying an engineering action for correction of inadequate conditions and starting planning for future repair and maintenance requirements. For this purpose, the presented quantity rating system can be applied in a concrete structure in order to determine the components needed repair. Also, with completion of inspection and visualization forms and periodic investigations, the inspector could prevent the extent of deteriorations and enhance the service life of concrete structures.

ACKNOWLEDGEMENT

A note of appreciation and special thanks to Engineer Shahriari , Deputy of Technology, Dr Ezadi, Director of Research and Development, and Engineer Aghajani ,Director of Technical Support , Mobarekeh Steel Complex for their support and help during this research.

REFERENCES

1. Ramezanianpour A.A., Moodi F. and Peydayesh M., Providing Code of Practice for Inspection and Evaluation of Concrete Structures in the Mobarekeh Steel Complex, Reports No 1, 2, 3 and 4, Mobarekeh Steel Complex, 2008.
2. Mehta P.K. and Monterio D.J.M., Concrete (Microstructure, Properties, and Materials) (Advanced Concrete Technology), Translated by Ramezanianpour A.A., Ghoddusi P. and Ganjian E., Amirkabir University of Technology Press, 2004, Iran.
3. Mailvaganam N.P., Repair and Protection Concrete Structures, Translated by Ramezanianpour A.A. and Pashaei R., Norpardazan Press, 2007, Iran.
4. Moodi, F, Development of a Knowledge-Based Expert System for the Repair and Maintenance of Concrete Structures, PhD. Thesis, Newcastle upon Tyne University, Newcastle upon Tyne, 2001, UK.
5. USACE, Engineering and Design: Evaluation and Repair of Concrete Structures, Engineer Manual 1110-2-2002, U.S. Army Corps of Engineers, 1995, USA.
6. Bungey J.H., Testing of Concrete in Structures, 2nd Edition, Surrey University Press, 1989, England.

7. Campbell D.A., and Roper H., Concrete Structures: Materials, Maintenance and Repair, Longman Group UK Ltd., 1991, England.
8. Cordon W.A., Repair of Concrete; Concrete Construction Handbook, 2nd Edition, McGraw-Hill Ltd., 1974, USA.
9. ICRI, Guide for Selecting Application Methods for Repair of Concrete Surfaces, Guideline No. 03731, International Concrete Repair Institute, 1992, USA.
10. Rilem, 'Draft Recommendation for Damage Classification of Concrete Structures', Journal of Materials and Structures, No. 27, 1994, pp 362-369.
11. Rilem, Durability Design of Concrete Structures, Technical Report No. 14, Chapman and Hall Ltd., 1996, London.
12. Federation International DU Beton, Assessment; Maintenance and Rehabilitation, Task Group 5.3, Document A: Technical Report on Assessment and Rehabilitation of Concrete Structures, TG 5.3, Fib, 2007, Switzerland.

CD04-008

EXPERIMENTAL AND NUMERICAL STUDY OF DAMAGED-RC BEAMS BEHAVIOR RETROFITTED BY FRP

A.R. Rahai[1], M.R. Saberi[2]
[1]Professor, Dept of Civil Eng. Amirkabir University of Technology, Tehran, Iran
[2]Msc. Student, Dept of Civil Eng. Amirkabir University of Technology, Tehran, Iran

ABSTRACT
Strengthening of structures to avoid future damages is inevitable in different conditions. In recent years, fiber reinforced polymer (FRP) sheets are vastly used for strengthening of different concrete members. In this paper, to evaluate the effect of FRP plates on damaged or non-damaged members, an extensive experimental and numerical program is prepared. For this purpose, 10 beam specimens are built. Some of the beams are made under loading condition and their load - deformation curves are prepared; then, the damaged beams are strengthened with CFRP and GFRP using epoxy resin and have been tested under loading. The second part of the beam specimens are strengthened before loading and then their load- deformation curves are prepared. Some specimens are analyzed using Finite Element Method [1]. The results of numerical model and experimental research work show the improvement of bearing capacity of strengthened damaged beams compared to the non-damaged ones.

Keywords: concrete, damaged- beams, CFRP, GFRP, retrofit

1. INTRODUCTION
In recent years, the use of fiber reinforced polymers (FRP) as an externaly strip have achieved considerable popularity for the strengthening and repair of concrete structures. The FRP composites have been used successfully for rehabilitation and strengthening of deficient reinforced concrete elements. The potential market for such applications is huge since the estimated annual cost of repairing bridges in the United States alone is 9.4 billion dollars [2].
Chen and Teng (2003) presented a simple, accurate and rational method to study the shear capacity of FRP-strengthened beams which fail by FRP debonding. A new shear strength model is then developed, which was validated using experimental data collected from the existing literature [3].
In 2006 a series of 4-point bending experiments of the proposed hybrid FRP–concrete beam model were carried out by Wu et al. In addition, based on the principles of strain compatibility and equilibrium, an iterative analytical model was developed to analyze the flexural behavior of hybrid system [4].
Chen et al. (2006) presented a finite element analysis on the stress distributions in a typical shear test set-up for FRP-to-concrete bond strength. They show that the stress distribution is significantly different from plane stress assumption primarily

because of the difference between the width of the tested FRP plate and that of the concrete block [5].
Aram et al (2007) investigate the Debonding failure modes of flexural FRP-strengthened RC beams. In this paper, different types of de bonding failure modes are described. Then, experimental results of four-point bending tests on FRP strengthened RC beams are presented and debonding failure mechanisms of strengthened beams are investigated using analytical and finite element solutions [6].
Oehlers et al (2007) presented intermediate crack debonding resistance of groups of FRP NSM strips in reinforced concrete beams. This paper develops a mathematical model for the intermediate crack debonding resistance of groups of NSM plates for use in the flexural and shear strengthening of reinforced concrete beams [7].
Following the above mentioned researches, in this paper the strength and behavior of Damaged-Concrete Beams retrofitted by FRP layers are studied and their difference with non damaged ones are presented.

2. EXPRERIMENTAL INVESTIGATION

2.1. Specimen Design

Ten beam specimens were fabricated and tested. Two of these specimens were tested in their virgin conditions to serve as control, while the remaining eight beam specimens were tested after being strengthened using carbon and glass fibers. All of the RC beams were designed to have the same nominal dimensions: 2000 mm long, 200 mm wide and 300 mm height, with a span of 1800mm. As shown in Figure1, the flexural reinforcement consisted of 2T12 deformed bars. The shear reinforcement consisted of 1T8 distanced of 50 mm. Strengthening of specimens was achieved by the external strip of unidirectional carbon and glass fiber sheets using epoxy resin.

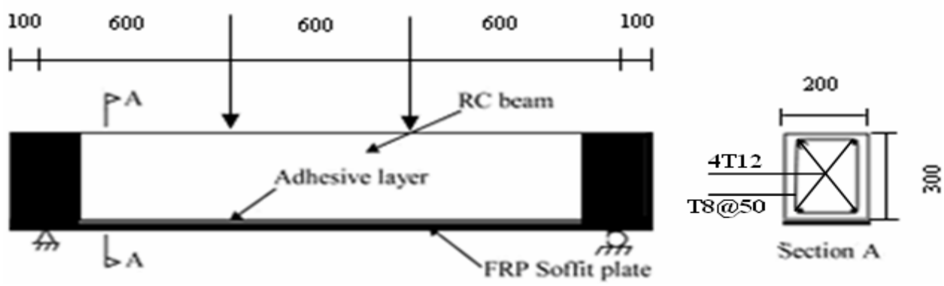

Figure 1. Detail of RC beam bonded with CFRP

2.2. Specimens Preparation

All eight RC beam specimens were fabricated with a normal density concrete mix. After the specimens strengthening was achieved by the external strip of unidirectional carbon and glass fiber sheets. Large-scale retrofitted RC beam tests indicate that failures of FRP plated systems may take place through various possible mechanisms, depending on the concrete grade, rebar provision, FRP properties, and service environments. Identified failure modes include: (1) concrete crushing before steel yielding; (2) steel yielding followed by concrete crushing; (3) steel yielding followed by FRP rupture; (4) Shear failure; (5) concrete cover de lamination and (6) de bonding in the vicinity of the FRP / epoxy / concrete Bond interface. Debonding in a FRP bonded concrete system is a complex phenomenon. At the bottom of the concrete core, CFRP and GFRP strips are axially bonded to carry tensile load and assure the stiffness of the member. Outside the CFRP and GFRP strips, CFRP and GFRP strips are hoops directionally wrapped to provide confinement to the end of concrete core and also to prevent the premature debonding of interior CFRP and GFRP strips (Figures 2, 3). Certain layers of carbon and glass fiber sheets were bonded along the axial direction (at 0 angle) at the bottom surface of the concrete core by epoxy resin and then carbon fiber sheets were wrapped round the beam at 90 angle. Electro-thermal blanket was used in some cases to maintain the curing temperature above 25C.

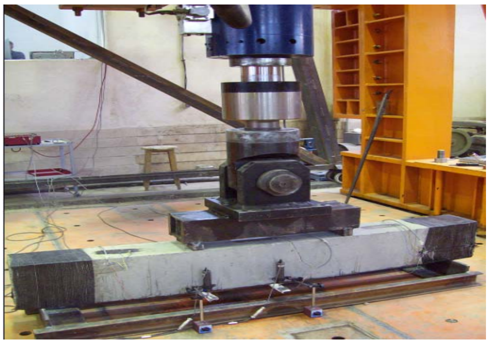

Figure 2. RC beam bonded with CFRP

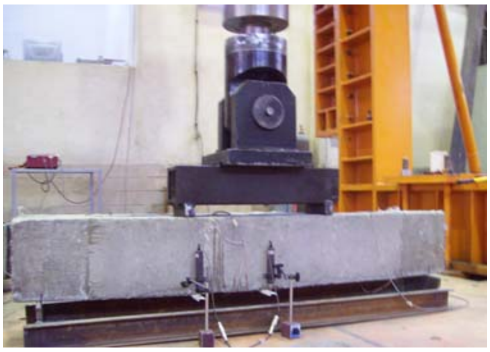

Figure3. RC beam bonded with GFRP

2.3. Material Properties

The compressive strength of concrete which has been prepared in the laboratory was equal to 33 MPa. The flexural reinforcement consisted of 2T12 deformed bars of yield strength 485 MPa. The shear reinforcement consisted of 1T8 distanced of 50 mm deformed bars of yield strength 430 MPa.

The tensile properties of the CFRP and GFRP materials are listed in Table 1, which were determined according to ASTMD3039/D3039M-95a [8]. The corresponding mechanical properties of resin used in experiments are listed in Table 2.

Table 1: Properties of strengthening materials

CFRP material	Strip	Wrap
Width (mm)	200	300
Thickness (mm)	0.61	0.61
Tensile strength (MPa)	3800	3800
Tensile modulus of Elasticity (GPa)	242	242
Failure strain (%)	1.5	1.5

Table 2. Properties of resins

Resin type	Epoxy (ML 506)	Polyester (HN160)
Density (gr/cm^3)	1.11	1.08
Adhesive Tensile Strength (MPa)	76.1	55
Modulus of Elasticity (GPa)	2.789	1.833

2.4. Strengthening Materials and Methods

Beam specimens B1 and B2 were tested in its virgin condition to serve as control (Figure 6). Beam specimens B3 and B4 were strengthened with CFRP strip. Its dimension was: 2000 mm long and 200 mm. Beam specimens B5 and B6 were strengthened using GFRP, the strips were similar to beams B3 and B4. The beam specimens B7 to B10 were loaded before strengthening until the maximum crack width was reached to 0.4mm and then the beam specimens B7 and B8 were strengthened with CFRP strips similar to B3 and B4. The beam specimens B9 and B10 were strengthened with GFRP similar to B5 and B6.

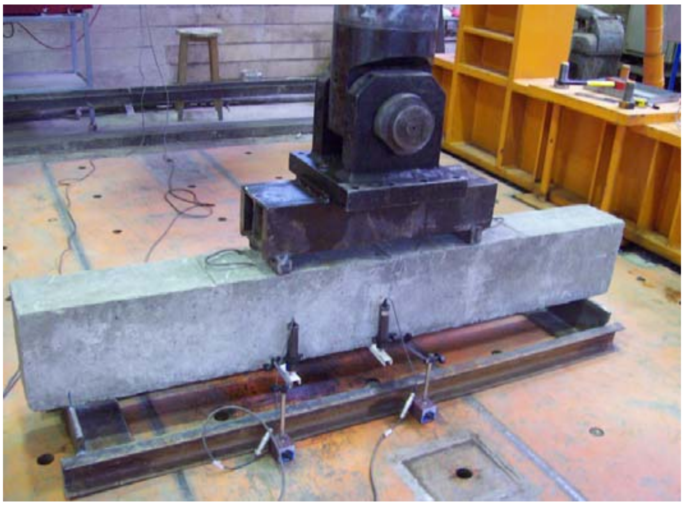

Figure 6. RC beam in its virgin condition

2.5. Instrumentation and Test Procedure

The beam specimens were simply supported over a span of 1600mm(L) and tested in flexure under two symmetrical point loads, thus giving a L/h ratio of 5.33 and an a/h ratio of 2, where a is the shear span. The load was applied using a servo controlled hydraulic actuator with a maximum capacity of 1000KN according to ASTMC78-00 [9]. The load rate constantly increased the extreme fiber stress between 0.86 and 1.21 MPa/min. The load was applied monotonically up to failure. First linear variable displacement transducer (LVDT) was placed under the mid-span and second LVDT were similarly placed under the beam at the load position. Figure 6 gives the positions of LVDTs.

3. TEST RESULT AND DISSCUSSIN

The loads vs. mid-span deflections of the beams are presented in Figures 7-11.

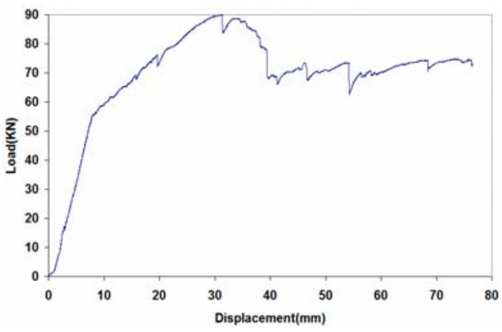

Figure 7. Load–Displacement for B1 and B2 specimens

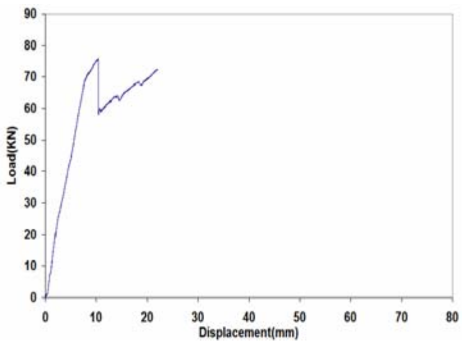

Figure 8. Load–Displacement for B3 and B4 specimens

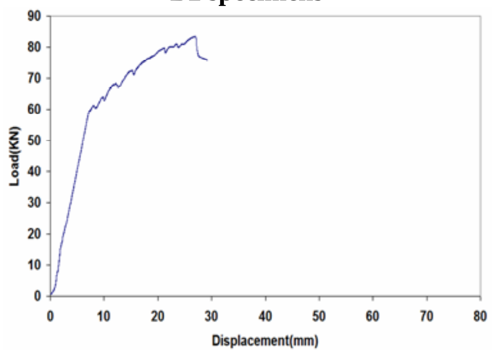

Figure 9. Load–Displacement for B5 and B6 specimens

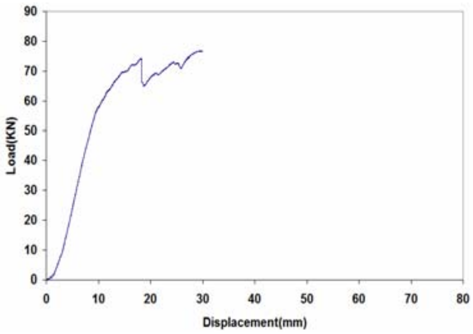

Figure 10. Load – Displacement for B7 and B8 specimens

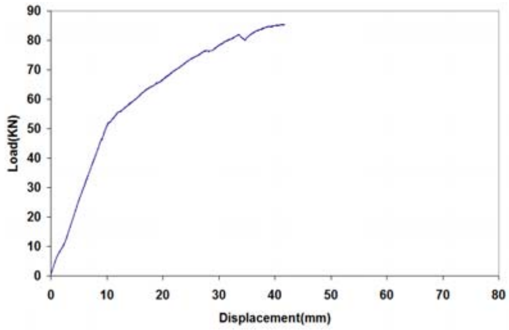

Figure 11. Load–Displacement for B9 and B10 specimens

As expected, beams strengthening by external bonding of different FRP materials resulted in an increase in stiffness, the highest increase being exhibited in beam specimens B3 and B4 that strengthened by CFRP and epoxy (ML-506) resin. The loads corresponding to the appearance of flexural crack are presented in Table 3. The first crack appeared at the bottom of mid-span section and then propagated to the top of zone.

All the beam specimens failed in bending. The beams B1, B2 failed by crushing of compressive concrete in load of 51KN. B3, B4 which were strengthened by CFRP and resin epoxy failed at a load 33% higher than the beams B1, B2 that its load was 68KN. Beams B5, B6 also show a 15% increase in yielding strength where FRP strip failed that its load was 59KN. Specimens B7, B8 failed at a load lower than B3, B4. Their yielding loads were almost half of yielding load of B3, B4 because of they were damaged. They failed at a load 14% higher than the specimens B1, B2 that its load was 58KN. B9, B10 show a 7% increase in yielding strength its yielding load that FRP strip failed was 54KN. Similar to B7, B8 their yielding load were almost half of the yielding load of B5, B6. The failure of all of strengthening beams was initiated due to failure of the bottom strip. In the table 3, the yield load where FRP strips failed is presented.

Table 3. Test result

Beam	Yield Load (KN)	Increase in yielding load after strengthening (%)
B1, B2	51	
B3, B4	68	33
B5, B6	59	15
B7, B8	58	14
B9, B10	54	7

4. FINITE ELEMENT MODELING

Linear elastic FE analyses were carried out to investigate the Load – Displacement. The concrete block was taken to be 1000 mm long, 300 mm thick and100 mm wide. The Youngs modulus was assumed to be 200, 2.789 and 31.6GPa, respectively for the plate, adhesive and concrete. The corresponding Poissons ratios were 0.3, 0.3 and 0.15, respectively. The geometry, loading, boundary conditions and adopted coordinate system are shown in Figure 12. Only a quarter of the beam was modeled using the symmetrical conFigureuration in the x–y plane. Numerical analyses were conducted using ANSYS.9. Concrete was modeled using solid65 and plate, adhesive, CFRP and GFRP layers were modeled using solid45, and reinforcing bars were modeled using link8 [1]. The element size for all meshes was 25 mm. In most tests, failure occurs within the concrete in top of beams. The comparison between numerical analysis and experimental test results are shown in Figures 13-17.

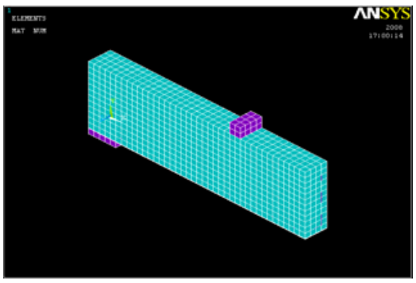

Figure 12. Ansys model

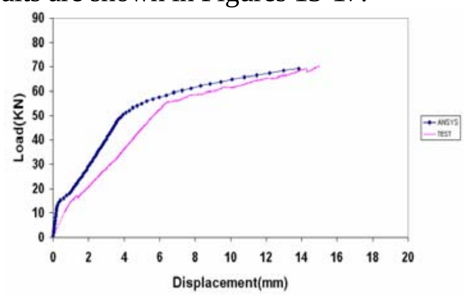

Figure 13. Comparison between ANSYS and TEST for beams B1, B2

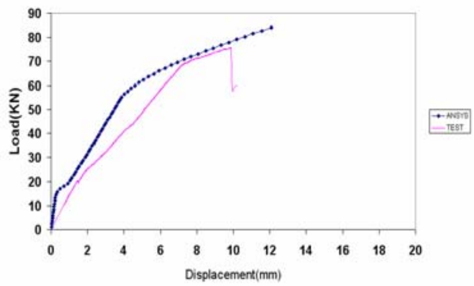

Figure14. Comparison between ANSYS and TEST for beams B3, B4

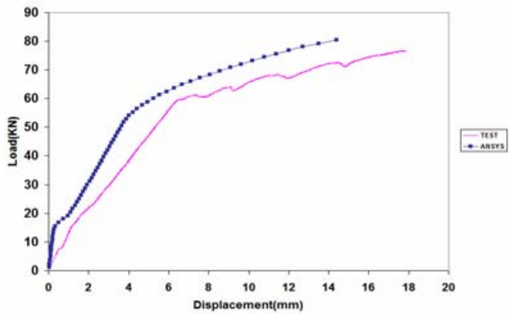

Figure15. Comparison between ANSYS and TEST for beams B5, B6

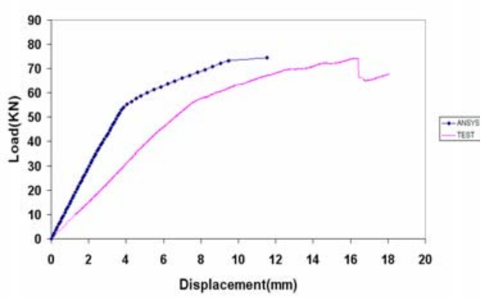

Figure16. Comparison between ANSYS and TEST for beams B7, B8

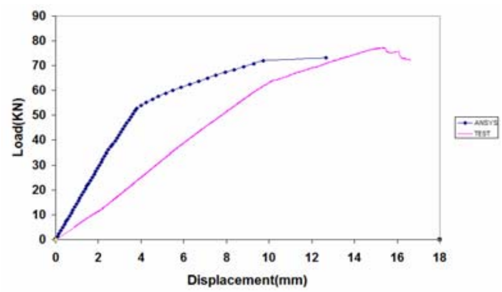

Figure17. Comparison between ANSYS and TEST for beams B9, B10

5. COMPARISON OF NUMERICAL AND TEST RESULTS

Comparison in terms of load–midspan displacement curves, with the numerical results obtained by the finite element analysis are shown in Figures 13-17. It can be initially observed from the Figures that the straight lines obtained by the FEM analysis provide a good approximation for the curves obtained experimentally, with close agreement regarding the beam stiffness. On comparing now the experimental results from the bending tests with the numerical ones, it can be observed that, for the all specimens the FEM analyses curve lies a little above the curves from the experimental, giving slightly lower displacements for the same applied load value. These differences are probably caused by the differences between the elastic properties estimated in the analyses and the true ones, and also due to difficulties in reproducing the true boundary conditions of the experimental tests in the models. It should be noted, however, that the differences are small in comparison with the variations observed in the experimental measurements.

6. CONCLUSIONS

This paper deals with bending strength of the reinforced concrete damaged beams using an externally CFRP and GFRP strip. Test result of ten retrofitted beams in states of before and after damage are presented and discussed. This paper clearly shows that there is difference in strength between using CFRP with epoxy resin or GFRP with epoxy resin in concrete beams; moreover, there is a high difference between retrofitting of damaged or non damaged beams.

REFERENCES

1. Sadeghian. P & Rahai. A. R & Ehsani. M. R, Numerical modeling of concrete cylinders confined with CFRP composites, journal of reinforced plastics and composites, 2008, 27:1309.
2. ASCE report card for America's infrastructure available from: www.asce.org/reportcard. 23 January 2005.
3. Chen. A. T & Teng. J. G, Shear capacity of FRP-strengthened RC beams: FRP debonding, Construction and Building Materials Journal, 2003, 27-41.
4. Wu. Zhishen & Li. Wenxiao & Sakuma. Naoki, Innovative externally bonded FRP/concrete hybrid flexural members, Composite Structures Journal, 2006, 72, 289-300.
5. J.F. Chen & W.K. Pan, Three dimensional stress distribution in FRP-to-concrete bond test specimens, Construction and Building Materials Journal, 2006, 20, 46-58.
6. Aram. M. R & Czaderski. Ch & Motavalli. M, Debonding failure modes of flexural FRP-strengthened RC beams, Composites, 2008, 39, Part B, 826–841.
7. Oehlers. D. J & Rashid. R & Seracino. R, IC debonding resistance of group of FRP NSM strips in reinforced concrete beams, Construction and Building Materials, 2008, 22, 1574-1582.
8. ASTMD3039/D3039M-95a, Standard test method for tensile properties of polymer matrix composite materials, Philadelphia (USA), American Society for Testing and Materials (ASTM), 1995.
9. ASTMC78-00, Standard test method for Flexural strength of concrete (Using simple beam with third-point load), USA, American Society for Testing and Materials (ASTM), 2001.

CD04-009

REPAIR AND RETROFIT OF RC COLUMNS WITH PRE-STRESSED BANDS FOR IMPROVED SEISMIC BEHAVIOUR

H. Moghaddam[1], M. Samadi[2]
[1]Sharif University of Technology Tehran, Iran
[2]Islamic Azad University of Mashhad, Iran

ABSTRACT
A new technique of seismic retrofit of RC columns has been applied in this paper. Pre-stressed high strength metal strips are externally applied to RC columns. Eight large-scale RC columns with insufficient transverse reinforcements were tested under constant axial and cyclic lateral load reversals. The level of axial load and the pattern of strengthening were parameters of this study. The ability of the technique for improving the ductility of RC columns and increasing the lateral strength of columns as well as repair of damaged columns was studied. It was observed that the technique is capable to enhance the lateral behavior of RC columns significantly. Very ductile behavior was achieved. The height-wise variations of lateral strain on confining strips are studied.

Keywords: RC column, seismic behavior, earthquake, repair, seismic retrofit

1. INTRODUCTION
Major failure modes that have been reported for RC columns in previous earthquakes or laboratory tests including shear failre, lap-splice failure, buckling of longitudinal bars inflexural failure, insufficient capacity of plastic hinge rotation can mainly be interpreted due to the inadequte confinement. Several experimental studies have been performed on application of various techniques of seismic retrofit of reinforced concrete columns such as RC jacketing, steel jacketing, glued steel bands, FRP jacketing, FRP collars, post-tensioned cables, etc. [1-5]
In this paper, an easy and innovative technique of retrofit of concrete is applied for enhancing the lateral behavior of concrete columns. This technique involves post-tensioning high-strength packaging straps around the column and subsequently locking their ends in metal clips. Various conFigureurations have been applied in laboratory tests of reinforced concrete columns including cantilever, double curvature, double ended, flexible base and hammerhead. [7] In this study the cantilever conFigureuration was selected in which a constant axial load is applied and then lateral reversal cyclic displacements are applied by means of hydraulic jacks. This paper presents the experimental results of a study on the application of this retrofit technique on large-scale models of building columns. The main objective of this research was quantification of the improvement of RC columns behavior by applying this technique. This technique was previously applied for retrofitting the compressive behavior of small scale concrete columns with various

shapes and sizes [8]. It could also increase the compressive strength and ductility of spirally reinforced cylindrical columns [9].

2. APPLIED RETROFIT TECHNIQUE

The technique used for retrofitting concrete columns in this study, involves post-tensioning high-strength packaging straps around the column (by using standard strapping machines used in the packaging industry) and subsequently locking their ends in metal clips, as shown in Figure 1.

Figure 1. strapping mechanism and devices for retrofit of rc members

Commercially available strapping tensioners and sealers make it easy to pretension the strip and fix the strip ends in the clamps. The available straps have widths of 10 to 50 mm and thicknesses of 0.5 to 1.12 mm. In terms of strength, high strength strips in excess of 10000kg/cm^2, are available in the market. The strips are tensioned to 30 percent of their yield stress. Hence, an effective lateral stress is applied on the column prior to loading. This has many benefits such as full utilization of the strip capacity and prevention from premature crushing of the confined concrete, as would be the case with not properly tightened strips.

The low cost of strip and speed and ease of application of the strapping technique make this method efficient for use as a repair and strengthening technique for RC structural members. An RC column would normally require six man days' work to be jacketed whilst a maximum of two days' work is required for external strapping, which clearly demonstrates the cost saving when using the proposed technique. (Frangou & Pilakoutas 1995)

3. EXPERIMENTAL PROGRAM

Eight 2/3 scale models of reinforced concrete building columns with inadequate transverse reinforcement were made and tested under constant axial load and cyclic lateral displacement reversals. In Figure 1 details of reinforcement of these columns is shown. The specimens were tested under one of the two considered levels of axial compression that were equal with 0.19f'cAg and 0.38 f'cAg.

The yield strength of longitudinal and transverse bars for all specimens was 550MPa and 600MPa, respectively. The average strength of concrete was 26MPa. The retrofit technique that was applied in this study involves strapping the concrete columns with high strength metal strips. The strips are tensioned with a pneumatic tensioner and then the both ends of the strip are locked in a seal by means of a

sealer. Calibration tests were initially conducted and a linear relationship was obtained between air pressure and tensioning force in the strip. This linear relationship was then used in retrofit of RC columns. The yield and ultimate strength of applied metal strips were 850 and 950 MPa, respectively.
Four distinctive failure modes have been reported for RC columns under seismic conditions, including flexural failure, shear failure, shear-flexural failure and lap-splice failure. Typically, in columns of building structures, the aspect ratio and shear span to depth ratio are greater than 8 and 3, respectively. Therefore, the flexural and shear-flexural failure modes have more frequently been reported for building columns. Design of columns was conducted with the aim of achieving a shear-flexural failure mode. So, the ratio of Vp/Vn was so designated that the failure mode of column would be shear-flexural mode, in which shear failure occurs following to the flexural failure.
Test parameters included axial load and retrofitting pattern. Details of column specimens are presented in table 1. Two different amounts of strips were applied through height of columns. As shown in Figure 2, the column height was divided into two different regions of L1 and L2. Generally more confinement was provided in the first region.

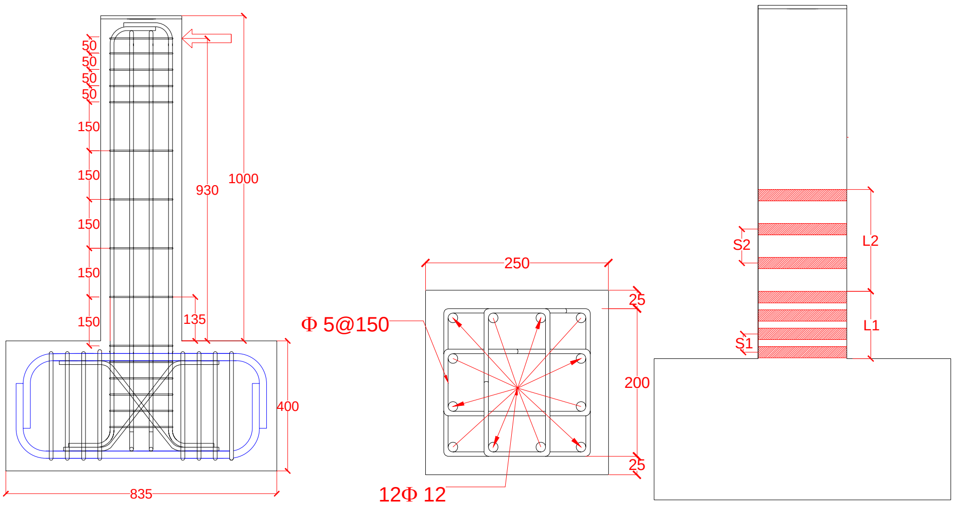

Figure 2. Details of test specimens and retrofit layout

For each level of axial load, a control specimen was tested as the basis for quantification of the improvement developed due to strapping the column. One of the retrofitted columns, i.e. C2 was tested under the first level of axial load. This specimen was slightly retrofitted with strips placed at the middle between the internal ties.

Table 1: Test Matrix

Specimen	Axial load	Retrofit layout						
		L1 (mm)	Number of strip layers	S1 (mm)	L2 (mm)	Number of strip layers	S2 (mm)	
C1	0.19 Ag. f'c	Control specimen for fist level of axial load						
C2	0.19 Ag. f'c	65	1	32	687	1	150	
C3	0.38 Ag. f'c	Control specimen for second level of axial load						
C4	0.38 Ag. f'c	198	2	33	285	1	36	Encircled with wood
C5	0.38 Ag. f'c	198	2	33	285	1	36	
C6	0.38 Ag. f'c	132	2	33	250	1	83	
C7	0.38 Ag. f'c	280	2	71	213	1	71	Damaged and repaired
C8	0.38 Ag. f'c	132	2	33	332	1	83	NSM lon. bar

Three columns were tested under the second level of axial load. Specimens C4 and C5 were retrofitted with the same layout. The only difference between these specimens was the form of column section. Four wood pieces were attached to each side of column and the form of column section was changed from square to circular. This increases the confinement effectiveness. The lower part of the last column, C6, was fully jacketed with two layer strips from column base to an elevation of 132mm which is the elevation of the first internal tie. From this elevation to elevation of 382mm, which is about 1.5 times the column width, one layer strips were applied at a spacing of 83 mm. Along the vertical edges of the columns a radius of 25mm fillet was formed by including suitable block outs in the formwork to prevent stress concentration that may cause premature failure of strips at the corners as well as to increase the geometrical confinement effectiveness.

The column specimen C7 was initially tested without any retrofit under the higher level of axial load until the lateral strength decreased by 20% of the peak lateral strength. Parts of the cover concrete that have been crushed during the first test were removed and re-filled with a cement based mortar with addition of the epoxy adhesive. The damaged specimen was then retrofitted with steel strips and re-tested. (Figure 3)

(a) (b)

Figure 3. Column C7; a) damaged state, b)end of test of repaired column (15% drift ratio)

In order to assess the possibility of increasing the lateral strength of RC columns with application of "Near Surface Mounted" reinforcement together with the strapping technique, column specimen C8 was made and tested. Increasing the strength of a RC column is a necessary issue in the cases of a weak column and strong beam in RC frame buildings. A longitudinal groove was created at each one of the two tensile-compressive faces of column (Figure 4).Then a deformed 12 mm diameter bar was glued inside the groove and the groove was filled with a cement-based mortar. No chemical adhesive was applied.

(a) (b)

Figure 4. Column specimen C8; A) NSM longitudinal bar, B) final damage state (11% drift ratio)

3.1. Test Setup and Instrumentation

The column stubs were fastened to the strong floor with eight high-strength rods, and each rod was pre-stressed to 200 KN to prevent slip and overturning under large lateral load. A vertical hydraulic jack was used to apply the constant axial load which was controlled by a load cell. Two horizontal hydraulic jacks were utilized to apply lateral cyclic loading. Six vertical LVDTs, four horizontal LVDTs and four inclined LVDTs were used to measure the columns curvature, lateral displacement and shear deformation, respectively. In addition, two LVDTs were used to measure the width of developed crack at the interface of the column and end beam. Ten Electrical resistance strain gages glued to longitudinal and transverse reinforcements and twenty strain gages for measuring the strip strains were used.

The axial load was held constant during the test by vertical hydraulic jack shown in Figure 2. The effect of earthquake on the column specimens was simulated by reversed cyclic loading. Two hydraulic jacks in the test setup were used to displace the top of the columns to achieve a predetermined displacement level. Then the loading direction was reversed to achieve the same displacement level in the opposite direction. The lateral force was applied in the displacement control mode, consisting of incrementally increasing lateral drift cycles at 0.5, 1.0, 2.0%, etc., until the load resistance dropped by 30%.

4. TEST RESULTS AND OBSERVATIONS

Since fraction of the applied lateral load is cancelled with the horizontal component of the axial load, especially in large drifts, it is necessary to calculate the net applied lateral load. Instead, since the failure modes of retrofitted columns were flexural, the moment at the base of column was drawn versus lateral drift. This drawn moment includes the moment induced by the axial load, i.e. known as the effect of P-$\tilde{\Delta}$

In Figure 5, the moment versus drift ratio for columns tested under the lower level of axial load are shown. The first control specimen, i.e. C1, behaved quite well. Although the distance between internal tie reinforcements was very large, but due to the large yield strength and suitable conFigureuration of these reinforcement and also the small amount of axial load, C1 showed a ductile behavior. In this specimen, after concrete cracking in tension and yield of longitudinal reinforcements, cover concrete spalled off and subsequently longitudinal reinforcements buckled and considerable loss in lateral strength occurred. Specimen C2 was slightly reinforced with one layer of metal strips. The small amount of confining strips could enhance the behavior of column. The inclined shear cracks were eliminated. Since the first two strips from the column base were applied with no spacing, the cracking and crushing of cover concrete occurred only between the second and the third strips. Longitudinal bar buckling was observed after cover spalling and subsequently longitudinal bars ruptured one by one. It was concluded that the ductility of a relatively ductile column can be enhanced with a small amount of metal strips.

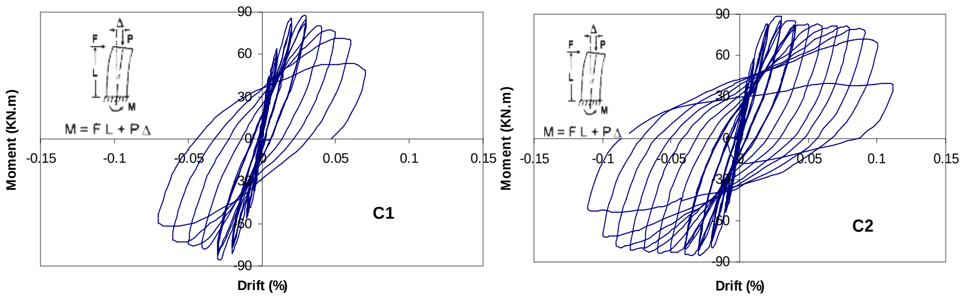

Figure 5. Hysteretic lateral behavior of columns tested under the lower axial load level

In contrast, the second control specimen, C3, that was tested under higher axial load showed a brittle behavior. At 3% drift, suddenly the cover concrete spalled off and longitudinal bar buckling occurred. Shear cracks were also observed on side faces (Figure 6).

Specimen C4 showed a very ductile behavior. Due to the effective confinement applied no cracks or damage was created in the column until failure except crack at the interface of column base and foundation. By increasing the lateral drift, this crack was opened until the longitudinal bars ruptured. In addition to the ductility, the lateral strength of this column was also increased. None of the strips failed until the end of the test. In this specimen the length of plastic hinge was very small, about 3cm!

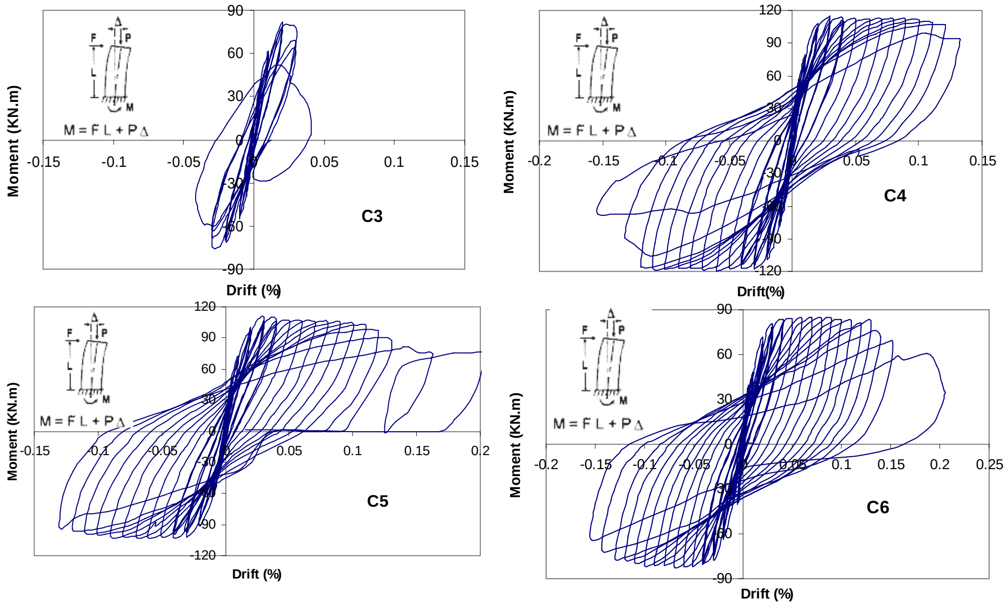

Figure 6. Hysteretic lateral behavior of columns tested under the higher axial load level

Both strength and ductility of column C5, with a retrofit layout the same as that of C4 but without wood, enhanced considerably. Cracks took place between adjacent strips in addition to the interface crack. So, on the contrary to C4 in which the damage was concentrated only at the interface of column and foundation, the plasticity was distributed over a particular length and therefore longitudinal bar rupture did not occur. Loading was continued to very great values of drift ratio but no rupture was observed in strips or bars.

Similarly, column specimen C6 showed a very ductile behavior. No rupture was observed in confining strips. The main difference between C6 with lower amount of confinement with C5 was its smaller lateral strength. In terms of ductility, both columns behaved very ductile and no strip rupture occurred. The moment-drift relationships of these specimens are shown in Figure 4. It can be observed that the fully jacketed specimens, C4 and C5, have achieved higher strength values. This is because the strips of compressive face lean on each other and resist some compressive forces.

In Figure 7A, envelope of recorded hysteretic moment-drift response of column specimen C7 before and after repair with strapping is shown. The column was initially tested without any retrofit until its lateral load carrying capacity decreased by 20%. The dashed line shows the rest of the curve obtained form control specimen (C3). The imposed damage level was really significant including complete spalling of the cover concrete in the plastic hinge region, yielding of longitudinal reinforcement in tension and buckling in compression as shown in Figure 3. Such a damage state has been defined as the failure or collapse performance level in the literature. After repairing the column with strapping, the column behaved acceptably. Although it showed less stiffness than the initial undamaged column but it could suffer large lateral displacement and very ductile behavior.

Hysteretic behavior of column C8 with addition of near surface mounted longitudinal bars and external strapping is compared with that of control specimen C3 in Figure 7B. This technique could provide 30% increase in lateral strength as well as considerable enhancement in column ductility.

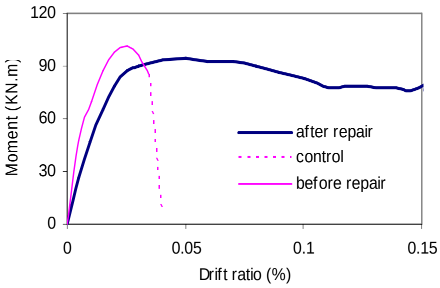

(a)

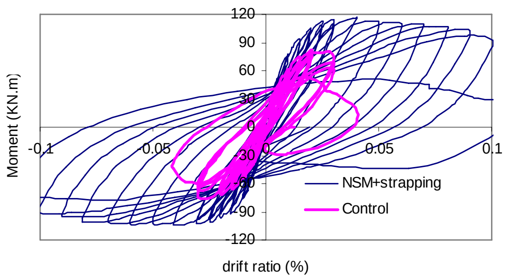

(b)

Figure 7. a) behavior of C7 before and after repair, b) Hysteretic behavior of column C8

5. ANALYSIS OF THE RESULTS

5.1. Envelope of Moment-Drift Ratio

The lateral displacement of a RC column consists of several fractions including flexural deformation, shear deformation and bar slip. The lateral displacement due to flexural deformations is usually obtained by using fiber modeling approach. In this approach, the uniaxial stress-strain behavior of the three parts of column section, i.e. cover concrete, longitudinal bars and core concrete is assigned to the corresponding part. The moment-drift ratio of two columns were obtained by this method and compared to the experimentally obtained relationship. It shall be noted that the shear deformations were not taken into account in these analyses and Mander et al. 1988 confinement model was used for estimation of the stress-strain of concrete confined with strips or internal strips. In analysis of specimen C5 that is confined with external strips, the stress-strain behavior of cover concrete and was calculated based on lateral pressure created by external metal strips. On the other hand, the stress-strain of core concrete was obtained by a two step approach. At the first step, peak strength and corresponding strain of the core concrete confined with internal transverse reinforcements is obtained by application of any confinement model. At the second step, the aforementioned properties are assumed as the properties of plain concrete that is confined with external strips.

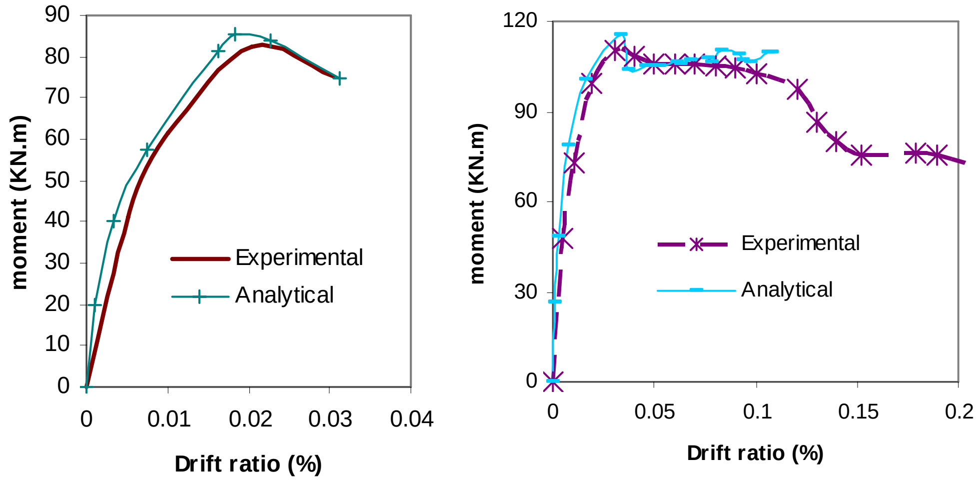

(a) (b)

Figure 8. A Comparison of the analytically and experimentally obtained moment-drift envelopes for A) column C3 and B) column C5

As can be seen in this Figure, the analytically obtained curve is relatively in good agreement with experimental results. For both specimens, the analysis has overestimated the stiffness of pre-peak branch of curve. This is mainly because the lateral displacement due to shear deformations has not been considered in the analyses.

5.2. Evolution of the Lateral Strains in Strips

The recorded strains of confining strips were studied for column specimen C4 at he peak of each loading cycle. In Figure 9, strains of five strain gages that were attached on strips of a side face of column, recorded at various drift ratios, are drawn versus elevation of the strip from column base. It can be observed that at an elevation of about 13.5 cm, i.e. the elevation of internal transverse reinforcement, the strip strains has not been increased with increasing the lateral displacement. This is mainly because the internal ties have prevented the dilation of concrete, decreased the shear deformations, reduced the lateral deformation due to longitudinal bar buckling and also decreased the opening of cracks at that elevation. The strains of the lowest strip show the greatest values among the height of column. This implies that the column behavior has been flexural, because for a column with shear deformations the inclined shear cracks at a height of equal with one column width tend to widen and therefore induce tension in lateral confinement over this height. It is also observed in this Figure that there is not any significant difference between the strain values of each strain gage in push and pull cycles.

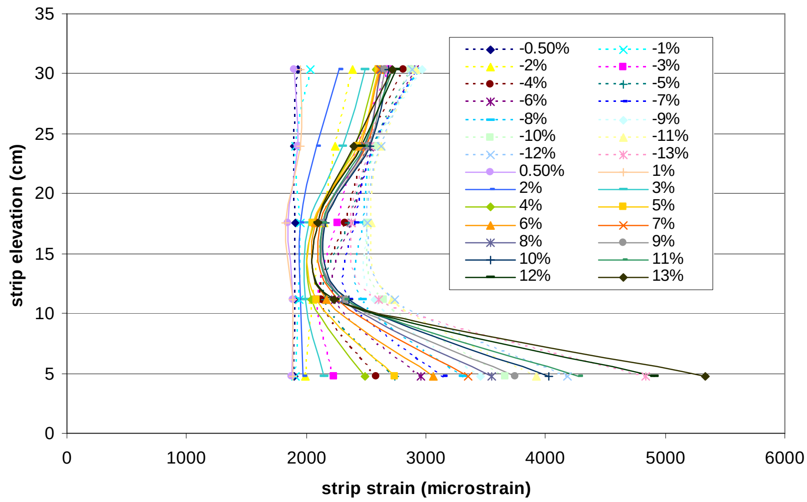

Figure 9. Heightwise variation of strains of strips at side face of C4

Variation of strains of each strain gage at the peak points of each loading step are drawn in Figure 10. It can be observed that although in push and pull cycles, strains at side faces are the same, but they result in an asymmetry in curves corresponding to strains at column corners. In addition, Figure 10 shows that only the strains of the first three strips from column base has evolved noticeably and very small strain values have been induced in upper strips.

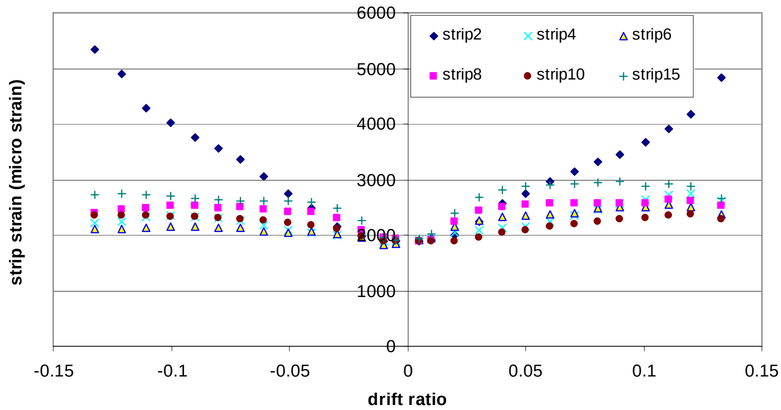

Figure 10. Variation of strains of strips at side face of C4 with column drift ratio

6. CONCLUSION

A new retrofit technique for seismic enhancement of RC columns was described and applied to eight square sectioned RC columns with inadequate transverse reinforcement. Column specimens were tested under constant axial load and cyclic lateral displacement. It was observed that this technique is capable to enhance ductility of brittle RC columns considerably. By application of ductile confining strips with effective sealing type, none of the strips fail even under large lateral displacements. The fiber modeling approach can reasonably estimate the lateral behavior of flexural RC members. Due to the flexural behavior of RC columns, only the first three strips from the base of column experience large strains. Mainly the strips that are located between column base to the first internal reinforcement are stressed that by suitable confining this region, considerable ductility enhancement is achieved. Place and length of plastic hinge in retrofitted column is directly dependent to the layout of retrofit. The technique was also successfully applied in repair of severely damaged RC column. In addition, it can be employed together with NSM bar technique to increase the strength as well as ductility of columns.

REFERENCES

1. Saatcioglu, M. and Yalcin, C. "External Prestressing Concrete Columns for Improved Seismic Shear Resistance", *Journal of Structural Engineering, ASCE*, Vol. 129, No. 8, 2003.
2. Aboutaha R.S., Engelhardt, M.D. Jirsa, J.O. Kreger, M.E. "Seismic Retrofit of R/C Columns Using Steel Jackets". *Seismic Rehabilitation of Concrete Structures,* ACI-SP 160, 1997.
3. Teran, Ruiz, "R/C jacketing of existing structures".. *10th WCEE,* Spain 1992, pp 5107-5113.
4. Saadatmanesh, H. Ehsani, M. R. and Jin, L. "Seismic strengthening of circular bridge pier models with Fiber Composites", *ACI Structural Journal,* Vol. 93, No. 6, November-December 1996.
5. Moghaddam, H.A. and Mehdizad, S. “behavior of square reinforced concrete columns retrofitted with CFRP and AFRP “,*First European Conference on Earthquake Engineering and Seismology, Geneva, Switzerland,* 2006.
6. Frangou M, Pilakoutas K (P) and Dritsos S., "The Structural Repair/Strengthening of RC Columns", *Journal of Construction and Building Materials*, Vol.9, No 5, October 1995, pp 259-266.
7. Berry, M., Parrish, M., Eberhard, M. “PEER Structural Performance Database User’s Manual”, 2004.
8. Moghaddam, H., Samadi, M. “on the effect of external active confinement on spirally reinforced concrete columns”, 14th world conference on earthquake engineering, china, 2008.
9. Moghaddam, H., Samadi, M., Mohebbi, S. “Behavior and modeling of high-strength concrete columns confined by external post-tensioned strips”, SEI08 conference, Canada, 2008.

CD04-010

A COMPARATIVE STUDY ON COMPRESSIVE BEHAVIOR OF H.S. STEEL VS. FRP CONFINED CONCRETE

H. Moghaddam[1], M. Samadi[2]
[1]Sharif University of Technology Tehran, Iran
[2]Islamic Azad University of Mashhad, Iran

ABSTRACT
This paper presents the results of an experimental and analytical study on application of “high strength steel strapping” technique and comparing it with FRP for retrofit of concrete columns. Various parameters were found to influence the compressive strength and ductility of confined concrete, including confinement mechanical volumetric ratio, number of confinement layers, strength of plain concrete and ductility of confining material. Among these parameters, the latter was found to play the most important role in determining the ultimate strain and post peak behavior of concrete. Axial compressive tests were performed on small-scale circular or square section concrete columns. Three different materials were applied for confining concrete specimens, including CFRP jacket, brittle high-strength steel strips and ductile steel strip. Test Results showed significant increase in strength and ductility of columns due to active confinement by metal strips. CFRP confined concrete also showed enhanced behavior. A database of results of compressive tests on concrete confined with various materials was collected from the literature. An analytical model was proposed based on results of this study and the collected database to determine the strength and ultimate strain of confined concrete. The proposed model takes the confinement ductility into account and shows good agreement with the experimental results.

Keywords: concrete, confinement, FRP, steel strip, ultimate strain

1. INTRODUCTION
It is well known and proven that lateral confinement improves the strength and ductility of concrete. Confinement reinforcement is generally applied to compressive members as lateral reinforcement with the aim of increasing their load carrying capacity and their ductility in case of seismic upgrading. In addition, lateral confinement prevents slippage and buckling of the longitudinal reinforcement (Saadatmanesh et al., 1994). Lateral reinforcement can be provided by using circular hoops, rectangular ties, jacketing by steel, FRP, ferrocement, etc.
Since many of the existing RC columns are vulnerable under severe earthquakes due to low ductility, increasing the concrete compressive displacement capacity by confinement becomes a vital issue. Several researches have been conducted in the field of strength and ductility enhancement of concrete by confinement with various materials.

In addition, various models have been proposed for approximating the gain in strength, peak strain and ultimate strain due to confinement. Since the confinement ductility has not been considered as a parameter of study, in almost all of the existing experiments and models, the effect of ductility of confining material on ductility enhancement of concrete has been missed. This paper presents the results of an experimental and analytical study that focuses on this issue. This study was part of a comprehensive investigation on different techniques of concrete retrofit. The study included axial compressive tests on concrete specimens with square or circular sections with or without internal confining bars that were retrofitted with two types of metal strips as well as CFRP jackets.

Confinement models for peak of the compressive behavior a review of the available confining models in the literature shows that almost all of the existing confinement models include an identical form in which strength of confined concrete and the corresponding peak strain is a function of effective lateral pressure f_{le} and strength of plain concrete f'_c as rewritten in Table 1. One of the main differences of these models is the assumed parameters or approaches in computing the effective lateral pressure. Some models use the yield force of confining material for computing the lateral pressure, while a few of these models try to obtain the existing stress in the confining material at the peak axial stress. However, this issue is more important for estimating the strength of steel-confined concrete.

In addition, in some models, the lateral pressure is decreased to account for the ineffectively confined zones of concrete columns which was firstly introduced by Sheikh and Uzumeri 1982 and by Mander et al. 1984 and then applied in EC8. Therefore, according to the most advanced confinement models, the effective lateral pressure is a function of mechanical volumetric ratio of confining material and geometry and dimensions of concrete column and its longitudinal and transverse reinforcements.

Confinement Models for Ultimate Compressive Strain

In contrast to the peak point in stress-strain behavior of concrete, ultimate compressive strain has not been consistently defined with various researchers. In contrast to the tensile tests, in which an apparent rupture could be observed, the definition of the ultimate point in compressive tests of concrete is a controversial issue. For steel-confined concrete, CEB model code 90 (1993) uses the strains on the post-peak branches of stress-strain curves of confined and unconfined concretes that corresponds to a stress level of 85% of strength of unconfined concrete as the ultimate strain of confined and unconfined concretes, respectively.

Cusson and Paultre (1995) used the strains at which the stress drops to 50% of corresponding strengths of confined or unconfined concrete as the ultimate strains of confined or unconfined concretes, respectively. Razvi and Saatcioglu 1999 used an approach similar to that of Cusson and Paultre 1995, in which strains at 85% of strength of confined and unconfined concretes are applied as the ultimate strains of confined and unconfined concretes, respectively. It is observed that there is much difference between theses measures.

However, for FRP confined concrete an obvious ultimate point can be observed which corresponds to the rupture of FRP jacket. Lam and Teng 2003

Table 1: A Summary of Famous Steel-Based Confinement Models

Model	Confined concrete strength	Strain at peak stress
Richart 1928	$f_{cc}^{'} = f_{co}^{'}[1+4.1 f_{le}]$	
Newman 1971	$f_{cc}^{'} = f_{co}^{'}\left[1+3.7\left(\frac{f_{le}}{f_{co}^{'}}\right)^{0.86}\right]$	
Sheikh and Uzumeri 1982	$f_{cc}^{'} = Kf_{co}^{'}$ $K = 1.0+\frac{b_c^2}{140P_{acc}}\left[\left(1-\frac{ns_l^2}{5.5b_c^2}\right)\left(1-\frac{s}{2b_c}\right)^2\right]\sqrt{\rho_s f_{sh}}$	$\varepsilon_{cc} = 80Kf_c^{'}\times 10^{-6}$
Park 1982	$f_{cc}^{'} = f_{co}^{'}(1+2\frac{f_l}{f_c^{'}})$	$\varepsilon_{cc} = \varepsilon_{co}(1+2\frac{f_l}{f_c^{'}})$
Fafitis and Shah 1985	$f_{cc}^{'} = f_{co}^{'}+(1.15+\frac{3048}{f_c^{'}})f_l$	
Saatcioglu and Razvi 1992	$f_{cc}^{'} = f_{co}^{'}+6.7(f_{le})^{0.83}$	$\varepsilon_{cc} = \varepsilon_{co}(1+33.5\left(\frac{f_{le}}{f_{co}^{'}}\right)^{0.83}$
Ahmad & Shah 1982	$f_{cc}^{'} = f_{co}^{'}\left[1+4.2556\left(\frac{f_l}{f_{co}^{'}}\right)\right] \quad if\ \frac{fl}{f_{co}^{'}} < 0.68$ $f_{cc}^{'} = f_{co}^{'}\left[1.7757+3.1171\left(\frac{f_l}{f_{co}^{'}}\right)\right] \quad if\ \frac{fl}{f_{co}^{'}} > 0.68$	
Mander et al 1988	$f_{cc}^{'} = f_{co}^{'}\left[2.254\sqrt{1+7.94\frac{fl}{f_{co}^{'}}}-2\frac{fl}{f_{co}^{'}}-1.254\right]$	$\varepsilon_{cc} = \varepsilon_{c0}\left[1+R\left(\frac{f_{cc}}{f_{c0}}-1\right)\right]$
Karabinis 1994	$f_{cc}^{'} = f_{co}^{'}+4.269 f_l^{0.587}$	
Hoshikuma et al. (1997)	$f_{cc}^{'} = f_{co}^{'}(1+7.6\frac{f_{ley}}{f_{co}})$	
Cusson & Paultre 1995	$f_{cc}^{'} = f_{co}^{'}(1+2.1(\frac{f_{ley}}{f_{co}^{'}})^{0.7})$	$\varepsilon_{cc}-\varepsilon_{co} = 0,21\left(\frac{f_{le}}{f_{co}}\right)^{1,7}$
EC8 2001	$f_{cc}^{'} = f_{co}^{'}(1+5(\frac{f_{ley}}{f_{co}^{'}})) \quad \alpha\omega_w \leq 0.1$ $f_{cc}^{'} = f_{co}^{'}(1.125+2.5(\frac{f_{ley}}{f_{co}^{'}})) \quad \alpha\omega_w \geq 0.1$	$\varepsilon_{cc} = \varepsilon_{co}(1+2.5\,\alpha\omega_w)^2$ $\varepsilon_{cc} = \varepsilon_{co}(1.125+1.25\alpha\omega_w)^2$

Table 2: Models for ultimate compressive strain of concrete

Model	Ultimate strain of confined concrete
CEB model code 90 (1993)	$\varepsilon_{85C} = \varepsilon_{85U}+0.1\left(\frac{f_{le}}{f_{co}^{'}}\right)$
Cusson and Paultre (1995)	$\varepsilon_{50C} = \varepsilon_{50U}+0.15\left(\frac{f_{le}}{f_{co}^{'}}\right)$
Seible et al. (1995)	$\varepsilon_{cu} = 0.004+1.4\left(\frac{f_{le}}{f_{cc}^{'}}\varepsilon_{ju}\right)$ steel $\varepsilon_{cu} = 0.004+2.65\left(\frac{f_{le}}{f_{cc}^{'}}\varepsilon_{ju}\right)$ FRP
Cusson and Paultre (1995)	$\varepsilon_{50C} = \varepsilon_{50U}+0.15\left(\frac{f_{le}}{f_{co}^{'}}\right)$
Razvi and Saatcioglu (1999)	$\varepsilon_{85C} = \varepsilon_{85U}+260k_3\rho\varepsilon_{cc}[1+0.5k_2(k_4-1)]$

2. EXPERIMENTAL PROGRAM

This paper presents parts of the results of a comprehensive study on application of the strapping technique for concrete strengthening. The Experiments presented in this paper included axial compressive tests on 30 prismatic 15*30 concrete columns. The axial and lateral stress-strain behaviors of concrete specimens were obtained by simultaneously measuring the force and axial and lateral displacements of specimens. Several parameters were considered for column specimens and retrofitting including compressive strength of concrete, yield strength, ductility, spacing and size of confining strips. A detailed description of the results of strapped concrete columns with various shapes and sizes has been presented by the authors [13], in which several other parameters affecting the response of strapped concrete is discussed in detail. But the main aim of this paper is studying the effect of mechanical properties of confining material on behavior of confined concrete. Three different materials were used for confining concrete columns, including two different types of strips that are called S and T types, as well as CFRP.

Prismatic specimens were fabricated in the structure and concrete Laboratory at the building and housing research center. Three different concrete mixtures were used to study the effect of strength of plain concrete on response of confined concrete as listed in Table 3. The first set (B1) was used to study the strapping technique and compare the application of ductile and brittle metal strips (i.e. S and T type strips). The two latter sets (B2 and B3) were especially made for comparing CFRP with the two types of strips for concrete confinement. The corners of prismatic specimens of the second and the third sets (i.e. B2, B3) were rounded with a radius of 2.5 cm, making it suitable for CFRP wrapping.

The material used for the concrete specimens included type I portland cement, local sand and gravel. The maximum size of the gravel was 12 mm. No additive was used in any of the mixes.

Applied strips had different widths, thicknesses and mechanical behaviors. Standard tensile tests were performed on three samples of each size of these materials and their average mechanical properties are shown in table 4. The moduli of elasticity of strips and FRP were 200 and 220 GPa, respectively. Ultimate strength, elastic modulus, ultimate strain and thickness of each layer of CFRP was 2800 MPa, 220 GPa, 1.55% and 0.176 mm, respectively. A summary of the mechanical properties of these materials are reported in the following table.

Table 3: Concrete Mix Designs (per Cubic meter)

Element	Batch1 (B1)	Batch2 (B2)	Batch3 (B3)
Cement	241	336	436
Water	205	205	205
Coarse aggregate	874	874	874
Fine aggregate	1025	930	830
W/C ratio	0/85	0/61	0/47
Design compressive strength (Mpa)	10	25	35
Corners radius	0	2.5	2.5
Number of specimens	14	8	8

Table 4: Mechanical Properties of Applied Strips

Material	Width (mm)	Thickness (mm)	Yield stress (kg/cm^2)	Ultimate stress (kg/cm^2)	Ultimate strain
S strip	16	0.5	1033	1033	0.01
T strip	32	0.8	8746	9975	0.07
CFRP	---	0.176	28000	28000	0.0155

(a) (b)

Figure 1. Test setup and instrumentation a) strapped b) FRP wrapped

3. AXIAL STRESS-STRAIN BEHAVIOR

Axial and lateral strains of column specimens were obtained by measuring specimen deformations by LVDT. In Figure 2, axial and lateral stress-strain behaviors of two specimens of the first set of specimens (B1) are shown. These specimens were confined with brittle S strips at two distinctive spacing values.

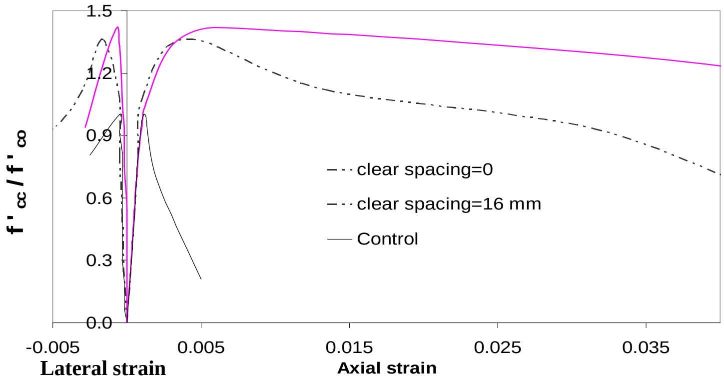

Figure 2. Normalized stress-strain of two confined specimens of B1 set strengthened with S strip

The vertical axis shows the provided increase in strength which is obtained by normalizing the measured stress to strength of plain concrete. It can be seen that the amount of volumetric ratio of confinement affects concrete strength and ductility. However because of the low strength of these specimens (in contrast to other results) the increase in strength is not as much as ductility enhancement. By considering the evolution of the lateral strains, it is obvious that the more confined specimen experiences less dilation.

Similarly, the stress-strain behavior of specimens of B2 and B3 sets that have been confined with one of the three applied confining materials are drawn in Figure 3. By comparing the behavior of specimens confined with brittle strips, ductile strip and CFRP it can be concluded that:

1. For a particular confining material, both strength and ductility of confined concrete increase with increasing the level of confinement.
2. For a similar confinement pattern, ductility of confined concrete is lower for specimens with higher strength concrete.
3. Although all of the three confining materials have similar elastic stiffness and both metal strips have similar strength values, but the form of stress-strain behavior of the triple sets of specimens differ apparently. As a matter of fact, ductility of confining material has dominated the stress-strain curve of confined concrete. As can be seen in the Figures, for a particular confining material, a similar form of stress-strain curve can be observed for various levels of confinement.
4. For a constant level of confinement with several confining materials, the higher the ductility of confining material, the higher the compressive ductility of confined concrete.

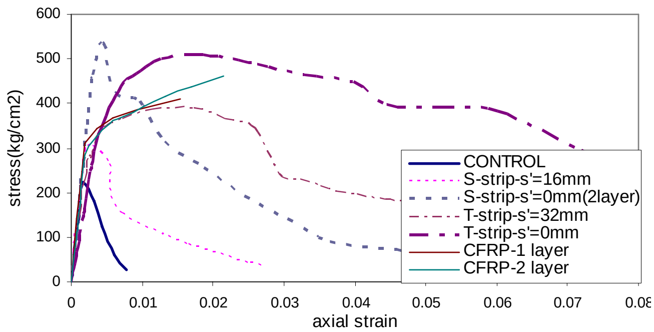

(a)

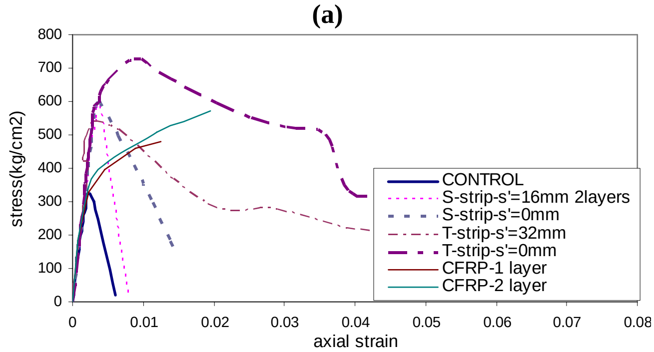

(b)

Figure 3. axial stress-strain of specimens confined with different materials for concrete specimens of a) B2 and b) B3 sets

It is also observed from these Figures that by using a ductile confining material, a very ductile compressive behavior for concrete can be achieved. This means great ultimate strain, better post-peak behavior and more thoughness and capability to absorb energy. It should be noted that theses curves correspond to prismatic specimens that traditionally can not be confined effectively and the obtained results for cylindrical specimens show much more ductility. For cylindrical specimens, it was observed that the ductile strip is capable to provide a very ductile behavior even for high strength concretes.[13]

From the above results and the results of other specimens presented by the authors [13], it can be concluded that for a similar confinement level, i.e. equal confinement pressure, ultimate strain and post-peak behavior of confined concrete is mainly dependent to the deformation capacity of the confining material.

4. ANALYSIS OF THE RESULTS

One of the measures for confinement level that has been widely used in the literature is the effective mechanical volumetric ratio of confining material, i.e. $K_e.\frac{\rho.f_y}{f_c^{'}}$. This has been also known as the effective confinement index. In this index, K_e is a ratio between 0 and 1 that takes the ineffectively confined regions between the longitudinal and transverse reinforcements into account. ρ is the volumetric ratio of the confining material , f_y and $f_c^{'}$ are yield strength of confinement and strength of plain concrete.

By considering the equilibrium of confined concrete, it can be shown that the effective confinement index equals with $K_e.\frac{2f_{ly}}{f_c^{'}}$, in which f_{ly} is the lateral confining pressure corresponding to the yield of confinement. This has also been shown by defining the concept of effective yield-based lateral confining pressure, i.e. $\frac{2f_{ley}}{f_c^{'}}$.

By analyzing the experimentally obtained results of this study and also experiments performed by Moghaddam and Samadi 2008, Frangou and Pilakoutas 1995 and also Mortazavi and Pilakoutas 2004, it was observed that the improvement of strength of confined concrete is strongly dependent to the effective confinement index. As can be observed in Figure 4, there is a fair relationship between the strength gain of confined concrete and the effective confinement index. Although, the available models for strength of confined concrete give relatively different formulas the upper and lower bounds of strength improvement ratio, can reasonably be determined with Richart1928 and Ahmad & shah 1982 models, respectively.

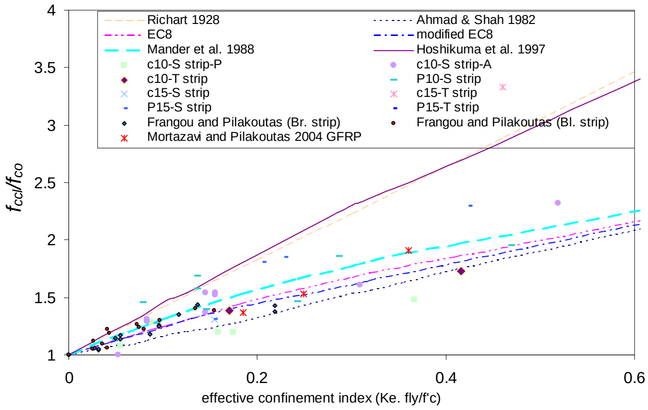

Figure 4. the relationship between effective confinement index and gain in strength

This strong relationship between effective confinement index and strength increase ratio can also be studied in particular for the three sets of specimens of this study which had different plain strengths. Figure 5 shows the strength gain ratio for specimens of this study that were retrofitted by any of the three confining materials of S strips, T strips and CFRP. It is observed that a close relationship exists between the variation of the strength increase ratio and the effective confinement index. This relationship is approximately the same for the three confining materials and three plain strength values.

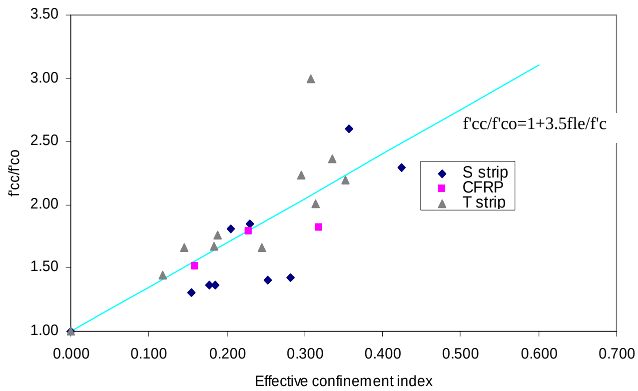

Figure 5. Strength Gain for Specimens of Three Batches Confined with one of the Triple Confining Materials

However, as observed in Figures 3, the gain in ductility of confined concrete is also dependent to the ductility of confining material and can not be described as only a function of confinement index. Therefore, a modification to the effective confinement index was done to take the deformation capacity of confining material into account. An equation with a form similar to that of Seible et al. 1995 as shown in table 2 was selected to predict the ductility gain of confined concrete and the modified confinement index was defined as the effective confinement index multiplied by the ultimate strain capacity of confining material. In order to study the ductility of confined concrete, ductility measure of CEB model code 90 was applied. A database of results of compressive tests on concrete confined with various materials was collected from the literature. The first data set of the database was the results of axial compressive tests on cylindrical 10*20 and 15*30 and prismatic 10*20 and 15*30 specimens that were confined with the two types of metal strips. These tests were previously conducted by the authors[13]. The second set of data includes test results of cylindrical 10*20 specimens confined with carbon or aramid FRP sheets by Watanabe et al. 1997. The third data set includes results of tests on cylindrical 15*30 specimens confined with CFRP sheets. The ratio between ultimate strains of confined and unconfined concrete specimens are drawn in Figure 8 versus the modified confinement index. As can be seen, the models of Seible et al. 1995 and EC8 did not suitably predict the ductility gain for neither of the steel-confined nor CFRP-confined concrete specimens. An analytical formula was obtained statistically and is as follows.

$$\varepsilon'_{cc}/\varepsilon'_{co}=1+2500\ (f_{le}/f'_c).\ \varepsilon_{ju}\ \ (f_{le}/f'_c)<0.001 \qquad (1)$$

$$\varepsilon'cc/\varepsilon'co=3.5+550\ (f_{le}/f'_c).\ \varepsilon_{ju}\ \ (f_{le}/f'_c)>0.001$$

The obtained formula of equation 1 is compared to the experimental data of the collected database. Figure 6 shows that, although the ductility gain data are more scattered than strength increase ratio values as presented in Figure 4, but equation 1 can give a better estimation of the increase in ductility due to confinement than the previous models. It is important to note that the experimental data of Figure 6 includes specimens with various shapes, sizes and confining materials and therefore the modified confinement index and equation 1 seem to have given good approximation of the ductility gain.

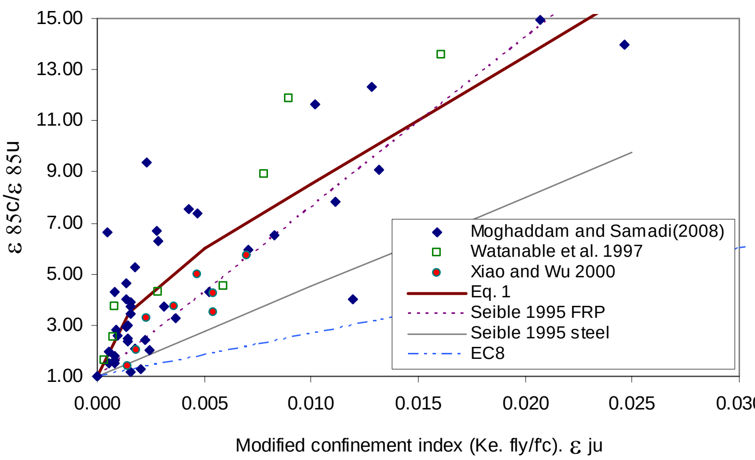

Figure 6. The Gain in Ultimate Strain for Concrete Confined with Various Materials

In order to verify the accuracy of the proposed equation, the experiments of this study were conducted. As mentioned earlier, prismatic 15*30 specimens with three levels of concrete strength were retrofitted with three confining materials, i.e. S type strips, T type strips and CFRP. The ratio of ultimate strain of confined concrete to that of unconfined one are drawn against the proposed ratio of modified confinement index in Figure 7. As can be seen in this Figure, the modified index for confinement and the proposed equation for ductility enhancement ratio due to confinement could give good approximation of the experimentally obtained values of this study. Adequate correlation can be observed between the experimental and analytical values especially when considering numerous differences than exist between the data points including strengths of plain concrete, confinement levels and confining materials.

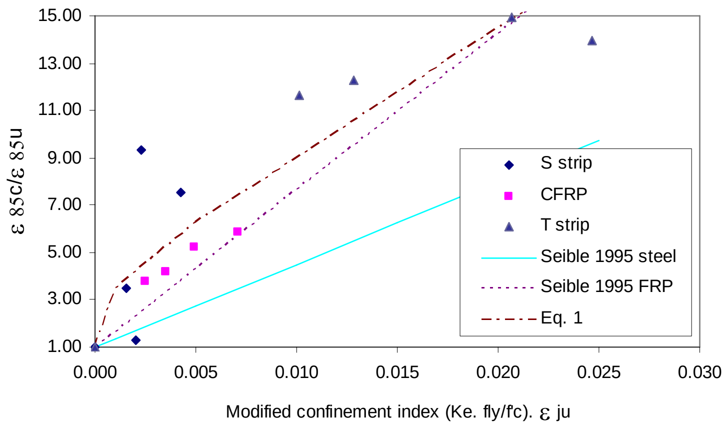

Figure 7. Gain in Ultimate Strain Versus Modified Confinement Index

5. CONCLUSION

Compressive tests were conducted on concrete specimens confined with various confining materials. In addition, some other test results were collected from the literature. Based on these results, some conclusions can be made. For all confining materials, by increasing the level of confinement, both strength and ductility of confined concrete increase. The confinement index (defined as the ratio of effective lateral pressure to strength of plain concrete) shows good correlation with the increase of strength of confined concrete for specimens with any size, shape and strength confined with both steel or FRP. Among various parameters, ductility of confining material plays the main role in determining the post-peak response of confined concrete. Then, for a particular confining material, by increasing the level of confinement the strength and ultimate strain of confined concrete are scaled without any significant change in the form of stress-strain curve of concrete.

The confinement index alone can not be used for approximating the ultimate strain of confined concrete. The modified confinement index, that was defined and applied in this paper, showed relatively good correlation with the gain in ductility.

ACKNOWLEDGEMENT

The authors would like to express their sincere thanks to Dr. Parhizkar and all administrative staff of structures laboratory of building and housing research center.

REFERENCES

1. Xiao Y, Wu H., Compressive behavior of concrete confined by carbon fiber composite jackets, *J Mater Civ Eng ASCE*, Vol. 12, No. 2, 2000, 139-46.
2. Watanable K, Nakamura H, Honda T, Toyoshima M, Iso M, et al., "Confinement effect of FRP sheet on strength and ductility of concrete cylinders under uniaxial compression" *Non-Metallic (FRP) Reinforcement for Concrete Structures, Proceedings of the Third International Symposium*, vol. 1, Sapporo, Japan: Japan Concrete Institute, 1997:233-240. Cited from Lam, L. and Teng J.G. 2003.
3. Cusson D. And Paultre P. "Stress-Strain Model For Confined High Strength Concrete'' *J. Of Structural Engineering, ASCE*, Vol. 121, No 3, 1995.
4. Razvi, S. and Saatcioglu, M. "confinement model for high-strength concrete", *J. of structural engineering, ASCE*, Vol. 125, No. 3, 1999, 281-289.
5. Seible, F., R., Abdallah, M. G., and Nuismer, R. ''Advanced composite carbon shell systems for bridge columns under seismic loads.'' *Progress in Res. and Pract., Proc., Nat. Seismic Conf. on Bridges and Highways*, San Diego, Calif. 1995.
6. Sheikh, S.A. And Uzumeri, S.M. "Analytical Model for Concrete Confinement in Tied Columns". *Journal of Structural Engineering (Asce)*, Vol. 108, No. St12, 1982, Pp. 2073-2722.
7. Mander, B. J., Priestley J. N. M. and Park R. "Theoretical Stress-Strain Model for Confined Concrete", *ASCE Journal of Structural Engineering*, Vol. 144, No. 8, 1988, 1804-1826.
8. [8] Karabinis, A.I. and P.D. Kiousis, "Effect of Confinement on Concrete Columns: Plasticity Approach". *Journal of Structural Engineering (Asce)*, Vol. 120, No. 9, 1994, Pp. 2747 - 2767.
9. Ahmad, S.H. and S. P. Shah, "Complete Triaxial Stress - Strain Curves For Concrete". *Journal of Structural Engineering (Asce)*, Vol. 108, No. St4, 1982, Pp. 728-742.
10. Saatcioglu, M. and Razvi, S. R., "Strength and Ductility of Confined Concrete". *Journal of Structural Engineering (ASCE)*, Vol. 118, No. 6, 1992, pp. 1590-1607.
11. Lam, L. and Teng, J.G., "Design-oriented stress–strain model for FRP-confined concrete", *Construction and Building Materials*, 17, 2003, PP 471-489.
12. Seible, F., Priestley, M.J.N., and Innamorato, D. ''Earthquake retrofit of bridge columns with continuous fiber jackets, Vol. II, Design guidelines", *Advanced Compos. Technol. Transfer Consortium, Rep. No. ACTT-95/08*, University of California, San Diego., 1995.
13. Moghaddam, H. and Samadi, M. "lateral post-tensioned metal strips for strength and ductility enhancement of concrete columns: investigation of size and shape effects" *14th world conference on earthquake engineering*, China, 2008.

CD04-011

IMPROVEMENT IN AXIAL STRESS-STRAIN BEHAVIOR OF COLUMNS USING PRE-STRESSED NON-LAMINATED FRP

H. Hajiloo[1], M.Motavalli[2, 3], A.Hosseini[2]
[1]M.Sc. Student, School of Civil Engg. Tehran University, Tehran, Iran
[2]Assistant Professor, School of Civil Engg. Tehran University, Tehran, Iran
[3]Swiss Federal Laboratories for Materials Testing and Research (Empa)

ABSTRACT
As a new approach to obtain high efficiency from FRP confinement, pre-stressing of FRP composites have been introduced. Pre-stressed FRP straps change confinement situation from passive to active confinement. At active confinement, without considerable axial stress, confining stresses due to pre-stressed FRP composites are present in perimeter of column. In this paper, an innovative method is presented to confine square reinforced concrete columns using non -laminated CFRP straps. Tests were carried out on three medium scale columns (2.0 m high with a cross section of 0.4 m x 0.4 m). Numerical analyses are performed to predict the effects of the pre-stressing at square column. In this paper, a new geometrical model to account for the effects of FRP pre-stressing and shape modifying of the section is proposed which describes better distribution of confinement stresses. Using FE modeling and proposed model, effectiveness of FRP confinement is revised and effectively confined area increased.

Keywords: columns, finite element, confinement, effectiveness, pre-stressing

1. INTRODUCTION
The use of externally applied fiber-reinforced polymer (FRP) has gained popularity for strengthening and repair of concrete structures. Retrofitting concrete structures with fiber reinforced polymer (FRP) has today grown to be a widely used method throughout most parts of the world. The main reason for this is that it is possible to obtain a good strengthening effect with a relatively small work effort. It is also possible to carry out strengthening work without changing the appearance or dimensions of the structure. Nevertheless, when strengthening a structure with external FRP, it is often not possible to make full use of the FRP. The reason for this depends mainly on the fact that a strain distribution exists over the section due to dead load or other loads that cannot be removed during strengthening. This implies that steel yielding in the reinforcement may already be occurring in the service limit state or that compressive failure in the concrete is occurring. By pre-stressing, a higher utilization of the FRP material is made possible [1]. It is extremely important to ensure that, if external pre-stressing is used, the force is properly transferred to the structure. All over the world, there are structures intended for living and transportation. These structures are of varying quality and

function, but they are all aging and deteriorating over time. Of the structures that will be needed 20 years from now, about 85–90% of these are probably already built. Some of these structures will need to be upgraded or replaced, because they are in such poor condition. This is due not only to deterioration processes, but also to errors that may have been made during the design or construction phase so that the structure needs to be strengthened before it can be fully used.

FRP materials were used successfully for confining circular concrete columns. Their effectiveness for confining rectangular columns, however, is still not fully recognized. Rectangular columns behave quite differently from circular columns. Rectangular specimens engage high confining pressure at their corners, but little pressure on their flat sides. The cross section is therefore only partially confined, which results in a smaller increase in compressive strength. This shape-related negative effect, however, can be reduced by rounding off the corners of a rectangular member. The presence of steel ties near the corners limits the possibility of rounding the corner radius in existing square and rectangular columns.

Lower FRP confinement effectiveness results in softening behavior for square and rectangular sections; the high strength of FRP composites is not fully used and the FRP composite ruptures prematurely. Shape modification of section and active confinement due to pre-stressing of FRP straps can reduce the effect of column corners and flat sides, thereby improving the axial strength capacity of FRP-confined square and rectangular concrete columns [2]. Active confinement method causes relative increase in axial strength of circular columns, but limits axial confined strains. In rectangular and square columns pre-stressing of FRP sheets need to shape modification of section. Shape-modification of rectangular sections prevents premature rupture of FRP due to stress concentration in corners.

In this paper, an innovative method is presented to confine square reinforced concrete columns using non -laminated CFRP straps. The CFRP straps can be either unstressed at the beginning or pre -stressed. Tests were carried out on three medium scale columns (2.0 m high with a cross section of 0.4 m x 0.4 m) [3]. The experimental results demonstrate the effectiveness of shape modification with prefabricated parts (mortar filled hoses) which are arranged on the surface of column at the flat sides. In contrast to other researches, presence of longitudinal and transverse steel reinforcement and medium scale columns leads to real assessment behavior of the columns, which is appropriate for existing deficient concrete columns. Models for column confinement are generally based on laboratory tests carried out on small size specimens, generally between 75 and 200 mm (3 and 8 in.) side dimension. For such small size columns, few layers of FRP wrap represent a high volumetric ratio and generally provide a rigid confinement. As a result, a substantial increase in the confined concrete strength can be obtained. In the case of full-scale columns, results are generally extrapolated from such tests and the concept of FRP volumetric ratio is used. The FRP volumetric ratio in real applications is normally less than that of the tested specimens. With the FRP jacket, increasing the column size decreases the FRP volumetric ratio and, therefore, the confined concrete strength also decreases.

2. TESTS SETUP

In this paper an innovative method is presented to confine square reinforced concrete columns using non-laminated CFRP straps. The CFRP straps can be either unstressed at the beginning or pre-stressed. Tests were carried out on three medium scale columns. The first column was the unconfined reference column, the second column was confined with pre-stressed non-laminated CFRP straps and the third column was confined with non pre-stressed non-laminated CFRP straps. Three medium scale reinforced concrete columns were tested under increasing axial loading. The columns had a height of 2 m and a square cross section of 400 x 400 mm (Figure 1). Table 1 summarizes the Non-laminated CFRP straps properties.

Table 1: Material properties of non-laminated CFRP straps

Thickness [mm]	width [mm]	ultimate strain [-]	E-modulus [GPa]
0.125	30	0.0183	131

3. SPECIMENS' CONSTRUCTION AND PRESTRESSING METHOD

Column (1) was tested without confinement and was used as a reference column. Column (2) was confined with pre-stressed non-laminated CFRP straps and column (3) was confined with non-laminated CFRP straps but without pre-stressing. At each side of the column, two hoses with an outer diameter of 42 mm were fixed over the whole length of the column. This ensured reasonably uniform application of confinement forces on each face of column. The column was confined by 6 layers of CFRP straps with a total thickness of 0.75 mm. After this, a mortar mixture of cement, water and additives, normally used for filling the gaps between concrete and post-tensioned cables, was pumped inside the hoses. For column (3) with non pre-stressed CFRP straps the hoses were filled with mortar before the wrapping of the CFRP layer. In order to achieve the same geometric shape, the hoses were filled between two wooden plates and only then attached to the column. The CFRP straps were then wrapped around the perimeter of the column in the same manner as for column (2). The confined columns (2) and (3) were instrumented for displacement and strain measurements according to Figure 1.

4. OBSERVED BEHAVIOR OF SPECIMENS

FRP-confined concrete compression members exhibit either a hardening or a softening behavior. This separation has been used in the past by other researchers [4]. Effectively confined concrete compression members exhibit hardening behavior. Figure 2 shows the load-deformation behavior of the column (2) with pre-stressed non-laminated CFRP straps which exhibits large deformations with a distinct plateau. Figure 3 shows behavior of Column (3) with non pre-stressed CFRP straps exhibits even larger deformations than column (2). Column (2) and (3) in Figure 2 and 3 compared with behavior of column (1) that predicted by analytical Mander's model.

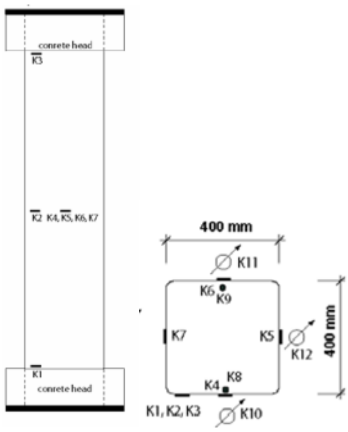

Figure 1. Arrangement of measurement instruments

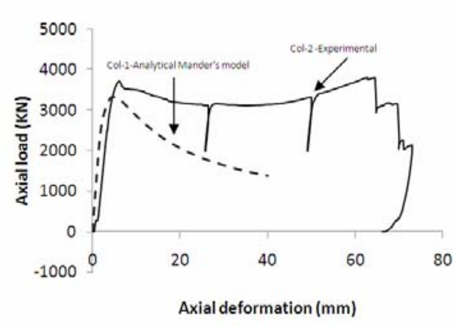

Figure 2. Axial load-deflection behavior of Column (2)

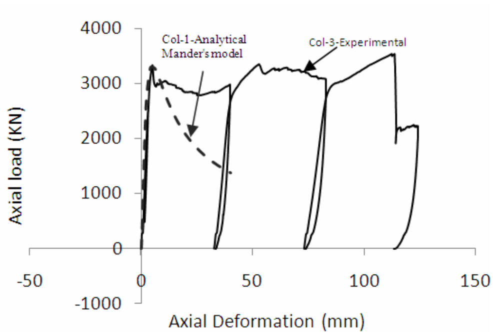

Figure 3. Axial load- deflection behavior of column (3)

5. INITIAL POST-TENSIONED TRANSVERSE FIBER STRAIN IN FRP SHELLS

One way of overcoming low utilized strength of FRP composites in rectangular columns is to reduce the lateral strain of the concrete at failure through pre-tensioning of the confinement materials. This method is particularly useful for low modulus materials (like glass) or when relatively low amounts of confinement are applied, such as in full-scale structures [12]. In addition, existing structures may already have very large strains due to existing loading. Adding pre-tensioned FRP wraps can help reduce the stress from the internal links and provides active confinement to the structure in its service condition [13]. Lateral pre-tensioning of composites is not easy to achieve unless the fibres are stretched before the resin hardens. Resin injections under pressure were adopted by some researchers [14, 15] when trying to address the problem of inadequate starter bar lap length in columns. However, the active pressure created by this method (resin injection) is generally quite small in comparison with the passive pressure generated by concrete dilation [16] Confinement of concrete, using shape modification of square and rectangular compression members using post-tensioned FRP composite shells with expansive cement concrete was investigated by Yan et al.(2006) and

Mortazavi et al(2003). From the experiments carried out (Yan 2005), an empirical relationship was developed as; [17]

$$\varepsilon_{j,ini} = c_1 - 0.00041\left(\frac{B_j}{D_j}\right); 3 \geq \left(\frac{B_j}{D_j}\right) \geq 1 \tag{6}$$

The initial post-tensioned transverse fiber strain $\varepsilon j,ini$ depends on the aspect ratio (Bj /Dj) of the prefabricated FRP shell, which is the ratio of the cross section major axis Bj to the minor axis Dj. for shells with two layers of CFRP composite $c1$=0.0020, and for shells with six layers of GFRP composite $c1$= 0.0025; the value of constant $c1$ is material dependent and decreases with increasing elastic modulus of the FRP composite.

6. FINITE ELEMENT MODELING

Concrete damage plasticity model is used for confined concrete [18]. Suitable elasticity models are used for fiber-reinforced polymers. A nonlinear static analysis was performed where the load was applied incrementally as axial direction displacements uniformly impose at top surface of column. Concrete is modeled using a solid 8-node element (C3D8R) with linear reduced Gauss integration points and enhanced hourglass control. FRP jacket could be modeled as quadrilateral lamina element with either membrane or shell properties. Membrane elements are surface elements that transmit in-plane forces only (no moments), and have no bending stiffness, but shell section has bending stiffness (Figure 4). Therefore for modeling FRP sheets saturated by a resin which has bending stiffness, using shell section is suitable. For unbounded FRP sheets that wrapped around column without resin, no bending stiffness was considered, thus membrane elements are recommended. Therefore in this study, FRP jacket is modeled as quadrilateral lamina element with membrane properties (M3D4), linear reduced Gauss integration points (one point per element), and enhanced hourglass control. Displacement compatibility is considered between concrete and composite material in the lateral direction.

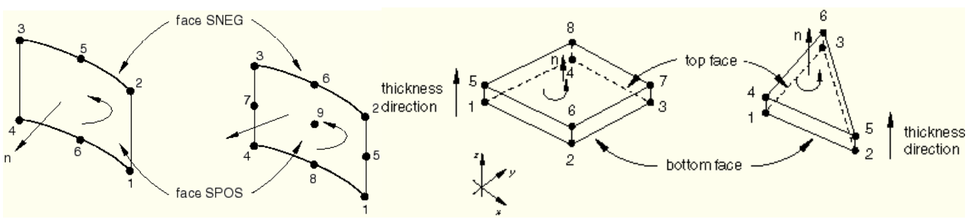

Figure 4. Continuum shell elements (left), membrane elements (right)

A simplified model has been made with totally 2 tubes that were placed on straight face of square columns (Figure 5). A major output of this model is describing stress distribution in concrete core due to lateral confinement produced by pre-stressed FRP non-laminated straps. Tubes are shells with low stiffness where pressure loads are inserted in the internal surface of tubes. Several interactions have been assigned between tubes concrete and tubes–FRP and concrete–FRP. Initial strains due to pre-stressing of FRP straps are 20% of amount strains in EMPA tests. A large stress is inserted onto the concrete surface due to expansion of tubes. As Figure 5 shows at pre-stressing phase, there are no significant confinement stresses of corners, but large lateral stress from below tubes developed and extended to the inside of concrete. As similar to Fig 5, if two other tubes are placed on the other flat sides, similar behavior and lateral stresses is brought about from tubes on the vertical sides.

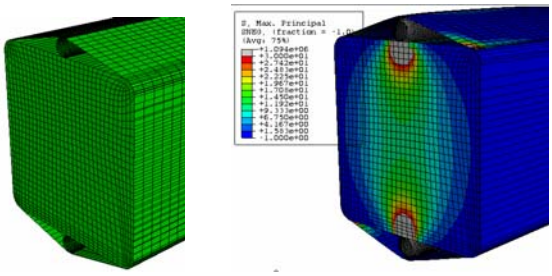

Figure 5. FE Model of the FRP Per-stressing; Right) before tube expansion; left) after expansion

A simplified numerical model to illustrate the advantages of shape modified section has been built. A triangular part with 20 mm height and equal width to column section width is placed at the flat sides. It is similar to column (3) which has two tubes on the flat sides. As shown in Figure 6, confinement stresses at the section of shape modified column are well distributed than conventional square column (right). At square and rectangular, because of low flexural stiffness of FRP jacket, there is a low amount of confinement stresses. Therefore, some researchers concluded that a parabola area at each of the flat sides, with depth of $w/4$, is unconfined area, ($w=a-2r$), and introduces a coefficient that is the ratio effectively confined to the gross area from which actual confinement stresses which assumed uniformity at the whole of the section is obtained. Then confinement ratio (f'_{cc}/f_c) is gained. As shown in Figure 6 (left) unconfined length is divided into two parts at each flat side. Therefore, unconfined area is reduced. In Figure 6, the area in white color has confinement stresses that are less than the assumed confinement stresses which are needed to consider an area as confined area.

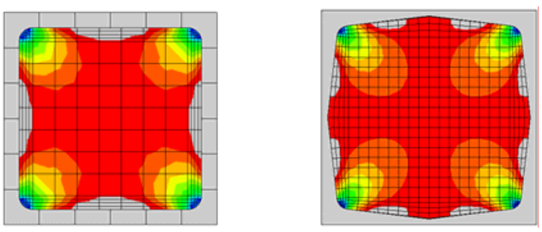

Figure 6. Confinement stresses at 400x400(mm) column; Right)conventional square column; Left)shape modified column similar to cloumn(3)

7. FRP AND STEEL CONFINED AREA

Figure 7 shows the deformed shape of stirrups in conventional column. Lack of constraint at flat sides of section causes large deformation of stirrups towards the outside. If cross ties are implemented at cross section of column, deformations have been limited. But older concrete columns demonstrated deficiency in reinforcement detailing. At tested columns, there are no cross ties. Therefore, deformation of stirrups becomes somewhat as shown in figure 7-a. Using new innovative method tested, deformation of transverse reinforcement has been changed and limited. Indeed, tubes on the flat side act as cross ties. Figure 7-b shows modified deformation of transverse reinforcement in column (2) and (3). According to this modified behavior of transverse reinforcement new effectively confined area is proposed for steel confined area of mentioned columns. Figure (8-a) and (8-b) present effectively confined area by steel transverse reinforcement.

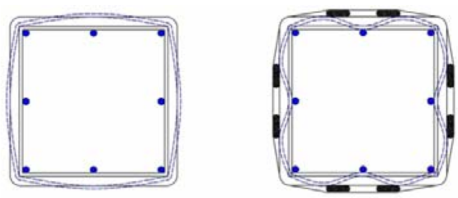

Figure 7. Deformation of ties in Conventional and sections with tubes

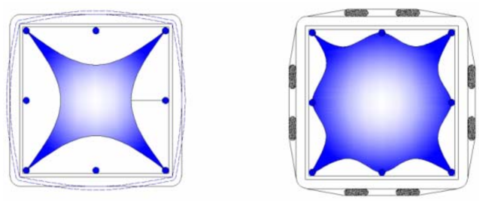

Figure 8. Effectively confined area by ties in conventional and sections with tubes

In tube injection phase, considerable stresses are produced between tubes and concrete. In this phase, confining stresses in corners is lower than tube interaction faces. At axial loading phase, due to FRP confining effects on the square and rectangular sections, confining stresses at corners increase. At axial loading phase, increasing of lateral confining stresses at corners is higher than flat sides and tube interaction faces.

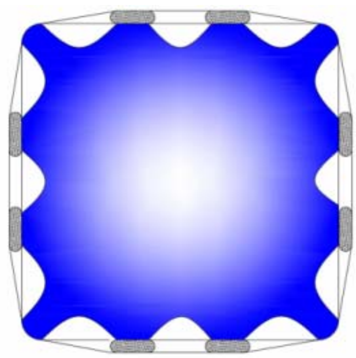

Figure 9. FRP confined area in column (2) and (3)

Therefore, using this method can modify efficiency of FRP confinement in square and rectangular sections, (Figure 9).

8. PROPOSED GEOMETRICAL AND MECHANICAL MODELS

In this study, a geometrical relationship of the investigated method to produce pre-stressing at FRP and shape modifying of square section column is proposed. According to the new proposed model, confining stresses are developed between pre-stressing devices or shape modifying parts and concrete. Confinement stresses relationships are basically derived from dimensions of the column and diameter of tubes and corner radius, as well as FRP material properties. By virtue of symmetrical condition, one quarter of the section has been considered (Figure 10-a). Following the simple approach of Karam et al. [19] for a generic rectangular cross section column (Figure 10-b), it is proposed that the action of the confining wrap on a square column with pre-stressing tubes on the center of flat sides of column (Figure 10-c) with a side *2a*, and a corner radius *R*, and a tube diameter D_t should be observed. The concrete is assumed to be subjected to uniform confining stresses at its middle sections with f_a acting along the sides. The relationship between f_a and the FRP tensile stress f_j is obtained from statics equilibrium of forces in the in plain *x* and *y* directions. At first and before tube expansion, a common form of FRP confinement, FRP has been positioned approximately in contact with the flat sides of column. After mortar injection and due to expansion of tube, non-laminated and un-bonded FRP straps separates from flat sides and takes an angle (θ) with the sides.

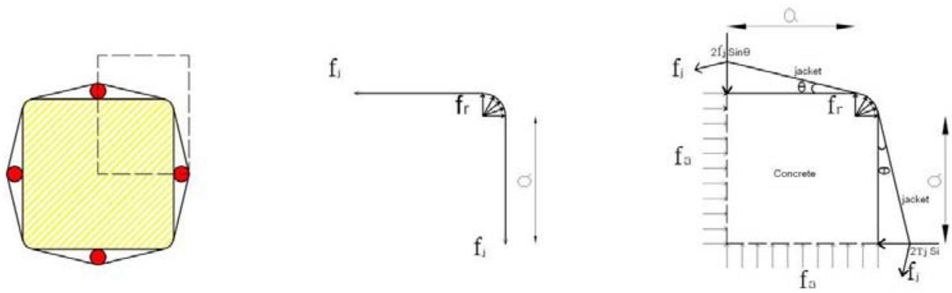

(a) (b) (c)

Figure 10. a) Square cross section with expanded tubes on the sides; b) Free-body diagram of FRP wrap; c) Free-body diagram of FRP wrap with pre-stressing effects

In Figure 10-c, status of FRP before and after tube expansion and tensile stress and concentric force after tube expansion has been illustrated. Confining stresses at middle sections and at the corners motivated through the tube expansion. Wrap is assumed to act as a cable around the corner. Assuming no friction, the relationship between f_j and the confining stresses at the corner region is also found from statics. (Eq.7)

$$f_j \times t\cos\theta = \int_0^{\pi/2} (f_r \times \cos\alpha)(R \times d\alpha) = Rf_r$$

$$f_r = \frac{f_j \times t\cos\theta}{R} \tag{7}$$

f_j and f_r are tensile stress of FRP and confinement stress at corner zone, and θ is angle between straps and concrete flat side in degree, and t, is the thickness of FRP jacket. Using Statics, equilibrium of forces in the horizontal direction results in confining stresses f_a at middle sections. On the contrary with common FRP-confined sections, an additional term appears in equation, ($tf_j \times sin\theta$). It demonstrates effects of stresses which the tube has produced. Tubes in middle of the side introduce something like line load toward the core of concrete.

$$f_a \times a = t \times f_j \times \cos\theta + t \times f_j \times \sin\theta$$
$$f_a = \frac{f_j \times t(\cos\theta + \sin\theta)}{a} \tag{8}$$

Now tensile stresses of FRP should be expressed as a function of parameters which changes during tube expansion and pre-stressing process. A point at middle of the corner arc is taken as base point from which FRP elongation is measured. At the other side of the selected point there is a similar situation, thus the selected point could be immovable. Using this approach, tensile stress of FRP during pre-stressing has been expressed as a function of tube diameter (D_t), side length, corner radius, and θ. Eqs. 9 to 12 describe mentioned approach, and finally confining stresses at corner and middle section have been derived.

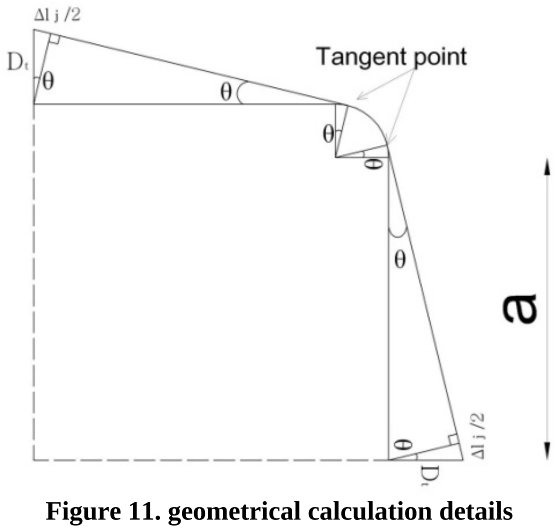

Figure 11. geometrical calculation details

$$\Delta l_j = \frac{D_t \times \sin\theta}{2} \qquad l_{jo} = a + \left(R\theta \pi/180\right)$$
$$\varepsilon_j = \frac{\Delta l_j}{l_{jo}} = \frac{D_t \times \sin\theta}{2(a + R\theta \pi/180)} \tag{9}$$

Where ε_j = strap strain, Δl_j = elongation of straps, l_{j0}= initial length of strap that was measured from tangent point, D_t=diameter of tube;

$$\tan^{-1}\left(\frac{D_t}{a-R}\right)=\theta \tag{10}$$

$$f_r=\frac{E_j\varepsilon_j t\times\cos\theta}{R}=\frac{E_j D_t\times\sin\theta\times t\times\cos\theta}{2R(a+R\theta\,\pi/180)} \tag{11}$$

$$f_a=\frac{tE_j D_t\times\sin\theta(\cos\theta+\sin\theta)}{2aR(a+R\theta\,\pi/180)} \tag{12}$$

Using this proposed equation, the uniformly distributed confinement stresses is calculated which considers all usable forces and stresses that are there to produce confinement stresses.

As diameter of the tube increases, the angle between FRP and side of column increases. Then FRP at the corner and rounded region separates from concrete core and as illustrated in Figure 12 this results in lessening of direct contact between FRP and concrete. Due to mentioned reason, concentration of stresses at the corner increases. Changing angle between FRP and concrete from 90 degrees to a higher amount is advantageous to transform confinement condition from square to circular column, but lesser contact between FRP and concrete at the corner will reduce effectiveness of this method. At highest possible angle which is 45 degree, contact between FRP and concrete at the corner transforms to a point. The Tangent point which from FRP starts to separate from concrete is shown in Figure 11.

9. CONCLUSIONS

A study is performed on the new FRP confining approach for pre-stressing of FRP straps which proposed and tested by EMPA laboratories. A numerical model using advanced concrete model is performed to study the effects of pre-stressing of FRP non-laminated straps on the confinement stress distribution across the section and the effects of shape modifying. Results have presented that expansion of the tubes imposes lateral stress on the flat sides of rectangular section and this leads to increase in effectiveness of FRP confinement and delays the buckling of longitudinal reinforcement. FRP confinement stress from pre-stressed straps are present before axial loading and results in increasing of initial peak axial stress in comparison with usual using of FRP and a higher strength is achieved in less lateral expansion. A geometrical model for evaluating the confinement stress across the section due to expansion of tubes to produce pre-stressing at FRP is proposed. Using this model and based on developed changes in initial position of the FRP, confinement stress due to pre-stressed FRP straps is calculated.

REFERENCES

1. Nordin, H., Täljsten, B., “Concrete Beams Strengthened with Prestressed Near Surface Mounted CFRP”, journal of composites for construction, 2006, 10, 1, pp 61-68.
2. Yan, Z., Pantelides, CP. and Reaveley, L., “Fiber-Reinforced Polymer Jacketed and Shape-Modified Compression Members: I-Experimental Behavior”, ACI Structural Journal, 2006 103, 6, pp 885-893.
3. Pfyl-Lang, K., Huth, O., Green, M.F., Motavalli, M., “Square RC columns confined with non-laminated CFRP straps”, CICE2008, Zurich, Switzerland, 2008.
4. Lam, L., Teng, J. G., “Design-Oriented Stress-Strain Model for FRP-Confined Concrete in Rectangular Columns,” Journal of Reinforced Plastics and Composites, 2003, 22, 13, pp 1149-1186.
5. Pilakoutas, K. Mortazavi, A., “Laterally Pre-stressed Concrete with Composites”, Proceedings of the Fifth International Conference on Fibre reinforced Plastics for Reinforced Concrete Structures”, Cambridge, UK: Thomas Telford Ltd, July2001, 2, pp 855-864.
6. Mortazavi Ali A. “Behavior of confined concrete with variable lateral pressure”, Ph.D. Thesis (expected 2002), The University of Sheffield, UK.
7. Saadatmanesh, H., “Wrapping with composite materials”, Non-Met (FRP) Reinf Concr Struct E and FN Spon, 1995, 1, 1, pp 593-600.
8. Priestley, MJN., Seible, F., “Design and seismic retrofit measures for concrete and masonry structures”. Constr Build Mater, 1995, 9, 6, pp 365-77.
9. Harries, KA. Kharel G. “Behaviour of modelling of concrete subject to variable confining pressure”, ACI Mater J, 2002, 99, 2, pp 180-9.
10. Pantelides, C. P., Yan, Z., and Reaveley, L. D., “Shape Modification of Rectangular Columns Confined with FRP Composites,” Research Report CVEEN-04/4, Department of Civil and Environmental Engineering, University of Utah, Salt Lake City, Utah, Dec. 2004, 166 pp.
11. Abaqus Documentation Version. 6.6. ABAQUS Inc (2006).
12. Karam,G., Tabbara, M., “Confinement Effectiveness in Rectangular Concrete Columns with Fiber Reinforced Polymer Wraps”, journal of composites for construction, 2005, 9, 5, pp 388-398

CD04-012

APPLICATION OF FIBER REINFORCED PLASTICS FOR CONCRETE T-BEAM BRIDGE STRENGTHENING

K. Siamardi [1], A.A. Mounesan [2], M.M. Khodavirdi Zanjani[3]
[1]Civil Engineer, Concrete Research Center, Atisaz Company
[2]Civil Engineer, Sharif University of Technology, Head Manager of Atisaz Company
[3]Civil Engineer, Concrete Research Center, Atisaz Company

ABSTRACT
A strengthening method using fiber reinforced plastics (FRP) has been widely applied for deteriorated reinforced concrete bridges. Advantages of this method may include that the strengthened structures do not increase dead weight and that no corrosion is concerned. From various experimental studies, behavior characteristics of the FRP strengthened structural members have been generally well evaluated. The majority of those studies, however, have been performed on laboratory sized structural members rather than actual full scale bridges. The study herein used a full scale actual deteriorated bridge to evaluate the strengthening effects with three different FRP materials, carbon fiber sheet, glass fiber reinforced plastics and aramid fiber sheet. In the field load tests, concrete weight blocks were used as a loading system instead of commonly used a live-truck load or hydraulic jacking force. The strengthening was designed as specified in ACI 440.1R which is based on the ultimate strength design concept. From the measured behaviors, it was confirmed that the strengthening using FRP materials successfully improved the flexural capacity of the aged and deteriorated concrete bridge. The strengthened girders behaved linearly up to the design moment even though the applied stress distribution mechanisms were different depending on the FRP materials. Therefore, it is concluded that the strengthening design method specified in ACI 440.1R can be successfully used for actual full scale bridges strengthened with external FRP bonding.

Keywords: strengthening, CFS, FRP, T-beam bridge, USD

1. INTRODUCTION

For deteriorated concrete bridges, an external strengthening method with fiber reinforced plastics (FRP) has been widely applied with some advantages. Among others, the method does not increase dead weight and no corrosion consideration is needed. Therefore, it could be a good alternative method for the ordinary steel plate strengthening method. In the early stage of the application of FRPs, most research studies were to evaluate the material properties of FRPs. Since late 90s, the strengthening in various forms of FRPs has been rigorously studied and its effectiveness was successfully proven. In the last decade, engineers and researchers have been intended to develop design and construction specifications for the

practical applications of the FRP strengthening in the field [1, 2, 3].
Through a variety of experimental studies, structural behaviors of the FRP strengthened bridges have been generally well evaluated, and the problems of stress concentration at the end section of the bonded FRP have been improved [4, 5, 6, 7]. Most of these studies, however, have been performed on scaled down in-laboratory specimens rather than actual full scale bridges. There must be limitations in representing deteriorating conditions in the field, such as the difference in environmental conditions, dependency on neighboring structures, and girder-slab composite behavior [8]. In addition, depending on field construction conditions and workmanship, the accurate installation of the FRP strengthening materials may not be expected as desired. Therefore, in order for the strengthening method using external FRP bonding to be practically applied to deteriorated bridges, the performance of the strengthening should better be evaluated using a full-scaled field bridge. Results or data from the evaluation using the actual bridge might also be used as basic information for the specifications or provisions for strengthening design and installation.

The study herein used a full-scaled actual deteriorated bridge to evaluate the strengthening effects from three different FRP materials, carbon fiber sheet (CFS), glass fiber reinforced plastics (GFRP), and aramid fiber sheet (AFS).
Another interesting feature of this study is the use of concrete weight blocks as a loading system instead of a truck load or a hydraulic jacking force, which are commonly used in the performance evaluation of bridges. However, some shortcomings of the later methods are: The field loading test using the truck load may provide information only up to a limited elastic range. The hydraulic jacking method costs relatively too high, and sometimes is not feasible to install reaction frames [9].

In addition to these reasons, the target bridge was no longer in-service so that the loading method using the concrete weight blocks was thought very appropriate and challenging for this study.

2. EXPERIMENTAL STUDY

2.1. Bridge Description

The target concrete T-beam bridge originally consisted of two continuous three-spans, but south two spans were replaced with steel I girder after severe damage from accident impact load. When tested, the bridge consisted of one continuous three-span T girder, one simple span T girder and two of simple spans of steel I girder. It should be noted that the concrete bridge age is 80 years.

Based on visual inspection report, the selected three spans were repaired using an epoxy injection and mortar prior to the strengthening. This repair process was to provide a theoretically identical level of deterioration condition. Compressive strengths of the girders were measured using the Schmidt Hammer and appeared to be from 16.9 to 18.5MPa. based on non-destructive tests and concrete power peeling off, it was revealed that the span 1 and 3 had 25mm diameter rebars and the span 2 20mm diameter rebars as shown in figure 1. Tensile strength of the steel rebars was assumed to be 300MPa.

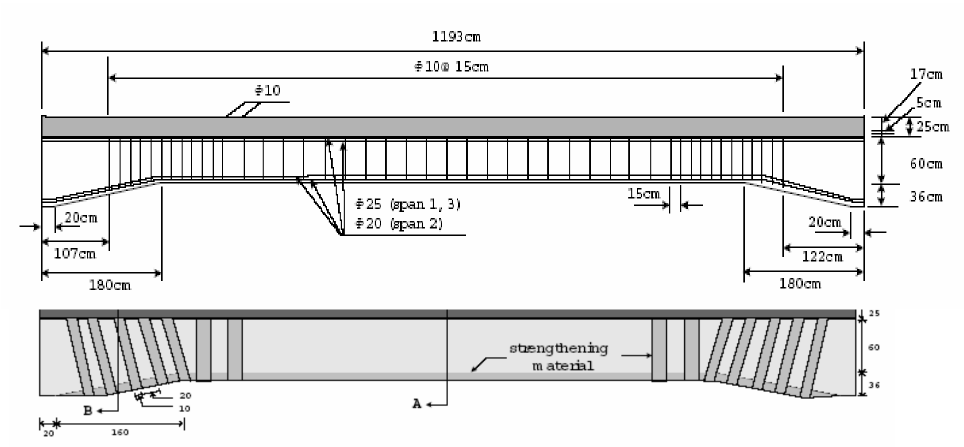

Figure1. Detail of sections and strengthening

2.2. Strengthening Design

In this experimental study, three different FRP strengthening materials were considered and they were CFS, GFRP and AFS. The strengthening was designed according to ACI 440.1R [10] which is based on the ultimate strength design (USD) method that provide 10% higher flexural capacity than the repaired condition. An equation is given below to compute the nominal flexural capacity of the FRP strengthened beams.

$$M_n = A_s f_y \left(d - \frac{\beta_1 c}{2} \right) + \psi_{frp} A_{frp} f_{frp} \left(d - \frac{\beta_1 c}{2} \right) \tag{1}$$

where *Mn* is a nominal moment, *As* and *Afrp* are cross sectional areas of rebar and FRP strengthening material, *fy* and *ffrp* are yielding and ultimate strength of rebar and FRP strengthening material, *d* is an effective depth of beam, *c* is a distance from extreme compression fiber to the neutral axis, *β1* is taken as 0.85 for the given concrete strength and, *ψfrp* (=0.85) is a additional reduction factor to account for more brittleness of the FRP reinforcement. The equivalent steel ratios of the FRP strengthened girders were less than the balanced ratio that was intended not to cause an unexpected brittle failure. The span 1 was strengthened with CFS, the span 2 with GFRP and the span 3 with AFS as shown in Figure 2. The Properties of the strengthening materials provided from the manufacturers are given in Table 1. Table 1 also details the strengthening details and the design flexural capacity.

2.3. Field Load Testing

For the three spans strengthened with each different FRP, loading test were conducted using the concrete weight blocks which had two different weights, 12.8KN and 25.5KN. The concrete weight blocks were loaded until the weight reached 95% of the design flexural capacity for the safety concerns considering the age of the target bridge. Before the weight blocks were loaded by a crane, an accurate weight of the each block was measured. When each block was loaded, vertical mid-span deflections and strains of the rebar and the strengthening materials were measured by LVDTs and strain gages.

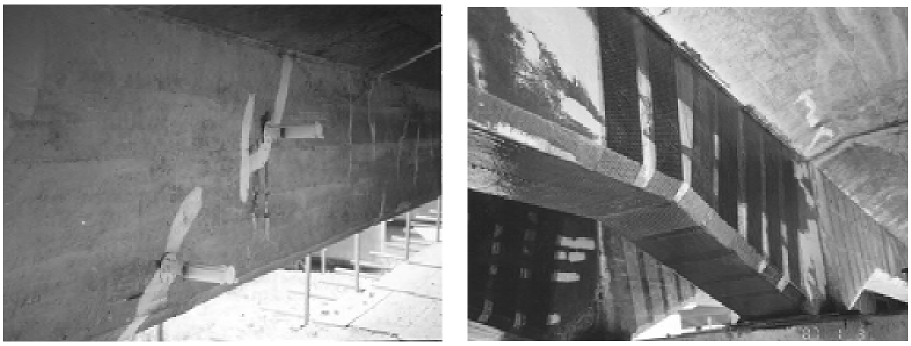

Figure 2. Epoxy repair and strengthening views

Table 1: Properties of strengthening materials and strengthening design capacity

Test Span	Material	Ultimate Strength (MPa)	Ultimate Strain	Thickness (mm)	Width (cm)	No. of Layer (ply)	$M_n - M_d$ (KN.m)	
							before	After
1	AFS	2,942	0.026	0.193	35	1	2,706	3,119
2	GFRP	441	0.020	1.300	35	2	1,363	1,783
3	CFS	3,481	0.015	0.110	35	1	2,706	3,285

3. DISCUSSION OF TEST RESULTS

3.1. Span 2: GFRP Strengthened

The maximum applied load was 535KN and 677KN for the non-strengthened and the GFRP strengthened girders, respectively. As the load increased, a certain amount of the flexural cracks occurred and then the diagonal shear cracks formed. in the girder 3, some of the diagonal shear cracks occurred before the flexural cracks. This might be because of the degradation of stirrups due to corrosion and an incomplete epoxy repair for the inside of the girder. After the strengthening, the crack patterns were similar but the numbers and the widths of the cracks smaller by visual inspection. No delamination of the strengthening material, GFRP, was observed at the bonded interface due to the attached U-shaped strengthening at the both ends.

For the non-strengthened girder, initial cracks developed at about 100KN of loading with a slight decrease of stiffness. It was also observed that there was a secondary stiffness reduction at about 480KN. This might be, even though the yielding strain of the rebar was assumed as 0.0015, because the rebar in the bridges already experienced a significant amount of plastic deformation accumulated during more than 60 years of the service period and also because of the steel grade for the old bridge. For the GFRP strengthened girder, the deflection and rebar strain increased momentarily to some degree at 640KN.

3.2. Span 1 and 3: CFS and AFS Strengthened

The spans 1 and 3 were also repaired before the loading test with an epoxy and mortar, and then strengthened with CFS and AFS for the span 1 and 3, respectively. During the loading blocks were loaded, both the CFS and AFS strengthened girders developed some bending cracks followed by the shear cracks at the bottom with no rupture or delamination of the strengthening material.

The AFS strengthened girder developed initial flexural cracks at about 245KN at girder 1 and 2, and then diagonal shear cracks. For the CFS strengthened girders more cracks developed but the widths were relatively smaller. The load-deflection behaviors were linear but as the loading approached to the maximum there was slight increase in deflection for both cases. Once the loading was removed the girders exhibited residual strain greater than 200µ, which was similar to the span 2.

In the CFS strengthened girder, above 500KN, the applied load seems to be suspended more by CFS rather the rebar. In the AFS strengthened girder, the applied load is carried more by the rebar. In the experiments, small scale localized ruptures occurred on the surface of AFS. None of the CFS and AFS strengthened girders examined any significant reduction of load-carrying capacity during the testing and the measured load deflection behaviours (figure 3) seems as if the girders are within the elastic ranges, even though the stress distribution mechanisms are different for both strengthening materials. These observations imply that the strengthening design method used in this study appropriately takes account of the material properties of CFS and AFS. Therefore, it can be concluded that the strengthening design method specified in ACI 440.1R [10], which is based on the USD concept, can be successfully used for actual full scale bridges which are strengthened with external FRP bonding.

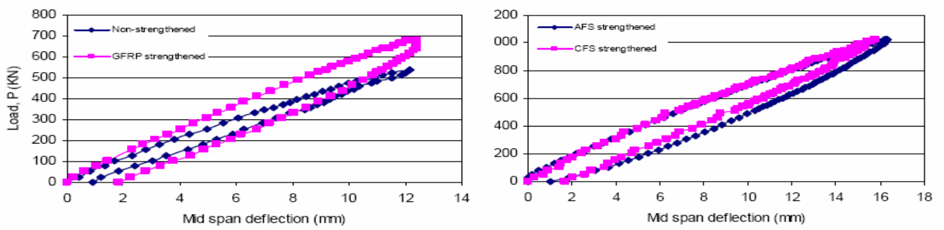

Figure 3. Load-deflection , left: span 2, right: span1 and3

4. CONCLUSIONS

This study conducted field load tests on an existing full scale reinforced concrete T-typed girder bridge to evaluate the performance of structural strengthening. In the field load tests, the loading system used concrete weight blocks rather than using a live-truck load or hydraulic jacking force. The method was found to be safe and efficient especially when failure behavior over elastic limit is interested. The strengthening used three different types of FRP materials, AFS, GFRP, and CFS, which were bonded on the bottom of the girders to enhance the flexural load carrying capacity. The strengthening was designed as specified in ACI 440.1R which is based on USD concept. It was confirmed that AFS, GFRP and CFS strengthenings successfully improved the flexural capacity of the aged and deteriorated concrete bridge. The strengthened girders behaved linearly up to the design moment even though the applied stress distribution mechanisms were different depending on the FRP materials. Therefore, it is concluded that the strengthening design method specified in ACI 440.1R [10] can be successfully used for actual full scale bridges which are strengthened with external FRP bonding.

ACKNOWLEDGEMENTS

The Atisaz company has provided this research study for concrete research center.

REFERENCES

1. Sim, J. Standardization of Repair/Rehabilitation of Concrete Bridge. Korea Infrastructure Safety and Technology Corporation, Korea, 1999.
2. Oh, H., Sim, J., and Meyer, C. Experimental Assessment of Bridge Deck Panels Strengthened with Carbon Fiber Sheets. *Composites: Part B-Engineering*, Vol. 34, 2003, pp. 527-538.
3. Oh, H., and Sim, J. Interface Debonding Failure in Beams Strengthened with Externally Bonded GFRP.*Composite Interface*, Vol. 11, No. 1, 2004, pp.25-42.
4. Sim, J., and Oh, H. Experimental Study of Strengthening Technique using Carbon Fiber Sheets on *Prototype Reinforced Concrete Bridge Deck Specimens*, ACI SP 193, American Concrete Institute, Michigan, 2000, pp. 343-359.
5. Quantril, R. J., Hooaway, L. C., and Tbrone, A. M. Experimental and Analytical Investigation of FRP Strengthened Beam Response. *Magazine of Concrete Research*, Vol. 48, No. 177, 1996, pp. 331-342.
6. Smith, S. T., and Teng, J. G. FRP-Strengthened RC Beams I: Review of Debonding Strength Models. *Engineering Structures*, Vol. 24, Issue 4, 2002, pp. 385-395.
7. Smith, S. T., and Teng, J. G. FRP-Strengthened RC Beams II: Assessment of Debonding Strength Models. *Engineering Structures*, Vol. 24, Issue 4, 2002, pp. 397-417.
8. Oh, B., Kim, K., You, Y., and You, D. Ultimate Behavior and Characteristics of Load Distribution of PSC Composite Girder Bridge. *Journal of Korean Society of Civil Engineers*, Vol. 21, No. 5, 2001, pp. 761-771.
9. Sim, J., and Moon, D. Y. A Proposal for Structural Performance Evaluation of Old Bridge using Concrete Weight Blocks. Proceedings of Structural Engineers Would Congress, *SEWC 2002*, Yokohama, Japan, 2002, Paper No. T9-1-b-3.
10. American Concrete Institute Committee 440.1R-01. Guide for the Design and Construction of Externally *Bonded FRP Systems for Strengthening of Concrete Structures*, American Concrete Institute, Farmington Hills, Michigan, 2001.

CD04-013

DURAPGULF, A PROBABILISTIC APPROACH FOR DURABILITY DESIGN OF RC STRUCTURES IN THE PERSIAN GULF USING

M. Shekarchi[1], A. Rafiee[2], H. Layssi[3], F. Moradi-Marani[4]
[1]Director of Construction Materials Institute (CMI), University of Terhran
[2]PhD Student of Kassel University, Kassel, Germany
[3]PhD Student of McGill University, Montreal, Canada
[4]Research Assistance of Construction Materials Institute (CMI), University of Tehran, Iran

ABSTRACT

A probabilistic approach in durability design of reinforced concrete structures has been studied using DuraPGulf model. DuraPGulf is a service life design model, the first version of which provides a realistic prediction of corrosion initiation for RC structures in Persian Gulf region. Output parameters are interpolated using a complete database of conducted experiments in this region.

Although relevant data is still lacking, this approach has been successfully applied to a concrete structure in Persian Gulf environment. In order to facilitate the probability-based durability analysis, simple analysis has been developed, where the probabilistic approach is based on a Monte Carlo simulation. A comparative study of deterministic and probabilistic approach has been carried out using the data available from durability assessment of a jetty in Persian Gulf. In particular, probability based design seems to provide more realistic results than deterministic durability design analysis.

1. INTRODUCTION

Reinforced concrete has proved to be a reliable structural material with good durability performance when used properly. It has been one of the most used building materials in the last decades. However, there are many structures which show early, premature deterioration, and sometimes failure, namely those exposed to aggressive environments (Vaysburd & Emmons 2004).

The Persian Gulf environment has a long record of stigma for its harsh climate, desert features and saline waters, that increases the chloride penetration and consequently chloride induced reinforcement corrosion rates (Haque et al. 2007).

In many cases in the Persian Gulf, even structures which have been designed and constructed in compliance with Iranian code for durability of concrete structures in Persian Gulf region (BHRC-PNS428 2005), express corrosion problems in early age of their service life. In order to solve this problem, besides changing the code requirements in respect of durability, one should represent methods of durability design so that to find the most economical solution according to the desired service life for reinforced concrete structures (Ghalibafian et al. 2003). Since all parameters both for concrete durability and environmental exposure typically show a high scatter, a probability-based approach provides a very powerful basis for

durability analysis (Gehlen & Schiessl 1999, Bentz 2003).
This approach is primarily applied in order to obtain more controlled durability and long-term performance of new concrete structures.
During the past decades, many physical and mathematical models have been introduced to calculate the chloride diffusion parameters into concrete and to estimate the time to corrosion initiation. DuraPGulf (Chini et al. 2004, Ghods et al. 2007), like many other programs, was deterministic in its operation, meaning that it will produce only one predicted time to nitiation
of corrosion for one set of input parameters. This single output contrasts with the well-known fact that concrete structures are quite variable in properties both throughout the structure and in terms of quality of construction and materials from one project to another. It would be useful if programs like DuraPGulf were able to predict a range of expected times to initiate corrosion rather than a single value to allow owners in a better risk management (Bentz 2003).
This paper describes the DuraPGulf model structure. The demonstration of this practical application is also explained through an example in this paper.
Results obtained from the model have been verified with the data available from durability assessment of a jetty in Persian Gulf region.

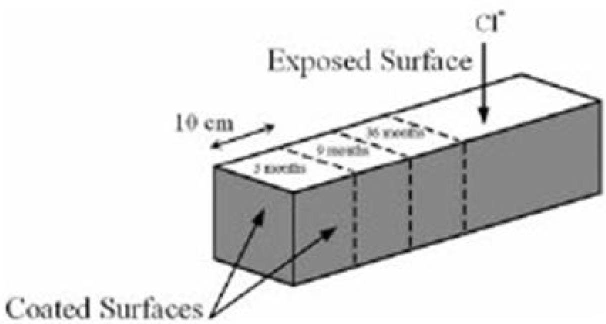

Figure 1. Concrete prism specimens (150×150×600 mm) exposed to marine environment for long-term durability studies.

2. EXPERIMENTAL PROGRAM

Concerning the fact that there was few data available for concrete durability studies specially regarding the chloride diffusion in Persian Gulf region, a complete set of field experiments were conducted in order to investigate the effect of different parameters on chloride diffusion such as water to cement ratio, silica fume content, curing condition, exposure condition, environment temperature and surface coating. A detailed review regarding this experiment can be found elsewhere (Chini et al. 2004, Ghods et al. 2007). In this project, 120 prism specimens measuring 150×150×600 mm were exposed to marine environment of Bandar-Abbas city. Sampling of the specimens for chloride diffusion has been carried out at the ages of 3,9 and 36 months. Figure 1 shows the concrete prism specimens for the long-term durability studies.
By curve fitting of chloride profiles of each specimen to Fick's second law (Crank

1975), data for diffusion coefficient and surface chloride content were calculated. Data have been used in order to develop the DuraPGulf database.

3. NUMERICAL MODELING

DuraPGulf uses advanced mathematical concepts for analyzing input data in order to predict Diffusion Coefficient (D_c) and Surface Chloride Content (C_c) values for new cases. Moving Least Squares method (MLS) is used for data regression. Accordingly, for each set of new input data in the n-dimensional space of primary data, a regression is conducted so that the nearby primary data have the highest effect on the final output (i.e. diffusion coefficient and surface chloride content).
According to the Figure 2, in the Moving Least Squares approach the weighting function F is defined in shape and size, and is translated over the domain so that it takes the maximum value over the point k identified by the coordinate X_k where the unknown function û is to be evaluated. The weight factor in this regard, which influences the effect width, can be calibrated after trial and error for new set of experiments (Lancaster & Salkauskas 1981).

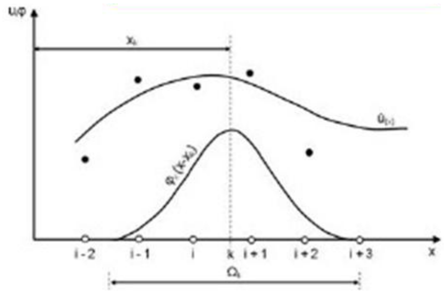

Figure 2. Schematic illustration of Moving Least Squares (MLS) method.

Finite Difference Method (FDM) is used to solve differential equation of the Fick's second law of diffusion over time:

$$\frac{\delta C}{\delta t} = Dc^2 \frac{\delta_2 C}{\delta X} \tag{1}$$

Considering the following boundary conditions:

$$C(X > 0, t = 0) = 0$$
$$C(X = 0, t > 0) = Cs$$
$$C(X = \infty, t > 0) = 0$$

The solution for this differential equation is:

$$C(X,t) = Cs.1 - erf \quad \frac{\sqrt{X}}{2Dct} \tag{2}$$

Where D_c is the chloride diffusion coefficient, Cs is the equilibrium chloride concentration on concrete surface and C is the chloride content at the depth of X from the surface at the time. The time, at which chloride content on the reinforcement surface reaches the chloride threshold value, is considered as the corrosion initiation time. In the DuraPGulf software, the percentage of chloride threshold is depended on mixture proportion and thickness of concrete cover. The time dependence of the diffusion coefficient is normally expressed as (Thomas & Bentz 2001):

$$D(t) = D0. \quad \frac{t}{t0}^{\alpha} \tag{3}$$

Where D_0 is the diffusion coefficient at a given time t_0 and the exponent α represents the time dependence of the diffusion coefficient or the increased ability of the concrete to resist chloride penetration over time.

Table 1. Input data for initial probability analysis

Parameter	Average	Coefficient of Variation	Standard Deviation	Distribution
Chloride diffusivity (m2/s. 10-12)	0.56	0.25	0.140	Normal
Surface chloride content (%weight of concrete)	0.80	0.30	0.24	Normal
Critical chloride content (%weight of concrete)	0.13	0.20	0.027	Normal
Concrete cover (mm)	75	0.10	7.5	Normal
Aging factor	0.31	0.25	0.078	Noraml

Employing Ahrenius equation, the effect of temperature is considered on the diffusion coefficient for different months during the year (Page et al. 1981):

$$\frac{D_T}{D_0} = \exp \quad \frac{U}{R} \times \frac{1}{T_0} - \frac{1}{T} \tag{4}$$

Where T and T_0 are temperature in Kelvin degree, R is the gas general constant value and U is the activation energy of the diffusion process. A special value of 2948 for U/R was suggested in this study for DuraPGulf based on the experiments at the Construction Materials Institute (Chini et al. 2004). Similar to the temperature, the effect of humidity on the diffusion coefficient is considered through the model proposed (Bazant & Najar 1972):

$$\frac{D_H}{D_0} = 1 + 256(1 - \frac{h_4}{100})^{-1} \tag{5}$$

Where h is the humidity of environment (%).

4. PROBABILISTIC APPROACH

The probabilistic approach is based on the Monte Carlo Method, which can be briefly described as a statistical simulation method, where sequences of random numbers are applied to perform the simulation (Gehlen & Schiessl 1999, Bentz 2003). In the present application of the simulation, the physical process is simulated directly by use of the modified Fick's Second Law of Diffusion for describing the transport process. The only requirement is that all the input parameters to the equation be described by a probability density function. Once the probability density functions of the various durability parameters of the system are known, the probability of failure is based on the evaluation of the limit state function for a large number of trials. Figure 3 shows a normal curve divided into eight sections, each with a probability of 0.125 (Bentz 2003). At about the centroid of each region is a discrete point that represents the characteristic value for that region. The locations of these points are positive and negative 1.65, 0.89, 0.47 and 0.155 standard deviations from mean. By varying each set of the input parameters through all eight of these calculation points, it becomes possible to know exactly the number of iterations necessary to fully cover the input domain and produce a reasonable estimate of the solution. The accuracy of the Monte Carlo Method depends mainly on the number of trials undertaken and the method is easy to implement, a simulation based on this method appears to be both simple and intuitive.

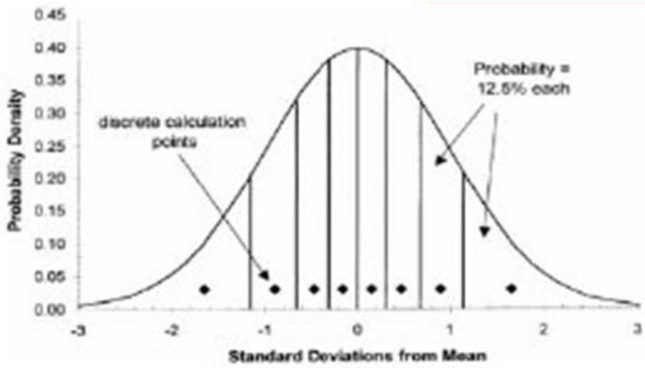

Figure 3. Division of normal curve into discrete regions (Bentz 2003).

5. PROGRAMMING

DuraPGulf software has been developed based on data regression and analyses according to the mathematical methods mentioned earlier. The program uses a FDM kernel and graphic user interface (GUI) provided by VISUAL BASIC programming.

6. EXAMPLE

A typical reinforced concrete pier of a jetty in Bandar-Emam port is subjected to the tidal zone exposure of the Gulf. The thickness of the concrete cover is assumed

to be 75 mm. Temperature diagram of Bandar-Emam is also shown in Figure 4. Concrete has been cured for 3 days after demolding in July. The concrete mixes were developed at the water to cementitious ratios of 0.38, cementitious materials content of approximately 450 kg/m3 and 6.5% silica fume. These parameters were used as input to the program. Running DuraPGulf, the calculated profile of chloride concentration versus depths for a given time of 27 months and the result of the sampling are shown in Figure 5. The corrosion initiation time is calculated with the deterministic approach to be 128 years, which is very high.
In order to analyze the probability levels of the above combinations of concrete quality and concrete cover, initial probability analysis with input parameters as shown in table 1 were carried out. In this table, the surface chloride content of 0.8% by weight of concrete, which reflects the exposure conditions in tidal zone, was adopted. Based on a complete database of experiments, a threshold chloride content of 0.13% (Frederiksen, J.M., 2000) by weight of concrete and aging factor of 0.31 was assigned. Using Monte Carlo simulation, the probability of steel corrosion and development of further chloride penetration is illustrated in Figure 6. In most codes for reliability of structures, an upper level of 10% for probability of failure is normally accepted (NS 3490, 2004). As can be seen from Figure 6, a 10% level for the risk of steel corrosion will result in a service period of 32 years and for a service period of 128 years, the level of risk would be 65%.

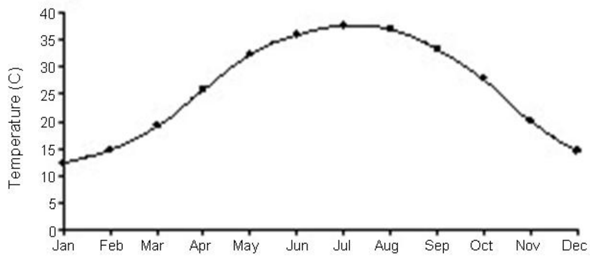

Figure 4. Annual temperature diagram of Bandar-Emam

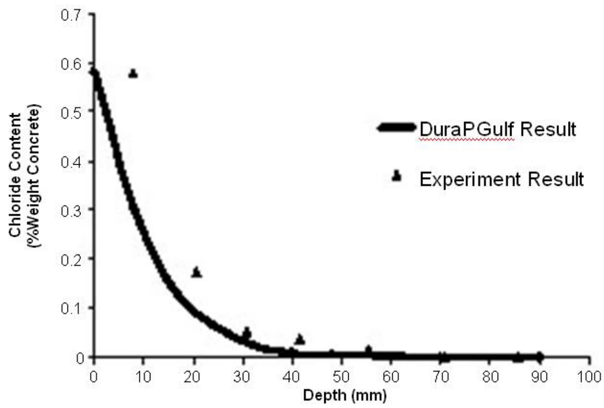

Figure 5. Comparison of the results of experiment with the results predicted by DuraPGulf model

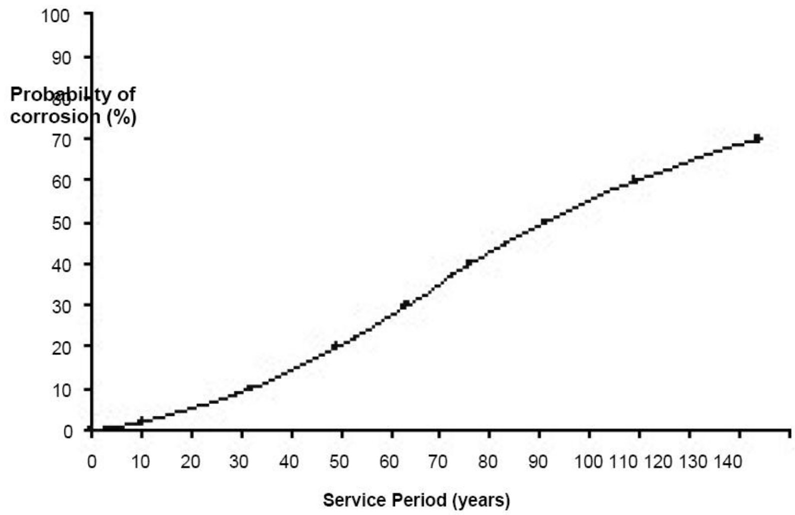

Figure 6. Development of risk for steel corrosion

7. CONCLUSIONS

Regarding results and experiments following conclusions can be drawn:

1. Durability design of RC structures has received a great concern in the recent decades;
2. In Iran, the need for a model for service life design of concrete structures in Persian Gulf region is highly necessary;
3. The predicted chloride profile by DuraPGulf model is generally in agreement with the experimental results.
4. Probabilistic durability model provides more realistic solutions than deterministic durability design.

ACKNOWLEDGEMENTS

Authors are deeply indebeted to Late Professor M. Ghalibafian for his continuous support and discussions. The financial support of Management and Planning Organization of Iran is greatly acknowledged.

REFERENCES

1. Bazant, Z.P. & Najjar, L.J. 1972. Nonlinear water diffusion of nonsaturated concrete. Materials and Structurals Journal, 5 (1): 3–20.
2. Bentz, E.C. 2003. Probabilistic modeling of service life for structures subjected to chlorides. ACI Materials Journal, 100 (5): 391–397.
3. BHRC-PNS428. 2005. National code of practice for concrete durability in the Persian Gulf and Omman Sea (proposed). Building and Housing Research Center, Ministry of Housing and Urban Development, Tehran: Iran.
4. Chini, M. Ghods, P. Alizadeh, R. Hoseini, M. Montazer, Sh. Shekarchi & M. Ghalibafian, M. 2004. Developing the first version of the model for service life prediction of reinforced concrete structures in Persian Gulf and Oman Sea. 2nd report, NO. CMI8309144, Construction Materials Institute at the

University of Tehran: Tehran, Iran.

5. Crank, J. 1975. The mathematics of diffusion (2nd Ed.). Oxford Press: London.
6. Frederiksen, J.M., 2000 (approved 2002–03). Method for determination of chloride threshold values for steel in concrete. Nordtest report TR 500.
7. Gehlen, C. & Schiessl, P. 1999. Probability-based Durability design for the Western Scheldt Tunnel. Structural Concrete, No 2: 1–7.
8. Ghalibafian, M. Shekatchi, M. Zare, A. & Tadayon M. 2003. Chloride penetration testing of silica fume concretes under Persian Gulf conditions. Proc. 6th CANMET/ACI intern. Confe On durability of concrete, SP-212-46, Thessaloniki, Greece: 737–754.
9. Ghods, P. Alizadeh, R. Chini, M. Hoseini, M. Ghalibafian, M. & Shekarchi, M. 2007. Durability-based design in the Persian Gulf, Concrete International, 29(12): 50–55.
10. Haque A.M. Al-khaiat, H. & John B. 2007. Climatic zones-A prelude to designing durable concrete structures in the Arabian Gulf. Building and Environment, 42(6): 2410–2416.
11. Lancaster, P. & Salkauskas, K. 1981. Surface generated by moving least square methods. Mathematics and Computer, No. 37: 141–158.
12. NS 3490. 2004. Design of structures. Requirements to reliability, Standards Norway, Oslo.
13. Page, C.L. Short, N.R. & Tarras, A. El. 1981. Diffusion of chloride ion in hardened cement pastes. Cement and Concrete Research, 11(30): 395-406.
14. Thomas, M.D. A & Bentz E.C. 2001. Life 365: Computer program for predicting the service life and life cycle coass of reinforced concrete exposed to chlorides. American Concrete Institute, Committee 365, Service life prediction, Ditroit, Michigan.
15. Vaysburd, A.M. & Emmons, P.H. 2004. Corrosion inhibitors and other protective systems in concrete repair. Cement and Concrete Composites, 26(3): 255–263.

CD05

Durability and Evaluation

CD05-001

MODELING THE CORROSION OF REINFORCED CONCRETE STRUCTURES BASED ON THE FUZZY SYSTEMS

J. Sobhani[1], A.A. Ramezaninpour[2]
[1]Assistant professor, Building and Housing Research Center, and Member of CT&D Research Center of Amirkabir University of Technology, Tehran, Iran
[2]Professor, Dep. of Civil & Evil Engineering, and head of CT&D Research Center of Amirkabir University of Technology, Tehran, Iran

ABSTRACT

Reinforced concrete structures are susceptible to be deteriorated in harsh environments. One of the major causes of deterioration of RC structures in these environments is the corrosion of their reinforcements. Generally the corrosion of reinforcements involves some uncertainties. In brief these uncertainties can be categorized into classes: 1) random nature of corrosion process and 2) linguistic terms of construction process. The first one is successfully handled by probabilistic methods, but to deal with the linguistic ambiguities, the fuzzy systems are general form of confrontation. One main problem is to obtain the fuzzy membership functions of corrosion process; in particular, the corrosion initiation and propagating time periods. In this paper we developed an algorithm to extract the fuzzy membership functions from the available stochastic information. In this regard, an integrated system proposed to convert the probabilistic information into the corresponding fuzzy sets. In this process, a genetic algorithm optimization utilized to gain the standard Triangular and Trapezoidal fuzzy sets, by means of minimizing the distance of fuzzy sets from the corresponding normalized probability density functions.

Keywords: reinforced concrete, corrosion, service life, probability, fuzzy variables, genetic algorithm

1. INTRODUCTION

Reinforced concrete structures are susceptible to be deteriorated in harsh environments. There may be many detrimental agents at the environment of structures, that could cause some serious damages on both reinforcement and concrete. ACI's guide to durable concrete [1] recognized five general classes of concrete deterioration as: a) Freezing and thawing, b) Aggressive chemical exposure, c) Abrasion, d) Corrosion of steel and other materials embedded in concrete, and e) Chemical reactions with aggregates.

Among these deteriorative mechanisms, the corrosion of reinforcement is very important for the structures located in the harsh environment of the southern parts of Iran, especially in the region of the Persian Gulf and Oman Sea. In these regions, high humidity along with high temperature, and availability of detrimental agents like chloride ions, are preparing a suitable environment for premature deterioration of RC infrastructures which has been built there. In this view, one of the important issues that should be considered is the corrosion of the built RC structures at these regions. Up to now well-established models have been proposed for estimating of the rate of chloride ingress and corrosion rate. Unfortunately the most of these models are based on deterministic variables that can not handle the associated uncertainties. The stochastic models are also established to deal with some uncertainties regarding the randomness nature of the corrosion. While the uncertainties regarding the linguistic terms are usually dismissed and can not be handled by the stochastic methods. The fuzzy systems are famous for their capabilities to consider the verbal rules and regulations. Therefore in this paper we try to extend the appropriate stochastic modes to the fuzzy models, to be used in the framework of fuzzy systems that could be simultaneously handled by fuzzy-logic operations and knowledge processing techniques.

2. CONCRETE AND DURABILITY

Over the millennia, concrete prepared by the Romans using lime, pozzolana and aggregates has survived the elements, giving proof of its durability [2]. Prestigious concrete works have been handed down to us: buildings such as the Pantheon in Rome, whose current structure was completed in 125 A.D. and also structures in marine environments have survived for over two thousand years. This provides a clear demonstration that concrete can be as durable as natural stone, provided that specific causes of degradation, such as acids or sulphates, freeze-thaw cycles, or reactive aggregates, are not present [2]. Today, thanks to progress made over the past few decades in the chemistry of cement and in the technology of concrete, even these causes of deterioration can be fought effectively. With an appropriate choice of materials and careful, adequately controlled preparation and placement of the mixture, it is possible to obtain concrete structures which will last in time, under a wide variety of operative conditions. The case of reinforced concrete is somewhat different. These structures are not eternal, or nearly eternal, as was generally supposed up until the 1970s [2]. Instead, their service life is limited precisely because of the corrosion of reinforcement. Actually, concrete provides the ideal environment for protecting embedded steel because of its alkalinity. If the design of a structure, choice of materials, composition of the mixture, and placement, compaction and curing are carried out in compliance with current standards, then concrete is, under most environmental conditions, capable of providing protection beyond the 50 years typical of the required service life of many ordinary structures, at least in temperate regions. In fact, cases of corrosion that have been identified in numerous structures within periods much shorter than those just mentioned, can almost always be traced to a failure to comply to current standards or to trivial errors in manufacturing of the concrete. However, under environmental conditions of high aggressiveness (generally relate to the presence of chlorides), even concrete which has been properly prepared and placed may lose its protective properties and allow corrosion of reinforcement long before 50 years have elapsed, sometimes resulting in very serious consequences [2].

3. CORROSION OF REINFORCED CONCRETE STRUCTURES

As emphasized in previous section, the problem of corrosion in reinforced concrete structures is a very crucial matter and must be given special considerations.

The durability of reinforced concrete structures is impacted by the chloride penetration and susceptibility of the reinforcement to chloride-induced corrosion, when exposed to chloride-laden environment or deicing salts. Once the chloride content at the reinforcement reaches a threshold value and enough oxygen and moisture are presented, the reinforcement corrosion will be initiated. Corrosion products then accumulate in the concrete–steel interface transition zone (ITZ), generate expansive pressure on the surrounding concrete, and cause crack initiation and propagation [3]. In this paper we are aimed to study the corrosion initiation and corrosion-induced cracking periods in the fuzzy sets vision. To develop such models it is needed to find a way to establish fuzzy model and their sets conFigureurations. To this aim, we developed our fuzzy models based on the statistical information that reflects the real distributions of the basic variables which is gained from the available information in the literature.

4. TRANSFORMING THE PROBABILISTIC INFORMATION INTO FUZZY SETS

In many engineering problems which involve a number of variables, sufficient information may be available to model some of the variables using probability distribution functions (pdf), while the other variables are treated as fuzzy. But, in some cases, such as steel corrosion analysis, it may be more realistic to carry out the decision analysis in the framework of fuzzy set theory. In fact, it is easy to deal with fuzzy sets than the probability distributions. So, obtaining the corresponding fuzzy sets from its known probability distribution could be very crucial issue in the framework of fuzzy experts systems and some further decision making processes.

4.1. Fuzzy Probability

A usual method, used for converting a probability distribution into a fuzzy set, is by dividing the pdf of the distribution by the peak value of the pdf [4]. While this method is simple, as pointed out by Dubois and Prade [5] there is a need to explicitly check the resulting fuzzy set for possibility/probability consistency principle. Using this method, a probability distribution with given pdf, p(x), can be converted into a fuzzy set by

$$f_p(x) = \frac{p(x)}{\sup_{x\in\Re}(p(x))} \tag{1}$$

where $f_p(x)$ is the membership function of the fuzzy set. The resulting fuzzy set is of the same form as that of the probability distribution. But, for typical engineering applications involving several uncertain variables, fuzzy sets with triangular or trapezoidal form are preferred due to the computational simplicity.

4.2. Extracting the Standard Fuzzy Memberships

Klir and Yuan [6] proposed the method of least-square curve fitting for constructing a membership function from samples of membership grades for some elements in the universal set X. Given the sample data (x_i,a_i), i = 1,. . . ,n, where a_i is the grade of membership of x_i in fuzzy set A, and a suitable class of functions $f(x;\alpha,\beta,...)$ where $\alpha,\beta,...$ are parameters whose values distinguish functions in the class from one another, the method of least-square curve fitting selects that function $f(x;\alpha_0,\beta_0,...)$ from the class for which the following norm reaches its minimum (discrete form).

$$E=\sum_{i=1}^{n}\left[f(x_i;\alpha,\beta,...)-f_p(x_i)\right]^2 \tag{2}$$

This method can be used to convert the probabilistic fuzzy set into the equivalent triangular or trapezoidal fuzzy set. The equivalent fuzzy set, $f(x;\alpha_0,\beta_0,...)$, is the one which minimizes the function F, given by (continuous form)

$$F=\int_X\left[f(x;\alpha,\beta,...)-f_p(x)\right]^2dx \tag{3}$$

where $f_p(x)$ is the membership function of the probabilistic fuzzy set given by Eq. (1). For a triangular fuzzy set, $f(x;\alpha,\beta,...)$ is given by (Figure 1(a))

$$f(x;\alpha,\beta,\gamma)=\begin{cases}0 & x<\alpha\\ \dfrac{\alpha-x}{\alpha-\beta} & \alpha\le x\le\beta\\ \dfrac{\gamma-x}{\gamma-\beta} & \beta<x\le\gamma\\ 0 & x>\gamma\end{cases} \tag{4}$$

For a trapezoidal fuzzy set, $f(x;\alpha,\beta,...)$ is given by (Figure 1(b))

$$f(x;\alpha,\beta,\gamma,\delta)=\begin{cases}0 & x<\alpha\\ \dfrac{\alpha-x}{\alpha-\beta} & \alpha\le x\le\beta\\ 1 & \beta<x<\gamma\\ \dfrac{\delta-x}{\delta-\gamma} & \gamma\le x\le\delta\\ 0 & x>\delta\end{cases} \tag{5}$$

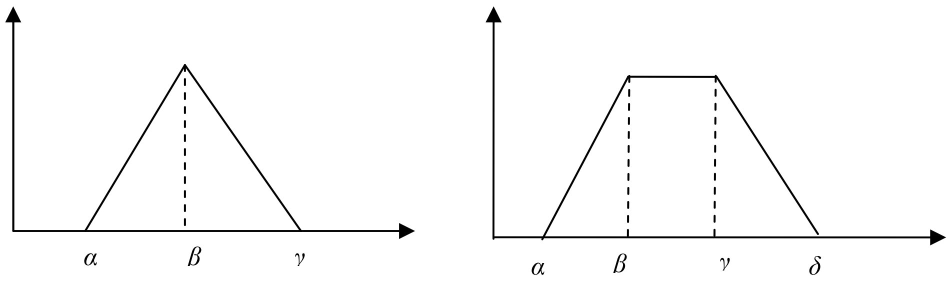

Figure 1. a) Triangular fuzzy set b) Trapezoidal fuzzy set

In this paper, genetic algorithm would be used to optimization process to find the standard fuzzy membership functions of corrosion initiation and corrosion propagation periods.

5. FUZZY MODEL FOR CORROSION INITIATION PERIOD

The steel remains passive in the concrete due to the alkalinity of the environment. Once the chloride ions attack the reinforcement, the passive oxide layer on the steel surface would be broken. This stage, known as the corrosion initiation time. The ingress of chloride ions into the concrete media is directly depends on the permeability of the concrete that is affected by the quality of the concrete practice. If we suppose that there is no initial chloride ion in the concrete (C_i=0), then the Fick's second law of diffusion could be applicable in the form of Eq. 6.

$$\overline{T}_i = \frac{\overline{C}^2}{4\overline{D}_c}\left[erf^{-1}\left(\frac{\overline{C}_s - \overline{C}_{cr}}{\overline{C}_s} \right) \right] \tag{6}$$

where $\overline{C}$ is the random concrete cover depth, $\overline{D}_c$ is the random diffusion coefficient of concrete, $\overline{C}_s$ is the surface chloride concentration and $\overline{C}_{cr}$ is the random critical chloride concentration. This is a probability or stochastic form for the corrosion initiation time. Note that in this equation, *erf* is error function and equals to $(2/\sqrt{\pi})\int_0^x e^{-t^2}\,dt$. Now if we exert section 4 method to convert the random representation of parameters into the fuzzy ones, we can reach the fuzzy model for corrosion initiation time as follow:

$$\hat{T}_i = \frac{\hat{C}^2}{4\hat{D}_c}\left[erf^{-1}\left(\frac{\hat{C}_s - \hat{C}_{cr}}{\hat{C}_s} \right) \right] \tag{7}$$

where $\hat{C}$ is the fuzzy concrete cover depth, $\hat{D}_c$ is the fuzzy diffusion coefficient of concrete, $\hat{C}_s$ is the fuzzy surface chloride concentration and $\hat{C}_{cr}$ is the fuzzy critical chloride concentration.

5.1. Probability Distribution for Corrosion Initiation Time

The probability distribution for the corrosion initiation could be gained based on the simple Monte Carlo Simulation (MCS) method. The basic variables for MCS of corrosion initiation are summarized in Table 1.

Table 2, summarizes ANOV results for lognormal distribution fitted on the MCS of Eq. 6. According to the results of this table, the corrosion initiation lognormal pdf is:

$$\overline{T}_i \approx \frac{1}{1.478t} e^{\frac{-(\ln t - 3.89)^2}{0.6956}} \tag{8}$$

The supreme value for $\overline{T}_i$ is 0.0163. By dividing the Eq. (8) to the supreme value, the fuzzy model for corrosion initiation can be gained as follows:

$$\hat{T}_i = \frac{1}{0.0241t} e^{\frac{-(\ln t - 3.89)^2}{0.6956}} \tag{9}$$

Figure 2 shows the visualization of the fuzzy distribution of corrosion initiation.

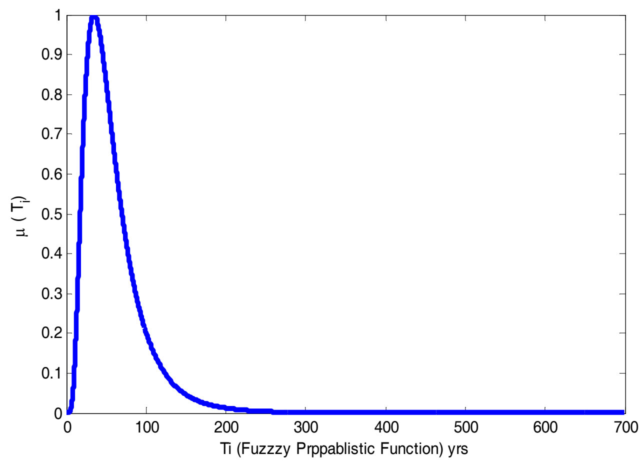

Figure 2. Fuzzy probabilistic function visualization for T_i

Table 1: Basic variables for T_i

Variable	pdf type	Mean	Standard division	unit	reference
$\overline{C}$	normal	40	8	[mm]	[7]
$\overline{D}_c$	normal	30	5	[mm^2/year]	[7]
$\overline{C}_{cr}$	normal	0.3	0.05	[%]	[7]
$\overline{C}_s$	normal	0.650	0.03	[%]	[7]

Table 2: Lognormal pdf fitting ANOV results for T_i (mu=58.7226, sigma=1434.28)

Parameter Estimated Std. Err.:	mu	3.89893	0.00589736
	sigma	0.589736	0.00417038
		mu	sigma
Estimated covariance of parameter estimates:	mu	3.47789e-005	2.9251e-019
	sigma	2.9251e-019	1.7392e-005

Table 3: GA to adjust $\hat{T}_i$ MF parameters

	Type	Fitness function	Variable
Membership function	Triangular	@Ti_fuz_tri_nor	$[\alpha\ \beta\ \gamma]$
	Trapezoidal	@Ti_fuz_trap	$[\alpha\ \beta\ \gamma\ \delta]$
Population type	double		
Population size	30		
Fitness scaling	rank		
Selection	stochastic uniform		
Mutation	adaptive feasible		
Crossover	scattered		
	Optimized parameters		
MF type	Triangular	Trapezoidal	
Variables	$[\alpha\ \beta\ \gamma]$	$[\alpha\ \beta\ \gamma\ \delta]$	
Adjusted result	[6.7813 29.0 119.0]	[7.5625 28.0 31.0000 118.50]	

5.2. Genetic Algorithm to Get Standard Fuzzy MF Of $\hat{T}_i$

To extract the standard fuzzy membership functions for the corrosion initiation time, Eq. 2 or 3 should be minimized. In this paper we use genetic algorithm for its robustness in optimization task with detail summarized in Table 3. Moreover, Table 3 summarized the GA-optimized variables for each of triangular and trapezoidal standard fuzzy membership functions. Moreover, optimized fuzzy triangular and trapezoidal MF functions are demonstrated in Figure 3a and Figure3b respectively.

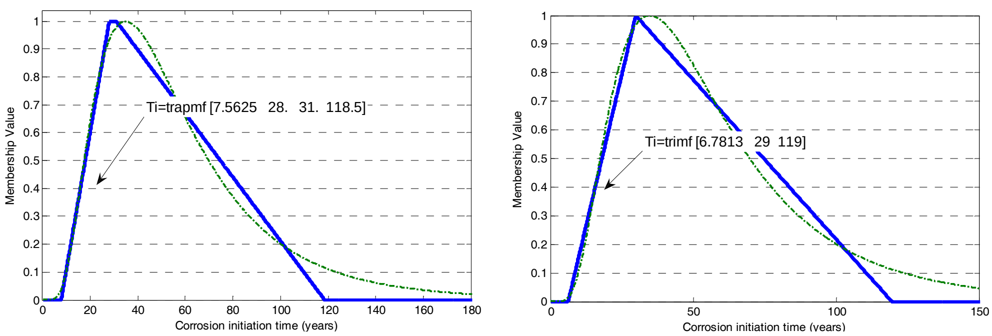

Figure 3. a) Optimized triangular MF for $\hat{T}_i$, b) Trapezoidal MF for

6. FUZZY MODEL FOR CORROSION-INDUCED CRACKING TIME

The corrosion of reinforcing bar in the concrete has very wide ranges of deteriorative effects. Figure 4 shows some effects of corrosion on residual strength [8]. In this paper we consider the cracking of cover concrete due to the radial forces of expansive corrosion products.

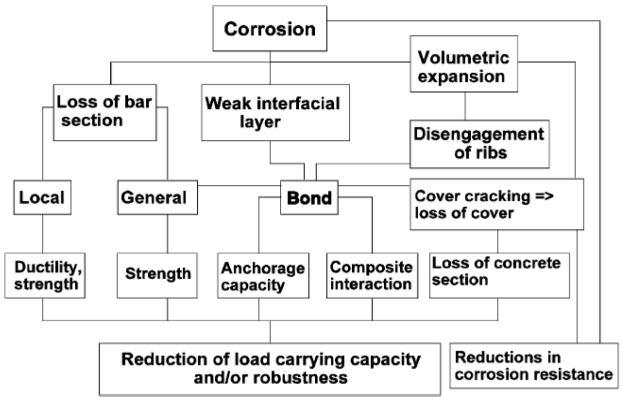

Figure 4. Effects of corrosion on residual strength [8].

Table 4: α for various corrosion products [10]

corrosion product	FeO	Fe_3O_4	Fe_2O_3
α	0.777	0.724	0.699
corrosion product	$Fe(OH)_2$	$Fe(OH)_3$	$Fe(OH)_3 \cdot 3H_2O$
α	0.622	0.523	0.347

Table 5: Basic variables for T_{cr}

Variable	Distribution type	Mean	Standard deviation	Unit	Reference
$\overline{C}$	normal	40	8	[mm]	[7]
$\overline{D}_c$	<<<	30	5	[%]	[7]
$\overline{C}_{cr}$	<<<	0.3	0.05	[%]	[7]
$\overline{C}_s$	<<<	0.650	0.03	[mm^2/year]	[7]
$\overline{D}$	<<<	12	0.15	mm	[11]
$\overline{i}_{cor}$	uniform	1.5	2.5	$\mu A/cm^2$	[7]
d_0	deterministic	12.5	---	μm	[7]
υ_c	<<<	0.18	---		[11]
$\overline{E}_{ef}$	normal	18.82	0.12	GPa	[12]
f'_t	deterministic	3.3	---	MPa	[12]
f'_c	<<<	31.5	---	MPa	[12]
α	<<<	0.57	---	---	[12]
ρ_{rust}	<<<	3,600	---	kg/m^3	[12]
ρ_{st}	<<<	7,850	---	kg/m^3	[12]

Table 6: Normal pdf fitting ANOV results for T_{cr}:(mu=0.552096, sigma=0.0143802

Parameter Estimated Std. Err.:	mu	0.552051	0.00119047
	sigma	0.119047	0.000841853
		mu	sigma
Estimated covariance of parameter estimates:	mu	1.41722e-006	1.41722e-006
	sigma	7.08717e-007	-3.40944e-020

Table 7: GA-optimized MFs for $\hat{T}_i$

Optimized parameters		
MF type	Triangular	Trapezoidal
Variables	[α β γ]	[α β γ δ]
Adjusted result	[0.2729 0.5487 0.8339]	[0.2696 0.5346 0.5754 0.8229]

Extended probabilistic formulation for the time to corrosion-induced cracking time period was proposed as follows [9]:

$$\overline{T}_{cr} = \frac{\overline{W}_{crit}^2}{2\overline{k}_P} \tag{10}$$

Here we convert this formulation to its fuzzy model using the method described in section 4 as follows:

$$\hat{T}_{cr} = \frac{\hat{W}_{crit}^2}{2\hat{k}_P} \tag{11}$$

where $\hat{T}_{cr}$ is the fuzzy time to crack initiation, $\hat{W}_{crit}$ is the fuzzy critical amount of corrosion products, $\overline{k}_P$ is the fuzzy rate for rust production as the corrosion product. These quantities can be obtained using the following formulas:

$$\hat{W}_{crit} = \rho_{rust}\left(\pi\left[\frac{\hat{C}f_t'}{\hat{E}_{ef}}\left(\frac{a^2+b^2}{b^2-a^2}+\nu_c\right)+d_0\right]\hat{D}+\frac{\hat{W}_{st}}{\rho_{st}}\right) \tag{12}$$

where $\hat{D}$ is the fuzzy diameter of rebar and $\hat{W}_{st} = \alpha\hat{W}_{crit}$ and,

$$\hat{k}_P = 0.105(1/\alpha)\pi\hat{D}\cdot\hat{i}_{cor} \tag{13}$$

where $\bar{i}_{cor}$ is the fuzzy annual rate of corrosion in μA/cm^2 and α depends on the type of corrosion product which can be adopted from the Table 4.

6.1. Probability Distribution for Corrosion-Induced Cracking Time

The probability distribution for the corrosion cracking could be gained based on the simple Monte Carlo Simulation (MCS) method. The basic variables for MCS of corrosion cracking are summarized in Table 5.

Table 6, summarizes ANOV results for normal distribution fitted on the MCS of Eq. 11. According to the results of this table, the corrosion initiation lognormal pdf is:

$$\overline{T}_{cr\_\mathrm{Norm}} \approx \frac{1}{0.552} e^{\frac{-(t-0.552051)^2}{0.0283}} \tag{14}$$

The supreme value for $\overline{T}_{cr}$ is 3.35. By dividing the Eq. (14) to the supreme value, the fuzzy model for corrosion initiation can be gained as follows:

$$\hat{T}_i = \frac{1}{0.0241t} e^{\frac{-(\ln t-3.89)^2}{0.6956}} \tag{15}$$

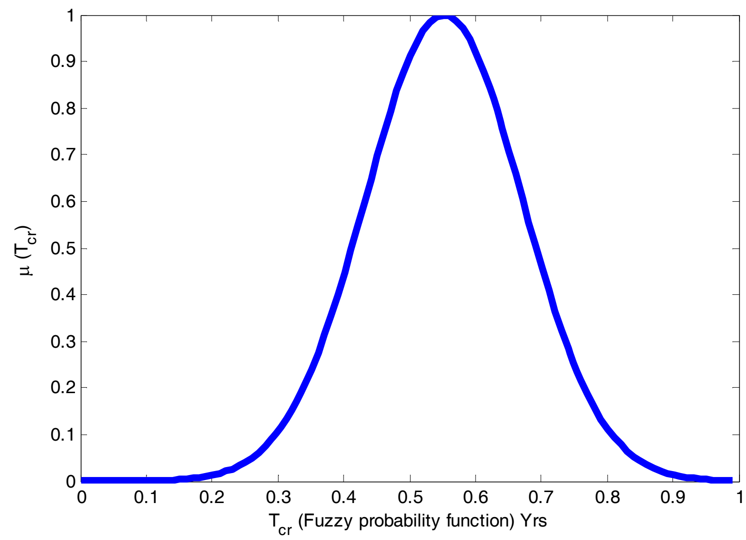

Figure 5. Fuzzy probabilistic function visualization for T_{cr}

6.2. Genetic Algorithm to Get Standard Fuzzy MF Of $\hat{T}_{cr}$

Figure 5 shows the visualization of the fuzzy distribution of crack-initiation time. To extract the standard fuzzy membership functions for the corrosion initiation time, Eq. 2 or 3 should be minimized. As said before, in this paper we use genetic algorithm for its robustness in optimization task with detail similar to Table 3 with minor modifications. Table 7 summarized the GA-optimized variables for each of triangular and trapezoidal standard fuzzy membership functions. Moreover, optimized fuzzy triangular and trapezoidal MF functions are demonstrated in Figure 6a and Figure 6b respectively.

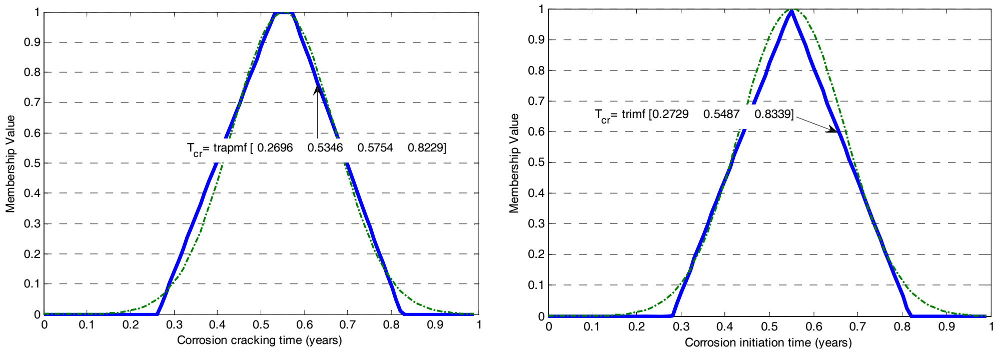

Figure 6. a) Optimized triangular MF for $\hat{T}_{cr}$, b) Trapezoidal MF for

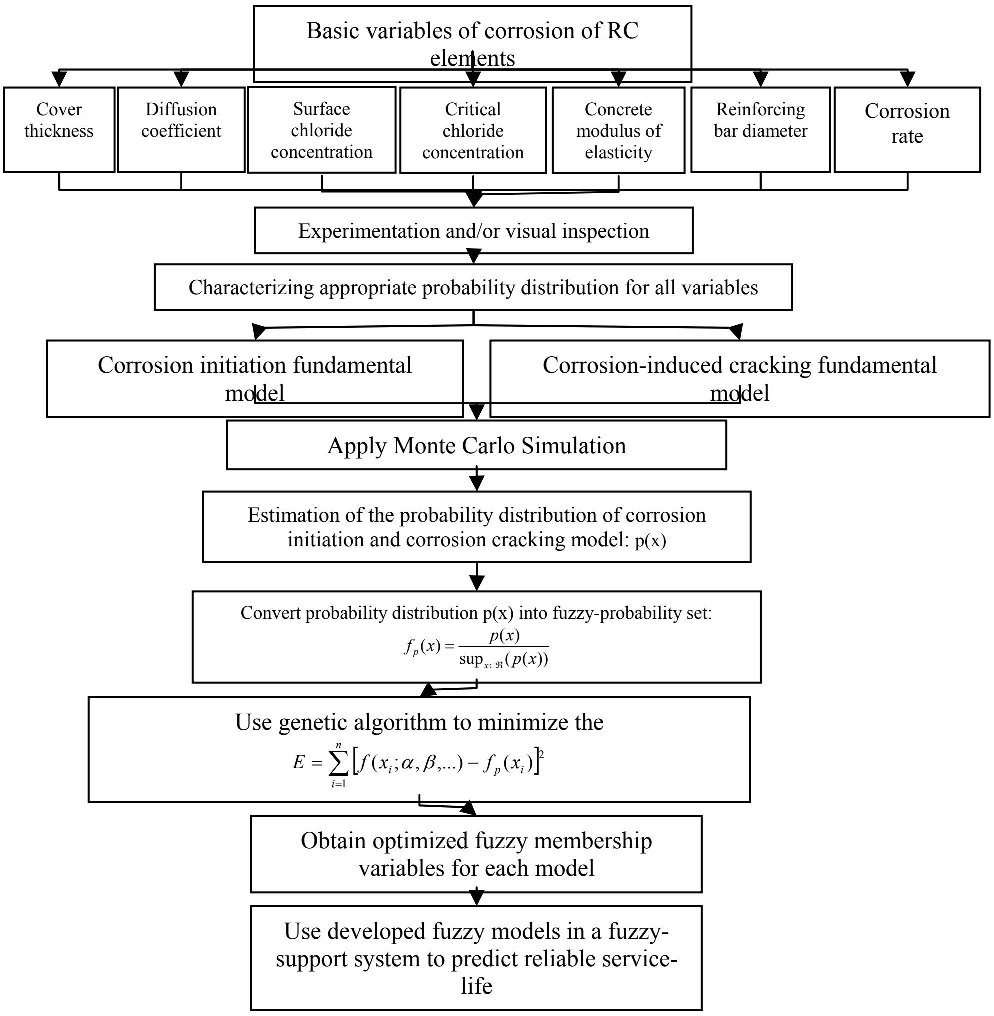

Figure 7. Integrated algorithm to model to model the corrosion initiation and propagation periods

7. FUZZY-BASED ALGORITHM TO MODEL THE CORROSION OF RC ELEMENTS

At previous sections, we discussed about how to develop a fuzzy model from available stochastic models. Here we integrate these steps in an algorithm to be more useful. This algorithm is shown in Figure 7.

8. SUMMERY AND CONCLUSION

In this paper, we introduced a method to communicate with the available probabilistic information and conversion of them into the fuzzy sets. In this sense, the probability distribution functions for corrosion initiation and corrosion-cracking time period were converted into the fuzzy sets. The fuzzy sets are famous for their capabilities in processing the linguistic information rather than the random nature. So the constructed fuzzy sets could be used in a decision support system to eliminate the linguistic ambiguities of the corrosion in the RC structures. Thus the method introduced in this paper, is a major modules for developing a so-called Structural Health Monitoring System (SHMS) for reinforced concrete infrastructures.

REFRENCES

1. ACI committee 201, "Proposed revision of: Guide to durable concrete", ACI Material Journal 1991, Vol. 88, No. 5, pp. 544-582.
2. Bertolini L., Elsener B., Pedeferri P., Polder R.P., "Corrosion of steel in concrete", WILEY-VCH Verlag GmbH & Co. KGaA, Weinheim, Germany, 2004.
3. Chen D., Mahadevan S., "Chloride-induced reinforcement corrosion and concrete cracking simulation", Cement and Concrete Composites 2008, Vol. 30, pp. 227-238.
4. De Lima B.S.L.P., Ebecken N.F.F., "A comparison of models for uncertainty analysis by the finite element method", Finite Elements in Analysis and Design 2000; Vol. 34, pp. 211-32.
5. Dubois D, Prade H. "Fuzzy sets and systems: theory and applications", Academic Press; 1980.
6. Anoop, M.B., Rao, K. B., Gopalakrishnan, S., "Conversion of probabilistic information into fuzzy sets for engineering decision analysis", Computers and Structures 2006, Vol. 84, pp. 141-155.
7. Thoft-Christensen P., "Assessment of the reliability profiles for concrete bridges", Engineering Structures 1998, Vol. 20. No. 11, pp. 1004-1009.
8. Cairns J., Du Y., and Law D., "Influence of corrosion on the friction characteristics of the steel/concrete interface", Construction and Building Materials 2007, Vol. 21, pp.190-197.
9. Sobhani J., "A Soft Computing Approach for Service-Life Prediction of RC Bridge Deck in Chloride-Laden Environments", PhD Dissertation, Amir Kabir University of Technology, 2007.
10. Bhargava K., Ghosh A.K., Mori Y., Ramanujam S., "Model for cover cracking due to rebar corrosion in RC structures", Engineering Structures

2006, Vol. 28, pp. 1093-1109.
11. Li C.Q.; Lawanwisut W., and Zheng J.J., "Time-dependent reliability method to assess the serviceability of corrosion-affected concrete structures", Journal of Structural Engineering 2005, Vol. 131, No 11, pp. 1674-1680.
12. Liu Y., and Weyers R.E., "Modeling the time-to-corrosion cracking in chloride contaminated reinforced concrete structures", ACI Material Journal 1998, Vol. 95, No. 6, pp. 675-681.

CD05-002

SCC CONTAINING POZZOLANIC MATERIALS AS FILLER REPLACEMENT AT ELEVATED TEMPERATURES

A.A. Ramezanianpour[1], R. Esmaili[2]
[1]Professor in Civil Engineering, Amirkabir University of Technology, Tehran, Iran
[2]BSc. Student in Civil Engineering, Amirkabir University of Technology, Tehran, Iran

ABSTRACT

Few investigations have been reported on the properties of Self-Compacting Concrete (SCC) when it is exposed to elevated temperatures; because it is commonly understood that concrete can resist very well against elevated temperatures. Even so, it's necessary to evaluate all structures after they exposed to elevated temperatures.

Mechanical properties of SCC containing two types of Pozzolans (Silica Fume and Pumice) as filler replacement at elevated temperatures were experimentally investigated in this paper. At the age of 28 days, the specimens were placed in an electrical furnace and heating was applied up to the maximum temperatures of 200, 450, 600 and 800°C for 2 hr. Then, the specimens were allowed to be cooled in the furnace and subsequently tested for compressive strength, rebound hammer, ultrasonic pulse velocity and weight loss. The results show that concretes without Silica Fume and Pumice as a replacement for filler show slightly better performance in terms of lower strength loss.

Keywords: SCC, pozzolanic materials, elevated temperatures, mechanical properties, filler

1. INTRODUCTION

Self-Compacting Concrete (SCC) was first developed in 1988 to achieve durable concrete structures. Since then it has been used for a wide range of structures and infrastructures, such as bridges and tunnels. SCC is usually considered as a special type of High-Performance Concrete (HPC) produced with higher amounts of filler materials and lower water/binder ratios as compared with other concretes. Thus, porosity of SCC is usually reduced and the material is characterized by a high diffusion resistance [1]. Concrete mixture of high diffusion resistance such as SCC and HPC, are usually considered as more vulnerable to fire attack. Due to the lower porosity and lower connectivity of pores in SCC and HPC, the accumulating moisture and water vapor can hardly escape from the structure. So, very high pore pressure may be built up as functions of temperature, heating rate, and size of the specimens [2].

The cracking starts around the $Ca(OH)_2$ crystals and then progresses to areas near the unhydrated cement grains, as supported by Scanning Electron Microscopy (SEM) observations [3]. Cracking increases significantly as the temperature is raised beyond 300°C [3,4]. When the maximum exposure temperature is below 300°C, concrete damage is dominated by only localized boundary cracking between the aggregates and the cement paste [5]. Cracks of the heated concrete could be further extended and developed during postcooling [6]. Therefore, a reduction of $Ca(OH)_2$ content in the cement paste containing supplementary cementing materials such as Silica Fume (SF), Pumice, etc., due to the pozzolanic reaction could help to reduce cracking due to postcooling. However, it should be noted that, above the dissociation temperature of $Ca(OH)_2$ at about 500°C, most concretes are likely to lose their structural properties [5].

Pozzolanic concretes are used extensively throughout the world; the oil, gas, nuclear, and power industries are among the major users. The applications of such concretes are increasing day by day due to their superior structural performance, environmental friendliness, and energy conserving implications [7]. As the use of Pozzolanic concretes becomes common, the risk of exposing them to elevated temperatures increases. So, it's necessary to evaluate all these structures after they are exposed to elevated temperatures.

This paper presents the results of an experimental investigation studying the mechanical properties of SCC containing two types of Pozzolans; Silica Fume (SF) and Pumice (P) that were used as filler replacement, subjected to elevated temperatures.

2. EXPERIMENTAL PROGRAM

2.1. Materials and Mix Designs

A total of four different mixtures were made; control SCC, Traditional Concrete (TC), one SCC with 7.5% Silica Fume (SF) replacing filler by weight and the other with 15% Pumice (P) replacing filler by weight.

Table 1 lists mix design proportions of SCCs and the TC. Properties of fresh and hardened concretes are depicted in Table 2. Local natural aggregate with maximum size of 10 mm; city potable water and Type I Portland cement were used. Limestone was used as filler. Superplasticizer was used according to the results obtained for the slumps. SCCs were prepared and tested in fresh conditions according to the EFNARC specifications [8].

2.2. Preparation of Specimens and tests

The specimens prepared were 100 (mm) cubes. Concrete test specimens were kept protected after casting to avoid water evaporation. After 24 hr the 100 (mm) cubes were cured for 28 days in lime-saturated water at 23 ± 2 °C to prevent possible leaching of $Ca(OH)_2$ from these specimens. Then the specimens used for measuring the 28 day compressive strength, rebound hammer number, pulse velocity and weight loss. At the age of 28 days, specimens were placed in an electrical furnace with heat applied at the rate of 2.5 (°C /min) until the desired temperature was reached (Figure 1). Before fire testing, two cubes were dried to reach to a constant mass.

A maximum temperature of 200, 450, 600 and 800 ^{o}C was maintained for 2 hr under the same conditions and without any imposed load. Specimens were then allowed to cool in the furnace and tested for compressive strength, rebound hammer, pulse velocity and weight loss. Control tests were also performed on specimens cured at room temperature (23 ± 2°C).

Residual compressive strength was determined as the mean value of two cubes tested per temperature, whereas rebound hammer was determined as the mean value of two measurements (two opposite sides of the cubes used for compressive strength measurements). Pulse velocity measurements were determined as the mean value of four measurements (two other opposite sides of the cubes used for compressive strength measurements) at any temperature. The weight loss of specimens was determined as the mean value of two cubes' weight loss, with which their weight being measured before and after the fire testing.

Table 1: Mix design proportions of self-compacting concretes and the traditional concrete

Mixture				
P2	**SF2**	**SCC**	**TC**	**Constituents (Kg/m^3)**
450	450	450	450	Type I Portland cement
—	34	—	—	Silica Fume (SF)
67.5	—	—	—	Pumice (P)
82.5	116	150	—	Filler
890	898	900	900	Coarse Aggregate
593	598	600	600	Fine Aggregate
180	180	180	180	Water
0.4	0.4	0.4	0.4	w/c
1.1	0.9	0.85	1	Superplasticizer (lt/100 kg of binder)

Table 2. Proportions of fresh and hardened concretes

Mixture				
P2	**SF2**	**SCC**	**TC**	**Mixture properties**
—	—	—	100	Slump (mm)
700	680	720	—	Slump flow (mm)
1.1	0.97	0.95	—	L Box (H_2/H_1)
5.7	5.16	9	—	V-funnel (s)
69	70	55	60	f_{c28} (Mpa)

Figure 1. Specimens in the electrical furnace

3. RESULTS AND DISCUSSION

3.1. Compressive Strength

The residual compressive strength at the age of 28 days for all mixtures is shown in Figure 2. When concretes are exposed to high temperatures, there are changes in the mechanical properties and the durability of them. However, the mechanisms causing these changes in properties is quite complex as a result of the concurrence of chemical and physical changes in hardened cement paste (HCP) , aggregate, and at the interfaces.

The results show that all mixtures had an increase in their residual compressive strength up to 200 °C and then a sudden decrease occurred in SCC mixtures containing silica fume and pumice as replacement for filler. No spalling occurred at any temperature for all mixtures. In general, SCC with 15% pumice and another one with 7.5% silica fume replacement with filler (P2 & SF2) have higher strength loss with increasing temperatures than other mixtures without pozzolanic materials. The increase in compressive strength can be partially due to the strengthened HCP during the evaporation of free water [9,10]. Further hydration of cementitious materials is another important cause of the hardening of HCP [9].

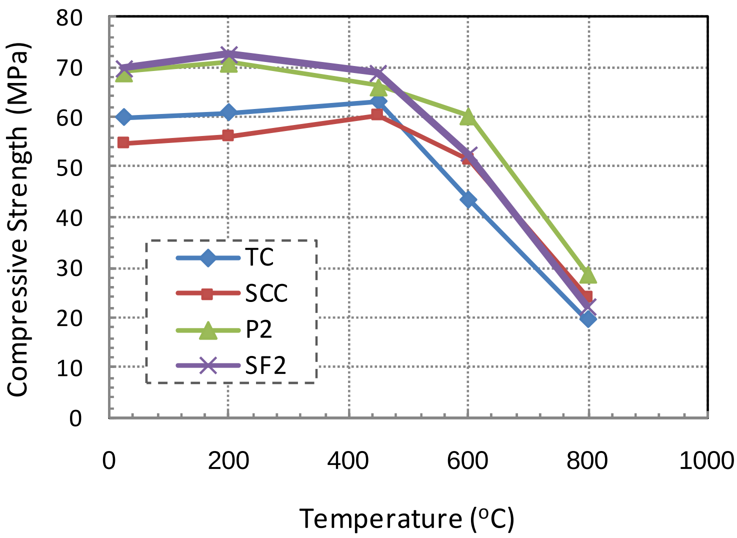

Figure 2. Residual compressive strength of all mixtures

3.2. Rebound Hammer

The residual rebound hammer number at the age of 28 days for all mixtures is shown in Figure 3. The rebound values are influenced mainly by the condition of the surface of concrete to a depth not exceeding 3 cm approximately [11].

Since a temperature rise up to 200°C causes drying and hardening of the surface layer, rebound measurements present a small increase. At temperatures above 450°C, intensive internal cracking and chemical decomposition of the surface layer become more significant and rebound numbers show a significant reduction.

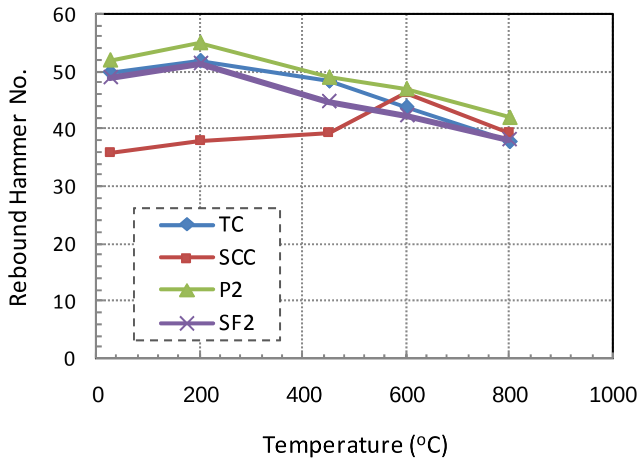

Figure 3. Residual rebound hammer number of all mixtures

3.3. Ultrasonic Pulse Velocity

The residual pulse velocity at the age of 28 days for all mixtures is shown in Figure 4. It is clearly seen that pulse velocity reduces almost linearly with increasing temperature.

It is obvious that the transmission of pulse waves through a concrete mass is highly influenced by the microcracking of concrete. Thus, the decrease in pulse velocity with increasing temperature is a sensitive measure of the progress of microcracking in the material.

Because microcracks might have developed along the boundary due to the swelling of physically bound water layers and the thermal incompatibility between aggregates and cement pastes [12]. Microcracking also increased significantly beyond 300°C, which is responsible for further durability loss in specimens heated to 450, 600, and 800°C [4,13].

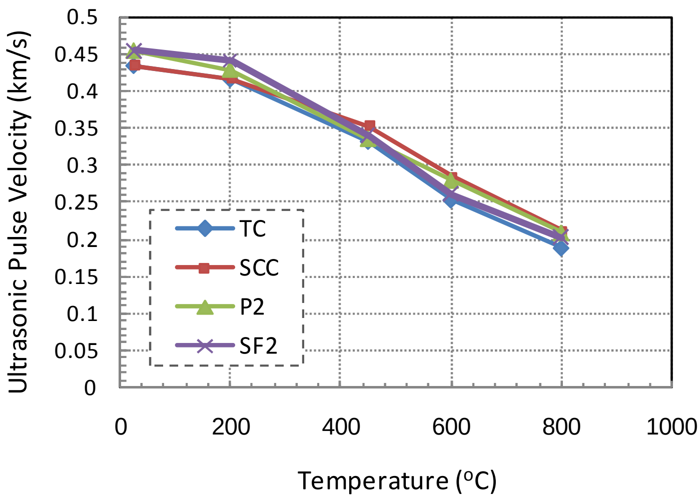

Figure 4. Residual ultrasonic pulse velocity of all mixtures

3.4. Weight Loss

Figure 5 shows the weight loss at the age of 28 days for all mixtures at various temperatures. It can be observed that the TC samples show higher levels of weight loss than the others. Between 23 ±2°C and 200°C, a quick weight loss occurred in all samples, especially the TC and control SCC samples. This corresponds to the loss of the evaporable water and part of the physically bound water [2].

From 200 to 600°C, the weight loss includes the loss of chemically bound water from the decomposition of the CSH [2]. The weight loss of TC is higher than the others for temperatures up to 800°C. However, when the temperature is higher than 600°C, a dramatic loss of weight was observed in all samples. This is due to the decomposition of limestone filler, releasing carbon dioxide [14]:

$$CaCO_3 \rightarrow CaO + CO_2 \quad (1)$$

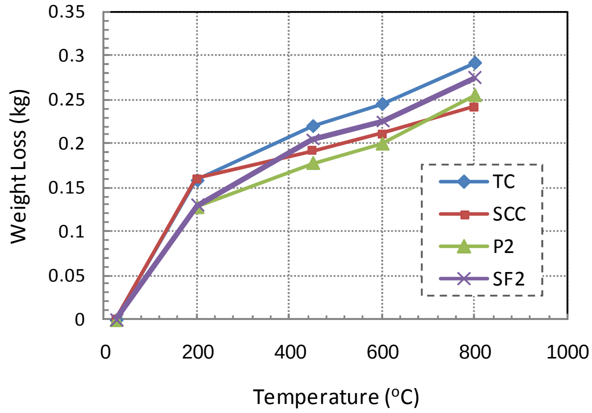

Figure 5. Weight loss of all mixtures

3.5. Residual Compressive Strength and Residual Ultrasonic Pulse Velocity

Figure 6 shows the relation between residual compressive strength and residual ultrasonic pulse velocity for all concrete mixtures. At temperatures above 450°C, both compressive strength and ultrasonic pulse velocity decrease almost linearly with increasing temperature because of intensive internal cracking progress in the samples.

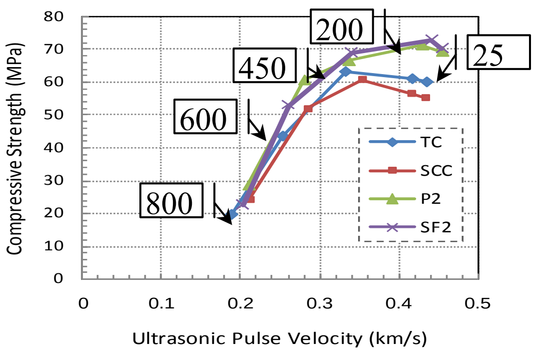

Figure 6. Relation between residual compressive strength and residual ultrasonic pulse velocity for all mixtures

It can be seen that in spite of the residual ultrasonic pulse velocities of all concrete mixtures were nearly equal, the residual compressive strength loss of SCC with 7.5% Silica Fume replacement with filler (SF2) was higher than others.

3.6. Residual Compressive Strength and Weight Loss

Figure 7 shows the relation between residual compressive strength and weight loss for all concrete mixtures. It is observed that the SCC mixtures with 15% pumice replacement with filler (P2) and the one with 7.5% silica fume replacement with filler (SF2) had higher residual compressive strength than the other specimens. As shown in this Figure, a linear relationship can be obtained for compressive strength and weight loss at temperatures between 450-800 °C.

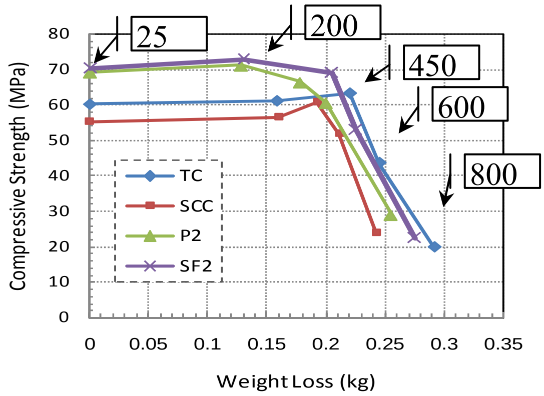

Figure 7. Relation between residual compressive strength and weight loss for all mixtures

3.7. Residual Ultrasonic Pulse Velocity and Weight Loss

The relation between residual ultrasonic pulse velocity and weight loss at the age of 28 days for all mixtures is shown in Figure 8. It can be seen that higher temperature has resulted in higher weight losses due to the chemical decomposition of materials. This has caused microcracks in the cement pastes and micro-structure change and hence lower pulse velocity results. There is also no linear relationship between Ultrasonic Pulse Velocity (UPV) and weight loss at all temperatures.

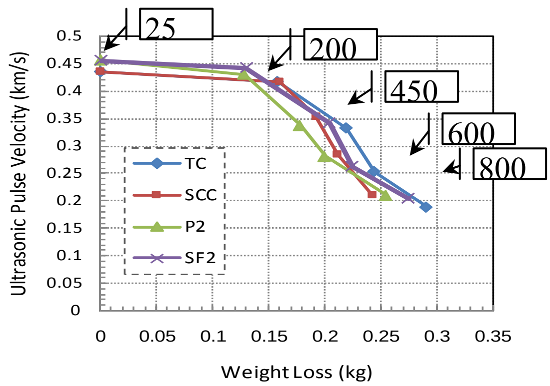

Figure 8. Relation between residual ultrasonic pulse velocity and weight loss for all mixtures

4. CONCLUSIONS

The following conclusions were drawn from the study:

(1) In the range of 25–200°C, an increase in strength was observed in all concrete mixtures which can be resulted due to the evaporation of free water and further hydration of cementitious materials. From 200 to 450°C, a decrease in strength was observed in SCCs containing Silica Fume and Pumice as a replacement for filler. A loss in strength within the range of 70–75% was observed in the 400–600°C temperature range. At 800°C residual strength of SCCs varies between 25 and 30%. The sever loss in strength at an elevated temperature is probably due to the intensive internal cracking and chemical decomposition of concrete components.

(2) In general, concretes without Silica Fume and Pumice as a replacement for filler show slightly better performance in terms of lower strength loss.

(3) Results obtained for residual strength of heated samples by standard crushing test, rebound hammer and pulse velocity are different. This variation is attributed to the surface hardness measurement by hammer test and the influence of the microcracks on UPV test results.

(4) It is important that building designers, building officials, and the fire service organization be aware of the loss in mechanical properties of concretes which could reduce the load carrying capacity and durability of affected structural components.

REFERENCES

1. Kosmas K. Sideris, Mechanical Characteristics of Self-Consolidating Concretes Exposed to Elevated Temperatures, Journal of Materials in Civil Engineering, 2007, Vol. 19, No. 8, 648-654.
2. Bazant, Z.P., Kaplan, M.F., Concrete at high temperatures: Material properties and mathematical models, Longman, London, 1996.
3. Piasta, J., Heat deformations of cement phases and the microstructure of cement paste, Mater. Struct. 1984, 17(102) 415-420.
4. Riley, M. A., Possible new method for assessment of fire damaged concrete, Mag. Concrete Res., 1991, 43(155) 87-92.
5. Khandakar M. Anwar Hossain, Macro and Microstructural Investigations on Strength and Durability of Pumice Concrete at High Temperature, Journal of Materials in Civil Engineering, 2006, Vol. 18, No. 4, 527-536.
6. Petzold, A., Rohr, M., Concrete for high temperatures, Maclare, London, 1970.
7. Mehta, P.K., Advancements in concrete technology, Anim. Reprod. Sci. 1999, 96(4), 69-76.
8. Efnarc, Specification and Guidelines for Self-Compacting Concrete, Feb. 2002.
9. Khoury, G.A., Compressive strength of concrete at high temperatures: A reassessment, Mag. Concrete Res., 1999, 44(161), 291-309.
10. Dias, D.P.S., Khoury, G.A., Sullivan, P.J.E., Mechanical properties of hardened cement paste exposed to temperatures up to 700°C (1,292°F), ACI Material Journal, 1990, 87(2) 160-165.
11. A. Savva, P. Manita, K.K. Sideris., Influence of elevated temperatures on the

mechanical properties of blended cement concretes prepared with limestone and siliceous aggregates, Cement & Concrete Composites, 2005, 27, 239-248.

12. Malhotra, H.L., Effect of temperature on the compressive strength of concrete, Mag. Concrete Res., 1956, 8(23) 85-94.
13. Lin, W.M., Lin, T.D., Powers-Couche, L.J., Microstructures of fire-damaged concrete, ACI Mater. J., 1996, 93(3) 199-205.
14. G. Ye, X. Liu, G. De Schutter, L. Taerwe, P. Vandevelde., Phase distribution and microstructural changes of self-consolidating cement paste at elevated temperature, Cement & Concrete Research, 2007.

CD05-003

INVESTIGATION OF DURABILITY OF REINFORCEMENT CONCRETE IN SEVERE CORROSIVE MARINE ENVIRONMENT

A. Mahmoodi[1], H. Afshin[2], H. Hakimzadeh[3], D.Jalali[4]
[1]M.Sc. Student, Dept. of Civil Engineering, Sahand Industrial University, Tabriz, Iran
[2]Assistance Professor, Dept. of Civil Engineering, Sahand Industrial University, Tabriz, Iran
[3]Associate Professor, Dept of Civil Engineering. Sahand Industrial University, Tabriz, Iran
[4]Associate Professor, Dept. of Mechanical Engineering, Sahand Industrial University, Tabriz, Iran

ABSTRACT
The intensity of damage in concrete structures has a vital relationship to the position of concrete versus the sea water level. With regard to this concept, the environment of located structures near the coast (i.e. coastal structures) can be divided into four zones: marine atmospheric, splashing, tidal and submerged [1, 2]. A hydraulic model consists of a channel with 10 meters in length, 0.7 meters width, 1 meter depth and a wave maker machine capable of making regular waves with various heights and periods, has been designed and constructed in hydraulic laboratory of Sahand University of Technology to simulate the marine environment and conditions in this research study. The Oroomiyeh lake water was used to reproduce severe corrosive marine environment. Two water/ cement ratios (0.45 and 0.55) and two cement contents (350 and 400 kg/m^3) were selected for reinforcement and plain concrete specimens. Furthermore, silica fume was used as supplementary cementing material.
After standard curing, these specimens were kept in different conditions: submerged, tidal, splash, atmospheric and outdoors.
A series of tests such as corrosion potential measurement, electrical resistivity and reinforcement corrosion intensity, chloride ion concentration and compressive strength were carried out at different ages of concrete. In this paper, the function of specimens' durability in different zones have been investigated and compared with one to the others.

Keywords: reinforcement corrosion, chloride ion concentration, corrosion potential, splashing zone, atmospheric zone

1. INTRODUCTION
Due to the importance of the oil industry, marine transportation and mining in seas, construction of various structures (e.g. jetty, platform, etc) has been increased remarkably in recent years. Although concrete is a durable material, there are some reasons that can damage it in its lifetime. In designing the concrete structures, it is necessary to consider various factors to which the concrete should be exposed [3].
Research in real marine environment is very difficult to do as it needs many tools, equipments, etc. However, the marine conditions can be simulated partly in the

laboratory to perform experiments on specimens.

Investigations have been done in durability of concrete in marine environment across the world. For instance, marine durability of some concrete specimens in tidal condition in Japan coasts was reported in late 20th century [4]. Also, in I.R.Iran durability of concrete specimens in different conditions in Persian Gulf has been investigated by Building and Housing Research Center (BHRC) in 2006[5]. The specimens in latter research had been kept in real coastal environment, tidal and submerged conditions. In most researches, durability of concrete has been reported only for submerged, tidal and outdoors conditions. However, there were no reports in atmospheric and splashing conditions. In this research, durability of concrete in splashing and atmospheric conditions has been investigated in addition to submerged, tidal and outdoors conditions.

2. EXPERIMENTAL PROGRAM

2.1. Materials

Cement type 2 and silica fume have been used. The chemical analysis of cement and silica fume is shown in table 1.

Table 1: Chemical analysis of cement and silica fume

Chemical composition (%)	SiO_2	Al_2O_3	Fe_2O_3	MgO	CaO	SO_3	C_3S	C_2S
Cement type 2	21.97	4.62	3.55	2.33	64.56	1.65	50.68	24.76
Silica fume	95.1	1.32	0.87	0.97	0.49	0.1	-	-

Gravel, having the size of 19mm at maximum and sand with a stiffness module of 2.94 were used. Gravel and sand unit weights are 2650, 2560 kg/m^3, respectively. Tap water was used for mixing.

2.2. Mix Proportion, Specimens' Details, Exposure Conditions and Tests

In this research, two water/cement ratios (0.45 and 0.55) and two cement contents (350 and 400 kg/m^3) were selected. Silica fume was used as supplementary cementing material. Expected slump in all mixes gained by adding plasticizer up to 1% of total mass of cementitous material. Concrete mix proportions are shown is Table 2.

Table 2: Concrete mix proportions made (1 m^3)

Abbreviation Symbol	Concrete mix	$\frac{W}{C}$	Weight (kg)				
			Cement type 2	Silica fume	Sand	Gravel	Water
M1	Cement type 2	0.55	350	-	977	825	192
M2	Cement type 2 + 10% Silica fume	0.45	360	40	787	977	180

All specimens were kept in mold for 24 hours, then in tap water in laboratory environment for 72 hours and finally they were moved to different conditions:

- Outdoors: laboratory environment
- Reference environment: pond tap water in the laboratory conditions
- Submerge zone: A pond containing Oroomiyeh Lake water (the water was renewed every month) in the average temperature of 30˚C.
- Tidal zone: Composed of two ponds containing Oroomiyeh Lake water. The water was pumped from the first pond to the second and vice versa. The specimens were on average subjected to 10h of wetting and 14h of drying per 24h. The average pond water temperature was approximately 30˚C.
- Splashing zone: A channel with 10 meters length, 0.7 meters width, 1 meter depth and a wave maker machine capable of making regular waves. This channel contained Oroomiyeh Lake water. The specimens were kept at the still water level to be exposed to the waves and splashes.
- Atmospheric zone: In this simulation, a pump and several nozzles were used to spray water into the system. The specimens were kept at a short distance from nozzles to get more accurate results.

In Table 3, a comparison between the constituents of Oroomiyeh Lake and Persian Gulf water is shown.

Tabel 3: Chemical analysis of Oroomiyeh lake water

	K^+	Ca^{2+}	Mg^{2+}	So_4^{2-}	Na^+	Cl^-
Oroomiyeh lake	1404	1360	12418	22752	86066	143704
Persian Gulf	450	430	1460	2720	12400	21450
Ratio of Oroomiyeh lake water constituents to Persian Gulf's water	3.12	3.16	8.5	8.3	6.9	6.7

The details of specimens and keeping conditions for each test are shown in Table 4.

Table 4: Details and characteristics of specimens and the keeping conditions

Test	Specimens size (cm)	Characteristics	keeping conditions
compressive strength	$10\times10\times10$	-	submerged, tidal, splash, atmospheric and Reference environment
chloride ion concentration	$10\times10\times10$	–	submerged, tidal, splash, atmospheric
corrosion potential and intensity	$10\times10\times20$	2.5 cm concrete cover	submerged, tidal, splash, atmospheric and outdoors
electrical resistivity	$10\times10\times10$	–	submerged, tidal, splash, atmospheric and Reference environment

3. TESTS AND RESULTS

Compressive strength of specimens in different conditions was measured at ages of 28 and 90 days. Furthermore, corrosion potential, reinforcement corrosion intensity and electrical resistivity were measured at different ages and conditions. The half cell apparatus with Ag/AgCl reference electrode was used to measure the rate of corrosion potential [6]. Reinforcement corrosion intensity was also measured by Potentiostat [7, 8]. Electrical resistivity was measured by using Weston (standard) cell [9]. Chloride ion concentration was measured at the age of 3 months used concrete by powder sample from the depth of 2-3 cm and chloride ion (% wt. of concrete) determined.

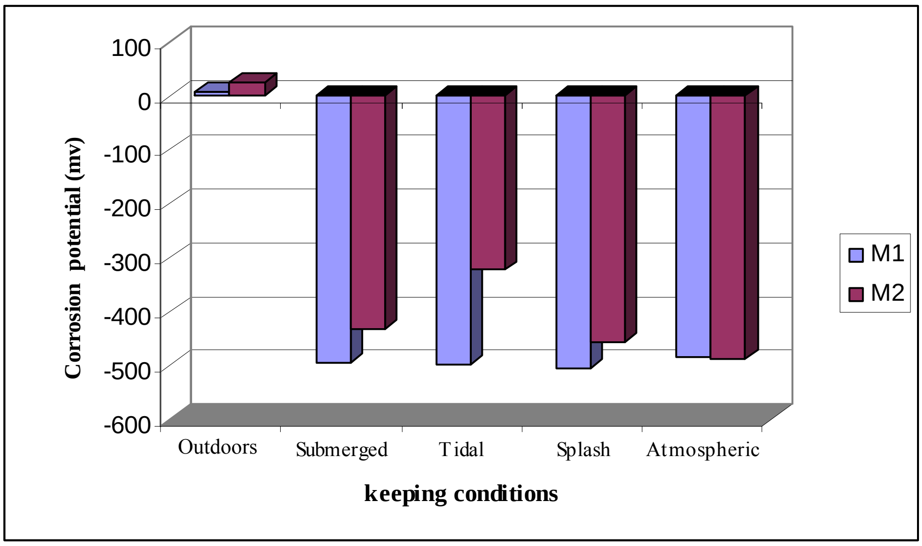

Figure 1. Half cell potential for various mixes in different conditions at the age of 90 days

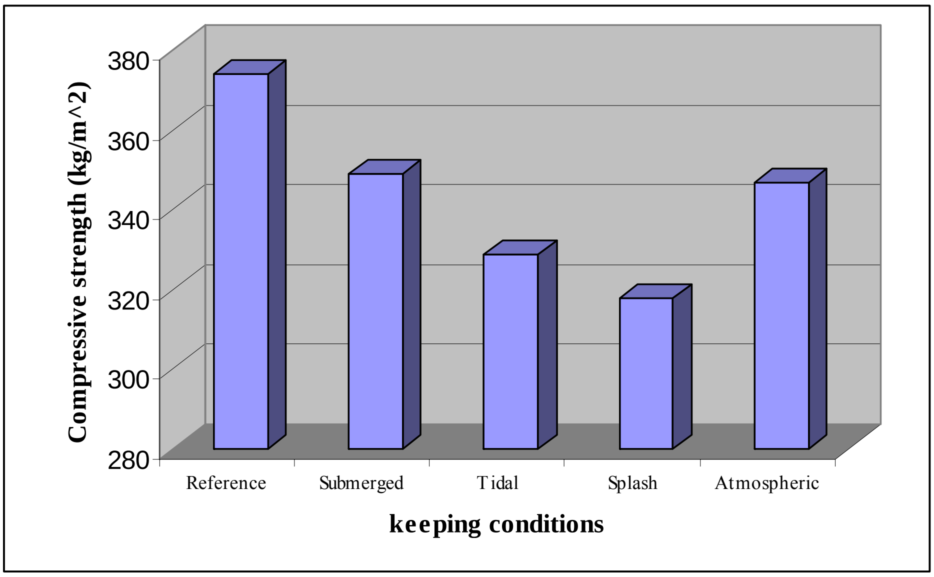

(a)

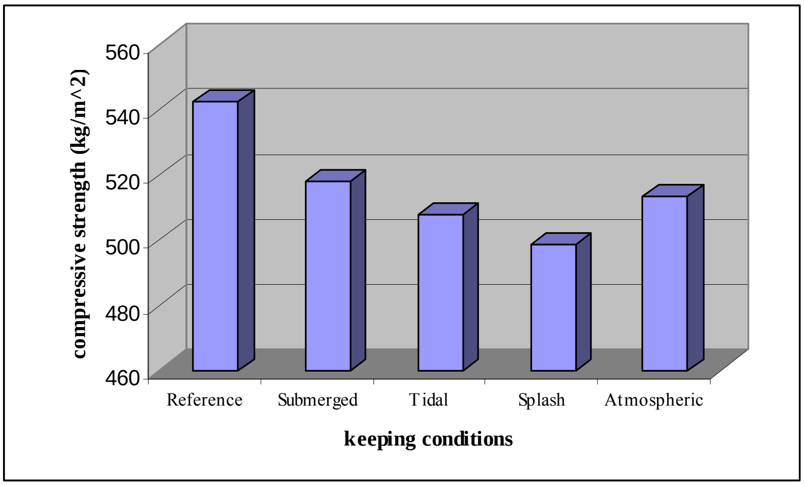

(b)

Figure 2. Compressive strength in different conditions at the age of 90 days for a) M1 mix b) M2 mix

Table 5: Corrosion potential range and corrosion probability based on ASTM-C876 for Ag/AgCl Half Cell [6]

Corrosion potential range	Corrosion probability
≤-84 mv	There is 90% probability that corrosion does not exist.
-234 mv≤ ≤ -84 mv	Corrosion does not exist positively but is absolutely possible
≤-234 mv	There is 90% probability for corrosion

Table 6: Chloride ion (% wt. of concrete) in different conditions at the age of 90 days.

Abbreviation Symbol	Concrete mix	$\frac{W}{C}$	Chloride ion(% wt. of concrete)			
			Submerged zone	Tidal zone	Splash zone	Atmospheric zone
M1	Cement type 2	0.55	0.19	0.25	0.28	0.22
M2	Cement type 2 + 10% Silica fume	0.45	0.11	0.15	0.17	0.13

Table 7: Corrosion current density for various mixes in different conditions at the age of 180 days.

Abbreviation Symbol	Concrete mix	$\frac{W}{C}$	Corrosion current density ($\mu A/cm^2$)			
			Submerged zone	Tidal zone	Splash zone	Atmospheric zone
M1	Cement type 2	0.55	0.839	1.24	1.609	0.95
M2	Cement type 2 + 10% Silica fume	0.45	0.333	0.412	0.423	0.398

Table 8: Corrosion intensity range and its interpretation [8]

Corrosion Current Density($\mu A/cm^2$)	Extent of Corrosion
$I_{corr} < 0.1$	Passive condition
$0.1 < I_{corr} < 0.5$	Low to moderate corrosion
$0.5 < I_{corr} < 1$	Moderate to high corrosion
$I_{corr} > 1$	High corrosion

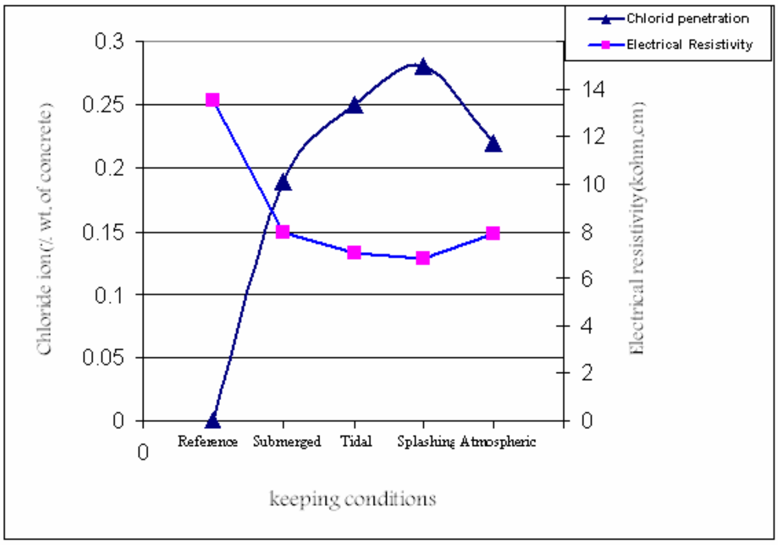

(a)

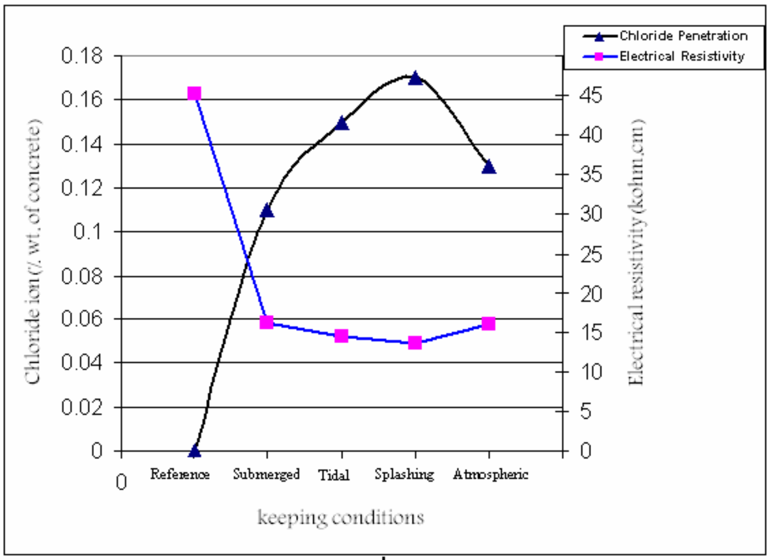

(b)

Figure 3: Chloride ion (% wt. of concrete) and Electrical resistivity in different conditions at the age of 90 days for a) M1 mix b) M2 mix

4. EXPERIMENTAL RESULTS AND DISCUSSION

4.1. Chloride Ion Penetration

For the splashing zone, due to capillary absorption and surface condensation phenomenon, concrete is more prone to be damaged [10].

In the second mix, because of the reduction of water/cement ratio and effects of silica fume on making concrete pores smaller, the rate of chloride ion penetration decreased.

4.2. Corrosion Potential and Intensity

In terms of corrosion, the splashing zone has the worst conditions, by increasing moisture, free chloride ion concrete and enough oxygen, corrosion intensity also increased.

In submerged condition, because of thin air, although corrosion potential of reinforcement was high, the rate of corrosion intensity was low.

4.3. Compressive Strength

Presence of Sulphate (SO_4^{2-}) ion in corrosive environment caused some decreases in compressive strength for all concrete mixes in comparison with reference specimens. Specimens in splashing zone have the highest strength deterioration factor (SDF) because of leach out, efflorescence under cyclic consequence wetting, drying and salt crystallization (which creates internal pressure and causes cracking of concrete).

In the second mix, decreasing of water/cement ratio and using silica fume caused lower SDF [11].

5. CONCLUSION

1. The main reasons of destruction of marine concrete structures are the chloride ion penetration and reinforcement corrosion which result in cracking of concrete.
2. Splashing condition has the highest chloride ion penetration in concrete which decreases electrical resistivity and increases reinforcement corrosion intensity.
3. Specimens in splashing condition have the highest strength deterioration factor.
4. In marine environment, concrete in splashing zone, which is exposed to waves and splashes, is more vulnerable in comparison with other zones and needs special attention in the curing of buildings.
5. In submerged condition, because of thin air, although corrosion potential of reinforcement is high, the rate of corrosion intensity is low.
6. In all specimens kept in various conditions, electrical resistivity was decreased as time passed. This attenuation may result in an increase in corrosion intensity.
7. Comparison between the experimental results shows that reinforcement corrosion intensity reduces in splashing, tidal, atmospheric and submerged condition, respectively.

REFERENCE

1. Allen, R.T.L, "Concrete in coastal structures" , 1998 , Thomas Telford.
2. M.N.Haque, H. Al-Khaiat , B. John , " Climatic zones_ A prelude to designing durable concrete structures in the Arabian Gulf ", Building and Environment journal PP.2410-2416 4 April 2006.
3. Kumar Mehta, "Concrete in the marine environment", 1991.
4. Tarek Uddin Mohammed, Toru Yamaji, Toshiyuki Aoyama, and Hidenori Hamada, " Marine Durability of 15- Year old concrete Specimens Made with Ordinary Portland, Slag and Fly Ash Cements, ACI SP 199-30-2000,PP.451-560.
5. Ramazanianpour, A.A., Parhizkar, T., Pourkhorshidi, R., Raisghasemi, M., "Assessing Concrete Durability with Different Cements and Pozzolans in Persian Gulf Environment", Concrete journal, Research Report, BHRC Publication No. R-434, 2006.
6. ASTM(American Society for Testing and Materials), Standard Test method of Half- Cell Potential of Uncoated Reinforced Steel in Concrete, ASTM C876, ASTM Publication, 1995.
7. A.Benture, S.Diamond and N.S.Berke, "Corrosion of steel in concrete", 1988.
8. Ping Gu, .J.J. Beaudoin, Min-Hong Zhang, and V. M. Malhotra, " Performance of Reinforcing Steel in Concrete Containing silica fume and Blast- Furnace Slage Ponded with Sodium Chloride Solution ", ACI Materials Journal / May-June , 2000.
9. David A. Whiting and Mohamad A. Nagi, "Electrical Resistivity of concrete-A Literature Review ", Portland Cement Association, 2003.
10. Maruya, T.Tangtermsirikui S. "Simulation of chloride penetration in to hardened concrete", Third conment/aui International conference on Durability of concrete, france sp 145-27, 1994, PP.519.
11. R.D.Hootan, "Influence of silica fume replacement of cement on physical properties and resistance to sulfate attack, freezing and thrawing, and alkali-silica reactivity ", ACI Material Journal, March- April, 1993.
12. Troconis de Rincon, M. Sanchez, V. Millano, R. Fernandez,…" Effect of the marine environment on reinforced concrete durability in Iberoamerican countries", Corrosion Science Journal, PP. 2832-2843, 16 March 2007.

CD05-004

CONTRADICTORY EFFECTS OF SILICA FUME CONCRETES IN SULFURIC ACID ENVIRONMENTS

H. Rahmani[1], A.A. Ramazanianpour[2], T. Parhizkar[3], B. Hillemeier[4]
[1]Ph.d candidate, Amirkabir University, Civil Engineering Department, Tehran, Iran
[2]Professor, Amirkabir University, Civil Engineering Department, Tehran, Iran
[3]Assistant Professor, Building and Housing Research Center, Tehran, Iran
[4]Professor, TU Berlin, Institute of Civil Engineering, Berlin, Germany

ABSTRACT
In certain industrial activities sulfuric acid is used during the production process, which may cause degradation of concrete structures. Another important phenomenon where sulfuric acid is responsible for concrete corrosion is biogenic sulfuric acid corrosion, which occurs often in sewer systems. Therefore, researchers used sulfuric acid solutions to simulate of such aggressive environments. Also, they used suitable cement replacement materials such as silica fume to improve acid resistance of concretes. But some researchers reported lowest susceptibility of concrete containing silica fume to corrosion at such environments while the other groups reported unsuitable performance of silica fume.
In this paper, control specimens and specimens containing 8% silica fume as cement replacement materials were immersed in sulfuric acid solutions with pH of 1.0 and 2.0. The dense packing of siliceous aggregates and cementitious materials were used to achieve low porosity concretes. They were periodically examined for appearance and measured for mass change up to 315 days. Total porosity of samples at the age of 90 days was measured. Results show that the porosity plays an important and twofold role in the mass loss of mortar specimens immersed in sulfuric acid solutions. In low pHs such as 1.0 corrosion rate of low porosity concretes is more than that of high porosity concretes. But, in the high pHs such as 2.0 corrosion rate of low porosity concretes is less than that of the high porosity concretes. In the low and high pHs of sulfuric acid solutions internal and external or surface degradations were observed respectively.
Contradictory results were obtained for the concretes containing silica fume because of its effect on the porosity and the production of silica gel at ITZ by reacting of portlandite. Investigations by optical microscopy on thin section samples indicate that the use of silica fume makes mixtures more homogeneous and hence lowers the corrosion rate in sulfuric acid environments.

Keywords: silica fume, sulfuric acid attack, dense concretes, porosity

1. INTRODUCTION
Concrete is the most widely used construction material for sewer structures. However, the environment in some sewer structures can become very acidic due

mainly to formation of sulfuric acid converted from hydrogen sulfide by bacterial action. Significant deterioration of concrete in such harsh environments has been reported all over the world [1,2,3]. Also several reports were published elucidating the mechanisms of concrete deteriorations in sewer environments [4,5,6]. Although, it has been reported that some new materials such as high performance coating, glass fiber reinforced lining, special mortars and high proportions of polymer modified binder can be more acid resistant, but they are too costly for most practical applications [7,8,9]. Therefore, the research on evaluation of acid resistance of normal concretes is still attractive.

It is well known that the porosity of the cement paste is the most important parameter determining mechanical properties and consequently, the durability of the material in the hardened stage. Therefore, information on porosity is a paramount importance for engineering concrete applications. The densest packing of the complete mixture made of aggregates and binder can lead to an extremely high density, low porosity system, and at the same time to the minimum binder content requirement.

In this paper, the dense packing of siliceous aggregates was obtained by replicating ASTM C29 standard test method for the aggregate fractions. The Fuller ideal grading curve for particle size distribution (PSD) of cementitious material including ultra fine filler was used. Finally, the effect of different pHs of sulfuric acid solutions, silica fume and ultra fine filler on resistance of mixtures to sulfuric acid attack were investigated. Sulfuric acid solution with pH of 1.0 and 2.0 were considered to represent the aggressive sewer environments. The pH of 1.0 is widely used in many laboratory tests to investigate the acid resistance of concretes for sewer structures [6,7,10]. But the pH of 2.0 is considered by some researchers to simulate the aggressive environments [11, 12]. Three mixtures including control mixture, mixture containing ultra fine filler and mixture containing 8% silica fume and ultra fine filler were investigated. Mortar and concrete samples were immersed in sulfuric acid solution for over 315 days. Water binder ratio and cementitious material content were considered as 0.42 and 325kg/m^3 respectively. Specimens were regularly investigated by visual inspection of surface deterioration and measuring mass change. Porosity of mortar samples was investigated to find more knowledge about the mechanism of sulfuric acid attack. Also cement matrix and protection layer in samples that is formed during the sulfuric acid attack were investigated by optical microscopy on thin section samples.

2. EXPERIMENTAL PROGRAM

2.1. Materials

The materials used in this investigation were locally sourced and they satisfied the requirements of respective National Standards. Table 1 presents the results for typical chemical compositions of the Type II Portland cement, silica fume, and Quartz powder. The coarse and fine aggregates used in this investigation were 5-20mm and 0-5mm siliceous crushed river gravel and silica river sand respectively. A superplasticizer was used in the concrete mixtures to achieve a slump between 50-100mm.

Table1.Chemical composition of cement, silica fume and Quartz powder

Oxide	CaO	SiO_2	Al_2O_3	Fe_2O_3	SO_3	MgO	$(Na_2O)_{eq}$
Cement	62.94	21.1	5.05	3.08	1.5	3.4	0.87
Silica fume	1.02	95.1	0.6	1.1	1.2	0.6	-
Quartz powder	1.05	96.45	1.08		-	0.5	-

2.2. Material Proportions
2.2.1. Aggregates
Aggregates take up 60-90% of the total volume of concrete. Proper selection of aggregate type and particle size distribution affects the main properties of concrete such as workability, mechanical strength, permeability, durability and the total cost of hardened concrete. High density along with low specific surface of aggregates is used to achieve minimum cement consumption and low porosity concrete production by replicating ASTM C29 standard test method. Process of aggregate proportion selection was published in the previous works [13-16]. Grading curve of selected aggregates and BS standard limits are shown in Figure 1.

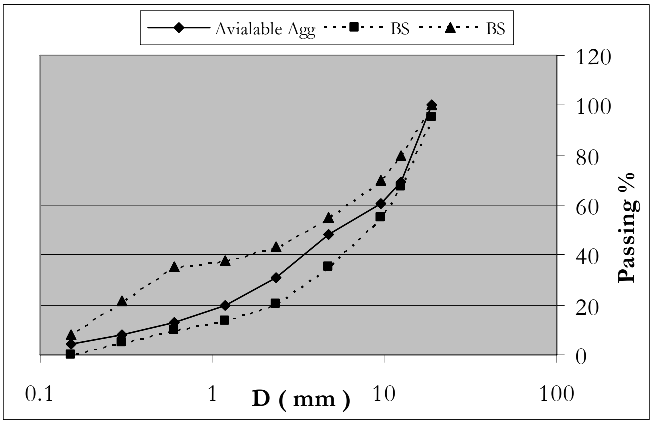

Figure 1. Grading curve of aggregates and BS standard limits.

2.3. Quartz Powder Content
It is well known that porosity has an important role on many properties of concrete such as strength, permeability and durability. To obtain a dense structure in the hardened mortars, the density of dry binder should be maximized [17]. The packing density of the commercial cement powder is relatively low because of its narrow PSD obtained through a closed-circuit grinding process. It could be demonstrated mathematically that the cement powder lacks the section of super fine particles compared with the dense packing powder [18, 19]. In order to achieve the dense packing powder in the cementitious material, a very fine Quartz powder as a filler with particle size between 0-16 microns was added to the cementitious material. Proportion of super fine Quartz powder (k) was calculated from optimization of

followed objective function:

$$F = \sum_{i=1}^{n} \left[U_1(D_i) - \left((1-k) U_2(D_i) + k U_3(D_i) \right) \right]^2 \tag{1}$$

Where n: is the number of sieves, $U_1(D_i)$: is the PSD of ideal grading curve according to Fuller ideal curve by $n = 0.38$, $U_2(D_i)$: is the PSD of cementitious material and $U_3(D_i)$: is the PSD of ultra fine filler or Quartz powder. Optimization process has been published elsewhere [13, 14]. Results indicated that the use of 22% and 13.7% ultra fine filler in the second and third mixtures could lead to the production of low porosity concretes. Exception was the control concrete mixture which had no filler addition. Quartz powder was used as aggregate replacement in the second and third mixtures.

2.4. Preparation of Test Specimens

Three concrete mixtures were designed with constant cementitious material contents and water binder ratios to investigate their mechanical properties and resistance in sulfuric acid solution with pH of 1.0 and 2.0. Water binder ratio and cementitious material content were considered 0.42 and 325kg/m^3 respectively. Mixture proportions are shown in Table 2. Mortar plates (10×10×2cm) and concrete cubes (10×10×10cm) were cast from each mixture according to ASTM C192 test method. In addition, mortar prisms (4×4×16cm) and concrete cubes (10×10×10 cm and 15×15×15cm) were cast for flexural, compression and water permeability tests respectively. All mortars were obtained by sieving concretes using No. 4 sieve. After 24 hours, specimens were demoulded and cured up to 28 days in the control room. Some specimens remained in the control room up to 90 days for flexural, compression and water permeability tests. The samples were then immersed in acid solution for a period of 315 days. Specimens were periodically washed during the test period and then their mass changes were measured. All measurements were carried out at the saturated surface dry condition (SSD).

Table 2. Mixture proportions

Mixture	W/C	Cement (kg)	Silica fume (kg)	Trass (kg)	Pumice (kg)	Filler (kg)	Sand (kg)	Gravel (kg)
C_1	0.42	325.0	---	---	---	---	889.4	1019.9
C_2	0.42	325.0	---	---	---	71.5	852.7	977.70
C_3	0.42	299.0	26	---	---	44.5	863.4	990.00

2.5. Sulfuric Acid Solution

The ASTM C267 test method was modified to investigate mortars and concretes in sulfuric acid solution. A sulfuric acid solution with pH of 1.0 and 2.0 were chosen to simulate the aggressive environment of sewer structures. The pH of sulfuric acid solution was kept constant in the range of 0.97 to 1.07 for pH of 1.0 and 1.87 to

2.23 for pH of 2.0 by adjusting the pH weekly using 98% sulfuric acid. All specimens were continuously immersed in monthly refreshed sulfuric acid solution during the test period. Test setup is shown in Figure 2.

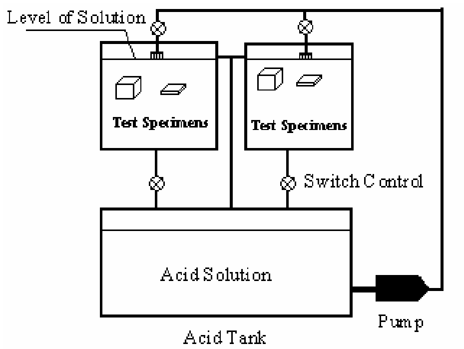

Figure 2. Test setup for simulation of sewer structures

3. TEST RESULTS AND DISCUSSIONS

3.1. Air Content, Water Absorption and Water Penetration Depth

Air content of fresh concrete, half an hour and 24 hour water absorption at the age of 28 days and water penetration depth of hardened concretes at the ages of 28 and 90 days were measured according to ASTM C231, BS1881-122, ASTM C642 and DIN 1048 test methods, respectively. Test results are summarized in Table 3. Selection of dense packing aggregate proportions decreased the air content, water absorption and water penetration depth of the control mixture in comparison with the plain concretes. Utilization of ultra fine Quartz powder that improves PSD of cement decreases the air content, water absorption and water penetration depth of the second mixture (C_2) when compared with the control one. In addition using silica fume that improve the interfacial transition zone (ITZ) decrease the above parameters in comparison with the second mixture (C_2). The dense packing of aggregates and dry binder seems to disconnect the capillary pores. Disconnection of voids in the C_2 and C_3 mixtures seems to be greater than the control mixture due to the usage of ultra fine filler and silica fume.

Table 3: Air content of fresh concrete, water absorption and water penetration depth (WPD)

Mixture	W/C	Cementitious material (kg)	Air content %	Water Absorption Half hour (%)	Water Absorption 1 day (%)	WPD (28 days) mm	WPD (90 days) mm
C_1	0.42	325	2.8	1.72	5.55	8	7
C_2	0.42	325	2.0	1.49	4.07	3	2-3
C_3	0.42	325	1.5	1.62	4.01	0	0

3.2. Mechanical Properties of Concretes and Mortars

Compressive and flexural strengths test results for concrete mixtures under standard curing conditions are shown in Figure 3 and 4. Higher compressive strengths with low cementitious material content (325kg/m^3) are due to the dense packing of aggregates. Flexural strength of the third mixture or C_3 at the age of 28 days is higher than other mixtures because of the high pozzolanic activity of silica fume. Also, higher compressive and flexural strengths of control mixture were probably obtained due to low porosity production (see Table 4). Total porosity of mixtures containing ultra fine filler is more than the control mixture probably due to satisfactory compaction of control mixture. Therefore, compressive and flexural strengths of these mixtures were less than the predicted values.

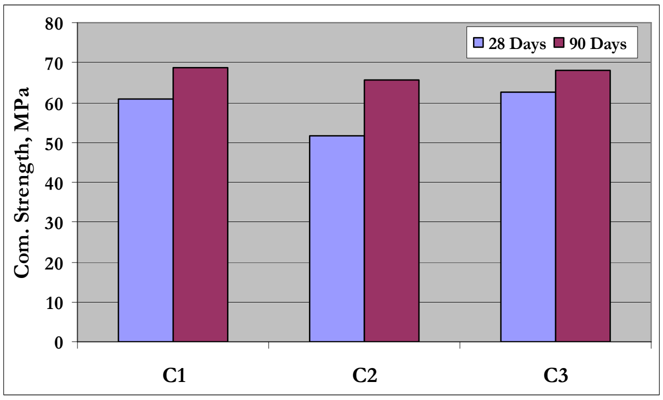

Figure 3. Compressive strength of concrete mixtures

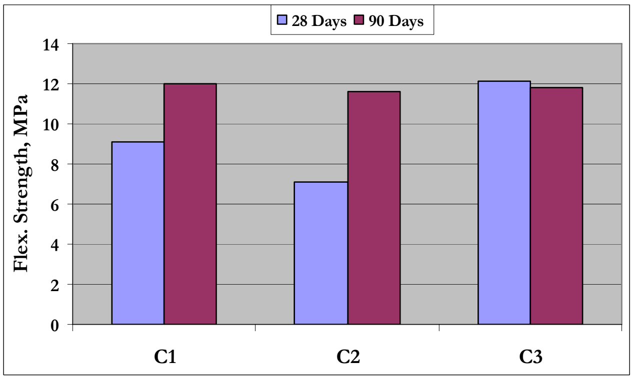

Figure 4. Flexural strength of mortar prisms

3.3. Acid Attack Test Results

3.3.1. Visual Inspection of Mortar and Concrete Specimens

During the immersion period in sulfuric acid solutions, the samples were periodically retrieved from the acid solutions for measurements and visual inspection of the surface appearance. At the early age of immersion, surface of specimens changed to white and yellow color for specimens subjected to sulfuric acid solution with pH of 1.0 and 2.0 respectively as shown in Figure 5. Then, softening of the cement matrix due to excessive expansion and dissolution was also observed during visual inspections of the concrete and mortar samples. The expansions of mortar and concretes were increased by exposure of aggregates. Typical surface appearances of concrete cubes after 3 and 6 months immersion in sulfuric acid solution with pH of 1.0 are shown in Figure 6. After 3 months of immersion, it is clearly seen that the control concrete (C_1) containing Portland cement has suffered the most severe damage with exposure of coarse aggregates and significant loss of cement mortar at all external surfaces. For C_2 and C_3 concrete mixtures, the acid affects the edges, corners, and part of the surfaces of the specimens. After 6 months immersion, surfaces of the mixtures were corroded by acid with exposure of aggregates. After 315 days immersion, all specimens were corroded at different depths. It should be noted that, there is a tan layer between corroded and uncorroded concrete which is more resistant to acid (see Figure 10). Apparently this protective layer is formed near the surface of specimens subjected to sulfuric acid solutions with pH of 2.0. Also, typical surface appearances of mortar plates after 2 and 6 months immersion in sulfuric acid solution with pH of 2.0 are shown in Figure 7. After 2 months immersion, all mortar plates have suffered damage with exposure of aggregates and significant loss of cement mortar. After 6 months immersion, C_1 mixture performed better when compared with other mixtures.

Figure 5. Mortar plates of C_2 mixture after 1 week immersion in sulfuric acid solutions with pH of 1.0 and 2.0

C_1 ***C_2*** ***C_3***

Figure 6. Concrete cubes after 3 and 6 months immersion in sulfuric acid solution with pH of 1.0

Figure 7. Mortar plates after 2 and 6 months immersion in sulfuric acid solution with pH of 2.0

3.4. Mass Change Measurement

The mass change of a sample as a percentage of the initial mass is a widely used indicator for assessment of the deterioration of concrete subjected to acid attack. In this investigation the initial mass of samples was determined under saturated surface dry (SSD) conditions at the age of 28 days. Then, the specimens were immersed in sulfuric acid solutions. The measurements of mass change of samples at SSD condition were taken weekly within the first and second months and monthly afterwards until 11 months except for the third, fifth and seventh week and eighth and tenth month. During measurement, the samples were rinsed with tap water, brushed gently with a plastic brush to remove loose particles and then measured for their SSD masses. Test results of mortar and concretes in sulfuric acid solution with pH of 1.0 are shown in Figure 8. Also weight loss of mortar plates in sulfuric acid solution with pH of 2.0 is shown in Figure 9. As shown in Figure 8, the control concrete or C_1 samples showed mass gain over the first 14 days immersion in the acid solution. But, the C_2 and C_3 concrete mixtures had net mass gains over 45 days after immersion. In the mortar specimens, mass loss of C_1 begins after 14 days immersion. However, mass loss of C_2 and C_3 begins after 30 days immersion. Deterioration of mortar specimens is higher than the concrete samples because of their low thicknesses and higher cementitious material contents. Also, mass loss of the control mixture or C_1 in the concrete and mortar specimens is higher than the other mixtures. After 315 days immersion, the C_1 to C_3 concrete specimens showed a reduction in mass loss of about 31,9%, 30,1% and 30,6%, respectively. However 69.1%, 64.0% and 57.2% mass reduction in the mortar specimens after 7 months immersion were observed respectively. Some of the mortar specimens after 7 months immersion were failed. Therefore, based on visual inspections and weight loss test results, it can be seen that the usage of silica fume and ultra fine filler may enhance the service life of concretes against high concentration of sulfuric acid solutions.

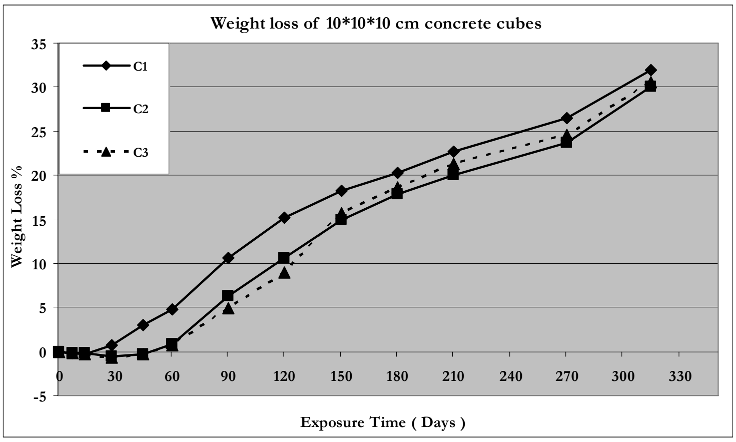

(a)

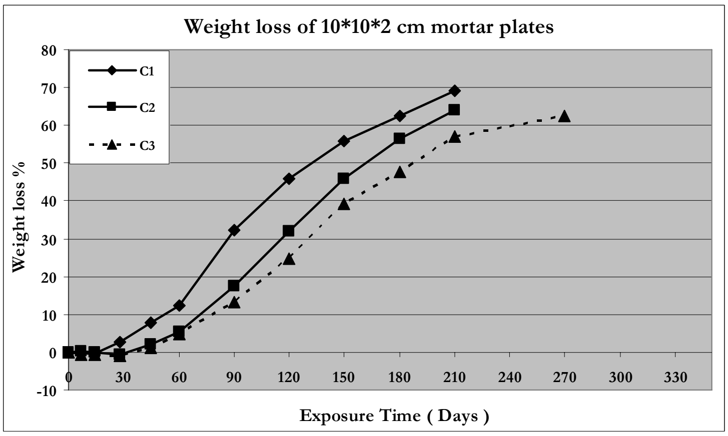

(b)

Figure 8. Weight loss of samples after 315 days immersion in pH of 1.0 a) concrete cubes b) mortar plates

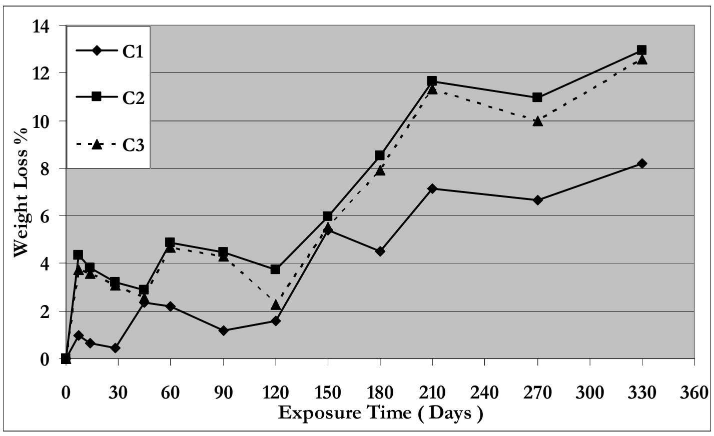

Figure 9. Weight loss of mortar samples after 11 months immersion in pH of 2.0

But, performance of mortars in sulfuric acid solutions with pH of 2.0 is quite different. The control mixture that had the worst performance in the sulfuric acid solution with pH of 1.0 showed minimum weight loss at about 8.2%. The C2 and C_3 specimens showed a reduction of about 12.9% and 12.6% respectively. Based on visual aspects and weight loss test results, mechanism of sulfuric acid attack with different pHs is different. Therefore, micro structural analysis should be carried out on the samples for further clarifications.

Figure 10. Tan layer formation between corroded and uncorroded concrete in mixture

3.5. Micro Structural Analysis

3.5.1. Porosity Study

Mortar samples were taken from freshly broken prisms after 90 days curing in control room. Samples dried at $105^{\circ c}$ until mass stabilization and then their total porosity were measured by using following equation:

$$P_t = \left(1 - \frac{\rho}{\rho_0}\right) \times 100\% \qquad (2)$$

Where, ρ and ρ_0 are dry bulk and solid phase densities and P_t is the volume percent of total porosity. Test results are summarized in Tab. 4. Also, total porosity of C_1 and C_2 samples that is measured by mercury porosimeter is shown in Tab. 4. Comparison of total porosity that is measured by mercury porosimeter with total porosity obtained according to equation (2) indicates that the compaction of control mixture was satisfactory. Also, actually porosity plays a twofold role in sulfuric acid attack to concrete. When a sulfuric acid solution with low pHs such as 1.0 attacks the concrete with low porosity or dense concrete, the dense structure prevents the absorption of acid by the concrete. Consequently the acid reacts with the cement paste at the narrow depth of concrete causing significant degradation due to expansion of gypsum or ettringite. For high porosity concretes, owing to a more porous structure, concrete absorbs the acid which reacts with hydration products to form gypsum and ettringite, which would fill the pores of the concrete, and create a protective layer. This layer forms within the depth of specimens between corroded and uncorroded concrete causes reduction in chemical reactions (see Figure 10). Thus the depth of degradation which is a function of exposure time, pH of sulfuric acid solution and mixture parameters should be investigated separately.

Table 4: Total porosity of mixtures after 90 days curing

Samples ID	ρ (g/cm^3)	ρ_0 (g/cm^3)	P_t $Vol.\%$	P_t %, Mercury porosimeter
C_1	2.23	2.557	12.8	10.4
C_2	2.17	2.586	16.1	10.1
C_3	2.17	2.632	17.6	-

Also, this layer formed near the surface of specimens in low porosity concretes and deteriorated at a shorter time. Therefore, based on test results, using an air-entraining agent could improve the resistance of concretes against sulfuric acid solutions with low pHs as was investigated in the literature [20]. Also, improvement of concrete resistance against sulfuric acid by increasing of water to cement ratio have been reported by several researchers without investigation of corrosion depth [13,21,22]. However, in case of higher pH of sulfuric acid solutions such as 2.0, sulfuric acid solutions couldn't penetrate in the depth of concretes owing to low concentration of sulfate ions. Consequently the acid reacts with the cement paste at the narrow depth or surface of concretes in both low and high porosity concretes causing degradation. Surface of high porosity concretes is more than that of low porosity concretes. Therefore corrosion rate of high porosity concretes is higher than that of low porosity concretes. Therefore, based on twofold effect of porosity against sulfuric acid solutions, contradictory effect of silica fume could be elaborated.

3.6. Investigate of Samples by Optical Microscopy

Mixture characteristics, Thickness of tan layer that is formed during the sulfuric acid attack between corroded and uncorroded concrete and products of degradation were investigated on thin sections using transmitted light microscopy. Mortar samples were taken from freshly broken prisms after 315 days immersion in sulfuric acid solution with pH of 1.0. Effect of ultra fine filler and silica fume on portlandite consumption which resulted in homogeneous mixtures is shown in Figure 11. Comparison of cement matrix of C_2 with control mixture indicates that the mixtures containing ultra fine filler is more homogeneous than that of the control mixture. Also using silica fume reduces calcium hydroxide content. In Figure 12, typical micrographs of transmitted light microscopy on thin section samples of C1 and C_3 mixtures in the corroded area are shown. Also, average thickness of tan layers measured by optical microscopy is summarized in Table 5. It is clearly seen that the thickness of the tan layer depends on the cementitious materials composition. In other words, a corrosion rate depends on stiffness of cement matrix. Usage of silica fume increases the thickness of tan layer owing to silica gel formation in the ITZ. Gypsum is observed in all samples in front of the tan layer as a product of degradation (see Figure 12). Based on Figure 8, Table 4 and 5, weight loss of high porosity concretes begins at the later ages, but corrosion depth of high porosity concretes is probably more than that of the low porosity concretes.

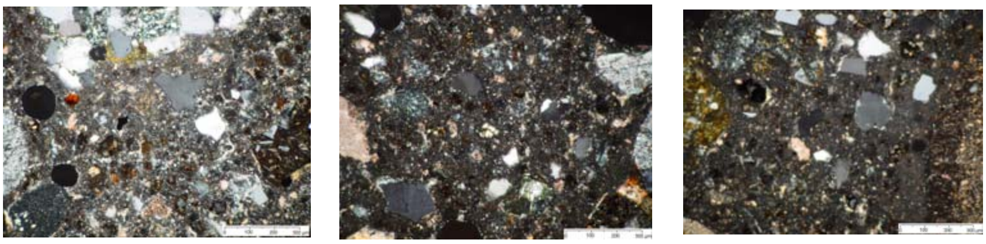

C_1 C_2 C_3

Figure 11. Cement matrix of different mixtures

Table 5. Thickness of tan layer for different mixtures

Mixture code	C_1	C_2	C_3
Thickness of tan layer (μm)	200	200	290

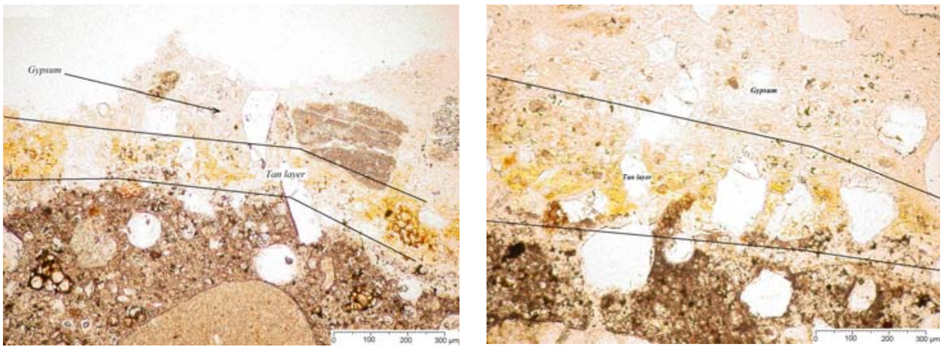

C_1: 200 μm **C_3: 290 μm**

Figure 12. Thickness of tan layer in C_1 and C_6 mixtures

4. CONCLUSIONS

Based on the test results, the following observations and conclusions are drawn:

1. Using an ideal aggregate grading decreases the porosity of mortars and concretes and increases their durability.
2. Most properties of concretes containing ultra fine filler such as compressive and flexural strengths, density, air content of fresh concrete and porosity were further improved.
3. Porosity plays a twofold role in different concentration of sulfuric acid solutions. External and internal corrosion was observed for high and low concentration, respectively.
4. For high concentration of sulfuric acid solutions that is caused internal corrosion, higher porosity concretes showed less mass loss. But, their

corrosion depths should be investigated separately.
5. Utilization of ultra fine Quartz powder reduces porosity and hence increasing the resistance of concretes against sulfuric acid attack.
6. Utilization of silica fume prepared with an ideal grading curve of the cementitious materials improved the durability of concretes in sulfuric acid environments.
7. Corrosion rate varies with variation in micro structure of cement matrix.
8. Gypsum is observed in all specimens subjected to sulfuric acid solutions with pH of 1.0 as a product of degradation.
9. Application of ideal grading curve for cementitious materials enhances the homogeneity of the mixtures.

REFERENCES

1. Parker, C., the Corrosion of Concrete Isolation of a Species of Bacterium Associated with the Corrosion of Concrete Exposed to Atmospheres Containing Hydrogen Sulphide", Aust J Exp Biol Med Sci, 23 (3) pp.14-17, 1945.
2. Mori, T., Nonaka, T., Tazaki, K., Koga, M., Hikosaka,Y., Noda,S.," Interaction of Nutrients, Moisture and pH on Microbial Corrosion of Concrete Sewer Pipe", Water Research, 26 (1), pp.29-37, 1992.
3. Saricimen, H., Maslehuddin, M., "Case Study of Deterioration of Concrete in Sewerage Environment in an Arabian Gulf Country", Durability of Building Materials, 5, pp.145-154, 1987.
4. Zivica, V., Bajza, A., "Acidic Attack of Cement Based Material – a Review. Part 1 Principle of Acidic Attack", Construction and Building Materials, 15, pp.331-340, 2001.
5. Monteny, J., Belie, N.D., Vincke,E., Verstraete,W., Taerwe,L., "Chemical and Microbiological Tests to Simulate Sulfuric Acid Corrosion of Polymer-Modified Concrete", Cement and Concrete Research, 31, pp. 1359-1365, 2001.
6. Monteny, J., Vincke, E., Beeldens, A., Belie, N.D., Taerwe, L., Gemert, D.V., Verstraete,W., "Chemical, Microbiological, and in situ Test Methods for Biogenic Sulfuric Acid Corrosion of Concrete", Cement and Concrete Research, 30 , pp. 23-634, 20006.
7. Saricimen, H., Shameem, M., Barry, M.S., Ibrahim, M., Abbasi, T.A., "Durability of Proprietary Cementitious Materials for use in Wastewater Transport Systems", Cement and Concrete Composites, 25, pp. 421-427, 2003.
8. Vipulanandan, C., Lium,J., "Glass-Fiber Mat Reinforced Epoxy Coating for Concrete in Sulfuric Acid Environment", Cement and Concrete Research, 32, pp.205-210, 2002.
9. Vincke, E., Wanseele, E.V., Monteny, J., Beeldens, A., Belie, N.D., Taerwe, L., Gemert, D.V., Verstraete, W., "Influence of Polymer Addition on Biogenic Sulfuric Acid Attack of Concrete", International Biodeterioration & Biodegradation, 49, pp. 283-29, 2002.
10. Chang, Z.T., Song, X.J., Munn, R., Marosszeky, M., "Using Limestone Aggregates and Different Cement for Enhancing Resistance of Concrete to

Sulfuric Acid Attack", Cement and Concrete Research, 35, pp. 1486-1494, 2005.
11. Hewayde, E., Nehdi, M., Allouche, E., Nakhla, G., Effect of Mixture Design Parameters and Wetting-Drying Cycles on Resistance of Concretes to Sulfuric Acid Attack, Journal of Materials in Civil Engineering, Vol. 19, No. 2, pp 155-163, February 2007.
12. Hillemeier, B.H.A., "High Performance concrete Specialized for Acid Resistance", 1st International Conference on Concrete & Development, 30April-2May, Tehran, Iran, 2001.
13. Rahmani, H., Ramazanianpour, A. A.,"Effect of Binary Cement Replacement Materials on Sulfuric Acid Resistance of Dense Concretes", Magazine of concrete research, Vol. 60, No. 2, March 2008, pp. 145-155.
14. Rahmani, H., Ramazanianpour, A. A.," Effect of Silica fume and Natural Pozzolanas on Sulfuric Acid Resistance of Dense Concretes", Asian Journal of Civil Engineering (Building and Housing), Vol. 9, No. 3, 2008, pp. 245-261.
15. A.A.Ramezanianpour, H.Rahmani,"Low Porosity Concretes for Sulfuric Acid Attack", third international symposium on sustainability in cement and concrete, 21-23 May, Istanbul, Turkey, 2007.
16. Ali A. Ramzanianpour, Hamid Rahmani," Effect of Silica fume and Ultra Fine Filler on Acid Resistance of Concrete", Iranian Corrosion/ICA International Congress, 14-15 May; Tehran, Iran, 2007.
17. Lange,F., et al, "Dense Packing of Cement Paste and Resulting Consequences on Mortar Properties", Cement and Concrete Research, Vol. 27, No 10, pp 1481-1488, 1997.
18. Niu, Q., "Effect of Superfine Slag Powder on Cement Properties", Cement and Concrete Research, Vol32, pp 615-621, 2002.
19. Dinger, D. R., Funk, J. E., "Particle-Size Analysis Routines Available on Cerabull", American Ceramic Society Bulletin, Vol. 68, No. 8, pp 1406-1408, 1989.
20. Safwan, A. K, Abouzeid, M. N., Jane, M. A., " Response of Air-Entrained Concrete to Severe Chemical Aggression", Journal of Materials in Civil Engineering, Vol. 18, No. 1, pp 155-163, February 2006.
21. Hewayde,E.,Nehdi,M.,Allouche,E.,Nakhla,G.," Effect of Mixture Design Parameters and Wetting-Drying Cycles on Resistance of Concretes to Sulfuric Acid Attack", Journal of Materials in Civil Engineering, Vol. 19, No. 2, pp 155-163, February 2007.
22. Fattuhi, N. I., Hughes, P. B.," Ordinary Portland Cement Paste and Concrete Subjected to Sulfuric Acid attack", Cement and Concrete Research, Vol. 18, No 4, pp 545-555, 1988.

CD05-005

THE ANALYSIS OF CHLORIDE DIFFUSION COEFFICIENT IN CONCRETE BASED ON NEURAL NETWORK MODELS

A. Delnavaz[1], A.A. Ramezanianpour[2], H.R. Ashrafi
[1]Ph.D. Candidate, Dept. of Civil Engineering, Amir Kabir University of Technology, Tehran, Iran
[2]Professor, School of Civil Engineering, Amir Kabir University of Technology, Tehran, Iran

ABSTRACT
Chloride diffusion is one of the major causes of deterioration of concrete structures. A large amount of research has been conducted to study the chloride diffusion of concrete, both experimentally and theoretically. Because chloride diffusion experiments are time consuming, it is desirable to develop a model to predict the chloride profiles in concrete. This paper studies the feasibility of using a neural network as an adaptive synthesizer as well as a predictor to meet such a requirement.

So some neural network models to predict chloride diffusion coefficient were made. The models were trained by results of chloride profile experiments. Input parameters were water to binder ratios, the amount of silica-fume and environmental condition of samples. The output parameter was chloride diffusion coefficient.

Neural network models are multi layer Perspetron models and they differ in the number of hidden layers and neurons. To control the accuracy of the model, an ANNs model was made and the result of the model was compared with test specimens. The result demonstrates that both neural network models have the ability of predicting the chloride diffusion coefficient with good accuracy.

Keywords: neural network model, chloride diffusion coefficient

1. INTRODUCTION
Steel reinforced concrete is one of the most durable and cost effective construction materials. The durability of reinforced concrete depends on the surrounding environment and exposure conditions, including the factors such as carbonation, corrosion, alkali-slices reaction and freezing/thawing [1,2]. Corrosion of reinforced steel resulting from the ingress of chloride ion is one of the most important issues concerning the durability of concrete structures. The prevention of reinforcement corrosion is primarily in the design stage with the use of high quality concrete and adequate cover. It is well known that steel is protected from corrosion by a microscopically thin oxide layer (Passive film: γ-Fe_2O_3-H_2O) that is formed in the highly alkaline condition of concrete pore solution. This protective film suppresses the iron dissolution to negligibly low values and furthermore, this oxide is insoluble and highly stable [3]. Corrosion occurs by loss of the alkalinity of concrete in the form of carbonates, thereby providing a direct route for chlorides to

approach the reinforcing steel and prevent re-passivation reaction that leads to pitting corrosion [4].Carbonates, chlorides and sulphates media can be found in concrete when using contaminant aggregate, or adding $CaCl_2$ during the mixing step or they are found under the effect of sea-water or ground water on concrete and they can also result from an attack on concrete by the surrounding environment in coastal regions. Carbonation destroys the protective oxide layer presented on the surface of embedded steel in concrete leading to corrosion. As the corrosion of embedded steel continues, the products formed exert enormous stress on the surrounding concrete leading to cracking and later sapling of the concrete. These stresses have been reported to be as high as 450 Mpa [5]. Methods of corrosion control include cathodic protection, surface treatments of the rebar and the use of admixtures in concrete [6]. Use of blended cements incorporating supplementary cementing materials such as silica-fume, blast furnace slag, fly ash or natural pozzolan, is a solution that leads to mixtures with greater resistance against chloride [7].

There are a number of computational analysis techniques that deal with concrete [8-12]. One of the most known techniques is artificial neural network (ANNs) [13, 16]. Topcu and Sndemire [17] that used ANNs and Fuzzy logic for prediction of mechanical properties of recycled aggregate concretes containing silica fume. They obtained successful simulation result from both ANNs and fuzzy logic. Altun et al. [18] used ANNs for predicting the compressive strength of steel fiber added lightweight concrete and they compared ANN result with multi layer regression technique results. They concluded that ANNs predicts the compressive strength of steel fiber added lightweight concrete more accurately than multi layer regression. Sakla and Ashour [19] predicted tensile capacity of single adhesive anchors using ANNs. They concluded that ANN is a useful technique for predicting of tensile capacity of adhesive anchors. Since ANNs has taken into account nonlinear transfer functions, they can automatically consider the nonlinear relations between the data. Hence better prediction results than other statistical tools can be obtained in general. Topcu et al. [3] used ANNs to model corrosion currents of reinforced concrete. They used two types of cement and 3 different ratios of fly ash for their modeling. Their Ann model produced close prediction current values to currents measured in experiment. They concluded that ANN is an appropriate tool for modeling the corrosion currents. Parichatprecha, and Nimityongskul.[20] used ANNs to durability analysis of high performance concretes. Their results indicated that the ANN models can be used to efficiently predict the chloride ions permeability across a wide range of ingredients of HPC. Based on the simulated total charge passed model, built using trained neural networks, they also concluded that the optimum cement content for the design of HPC in terms of total charge passed ranges from 450 to 500 kg/m3.

The aim of this study is to construct an ANNs model to investigate the influence of mix proportion parameters on the resistance of chloride ion penetrability on concretes containing silica-fume. For this purpose, data for developing the neural network model are collected from the experiments. The design of the experimental program is based on the relevant parameters, namely W/B, cement content, silica fume content and some experimental data.

2. ARTIFICIAL NEURAL NETWORKS

Artificial neural networks are computing systems that simulate the biological neural systems of the human brain. They are based on a simplified modeling of the brain's biological functions exhibiting the ability to learn, think, remember, reason, and solve problems. Conceptually, a neural networks model consists of a set of computational units and a set of one-way data connection joining units or weights as shown in Figure 1.

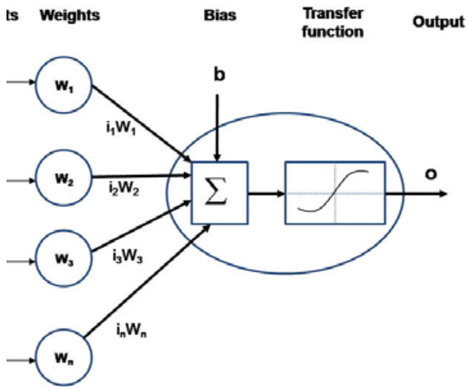

Figure 1. Single processing element of ANNs

Units that receive no input from others are called input nodes, while those with no outgoing links are called output nodes. All other intermediate units are called hidden nodes. The multi-layered model has several layers, and each layer consists of numerous neurons which are connected with each other. In this model, information is sent from input layer to output in one direction, and learning is preceded so as to minimize the difference between the output of the model and the target output. ANNs can solve challenging problems of interest to computer scientists and engineers such as pattern classification, categorization, function approximation, prediction and forecasting, optimization, content-addressable memory, and control robotics. Rumellhart et al. [21] developed a method called error back-propagation, or more simply back-propagation, for learning associations between input and output patterns using more than the two layers of Rosenblat's original perceptron. Back-propagation is a supervised learning technique that compares the responses of the output units to the desired response, and readjusts the weights in the network so that the next time when the same input is presented to the network, the network's response will be closer to the desired response. Errors that arise during the learning process can be expressed in terms of mean square error (MSE) and are calculated using Eq. (1).

$$MSE = \left(\frac{1}{p}\right) * \sum_{j} \left(t_j - \sigma_j\right)^2 \qquad (1)$$

In addition, the absolute fraction of variance (R^2) and mean absolute percentage error (MAPE) are calculated using Eqs. (2) and (3), respectively.

$$R_2 = 1 - \left(\frac{\sum_j (t_j - \sigma_j)^2}{\sum_j (\sigma_j)^2} \right) \tag{2}$$

$$MAPE = \frac{1}{p} \sum_j \left(\left| \frac{\sigma_j - t_j}{\sigma_j} \right| * 100 \right) \tag{3}$$

where t_j is the target value of j_{th} pattern, σ_j is the output value of j_{th} pattern, and p is the number of patterns.

3. EXPERIMENTAL STUDIES

3.1. Materials Used

3.1.1. Cement and silica-fume

In experimental studies, the CEM I 425 R Portland cement which is produced by Tehran cement factory were used.

3.1.2. Aggregates

Crushed sand and crushed stone aggregates were used. The maximum particle size of aggregates is 20 mm. As a result of the experiment, the specific gravities of sand and crushed stone are obtained as 2.62 and 2.71 kg/dm^3, respectively.

3.2. Mix Proportions

Cement type I.425 was used in concrete mixtures. Concretes are produced using 0, 7 and 10% replacement level of SF by weight of cement. These specimens were cured at 28, 90 and 270 days. The amounts of materials used in 1 m^3 concrete are given in Table 1.

Table 1: Mix design of specimens

Specimen code	W/B	csf/(c+csf)*	sand	gravel
M-35-0	0.35	0	800	1050
M-35-7	0.35	7	800	1050
M-35-10	0.35	10	800	1050
M-40-0	0.4	0	800	1050
M-40-7	0.4	7	800	1050
M-40-10	0.4	10	800	1050
M-50-0	0.5	0	800	1050
M-50-7	0.5	7	800	1050
M-50-10	0.5	10	800	1050

***csf : content of silica-fume in concrete**

4. EXPERIMENTAL PROGRAM AND DATA COLLECTION

The first step in developing the network is to obtain good and reliable training and testing examples. To obtain the data for developing the neural network models, different experiments were done on specimens. The aim of these experiments was to find a relationship between mix design and chloride diffusion coefficient in concrete. For this reason, the specimens were exposed to chloride in 3 different conditions for more than 270 days. The environmental conditions were submerge, tidal and atmospheric zone. Persian Gulf modeling room of Building and Housing Research Center (BHRC) was used to model the mentioned environment. In addition to this experiment, RCPT, concrete compressive strength and water permeability of concrete under pressure were done to find a relationship between concrete durability contents and chloride penetration coefficient. Results of experiments can be finding in ref. [22].

4.1. Variables Selected for Neural Networks

Considering the environmental conditions at the construction sites and in order to find the important variables that might strongly affect the chloride diffusion coefficient, 7 different ANNs were selected with different input variables and hidden layers. 1 variable was chosen as the desired output. Table 2 gives the list of the ANNs inputs and outputs. In this study, the neural networks were developed and performed under MATLAB programming. The learning algorithm used in the study was gradient descent with adaptive learning rate back-propagation, a network training function that updates weight and bias values according to gradient descent with adaptive learning rate [21]. The error incurred during the learning process was expressed in terms of mean-squared-error (MSE).

Table 2: Input and output parameters of ANNs

Code	Input				Output		Number of Data
	W/B	SF (%)	RCPT index	Time of exposing	RCPT index	Diffusion coefficient D	
M1	*	*			*		24
M2	*	*		*		*	16
M3	*	*		*		*	16
M4			*	*		*	24
M5			*	*		*	24
M6			*	*		*	24
M7			*	*		*	24

All model structures were based on the following cases:

1. The minimum and maximum neurons in the hidden layer were changing between 1.5 and 3 times the input number of parameters. For example, in the model with 2 input parameters, the number of hidden layer neurons was 3 to 6.
2. The number of iterations and MSE between output parameter of model and test data was the criteria used for selecting the best model.

5. RESULTS AND DISCUSSION

For 7 models, the summary of models has been collected in tables 3-9. According to the criteria mentioned for choosing the best model in each ANNs, the selected model has been shown in different colors in the rows.

Table 3: The summary of results of M1 ANNs model

Code	Number of iterations	Number of neurons in hidden layer	MSE ($*10^{-4}$)	MAPE
M1-3-1	6	3	6.52	7.93
M1-4-4	5	4	6.52	7.93
M1-5-6	5	5	6.52	7.93
M1-6-4	4	6	6.52	7.93

Table 4: The summary of results of M2 ANNs model

Code	Number of iterations	Number of neurons in hidden layer	MSE ($*10^{-4}$)	MAPE
M2-5-1	13	5	1	12.68
M2-6-5	9	6	1	22.93
M2-7-7	7	7	1	7.63
M2-8-2	7	8	1	11.97
M2-9-4	6	9	1	62.57

Table 5: The summary of results of M3 ANNs model

Code	Number of iterations	Number of neurons in hidden layer	MSE ($*10^{-4}$)	MAPE
M3-5-3	9	5	1	21.50
M3-6-1	9	6	1	20.61
M3-7-2	8	7	1	9.30
M3-8-3	6	8	1	1.76
M3-9-2	5	9	1	16.14

Table 6: The summary of results of M4 ANNs model

Code	Number of iterations	Number of neurons in hidden layer	MSE ($*10^{-4}$)	MAPE
M4-3-1	1000	3	5.01	120.4
M4-4-2	1000	4	1.19	84.97
M4-5-2	1000	5	0.02	92.90
M4-6-4	1000	6	0.0008	9894.78

Table 7: The summary of results of M5 ANNs model

Code	Number of iterations	Number of neurons in hidden layer	MSE ($*10^{-4}$)	MAPE
M5-3-3	1000	3	3.23	66.05
M5-4-3	1000	4	0.772	23.12
M5-5-2	1000	5	0.0002	150.07
M5-6-2	1000	6	0.0919	205.68

Table 8: The summary of results of M6 ANNs model

Code	Number of iterations	Number of neurons in hidden layer	MSE ($*10^{-4}$)	MAPE
M6-3-3	1000	3	1.27	7.30
M6-4-3	1000	4	0.0975	8.64
M6-5-1	1000	5	0.0448	36.79
M6-6-2	1000	6	$8.04*10^{-9}$	29.46

Table 9: The summary of results of M7 ANNs model

Code	Number of iterations	Number of neurons in hidden layer	MSE ($*10^{-4}$)	MAPE
M7-3-3	1000	3	5.7	9.46
M7-4-1	1000	4	0.0683	14.27
M7-5-3	1000	5	0.0683	23.10
M7-6-1	1000	6	$3.33*10^{-8}$	84.35

As it can be seen from the results, the selection of mix design parameter (W/B and S.F percentage) makes better output than RCPT. It is because of the uncertainties of RCPT. Furthermore, both the number of neurons in hidden layer and number of hidden layers in relation with each other has a positive effect in ANNs output. It's because of the nonlinear nature of chloride diffusion in concrete.

6. CONCLUSION

After the tests, it is observed that the diffusion of chloride in concrete changes by SF ratio used instead of cement and water to binder ration. As a result of the analysis, ANN structures that produce close prediction current values to measured ones are presented and the robustness of ANN structure is tested. 7 ANN model was tested and in each model, the input and output parameters was changed to find the best input variable for prediction of chloride diffusion coefficient in concrete. The results show that W/B ration and percentage of silica-fume in concrete are better inputs than RCPT results. Furthermore, the results show that both the number of neurons in hidden layer and number of hidden layers in relation with each other has positive effect in ANNs output. To sum up, it is concluded that ANN is an appropriate tool for modeling the diffusion coefficient of chloride in concrete.

REFERENCES

1. K. Sakr,” Effect of cement type on the corrosion of reinforcing steel bars exposed to acidic media using electrochemical techniques”, Cem. Concr. Res. 35 (2005) 1820-1826.
2. K.Y. Yeau, E.K. Kim, “An experimental study on corrosion resistance of concrete with ground granulate blast-furnace slag”, Cem. Concr. Res. 35 (2005) 1391-1399.
3. İlker Bekir Topçu, Ahmet Raif Boğa, Fatih Onur Hocaoğlu, “Modeling corrosion currents of reinforced concrete using ANN”, Autom. Const. (2008),
4. A.A. Gürten, K. Kayakırılmaz, M. Erbil, The effect of hiosemicarbazide on

corrosion resistance of steel reinforcement in concrete, Const. Buil. Mater. 21 (2007) 669-676.
5. T. Parthiban, R. Ravi, G.T. Parthiban, S. Srinivasan, K.R. Ramakrishnan, M. Raghavan, Neural network analysis for corrosion of steel in concrete, Cor. Sci. 47 (2005) 1625-1642.
6. J. Hou, D.D.L. Chung, Effect of admixtures in concrete on the corrosion resistance of steel reinforced concrete, Cor. Sci. 42 (2000) 1489-1507.
7. K.K. Sideris, A.E. Sava, Durability of mixtures containing calcium nitrite based corrosion inhibitor, Cem. Concr. Compos. 27 (2005) 277-287.
8. C.H. Lim, Y.S. Yoon, J.H. Kim, Genetic algorithm in mix proportioning of high performance concrete, Cem. Concr. Res. 34 (2004) 409-420.
9. E.M.R. Fairbairn, M.M. Silvoso, R.D.T. Filho, J.L.D. Alves, N.F.F. Ebecken, Optimization of mass concrete construction using genetic algorithms, Comp. Struc. 82 (2004) 281-299.
10. G. İnan, A.B. Göktepe, K. Ramyar, A. Sezer, Prediction of sulfate expansion of PC mortar using adaptive neuro-fuzzy methodology, Build. Environ. 42 (2007) 1264-1269.
11. İ.B. Topçu, M. Sarıdemir, Prediction of properties of waste AAC aggregate concrete using artificial neural network, Comput. Mater. Sci. 41 (2007) 117–125.
12. N.Yasuda, T. Tsutsumi T. Kawamura, “Assessment Of Deteriorating Reinforced Concrete Structures Using Artificial Neural Networks”, Ieee Xplore (1993).
13. İ.B. Topçu, M. Sarıdemir, Prediction of compressive strength of concrete containing fly ash using artificial neural networks and fuzzy logic, Comput. Mater. Sci. 41 (2008) 305-311.
14. B.B. Adhikary, H. Mutsuyoshi, Prediction of shear strength of steel fiber RC beams using neural networks, Const. and Buil. Mater. 20 (2006) 801-811.
15. A. Mukherjee, S.N. Biswas, Artificial neural networks in prediction of mechanical behavior of concrete at high temperature, Nucl. Eng. Des. 178 (1997) 1-11.
16. İ.B. Topçu, M. Sarıdemir, Prediction of compressive strength of concrete containing fly ash using artificial neural networks and fuzzy logic, Comput. Mater. Sci. 41 (2008) 305-311.
17. İ.B. Topçu, M. Sarıdemir, Prediction of mechanical properties of recycled aggregate concretes containing silica fume using artificial neural networks and fuzzy logic, Comput. Mater. Sci. 42 (2008) 74-82.
18. F. Altun, Ö. Kişi, K. Aydin, Predicting the compressive strength of steel fiber added lightweight concrete using neural network, Comput. Mater. Sci. 42 (2008) 259-265.
19. S.S.S. Sakla, A.F. Ashour, Prediction of tensile capacity of single adhesive anchors using neural networks, Comp. Struct. 83 (2005) 1792–1803.
20. R. Parichatprecha, P. Nimityongskul. “Analysis of durability of high performance concrete using artificial neural networks”, Construction and Building Materials 23 (2009) 910-917.
21. Rumellhert D, Hinto G, Williams R. “Learning internal representations by Error Propagation”. Cambridge, Mass: MIT Press; 1986.
22. H.R. Ashrafi, A.A Ramezanianpour, “The Assessment of Chloride Diffusion in concretes containing Silica-Fume”, Phd Thesis, 2007.

CD05-006

PREDICTION OF CHLORIDE COEFFICIENT IN CONCRETE WITH DIMENSIONAL ANALYSIS IN PERSIAN GULF

H.Beheshti Nezhad[1], M. M.Ranjbar[2], N.Nariman Zadeh[3], H. Ghare Babaee[4]
[1]Faculty Member, Department of Civil, Islamic Azad University, Birjand Branch, Iran
[2]Assistant Professor, Department of Engineering, Guilan University, Rasht, Iran
[3]Associate Professor, Department of Engineering, Guilan University, Rasht, Iran
[4]PhD. Student, Dept of Mechanic Engg. School of Engg. Guilan University, Rasht, Iran

ABSTRACT

One of important causes for failure of concrete structures particular in Persian Gulf region is diffusion of chloride in concrete .One of the parameters which can increase the diffusion chloride ion is level of diffusivity of the concrete. prediction of concrete diffusion factor is an important issue as a key parameter in life cycle of concrete structures.

Experimental method in this field have problems such as time consummation, high cost, lack of experimental instruments, existence of inconvenience ions during experiment, committing unwanted errors and distorting from the true model.

For this reason in this research singular value decomposition (SVD) for modeling the diffusivity of chloride ion in concrete has been used.

The aim of this modeling is to find mathematical relation between the concrete diffusivity coefficient with effective parameters on it which means the proportion of water per cement and percent of silica fume.

Keywords: prediction, dimensionless analysis, persian gulf, chloride diffusion, SVD

1. INTRODUCTION

Concrete is such a construction material that is widely used in the world. The advantages of concrete are low cost, availability of constituents, workability, durability and convenient compressive strength that make it popular near engineers and builders. However, these advantages seriously depend on the correct mix and placing and curing [1,2].

Per year millions dollars are spent as the result of destruction of concrete structures near seashore and industrial refineries which contain chloride ions. The concrete used in this structures-specially sea structures- should resist against factors such as chloride attack and steel corrosion. In middle east specially in Persian gulf and southern banks of the Iran, the problems in concrete processing with high reliability cause high cost for the country[3].

Economically the best solution for preventing the precocious destruction is increasing the concrete resistance against chloride permeation during the concrete life. By operating of laboratory instruments we can produce concrete which can fulfill our needs. But there is no clear way to determine the duration of concrete structures and predicting the diffusion of chloride. The main problem is the vast variation of mixing proportion and huge number of effective parameters [4]. One of the methods for predicting the life time of concrete in the world is gathering the result of experiments and the present structure information for making a model that its usage decreases costs and time, easing in application and flexibility in any concrete structure.

Prediction of concrete diffusion factor is an important issue as a key parameter in life cycle of concrete structures.

System identification and modeling of complex processes using input-output data have always attracted many research efforts. In fact, system identification techniques are applied in many fields in order to model and predict the behaviors of unknown and/or very complex systems based on given input-output data [5]. Theoretically, in order to model a system, it is required to understand the explicit mathematical input-output relationship precisely.

There have been many research efforts for theoretical modeling the properties of concrete to predict the relationship of concrete diffusion factor as a function of the water per cement ratio and silica fume percent [6].

In this paper, experimental data of Construction Materials Institute at the University of Tehran [7] In which parameters water per cement ratio and silica fume percent are considered as input variables are used to find an equation for predicting concrete diffusion factor as output variable using singular value decomposition (SVD) method. In this way, the above mentioned input variables are re-grouped as dimensionless parameters which are then used to obtain the closed-form equation of concrete diffusion factor under aggressive environment in Persian gulf experiments carried out by M.shekarchi zadeh and others [7]. Such hybrid application of SVD and dimensionless analysis modeling is very simple and promising in modeling of the complex processes such as concrete diffusion factor under aggressive environment.

2. EXPERIMENTAL PROCEDURE

Experiments were carried out on result of experimental data on concrete durability in the south of Iran region.

In that regard, 20 concrete prism specimens measuring 15×15×60cm were exposed to the marine environment of Bandar Abbas city in the south of Iran, see Figure 1.

All concrete specimens were made with 400kg/m^3 Portland cement type II and crushed coarse aggregate (maximum size of 12.5 mm). Among the variables, five percentages of cement replacement with silica fume (0, 5, 7.5, 10, and 12%), and four water to cement ratios (0.35, 0.40, 0.45, and 0.50) were Investigated [7,8].

The data for the chloride diffusion coefficient for the age of 86 days were obtained. In this age, a 10 cm part of the specimens was cut for measuring the chloride ion content at different depths from the surface, see Figure 2, and thereby obtain the associated chloride profile on the top and bottom surfaces of the specimen.

Figure 1. Bandar-Abbas exposure site on the southern Iranian coast

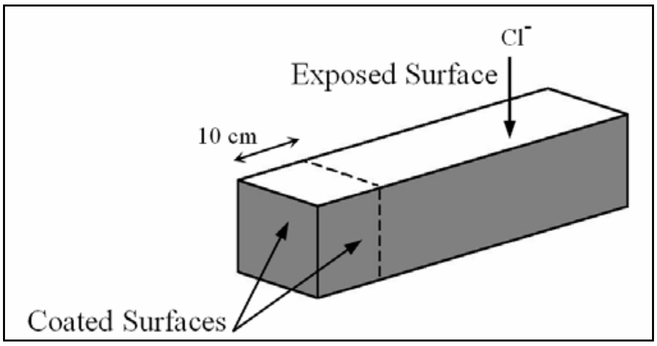

Figure 2. Concrete prism specimens exposed to marine environment for durability studies

3. DIMENSIONLESS MODELING OF CONCRETE DIFFUSION FACTOR USING SVD

The use of dimensionless parameter in modeling of concrete diffusion factor has been reported by Institute at the University of Tehran [7] using some experimental data, including those used by Beheshti Nezhad and Ranjbar [6]. They applied group method of data handling (GMDH)-type neural networks for modeling and prediction of concrete diffusion factor. However, singular value decomposition (SVD) and dimensionless parameters can be readily used together to obtain a simple equation for predicting the concrete diffusion factor based on the experimental data.

The formal definition of modeling is to find a function $\hat{f}$ so that can be approximately used instead of actual one, f, in order to predict output $\hat{y}$ for a given input vector $X = (x_1, x_2, x_3, ..., x_n)$ as close as possible to its actual output y. Therefore given M observation of multi-input-single-output data pairs so that

$$y_i = f(x_{i1}, x_{i2}, x_{i3}, ..., x_{in}) \quad i = 1,2,...,M \ , \tag{1}$$

it is now possible to obtain $\hat{f}$ to predict the output values $\hat{y}_i$ for any give input vector

$$X_i = (x_{i1}, x_{i2}, x_{i3}, ..., x_{in}) \tag{2}$$

Such that

$$\hat{y}_i = \hat{f}(x_{i1}, x_{i2}, x_{i3}, ..., x_{in}) \quad i = 1,2,...,M \tag{3}$$

The problem is now to determine $\hat{f}$ so that the square of different between the actual output and the predicted one is minimized, i.e.

$$\sum_{i=1}^{M} [\hat{f}(x_{i1}, x_{i2}, x_{i3}, ..., x_{in}) - y_i]^2 \rightarrow Min. \tag{4}$$

In dimensionless modeling, however, a dimensionless set, $\pi = \{\pi_0, \pi_1, \pi_2, \pi_3, ..., \pi_k\}$, rather than the set of real physical variable $\{y, X\} = \{y, x_1, x_2, x_3, ..., x_n\}$, is used to obtain $\hat{f}$, i.e.

$$\hat{\pi}_{0i} = \hat{f}(\pi_{1i}, \pi_{2i}, \pi_{3i}, ..., \pi_{ki}) \qquad i = 1,2,...,M \tag{5}$$

Such that

$$\sum_{i=1}^{M} [\hat{f}(\pi_{1i}, \pi_{2i}, \pi_{3i}, ..., \pi_{ki}) - \hat{\pi}_{oi}]^2 \rightarrow Min \tag{6}$$

In the order to construct such independent dimensionless parameters for modeling of concrete diffusion factor (D_f), total water per cement ratio (w/c) and silica fume percent (SF) have been considered. From the set of such input-output parameter, K=3 independent dimensionless parameters can be constructed according to three main dimensionless (M, L, T) as follows

$$\pi_1 = \log(1/D) \tag{7-a}$$

$$\pi_2 = \frac{W}{C}, \tag{7-b}$$

$$\pi_3 = 1 - \frac{SF}{100}, \tag{7-c}$$

So that,

$$\pi_1 = f(\pi_2, \pi_3)\,. \tag{8}$$

In order to use SVD to obtain the model, equation (8) can be represented as

$$\pi_1 = C(\pi_2)^{\alpha}(\pi_3)^{\beta} \tag{9}$$

Therefore, the problem of modeling is now to find coefficients C, α *and* β so that equation (6) is satisfied. By using natural logarithm, equation (9) can be represented as a linear relation with respect to the coefficients $(\eta = LnC)$, (α) *and* (β) as

$$\mathrm{Ln}(\pi_1) = \eta + \alpha \mathrm{Ln}(\pi_2) + \beta \mathrm{Ln}(\pi_3) \tag{10}$$

Consequently, a system of M Linear algebraic equation with K=3 unknown of the above mentioned coefficients is now constructed based on M input-output experimental data pairs as follows

$$\begin{cases} \eta + \alpha\zeta_{11} + \beta\zeta_{12} = \zeta_{10} \\ \eta + \alpha\zeta_{21} + \beta\zeta_{22} = \zeta_{20} \\ \vdots \\ \eta + \alpha\zeta_{M1} + \beta\zeta_{M2} = \zeta_{M0} \end{cases}, \tag{11}$$

where

$$\zeta_{ij} = Ln(\pi_{ij}) .\ i = 1,2,...,M \ , j=1,2 \tag{12}$$

and

$$\zeta_{i0} = Ln(\pi_{i0}) .\ i = 1,2,...,M \tag{13}$$

Such system of linear equations in which $M>>K=3$ can be represented as

$$AX = Y\,, \tag{14}$$

Where

$$X = [\eta \ \ \alpha \ \ \beta\,]^T\,, \tag{15}$$

$$Y = [\zeta_{10} \ \ \zeta_{20} \ \ ... \ \ \zeta_{M0}]^T\,, \tag{16}$$

And

$$A = \begin{bmatrix} 1 & \zeta_{11} & \zeta_{12} \\ 1 & \zeta_{21} & \zeta_{22} \\ \vdots & \vdots & \vdots \\ 1 & \zeta_{M1} & \zeta_{M2} \end{bmatrix} \tag{17}$$

The least-squares technique from multiple-regression analysis leads to the solution of the normal equation in the form of

$$X = (A^T A)^{-1} A^T Y \ , \tag{18}$$

Which determines the vector of the best $k = 3$ unknown of equation (9) for the whole set of M experimental observation data. However, such solution directly form solving normal equations (18) is rather susceptible to round off error and, more importantly, to the possible singularity of these equations. Therefore, SVD is used to solve equation (14) which leads to better results in comparison with those of using equation (18).

SVD is the method for solving most linear least-squares problems that some singularities may exist in the normal equations. The SVD of a matrix, $\mathbf{A} \in \Re^{M \times K}$, is a factorization of the matrix into the product of three matrices, column orthogonal matrix $\mathbf{U} \in \Re^{M \times K}$, diagonal matrix $\mathbf{W} \in \Re^{K \times K}$ with non-negative elements (singular values), and orthogonal matrix $\mathbf{V} \in \Re^{K \times K}$ such that

$$\mathbf{A} = \mathbf{U}\mathbf{W}\mathbf{V}^T \tag{19}$$

The most popular technique for computing the SVD was originally proposed in [9]. The problem of optimal selection of vector of the coefficients in equation (15) and (18) is firstly reduced to the modified inversion of diagonal matrix W [10] in which the reciprocals of zero or near zero singulars (according to a threshold) are set to zero. Then, such optimal X are obtained using the following relation

$$X = \mathbf{V}\left[diag\left(\frac{1}{w_j} \right) \right] \mathbf{U}^{\mathbf{T}}\ \mathbf{Y} \tag{20}$$

In order to demonstrate the prediction ability of SVD in such dimensionless modeling, the data have been divided into two different sets, namely, training and testing sets. The training set, which consists of randomly chosen N_t input-output data pairs, is used for training the $K = 3$ unknown coefficients involved in the dimensionless model of concrete diffusion factor. The testing set, which consists of N_P unforeseen input-output data samples during the training process, is merely used for testing to show the prediction ability of the obtained simple model.

4. RESULTS AND COMPARISONS

In order to obtain a simple model for concrete diffusion factor under aggressive environment (equation (9)), the experimental data of shekarchi [7] described in section of experimental procedure is now converted into a dimensionless data table based on definitions (7-a)-(7-d) and their natural logarithms equations (12)-(13).

The unknown $K=3$ coefficient involved in the simple model representing by equation (9) can now be determined by either solving normal equation (SNE) by pseudo- inverse of matrix A given by equation (18) or by SVD approach proposed in this work given by equation (20). Such approach is accomplished by randomly selecting N_t data pairs out of total N=20 data pairs. The remaining $N_p = N - N_t$ data pair is used to show the prediction ability of the obtained simple model in the form of equation (9).

In order to obtain the best possible model (as the amount of N_t can vary between $N_t = K = 3$ *to* $N_t = N$), series of runs in which N_t and N_p vary between (3 to N) and (N to 3), respectively, have been performed. The values of root mean squares of errors (RMSE) obtained using SVD and SNE are 0.959353 and 1.37529, respectively, which demonstrates the superiority of SVD over SNE. In this paper, $N_t = 5$ and $N_p = 15$ has been chosen to represent the simple dimensionless concrete diffusion factor in Persian gulf environment. The corresponding values of parameters are found as $C = 10.628$, $\alpha = -4.353519E-02$, $\beta = -3.952748E-01$ Hence, the model can now be given as

$$\log(1/D) = 10.628(\mathrm{w/c})^{-4.353519\mathrm{E}-02}(1 - sf/100)^{-3.952748\mathrm{E}-01} \qquad (21)$$

Figure (3) shows the comparison of $(\log 1/D)$ given by equation (21) with respect to the experimental values both for training and testing data sets. It is evident from this figure that equation (21) predicts the midpoint concrete diffusion factor successfully for the testing data.

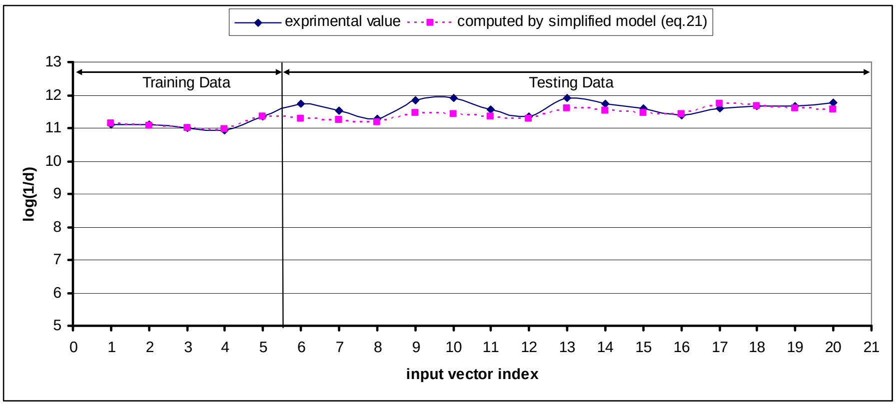

Figure 3. Variation of concrete diffusion factor using the simplified model (equation 21) in comparison with the experimental values

However, the obtained model given by equation (21) can be further simplified in order to compare with some other models in world.

5. CONCLUSION

Singular value decomposition and dimensionless analysis have been used to model the concrete diffusion under aggressive environment using some experimental input-output data. It has been shown that the simple obtained model can successfully predict the concrete diffusion factor compared with the actual experimental values. The methodology of this paper can be readily applied to find simple closed-form equations of complex real-world processes where some experimental input-output data pairs are available.

REFRENCES

1. Neville, A.M., “Properties of concrete.3rd edition”, Pitman publishing limited, London, 1981.
2. Tasdemir, C., et al. “The influence of aggregate type on the mechanical properties of concrete”, 12th European realy mixed concrete congress, 1998, Vol. 1. Lisbon-Portugal. June, PP. 564-573.
3. Alizadeh, R., “Effect of Curing Conditions on the Chloride Diffusion in Concrete in Persian Gulf”, *M.Sc. Thesis,* 1998, *University of* Tehran, (in Persian).
4. Andrade. C., (1993), Calculation of Chloride Diffusion Coefficients in Concrete From Ionic Migration Measurements, Cement and Concrete Research, 1993, Vol 23, pp. 724-742.
5. Astrom. K.J, Eykhoff. P, “System identification, a survey”, *Automatica*, 1971, Vol.7, pp. 123-62.
6. H. Beheshti Nezhad , M.M Ranjbar, N. Nariman Zadeh, ”Prediction of Concrete Diffusion Factor Under Aggressive Environment with GMDH-Type Neural Networks” ,Taylor& Francis Group publishing, 8th international conference on creep, shrinkage and durability mechanics of concrete structures, 2009 ,japan,1131-1137.
7. M. Chini, P. Ghods, R. Alizadeh, M. Hoseini, SH. Montazer, M. Shekarchi, and M. Ghalibafian, (2004), “Developing the First Version of the Model for Service Life Prediction of Reinforced Concrete Structures in Persian Gulf and Oman Sea” ,Technical Report, NO. CMI 8309144, Construction Materials Institute at the University of Tehran, Iran.
8. M. Ghalibafian, R. Alizadeh, P. Ghods, M. Chini, M. Hosseini, and M. Shekarchi, (2008), “Effect of Curing Conditions on the Service Life Design of RC Structures in Persian Gulf Region”, Journal of Materials in Civil Engineering, 20(1),pp. 2–8.
9. Golub, G.H., Reinsch, C., Singular value decomposition and least squares solutions, Numer. Math. 14 (5), 1970, PP. 403-420.
10. Press, W.H., Teukolsky, S.A., Vetterling, W.T., Flannery, B.P., Numerical Recipes in FORTRAN: The Art of Scientific Computing, 2nd Edition, Cambridge University Press, Cambridge, 1992.

CD05-007

EVALUATION OF MECHANICAL PROPERTIES AND DURABILITY OF CONCRETES CONTAINING RICE HUSK ASH

A.A.Ramezanianpour[1], P.Pourbeik[2], M.Mahdikhani[3], F.Moodi[4] , Gh.Ahmadibeni[5]
[1]Professor, Dept. of Civil Engineering Amirkabir University of Technology, Tehran, Iran
[2]M.Sc. Student, Dept. of Civil Engineering School of Engineering, Amirkabir University of Technology, Tehran, Iran
[3]Msc , Dept. of Civil Engineering School of Engineering, Amirkabir University of Technology, Tehran, Iran
[4]Assistant Professor, Dept. of Civil Engineering, Amirkabir University of Technology, Tehran, Iran
[5]Bsc, Dept. of Mechanical Engineering, Amirkabir University of Technology, Tehran, Iran

ABSTRACT
Replacement of cement with pozzolan in the production of concrete not only improves the mechanical properties and durability of concrete but also decreases the amount of consumed cement in construction projects as well.
For many decades, the concretes incorporating Rice Husk Ash (RHA) as an artificial Pozzolan have been noticed for its qualities and properties. The ash remaining from burning rice husk with high specific surface, decreases porosity and permeability and increases durability of concrete as a result of considerable pozzolanic activities and chemical activities with Calcium Hydroxide.
In this paper, in order to supply typical RHA, a special furnace was designed and constructed in Amirkabir University of Technology.
XRD and XRF techniques were used to determine the amorphous silica content of the burnt rice husk. Consequently, temperature of 650 degrees centigrade and 60 minutes burning time was found to be the best combination.
Then, various experiments were carried out to determine properties of concretes incorporating optimum RHA. The results show that RHA as an artificial pozzolanic material has increased the strength and reduced chloride permeability leading to higher durability. As an example, the tensile strength increased up to 13% after 28 days and up to 23% at 90 days.

Keywords: RHA, durability, special furnace, mechanical properties, RCPT

1. INTRODUCTION
Sustainable development of the cement and concrete industry requires the utilization of industrial and agricultural waste components. At present, for a variety of reasons, the concrete construction industry is not sustainable. Firstly, it consumes huge quantities of virgin materials which can remain for next generations. Secondly, the principal binder in concrete is Portland cement, the production of which is a major contributor to greenhouse gas emissions that are implicated in global warming and climate change. Thirdly, many concrete structures suffer from lack of durability which may waste the natural resources. So,

finding a solution to substitute a practical recycled product for part of the cement seems to be desirable for sustainable development. [1-7]

Recycling of waste components contributes to energy savings in cement production, to conservation of natural resources, and in protection of the environment. Furthermore, the use of certain components with potentially pozzolanic reactivity can significantly improve the properties of concrete [8-14]. One of the most suitable sources of pozzolanic material among agricultural waste components is rice husk, as it is available in large quantities and contains a relatively large amount of silica. When rice husk is burnt, about 20% by weight of the husk is recovered as ash in which more than 75% by weight is silica. Unlike natural pozzolan, the ash is an annually renewable source of silica. It is worth mentioning that the use of RHA in concrete may lead to the improved workability, the reduced heat evolution, the reduced permeability, and the increased strength at longer ages. [15-21]

In Iran, rice production has increased during these years, becoming the most important crop. Rice husks are residue produced in significant quantities. While in some regions, they are utilized as a fuel in the rice paddy milling process, in our county they are treated as waste, causing pollution of environment and disposal problems. Due to increasing environmental concern, and the need to preserve energy and resources, efforts have been made to burn the husks under controlled conditions and to utilize the resultant ash as a building material. In addition, rice husks are able to be an ideal fuel for electricity generation [11-14].

The use of Rice Husk Ash (RHA) in concrete was patented in the year 1924 [14]. Up to 1978, all the researches were concentrated to utilize ash derived from uncontrolled combustion. Mehta published several papers dealing with rice husk ash utilization during this period. He established that burning rice husk under controlled temperature-time conditions produces ash containing silica in amorphous form [22-26].

Depending on produce method, the utilization of rice husk ash as a pozzolanic material in cement and concrete provides several advantages, such as improved strength and durability properties. Rodrı´guez de Sensale [16] reported that mortars and concrete containing RHA have compressive strength values inferior or superior to that of OPC concrete. In addition, in most of the cases [18, 19, 26], mortars and concrete containing RHA improves durability of concrete at various ages.

Generally, there are two types of RHA in concrete. The type of RHA which is suitable for pozzolanic activity is amorphous rather than crystalline. Therefore, substantial research has been carried out on producing RHA containing high amount of amorphous silica. The results have shown that RHA quality depends on temperature and burning time.

In fact, for an incinerator temperature up to 700°C the silica is in amorphous form and silica crystals grew with time of incineration. The combustion environment also affects specific surface area, so that time, temperature and environment also must be considered in the processing of rice husks to produce ash of maximum reactivity [5, 7].

2. MATERIALS USED

The following materials were used in the preparation of the concrete specimens. Local natural sand according to ASTM Standard with maximum aggregate size of 4.75 mm; Crushed granite according to ASTM Standard with maximum aggregate size of 19 mm; Tehran potable water, Type I Portland cement and homogeneous rice husk ash produced by the special designed furnace at 650°C and 60 minutes burning time. Table 1 shows the physical and chemical characteristics of RHA (RHA-650-60) and cement.

Table 1: Physical and chemical characteristics of cement and RHA

	Physical Tests		Chemical Analyses, (%)								Bogue Composition, (%)			
	Specific Gravity	Blaine, (cm^2/gram)	SiO_2	Al_2O_3	Fe_2O_3	CaO	MgO	Na_2O	K_2O	LOI	C_3S	C_2S	C_3A	C_4AF
RHA	2.15	3600	89.61	0.04	0.22	0.91	0.42	0.07	1.58	5.91	—	—	—	—
Cement	3.21	3200	21.50	3.68	2.76	61.50	4.80	0.12	0.95	1.35	51.1	23.1	5.1	8.4

3. TEST METHODS

A total of 4 concrete mixtures were made; one corresponding to a control concrete (CTL) and three others with 7%, 10% and 15% RHA replaced with cement by weight. Table 2 lists the mix proportions of concrete. Slumps were kept constant at 70 ± 10 mm. Superplasticizer with polycarboxylate base was used at very low percentages according to the results obtained for the slumps. Concrete test specimens were compacted by external vibration and kept protected after casting to avoid water evaporation. After 24 hr. they were demolded and cured in lime-saturated water at 23 ± 2°C to prevent possible leaching of Ca (OH) 2 from these specimens.

Concrete cubes of 100×100×100mm dimension were cast for compressive strength and water penetration tests. The results obtained are reported as an average of two tests. While two 150×300 mm cylinder concrete specimens were prepared for the tensile strength test and static modulus of elasticity, samples of rapid chloride permeability tests (RCPT), according to ASTM C 1202, were prepared by cutting and discarding 25mm slices from the top and bottom of 100×200 mm cylinders, and the remaining section cut into three 50mm thick slices. The water permeability test was conducted using a high-pressure permeability cell. The specimens used were cubes of 150×150×150 mm dimension. In addition, 50×50×50 mm mortar samples were prepared for the pozzolanic activity test. All specimens were moist cured until the time of testing.

Table 2: Mix proportions of concrete

	RHA (kg/m^3)	cement (kg/m^3)	Aggregate (kg/m^3)		SP/cement (%)	water/ cement
			Fine	coarse		
CTL	0	420	815	995	0	0.45
7%RHA	29.4	390.6	815	995	0.15	0.45
10%RHA	42	378	815	995	0.25	0.45
15%RHA	63	357	815	995	0.40	0.45

4. TEST RESULTS

The results of pozzolanic activity test are shown in Table 3. Results demonstrate high pozzolanic activity index of RHA over that of the control in accordance with ASTM C-311/ASTM C-618 test method. On the other hand, produced rice husk ash is a high reactive pozzolanic material, and entirely satisfies other requirements. Figure 1 shows XRD patterns of the ash.

Table 3: Comparison in chemical and physical specifications of produced RHA with ASTM standard C618-03

	ASTM	RHA results
Chemical Requirements		
$SiO_2 + Al_2O_3 + Fe_2O_3$, min., %	70	89.9
SO_3, max., %	4	0.15
Moisture Content, max., %	3	0.23
Loss On Ignition (LOI), max., %	6	5.9
Physical Requirements		
Fineness: Amount retained when wet-sieved on 45 µm sieve, max., %	34	8
Strength Activity Index (20% RHA) at 3-day, min. % control	---	102
Strength Activity Index (20% RHA) at 7-day, min. % control	75	106
Strength Activity Index (20% RHA) at 28-day, min. % control	75	110

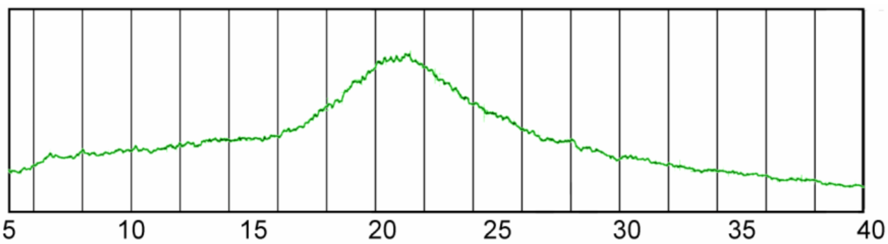

Figure 1. Results of XRD on rice husk ash sample

Results of the compressive strengths of concretes are given in Figure 2. In general, the RHA concrete had higher compressive strengths at various ages and up to 90 days when compared with the control concrete. The results show that it was possible to obtain a compressive strength of as high as 46.9 MPa after 28 days. In addition, strengths up to 63.2 MPa were obtained at 90 days.

Figure 3 shows that concrete containing RHA has a greater splitting tensile strength than that of the control concrete at all ages. It is clear that, as the amount of RHA increases, the tensile strength increases up to 20%. For instance, at 90 days the 15%RHA concrete had a compressive strength of 5.62 MPa compared with 4.58 MPa for the control concrete.

Figure 4 shows the static modulus of elasticity in compression of concrete mixed with different proportions of RHA at 28 and 90 days. After 90 days, mixture containing 15% of RHA showed 7% increase in static modulus of elasticity in compression as compared to the control concrete. On the other hand, concrete containing RHA depicts a higher static modulus of elasticity when compared to the control concrete.

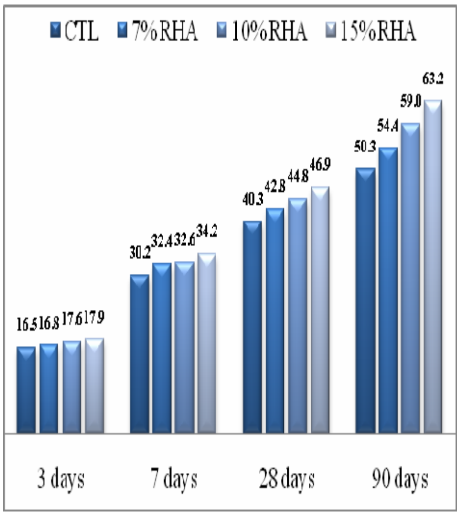

Figure 2. Compressive strength (MPa) at various ages for control (CTL) & RHA mixtures

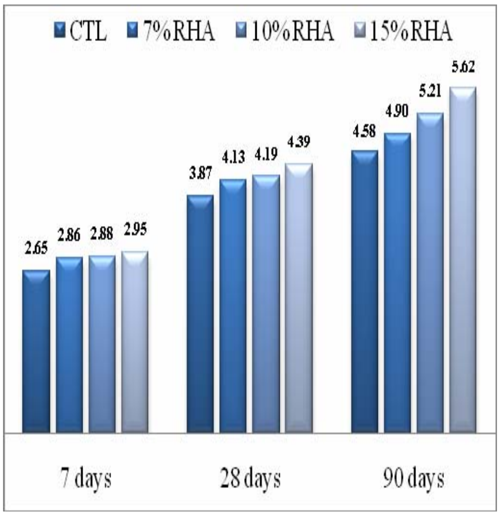

Figure 3. Tensile strength (MPa) at various ages for control (CTL) & RHA mixtures

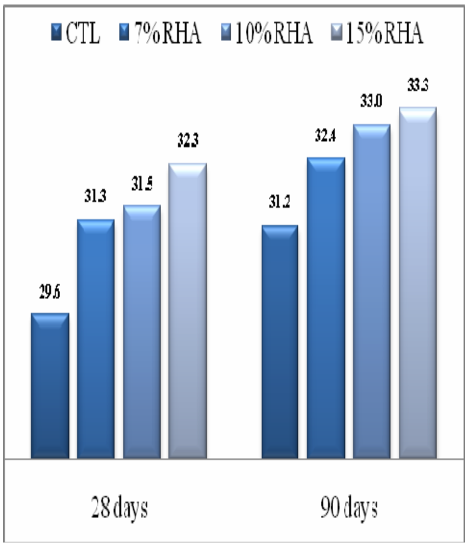

Figure 4. Modulus of elasticity (GPa) at various ages for control (CTL) & RHA control mixtures

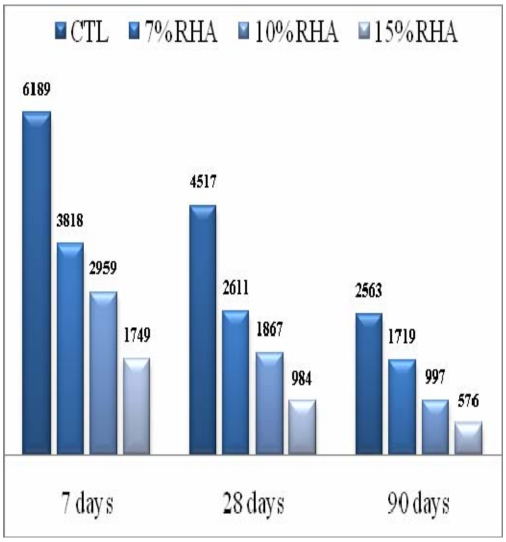

Figure 5. Resistance to chloride ion penetration (coulomb) at various ages for (CTL) & RHA mixtures

Results of the rapid determination of chloride permeability of concrete test (Figure 5) show that using RHA drastically enhances resistance to chloride penetration compared to control concrete on average, around 4~5 times higher for the 15% RHA. At 7 days, the control concrete showed the highest value of 6189 coulombs while the charge passed through the 15%RHA concrete was 1749 coulombs.

With a continuous moist-curing of up to 91 days, the charge passed through all concretes; was reduced. The charge for the 15%RHA concrete was reduced to 576 coulombs, which was well below that of the control concrete (2563 coulombs). According to ASTM C 1202, when the charge passed through concrete is below 1000 coulombs, it is categorized as a very high resistance concrete to chloride ion penetration.

The chloride permeability of the concrete specimens incorporating 15%RHA was "very low", while that of the concrete specimens with 0%, 7%, 10% RHA were "moderate", "low" and "low", respectively, as per ASTM C 1202 criteria.

In addition to RCPT, investigations of water permeability were carried out. In this test, water was forced into the concrete samples from one side for three days and under constant pressure of 0.5 MPa. Then, the samples were split in a plane parallel to the direction of water penetration, and the greatest depth of water penetration into the concrete sample was measured. The depth of water penetration of concrete incorporating RHA specimens is shown in Figure 6. As expected, depth of water penetration of concrete specimens decreased significantly with an increase in RHA content and curing period.

Figure 7 gives a linear relationship between compressive strength and tensile strength, it is significant. A good relationship was also found between RCPT and compressive strength, which is shown in Figure 8.

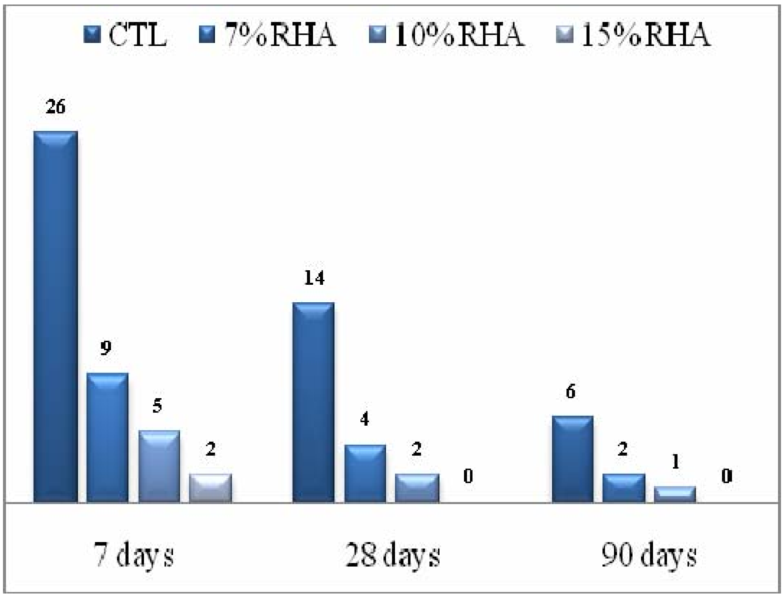

Figure 6. Depth of water penetration (mm) at various ages for control (CTL) & RHA mixtures

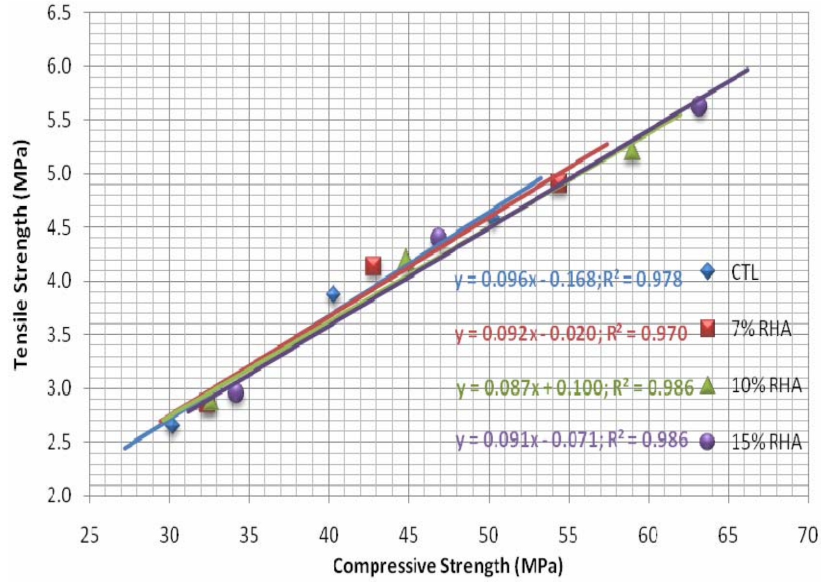

Figure 7. Relationship between compressive strength and tensile strength

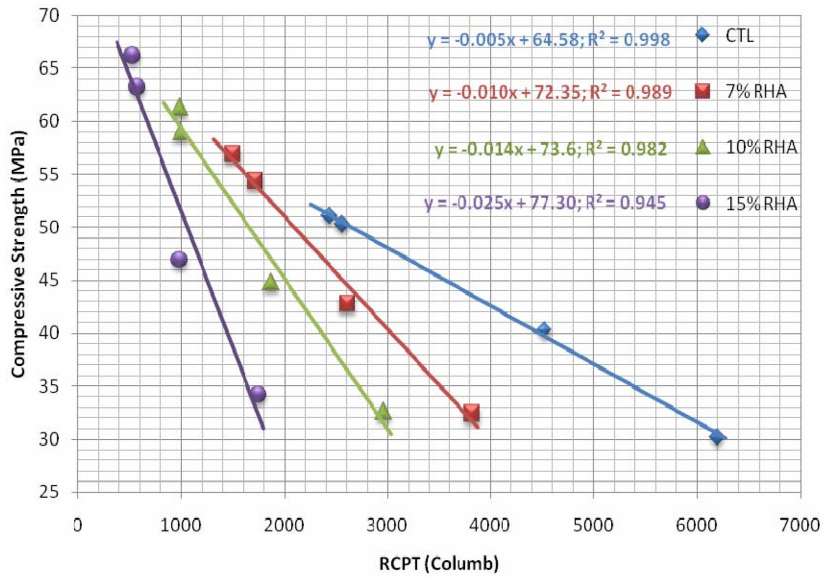

Figure 8. Relationship between compressive strength and RCPT test

5. DISCUSSION

Improvements in mechanical and durability properties of the concretes containing RHA can be explained by the chemical and physical effects of RHA. Chemical effect is mainly due to the pozzolanic reactions between the amorphous silica of RHA and calcium hydroxide (C-H) produced by the cement hydration to form calcium-silicate-hydrates (C-S-H). The physical effect which can also be considered as filler effect is that RHA particles increase the packing of the solid materials by filling the spaces between the cement grains in much the same way as cement fills the spaces between fine aggregates, and fine aggregates fill the spaces between coarse aggregates in concrete. Moreover, small particles of additions generate a large number of nucleation sites for the precipitation of the hydration products. This will accelerate the reactions and form smaller C-H crystals. RHA reduces the number of large pores and increases the probability of transforming the continuous pores into discontinuous ones. Therefore, all these mechanisms make the microstructure of the paste more homogeneous and denser.

6. CONCLUSIONS

Based on the results of the present experiments, the following conclusions can be drawn out:

1) The quality of the RHA cement is widely varied due to the differences in the methods of production. So, it is generally advocated to use special incinerators, which can guarantee controlled burning conditions. With the proper production method, rice husk ash of a pozzolanic reactivity comparable to other pozzolans can be obtained. A special furnace which was designed and constructed was able to produce RHA with various qualities.
2) The duration and temperature of furnace are important parameters, influencing the reactivity of RHA pozzolans. Silica in the rice husk initially exists in the amorphous form, but may become crystalline when rice husk is burnt at high temperature. In addition, silica in rice husk ash will not remain porous and amorphous, when combusted for a prolonged period at a temperature above 650°C, or during less than a few minutes at 1100°C, under oxidizing conditions. The results of XRD analysis show that quartz crystal is present in both types of ashes. So, investigation on the influence of combustion conditions on the amorphous silica suggests that the RHA-650-60 can be considered to be non-crystalline RHA and to save the RHA production time.
3) Huge amounts of crystalline silica or higher carbon content are detrimental to the pozzolanic reactivity of the ash. Presence of un-burnt carbon can adversely affect the reactivity even though it is rich in amorphous silica. The results of pozzolanic activity demonstrate high pozzolanic activity index of produced rice husk ash concrete over that of the control. In addition, the produced rice husk ashes containing up to 90 percent amorphous silica entirely satisfy other requirements of ASTM standard C618-03. This shows the high quality of produced rice husk ashes.
4) The RHA concrete showed higher compressive strength at various ages in comparison with that of the concrete without RHA. In addition, the RHA concrete had higher splitting tensile strength and modulus of elasticity in comparison with that of the concrete without RHA. It is concluded that produced RHA provides a positive effect on the compressive strength of concretes.
5) The performance of concrete with cement replacement by RHA is outstanding considering resistance to water and chloride ion penetration which is in many

cases the most important characteristic concerning durability and corrosion prevention.

REFERENCES

1. Mehta, P.K., "High-performance, high-volume fly ash concrete for sustainable development", Proceedings of the International Workshop on Sustainable Development and Concrete Technology, Beijing, China, May 20–21, 2004.
2. Mehta, P.K., "Mineral admixtures for concrete – an overview of recent developments". Advances in cement and concrete, Proceedings of an Engineering Foundation Conference, University of Newhampshire, ASCE, pp. 243-256, 1994.
3. A. Ramezanianpour, F. Gafarpour, M.H. Majedi, The use of rice husk ash in the building industry, Building and Housing Research Center (BHRC), winter 1995.
4. A. Ramezanianpour, G. Bina, and H. Rahimi "The role of rice husk ash in production of light-weight structural panels", Proceedings 3rd International Conference on Concrete, May 2000, Tehran, Iran.
5. P. K. Mehta, P. JM Monteiro, Concrete, Microstructure, Properties, and Materials, Translated into Persian by A.A. Ramezanianpour, P. Ghoddousi, E. Ganjian, Amirkabir University of Technology Press, Summer 2004.
6. A.A. Ramezanianpour, A.M. Ramezanianpour, "Chloride diffusion in silica fume concrete mixtures", International Symposium on Concrete, Toronto, Canada, 17 October 2005.
7. M. Nehdi, J. Duquette, A. El Damatty, "Performance of rice husk ash produced using a new technology as a mineral admixture in concrete", Cement and Concrete Research, (2003) PP. 1203-1210.
8. M. Zhang, V. M. Malhotra, "High-Performance Concrete Incorporating Rice Husk Ash as a Supplementary Cementing Material", ACI Materials Journal, November-December 1996, Tittle no. 93-M72, PP. 629-636.
9. A. Ramezanianpour, F. Gafarpour, M.H. Majedi, Use of rice husk in the production of masonary cements, Building and Housing Research Center (BHRC), September 1997.
10. Khoddam Razavi, S. R, "Rice husk ash a mineral admixture for high performance concrete", Msc Thesis, Amirkabir University of Technology Press, 2005.
11. Vosugh, Sh, "Mechanical properties and Durability of Concretes Containing of Rice Husk Ash", Msc Thesis, Amirkabir University of Technology Press, 2001.
12. Bui, D. D, "Rice husk ash a mineral admixture for high performance concrete", PhD Thesis, Delft University Press, 2001.
13. D.D. Bui, J. Hu and P. Stroeven, "Particle size effect on the strength of rice husk ash blended gap-graded Portland cement concrete", Cement and Concrete Composites, Volume 27, Issue 3, pp. 357-366, March 2005.
14. N. Pitt, "Process for the preparation of siliceous ashes", US Patent, 3959007, July 1972.

15. P.K. Mehta, “Siliceous ashes and hydraulic cements prepared therefrom”, US Patent, 4105459, August 1978.
16. Gemma Rodrıguez de Sensale, “Strength development of concrete with rice husk ash”, Cement & Concrete Composites, No. 28 (2006) PP. 158–160.
17. K. Ganesan, K. Rajagopal and K. Thangavel, “Rice husk ash blended cement: Assessment of optimal level of replacement for strength and permeability properties of concrete”, Construction and Building Materials, Article in Press, Available online 20 August 2007.
18. Prinya Chindaprasirt, Sumrerng Rukzon and Vute Sirivivatnanon, “Strength, porosity and corrosion resistance of ternary blend Portland cement, rice husk ash and fly ash mortar”, Construction and Building Materials, Article in Press, Available online 2 August 2007.
19. P. Chindaprasirt and S. Rukzon, “Strength, porosity and corrosion resistance of ternary blend Portland cement, rice husk ash and fly ash mortar”, Construction and Building Materials, Article in Press, Available online 10 August 2007.
20. Graciela Giaccio, Gemma Rodríguez de Sensale and Raúl Zerbino, “Failure mechanism of normal and high-strength concrete with rice-husk ash”, Cement and Concrete Composites, Volume 29, Issue 7, August 2007, Pages 566-574.
21. V. Saraswathy and Ha-Won Song, “Corrosion performance of rice husk ash blended concrete”, Construction and Building Materials, Volume 21, Issue 8, August 2007, Pages 1779-1784.
22. P. Chindaprasirt, S. Homwuttiwong and C. Jaturapitakkul, “Strength and water permeability of concrete containing palm oil fuel ash and rice husk–bark ash”, Construction and Building Materials, Volume 21, Issue 7, July 2007, Pages 1492-1499.
23. A.L.G. Gastaldini, G.C. Isaia, N.S. Gomes and J.E.K. Sperb, “Chloride penetration and carbonation in concrete with rice husk ash and chemical activators”, Cement and Concrete Composites, Volume 29, Issue 3, March 2007, Pages 176-180.
24. P. Chindaprasirt, S. Rukzon and V. Sirivivatnanon, “Resistance to chloride penetration of blended Portland cement mortar containing palm oil fuel ash, rice husk ash and fly ash”, Construction and Building Materials, Article in Press, Available online 16 January 2007.
25. M.R.F. Gonçalves and C.P. Bergmann, “Thermal insulators made with rice husk ashes: Production and correlation between properties and microstructure”, Construction and Building Materials, Article in Press, Available online 17 October 2006.
26. S.K. Agarwal, “Pozzolanic activity of various siliceous materials”, Cement and Concrete Research, Volume 36, Issue 9, September 2006, Pages 1735-1739.

CD05-008

INFLUENCE OF WATERPROOFING ADMIXTURE IN WATER PENETRATION OF CONCRETE

M. Haji Sotoudeh[1], F. Vazinram[2], M.M. Khodaparast[3], M. Jalal[4]
[1]Power and Water University of Technology, faculty member
[2]Power and Water University of Technology, faculty member

ABSTRACT
Nowadays, concrete plays an outstanding role in construction industry and variety of engineering infrastructures such as bridges, dams, jetties, piers and channels which are made of concrete. Since from one hand, these huge and critical concrete structures in which some cases are of lifelines of a country are of great importance and on the other hand, the necessity of conservation and durability of these structures is inevitable, the importance of concrete durability will become vividly apparent. One of the factors that can deteriorate the reinforced concrete condition by corrosion and cause cracking in severe cold weather, has turned out to be water penetration into concrete. With this respect, one of the practical and efficient ways ever used to countermeasure this situation is to use water proof additives in concrete mix in order to reduce water and waste water absorption and penetration into concrete. In this investigation, PN gel, PN liquid and PN liquid along with micro silica powder as waterproofing additives, were used in separate mix designs to make specimens and then these specimens and the witness were tested by two methods in order to determine water absorption and penetration depth in concrete. in one of these two methods, water absorption percentage was just determined and in the other one which was more accurate and was implemented by triaxial apparatus, both water absorption and penetration depth in the specimens were investigated. Finally, the tables and diagrams for gained results concerning specimens containing PN additives and witness were prepared and compared. The results showed about more than 50% improvement in water penetration reduction.

Keywords: concrete, durability, waterproof additives, penetration depth, water absorption

1. INTRODUCTION
In the present research, the methods and results of water absorption and penetration depth tests are presented which have been carried out for four groups of specimens including waterproofing additives PN gel, PN liquid, PN liquid along with micro silica powder. These additives are produced by 'Vand Chemie Sakhteman" company, and the tests have been implemented on 28-day concrete specimens in Material and Concrete Technical Unit laboratory of Power & Water University of Technology (PWUT).
General characteristics of materials used in concrete mix designs are presented in

the following tables:

Table 1: Materials used in mix designs

Materials	Characteristics
Cement	Tehran Portland cement Type I
Aggregates	Materials and Concrete Technical Unit lab
Water	Tehran drinking water
Water proofing gel	PN additives (produced by 'van shimi' Co.)
Water proofing liquid	PN additives (produced by 'van shimi' Co.)
Micro silica	Powder (produced by 'van shimi' Co.)

Table 2: Mix design characteristics of specimens

Group NO.	Mix design	w/c ratio	Slump no. (cm)	Cement content (kg/m^3)	Aggregate content (kg/m^3)	Coarse aggregates (kg/m^3)	Fine aggregates (kg/m^3)	Weight ratio of additives to cement (%)
1	witness	0.63	5	350	945	473	473	0
2	PN gel	0.63	16	350	945	473	473	7
3	PN liquid	0.63	17	350	945	473	473	0.5
4	PN liquid + microsilica powder	0.63	16	350	945	473	473	0.5 +10

2. DEFINITIONS AND CALCULATIONS FORMULAS

1. Saturated with dried surface weight or SSD (Saturated Surface Dry):
Weight of aggregates in saturated state with dried surface or weight of concrete specimen in saturated state with dried surface.
2. Water absorption:
Weight difference ratio for two states as SSD (Saturated Surface Dry) and fully dried (heated in the oven for at least 48 hours in $110^{\circ C}$) to fully dried specimen weight described in percentage
3. Dry weight:
Specimen weight after being heated in oven for 48 hours at $110^{\circ C}$.

2.1. Construction and Test Procedure

2.1.1. Specimens construction

According to the mix design prepared as witness, at first aggregates and half of the mix water were poured into the mixer and then cement and the rest of the water were added into the mixer. The slump was tested in order to reach the specified slump to the amount of *5cm.* therefore, water to cement ratio was determined as *0.63* and this ratio was used in other mix designs of the specimens.The molds were opened 24 to 26 hours after placing the concrete.[1]

2.1.2. Construction standards

Steps of making and curing of the specimens have been done as presented in the following table:

Table 3: Standards of making the concrete specimens

Row No.	Description	ABA standard (Iran concrete standard)
1	Making concrete specimens for concrete tests	د.ت. 503
2	Curing the specimens in the laboratory	د.ت. 503
3	Determination of concrete workability (slump)	د.ت. 505
4	Determination of fresh concrete unit weight	د.ت. 509

2.2. Curing Condition of the Specimens

The specimens were kept in water with the temperature of 23°C until the age of 28 days.

Figure 1. Water pool where the specimens were kept

2.3. Implementation of Penetration Test

In order to do the penetration test by triaxial apparatus (Figures. 2-1 to 2-4), since the maximum height of the apparatus was less than *20 cm*, the specimens were cut *2 cm* in length and their heights reached *18 cm*.

Figure 2.1. General view of tri axial apparatus

Figure 2.2. Digital sensor for axial force

Figure 2.3. Digital sensor for water input measurment in to the specimen(volume change)

Figure 2.4. Measurement gauge for confining and injection pressure with continuous control

2.4. Sealing the Specimens and Test Procedure Selection

Since the water must be just entered from top surface of the specimen, its lateral sides ought to be completely sealed. For this purpose, an elastic cover was used and all of the seams were sealed with silicon glue and the cover was fully attached to the top and bottom supports by special elastic rings, Then the confining pressure which was higher than injection pressure was applied to the specimen and sealed it completely (Figure 3).

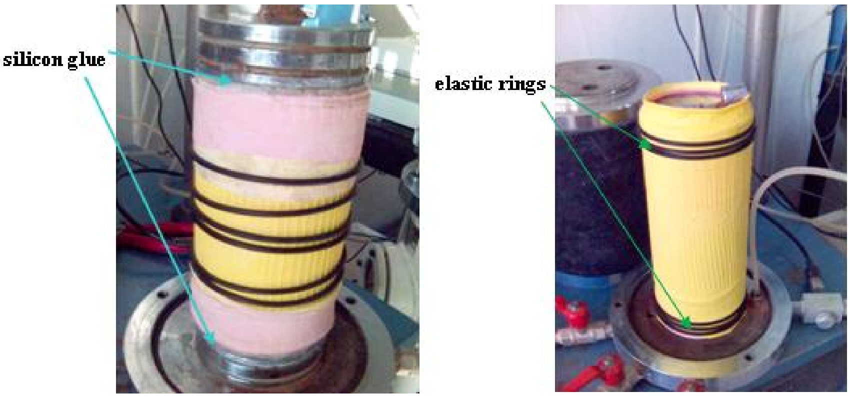

Figure 3. Covering the specimen with elastic jacket

Then the witness specimen kept in the oven for 48 hours at 110°C was placed in the triaxial apparatus and injection and confining pressures were applied as much as *490Kpa(4.9bar)* and *500Kpa(5bar),* respectively. With these preparations, the time period which lasted until the water reached the other side of the specimen could be determined. Since in the period of one hour, no water output considered, this time period was used as a criterion for time period test of the specimens and this procedure was finalized after two series of tests. [2]

2.5. Test Standard of Water Penetration Depth

According to implemented steps, standard method for the test is summarized as following:

- First all of the specimens should be kept in the oven for 48 hours at 110°C.
- Then the specimens should be placed into the triaxial apparatus for 60 minutes and under injection and confining pressures equal to 490Kpa and 500Kpa, respectively.
- Finally the specimens are brought out of the apparatus and broken in Brazilin way into two pieces. By considering the wet part of the half of the specimen, the wet distance measured from top surface of the specimen can be determined as water penetration depth.

It should be mentioned that the final penetration depth has been determined as average of five readings of middle, 1/2 from sides and 1/4 from sides of diameter of the specimens.

2.6. Characteristics of Test Specimens

2.6.1. Characteristics of Fresh Concrete

Characteristics of fresh concrete such as slump, density and ambient temperature are listed in Table (4).

Table 4: Fresh concrete characteristics

Mixture design	Ambient temperature (°C)	Slump (cm)	Fresh concrete density (gr/cm^3)
Witness	15	5	2.5
PN gel	15	16	2.53
PN liquid	15	17	2.5
PN liquid + micro silica powder	15	16	2.54

It can be concluded from the above table that slump variation of the concrete containing water proof materials is considerable in comparison to the witness specimen. Figure (4) demonstrates these variations properly. This vividly reveals the improvement of concrete workability.

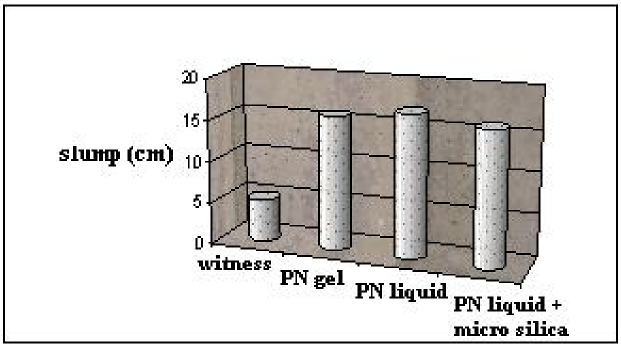

Figure 4. Slump comparison in different mixture designs

2.7. Characteristics of Hardened Concrete

2.7.1. Water absorption

Two procedures were used to measure water absorption of the specimens. The first one was mentioned in section 1-1 and the second one was in such a way that having the specimens placed in the oven for 48 hours at 110 °C and let them to be cooled in the air for two hours, they were placed in water for two hours and then water absorption of the specimens were measured.

The results of both methods are presented in the table below:

Table 5: Characteristics of hardened concrete and water absorption (first method-SSD)

Row No.	Specimen	Age (days)	SSD Weight (gr)	Dry weight 48hours (gr)	Specimen dimensions (cm)		Volume (Cm^3)	SSD density (gr/cm^3)	Dry density	Water absorption (%)
					diameter	height				
1	witness 1	28	3538	3244	10	18	1413.7	2.5	2.29	9.06
2	PN gel 1	28	3480	3226	10	18	1413.7	2.46	2.28	7.87
3	PN liquid 1	28	3954	3686	10	20	1570.8	2.52	2.35	7.27
4	PN liquid + Ms 1	28	3835	3586	10	20	1570.8	2.44	2.28	6.94

Calculation results can be seen in figure (5).

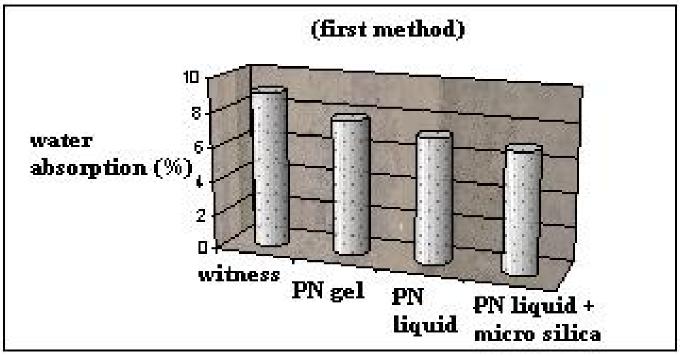

Figure 5. Water absorption comparison of the specimens in the first method

Table 6: Characteristics of hardened concrete and water absorption in second method

Row No.	Specimen	Age (days)	Wet Weight (gr)	Dry weight 48hours (gr)	Specimen dimensions (cm)		Volume (Cm^3)	wet density (gr/cm^3)	Dry density	Water absorption (%)
					diameter	height				
1	witness 1	28	3428	3244	10	18	1413.7	2.42	2.29	5.67
2	PN gel 1	28	3370	3226	10	18	1413.7	2.4	2.28	4.46
3	PN liquid 1	28	3843	3686	10	20	1570.8	2.45	2.35	4.26
4	PN liquid + Ms 1	28	3701	3586	10	20	1570.8	2.36	2.28	3.21

Water absorption variations in second method are demonstrated in Figure (6).

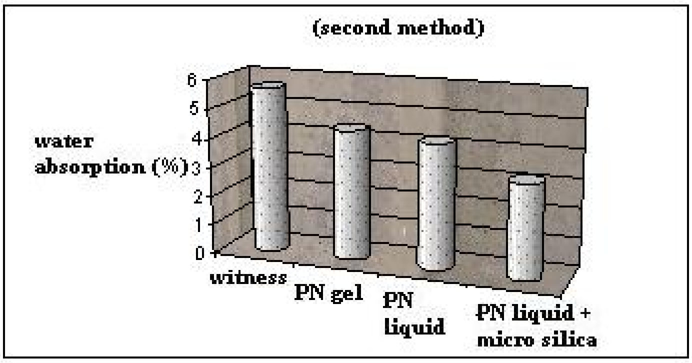

Figure 6. Water absorption comparison of the specimens in the second method

2.8. Water Penetration Depth

In order to start the test, the specimens were placed in standard conditions and tests were carried out for 4 specimens and the results are presented in the table and figure below:

Table 7: Results of water penetration depth tests

Row No.	Specimen	Age (days)	Specimen dimensions (cm)		Water penetration depth (cm)					Average (cm)
			diameter	height						
1	witness 2	28	10	18	15	14	13	14.5	15	14.3
2	PN gel 2	28	10	18	*	3.8	4.9	5.1	*	4.6
3	PN liquid 2	28	10	18	6	5.5	6	5.5	6	5.6
4	PN liquid + Ms 2	28	10	18	5.1	4.5	4	4	5	4.52

***since in the specimens containing PN gel, a small part of upper surface has become water resistant by the glue, therefore the values for the sides were invalid and measurements were made at three middle points.**

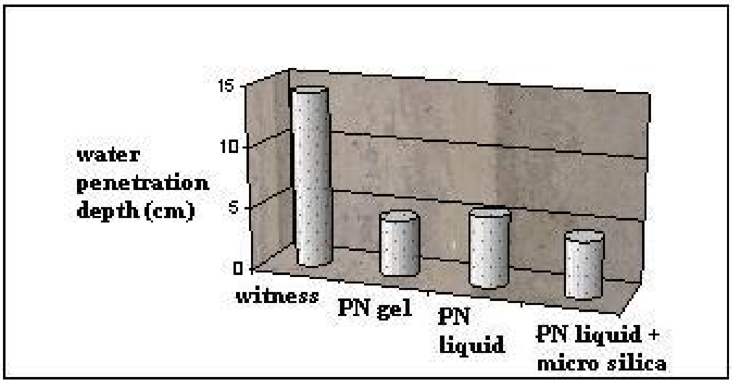

Figure 7. Water penetration depth comparison based on the mentioned standard

Figure 8. Water penetration depth in witness specimen

Figure 9. Water penetration depth in the specimen containing PN gel

Figure 10. Water penetration depth in the specimen containing PN liquid

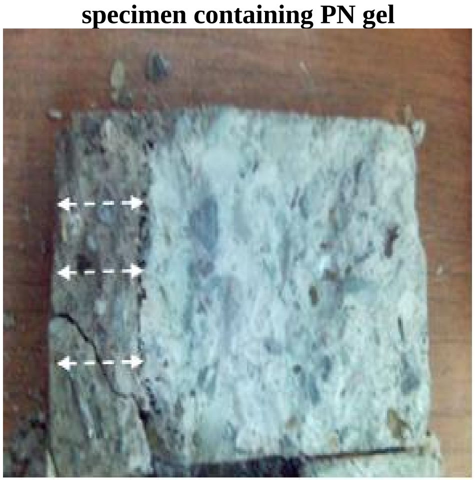

Figure 11. Water penetration depth in the specimen containing PN liquid + Ms

3. CONCLUSION

All of the obtained results for different tests on 28-day specimens have been listed in the following table. In this table, water absorption and penetration depth improvements for two methods are presented.

The results can be interpreted as following:

- Using PN water resistant additives, penetration depth can be reduced by 60% in average.
- Based on the fist method, concrete water absorption decreases by 13% to 23%.
- Based on the second method, concrete water absorption decreases by 21% to 43%.
- Using PN water resistant additives, the workability of concrete increased considerably, i.e. the slump value increased three times compared to the witness.

Table 8: Results add up and Comparison

Row NO.	Test type	Specimen age (days)	Improvement percentage
1	Water penetration depth in witness specimen	28	-
2	Water penetration depth in the specimen containing PN gel	28	67.83
3	Water penetration depth in the specimen containing PN liquid	28	60.84
4	Water penetration depth in the specimen containing PN liquid + Ms	28	68.39
	Water absorption percentage (first method)		
5	Water absorption depth in witness specimen	28	-
6	Water absorption depth in the specimen containing PN gel	28	13.13
7	Water absorption depth in the specimen containing PN liquid	28	19.76
8	Water absorption depth in the specimen containing PN liquid + Ms	28	23.4
	Water absorption percentage (second method)		
9	Water absorption depth in witness specimen	28	-
10	Water absorption depth in the specimen containing PN gel	28	21.34
11	Water absorption depth in the specimen containing PN liquid	28	24.87
12	Water absorption depth in the specimen containing PN liquid + Ms	28	43.39

REFERENCES

1. Concrete and aggregates. 1988. Annual Book of ASTM Standards, part 04.02 ASTM, Philadelphia, PA, 751pp.
2. Olsen, H. W., Morin, R. H., and Nichols, R. W., "Flow Pump Application in Triaxial Testing," Symposium on Advanced Triaxial Testing of Soil and Rock, ASTM STP 977, ASTM, 1988, pp. 68-81.

CD05-009

APPLICATION OF GENETIC ALGORITHM IN OPTIMIZATION OF FIBERS DIRECTION IN COMPOSITE FRP JACKETS FOR LATERAL RETROFITTING OF RC COLUMNS

H.R.Ashrafi[1], M.Jalal[2], K.Garmsiri[3]
[1]Assistant professor, Dept of civil Engg. School of Engg. Razi University, Kermanshah, Iran
[2]M.Sc. Student, Dept of civil Engg. School of Engg. Razi University, Kermanshah, Iran
[3]M.Sc. Student, Dept of mechanical Engg. School of Engg. Razi University, Kermanshah, Iran

ABSTRACT

In the recent years, many researches have been implemented in the field of composite fibers in concrete. One of the effective and efficient methods of rehabilitation and strengthening of RC members is application of composite materials and FRP jackets and laminates. These laminates are made in different ways with respect to the direction and orientation of fibers forming the layers. Generally 1D, 2D or 3D layers are used for this purpose for which the direction of fibers varies for different types. Selection of the best and optimized direction of fibers is of great importance to fully utilize the strength capacity of composite fibers and the layers.

In this paper, genetic algorithm is considered to be used to find the optimized direction of fibers in composite layers. In this way, different angles of fibers in the layer are tested by genetic algorithm to so that the best performance of the composite layers is obtained. It should be considered that by this optimization, lateral resistance of concrete members wrapped by composite layers can be improved.

Keywords: genetic algorithm, fibers direction, composite fibers, optimization, FRP jackets

1. INTRODUCTION

As a result of development of composite materials technology and their cost decrease during last three decades, application of such materials as a good replacement of metallic alloys has been promoted. Generally, a composite is combination of at least two materials which are combined to produce desirable characteristics. In practice, most of composites contain a base material and a strengthening element which is added to the base material to increase its strength. The most common composite materials are those composed of a series of strong fibers tightly packed together by means of a bonding material. In fact, the bonding material acts as a paste or matrix and let the stress transfer from one fiber to another so that a uniform and integrated formation is produced.

Composites offer variety and combinations of characteristics which are not available in traditional materials. It is possible for the fibers in high stress areas to be in the position, orientation and volume so that maximize the efficiency and functionality and again in another area of low stress in the same member, the characteristics may be changed to satisfy the requirements. Other advantages include: light weight, corrosion resistance, flexibility and desirable functionality in structures.

Fibers form an important element of composite materials. Totally, 30 to 70 percent of composite volume consists of fibers which may be in individual or woven form.

Regardless of the geometry, fibers are mad of different materials the most common of which in structural applications are glass, carbon and aramid. Also new fibers of high strength have been developed which are known as 'Advanced fibers'. Composites made of such materials are also called 'advanced' composites. Mechanical properties of composites are dependant on different parameters such as fibers type, volume and orientation. These materials are anisotropic and their strength varies in different directions. Their stress-strain curve shows a sudden failure at the yielding point. Although the resin shows visco-elastic behavior under applied loads and bear creep and relaxation, the total composite is design so as to satisfy the needed requirements.

A kind of composites known as FRP are made of different fibers as mentioned earlier such as carbon (CFRP) and glass (GFRP) and also aramid (AFRP). These products are being widely used in different applications such as cylindrical shells and in different forms like jackets and laminates for structures retrofitting. In the latter application, FRP may be used as lateral confinement around the concrete member to enhance its load bearing capacity.

For example in Europe and New Zealand, the seismic philosophy for achieving ductility is different, relying more on increasing the non-linear concrete stains through concrete confinement [3]. The advantage of this philosophy is that apart from smaller cross-sections, a significantly higher amount of lateral reinforcement is required. This lateral reinforcement, which is there to confine the concrete, is also beneficial in resisting additional shear and preventing splice and anchorage failures.

The enhancement of concrete ductility by confinement is central to the principles of Eurocode 8. However, researchers dealing with FRP confinement do not always consult the huge wealth of published work, which is derived from the earthquake engineering research.

From Figure 1, it can be easily recognized that lateral confinement has effectively improved the load bearing capacity of the RC columns confined by CFRP and GFRP. Physical and mechanical properties of the composites are presented in the following tables:

E_{frp}	Young’s modulus of elasticity
f_{frpu} ε_{frpu}	Ultimate tensile strength and elongation of pultruded laminate
T_{GM}	Glass transition temperature
V_{f+}	Volumetric fibre content

Table 1: Physical and Mechanical properties of Fibre sheets [6]

Fibre	E_{frp} GPa	f_{frpu} MPa	ε_{frpu} %	Density gr/cm^3	T_{GM} C^o	V_f %	Composition
GFRP AR	65	1700	2.88	2.6	-	100	Bi-Directional
CFRP 240	240	3900	1.55	1.7	100-130	100	Uni-Direction

Table 2: Physical and Mechanical properties of Epoxy Plus Structural Adhesive [6]

Epoxy	Colour	Strength MPa	$E_{m\ flexural}$ GPa	Density kg/litre	T_{GK} C^o	Manufacturer U.K.
Adhesive	Mid grey	19	9.8	1.535	60	SBD
Primer	Translucent	-	-	1.12	-	SBD

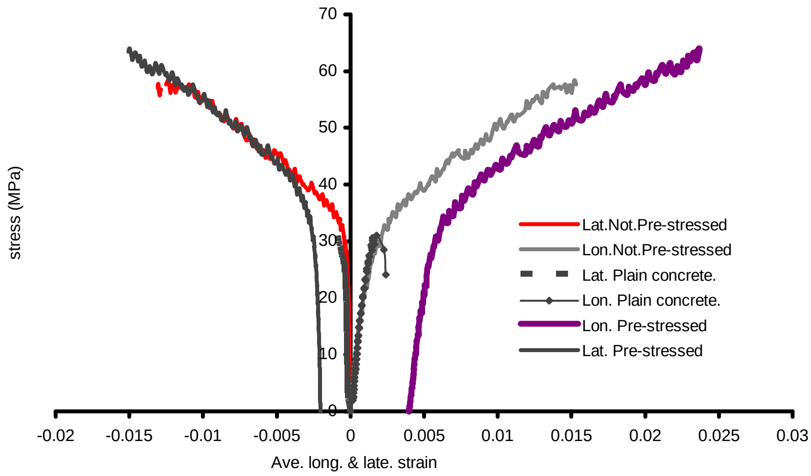

Figure 1. Comparison of Ave. longitudinal and lateral strain measured by strain gauges VS. stress

2. CLASSIFICATION OF COMPOSITES BASED ON GEOMETRY AND STACKING OF LAYERS

Classification of composites varies depending on geometry and stacking of layers. The basic form is the unidirectional layers with continuous fibers. The one layer may itself be composed of several layers however; all of the fibers are oriented in the same direction, weather in simple or woven form.

Multi layer laminates are made by stacking of unidirectional layers each of which having different fiber orientation. Efficient properties of multi layer laminates vary by fibers orientation, layers thickness and stacking order. Hybrid composites which are used in many applications include more than one kind of fiber or combination of fibers and metallic materials. Different types of fibers are combined in a composite to achieve the best performance and lowest cost. Nevertheless, in many applications one kind of fibers may be used in different layers with various fibers orientation and in order to achieve the best performance, the angle of the fibers should be optimized (Figure 2)

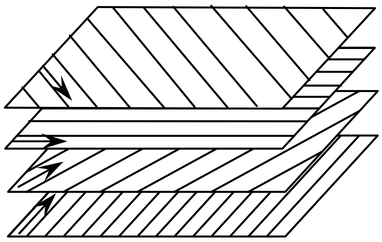

Figure 2. Different fibers orientation in different layers of composite material

3. GENETIC ALGORITHM (GA) METHOD

Optimization algorithms are divided into two basic types, one based on differential equations and other based on numerical methods. The former one uses gradient-based search with a suitable primary guess. These algorithms search range is local and concerning ill-posed target functions, they are instable and get involved in local optimized points. Many numerical methods have been proposed to overcome the local optimized problem however; these methods increase the calculations volume. Genetic algorithm which belongs to the latter type of optimization algorithms is the most applicable evolutionary algorithms. In spite of many methods, the genetic algorithm utilizes the probabilistic rules instead of deterministic ones for conducting the search process to the more suitable search space.

GA algorithms basically were developed to study intelligent systems nevertheless; they were used from the beginning in optimization of practical engineering problems. GA usually include a population of individuals, fitness function, crossover operator and new generation replacement. Figure 3 shows the cycle of classic GA (CGA) and basic elitist GA (BEGA).

In the GA, first a determined numbers of inputs, which belong to the sample space X are selected and displayed as a vector, X=(x_1, x_2,…x_n), which is called 'chromosome'. A group of chromosomes form 'colony' or 'population'. In each step, the population evolves based on determined rules. There is a fitness for each chromosome as $f(x_i)$. Stronger elements or chromosomes the fitness of which is closer to the optimized of the colony would have more chance to survive in next generations. In other word, inputs closer to the optimized solution will remain and others will be disregarded.

Another important step is the birth which is occurred once in each period. In this process, two suitable chromosomes are combined to generate more optimized chromosome. Furthermore, during each period a series of chromosomes might have mutation.

4. DIFFERENCE BETWEEN GA AND TRADITIONAL OPTIMIZATION METHODS

The difference between GA and other optimization methods may be summarized as follows:

- Despite the other methods, GA uses several search points (as a set of individuals) which are convergent instead of one search point. Therefore, the possibility of getting involved in local optimized points decreases significantly and on the other hand, the access probability of the global optimized point will increase.

- GA takes advantage of the data obtained (from fitness function) instead of the derivatives or subordinate data.
- It is applicable to optimization problems with multi-objective functions.
- It is applicable to linear, nonlinear and ill-posed problems
- It can be combined with other optimization methods
- It s a powerful algorithm to approach the nearest optimized solution with high probability.

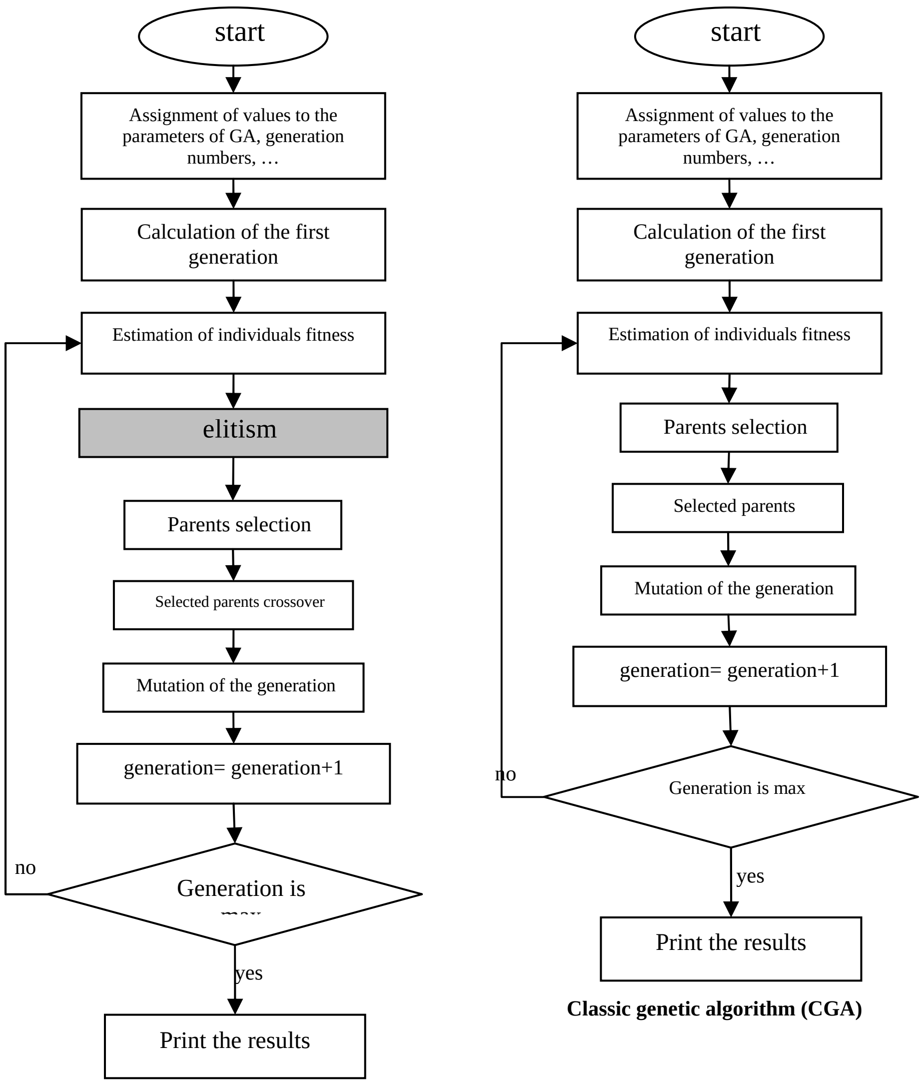

Classic genetic algorithm (CGA)

Basic elitist genetic algorithm (BEGA)

Figure 3. diagram of CGA and BEGA cycles

5. THE ROLE OF NEURAL NETWORK IN GA OPTIMIZATION

GA is a powerful method in optimization problems especially multi-objective optimization, however, one of disadvantages of GA is high CPU time. This reason and also stochastic nature of GA in solving the optimization problems make the process of optimization slow down. Using ANN, this problem can be overcome while maintaining the other useful characteristics of GA.

In this study, first the neural network was trained and then tested and the trends obtained from ANN was used in GA to optimize fibers angles and also final value of objective function.

6. SIMPLE OPTIMIZATION OF NATURAL FREQUENCY OF FOUR-LAYER FRP CYLINDRICAL SHELL

Characteristics of the composite cylindrical shell are illustrated in Figure 4.

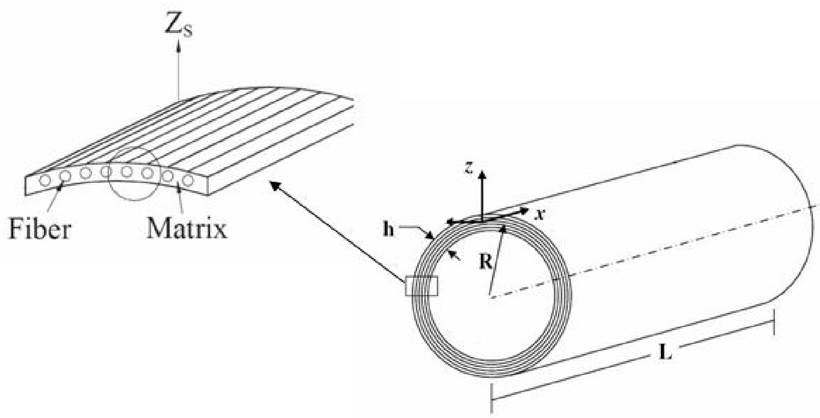

Figure 4. Sketch of a Multi-layer composite cylindrical shell

In this study, the ANN trained and tested to be used in GA was one of the back propagation algorithms called *Levenberg-Marquardt* which had the best results and less errors compared to other algorithms. This four-layer network has 4 neurons in input layer and one neuron in output layer. The characteristics of the network are presented in Table 3.

Table 3. Characteristics of trained ANN to model natural frequency of four-layer shell for h/r=0.01

Number of inputs	Hidden layers				Output layer	
	First layer		second layer		Third layer	
4	Transition function	Number of neurons	Transition function	Number of neurons	Transition function	Number of neurons
	Tangent sigmoid	25	Tangent sigmoid	12	Pure lin	1

In order to assure the appropriate performance of the network, it should be tested and the training error should be determined. Figure 4 shows MSE curve with respect to the cycles of ANN for modeling of first natural frequency.

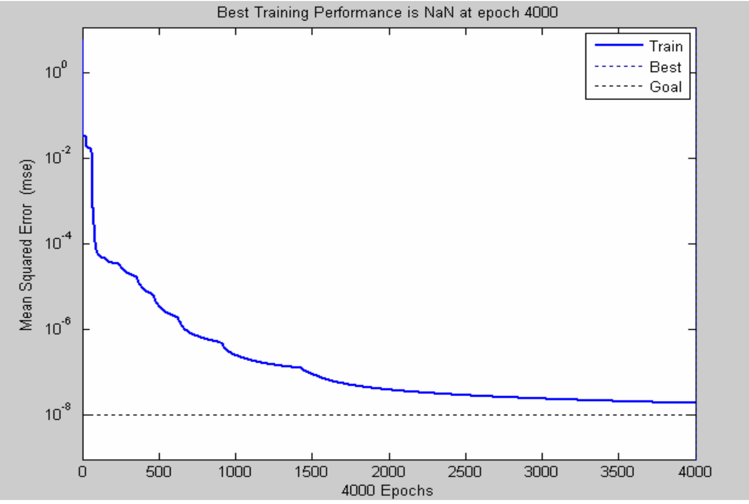

Figure 5. MSE curve with respect to the ANN cycles to train first natural frequency in four-layer shell for h/r=0.01

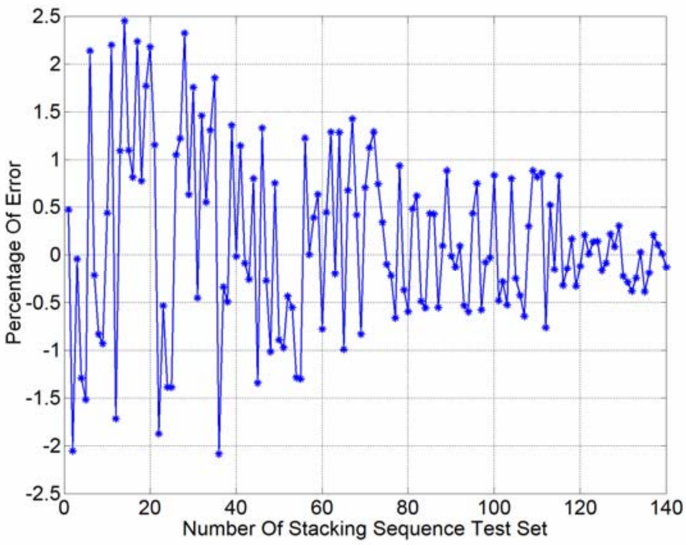

Figure 6. Errors of the trained ANN for natural frequency in test space

As can be seen in Figures 4, 5 MSE in the network is around 10^{-8} and maximum error in the trained network in test stage is about 2.5% which shows appropriate accuracy of the network.

When the network is tested and its performance is assured, the process of optimization starts. Increase of fitness function of GA using analytical solution and ANN for following state is compared in Figure 7.

$$L = 1(m)\ ,\quad R_m = \frac{L}{2}\ ,\quad h = \frac{R_m}{100}$$

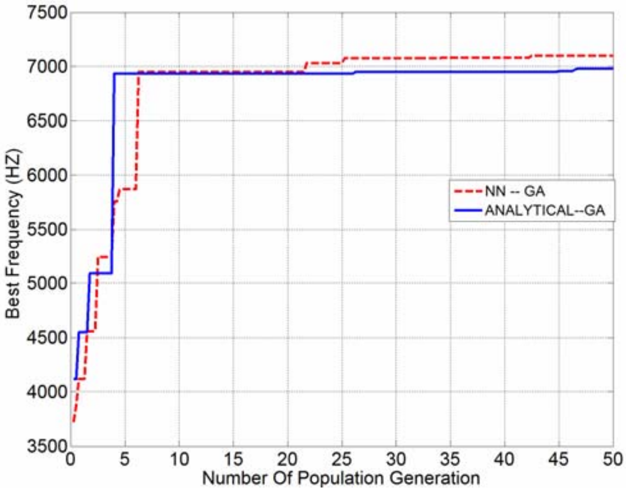

Figure 7. Comparison of two fitness function increase in GA obtained by analytical solution and ANN for four-layer shell in the case of h/r=0.01

According to Figure 7, the best frequency obtained from GA and analytical solution is equal to 7016 (Hz) which was reached after 46 generation and after that no improvement in frequency observed. Angles of layers stacking are as following:
$\theta = [-45^\circ\ \ 46^\circ\ \ 40^\circ\ \ 45^\circ]$

However, the frequency obtained from GA and neural network is equal to 7152(Hz) which was reached after 42 generation. In this method, Angles of layers stacking are as following:

$$\theta = [73^\circ\ \ 58^\circ\ \ -48^\circ\ \ 73^\circ]$$

It should be mentioned that in this process, number of 50 generation was considered as stop criterion of the cycle.

As it is obvious in Figure 8 increase of fitness function in both methods are in good agreement and the final result which is the optimized frequency has rather small error. Therefore, using ANN has speeded up the optimization while keeping the error desirably small. The error due to application of ANN in GA instead of analytical solution is presented in Table 4.

Table 4. Results comparison of ANN and analytical solution in GA for frequency calculation of four-layer shell in the case of h/r=0.01

Maximum of fitness function(GA and analytical solution)	Optimized fibers angle in the layers	g^*	Maximum of fitness function (GA and ANN)	Optimized fibers angle in the layers	g^*	Error percentage in frequency calculation
7016	[-45,46,40,45]	46	7152	[73,58,-48,73]	42	1.94

Figure 8 shows average of fitness functions in generation of sequential populations for four-layer shell which is calculated by following equation:

$$f_m = \frac{\sum_{i=1}^{n_s} f(c_i)}{n_s}$$

Where:
c_i is i^{th} member of the population.
Also fitness function increase and fitness functions average in GA for four-layer shell for h/r=0.01 are presented in the same plane in Figure 9.
It can be observed that average of fitness functions increases at 45^{th} generation until reaches its maximum which the corresponding frequency of 45 is 4400(Hz) that implies the appropriate performance of the process.
Having made sure the proper performance of ANN in GA for h/r=0.01, ANN may be used for other conditions such as h/r=0.05, 0.1 to find the optimized frequency.

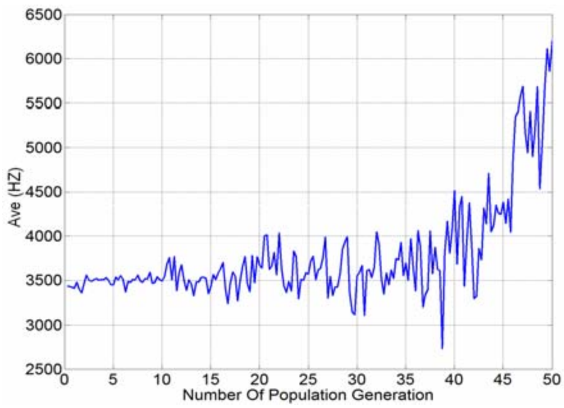

Figure 8. average of fitness functions in generation of sequential populations for four-layer shell in the case of h/r=0.01

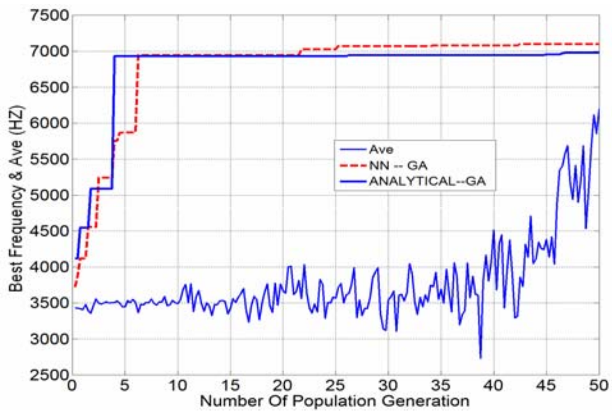

Figure 9. presentation of fitness function increase and fitness functions average in generation of sequential populations for four-layer shell in the case of h/r=0.01

The best frequency obtained for four-layer shell for h/r=0.05 was equal to 7222(Hz) that was reached after 20 generations. The corresponding stacking of layers is as below:

$$\theta = [-74^\circ \;\; 56^\circ \;\; 71^\circ \;\; -18^\circ]$$

Also the best frequency obtained for four-layer shell for h/r=0.1 was equal to 7243(Hz) that was reached after 46 generations. The corresponding stacking of layers is as below:

$$\theta = [-73^\circ \;\; 73^\circ \;\; -73^\circ \;\; 72^\circ]$$

In both cases number of 50 generations considered as end of the cycle. All of the optimization results for four-layer shell for different thicknesses are presented in Table 5.

Table 5: optimization results of layer stacking in four-layer shell

h/r	Maximum frequency(Hz)	Optimized fibers angle in the layers	Number of generations for maximum frequency(Hz)
0.01	7152	[73,62,-48,73]	42
0.05	7222	[-74,-56,71,-18]	20
0.1	7243	[-73,73,-73,72]	46

7. CONCLUSION

Since the strength of FRP shell composed of several layers is affected by orientation of fibers in different layers, so finding the best angle of fibers in each layer to optimize the strength of FRP shell is of great importance. With this respect, GA was applied to do this optimization. In the process, ANN was used to speed up the optimization process while keeping the errors small. Results comparison of analytical solution and ANN showed good agreement.

The results of optimization showed that the increase of thickness and number of layers would result in increase of optimized solution and frequency.

REFERENCES

1. Grosset L., Le Riche R., and Haftka, R.T., “A comparison of an estimation of distribution algorithm and a stochastic hill-climber for composite optimization problems” Proceedings of the American Society for Composites 18th Technical Conference, Gainesville, FL, October 19-13, 2003, paper No. 168.
2. B. Krose, P. Smagt, "An Introduction To Neural Networks", Ninth Edition, November 2001.
3. C. Fyfe, "Artificial Neural Networks", Department of Computing and Informationn Systems, Second Edition, 1998.
4. Fukunaga, H., Vanderplaats, G.N.,” Stiffness Optimization of Orthotropic laminated Composite using lamination parameters”, AIAA Journal, vol 29 No.4, 641-646, (1991).
5. C.W. Bert, “Optimal Design of a Composite Material Plate to Maximize its Fundamental Frequency”, J .of sound and vibration vol. 50(2) pp.229-237,

(1977).
6. Pilakoutas K. and Mortazavi A. "Ductility through external lateral confinement of RC members with FRP". Non-metallic (FRP) reinforcement for concrete structures, proceeding of the third international Symposium, Vol. 1. 107, No. ST1, Oct. 1997, pp 225-232.
7. Pilakoutas K., "Ductility design of reinforced concrete members", 16th European Seminar on Earthquake Engineering, Stara L., Czechoslovakia 6-12 Oct. 1991, pp 62-71.
8. Mortazavi A., "Strengthening, ductility and repair of RC structures by lateral confinement", MPhil thesis, University of Sheffield, Oct. 1998.

CD05-010

PREDICTION OF COMPRESSIVE STRENGTH OF COMPOSITE FIBER REINFORCED CONCRETE (FRC) USING ARTIFICIAL NEURAL NETWORK

H.R.Ashrafi[1], M.Jalal[2], K.Garmsiri[3]
[1]Assistant professor, Dept of civil Engg. Faculty of Engg. Razi University, Kermanshah, Iran
[2]M.Sc. Student, Dept of civil Engg. Faculty of Engg. Razi University, Kermanshah, Iran
[3]M.Sc. Student, Dept of mechanical Engg. Faculty of Engg. Razi University, Kermanshah, Iran

ABSTRACT
Within the framework of studies on FRC, a series of tests were undertaken in the laboratory in order to better understand the behavior of FRC and composite fibers to characteristic loading. The results obtained in the tests vary according to the type and arrangement of fibers, the water content, the size of grains (grains size distribution) and percentage of composite fibers. Therefore, it is important to estimate the strength of concrete according to available data and in the case of lacking of enough experimental data. For this purpose, neural network technique was used to predict the strength of concrete based on mix proportions. At first the results of experimental tests carried out in PWUT laboratory on fiber reinforced concrete specimens are presented and then the missing experimental data and gaps in compressive strength trends are predicted by back propagation method in neural network. It is worth mentioning that it can also be used to study the different mix parameters on concrete strength.

Keywords: neural network, back propagation, fiber reinforced concrete, composite fibers

1. INTRODUCTION
Compressive strength of the hardened concrete is the most important property that describes its quality and suitability for construction works. Also, it considers the mother strength, where most of other properties and strengths; such as tension, flexural, shear and bond with steel reinforcement are improved with the improvement in compressive strength and vice versa. Most often, an ultimate target in the mixture design is the 28-day compressive strength. This strength is usually determined based on a standard uniaxial compression test, and is accepted universally as a general index of concrete strength.
Most research in material modeling aims to construct mathematical models to describe the relationship between components and material behavior. These models consist of mathematical rules and expressions that capture these varied and complex behaviors. Concrete is a highly nonlinear material, so modeling its behavior is a difficult task. However, the artificial neural network (ANN) was proved to be able in predicting the concrete compressive strength, without the need

of specific equations (Yeh 1998, Guang and Zong 2000, Lee 2003, Kim et at. 2004). Also, its application would reduce the time and cost required for making specimens and the 28 day waiting period before they could be tested. The ANNs have recently been widely used to model some of the human activities in many areas of science and engineering. They need sufficient input-output data, which may be theoretical, experimental or empirical. ANNs can deal with incomplete and noisy data, which is the predominant case in engineering applications.

In this study, the back-propagation neural network (BPNN) was used to predict the fiber reinforced concrete compressive strength based on the mix proportions and fiber percentages. Training and testing patterns of the network were prepared using the data sets containing the mix proportions of two ready-mixed concrete companies and fiber percentages from specimens tested in the laboratory. The estimated strengths were compared with those tested in the laboratory.

2. ARTIFICIAL NEURAL NETWORKS

As in the biological neurons, the information processing system of the ANN consists of three main aspects: transmission of information, processing of information and storage of information. The counterparts in ANN are the input layer, one or more hidden layer and the output layer. The input layer consists of number of nodes each of which receives input data of an independent variable. Thus, the total number of nodes in the input layer is equal to the total number of the input variables of the problem.

The hidden layer receives information from input layer, using the applied weights and pre-specified activation functions (Waszczszyn, 1998). The output layer receives the processed information from the hidden layer and sends the results to an external recreant. The number of nodes in the output layer is equal to the number of output variables.

The number of hidden layers and the number of nodes in each hidden layer are important factors in the design of the network, and there are no generally applicable rules to determine these numbers exactly (Flood and Kartam, 1994). l-lowcvcr, there are some suggestions, which were proposed to aid in selecting the optimum number of nodes and layers in the hidden part (Flood and Kartam 1994, Hajela and Berke 1991).

The collected data for the problem is divided into training and testing data sets. Depending on the available data, about 60-70% of the total data is used as a training data. The number and distribution of training patterns affect the generalization ability of the ANN (Flood and Kartam, 1994). The training pattern must cover all the possible ranges of the study.

Once the topology of the ANN is determined, the training process is started by assigning values to the training parameters and specifying the activation function and learning algorithm. Different learning algorithms could be used; among of which the back- propagation algorithm is predominant one used in civil engineering applications (Adeli, 2001). This algorithm looks for the minimum of the error function in weight space using the method of gradient decent.

3. PROPOSED ANN MODEL FOR THE PRESENT CASE

The data used in this study consisted of actual mix proportions provided by two different ready mixed concrete companies and also the data of force-deflection curve of the specimens containing different percent of fibers. The back propagation neural network was applied on these data using the MATLAB software. Several MATLAB subroutines were developed and various other commands were used to perform the task. Constructing the proposed ANN model consisted of the following steps:

3.1. Preparation of Training and Testing Data Sets

The total number of records obtained was about 70; table 1 gives the minimum maximum and average values of each parameter of the concrete mix proportions and fiber percentages. Two-third of the data set (i.e., 47 records) was used for training and one-third (i.e., 23 records) was used for testing the ANN. Due to the large difference in the values of the data provided to the ANN and since the activation functions are often varied within 0 to 1 or -l to 1, the training patterns were normalized before they were applied to the ANN.

Table 1: Minimum maximum and average values of each mix parameter

	slump cm	w/c	unit water content kN/m^3	unit cement content kN/m^3	natural sand kN/m^3	coarse agg. kN/m^3	fiber percentage %	Admix %	strength Mpa
Min	1	0.32	1.3	2.66	2.5	8.9	0	0.74	19.3
Max	9	0.6	1.6	5.67	9.2	10.1	5	2.2	44.1
Ave.	5	0.46	1.45	3.75	5.35	9.5	2.5	1.47	31.7

3.2. Determination of Mean Square Error (MSE)

MSE is an important parameter to be specified in training and testing ANNs. To identify its value, an ANN having one hidden layer with 20 nodes was used with MSE decreasing up to about 10^{-6}. The curves of MSE for different percent of fibers are presented in Figure 1.

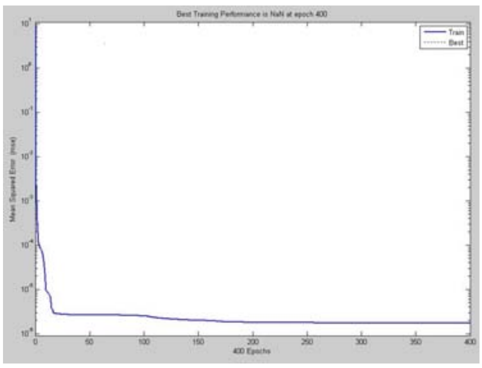

Figure 1a. MSE curve for specimens containing 1% of fibers

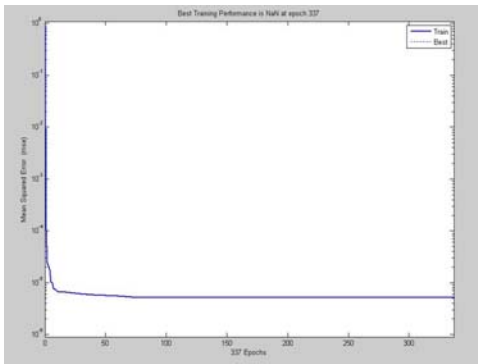

Figure 1b. MSE curve for specimens containing 2% of fibers

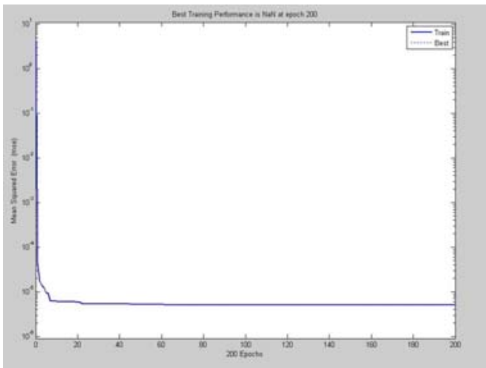

Figure 1c. MSE curve for specimens containing 3% of fibers

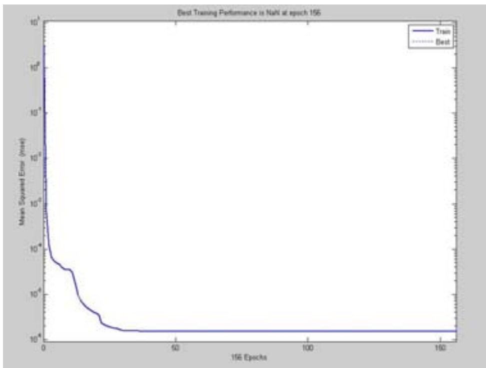

Figure 1d. MSE curve for specimens containing 5% of fibers

3.3. Training of the ANN

Computer subroutines were developed to utilize the ANN tools in MATLAB environment and used in training the suggested ANN. It consisted of the following main steps:

a. Reading the training data set and specifying the input and output variables to the ANN.

b. Normalizing the training data according the normalization rule selected.

c. Defining the topology of the ANN. This was achieved by specifying the number of hidden layers in excess of the input and output layers. The number of hidden layers was selected to be 1 and 2. In each one of these ANNs, the number of nodes in the input and output layers was 8 and 1, respectively, see figure 2 for the one-hidden layer ANN. The number of nodes in the hidden layer was varied and searching was carried out to determine the optimum number of nodes that satisfies the acceptable value of MSE with a minimum possible time (number of epochs) consumed during the run.

d. Specifying the transfer functions used for the hidden and output layers; they were log-sigmoid (logsig) and linear (purline), respectively.

e. Specifying the learning rule used, which was the evenberg_MarqUdt algorithm with the identity acronyms within the MATLAB - Trainlm (Demuth et aL., 2006).

f. Specifying the training parameter required for convergence (MSE) and the limiting maximum number of epochs.

g. Training the ANN defined according the above steps.

h. Computing the normalized target variables, then converting them to the same units of the original targets.

i. Evaluating the ANN training efficiency by plotting the output of ANN versus the original target values.

X1	**The slump**
X2	**The water to cement ratio**
X3	**The unit water content**
X4	**unit natural sand content**
X5	**The unit natural sand content**
X6	**The unit coarse agg. content**

X7	**The fiber percentage**
X8	**The admixture ratio**
Y	**The compressive strength**

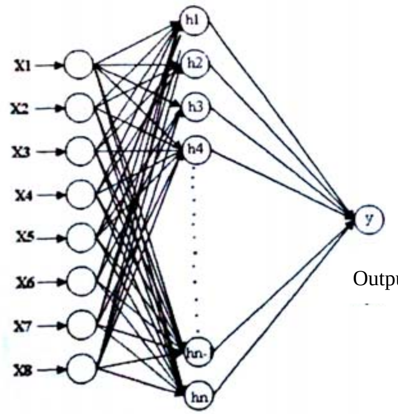

Figure 2. Topology of one-hidden layer ANN

3.4. Determination of the optimum topology for the ANN

At each suggested number of nodes, the maximum error and the total number of epochs required to converge the specified MSE were recorded and. As clarified, the ANN with 22 nodes was considered the optimum for the case of one hidden layer. It gave reasonable maximum % error with very low number of epochs; 1.3526 at 8, respectively. Also, the ANN with 6 nodes in the first hidden layer and 5 nodes in the second hidden layer (6-5) was considered as the optimum for the case of two hidden layers, because it gave the lowest value of the maximum % error with reasonable number of epochs; 1.2268 at 98, respectively.
Comparing the performance of the above mentioned ANNs showed that the both types of ANN were performed well with this type of data. The one-hidden layer ANN with 22 nodes was the optimum in view of the time consumed (number of epochs), however, the two-hidden layers ANN with 6-5 nodes was the optimum in view of the maximum percent of error. In fact the difference in accuracy between the two types of ANN was very small when compared with the higher reduction in the number of epochs, so the one-hidden layer ANN was more preferable.

3.5. Testing of the Optimum ANN

Once trained, the optimum ANN need to be tested to evaluate whether it can successfully estimate the force-deflection curve (stress-strain behavior) and compressive strength of fiber reinforced concrete based on mixing proportions. The testing data set was used for this task. Again this set contained actual data provided by companies and empirical results from laboratory, but completely different from those used for training the ANN. Figure 3 shows the train error curves of ANN method.

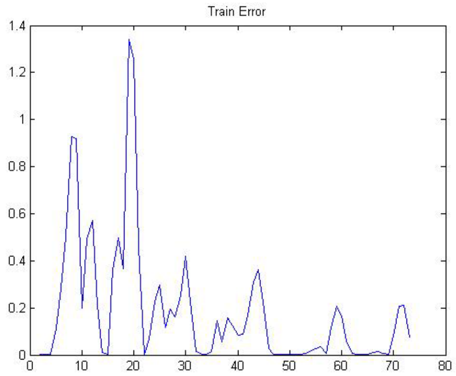

Figure 3a. training error for 1% of fibers

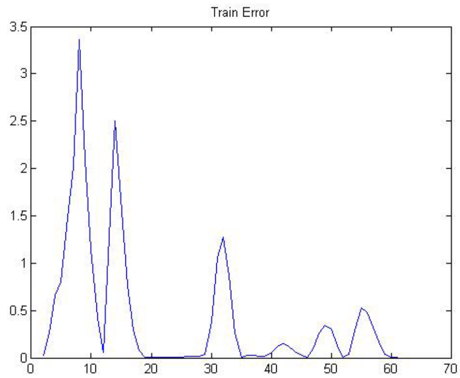

Figure 3b. training error for 2% of fibers

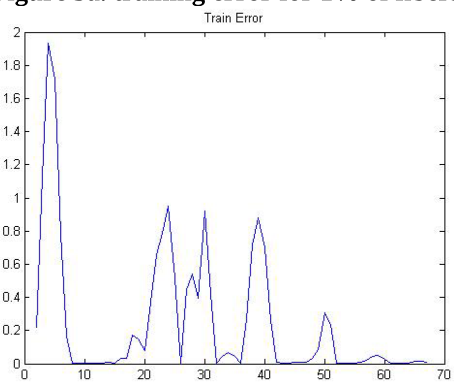

Figure 3c. training error for 3% of fibers

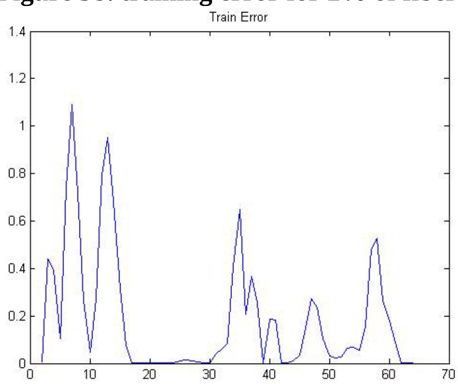

Figure 3d. training error for 5% of fibers

4. FACTORS AFFECTING PERFORMANCE OF ANN

4.1. Effect of Learning Algorithm

There are a lot of learning algorithms available in the neural network toolbox for use with the MATLAB (Demuth et. al., 2006). The Trainlm or Levenberg-Marquardt algorithm was used in the training process of the optimum ANN. As well observed the Training algorithm was the best, since it had the lower value of the maximum % error at smaller number of epochs.

4.2. Effect of Normalization Method

The normalization method used in obtaining the optimum ANN was the mean and standard deviation (mean-std) method. To study the effect of the normalization method, the optimum ANN was trained and tested using the minimum and maximum (mm-max) normalization method. The results showed that a lower error in the target was obtained by the use of the mean-std method. This means that the mean-std normalization method can be considered as more suitable for this type of data.

5. APPLICATIONS USING OPTIMUM ANN

The use of ANN extended to be applied for studying the effect of certain parameters on the 28-day FRC strength and force-deflection curve. For example, figure 4 shows the effect of fibers on the 28-day force-deflection curve and final compressive strength of concrete. Figure 5 shows the fitness curves of experimental and predicted values.

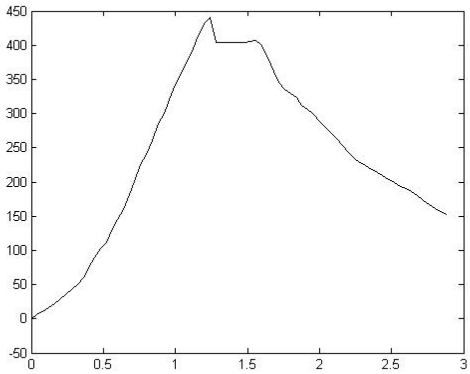

Figure 4a. predicted force-deflection curve for 1% fiber specimens

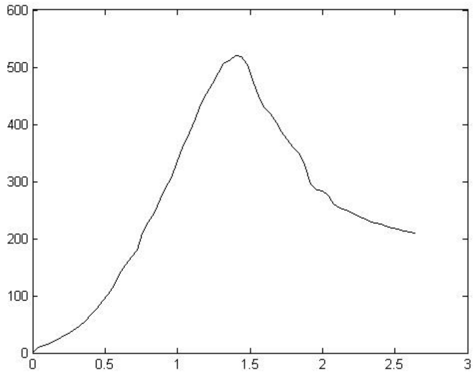

Figure 4b. predicted force-deflection curve for 2% fiber specimens

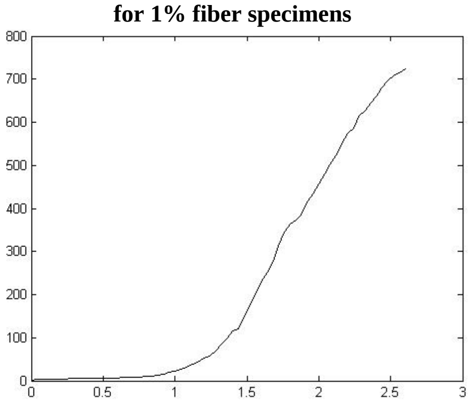

Figure 4c. predicted force-deflection curve for 3% fiber specimens

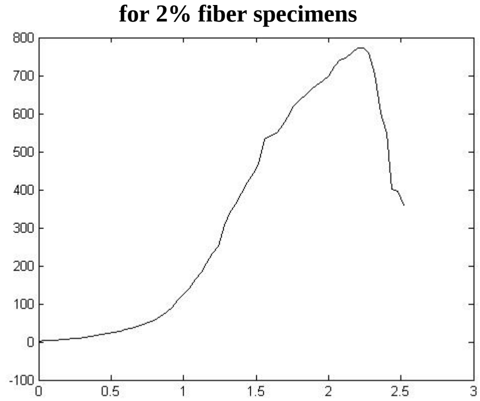

Figure 4d. predicted force-deflection curve for 5% fiber specimens

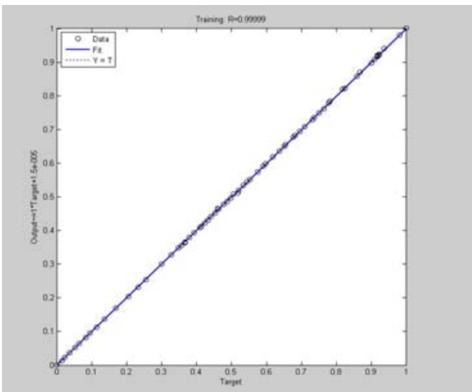

Figure 5a. Fitness curve for 1% of fibers

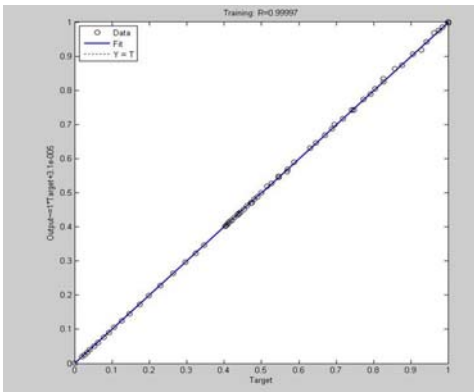

Figure 5b. Fitness curve for 2% of fibers

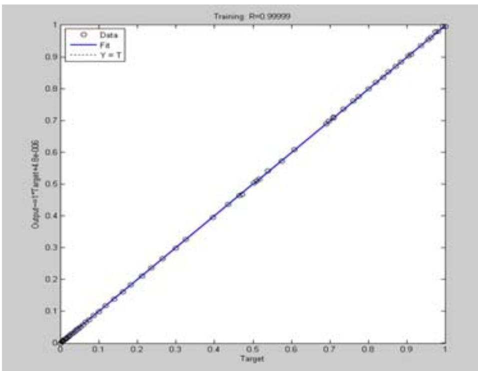

Figure 5c. Fitness curve for 3% of fibers

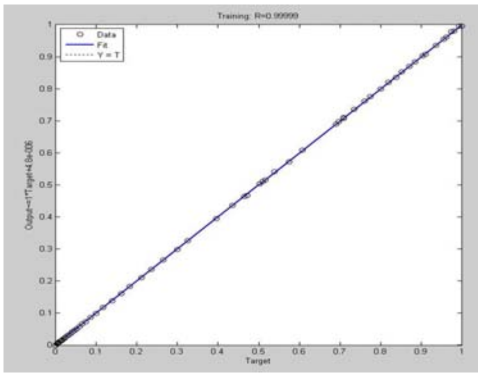

Figure 5d. Fitness curve for 5% of fibers

6. CONCLUSION AND PERSPECTIVES

In this study the feed-forward back-propagation ANN was used to predict the force-deflection curve and compressive strength of concrete based on mix proportions and also fibers percentages. The results showed that the one-hidden layer ANN with 22 nodes and the two-hidden layers ANN with 6-5 combination of nodes could accurately estimate the Concrete force-deflection curve and compressive strength. However, the one-layer ANN was more preferable. The optimum ANN was also used to study the effect of certain mix parameters on the 28-day compressive strength and stress-strain behavior; the relations developed showed trends similar to the experimental ones. The standard deviation normalization method and the Levenberg-Marquardt learning algorithm were proved to be more efficient for the present study.

REFERENCES

1. Adeli, H. (2001) Neural networks in civil engineering: 1989-2000, Computer-Aided Civil and infrastructure Engineering, Vol. 16, pp. 126-142.
2. Demuth H., Beale M. and Hagan M. (2006) Neural network toolbox for use with MATLAB, The Mathworks Inc., 3 Apple Hill Drive, Natick, MA, User’s guide, Version 5, Chapter 5, l05p.
3. Flood, I. and Kartam, N. (1994) Neural networks in civil engineering 1: principals and understanding, Jr. v/Computing in Civil Engineering. Vol. 8, No. 2, pp. 131-148.
4. Guang, N.H. and Zong, W.J. (2000) Prediction of compressive strength of concrete by neural networks, Cement and Concrete Research, Vol. 30, pp 1245-1250.
5. Hajela, P. and Berke, L. (1991) Neurobiological computational models in structural analysis and design, Jr. of computers and Structures, Vol. 41, pp 657-667.
6. Kim J.L., Kim D.K., Feng M.Q. and Yazdani F. (2004) Application of neural network for estimation of concrete strength, Jr. of Materials in Civil Engineering, pp. 257-264.
7. Yeh, I.C. (1998) Modeling concrete strength with augment-neuron networks. Jr. of Materials in Civil Engineering, Vol. 10, No. 4, pp. 263-208.

CD05-014

EXPERIMENTAL STUDY ON SHORT CONCRETE COLUMNS STRENGTHENING BY COMPOSITE FIBERS

F. Rezaie[1], S.M. Nasr Azadani[2], S. Razzaghi[3]
[1]Professor assistant of Bu Ali Sina University
[2]Professor assistant of Iran University Science& Technology
[3]M.S in structural Eng of Tabriz University

ABSTRACT

Nowadays, the concrete structures are strengthening in several ways. One of these ways that has drawn considerable attentions in the recent years is using composite fibers (FRP) in concrete structures strengthening. There have been many studies on the effects of these fibers on resistance and ductility of the structures. The present study intends to focus on the effects of two types of composite fibers, Carbonic and glass fibers, with three different arrangements that are being currently used in strengthening of the columns. At first, we referred to how the samples have been developed, and then introduce the arrangements that are being used. The results indicate that strengthening the short columns by carbonic composite fibers with complete wrapping which is perpendicular to the direction of loading, along the fibers; have the highest effect on the resistance and formability.

Keywords: composite fibers, short concrete columns, structure strengthening, confinement CFRP, GFRP

1. INTRODUCTION

The studies on the effect of wrapping on resistance and shape of concrete began by introducing enclosed columns with wrapping reinforcement columns. Enclosing or wrapping by cross-sectional reinforcement are inactive. It means that the wrapping pressure is created after the pressure resulting from Poisson's ratio of the enclosed concrete and the strain of the ring material of wrapper. One way which is nowadays used to wrap the concrete is using the FRP composite sheets. The sheets have been drawn considerable attention during the recent yeas in improvement and repairing the structures especially concrete structures due to their high resistance compared to their high weight (FRP layer with a weight of 20% of steel and stress resistance of app. 200 to 1000% of steel) and Resistance to the scratch and chemicals, resistance to exhaustion arising out of loading and immediate installation. FRP composites are made up of two fibrous and resin materials which may strengthening the column or stake of the related element.

Since this is a new technique of supporting, there has been considerable attempt on the behavior of these polymers in making the concrete buckle resistance by attaching these fibers to the intersection which is under stress which all highlight the mechanical behavior and increased buckling resistance buckling. Present article reviews the effect of FRP sheets in the both kinds, carbonic and glass, on the compressive resistance of the short concrete columns.

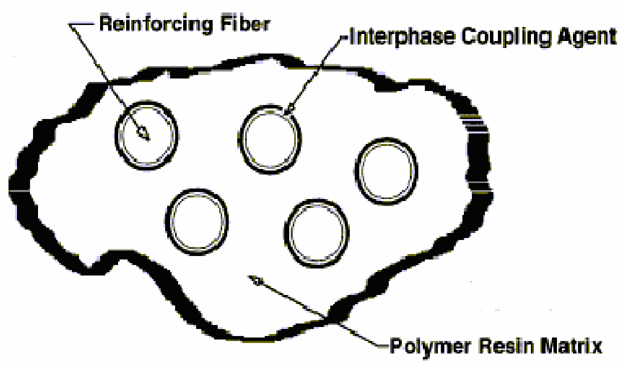

Figure 1. The components of FRP

2. GEOMETRICAL SPECIFICATIONS OF CONCRETE COLUMNS EXPERIMENTAL SAMPLES

The present study uses cylindrical columns with 500mm length and 200mm diameter which fulfills the requirements of short columns. In the improvement process or seismic resisting by composite fibers, the column that was introduced earlier may be slender due to increased loading. Therefore, prior to strengthening and for avoidance of possible breaking as a result of extreme buckling, the column's behavior was controlled. To review the effect of FRP on the resistance of columns, six cylindrical samples were used in the experiments. Two samples were used without cover of FRP and two other samples had the GFRP, other two samples were wrapped with CFRP. Concrete samples were developed in a standard environment within 28 days from producing. After the development process completed, 2 samples, E and F, remained as controller samples. B and A samples with CFRP sheets were strengthen with one layer in the form of complete ring and spiral cover with null phase and a 1cm cover with approximately 30C angel then tested (Figure 2). D and C samples were strengthen with GFRP sheets as well.

Figure 2. Sample A&B confined with CFRP- C&D confined with GFRP

To prepare the surfaces, the concrete surface was cleaned and dried completely, then an even resin layer was distributed on the surface that was going to be confined. The fibers were cut into the various numbers, and then it was put on the resin layer without any compression. Another resin layer was distributed on the surface. Resin development is a phenomenon depending on the heat and time. Contraction of the resin completely takes place normally in standard conditions. In the samples under test, the development of resins in environmental conditions took place under the temperature of 11^0C. during this phase, all necessary actions was taken to prevent direct contact of sunlight, rain, dire heat changes as well as any pollution, dust and moisture exposition. The quality of the samples was satisfactory with no spume observed.

3. CONCRETE MIX DESIGN AND SPECIFICATIONS OF COMPOSITE FIBER

Concrete mix design in producing the cylindrical columns per 1 m^3 of volume is as follows:

Table 1: Specification of consumed concrete in tests

Gravel	800 kg
Sand	1100kg
Cement	350kg
Water to cement Ratio	0.48
Type of cement	Portland Type 2

No additives were used in concrete producing procedure. The results obtained from tests that were conducted on the concretes indicate that the utilized concrete has compression resistance of cylindrical sample of about 25MPa. Also, the specifications of the material of FRP are presented in the following table:

Table 2: Material specification of FRP

Material	Sheet thickness	Layers Number	E (GPa)	σ_y (MPa)
GFRP	0.6	1	76	2300
CFRP	0.17	1	240	4900

4. HOW TO CONDUCT THE AXIAL COMPRESSION TESTS

The final step of the test is breaking the samples under the compression. Prior to breaking the samples, their surface were saturated with melt sulfur in order that even power exert on the surface. Breaking the samples by two jacks of 100 and 300 tons was conducted in the laboratory. Considering the facilities, the test was conducted in the controlled form. The jack of 100tons was calibrate digitally; while, the jack of 300tons lacked this advantage. So it was essential to read the force and displacement changes manually. Consequently, the of human error also affected the results. Unconfined samples which were E and F sample broken by jack of 100tons and confined samples were broken by jack of 300tons due to lack of needed capacity. In order to registering the displacement and longitude strain of the samples along the cylinder axis, two LVDT devices were used in both sides of the jack. The precision of these devices were 0.01mm.

4.1. Results of Tests

The conducted tests on controlled samples of E and F indicated that the average compression resistance of short columns was 70.5 MPa which has approximately 5% difference with analytical equations.

Figure 3. Sample A during the test and after the failure

Diagram 1 shows the stain-stress behavior of the enclosed columns by CFRP. In the confined sample in the form of a ring, the weakness of performance of integrated column and supporter layer causes a local yielding in strain of approximately 0.00135. After the force was increase from this phase onward, in fact, the confined layers are activated. It can create a confinement behavior in the wrapping in a form of spiral. Probably, correct implementing the CFRP is a main reason for good performance of the column that indicates the role and importance of the implementation in practice. Behaviors suggest that elasticity module of diagram A. had decreased but had reached the same after loading with column B. also, the wrapped column in the form of ring indicated resistance and forming. In fact, enclosing the ring exerts better control compared to the lateral strains perpendicular to the axis of the column. Increased strain such as breaking (app.90%) is more significant than the resistance of (app.22%) compared to that of column B.

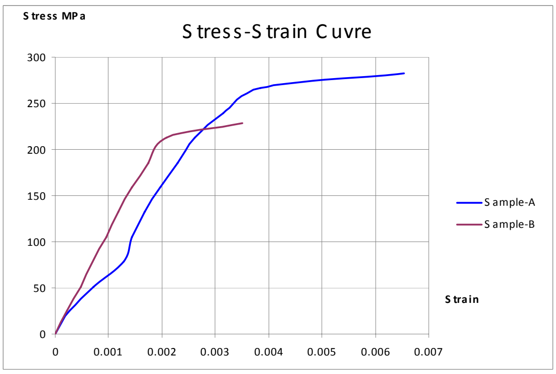

Diagram 1. Strain-Stress of Sample A&B confined with CFRP

In diagram 2 the strain-stress graph of the confined columns with GFRP has been indicated. Column B broke just like the columns of wrapped with carbon composite fibers. In continuing, the GFRP was used. In column B, failure strain increased (app.38%) was more significant than resistance increasment (app.20%) the column B.

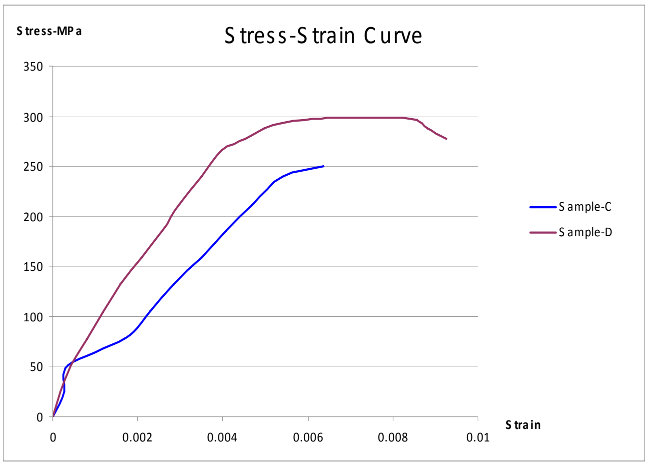

Diagram 2. Strain-Stress of Sample C&D confined with GFRP

Finally all 4 Samples strain-stress graph gathered for comparison in diagram 3.

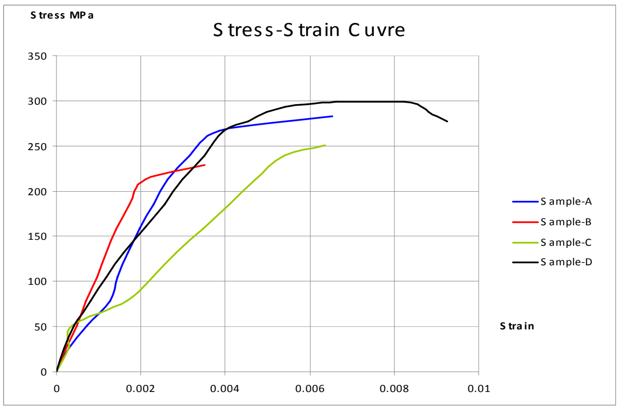

Diagram 3. Strain-Stress of all 4 Samples

5. CONCLUSION

Confined columns had resistance with an average of 265MPa. It clearly indicates that Samples A&C in the compression resistance tests whose results are being observed in diagrams 1&2, the failure observed double. This has caused that FRP has not loaded from the beginning and after the early concrete beating, the samples are equipped with FRP, then the loading capacity is increased. This indicates the need to focusing on the proper manner of covering, involvement of composite fibers with concrete samples when strengthening the columns using these fibers.

In both models of GFRP and CFRP, the samples that have been taken a form of complete wrap can be tested compared to other samples. They may have stronger resistance and formability. It, therefore, seems that using these fibers in the form of wrapped may has highest effect on the resistance and formability of the concrete columns.

Although, sample C has the form of wrapped, it may has the least elasticity module, consequently, its resistance may be least. But the results obtained indicate that using these composite fibers, even if they are being used in some sections of the column, may exert considerable effect on the resistance and formability.

Samples A and B as well as C and D have the same slope in most part of the diagram which suggests the effect of FRP on elasticity module of equipped columns and the arrangement and manner of using FRP has little effect on this module.

REFERENCES

1. 2003, Bonded Repair and Retrofit of Concrete Structures Using FRP Composites, NCHRP Report 514.
2. Teng, J. G., Chen, J. F., Smith, S. T., and Lam, L. 2002. "FRP strengthened RC structures", Wiley, West Sussex, U.K.
3. American Concrete Institute. ACI "440.2R-02 guide for the design and construction of externally bonded FRP systems for strengthening concrete structures"; 2002.
4. Concrete Code of Iran No. 120.

CD05-015

ارائه شبکه عصبی مناسب برای طرح اختلاط بهینه سدهای بتنی غلتکی

حمید رضا وثوقی فر[1]، عباس منصوری[2]، وحید خلیلی خرّم[3]
۱. استادیار دانشکده مهندسی عمران، دانشگاه آزاد اسلامی‌واحد تهران جنوب
۲. استادیار دانشکده مهندسی عمران، دانشگاه آزاد اسلامی‌واحد تهران جنوب
۳. دانشجوی کارشناسی ارشد سازه‌های هیدرولیکی، دانشگاه آزاد واحد تهران جنوب

چکیده
یکی از روش‌هایی که در ساخت سدهای بتنی و خاکی به عنوان جایگزینی مناسب مطرح است روش ساخت سدها به شیوه بتن غلتکی می‌باشد. صرف بودجه کمتر، استفاده ازماشین آلات راهسازی، کوتاه شدن زمان ساخت و تداوم ساخت، همگی از ویژگیهای این نوع روش ساخت سدها می‌باشد که باعث برتری یافتن این روش شده است و در نهایت این شیوه برای ساخت سدها در نقاط مختلف جهان به عنوان جایگزینی مناسب مطرح شده است. از طرفی گستردگی مواد و مصالح مورد استفاده در این نوع بتن و پیچیدگی طرح اختلاط آن و متاثربودن طرح اختلاط آن ازپارامترهای مختلف ونیز یافتن روابط بین پارامترهای مختلف طرح اختلاط آن، باعث شده اند تا ارائه مدلی برای طرح اختلاط بتن غلتکی ضروری به نظربرسد. شبکه‌های غصبی مصنوعی از جمله روشهای مدل سازی می‌باشند که قدرت بسیارزیادی جهت تطبیق با مسائل مهندسی ازخود نشان داده اند. نوعی از این شبکه‌ها با عنوان شبکه‌های عصبی چند لایه پرسپترون (MLP) به همراه الگوریتم آموزش پس انتشار خطا، که بیشتر در زمینه مدل‌سازی رفتارهای نگاشت گونه کاربرد داشته اند به عنوان هسته اصلی مدل سازی در این مقاله، استفاده شده‌اند.

با استفاده از این نوع شبکه عصبی، که دارای یک لایه پنهان باشد و بر اساس داده‌هایی که از طرح‌های اختلاط سد بتن غلتکی زیردان جمع‌آوری شده‌اند، مدل‌هایی به منظور پیش بینی مقاومت فشاری این نوع بتن آموزش داده شده‌اند که می‌توان ازآنهاجهت پیش بینی‌های مهندسی استفاده کرد و همچنین با استفاده از روشهای بهینه‌یابی به اقتصادی‌ترین و یا بهینه‌ترین طرح اختلاط دست یافت.

کلیدواژه: شبکه‌های عصبی، بتن غلتکی، پیش بینی مقاومت فشاری، شبکه‌های عصبی چند لایه پرسپترون

۱- مقدمه
با کشف این حقیقت که مغز انسان محاسبات را با روشی کاملاً متفاوت از کامپیوترهای دیجیتال متداول انجام می‌دهد، مطالعات بر روی شبکه‌های عصبی مصنوعی که معمولاً شبکه‌های عصبی نامیده می‌شوند، آغاز شد. مغز در حقیقت یک کامپیوتر بسیار پیچیده، غیر خطی و با ساختار موازی می‌باشد. به دلیل توانایی در سازمان دهی عناصر بنیادی یعنی نرون‌ها، مغز توانایی انجام بسیاری از محاسبات (مانند تشخیص الگو، ادراک و...) را با سرعتی

بسیار بالاتر از سریع ترین کامپیوترهای دیجیتال امروزی دارا می‌باشد[7]. الگوریتم ژنتیک که بر پایه تئوری تکامل داروین استوار است اولین بار توسط هولند در (۱۹۷۵) مطرح شد و بعد از آن گلدبرگ (۱۹۸۹) و میشویکس (۱۹۹۲) معرفی کامل و دقیقی از این روش ارائه دادند [12].

شبکه‌های عصبی مصنوعی از کاربردهای هوش مصنوعی هستند که به طور وسیع در مدلسازی تعداد زیادی از مسایل مهندسی وعلمی‌مورد استفاده قرار می‌گیرد. تعداد زیادی مطالعه وتحقیق در مورد پیش بینی مقاومت فشاری بتن به وسیله شبکه‌های عصبی صورت گرفته است [17].

بتن غلتکی یکی از شیوه‌های نسبتا جدید ساخت سد در ایران است. پیش بینی و مدل سازی طرح اختلاط و مقاومت این بتن بر اساس پارامترهای ورودی به مانند انواع دیگر بتن و چه بسا بیشتر ازدیگر انواع، از پیچیدگی خاصی برخورداراست. از طرفی ورود انواع پوزولانها، مواد افزودنی جدید در طرح اختلاط این نوع بتن و همچنین متاثر بودن این بتن از روشهای متفاوت بتن ریزی، اختلاط وتراکم، پیچیدگی طرح اختلاط آن را مضاعف نموده است [13]. مدل سازی مقاومت بتن غلتکی توسط شیوه‌های سنتی و رگرسیونی با توجه به پیچیدگی‌های موجود در این موضوع، قادر به پیش بینی‌های مناسب نخواهد بود، چرا که رفتار مقاومتی بتن تحت تاثیر شرایط غیر خطی است و از کوچکترین جزئیات اجزای موجود در مخلوط و تعامل بین این اجزا متاثر می‌باشد [17]. خصوصیات شبکه‌های عصبی با الگوریتم پس انتشار خطا باعث شده تا استفاده از این شیوه مدل سازی غیر خطی برای پیش بینی مقاومت انواع بتن بسیار جذاب ومناسب باشد [15]. لذا این تکنیک به عنوان پایه اصلی مدل‌سازی در این تحقیق به کار برده شده است.

۲- روش تحقیق

- شبکه‌های عصبی به کار رفته جهت مدل سازی

شبکه‌های عصبی چند لایه پرسپترون (MLP) با الگوریتم پس انتشار خطا یکی از پر کاربردترین ابزارهایی هستند که توانایی فوق العاده ای در انواع مدل سازی‌های غیر خطی و خطی از خود نشان داده اند[16]. در این تحقیق از شبکه‌های عصبی MLP با یک لایه مخفی که مطابق با شکل 1 عمل می‌کنند، استفاده شده است چرا که این ساختار با تعداد المان پردازشگر (سلول عصبی) مناسب در لایه مخفی قادر به شبیه سازی انواع توابع و نگاشتهای مختلف می‌باشد [15]. شکل شماره 1 ساختار شبکه به کار رفته جهت مدل سازی را نشان می‌دهد که از سه لایه ورودی و مخفی و خروجی تشکیل شده است که xp1 , xp2 ,…, xpN ورودی‌های N عنصری، Whi و Wjh اوزان قابل تنظیم شبکه را تشکیل می‌دهند.

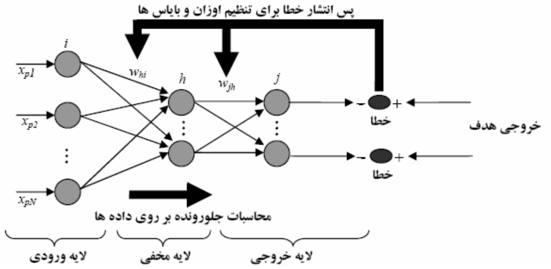

شکل ۱- ساختار شبکه‌های عصبی با الگوریتم پس انتشار خطا

این شبکه‌ها براساس المانهای پردازشگری به نام سلول عصبی عمل می‌کنند (شکل۱). سلول‌های لایه ورودی مقادیر عناصربردار ورودی هر یک از الگوها را بدون هیچ پردازشی به لایه پنهان منتقل می‌کنند و سلول‌های لایه پنهان و لایه خروجی بر اساس شکل 2 بر روی مقادیر ورودی خود به پردازش اطلاعات دست می‌زنند. تابع f در این شکل با نام تابع تحریک در این شکل شناخته می‌شود ومی‌تواند از نوع تابع سیگموئید ویا تانژانت هیپربولیک و یا خطی باشد [14].

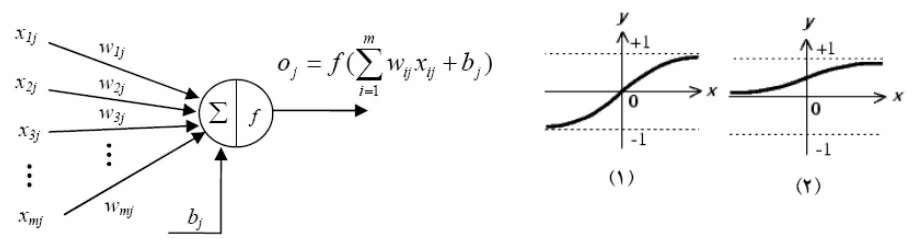

شکل ۲- (چپ) سلول عصبی وعملیات ریاضی آن،(راست۱)تابع تانژانت هیپربولیک (راست۲) تابع سیگموئید

در این شبکه‌های عصبی دو روال انجام می‌شود. روال تابعی که شامل اعمال الگوها و مثال‌های ورودی به شبکه و تعیین خروجی‌های سلولی هر لایه و انتقال خروجی هر لایه به لایه بعدی است. روال پس انتشار خطا، با مقایسه نتیجه لایه خروجی با مقدار هدف هر الگو وتعیین خطای این مقایسه آغاز می‌شود (رابطه۱) و بر اساس الگوریتم‌های مختلف آموزش این خطا را از لایه‌های انتهایی به لایه‌های قبلی انتقال داده و در حین این انتقال اوزان و بایاس‌ها رابه گونه ای تنظیم می‌کند که خطای شبکه به پایین ترین سطح برسد [14].

$$mse = \frac{1}{N.S_0} \sum_{j=1}^{S_0} \sum_{i=1}^{N} (t_{ij} - 0_{ij})^2 \qquad (۱)$$

تابع خطا و عملکرد شبکه
در رابطه (۱)
t هدف
0 خروجی مدل
iامین سلول خروجی
jامین الگو
N تعدادسلول درخروجی
S0 تعدادالگو

- پارامترهای مختلف شبکه عصبی در مدل‌سازی مقاومت

شبکه‌های BP با یک لایه پنهان و تابع تحریک خطی در لایه خروجی اساس مدل سازی قرار گرفته است. همچنین از تابع تحریک تانژانت هیپربولیک (Tanh) در لایه مخفی استفاده شده است. در ضمن از نرم افزار

MATLAB برای برنامه نویسی‌های مورد نیاز مدل سازی استفاده شده است.

- مجموعه داده‌های مدل‌سازی

اطلاعات به کار رفته در این مدل سازی از میان طرح اختلاط‌های آزمایشگاهی سد زیردان گردآوری شده است. رکوردهای جمع آوری شده شامل ۱۹۰ طرح اختلاط می‌باشد که پس از بازبینی آنها داده‌های با خطای چشمگیر و همچنین داده‌های با نقصان در پارامترهای موثر بر طرح اختلاط و مقاومت کنار گذاشته شدند و در نهایت ۱۱۱ طرح اختلاط به عنوان پایگاه اصلی مدل سازی‌های مختلف به کار گرفته شده اند.

- مدل‌سازی مقاومت ۷، ۲۸، ۹۰ و ۱۸۰ روزه

با توجه به اینکه طرحهای اختلاط حاوی مجموع مواد سیمانی ۷۰ تا ۱۹۰ کیلوگرم بر متر مکعب و با پله‌های ۱۰ کیلوگرم ساخته شدند برای ایجاد مدل پیش بینی مقاومت از میان اطلاعات گردآوری شده نیز به این ترتیب عمل شد که برای هر طرح اختلاط روابط مقاومت فشاری آن در سنین مخلتف محاسبه شود.

- پارامترهای ورودی مدل

پارامترهای متفاوتی بر مقاومت بتن غلتکی تاثیرگذار هستند که ازجمله این پارامترها می‌توان به میزان و نوع سیمان و پوزولان، شن و ماسه، ریزی ذرات سیمان،مقدارآب، مدول ریزی ماسه، حداکثربعد سنگدانه، دانه بندی سنگدانه‌ها و میزان و نوع مواد افزودنی اشاره کرد. علاوه بر این موارد پارامترهای ترکیبی نیز وجود دارندکه از آنها به عنوان شاخص‌های موثر بر مقاومت یاد شده است[9]. از میان پارامترهای مستقل موثر بر مقاومت بتن غلتکی آن دسته از پارامترها و ویژگیهایی که در اطلاعات گردآوری شده حضور داشتند انتخاب شده به نحوی که بتوان ازآنها در شرایط گوناگون استفاده نمود، به کار گرفته شدند. این پارامترها به ترتیب عبارتند از:

- شن ۵۰~۲۵، شن ۲۵~۵، ماسه ۵~۰، ماسه ۳~۰، سیمان، پوزولان خاش، آب،
- افزودنیهای Chrysoplast CER ، Chryso Tard CHR و Conplast RP264M و شسته یا نشسته بودن مصالح

- آماده‌سازی و استاندارد کردن داده‌ها

جهت انجام محاسبات در ابتدا لازم است که داده‌های خام بین ۰ و ۱ استانداردسازی شوند [7]. بنابراین داده‌های ورودی با توجه به میزان داده‌های حداکثر و حداقل استاندارد شدند. این عمل که نرمالیزه کردن داده‌ها خوانده می‌شود از روشهای استاندارد سازی دیگر کاربردی تر است. بعد از خروجی گرفتن از شبکه، خروجی‌های استاندارد شده بایستی به داده‌های واقعی تبدیل شوند تا با مقادیر مشاهده شده مورد مقایسه قرارگیرند. همچنین محدوده ماکزیمم و مینیمم داده به شرح جدول ۱ می‌باشند:

جدول ۱: محدوده داده‌های طرح اختلاط‌ها

۰~۳ (kg/m3)	۰~۵ (kg/m3)	۵~۲۵ (kg/m3)	۲۵~۵۰ (kg/m3)	محدوده داده‌ها	مجموع مصالح سیمانی
۴۴۴	۳۵۳	۸۰۶	۴۰۳	ماکزیمم	۱۱۰
۶۰۸	۴۸۸	۹۰۲	۴۵۱	مینیمم	
۴۴۰	۳۳۵	۸۴۳	۳۹۹	ماکزیمم	۱۲۰
۵۷۶	۴۸۳	۹۱۴	۴۶۸	مینیمم	
۴۳۲	۳۳۲	۸۳۰	۳۹۳	ماکزیمم	۱۳۰
۵۶۷	۴۶۰	۹۰۷	۴۶۵	مینیمم	
۴۱۳	۳۲۷	۷۵۱	۳۹۲	ماکزیمم	۱۴۰
۵۶۰	۴۸۰	۹۰۶	۴۸۶	مینیمم	
۴۹۶	۳۳۲	۷۲۸	۴۴۱	ماکزیمم	۱۵۰
۵۷۳	۳۸۳	۹۰۷	۵۶۱	مینیمم	

۳- یافته‌ها

پس از تحلیل داده توسط شبکه عصبی نرم افزار متلب خروجی‌ها به صورت وزن هر یک از داده‌ها برای مقاومت ۷روزه در جداول ۲ و ۳، برای مقاومت فشاری ۲۸ روزه در جداول ۴ و ۵، برای مقاومت فشاری ۹۰ روزه درجداول ۶ و ۷ و همچنین برای مقاومت فشاری ۱۸۰ روزه درجداول ۸ و ۹ که به ترتیب در جدول اول شامل وزن W(1,1)ها و در جدول دوم شامل w(2,1)، b1، b2 ، و ماکزیمم مقاومت فشاری طرح مورد نظر می‌باشند ارائه شده است.

جدول ۲: نتایج W(1,1) مقاومت فشاری ۷ روزه

1=نشسته	فزودنی	فزودنی	افزودنی	آب	پوزولان	سیمان	0-3	0-5	5-25	25-50	مقاومت فشاری ۷روزه
0= شسته	Conplast RP264M	ChrysoTard CHR	Chrysoplast CER	آزاد	خاش	(kg/m^3)	(kg/m^3)	(kg/m^3)	(kg/m^3)	(kg/m^3)	W(1,1)
26128.3625	-1312.877	960.5746	2586.4581	2331.84	-30.1465	-271.3188	1018.7599	744.7871	862.765	857.6825	110
1315.5817	-3078.1852	494.7499	3614.0623	-1994.0385	24.5908	221.3177	-1259.5986	-1242.9058	1575.4713	-4014.6545	120
-279.3159	-1446.9252	-326.5085	-2178.5697	701.6738	-10.6125	-95.5121	354.4187	344.5169	-20.6556	687.2884	130
-38.9949	-238014.0819	1028.3934	238130.8079	220886.0558	-3931.0348	-22969.298	59492.9423	63439.0382	59919.6422	61232.0142	140
-151.003	-439.9155	-209.5466	-644.9751	-106.7477	1.739	15.6507	54.2189	-192.0378	-48.2741	-48.2507	150

جدول ۳: نتایج w(2,1) و b1 و b2 و ماکزیمم داده‌های مقاومت فشاری ۷ روزه

ماکزیمم دادها	b2	b1	w(2,1)	مقاومت فشاری ۷روزه
59.3	68.6172	-2455.6	67.8715	110
64.9	0.83419	1856.336	0.18378	120
75.9	0.84413	-732.407	-0.23585	130
88.4	0.87284	-173501	-0.08802	140
119.5	71.3546	128.3482	-70.8489	150

جدول شماره ۴: نتایج W(1,1) مقاومت فشاری ۲۸ روزه

1= نشسته	فزودنی	فزودنی	افزودنی	آب	پوزولان	سیمان	0-3	0-5	5-25	25-50	مقاومت فشاری ۲۸روزه
0= شسته	Conplast RP264M	ChrysoTard CHR	Chrysoplast CER	آزاد	خاش	(kg/m3)	(kg/m3)	(kg/m3)	(kg/m3)	(kg/m3)	W(1,1)
1948.0145	826.065	-688.766	2772.5523	728.9701	-9.7292	-87.5631	304.3659	284.6204	271.5006	304.2699	110
-10468.0368	12054.4859	-2073.7938	-6904.3204	3257.0184	-32.5199	-292.6772	2322.3635	2384.6857	-4926.4887	9545.2621	120
-1939.9944	-186.3095	47.9842	347.6326	1.5363	-0.636	-5.724	-7.2057	15.0429	33.9636	-30.6109	130
36068.8599	16241.0049	-181491.7105	129567.3362	440296.6899	-6270.6733	-59248.174	156777.2375	157656.2341	151744.3845	152788.9625	140
-504.9597	-35.5678	3740.8166	-320.4495	-1737.1075	34.339	309.3358	537.8686	-2744.5241	-798.184	-783.1546	150

جدول ۵: نتایج (w(2,1 و b1 و b2 وماکزیمم داده‌های مقاومت فشاری ۲۸ روزه

ماکزیمم داده‌ها	b2	b1	w(2,1)	مقاومت فشاری ۲۸روزه
94.3	82.99	-802.513	82.2571	110
88.9	0.8724	-2490.37	-0.12829	120
106.6	33.7257	-21.8034	33.4206	130
123.8	0.878	-423751	-0.09141	140
165.5	0.73674	2083.601	-0.14299	150

جدول ۶: نتایج (W(1,1 مقاومت فشاری ۹۰روزه

1=نشسته	افزودنی	افزودنی	افزودنی	آب	پوزولان	سیمان	0-3	0-5	5-25	25-50	مقاومت فشاری ۹۰روزه
شسته0=	Conplast RP264M	ChrysoTard CHR	Chrysoplast CER	آزاد	خاش	(kg/m3)	(kg/m3)	(kg/m3)	(kg/m3)	(kg/m3)	W(1,1)
-155.6943	1201.9453	1383.355	1561.3317	219.7201	-3.2325	-29.0929	88.9994	90.6119	84.8313	90.5575	110
20662.366	415.202	-12040.6101	-15222.0467	-7883.7779	88.345	794.9786	-1422.8069	-1647.4708	-5862.5253	2863.2778	120
9276.0029	-1522.8943	22572.0953	28096.9814	5052.3912	-38.62	-348.7599	-97.4022	-191.8954	4311.5341	-4148.688	130
665.3672	873.041	1983.6598	-4896.7036	152.4836	-82.8525	-29.0349	235.6504	191.8984	197.6006	194.7366	140
18.8333	-631.5906	-10421.1236	-441.2291	60.7262	-2.4661	-22.1758	-122.8437	332.6311	64.6324	60.6244	150

جدول ۷: نتایج (w(2,1 و b1 و b2 و ماکزیمم داده‌های مقاومت فشاری ۹۰ روزه

ماکزیمم داده‌ها	b2	b1	w(2,1)	مقاومت فشاری 90روزه
104.4	16.6011	-245.634	16.3178	110
109.1	0.83464	6719.227	0.12899	120
123.6	-163.517	-2719.67	-164.474	130
141.6	0.90005	-507.018	0.11192	140
188.3	0.86241	-154.494	0.13146	150

رابطه ای که برنامه MATLAB طبق آن محاسبات را انجام می‌دهد به صورت رابطه (۲) می‌باشد:

$$Purlin(W2,1*Tansig(W1,1*A+b1)+b2 \qquad (۲)$$

که :

W1,1 و W2,1 و b1 و b2 ضرائب محاسباتی توسط نرم افزارمی‌باشد و A نیز مقادیر اولیه طرح اختلاط می‌باشد.

به طور مثال اگر مقاومت فشاری ۹۰ روزه طرحی با مجموع مصالح سیمانی ۱۲۰ کیلوگرم بر متر مکعب و با

نسبتهای اختلاط مطابق جدول ۱۰ مدنظرباشد به صورت زیر عمل میشود:

جدول ۸: نتایج W(1,1) مقاومت فشاری ۱۸۰ روزه

مقاومت فشاری ۱۸۰روزه	25-50	5-25	0-5	0-3	سیمان	پوزولان	آب	افزودنی	افزودنی	افزودنی	1=نشسته
W(1,1)	(kg/m3)	(kg/m3)	(kg/m3)	(kg/m3)	(kg/m3)	خاش	آزاد	Chrysoplast CER	ChrysoTard CHR	Conplast RP264M	0=شسته
110	-220.5406	-212.9597	-220.6838	-222.7109	68.5733	7.6193	-535.4856	34.565	474.101	2996.6691	144.7062
120	2047.2502	-1010.1246	479.459	548.0719	-72.9755	-8.1094	1070.651	-63.7307	85.621	-262.3356	5485.6287
130	-3199.9818	3743.3125	52.0612	111.5684	-365.7089	-40.6449	4879.5062	25025.2947	20247.5529	-1898.339	6023.9677
140	-71943.8467	-70414.2492	-74495.9859	-69988.6009	26582.4219	4843.492	-257860.4159	155.6007	698.62	-279.1942	-397.4239
150	295.3008	297.0688	262.3528	343.8102	-121.5758	-13.5086	891.4534	1363.1841	13469.3763	2011.4399	-7224.7236

جدول ۹: نتایج w(2,1) وb1 و b2 و ماکزیمم دادههای مقاومت فشاری ۱۸۰ روزه

مقاومت فشاری 180روزه	w(2,1)	b1	b2	ماکزیمم دادهها
110	-25.2946	603.6801	26.1003	106.2
120	-0.17735	-644.509	0.82266	112.7
130	-185.065	-2814.37	-184.077	122.4
140	0.058119	203536.5	0.87403	151.5
150	-0.12929	-828.736	0.85081	211.8

جدول ۱۰: دادههای اولیه مثال

مقاومت فشاری ۹۰روزه	25-50	5-25	0-5	0-3	سیمان	پوزولان	آب	افزودنی	افزودنی	افزودنی	1=نشسته
	(kg/m3)	(kg/m3)	(kg/m3)	(kg/m3)	(kg/m3)	خاش	آزاد	Chrysoplast CER	ChrysoTard CHR	Conplast RP264M	0=شسته
120	401	846	483	482	108	12	120	0.6	0	0	1

ابتدا مقادیر هر یک از مصالح را در اوزان مربوط به ردیف دوم جـدول ۶ کـه مخـتص مقاومـت فـشاری ۹۰ روزه (جدول۶) که همان(W(1,1ها هستند ضرب شده آنگاه حاصل را با مقدار b1 ردیف دوم جدول ۷ جمع میشود.

جدول۱۱: W(1,1) های مقاومت ۹۰ روزه طرح اختلاط با ۱۲۰کیلوگرم مواد سیمانی

مقاومت فشاری ۹۰روزه	25-50	5-25	0-5	0-3	سیمان	پوزولان	آب	افزودنی	افزودنی	افزودنی	1= نشسته
W(1,1)	(kg/m3)	(kg/m3)	(kg/m3)	(kg/m3)	(kg/m3)	خاش	آزاد	Chrysoplast CER	ChrysoTard CHR	Conplast RP264M	0= شسته
120	2863.2778	-5862.5253	-1647.4708	-1422.8069	794.9786	88.345	-7883.7779	-15222.0467	-12040.6101	415.202	20662.366

سپس جواب را برابر x درنظرگرفته و در رابطه (۳) قرار داده میشود:

$$z = \frac{1-e^{-2x}}{1+e^{-2x}} \qquad (۳)$$

حال z را در مقدار w(2,1) ردیف دوم جدول ۷ ضرب شده و با عدد b2 جمع می‌شود و در انتها به دلیل اینکه روابط براساس اعداد نرمالیز شده است جهت رسیدن به مقاومت موردنظر باید حاصل را در ماکزیمم داده‌هاکه برابر با $109.1kg/cm^2$ است ضرب شده که جواب نهایی برابر با $100.3kg/cm^2$ می‌شود.

۴- بحث

استفاده از شبکه‌های عصبی، مدل سازی مقاومت بتن غلتکی را دچار تحول ساخته است و نتایج بسیار مناسب و دقیقی را در برداشته است. درتحقیقی که توسط سورکن و همکارانش صورت گرفته نیز نتایج بسیار دقیقی به واسطه شبکه‌های عصبی در رابطه با پیش بینی مقاومت فشاری بتن صورت گرفته است[9]. این مدل تنها یک بار ساخته شده است و دست یابی به پیش بینی مقاومت را به صورت آنی و با دقت بسیار مناسب انجام می‌دهد و می‌تواند بسیاری از هزینه‌های نمونه سازی طرح اختلاط بتن غلتکی را کاهش دهد. مقاومت فشاری ملاتهای سیمانی شامل انواع متفاوتی از پوزولانها بر اساس شبکه عصبی بدون نیاز به انجام هیچ گونه مطالعات آزمایشگاهی سبب صرفه جویی هزینه‌ها به مقدار بسیار زیادی در پروژه‌ها می‌گردد[13].

با به کاربردن این مدل‌های پیش بینی مقاومت و استفاده ازروش‌های مینیمم سازی می‌توان با درنظرگرفتن بسیاری ازویژگی‌های طرح اختلاط و بدون ساخت نمونه‌های آزمایشگاهی به طرح اختلاط‌های بهینه ازجنبه‌های سازه ای و مالی دست یافت. به کارگیری این مدل‌ها برای بررسی بیشتر پارامترهای موثر بر بتن غلتکی بسیارسودمند است. استفاده از خصوصیات بیشتری از سنگدانه‌ها (نوع کانی، شرایط سنگدانه‌ها برای جلوگیری ازجدایی و...)، نوع سیمان مصرفی و شرایط ساخت نمونه‌ها (زمان اختلاط، نحوه اختلاط، فاصله زمانی بین اتمام اختلاط و بتن ریزی و...) درکنار دیگرپارامترهای ورودی پیش بینی مقاومت را دقیق تر میکند.

تشکر و قدردانی

بدینوسیله ازمهندس محسن جعفربیگلو و تکنسینهای آزمایشگاه بتن شرکت جهان کوثر (پیمانکار سد زیردان) که در کلیه مراحل ساخت مخلوطهای بتن و انجام آزمایشها، صمیمانه همکاری فراوانی را مبذول داشته اند سپاسگزاری و قدردانی می‌شود.

مراجع

۱- منهاج، م، «هوش محاسباتی (جلد اول)، مبانی شبکه‌های عصبی»، مرکز نشر پروفسور حسابی، چاپ اول، تهران، (۱۳۷۷).

۲- روشهای طرح اختلاط بتن‌های غلتکی پروژه‌های سدسازی-دکتر علیرضا باقری گزارش فنی سد زیردان، مهندسین مشاور آبفن و پژوهاب ۱۳۷۷

۳- رابرت جی شالکف، شبکه‌های عصبی مصنوعی، ترجمه دکتر محمود جورابیان، انتشارات دانشگاه شهید

چمران اهواز، ۱۳۸۲

۴- پور ذاکر عربانی، سودابه، مفاهیم هوش مصنوعی، انتشارات ندای سبز شمال، ۱۳۸۵

۵- رمضانیانپور علی اکبر،نیاعمران محمد اسماعیل، «کاربرد شبکه‌های عصبی مصنوعی در طرح اختلاط بتن غلتکی»،کنفرانس بین المللی مهندسی عمران،۱۳۸۲.

۶- بصیری فرزانه،خسروانی سارا، «بتن غلتکی»، دوازدهمین کنفرانس سراسری مهندسی عمران، دانشگاه علم و صنعت ایران، آبان ۱۳۸۴.

7- Demuth,H. "Neural Network Toolbox for Use with MATLAB-User Guide",The Mathwork Inc, (1998).

8- ASTM C1170," Standard Test Methods for Determining consistency and Density of Roller- Compacted Concrete Using a Vibrating Table".

9- Guide for Selecting proportions for No-Slump Concrete. Reported by ACI Committee 211.3R-02.

10- ASTM C1176,"Standard Practice for Making Roller-Compacted Concrete in Cylinder Molds Using a Vibrating Table".

11- Roller compacted concrete dam for the Petit Saut dam, published in Travaux agazine,Jine 1993.

12- Goldberg D.E.,"Genetic algoritm in search,optimization and machine learning",Addison-wesley,Reading Mass(1989).

13- Yeh IC,Modeling of strength of HPC using ANN.Cement Concrete Res 1998;28(12):1797-808.

14- Metin Hakan Severcan,Mustafa Saridemir,"Prediction of Long-term effects of GGBFS on compressive strength of concrete by artifitial neural networks and fuzzy logic"2008 elsevier scince.

15- per-wei Gao,"The characteristics of air voids and frost resistance of RCC with.fly ash and expansive agent"2005 elsevier Science.

16- V.G.Papadakis, S.Tsimas, "Supplementarycementingmaterials in concrete". 2002 elsevier Science.

17- Y. Xie, B. Liu, J. Yin, S. Zhou, "Optimum mix parameter sof high strength concrete". Concr. Res. 32(2002)477-480.

18- C.D.Atis,U.K.Svin,O.Karahan,"Strengh properties of roller compacted concrete contaning a non-standard high calcium fly ash"2003 Elsevier Science.

19- Ilker Bekir Topcu, Cenk Karakurt, Mustafa Sarıdemir," Predicting the strength development of cements produced with differentpozzolans by neural network and fuzzy logic"2008 Elsevier Science.

20- Alshihri M, Azmy AM, El-Bisy MS. Application of neural networks in the prediction of compressive strength of high strength concrete. Al-Azhar Univ, Civil Eng Res Mag Cem 2007;29(2):573–89.

CD05-016

بررسی اثر C_3A سیمان پرتلند بر کاتیون‌های مختلف کلرید در ایجاد پیوند شیمیایی و روش اندازه گیری کلرید آزاد در سیستم‌های سیمانی

فاطمه جعفرپور[۱]، فهیمه فیروزیار[۲]
۱. عضو هیات علمی‌مرکز تحقیقات ساختمان و مسکن
۲. کارشناس تحقیقات مصالح ساختمانی مرکز تحقیقات ساختمان و مسکن

چکیده

هنگامی‌که کلرید محلول در آب در یک سیستم سیمانی مانند ملات یا بتن وجود داشته باشد، می‌تواند سبب خوردگی فلزاتی نظیر فولاد گردد. یون‌های کلرید با فاز C_3A ترکیب می‌شوند و کلرور آلومینات تولید می‌شود. بنابراین سیمان‌هایی که دارای مقدار بیشتر C_3A می‌باشند قادرند مقداری از کلرید را پیوند دهند. وقتی که یون‌های کلرید با C_3A پیوند می‌یابند به حالت غیر محلول تبدیل شده و بنابراین غیر فعال می‌شوند، به عبارت دیگر کلریدهای پیوند یافته و غیر محلول در فرآیند خوردگی نقشی ندارند. همچنین نوع کاتیون‌های کلرید نیز در خوردگی آرماتور اثر دارند و شدت خوردگی به طور قابل توجهی تابع نوع کاتیون است.برخی سنگدانه‌ها حاوی مقدار قابل توجهی کلرید هستند که در سنگدانه محبوس بوده و در واکنش خوردگی شرکت نمی‌کنند. درروش آزمون استاندارد ملی ایران شماره ۸۹۴۷، بخشی از کلریدی که در این سنگدانه‌ها وجود داشته و درواکنش خوردگی نقشی ندارند نیز اندازه‌گیری می‌شود. با توجه به اینکه مقدار کلرید اندازه‌گیری شده به شدت به درجه نرمی‌سنگدانه‌ها هنگام تهیه آزمونه بستگی دارد، بنابراین در این روش، کلریدهای اندازه‌گیری شده که عموماً در واکنش خوردگی شرکت نمی‌کنند نیز اندازه گیری می‌شود.

در این مقاله نتایج حاصل از انجام یک پروژه تحقیقاتی در زمینه «بررسی تأثیر میزان C_3A سیمان در ایجاد پیوند شیمیایی یون کلرید»، «بررسی تأثیر کاتیون‌های مختلف کلرید در ایجاد پیوند شیمیایی» و «بررسی روش اندازه‌گیری کلرید عصاره‌گیری شده در سیستم‌های سیمانی» ارائه شده است.

کلیدواژه: میزان C_3A، کلرید آزاد، کاتیون‌های مختلف، پیوند شیمیایی، کلرید عصاره‌گیری‌شده، سیستم‌های سیمانی

۱- مقدمه

بتن ترکیبی است که خاصیت قلیایی بسیار زیادی دارد. این خاصیت آن را از بسیاری از صدمات که بر اثر عوامل خورنده ایجاد می‌شود، حفظ می‌کند. فولاد داخل بتن تحت چنین شرایط قلیایی در حالت غیر فعال باقی مانده و از آسیب دیدگی محفوظ خواهد ماند. ولی با ورود عوامل مخربی مانند کلریدها، سولفیدها و دی‌اکسیدکربن و... به بتن خاصیت قلیایی آن از بین رفته و فولاد حفاظت شده داخل آن در معرض خوردگی واقع می‌شود. ازاین رو

جلوگیری از ورود این عوامل به بتن یکی از عوامل ضروری در حفظ دوام بتن است.
ازجمله عوامل مهاجم به بتن و آرماتور داخل آن، یون کلرید و ترکیبات آن است این ماده می‌تواند از طریق منافذ موجود در بتن که در اثر اضافه کردن آب به مخلوط سیمان و شن وماسه تولید شده است وارد بتن شده و در کنار فولاد قرار گیرد. مقداری از این یون‌ها با ترکیبات داخل سیمان (توسط C_3A سیمان) واکنش و ایجاد پیوند کرده که به نمک فریدل معروف است. مشکل عمده، یون‌هایی است که پیوند نداده و به طور آزاد در محلول منافذ و اطراف فولاد درحرکت می‌باشند. یون‌های کلرید با رسیدن به فولاد حفاظت شده که لایه هیدروکسیدی در اثر pH بالای بتن بر سطح آن تشکیل داده است، این لایه محافظ را از بین برده و فولاد بدون پوشش را در معرض محیط خورنده قرار می‌دهد که باعث از بین رفتگی شدید فولاد می‌گردد.
در این خصوص، در مرکز تحقیقات ساختمان و مسکن پروژه‌ای تحت عنوان «بررسی اثر C_3A سیمان پرتلند بر کاتیون‌های مختلف کلرید در ایجاد پیوند شیمیایی و روش اندازه گیری کلرید آزاد در سیستم‌های سیمانی» انجام شده است. در این راستا، اثر C_3A سیمان در پیوند کلریدی، از طریق ساخت C_3A خالص در آزمایشگاه و افزودن آن به مقادیر مختلف به سیمان و اضافه کردن دو نوع نمک کلریدی به نسبت‌های مختلف و همچنین در نمونه‌های ساخته شده با سیمان دارای C_3A مختلف که شرایط واقعی را فراهم سازد، مورد بررسی قرار گرفته است.

۲- بررسی ساختار شیمیایی بتن

ساختار شیمیایی بتن نقش عمده‌ای در روند آسیب‌دیدگی دارد و شناخت اصول و مفاهیم ساختار برای درک فرآیندهای آسیب‌دیدگی و جلوگیری از تخریب بتن ضروری است. ساختار شیمیایی بتن، در واقع واکنش‌های شیمیایی (هیدراتاسیون) است که بین سیمان وآب انجام می‌شود. این ساختار همچنین شامل اندرکنشی است که افزودنی‌های شیمیایی و معدنی با بتن تازه و سخت شده دارد. اندرکنش بین بتن با محیط نیز در ساختار شیمیایی اثر می‌گذارد، که کلاً به دوام بتن مربوط می‌شود. به طور کلی، خمیر سیمان هیدراته شده شامل سه سیستم مهم به شرح زیر است:

- سیستم جامد
- سیستم منافذ
- سیستم محلول در منافذ

سیستم‌های جامد و محلول در منافذ مربوط به ساختار شیمیایی است، سیستم منافذ محدود به ساختار فیزیکی است. سیستم جامد در واقع محصولات هیدراتاسیون است که شامل ژل C- S- H، هیدروکسید کلسیم و فازهای آلومینات و فریت است. قسمتی از ذرات سیمان در میان ژل بدون واکنش هیدراتاسیون باقی می‌ماند که ناشی از بزرگ بودن آن ذرات است.
سیستم منافذ شامل منافذ ژل است که اندازه آنها بسیار کوچک و منافذ مویین که نسبتاً بزرگترند. به علاوه منافذ دیگری نیز وجود دارند که اندازه آنها بزرگتر از منافذ مویین است که در نتیجه تراکم ناقص بتن ایجاد می‌شود.
بخشی یا تمام سیستم منافذ با محلول پر می‌شود، که این محلول عمدتاً شامل هیدروکسید سدیم (NaOH)، هیدروکسید پتاسیم (KOH) و هیدروکسید کلسیم ($Ca(OH)_2$) است. تغییرات در هریک از سه سیستم یاد شده سبب تغییر در دو سیستم دیگر می‌شود.

معمولاً اجزای تشکیل دهنده سیمان به دو گروه اجزای اصلی و فرعی تقسیم می‌شود. اجزا یا ترکیبات اصلی شامل آلیت (C_3S)، بلیت (C_2S)، سیلیت (C_4AF) و فاز کلسیم آلومینات (C_3A) است. این گروه حدود ۹۰ درصد جرم سیمان را تشکیل می‌دهند. ترکیبات فرعی عبارتند از: MgO، TiO_2، Mn_2O، K_2O و Na_2O که مهمترین آنها قلیایی‌ها، یعنی K_2O و Na_2O است.

آلیت یا سه کلسیم سیلیکات ($3CaO, SiO_2$) یا C_3S حدود ۴۵ تا ۵۰ درصد سیمان پرتلند معمولی را شامل می‌شود. این ماده نقش عمده‌ای در رفتار و خواص خمیر سیمان دارد. آلیت نسبت به بقیه ترکیبات دارای مقاومت فشاری زیادی است.

بلیت یا دو کلسیم سیلیکات ($2CaO, SiO_2$) یا C_2S حدود ۲۵ درصد سیمان پرتلند معمولی را تشکیل می‌دهد. برخلاف C_3S که گیرش و سخت شدن آن چند ساعت به طول می‌انجامد، هیدراتاسیون C_2S به آهستگی انجام می‌شود و گیرش آن ممکن است چند روز طول بکشد.

سه کلسیم آلومینات ($3CaO, Al_2O_3$) یا C_3A با آب واکنش سریع می‌دهد و در نتیجه باعث گیرش ناگهانی خمیر سیمان می‌شود. برای کاهش زمان گیرش C_3A و جلوگیری از گیرش ناگهانی، به کلینکر سیمان مقداری گچ ($CaSO_4 . 2H_2O$) افزوده می‌شود. C_3A نقش کمی‌در کسب مقاومت خمیر سیمان دارد ولی ممکن است در طی یک یا دو روز به مقاومت نهایی خود برسد. سیمان پرتلند معمولی بـه طـور متوسط دارای تقریباً ۱۰ درصد C_3A است.

سیلیت، فاز آهن‌دار سیمان است، بنابراین گاهی اوقات از آن به عنوان فاز فریت نام می‌برند. این ماده چهار کلسیم آلومینو فریت ($4CaO , Al_2O_3 , Fe_2O_3$) یا C_4AF است که حدود ۸ تا ۱۰ درصد سیمان را تشکیل می‌دهد. کسب مقاومت C_4AF بسیار سریع ولی مقاومت نهایی آن بسیار کم است. شایان ذکر است که شرکت اجزای سیمان در کسب مقاومت خمیر سیمان متفاوت است و هریک از ترکیبات درصدی از کسب مقاومت را به‌عهده دارند.

مقدار تقریبی هر یک از ترکیبات اصلی سیمان و خلاصه عملکرد آنها در جدول ۱ ارائه شده است.

جدول ۱: مقدار و عملکرد ترکیبات اصلی سیمان

ترکیبات اصلی	مقدار (درصد)	عملکرد
C_3S	۵۰–۴۵	بسیار فعال، حرارت هیدراتاسیون بالا و مقاومت اولیه زیاد
C_2S	۲۵	حرارت هیدراتاسیون پایین و فعالیت کم
C_3A	۱۰	ایجاد مشکلات در اثر حمله سولفاتی و حرارت هیدراتاسیون بالا
C_4AF	۱۰–۸	کسب مقاومت سریع و مقاومت نهایی بسیار کم
گچ	۵	کنترل گیرش سیمان

۳- خوردگی کلریدی

خوردگی بر اثر نفوذ یون کلرید یکی از عوامل اصلی و مهم تخریب سازه‌های بتن مسلح است کـه در معـرض آب دریا یا نمک‌های یخ زدا قرار دارند. همچنین کلریدها می‌توانند روی سطح بتن رسوب کنند. این رسوب‌ها از طریق قطرات بسیار ریز آب دریا و گردوغبار معلق در هوا تشکیل می‌شود.

هنگامی‌که کلرید در بتن مسلح شده وجود داشته باشد می‌تواند سبب خوردگی‌های بسیار شدید آرماتور شود. منشأ کلریدها از دو منبع عمده به شرح زیر است:

الف – کلرید با منشأ داخلی

این نوع کلریدها در هنگام اختلاط به بتن وارد می‌شوند. مانند استفاده از افزودنی‌های زودگیرکننده (کلرید کلسیم)، سنگدانه‌ها و آب دریا یا سایر آب‌های شور.

ب- کلرید با منشأ خارجی

این نوع کلریدها در زمان سخت شدن به بتن وارد می‌شوند. مانند استفاده از نمک ضدیخ در ساخت بزرگراه‌ها و کلریدهای ناشی از آب دریا در سازه‌های دریایی (اسکله).

اثر نمک‌های کلریدی تا حدی به شیوه وارد شدن آن دارد. چنانچه کلرید هنگام اختلاط اجزای متشکل بتن وجود داشته باشد. فاز تری کلسیم آلومینات (C_3A) سیمان تا حدی با کلرید واکنش داده و تشکیل پیوند شیمیایی کلروآلومینات کلسیم می‌دهد. دراین حالت، کلرید در محلول منافذ غیر محلول بوده و در واکنش‌های خوردگی شرکت نمی‌کند. قابلیت سیمان برای تشکیل کمپلکس کلرید محدود است و بستگی به نوع سیمان دارد. به عنوان مثال، سیمان ضدسولفات که دارای C_3A کم است در تشکیل کمپلکس کلریدی در حد کمی شرکت می‌کند. همچنین، تجربیات نشان می‌دهد که میزان کلرید بیش از ۰/۴ درصد وزنی‌سیمان، خطر خوردگی را افزایش می‌دهد. شایان ذکر است که این حد به این معنا نیست که بتن‌های دارای میزان کلرید بیشتر از حد ذکر شده محتملاً سبب خوردگی شدید آرماتور می‌شوند. خوردگی به نفوذپذیری بتن و عمق کربناتاسیون در ارتباط با پوشش آرماتور بستگی دارد.

هنگامی‌که بتن در اثر واکنش با دی‌اکسید کربن هوا کربناته می‌شود، کلریدهای پیوند یافته آزاد می‌شوند. در اثر این فرآیند، غلظت کلریدهای محلول در مجاور منطقه کربناتاسیون زیادتر می‌شود و در نتیجه سبب مهاجرت کلرید در داخل بتن می‌شود.

۴- کلریدهای پیوندی و آزاد

مهمترین پیوند یون‌های کلرید، واکنش آنها با C_3A است که تشکیل کلسیم کلروآلومینات $3CaO.\ Al_2O_3.\ CaCl_2.\ 10H_2O$ می‌دهد که نمک فریدل نامیده می‌شود. یون کلرید با C_4AF نیز واکنش مشابهی انجام داده وتشکیل کلسیم کلروفریت می‌دهد. بنابراین وقتی مقدار C_3A سیمان بالا باشد و همچنین وقتی مقدار سیمان در مخلوط زیاد باشد، یون‌های کلرید بیشتری پیوند برقرار می‌کند. بنابراین این طور استنباط می‌شود که استفاده از سیمان با C_3A بالا منجر به ایجاد مقاومت مناسب در برابر خوردگی می‌شود. این مساله ممکن است هنگامی‌صدق کند که از ابتدا یون‌های کلرید موجود باشند و به سرعت با C_3A واکنش دهند. در نتیجه وقتی یون‌های کلر از خارج وارد بتن شوند مقدار کمتری کلروآلومینات تشکیل می‌شود.

همچنین ممکن است تحت شرایطی کلروآلومینات تفکیک شده و یون‌های کلرید آزاد توسط آب منافذ به سطح فولاد منتقل شوند. عامل دیگری که تعیین کننده مقدار مطلوب C_3A در سیمان می‌باشد مشکل حمله سولفات‌ها

است. شایان ذکر است که برای مقاومت در برابر سولفات لازم است مقدار C_3A سیمان پایین باشد. به این دلیل آیین نامه ASTM، سیمان نوع II را که دارای مقاومتی متوسط در برابر سولفات است سازگارترین سیمان برای سازه‌های بتنی قرار گرفته در معرض حمله سولفات‌ها معرفی می‌کند. در جدول۲ میزان C_3A انواع سیمان مشخص شده است.

جدول ۲: درصد ترکیبات متشکل انواع مختلف سیمان

نوع سیمان	C_3S	C_2S	C_3A	C_4AF
I	۴۲ –۶۵	۱۰ –۳۰	۳ –۱۷	۶ –۱۸
II	۳۵ –۶۰	۱۵ –۳۵	۳ –۸	۶ –۱۸
III	۴۵ –۷۰	۱۰ –۳۰	۳ –۱۵	۶ –۱۸
IV	۲۰ –۳۰	۵۰ –۵۵	۳ –۶	۸ –۱۵
V	۴۰ –۶۰	۱۵ –۴۰	۳ –۵	۱۰ –۱۸

اثر نوع و مقدار سیمان در نفوذ کلرید

در صورت نفوذ کلرید به داخل بتن و یا به دلیل آلوده بودن مصالح بتن، یون‌های کلرید به سه حالت آزاد در محلول منافذ، جذب فیزیکی با محصولات هیدراتاسیون و پیوند یافته با C_3A در بتن یافت می‌شود. از دیدگاه خوردگی فقط کلریدهای آزاد اهمیت دارند. کلرید با C_3A ترکیب شده و تشکیل نمک فریدل $CaO.\ Al_2O_3.\ ۳CaCl_2.\ 10H_2O$ می‌دهد و در نتیجه کلریدها پیوند می‌یابند. بنابراین می‌توان نتیجه گرفت که ظرفیت پیوند سیمان پرتلند توسط مقدار C_3A تعیین می‌شود و سیمان با مقدار بیشتر C_3A ترجیح دارد. انتظار می‌رود که سیمان با ظرفیت پیوندی زیاد، سبب کاهش سرعت نفوذ یون‌های کلرید در بتن شود و در نتیجه زمان شروع خوردگی میلگرد افزایش یابد. این نظریه شاید درباره سیمان‌های پوزولانی صادق نباشد، زیرا بعضی از پوزولان‌ها دارای ظرفیت پیوندی کم بوده، اما توسط سازوکارهای دیگر (مانند نفوذپذیری کم) سبب کاهش سرعت نفوذ یون‌های کلرید می‌شوند.

به‌هرحال، در محیطی که یون‌های کلرید به عنوان عامل مخرب محسوب می‌شود، سیمان پرتلند معمولی نوع I با مقدار زیاد در مقایسه با سیمان پرتلند ضدسولفات (با مقدار C_3A کم) عملکرد بهتری دارد.

تحقیقات انجام شده نشان می‌دهد که علاوه برمقدار C_3A سیمان در پیوند دادن یون‌های کلرید، عوامل زیر نیز مؤثرند:

- ترکیبات سیمان
- ترکیبات محلول منافذ

پیوند یافتن یون‌های کلرید فقط تابع مقدار C_3A نیست، بلکه C_4AF و همچنین C_3S و C_2S نیز مؤثرند.

ترکیبات محلول منافذ نیز در مقدار یون‌های کلرید پیوند یافته، اثر دارد. به عبارت دیگر، یون‌های موجود در محلول منافذ مانند OH^- و SO_4^{2-} در پدیده پیوند با یون‌های کلرید رقابت می‌کنند.

ترکیبات محلول منافذ به ترکیبات سیمان، مواد افزودنی شیمیایی و معدنی و شرایط محیط بستگی دارد. برای مثال اگر به مقادیر OH^- و SO_4^{2-} در منافذ بتن افزوده شود، از مقدار یون‌های کلرید پیوند یافته کاسته می‌شود، زیرا قسمتی از ظرفیت پیوند سیمان برای یون‌های OH^- و SO_4^{2-} صرف می‌شود.

کاملاً واضح است که فقط ترکیبات سیمان در مقدار کلریدهای پیوند یافته نقش ندارند، بلکه مقدار سیمان نیز مؤثر است. بنابراین با افزایش مقدار سیمان در بتن، از مقدار نفوذ کلریدها کاسته می‌شود.

اثر نوع کاتیون‌ها

با تحقیقات انجام شده مشخص شده است که نوع کاتیون‌های کلرید در خوردگی آرماتور اثر دارد. وقتی مقدار مساوی Cl^- اما با کاتیون‌های مختلف به ملات سیمان پرتلند افزوده شود، اثرات متفاوتی را نشان می‌دهد. در این تحقیق از $CaCl_2$، $NaCl$ و KCl استفاده شده است. نتایج این پژوهش نشان می‌دهد که شدت خوردگی به طور قابل توجهی تابع نوع کاتیون بوده و $CaCl_2$ بیشترین اثر تخریبی را داشته است. همچنین مشخص شده است که کل تخلخل و غلظت کلرید در محلول منافذ و یا pH، عوامل کنترل کننده در شدت خوردگی نمی‌باشند، زیرا این عوامل در تمام نمونه‌های مورد تحقیق تقریباً مشابه بوده است. تفاوت در مقاومت الکتریکی عامل اختلاف در شدت خوردگی است. از آنجایی که مقاومت الکتریکی تابع توزیع اندازه منافذ ملات است، در نتیجه تغییر در کاتیون باعث تغییر در توزیع اندازه منافذ می‌شود. بنابراین $CaCl_2$ منافذ بزرگتری ایجاد می‌کند و در نتیجه انتشار کلرید آسانتر انجام می‌شود و هدایت الکتریکی افزایش می‌یابد. همچنین براساس نتایج تحقیقات انجام شده مشخص شده است که، کلرید سدیم باعث کاهش اندازه منافذ می‌شود. بنابراین تخلخل بتن تابع کاتیون و نوع مخلوط بتن می‌باشد.

بررسی‌های انجام شده در مرکز تحقیقات ساختمان و مسکن

بررسی‌های انجام شده در مرکز تحقیقات ساختمان و مسکن در سه زمینه به شرح زیر بوده است:

- بررسی تأثیر میزان C_3A سیمان در ایجاد پیوند شیمیایی یون کلرید.
- بررسی تأثیر کاتیون‌های مختلف کلرید در ایجاد پیوند شیمیایی.
- بررسی روش‌های اندازه‌گیری کلرید آزاد در سیستم‌های سیمانی.

در این راستا، با ساخت C_3A خالص (براساس نسبت‌های استکیومتری) در آزمایشگاه و افزودن آن به نسبت‌های ۵، ۸، ۱۰ و ۱۲ درصد به سیمان و ساخت ملات با سیمان‌های ساخته شده و افزایش کلرید سدیم و کلسیم به نسبت‌های ۰/۵، ۱ و ۲ درصد به آب اختلاط، روند پیوند کلریدی مورد بررسی قرار گرفت. پس از عمل‌آوری نمونه‌های ساخته شده و آماده‌سازی آنها براساس روش‌های استاندارد، میزان کلرید محلول در آب و محلول در اسید آنها اندازه گیری شد.

همچنین به‌منظور بررسی اثر C_3A در پیوند کلریدی در شرایط واقعی، از چهارنوع سیمان با درصدهای مختلف C_3A (۳/۴۲، ۶/۶۵، ۸/۲۴ و ۱۱/۵۷درصد)، در ساخت نمونه‌ها استفاده شد. عمل‌آوری نمونه‌ها و آماده‌سازی آنها مشابه نمونه‌های ساخته شده با سیمان دارای C_3A خالص بوده است.

اثر میزان C_3A سیمان در پیوند کلریدی

– بررسی نتایج به دست آمده از اندازه‌گیری کلرید نمونه‌های ساخته شده با سیمان با C_3A خالص (ساخته شده در آزمایشگاه) با درصدهای ۵، ۸، ۱۰ و ۱۲، نشان می‌دهد که با افزایش میزان C_3A سیمان، پیوند کلریدی

نیز افزایش یافته است. همچنین کلریدهای محلول در آب (کلریدهای آزاد) نیز با افـزایش C_3A، نتیجـه کمتـری به‌دست داده که مؤید پیوند کلریدی بیشتری است.
در شکل‌های ۱ و ۲ روند افزایش پیوند کلریدی با افزایش میزان C_3A سیمان، به‌ترتیب در نمونه‌های ساخته‌شده با کلرید سدیم و کلرید کلسیم مشاهده می‌شود.

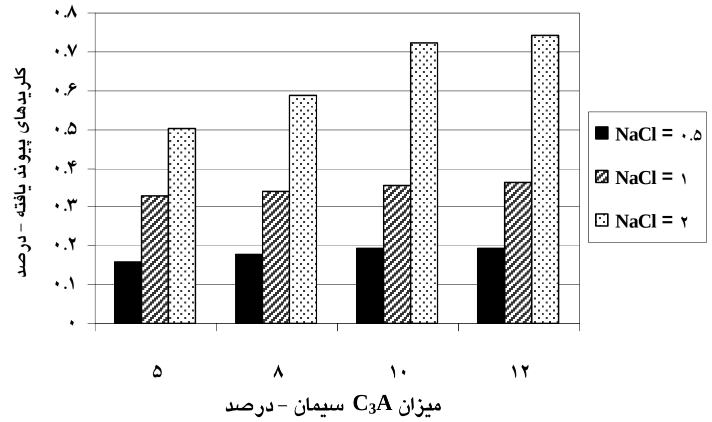

شکل ۱- هیستوگرام روند افزایش کلریدهای پیوند یافته با افزایش میزان C_3A (در نمونه‌های ساخته شده با سیمان با C_3A خالص و کلرید سدیم)

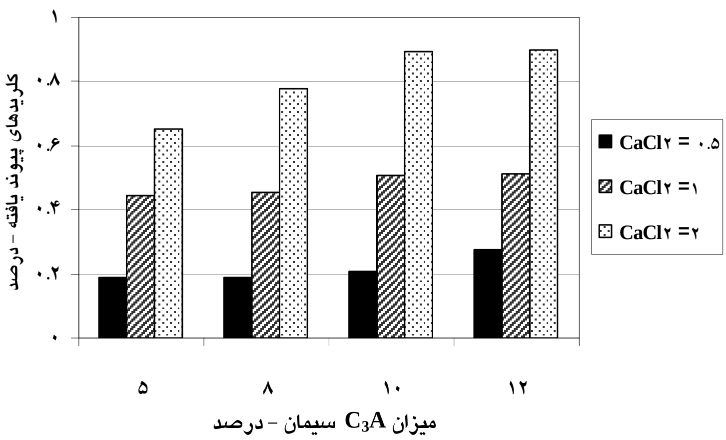

شکل ۲- هیستوگرام روند افزایش کلریدهای پیوند یافته با افزایش میزان C_3A (در نمونه‌های ساخته شده با سیمان با C_3A خالص و کلرید کلسیم)

- بررسی نتایج به دست آمده از اندازه‌گیری کلرید نمونه‌های ساخته شـده بـا سـیمان دارای C_3A مختلـف (بـا درصدهای ۳/۴۲، ۶/۶۵، ۸/۲۴ و ۱۱/۵۷)، نشان می‌دهد که با افزایش میزان C_3A سیمان، پیوند کلریـدی نیـز افزایش یافته است. همچنین کلریدهای محلـول در آب (کلریـدهای آزاد) نیـز بـا افـزایش C_3A، نتیجـه کمتـری به‌دست داده که مؤید پیوند کلریدی بیشتری است.

در شکل‌های ۳ و ۴ روند افزایش پیوند کلریدی با افزایش میزان C_3A سیمان، به‌ترتیب در نمونه‌های ساخته‌شده با کلرید سدیم و کلرید کلسیم مشاهده می‌شود.

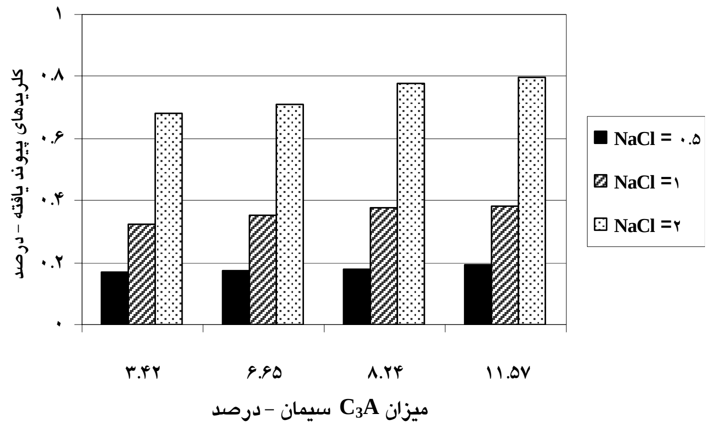

شکل ۳- هیستوگرام روند افزایش کلریدهای پیوند یافته با افزایش میزان C_3A (در نمونه‌های ساخته شده با سیمان دارای C_3A مختلف و کلرید سدیم)

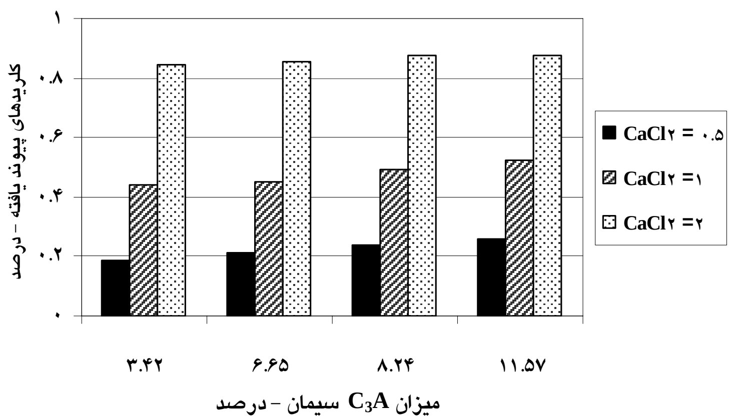

شکل ۴- هیستوگرام روند افزایش کلریدهای پیوند یافته با افزایش میزان C_3A (در نمونه‌های ساخته شده با سیمان دارای C_3A مختلف و کلرید کلسیم)

تأثیر نوع کاتیون کلرید در ایجاد پیوند کلریدی

- بررسی نتایج به دست آمده از اندازه‌گیری کلرید نمونه‌های ساخته شده با سیمان با C_3A خالص (ساخته شده در آزمایشگاه) با درصدهای ۵، ۸، ۱۰ و ۱۲، نشان می‌دهد که در همه موارد با یک نسبت مشابه کلریدسدیم و کلرید کلسیم، نمونه‌های دارای کلرید کلسیم، پیوند کلریدی بیشتری ایجاد کرده است.
- بررسی نتایج به دست آمده از اندازه‌گیری کلرید نمونه‌های ساخته شده با سیمان دارای C_3A مختلف (با درصدهای ۳/۴۲، ۶/۶۵، ۸/۲۴ و ۱۱/۵۷، نشان می‌دهد که در همه موارد با یک نسبت مشابه کلریدسدیم و

کلرید کلسیم، نمونه‌های دارای کلرید کلسیم، پیوند کلریدی بیشتری ایجاد کرده است.

در شکل ۷ میزان کلرید پیوند یافته درنمونه‌های ساخته شده با کلرید سدیم و کلرید کلسیم به نسبت‌های مختلف (سیمان با ۱۲ درصد C_3A خالص) مقایسه شده است.

در شکل ۸ میزان کلرید پیوند یافته درنمونه‌های ساخته شده با کلرید سدیم و کلرید کلسیم به نسبت‌های مختلف (سیمان دارای ۱۱/۵۷ درصد C_3A) مقایسه شده است.

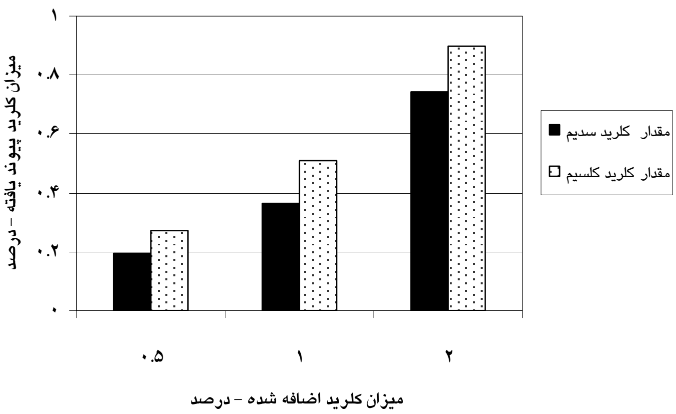

شکل ۷- هیستوگرام میزان کلرید پیوند یافته درنمونه‌های ساخته شده با کلرید سدیم و کلرید کلسیم به نسبت‌های مختلف (سیمان با ۱۲درصد C_3A خالص)

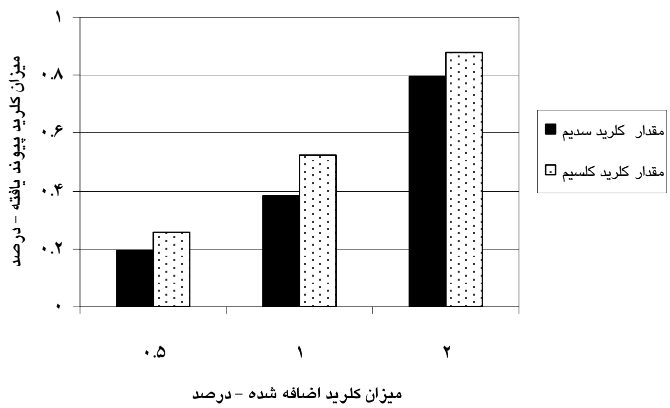

شکل ۸- هیستوگرام میزان کلرید پیوند یافته درنمونه‌های ساخته شده با کلرید سدیم و کلرید کلسیم به نسبت‌های مختلف (سیمان دارای ۱۱/۵۷ درصد C_3A)

کلرید عصاره‌گیری شده در سنگدانه و سیستم‌های سیمانی

برخی سنگدانه‌ها حاوی مقداری کلرید هستند که در سنگدانه محبوس بوده و در واکنش خوردگی شرکت نمی‌کنند. این نوع کلریدها از طریق روش عصاره‌گیری اندازه‌گیری می‌شوند.

هنگامی‌که کلرید محلول در آب به مقدار کافی وجود داشته باشد، می‌تواند سبب خوردگی فلزاتی نظیر فولاد شده

که در داخل یک سیستم سیمانی مانند ملات، گروت یا بتن قرار دارد یا در تماس با آنها می‌باشد. این روش آزمون در مورد سنگدانه‌هایی که به طور طبیعی دارای کلرید هستند، قابل عمل است.

روش آزمون شرح داده شده در استانداردملی ایران شماره ۸۹۴۷، بخشی از کلریدی را که در این سنگدانه‌ها وجود دارند اندازه گیری می‌کند. شایان ذکر است که مقدار کلرید اندازه‌گیری شده به شدت به درجه نرمی‌سنگدانه‌ها که هنگام تهیه نمونه آسیاب می‌شوند بستگی دارند.

در روش‌های آزمون استاندارد ملی ایران شماره‌های ۸۹۴۶ و ۸۹۴۷ به ترتیب کلریدهای محلول در اسید و محلول در آب را تعیین می‌کند. در هر دو روش نمونه به شکل پودر ریزدانه یا به صورت مواد دانه‌ای ریز آسیاب می‌شود و کلریدهای محبوس در سنگدانه‌ها را که در واکنش خوردگی شرکت ندارند، نیز اندازه‌گیری می‌کند.

روش اندازه‌گیری این نوع کلریدها دراستاندارد ASTM C 1524 - 02a و آیین نامه بتن آمریکا (ACI 222.1-96) ارائه شده است. در این روش با استفاده از دستگاه عصاره‌گیر Soxhlet، مقادیر بسیار کم کلرید را که در برخی سنگ‌ها باقی می‌ماند و در واکنش خوردگی شرکت نمی‌کنند، عصاره‌گیری می‌شود.

دستگاه عصاره گیر Soxhlet

به منظور بررسی کلریدهای محبوس در برخی از سنگدانه‌ها که در واکنش خوردگی شرکت نمی‌کنند، از دستگاه عصاره گیر Soxhlet استفاده می‌شود.

این دستگاه متشکل از یک گرمکن، یک بالن ته صاف، یک نمونه‌گیر و یک مبرد است. عملکرد دستگاه عصاره گیر به گونه‌ای است که با اضافه کردن ۲۰۰ میلی لیتر آب مقطر در بالن ته صاف و اعمال گرما به آب داخل بالن، بخار حاصل از آب جوش از قسمت مبرد عبور کرده و مایع حاصله در نمونه‌گیر جمع می‌شود. نمونه در داخل نمونه گیر مخصوص قرار گرفته و مایع گرم حاصل از تبخیر آب جوش اطراف آن جمع می‌شود. هنگامی‌که عصاره حاصله به ارتفاع بحرانی رسید به داخل بالن ته صاف برگشته و این فرآیند تکرار می‌شود. ترکیبات غیر فرار عصاره گیری شده که حاوی آب مقطر گرم نیز می‌باشد در بالن ته صاف جمع می‌شود. شایان ذکر است که ورودی گرما باید به اندازه کافی بوده تا یک چرخه عصاره گیری در حدود هر ۲۰ دقیقه یک بار تکرار شود.

در شکل ۹ شمای این دستگاه مشاهده می‌شود.

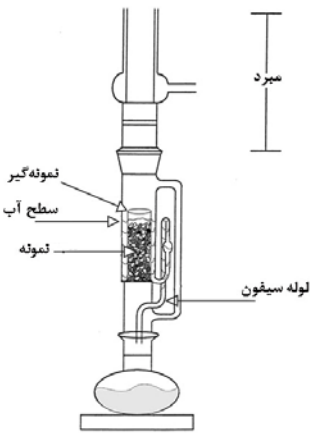

شکل ۹- دستگاه عصاره گیر Soxhlet

مراجع

۱- قدوسی، پرویز، گنجیان، اسماعیل، پرهیزکار، طیبه، رمضانیانپور، علی‌اکبر، فن‌آوری بتن در شـرایط محیطـی خلیج فارس – آسیب‌شناسی بتن و ارزیابی آن، شماره ۲۸۳، بهار ۱۳۷۸، مرکز تحقیقات ساختمان و مسکن.

۲- پروفسور نویل، ترجمه: فامیلی، هرمز، بتن شناسی (خواص بتن)، ۱۳۶۸، جهـاد دانـشگاهی، دانـشگاه علـم و صنعت ایران.

3- Hewlett, Peter C., LEA'S Chemistry of Cement and Concrete. Fourth Edition, Arnold, 1988.

۴- حسینی، عبدالله، پرهیزکار، طیبه، استخراج یون کلرید از بتن به منظور توقف خوردگی آرمـاتور، شـماره ۳۹۷، ۱۳۸۴، مرکز تحقیقات ساختمان و مسکن.

5- Lambert, P., Page, C.L. and Short, N.R., Pore Solution Chemistry of the Hydrated System Tricalcium Silicate/ Sodium Chloride/Water, Cement and Concrete Research, Vol 15, pp.675-680,1985.

۶- قدوسی، پرویز، پرهیزکار، طیبه، رمضانیانپور، علی‌اکبر، مظفری، نرگس، فـن‌آوری بـتن در شـرایط محیطـی خلیج فارس –جلد دوم - روش‌ها و توصیه‌ها برای افزایش عمر مفید سازه‌های بتنی، شـماره ۳۷۰، ۱۳۸۳، مرکز تحقیقات ساختمان و مسکن.

7- Hansson, C.M., Frolund, T. and Markussen, S.B., the Effect of Chloride Cation Type on the Corrosion of Steel in Concrete by Chloride Salts, Cement and Concrete Research,Vol. 14,1985, PP. 65-73.

8- Midgley, H.G. and Illston, J.M., Effect of Chloride Penetration on the Properties of Hardened Cement Pastes, Proc. 8th International Symposium on Chemistry of Cement , Rio de Janeiro, Part VII, pp.101-103, 1986.

۹- جعفرپور، فاطمه و همکاران، بررسی روش‌های اندازه گیری کلرید در بتن‌های سخت شـده و انتخـاب روش بهینه و تهیه دستورالعمل آن، شماره ۴۶۱، ۱۳۸۶، مرکز تحقیقات ساختمان و مسکن.

10- Tritthart, J., Chloride Binding in Cement. I. Investigations to Determine the Composition of Porewater in Hardened Cement, Cement and Concrete Research, Vol 19 , pp.586-594, 1989.

11- Al - Hussaini, M.J., Sangha, C.M., Plunkett, B.A. and Walden, P.J., The Effect of Chloride Ion Source on the Free Chloride Ion Percentages in OPC Mortars, Cement and Concrete Research, Vol 20 , pp.739-745, 1990.

12- Arya, C., Buenfeld, N.R. and Newman, J.B., Factors Influencing Chloride-Binding in Concrete, Cement and Concrete Research, Vol 2 , pp.291-300, 1990.

13- Chatterji, S., Transportation of Ions Through Cement Based Materials, Part 3, Experimental Evidence for the Basic Equations and Some Important Deductions, Cement and Concrete Research, Vol 24 , pp.1229-1236,1994.

14- Nevile, A., Chloride Attack of Reinforced Concrete in Overwiew, Materials and Structures, Vol 28 , pp.63-70,1995.

15- Delagrave, A., Marchand, J., Ollivier, J.P., Julien, S. and Hazarti, K., Chloride Binding Capacity of Various Hydrated Cement Paste Systems, Adv.Cem. Bas. Mat., Vol 6 , pp.28-35, 1997.

16- Lambert, P., Page, C.L. and Short, N.R., Diffusion of Chloride Ions in Hardened Cement Pastes Containing Pure Cement Minerals, Br. Ceram. Proc., Vol 35, pp.267-276, 1984.

17- Brown, P.C., Kinetics of Tricalcium Aluminate and Tetra Calcuim Aluminoferrite

Hydration in the Presence of Calcium Sulphate, J. American Ceramic Society, Vol 76, No. 12, pp.2971-2976, 1993.

18- Traetteberg, A., The Mechanism of Chloride Penetration in Concrete, SINTEF Report STF65 A77070, 1977-12-30, 51 pp.

19- Tang, L. and Nilsson, L.O., Chloride Binding Capacity and Binding Isotherms of DPC Paste and Mortars, , Cement and Concrete Research, Vol 23 , pp.247-253, 1993.

20- Dr. Harald Justnes,A Review of Chloride Binding in Cementitious Systems, Cement and Concrete, N-7034 Trondheim, Norway, 2005.

۲۱- مؤسسه استاندارد و تحقیقات صنعتی ایران، بتن- اندازه‌گیری کلرید محلول در آب در ملات و بتن سخت شده - روش آزمون، شماره ۸۹۴۷، سال ۱۳۸۵.

۲۲- مؤسسه استاندارد و تحقیقات صنعتی ایران، بتن- اندازه‌گیری کلرید محلول در اسید در ملات و بتن سخت شده - روش آزمون، شماره ۸۹۴۶، سال ۱۳۸۵.

23- ASTM C1524-02a Standard Test Method for Water-Extractable Chloride in Aggregate (Soxhelt Method).

24- American Concrete Institute, Provisional Standard Test Method for Water –Soluble Chloride Available Corrosion of Embedded Steel in Mortar andConcrete Using the Soxhelt Extractor, Committee 222.1-96 , ACI, 2003.

25- Brian B. Hope, John A. Page and John S. Poland, The Determination of the Chloride Content of Concrete, Cement and Concrete Research, Vol 15, No.5, pp.863-870, 1985.

CD06

Maintenance Repairing and Strengthening

CD06-001

BENDING AND SHEARING STRENGTH OF T-FORMED BEAM MADE OF STRUCTURAL LIGHT CONCRETE USING FRP SHEETS

A. Ghods[1], M.H.Beygi[2] , M. Miri[3], H. Navaee[4]
[1,3]Department of Civil Engineering, University of Sistan and Baluchestan, Iran
[2]Department of Civil Engineering, Babol University of Nushiravan
[4]Department of Civil Engineering, Azad University of Tehran, South Branch

ABSTRACT

To study enforcement effect of T-formed beams made of Structural lightweight concrete by binding CFRP with use of epoxy resin on the bending & shearing resistance, nine lab samples were designed, built and tested. These samples were divided into A, B & C groups, regarding their weakness. In all beams, two rods # 12 were used as compressive armature. In A, designing was such that beams have bending weakness. In these beams, two rods #12 were used as tensile armature and rod # 10 were used as shearing armature with a distance of 7.5 cm. In B, designing was such that beams have shearing weakness and 4 rods # 16 were used as tensile armature , the distance of stirrup was 30 cm. In c, designing was such that beams have shearing and also flexural weakness , In these beams , two rods # 12 were used as tensile armature and the distance of stirrups was 30 cm.

According to observed studies, in flexural strengthening, beams have had a strength increase of 60%, although breaking was shearing and CFRP sheets didn't reach the rupture stage. Studying beam's shearing strengthening represents loading capacity increase of 20% and breaking was as stratified cutting of concrete with CFRP sheet. Also, we observed 45% increase of beam's loading capacity from bending and also shearing strengthening together. In this case, failure mode was as stratified cutting of concrete with CFRP sheet from the beam's side.

Keyword: strengthening, tensile armature, CFRP, flexural

1. INTRODUCTION

Due to several causes such as damages resulting from corrosion or blasting severe wind, members weakness resulting from incorrect maintenance, damages from war or earthquake, usage changes, request for increasing foundation or number of stories and changes of used parameters, maybe the structures of armature concrete don't have necessary ductility and resistance against imposed loads.[1]

To remove the deficiency of using steel plates in the strengthening of concrete members, using fiber reinforcing polymers (FRP) has some advantages.

Several researchers have studied on bending and shearing strengthening by FRP sheets in worldwide scientific centers & universities. The polymeric sheets are not under the effect of corrosive factors, unlike the steel plates and are resistant against damaging effects and also tolerate the relatively high temperatures well. So, using these sheets doesn't need special arrangements before attachment and their maintenances are easier after the installation in comparison with steel plates.[2]

2. LABORATORIAL PLAN

In this study, nine T-formed beams of light concrete with a total length of 1900mm were built and tested over supports with a span of 1800mm. Lab samples are in A,B and C groups and each group has 3 beams. For labs, one is as un-strengthened and the other two are strengthened based on the kind of weakness in the beam.

3. SPECIFICATIONS OF USING MATERIALS

3.1. Armature

Internal armature is ribbed bar and from A_2 type. The yielding stress for bars of 16 is 3300 kg/cm_2, for bars of 12, 3800 kg/cm_2 and for bars of 10 3650 kg/cm_2. The results of the using steel bars are given in.

Table 1: Tensile experiment results for steel bars

Number	Steel bar's diameter mm	Area cm^2	Yield stress kg/cm^2	Rupture stress kg/cm^2	Percentage of length increase	Elasticity modulus kg/cm^2
1	10	0.785	3650	5600	15	2039000
2	12	1.13	3800	5600	15	2039000
3	16	2.01	3800	5600	15	2039000

3.2. Concrete

Regarding the first mix designs, an effort has been made to obtain a suitable mixture regarding the effective factors on the compressive resistance increase and also economic and administrative conditions.
To provide needed experimental concrete, the following mixing ratio was used.

Table 2: Mixing design

Sources	Material weight
Cement	450
Water	180
Gravel	234
Sand	561.6
Lecca	374.4
Super Plasticizer	6.75
Water to cement ratio	0.4
Sources	1800

Lecca grains are products of Saveh lecca factory and the fine grains were used in this plan. The used sand was provided from washed one in the Ganjafrooz mine in Babol. The kind of used cement is type, II Portland produced in Neka cement factory. The using superplastilizer is PCE from Vandshime factory and the water is from urban potation one.

3.3. Glus
To make glue, a mix including two parts of epoxy resin and one part of hardening is used that will gain its complete stick after one week.

3.4. CFRP Sheet
The CFRP sheets used in beam strengthening are uni- lateral yarn with the yielding stress of 3800 and elasticity modulus of 240.000 MPa. Their thickness is 0, 11 mm.

4. LOADING SYSTEM
Loading system is shown in Figure (6-3). In this system, we used rigid metal frames assumed to install jack. Samples are put on the part of this rigid frame for beam support. In this study, beams are tested as Simple beam.

5. MEASURING TOOLS
Measuring special buttons of strain are installed on the beam lateral surface in its upper and lower arrays with a distance of 200mm. These buttons are installed by using concrete glue on the beam in order to measure concrete strain and its stick strengthening sheets by strain gage.

5.1. Data Logger
The available Data Logger is cr10x that has high compatibility in data recording & sending, even through modem & internet.

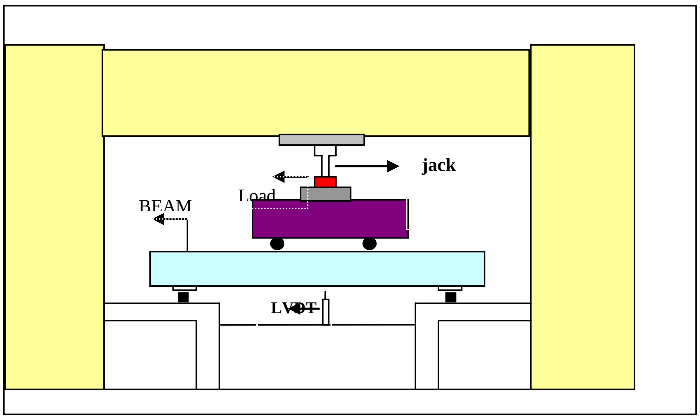

Figure 1. Loading specification

5.2. Samples Introduction
In this study, nine T-formed beams of light concrete with a total length of 1900mm were loaded and tested on the supports with a span of 1800mm. The compressive strength of used concretes in all beams has been designed for f_c=410 kg/cm^2

5.3. “A” Group Beams

“A” Group relates to the beams having weakness in bending. In this group, we used two ribbed bars # 12 as tensile armature and two ribbed bars #12 as compressive ones. For shearing armature, we used ribbed bars # 10 as rectangular ones with the distance of 75mm axis to axis.

Selecting the above armature for A was due to strength of these beams in shearing & their weakness in bending. The specifications of “A” are given in figure 5.

5.4. “B” Group Beams

“B” Group relates to the beams having weakness in shearing. In this group, we used four ribbed bars # 16 as tensile armature in two double arrays and two ribbed bars # 12 as compressive ones.

For Shearing armatures, we used ribbed bars # 10 as a rectangular form with a distance of 300 mm from axis to axis. The specifications are given in figure 6.

5.5. “C” Group Beams

C Group relates to the beams having both bending & shearing weakness. In this group, we used two ribbed bars # 12 as tensile armature and two ribbed bars # 12 as compressive ones. For shearing armatures, we used ribbed bars # 10 as rectangular ones with a distance of 300 mm axis to axis. The specifications are given in Figure 7.

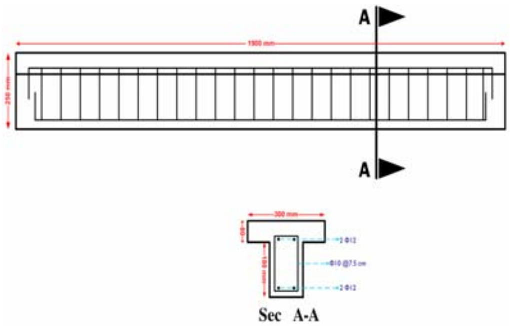

Figure 2. Specifications relating to “A” beams

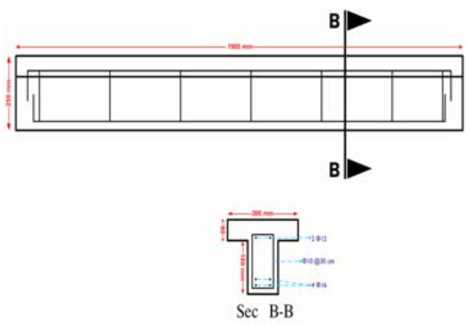

Figure 3. Specifications relating to “B” beams

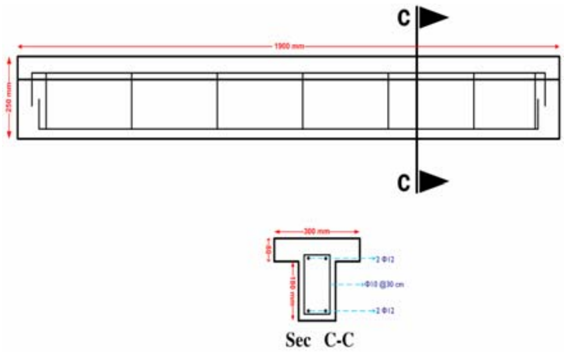

Figure 4. Specifications relating to “C” beams

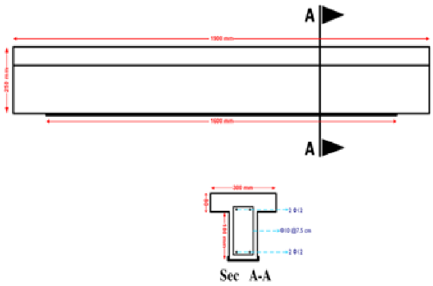

Figure 5. Strengthening method of A_1, A_2 beams

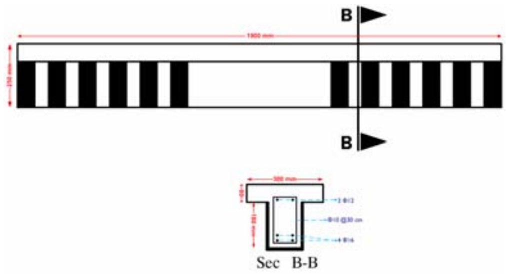

Figure 6. Strengthening method of B_2, B_3

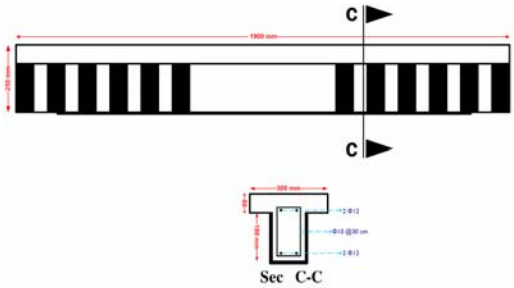

Figure 7. Strengthening method of beams

6. BEAM'S STRENGTHENING METHOD

6.1. Strengthening of A Grap Beams

"A" beams are included in A_1, A_2 and A_3 with the same specifications. In this study, we regard A_3 as a reference beam and strengthen A_1 and A_2. To strengthen A_1 and A_2, we used uni-lateral CFRP sheets by the yielding stress of 3800 Mpa and elasticity modulus of 240,000 Mpa. The width of reinforced sheet is 16 cm and its length is 160cm. Its pure thickness is 0.11mm and its strengthening method is given in Figure 8.

6.2. Strengthenin of B Grap Beams

"B" beams are included in B1, B_2 and B_3 with the same specifications.

In this study, we regard B_1 as a reference beam and strengthen B_2 and B_3; we used CFRP sheets having a width of 7cm & length of 48cm in U form. Its strengthening method is given in Figure 9.

6.3. Strengthening of "C" Group Beams

"C" beams include C_1, C_2 and C_3 with the same specifications. In this study, we regard C_1 as a reference beam and strengthen C_2 and C_3. To strengthen this beam, we used first the FRP sheet having a width of 16cm & length of 160cm for Flexural strengthening of the beam. Then, we used the 48*7cm sheets for shearing strengthening (figure 10). The cause of installing bending CFRP first and them shearing CFRP is that bending CFRP transfers the tensile forces relatively to the CFRP and this decreases the possibility of debonding risk beneath concrete.

6.4. Results

Cracking ultimate loads and strength failure mode:

Tables 3, 4 and 5 represent cracking loads, and increasing percentage in comparison to the control beam, and also ultimate load that can be carried by beams resulting from carrying out strengthening as well as maximum deflection in beams middle Span while rupturing in 3 different groups.

Table 3: Results of "A" group beams

Sample	compressive strength kg/cm^2	ultimate load ton	Increase of ultimate load relative to control beam %	maximum deflection mm	Bending cracking load kN	Shearing cracking load kN	Load increase of bending crack %	Load increase of Shearing crack %	Failure mode
A_3	525	112	-	14.8	29	59.6	-	-	Bending accompanied with yielding of tensile bars
A_1	525	175	56%	1.5	43	60	48%	0.67%	shearing
A_2	540	189	69%	10	46	59.6	59%	0	Shearing with CFRP removing accompanied with a layer of concrete

Table 4: Results of "B" group beams

Sample	compressive strength Kg/cm^2	ultimate load kN	Increase of ultimate load relative tocontrol beam%	maximum deflection mm	Bending cracking load kN	Shearing cracking load kN	Load increase of bending crack%	Load increase of Shearing crack%	Failure mode
B_1	550	185	-	8.8	43	55	-	-	Shearing with bursting compressive flange
B_2	560	210	14%	9	43	111	0	102%	Shearing with CFRP removing accompanied with a layer of concrete
B_3	560	225	22%	9.4	55	140	28%	155%	Shearing with bursting compressive flange

Table 5: Results of "C" group beams

Sample	compressive strength Kg/cm^2	ultimate load kN	Increase of ultimate load relative tocontrol beam%	maximum deflection mm	Bending cracking load kN	Shearing cracking load kN	Load increase of bending crack%	Load increase of Shearing crack%	Failure mode
C_1	555	105	-	21.8	32	56	-	-	shearing
C_2	545	150	43%	19.6	40	75	25%	34%	Shearing with CFRP removing accompanied with a layer of concrete
C_3	550	141	34%	15.7	38	71	19%	27%	shearing

6.5. Comparison of “A” Group Beams

In loading “A” group beams, there are some results. The first created bending crack in A_3 was in a load of 2.9 ton, while in A_1 and A_2 it was 4.3 and 4.6 tons. It was observed that the first crack of these beams is created in a load of 1.5 times for A_1 and 1.6 times for A_2.

The first created shearing crack in A_3 was in a load of 5.96 tons, while in A_1 and A_2 it was 6 and 5.9 tons. It was expected that these beams would reach the first shearing crack in the same load.

The A_3 failing was in a load of 11.2 tons and it was flexural failure with yielding tensile bars, while in A_1 and A_3, failing was in 17.5 and 18.9 tons and shearing.

As it was observed, the created strength increase in A_1 was about 56% and in A_2, about 70%. We should consider the fact that the real amount of loading capacity increase could be much more than this. Because, first the breaking of A_1 and A_2 was shearing and the beam fails before using its total flexural capacity. Secondly, if we compare the imposed load in the first crack, we can see that the load of the first crack in A_1 and A_2 was about 1.5 times for A. So, the flexural strength increase of A2 and $A_{1\ \text{is}}$ much more than the observed amount.

6.6. Comparing Of “B” Beams

Comparing B_1, B_2 and B_3, we can see that the first bending crack in B_1 was in load 4.3 ton, while it was expected that the first bending crack of B_1 and B_2 is created in the same load. But the first bending crack in B_3 was in 5.5 tons that is a little more than the other event.

The first shearing crack in B_1 was in 5.5 ton, while in B_2 and B_3; it was in 11.1 and 14 tons that increases the resistance against the first shearing crack. The B_1 failure was in 18.5 tons and shearing and for B_2 and B_3 it was 21 and 22.5 tons and shearing. As we can see, the increase of B_2 strength against B_1 was about 15% and B_3 against B_1, was about 22% that is not remarkable. Due to the shearing failure of B_2 and B_3, we conclude that there is no suitable strengthening, beams still have shearing weakness and CFRP sheets haven’t been broken, but they were removed by a concrete layer. This shows that CFRP sheets can still tolerate more loads.

6.7. Comparing “C” Beams

Comparing C_1, C_2 and C_3, we can see that the first bending crack is created in 3.2 for C_1 and 4 and 38 tons for C_2 and C_3.

The first created bending crack in C_1 was about 5.6 tons and in C_2 and C_3 it was about 7.5 and 7.1 tons, and its increase against C_1 was 35% for C_1 and 28% for C_3.

The breaking of C_1 was in 10.5 tons and shearing, while for C_2 and C_3 it was in 15 and 14.1 tons and shearing. As we can see, there is a good strength increase that is 45% for C_2 and 35% for C

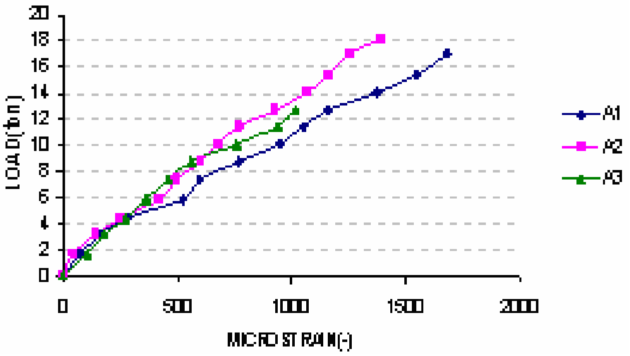

Figure 8. Load- tensile strain graph for A beams

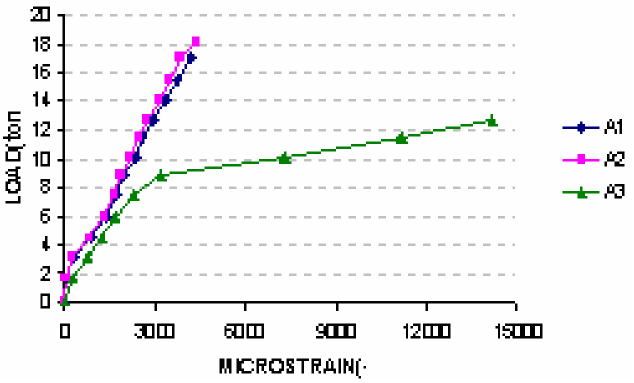

Figure 9. Load compressive strain graph for B beams

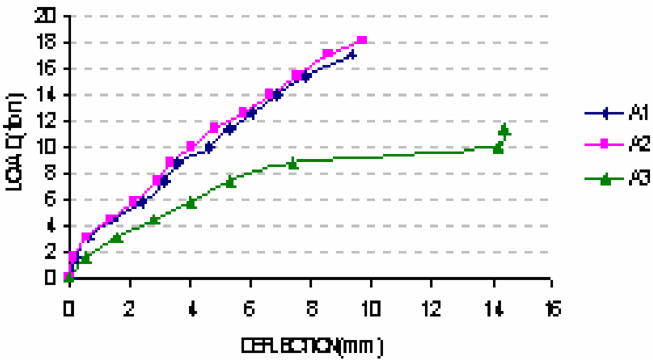

Figure 10. Load- deflection graph for A beams

7. DISCUSSION AND RESULTS

7.1. Strain in Strengthened Frp

Observing figures 8-10 relating to the load-compressive strain and load-tensile strain graph we can see increasing of compressive strain and decreasing of tensile strain in a defined load, that can be due to displacement of neutral cord because of strengthening.

8. CONCLUSION

Based on experiments and calculations, we obtained the following results:

1. The modes of shearing failure in strengthened beam were:

a) Resulting from FRP failure, b) without FRP failure, c) resulting from FRP debonding.

2. Bending & shearing strengthening on different samples, shows that the compressive strain increases remarkably.
3. With strengthening the beams, the cracking load in beams increases.
4. Deflection of flexural strengthened beams is lower than non- strengthened one.
5. Strengthening the beams, the neutral cord moves upwards at a lower speed.

REFRENCES

1. Guide of strengthening & retrofitting the concrete structures using FRP composite under ACI-440 Committee Report.
2. Al-Sulaimani GJ, Sharif A, Basun bul A, Baluch M H and Ghaleb BN (1994), Shear repair for reinforced concrete by fiberglass plate bonding, ACI Structj 91(4), 458-464.
3. Allen, D.C. and Roper, H. (1991), “Concrete Structures Materials Maintenance and Repairs”, UK, Concrete Design and Construction Scientific & Technical, 369p.
4. Noghabai K., "Beam of fibrous concrete in shear and bending: experiment and model", J. Of struct. Eng. Feb., Vol. 126, No.2, 2000.
5. Chajes MJ, Thomson T A, Finch W W and Januszka TF (1994), Flexural Strengtheing of concrete beams using externally bonded composite materials, Construct Build Mater 8(3) 191-210.

INVESTIGATION OF BENDING BEHAVIOR OF REINFORCED CONCRETE BEAMS STRENGTHENED WITH CFRP SHEETS

A.R. Mardookhpour[1], H. Jamasbi[2]
[1]Ph.D Department of Civil Engineering, Islamic Azad University of Lahijan. Iran
[2]M.Sc. Department of Civil Engineering, Islamic Azad University of Lahijan. Iran

ABSTRACT
The effect of FRP (Fiber Reinforced Polymers) sheets on bending strength of beams is one of the advantages of utilizing carbon fibers in concrete structures. By utilizing FRP sheets, reinforcing bar ratio which is used as longitudinal tensile reinforcements would increase in specimens and bending strength would be improved. In this research study, by testing 12 concrete beam specimens with known dimensions with 3 different reinforcing bar ratios the effect of FRP in flexural behavior strength, displacements, ultimate load and stiffness of the concrete beams have been investigated. The results show that in addition to increased strength, failure may occur with high adequate ductility in reinforced concrete beams.

Keywords: FRP sheets, bending strength, concrete beam, bar ratio

1. INTRODUCTION
Retrofitting and strengthening of a constructed structure are currently very significant in modern civil engineering. One of the modern methods in strengthening concrete structures is utilizing fiber reinforced polymers (FRP) bonded to concrete beams as strips made of carbon fibers [3]. This method has several advantages over traditional ones, especially increasing high strength, decreasing beam weight and creating durability of concrete structures. Based on experimental results obtained by Teng et al, Bonacci, Maalej and Feo [1, 8], the most common failure mode is derived from debonding of FRP plate or ripping of the concrete cover. In addition, some premature failures are generally associated with reduction in deformability of the strengthened tensile members.[2]. Numerous experiments have been carried out to determine failure mode and behavior of concrete beams. [5]. Based on existing studies typical failure modes observed in experiments is shown in Figure.1. [4,8]. These failure modes are type (1), type (2) , type (3) and type (4) as the following schematic representation [8].

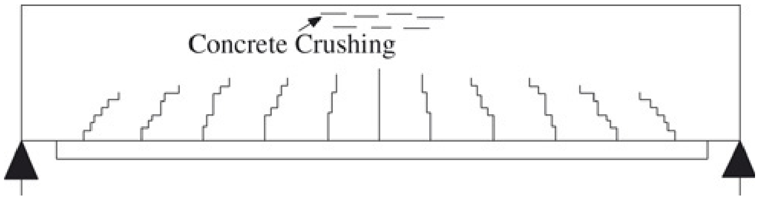

Figure 1. (a) - failure type -1-

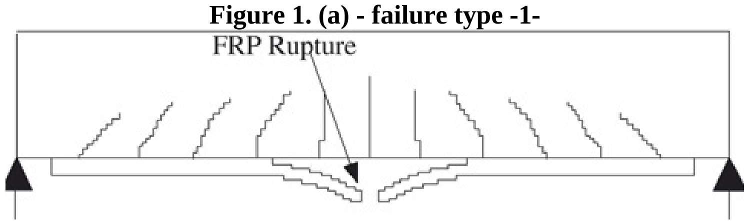

Figure 1. (b) failure type -2-

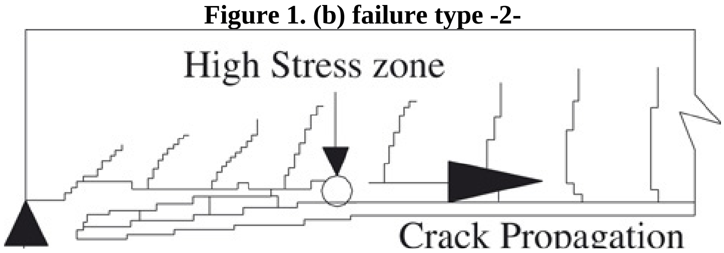

Figure 1. (c) failure type – 3-

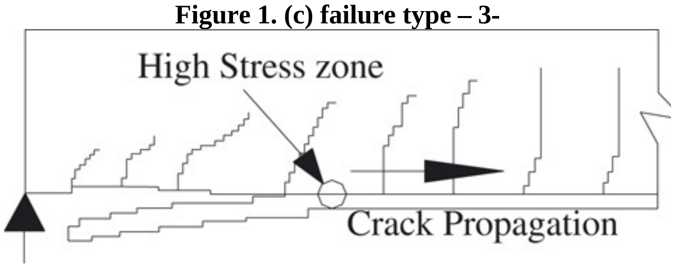

Figure 1. (d) failure type – 4 (a)

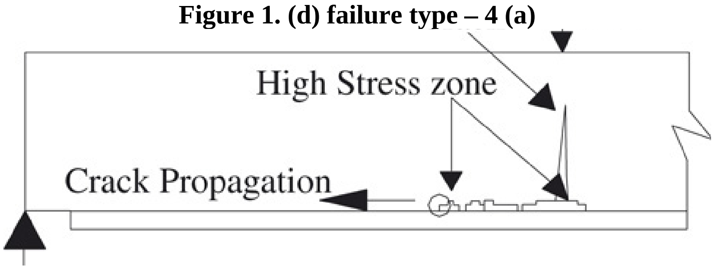

Figure 1. (e) failure type – 4 (b)

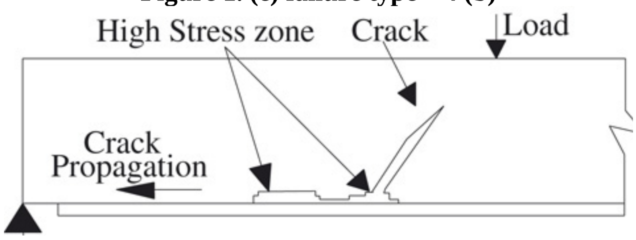

Figure 1. (f) failure type – 4 (c)
Figure 1. failure modes of concrete beams

According to Sebastian and Teng the corrosion of tensile longitudinal steel bars , changing of reinforcing bar ratio and shear forces may increase the probability of these types of failures [6]. The ratio of reinforcing bar of beams affects the above patterns and bending behavior and the width of cracks.[8]. The influence of FRP, bond around tensile longitudinal bars, on flexural strengthening of reinforced concrete beams and the ductility of beams are investigated in this paper by the test results of 12 beam specimens strengthened by carbon fiber reinforced polymers (CFRP).

2. EXPERIMENTAL SET UP

In order to perform research on the materials some tests carried out have been introduced.

2.1. Materials

For the beam specimens the compressive strength is 240 MPa. The concrete mixture proportions are shown in Table 1.

Table 1: Concrete mixture design (kg / m^3)

Coarse aggregate	sand	cement	water
750	1000	300	160

***-maximum size of aggregate is 12 mm**

Also different sizes of tensile bars which have been used in beams are 8,10,12,16 and 20mm.The yield and ultimate strength of bars is indicated in Table 2.

Table 2: Characteristics of reinforcing bars

Diameter	8	10	12	16	20
Yield stress (MPa)	350	365	400	420	450
Ultimate stress (MPa)	460	570	575	585	590

Mechanical properties of CFRP sheets are presented in Table 3.

Table 3: Mechanical properties of CFRP sheet

Layer thickness (mm)	Ultimate strain	Tensile strength (MPa)	Modulus of elasticity (GPa)
0.170	0.0160	3750	230

Also the stress – strain relationship is sketched in Figure 2.
The adhesive used for binding the CFRP sheet on the concrete surface is hand-mixed epoxy and the air between concrete surface and CFRP sheet is removed. The adhesive curing time is 6 days according to instructions of the manufacturer.[9,11]

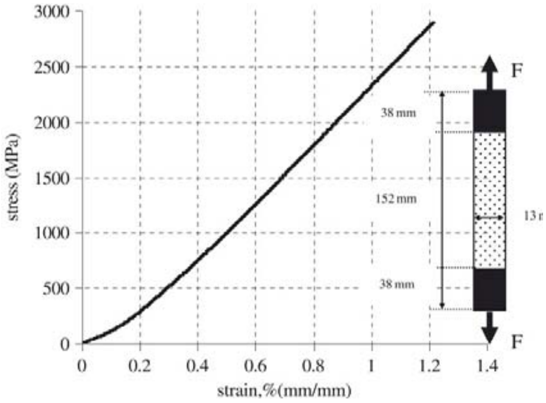

Figure 2. Stress-strain diagram of CFRP sheets

2.2. Experiments on Specimens

12 concrete beam specimens with dimensions according to Figure 3 are manufactured. The reinforcing bar ratios are 20%, 40% and 70% of the tensile reinforcement balanced ratio.

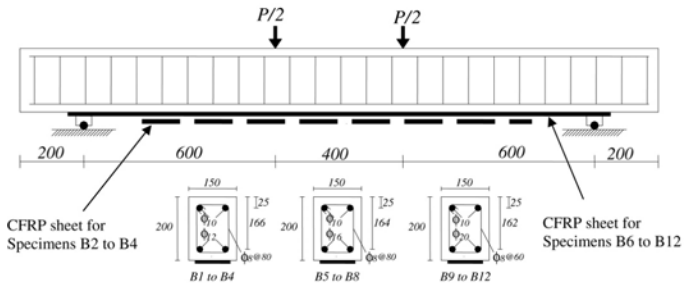

Figure 3 (a): concrete bream in tests

The dimensions and details of reinforced specimens are shown in Table 4.

Table 4: Details of constructed beams

Specimens	CFRP width (mm)	f' 'c (MPa)	As (mm^2)	A's (mm^2)	d (mm)	d' (mm)
B1	0	240	226	157	170	25
B2	10	240	226	157	170	25
B3	20	240	226	157	170	25
B4	25	240	226	157	170	25
B5	0	240	402	157	170	25
B6	10	240	402	157	170	25
B7	20	240	402	157	170	25
B8	25	240	402	157	170	25
B9	0	240	628	157	170	25
B10	10	240	628	157	170	25
B11	20	240	628	157	170	25
B12	25	240	628	157	170	25

As shown in Table 4, seven specimens are strengthened by CFRP sheets. Also three specimens are kept as control specimens without strengthening.
After loading the deflection of the specimens the strains at the mid- spans are measured by gauge. Also, the strain of concrete at the level of the tensile and compressive reinforcing bars and the strain of CFRP sheets at the mid- span of beam are measured by gauge according to Figure 4:

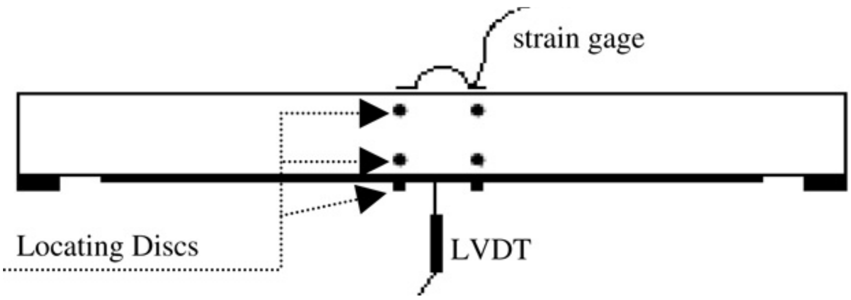

Figure 4. Measuring instruments

The output data are recorded by a computer.

2.3. Results and Discussion

The control specimens B1, B5 and B9 failed after straining of tensile bars in a very ductile manner. In B2 failure occurred due to fracture of CFRP sheet but the beam carried a higher load than B1 .Specimens B3 and B4 failed in Type three due to high shear and normal stresses at the ends of the CFRP sheets due to debonding of CFRP. B6, B7 and B8 failed due to fracture of CFRP sheets (Type 2) after yielding of reinforcing bars. Specimens B10 failed in Type 2 due to fracture of CFRP sheets around the mid-span after yielding reinforced bars. Specimens B11 and B12 failed in Types (4-b) and (4-c) .In both of them debonding of CFRP sheet started due to shearing cracks. Compared to other specimens more shearing cracks with closer spacing occurred in B11 and B12.
Figureure 6(a)-(c) shows the load versus mid-span displacement relationship of beams. According to these Figureures, at earlier stages, before flexural cracking the load-displacement curves are close to each other. With increasing the load, the strengthened specimens exhibited larger stiffness. After yielding of reinforcing bars, the strength and stiffness of the strengthened specimens were larger compared to the control specimens. In specimens B11 and B12, the load – displacement curves continued without dropping and failure was initiated due to separation of FRP. However, the specimens failed due to crushing of concrete with adequate ductility as indicated in Figureure 6 (c).
As shown in Figureure 6, by increasing the load, the strengthened specimens demonstrate larger stiffness. After yielding tensile bars the strength and stiffness of specimens reinforced by CFRP are larger compared to the control specimens. Also, after failure of CFRP the load- displacement curves of strengthened drops.

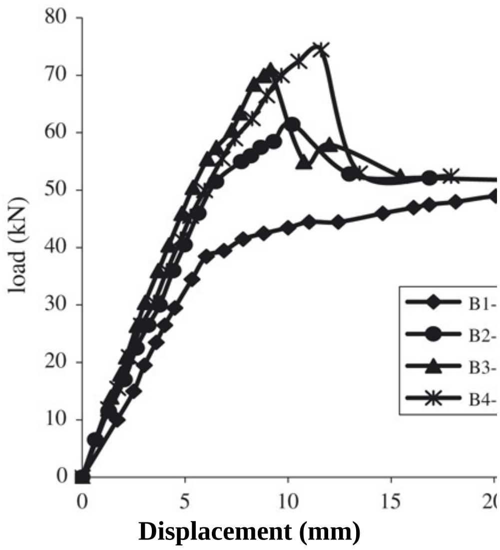

Figure 6 (a). B1, B2, B3 and B4

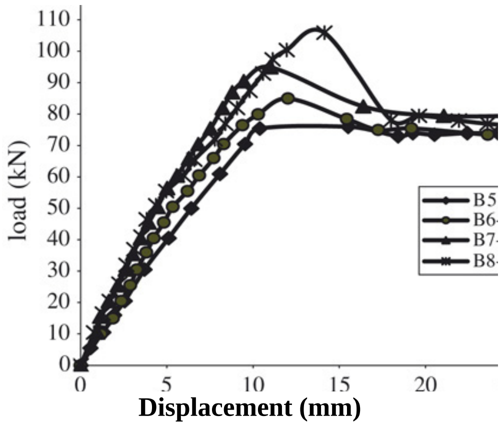

Figure 6 (b). B5, B6, B7 and B8

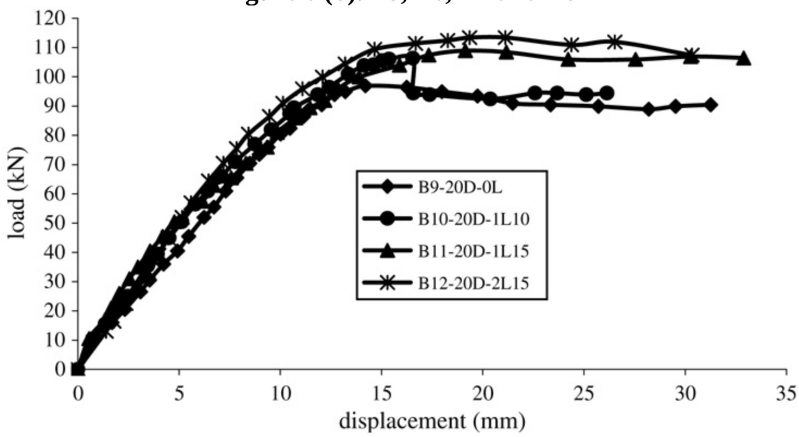

Figure 6 (c). B9, B10, B11 and B12

The displacement and ultimate strength Pu of concrete beams are shown in Table 5 .The increase in strength of beams reinforced by CFRP sheets which varies with the reinforcing bar ratio are also submitted in this table.

Table 5: Results of tests

Specimens	Bar ratio/ Bar balance	Pu (kN)	P=Pu-Pu0 (kN)	P/ Pu0 %	displacement at Pu (mm)
B1	0.2	Puo= 39.6	-	-	22.3
B2	0.2	51.3	11.7	29.5%	10.5
B3	0.2	62.58	22.98	58%	9.2
B4	0.2	64.5	24.9	62.8%	11.5
B5	0.4	Puo= 65.6	-	-	15.3
B6	0.4	73.5	7.9	12%	12.1
B7	0.4	82.66	17.06	26%	11.1
B8	0.4	95.43	29.83	45.5%	14.2
B9	0.7	Puo=85.3	-	-	16.1
B10	0.7	93.21	7.91	9.2%	16.2
B11	0.7	95.63	10.33	12.1%	18.5
B12	0.7	105.44	20.14	23.6%	19.5

2.4. Comparison Between Experimental Results and Theoretical Predictions

According to proposed equations by ISIS Canada, a linear variation over the depth of concrete section and the value of 0.0035 for the maximum concrete strain are being considered .[3] Also ISIS supposes the reduction factors of 0.6 , 0.85 and 0.75 for concrete , steel and FRP sheet respectively [3] . The ratios of ultimate test loads to the calculated values supposed by ISIS are given in Table 6.

Table 6: Comparison between test results and the value calculated by ISIS

Specimens	bar ratio/bar balance %	Ptest (kN)	PISIS (kN)	Ptest /PISIS
B1	0.4	39.6	32.4	1.22
B2	0.4	51.3	40.3	1.27
B3	0.4	62.58	50.5	1.23
B4	0.4	64.5	53.2	1.21
B5	0.8	65.6	55.6	1.18
B6	0.8	73.5	61.7	1.19
B7	0.8	82.66	71.3	1.16
B8	0.8	95.43	80.5	1.19
B9	1.0	85.3	78.2	1.09
B10	1.0	93.21	83.9	1.11
B11	1.0	95.63	88.5	1.08
B12	1.0	105.44	98.5	1.07

Comparing the test results of specimens B2, B6, B7, B8, B10, B11 and B12, ISIS overestimates the ultimate bending strength in the case of strengthened beams with small reinforcing bar ratios. According to Table 6 by increasing the reinforcing bar ratio in concrete beams, the ratio of Ptest / PISIS increases. Therefore, the equations proposed by ISIS are more appropriate for concrete beams with high reinforcing bar ratios. [8,10].

3. CONCLUSION

Generally from the test results and calculated values the following conclusion has been obtained:

1. The flexural strength and stiffness of RC beams increases by CFRP.
2. While the reinforcing bars increases, the ratio of the test load to the Load calculated (Ptest / PISIS) increase.
3. With high reinforcing bars near balanced reinforcement ratio failure of the concrete beams occurs in either Type - 4 (b) and 4 (c) with adequate ductility.

ACKNOWLEDGMENTS

The authors wish to thank the University of Science and Research Islamic Azad University (Tehran) and the Islamic Azad University of Lahijan for their experimental instruments and scientific labors.

REFERENCES

1. Bonacci J.F, Maalej .M. Behavior trends of RC beams strengthened with externally bounded FRP. Journal of Composite for Construction. 2001.
2. Esfahani, M.R., et al .Flexural behavior of reinforced concrete beams strengthened by CFRP sheets, Engineering structures. 2007. doi: 10.1016/j.engstruct.
3. Feo.l. Modeling of composite / concrete interface of RC beams strengthened with composite laminates. Composite Part B: Engineering. 2000.
4. ISIS Canada strengthening reinforced concrete structures with externally-Bounded fiber reinforced polymers. Design manual. No 4. 2001.
5. Nguyan. D.M., Chan. T.K. Brittle failure and bond development length of CFRP concrete beams. Journal of Composite for Construction.ASCE.2001.
6. Rahimi. H, Hutchinson. A. Concrete beams strengthened with externally bonded FRP plates. Journal of composite for construction. ASCE. 2001.
7. Ross.C.A., Jerome. D.M., Tedesco. JW., Hughes. M.L. Strengthening or reinforced concrete beams with externally bonded composite laminates. ACI structural Journal. (1999) .96(2): 212-220.
8. Saadatmanesh. H. Ehsani. M.R. RC beams strengthened with FRP plates. I: Experimental study. Journal of Structural Engineering. 1991.
9. Shahawy. M.A., Arockiassamy. Reinforced concrete rectangular beams strengthened with CFRP laminates. Composites: Part B.1996.
10. Tajari. A.R., esfehani.M.R. Flexural behavior of reinforced concrete beams strengthened by CFRP sheets. Elsevier. 2006.
11. Teng .JG. Smith. ST. Intermediate crack-induced debonding in RC beams and slabs. Construction and building material. 2003.

CD06-003

SHAPE AND DIMENSIONAL EFFECT ON BEHAVIOR OF CONCRETE COLUMNS CONFINED WITH FRP SHEETS

H. R. Salehian[1], A. Kheyroddin[2]
[1]Lecturer of Civil Engineering Dept., Islamic Azad University, Semnan Branch, Semnan, Iran
[2]Associate Professor, Civil Engineering Faculty, Semnan University, Semnan, Iran

ABSTRACT
In recent years, the use of FRP jackets for strengthening of weak concrete columns has become increasingly popular. The confinement effect of the externally bonded FRP systems in rectangular and square sections of concrete columns is known to be complicated and less than those in circular sections. In this article, the predictive design equations for calculating the compressive strength of FRP-confined concrete columns in three current international guidelines and five theoretical models have been introduced and effective parameters in each of them have been investigated. For a comparative study, also, a database consists of experimental results of 43 prismatic specimens of different cross-sectional shapes and confinement details have been collected. The analytical results show that the section’s shape and dimensions are effective parameters in diversity of experimental and theoretical results. Also, by defining the effective factors, a model has been expanded for prismatic FRP-confined concrete columns. Based on the analytical results, the expanded model indicates acceptable predictions in comparison with the other models and guidelines.

Keywords: FRP, concrete column, confinement, shape factor, compressive strength

1. INTRODUCTION
In recent years, earthquake damage to many reinforced concrete columns in bridges and buildings has indicated inadequate strength and deformation of reinforced concrete columns built before the 1970’s and urgent need to retrofit them [1]. These structures were rather constructed according to older codes or without an adequate construction practice. The structural members of this type of buildings may experience sever damage due to low deformability and axial capacity (Figure 1). The initial application for retrofitting of weak columns involved the use of steel hoops and straps to provide lateral confinement. Some analytical models have been developed to provide a theoretical base for retrofitting concrete columns [1]. These models are satisfactory for the prediction of strength and ductility of concrete columns confined by steel stirrups.

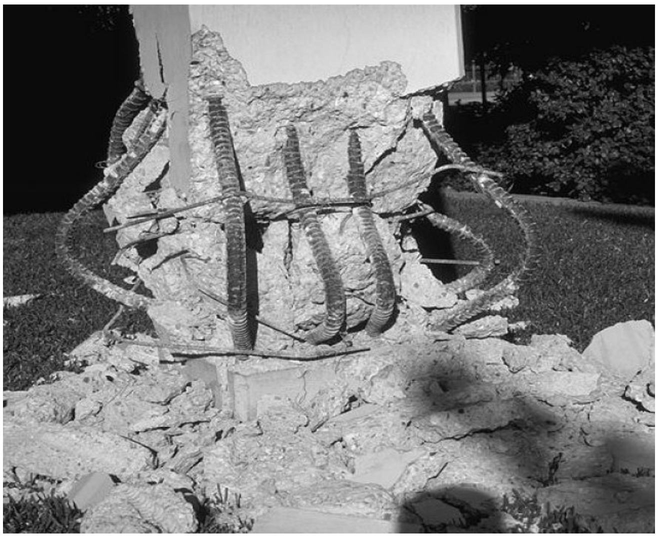

Figure 1. Buckling of the longitudinal bars, because of loss of the concrete in an earthquake damaged column

Rather to some disadvantages of steel jacket, such as heavy weight and high potential for corrosion, the use of fiber reinforced polymer (FRP) composites has been developed in recent decades. This material has some unique properties such as light weight, high stiffness and high strength to weight ratio. Moreover, FRP has great resistance to corrosion. These new materials have shown a great potential in replacing the traditional steel reinforcement as retrofit material. Based on the results of many experimental researches, when reinforced concrete columns confined laterally with FRP sheets, its ductility and axial load capacity will be enhanced [2].

2. CONFINING EFFECT OF FRP

The strength enhancement in columns using lateral FRP sheets may be the confinement effect of transverse fiber sheets. When a concrete column is affected by axial compressive load, concrete core will expand laterally. In jacketed column, however, lateral expansion is limited by the effect of lateral confining material. In these cases concrete core of the column section will be affected by a kind of passive pressure named confining stress. An important aspect of the behavior of confined concrete is that at the rupture of FRP, the hoop strain reached in the jacket is generally considerably smaller than the ultimate tensile strain found from flat coupon tensile tests. The FRP efficiency factor had been suggested for calculation of the actual hoop rupture strain of FRP jacket. According to the stress distribution of confined circular section (Figure 2), confining pressure provided by the transverse FRP sheet (f_l) is given by [3 and 4]:

$$f_l = \left(\frac{2}{D}\right) E_{FRP} k_{\varepsilon} \varepsilon_{FRP} t_{FRP} \tag{1}$$

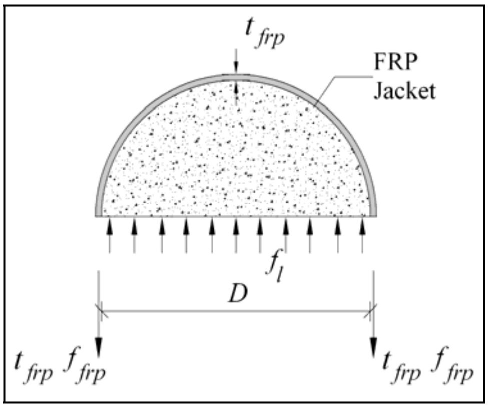

Figure 2. Stress distribution of confined circular section

Where D = diameter of column section, t_{FRP} = whole thickness of FRP sheets, k_{ε} =FRP efficiency factor and E_{FRP} and ε_{FRP} = the modulus of elasticity and ultimate tension strain of FRP sheet. Based on experimental results the advantages of FRP in circular section column are different from rectangular section. In a circular concrete column, the confining pressure is constant around circumference and small variation due to factors such as in homogeneity of concrete is ignored. In rectangular section of columns, the confining pressure of FRP does not distribute uniformly over the section and only a portion of the section is affected by confining pressure (Figure 3). Because of it the performances of FRP in this kind of sections are different and lower than that of FRP-confined circular sections [4].

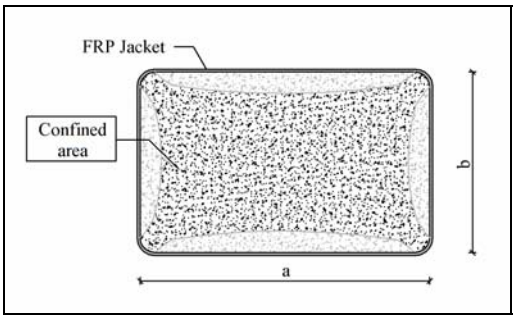

Figure 3. Confined area in a rectangular section of confined concrete column

In rectangular section, due to stress concentration in FRP jacket, premature failure of FRP occurs and whole capacity of FRP is not used. In this section, the confining pressure provided by the FRP sheet must be decreased by introducing the shape factor that is less than 1.0. In rectangular sections it is given by [5]:

$$f_l = k_s k_{\varepsilon} E_{FRP} \varepsilon_{FRP} t_{FRP} \tag{2}$$

Where k_s = shape factor of section and is related on section's geometrical dimensions and often different in each model.

3. EXISTING MODELS FOR FRP-CONFINED CONCRETE

Most of the available models for evaluating the compressive strength of FRP-confined concrete columns are based on the confinement model that was derived experimentally for specimens under active hydrostatic pressure [6]. In this article, five existing models for rectangular and square columns are investigated. Those models had been presented by Mirmiran et al. [7], Pantelides and Yan [8], Al-Salloum [9], Lam and Teng [2], and Illki et al. [10] and summarized in Table 1. *a*, *b*, and *r* in this table are large having a small dimension and corner radius of cross section. Lateral confining pressure f_l in each model is calculated from Eq. (2) where FRP efficiency factor and shape factor in each model are given in Table 2.

4. REVIEW OF DESIGN GUIDELINES

The document considered in this article is as follows: "Guide for the Design and Construction of Externally Bonded FRP Systems for Strengthening Concrete Structures" reported by the American Concrete Institute (ACI Committee 440.2R-02 2002) [11], "Design and Construction of Building Components with Fiber Reinforced Polymers" Reported by the Canadian Standard Association (CSA S806-02 2002) [12], and "Externally Bonded FRP Reinforcement for RC Structures" Technical Report by the Fédération Internationale du béton (*fib Bulletin 14* 2001) [13]. Each of the design guidelines has some limitations and conditions in nonlinear cross sections, which are related to the type of compressive load application, maximum dimensions, maximum side-aspect-ratio (a/b), and minimum corner radius of cross section (*r*). In Table 3 the mentioned limitations in each guideline had been summarized. Approach presented by the current ACI committee 440 (ACI 2002) for compressive strength enhancement is conservative. This guideline specifies that although confining square and rectangular members with FRP jackets can provide marginal increases in the axial compression strength of the member, there are no recommendations provided at this time on the use of FRP. The model provided by ACI guideline for estimation ductility of confined rectangular column is given as follows:

$$f'_{cc0} = f'_{c0}\left(2.25\sqrt{1+7.9 f_l / f'_{c0}} - 1.25\right) - 2 f_l \tag{14}$$

Eq. (14) had been primary presented for steel-confined concrete. Some research showed that it is applicable for the case of FRP-confined concrete [2]. According to the ACI guideline FRP confining pressure in prismatic column can be obtained by Eq. (2) where the shape factor k_s and FRP efficiency factor k_ε are calculated by Eqs. (10) and (15):

$$k_\varepsilon = MIN.\left\{0.75, \frac{0.004}{\varepsilon_{FRP}}\right\} \tag{15}$$

Table 1: Estimating models for compressive strength of confined concrete column.

Author's name	Compressive strength of confined concrete column	
Mirmiran et al.	$f'_{cc0}=\left(1+6.0\dfrac{f_l^{0.7}}{f'_{c0}}\right)f'_{c0} \qquad for: \left(\dfrac{2r}{a}\right)\left(\dfrac{f_l}{f'_{c0}}\right)\geq 0.15$	(3)
Pantelides and Yan	$f'_{cco}=\left(-4.322+4.271\sqrt{1+4.193\dfrac{f_l}{f'_{c0}}}-2\dfrac{f_l}{f'_{co}}\right)f'_{c0} \qquad \dfrac{f_l}{f'_{co}}\geq 0.2$	(4)
	$f'_{cco}=MAX\left[\left(\dfrac{-4.322+4.271\sqrt{1+4.193\dfrac{f_l}{f'_{c0}}}-2\dfrac{f_l}{f'_{co}}}{0.0768\ln(\dfrac{f_l}{f'_{co}})+1.122}\right)f'_{c0}\ ,\ f'_{c0}\right] \qquad \dfrac{f_l}{f'_{co}}<0.2$	(5)
Al-Salloum	$f'_{cc0}=\left(1+3.14\dfrac{f_l}{f'_{c0}}\right)f'_{c0}$	(6)
Lam and Teng	$f'_{cc0}=\left(1+3.3\dfrac{f_l}{f'_{c0}}\right)f'_{c0}$	(7)
Illki et al.	$f'_{cc0}=\left(1+2.54\dfrac{f_l}{f'_{c0}}\right)f'_{c0}$	(8)

Table 2: FRP efficiency factor and section's shape factor in each model

Author's name	FRP efficiency factor(k_ε)	Section's shape factor (k_s)	
Mirmiran et al.	1.0	$k_s=\dfrac{4r}{a^2}$	(9)
Pantelides and Yan	0.5	$k_s=\left(1-\dfrac{(a-2r)^2+(b-2r)^2}{3ab}\right)\left(\dfrac{(a+b)}{ab}\right)$	(10)
Al-Salloum	1.0	$k_s=\left(\dfrac{2a}{\left(\sqrt{2}a-2r\left(\sqrt{2}-1\right)\right)^2}\right)\left(1-\dfrac{2}{3}\left[\dfrac{(1-2(r/a))^2}{1-(4-\pi)(r/a)^2}\right]\right)$	(11)
Lam and Teng	0.57	$k_s=(\dfrac{b}{a})^2\left(\dfrac{2}{\sqrt{a^2+b^2}}\right)\left[\left(1-\dfrac{(b/a)(a-2r)^2+(a/b)(b-2r)^2}{3\left(ab-(4-\pi)r^2\right)}\right]$	(12)
Illki et al.	0.85	$k_s=\left(\dfrac{a+b}{ab}\right)\left[1-\left(\dfrac{(b/a)(a-2r)^2+(a/b)(b-2r)^2}{3(ab-(4-\pi)r^2)}\right)\right]$	(13)

Regarding CSA S806-02 guideline (CSA2002), the maximum confined concrete compressive strength is given by Eq. (16). This equation is similar to well-known equation provided by Richart et al. [2].

$$f'_{cc0}=0.85f'_{c0}+2.12f_l^{0.83} \qquad (16)$$

Table 3: Design Guidelines Limitations and conditions

Guideline	Kind of Loading	Side Dimensions (mm)	Ratio of Side Dimension	Corner Radius (mm)
ACI	Concentric Axial loading	$b, a \leq 900$	$a/b < 1.5$	$r \geq 13$
CSA	Concentric Axial loading	-	$a/b \leq 1.5$	$r \geq 20$
fib	Concentric Axial loading	-	-	Recommended: $15 \leq r \leq 25$

Confining pressure in above equation is calculated by Eq. (2), where FRP efficiency factor is calculated from Eq. (15) and shape factor is given by:

$$k_s = \left(\frac{2}{D}\right) \text{ , } D = \text{lesser of } a \text{ and } b \tag{17}$$

The design recommendations provide by *fib* for prismatic columns are based on the model proposed by Spoelstra and Monti [2]. In this code, the maximum amount of confined concrete compressive strength determined from cube calculated is given by:

$$f'_{cc0} = f'_{c0}\left(0.2 + 3\sqrt{\frac{f_l}{f'_{c0}}}\right) \tag{18}$$

Confining pressure in *fib* is determined from Eq. (2), in which shape factor are given by Eq. (13). *fib* highlights that the hoop rapture strain of the FRP jacket, based on experimental evidence, is lower than the ultimate strain obtained by tensile testing of the material. The guideline points out that this reduction is due to several reasons, such as the quality of construction, the size effect when applying several layers, the effect of wrapping the material on the corners of low radius, and the combined state of stress of the FRP wrapping. Because of the lack of data no appropriate reduction factors are suggested in this guideline. In other words *fib* provides FRP efficiency factor equal to the value of 1.0 for a confinement by full wrapping. In this design guideline, FRP safety factors γ_f are applied individually to each of the material components of the FRP during the computation of lateral confining pressure.

Table 4: FRP safety factors in normal control quality

FRP type	CFRP	AFRP	GFRP
γ_f	1.20	1.25	1.30

Table 5: Experimental details of FRP-confined square and rectangular concrete specimens

Authors	No.	*a* (mm)	*b* (mm)	*r* (mm)	f'_{c0} (MPa)	FRP type	E_{frp} (GPa)	ε_{frp} (%)	t_{frp} (mm)	Exp. f'_{cc} (MPa)
Parvin and Wang	1	108	108	8.26	21.40	CFRP	188.9	1.60	0.138	36.630
	2	108	108	8.26	21.40	CFRP	188.9	1.60	0.268	45.230
Al-Salloum	3	150	150	5	29.81	CFRP	75.1	1.00	1.200	41.840
	4	150	150	25	30.16	CFRP	75.1	1.00	1.200	46.920
	5	150	150	38	29.00	CFRP	75.1	1.00	1.200	55.960
	6	150	150	50	27.49	CFRP	75.1	1.00	1.200	62.680
Kumutha et al.	7	125	125	0	34.31	GFRP	10.5	3.50	0.680	50.300
	8	125	125	0	34.31	GFRP	10.5	3.50	1.360	60.160
	9	140	112	0	34.31	GFRP	10.5	3.50	0.680	49.410
	10	140	112	0	34.31	GFRP	10.5	3.50	1.360	58.880
	11	161	97	0	34.31	GFRP	10.5	3.50	0.680	49.280
	12	161	97	0	34.31	GFRP	10.5	3.50	1.360	55.040
Shehata et al.	13	188	94	10	23.70	CFRP	235	9.10	0.165	25.810
	14	188	94	10	23.70	CFRP	235	4.60	0.330	33.200
	15	188	94	10	29.50	CFRP	235	9.10	0.165	25.710
	16	188	94	10	29.50	CFRP	235	4.60	0.330	38.700
Rochette and Labossiere	17	152	152	5	42.00	CFRP	82.7	0.23	0.900	39.48
	18	152	152	25	42.00	CFRP	82.7	0.56	0.900	41.58
	19	152	152	25	42.00	CFRP	82.7	0.63	0.900	43.26
	20	152	152	38	42.00	CFRP	82.7	0.71	0.900	47.46
	21	152	152	38	42.00	CFRP	82.7	1.61	0.900	50.40
	22	152	152	5	43.90	CFRP	82.7	0.44	1.500	43.90
Rochette and Labossiere	23	152	152	25	43.90	CFRP	82.7	0.59	1.200	50.92
	24	152	152	25	35.80	CFRP	82.7	0.70	1.200	52.27
	25	152	152	25	35.80	CFRP	82.7	0.65	1.500	57.64
	26	152	152	38	35.80	CFRP	82.7	0.89	1.200	59.43
	27	152	152	38	35.80	CFRP	82.7	0.86	1.500	68.74
	28	152	152	5	43.00	AFRP	13.6	0.79	1.260	50.74
	29	152	152	5	43.00	AFRP	13.6	1.30	2.520	51.60
	30	152	152	5	43.00	AFRP	13.6	1.48	3.780	53.75
	31	152	152	5	43.00	AFRP	13.6	0.90	5.040	54.18
	32	152	152	25	43.00	AFRP	13.6	1.12	1.260	51.17
	33	152	152	25	43.00	AFRP	13.6	1.27	2.520	51.17
	34	152	152	25	43.00	AFRP	13.6	0.94	3.780	53.32
	35	152	152	25	43.00	AFRP	13.6	1.04	5.040	55.04
	36	152	152	38	43.00	AFRP	13.6	1.05	2.520	50.74
	37	152	152	38	43.00	AFRP	13.6	0.97	3.780	52.89
	38	203	152	25.0	42.00	CFRP	82.7	1.50	0.900	42.000
	39	203	152	38.0	42.00	CFRP	82.7	1.50	0.900	43.680
	40	203	152	5	43.90	CFRP	82.7	1.50	1.500	44.340
	41	203	152	25	43.90	CFRP	82.7	1.50	1.500	44.340
Pessiki et al.	42	152	152	38	26.40	CFRP	38.1	0.83	1.000	41.40
	43	152	152	38	26.40	CFRP	38.1	0.90	2.000	55.10

These material safety factors are summarized in Table 4 and used as dividers. These are mainly based on the observed differences on the long term behavior of composites (basically depending on the type of fibers), as well as influence of application methods.

4.1. Test Database

A large number of existing studies have been concerned with the compressive behavior of rectangular concrete columns confined by wrapped FRP. In this article for a comparative study of mentioned model with actual results, a test database containing a total of 43 FRP-confined plain concrete rectangular specimens have been assembled from experimental studies of Parvin and Wang [14], Kumutha et al. [15], Shehata et al. [16], Rochette and Labossiere [17] , Pessiki et al. [18], and Al-Salloum [9] presented in Table 5. Those data are over square and rectangular specimens with the section depth ranging from 94 to 203 mm, and the corner radius from 0 to 50 mm. The unconfined concrete strength of these specimens ranges from 21.4 to 43.9 MPa. Lateral confinement of these specimens was provided by aramid FRP (AFRP), carbon FRP (CFRP) or glass FRP (GFRP).

4.2. Performance of Models and Guidelines

The compressive strength of each experimental case (Table 5) and the theoretical results of each of the models and guidelines are presented in Figure 4. It is observable that if any experimental case doesn’t satisfy the limitation and conditions of each of the models and guidelines, corresponding lateral confining pressure is considered equal to zero. As Figure 4 shows, the models of Mirmiran et al. and ACI and CSA guidelines, significantly underestimate the compressive strength (Figure 4(a) and (h)). According to the Figure 5, models of Lam and Teng, Illki et al, and Al-Salloum predict the correct trend for both square and rectangular specimens with different amount of geometrical dimensions and lateral confining pressure (Figure 4(d), (e), and (c)). Models of Lam and Teng, and Al-Salloum suppose less than 1.0 amount for FRP efficiency factor. But this factor in Illki et al.'s model is equal to 1.0. The results of Panteledis and Yan's model and *fib* guidelines are overestimated for rectangular cross sections (Figure 4(b) and (g)). In those models, by increasing the side-aspect-ratio (*a/b*), the deviation of theoretical results are noticeable. Regarding the amount of the FRP efficiency factor and the shape factor in Panteledis and Yan, it can be concluded that the suggested relation for calculating the compressive strength of confined concrete in this model is affected by cross section of columns and its side-aspect-ratio. Overestimation of *fib* guideline can depend on the amount of FRP efficiency factor presented in this guideline.

4.3. Proposed Model for Prismatic Columns

Kheyroddin et al. [19] suggested a model for calculating compressive strength of concrete column confined by FRP which is given as follows:

$$f'_{cc0} = f'_{c0}\left[0.622 + \frac{f_l}{f'_{c0}} + 1.577\sqrt{\left(\frac{f_l}{f'_{c0}} + 0.058\right)}\right] \qquad (19)$$

In this model that is suggested for columns with circular cross sections, lateral confining pressure is calculated from Eq. (1). For adaptation of the above equation for prismatic FRP-confined columns, FRP efficiency factor and shape factor of section should be defined. According to the structure of models that have been investigated, the shape factor k_s in this model suggested is the same as shape factor in Lam and Teng as given by Eq. (12).

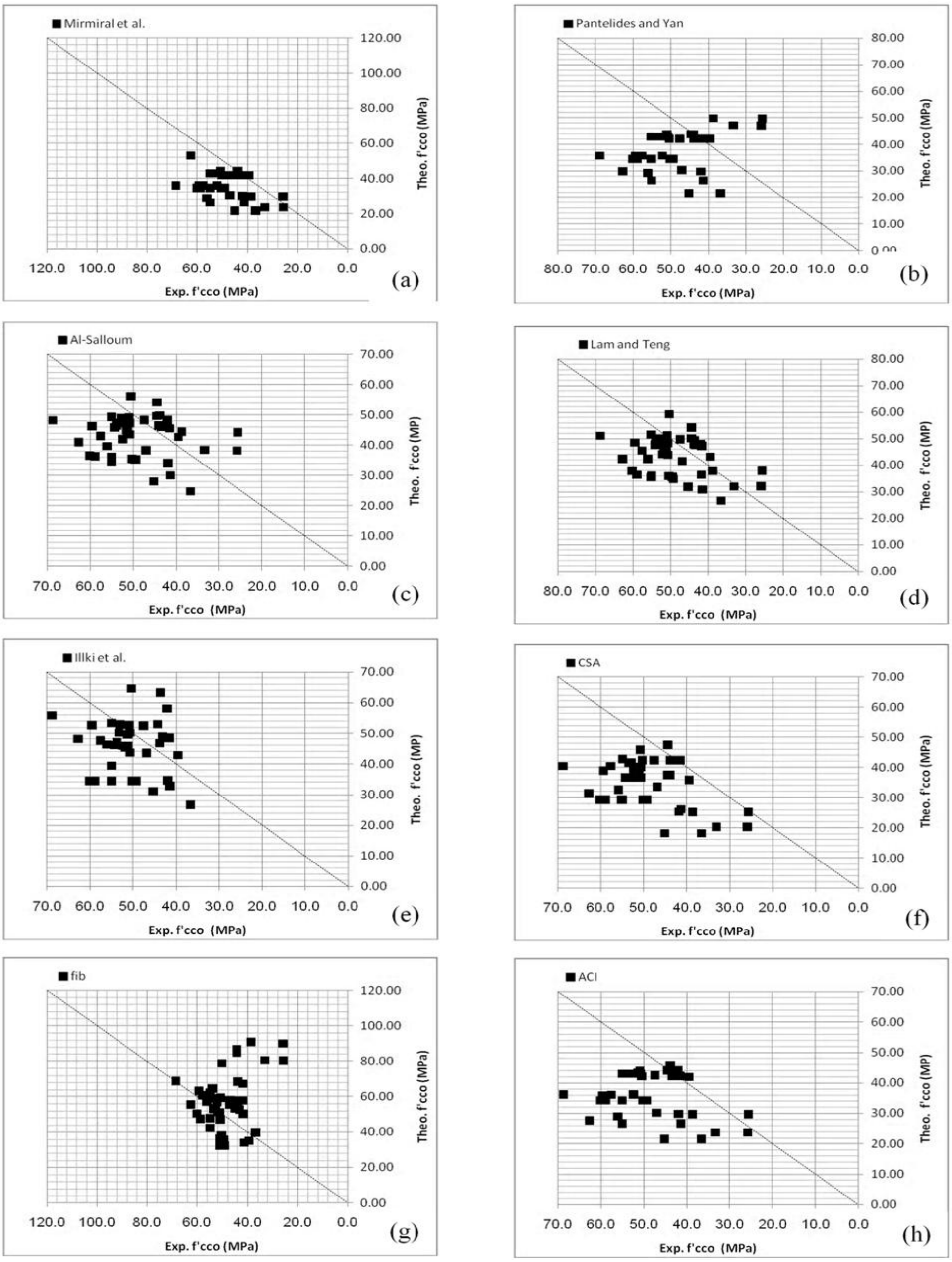

Figure 4. Performance of the models and the guidelines

By a trial and error method the FRP efficiency factor k_ε for this model is obtained as the value equal to 0.650. The performance of the new proposed model is presented in Figure 6. As this figure shows, Kheyroddin et al.'s model with adopted factors predicts acceptable result for prismatic concrete columns confined by FRP in the range of collected experimental database.

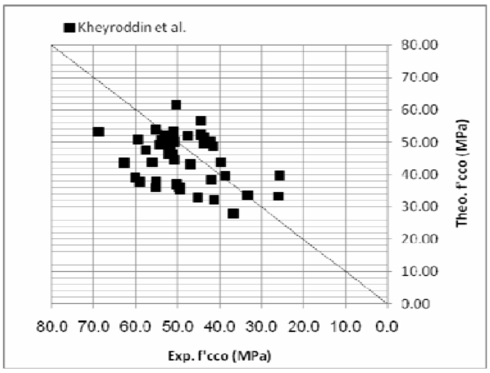

Figure 5. Performance of proposed models

4.4. Accuracy of Models

Cusson and Paultre [20] in their comparative studies between experimental and theatrical results applied index error, as follows:

$$Index\ Error = \sqrt{\sum\left(\frac{Experimental - Theoretical}{Experimental}\right)^2} \tag{20}$$

This equation has been used for all predicted results of models and guidelines for collected database and obtained results are comparable with the proposed model in Table 6. According to the obtained results, Kheyroddin et al.'s with suggested factors has been indicated acceptable approximations in comparison with other models and guidelines.

Table 6: Total differences between experimental and theoretical results

Models	Mirmiran et al.	Pantelides and Yan	Al-Salloum	Lam and Teng	Illki et al.	ACI	CSA	*fib*	Proposed Model
Index Error	1.82	3.08	1.65	1.38	1.36	1.90	2.11	4.34	1.37

5. CONCLUSIONS

In this paper, the performance of some current models and guidelines for estimating the compressive strength of FRP-confined concrete columns has been investigated. Studied models and guidelines had been affected by section's shape. Some of models such as Mirmiran et al.'s model and ACI and CSA underestimate the compressive strength. The results of Panteledis and Yan's model and *fib* guidelines are overestimated for rectangular cross sections. Models of Illki et al., Lam and Teng, and Al-Salloum had acceptable predictions. Index error in those models was 1.36, 1.38, and 1.65. Moreover, by definition some effective factors, a model had been expanded for prismatic FRP-confined concrete columns showed the proposed model has acceptable predictions in comparing to the other investigated models and guidelines. Index of error for this model obtained is equal to 1.37.

REFERENCES

1. Kheyroddin, A., Naderpour, H., "*Nonlinear finite element analysis of composite RC shear walls*", Iranian J. of Science and Technology, Transaction B: Engineering, 32(B2), 79-89.
2. Lam, L. and Teng, J.G., "*Design-oriented stress-strain model for FRP-confined concrete in rectangular columns*", J. of Reinforced Plastics and Composites, 2003, 22(13), 1149-1186.
3. M.R. Esfahani, H. R. Salehian, "*Investigation in Behavior of RC Columns Confined by CFRP under Eccentric Compression loading*", J. of Faculty of Engineering of Tehran University, (Special Issue: Civil and Survey Engineering), 2005, 39(5), 559-569.
4. Kheyroddin, A., Salehian, H.R., "*Investigation of effective parameters in compressive strength of FRP-confined concrete columns*", 1th Int. Conf. on Seismic Retrofitting of Buildings, 2008, 20-22 October, Tabriz, Iran.
5. H.R. Salehian, R. Esfahani, "*Behavior of confined RC column under eccentric compression loading*", Second Int. conf. on Concrete and Development, 2005, 27-29 April, Tehran, Iran.
6. Kheyroddin, A., Naderpour, H., "*Nonlinear finite element analysis of composite RC shear walls*", Iranian J. of Science & Technology, 2008, 32(B2), 79-89.
7. Mirmiran, A., Shahawy, M., Samman, M., Echary, H., Mastrapa, J. C., Pico, O.,"*Effect of column parameters on FRP-confined concrete*", J. of composites for construction, 1998, 2(4) 175-185.
8. Pantelides, C. P., Yan, Z, "Confinement model of concrete with externally bonded FRP jackets or post tensioned FRP shells", J. of Structural Engineering, 2007, 133(9), pp 1288-1296.
9. Al-Salloum, Y. A., "Influence of edge sharpness on the strength of square concrete columns confined with FRP composite laminates", Elsevier: Composites, B: engineering, 2007, 38, 640-650.
10. Illki, A., Peker, O., Karamuk, E., Demir, C. Kumbasar, N., "*FRP retrofit of low and medium strength circular and rectangular concrete columns*", J. of Materials in Civil Engineering, 2008, 20(2), 169-188.
11. American Concrete Institute (ACI), "Guide for the design and construction of externally bonded FRP systems for strengthening of concrete structures" 2002 , ACI 440.2R-02, Farmington Hills, Mich.
12. Canadian Standards Association (CSA), "Design and construction of building components with fiber-reinforced polymer", 2002, *CSA-S806*, Rexdale, Ont., Canada.

13. Fédération Internationale du Béton (*fib*), "Externally Bonded FRP Reinforcement for RC Structures", 2001, *Bulletin No. 14*, Technical Rep., Lausanne, Switzerland.
14. Parvin, A. and Wang, W., (2001) "Behavior of FRP jacketed concrete columns under eccentric loading" J. of Composites for Construction, 5(3), pp 146-152.
15. Kumutha, R., Vaidoyanathan, R. And Palanichamy, M. S., (2007), "Behavior of reinforced concrete rectangular columns strengthened using GFRP", Elsevier: Cement & Concrete Composites, 29, 609-615.
16. Shehata, I.A.E.M., Carneinro, L.A.V. and Shehata, L.C.D. (2002), "Strength of short columns confined with CFRP sheets", J. of Material and Structures, 35(1), 50-58.
17. Rochette, P. and Labossiere, P., (2000), "Axial testing of rectangular column models confined with composites", J. of Composites for Construction", 4(3), 129-136.
18. Pessiki, S., Harries, K. A., Kestner, J. T., Suase, R., Ricles, J. R., "*Axial behavior of reinforced concrete columns confined with FRP jackets*", 2001, J. of composites in construction, 5(4), 237-245.
19. Kheyroddin, A., Naderpour, H., Hoseynie vaez, S. R., "*Investigation of the effects of confining FRP sheets in ductility of RC members*", 4th National congress of civil engineering, 2007, 8-10 May, Tehran, Iran.
20. Cusson, D., Paulter, P., "*Stress-strain model for confined high-strength concrete"*, J. of Structures Engineering, 121(3), 468-477.

CD06-005

STUDYING THE EFFECT OF FREEZE AND THAW CYCLES ON BOND STRENGTH OF CONCRETE REPEIR MATERIALS

K. Behfarnia
Assistant professor, Dept. of Civil Engg. Isfahan Univ. of Technology, Isfahan, Iran

ABSTRACT
The mechanisms of damage to concrete from repeated cycles of freezing and thawing are not well understood and continue to be intensively studied. Original research was based on the fact that water expands 9 percent when it freezes. Further researches proposed more mechanisms. Hydraulic pressure theory proposes that destructive stresses can develop if water is displaced to accommodate the advancing ice front in concrete. If the pores are critically saturated, water will begin to flow to make room for the increased ice volume. The concrete will rupture if the hydraulic pressure exceeds its tensile strength.
In this paper the results of an experimental study of the effect of freeze & thaw cycles on the bond between repair materials and concrete substrate is presented. The work was aimed at studying the effect of various factors such as initial curing periods and surface preparation method on bond strength. Old concrete samples were made based on BS6319, Part 4 standard. Smooth as-sawn and acid etching methods were used for preparation of concrete substrate surface. Ordinary concrete with cement type II and concrete containing microsilica were used as repair materials. Repaired samples were subjected to 10 to 100 freeze and thaw cycles based on ASTM C666. The bond between repair materials and concrete substrate was evaluated based on slant shear test method (BS, 1984). The obtained results are tabulated and presented in this paper.

Keywords: freeze & thaw, concrete, repair, bond strength

1. INTRODUCTION
The serviceability of construction materials in general is of significant economic importance. This is especially so with structures and materials which are part of the infrastructure of a modern society. Concrete is a material heavily used in urban development, meeting the requirements of codes of practices by means of strength and durable structures. Reduced service life of concrete members in the sense of lack of durability may be due to a number of different reasons, e.g. planning/capacity (over loading), improper structural or material design, construction practice or inadequate maintenance – or lack of knowledge.
Widespread use of de-icing salts in many parts of the world is considered one of the major cause of rapid degradation of concrete structures. Further, the de-icing salt together with repeated freezing and thawing may cause failure of the concrete

cover by surface scaling, which combined with steel corrosion may critically reduce the structure’s service life. It is very difficult to estimate the direct repair and maintenance costs caused by freeze-thaw damages of concrete structures. However, due to its still nonrevealed secrets concerning deterioration mechanisms, freeze-thaw resistance has received significant attention for several decades.

The mechanisms of damage to concrete from repeated cycles of freezing and thawing are not well understood and continue to be intensively studied. Original research was based on the fact that water expands 9 percent when it freezes. Thus, the term "critical saturation" was coined to describe the point at which the concrete pores were 91.7 percent saturated and, therefore, assumed to be susceptible to damage due to freezing and thawing. Further investigation determined that deterioration due to freezing and thawing can affect concrete with lower degrees of saturation [1].

Four theories have gained wide acceptance in describing the mechanisms of frost action. Although most of these theories were originally used to describe the frost action in cement paste, they are also applicable to concrete [2]. The first was the hydraulic pressure theory Powers proposed in 1945. This was followed by the diffusion and growth of capillary ice theory constructed by Powers and Helmuth in 1953, the dual mechanism theory by Larson and Cady in 1969, and the desorption theory by Litvan in 1972. Other theories have been proposed, but these four form the basis of most research in the area of frost resistance of concrete.

While these theories disagree as to whether water moves toward or away from the point of ice formation, they agree that the amount of water in the pores and the resistance to movement of that water play a role in the frost resistance of concrete. In the case of concrete, it is generally accepted that the pore system is potentially susceptible to damage from freezing and thawing. Efforts to produce frost-resistant concrete have primarily focused on providing a proper system of entrained air voids. In the case of aggregates, some pore systems do not show susceptibility to damage from freezing and thawing while other pore systems do. In addition to the air-entrainment of concrete as mentioned above, efforts have also focused on identifying the aggregates with acceptable pore systems for use in concrete exposed to freezing and thawing.

The causes of concrete deterioration have always been the object of concern and research. This interest is increasing due to the high cost associated with the repair and maintenance of the concrete structure. Repairs, however, are successful in the long-term if the causes of the original damage have been understood and appropriate repair materials are applied to resist future deterioration. Repair materials should be compatible with old concrete and have good adhesion. In repair of concrete, the bond strength between repair materials and old concrete is of vital importance.

The objective of this study was to investigate the effect of freeze and thaw cycles on bond strength of repair materials. Strength and integrity of the bond depends on not only the physical and chemical characteristics of the repair component, but also other factors such as surface preparation method and environmental conditions. The effects of these factors were studied in this work.

2. EXPERIMENT

Old concrete samples were made based on BS6319 Part 4 standard [3]. It is shown that surface preparation method has significant effect on bond strength [4], therefore, two methods including, smooth as-sawn and acid etching were used in order to prepare the surface of old concrete samples. Ordinary concrete, made with type II portland cement, and concrete containing 15 percent microsilica were used as repair materials. Repaired samples were subjected to 10 to 100 freeze and thaw cycles based on ASTM C666 procedure B. The bond between repair materials and concrete substrate was evaluated based on slant shear test method (BS, 1984).

2.1. Mix Proportions

Type II portland cement (ASTM C 150 specification) was used in this research. Crushed stone with a maximum size less than 9.5 mm and sand with a fineness modulus of 2.9 were used for producing concrete. The composition of old concrete mixes (OC mix) was 0.5:1.0:2.35:1.04 (water: cement: sand: gravel) by weight. The uniaxial compressive strength of old concrete samples was 35 MPa. MSOC mix was produced with replacement of 15% of cement in OC mix (by weight) with microsilica in order to investigate the effect of microsilica on bond strength.

2.2. Specimen Preparation

Old concrete samples were made based on BS 6319: Part 4 standard, figure 1. They were cast as 55x100x150 mm prisms and cured in water for 28 days in laboratory. Then cut at 30 deg to the vertical axis using a diamond saw. The acid etching method with use of hydrochloric acid was used to prepare the surface of 1/2 of samples.

Figure 1. Concrete samples prepared based on BS 6319: Part 4

For acid etching, with reference to ACI committee 549 [4], a hydrochloric acid solution was chosen. HCl can primarily react with the $Ca(OH)_2$ of the hydrated cement paste to form $CaCl_2$, making the substrate more porous. Because no adequate information concerning the influence of acid consistency on bond strength was available in current literature, hydrochloric acid solutions of 5% were chosen for testing [5]. The etching of surface was carried out in such a way that the hydrochloric acid solution was brushed on the surface of concrete substrate with a soft nylon brush at a rate of 20 times/min. The etched surface was then flushed under flowing tap water for 2 minutes.

2.3. Repair and Test Procedure

Concrete samples were formed in the moulds in which they were cast. The repair material, OC or MSOC mixes, was then applied and hand-compacted. Samples were stripped after 24 hr and placed in curing tank for 7, 14, and 28 days.

To evaluate the effect of freeze and thaw cycles on bond strength of repair materials, concrete samples after curing were subjected to 10 to 100 freeze and thaw cycles based on ASTM C666 Procedure B, figure 2. The loss of the weight in the concrete specimens were also measured and recorded.

Figure 2. Samples of freeze and thaw test

A wide range of test method has been proposed to evaluate bond properties and performance of repair materials in general. The slant shear test has become the most widely accepted test for evaluating the bond of resinous repair materials to concrete. However, there seems to be no standard test for testing the bond to concrete of cementitious and modified cementitious repair materials. To compare the bond strength of repair materials, slant shear test method was used in this work. This method, which puts the bond interface into a combined state of compression and shear is adopted in BS6319: Part4 [3], was used as a test method for evaluating bond strength of repair materials, Figure 3.

Figure 3. Slant shear test

2.4. Test Results and Discussion

Strength and integrity of the bond depends on not only the physical and chemical characteristics of the repair component, but also other factors such as initial curing periods, surface preparation method and environmental conditions. The effects of these factors were studied in this work. The obtained results are presented and discussed briefly in this section.

The results given in Table 1, shows the effect of initial curing periods on durability of samples subjected to 100 freeze and thaw cycles. Based on the results, the curing period has an important effect on durability of concrete samples subjected to freeze and thaw cycles.

Table 1: The effect of initial curing on durability

Repairing Material	OC			MSOC		
Curing Period (day)	7	14	28	7	14	28
Weight Loss (%)	3.05	2.25	2.11	2.1	1.64	1.43

As shown in the above table with increase in curing period weight loss decreases. For concrete samples repaired with ordinary concrete, the weight loss has decreased from 3.05% to 2.11% with increase in curing period from 7 to 28 days, respectively, which means 31% increase in durability, or in other words, increase in resistance to freeze and thaw cycles. With increase in strength of repair material, the weight loss of samples is decreased. Based on the obtained results, samples repaired with MSOC material show about 30% more resistance to freeze and thaw cycles than concrete samples repaired with OC material. For concrete samples repaired with microsilica concrete, the weight loss has decreased from 2.1% to 1.43% with increase in curing period from 7 to 28 days, respectively, which means 32% increase in resistance to freeze and thaw cycles.

To study the effect of freeze and thaw (F&T) cycles on bond strength, samples were cured for 28 days in curing tank and then were subjected to 10 to 100 freeze and thaw cycles based on ASTM C666 Procedure B. Test results are given in Table 2. Based on the obtained results freeze and thaw action decreases the bond strength considerably. With increase in number of F&T cycles bond strength decreases. After 100 cycles of F&T, the bond strength of samples repaired with OC and MSOC materials is reduced by 85.6% and 61.2%, respectively. Moreover, microsilica concrete not only increases the bond strength [6-7], but also increases durability regarding F&T cycles.

Table 2: The effect of F&T cycles on bond strength

Repairing Material	OC						MSOC					
No of F&T cycles	0	10	20	50	70	100	0	10	20	50	70	100
Bond Strength (MPa)	21.5	20.4	19.2	17.6	10.3	3.1	24.0	23.3	21.4	19.5	15.1	9.3

In Figure 1, the bond strength of samples subjected to F&T cycles is compared to that of samples which were not subjected to F&T cycles (FT/NFT).

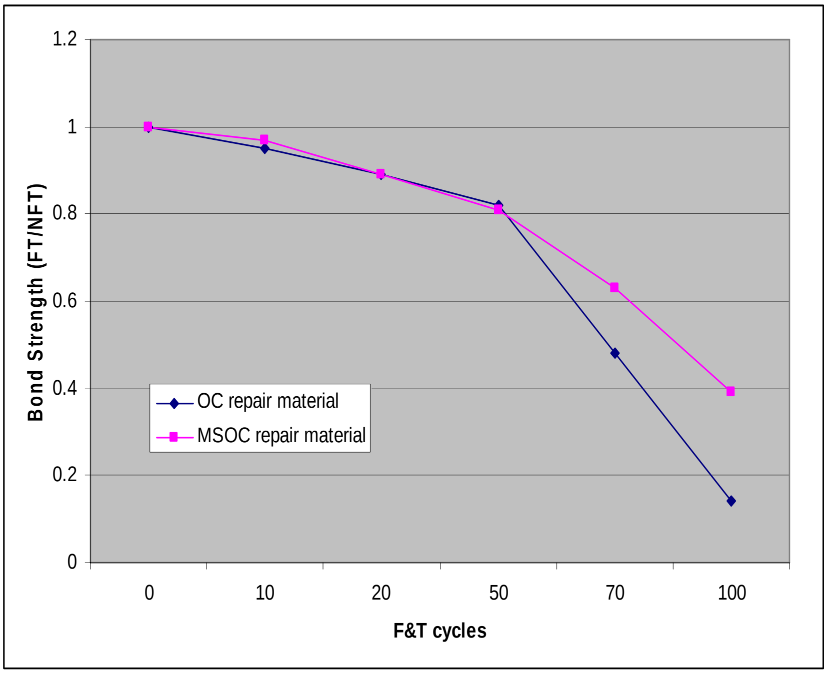

Figure 1. Ratio of bond strength of samples subjected to F&T with that of observation samples

As the above figure shows, the bond strength of repair materials is not much affected in the first 50 cycles of F&T and reduction is less than 20 percent. However, during the second 50 cycles, the bond strength of repair materials reduces sharply in both OC and MSOC materials. As can be seen, reduction of bond strength in OC repair materials is more than that of MSOC repair material.
Two surface preparation methods, smooth as-sawn (SS) and acid etching (AE) were used to prepare the MSOC samples. After repair, samples were cured for 28 days in curing tank and then were subjected to 70 freeze and thaw cycles. Slant shear test was used for evaluating the bond of MSOC repair materials to concrete. In Table 2, the 28-day bond strength of samples is given.

Table 2: The effect of surface preparation method on durability and bond strength

Surface Preparation Method	SS			AE		
No of F&T cycles	50	70	100	50	70	100
Bond Strength (MPa)	19.5	15.1	9.3	22.1	17.5	11.1

Based on the obtained results, the surface preparation method has a considerable effect on bond strength of repair materials subjected to F&T cycles. With use of acid etching method, the bond strength of MSOC repair material is increased by 13%, 16%, and 19% after 50, 70, and 100 F&T cycles, respectively, compare to those of samples prepared by SS method.

3. CONCLUSIONS

In this study the effect of Freeze and thaw cycles on bond strength of cementitious repair material is investigated. The work was aimed at studying the effect of various factors such as initial curing periods and surface preparation method on bond strength. Old concrete samples were made based on BS6319, Part 4 standard. Smooth as-sawn and acid etching methods were used for preparation of concrete substrate surface. Ordinary concrete (OC) with cement type II and concrete containing microsilica (MSOC) were used as repair materials. Repaired samples were subjected to 10 to 100 freeze and thaw cycles based on ASTM C666B. The bond between repair materials and concrete substrate was evaluated based on slant shear test method (BS, 1984). The following conclusions can be drawn from the obtained results:

2) the curing period has an important effect on durability of concrete samples subjected to freeze and thaw cycles. With increase in curing period weight loss of samples decreases. In this study, for concrete samples repaired with ordinary concrete, the weight loss has decreased with increase in curing period from 7 to 28 days by 31%.
3) freeze and thaw phenomena decreases the bond strength considerably. With increase in number of F&T cycles bond strength of repair materials decreases. After 100 cycles of F&T, the bond strength of samples repaired with OC and MSOC materials reduced by 85.6% and 61.2%, respectively. Moreover, microsilica concrete not only increases the bond strength but also increases durability regarding F&T cycles.
4) with application of an effective surface preparation method one can improve the bond strength of repair material considerably. In this study, with use of acid etching method, the bond strength of MSOC repair material could be increased by 13%, 16%, and 19% after 50, 70, and 100 F&T cycles, respectively, compare to that of samples with smooth as sawn surface.

REFERENCES

1. Roning, T.F., Freeze-Thaw resistance of concrete, PhD thesis, The Norwegian Institute of Technology, 2001, 417 pp.
2. Janssen, D.J., Resistance of concrete to freezing and thawing, Technical report, Strategic highway research program, NRC, Washington DC, 1994, 217 pp.
3. British Standard Institute, Testing of resin composites for use in construction, BS 6319, Part 4: method for measurement of bond strength: slant shear method, 1984.
4. ACI Committee 549. Guide for the Design, Construction, and Repair of Ferrocement. ACI Struct J. Vol 85, 1988. pp 325-335.
5. Xiong, G., Cui, Y, Chen, L and Jiang, H. Influence of hydrochloric acid

etching on bond strength between concrete substrate and repair materials. Cement and Concrete composites. Vol 26, 2002. pp 41-45.
6. Behfarnia, K., Jonesari, H., Mosharaf, A., The bond between repair materials and concrete substrate in marine environment., Asian Journal of Civil Engineering, Vol 6, No. 4, pp 267-272.
7. Behfarnia, K., Jonesari, H., Mosharaf, A. Studying the bond between repair materials and concrete substrata, The 6th International Congress, Global Construction: Ultimate Concrete Opportunities, Dundee, Scotland, July 2005.

CD06-006

AN EXPERIMENTAL STUDY ON STRUCTURAL BEHAVIOR OF RECTANGULAR RC COLUMNS DAMAGED BY REBARS CORROSION AND STRENGTHENING THEM WITH FRP

S.M. Kadkhodaee[1], A. Hosseini[2]
[1]MSc. Student, Dept of Civil Engg., School of Engg., Tehran University, Tehran, Iran
[2]Assistant Professor, School of Engg. Tehran University, Tehran, Iran

ABSTRACT
This paper presents the results of an experimental study on the structural behavior (strength and ductility) of rectangular RC columns which have been damaged by rebar corrosion. 22 small-scale reinforced concrete columns with dimensions of 160×160 mm in section and 340 mm in height were tested. Ten specimens were conditioned to three levels of accelerated corrosion and six were conditioned to natural corrosion. The specimens were subjected to concentric compression load in order to assess the change of their mechanical properties due to the corrosion effects. Twelve specimens were strengthened with carbon and glass fiber reinforced polymer (CFRP and GFRP) to see the efficiency of different strengthening schemes. Based on this research it was concluded that the damaged columns show less strength and ductility in comparison with two undamaged columns and, FRP wraps could greatly enhance the strength and ductility of damaged specimens.

Keywords: corrosion, fibre reinforced polymer (FRP), strength, ductility, strengthening

1. INTRODUCTION

The structural degradation of concrete structures, due to reinforcement corrosion is a major worldwide problem. For instance, corrosion of reinforcement in bridge piers is encouraged by chloride contamination from exposure to marine environment and from deicing salts used in bridges during winter. Premature failure of RC structures due to corrosion of reinforcement is a significant issue. Corrosion products generally occupy greater volume than the original material; expansive forces are generated in concrete leading to cracks and spalling of the cover, reducing steel cross-section, deterioration of bond between reinforcement and concrete and finally further acceleration of the reinforcement disintegration [2] (Figure 1). Jacketing of such structures by fiber reinforced composite sheets is an effective remedy, not only as a means of slowing down the rate of the reaction, but also by confining the concrete core thereby imparting to it ductility and strength [3]. Fiber-reinforced polymers (FRP), consisting of continuous carbon (C), glass (G), or aramid (A) fibers bonded together in a matrix of epoxy, vinyl ester, or polyester, are being employed extensively for rehabilitation of concrete structure.

Despite their relatively high material costs, the high strength-to-weight ratio of FRP, their immunity to corrosion, and easy handling and installation are making them the material of choice in an increasingly large number of rehabilitation projects [7].

In order to ensure safety of reinforced concrete structures whose reinforcing steel has been severely corroded, it is necessary not only to repair the damage appropriately, but also to evaluate the strength of RC members according to the degree of rebar corrosion [3, 4]. RC columns, are the main members of RC structures, usually sustain axial forces of dead loads and live loads. There are currently some reports on beams subjected to bending, but only a few attempts have so far been made at columns, in which axial force is not predominant [4].The authors of this paper try to carry out some experimental studies on the structural behaviour of rectangular RC columns damaged by accelerated rebar corrosion in different levels and natural rebar corrosion under concentric axial load. In this research also strengthening method using carbon fibre and glass fibre sheets (CFS and GFS) and the comparison between them is considered.

2. EXPERIMENTAL PROGRAM

2.1. Material and Design

Twenty two specimens were made in the laboratory. All the specimens had a 160 mm square cross-section and a 340 mm height between the test-region. The mix proportion and the mechanical properties of the specimens are given in table 1. The rebars mechanical properties are given in table 2. Figure 2 shows the geometric details of the specimens.

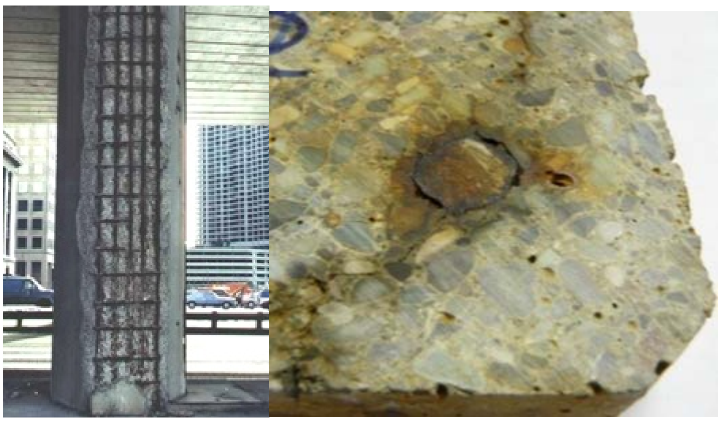

Figure 1. Spalling of the covers and Corrosion cracks.

Table 1: Mixing and mechanical properties of concrete

W/C (%)	Slump (cm)	Unite weight (kg/m^3)				Compressive Strength (MPa)
		W	C	S	G	
68	19	238	350	982	700	21.55

Table 2: Mechanical properties of rebars

Type	Yield Strength (MPa)	Tensile Strength (MPa)	Elastic modulus (GPa)
D16	575	696	197
D6	260	435	172

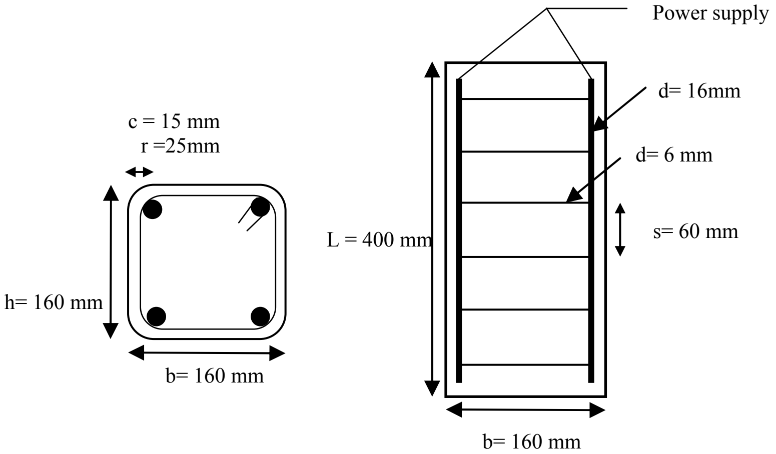

Figure 2. Geometry of the specimens.

2.2. Conditioning to Accelerated and Natural Corrosion

After 28 days of curing, 10 of the 22 specimens were connected to the electrochemical corrosion cell aiming to stimulate, the corrosion. The chemical effects can be created naturally around the reinforcement and concrete cover by depletion of iron and rust accumulation. Although admittedly, the exact chemical composition of rust produced in natural conditions is hard to duplicate under electrochemical conditions, by securing adequate supply of oxygen to the corrosion cell, the aim here was to generate expansive rust products that would cause a network of fine cracks to build upon the specimen surface similar to what is seen in the field. Based on earlier research, a mass loss of approximately 5% calculated with Faraday's Law, assuming constant rate of steel consumption and uniform corrosion over the reinforcing cage is a critical threshold for generating crack widths of 0.2-0.4 mm that are thought to correspond to the Serviceability Limit State of a structure [8]. To this end, specimens were placed in a corrosion basin containing 3% by weight water solution of NaCl. The reinforcement cage of each specimen was connected to the circuit so as to serve as the anode in the corrosion cell, whereas an external steel bar immersed in the basin was used as cathode. Anode and cathode were connected to a constant power supply of 6 V. This voltage has been found to be suitable for generation of similar corrosion products as would occur in nature in a realistic time period so as to enable systematic study of the depletion process and rust accumulation in the laboratory [3, 6]. The electric current passing through each specimen was measured by interpolating ampere meters between anode and the power supply. Three levels of corrosion were considered by the volume of integrated electric current. The categories of the levels were as follows: level one 435 hours, level two 653 hours and level three 870 hours were considered. Figure 3 shows the mechanism of accelerated corrosion applied through each specimen.

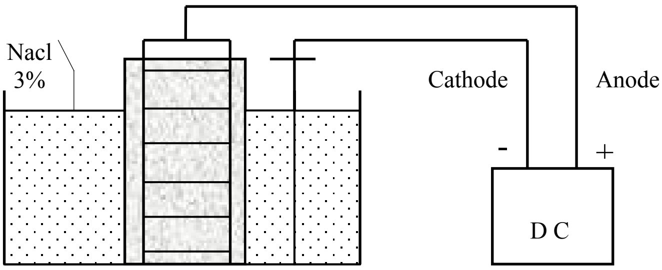

Figure 3. Mechanism of accelerated corrosion.

The propagation of cracks due to corrosion at each level was observed. Figure 4 shows the overall views of cracking in the specimens after carrying out electrolytic corrosion. Although map cracking has been observed, most of the cracks were alongside of the reinforcement and it looks as cracks in the longitudinal directions were more than the lateral directions. The characteristic of the corrosion observed was that the rust concentrated on or near corrosion cracks and on the corners of hoops. The reason for this seems to be that cracks are prone to water infiltration and that the corners of the hoops are under high stresses induced when being bent in the preparation of rebars [4].

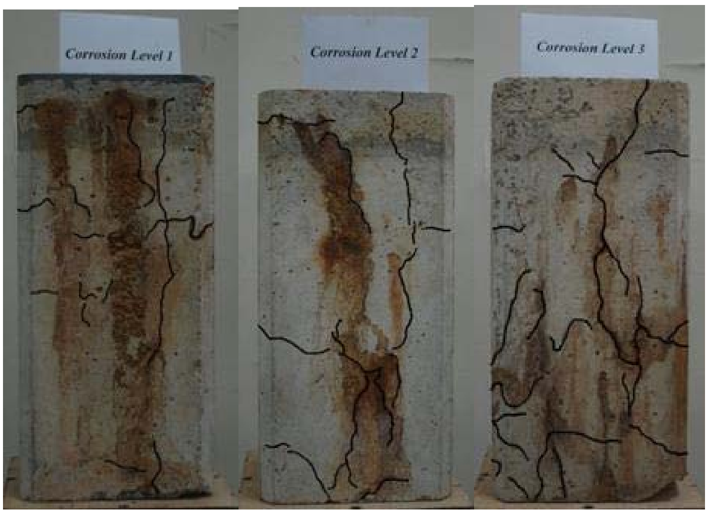

Figure 4. Overall views of cracking in the specimens

The depleted mass of iron ΔW (gr) consumed over the time Δt (s) was estimated from the current I_{corr} flowing through the cell using Faraday's Law (Equation 1), which assumes a constant rate of iron depletion:

$$\Delta W = \frac{I_{corr}\ \Delta t\ A_m}{Z\ F} \qquad (1)$$

Where A is the atomic mass of iron (55.87 gr), Z is the valence of the reaction usually taken as 2 (assuming the corrosion product is Fe(OH)2) and F is Faraday's constant equal to 96490 C (g/equivalent)[1]. The experimental values concerning steel mass consumption are listed in Table 5.
Six of the specimens were subjected to long term (one year) natural corrosion. In order to carry out the natural corrosion the specimens were placed in a basin of salt solution (NaCl 3%) and conditioning to a dry and wet situation once in a day. To evaluate the rebars corrosion activity, corrosion potential readings of the specimens were registered by using calomel electrode once a month. Table 3 shows the results of half cell potential test. The results of the table indicate that corrosion activity was started from the fifth month with 90% probability according to [1].

Table 3: Half cell potential test result for specimens with natural corrosion

Month	1	2	3	4	5	6	7	8	9	10	11	12
Potential (mV)	-260	-320	-360	-440	-530	-530	-540	-550	-570	-570	-570	-570

2.3. Repair Procedures

Two types of FRP sheets were used for the retrofitting of 12 specimens, with different fibre materials: Carbon versus Glass. The carbon fibre sheet (CFS) consisted of fibres arranged in a uniform direction and the glass fibre sheet (GFS) consisted of fibres arranged in two directions with proportions of 100% and 10%. Table 4 gives the mechanical properties of CFS and GFS in the main direction. Six of the specimens wrapped with CFS and the other six specimens wrapped with GFS. Initially the corner of specimens were rounded by a radius of 25 mm. Surface of the specimens were cleaned from rust and dust and then coated by resin primer. After 24 hours, columns were wrapped with 2 layers of FRP using resin glue.

Table 4: Mechanical properties of FRP

Type	Weight (g/m^2)	Thickness (mm)	Tensile strength (MPa)	Elastic modulus (GPa)
CFS	300	0.176	4000	240
GFS	440	0.15	3450	77

3. EXPERIMENTAL RESULTS AND DISCUSSIONS

In the fourth phase of the experimental program all specimens were tested to failure under monotonically increasing concentric compression. Axial strain was measured as the average of two LVDTs placed on opposite sides of the specimen.
In Table 5, columns 6–8 outline the most important indices of mechanical response measured during the load tests. In particular the ratio of P_{max}/P_{cont} quantifies the

increase and decrease in load carrying capacity (P_{max}) as compared to that of identical uncorroded-control specimens (P_{cont}). The specimens named as; U = uncorroded, ACi = accelerated corrosion with different levels, N=natural corrosion, W = without confinement, C = CFRP confinement and G = GFRP confinement. Figures 5 plot is a representative of histories of compressive stresses versus axial strain for the specimens.

Table 5: Experimental Result

specimen I.D.	number of specimen	level of corrosion	Mass loss $\Delta M_s/M_{cage}$ (%)	layer and type of FRP	P_{max} (kN)	P_{max}/P_{cont}	$\varepsilon_{ax,peak}$ (%)
U-W	2	–	–	–	960	1	0.42
U-C	2	–	–	2-CFRP	1530	1.59	0.81
U-G	2	–	–	2-GFRP	1310	1.36	1.03
AC1-W	2	1	6.08	–	875	0.91	0.34
AC2-W	2	2	9.35	–	820	0.85	0.27
AC3-W	2	3	12.15	–	790	0.82	0.08
AC3-C	2	3	12.15	2-CFRP	1470	1.53	0.66
AC3-G	2	3	12.15	2-GFRP	1205	1.25	0.90
N-W	2	Natural	–	–	925	0.96	0.39
N-C	2	Natural	–	2-CFRP	1505	1.56	0.78
N-G	2	Natural	–	2-GFRP	1300	1.35	0.98

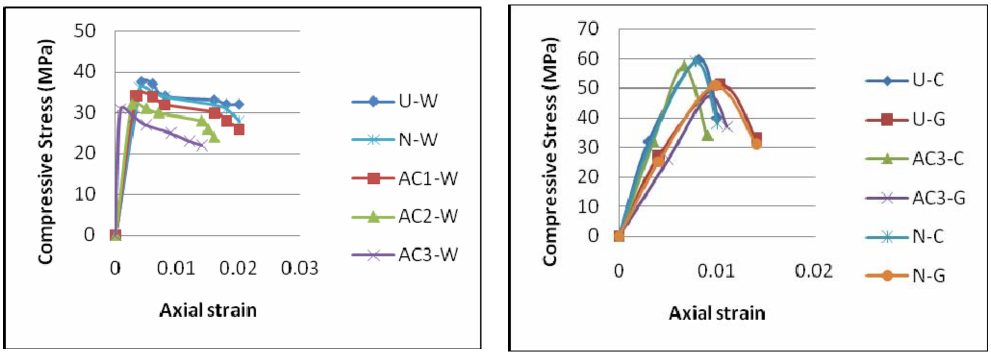

Figure 5. Stress-strain curves of compressive tests

Generally, the FRP jackets improved the performance of columns under compression in terms of load carrying capacity, deformation capacity up to peak load and ductility. Their passive confining action was mobilized progressively in response to lateral dilation of the concrete core. In most_cases failure started in the corroded portion and extended over the entire specimen with abrupt rupture of the jacket and disintegration of the concrete cover and core. This premature mode of failure was accompanied by simultaneous buckling of longitudinal reinforcement owing to the failure of corroded stirrups.

According to the experimental results in table 5, it is concluded that corrosion level 3 of the specimens reduces 18% strength and 80% ductility with respect to the

reference specimens (U-W). The sever loss of ductility is due to the effect stirrups being more corroded than the longitudinal reinforcements, due to the fact that cover on the stirrups is less than the longitudinal bars.
Strength and ductility of specimens that are corroded naturally are between the results of U-W and AC1-W specimens. Strengthening of the specimens corroded intensively using CFRP and GFRP wrap increase the strength and ductility more than the U-W specimens. This strength and ductility values could reach also close to U-C and U-G values. Regarding all the cases CFRP gives better performance towards strength and GFRP gives better performance towards ductility. According to the last reports [3, 5] and results of this paper it is concluded that because of geometry of column's section and stresses concentration on the corner of rectangular section, FRP wrap has the lower performance in comparing with columns with circular section.

4. CONCLUSIONS

The following conclusions are deduced from the experimental results:

- Intensive corrosion of the specimens reduces 18% strength and 80% ductility with respect to the reference specimens (uncorroded).
- The sever loss of ductility is due to the effect stirrups being more corroded than the longitudinal reinforcements.
- Generally, the FRP jackets improved the performance of columns under compression in terms of load carrying capacity, deformation capacity up to peak load and ductility. Their passive confining action was mobilized progressively in response to lateral dilation of the concrete core.
- Regarding all the cases CFRP gives better performance towards strength and GFRP gives better performance towards ductility.

REFERENCES

1. Bertolini, L., Elsener, B., Pedeferri, P. and Polder, R., *Corrosion of Steel in Concrete*, WILEY-VCH Verlag Gmbh & Co.KGaA, Weinheim, Germany, 2004, 392 pp.
2. Mehta, P.K., and Monterio, P.J.M., Concrete Microstructure, Properties and Materials, first ed, Indian Concrete Institute, Chennai, India, 1997.
3. Pantazopoulou, S.J., Bonacci, J.F., Sheikh, S., Thomas, M.D.A., and Hearn, N., "Repair of Corrosion-Damaged Columns with FRP Wraps", *Journal of Composites for Construction*, 2001, 5, 1, pp 3-11.
4. Lee, H.S., Kage, T., Noguchi, T., and Tomosawa, F., "An Experimental Study on the Retrofitting Effects of Reinforced Concrete Columns Damaged by Rebar Corrosion Strengthened with Carbon Fiber Sheets", *Journal of Cement and Concrete Research*, 2003, 33, pp 563-570.
5. Tastani, S.P., and Pantazopoulou, S.J., "Experimental evaluation of FRP Jackets in Upgrading RC Corroded Columns with Substandard Detailing", *Journal of Engineering Structures*, 2004, 26, pp 817-829.
6. Lee, C., Bonacci, J., Thomas, M.D.A., Maalej, M., Khajenpour, S., Hearn, N.,

et al., “Accelerated Corrosion and Repair of Reinforced Concrete Columns Using CFRP Sheets”, *Canadian Journal of Civil Engineering*, 2000, 27, 5, pp 949-59.

7. Bousias, S.N., Triantafillou, T.C., Fardis, M.N., Spathis, L. and ORegan, B.A., “Fiber-Reinforced Polymer Retrofitting of Rectangular Reinforced Concrete Columns With or Without Corrosion”, *ACI STRUCTURAL JOURNAL*, 2004, 101, 4, pp 512-20.
8. Andrade, C., Alonso, C., and Molina, F., “Cover cracking as a Function of Bar Corrosion”, *Part I – experimental test, RILEM Material and Structures*, 1993, 26, pp 453-64.

CD06-007

DESIGN AND DEVELOPMENT OF RESIN CAPSULE ANCHORING SYSTEMS FOR STRENGTHENING THE CONCRETE SURFACE USING DESIGN-EXPERT SOFTWARE

B.Kaffashi[1], M.Moosavi[2], I. Fotovat Ahmadi[3]
[1]Associate Professor, School of Chemical Engineering, University of Tehran, Tehran, I. R. Iran
[2]Associate Professor, School of Mining Engineering, University of Tehran, Tehran, I. R. Iran
[3]M.S Student, School of Chemical Engineering, University of Tehran, Tehran, I. R. Iran

ABSTRACT
The demand for strengthening of concrete structures has resulted in an increased use of chemical bonded anchors. Therefore, investigating the formulation and mechanical properties of adhesive grout layer has become an important issue. Different formulations of polyester resin grout were designed by Design-Expert software and their uniaxial compressive strength, volume shrinkage, gel time and maximum exotherm temperature were obtained. In addition, their rheological behaviors once the reinforcing bar is inserted were evaluated. Having optimized the above parameters by means of mixture D-optimal method, the most efficient formulation of chemical bonded anchors was developed. The effect of adding thixotropic additives and different rotational speed of anchors on the rheological behavior of optimum mixture were investigated and the resin capsule was produced. The most significant factors increasing compressive strength and volume shrinkage are resin and monomer content. Inhibitor concentration decreases both responses dramatically. Silica fume not only improves the rheological behavior of the grout, but also increases its storage time.

Keywords: chemical bonded anchors, polyester resin grout, mixture d-optimal, thixotropic behavior

1. INTRODUCTION
Grouting is a widely used method for strengthening and sealing rock, soil and concrete. Grouts application in the construction and repair of structures include returning disintegrated concrete and masonry into a monolithic mass, repair and welding of cracks in structural concrete members, securing of bolts, rods and anchors in drilled hole, casting of preplaced aggregate concrete and corrosion protection for anchors and tendons [1]. The demand for more flexibility in planning, design and strengthening concrete structures has resulted in an increased consumption of chemical grouted anchors. In addition, due to reducing the average-time of construction, chemical bonded anchors or grouted anchors provide a viable and economical method for adding new concrete sections or steel members to existing concrete structures.
The chemical bonded anchor consists of a structural adhesive grout such as

unsaturated polyester resin and a threaded rod or a reinforcing bar which is inserted in a drilled hole. They develop their holding capacities by bonding of the adhesive grout to both the anchor and concrete [2]. Resin adhesive grouts are available as prepackaged glass or plastic film capsules or dual cartridge injection systems. Plastic films capsules are better suited for use on construction sites since they are more robust. Because of their flexibility they adapt themselves to the hole geometry and can easily be installed overhead [3]. The capsules contain two separated compartments. The outer compartment contains the resin mixture while the inner compartment contains the catalyst mixture. The capsule is inserted into the hole, the threaded rod is then rotary-hammered into the capsule, rupturing the plastic film and mixing the two compartments. Chemical reaction between resin and catalyst mixture hardens the resin adhesive and creates a high strength bond. Factors influencing the performance of load transfer in and strength of chemical bonded anchor systems are reinforcing bar properties, adhesive grout characteristics and installation conditions. Resinous grout properties can be determined by its compositions. The cross-linking reaction between unsaturated polyester resins and vinyl monomers allows one polymer chain to connect with other polymer chains and produce a three dimensional network, which converts the resin from a viscous liquid into a hard, thermoset solid. Unsaturated polyester resins (UP) are cured in the presence of free radicals that are derived from a catalyst such as organic peroxides.

The resin adhesive should have good mechanical properties after setting. Viscosity alteration is also needed especially during installation in order to ensure proper mixing; moreover, maximize contact with concrete and rod surfaces. Residual stresses and possible formation of cracks and voids due to volume shrinkage can present serious problems for chemical bonded anchors. In vertical concrete surfaces, Thixotropic behavior of the resin can reduce run out and sagging before gelation takes place.

The main objective of the present work is to design different adhesive grout formulations and analyze their influence on uniaxial compressive strength, volume shrinkage and rheological behavior of the resinous grout with the latest version of Design-Expert software. Various compounds were designed by mixture D-optimal method. Finally the effect of thixotropic agent on rheological properties of the optimized compound will be evaluated.

2. EXPERINMENTAL PROCEDURE

2.1. Materials

Design variables include unsaturated polyester resin (A), mineral filler (B), monomer (C) and initiator-inhibitor mixture (D). Amount of plasticizer and promoter are kept constant in order to increase the efficiency of the predicted models which are suggested by software. The ratio of the initiator to inhibitor for the mixtures with more than 2% peroxide is 0.25. The amount of orthophthalic polyester resin -provided by Resitan Co., containing 30 wt. % styrene- in the formulation was kept between 20 to 30 wt. %. Limestone powder (200 mesh) was chosen as filler having a mean particle size of about 30 – 50 microns from Iran

Micronized Powder Co. (55-68 wt. %). Styrene monomer was used as crosslink agent in the curing reaction of unsaturated polyester resin (4-9 wt. %). The initiator used in this study was 55 wt. % solution of benzoyl peroxide (BPO) in phthalate solvent (2-5 wt. %). N, N dimethyl aniline (DMA) was employed as promoter because of its high reactivity to decompose the initiator at low temperatures. Inhibitor was 3 wt. % solution of hydroquinone in dipropylene glycol. Constant amount of 4% Dibutyl phthalate was added as plasticizer in order to adjust the viscosity of the resinous grout. Silica fume from I.F.I Co. was used as thixotropic agent in three different percentages (0.2%, 0.7% and 1.5%) with mean particle size of 0.05-0.015 microns.

2.2. Methods

Depending on the number of design variables and applied constraints, 22 combinations were designed by the software; their results are presented in Table 1. Among these combinations, 5 are allocated to replicates; another 5 are for testing the lack of fitness. Test method for gel time and maximum exotherm temperature during curing of each designed mixture was performed using ASTM D2471-99 [4]. The compressive strength test was performed according to ASTM-C579-01 [5]. Three cylindrical test specimens were cast for each composition; each specimen was Design and Development of Resin Capsule Anchoring Systems for Strengthening the Concrete Surface Using Design-Expert Software.

Table 1: Different adhesive grout formulations and their response values

Sample	Gel Time (s)	Compressive Strength (MPa)	Volume Shrinkage (%)	Max Temp. (˚C)	Density g/cm^2
1	75.41	78.1337	9.42276	79.2	1.84384
2	69.56	60.6298	4.79809	65.2	1.9272
3	304.50	56.8142	6.43913	74	1.7577
4	91.80	76.2515	7.84562	75	1.85682
5	77.87	81.4337	10.2696	84	1.74617
6	211.47	51.5387	7.25721	67	1.9495
7	193.37	72.2084	9.102	80.3	1.8155
8	94.88	73.6807	9.14743	71	1.88868
9	231.52	54.6982	6.9195	74.8	1.89086
10	234.86	55.723	6.54811	77	1.84909
11	318.64	46.6478	7.75762	73.9	1.78145
12	83.19	75.256	10.0429	78.8	1.8276
13	325.41	41.7709	7.11796	70.1	1.81973
14	71.33	84.3686	11.327	78.4	1.76077
15	308.12	48.9402	7.72005	80	1.72894
16	375.17	35.5334	4.0159	56.2	1.86675
17	334.32	47.6118	6.32899	71	1.79352
18	353.03	40.8754	4.03017	63.5	1.85196
19	286.41	57.0403	8.40159	69.7	1.76715
20	352.18	33.3691	2.55093	52.6	1.86198
21	79.63	57.9861	6.71264	65.5	1.91125
22	61.79	81.4481	8.40954	78.8	1.81908

3. RESULTS AND DISCUSSIONS

3.1. Compressive Strength

In accordance with the obtained results of compressive strength for each grout mixture (Table 1), analysis of variance (ANOVA) is conducted by the software and the quadratic model is recommended for estimating the outcomes. As is demonstrated in Table 2, each design variable solely has a significant role in determining the compressive strength of grout. Moreover, the CD factor which represents the interaction effect between monomer and initiator-inhibitor mixture is known as a fairly influential factor in verifying compressive strength of resinous grout.

According to Figure 1 and Figure 2, increase in percentages of resin and initiator-inhibitor mixture has the most significant effect on compressive strength of the grout. By increasing the concentration of initiator- inhibitor mixture, compressive strength is declined dramatically; this is originated from the increase of inhibitor content in the mixture, despite the increment of initiator concentration. Similar results have been observed in the Cook and Lau's research concerning the curing process of polyester resin in presence of different percentages of initiator and inhibitor [6].

Adding the promoter leads to decomposition of initiator into free radicals. Inhibitor consumes the generated free radicals; as a result the efficiency of initiator will be diminished.

The increase of resin percentage is similar to increase of matrix component of the grout. Therefore, filler particles are dispersed better in the resin matrix. The reduction of viscosity due to higher resin content and lower filler content assist in better wetting and screening of the particles. Consequently, by curing the matrix component a more densified network is formed and the compressive strength is increased. Figure 2 illustrates a decrease in compressive strength in high percentages of filler. Increasing the monomer concentration has led to a higher compressive strength. This is due to increase of probability of reaction between styrene and free radicals in polyester resin chains.

Table 2. Analysis of variance (ANOVA) for compressive strength results

Source	SS	DF	MS	F-value	P- value	Significance
Mean	5213.35	9	579.26	115.56	<0.0001	S.
Linear	5035.37	3	1678.46	334.86	<0.0001	
AB	5.59	1	5.59	1.12	0.3116	
AC	3.53	1	3.53	0.7	0.418	
AD	11.65	1	11.65	2.32	0.1532	
BC	0.6	1	0.6	0.12	0.736	
BD	9.4	1	9.4	1.87	0.1961	
CD	25.84	1	25.84	5.15	0.0424	
Residual	60.15	12	5.01			
LOF	44.49	7	6.36	2.03	0.2267	Not S.
Error	15.66	5	3.13			
Total	5273.5	21				

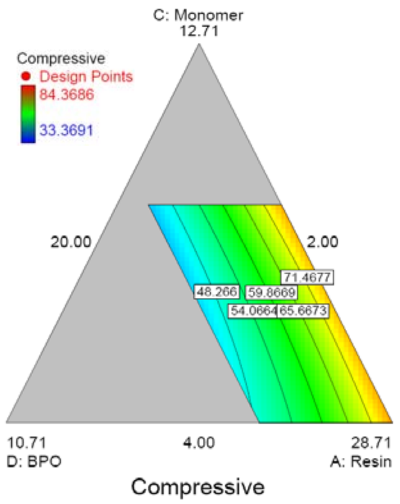

Figure 1. Contour plot for compressive strength (constant filler content: 61.29%)

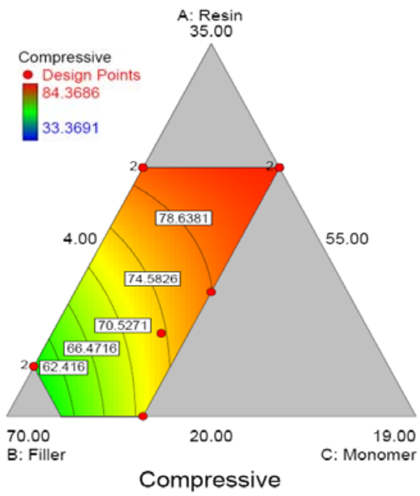

Figure 2. Contour plot for compressive strength (constant initiator content: 2%)

When the curing reaction begins, viscosity increases and after gelation a three dimensional network is produced in resinous grout bulk. Therefore, polyester resin chain's motions are limited, resulting in increased rate reaction between small molecules of styrene monomer and free residual radicals. The result is autoacceleration of the reaction at higher conversions known as Norish-Trommsdof effect. Van Assache concluded that the autoacceleration is mainly an acceleration of the styrene consumption. Also the autoacceleration is because of depletion of the styrene monomer that causes a further increase in the viscosity [7]. Hence, as a result of autoacceleration, higher degrees of conversion of the grout are achieved, thus raising the compressive strength of the samples.

3.2. Volume Shrinkage

Considering the empirical and predicted results, the Design-Expert software suggested a linear model for estimating the volume shrinkage of the grouts (Table 3).
According to trace plot in Figure 3, the slope of design variables shows that the resin and monomer concentration have the most significant influence on increase of the volume shrinkage of the resinous grout.

Table 3: Analysis of variance (ANOVA) for volume shrinkage results

Source	SS	DF	MS	F value	P value	Significance
Model	85.96	3	28.65	37.24	<0.0001	S.
Linear	85.96	3	28.65	37.24	<0.0001	
Residual	13.85	18	0.77			
LOF	7.94	13	0.61	0.52	0.843	Not S.
Error	5.9	5	1.18			
Total	99.81	21				

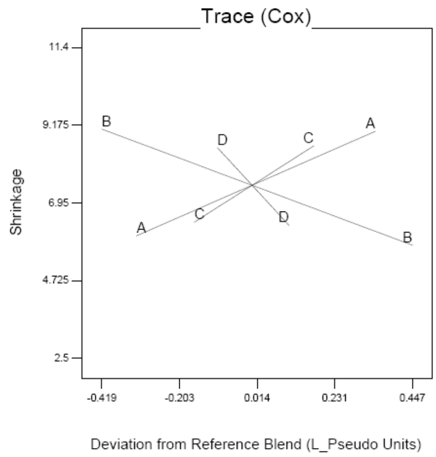

Figure 3. Trace (cox) plot for volume shrinkage, each line represents a primary trace for that component

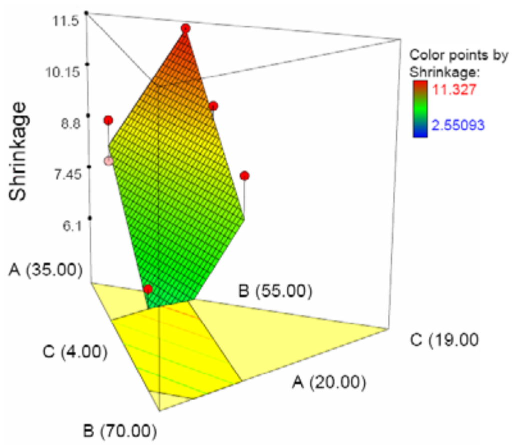

Figure 4. 3D surface plot for volume shrinkage (initiator-inhibitor mixture: 2%)

The opposite effect is observed while increasing the concentration of filler and initiator-inhibitor mixture (D). Higher amount of inhibitor in the mixture consumes more generated free radicals which lessens the degree of conversion. Higher conversion would result in a higher amount of shrinkage. Therefore, the polyester resin network shrinks less compared to the state which no inhibitor exists. Monomer's effect on the shrinkage of the grout is more considerable than that of the resin. This is because of the major role of the styrene monomer in increasing the conversion during curing of the polyester resin. As was mentioned before, small molecules of styrene can diffuse easily among the long crosslinked polyester chains and react with free radicals, making the network denser.
Increasing the filler content reduces volume shrinkage linearly. This is because of the decrease in the resin content in the mixture (Figure 4). Filler component acts similar to thermal insulation in the resin matrix and prevents heat transfer through the matrix bulk. By absorbing the exotherm heat, filler particles can hinder the volume shrinkage of the grout and prevent the development of internal stresses. Rate of relaxation of the internal stresses in polymers can be increased by adding substances such as fillers [8].

3.3. Comparing the Results

In Figure 5, higher compressive strengths are seen in the samples which have higher maximum exotherm temperature; this represents higher conversion in these samples. Therefore the resinous matrix of the grout is stiffer and can resist more loads before failure. Figure 6 confirms that higher volume shrinkage would occur in the samples which have higher exotherm temperatures. By examining different formulations, it is clarified that filler content cannot increase the compressive strength, but it even reduces the compressive strength by decreasing the concentration of the resin and monomer.

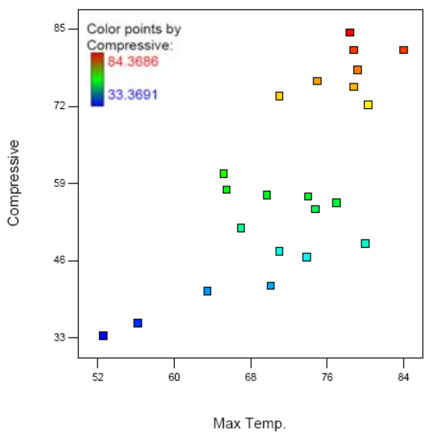

Figure 5. Compressive strength results vs. maximum exotherm temperature

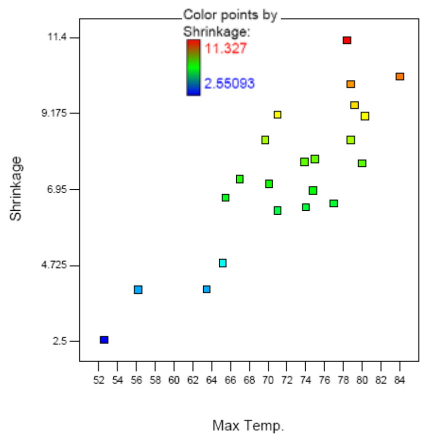

Figure 6. Volume shrinkage results vs. maximum exotherm temperature

According to previous results, it is essential to estimate the optimized formulation in order to gain the highest compressive strength and the lowest volume shrinkage. The software introduces the compound formulations as ideal grouts with optimized responses as mentioned in Table 4. In order to compare the outcomes with predicted results achieved by the software, it is necessary to implement the conducted experiments on the optimized compound #1 as well.

One of the significant characteristics of chemical bonded anchors is their high compressive strength in the beginning of the installation of the anchors. Hence, the compressive strength of the optimized compound was examined in the first one hour and 24 hours right after grout curing in order to reassure its strength from the beginning of the installation.

According to Table 5, about 79% of the final strength was achieved after 24 hours of installation the anchor in concrete hole. The outcomes of the designed models for evaluating each response show a good correlation with empirical results. This means that the suggested models can perfectly predict the different formulation properties. Therefore, by using these models, ideal formulations can be suggested and different kinds of grouts can be designed based on consumer demands. This will considerably decrease the price of the final product.

3.4. Thixotropic Agent

It is essential to evaluate rheological behavior of the optimized compound in the presence of three different percentages of fumed silica (0.2%, 0.7% and 1.5%) as a thixotropic agent. Therefore, the rheological measurements were designed in such a way that stimulates similar circumstance which grout has in a concrete hole. That is, first the grout sample was subjected to shear rate of 0.01 s^{-1} in 100 seconds (stage1), then it was promptly exposed to rotation speed of 100 rpm for another 100 seconds (stage2). Then, the sample was remained in holding time period in which the rotation was stopped and the shear rate returns to 0.01 s^{-1}(stage3). This test determines the thixotropic and flow behavior of the optimized grout compound in each of the three defined intervals.

Table 4: Optimized formulations and their predicted results are suggested by the software

	V.Shrinkage (%)	Compressive (MPa)	Max.Temp. (°C)	Density (g/cm^3)	Gel Time (s)	Desirability
1	7.60287	71.2102	74.6882	1.87189	63.1655	0.822
2	7.7851	69.0389	68.7493	1.90448	107.2	0.804
3	8.51495	75.8757	80.5386	1.83724	108.495	0.8
4	8.65867	74.6901	75.6227	1.8573	95.09888	0.789

Table 5: The actual properties of optimized compound

	Gel Time	V.Shrinkage	Compressive Strength (MPa)			Max.Temp	Density
Optimized	s	%	1hr	24hr	7days	˚C	g/cm^3
compound	79.56	7.40816	49.3914	61.04594	76.77016	72.4	1.843463

Figure 7 shows how the optimized compound behaves in the presence of three different percentages of silica fume. In spite of the high amount of filler in the compound during shearing interval (stage 2), viscosity decreases dramatically. Furthermore, it is observed that increase in the silica fume content enhances the thixotropic properties of the samples and after the rotation of anchor is terminated, the viscosity returns to plateau state rapidly. Silica fume particles are reactive pozzolanic materials and in consequence of their method of producing, they have silanol groups on their surfaces. Researchers have shown the interaction and forming of hydrogen bridging between carbonyl groups and hydroxyl end groups of the polyester resin with silanol groups [9]. Structures based on hydrogen bond through silanol groups are temporary and they will break if exposed to high shear mixing.

In order to examine the grout structure, frequency sweep test is conducted on grout samples (Figure 8). It is observed that by adding silica fume to the optimized compound, storage modulus is increased. According to the trend of storage modulus and loss modulus in Figure 8, all the samples except the one with 1.5% silica fume, show viscous behavior at low frequencies. However, in the sample with 1.5% silica fume, by increasing frequency, the storage and loss modulus remain approximately unchanged. Hence, the mentioned sample would resist against deformation. When the storage modulus as a function of frequency turns into horizontal line, a three dimensional structure is formed; this is occurred in the sample with 1.5% silica fume. In fact by increasing the amount of silica fume in grout, interactions between filler's metal oxides and silanol groups with acid groups in polyester resin chains would increase and this would result in a network structure as shown in frequency sweep test. The elastic behavior of sample with 1.5% silica fume would provide longer storage time. This structure is temporary and according to Figure 7 during shearing interval resinous grout represents the good thixotropic behavior.

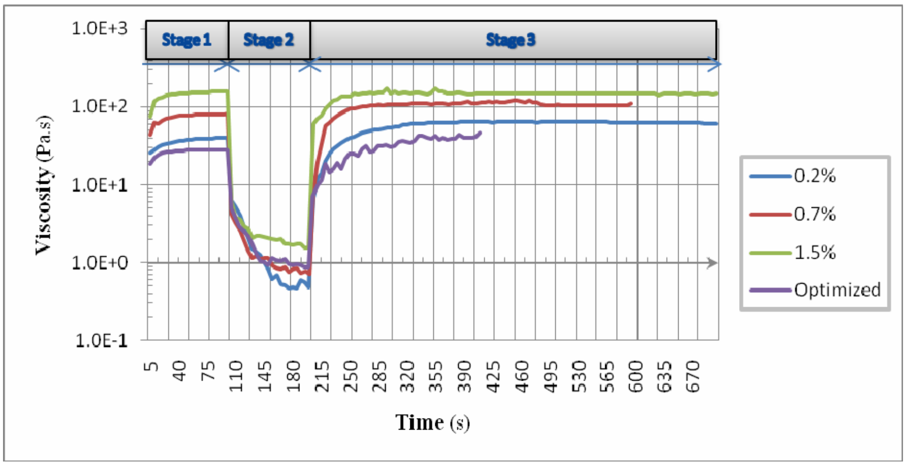

Figure 7. The thixotropic behavior of the optimized grout compound (■) in presence of three different percentages of silica fume. 0.2% (■), 0.7% (■), 1.5% (■)

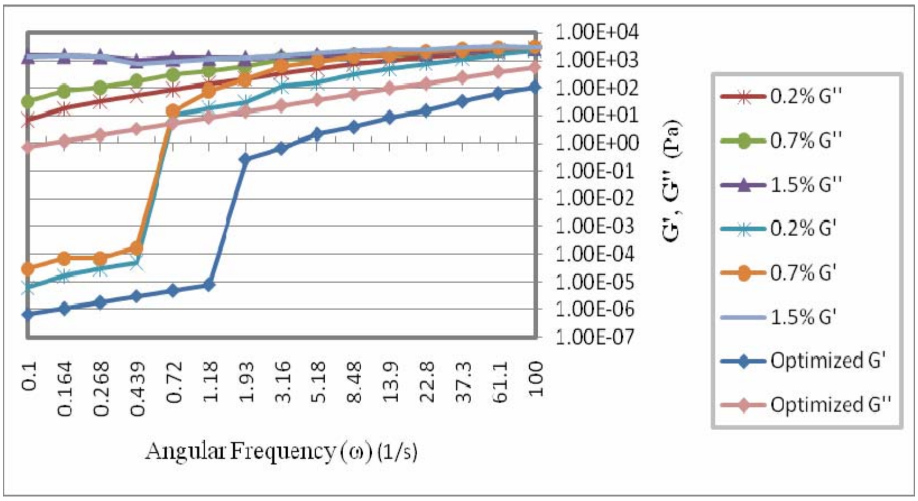

Figure 8. Loss and storage modulus of optimized compound as a function of frequency in presence of different percentages of silica fume (0.2%, 0.7% and 1.5%) in frequency sweep test

The rheological test, designed for observing the thixotropic properties in three different rotation speeds (100 rpm, 300 rpm and 600 rpm), has been evaluated. In Figure 9, it is illustrated that in all three presumed rotation speeds, grout samples show good thixotropic behavior and would return to the plateau state in a short while. Viscosity drop in higher shear rates is more considerable and it assists to better mixing of components. Because all three samples return to plateau state approximately at the same time, the higher rotation speed of the anchor is preferred due to the more viscosity drop it causes in second interval.

The plastic film used for packaging the resinous grout into the capsule shape is called Myler film.

The Myler film is polyethylene terphthalate transparent barrier film with 30-40 microns thickness. The catalyst formulation compartment would be located inside the resin formulation compartment. (Figure 10)

4. CONCLUSION

Polyester resin, as the matrix component of the adhesive, has the most significant effect on increasing the compressive strength of the grout. Increasing the initiator-inhibitor mixture decreased the compressive strength dramatically because the inhibitor consumed the free radicals. The low filler content had no effect on compressive strength of the grout but higher amounts of the filler reduced the compressive strength. It was observed that monomer content has the most significant influence on increasing the volume shrinkage. Increasing the initiator-inhibitor mixture and filler content reduced the volume shrinkage linearly while higher resin concentration led to increased shrinkage.

Good correlation between the maximum exotherm temperatures and other responses were obtained. Moreover, the results of the experiments for the optimized compound are in good agreement with the estimated values. According to the designed rheological test, improved thixotropic behavior was achieved by adding fume silica to polyester resin grout. The higher rotation speed of anchor caused better mixing and thixotropic behavior.

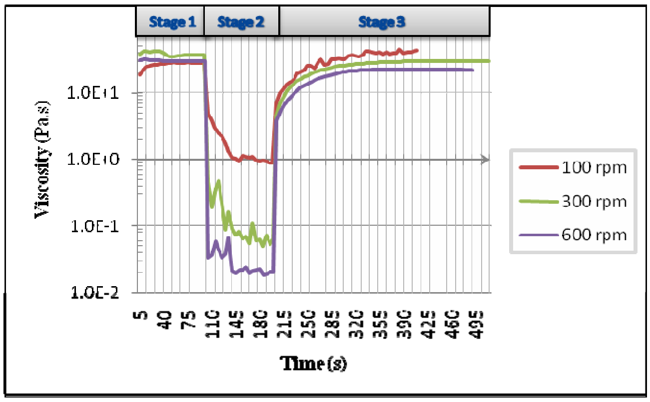

Figure 9. Thixotropic behavior of the optimized grout in three different rotation speeds

Figure 10. Resin capsule anchoring system

REFERENCES

1. J. Warner, Practical Handbook of Grouting: Soil, Rock and Structures, John Wiley and Sons, USA, 2004, 700 pages.
2. Concrete Repair Manual, Vol.1, International Concrete Repair Institute (ICRI), USA, 2003, 2093 pages.
3. K.R Wisser, J. Kunz, P.L. Geiss, Behavior and Design of Adhesive Anchors Under Tensile Load, 23rd Annual Meeting of the Adhesion Society, USA, 2000, 19-23 February, 6 pages.

4. American Society for Testing and Materials, Standard Test Method for Gel Time and Peak Exothermic Temperature of Reacting Thermoset Resins, D2471-99, Annual Book of ASTM Standards, USA, 2004.
5. American Society for Testing and Materials, Standard Test Method for Compressive Strength of Chemical-Resistant Mortars, Grouts, Monolithic Surfacings and Polymer Concretes, C579-01, Annual Book of ASTM Standards, USA, 2004.
6. W.D. Cook, M. Lau, M. Mehrabi, K. Dean, M. Zipper, Control of Gel Time and Exotherm Behavior During Cure of Unsaturated Polyester Resins, , Polymer International Journal, 2001, Vol.50, 129-134.
7. G. Van Asschea, E. Verdonck, B. Van Mele, Interrelations between Mechanism, Kinetics, and Rheology in an Isothermal Cross-linking Chain-Growth Copolymerization, Polymer International Journal, 2001, Vol.42, 2959-2968.
8. R.A. Veselovskiĭ, V.N. Kestelman, Adhesion of Polymers, McGraw-Hill Professional, USA, 2002, 403 pages.
9. S. Frings, Organic-Inorganic Hybrid Coatings based on Polyester resins and In Situ Formed Silica, University of Eindhoven, 1999, 147 pages

CD06-008

PERFORMANCE INVESTIGATION OF RC SHORT COLUMNS RETROFITTED WITH FRP COMPOSITES IN PASSIVE & ACTIVE STATES

G. Ghodrati Amiri[1], A. Emdadi[2] and H. Hamidi Jamnani[3]
[1]Professor, Center of Excellence for Fundamental Studies in Structural Engineering, School of Civil Engineering, Iran University of Science & Technology, Tehran, Iran
[2]M.Sc., Azad Islamic University, South Branch, Tehran, Iran
[3]PhD Candidate, School of Civil Engineering, Iran University of Science & Technology, Tehran, Iran

ABSTRACT
Short columns and columns having weakness in transverse reinforcement have shown inappropriate behaviour in confronting with shear forces during different earthquakes and the shear failure mode of these columns is the main failure mode. One of the most conventional methods for improving the behaviour of these columns is the application of wrapped FRP jacket. These FRP jackets are lightweight, high strength and have a convenient installation process. These jackets can be utilized both in active and passive states. In this study, weak and retrofitted columns have been modelled using "Seismostruct" software and have been compared with experimental conclusions as well. In passive retrofitted specimens, the improvement in value of energy dissipation observed was about 1.7 to 4 times greater than control specimens. Furthermore, drift angle was increased about 1.4 to 2.5 times greater. Moreover, active retrofitted specimens have demonstrated a better behaviour than passive ones. In most of the specimens the growth was about 20% and 30 to 40 percent in shear strength and quantity of energy dissipation, respectively. Finally, AFRP composites have demonstrated higher ductility than CFRP composites, despite the fact that the shear strength of CFRP was higher than AFRP type.

Keywords: AFRP, CFRP, confinement, fibre analysis, drift angle, wrapped jackets

1. INTRODUCTION
Shear failure has been one of the most common failure modes for RC structures subjected to earthquakes. Recent studies and experimental researches have shown that short RC columns of buildings are vulnerable in brittle failure. Due to this weakness, a great number of studies have been done to find appropriate methods for increasing the shear strength of such columns in order to change the brittle failure mode to a ductile one. A majority of columns are primarily designed as flexural members but unexpectedly change into short columns by adding walls and infill to the structure. In addition, most of the columns, which have been designed according to codes before 1970 (strength based design) lack enough transverse bars, so their dominant failure mode is the shear mode. This failure mode happens

suddenly and the brittle shear failure decreases the capacity of energy dissipation of the column. Shear capacity of short RC columns is a function of parameters like: 1- Area of longitudinal and transverse bars, 2- Compressive strength and confinement of concrete and 3- Coherence between steel and concrete [1 & 2].

2. HISTORY

A large number of numerical and experimental researches have been done for strengthening and retrofitting RC columns using passive confinement so far, such as the works of Galal et al. [1&3], Saatcioglu [4] and Ehsani [5]. Nevertheless, a few studies have been done using active confinement. The researches of Yamakava et al. [6] and Saadatmanesh [7] are the sample of these studies. In this study, both active and passive confinements were investigated. The active confinement has been considered with the use of prestressed Carbon & Aramid fibres.

3. METHODOLOGY

In the present study, 5 short cantilever RC columns have been chosen and retrofitted in both active and passive states. The ratio of their shear span to depth is 2.5. For considering confinement effect in the concerned software, the relationships of Mander et al. [8] have been used for evident specimens. For passive retrofitted specimens, the relationships introduced by Galal et al. [1&9] and for active retrofitted specimens, those introduced by Yamakava et al. [6] have been used for obtaining confinement factor. The mentioned specimens have been subjected to a constant perpendicular and cyclic lateral load with the help of “Seismostruct” software [10]. The results of analyses have been evaluated and then compared with those of experimental studies [11] held in advance. There is a satisfying compatibility between the hysteresis curves obtained from either analytical specimens or experimental studies.

4. GENERAL PROPERTIES OF THE SPECIMENS

All the specimens have been considered rectangular, having 250x250 mm^2 dimensions and a height of 620 mm. The compressive strength of concrete is 18MPa. As shown in Figure (1), the longitudinal bars used for reinforcement is $12\phi12$ and $\phi4$ bars are used for transverse reinforcement. The spacing of transverse reinforcement was considered to be 50 mm at the beginning of the column and at the column-foundation connection, and 100 mm for the rest. For the passive retrofitted specimens, Aramid & Carbon FRP have been used and wrapped up to the height of 30 mm of the columns. The mechanical properties of these composites are shown in Table (1). For the active retrofitted specimens, prestressed FRP fibres having 40 mm width and spacing of 70 mm have been utilized.

Table 1: Mechanical properties of used FRP

Fiber Types	Tensile Strength (MPa)	Ultimate Strain (%)	Modulus of Elasticity (GPa)	Thickness (mm)
Carbon	3800	1.55	240	0.165
Aramid	2900	2.50	120	0.440

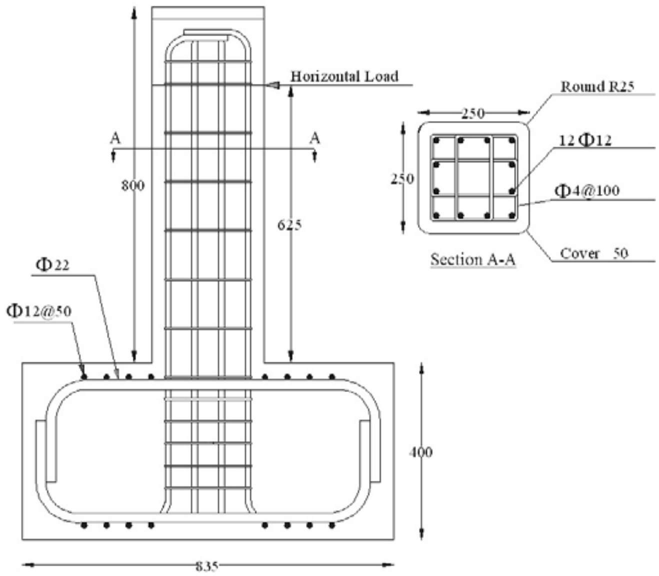

Figure 1. Section and elevation of the specimen

For convenience of studying, the specimens have been nominated as regarded in Table (2).

Table 2: Names adopted for the specimens

Description	Parameter	description	parameter
One layer CFRP	C1	Evident Column	C
One layer AFRP	A1	Passive Retrofit	PR
Prestressed CFRP fibre	SC	Active Retrofit	AR
Prestressed AFRP fibre	SA	Level 1 axial force ($N=0.2 \times A_g \times f'c$)	L1
Prestressed strain (ratio of ultimate strain of FRP)	1/n	Level 2 axial force ($N=0.4 \times A_g \times f'c$)	L2

5. INTRODUCING SEISMOSTRUCT SOFTWARE

SeismoStruct is a Finite Element program capable of predicting large displacement behaviour of space frames under static or dynamic loading, taking into account both geometric nonlinearities and material inelasticity. The spread of inelasticity along the member length and across the section depth is explicitly modelled, allowing for accurate estimation of damage distribution. The sectional stress-strain state of beam-column elements is obtained through the integration of a nonlinear uniaxial stress-strain response of the individual fibres in which the section has been subdivided. The subdivision of a typical reinforced concrete cross-section is depicted in the Figure (2). By employing a sufficient number of fibres (200-400 in spatial analysis), the distribution of material nonlinearity across the section area could be accurately modelled, even in the highly inelastic range. In this study, the number of fibres has been chosen to be 250 [10].

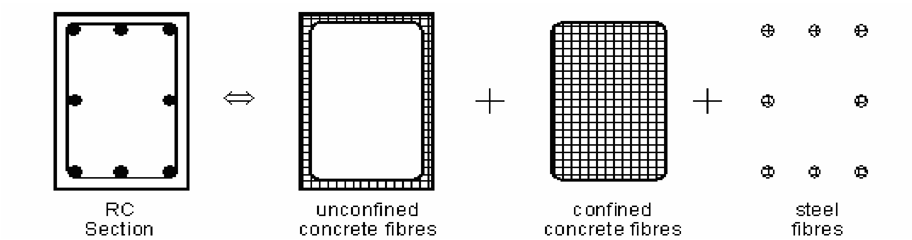

Figure 2. Fibres employed for RC section [10]

5.1. Loading

The aforementioned models have been subjected to two simultaneous loads; 1- Constant perpendicular axial load and 2- Time history lateral load. The analysis operation is based on time history static procedure. The constant perpendicular load is considered as a ratio of compressive strength of concrete column ($0.2\times A_g\times f'c$) which is equal to 225 KN. The time history lateral load is employed as "applied displacement", where the corresponding values are the displacement of column and time. These values are obtained by dividing lateral displacement of column (Δ) over its height (h) which is defined as "drift angle". At each drift angle (R), 3 successive cycles with the values of 0.5, 1.0, 1.5, 2.0 and so on have been applied as shown in Figure (3).

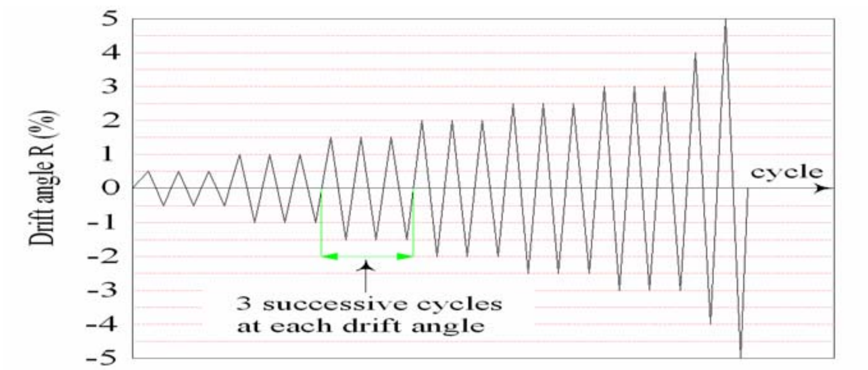

Figure 3. Time history lateral load versus drift angle

5.2. Analysis Results

5.2.1. Hysteresis Curves of Shear-Displacement Index

The obtained hysteresis curves of retrofitted columns wrapped with Carbon (PR-C1-L1) and Aramid (PR-A1-L1) in the passive state and the evident specimen (C-L1) have been shown in Figures (4 and 5). By the comparison of the given curves, the high efficiency of application of wrapped FRP can be observed on increasing the ductility and shear strength of retrofitted ones. Furthermore, the specimens retrofitted with Aramid have shown more adequate ductility than the Carbon though there is a negligible difference for shear strengths.

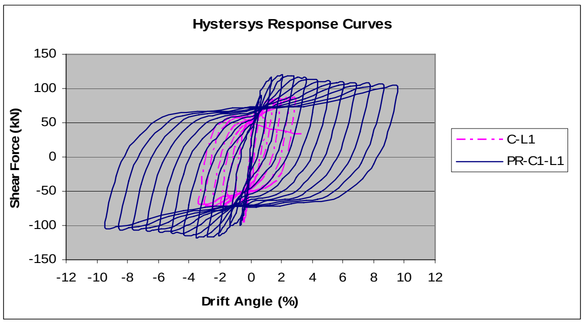

Figure 4. The hysteresis curves of PR-C1-L1 and C-L1

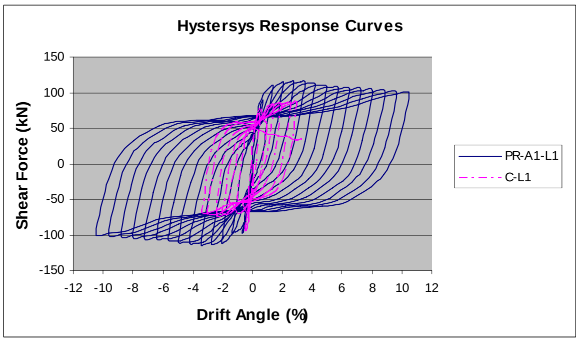

Figure 5. The hysteresis curves of PR-A1-L1 and C-L1

The obtained hysteresis curves of retrofitted columns wrapped with prestressed Aramid fibres (AR-CA-SA-1/2-L1) and unwrapped prestressed Carbon fibres (AR-SC-1/6-L1) where the prestressing values are considered as $\frac{1}{2}\varepsilon_{frp}$ and $\frac{1}{6}\varepsilon_{frp}$ respectively have been shown in the Figures (6 and 7). Regarding to the hysteresis curves, it can be found that prestressing of AFRP fibres results in more efficient to increase ductility and shear strength than the passive retrofitted one, especially for shear strength enhancement.

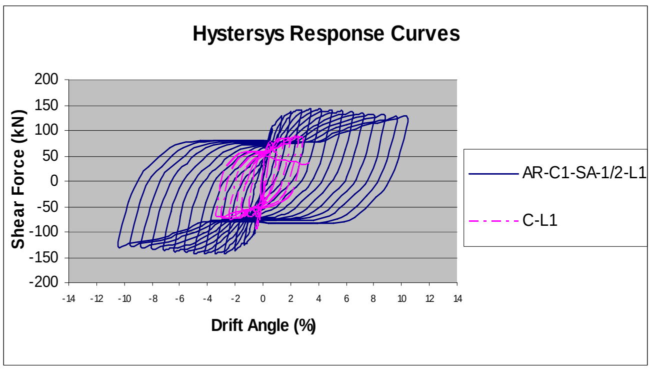

Figure 6. The hysteresis curves of AR-C1-SA-1/2-L1 and C-L1

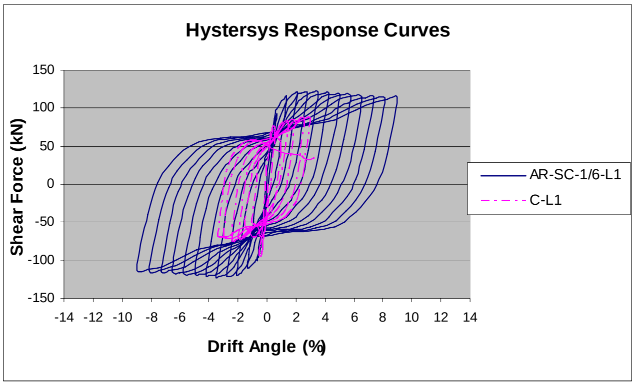

Figure 7. The hysteresis curves of AR-SC-1/6-L1 and C-L1

Regarding Figure (8), it is obvious that the active retrofitted specimen (AR-C1-SA-1/2-L1) in comparison to passive retrofitted one experiences more ductility and shear strength.

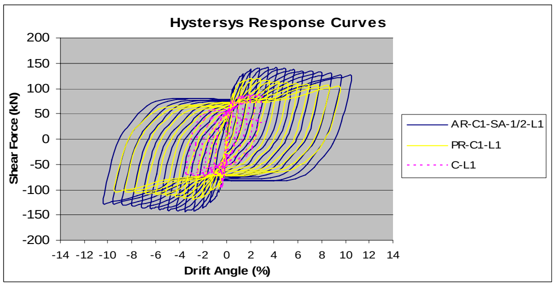

Figure 8. The hysteresis curves of AR-C1-SA-1/2-L1, PR-C1-L1 and C-L1

5.3. Energy Dissipation Diagrams

The amount of energy dissipation of the studied specimens, have been shown in Figure (9). The energy dissipation has a direct relation to the ductility of a structure. Regarding the mentioned figure, the amount of energy dissipation for active retrofitted specimen is more than the passive one.

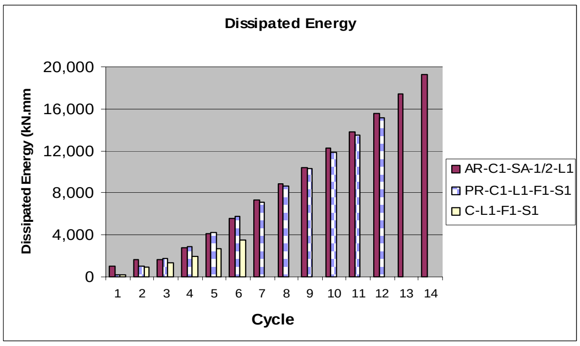

Figure 9. The energy dissipation of the specimens, loaded in level 1 (225 KN)

5.4. Shear Force Envelop Curve

The decrement or increment of the column shear force versus drift angle has been illustrated in Figure (10). The active retrofitted specimens have shown more suitable performance than the passive ones.

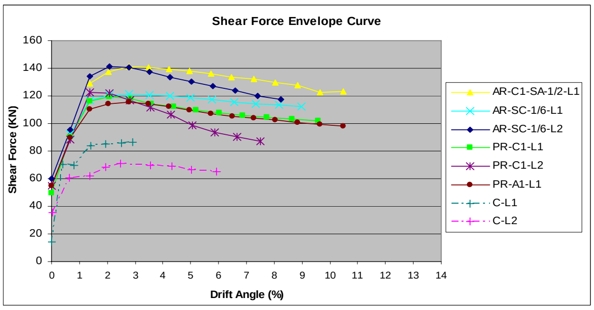

Figure 10. Shear force envelope curve

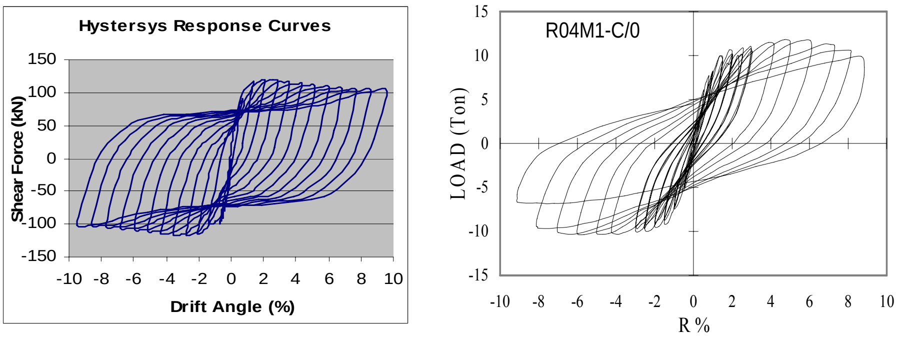

a. analytical model **b. experimental model [11]**

Figure 11. Analytical (PR-C1-L1) and experimental models

5.5. Comparison of Analytical Hysteresis with the Experimental Studies

On account of probable errors in analysis and also the differences between material properties in theory and experiment, a comparison has been done between the two analytical models and two concerned experimental ones. As shown in Figures (11 and 12), there is an acceptable conformity among analytical and experimental models.

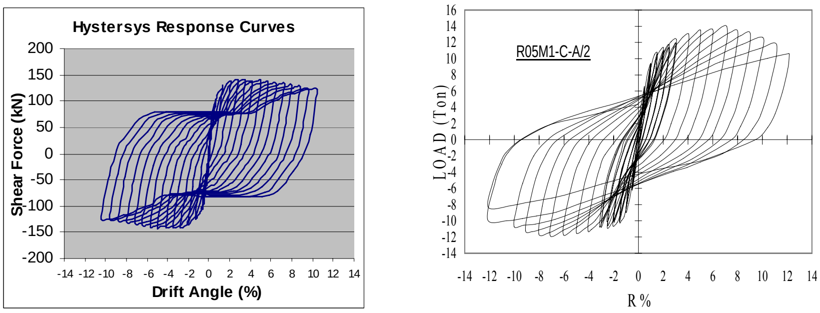

a. analytical model **b. experimental model [11]**

Figure 12. Analytical (AR-C1-SA-1/2-L1) and experimental models

6. CONCLUSIONS

The results derived from the abovementioned analyses are stated as below:

1. The amount of ductility, energy dissipation and shear strength of the columns would increase by retrofitting them using passive wrapped FRP.
2. AFRP composites have shown more ductility than CFRP composites as a consequence of higher strain capacity, though the shear strength of CFRP was higher than AFRP type.
3. By prestressing the FRP fibres especially AFRP, the amount of confinement and accordingly the shear and compressive strength of concrete would increase.
4. The ratio of increment of energy dissipation for retrofitted specimens varies from 1.7 to 4 times than evident specimens. Also the drift angle increases from 1.4 to 2.5 times.
5. Active retrofitted specimens have shown better behaviour than passive ones, around 20% increment in shear strength and 30-40% in energy dissipation.

REFERENCES

1. Galal, K. and Ghobarah, A., 2004. "Seismic Rehabilitation of Short Rectangular RC Columns", Journal of Earthquake Engineering, 8(1): pp. 45–68.
2. Rahaei, A. and Zomorodian, A., 2005. “Retrofitting of RC Structures Using Composite FRP”, Publication of University of Tafresh.
3. Galal, K., Arafa, A., and Ghobarah, A., 2005. "Retrofit of RC Square Short Columns", Journal of Engineering Structures, 27: pp. 801-813.
4. Saatcioglu, M. and Ozbakkaloglu, T., 2004. “Seismic Performance of High-Strength Concrete Columns Cast in Stay-in-Place FRP Formwork”, 13th World Conference on Earthquake Engineering, Vancouver, B.C., Canada. Paper No. 2719.
5. Saadatmanesh, I I. and Ehsani, M.R., 1997. “Repair of Earthquake Damaged Reinforced Concrete Columns with FRP Wraps”, ACI Structural Journal, 94(2): pp. 206-215.
6. Miyagi, T., Yamakawa, T., Li W. and Rahman, N., 2004. "A Study on Emergency Retrofit Using Prestressing Bars and Steel Plates for Damaged Columns", 13th World Conference on Earthquake Engineering, Vancouver, B.C., Canada. Paper No. 1169.
7. Saatmanesh, I I., Ehsani, M.R. and Li, M. W., 1994. “Strength and Ductility of Concrete Columns Externally Reinforced with Composite Straps”, ACI Structural Journal, 91 (4): pp. 434-447.
8. Mander, J. B., Priestly, M. J. N., and Park, R., 1988. "Theoretical Stress-Strain Model for Confined Concrete", Journal of Structural Engineering, ASCE, 114(8): pp. 1804-1826.
9. Galal, K. and Ghobarah, A., 2004. "Shear Capacity of Retrofitted Rectangular RC Short Columns", 13th World Conference on Earthquake Engineering, Vancouver, B.C., Canada. Paper No.1495.
10. SeismoStruct, 2005. European School for Advanced Studies in Reduction of Seismic Risk (ROSE School), University of Pavia, Italy.
11. Moghadam, H. and Mahdizadeh, M., 2005. “Retrofitting of Short RC Column Using FRP in Active and Passive States”, MSc Dissertation, Sharif University of Technology.

CD06-009

NUMERICAL MODELING OF UPLIFT RESISTANCE OF BURIED CONCRETE DUCTS & PIPES

M.S. Karimi[1], A. Arbabi[2], A. Haddad[1], E. Maroofi[2]
[1]Associated professor, School of Civil Eng., Semnan University, Semnan, Iran
[2]Graduated Student, School of Civil Eng., Semnan University, Semnan, Iran

ABSTRACT

This paper presents simulation of the pipe and soil system behavior during uplift displacement of pipelines in dense and loose sand by a 2D Finite Element modelling. As the first part of an ongoing research, this study focuses on the type of the soil failure mechanism which occurs in saturated condition at different burial depths and soil densities for constant pipe diameter.

Then, at this stage, pipe is considered as a linear elastic but very stiff material (compare to the soil). Using conventional continuum elements for the soil, its material behavior is modelled by the Drucker-Prager criterion. The numerical results compared to the laboratory observations and results as well as theoretical aspects.

Different laboratory failure mechanisms in loose and dense soils and also load-displacement curves impressively reproduced by the numerical modellings. Even, development of a gap below the pipeline in dense sand well captured by the FEM results. The essential effect of the soil density on the resistance force against uplift displacement is also well illustrated by the numerical results. To obtain a normalized upheaval load-displacement curve for this phenomenon, displacements were nomalised by the pipe diameter and also burial depth, however, another more suitable length parameter is under investigation.

Keywords: buried pipeline, uplift, sand, numerical modeling, FEM

1. INTRODUCTION

Lifeline pipes and ducts are commonly buried to provide environmental stability, thermal isolation and mechanical protection. In shallow trenches of saturated sand soils, buried pipelines and ducts are under threaten of progressive upheaval creep failure, during long term operation. This phenomenon called as upheaval buckling. This type of failure can cause the pipe to resurface at its bed-line and causes probable fracturing and damages, specially on the concrete ducts. This presents considerable operational problems and would have significant costs. The backfill soil in the trench and the pipe weight contribute to prevent the upheaval buckling load imposed to the pipeline. However, the resistance to the upheaval load provided by the soil is difficult to calculate.

A number of theoretical models has been developed to predict the resistance to upward movement provided by the pipeline/soil system. Generally, the models have considered the backfill soil without considering imperfections of the material during pipe placement. Also, no roughness effect of the pipe-soil contact surface was considered. It is widely accepted that the uplift resistance is complex and it is related directly to the geotechnical properties of the soil.

Most theoretical analyses assume some failure surfaces extending through the soil above the pipe. The simplest of these, reported by Matyas and Davies (1983) [1], is to assume a vertical slip surface extending above the pipe, Figure 1(a). The uplift resistance per unit length derived from the weight of soil above the pipe, the weight of soil displaced by the upper half of the pipe and the shearing resistance along the vertical slip surface, is given by the expression (1):

$$F_u = (1 - \frac{\pi D}{8H} + K \tan\phi_{ps} \frac{H}{D})\gamma' HD \tag{1}$$

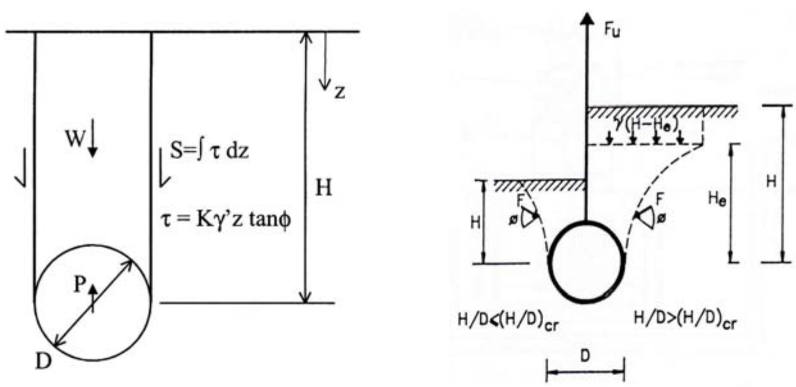

(a) (b)

Figure 1. Assumed failure mechanism by (a) vertical slip surface model [1], and (b) Curved slip surface [2]

in which γ'= effective soil unit weight, H= depth to centre of pipe, D= pipe diameter, φ_{ps} = angle of soil friction in plain strain, and K= lateral earth pressure coefficient. The value of K is often taken as K_0 , the at rest coefficient for loose sand, but its value in case of the dense sand is difficult to assess and can often be greater the one. Trautmann *et al* (1986) found [3], this theory has good agreement with the experimental data with K values of 0.5, 0.65 and 0.75 for pipes in loose, medium and dense sand, respectively. However, rupture surface above pipes are generally curved in broad agreement with the pyramidal shaped geometry analyzed by Meyerhof and Adams (1968) [2], shown in Figure 1(b). For shallow embedment, they ignored the second term in Eq. 1, and assumed K=0.95, while at greater depths the Eq. 2 was proposed:

$$F_U = \left(1 + \left(\frac{2H}{D} - \frac{H_e}{D}\right)\left(\frac{H_e}{H}\right) K \tan\phi_{ps}\right)\gamma' HD \tag{2}$$

where H_e= vertical extent of the rupture surface and depends on φ_{ps} and D .
The uplift force, N_u can be non-dimensionalised and re-expressed as uplift factor, f_d, as suggested by Schaminee *et al* (1990) [4]. This calculated using:

$$f_d = \frac{N_u - 1}{\left(\frac{H}{D}\right)} \text{, in which: } N_u = \frac{F_u}{\gamma' HDL} \quad (3)$$

where H is the instantaneous embedment depth measured to the crown of the pipe.

2. PREVIOS MODELLINGS' RESULTS

Over the last decade, the geotechnical aspects associated with upheaval resistance of the buried pipes have received considerable attention by the researchers. The focus of this attention has been aimed at the mechanism of soil failure and measurement of uplift load for various soil types. Because of practical difficulties and the high cost of conducting full scale field tests, the majority of these works has been done at small scale, or using geotechnical centrifuge modelling to simulate full scale conditions [5]. Barnsby *et al* (2001) [6] undertook a combined study using numerical FE analysis and scaled physical model testing to investigate soil resistance to upwards pipeline movement. Rezaee *et al* (2005) [7] carried out full scaled laboratory tests by improving the conditions of the experiments done by the Trautmann *et al* (1986) [3], which the FEM modellings of these experiments are presented in here.

3. EXPERIMENTAL OBSERVATION

The laboratory model built by Rezaee *et al* (2005) [7],[8], was including four parts: test box, coarse sub-grade, transducers & gauges, and water intake system to apply loading.
Rigid boundaries have to be located remote from the pipe so as not to interfere with failure mechanisms or effect on the effective stresses in deforming zone. According to the Trautmann suggestion [3], the width and height of the model should be chosen at least five times and its length nine times of the pipe diameter. Then, the test box dimensions- in toughened glass material of 1 cm thickness- considered 69cm of width and height, and 177cm of length, comparing to 11cm of the P.V.C pipe diameter. The test box was well braced not to deform during the loading. As it was necessary to increase the water surface uniformly, a coarse graded layer in 10 cm thickness spread over the test box floor. This layer also prevented cavitations and water worn effect on the soil. In Trautmann's test load was applied mechanically to the pipe, while in here, real uplift force of the water is applied to.
According to the tests done on the local area soil which used in this study, it classified as a poor aggregated sand (SP) with 2.66 of the solid density and 0.00225 cm/sec of the permeability rate. Its minimum and maximum specific weight were 1.38 and 1.78gr/cm^3, respectively. The internal friction angle for its loose case was equal to 32.9° and in dense case was 37.6°.

3.1. Laboratory Failure Mechanisms

In initial tests [7] using dense sand (γ=1.78 gr/cm^3), pipe was placed in depth equal to its diameter, i.e. 11 cm- from its center level to the soil surface. During the loading, two mechanisms of failure was observed; first, an **angled sliding block mechanism,** when the soil resistance reached to its utmost strength against upheaval forces, an inclined slip surface (about 20° diversion from the normal direction) created. This failure mechanism happened under small upheaval displacement (about 2mm)- as shown in Figure 2(a)- and this followed by a quick reduction in resistance upheaval force. By increasing the upheaval displacement, uplift resistance more decreased, and a second mechanism called **circulation mechanism**, observed around the pipe. At this stage, two gaps below the pipe formed [Figure 2(b)] and by progressing the upward moving of the pipe, these gaps were filled by flow dropping of the upper soils [Figure 2(c)]. As the curve in Figure 2 depicts after 10mm of displacement, uplift resistance force reaches to a constant amount, called as the residual force, with breaking of the inter-locking between the soil particles and make the pipe buoyant , and a considerable uplift displacement.

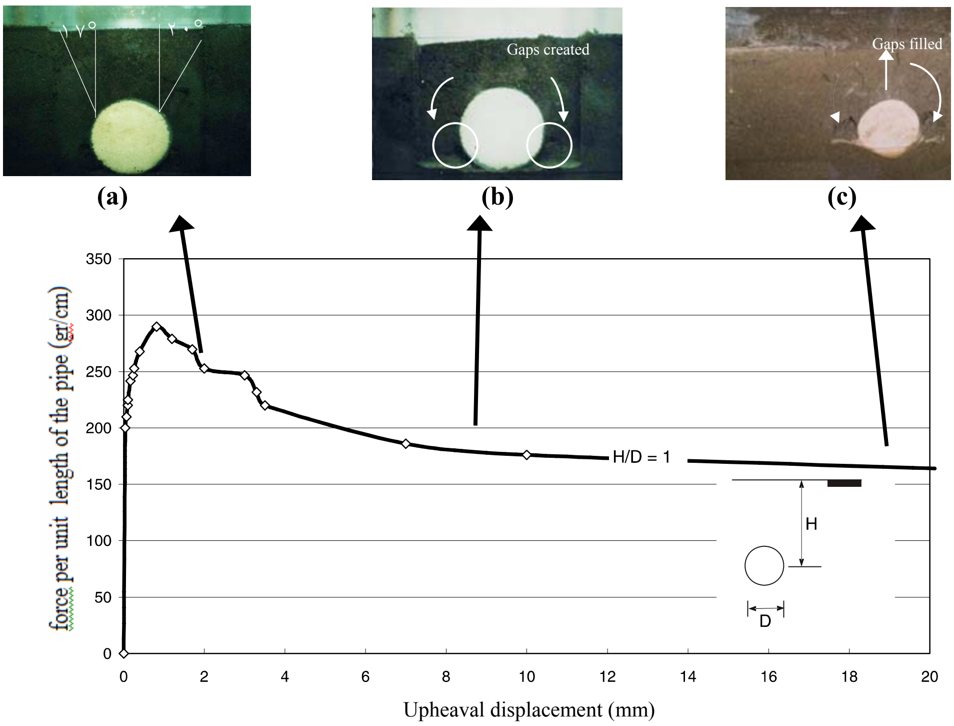

Figure 2. Load- displ. diagram of dense soil on the top of the buried pipe under upheaval force [7]

For the loose sand, only a circular mechanism observed as the failure mechanism of the soil. In this case, there was no sign of the sliding surfaces (trivial inter-locking) and from the beginning, only the two gaps created under the pipe, and further on, they were filled by flow dropping of the upper soil. Figure 3, illustrates the variation curves of the resistance load against upheaval displacement for different burial depths as well as sand densities.

As the curves depict, for embedment ratio of 0.7 and 1, the residual force in dense sand is less compare to the loose one. Its reason can be stated by this fact when the angled sliding block happened in dense soil, the soil reminds above the pipe is less than the amount in case of loose sand. As the resistance shear force depends on the surcharge loads, then the experimental results is justified. Also, as the curves show the effect of the density is more than the burial depth ratio in uplift load carrying capacity of the soil .

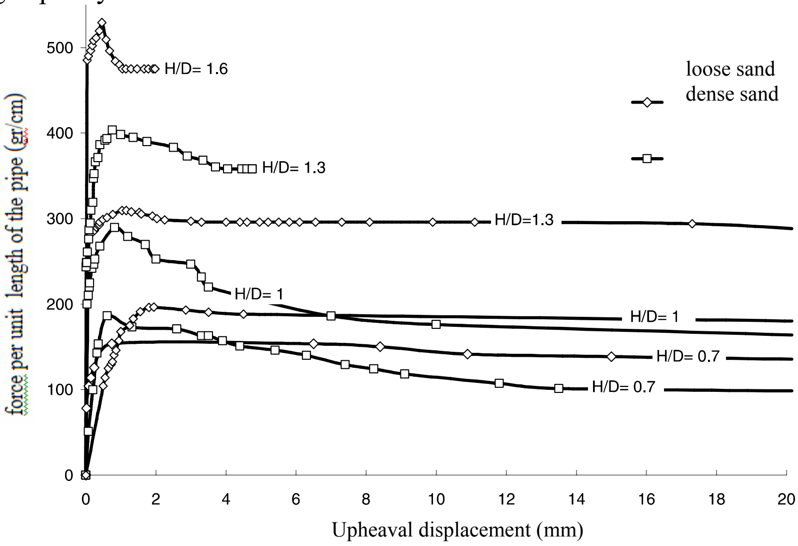

Figure 3. Upheaval load-displ. curves for different burial depths of loose and dense sand [8]

4. FINITE ELEMENT MODELLING

2D finite element plane-strain analyses was carried out to investigate the uplift behavior of circular pipeline to identify the effect of the most important parameters- i.e. the soil density and the embedment depth ratio- for further studies as well as to understand the mechanics of the soil around the pipeline in more details. Uplift capacities and soil failure mechanisms were found for different soil conditions and burial depth ratios. The influence of the mesh size, soil stiffness, ratio between the soil permeability and the loading rate as well as the soil/pipe contact surface effect has not been considered at this instance.

4.1. Soil & Pipe Characteristics

Conventional 8-noded quadrilateral serendipity element used to model the pipe and soil. Each node has two degrees of freedom of displacement. A non-associated Drucker-Prager elastic- perfectly plastic criterion chose to model soil material. This has a constant friction angle **φ**, a non-associated dilatancy angle **ψ**, and cohesion stress **c**, apart of its elastic parameters E, G and υ . For this example some of the parameters have been speculated to fit suitably the behavior of the soil/pipe system. This can be supported by the facts which are explained in below;

1. Experimental data in the literature are not enough to provide all values of parameters are needed in the numerical modelling. Then some of the values (listed in Table١) have been picked from other sources. This, would be the main source of discrepancy in the FEM results compared with the experiments, as the predictions are sensitive to in situ stresses and soil stiffness.
2. It should be pointed out that all analyses were run under plane-strain formulation which results more stiffer and higher load-carrying capacity structure compare to the plane-stress one, which is the more realistic option in 2D analyses for the tested buried pipe.
3. No potential cracking and fracture is modelled or allowed in the soil elements by loading progress. This also results a stiffer response of the numerical model.

Table 1: Soil and pipe material properties in numerical analysis

Material characteristics	soil		pipe
	Loose	Dense	
E	3-4 MPa	8-10 MPa	2.6×10^3 MPa
γ	1.45 gr/cm^3	1.78 gr/cm^3	------
υ	0.33	0.33	0.3
φ	32.9°	37.6°	------
c	2 KPa	5-10 Kpa	------
ψ	0°	0°	------

4. Dilatancy angle, measured by *tan* ψ, was constant and set to zero. This means that soil material can slide over the other without producing any vertical displacement and this should affect only marginally the results. However, this is reasonable for the loose soil, but for the dense one, more explanation is presented. As laboratory tests show, dilatancy angle decreases to zero with increasing plastic shear slipping or increasing normal confining pressure. These phenomena occur often combined, particularly in confined structures (for instance deep soil, in here), because shear slip with dilatancy necessarily induces normal compressive stresses. For the concerned case in here, the combined action of these two factors will also produce a faster degradation of the dilatancy angle under increasing confining pressure on the soil.

5. NUMERICAL RESULTS

5.1. Dense Sand

Figure 4-left gives upheaval load-displacement curve of FEM analysis for the dense soil with embedment depth ratio (H/D) equal to 1, which well correlates with

the experimental results, with about 10 percent difference in peak load. The numerical results show a steeper initial slope of the curve compare to that obtained from the experimental results. This may be due to a much higher values of the stiffness parameter E, which has not been provided in the reference text [7]. The higher initial stiffness caused increase in resistance of the soil against more shear deformation by resulting delay in forming the sliding surface, and increasing the stiffness of the soil. Also, Figure 5-left depicts contours of ε_{yy} on deformed mesh and Figure 5-right shows contours of the upheaval displacement, both at 0.4cm of vertical applied displacement. These pictures well demonstrate the sliding surface in dense sand which complies with the experiment.

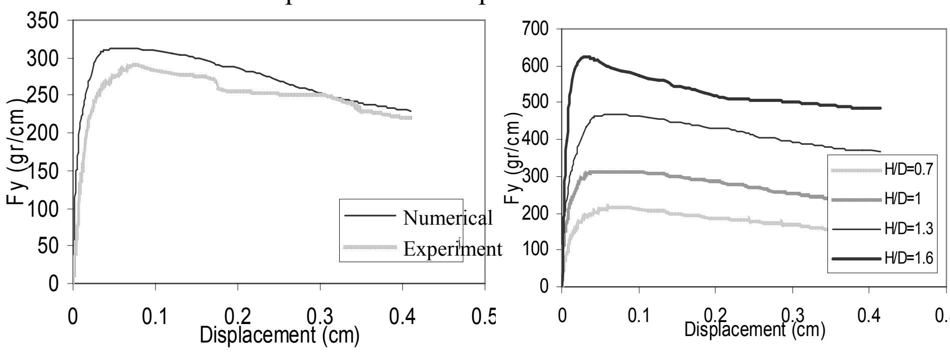

Figure 4. (left) Comparing numerical & experimental load-displacement curves for H/D=1 and; (right) comparing the same curves for different ratios of H/D, all for dense soil

More over, it is clear that none of the experimental and numerical results of the failure mechanism in dense soil, obeyed the vertical sliding surface theory.

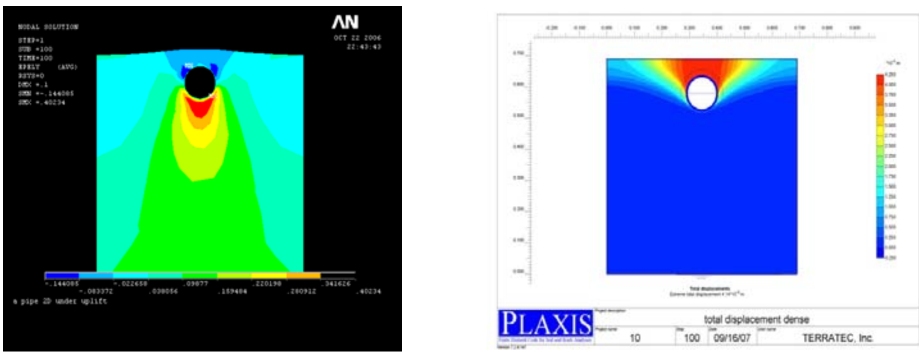

Figure 5. (left) Contours of the vertical strain and, (right) contours of the upheaval displacement at 0.4 cm of displacement in dense sand for H/D=1

As it was explained before, for dense soil, uplift resistance force reaches to its peak amount in small upheaval deflections. At this stage, the soil above the pipe has failed and this causes a progressive reduction in uplift force (the descending branch of the curve), to get its residual value in large displacements. Figure 4-right compares load-upheaval displacement curves for other ratios of H/D, obtained from the numerical analyses. These curves show the amount of deduction in resistance force varies with the ratio of H/D. Numerical results give lesser reduction in the peak resistance load compare to the experimental ones.

5.2. Loose Sand

Figure 6 draws load-displacement curves obtained numerically for the loose soil.

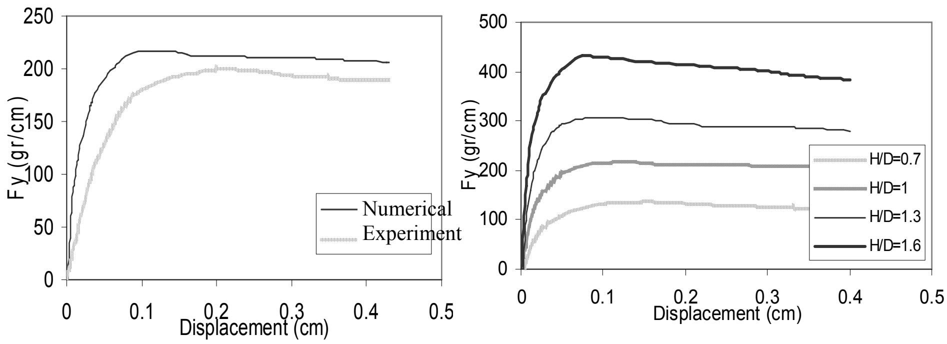

Figure 6. (left) Comparing numerical & experimental load-displacement curves for H/D=1 and; (right) comparing the same curves for different ratios of H/D, all for loose soil

All show by increasing the burial depth, upheaval load capacity has increased, but upheaval displacement corresponding to the peak load has decreased. However, numerical results in Figure 6-left gives a stiffer model compare to the experimental one with a steeper initial slope of the curve as well as a higher resistance peak load, but its failure mechanism has been well captured by the FEM results. As Figure 7.right shows, in loose sand, a lager region of deformed soil under circulation mechanism of the soil flow underneath the pipe has created (from beginning of the failure procedure). Figure 6-right compares load-upheaval displacement curves for other ratios of H/D, obtained by the numerical analyses which have the same trend explained for the dense sand. Figure 7-left also pictures deformed mesh at 0.4 cm of upheaval displacement for H/D = 1.3 (deflections magnified).

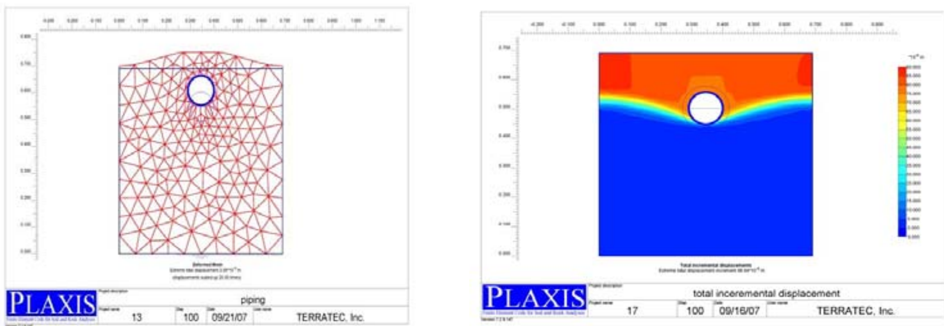

Figure 7. (left) Mesh deformation and, (right) contour of upheaval displacement at 0.4 cm of displacement in loose soil for the H/D=1.6

5.3. Further Studies

Figure 8-left depicts non-dimensional curves of the upheaval load-displacement variations for different ratios of the burial depth. The load-displacement results are re-plotted normalized by peak load and embedment depth, respectively. There is an excellent agreement between the results for the different embedment ratios, with all showing similar normalized stiffness and that d/H equal to 1% for dense sand and 1.5% for the loose sand. However, there is a bit concern for the correlation of the curves after peak load, specially in dense sand, which is, of course, of some shortcomings data, explained earlier. Also, there is less good agreement between the normalized curves when the results are normalized by pipe diameter (not presented here).

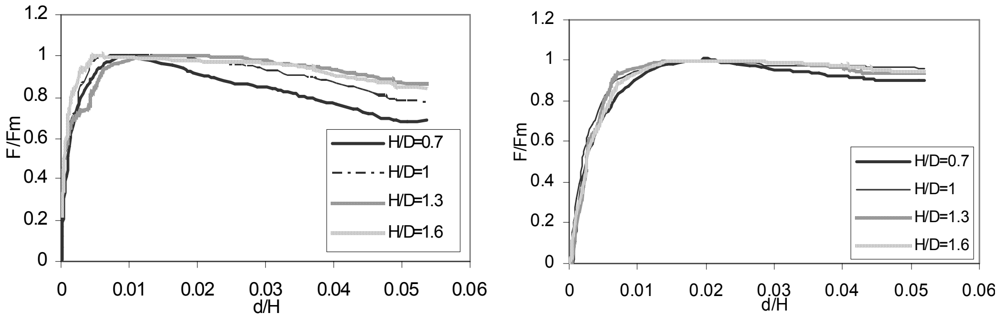

Figure 9. Normalized load -displacement curves (left) for dense sand and; (right) for loose sand

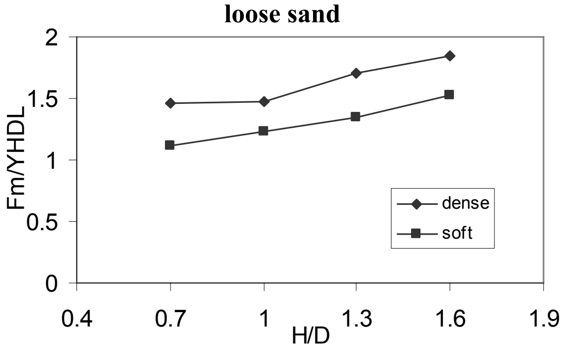

Figure 9. Normalized uplift peak load for various H/D ratios of dense and loose sand

Also, according to Eq. 3, normalized uplift peak load (N_u) has drawn as a function of H/D, in Figure 9, for dense and loose sand. As this figure shows, normalized peak load is increased by increasing the burial depth and it is more in dense sand compare to loose one for an equal depth ratio.

6. CONCLUSION

A series of Finite Element analyses have been described to examine the soil density and the embedment depth ratio on the uplift capacity and corresponding displacement on the failure of a circular buried pipeline subjected to vertical uplift. Finite Element model gave a very good approximation to the system behavior and was able to reproduce the complete deformation pattern of the system up to and beyond the peak load until total degradation of strength, without major numerical difficulties. The following conclusions have been drawn from this study:

1. Type and mechanism of failure differs in dense and loose sand. In dense sand, only sliding block mechanism with angled surfaces is formed, in small upheaval deformations, while in loose sand, deformation of wide range of the soil above the pipe is happening.
2. Corresponding displacement for the uplift peak load is much more in loose sand compare to the dense one, in the same H/D ratio.
3. Effect of the increase in soil density on uplift capacity is more than the effect of increase in burial depth ratio, which is very important of economical view.
4. Deduction in peak resistance force capacity to reach the residual force in dense sand is more then the loose one, as a result of different failure mechanisms.
5. Normalized N_u is increased with the embedment ratio, and its peak amount is more in the dense sand compare to loose one, for an equal H/D.
6. FEM results suggest that displacement should normalized by embedment depth, H, rather than pipe diameter, D.
7. Obtaining some crucial parameters carefully and some more refinement, FEM has potential for use in defining advanced design parameters and rules.

REFERENCES

1. Matyas, E. L., Davies, J. B. Prediction of vertical earth loads on rigid pipes. *Journal of Geotechnical Eng. ASCE, Vol. 109, No. GT2, Paper 17716.* 1983, pp. 190-201.
2. Meyerhof, G. G., Adams, J. I. The ultimate uplift capacity of foundations. *Canadian Geotechnical Journal.* 1968, Vol. 5, 4, pp. 225-244.
3. *Soil Response for Pipeline Upheavall Buckling Analyses: Full-scale Laboratory tests and Modelling.OTC 6486.* Schaminee, P.E.L., Zorne, N.F., and Schotman, G.J.M. Houston, Texas : s.n., May 7-10, 1990. 22nd Annual Offshore Technology Conference. pp. 563-572.
4. Dickin, E.A.,. Uplift Resistance of Buried Pipelines in Sand. *Soils and Foundations.* 1994, Vol. 34, 2, pp. 41-48.
5. *Numerical and Centrifuge Modelling of the Upheaval Resistance of Buried Pipelines.* Barnsby, M.F., Newson, T.A., Brunning, P. Rio de Janeiro, Brazil: S.N., June 3-8, 2001. 20th International Conference on Offshore Mechanics and arctic engneering .
6. Trautmann, C. H. O'Rourke, T.D. and Kulhawy, F. H. Uplift force-displacement response of buried pipe. *Journal of Geotechnical Eng. Division, ASCE.* 1985, Vol. 111, 9, pp. 1061-1075. Paper 1986.
7. *Laboratory modelling of the buried pipe behaviour under uplift load.* Rezaee, D., Janalizadeh, A., Mirzagoltabar, A.R. Teharn, Iran : University of science and industry, 2005, in Farsi.
8. *Laboratory study of the buried pipe behaviour under uplift load.* Rezaee, D., Janalizadeh, A., Mirzagoltabar, A.R. Teharn, Iran : University of science and industry, 2005, in Farsi.

A SENSITIVITY ANALYSIS ON THE CHLORIDE-INDUCED CORROSION INITIATION TIME OF RC ELEMENTS

J. Sobhani[1], A.A. Ramezaninpour[2]
[1]Assistant professor, Building and Housing Research Center, and member of CT&D Research Center of Amirkabir University of Technology, Tehran, Iran
[2]Professor, Dept of Civil Eng., and head of CT&D Research Center of Amirkabir University of Technology, Tehran, Iran

ABSTRACT
One of the most important causes for reinforcing steel corrosion is the presence, ingress and attack of chloride ions on RC elements. Reinforcement corrosion has been widely reported in the literature over the last two to three decades. They cause localized breakdown of the passive film that initially formed on steel as a result of the alkaline nature of the pore solution in concrete. In this paper, a sensitivity study was carried out on the influence of the effective parameters of corrosion on the corrosion initiation time, both in uncracked and cracked concrete elements. The results of the study shows a high sensitivity of the corrosion initiation time, regarding C_s (chloride surface concentration) and C (cover depth), in uncracked concrete, and on the other side, more sensitivity of the ratio of the w/l (crack width to crack spacing) in cracked concrete elements.

Keywords: reinforcement corrosion; sensitivity analysis; electrochemical process; corrosion initiation time cracked concrete

1. INTRUDUCTION
Reinforcement corrosion has been widely reported in the literature over the last two to three decades 1, 1. Chloride-induced corrosion of the reinforcing steel is known to be a major cause of premature rehabilitation of many RC structures like bridge decks 3. Moreover, reinforcement corrosion in concrete is the predominant causal factor for the premature deterioration of reinforced concrete structures, leading to structural failure. Failure does not necessarily mean structural collapse only, but also includes loss of serviceability, characterized by concrete cracking, spalling, and excessive deflection. Clearly detection and monitoring of reinforcement corrosion in concrete is of significant practical importance if premature failure of RC structures is to be prevented 3. In this regard, the present paper tries to define the corrosion of reinforcements in concrete, mostly due to the chloride ion ingresses, develop and describe the advanced models for chloride-induced corrosion both in cracked and uncracked elements and finally, study the influence of various factors on the corrosion initiation life period.

2. CORROSION OF REINFORCEMENTS

Because of high alkalinity of concrete media 1, 1, 4, 5, (pH >13.5), steel remains passive within the concrete by forming a thin oxide layer on steel rebar surface. In addition, well-consolidated and properly cured concrete with a low w/c ratio has a low permeability, which minimizes ingress of detrimental stuffs either gaseous or liquid, such as chloride, carbon dioxide, oxygen, moisture, and etc. to the steel surface. Furthermore, high electrical resistivity of concrete 1 restricts the rate of corrosion by reducing the flow of electrical current from the anodic to the cathodic sites. The passive film remains stable as long as the composition of the pore solution remains constant. The protective film is destroyed when there is a sufficient concentration of chloride ions and or carbonation around the reinforcement. Therese ions and other detrimental, stemming from environment, deicing salts, and etc penetrate into concrete. Once the reinforcing steel was depassivated and it was supplied with oxygen and water (humidity), metal dissolution (corrosion in the form of rust formation, loss in cross section) may start. 6

3. ELECTROCHEMICAL PROCESS OF CORROSION

Reinforcement corrosion is an electrochemical process. Similar to a flash battery, corrosion take place by coupled cathodic and anodic reactions in an electrolyte like concreter pore water (known as complex electrolyte). The surface of the corroding steel functions as a mixed electrode that is a composite of anodes and cathodes electrically connected through the body of steel itself, upon which coupled anodic and cathodic reactions take place. Concrete pore water functions as an aqueous medium, i.e., a complex electrolyte. Therefore, a reinforcement corrosion cell is formed.

3.1. Anodic and Cathodic Reactions

Generally, anodic and cathodic reactions are referred as oxidation and reduction process respectively. At anode, dissolution of metallic steel occurs, while at the cathode the reaction leads to reduction of dissolved oxygen to form hydroxyl ions. By the way, the possible anodic and cathodic reactions are as follows 1, 7, 1, and 7.

At anode;

$$3Fe + 4H_2O \rightarrow Fe_3O_4 + 8H^+ + 8e^- \quad (1)$$

$$2Fe + 3H_2O \rightarrow Fe_2O_3 + 6H^+ + 6e^- \quad (2)$$

$$Fe + 2H_2O \rightarrow HFeO_4^- + 3H^+ + 2e^- \quad (3)$$

$$Fe \rightarrow Fe^{2+} + 2e^- \quad (4)$$

At cathode;

$$2H_2O + 4O_2 + 4e^- \rightarrow 4OH^- \quad (5)$$

Or

$$2H^+ + 2e^- \rightarrow H_2 \quad (6)$$

Table 1: State of reinforcement corrosion at various ph levels 1

pH of concrete	State of reinforcement corrosion
Below 9.5	Commencement of steel corrosion
At 8.0	Passive film on the steel surface disappears
Below 7	Catastrophic corrosion occurs

Table 2: Corrosion risk in concrete containing chlorides 11

Total chloride (wt.% of cement)	Condition of concrete adjacent to reinforcement	Corrosion risk
Less than 0.4% Carbonated High	carbonated	High
	Uncarbonated, made with cement containing less than 8% C_3A	Moderate
	Uncarbonated, made with cement containing 8% or more C_3A	Low
0.4% - 1.0 %	As above	High
	As above	High
	As above	Moderate
More than 1.0%	All cases	High

4. FFECT OF ACIDIC GASEOUS AGENT IN CORROSION

The corrosive effect of carbonation and other acidic gases, such as So_2 and No_2 are due to their tendency to reduce the pH of the concrete. The fall of pH to a certain level may cause commencement of reinforcement corrosion, loss of passivity of concrete against reinforcement corrosion, and catastrophic reinforcement corrosion as indicated in Table 1.

Chloride in concrete may be in the forms of: i) Acid soluble chloride, which is equal the total amount of chloride present in the concrete or that is soluble in nitric acid 8, ii)Bound chloride, which is the sum of chemically bound chloride with hydration products of the cement, such as the C_3A or C_4AF phases, and loosely bound chloride with C–S–H gel, and iii) Free or water-soluble chloride, which is the concentration of free chloride ions (Cl^-) within the pore solution of concrete, and is extractable in water under defined conditions. It is generally recognized that only the free chloride ions influence the corrosion process 9. It is reported 10 that the receptivity decreases and corrosion rate increases with an increase in the chloride content. However, the change in pH is found to be insignificant due to a change in the chloride content of concrete 10. The risk of reinforcement corrosion associated with the levels of chloride content in both uncarbonated and carbonated concrete is presented in Table 2 11.

5. CHLORIDE-INDUSED CORROSION MODELING

5.1. Chloride Diffusion Model

Chloride (or ion) diffusion is a specific case of scalar field problem that are encountered in almost all branches of engineering and physics. Most of them can viewed as special forms of the general Helmholtz equation given by 12

$$\frac{\partial}{\partial x}\left(k_x \frac{\partial \phi}{\partial x}\right)+\frac{\partial}{\partial y}\left(k_y \frac{\partial \phi}{\partial y}\right)+\frac{\partial}{\partial z}\left(k_z \frac{\partial \phi}{\partial z}\right)+Q=c\rho\frac{\partial \phi}{\partial t} \tag{7}$$

where $\phi(x,y,z)$ is the field variable to be solved.
For the diffusion of Chloride in one dimension, it can be shown that the governing equation reduced to Fick's Second Law of Diffusion:

$$\frac{\partial c}{\partial t}=-D\frac{\partial^2 c}{\partial x^2} \tag{8}$$

Clifton (1993) derived a closed form solution to Fick's Law using an apparent diffusion constant D_{ac}. Beginning with Fick's Law and assuming a constant surface chloride concentration and an initial chloride-free surface, the closed form solution is 14

$$C(x,t)=C_0\left(1-erf\left[\frac{x}{2\sqrt{D_{ac}t}}\right]\right) \tag{9}$$

Where C_0 is the constant surface concentration, kg/m^3, t is the time of exposure to C_0, *years* and D_{ac} is the apparent diffusion constant, $cm^2/year$. By solving the Eq. 9 on a continuum media like a RC bridge deck shown in Figure 1, the time to corrosion initiated could be gained as follows:

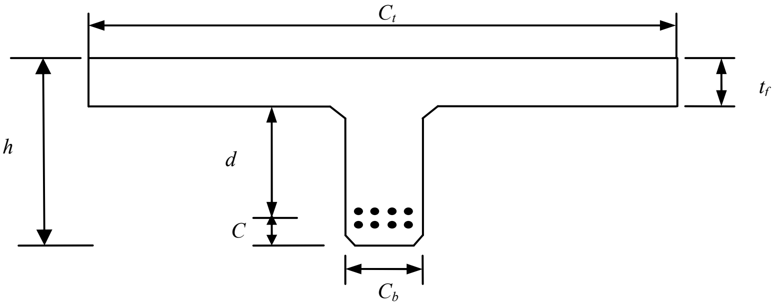

Figure 1. Schematic of a typical RC element.

$$T_i=\frac{C^2}{4D_c}\left[erf^{-1}\left(\frac{C_s-C_{cr}}{C_s}\right)\right]^{-2} \tag{10}$$

Where T_i is the corrosion initiation time and other terms are defied before.

5.2. Time-Dependent Diffusion Coefficient

Midgley et al. (1984) conducted experiments using samples of hardened cement pastes 12. They calculated apparent diffusion coefficient from the quantity of chloride ions present in at the distance of penetration. Mange and Molloy (1994) derived a closed form solution to Fick's Law for a time-dependent diffusion coefficient 13.

$$\frac{\partial c}{\partial t} = \underbrace{D_i t^{-m}}_{D_c} \frac{\partial^2 c}{\partial x^2} \tag{11}$$

Where D_i is a time dependent diffusion coefficient and m is an empirical coefficient based on the concrete water-cement ratio (*w/c*). They 12 cited work by Conjeaud and Buenfeld and Newman that indicated that the rate of ingress of chloride ions into concrete decreased with time. This finding has been strengthened by the work of Weyers et al. (1994) reported previously 12. Mangat and Molloy concluded that the underlying common cause of the time-dependence of chloride ion diffusion on the pore structure of concrete, which changes with time 13. They exposed mixes of concrete-to-sea water and monitored the chloride diffusion. All results showed that D_{ac} decreased with time 13.

5.3. Effect of Chloride Binding

Clifton, (1993) expressed that because chloride ions may react with the tricalcium aluminate of Portland cement (C_3A), the concentration has two components: concentration of bound chloride ions C_b and concentration of free ions C_f related by constant R 14

$$C_b = R.C_f \tag{12}$$

However, carbonation or sulfate ions can release the bound chloride ions, and usually R assumed to be 0 14. Moreover, Oh and Jang (2003) consider the effect of chloride binding in the ingress of the chloride into the concrete 15. They study the general form of Fick's law in the form as follows 15

$$\frac{dC_f}{dt} = \frac{dC_f}{dC_t} div\left[D_{cl} grad\left(C_f\right)\right] \tag{13}$$

where C_t is the total chloride ions (per weight g/g), C_f is free chloride ions (per weight g/g), t is time, D_{cl} is diffusion coefficient, and dC_f / dC_t is the binding capacity 15. The binding capacity is herein defined as the ratio between the free chloride and total chloride ions and can be rewritten as follows 15

$$C_t = C_f + C_b \tag{14}$$

$$\frac{dC_f}{dC_t} = \frac{1}{1 + (dC_b / dC_f)_b} \tag{15}$$

where C_b is the bound chloride ions (per concrete weight g_{cl}/g_{con}), and $dC_b\ /dC_f$ represent binding isotherm is usually affected by concrete mixture characteristics, and some features have been considered in their study. The base of chloride isotherm is that some chloride ions penetrated in to the concrete are bound and do not affect the corrosion of steel bars. This isotherm is directly related to the amount of calcium silicate hydrate (C-S-H) that is found during the hydration process of cement. Xi, and Bazant (1999) 16 and Jennings and Tennis (1994) 17 are also proposed modified Powers Model to represent the chloride binding isotherm. The overall form of the model is 15, 16, and 17

$$C_b' = (C_f')^A 10^B \tag{16}$$

where C'_b is the bound chloride ions (per gel weight mg_{cl}/g_{gel}), C'_f is the free chloride ions (per gel weight mg_{cl}/g_{gel}), A and B are constants 15.

5.4. Cracked Concrete

Boulfiza et al. (2003) [19] used Darcy's Law to predict the chloride ions ingress in uncracked and cracked concrete. They developed a rational model for this purpose [19]. This model considers water flow properties in matrix and crack, both in saturated and unsaturated cases. Boulfiza et al, proposed a Simplified Smeared Approach (SSA) to model the chloride ions ingress into the cracked concrete 18. In this approach, it is assumed that chloride ions ingress into cracked concrete can be approximated using Fick's Second Law of Diffusion in which the following average coefficient is used

$$D_{av} = D_0 + \frac{w}{l} D_{cr} \tag{17}$$

where D_{av} is the average diffusion coefficient, D_0 is the diffusion coefficient of uncracked concrete, w is the crack width, l is the crack spacing, and D_{cr} is the diffusion coefficient inside the crack, as shown in Figure 3 18. Hence, the average diffusion coefficient is proportional to the crack width and inversely proportional to the crack spacing. Also, they proposed a Simplified Discrete Approach (SDA) 18 to evaluate the chloride ingress into the concrete. In this approach, chloride diffusion through the crack has been shown to obey the following equation which proposed by Tsukahara and Umoto (2000) 18 , and Kato et al. (2005) 19.

$$C_c(x,t) = \alpha\sqrt{x} + s\sqrt{t} \tag{18}$$

where, C_c is the chloride concentration, $\boldsymbol{x}$ is the location along the crack wall starting from spacemen surface, t is time, and α and s are two empirical constants. Chloride diffusion through the matrix is assumed to obey Fick's law under variable conations and given by

$$C_c(x,t) = \alpha\sqrt{t}\left\{\exp\left[\frac{x^2}{4Dt}\right] - \frac{x\sqrt{\pi}}{2\sqrt{Dt}}\, erfc\left[\frac{x}{2\sqrt{Dt}}\right]\right\} \tag{19}$$

Boulfiza et al. showed that the two methods (13 and 14) have a good agreement between in their predictions 18.

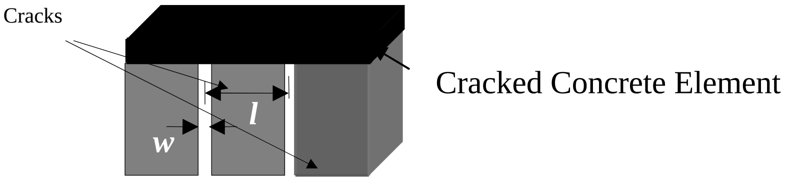

Figure 2. Schematic representation of crack l and crack width

Li et al. (2003) 20, proposed a new solution for prediction of chloride ingress in reinforced concrete flexural members. They use fundamental mechanism of diffusion of chloride ions in concrete. Based on a combination of Knudsen flow and viscous flow, an analytical solution is derived for the prediction of chloride ingress in concrete flexural members (Figure 5) 20. Also they verified the proposed model by experimental results. By applying some boundary and initial condition on Fick's Law, Li et al., proposed the following equations for chloride ingress in the cracked-concrete:

when $C_s(t) < C_r$

$$C(x,t) = C_s(t) + \left[C_i - C_s(0)\right] \sum_{n=1}^{\infty} U_n(x,t,D_{c1}) - \sum_{n=1}^{\infty}\int_0^t C_s^{'}(\tau) U_n(x,t-\tau,D_{c1}) d\tau \tag{20}$$

if $C_s(t)$ assumed to be constant as for almost all current solution, then the equation (14) becomes

$$C(x,t) = C_s + \left[C_i - C_s\right] \sum_{n=1}^{\infty} U_n(x,t,D_{c1}) \tag{21}$$

when $C_s(t) > C_r$,

$$C(x,t) = C_s(t) + \sum_{n=1}^{\infty} \bar{h}_n U_n(x,t,D_{c2}) - \sum_{n=1}^{\infty}\int_0^t C_s^{'} U_n(x,t,D_{c2}) d\tau \tag{22}$$

where,

$$\bar{h}_n = \left[C_i - C_s(0)\right]\frac{U_n(x,T_r,D_{c1})}{U_n(x,T_r,D_{c2})} - \int_0^{T_r} C_s^{'}(\tau)\frac{\left[U_n(x,T_r-\tau,D_{c1}) - U_n(x,T_r-\tau,D_{c2})\right]}{U_n(x,t,D_{c2})} d\tau \tag{23}$$

and when $C_s(t)$ assumed to be constant, then the equation (17) becomes

$$C(x,t) = C_s + (C_i - C_s)\sum_{n=1}^{\infty}\frac{U_n(x,T_r,D_{c1})U_n(x,t,D_{c2})}{U_n(x,T_r,D_{c2})} \qquad (24)$$

where, in the above equations, C_i is the initial chloride concentration, C_s is the surface chloride concentration, C_r is the critical chloride concentration, t is the time, T_r is the time at which the critical chloride concentration is attained and, x is the location. And,

$$U_n(x,t,D_c) = \frac{4}{(2n-1)\pi}e^{\frac{D_c 2n-1^2\pi^2}{4l^2}t}\sin\frac{(2n-1)\pi x}{2l} \qquad (25)$$

where, $D_c = 2\overline{v}_c\lambda_c$, $D_{c1} = 2\overline{v}_0\lambda_c$, where λ_c is the mean free path of chloride ions, and υ_c is the average velocity of chloride ions, and $D_{c2}=\xi w^2$; in which ξ is an empirical calibration factor, w is the width of crack, and l is the length of crack 20[21].

5.5. Non-Constant Surface Chloride Concentration

In concrete bridge decks, surface chlorides are derived from the deicing salts used during winter maintenance operations, and in particular locations, from exposure to sea water 21. Kassir and Ghosn 2002), showed that surface chloride concentration may not be constant 21. Phurkhao and Kassir (2005) modeled surface chloride by a ramp-type variation 22, so in this case the boundary condition change to

$$C(0,t) = f(t) \qquad (26)$$

where

$$\begin{aligned} f(t) &= \frac{C_0}{t_0}t, && 0 \le t \le t_0 \\ f(t) &= C_0 && t \ge t_0 \end{aligned} \qquad (27)$$

They solved the Fick's law (Eq. 7) for the above boundary condition 22. By applying some mathematical techniques, they derived a closed form solution to initiation time of chloride-induced corrosion as follows

$$\begin{aligned} \frac{C(x,t)}{C_0} &= g(x,t), && t \le t_0 \\ \frac{C(x,t)}{C_0} &= g(x,t) - g(x,t-t_0), && t \ge t_0 \end{aligned} \qquad (28)$$

where

$$g(x,t) = \frac{t}{t0}\left[-\frac{x}{\sqrt{\pi D0t}}e^{(-x^2/4tD_0)} + \left(1+\frac{x^2}{2D_0t}\right)\mathrm{erfc}\left(\frac{\mathrm{x}}{\sqrt{4\mathrm{D}_0t}}\right)\right] \qquad (29)$$

The result of numerical study showed that in the ramped-type chloride case, the time predicted to initiate corrosion is grater than the constant chloride concentration one 21-23].

6. SENSITIVITY ANALYSIS STUDY

Here some numerical results are presented to verify the above mentioned models. The effect of the various terms in the diffusion of chloride ions into the uncracked and cracked RC structures are evaluated respectively:

6.1. Uncracked Concrete

Sensitivity of diffusion coefficient (D_c)

Figure 3 shows the effect of diffusion coefficient on the corrosion initiation time. It can be seen that by 10 times decrease in diffusion coefficient the initiation time increased up to 10 times. This shows a linear inverse relationship between T_i and D_c as in model Eq. 9.

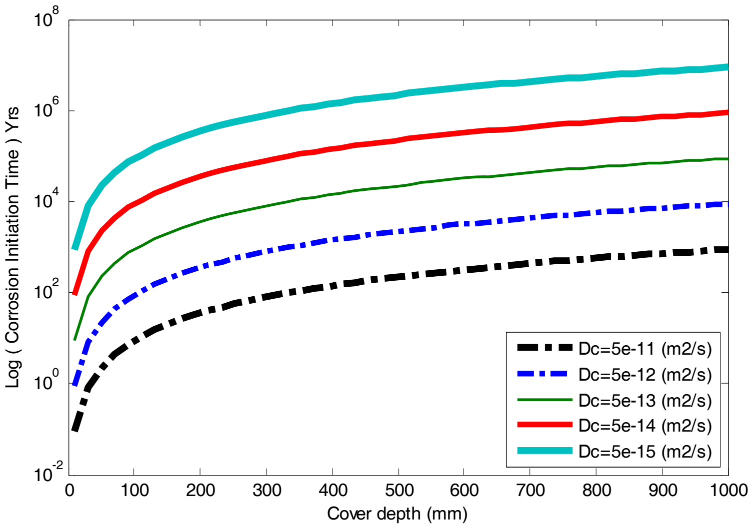

Figure 3. Effect of D_c on corrosion initiation time (C_s=0.5%, C_{cr}=0.275%)

6.2. Sensitivity of Surface Chloride Concentration (C_S)

The effects of surface concentration of chloride ions are shown in Figure 4. As seen in this figure, two times increasing in C_s leads to 224 times decrease in corrosion initiation time. This finding shows a strong relation between C_s and T_i.

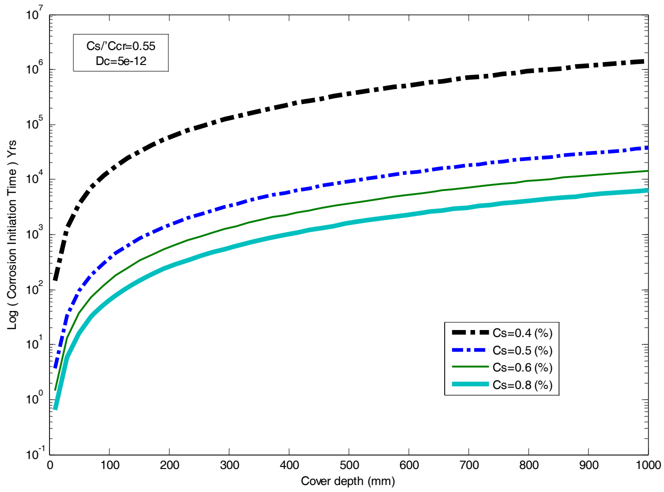

Figure 4. Effect of *C*s on corrosion initiation time (C_s / C_{cr}=0.55, D_c=5×10^{-12})

6.3. Sensitivity of Critical Chloride Concentration (C_{CR})

It is a natural effect that by increasing the threshold value for corrosion initiation which here, is the critical chloride concentration, leads in longer time for corrosion initiation. This effect is shown in Figure 5. It can be seen that three times increase of C_{cr} would increase T_i about 3.9 times.

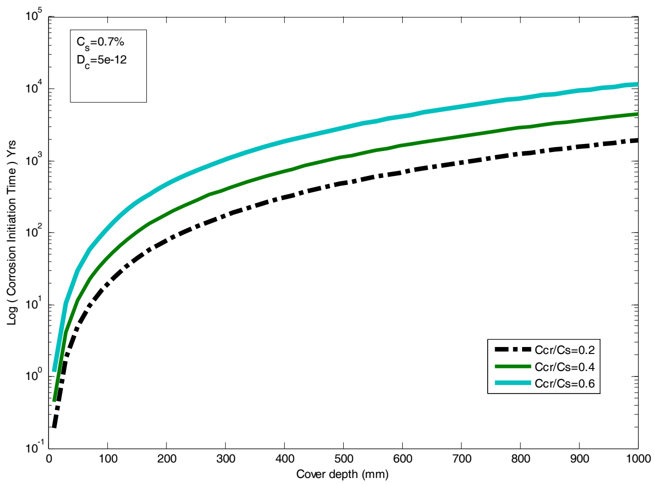

Figure 5. Effect of C_{cr} on corrosion initiation time (C_s =7%, D_c=5×10^{-12})

6.4. Sensitivity of Cover Depth Thickness (C)

Figure 6 shows the effect of cover depth on the corrosion initiation time. It is obvious that the more concrete available at the outer surface of the reinforcements, the time to chloride ions to reach the steel surface would be reduced. This can be verified in Figure 6, when 3 times increase in cover depth leads to 9 times decrease in corrosion initiation time.

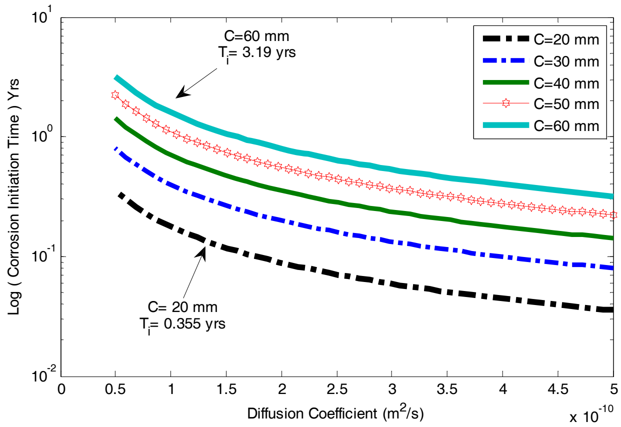

Figure 6. Effect of cover depth (C) on the corrosion initiation time (D_c=5×10^{-12})

6.2. Sensitivity of crack effect

Based on the Simplified Smeared Approach (SSA) developed by Boulfiza et al., three crack types assumed for RC elements (Figure 2) and the corrosion initiation time was estimated as shown in Figure 7. As depicted here, by increasing the crack width and crack spacing, the corrosion initiation time would be reduced in a logarithmic manner. By doubling the crack width, T_i increase up to 1.5 times, however, by 10 times increase in crack spacing, cause T_i to be decrease up to about 6 times.

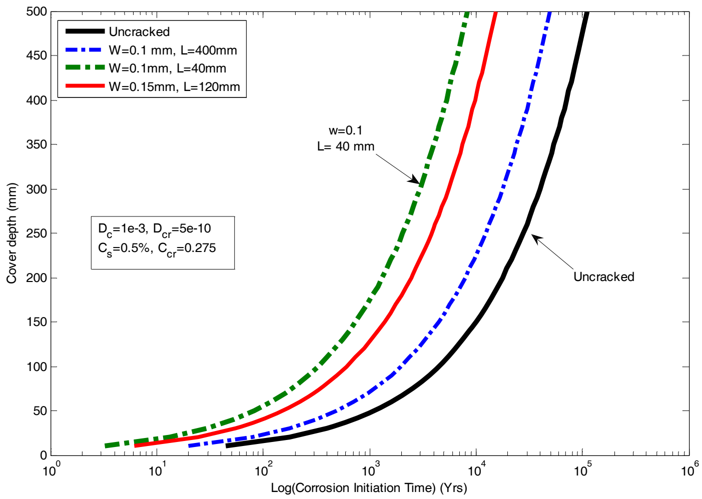

Figure 7. Effect of crack on the corrosion initiation time

7. CONCLUSION

In this paper, the corrosion of steel embedded in concrete as the reinforcements was studied. The main factors affecting the electrochemical corrosion process of reinforcements were described and anodic-cathodic reactions of corrosion were introduced. Various chloride-induce corrosion models were explained based on the conceptual differential equations. The time to corrosion initiation was explored both in uncracked and cracked concrete. Moreover a numerical study was carried out on the effects of the main factors of the corrosion process on the corrosion initiation time in intact concrete structures and also in cracked concrete structures. It was concluded that the surface chloride concentration has main influence on the corrosion initiation time. Moreover it was found that corrosion initiation time is very sensitive to the cover depth of concrete and the ratio of crack width to the crack spacing.

REFERENCES

1. Ahmad S., "Reinforcement corrosion in concrete structures, its monitoring and service life prediction–a review" Cement & Concrete Composites 2003, Vol. 25, pp. 459-471.
2. Sobhani J., and Ramezanianpour A.A., "chloride-induced corrosion of RC structures, ASIAN Journal of Civil Engineering (Building and Housing) 2007, Vol. 8, No. 5, pp. 531-547.
3. Kirkpatricka T.J., Weyersa R.E., Sprinkelb M.M., and Anderson-Cookc C.M., "Impact of specification changes on chloride-induced corrosion service life of bridge decks", Cement and Concrete Research 2002, Vol. 32, pp. 1189-1197.
4. Li C.Q., "Life Cycle Modeling of Corrosion Affected Concrete Structures-Initiation", ASCE Journal of Materials in Civil Engineering 2003, Vol. 15, No. 6, pp. 594-601.
5. Yeih W., and Chang J.J., "A study on the efficiency of electrochemical realkalisation of carbonated concrete", Construction and Building Materials 2005, Vol. 19, pp. 516-524.
6. Neville A.M., "Properties of Concrete". Final Version, Prentice Hall, 2000.
7. G. Roelfstra1, R. Hajdin B. Adey and E. Bruhwiler, "Condition Evolution in Bridge Management Systems and Corrosion-Induced Deterioration", ASCE Journal of Bridge Engineering 2004, Vol. 9, No. 3, pp. 268-277.
8. Montemor M.F., Simoes A.M.P., and Ferreira M.G.S., "Chloride-induced corrosion on reinforcing steel: from the fundamentals to the monitoring techniques", Cement & Concrete Composites 2003, Vol. 25 pp. 491-502.
9. Standard test method for acid-soluble chloride in mortar and concrete", ASTM C: 1152-" pp. 609-10, 1990.
10. Arya C., Buenfeld N.R., and Newman J.B., "Assessment of simple methods of determining the free chloride ion content of cement pastes. Cement & Concrete Research 1987, Vol. 17, pp. 907-18.
11. B.B. Hope, I.K., Alan "Chloride corrosion threshold in concrete" ACI Material Journal, Vol. 84, pp. 306-3014, 1987.
12. Pullar-Strecker P., "Corrosion damaged concrete: assessment and repair" London: Butterworths; 1987.
13. Hansen E.J. and Saoma E., "Numerical Simulation of Reinforced Concrete Deterioration-Part 1: Chloride Diffusion", ACI Material Journal 1999, Vol. 96, No. 2., pp. 173-180.

14. Mangat P., and B. Molley, "The penetration of chlorides into hardened cement pastes", Cement and Concrete Research 1994, Vol. 14, No. 4, pp. 546-558.
15. Clifton J.R., "Predicting the service life of concrete", ACI Material Journal 1993, Vol. 90, No. 6, pp. 611-617.
16. Oh B.H., and Jang S., Chloride Diffusion Analysis of Concrete Structures Considering Effects of Reinforcements", ACI Material Journal 2003, Vol. 100, No. 2.
17. Xi Y., and Bazant Z.P., "Modeling chloride penetration in saturated concrete", ASCE Journal of Materials in Civil Engineering 1999, Vol. 11, No. 1, pp. 58-65.
18. Jennings H.M., and Tennis P.D., "Model for developing microstructures in portland cement paste", Journal of American Ceramic Society 1994, Vol. 77, No. 12, pp. 3161-3127.
19. Boulfiza M., Sakai K., Banthia N., and Yoshida H., "Prediction of Chloride Ions Ingress in Uncracked and Cracked Concrete", ACI Materials Journal 2003, Vol. 100, No. 1, pp. 38-48.
20. Kato E., Kato Y., and Umoto T., "Development f simulation model of chloride ion transportation in cracked concrete", Journal of Advanced concrete technology 2005, Vol. 3, No. 1, pp. 85-94, Ava. Free. on: www.j-act.org/
21. Li C.Q., Zheng J.J., and Shao L., "New Solution for Prediction of Chloride Ingress in Reinforced Concrete Flexural Members", ACI Material Journal 2003, Vol. 100, No. 2, pp. 319-325.
22. Kassir M.K., and Ghosn M., “Chloride-induced corrosion of reinforced concrete bridge decks,” Cement & Concrete. Research 2002, Vol. 32, pp. 139–143.
23. Phurkhao P., and Kassir M.K., "Note on Chloride-Induced Corrosion of Reinforced Concrete Bridge Decks", ASCE Journal of Engineering Mechanics 2005, Vol. 131, No. 1, pp. 97-99.

CD06-011

EFFECT OF REBAR ON COMPRESSIVE STRENGTH OF CONCRETE CORES

M. Tadayon[1], H.T.P Moghadam[2], M.H. Tadayon[3]
[1]Associate professor, Civil Eng. Dept., Engineering Faculty, Bu-AliSina University, Hamedan, Iran
[2]Graduate of Iran University of Science and Technology Civil Engineering Faculty, Tehran, Iran
[3]M.S. Student, Dept of civil Eng., Engineering Faculty, University of Tehran, Tehran, Iran

ABSTRACT
Concrete coring is used for determining compressive strength of hardened concrete of elements to evaluate low-strength-test-result concrete or to understand concrete placing quality of existing structure. In safety evaluation of existing structures that need rehabilitation and retrofitting, it's necessary to have some information about existing concrete. The best and most accurate method to determine compressive strength of existing concrete is coring. Rebars always make difficulty in coring of reinforced concrete structures. Sometimes it is not possible to core from plain concrete areas. There are serious considerations for effects of rebar on compressive strength of concrete cores in some countries. There is no strength correction for the effect of rebars in ACI and also in Iranian related codes and specifications. There is only an Concrete Society equation in publication no.207 of BHRC based on result corrections of cores contained rebars perpendicular to cores longitudinal axes. This correction does not exceed 10%. Dealing with such problems in a project and because there was sureness about strength of placed concrete, but strength of cores was highly lower and it was not possible to obtain plain core as there was heavy rebar concentration, it was necessary to study rebar effects on core strength. In this research, strength of cores of an element contained rebars and plain ones were compared to evaluate above mentioned equations. Also some cylindrical samples were made and tested with placed rebars. In addition if the core has uncut rebars, there will be no significant reduction in its strength. It seems that cutting of rebars in coring process has little effects on concrete quality. It is due to cracks formation between concrete and rebars that reduce the concrete strength.

Keywords: compressive strength, core, rebar, reinforced concrete, structure

1. INTRODUCTION
If any strength test of laboratory-cured cylinders falls below fc′ by more than the given values or if tests of field-cured cylinders indicate deficiencies in protection and curing, steps shall be taken to assure that load-carrying capacity of the structure is not jeopardized [1].
If the likelihood of low-strength concrete is confirmed and calculations indicate that load-carrying capacity is significantly reduced, tests of cores drilled from the area in question in accordance with “Method of Obtaining and Testing Drilled

Cores and Sawed Beams of Concrete" (ASTM C 42) shall be permitted [1,3,4].
If by structural analysis, again it can not be accepted, ordinary solution to accept concrete structurally and according to strength criterion, especially in Iran, is coring critical parts of concrete structure [3,4].
Nondestructive tests of the concrete in place, such as by probe penetration, impact hammer, ultrasonic pulse velocity or pull out may be useful in determining whether or not a portion of the structure actually contains low-strength concrete. Such tests are of value primarily for comparisons within the same job rather than as quantitative measures of strength. For cores, if required, conservatively safe acceptance criteria are provided that should ensure structural adequacy for virtually any type of construction [1].
Some specific consideration such as preparing suitable diameter and height, not contacting with reinforcements if possible, positioning critical areas, and some non destructive tests such as rebar locating test, impact hammer and ultrasonic pulse velocity are needed for coring.
In any case, if rebars are closely spaced or rebars positions can not be determined, rebars will be cut and core will contain them.
Rebar existing in the core has always been debatable subject. Some consider that rebar increase sample strength; others believe that strength will be reduced when rebar exist; the others believe in very low effect of rebar presentation [6].
In some codes and standards like ACI, ASTM, EN, Iranian Concrete code and other Iranian codes, there is no consideration for rebar effect on core, therefore there is not any correction for core test result [1,2,3,4].
In some European countries there is no correction, but BS 1881:1983 and Concrete Society presented corrections for rebar existing in concrete cores [6].
Equation (1) generally works for samples that rebar are parallel to ends of sample.

$$StrengthCorrectionFactor = 1 + \frac{3\sum_{i=1}^{n}\left(d_{r,i}h_i\right)}{2d_c L} \quad (1)$$

Where, $d_{r,i}$ is rebar diameter, d_c is core diameter, h_i is rebar axis distance to next core surface and L is core length[5].
In equation (1), effects of rebar depend on diameter, location and number of rebar, but this correction does not exceed 25% of core strength [7].
If it is possible, the best solution is obtaining cores from plain concrete areas. Perhaps rebars cutting leads to adverse effects on structural strength, concrete quality and core strength [6].
Existing no quality control in precast concrete beams construction for bridges of a road in the South of Iran, supervisor selected coring as only practical solution for quality control of concrete of these beams. Compressive strength of cores was astonishing because there was enough confidence in strength of placed concrete, but strength of cores was too low. Accordingly, it was necessary to study rebar effects on core strength.

2. EXPERIMENTAL PROGRAM AND MATERIALS

To determine rebar effect on concrete core strength, two groups of concrete beams is used. In the first group, there are beams without rebar, and beams with rebars were the second group (Figure 1). The concrete that is used for construction of each group, is similar and also with same consolidation and curing conditions. By coring plain beams and determining their strengths, it is possible to compare results. In some beams, one, two and even three rebar was placed. Beam is a concrete block with dimension of 15× 15×60 cm and core is a cylinder with 10cm diameter and 15cm height (Figure2 and 3). As shown in Table 1, two different kinds of concrete mix proportion were used in this research. Nominal maximum size of aggregates was 20 mm.

Figure 1. Rebars placement in beams

Figure 2. Coring of beams

Figure 3. Cored beams

Table 1: Details of Mix Proportions

Mix No.	Cement kg/m^3	SilicaFume kg/m^3	W/C	Sand (SSD) kg/m^3	Coarse Aggregate (SSD) kg/m^3	Fresh Concrete Density kg/m^3	Slump mm.	HRWRA Admixture kg/m^3	Air Content %
1	370	30	0.4	925	850	2328	120	3.2	2.4
2	400	-	0.43	980	775	2328	140	2.8	2.1

Concretes without rebar are determined by CP and ones with rebar by CR. Three cores were prepared for each mix proportion. Rebar sizes are 10, 12, 16, 20, 32 mm diameter and different rebar arrangement, as shown in table 2, was used. These arrangements tried to be same as real rebar arrangements in real beams.

In another part of this research, some cylindrical samples with mix proportion no.2 and with or without rebar were prepared. Rebars placed in some samples are shorter than sample diameter and they are not cut. After 28-day same curing, tests were fulfilled. Cylindrical samples with rebar are distinguished with P and ones without rebar with letter R.

3. EXPERIMENTS RESULTS AND ANALYSIS

28-day Compressive strength results of cores in saturated state after capping as well as weights, number, diameter and arrangement of rebars are presented in Table 2. Also corrected strength of cores with rebar by using Concrete Society equation (mentioned above) is presented in this table.

Also results of cylindrical samples with and without rebar are shown in table 3. Cylindrical samples are with 150 mm diameter and 300 mm height.

According to Tables 2 and 3, in all cores with rebar there is a reduction of 25 to 60 percent than cores without rebar.

It seems that existing of rebars results in weakening of cores. In cylindrical samples, existence of rebar has reduced sample strength 16 to 24 percent.

After core breaking-up, it observed that usually rebar were separated from adjacent concrete matrix (Figure 4).

It also seems that in addition to weak connection resulting from bleeding that water gathers under rebar, act of rebar cutting weakens connection of rebar and concrete.

Cores strength variation does not follow any rule and there is much variation.

Cores strength correction result from Concrete Society equation does not show good proximity to strength of cores without rebar except CR-2-1, CR-2-2 and CR-2-4 cores.

Results of cylindrical samples with rebar after correction by Concrete Society equation show better correlation with samples without rebar. This demonstrates that rebar cutting weakens concrete samples.

Figure 4. Separation of rebars after compression test of cores

Table 2: Concrete Cores Test Results

Core No.	Rebar quantity and diameter(mm)	Rebar location (mm)	Core weight (kg)	Measured compressive strength (kg/cm^2)	Corrected strength by Concrete Society equation (kg/cm^2)
CP-1-1	-	-	2.240	490	-
CP-1-2	-	-	2.235	461	-
CP-1-3	-	-	2.235	475	-
CR-1-1	1Φ32	75	2.380	260	322.5
CR-1-2	1Φ32	75	2.365	231	286.5
CR-1-3	1Φ12 1Φ20	50	2.370	260	301.5
CR-1-4	1Φ12 1Φ20	50	2.375	212	246
CR-1-5	2Φ16	50	2.380	360	417.5
CR-1-6	2Φ16	50	2.375	320	371
CP-2-1	-	-	2.220	375	-
CP-2-2	-	-	2.235	404	-
CP-2-3	-	-	2.280	388	-
CR-2-1	1Φ32	75	2.310	303	375.5
CR-2-2	1Φ32	75	2.325	303	375.5
CR-2-3	1Φ32	50	2.310	245	284
CR-2-4	1Φ32	75	2.310	303	375.5
CR-2-5	2Φ10 1Φ20	50 50	2.360	231	277
CR-2-6	2Φ10 1Φ20	30 30	2.320	274	323
CR-2-7	1Φ12 1Φ20	50	2.330	260	301.5
CR-2-8	1Φ12 1Φ20	75	2.330	144	178.5
CR-2-9	1Φ16 1Φ20	50	2.300	216	255
CR-2-10	1Φ16 1Φ20	75	2.315	122	155
CR-2-11	2Φ16	75	2.325	260	322.5
CR-2-12	2Φ12	50 50	2.320	231	259

Table 3: Cylindrical Concrete Samples Test Results

Sample No.	Rebar quantity and diameter(mm)	Rebar location (mm)	Measured compressive strength (kg/cm^2)	Corrected strength by Concrete Society equation (kg/cm^2)
P-2-1	-	-	342	-
P-2-2	-	-	328	-
P-2-3	-	-	323	-
P-2-4	-	-	337	-
R-2-1	1Φ16 1Φ12	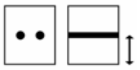 150	253	288.5
R-2-2	1Φ16 1Φ12	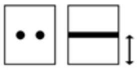 150	267	304.5
R-2-3	2Φ16 1Φ32	 150	252	-
R-2-4	2Φ16 1Φ32	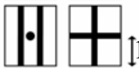 150	257	-
R-2-5	2Φ16 1Φ32	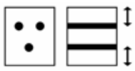 100 100	279	338.5
R-2-6	2Φ16 1Φ32	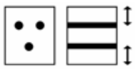 100 100	266	322.5

CONCLUSION

According to obtained results and their analysis, following conclusions can be deduced.

1. The equation given by Concrete Society does not predict the core results accurately.
2. Compressive strength of core with cut rebar is always less than corresponding strength of core without rebar.
3. It appears that strength reduction due to existence of rebar in cores is between 25 to 60 percent. This reduction in cast cylindrical samples is about 16 to 24 percent.
4. It seems that rebar cutting leads to weakness in cores compressive strength due to crack formation between concrete and rebars.
5. There is not reliable relationship for correcting compressive strength results of cores with rebar. But in limited cases, correction of Concrete Society equation can give acceptable results.
6. Strength reduction of cast cylindrical samples with rebar is usually less than that of concrete cores.

ACKNOWLAGEMENTS

Authors would like to thank Managing Director of Rah Sahel-Ghorb Nooh-Khatam alAnbia Reconstruction Center, Manager and Project director of Asalouye Concrete Plant.

REFERENCES

1. ACI Committee 318, “Building Code Requirements for Structural Concrete (ACI 318-05)", *ACI Manual of Concrete Practice, Part3, 2006.*
2. ASTM, "Standard Test Method for Obtaining and Testing Drilled Cores and Sawed Beams of Concrete", ASTM C42-99, Book of ASTM Standards, Concrete and Aggregates 04.02., 2000.
3. State Management and Planning Organization, "Concrete Code of Iran", Office of Technical Affairs Deputy, Iran, 2000, 94-96 (in Farsi).
4. Ministry of Housing and Urban Development, "Iranian National Building Code", Part 9, Iran, 2006, 94-96 (in Farsi).
5. Concrete Society Technical Report no.11, "Concrete Core Testing for Strength", Concrete Society, London, 1976.
6. Neville, A.M., “Properties of Concrete”; Forth Edition, Wiley & Sons, New York, 1996 (Translated into Farsi by Famili, H.).
7. Ramezanianpour, A.A., Hamidian, M.R., "Non-Destructive Testing of Concrete Core Tests", BHRC, Tehran, 1994 (in Farsi).

CD06-012

STUDY OF NEW GROUTING TECHNIQUES IN REPAIR AND STRENGTHENING OF SOFT SOILS

S. Kazemian, Bujang. B. K. Huat, A. Asadi, V. Ghiasi
Department of Civil Engineering, Universiti Putra Malaysia, Serdang, Selangor, Malaysia

ABSTRACT

Demands for soft land strengthening and contaminated soil solidification have been increased due to the explosion population, development of technology, industry, and transportation systems.

Deep mixing methods (DMMs) are conventional methods for strengthening the soft soils. Cement (or binder) with soil have being mixed in this method. Injection of cement and additives with a high pressure and displacing the gases and liquids from within soil grains in combination with DMMs is a new wedding technique for increasing the efficiency of soil stabilization.

In this paper, different kinds of deep mixing methods (conventional and new techniques) were studied. By considering the type and alternative layers of soil, load size, the situation, cost and type of project selecting the right stabilizing method for repair and strengthening of soft soils recommended and it is believed that it could prompt engineers to resolve soil strengthening difficulties from the geotechnic-al view point.

Keywords: grouting, stabilizing, injection, mixing, soft soil, cement and binder

1. INTRODUCTION

1.1. Deep Mixing Methods (dmms)

The DMMs refers to the rotary methods for the penetration of soil or rock and mixing of soil with suitable binder and at times with pneumatically dry or wet end for enough depth. This technique has been used for construction of tunnels by injecting binder in the rock too.

Based on design requirements, site conditions, soil layers, restraints, and economics, the use of DMMs is increasingly spreading. The demand for improving and stabilizing land for different purposes is expected to increase in the future and the best way to fulfill it is by using DMMs. The main advantage of these methods is long term increase in strength, especially for some of the binders used. It has been mentioned that DMMs is the best way to improve soils and rocks. The following are the characteristics of the improved soils and rocks when these methods are employed [1]:

(i) Reduction of settlements, (ii) increase of stability, (iii) increase of bearing capacity, (iv) prevention of sliding failure, (v) reduction of vibration, (vi) liquefaction mitigation, and (vii) remediation of contaminated ground.

The Federal Highway Administration has suggested that these techniques can be

classified based on [2]:
1) Method of additive injection (i.e. wet or dry injection).
2) Method by which additive is mixed (i.e. rotary, mechanical energy or by high pressure jet).
3) The location of the mixing tool (i.e. near the end of the drilling rods or along a portion of the drilling rods).
Majority of the companies which are working in these fields agree that the DMMs can be divided into three common techniques [9]:
1. Shallow soil mixing (SSM), which uses a single mechanical mixing auger located at the end of the drilling tool (Kelly bar).
2. Deep soil mixing (DSM), which utilizes a series of overlapping augers and mechanical mixing shafts.
3. Jet grouting which can be considered a type of soil mixing. In order to inject a liquid into voids within a structure, it is necessary to displace the gases and liquids from within these. This utilizes high velocity ranges from 28 to 42 Mpa backpressure and jets to hydraulically shear the soil and blends a cement grout or suitable binder to form a soil-cement column or column with soil and special binder.
Table 1 clearly names the methods which are utilized in each part. The explanation and comparison of each part will be made subsequently.

Table 1: The methods are utilized in DMMs parts.

Shallow soil mixing (SSM)	Deep soil mixing (DSM)	Jet grouting systems			
		Single phase	Dual phase	Triple phase	Super jet grouting
Ras-Columns	Cement Deep Mixing System (CDM)	I. Maxperm grouting system II. Navigational drilling system III. Vacuum grouting injection	Dry jet mixing system (DJM)	Jumbo ECO pile system (JEP)	Ras-jet system

The researchers have come up to four basic jet grouting systems to be used, which are [4]:
(i) Single phase (grout injection only), (ii) dual phase (grout + air injection), (iii) triple phase (water+air injection and followed by grout injection), and (iv) super jet grouting (air injection+drilling fluid by grout injection). Figure 1 shows the sketches of the jet grouting systems.

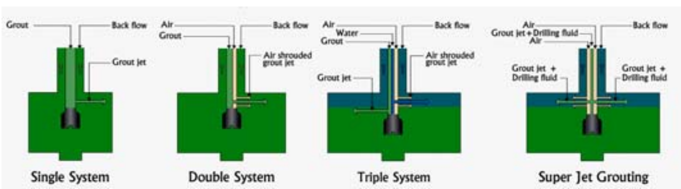

Figure 1. The systems in jet grouting.

2. SHALLOW SOIL MIXING (SSM)

2.1. Ras-Columns

Ras-Columns are one of the most common soils mixing in DDMs which are based on mechanical soil mixing technology. This method has been used for improving shallow soils and seldom in deep mixing.

The mixing head is combined with blades which can rotate inversely. In other words, in bottom auger the mixing blades rotate clockwise and in the upper auger, the mixing blades rotate anti clockwise [3].

This technique causes the cement to mix with soil homogenously, and thus produces higher quality soil-cement columns. The first step of this method is Rig positioning. This is followed by penetration whereby after passing dry excavation zone, injecting slurry without any jetting should start. The third step is churning or moving the head up and down to mix homogenous thoroughly. Finally is the completion step, where the head is withdrawn and soil column cement is completed (Figure 2).

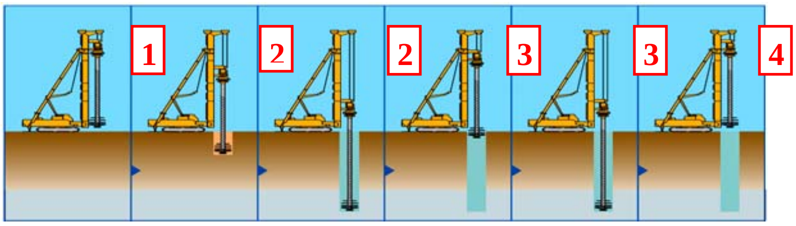

Figure 2. The steps in ras-columns system [3].

2.2. Advantages and Main Points

1. Ability to produce soil-cement column of 1.4 to 2.5 m diameter.
2. Applicable to a wide range of soils hence providing excellent quality improvement.
3. Uniform mixing and homogenous product quality due to counter-rotation mechanism (in comparison with traditional equipment).
4. Low noise and low vibration system.
5. Computer-based control and monitoring system ensures quality improvement (in some latest ones).

3. DEEP SOIL MIXING (DSM)

3.1. Cement Deep Mixing System (CDM)

The second method which is related to deep soil mixing and is one of the DMMs is CDM. As mentioned before, in this method a series of overlapping augers and mechanical mixing shafts are applied. Figures 3(a) and 3(b) show CDM machines with 2 and 3 augers respectively.

CDM is normally utilized in soft soil that contains mineral soils such as clay or sand. In some conditions where mineral soils are absent, sand should be added before mixing in cement slurry. CDM is a soil stabilization method which mixes cement slurry with soft soil in situ to attain a required strength. Soft soil is stabilized by the 2-phase chemical reaction. A hydration reaction occurs and an ettringite of capillary crystals is generated when the cement mixes with water. Then a pozzolanic reaction follows, as the age grows, where the hydration product reacts with the clay minerals in the soil [3].

Figure 3: (a) The CDM machine with 2 augers (b) The CDM machine with 3 augers

3.2. Advantages and Main Points

1. CDM is a drilling and mixing operation with low noise and low vibration, and does not generate dust.
2. CDM method mixes soft soil in situ with cement slurry without any jetting. The soil should have mineral soils like sand and clay for hydration product with cement.
3. Because of a series of overlapping augers, it saves soil mixing time and labor while maintaining efficiency in comparison with previous method.
4. Computer-based control and monitoring system ensures quality improvement (in some latest ones).

4. JET GROUTING SYSTEMS

Jet grouting systems, which is the third part of DMMs, have some similarities with the previous methods. Apart from having the same mixing tools, this method also applies the same process whereby the in-situ soil will be cut and broken by high pressure jet of slurry and produce homogenously improved zone around the mechanically mixed core.

In addition, for underwater applications, it is desirable to have highly flowable grout that can resist water dilution and segregation, and spread readily into place. The slump of concrete or grout is a good measure of the consistency and flow characteristics of a concrete or grout mixture. This equates (to) a mid range slump. A very high slump grout gives maximum water dilution. A very low slump grout results in little or no flow characteristics. For underwater grout, the slump flow is influenced (in order of influence) by the anti-washout admixture concentration and the binder content, the water-cementitious material ratio, and the water reducer concentration [10, 11].

4.1. Single Phase

4.1.1. Maxperm Grouting System

It has been mentioned that the jet grouting is divided into 4 phases. The first part which is single phase has 4 common methods. One of the newest methods in jet grouting system is Maxperm grouting system. This method is commonly utilized around the world by several names such as dual-tube double-packer grouting system.

In this method, the contractor can inject several materials in the soil which has several layers with different characteristics. On the other hand, the ground is made up of alternative layers, consisting of different particle sizes, and permeability can be stabilized by this method. The pre-defined region is improved and its sketches are shown in Figure 4.

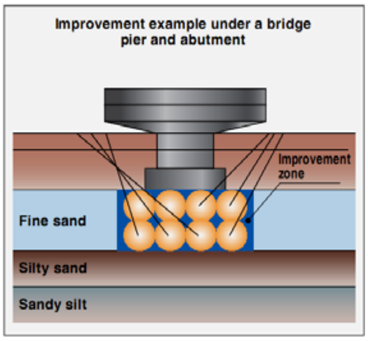

Figure 4. Pre-defined region can be improved by maxperm grouting system.

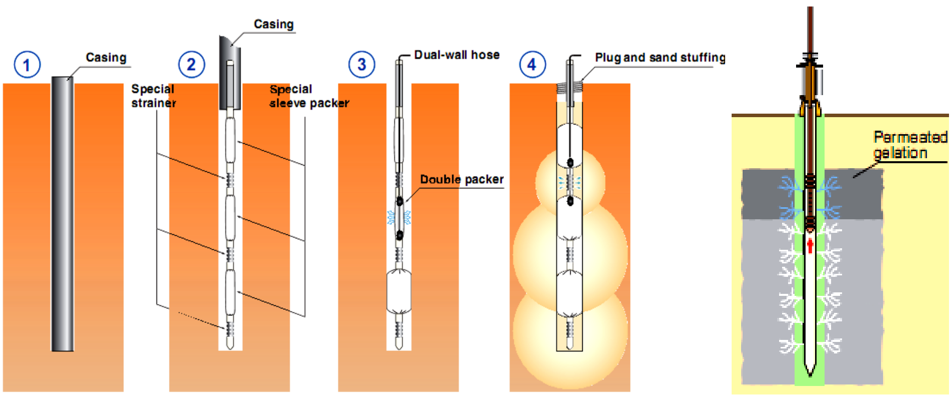

Figure 5. The steps and detailing of Maxperm grouting system

The following are the steps that take place in this method which are also shown subsequently in Figure 5[3]:

2. Apply casing drilling (φ=100 mm to a pre-defined depth).
3. Install the grout pipe with special sleeve packers and strainers then withdraw the casing.
4. Install the dual-wall inner tube equipped with double packer which inflates the

special slee-ve packers.

5. Inject grout through the strainer section. re-install the dual-wall inner tube equipped with double packer.

4.1.2. Advantages and Main Points

1. Cost-effective and labor saving alternative, because it can be separated and cause large borehole spacing.
2. Special layers, regions, any pre-defined point, a narrow area and ground with underground obstacles in soil can be improved by this method.
3. Large size improvement.
4. A pre-defined zone is homogenously stabilized by injecting grout from discrete injection points.
5. The system allows repetitive grouting at the same Injection point with different grout materials even after the work is completed.
6. This method can be used as a remedial method for structures.

4.1.3. Navigational Drilling System

The second method in single phase jet grouting is navigational drilling system. This is a new method which is broadly used. By using 3D navigational drilling system, horizontal grout holes can be installed from the surface without excavating a shaft.

The bit locator system monitors exact location of the drill bit with special locator sensors free from magnetic disturbance. The system gives the operator in real time such information as direction and inclination of drill bit, tool face orientation, and deviation from preplanned alignment. Figure 6 shows the schematic representation of the flexible borehole alignment.

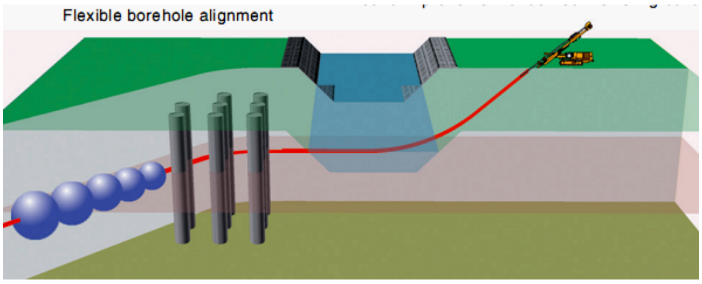

Figure 6. The schematic representation of the flexible borehole alignment which can be made by navigational drilling system [3]

Below are the steps that take place in this method:

1. Operator starts drilling while monitoring bit location (with the tool face oriented to the goal).
2. Withdraw the inner steel rod.
3. Install a grout pipe.
4. Withdraw the outer pipe.

Figure 8 clarifies the steps that take place in the navigational drilling system.

4.1.4. Advantages and Main Points

1. Drills of this method are the most flexible among injection and grouting tools (it can carve with various radiuses, e.g. 20)
2. Drills are able to drill at a long-distance.
3. Drills can solve the underground obstacle problems with special bit locator system.
4. Enable ground improvement and soil remediation under or behind existing structures with-out affecting operation or damaging underground structures
5. This method can be used as a remedial method for structures.

4.1.5. Vacuum Grouting Injection

It is worth pointing out that pressure injection may be less successful when the pressures needed to dispel gases and liquids from the voids are so high as to risk disrupting the structure. For instance this may happen when the voids consist of many fine interstices and are not always interconnecting (which may result in the need for a very large number of injection points), when complete filling is very difficult to achieve, or when it is difficult to confine the grout to the area to be injected.

The third part of single phase of jet grouting is Vacuum Grouting Injection. In this technique a partial vacuum is first established in a portion of the structure (or the whole of the structure if it is small enough), drawing off gases and liquids from the voids and interstices.

This vacuum holds the structure together, rather than exerting any potentially disruptive forces as in pressure injection. After achieving a stable vacuum, the injection liquid is introduced either through injection pipes set at appropriate intervals and depths or, over the surfaces and into the structure through cracks, fissures and porous areas [6]. In Figure 7 the proceeding of Vacuum Grouting Injection and its instrument are displayed.

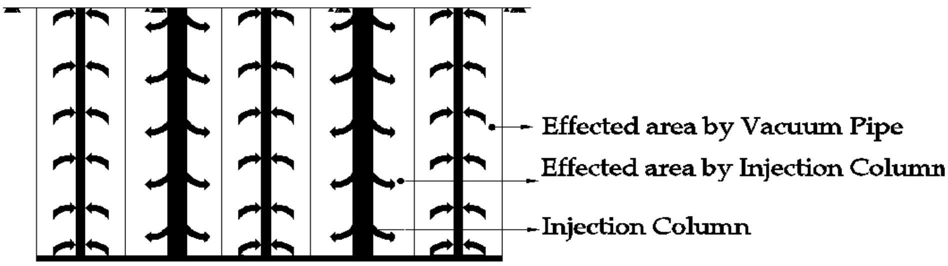

Figure 7: The proceedings of vacuum grouting injection.

4.1.6. Advantages and Main Points

1. It can be used for filling small, essentially air-tight voids through a single hole, where difficult access complicates the provision of vent holes (like Dam's concrete) [7].
2. It has been employed for filling small voids under steel liners, as well as defects in the original grouting of post-tensioning ducts. In other words, it can

fill off closely spaced fine defects in concrete or masonry.

3. It can be seen clearly which part of the voids are filled by grouting (in part 2). Whenever the plastic cover saturates the entire area under plastic sheeting, all air will be sucked in including any void space as well (Figure 8).
4. This method can be used as a remedial method for structures.
5. The mixing machine used is mobile and can be easily relocated to the next soil mixing location at /on site.
6. This method can be used as a remedial method for structures.

Figure 8. The plastic cover is used for all air to be sucked into any void spaces as well [12]

5. DUAL PHASE SYSTEM

5.1. Dry jet Mixing System (DJM)

The second part of jet grouting systems is dual phase system. The DJM is a highly effective ground treatment system used to improve the load performance characteristics of soft clays, peats and other weak soils. The concept of using dry binder for deep soil mixing was first presented in Scandinavia in 1967 by Mr. Kjeld Paus from Sweden. A period of thirty years has passed since then but the technique has been evolved considerably. The method is based on injecting dry binder carried by compressed air into soil [8]. The DJM uses mixing blades to mix dry reagents, such as cement or lime, with in-situ soils for remediation.

In this method, the process employs the effects of both hydration and the bonding of soil particles to increase the shear strength and reduce the compressibility of the soil mass [4].

Advantages and Main Points

1. The use of air instead of water to transport the binder in pipes and hoses is a big advantage where the temperature drops below the freezing point many months of the year or in the high ground conditions [8].
2. Additives to cement and lime can be used with particles of sizes less than 5 mm [3].
3. DJM does not need water or slurry preparation. Operation without water keeps the site clean.
4. Little dust is introduced into air and the operation is safe with minimum noise

and minimum ground vibration.

5. The mobility and automatic monitoring system (the latest one) of mixing machine records help in getting high quality performance and saves on labor.
6. Soil mix column with diameters of 600mm to 1000mm can be constructed to controlled height and depth. The amounts of binder agents commonly used are 80-100 kg/m^3 in soft clay and 150-200 kg/m^3 in peat [4].

5.2. Triple Phase

5.2.1. Jumbo Eco Pile System (JEP)

The next part of JEP is triple phase system. It can be said that the JEP is the most popular method in this system. Most frequently, the applications of JEP, which is also named soilcrete-jet grouting, are: underpinning, tunnel protection, foundation restoration and modification, shaft supports, deep foundation, earth pressure relief, panel walls, vault slabs, column walls, sealing cover, dam sealing, joint sealing, sealing slabs, and groundwater exits. Figure 9 shows the steps of this method.

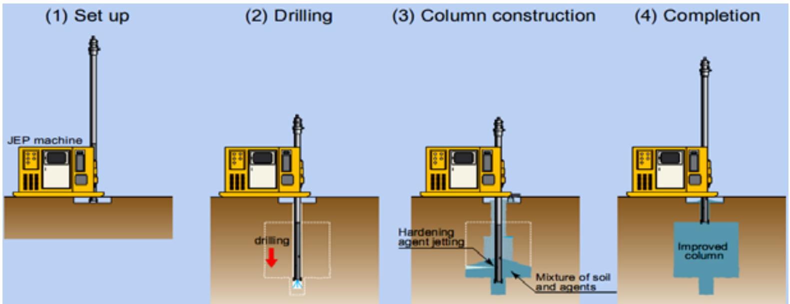

Figure 9. The steps of jumbo ECO pile system (JEP)

This method is also recognized as cement soil stabilization. With the aid of high pressure cutting jets of water or cement suspensions having a nozzle exit velocity〈100 m Sec^{-1}; eventually the air shrouding the soil around the borehole is eroded [4]. It has been suggested that when the cohesion of the ground exceeds 50 kNm$^{-2,}$ a separate study is required. A separate study is also required for the sand and gravel layer [3].

Advantages and Main Points

1. Large diameter column improvement from double jet monitors.
2. Double jet shortens construction time.
3. Tow jet crosses and cuts soil to smaller size, thus producing high quality product.
4. In comparison with the conventional method, this method is more cost-effective and time saving alternative.
5. The compressive strength of JEP system is from 2-25Mpa.

5.3. Super Jet Grouting

5.3.1. Ras-Jet System

Ras-Jet System is used in super jet grouting method. This method is the same as the Ras-Columns which have been elaborated in the first part of this paper. However, in Ras-Jet System, while the mixing blades are rotating; the same slurry is jetted simultaneously. With this system, the homogenous soil-cement column mass of a large diameter will be installed underground.

Grout slurry, air, and drilling fluid are pumped through separate chambers in the drill string. Upon reaching the designed drill depth, jet grouting is initiated with high velocity, coaxial air and grout slurry to erode and mix with the soil, while the pumping of drilling fluid is ceased. This system uses opposing nozzles and highly sophisticated jetting monitor specifically designed for focus of injection media [4]. Figure 10 shows the soil cement columns which are produced by Ras-Jet system.

Advantages and Main Points [3]

1. Applicable to a wide range of soils, providing excellent quality improvement.
2. Large diameter column improvement of diameter (1.6 - 2.0m, excluding the jet grouting part).
3. Uniform mixing and homogenous product quality due to counter-rotation mechanism.
4. Computer-based control and monitoring system for quality assurance.
5. Super high pressure jet of slurry cuts and breaks in-situ soil and produces homogenously improved zone around the mechanically mixed core.

Figure 10. The soil cement columns which have been made by ras-jet system

6. CONCLUSIONS

1. The DMMs which are applied to stabilize and improve soils are spreading increasingly and have been accepted worldwide as a soil improvement method. DMMs are based on mixing binders such as cement, and/or lime and other additives with soil grains, using rotating mixing tools or jetting, simultaneously.
2. These methods have been suggested and applied for soil and rock stabilizing, slope stability, liquefaction mitigation, vibration reduction (along the railway),

roads and railroads bridge foundations, embankments, construction of excavation support systems or protection of structure close to excavation sites, solidification and stabilization of contaminated soils, and remedial grout injection of building.

3. Based on conditions such as the types of soil and rock layers, time table of project, location, importance of project, and the economic situation, the use of multiple-auger or single auger deep mixing methods, jet grouting methods, or a combination of several methods may be required.

REFRENCES

1. Holm, G. "Dry Mix Method for Deep Soil Stabilization". Balkema, Rotterdam, 1999, ISBN 90 5809 108 2, Pp: 3-13.
2. Elias V., Welsh J., Warren J. and Lukas R. "Ground Improvement Technical Summaries, Volume II, Demonstration Project 116," U.S. Department of Transportation, Federal Highway Administration, 1998, Publication No. FHWA-SA-98-086.
3. Raito Company. Retrieved Jun of 2006 from: Http://www.raito.co.jp/english/.
4. Keller Company. Retrieved Sept of 2005 from: Http://www.kellergrundbau.com.
5. Williamson C. "Remedial Grout Injection of Building," Construction & Building Materials, 1988, Vol.2, No.3, September, Pp: 145-147.
6. Warner J. "Practical Handbook of Grouting: Soil, Rock, and Structures," Published by John Wiley and Sons, 2004, ISBN 0471463035, 9780471463030.
7. Bredenberg H. "Dry Mix Method for Deep Soil Stabilization". Balkema, Rotterdam, 1999, ISBN 90 5809 108 2, Pp: 323-331.
8. Andromalos K. B., Hegazy Y. A. and Jasperse B. H. "Stabilization of Soft Soils by Soil Mixing," Soft Ground Technology Conference, 2000, United Engineering Foundation and ASCE Geo-Institute, Noorwijkerout, Netherlands, May 28-June 2.
9. Khayat K. H., Sonebi M., Yahia A. and Skaggs C. B. "Statistical Models to Predict Flow ability, Washout Resistance and Strength of Underwater Concrete," Proceedings, RILEM Conference on Production Methods and Workability of Concrete, 1996, Glasgow, Pp 463-481.
10. Khayat K. H. and Sonebi M. "Effect of Mixture Composition on Washout Resistance of Highly Flowable Underwater Concrete," ACI Material Journal, 2001, July-August, Pp: 289-295.
11. Balvac Company. Retrieved Jan of 2008 from: Http://www.balvac.co.uk/.

CD07

Special Concretes

CD07-001

THE STUDY OF VELOCITY AND FREQUENCY OF PASSING WATER THROUGH A MAGNETIC FIELD AND ITS EFFECT ON THE COMPRESSIVE AND TENSILE STRENGTH OF CONCRETE

H. Safaye Nikoo
Faculty member of Chabahar Maritime University, Chabahar, Iran

ABSTRACT

Concrete is a material which can have a range of different strengths with using different ratio s of its composites. In this regard, every factor that can help us reach better mechanical properties and other characteristics of concrete is worth studying. In our study, regarding above information, we study the effects of water properties (considering magnetizing water) of concrete on some of the mechanical features of concrete containing microsilica such as compressive and tensile strength at different curing ages. The water in concrete has been passed through magnetic field with velocities such as Q, Q/2, Q/3, Q/6 and with 1, 3 and 6 passing times. The results indicate that increasing the number of times water is passed (from 1 to 6), improves the compressive and tensile strength of concrete, and decreasing the velocity of passing water through magnetic field in one cycle (from Q to Q/6) has a similar result. The improvement of decreasing the velocity in one cycle is more significant than the improvement caused by passing water through a number of times, and the compressive and tensile strength will be improved substantially. the compressive and tensile strength of concrete will be increased up to 15 % .This method is considered very economical and does not need special equipments in industry.

Keywords: microsilica, magnetic water, superplasticizer, compressive

1. INTRODUCTION

Henrico Anton Lorenz (1920) introduced the effect of the magnetic field on water that got the Nobel Prize. He found that, under the effect of a magnetic field, polar molecules are arranged and separated, therefore, water becomes lighter. When the molecules pass through a magnetic field, a change in their arrangements appears. Since each water molecule is like a little magnet, as shown in Figure 1, by passing through the magnetic field, they arranged in an end - to - end way; This is called polarity. Water molecules are not separated; they are attached to each other as a group by a hydrogen bond. The lesser the number of molecules are in this group of molecules, their activity will be more. The magnetic field helps to this process (Figure 2).

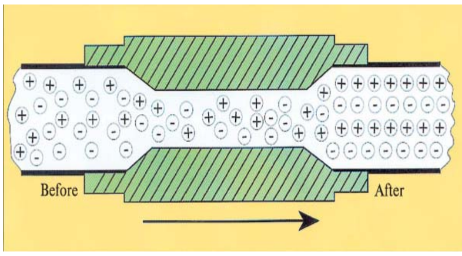

Figure 1. Effect of the magnetic field on molecules arrangement

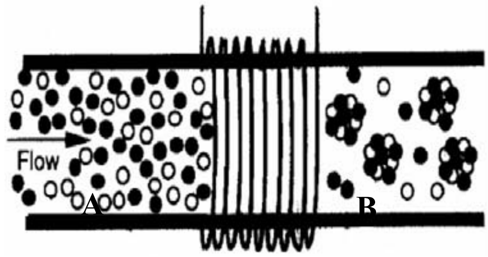

Figure 2. Effect of the magnetic field gathering of water molecules A) Before passing through the magnetic field B) After passing through the magnetic field

The general principle of magnetic technology is based on the interactions between a magnetic field and a moving electrical charge, in form of an ion in this system. When the ions pass through a magnetic field, some force is given to each single ion. In case, the orientation and the charge of the ions are against each other, it causes a fluctuation in the ions which, as a result, leads to the formation of sediment. The magnetic fields lead to the induction of electrical charge through positive and negative ions. As a consequence, ions of different charges repel each other instead of attracting each other. Therefore, a negative and a positive ion of the same charge that should form sediment, cannot approach enough to each other. Magnetic processing of water system is categorized in two and three, forms of installation and operation, respectively. Magnetic system may be installed inside or outside the flow. The inner systems are those which all or part of them is on the way of the flow. The outer systems are completely out of the water flow, thus they can be installed on the pipe (Figure 3) [1].

In terms of the kind of the operation these systems are categorized in the following way:

1. Magnetic: Mostly a permanent magnet.
2. Electromagnetic: In which the magnetic field is provided by the electromagnetic.
3. Electrostatic: In which the electrical field is forced into the water flow, which leads to the production of a magnetic field and, as a result, it attracts or repels the ions. The electrostatic units are always inside, whereas the other two kinds can be either inside or outside (outer) [1].

The degree of magnetization of water depends on three factors:

- The amount of the liquid in contact with the magnet.
- The power of the used magnet.
- The period of time that the liquid is in contact with the magnet.

During the recent years, there have been few researches carried out about the effect of magnetized water on the properties of normal concrete. In these researches, normal water was passed through a magnetic field in a frequency and with a specified velocity, and then this water was used in the mix designing. The result of these researches was an increase in the strength and other mechanical properties of concrete.

If water passes through a magnetic field during one or more frequencies or with different velocities, the behavior of the strength properties of the concrete containing Microsilica is studied in this research.

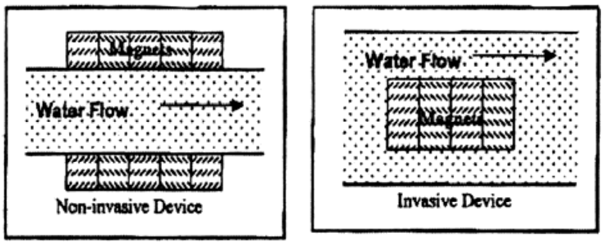

Figure 3. Different kinds of magnetic systems in terms of the place of installation

2. EXPERIMENTAL PROCEDURES

2.1. Properties of the Used Materials

2.1.1. Cement

The cement used in making concrete specimens of normal Portland cement type II of KHASH cement factory is based on the ASTM standard [3]. The unite weight obtained is 3.157 gr/cm^3. Tables 1 and 2 represent physical properties and results of the chemical analysis of the specimen, respectively.

2.1.2. Aggregates

Natural coarse (Gravel) and fine aggregates (Sand) are used to make the specimens. Different properties of the aggregates used, such as the unit weight (in terms of dry, saturated, and apparent), water absorption and their grading are obtained (Tables 3 and 4). Water absorption of the aggregates, represents the amount of the moisture of the aggregates in a saturated - dry surface (SSD).

Table 1: Physical and mechanical properties of Portland cement type II [3]

Compressive strength (Kg/cm^2)			Setting time (minute)		Hydration heat (cal/gr)	
28 days	7 days	3 days	final	initial	7 days	28 days
> 380	> 270	> 170	< 200	> 70	< 70	< 80

Table 2: Results of the chemical analysis of Portland cement type II [3]

SO_3	MgO	CaO	Fe_2O_3	Al_2O_3	SiO_2	Chemical compound
<2.0	<2.3	63.2-64.8	3.6-4.3	4.7-5.4	21.0-22.2	percentage
Na_2O+0.658K_2O		F.Cao	L.O.I	Lns.Res	Cl	Chemical compound
<1.0		<1.3	<1.0	<0.65	<0.05	percentage

Grading represents the amount of distribution and presence of different sizes of aggregates in a sand or gravel specimen. The size of an aggregate is the average diameter that can be considered for the aggregate. Therefore, dividing an aggregate into grains of the same size, is the definition of grading [4]. This grading of fine aggregate (sand) and coarse aggregate (gravel), as shown in diagrams 1 and 2, is experimentally obtained.

Table 3: Unit weight based on the results of the test (Kg/m^3)

The apparent unit weight	The actual saturated unit weight	The actual dry unit weight	Aggregate
2718	2673	2646	Gravel
2607	2576	2556	Sand

Table 4: The 24-hour water absorption aggregates based on the results of the test

Percentage of water absorption	Aggregate
1.005	Gravel
0.76	Sand

2.1.3. Water

Drinking water is used in carrying out tests and making specimens. To magnetize water it was first poured in to a system (at the end of which a pipe was attached from outside and in some parts of the pipe the AQUA apparatus (Figure 5) was installed, and there were two valves before and after the apparatus (Figure 4)), and after the water went out of the vessel and passed through a magnetic field, in case the valve installed at the end of the AQUA was turned on, it would pass through the pipe into the vessel 2 and it would be used in making specimens, immediately. If the objective was to repass the water through the magnetic field, the water in vessel 2 would be re-poured into vessel 1, and this would be done as many times as required. If the objective was passing the water with a lower velocity less than that of the basis, the valve before the AQUA was turned on so that the water could pass through the magnetic field with the desired discharge. Flow meters were used to control of the velocity of the water.

2.1.4. Admixtures

In this study silica fume (S.F) was used with the average grain of 0.2 μm and an actual specific weight of about 2.2 gr/cm^3. To study the extra effect of silica fume in concrete, specimens of 10% and 20% of silica fume were made as substitutes for cement and different results of the compressive and tensile strengths were obtained from magnetized water. Because of an increase in the viscosity and cohesiveness of the matrix and a decrease in the workability of concrete due to the use of silica fume, superplasticizer was used.

2.1.5. Superplasticizer

Superplasticizers are used in naphthalene formaldehyde sulphonate tests. This material is used as liquid in the form of solution in water. It is dark brown and has a specific weight of 1.2gr/cm^3.

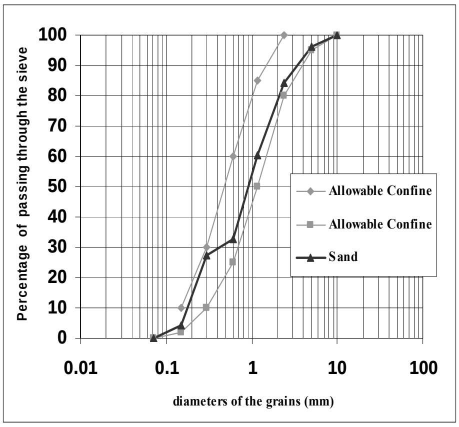

Diagram 1. Grading graph of fine aggregate (sand) and ASTM domain

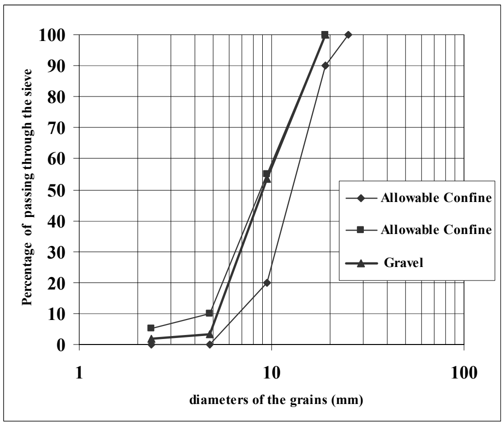

Diagram 2. Grading graph of coarse aggregate (gravel) and ASTM domain

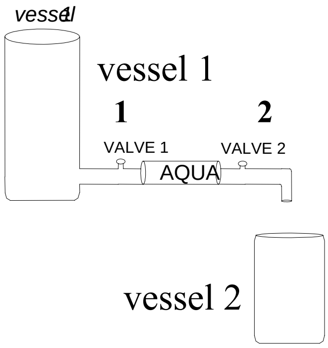

Figure 4. Water magnetizing system

Figure 5. Aqua-correct system

2.2. Properties of the Mix Designings

Properties of parts of the concrete mixture made with magnetized water (during different frequency or different velocities in a frequency) are calculated with absolute volume method and are shown in Table 5. CO_1 to CO_4 represent specimens made with normal water and are considered as the observer concrete. CN and CV represent specimens made with magnetized water in different frequencies and specimens made with magnetized water in different velocities, respectively.

Notes:

1. Q is the base discharge and is 105.8 cm^3/s.
2. In all Tables, the quantity of Q is cm^3/s.
3. In represents the number of magnetization of water cycles.
4. In this study, concrete specimens were made in which density of the cement
5. as 400 kg/m^3, the water to cement were 0.5 and 0.4 ratios and also 10% and 20% of Microsilica.
6. According to the fact that silica fume is a cement material, cement materials (B=C+S.F.) are used instead of cement, and water to cement material ratios

(W/B) instead of water to cement (W/C) in the calculations and Table of the mix designings.

7. The maximum amount of the superplasticizer is limited to 2% of the weight of the cement materials.
8. The amount of the air in these specimens is 2% of the volume of the concrete.
9. The average amount of slump is 60 mm.
10. The maximum size of the aggregates is 19 mm.

2.3. Details of the Specimens and the Preserving Method

Specimens were made to carry out the concrete compressive and tensile strength tests, which will be discussed later.

Table 5: The amounts of the mix designing (Kg/m^3)

Calculated specific weight	Amount of the basic passing discharge	Number of water magnetic frequency (n)	Superplasticizer	B= C+S.F	Microsilica (S.F)	Cement (C)	Water (W)	Sand (S)	Gravel (G)	Percentage of microsilica	ratio of water to cement	specimen
٢٣٤٨,٦٩	١٠٥,١٨	٠	٤,١٠ ٠,١١	٤٠٠ ١١,١٦	٨٠ ٢,٢٣	٣٢٠ ٨,٩٣	١٦٠ ٤,٤٦	٦٥٤,٣٤ ١٨,٢٦	١١٣٠,٢٥ ٣١,٥٤	٢٠	٠,٤	CO1
٢٣٥٨,٩٧	١٠٥,١٨	٠	١,٦٠ ٠,٠٤	٤٠٠ ١١,١٦	٤٠ ١,١٢	٣٦٠ ١٠,٠٤	١٦٠ ٤,٤٦	٦٦٧,١٢ ١٨,٦١	١١٣٠,٢٥ ٣١,٥٤	١٠	٠,٤	CO2
٢٢٨٤,٤٨	١٠٥,١٨	٠	٢,١٤ ٠,٠٦	٤٠٠ ١١,١٦	٨٠ ٢,٢٣	٣٢٠ ٨,٩٣	٢٠٠ ٥,٥٨	٥٥٢,٠٩ ١٥,٤٠	١١٣٠,٢٥ ٣١,٥٤	٢٠	٠,٥	CO3
٢٢٩٧,٠٥	١٠٥,١٨	٠	١,٩٢ ٠,٠٥	٤٠٠ ١١,١٦	٤٠ ١,١٢	٣٦٠ ١٠,٠٤	٢٠٠ ٥,٥٨	٥٦٤,٨٨ ١٥,٧٦	١١٣٠,٢٥ ٣١,٥٤	١٠	٠,٥	CO4

Table 6: comparison of the specimens W/B=0.4 , S.F=20%

specimen	CO1	CN1	CN5	CN9	CV1	CV5	CV9
n	٠	١	٣	٦	١	١	١
Q	١٠۵,١٨	١٠۵,١٨	١٠۵,١٨	١٠۵,١٨	٥٢,٥٩	٣٥,٠٦	١٧,٥٣

Table 7: Comparison of the specimens W/B=0.4 , S.F=10%

specimen	CO2	CN2	CN6	CN10	CV2	CV6	CV10
n	٠	١	٣	٦	١	١	١
Q	١٠۵,١٨	١٠۵,١٨	١٠۵,١٨	١٠۵,١٨	٥٢,٥٩	٣٥,٠٦	١٧,٥٣

Table 8. comparison of the specimens W/B=0.5 , S.F=20%

specimen	CO3	CN3	CN7	CN11	CV3	CV7	CV11
n	٠	١	٣	٦	١	١	١
Q	١٠۵,١٨	١٠۵,١٨	١٠۵,١٨	١٠۵,١٨	٥٢,٥٩	٣٥,٠٦	١٧,٥٣

Table 9. comparison of the specimens W/B=0.5 , S.F=10%

specimen	CO4	CN4	CN8	CN12	CV4	CV8	CV12
n	٠	١	٣	٦	١	١	١
Q	١٠٥,١٨	١٠٥,١٨	١٠٥,١٨	١٠٥,١٨	٥٢,٥٩	٣٥,٠٦	١٧,٥٣

A) Compressive strength test

Standard 10*10*10 cm moulds were used in making compressive specimens. To specify the compressive strength three specimens were made to be tested at each age, meaning that for each design, three cubic specimens for the compressive strength test at the age of 7 days, three cubic specimens for the compressive strength test at the age of 14 days and three cubic specimens to be test at the age of 28 were made and the average results of the test of the three specimens were placed into the pervious results. On the whole 252 cubic 10*10*10 cm specimens were made to specify the strength terms of 7, 14 and 28 days. To convert the compressive strength resulted from the cubic specimens to the standard cylinder, the proposed factors of Iranians Concrete Regulations were used. The strengths obtained, are the average of the strengths of the three concrete specimens made in the laboratory, and are shown in the table. [5]

B) Tensile strength test

15*30 cylindrical specimens and the Brazilian test method were used to achieve the tensile strength. Three models were made for each specimens and the average of the result are shown in Tables and Figures. All the tensile specimens of the age of 7 and 28 days were tested. Totally, 168 cylindrical specimens (15*30) were made of the age mentioned.[5]

3. RESULTS

Two subjects are studied in this part of the research. The first section compares the effect of two techniques of magnetizing water (passing water through the magnetic field in different frequencies or passing it through this field with different velocities) on the compressive and tensile strength. The results of the two techniques are studied in the second part.

3.1. Compressive and Tensile Strength

The results are shown in Table 10.

3.2. Results Discussing

In this part, due to the variety of the existing designs and the results obtained in the previous parts, examining and comparing the concretes made with the maximum compressive and tensile strengths (the designs with magnetized water in six frequencies or magnetized water with water passing through a magnetic field as much as 1/6 of the base passing discharge) with the observer concrete are studied.

Table 10. Results of average compressive and tensile strength of specimens of different ages (MPa)

Average 28-days tensile strength	Average 7-days tensile strength	Average 28-days compressive strength	Average 14-days compressive strength	Average 7-days compressive strength	Specimen
۳,۱۵	۲,۳۳	۴۰,۶	۳۴,۸	۲۳,۲	CO1
۲,۷۷	۱,۵۸	۳۴,۵	۲۹,۶	۱۹,۷	CO2
۲,۶۸	۱,۷۳	۳۳,۱	۲۸,۴	۱۸,۹	CO3
۲,۴۴	۱,۲۵	۲۸,۹	۲۴,۸	۱۶,۵	CO4
۳,۲۷	۲,۵۲	۴۳,۹	۳۷,۳	۲۳,۷	CN1
۳,۰۴	۱,۷۹	۳۹,۵	۳۳,۲	۲۰,۱	CN2
۲,۸۱	۱,۸۶	۳۸,۱	۳۲,۱	۱۹,۴	CN3
۲,۵۹	۱,۳۸	۳۳,۴	۲۸,۱	۱۶,۹	CN4
۳,۳۶	۲,۶۵	۴۴,۲	۳۷,۷	۲۴,۴	CN5
۳,۲۱	۱,۹۱	۴۰,۲	۳۳,۷	۲۰,۹	CN6
۳,۰۱	۲,۱۷	۳۸,۳	۳۲,۵	۲۰,۰	CN7
۲,۷۲	۱,۵۱	۳۳,۶	۲۸,۴	۱۷,۶	CN8
۳,۳۷	۲,۷۱	۴۴,۷	۳۸,۰	۲۴,۹	CN9
۳,۱۹	۲,۱۱	۴۰,۵	۳۴,۰	۲۱,۲	CN10
۳,۰۵	۲,۰۲	۳۸,۹	۳۲,۷	۲۰,۴	CN11
۲,۸۹	۱,۶۴	۳۴,۱	۲۸,۷	۱۹,۶	CN12
۳,۴۰	۲,۷۹	۴۴,۹	۳۸,۲	۲۴,۹	CV1
۳,۲۰	۱,۹۹	۴۱,۵	۳۶,۸	۲۲,۵	CV2
۳,۱۶	۲,۲۴	۴۰,۸	۳۴	۲۱,۱	CV3
۲,۸۹	۱,۶۰	۳۶,۴	۳۲,۴	۱۸,۷	CV4
۳,۵۱	۲,۹۰	۴۶,۸	۳۹,۶	۲۶,۱	CV5
۳,۴۱	۲,۱۳	۴۳,۲	۳۸,۳	۲۷,۱	CV6
۳,۲۷	۲,۳۹	۴۲,۶	۳۵,۹	۲۲,۸	CV7
۳,۰۰	۱,۷۷	۳۸,۲	۳۴,۴	۲۰,۲	CV8
۳,۴۵	۲,۵۹	۴۷,۹	۴۱,۱	۲۸,۱	CV9
۳,۳۵	۱,۸۱	۴۴,۷	۳۹,۸	۲۵,۹	CV10
۳,۳۴	۲,۵۱	۴۴	۳۷,۶	۲۱,۵	CV11
۳,۱۹	۱,۹۲	۴۰,۶	۳۵,۸	۲۱,۹	CV12

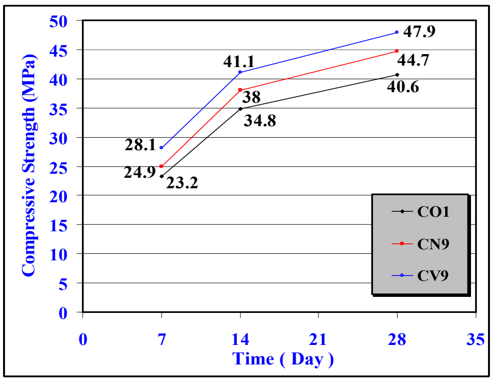

Diagram 3. Effect of magnetizing water on the compressive strength of concrete of different ages

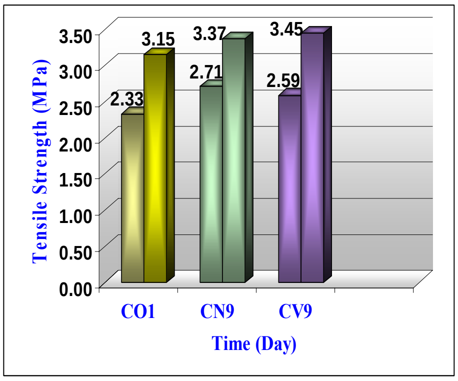

Diagram 4. Effect of magnetizing water on the tensile strength of concrete of different ages

3.2.1. Concrete with 0.4 Water to Cement Ratio and Containing 20% of Microsilica
The results of the comparison between this mix designing in the concrete with normal water and with magnetized water (in six frequencies and with a passing velocity of 1/6) are shown in diagrams 3 and 4. As illustrated in these figures, the magnetization of water causes an increase in the compressive and tensile strength. Furthermore, the induction of the magnetic property into water, by passing it through a magnetic field with 1/6 of the base velocity, compared with the number of processing frequencies causes more increase in the strength.

3.2.2. Concrete with 0.4 Water to Cement Ratio and Containing 20% of Microsilica
A comparison between the results of the diagrams 5 and 6 shows that due to magnetizing water, mechanical properties (including the compressive and tensile strength) will improve. For example, by increasing the number of magnetic processing frequencies of water, the 28 days compressive and tensile strengths of the concrete, in comparison with the observer specimen, will increase by 17.3 and 15.1, respectively.

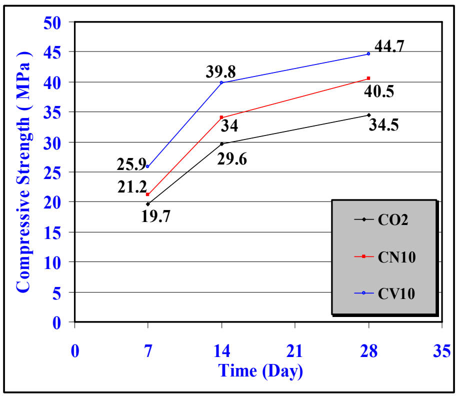

Diagram 5. Effect of magnetizing water on the compressive strength of concrete of different ages

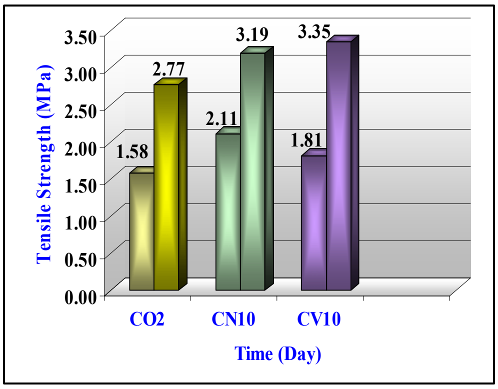

Diagram 6. Effect of magnetizing water on the tensile strength of concrete of different ages

Induction of magnetic property by decreasing the velocity of water passing through the field, causes an increase of 29.6% and 20.8% in these strengths. Therefore, magnetizing water via decreasing its velocity of passing through the magnetic field causes more increase in the compressive and tensile strengths of the concrete.

3.2.3. Concrete with 0.5 Water to Cement Ratio and Containing 20% of Microsilica
Results obtained from this comparison are shown in diagrams 7 and 8. According to these results, the concrete containing magnetized water, will have its maximum of tensile and compressive strength via decreasing the velocity of water passing through the magnetic field. For example, via this method of magnetizing water, the tensile and compressive strength will, in comparison with the observer concrete, increase by 24.6% and 32.9% respectively, whereas by increasing the number of magnetic processing, these two quantities will, in comparison with the normal

specimens of water, increase by 13.5% and 17.5%, respectively.

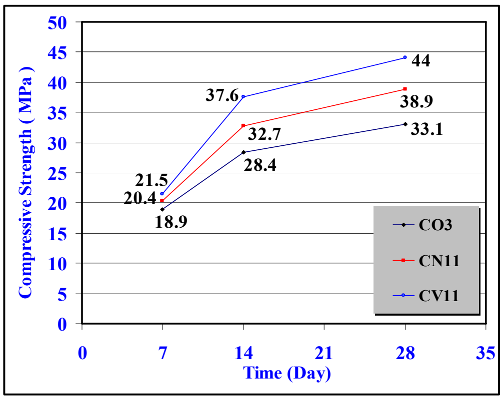

Diagram 7. Effect of magnetizing water on the compressive strength of concrete of different ages

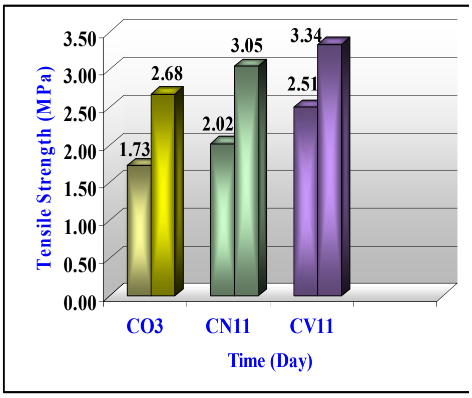

Diagram 8. Effect of magnetizing water on the tensile strength of concrete of different ages

4. CONCLUSION

Looking of the fact that, optimized strengths are obtained by magnetized water with six frequencies or 1/6 of the base discharge, the results of examining the laboratory results of this study and the final conclusion of the information there in are as follows:

- Generally, by once magnetizing water, the average changes in the compressive and tensile strength, will in comparison with normal water, be about 9% and 8.5%, respectively whereas the average amount of the increase in the compressive and tensile strength of all ages, by once to three times of magnetizing will, respectively be about 1.9% and 6.1% and with three to six times of magnetizing will be 2.1% and 1.8%. This is the case that magnetizing water via passing in through the magnetic field with the velocity of 1/2 of the discharge, the averages in the compressive and tensile strength, is respectively in comparison with normal water, about 17.6% and 20.4% whereas the average amount of the increase in the compressive and tensile strength from 1/2 of the discharge to 1/3 at all ages in respectively 6.5% and 5.6% and from 1/3 to 1/6 of the discharge is about 3.2% and 0.9%.

According to what has been mentioned:

1. Increasing the number of magnetizing water frequencies (from 1 to 6) and also decreasing the velocity of water passing through the magnetic field (from Q to Q/6), the average increase in the strength will face a decline.
2. six times of magnetizing water will change the average compressive and tensile strength, at all ages, to about 13% and 16.6% in comparison with the concrete made with normal water, where as by water passing with a velocity of 1/6 of the base passing discharge the average compressive and tensile strengths, at all ages, will respectively change about 27.3% and 25.1% in comparison with the

concrete made with normal water. Therefore,

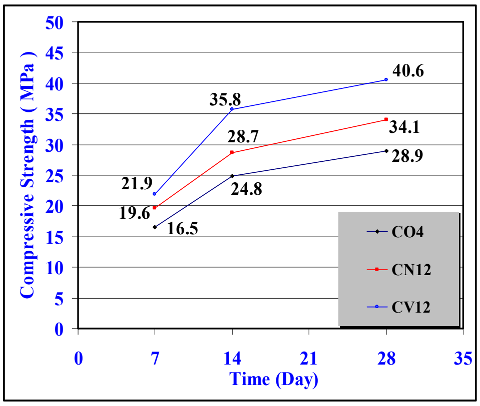

Diagram 9. Effect of magnetizing water on the compressive strength of concrete of different ages

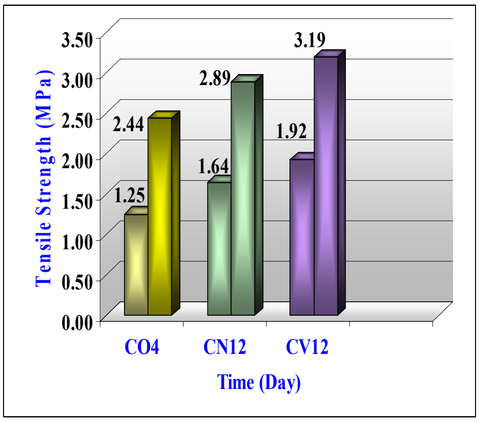

Diagram 10. Effect of magnetizing water on the tensile strength of concrete of different ages

A) Magnetizing water vi decreasing the velocity of water passing though the magnetic field, in comparison with the other technique of magnetizing water (by increasing the number of magnetic processing frequencies) is the most efficient technique, in a way that former technique causes an increase, in comparison with the later technique, of 14.3% and 8.5% in the compressive and tensile strength.

B) according to the results above, in the subject of tensile strength, water passing through the magnetic field with the velocity of 1/6 of the base discharge is not so cost-saving and caused a decline in the strength.

- The concrete containing 10% of Microsilica and a 0.5 water to cement ratio, shows the best response to magnetizing and the compressive and tensile strength, due to this change in the property of water (during six frequencies), the amount of the increase in the compressive strength will be about 16.9% while the concrete containing 10% of Microsilica and a 0.4 water to cement ratio has the maximum increase (about 22.5%), due to six times of increasing the number of the magnetic frequency, in the tensile strength. In case of magnetizing water (with the velocity of 1/6 of the discharge), the concrete containing 10% of Microsilica and a 0.5 water to cement ratio, shows the best response to the magnetizing in the compressive and tensile strength and due to this change in the property of water (during water passing will 1/6 of the base passing discharge), the amount of the increase in the compressive and tensile strength will be 26% and 37.9% respectively. Therefore, with a decrease in the percentage of Microsilica and an increase in the water to cement ratio, the concrete will have the maximum increase in the mechanical properties.

REFERENCES

1. H. Lotfi, “Effect of magnetic water on mechanical properties of lightweight concrete, master thesis, Sistan and Baluchestan university, 2007” 8-10;
2. Y. Salimpoor, “Effect of decline rigidity and sediment of water with electronically environment in heat and cold temperature, master thesis, Amir Kabir university, 2006” 12-14;
3. Khash factory, “First congress about recognition and consumption of cement types in cement factories, Khash, Sistan and Baluchestan, 2007”
4. A. Same, “ Quality and mix designing of concrete, Technical University of Isfahan, 2006”, 44-54;
5. M. Shahnazari, M. Sahab, “Recipes of concrete laboratory, Iran University Of Science & Technology, 2007,” 50-55;

CD07-002

MIX DESIGN OF STRUCTURAL SELF-COMPACTING CONCRETE USING VOID-BULK DENSITY METHOD

N. Abdizadeh[1], A.A. Zekavati[2], H. Afshin[3]
[1]M.Sc Student, Civil Eng. Faculty, Sahand University of Technology, Tabriz, Iran
[2]M.Sc Student, Civil Eng. Faculty, Sahand University of Technology, Tabriz, Iran
[3]Associated professor in Civil Eng. Faculty, Sahand University of technology, Tabriz, Iran

ABSTRACT
Self Compacting Concrete (SCC) was firstly developed in Japan in 1987. (Alternative: Pioneering works on Self Compacting Concrete returns to 1980s in Japan) In recent years, much research has been conducted in other to achieve a reasonable and also suitable mix design method for controlling the compaction experiment and determination of the compliance particular trait of SCC. But, just a few researches have been done in to propose a mix design method that can have both of highly fluid state and good viscosity, simultaneously. SCC is a special kind of concrete that can flow through and fill the gaps of reinforcement and corners of molds without any need for vibration and compaction during the placement process. In this paper Void-Bulk Density mix design method for structural SCC is investigated. In this method, firstly, the relationship between the void volume (or density of combined aggregates) and coarse-to-total aggregate volume ratio is established by packing different amounts of coarse and fine aggregates following ASTM C 29/C 29M, using the void volume of the dry binary aggregate (fine and coarse), is determined. Then, based on the optimum ratio that results from minimum void of aggregate and minimum bulk density, mix design is accomplished and finally in order to increase the flowability of the concrete have been added, some excess paste via reducing ratio of volume aggregate in unit volume concrete. Obtained results of the experiments on fresh concrete (Slump flow, L-box, V-funnel) and hardened concrete (compressive strength, tensile strength, elastic moduli and durability) show that this method is appropriate for SCC. In this study nine different SCC mixtures having the volume of paste and the ratio between sand and gravel as variables were compared with eight different mixtures of conventionally vibrated concrete (CVC).

Keywords: Self-compacting concrete, compressive Strength, Durability, elastic moduli, Mix design

1. INTRODUCTION
The development of Self-Compacting Concrete (SCC), also referred to as ‘‘Self-Consolidating Concrete’’ and ‘‘High-Performance Concrete’’, has recently been one of the most important developments in the building industry. It is a kind of concrete that can flow through and fill gaps of reinforcement and corners of

moulds without any need for vibration and compaction during the pouring process. It can be used in pre-cast applications or for concrete placed on site. SCC results in durable concrete structures, and saves labour and consolidation noise. Pioneering work in the development of SCC was carried out by Okamura [1] and Okamura and Ouchi [2], which will henceforth be referred to as Japanese Method. The method suggests that the gravel content in the concrete mix corresponds to 50% of its packed density, and that in the mortar the sand content corresponds to about 50% of its packed density (Figure 1).

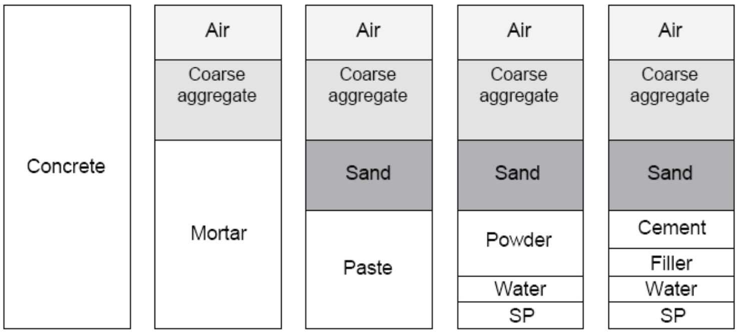

Figure 1. Schematic Composition of SCC [5]

This independent consideration of gravel and sand, results in SCC that has a relatively high content of paste. Many SCC mixes therefore attain a higher strength than actually required [3,4]. In the Netherlands, and many other European countries, the Japanese Method has been adopted and used as a starting point for the development of SCC [5]. More recently, Su et al. [6] and Su and Miao [7] developed an alternative method for composing SCC, henceforth referred to as Chinese Method. The Chinese Method starts with the packing of all aggregates (sand and gravel together), and later with the filling of the aggregate voids with paste. The method is easier to carry out, and results in less paste. This saves the most expensive constituents, namely cement and filler, and concrete of ''normal'' strength is obtained. This will also favour the technical performance of the concrete, as the largest possible volume of aggregate is advantageous in regard to strength, stiffness, permeability, creep and drying shrinkage.

Self-consolidating concrete (SCC) is a highly flowable, yet stable, concrete that can spread readily into place, fill the formwork, and encapsulate the reinforcement, if present, without any mechanical consolidation and without undergoing any significant separation of material constituents. The introduction of the modern SCC is associated with the drive towards better quality of concrete pursued in Japan in late 1980s, where the lack of uniform and complete compaction had been identified as the primary factor responsible for poor performance of concrete structures. SCC has many advantages over conventional concrete such as:

- Eliminating the need for vibration;
- Decreasing the construction time and labor cost;

2. MIXTURE DESIGN PROCEDURES FOR SCC

Several design procedures based on scientific theories or empirical experiences have been proposed for SCC [7-8]. In general, these procedures fall into the following two categories: 1) combination of high-range water-reducing admixture and high content of mineral powders, and 2) combination of high-range water-reducing admixture and viscosity-modifying admixture (VMA) with or without defoaming agent. Figure 2 illustrates the general principles for the design of SCC, as considered from the excess paste theory. The conventional concrete design method begins with the determination of the amounts of water and cement, and ends with the calculation of the amount of aggregates. Because aggregates are much less expensive and more stable than cement pastes, a quality concrete should contain as much aggregate and less cement paste as possible. Thus, the most reasonable approach to determine the amounts of cement pastes for the concrete should be based on the characteristics of the aggregates used and of the concrete designed. In this paper, a procedure has been developed to design SCC using a combination of the least void volume for a binary aggregate mixture, excess paste theory [9-10] and ACI 211.2,"Standard Practice for Selecting Proportions for Structural Concrete [11].

Figure 2(a) shows compacted aggregate particles. In order to obtain a concrete mixture with proper workability, it is necessary to have not only sufficient amount of cement paste to fill the voids among aggregate particles, but also enough paste to form a thin layer of coating on the surface of aggregates to overcome some frictions between aggregate particles, as shown in Figure 2(b). Without a film of cement paste around aggregates as a lubricant, the movement between aggregates would be difficult. To further increase the workability of the concrete mixture to become a self-consolidating concrete, it is necessary to increase the volume of excess paste or the distance between aggregate particles, as shown in Figure 2(c). The required volume of excess paste is dependent on gradation, shape, and surface texture of the aggregates used, and can be determined through laboratory experiments for concrete mixtures with desired properties.

To determine the volume of filled paste and excess paste, the void volume of the dry binary aggregate (fine and coarse) mixtures should be determined first. The relationship between void volume or density of combined aggregates and coarse-to-fine aggregate volume ratio can be established by packing different amounts of coarse and fine aggregates following ASTM C 29/C 29M,19 as shown in Figure 3. It can be seen from Figure 3 that the lowest void volume for the combined coarse and fine aggregates used in this project is around 280 L/m3 when the coarse-to-fine aggregate volume ratio is 0.4.

The target compressive strength fc′ of the designed SLC was 28 MPa (4000 psi) at 28 days using ASTM Type I Portland cement. Because no statistical strength data are available for this concrete, ACI 318 "Building Code Requirements for Structural Concrete" requires that an average strength of the tested concrete at 28 days be fc′ + 8 MPa (1200 psi), or 36 MPa (5200 psi). ACI 211.2 provides guidelines on relationships between compressive strength and cement content, and relationship between compressive strength and water cement ratio (w/c). Based on the strength requirement and ACI 211.2, a cement content of 420 kg/m3 and a w/c of 0.48 were used in this study. The volume of excess paste was determined by experiments.

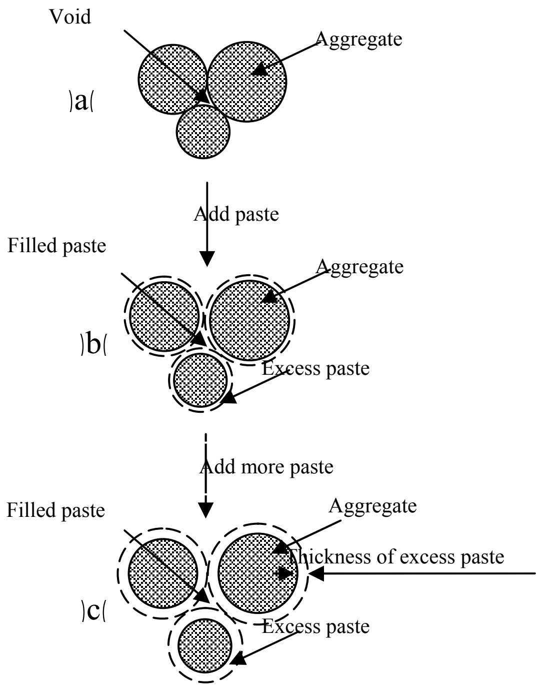

Figure 2. Scheme of compacted aggregate and concrete mixtures.

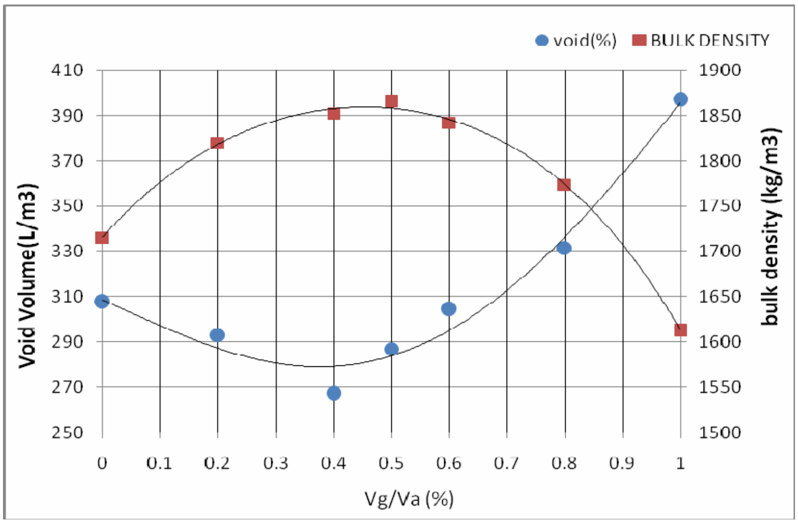

Figure 3. Effect of coarse-to-total aggregate volume ratio on bulk density and void volume of binary aggregate mixture consisting of coarse lightweight aggregate and fine natural siliceous sand

Different volumes of combined aggregates were replaced by cement paste with the same property. It was found that a replacement of 20% aggregate (by volume) by excess paste would give the concrete the required flowability and segregation resistance. The workability of the concrete mixture was adjusted by using a high-range water-reducing admixture. During the mixture proportioning, the cement content was fixed at 420 kg/m3; the rest of the paste was made from powders, such as Limestone and Silica fume.

Bulk Density ("Unit Weight") and Voids in Aggregate

Bulk Density-calculate the bulk density for the rodding, jigging, or shoveling procedure as follows:

$$M = (G - T)/V$$

Or

$$M = (G - T) \times F$$

Where:

M = bulk density of the aggregate, (kg/m^3),

G = mass of the aggregate plus the measure, kg ,

T = mass of the measure, kg ,

V = volume of the measure, m^3 , and

F = factor for measure, m^{-3}.

Figure 4. Cylindrical metal measure with Tamping Rod and piece of plate glass

Void Content-Calculate the void content in the aggregate using the bulk density determined by either the rodding, jigging, or shoveling procedure, as follows:

$$\%Void = \frac{100 \times [(S \times W) - (M)]}{S \times W}$$

Where:

M = bulk density of the aggregate, (kg/m^3) ,

S = bulk specific gravity (dry basis) as determined in accordance with Test Method C 127 or Test Method C 128, and

W = density of water, 998 (kg/m^3).

Relative Density (Specific Gravity) (OD)—Calculate the relative density (specific gravity) on the basis of oven-dry aggregate as follows:

Relative density (specific gravity) (OD) $= A/(B-C)$

Where:

A = mass of oven-dry test sample in air, g,

B = mass of saturated-surface-dry test sample in air, g, and

C = apparent mass of saturated test sample in water, g.

Powder Volume-Calculate the powder volume as follows:

$$V_P = V_W + V_C - V_{EXP} - Void$$

Where:

$V_P =$ Powder Volume (lit)

$V_W =$ Water Volume (lit)

$V_C =$ Cement Volume (lit)

$V_{EXP} =$ Excess Paste Volume (lit)

$Void =$ Void Volume (lit)

3. MIX DESIGN OF STRUCTURAL SCC USING VOID-BULK DENSITY METHOD

Nine batches of concrete were designed using the same mixture proportions, as shown in Table 1.

Concrete mixtures were mixed in a high-speed shear mixer. The properties of freshly mixed concretes were determined as described in the following. For each batch, two 100x200mm cylinders were cast for splitting strength testing and six 100x100x100mm cube were cast for compressive and elastic moduli testing. The specimens were cast in one layer without any compaction or vibration. After casting, all the molded specimens were taken to a fog room at 23±2°C. The curing and testing of these specimens for measurement of different properties are described in the following.

Table 1: Mixture proportions of SCC

Mixture No.	Coarse ggregate	Sand	Water	Cement	silicafume	limestone	sp
SCC1	684	884	191	458	46	149	6.8
SCC2	686	886	190	459	48	149	7.15
SCC3	699	907	169	429	36	165	7.01
SCC4	709	918	165	443	71	83	10.10
SCC5	711	924	180	444	63	107	9.8
SCC6	712	925	188	455	134	0	10.40
SCC7	705	917	186	451	87	61	9.47
SCC8	683	917	190	397	92	110	9.38
SCC9	692	900	205	439	116	33	10.10

3.1. Slump Flow Test

The slump flow test measures the horizontal free flow of SCC by using a regular slump cone. It was first developed in Japan for use in assessment of flowability of underwater concrete. This is a simple, rapid test procedure and is suitable for construction site use. The slump cone was filled with concrete mixtures without rodding, and then lifted up vertically. The diameters of spread mixtures in four directions after unconfined lateral spread were measured, and the average of the four measurements was used as the flowability of the concrete mixture. The slump flow of the mixtures was measured at 30, 60, and 90 min after the addition of mixing water to examine how the flowability of SCLC mixtures changed with time. Between measurements, the SCC mixtures were stored in a bucket covered with a damp cloth to avoid moisture loss.

3.2. V-funnel test

A V-funnel, as shown in Figure 5, was used to determine the flowability of the concrete. The funnel was filled with a concrete mixture without rodding or tamping, then the trap door at the bottom was opened to allow concrete to flow out under gravity. The time from opening the trap door until complete discharge of the concrete mixture was recorded as an indication of the flowability of the concrete.

Figure 5. Schematic illustration of V-funnel

3.3. L-box test

L-box tests assess the filling and passing ability of SCC. Serious lack of stability (segregation) can also be observed easily during the testing. The testing apparatus is shown in Figure 6. The vertical section was filled with a concrete sample without rodding or tamping, and then the sliding door was lifted. The time for concrete mixture to flow to the end of the horizontal section was recorded, and the distance H1 and H2 were measured. The flow time can give an indication of flowability. The ratio H2/H1 is called the blocking ratio. Obvious blocking of coarse aggregates behind the reinforcing bars can be visually observed easily.

Figure 6. Schematic illustration of L-box

Table 2: Properties of freshly mixed SCLC mixtures

Mixture no	Slump flow (mm)	Slump flow (s)	V-funnel (s)	L-Box H2/H1,%	L-Box flow t1 (s)	Segration resistance	Density kg/m3
SCC1	615.0	2.75	7.10	0.900	0.73	GOOD	2416.67
SCC2	625.0	2.65	6.70	0.910	0.54	GOOD	2425.00
SCC3	610.0	3.31	12.42	0.785	1.01	GOOD	2412.50
SCC4	655.0	4.05	9.25	0.875	0.68	GOOD	2400.00
SCC5	710.0	1.18	6.12	0.895	0.51	GOOD	2439.38
SCC6	585.0	2.25	6.45	0.805	0.74	GOOD	2424.38
SCC7	690.0	1.29	6.02	0.835	0.46	GOOD	2416.67
SCC8	670.0	1.28	5.88	0.885	0.43	GOOD	2397.78
SCC9	600.0	1.19	5.94	0.825	0.45	GOOD	2400.00

Table 3: Mixture proportions of CVC

Mixture no.	Coarse aggregate	Sand	Water	Cement	silicafume	limestone	sp
CVC1	691	895	176	393	81	180	5.86
CVC2	1062	806	159	413	36	0	6.88
CVC3	1042	877	148	385	38	0	7.16
CVC4	1041	914	138	352	39	0	7.45
CVC5	1001	849	165	447	23	0	7.9
CVC6	1038	886	146	426	22	0	8.80
CVC7	1040	823	167	437	22	0	7.05
CVC8	1071	884	156	372	20	0	7.16

ine different SCC mixtures, using the volume of paste and the relative amount of sand and gravel as variables, and four different mixtures of CVC were made (Tables 1 and 3). Natural sand and gravel with a high percentage of well rounded particles was used with a maximum grain diameter of 12.5 mm for SCC and 19.5 mm for CVC.

4. RESULT

The compressive strengths of SCC and CVC showed similar values for an identical w/b ratio (Figure 7).

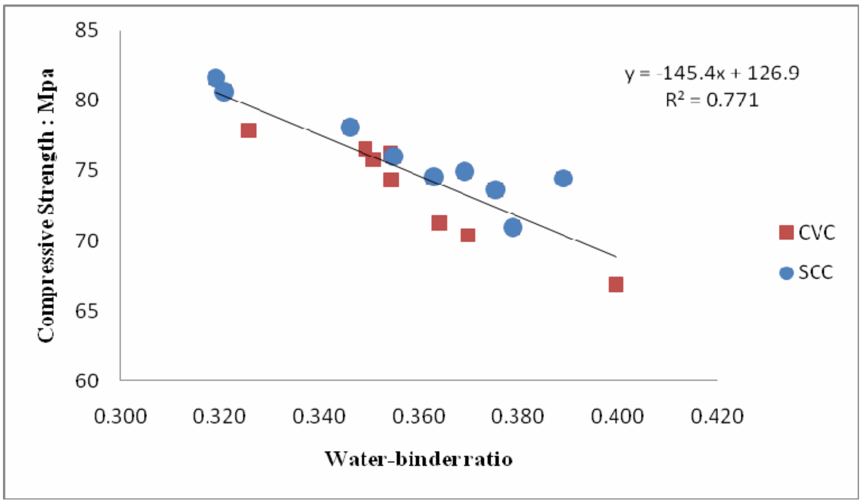

Figure 7. Compressive Strength at 28 days versus w/b ratio

The average E-modulus of SCC was about 8% lower than that of CVC for an identical compressive strength (Figure 8).

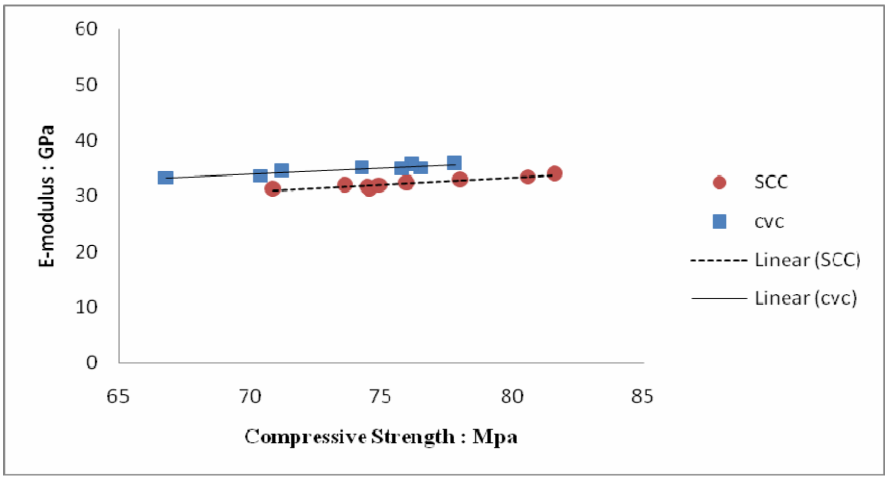

Figure 8. E-modulus versus Compressive Strength, both at 28 days

There was no significant difference in the relation between compressive and splitting tensile strength of SCC in comparison with CVC although the values for SCC showed a relatively high standard deviation (Figure 9).

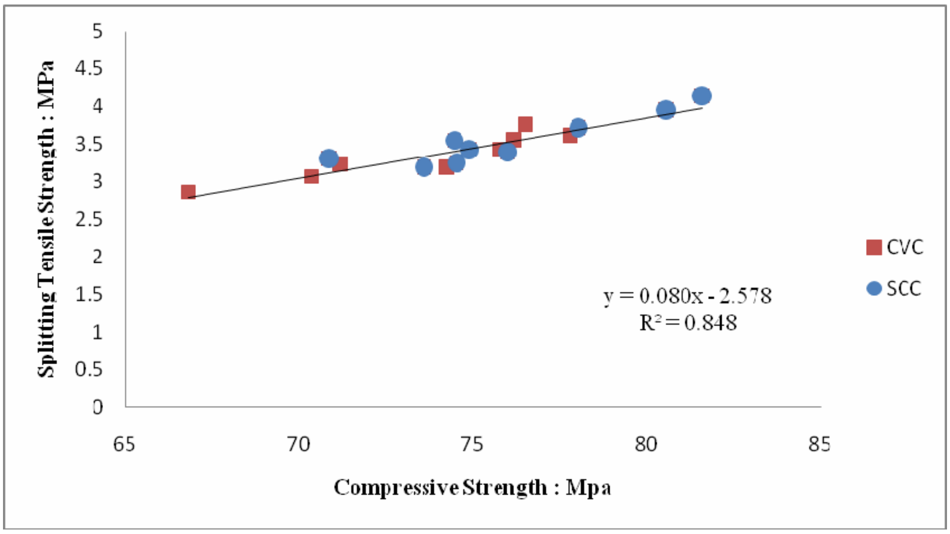

Figure 9. Splitting tensile strength versus Compressive Strength at 28 days

5. CONCLUSIONS

Based on the results of this study, the following conclusions can be drawn:

1. SCLC can be designed using a combination of the least void volume for a binary aggregate mixture, excessive paste theory, and ACI standard practice for selecting proportions for structural concrete. Both ground Limestone powder and Silicafume can be used satisfactorily as powder for making up the excessive paste for SCC.
2. Differences in the properties of SCC and CVC used in this study were mainly caused by their relative volume of paste:
3. The E-modulus of SCC was about 8% smaller than that of CVC for an identical compressive strength.
4. At the age of 28 days SCC and CVC displayed the same compressive and splitting tensile strength with a constant w/b ratio.

REFERENCES

1. H. Okamura, Self-compacting High-Performance Concrete, Concrete International 19 (7) (1997) 50-54.
2. H. Okamura, M. Ouchi, Self-Compacting Concrete-development, present, and future, RILEM, Proc. 1st International RILEM Symposium on Self-Compacting Concrete, 1999, pp. 3-14.
3. H. Ter Welle, Betoncentrale Twenthe, Hengelo, The Netherlands, Personal communications (2003).
4. B. Bos, BAS, Venray, The Netherlands, Personal communications (2003).

5. F.M.L. Ernst, Onderzoek zelfverdichtend beton. MSc Thesis TUE/CCO/00-09, Eindhoven University of Technology, Faculteit Bouwkunde, Capaciteitsgroep Constructief Ontwerpen, Eindhoven, The Netherlands, 2000 (in Dutch).
6. N. Su, K.C. Hsu, H.W. Chai, A simple mix design method for Self-Compacting Concrete, Cement and Concrete Research 31 (2001) 1799-1807.
7. Okamura, H., and Ozawa, K., "Mix Design for Self-Compacting Concrete," Concrete Library of Japan Society of Civil Engineers, No. 25, June 1995, pp. 107-120.
8. Hwang, C. L., and Chen, Y. Y., "The Property of Self-Consolidating Concrete Designed by Densified Mixture Design Algorithm," Proceedings of the 1st North American Conference on the Design and Use of Self Consolidating Concrete, Nov. 2002, pp. 121-132.
9. Kennedy, C. T., "The Design of Concrete Mixes," ACI JOURNAL, Proceedings V. 36, Feb. 1940, pp. 373-400.
10. Oh, S. G.; Noguchi, T.; and Tomosawa, F., "Toward Mix Design for Rheology of Self-Compacting Concrete," Proceedings of the first RILEM International Symposium, Å. Skarendahl and Ö. Petersson, eds., Stockholm RILEM Publications, France, Sept. 1999, pp. 361-372.
11. ACI Committee 211, "Standard Practice for Selecting Proportions for Structural Lightweight Concrete (ACI 211.2-98)," American Concrete Institute, Farmington Hills, Mich., 1998, 20 pp.

CD07-003

ENGINEERING PROPERTIES OF GEOPOLYMER CONCRETE BASED ON ALKALI ACTIVATED NATURAL POZZOLAN

D. Bondar[1], C.J. Lynsdale[2], N. Milestone[3], N. Hassani[4], A.A. Ramezanianpour[5]
[1]Ph.D. candidate of Sheffield University and P.W.U.T. Research Associate
[2]Dept. of Civil and Structural Engineering, (c) Dept. of Material Engineering Univesity of Sheffield, Mappin Street, Sheffield, S1 3JD, UK
[3]Research Center of Natural Disasters in Industry, P.W.U.T., Tehran, Iran
[4]Dept. of Civil Engineering, Amir Kabir University, Tehran, Iran

ABSTRACT
The development of alkali activated binders with superior engineering properties and longer durability have emerged as an alternative to OPC. It is possible to use alkali-activated natural pozzolans to synthesize environmental friendly sound geopolymeric cementitious construction materials. The main benefit of geo-polymeric cement is the reduction in environmental impact in harmony with the concept of sustainable development. This paper presents a comprehensive summary of the extensive studies conducted on the results of experimental investigations on the engineering properties of geo-polymer concrete using activated Iranian natural pozzolan namely, Taftan. Experimental work was conducted to determine mechanical strength; modulus of elasticity; ultrasonic pulse velocity and shrinkage of different concrete mixtures. Test data are used to identify the effects of salient factors such as water to binder ratios and curing conditions that influence the properties of the geopolymer concrete. The results show that mortar and concrete made with alkali activated natural pozzolan develop moderate to high mechanical strength and modulus of elasticity and shrink much less than ordinary Portland cement (OPC) concrete.

Keywords: alkali-activated binder; geopolymeric cement; natural pozzolan

1. INTRODUCTION
Portland cement concrete is a major construction material worldwide use is said to be second only to water. Unfortunate, the production of Portland cement releases large amount of CO_2 in to the atmosphere. This gas is a major contribution to the greenhouse effect and the global warming of the planet. To reduce greenhouse gas emissions, efforts are needed to develop environmentally friendly construction materials. Unlike with regular concrete the chemical reactions that form geopolymer concrete alternative do not give off carbon dioxide or require high temperatures, which also lead to CO_2 emissions.
In geopolymer concrete, the geopolymer paste serves to bind the coarse and fine aggregates, and any un-reacted material. Geopolymer concrete can be utilized to manufacture pre-cast concrete, structural and non-structural elements, to make

concrete pavements, immobilize toxic waste, and produce concrete products that are resistant to heat and aggressive environments [5, 6].

This paper presents the technology of making geopolymer concrete using natural pozzolan as its source material and presents the results of laboratory tests conducted on this material. The research data presented in this paper are useful to understand the engineering properties of geopolymer concrete.

2. PREVIOUS RESEARCH ON GEOPOLYMER MATERIAL

The term "geopolymer" describing a family of mineral binders those have a polymeric silicon-oxygen-aluminum framework structure. The mechanism of geopolymerisation may consist of dissolution, transportation or orientation, and polycondensation [15], and takes place through an exothermic process [3, 8].

Different pathways for preparation of a synthetic geopolymer, including the order of addition of the raw materials, show different evolutions of compressive strength of the materials. The best method is to prepare an alkaline solution (mixing MOH and water and stirring for 2 minutes), adding pozzolan to alkaline solution for 15 minutes in a mixer, followed by sodium silicate, and mixing for 15 minutes [10].

The geopolymer paste serves to bind the coarse and fine aggregates and any un-reacted material to prepare geopolymer concrete [5, 6].

The nature of the fresh geopolymer concrete is stiff paste with high viscosity hence it tends to have low workability [5, 6].

A geopolymer mix can be timed to set either fast or slow, by adjusting the mixture components. Depending on the synthesis conditions, structural integrity and reasonable strength were attained in a short time, sometimes in as little as sixty minutes [14]. With the use of granulated blast furnace slag as the source material with the addition of metakaolinite, Cheng and Chiu (2003) found that the setting time of geopolymer paste was affected by curing temperature, type of alkaline activator and the composition of source material. They stated that the setting time of above geopolymer paste was between 15 to 45 minutes at 60°C. The laboratory experience by Hardjito, Wallah, Sumajouw and Rangan (2004) showed that the fresh geopolymer concrete could be handled for at least 120 minutes after mixing, without any sign of setting and degradation in compressive strength. These have mostly depended on the compounds in the source material, for instance the higher the content of CaO, the faster the setting. The presence of compounds other than Al_2O_3 and SiO_2 in the source material may also delay the setting. The pfa based geopolymers show faster initial setting time at higher temperatures and the final setting of these mortars occurr from 15 to 25 minutes after the initial setting [7].

There are many different views as to which main parameters affect the compressive strength and other mechanical properties of geopolymer concrete. Palomo et al. (1999) stated that the significant factors affecting the compressive strength are the type of alkaline activator, the curing temperature and the curing time [5, 6]. Other researchers have reported that the important parameters for satisfactory polymerization are the relative amounts of Si, Al, K, Na, molar ratio of Si to Al in solution, the ratio of alumina silicate mineral to kaolinite, type of alkaline activator, water content, and curing temperature [1, 12, and 15]. The presence of silicate ions in the aqueous substantially improves the mechanical strength and modulus of elasticity values but has a slightly adverse effect on the otherwise very strong matrix/aggregate and matrix/steel bond [4]. Experimental results show that the H_2O/M_2O molar ratio in the mixture composition is a significant parameter affecting the compressive strength of fly ash based geopolymer concrete, whereas the influence of the Na_2O/SiO_2 molar ratio is less significant. An increase of the H_2O/M_2O molar ratio and water to geopolymer solids ratio decreases the compressive strength of geopolymer. In addition, Van Jaarsveld et al. (2002) found that curing at elevated temperatures for long periods of time may weaken the structure of hardened material. The research on fly ash-based geopolymer binder, Palomo, Grutzeck, and Blanco (1999) have confirmed that curing temperature and curing time significantly influenced the compressive strength but seems not to be same for different alumina silicate. Longer curing time and higher curing temperature increased the compressive strength in fly ash based geopolymer concrete, although the increase in strength may not be significant for curing at more than 60°C and for periods longer than 48 hours [5, 6]. In most cases 70% of the final compressive strength is developed in the first 4 hours of setting. Because the chemical reaction of the geopolymer paste is a fast polymerization process, the compressive strength does not vary with the age of concrete, after it has been cured for 24h. This observation is in contrast to the well-known behaviour of OPC concrete, where the hydration process extends over a long period and hence strength increases over time [5, 6]. Another Kinetic difference between the Portland and alkaline systems is the existence of a relatively low threshold temperature in the former, above which thermal curing can have an adverse effect on the mechanical development and even on material durability. In an activated ash, on the contrary, a suitable choice of reaction time and curing temperature can yield different reaction product without detracting from material durability, because according to Fernandez, Palomo, and Hombradoz (2006) increases in the curing temperature go hand-in-hand with decreases in the amount of Al incorporated into the final product and a concomitant improvement in mechanical properties. Such improvements parallel the formation of a homogeneous alumina-silicate matrix [3].

When alkali-activated slag cement concrete is cured in water, compressive strength of the concrete keeps increasing until 365 days. However, if the concrete is cured in sealed condition the strength stopped increasing at about 90 days. This may be attributed to the lack of moisture available for the hydration of slag inside the concrete. The concrete exposed to air exhibit the lowest strength all the time and strength retrogression at ages greater than 28 days. The strength reaches a maximum after 14 to 28 days of hydration, and then starts to decrease [13].

Puertas et al. (2003) reported that the elastic modulus of OPC mortars was 5679 MPa, also higher than the values for activated PFA mortars (4441 MPa).

Fernandez-Jimenez et al. (2006) found that the addition of soluble silicates in the alkali solution improves the modulus of elasticity. However, this improvement was not sufficient and the alkali activated PFA concrete showed a much lower static modulus of elasticity than expected. The values presented for OPC concrete ranged from 30.3 to 32.3GPa while for geopolymeric concrete ranged from 10.7 (without silicate) to 18.4 GPa (with silicate). Hardjito et al. (2004) observed better elastic modulus results for a concrete samples made in similar conditions: 22.95 to 30.84 GPa.

Geopolymers also attain shrink much less on setting (for 7days 0.2% & for 28days 0.5% of OPC) [14]. The explanation for this behaviour is to be found in the micro structural characteristic of the new binder and the main reaction product of the alkali activation of fly ash which causes a zeolite-type phase. Zeolite properties and microstructure are widely known to be unaffected by the loss of the water incorporated during their synthesis because not only water loss is reversible in most zeolites but also they are able to absorb water from the humidity in atmosphere [4].

3. EXPERIMENTAL WORK

3.1. Material and Mixing Procedure

In this research, Taftan andesite was selected as the most reactive natural pozzolan in Iran, used to produce Portland pozzolan cement by Khash Cement Factory. The chemical composition was analysed by XRF and presented on Table 1.

Potassium hydroxide was used as pellets to produce the alkaline solution for geopolymeric concrete production. It was a 98% pure KOH supplied by MERK International Ltd.

Sodium silicate was also provided by Iran Silicate Industrial Company in the form of granules, powder and solution (water glass). The chemical composition of the solution provided by the manufacture was:

8.5% of sodium oxide (Na_2O), 26.5% of silicon oxide (SiO_2) and 65% of water

Aggregate used in this study was obtained from deposits of Karaj River in northwest of Iran comprising 14mm and 4.75mm coarse aggregates and fine sand. The fineness modulus of combined aggregates was 2.08.

The proportioning of the concrete mixture was based on the BRE method targeting a 40 MPa (28 days) compressive strength and a slump of 70 mm. Then, the amount of cement was substituted with the same quantity of natural pozzolan and the amount of water was ignored since there was already water in the alkali solution. The BRE method was used only to decide what is a common ratio of binder, sand and coarse aggregates, it was not expected that the actual 28 days compressive strength or the slump would be in accordance with the values designed. The details of the different mixes are presented in Table 2 and the notation for the mixes is as follows:

CM1: PC control mix with w/c=0.45

CM2: PC control mix with w/c=0.55

ATAF1: Activated Taftan pozzolan with w/c=0.45

ATAF2: Activated Taftan pozzolan with w/c=0.55

The mixing of the geopolymeric concrete was carried out in two different mixers sequent. The paste was prepared in a Hobart mixer (2 litre capacity) and added to a horizontal pan mixer (20 litre capacity) which contains the aggregates.

Taftan specimens were de-moulded 24 hours after casting. Then they were cured in two curing regimes and at three different temperatures:

1. Sealed curing: Three series of specimens were sealed wrapped in a special plastic covering which was tested to be impermeable and stored in a controlled room kept at three different temperature equal to 20±2, 40±2 and 60±2°C.

Table 1: Chemical composition (oxide percent) of the materials used in this investigation reported by Kansaran Binaloud X-ray laboratory in Tehran, Iran (2005-2006)

Material	LOI	SiO_2	Al_2O_3	Fe_2O_3	CaO	MgO	TiO_2	K_2O	Na_2O
Taftan andesite	1.85	61.67	15.90	4.32	7.99	2.04	0.438	2.12	3.21

Table 2: Concrete Mix Proportion

Mix No.	Natural Pozzolan (Kg/M^3)	OPC (Kg/M^3)	Alkaline Hydroxide (Kg/M^3)	Water Glass (CC/M^3)	Water (Kg/M^3)	Total Water (Kg/M^3)	Total Binder (Kg/M^3)	Fine Agg. (Kg/M^3)	Coarse Agg. (Kg/M^3)	W/B%
CM1	_	403	_	_	180	181.3	403	577.82	1227.88	0.45
CM2	_	357	_	_	195	196.35	357	702	1119.65	0.55
ATAF1	391	_	66.27	34.18	157.78	180	403	578.17	1228.8	0.45
ATAF2	344	_	71.82	36.9	171	195	357	702	1121	0.55

2. Steam curing: Three series of the specimens were put in the steam curing chamber set at three different temperatures equal to 20±2, 40±2 and 60±2°C for measuring compressive and splitting tensile strength and one series was put at 40±2°C for other measurements.

3.2. Testing Procedures

In order to determine the compressive strength of geopolymeric concrete each of the subsequent mixtures were prepared in 100x100x100 mm cubes and the compressive strength for these samples were tested according to BS EN 12390-3:2000. Details of casting and curing are described in section 3.1. Three samples of each condition were tested for 1, 7, 14, 28, 90, 180 and 365 days, and the average compressive strength values reported as the results.

PUNDIT was used to measure the ultrasonic pulse velocity in accordance with BS 1881: part 203: 1986. The measurement was conducted on the 100mmx100mm end face of prism with a length of 500mm. Duplicate sets of samples were tested at 28, 90,180 days. For measuring ultrasonic pulse velocity, a pulse of longitudinal vibration is produced by means of 54 kHz an electro acoustical transducer of 50mm diameter and picked out by another transducer after travelling a known path length.

The splitting tensile strength of all mixes was measured using 100mm Φ x 200mm length cylinders. The samples were prepared and splitting tensile tests performed as described in BS EN 12390-6:2000. The specimens were tested in duplicate sets at 7, 14, 28, 90, 180 and the average results are reported.

The static modulus of elasticity is determined according to BS1881-121:1983 standard by subjecting a 100mmΦx200mm cylinder specimen to uni-axial compression and measuring the deformation by means of dial gauges fixed between certain gauge lengths. Dial gauge reading divided by gauge length will give the strain while load applied divided by area of cross section will give the stress. A series of readings are taken and the stress-strain relationship is established. The modulus of elasticity so found out from actual loading is called static modulus of elasticity.

In the present work the changes in length of 75x75x280mm concrete prisms were measured by commonly used mechanical equipment. Predrilled metal studs were fixed to either end of the concrete specimen with the adhesive at a preset spacing with the aid of a standard calibration bar. The distance between each two pins located into the stud holes was measured by an accuracy of about 0.0025 mm at certain times. One end of the reference rod was designed as the top and it was kept uppermost during all measurements. The prisms were placed in the apparatus with the marked end uppermost and were rotated slowly around the contact surfaces to measure the changes in length. For each mix two specimens were cast and cured for 3 and 7 days. The prisms were then left in a room controlled at 20°C and 70% humidity room and chemical shrinkage was measured using the length comparator in accordance with BS 812: Part 120: 1989.

4. RESULTS AND DISCUSSION

4.1. Compressive Strength

The results of the compressive strength tests on geopolymeric concrete using activated natural pozzolan and control Portland cement concrete mixes are presented in Figures 1.

In all cases, the strength of the concretes increased with age. The rate of strength gain is high at early ages and gradually decreases at longer ages. Geopolymeric concrete mixes mostly showed lower strengths than OPC control mixes at early ages, but they reached the same and even higher strengths than OPC mixes after long-term aging. ATAF1 have the highest compressive strength equal to 43.5 MPa. While ATAF2 mix has resulted compressive strength equal to 39.1 MPa after 365 days which is close to the amount resulted for OPC control mix.

It is well known that the lack of curing greatly affect the strength development. Figure 1 clearly shows the effect of different curing temperatures in two conditions of curing: sealed and steam curing. It generally sealed condition gives the best results in long term the same as OPC control concrete although the difference between the two conditions is not significant.

The results suggest that the optimum temperature for curing alkali-activated Taftan pozzolan is 60°C at early ages but curing at 40°C under sealed conditions gave the highest strength results in the long-term.

An increase of the water to binder ratio decreases the compressive strength of geopolymer concrete significantly (Figure 2).

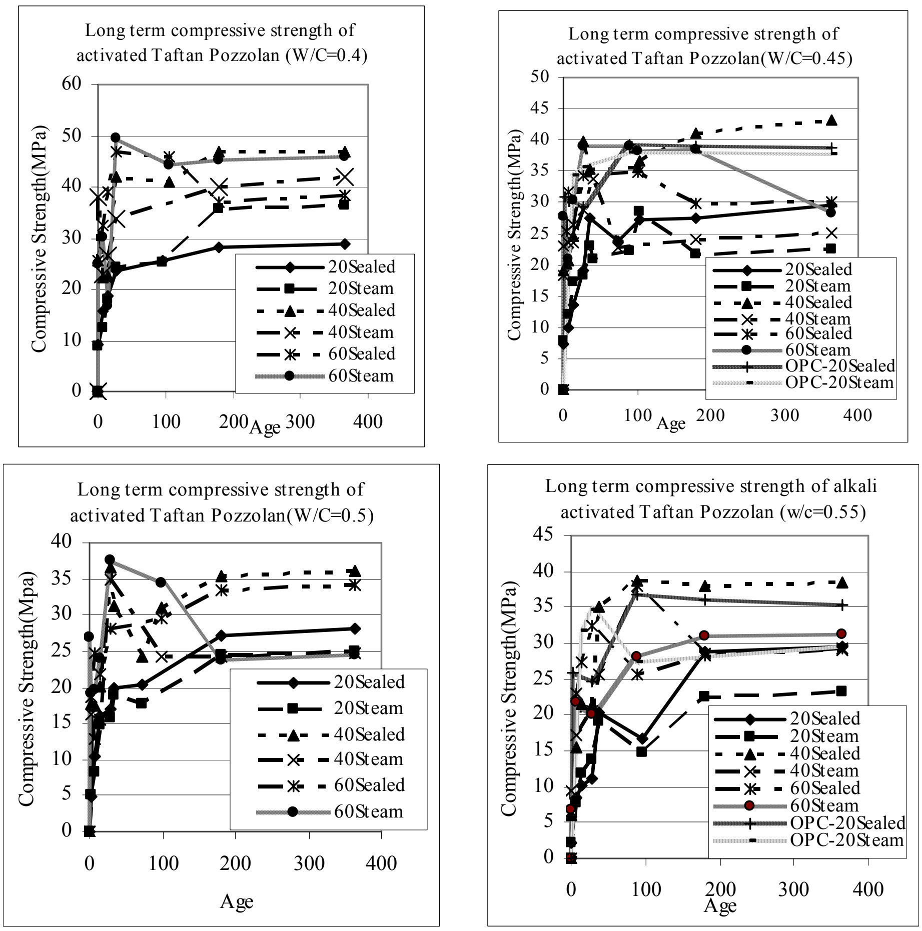

Figure 1. Effect of different curing condition and curing temperature on compressive strength development for activated Taftan pozzolan with different water to binder ratio

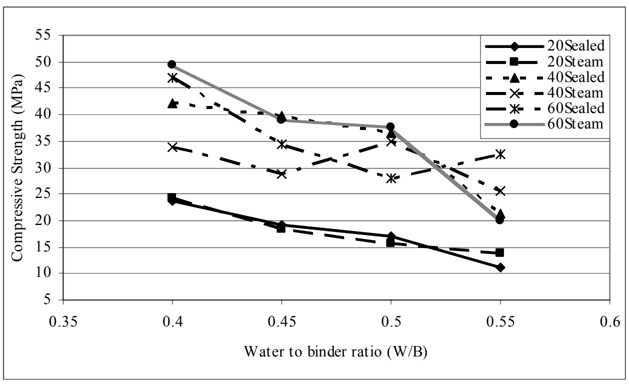

Figure 2. Compressive strength at 28 days versus water to binder ratio (W/B) for alkali activated Taftan pozzolan at different curing temperature

4.2. Ultrasonic Pulse Velocity

Figure 3 shows the results for the ultrasonic pulse velocity test for all mixes. The Figure shows that ATAF1 achieved the highest values followed by ATAF2. Tabular form of the results is shown in Table 3. Comparing the results with Table 4, which gives the pulse velocity rating as suggested by Central Water and Power research Station, Khadakwasla (India), presents lower velocity corresponding to the same compressive strength. It seems that in geo-polymeric concrete due to its lower density the velocity of pulses are lower than OPC concrete.

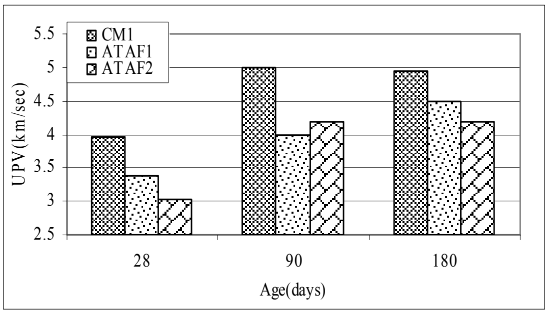

Figure 3. Ultrasonic Pulse Velocity for different mixes

Table 3: The pulse velocity and the corresponding compressive strength of different mixes

Mixes	Age(days)	Velocity(km/sec)	Compressive strength(MPa)
	28	3.95	29.8
CM1	90	5.0	39.23
	180	4.95	39
	28	3.5	24.78
CM2	90	4.7	36.78
	180	4.6	36
	28	3.39	39.7
ATAF1	90	4.0	35.6
	180	4.5	40.97
	28	3.03	21.36
ATAF2	90	4.2	38.72
	180	4.2	38.06

Table 4: Quality Criteria Suggested by Central Water and Power Research Station Khadakwasla (India)

Velocity (km/sec)	Classification (Quality)	Compressive strength(Kg/cm^2)
4.0 and above	Very good	300 to 350
3.5 to 4.0	Good	250 to 300
3.0 to 3.5	Medium	200 to 250
3.0 and below	Poor	150 to 200

4.3. Indirect Tensile Strength

The results of the indirect tensile strength tests up to 180 days are shown in Figure 4. The trend in tensile strength is similar to that obtained for compressive strength. Tensile strength increases as time proceeds. Figure 6 illustrates a difference development in tensile strength of different mixes. As far as the geopolymeric concrete mixes based on activated natural pozzolan are concerned, higher strength was observed at longer ages in comparison with control mixes. At early age, ATAF2 shows lower tensile strength results than OPC control mix. Although, the tensile strength of ATAF1 geopolymeric concrete mix is 3.57 MPa after 28 days and higher than the OPC control mix. The results of long term tensile strength show that Taftan geopolymeric concrete mixes have higher tensile strength than OPC control mix equal to 3.69 and 3.0 MPa after 365 days.

The tensile strength of this type of concrete as compared to its compressive strength, is more sensitive to improper curing, the same as OPC concrete. Figure 4 illustrates the effect of curing conditions and temperatures on tensile strength of concrete based on activated natural pozzlans. The optimum temperature of curing is 40ºC, the same as that found for compressive strength.

Figure 4 shows that the higher water to binder ratio results in lower tensile strength, same as OPC mixes.

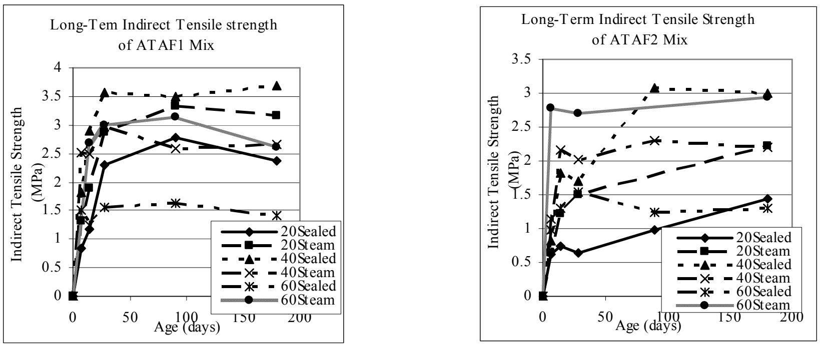

Figure 4. Effect of different curing condition and curing temperature on Indirect Tensile strength development for ATAF1 and ATAF2 mixes

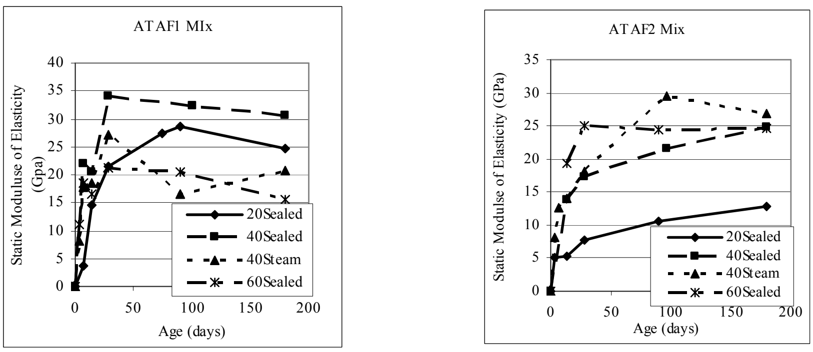

Figure 5. Effect of different curing condition and curing temperature on Static Modulus of Elasticity development for ATAF1 and ATAF2 mixes

4.4. Static Modulus of Elasticity

Results of the static modulus of elasticity are shown in Figure 5. Similar to the compressive strength results of the mixes, static modulus of elasticity increases with age. This improvement is fast in the first 28 days as the most of the modulus value is generally achieved in this period. During the first 14 days the mixes made with activated natural pozzolans have mostly shown lower values of static modulus of elasticity than OPC concrete mixes, except ATAF1 mix. The static modulus of elasticity for ATAF1, ATAF2 mixes after 14 days is 33.96, 14.033GPa, respectively with that for the CM1 mix is 26.55GPa. Long term results show that the static elastic modulus of some of alkali activated natural pozzolans such as ATAF1 are around 5% to 20% more than OPC mixes. The long term static modulus of elasticity of ATAF1, ATAF2 mixes were resulted at 32.664, 26.805GPa in compare with OPC concrete mixes which resulted 29GPa.

The elastic modulus was affected by the curing temperatures and conditions. Early age static modulus of elasticity increases with increasing the curing temperature to a limit which seems to be related to the water to binder ratio. For ATAF1 with water to binder ratio equal to 0.45, the elastic modulus increases with increasing curing temperature up to 40˚C and then decreases when the curing temperature rises up to 60˚C. This optimum temperature to achieve higher static modulus of elasticity raises to 60˚C for ATAF2 mixes with water to binder ratio equal to 0.55. However, the long term results drop to the same amount resulted for the mix cured at 40˚C.

4.5. Drying Shrinkage

The shrinkage time curves are shown in Figures 6. From this investigation the following observations are made:

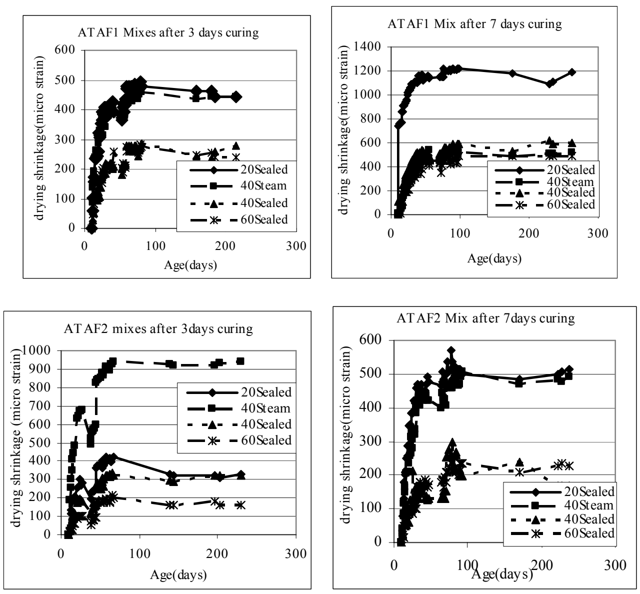

Figure 6. Effect of length, temperature and condition of curing on drying shrinkage development with age for ATAF1 and ATAF2 mixes

1) The graphs show that the magnitude of shrinkage increases with time and the rate of shrinkage decreases rapidly with time. The rate of shrinkage in Taftan pozzolan mixture was similar but not as rapid as the rate of development of strength and, seems to be constant after 60 days.
2) In OPC concrete one of the important factor which influences the magnitude of shrinkage is water to cement ratio of concrete and the values of shrinkage increases with the increasing of this ratio. The results indicate that the total water to binder ratio has a significant effect on the shrinkage properties of geopolymer concretes as well and seems to be contrary to the behaviour of OPC concrete, where the higher the water to binder ratio lowers the amount of drying shrinkage resulted. The maximum amount of final drying shrinkage for ATAF2 mix observed is 43% of that for ATAF1. The shrinkage of ATAF1 and ATAF2 mixes at 180 days at same curing conditions were $1185x10^{-6}$ and $514x10^{-6}$, respectively.
3) The results show that at a given water to binder ratio, the drying shrinkage at all ages varied with different curing regimes and temperatures. In concrete based on alkali activated natural pozzolan, the higher the curing temperature the lower the amount of drying shrinkage resulted. The lowest amount of drying shrinkage for different curing temperatures correspond to ATAF1 and ATAF2 mixes was 239×10^{-6} and 161×10^{-6}, respectively and achieved for mixes cured at 60ºC. It can be observed that steam curing shows higher amount of drying shrinkage. This phenomenon may be related to the pozzolan nature minerals and because of swelling properties of its minerals during absorbing moisture. When the samples are subjected to wetting condition, they start swelling. Swelling is due to the adsorption of water by the natural minerals in pozzolan gel. The water molecules act against the cohesive force and tend to force the gel particles further apart as a result of which swelling takes place. In addition, the ingress of water decreases the surface tension of the gel. The property of swelling when placed in wet condition, and shrinking when placed in drying condition. While in OPC concrete the magnitude of shrinkage is less sensitive to moisture movement in concrete.
4) The length of curing affects the amount of drying shrinkage as well. The specimens cured for a period of three days seem to absorb environmental humidity similar to zeolites but after 7days the property of water absorption reduces. Thus, the former show lower amount of shrinkage than the latter. In calcined Shahindej, this phenomenon is not observed.

5. CONCLUSION

The main conclusions drawn from the investigation of engineering properties of geopolymeric concrete based on activating natural pozzolans (i.e. alkali activated natural pozzolan or AANP) are summarized as follows:

1) Geopolymeric concrete mixes based on activated natural pozzolans have mostly shown lower strength than OPC mixes at early ages, but they have reached the same and even higher strength than OPC mixes after long-term.
2) It seems that the ultrasonic pulse velocity in the geopolymeric concrete due to

its inherent property caused lower density is lower than in OPC concrete having the same compressive strength.

3) During the first 14 days the mixes made with activated natural pozzolans have mostly shown lower values of static modulus of elasticity than OPC concrete mixes. However, long term results show that the static elastic modulus of alkali activated natural pozzolans concrete is generally around 5 to 20% more than OPC mixes.
4) The elastic modulus of AANP concrete was affected by the curing temperatures. Early age static modulus of elasticity increases with increasing the curing temperature to a limit which seems to be related to the water to binder ratio. That means if there be the lack of water due to its evaporation at higher temperature before the full strength is gained the static modulus of elasticity decreases at higher temperatures.
5) The AANP concrete mixes may exhibit lower drying shrinkage in comparison with the OPC mixes at the same water to binder and cement to aggregate ratio.
6) The results indicate that the total water to binder ratio have a significant effect on the shrinkage properties of geopolymer concretes and seems to behave differently to OPC concrete in this respect. Where, higher the water to binder ratio for geopolymer concrete the lower is the amount of drying shrinkage.
7) In concrete made with alkali activated natural pozzolan, the higher the curing temperature, the lower the amount of drying shrinkage resulted.
8) It can be observed that steam curing shows higher amount of drying shrinkage. This phenomenon may be related to the pozzolan natural minerals and because of swelling properties of its minerals during absorbing moisture.

REFERENCES

1. Barbosa, V.F.F., MacKenzie, K.J.D., and Thaumaturgo, C., “Synthesis and characterisation of materials based on inorganic polymers of alumina and silica: sodium polysialate polymers”, International Journal of Inorganic Materials, Vol. 2, 2000, pp. 309-317.
2. Cheng, T.W. and Chiu, J.P., “Fire-resistant geopolymer produced by granulated blast furnace slag”, Minerals Engineering, Vol. 16, 2003, pp.205-210.
3. Davidovits, J., “Chemistry of Geopolymeric Systems, Terminology”, Presented at the Geopolymer ’99 International Conference, France, 1999.
4. Fernandez-Jimenez, A.M., A. Palomo, et al. (2006). "Engineering properties of alkali activated fly ash concrete." ACI - Materials Journals **103**(2): 106-112.
5. Hardjito, D., Wallah, S. E., Sumajouw, D.M.J. & Rangan, B.V., “On The Development of Fly Ash-Based Geopolymer Concrete”, ACI Materials Journal, Accepted for publication, 2004a.
6. Hardjito, D., Wallah, S.E., Sumajouw, D.M.J. & Rangan, B.V., “The Stress-Strain Behaviour of Fly Ash-Based Geopolymer Concrete”, in ACMSM 18,A.A. Balkema Publishers - The Netherlands, Perth, Australia, 2004b.
7. Costa, J., Lynsdale, C.J., Milestone, N.B., “Alkali-activated fly ash”, M.S. Thesis, 2007.
8. Palomo, A., Grutzeck, M.W., and Blanco, M.T., “Alkali-activated fly ashes, a

cement for the future", Cement and Concrete Research, Vol. 29, 1999, pp. 1323-1329, 1999.

9. Palomo, A., Blanco-Varela, M.T., Granizo, M.L., Puertas, F., Vazquez, T., and Grutzeck, M.W., "Chemical stability of cementitious materials based on metakaolin", Cement and Concrete Research, Vol. 29, 1999, pp. 997-1004, 1999.
10. Palomo, A., Macias, A., Blanco, M.T., Puertas, F., "Physical, chemical and mechanical characterisation of geopolymers", Proceedings of the 9th International Congress on the Chemistry of Cement, 1992, pp. 505-511.
11. Puertas, F., Amat, T., Ferna´ndez-Jime´nez, A., Va´zquez, T., "Mechanical and durable behaviour of alkaline cement mortars reinforced with polypropylene fibres", Cement and Concrete Research, 33, 2003, pp.2031-2036.
12. Rowles, M. and O'Connor, B., "Chemical optimisation of the compressive strength of aluminosilicate geopolymers synthesised by sodium silicate activation of metakaolinite", Journal of Materials Chemistry, Vol. 13, 2003, pp.1161-1165.
13. Shi, C., Krivenko, P.V., Roy, D., "Alkali-Activated Cement and Concretes", Taylor & Francis, London and New York, 2006.
14. Van Jaarsveld, J.G.S., Van Deventer, J.S.J., Lorenzen, L., "The potential use of geopolymeric materials to immobilise toxic metals: Part I. Theory and applications. Miner", Eng. 10 _7, 1997, pp.659-669.
15. Xu, H. and van Deventer, J.S.J., "The geopolymerisation of aluminosilicate minerals", International Journal of Mineral Processing, Vol. 59, 2000, pp. 247-266.

CD07-004

USING SIMPLE PASTE AND MORTAR TESTS RESULTS TO OPTIMIZE SELF CONSOLIDATING CONCRETE

M. Khodadad-Saryazdi[1], H. Famili[2], T. Parhizkar[3], A.M. Raisghasemi[3]
[1]Civil Engineering Department, Yazd University, Yazd, Iran
[2]Civil Engineering Department, Iran University of Science and Technology, Tehran, Iran
[3]Building and Housing Research Center of Iran, Tehran, Iran

ABSTRACT

Self consolidating concrete (SCC) is usually proportioned with several mineral and chemical admixtures. A key factor for a successful formulation is a clear understanding of the role of the various constituents in the mix and their effects on the fresh and hardened concrete. In this research a three phase mix design procedure starting from designing the paste and then mortar leading to the design of a stable SCC was adopted. Selection of type and amount of paste ingredients was based on the result of a previous study presented elsewhere. A modified version of Marsh cone test, called FlowCyl, was utilized to quantify the viscosity related property of the paste. Also, using a miniature slump cone the spread diameter of the paste, which is related to its yield stress, was measured. Then, using a reduced size V-funnel and a mini slump cone, the influence of volume of selected paste on the flow behavior of mortar was studied and the mortar suitable for SCC was chosen. In this method if segregation or bleeding occurs in paste or mortar, the mix proportion would be adjusted at the corresponding design phase. Finally, by adding various quantities (volume) of the chosen mortar to the coarse aggregate, the effect of mortar volume on the flow behavior of SCC was studied and an optimized SCC with satisfactory workability was achieved.

1. INTRODUCTION

Over the last decade, SCC has been the most important subject in concrete research since it has unique properties and numerous advantages in practical applications. Self consolidating concrete is attractive for several reasons including the reduction of: manpower, construction time, noise disturbance on the job site, defects on the concrete surface, and the overall project cost [1-4].

The main factor in the mix design of SCC is the increase in the powder content, to increase the separation of the aggregate particles. As the use of cement for the entire powder fraction would be too expensive and detrimental for durability of the structure, as well as green environment, fine powdered mineral admixtures such as limestone powder, micronized quartzite, fly ash, silica fume etc. are usually substituted for cement. SCC also relies on the use of superplasticizers (SP) for achieving its fluidity and, often, viscosity modifying agents (VMA) to prevent segregation and to achieve robustness [1-4]. Due to the complexity of the mix design, with several chemical and mineral admixtures, the proportion design and compatibility of these admixtures should be optimized via testing the paste and mortar [5- 7]. The properties of paste and mortar can be established by using only a few liters of the material, while providing the designer with useful information for understanding the effects of various constituents on their fresh and hardened properties as well as predicting the behavior of fresh and hardened concrete.

Fresh SCC is a multiphase material but, from a practical viewpoint can be regarded as a two-phase material namely: a solute being suspended in a solution [8]. In the model the solute can be considered as either coarse aggregates, or fine and coarse aggregates in which case the solution would be either highly flowable mortar or paste, respectively. The flow properties and segregation resistance (stability) of SCC are consequently controlled via proper adjustment of the rheology of the mortar as well as that of paste and adequate selection of the content of aggregates [8-10].

Numerous researchers have successfully used the two point test, introduced by Tattersall [11], to measure the rheological properties of concentrated suspensions. In this model, using Bingham equation, two parameters define the flow of paste, mortar and concrete: yield stress and plastic viscosity [12-14]. The measurement of yield stress and plastic viscosity requires a rheometer and where it is not available, alternative simpler one point tests can be used to assess the workability. The slump spread-flow and flow time or rate of discharge from a funnel is used by many researchers to identify the yield stress and viscosity of paste, mortar and concrete [15, 16]. Obviously the size and shape of the apparatus used for testing concrete is bigger than that of mortar; and for testing the paste, mini-sized apparatus is used. Infact extensive concrete testing requires a large amount of materials and labor, which is expensive and is not always practical. While, testing paste and mortar is easier, cheaper, and needs much less material than concrete testing. There is, therefore, a need to engineer the mix design proportion of SCC starting from paste design and then mortar leading to a SCC with satisfactory desired properties.

The objective of this study was to use a three phase mix design procedure starting from designing the paste and then mortar leading to the design of a stable SCC. A modified version of Marsh cone test called FlowCyl, introduced by Mortsell [17] and widely used in European countries [18], was utilized to quantify the viscosity, called flow resistant ratio λ_Q, of the paste. Also, using a miniature slump cone (see Figure 1-a), the spread diameter of the paste, which is related to its yield stress, was measured. Then, the influence of paste volume on the flow behavior of mortar was studied via a reduced size V-funnel and mini slump cone suggested by EFNARC [1]. The self compactability of the mortar was examined by a small U-box suggested by Saak et al [2]. And the mortar suitable for SCC design was chosen. In this method if segregation or bleeding occurs in paste or mortar, the mix proportion would be adjusted at the corresponding design phase.

Finally, the flow behavior of SCC, using slump flow and V-funnel flow time, was studied by adding various quantities (volume) of the chosen mortar to the coarse aggregate and optimized SCC with satisfactory flow behavior was achieved. Passing ability of SCC was verified by L-box test. A mix design program based on volume proportioning and the objectives of this study was prepared using spread sheet software (EXCEL). The slump cones and funnels used in this study are shown in Figure 1.

Figure 1. Slump cones and Funnels used for testing (A) paste, (B) mortar, and (C) concrete

2. SIGNIFICANCE OF THE RESEARCH

For many years concrete was composed of only three materials (aggregate, cement, and water) and the simple mix design methods such as ACI-211 was used to proportion the ingredients. But in the recent years, the concrete mixture-proportioning problem has become more and more complicated. With the appearance of new components like organic admixtures and supplementary cementitious materials, SCC with several numbers of ingredients and high performance expectation has been emerged. Its design must be engineered starting first from the paste and then mortar, leading to an optimized SCC mixture with its required fresh and hardened properties fulfilled. It is shown that following this approach and using the results of very simple paste and mortar tests, not only simplifies the SCC mix design process, but also optimizes the mix proportion. The collection of test results utilizing this approach would make a valuable data base for the design engineer and ready concrete mix supplier.

3. EXPERIMENTAL PROGRAM

3.1. Materials and Test Variables

Type I-425 Portland cement with density=3.15 and silica fume with density=1.9 was used. Micronized quartzite with density of 2.65 was used as filler. The chemical properties of cement are given in Table 1. The density and absorbtion capacity of fine and coarse aggregates are given in Table 2 and their grain size distribution are given in Figures 2 and 3.

Table 1. Properties of Portland cement

SiO_2%	19.94
Al_2O_3%	4.12
Fe_2O_3%	4.08
MgO%	4.25
CaO%	60.15
SO_3	2.03
LOI%	4.10
C_3S%	54.02
C_2S%	16.41
C_3A%	4.01
$(Na_2O+0.658K_2O)$%	0.96

Table 2. Properties of the aggregates

Aggregate Type	SSD Density	Dry Density	Absorbtion Capacity %
Fine	2.59	2.51	3.24
coarse	2.58	2.53	1.97

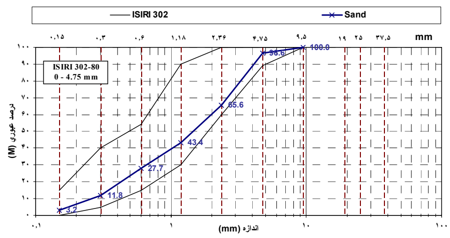

Figure 2. Grading curve of fine aggregate

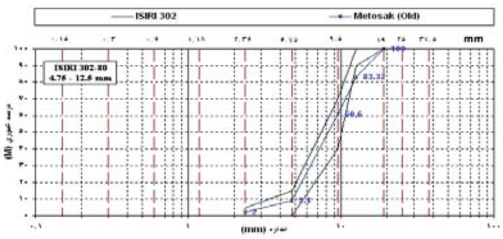

Figure 3. Grading curve of coarse aggregate

The superplastisizer used was based on carboxylic ether polymer with long lateral chains (Gelenium 110) and 40% solid content. It has density of 1.07. Two water powder ratios (W/P) of 0.25 and 0.30 were considered and utilizing the result of previous study presented elsewhere type and amount of powder and admixture was selected. The paste was designed and tested. Then mortar with paste volume of 50, 55 and 60 percent was made and its flow behavior was investigated; any necessary adjustments were made and the optimized mortar was selected. Finally SCC with mortar volume of 67.5, 70 and 72.5 percent was made from the selected mortar and the effect of mortar volume on the flow behavior of SCC was studied. At this phase, based on the design requirements, an optimized SCC would be selected. A data base of the collected mix design along with the result of performed tests could be used by design engineer and ready concrete mix supplier to obtain a reliable model for fast and smart mix design.

3.2. Mix Proportions and Measurements

A mix design program based on volume proportioning was prepared using spread sheet software (EXCEL). The experiments were carried out in three phases described as follows.

3.2.1. Flow Measurement and Properties of Paste

The mix proportion design of pastes is given in Table 3. The following mixing procedure was adopted, using a 3 speed Hobart 5 liter mixer equipped with a standard whisk: all dry constituents were mixed for 30 seconds at low speed. Then the mix water and HRWRA were added while the mixer was running at low speed. After wet mixing for 120 seconds, the mixer was stopped and undispersed cement paste was detached from the walls of the bowl during 30 seconds. In the next 2 minutes, the mixing was done at medium speed. The mixer was then stopped for 5 minutes, covered by a plastic sheet and finally it was allowed to run at medium speed for 60 more seconds. After mixing was completed, the paste was poured into a 3 liter plastic flask equipped with a tight cap for intermediate storage. Before the FlowCyl test was performed, the slump flow spread, temperature and density of paste was determined.

Table 3: Mix proportions of pastes

Paste ID	W/P	A/P	C/P	Sf/P	Fi/P
P1	0.25	0.6%	80%	10%	10%
P2	0.30	0.6%	80%	10%	10%

3.3. The Flowcyl Test

The FlowCyl apparatus is a modification of the Marsh Cone test apparatus originally developed to characterize oil well cements. The original cone of the Marsh Cone test has been replaced by a cylinder ending in a cone with a narrow outlet. This modification has been done in order to simplify the time - flow rate relation. The inner diameter of the cylinder is 80 mm and the outlet 8mm. The total length is 400 mm of which the cylindrical part is 300 mm. The cylinder is placed vertically in a rack. The FlowCyl test started 10 minutes after contact of water and powder. The flask containing the paste was shaken rigorously, and the paste was filled into the FlowCyl apparatus. During filling, the bottom outlet of the FlowCyl was closed by finger tip. When the FlowCyl cylinder was filled to the top level mark, the outlet was opened and a steel bowl placed on an electronic balance connected to a computer collected the paste flowing out of the cylinder and the weight was recorded by computer in 2 second intervals. Using a spread sheet program, the viscosity related parameter called "flow resistance ratio λ_Q" is calculated. λ_Q value can vary between 0 and 1. The larger value corresponds to more viscose paste. The corresponding λ_Q was 0.90 and 0.72 for P1 and P2 respectively.

3.2.1. Flow Measurement and Properties of Mortar

After selection of past with adequate viscosity, 6 mortar mixtures with paste volume of 50, 55 and 60 percent were made. The mixture proportion is given in Table 4.

Table 4: Mortar mix proportion design kg/m^3

	M1	M2	M3	M4	M5	M6
V_p %	50	55	60	50	55	60
W/P	0.25	0.25	0.25	0.30	0.30	0.30
C	656.6	722.4	788.2	605.8	666.5	727.2
Sf	82.1	90.3	98.5	75.7	83.3	90.9
Fi1	16.5	14.9	13.2	16.5	14.9	13.2
Fi2	65.5	75.4	85.3	59.2	68.4	77.7
W	194.7	214.2	233.7	217.5	239.3	261.1
Sp	16.6	18.3	20.0	15.3	16.9	18.4
FA	1280	1152	1024	1280	1152	1024

C=Cement, Sf=Silica fume, Fi1=Sand particles < 0.15mm, Fi2 = Micronized quartzite, W=Water, Sp = Superplastisizer, FA = Fine Aggregate, V_p= paste Volume

Mortar mixtures were prepared in 5 litter batches using an open pan forced action mixer. The mixing sequence consisted of homogenizing the dry materials (sand and powder) for 30 s, and then the water and super plasticizer were gradually added while the mixture was mixed for 180 seconds. After 300 s of rest, the mortar received another 120 seconds of mixing. The temperature and density of each mixture were measured.
The flow property of each mortar was evaluated using slump flow spread and V-funnel flow time tests. Both tests are based on the same principle as those for concrete but with a reduced scale version of the equipments. In the slump flow spread test the mini cone, placed on a smooth leveled surface, was filled with mortar and lifted. The final diameter of the mortar after self-weight flow on the smooth plate was measured in two perpendicular directions and the average was noted. In the V-funnel test, after filling the funnel the trap door was opened and the flow time was measured until the first sighting of daylight when looking down through the funnel. The passing ability and self compactability of mortar was verified using a small U-box with three steel rods spaced approximately 25 mm apart to act as obstacles, hindering the cohesive flow of the material. After filling one side of the box with mortar, the door separating the two chambers was lifted and the equilibrium height was measured. With regards to the results of these tests a suitable mortar was selected. Figure 1-B shows the apparatus used.

3.2.2. Flow Measurement and Properties of SCC

After selection of mortar with adequate flowability, 6 concrete mixtures with mortar volume of 67.5, 70, and 72.5 percent were made. The mixture proportion is given in Table 5.

Table 5: SCC mix proportion design kg/m^3

	C1	C2	C3	C4	C5	C6
V_m %	67.5	70	72.5	67.5	70	72.5
W/P	0.25	0.25	0.25	0.30	0.30	0.30
C	487.6	505.7	523.7	449.8	466.5	484.3
Sf	60.9	63.2	65.5	56.2	58.3	60.5
Fi1	26	27	27.9	26	27	27.9
Fi2	34.9	36.2	37.5	30.2	31.3	32.6
W	145.5	150.9	156.3	162.3	168.4	176.2
Sp	11.4	11.8	12.3	10.5	10.9	9.1
FA	786.7	815.8	845	786.7	815.8	845
CA	838.4	774	709.4	838.4	774	709.5

V_m=Volume of mortar, C=Cement, W=Water, P=Powder Sf=Silica fume, Fi1=Sand particles<0.15mm Fi2=Micronized quartzite, Sp=Superplastisizer, FA=Fine Aggregate, CA=Coarse Aggregate, Paste volume in mortar=55%

Preparation of concrete and its mixing sequence was similar to that of mortar described in the previous section. The air content, temperature, and density of each mixture along with its flow properties including Slump flow spread, T_{500}, V-funnel flow time, $V_{FT@5min}$, and L-box blocking ratio were measured. These tests were done according to “The European Guidelines for Self-Compacting Concrete” [18]. The slump flow and T_{500} time is a test to assess the flowability and the flow rate of self-compacting concrete in the absence of obstructions. It is based on the slump test described in ASTM C-143 or EN 12350-2. The result is an indication of the filling ability of self-compacting concrete. The T_{500} time is also a measure of the speed of flow and hence the viscosity of the self consolidating concrete. The fresh concrete was poured into a cone as used for the slump test. When the cone was withdrawn upwards, the time from commencing upward movement of the cone to when the concrete flowed to a diameter of 500 mm was measured and recorded as the T_{500} time. The largest diameter of the flow spread of the concrete and the diameter of the spread at right angles to it were then measured and the mean was recorded as the slump-flow.

The V-funnel test was used to assess the viscosity, filling ability, and passing ability of self consolidating concrete. The funnel was filled with fresh concrete and the time taken for the concrete to flow out of the funnel is measured and recorded as the V-funnel flow time. To assess the static segregation tendency of the mix, this test was repeated but a 5 minute rest period was enforced after filling the funnel; and then the trap door was opened and the time of SCC discharge was noted as $V_{FT@5min}$.

The L-box test, with three bars, was used to assess the passing ability of self consolidating concrete while flowing through tight spaces between reinforcing bars without segregation and blocking. The L-box, made from transparent pelexcy glass, was supported on a level horizontal base and the gate between the vertical and horizontal sections was closed. The concrete was poured into the vertical section of the L-box and after a minute the gate was raised so that the concrete could flow through the obstacle into the horizontal section of the box. When movement was ceased, the heights of concrete at the end of the horizontal section of the L-box (h1) and just behind the steel bars (h2) were measured and the blocking ratio h_1/h_2 was recorded.

4. RESULTS AND DISCUSSION

4.1. Appropriate Volume Percentage of Paste in Mortar

Mortar mixtures with the selected pastes consisting of 50, 55, and 60 percent paste were made to study the effect of amount of paste on the flowability of mortar. The test results are shown in figures 4 and 5. As shown in the figures increasing paste volume has a greater effect on the flowability of lower W/P mixture (higher λ_Q). Domone [19] has suggested that a mortar mini-slump spread range of 28 to 34 cm and mortar V-funnel flow time of 1 to 7.5 seconds would lead to SCC with satisfactory fresh properties recommended by European guidelines for SCC. With regards to this recommendation, as well as optimization purpose, it was decided to select the mortar with 55% paste volume for designing SCC.

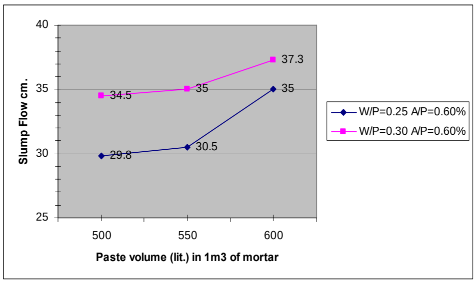

Figure 4. Slump Flow of mortar vs. Paste volume

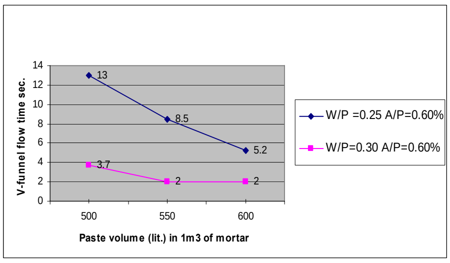

Figure 5. V-funnel flow time of mortar vs. Paste volume

4.3. Appropriate Volume Percentage of Mortar in SCC

Designing SCC using the results of paste and mortar tests was the last phase of this study. Mortar with 55% paste volume was selected and SCC with mortar volume of 67.5, 70, and 72.5 percent was made. W/P of 0.25 and 0.30 were considered and the fresh SCC was tested to study the effect of mortar volume on its flow properties. The test results are summarized in Table 6.

Table 6. Fresh SCC test results

	SF mm	T_{500} Sec	V_{Ft} Sec	$V_{Ft@5}$ Sec	L-Box h_1/h_2
C1	690	6	23	32	0.5
C2	700	4	16	28	0.6
C3	750	2	9	12	0.9
C4	710	3	14	21	0.6
C5	720	4	10	12	0.7
C6	760	3	5	7	1.0

The values of slump flow and v-funnel flow time vs. mortar volume of SCC are plotted in Figures 6 and 7 respectively. As shown the flowability is increased with increasing amount of mortar. Even though the slump flow of mixes C1, C2, C4 and C5 satisfies the requirement of SCC but the corresponding values of L-Box blocking ratio and V-funnel flow time at 5 minutes was not satisfactory and had tendency to segregate. Based on these results mixes C3 and C6 with mortar volume of 72.5% had excellent flowability and passing ability with no sign of segregation or bleeding.

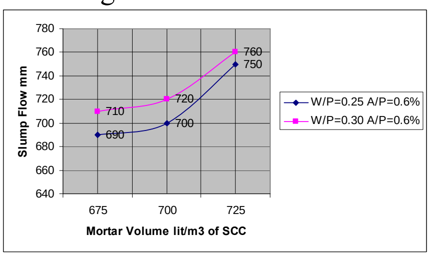

Figure 6. Slump Flow of SCC vs. Mortar volume

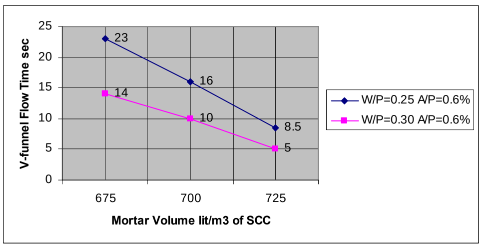

Figure 7. V-funnel flow time of SCC vs. mortar volume

Figure 6 shows that the more viscose the paste is the more mortar volume is needed in order to obtain the same slump flow and the difference in mortar volume gets smaller as the volume percentage of mortar increases beyond 70%. Also at this level the passing ability of SCC starts to improve significantly.

5. CONCLUSION

Investigation of new materials and evaluation of different combination of ingredients for selection of their most effective combination for making SCC can be done utilizing the single point tests mentioned in this paper. A three phase mix proportion design procedure starting from paste and then mortar leading to desired SCC was adopted and a spread sheet (EXCEL) program was prepared to fulfill this purpose. The effect of paste viscosity and its volume percentage on rheological properties of mortar was studied. Mortar with 55% paste volume was selected and the effect of mortar volume on fresh properties of SCC was investigated. As mortar volume increased beyond 70%, filling and passing ability of SCC was improved. A data base may be defined to collect the result of tests performed for each design phase which could be used by design engineer and ready concrete mix supplier to obtain a reliable model for fast and smart mix design.

ACKNOWLEDGEMENTS

The work presented here has been performed within a research project financed by the Building and Housing Research Center of Iran. Their support is gratefully acknowledged.

REFERENCES

1. EFNARC, "Specification and Guidelines for Self-Compacting Concrete", Feb. 2002, 32pp, http://www.efnarc.org.
2. Saak A. W., Jennings H. M., and Shah S. P., "New Methodology for Designing Self-Compacting Concrete", ACI Materials Journal, vol. 98, No. 6, Nov.-Dec. 2001, PP429-439.
3. Scrivener K.L., Kirkpatrick R.J., "Innovation in use and research on cementitious material", Cement and Concrete Research, Sep. 2007.
4. Domone P.L., "Self-compacting concrete: An analysis of 11 years of case studies", Cement & Concrete Composites, October 2005.
5. Ferrarisa C.F., HOblab K.H., Hill R., "The influence of mineral admixtures on the rheology of cement paste and concrete", Cement and Concrete Research, vol. 31, 2001, PP245-255.
6. Phan T.H., Chaouche M., Moranville M., "Influence of organic admixtures on the rheological behaviour of cement pastes", Cement and Concrete Research, vol. 36, 2006, PP1807-1813.
7. D'Aloia Schwartzentruber L., Le Roy R., Cordin J., "Rheological behaviour of fresh cement pastes formulated from a Self Compacting Concrete (SCC)", Cement and Concrete Research, vol. 36, 2006, PP1203-1213.
8. 8- Yahiaa, A., Tanimura M., Shimoyama Y., "Rheological properties of highly flowable mortar containing limestone filler-effect of powder content and W/C

ratio", Cement and Concrete Research, vol. 35, 2005, PP532-539.

9. Lachemi M., Hossain K. M. A., Patel R., Shehata M., and Bouzoubaa N., "Influence of paste/mortar rheology on the flow characteristics of high-volume fly ash selfconsolidating concrete", Magazine of Concrete Research, vol.59, No. 7, September 2007, PP517-528.
10. Domone, P., "Mortar Tests for Self-Consolidating Concrete: Simple evaluation of materials and mixture proportions", Concrete International, ACI, April 2006, PP39-45.
11. Tattersall G.H., Banfill, P.F.G., "Rheology of Fresh Concrete", Pitman, London, 1983, PP76-304.
12. Chao-Wei Tang, Tsong Yen, Chao-Shun Chang, and Kuan-Hung Chen, "Optimizing Mixture Proportions for Flowable High-Performance Concrete via Rheology Tests", ACI Materials Journal, Vol. 98, No. 6, Nov.-Dec.2001.
13. Wallevik OH, Gjorv OE., " Development of a coaxial cylinders viscometer for fresh concrete", In: Proceedings of the International Conference on Properties of Fresh Concrete, London, Chapman & Hall, 1990, PP213-224.
14. Petit J. Y., Wirquin E., Vanhove Y., and Khayat K., "Yield stress and viscosity equations for mortars and self-consolidating concrete", Cement and Concrete Research, 2007.
15. Roussel N., Le Roy R., "The Marsh cone: a test or a rheological apparatus?", Cement and Concrete Research, vol. 35, 2005, PP823-830.
16. Ferraris C.F., "Measurement of the Rheological Properties of High Performance Concrete: State of the Art Report", Journal of Research of the National Institute of Standards and Technology, Vol. 104, Number 5, Sep.–Oct. 1999.
17. Mortsell E., Smeplass S., Hammer T.A., and Maage M., "FLOWCYL – How to Determine the Flow Properties of the Matrix Phase of High Performance Concrete", 4th International Symposium on Utilization of High-strength/ High-performance Concrete, Paris 1996.
18. The European Union-Brite EuRam III, "Paste optimization based on flow properties and compressive strength", EuroLightCon Document BE96-3942/R10, March 2000, http://www.sintef.no/bygg/sement/elcon.

CD07-005

AN INVESTIGATION ON EFFECT OF USING PP FIBERS AND DIFFERENT CEMENTITIOUS MATERIALS ON MECHANICAL PROPERTIES OF EPS CONCRETE

A. Sadrmomtazi[1], M.A. Mirgozar Langeroudi [2], A. Fasihi[3], A.K. Haghi[4]
[1]Assistant professor, Dept of Civil Engg, Faculty of Engg, University of Guilan, Rasht, Iran
[2,3]M.S. Student, Dept of Civil Engg, Faculty of Engg, University of Guilan, Rasht, Iran
[4]Professor, Dept of Textile Engg, Faculty of Engg, University of Guilan, Rasht, Iran

ABSTRACT
The use of lightweight concrete in many applications of modern construction is increasing, owing to the advantages that lower density results in decreasing the magnitude of dead load of the structure which lead to smaller cross sections for load bearing elements. Expanded polystyrene (EPS) beads are a type of artificial lightweight nonabsorbent aggregates which can be used to produce low density concretes by replacing with normal aggregates, either partially or fully, depending upon the requirements of density and strength. Also plastic shrinkage is the dimensional change that occurs in all fresh cement based materials within the first few hours after it has been placed which is not unacceptable in itself, but it is some times accompanied by development of cracks that are unsightly and objectionable. Polypropylene and other synthetic fibers are added to concrete as secondary reinforcement in order to control this plastic shrinkage. On the other hand, the addition of fibers affects on the properties of hardened concrete like compressive and tensile strength, elastic modulus and toughness. The present study covers the use of polypropylene fibers at contents equal to 0.1%, 0.3%, 0.5% and 1% by volume of EPS concrete in order to study about the effects of its addition into the EPS concrete matrix on mechanical properties. Also the effects of using Silica fume and Rice husk as two supplementary cementitious materials were investigated.

Keywords: EPS concrete, PP fibers, silica fume, rice husk, mechanical properties

1. INTRODUCTION
Lightweight concretes can be produced by replacing the normal aggregates in concrete either partially or fully, depending upon the requirements of density and strength [1]. Historically, lightweight concrete is used for both structural and non-structural applications. use of lightweight concretes in construction of high rise buildings, offshore structures and long span bridges due to the advantage of its low density, results in a significant benefit in terms of load bearing elements of smaller cross section and a corresponding reduction in the size of the foundation [2]. Lightweight aggregates are broadly classified in to two types, natural (pumice, diatomite, volcanic cinders, etc.) and artificial (perlite, expanded shale, clay, slate, sintered PFA, etc.). One of the main problems associated with the use of

conventional lightweight aggregates produced from clay, slate and shale in concrete is that these porous aggregates absorb a very large quantity of the mixing water. This is known to affect the performance of the concrete, apart from the fact that it is difficult to maintain specific water content during the casting. Also, this absorption of water by the aggregate will mean that additional water will be required to maintain the slump at acceptable levels. These increased water contents necessitate higher cement contents, even without the benefit of higher strength [3]. Expanded polystyrene is a kind of stable foam with low density, nonabsorbent, closed cell nature aggregates consisting of discrete air voids in a polymer matrix. As a type of artificial ultra-lightweight aggregate, the polystyrene beads can easily be incorporated in mortar or concrete to produce lightweight concrete, with a wide range of densities, required for building applications like cladding panels and load-bearing concrete blocks. Also, they can be used as a construction material for floating marine structures, as an energy-absorbing material for the protection of buried military structures and as fenders in offshore oil platforms [4]. Also, it was reported that it can be used for other specialized applications like the sub-base material for pavement and railway track bed, as construction material for floating marine structures, sea beds, and sea fences, as an energy-absorbing material for the protection of buried military structures, and as fenders in offshore oil platforms [5,6]. Polypropylene fibers have been widely used for the reinforcement of cementitious materials to improve the toughness and energy absorption capability of matrix [7]. They were found to be extremely effective in reducing free plastic shrinkage, in retarding first crack appearance and in controlling crack development [8]. Although effectiveness of PP fibers in shrinkage cracking, impact resistance and ductility of cement matrices has been proved by many researchers, effect of PP fibers on compressive and flexural strength is not quit clear [9]. Presently, a comprehensive investigation on the mechanical behavior of the EPS concretes containing polypropylene fibers is not available. In this study, concretes with different EPS contents, were reinforced with polypropylene fibers and the effects of using fibers on mechanical properties were evaluated.

2. EXPERIMENTAL INVESTIGATION

2.1. Materials and Mix Proportions

Cement: The cement used in all mortar mixes was ordinary Portland cement which corresponds to ASTM type 1. The chemical analysis of Portland cement is shown in Table 1.

Silica fume: Silica fume has been used as supplementary cementing materials to partially replacement for many years. It has been also used for producing high performance concrete or achieving other desired properties. The silica fume used in this study contained 91.1% of SiO_2 with average size of 7.38 μm.

Rice husk ash: Rice husk ash has been used in many countries as a low cost concrete admixture because of its role as filler and a pozzolan [12]. It has been also used. For producing high performance concrete (HPC) or achieving other desire properties. RHA used in this experiment contained 91.62% of SiO_2 with average size of 15.83 μm.

Table 1: Chemical composition of Cement and Silica fume and Rice husk ash

Oxide	Portland cement	Silica fume	Rice husk ash
SiO2	21/00	91/10	91/62
Al2O3	4/60	1/55	0/49
Fe2O3	3/20	2/00	0/73
CaO	64/50	2/42	2/51
MgO	2/00	0/06	0/88
SO3	2/90	0/45	-
Na2O + K2O	1/00	-	2/39
LOI	1/50	2/10	-

Superplastisizer: Superplastisizers are now widely used as additives in concrete with high rheological requirements. The use of superplastisizers allows reducing the water to cement ratio (w/c) of mortar and concrete without significantly changing their flow properties. Sodium salts of formaldehyde condensates disperse the cement particles by electrostatic repulsion which results from the adsorption on cement surfaces [13, 14]. Due to high specific surface of silica fume and rice husk ash which need more water for complete hydration, workability of concrete will be affected. In order to achieve desire fluidity, polycarboxylate ether was incorporated in to all mixes. The content of super plastsizer was adjusted for each mixture to keep constant the workability of concrete.
Aggregates: Natural river sand was used with specific gravity of 2.51 gr/cm^3 and absorption capacity equal to 3.4%. Natural River gravel w used as coarse aggregate with specific gravity of 2.54 gr/cm^3 and absorption capacity equal to 2.57%.

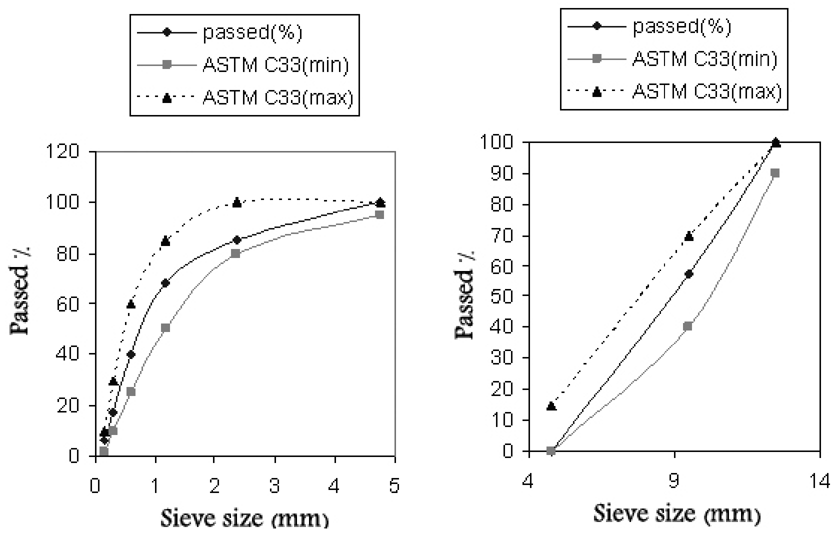

Figure 3 . Sieve Analysis of used Sand and Gravel based on ASTM standard

EPS: The grading shows that used EPS has mostly (85%) 3.5 mm size beads. The density of used expanded polystyrene was evaluated to be 0.0257 gr/cm^3.
Polypropylene fiber: polypropylene fibers which is used is waste carpet fibers,

has been cut by length of 6mm.

Table 2: Characteristics of the polypropylene fibers

properties	description
Morphology	Fibrillated or mono filament
Specific weight [gr/cm^3]	0.95
Diameter [µm]	20 – 200
Modulus of elasticity [GPa]	5 – 10
Tensile strength [MPa]	500 - 750
Ultimate strain [%]	5 - 15
Elongation at fracture [%]	Approx. 20
Melting point [°C]	160
Bonding with cement	Good
Stability in cement	Good

Mix proportions: Three percentages of using EPS of 15%, 25% and 40% by volume were listed. In order to investigate the effect of polypropylene fibers on mechanical properties of EPS concrete, it was used in mixes by four percentages of 0.1%, 0.3%, 0.5% and 1% by volume, silica fume and rice husk ash replacement were 10% and 20% by weight in the cementitious material, respectively. The complete details of the concrete mixes are presented in Table 3.

Table 3: Mix proportion of the specimens

mix No.	Cement (kg/m^3)	S.F %	R.H %	Water (kg/m^3)	w/(c+s)	0-3 (kg/m^3)	3-6 (kg/m^3)	6-12 (kg/m^3)	EPS %	PP %	Fresh Density (kg/m^3)
1	400	-	-	180	0.45	666	118	957	-	0% , 0.1% , 0.3% , 0.5% , 1% by Volume	2400
2	400	-	-	170	0.43	540	95	777	15%		1900
3	400	-	-	165	0.41	431	76	620	25%		1700
4	400	-	-	160	0.4	294	52	423	40%		1350
5	360	10%	-	190	0.48	652	115	940	-		2300
6	360	10%	-	175	0.44	524	93	755	15%		1900
7	360	10%	-	175	0.44	422	75	607	25%		1650
8	360	10%	-	170	0.43	282	50	406	40%		1300
9	320	-	20%	210	0.52	620	110	895	-		2250
10	320	-	20%	205	0.51	470	80	670	15%		1850
11	320	-	20%	205	0.51	385	68	555	25%		1600
12	320	-	20%	200	0.5	245	43	352	40%		1250

Production of EPS concrete: EPS beads were wetted initially with a part of the mixing water and superplasticizer before adding the remaining materials. Mixing was continued until a uniform and flowing mixture was obtained. The fresh concrete densities and slump values were measured immediately after the mixing which showed a variation between 50 and 70cm. The specimens were cured under wet gunny bags initially and, after demolding, were stored in water [11].

Specimens: Cube specimens of 100 mm were tested for the uniaxial compressive strength. Cylinders with a diameter of 150 mm and a height of 300 mm were tested for the splitting tensile strength and modulus of elasticity. The 50×50×200 mm beam specimens were tested in three point bending with the span of 180 mm with a cross head movement of 1 mm/min. all the tests were done by using a testing machine with a maximum load of 3000kN.

Test program: The main objective of the present investigation was to study the Effect of Using PP fibers and different Cementitious Materials on Mechanical Properties of EPS Concrete, over a wide range of concrete densities of 1250-2300 kg/m3, with the corresponding compressive strengths varying between 6.7 and 47.6 MPa. The flow values of the fresh concrete were measured according to ASTM C 124-1973. Compressive strength tests were carried out on 100 mm cubes at the age of 3, 7, 14, 28 and 90 days on a testing machine of 3000 kN capacity at a loading rate of 0.25 N/mm^2s. The splitting tensile strength test was conducted on cylinders of 150 mm in diameter and 300 mm in height, at 28 days as per ASTM C 496-89. Modulus of elasticity test was done at 28 days by using the mentioned machine based on ASTM C 469 [11]. the 50×50×200 mm beam specimens were tested in third-point loading over a span of 180 mm in accordance with ASTM C 1018 w21x. Flexural test was done on these specimens with a cross head movement of 1 mm/min at 28 days.

2.2. Result and Discossion

Fresh concrete: The main parameter, which is often used to determine the workability of fresh concrete, is the slump test. The slump value depends mainly on the water absorption and porosity of the aggregates, water content in the mixture, amount of the aggregate and fine material in the mixture, shape of the aggregates and surface characteristics of the constituents in the mixture. The slump values decreased significantly with the addition of polypropylene. With the use of sufficient compaction, the fresh concrete would flow satisfactorily again and the polypropylene fibers would be uniformly dispersed in the mixture. Furthermore, with the constant water-cement ratio, the slump values of the concrete mixtures containing polypropylene fibers were not significantly affected by the aggregate types. This was primarily caused by the good adhesion in the fresh concrete, which was created by the polypropylene fibers. The mixes having the higher percentage of silica fume and rice husk ash show higher flow values. All the concretes were flexible and easy to work with, and could be easily compacted using just hand compaction.

Compressive strength: With or without using of EPS in mixes, the addition of polypropylene fibers in the concrete did not significantly affect the compressive strength of concretes. Test results showed increase in value of compressive strength in some specimens and on the other hand, some other showed decrease on mentioned parameter. Also from the results, it is clear that the rate of strength gain in early ages increased using silica fume as a replacement of ordinary cement. But rice husk ash, as a replacement of ordinary cement needs more time to show its benefits as a pozzolanic material. In this case, an improvement in mechanical properties can be observed at the age of 90 days and upper. The desired density of EPS concrete can be determined by varying the EPS volume in the mix. The variations of compressive strength with the plastic density of concrete were observed to be linear. Moreover, the failure mode of the concrete specimens containing EPS aggregates under compressive loading observed to be gradual and the specimens were capable of retaining the load after failure without full disintegration. By adding polypropylene in EPS concrete matrix, the failure mode observed to be more gradual. This clearly shows the high energy absorption capacity of these concretes.

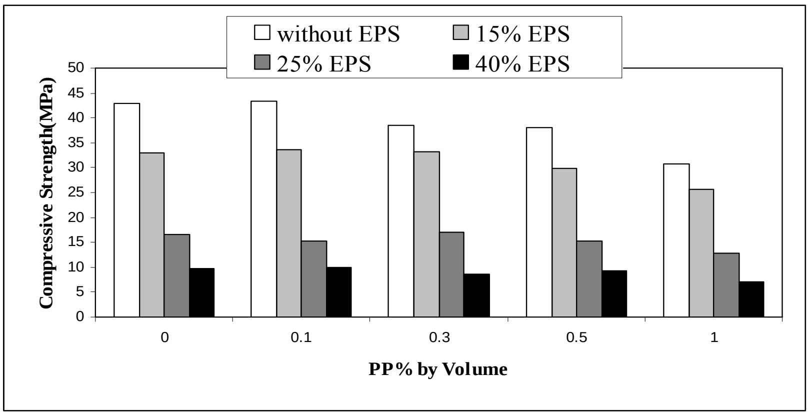

Figure 2. Compressive strength of concrete at different contents of EPS and PP fibers

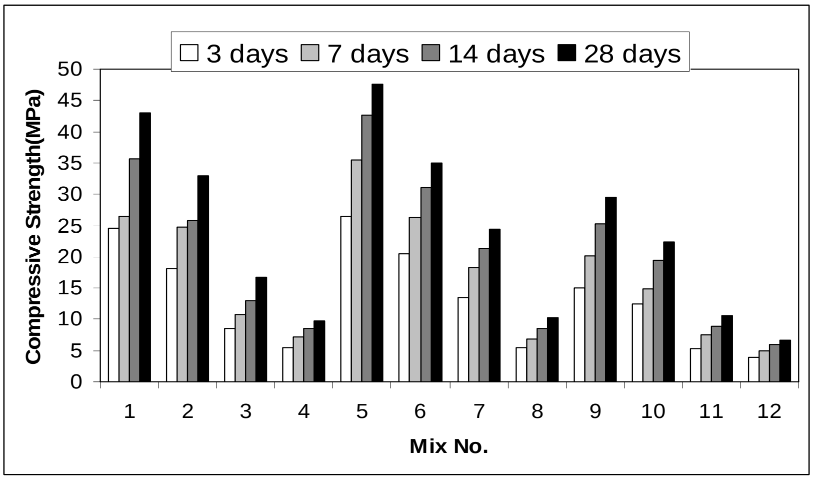

Figure 3. variation of compressive strength with age and cementitious replacement

Split tensile strength: The variation of tensile strength with the EPS and polypropylene content of admixture is given in Figure 4. From this, it can be seen that the tensile strength increased with decreasing EPS content of concrete.

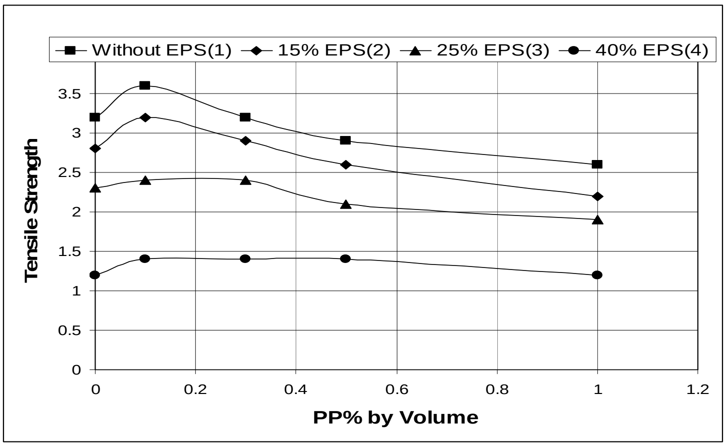

Figure 4. variation of Tensile strength with PP and EPS content of concrete

The splitting failure mode of the concrete specimens containing EPS aggregates also observed to be gradual. adding polypropylene fibers showed an increase in the value of tensile strength, as well by adding polypropylene in concrete matrix, the failure mode observed to be more gradual and specimens did not separate in two parts as shown in Figure 5. Effect of using silica fume and rice husk ash as a replacement of ordinary cement on split tensile is similar to the effects that observed during compressive strength tests.

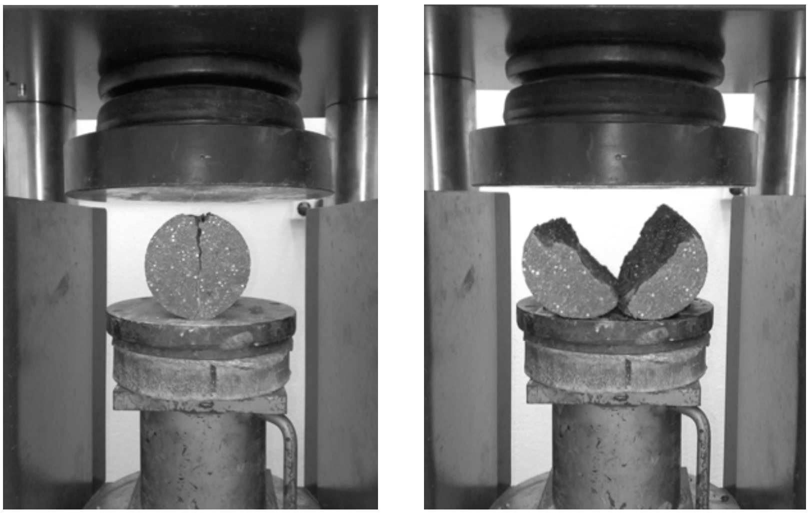

Figure 5. Effect of using polypropylene in concrete on failure mode

Modulus of elasticity: Static modulus of elasticity tests were carried out on the 150×300 mm EPS concrete cylinders. The results of these tests showed that this mechanical material property has a linear variation with the used volume of EPS in admixture, but vice versa. It means that an increase in the volume of EPS, used in concrete lead to decrease in the magnitude of the parameter modulus of elasticity which is expected. From the results, the addition of polypropylene fibers in the concrete did not significantly affect the modulus of elasticity of mixes. It means that the use of polypropylene fibers by the mentioned percentages in EPS concrete resulted in the low influence on modulus of elasticity of concrete rather than the influences contributed by the other constituents of concrete.

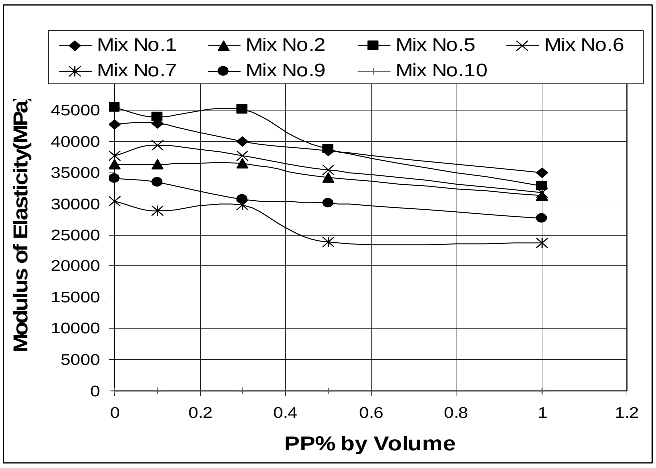

Figure 6. variation of Modulus of Elasticity with PP and EPS content of concrete

The results also indicated that adding silica fume to admixture caused an increase in modulus of elasticity in all mixes, however using rice husk ash as a supplementary cementitious material caused a decrease in value of the modulus of elasticity at 28 days.

Flexural behavior: from the results, the flexural capacity decreased with an increase in the volume of EPS in mixes. Also no effect on the flexural behavior was observed. However, by increasing used polypropylene's volume, flexural capacity was observed to be improved.

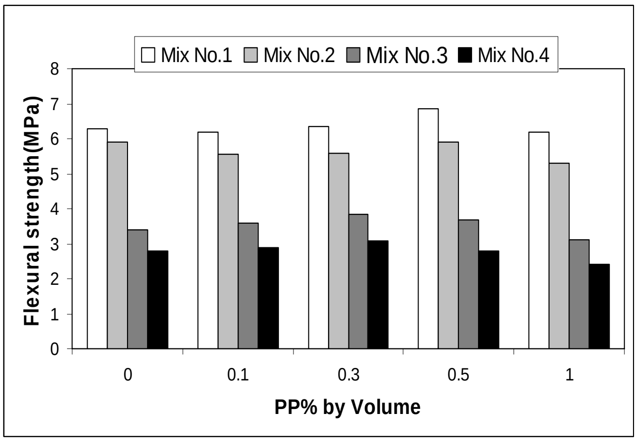

Figure 7. variation of Flexural strength with PP and EPS content of concrete

3. CONCLUSION

The mechanical strength of EPS concrete showed a linear increase with an increase in concrete density. The failure was observed to be gradual (compressible), and the specimens were capable of retaining the load after failure, without full disintegration. The strength of EPS concretes appears to increase linearly with an increase in concrete density, or with a decrease in the EPS volume. With or without using of EPS in mixes, the addition of polypropylene fibers in the concrete did not significantly affect the compressive strength of concretes. The rate of strength gain was increasing with using silica fume as a replacement of ordinary cement. But rice husk ash, as a replacement of ordinary cement needs more time to show its benefits as a pozzolanic material. In this case, an improvement in mechanical properties can be observed at the age of 90 days and upper. Be seen that the tensile strength increased with an increase in compressive strength. Modulus of Elasticity of concretes decreased with the incorporation of EPS. High amounts of EPS contents, decreased the elastic module more. Effect of polypropylene fibers on module of elasticity was not clear. Adding silica fume to admixture increased the modulus of elasticity however using rice husk ash had not positive effect in early ages. Results of flexural behavior test showed that, the flexural strength decreased with an increase in the volume of EPS in mixes. Results showed that application of PP fibers improved the flexural strength of concrete.

REFERENCES

1. K. Ganesh Babu, D. Saradhi Babu, Behaviour of lightweight expanded polystyrene concrete containing silica fume, Cement and Concrete Research 33(2003) 755-762.
2. ACI Committee 213R-0.3, Guide for structural lightweight aggregate concrete, American Concrete Institute, Farmington Hills, MI, 2003.
3. Sussman V, Lightweight plastic aggregate concrete, J Am Concr Inst Proc (1975) 321-372.
4. D.J. Cook, Expanded polystyrene concrete, concrete technology and design, New Concrete Materials, Surrey Univ. Press, London(1983) 41-69.
5. A.N. Hanna, Properties of expanded polystyrene concrete and applications for pavement sub-bases, Res. Develop. Bull-Portland Cem. Assoc. (Rd 055.01P).
6. C. Bagon, S. Frondistou-Yannas, Marine floating concrete made with polystyrene expanded beads, Mag. Concr. Res. 28 (1976) 225-229.
7. Sun W., Chen H., Luo X., Qian H., The effect of hybrid fibers and expansive agent on the shrinkage and permeability of high-performance concrete, Cement and Concrete Research (2001), 31,595-601.
8. Toledo Fileho R.D., Sanjuan M.A., Effect of low modulus sisal and propylene fibers on the free and restrained shrinkage of mortars at early age, Cement and Concrete Research 1999,29, 1547-1604.
9. Toutanji. H.A., Properties of polypropylene fiber reinforced silica fume expansive-cement concrete, Construction and Building Materials (1999), 13, 171-177.
10. D.J. Cook, Expanded polystyrene beads as lightweight aggregate for concrete,

Precast Concr. 4 (1973) 691-693.

11. 11. K. Ganesh Babu, D. Saradhi Babu, Behaviour of lightweight expanded polystyrene concrete containing silica fume, Cement and Concrete Research 33(2003) 755-762.
12. Jauberthie R., Rendell F., Tamba S., Cisse I., Origin of the pozzolanic effect of rice hisks, Construction and Building Materials 14(2000) 419-423.
13. Heikal M., Morsy M.S., Aiad I., Effect of treatment temperature on the early hydration characteristics of superplasticized silica fume blended cement pastes, Cement and Concrete Research 35 (2005) 680-687.
14. Leemann A., Winnefeld F., The effect of viscosity modifying agents on mortar and concrete, Cement & Concrete Composite 29(2007) 341-349.

CD07-005

AN INVESTIGATION ON EFFECT OF USING PP FIBERS AND DIFFERENT CEMENTITIOUS MATERIALS ON MECHANICAL PROPERTIES OF EPS CONCRETE

A. Sadrmomtazi[1], M.A. Mirgozar Langeroudi [2], A. Fasihi[3], A.K. Haghi[4]
[1]Assistant professor, Dept of Civil Engg, Faculty of Engg, University of Guilan, Rasht, Iran
[2,3]M.S. Student, Dept of Civil Engg, Faculty of Engg, University of Guilan, Rasht, Iran
[4]Professor, Dept of Textile Engg, Faculty of Engg, University of Guilan, Rasht, Iran

ABSTRACT

The use of lightweight concrete in many applications of modern construction is increasing, owing to the advantages that lower density results in decreasing the magnitude of dead load of the structure which lead to smaller cross sections for load bearing elements. Expanded polystyrene (EPS) beads are a type of artificial lightweight nonabsorbent aggregates which can be used to produce low density concretes by replacing with normal aggregates, either partially or fully, depending upon the requirements of density and strength. Also plastic shrinkage is the dimensional change that occurs in all fresh cement based materials within the first few hours after it has been placed which is not unacceptable in itself, but it is some times accompanied by development of cracks that are unsightly and objectionable. Polypropylene and other synthetic fibers are added to concrete as secondary reinforcement in order to control this plastic shrinkage. On the other hand, the addition of fibers affects on the properties of hardened concrete like compressive and tensile strength, elastic modulus and toughness. The present study covers the use of polypropylene fibers at contents equal to 0.1%, 0.3%, 0.5% and 1% by volume of EPS concrete in order to study about the effects of its addition into the EPS concrete matrix on mechanical properties. Also the effects of using Silica fume and Rice husk as two supplementary cementitious materials were investigated.

Keywords: EPS concrete, PP fibers, silica fume, rice husk, mechanical properties

1. INTRODUCTION

Lightweight concretes can be produced by replacing the normal aggregates in concrete either partially or fully, depending upon the requirements of density and strength [1]. Historically, lightweight concrete is used for both structural and non-structural applications. use of lightweight concretes in construction of high rise buildings, offshore structures and long span bridges due to the advantage of its low density, results in a significant benefit in terms of load bearing elements of smaller cross section and a corresponding reduction in the size of the foundation [2]. Lightweight aggregates are broadly classified in to two types, natural (pumice, diatomite, volcanic cinders, etc.) and artificial (perlite, expanded shale, clay, slate, sintered PFA, etc.). One of the main problems associated with the use of

conventional lightweight aggregates produced from clay, slate and shale in concrete is that these porous aggregates absorb a very large quantity of the mixing water. This is known to affect the performance of the concrete, apart from the fact that it is difficult to maintain specific water content during the casting. Also, this absorption of water by the aggregate will mean that additional water will be required to maintain the slump at acceptable levels. These increased water contents necessitate higher cement contents, even without the benefit of higher strength [3]. Expanded polystyrene is a kind of stable foam with low density, nonabsorbent, closed cell nature aggregates consisting of discrete air voids in a polymer matrix. As a type of artificial ultra-lightweight aggregate, the polystyrene beads can easily be incorporated in mortar or concrete to produce lightweight concrete, with a wide range of densities, required for building applications like cladding panels and load-bearing concrete blocks. Also, they can be used as a construction material for floating marine structures, as an energy-absorbing material for the protection of buried military structures and as fenders in offshore oil platforms [4]. Also, it was reported that it can be used for other specialized applications like the sub-base material for pavement and railway track bed, as construction material for floating marine structures, sea beds, and sea fences, as an energy-absorbing material for the protection of buried military structures, and as fenders in offshore oil platforms [5,6].
Polypropylene fibers have been widely used for the reinforcement of cementitious materials to improve the toughness and energy absorption capability of matrix [7]. They were found to be extremely effective in reducing free plastic shrinkage, in retarding first crack appearance and in controlling crack development [8]. Although effectiveness of PP fibers in shrinkage cracking, impact resistance and ductility of cement matrices has been proved by many researchers, effect of PP fibers on compressive and flexural strength is not quit clear [9]. Presently, a comprehensive investigation on the mechanical behavior of the EPS concretes containing polypropylene fibers is not available. In this study, concretes with different EPS contents, were reinforced with polypropylene fibers and the effects of using fibers on mechanical properties were evaluated.

2. EXPERIMENTAL INVESTIGATION

2.1. Materials and Mix Proportions

Cement: The cement used in all mortar mixes was ordinary Portland cement which corresponds to ASTM type 1. The chemical analysis of Portland cement is shown in Table 1.

Silica fume: Silica fume has been used as supplementary cementing materials to partially replacement for many years. It has been also used for producing high performance concrete or achieving other desired properties. The silica fume used in this study contained 91.1% of SiO_2 with average size of 7.38 μm.

Rice husk ash: Rice husk ash has been used in many countries as a low cost concrete admixture because of its role as filler and a pozzolan [12]. It has been also used. For producing high performance concrete (HPC) or achieving other desire properties. RHA used in this experiment contained 91.62% of SiO_2 with average size of 15.83 μm.

Table 1: Chemical composition of Cement and Silica fume and Rice husk ash

Oxide	Portland cement	Silica fume	Rice husk ash
SiO2	21/00	91/10	91/62
Al2O3	4/60	1/55	0/49
Fe2O3	3/20	2/00	0/73
CaO	64/50	2/42	2/51
MgO	2/00	0/06	0/88
SO3	2/90	0/45	-
Na2O + K2O	1/00	-	2/39
LOI	1/50	2/10	-

Superplastisizer: Superplastisizers are now widely used as additives in concrete with high rheological requirements. The use of superplastisizers allows reducing the water to cement ratio (w/c) of mortar and concrete without significantly changing their flow properties. Sodium salts of formaldehyde condensates disperse the cement particles by electrostatic repulsion which results from the adsorption on cement surfaces [13, 14]. Due to high specific surface of silica fume and rice husk ash which need more water for complete hydration, workability of concrete will be affected. In order to achieve desire fluidity, polycarboxylate ether was incorporated in to all mixes. The content of super plastsizer was adjusted for each mixture to keep constant the workability of concrete.
Aggregates: Natural river sand was used with specific gravity of 2.51 gr/cm^3 and absorption capacity equal to 3.4%. Natural River gravel w used as coarse aggregate with specific gravity of 2.54 gr/cm^3 and absorption capacity equal to 2.57%.

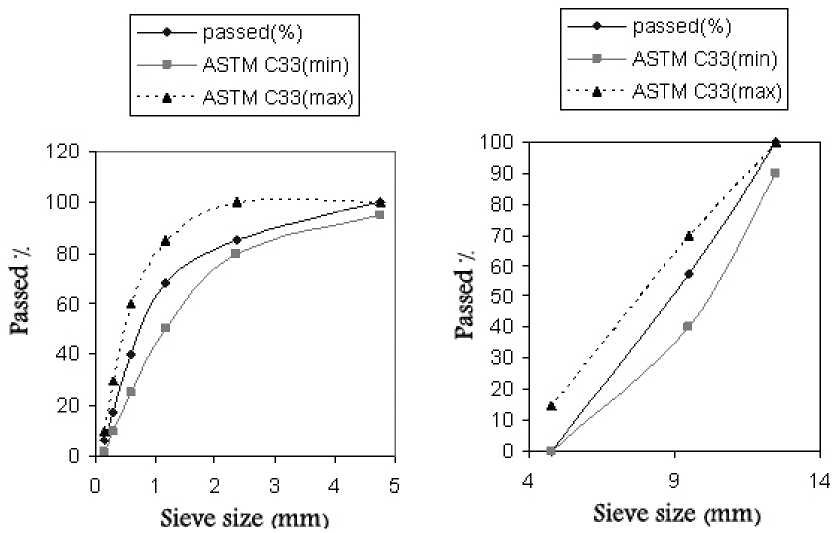

Figure 3 . Sieve Analysis of used Sand and Gravel based on ASTM standard

EPS: The grading shows that used EPS has mostly (85%) 3.5 mm size beads. The density of used expanded polystyrene was evaluated to be 0.0257 gr/cm^3.
Polypropylene fiber: polypropylene fibers which is used is waste carpet fibers,

has been cut by length of 6mm.

Table 2: Characteristics of the polypropylene fibers

properties	description
Morphology	Fibrillated or mono filament
Specific weight [gr/cm^3]	0.95
Diameter [μm]	20 – 200
Modulus of elasticity [GPa]	5 – 10
Tensile strength [MPa]	500 - 750
Ultimate strain [%]	5 - 15
Elongation at fracture [%]	Approx. 20
Melting point [°C]	160
Bonding with cement	Good
Stability in cement	Good

Mix proportions: Three percentages of using EPS of 15%, 25% and 40% by volume were listed. In order to investigate the effect of polypropylene fibers on mechanical properties of EPS concrete, it was used in mixes by four percentages of 0.1%, 0.3%, 0.5% and 1% by volume, silica fume and rice husk ash replacement were 10% and 20% by weight in the cementitious material, respectively. The complete details of the concrete mixes are presented in Table 3.

Table 3: Mix proportion of the specimens

mix No.	Cement (kg/m^3)	S.F %	R.H %	Water (kg/m^3)	w/(c+s)	0-3 (kg/m^3)	3-6 (kg/m^3)	6-12 (kg/m^3)	EPS %	PP %	Fresh Density (kg/m^3)
1	400	-	-	180	0.45	666	118	957	-	0% , 0.1% , 0.3% , 0.5% , 1% by Volume	2400
2	400	-	-	170	0.43	540	95	777	15%		1900
3	400	-	-	165	0.41	431	76	620	25%		1700
4	400	-	-	160	0.4	294	52	423	40%		1350
5	360	10%	-	190	0.48	652	115	940	-		2300
6	360	10%	-	175	0.44	524	93	755	15%		1900
7	360	10%	-	175	0.44	422	75	607	25%		1650
8	360	10%	-	170	0.43	282	50	406	40%		1300
9	320	-	20%	210	0.52	620	110	895	-		2250
10	320	-	20%	205	0.51	470	80	670	15%		1850
11	320	-	20%	205	0.51	385	68	555	25%		1600
12	320	-	20%	200	0.5	245	43	352	40%		1250

Production of EPS concrete: EPS beads were wetted initially with a part of the mixing water and superplasticizer before adding the remaining materials. Mixing was continued until a uniform and flowing mixture was obtained. The fresh concrete densities and slump values were measured immediately after the mixing which showed a variation between 50 and 70cm. The specimens were cured under wet gunny bags initially and, after demolding, were stored in water [11].

Specimens: Cube specimens of 100 mm were tested for the uniaxial compressive strength. Cylinders with a diameter of 150 mm and a height of 300 mm were tested for the splitting tensile strength and modulus of elasticity. The 50×50×200 mm beam specimens were tested in three point bending with the span of 180 mm with a cross head movement of 1 mm/min. all the tests were done by using a testing machine with a maximum load of 3000kN.

Test program: The main objective of the present investigation was to study the Effect of Using PP fibers and different Cementitious Materials on Mechanical Properties of EPS Concrete, over a wide range of concrete densities of 1250-2300 kg/m3, with the corresponding compressive strengths varying between 6.7 and 47.6 MPa. The flow values of the fresh concrete were measured according to ASTM C 124-1973. Compressive strength tests were carried out on 100 mm cubes at the age of 3, 7, 14, 28 and 90 days on a testing machine of 3000 kN capacity at a loading rate of 0.25 N/mm^{2}s. The splitting tensile strength test was conducted on cylinders of 150 mm in diameter and 300 mm in height, at 28 days as per ASTM C 496-89. Modulus of elasticity test was done at 28 days by using the mentioned machine based on ASTM C 469 [11]. the 50×50×200 mm beam specimens were tested in third-point loading over a span of 180 mm in accordance with ASTM C 1018 w21x. Flexural test was done on these specimens with a cross head movement of 1 mm/min at 28 days.

2.2. Result and Discossion

Fresh concrete: The main parameter, which is often used to determine the workability of fresh concrete, is the slump test. The slump value depends mainly on the water absorption and porosity of the aggregates, water content in the mixture, amount of the aggregate and fine material in the mixture, shape of the aggregates and surface characteristics of the constituents in the mixture. The slump values decreased significantly with the addition of polypropylene. With the use of sufficient compaction, the fresh concrete would flow satisfactorily again and the polypropylene fibers would be uniformly dispersed in the mixture. Furthermore, with the constant water-cement ratio, the slump values of the concrete mixtures containing polypropylene fibers were not significantly affected by the aggregate types. This was primarily caused by the good adhesion in the fresh concrete, which was created by the polypropylene fibers. The mixes having the higher percentage of silica fume and rice husk ash show higher flow values. All the concretes were flexible and easy to work with, and could be easily compacted using just hand compaction.

Compressive strength: With or without using of EPS in mixes, the addition of polypropylene fibers in the concrete did not significantly affect the compressive strength of concretes. Test results showed increase in value of compressive strength in some specimens and on the other hand, some other showed decrease on mentioned parameter. Also from the results, it is clear that the rate of strength gain in early ages increased using silica fume as a replacement of ordinary cement. But rice husk ash, as a replacement of ordinary cement needs more time to show its benefits as a pozzolanic material. In this case, an improvement in mechanical properties can be observed at the age of 90 days and upper. The desired density of EPS concrete can be determined by varying the EPS volume in the mix. The variations of compressive strength with the plastic density of concrete were observed to be linear. Moreover, the failure mode of the concrete specimens containing EPS aggregates under compressive loading observed to be gradual and the specimens were capable of retaining the load after failure without full disintegration. By adding polypropylene in EPS concrete matrix, the failure mode observed to be more gradual. This clearly shows the high energy absorption capacity of these concretes.

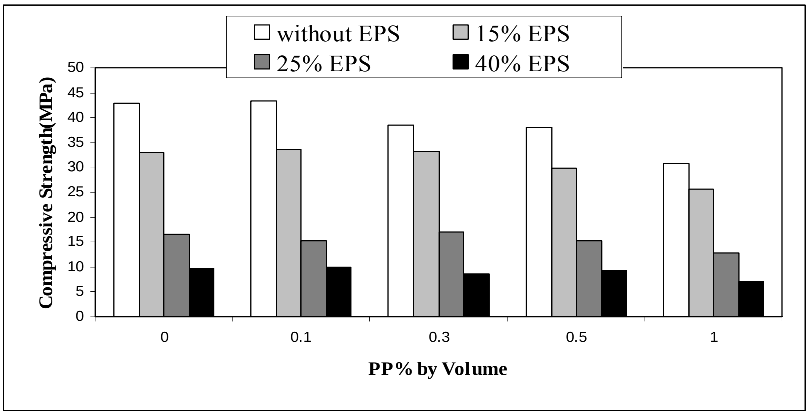

Figure 2. Compressive strength of concrete at different contents of EPS and PP fibers

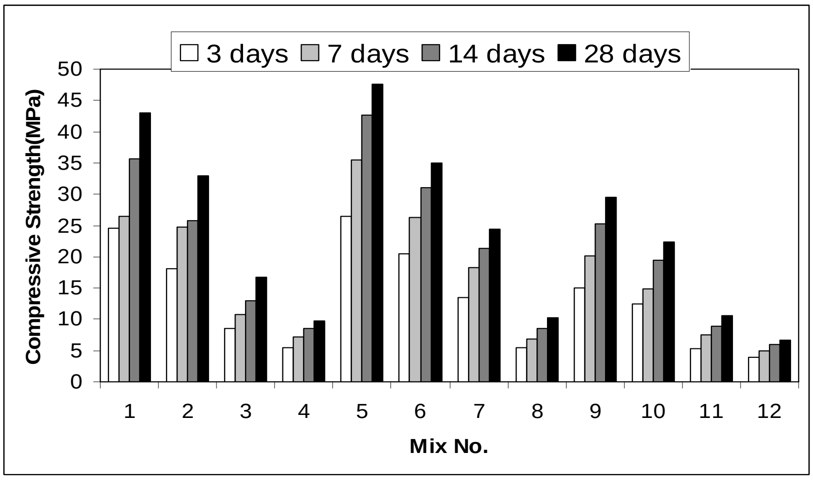

Figure 3. variation of compressive strength with age and cementitious replacement

Split tensile strength: The variation of tensile strength with the EPS and polypropylene content of admixture is given in Figure 4. From this, it can be seen that the tensile strength increased with decreasing EPS content of concrete.

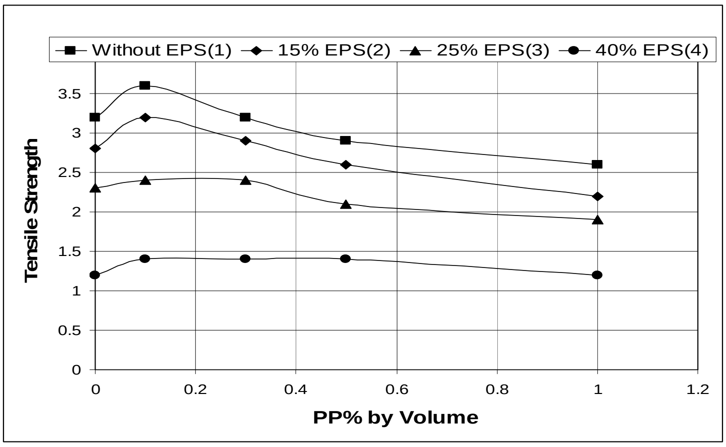

Figure 4. variation of Tensile strength with PP and EPS content of concrete

The splitting failure mode of the concrete specimens containing EPS aggregates also observed to be gradual. adding polypropylene fibers showed an increase in the value of tensile strength, as well by adding polypropylene in concrete matrix, the failure mode observed to be more gradual and specimens did not separate in two parts as shown in Figure 5. Effect of using silica fume and rice husk ash as a replacement of ordinary cement on split tensile is similar to the effects that observed during compressive strength tests.

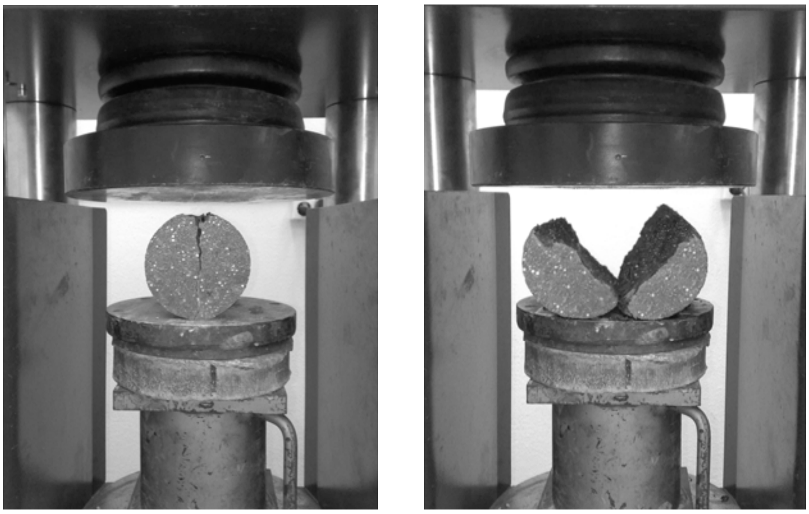

Figure 5. Effect of using polypropylene in concrete on failure mode

Modulus of elasticity: Static modulus of elasticity tests were carried out on the 150×300 mm EPS concrete cylinders. The results of these tests showed that this mechanical material property has a linear variation with the used volume of EPS in admixture, but vice versa. It means that an increase in the volume of EPS, used in concrete lead to decrease in the magnitude of the parameter modulus of elasticity which is expected. From the results, the addition of polypropylene fibers in the concrete did not significantly affect the modulus of elasticity of mixes. It means that the use of polypropylene fibers by the mentioned percentages in EPS concrete resulted in the low influence on modulus of elasticity of concrete rather than the influences contributed by the other constituents of concrete.

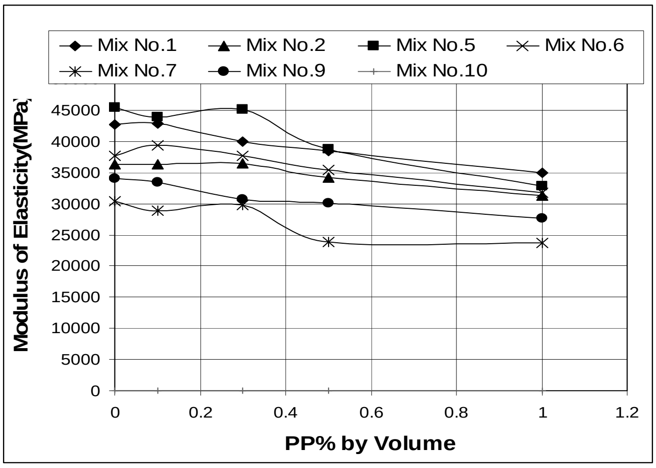

Figure 6. variation of Modulus of Elasticity with PP and EPS content of concrete

The results also indicated that adding silica fume to admixture caused an increase in modulus of elasticity in all mixes, however using rice husk ash as a supplementary cementitious material caused a decrease in value of the modulus of elasticity at 28 days.

Flexural behavior: from the results, the flexural capacity decreased with an increase in the volume of EPS in mixes. Also no effect on the flexural behavior was observed. However, by increasing used polypropylene's volume, flexural capacity was observed to be improved.

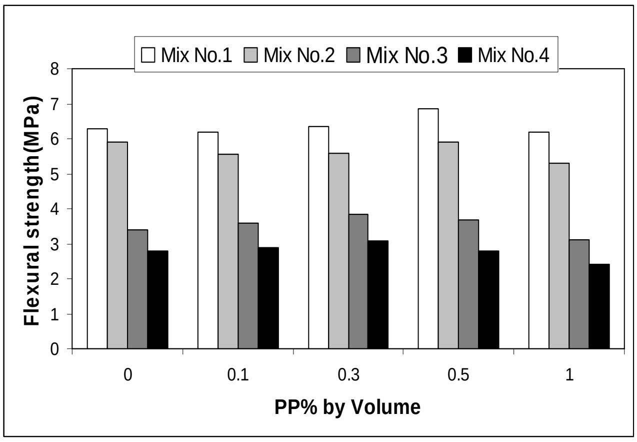

Figure 7. variation of Flexural strength with PP and EPS content of concrete

3. CONCLUSION

The mechanical strength of EPS concrete showed a linear increase with an increase in concrete density. The failure was observed to be gradual (compressible), and the specimens were capable of retaining the load after failure, without full disintegration. The strength of EPS concretes appears to increase linearly with an increase in concrete density, or with a decrease in the EPS volume. With or without using of EPS in mixes, the addition of polypropylene fibers in the concrete did not significantly affect the compressive strength of concretes. The rate of strength gain was increasing with using silica fume as a replacement of ordinary cement. But rice husk ash, as a replacement of ordinary cement needs more time to show its benefits as a pozzolanic material. In this case, an improvement in mechanical properties can be observed at the age of 90 days and upper. Be seen that the tensile strength increased with an increase in compressive strength. Modulus of Elasticity of concretes decreased with the incorporation of EPS. High amounts of EPS contents, decreased the elastic module more. Effect of polypropylene fibers on module of elasticity was not clear. Adding silica fume to admixture increased the modulus of elasticity however using rice husk ash had not positive effect in early ages. Results of flexural behavior test showed that, the flexural strength decreased with an increase in the volume of EPS in mixes. Results showed that application of PP fibers improved the flexural strength of concrete.

REFERENCES

1. K. Ganesh Babu, D. Saradhi Babu, Behaviour of lightweight expanded polystyrene concrete containing silica fume, Cement and Concrete Research 33(2003) 755-762.
2. ACI Committee 213R-0.3, Guide for structural lightweight aggregate concrete, American Concrete Institute, Farmington Hills, MI, 2003.
3. Sussman V, Lightweight plastic aggregate concrete, J Am Concr Inst Proc (1975) 321-372.
4. D.J. Cook, Expanded polystyrene concrete, concrete technology and design, New Concrete Materials, Surrey Univ. Press, London(1983) 41-69.
5. A.N. Hanna, Properties of expanded polystyrene concrete and applications for pavement sub-bases, Res. Develop. Bull-Portland Cem. Assoc. (Rd 055.01P).
6. C. Bagon, S. Frondistou-Yannas, Marine floating concrete made with polystyrene expanded beads, Mag. Concr. Res. 28 (1976) 225-229.
7. Sun W., Chen H., Luo X., Qian H., The effect of hybrid fibers and expansive agent on the shrinkage and permeability of high-performance concrete, Cement and Concrete Research (2001), 31,595-601.
8. Toledo Fileho R.D., Sanjuan M.A., Effect of low modulus sisal and propylene fibers on the free and restrained shrinkage of mortars at early age, Cement and Concrete Research 1999,29, 1547-1604.
9. Toutanji. H.A., Properties of polypropylene fiber reinforced silica fume expansive-cement concrete, Construction and Building Materials (1999), 13, 171-177.
10. D.J. Cook, Expanded polystyrene beads as lightweight aggregate for concrete,

Precast Concr. 4 (1973) 691-693.
11. 11. K. Ganesh Babu, D. Saradhi Babu, Behaviour of lightweight expanded polystyrene concrete containing silica fume, Cement and Concrete Research 33(2003) 755-762.
12. Jauberthie R., Rendell F., Tamba S., Cisse I., Origin of the pozzolanic effect of rice hisks, Construction and Building Materials 14(2000) 419-423.
13. Heikal M., Morsy M.S., Aiad I., Effect of treatment temperature on the early hydration characteristics of superplasticized silica fume blended cement pastes, Cement and Concrete Research 35 (2005) 680-687.
14. Leemann A., Winnefeld F., The effect of viscosity modifying agents on mortar and concrete, Cement & Concrete Composite 29(2007) 341-349.

CD07-007

DAMPER CONCRETE FOR SEISMIC WAVES

H. Khoshroo[1], F.Sinaeian[2]
[1]Apply Research Office of NAJA
[2]Building and Housing Research Centre (BHRC). I.R.Iran

ABSTRACT
When an earthquake happens, different kinds of compression and shear waves are produced. Structures in direction of compression waves P (sense's weight of structure) have good enforcement and main loss of structures is in sense of shear (sense of propagation S waves). By reducing amplitude of seismic waves, we can reduce damages to the building. Nowadays, one of the most important difficulties in front of engineering structure is finding ways for reducing side movement of structure and vibrations caused by the device measuring earthquakes in buildings especially high structures for adding to their factor of safety. Seismic waves are among mechanic waves and for propagation need material environment and their reduction has opposite environment's density. So, reducing density of propagation environment is one of ways for reducing amplitude of waves. On the other side, liquids do not have a stiffness shear and cannot effect and propagation S waves. So, in this plan, we have tried using this specifications and installing sphere full of fluid in the sample environment of ordinary concrete, make new concrete and evaluate its behavior so that has considerable reduce against shear waves.
For considering the made sample behavior and comparing it with ordinary concrete, cubic samples with sizes 10x20x20 and 10x20x60cm are made and were put under impulse loads. Comparing test results, it was observed that amplitude of registered wave on the concrete sample with fluid compare to sample of ordinary concrete has reduced on average %50. So, by using this damping concrete, we can reduce the seismic energy and acceleration effected to the structure and considering amount of this reduction, the structure weight is also reduced. Reduction of structure weight caused reduction of secondary seismic force.

Keywords: damper, shear wave, fluid

1. INTRODUCTION

Buildings are always subject to great dynamic loads which are caused by different environment factors, and the seismic load caused by earthquake is one of them. So, today one of the most important problems in front of structure engineers is finding ways for reducing side movement of structure and produced vibrations in buildings especially high structures for increasing the structure's factor of safety, ease and tranquility of inhabitants. Nowadays, in some buildings of advanced countries such as Japan and USA, passive dampers are used and they have different kind so bracing rod damper and pillar damper. You can see some pictures of the most useful ones in picture No. 1. Also, other kinds of dampers such as Viscous Damper (VEDs) and the one which can be adjusted for its weight (TMDs)… exist and by changing ductility of structure (R), it causes reduction of vibrations in the time unit or earthquake's rock. Using dampers is the base of reducing the seismic energy after entrance to structure. So, in this method, all changes are mechanic and do not have effect on nature of entrance waves. And, the seismic acceleration is exactly effected to the structure and is subject to dampers which constitute part of structure, are a mortised.

Although reducing R has effect in ductility, but another effective parameter is the structure weight which is independent of R. using the present dampers, for every structure, considering its weight, damping should be calculated separately. But, in this plan, we tried considering the nature of seismic waves, as much as effective acceleration on the structure is reduced, we can say definitely that we will have as much as force reduction for structure that has made a lighter structure design and this again will lead to reducing final shear force.

B **A**

Figure 1. Kinds of mechanical damp ions a) pillar. b) Bracing Rod

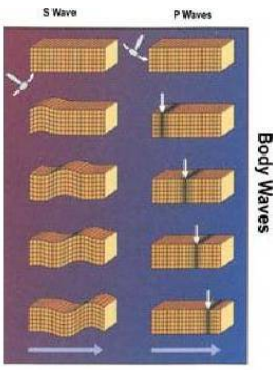

Figure 2. The style of production and diffusion of body waves

2. SEISMIC WAVES

When an earthquake happens, different types of body waves are produced which are mainly mechanic and are propagation only in material environments. These waves are produced in the center of earthquake and are distributed in all directions.

They are two main groups: compression waves (P) and shear waves (S). In picture No. 2, way of production and propagation of these waves is observed. The first group which is primary, compression and length waves cause compression and connection of materials which pass through them. Second group is secondary; shear or width waves cause vibration of environment particles in vertical line on distributing waves and perform shear waves on the distribution environment. Velocity of waves is subject to material and hardness of composed materials in the distributed environment and the steady fluid which does not have stiffness shear can not effected and distribute shear waves.

3. DAMPER CONCRETE

This concrete considering specifications of the propagation environment of shear waves and in order to amortize more these waves is made. Since sense of propagation compression waves is in line with the structure gravity and structures for effect this force in sense vertical are very rigidity designs, so that compression waves of the earthquake often are not serious damage. But, shear waves while happening of earthquake cause the most damages. But, if we can make shear waves before entrance to damped structure, we can reduce favorably the caused damages by earthquake. In this case, a lighter structure will have stability against earthquake. This in return causes reduction of the force to structure. If this cycle continues, we can achieve the below diagram is obtained. Some sentences of it are economical from engineering viewpoint. It means that we can do this several times and this cycle is effective depending on the structure weight.

$$Fn=aqn-1$$

Fn: Reduced earthquake force
A: Primary seismic force
Q: Amount of reduced seismic force in percent
N: No. of sentences

In making the sample concrete, sphere full of water have low shear resistance are available easily and are used as vertically sheets. Picture No. 3 shows a sample of these spheres. Shear waves of earthquake while passing these spheres because of their fluid are reduced. Amount of this reduction is subject to specifications and the amount of fluid inside the concrete and also the way of putting spheres in the concrete.

4. PERFORMING TESTS

Considering hypotheses and theories presented in the preface, we expect that waves and especially shear waves by passing this concrete are reduced. In this concrete, quite equal spheres by passage of time do not exit these spheres so that fluids are preserved for longer period in the environment. For primary considerations, effectiveness of the innovative concrete, at first a sample 20 x 20 x 10 cm is made and necessary considerations are made.

Figure 3. Arrangement of the beads full of fluid

Since the primary sample was cubic, one side of the cubic is chosen and a pounding device for impact shown in picture No. 4 is used for making waves.

Figure 4. The pounding is used in experiments.

Since our aim is comparing reduction of wave's amplitude in the made concrete sample and also waves amplitude in addition to distribution environment is the size is impact, the pounding device system is so made that it has equal conditions in all impact. Besides, by repeating the test and taking average, we tried to reduce the fault of these tests. Also, another parameter which is determining is time's impact. Impact should be in a way which is equal in time. So, in every test, equal impact with equal time intervals are used and in processes of data equal time window are considered. In these considerations on cubic samples, we observed that these spheres as expected by theory can cause amortization of shear waves and amplitude of vibrations is reduced. These changes are observed in picture No. 5-A and 5-B.
Since the primary sample was small, a second sample with sizes 60 x 20 x 10 were made, and results of the test were repeated.

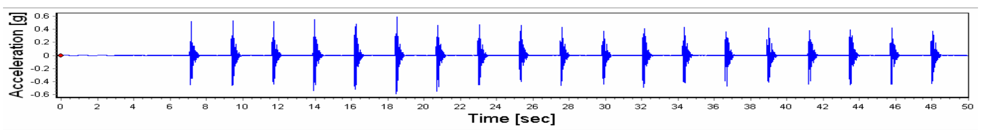

A)

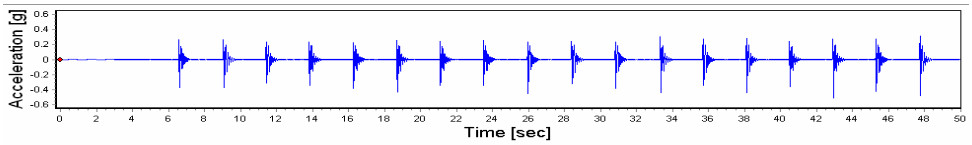

B)

Figure 5. Vibrations domain A) In sample of typical concrete B) In sample of damping concrete

During tests, two samples were used so that a suitable comparison is made in produced waves. I mean one sample of ordinary concrete and a sample of damping concrete in which fluid sphere existed. Difference of these samples is the spheres. And from other viewpoints such as: mixing design, amount of cement, type, grading of gravel and sand est. are considered the same. Before performing tests, it was necessary to get insured of producing shear waves by the pounding system. So, the test was done according to the picture No. 6. In this test, two horizontal single element sensors in two vertical lines were installed. And, from the side, we impact the samples. We expected that considering direction of the impact, the produced waves are shear; also the arrived polarity is changed. Results of this test shown in picture No. 7 confirm this hypothesis

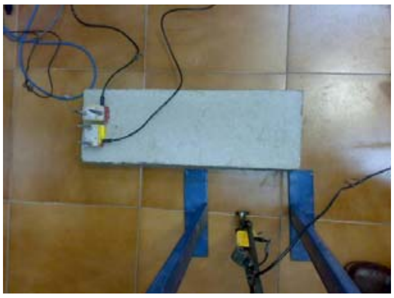

B

A

Figure 6. Using form uni-vector geophone for assessment of Shear wave production A) Sensors placement B) the way of doing impact

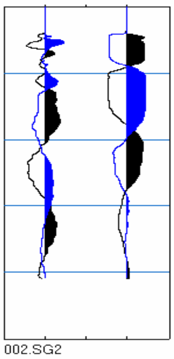

Figure 7. Polarity changing of wave with changing of impact direction is confirmation of producing shear wave in experiment

Continuing the tests, as observed in picture No. 8, hits are produced from side and instead of using geophone, horizontal device of systems measuring acceleration are very sensitive. 20 impacts are equally impact on the sample. The reason for using 20 impacts is getting average and reducing fault of impact size.

Figure 8. Testing in different environment.

In processing registered data, seismosignal is used and for omitting it, first it should pass though a filter in frequency limit of 1 to 25 Hertz. Considering acceleration response spectrum in damping %5, %10, and % 20 evaluation of data pseudo acceleration are received. Previous amount of them for both samples of concrete are measuring and reducing amplitude waves is got. And, by getting this ratio, we can say that the sample of produced concrete how much has role in reducing the amplitude and as result energy of seismic waves. Table No. 1 shows this ration in 10 samples tested for ordinary concrete and damping concrete.

Table 1: Obtained acceleration of data in typical and damping concrete and their ratios

Test number	Awc (g) Max acceleration in damping concrete	Acc (g) Max acceleration in typical concrete	Awc/Acc ratio
1	0.9	2.6	0.35
2	1.3	2.4	0.54
3	0.55	2.3	0.24
4	0.55	2.3	0.24
5	1.25	2.8	0.45
6	1.15	2.3	0.50
7	0.95	2.6	0.37
8	1.25	2.4	0.52
9	1.2	1.8	0.67
10	1.05	1.8	0.58

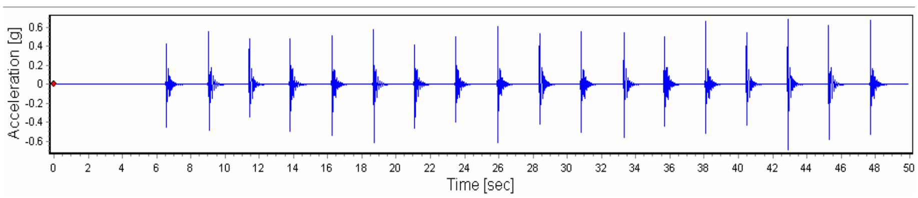

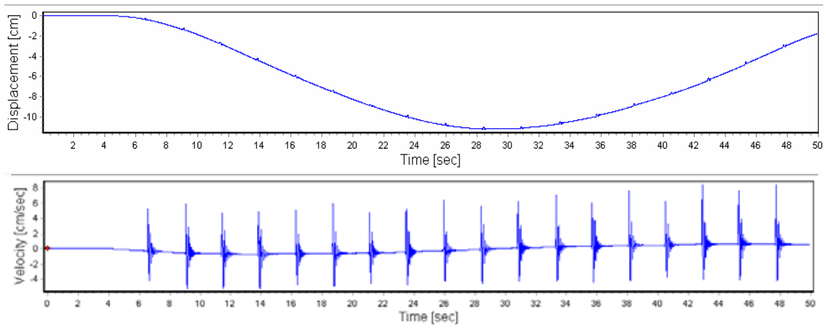

A)

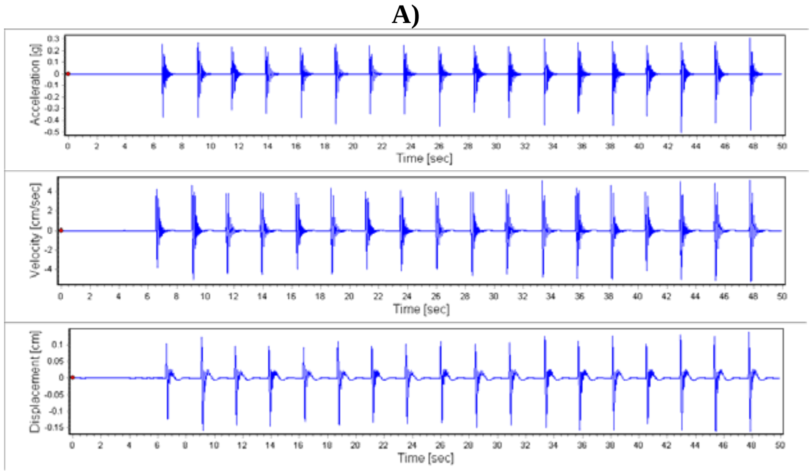

B)

Figure 9. Acceleration domain, speed and changes of recorded movement resulting form impacts, respectively A) before and B) after filter

Figure 10 is the response spectrum of amplitude figure of shear wave acceleration in the ordinary and damper concrete in 1.5 second compared together. In one test, amount of acceleration in damped concrete is less than ordinary concrete. And, in the figure of picture No. 11 the reduction ration of acceleration for 10 tests is shown.

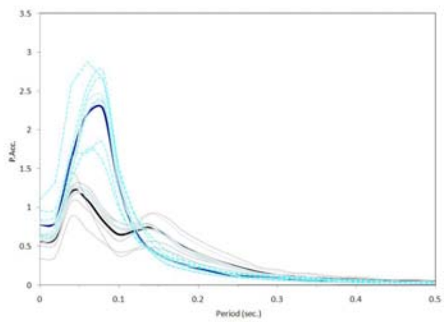

Figure 10. The comparison of acceleration response spectrums for section wave in damper and normal concrete- blue for normal concrete and balk & white for damper concrete

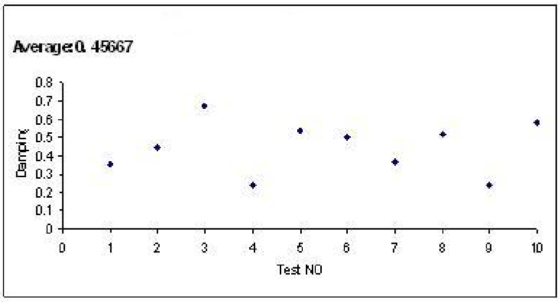

Figure 11. Shows the proportions ratio of acceleration decrease for 10 tests

As observed in pictures 10 and 11, using this damper concrete, we can seismic energy can be affected to structure. And, considering this amount of structure reduction is reduced. Also, reduction of structure weight causes secondary reduction of seismic force. This concrete reduces the wave acceleration directly and causes reduction of seismic force and reduces the structure weight indirectly. Later on, we intend to consider other parameters such as: dimensions, fluid volume, kind of fluid, arrangement of sphere and entrance of unit energy to the sample so that we achieve a reduction factor.

5. CONCLUSIONS

Since effect of spheres in small dimensions is considerable, we hope that by considering more, we can reduce seismic waves and consequently earthquake danger considerably. And, by reducing human losses, consumption of building materials, structure weight and seismic force are reduced. This is a useful method for reducing the seismic waves' intensity before entrance to structures.

ACKNOWLEDGEMENT

At the end, we would like to express our gratitude to Building and Housing Research Center BHRC presidency for providing the test facilities and engineer Mirzaei, management of center of controlling strong motion network of (BHRC) for his kind supports.

APPLICATION OF HYBRID FIBER REINFORCEMENT AND HIGH VOLUME COARSE FLY ASH IN SELF COMPACTING CONCRETE

A.A. Mounesan[1], K. Siamardi[2], M.M. Khodavirdi Zanjani[2]
[1]Civil Engineer, Sharif University of Technology, Head Manager of Atisaz Company
[2]Civil Engineer, Concrete Research Center, Atisaz Company

ABSTRACT
Self compacting concrete is termed as a concrete with high flow ability and cohesiveness which can fill its mold without the need of any extra vibration effort. Fiber inclusion to concrete enhances the mechanical properties, while making the concrete less workable. This article presents a study on the fresh and mechanical properties of a fiber reinforced self compacting concrete incorporating high-volume fly ash that does not meet the fineness requirements of ASTM C 618. A poly carboxylic based superplasticizer was used in combination with a viscosity modifying admixture. In mixes containing fly ash, 50% of cement by weight was replaced with fly ash. Two different types of steel fibers were used in combination, keeping the total fiber content constant at 60 kg/m3. Slump flow time and diameter, V funnel, and air content were performed to assess the fresh properties of the concrete. Compressive strength, split tensile strength, and ultrasonic pulse velocity of the concrete were determined for the hardened properties. It can be concluded that high-volume coarse fly ash could successfully be used in producing fiber reinforced SCC. Even though there is some reduction in the concrete strength, because of the use of high-volume coarse fly ash, it is possible to achieve self compaction with considerable fiber inclusion.

Keywords: self compacting concrete, fiber reinforcement, high volume coarse fly ash, fresh properties, ultrasonic test

1. INTRODUCTION
Use of self compacting concrete (SCC) in the construction industry has been increasing [1] because of its technical advantages such as flowing through the reinforcement and filling every corner of its mold without any need for vibration and compaction during its placement. Generally, SCC is achieved using new generation superplasticizers to reduce the water–binder ratio. In addition, supplementary cementitious or inert materials such as limestone powder, natural pozzolans, and fly ash is also used to increase the viscosity and reduce the cost of SCC. Among these materials, fly ash, a by-product of thermal power plants, has been reported to improve the mechanical properties and durability of concrete when used as a cement replacement material [2]. Concretes having large amounts

of fly ash are termed as high-volume fly ash (HVFA) concrete. HVFA concrete was initially developed for mass concrete applications to reduce the heat of hydration, but with its sufficient mechanical and excellent durability properties it has been used in structural and pavement applications [3]. Fly ash is usually separated at the power plants and high quality (fine) fly ash meeting the fineness requirement of ASTM C 618 can be used in producing blended cements or added as a separate ingredient at the ready mixed concrete batching plants. In addition to this fine fly ash, there are vast amounts of substandard (coarse) fly ash that can be utilized in the concrete industry. A successful application of the coarse fly ash in producing blended Portland cements was published by the researchers at CANMET [4]. Fly ash has also been increasingly used in the Turkish concrete industry. Recently, to increase the use of fly ash, investigations on HVFA in producing SCC are being performed [5]. In this article another application of this type of coarse fly ash will be presented on SCCs incorporating hybrid fiber reinforcement.

The term fiber reinforced concrete (FRC) is defined by ACI 116R, Cement and Concrete Terminology, as a concrete containing dispersed randomly oriented fibers. Inherently, concrete is brittle under tensile loading and mechanical properties of concrete may be improved by randomly oriented short discrete fibers which prevent or control initiation, propagation, or coalescence of cracks [6]. The character and performance of FRC changes depend on the properties of concrete and the fibers. The properties of fibers that are usually of interest are fiber concentration, fiber geometry, fiber orientation, and fiber distribution. Using a single type of fiber may improve the properties of FRC to a limited level. However, the concept of hybridization, adding two or more types of fiber into concrete, can offer more attractive engineering properties as the presence of one fiber enables more efficient utilization of the potential properties of other fibers [7-8]. Previous investigations showed that the use of steel fibers in SCC is feasible [9-10]. In these mixes, steel fibers can decrease workability of SCC as the fiber amount and slenderness ratio (length/diameter) increase.

However, in case of well-proportioned SCC the workability is not influenced by the steel fibers [10]. The incorporation of fibers in concrete improves mechanical properties of concrete such as ductility, toughness, tensile strength, impact resistance and fatigue.

The objective of this study is to assess the effects of HVFA replacement on the fresh and hardened properties of SCCs incorporating different types of steel fibers. Moreover, the fly ash used in this study was a coarse fly ash that does not meet the fineness requirements of ASTM C 618. Even though, the suitability of using such a substandard fly ash needs much detailed investigations, this study covers the fresh and some hardened properties of such mixes. In addition to the fly ash, two different sizes of steel fibers were used at different proportions in making the concrete. Total mass of cementitious materials is 500 kg/m3, in which 50% of cement is replaced by the coarse grained fly ash. For comparison, a control SCC mix without any fly ash was also produced. The commercially available chemical admixtures used in this study included a viscosity modifying admixture (VMA) and a polycarboxylic based superplasticizer (SP).

2. MATERIALS

2.1. Portland Cement

The cement used in all mixes was a commercially available Portland cement (PC), which corresponds to ASTM Type I cement. It had a specific gravity of 3.09 and Blaine fineness of 3030 cm2/g. Chemical composition of the PC is given in Table 1.

2.2. Limestone Powder

Limestone powder (LP) was used as a mineral viscosity enhancing admixture. LP was a by product of marble extraction with a CaCO3 content of 98% and a specific gravity of 2.70. The chemical composition of the limestone powder is also presented in Table 1.

2.3. Fly Ash

A fly ash (FA) from Çayırhan, Turkey was used in this study. Its chemical composition is given in Table 1. The FA had a relatively low specific gravity and Blaine fineness of 2.01 and 2420 cm2/g respectively. The percentage of fly ash retained when wet sieved on a 45-µm sieve was 46. Therefore, this FA failed to meet the fineness requirements of ASTM C 618. To confirm the fineness of the FA, the particle size distribution of the FA was also determined. Figure 1 shows the particle size distribution of the FA, as well as the LP, and PC used in this study. As can be seen from that plot, FA was much coarser compared to both PC and LP.

Table 1: Chemical composition of the Portland cement and mineral admixtures

Chemical analyses (%)	Portland cement	Fly ash	Limestone powder
CaO	61.94	11.31	54.97
SiO2	18.08	49.55	0.01
Al2O3	5.58	13.34	0.17
Fe2O3	2.43	8.51	0.05
MgO	2.43	4.10	0.64
SO3	2.54	1.70	0.00
K2O	0.99	1.99	0.00
Na2O	0.18	3.08	0.00
LOI	4.40	2.74	43.66

2.4. Fiber

Two cylindrical steel fiber types, one with hooked ends (SF1) and one straight (SF2) were used. Their specific gravities were 7.85 and 7.17 respectively. The length and aspect ratio of the SF1 was 30 mm and 55, respectively, compared to 6 mm and 37.5 of SF2. The SF2 fiber was made of high strength steel with a brass coating, which provides it a relatively smooth surface. The total fiber content was kept constant at 60 kg/m3 for all the mixes.

2.5. Aggregates

As for the aggregates, crushed limestone and crushed sand from the same local source were used. As can be seen from the gradation of the aggregates presented in Table 2, the maximum aggregate size was 19 mm. Both the coarse and fine aggregate had a specific gravity of 2.70, and water absorptions of 0.5 % and 1.2 % respectively.

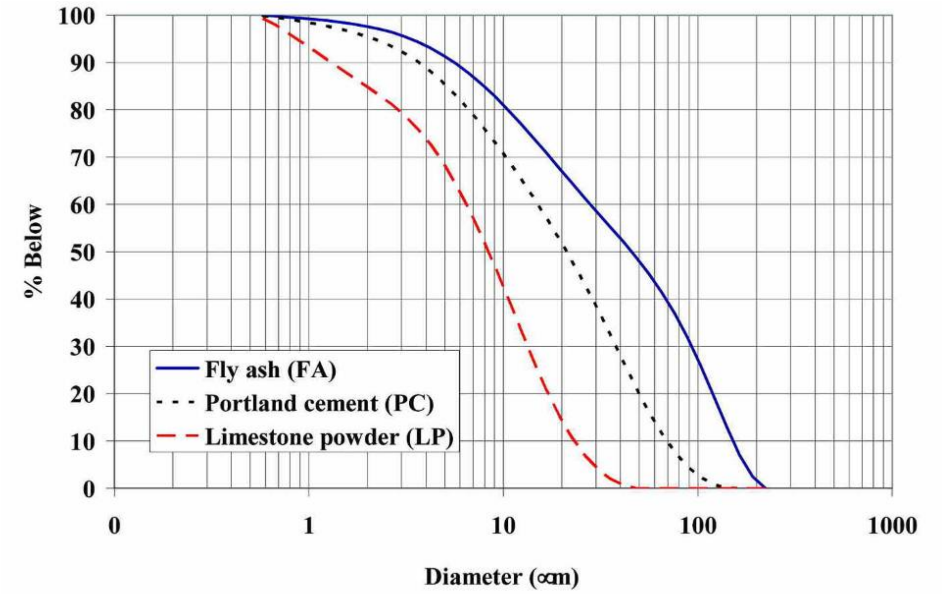

Figure 1. Particle size distribution of PC, FA and LP

Table 2: Aggregate grading

% passing		Sieve size (mm)
Coarse	Fine	
100	100	19
58.6	100	12.7
35.8	100	9.5
0	96.9	4.75
-	85.5	2.36
-	68.3	1.18
-	42.3	0.6
-	17.4	0.3
-	3.7	0.15

3. CHEMICAL ADMIXTURES

A polycarboxylic type superplasticizer (SP) was used in all concrete mixes. In addition to the SP a viscosity modifying admixture (VMA) was also used. The properties of both admixtures, as provided by their manufacturers, are shown in Table 3.

Table 3: Properties of chemical admixtures

Chemical Admixture	Specific gravity	pH	Solid content (%)	Main component
SP	1.08	5-7	40	polycarboxylic
VMA	1.00	-	20	dispersed carbohydrate

4. EXPERIMENTAL PROCEDURES

4.1. Mix Proportions

The mix proportions of the mixes are summarized in Table 4. As seen in that table, five concrete mixes are prepared. The two control mixes did not contain any steel fibers. As a binder, one of the control mixes included PC (Control_PC) and the other one had FA replacing 50 % by weight of PC (Control_FA). All of the remaining mixes had the same amount of FA as in Control_FA. These were named as FA_SF1, FA_SF1&SF2, and FA_SF2 indicating the type of steel fiber incorporated in the mix. For all the mixes, the total amount of binder (PC + FA), the amount of chemical admixtures, and the amount of LP were all kept constant. Water was added to the mix until the SCC characteristics were observed; therefore, the water/powder ratio was not kept constant and change was observed between 0.35 and 0.44.

Table 4: Mix proportions

Mix ID	Water	PC	FA	LP	Aggregate		Steel fiber		SP	VMA
					Fine	Coarse	SF1	SF2		
Control_PC	250	500	0	70	905	539	0	0	5.5	6.25
Control_FA	230	250	250	70	888	529	0	0	5.5	6.25
FA_SF1	226	250	250	70	889	530	60	0	5.5	6.25
FA_SF1&SF2	205	250	250	70	925	550	30	30	5.5	6.25
FA_SF2	205	250	250	70	924	549	0	60	5.5	6.25

4.2. Preparation and Casting of Test Specimens

The mixes were prepared at about 5 min. with a 70-liter rotating planetary mixer. The sand, coarse aggregate and fibers were first dry-mixed followed by the addition of fine materials and 1/3 of water. Finally, water and chemical admixtures were pre-mixed and added to the mix. After the mixing procedure was completed, tests were conducted on the fresh concrete to determine slump flow time and diameter, V-funnel flow time, and air content. Segregation and bleeding were visually checked during the slump flow test and was not observed in any of the mixes. From each concrete mix, six 150-mm cubes and six _100*200-mm cylinders were cast. All specimens were cast in one layer without any compaction. The cubes were used for the compressive strength and ultrasonic pulse velocity tests and the cylinders were used for the splitting tensile strength tests. After demolding, all specimens were stored in a curing room at 21±2 0C, and 95±5% relative humidity until testing.

4.3. Tests on Fresh Concrete

Deformability and viscosity of fresh concrete is evaluated through the measurement of slump flow time and diameter, and V-funnel flow time (Figure 2). The slump flow is used to assess the horizontal free flow (deformability) of SCC in the absence of obstructions. The procedure for the slump flow test and the commonly used slump test are almost identical. In the slump test, the change in height between the cone and the spread concrete is measured, whereas in the slump flow test the diameter of the spread concrete is determined as the slump flow diameter (D). According to Nagataki and Fujiwara, a slump flow diameter ranging from 500 to 700 mm is considered as the slump required for a concrete classified as SCC [11].

According to Specification and Guidelines for SCC prepared by EFNARC (European Federation of National Trade Associations), a slump flow diameter ranging from 650-800 mm can be accepted for SCC [12]. In the slump flow test concrete's ability to flow and its segregation resistance can also be measured. To measure these properties, the time (t50) it takes for the concrete to reach a 500 mm spread circle and any segregation border between the aggregates and mortar around the edge of spread are recorded. EFNARC suggests t50 of 2 to 7 sec. for SCC. In addition to the slump flow test, V-funnel test is also performed to assess the flowability and stability of the SCC. The funnel is filled completely with concrete and the bottom outlet is opened, allowing the concrete to flow. The V-funnel flow time is the elapsed time (tV-f) in seconds between the opening of the bottom outlet and the time when the light becomes visible from the bottom, when observed from the top. Good flowable and stable concrete would consume short time to flow out. According to Khayat, a tV-f which is less than 6 sec. is recommended for a concrete to qualify as a SCC [13]. According to EFNARC, tV-f ranging from 6 to 12 sec. is considered adequate for a SCC [12].


Figure 2. Workability tests on the HVFA-SCC

4.4. Tests on Hardened Concrete

Tests performed on cured concrete specimens consist of the specimen compressive strength, the splitting tensile strength, and the ultrasonic pulse velocity. For each mix, cubic specimens were loaded under compressive load to failure (ultimate load) at 28, and 56 days. The compressive strength was computed from the average of three specimens. The ultrasonic pulse velocities (UPV) of all six cubic specimens were measured on the two smooth sides of the specimen at 7, 14, 28, and 56 days. The UPV test was conducted with direct transducer arrangement using a pair of narrowband 54 kHz transducers using a commercially available PUNDIT system.

5. DISCUSSION OF TEST RESULTS

5.1. Fresh Concrete Properties

Table 5 lists the test results performed on fresh concrete. Included in that table are the w/p ratio of the mix, slump flow diameter (D) and time (t50), V-funnel flow time and air content. As seen in that table, the slump flow diameters of all mixes were in the range of 560 to 700 mm, slump flow times are less than 2.9 sec., and the V-funnel flow times (tV-f) were in the range of 2.4 to 4.3 sec. Therefore, all concrete mixes could be considered as SCC. In all of the SCC mixes, there was no segregation of aggregate near the edges of the spread-out concrete as observed from the slump flow test.

Table 5. Fresh properties

Mix ID	w/p*	Fiber factor	Slump flow		V-Funnel flow time tV-f (s)	Air Content (%)
			D (mm)	t50 (s)		
Control_PC	0.44	0	560	2.9	4.3	2.5
Control_FA	0.40	0	690	< 2.0	2.4	1.8
FA_SF1	0.40	42	660	< 2.0	2.8	4.2
FA_SF1&SF2	0.36	35	630	< 2.0	4.0	4.5
FA_SF2	0.36	29	700	< 2.0	2.7	3.6

Also observed in Table 5 is the change in w/p ratio for the same workability measure, i.e. the same D, t50, and tV-f. The Control_PC mix had the highest w/p ratio, but as part of the PC was replaced by FA the w/p ratio of all mixes decreased. This phenomenon is also observed by other researchers [4, 14]. In such studies, even though finer FAs were used, which is expected to increase the water requirement of a concrete mix, the smooth surface characteristics and spherical shape of the FA improved the workability characteristics of concrete mixes and the same workability was achieved by a smaller w/p ratio. Therefore, using a coarser FA with higher volumes is naturally going to decrease the water demand of a SCC mix for the same workability measure. The steel fibers also affected the fresh properties of the concrete mixes. The addition of SF1 type steel fibers did not affect the water requirement of the mix for the same workability. However, addition of SF2 type fibers which have smaller diameters and sizes reduced the amount of water. This could be explained by the geometry of the fibers as well as the surface characteristics of these fibers. SF2 fibers have smaller dimensions when compared with SF1 fibers, thus have less potential to prevent the movement of aggregates. In addition, SF2 fibers are coated with brass and have very smooth surfaces, which reduce the energy loss during the movement of particles.

5.2. Hardened Concrete Properties

The results of hardened concrete tests are presented in Table 6. Included in that table are the 28 and 56 day compressive and splitting tensile strength tests and 7, 14, 28, and 56 day ultrasonic pulse velocity tests. Even though the w/p ratio of the mix was reduced, substitution of PC with a coarse FA resulted in lower strengths both at 28 and 56 days. This reduction was 43% at 28 days and 31% at 56 days. The low pozzolanic activity can be attributed to the coarseness of the FA used. Fiber inclusion did not significantly affect the measured mechanical properties; however, as seen in Figure 3 as the volume of the SF2 type fibers increased the compressive strength slightly increased. This is due to the relatively small dimensions of SF2 type fibers, which give these fibers the ability to delay the micro crack formation and to arrest and prevent their propagation afterwards up to a certain extent. Another explanation to the increase in the compressive strength could be the decrease in w/p ratio which decreased as the amount of SF2 type fibers increased. However, when the split tensile strengths are examined (Figure 4) it can be seen that there is a reduction in the split tensile strengths as the volume of SF2 type fibers are increased or the w/p decreased. The reduction in the split tensile strength is explained by the loss of the presence of longer SF1 type fibers which are responsible for the increase in tensile strengths.

Table 6: Hardened properties

Mix ID	Compressive Strength(MPa)		Split Tensile Strength (MPa)		Ultrasonic Pulse Velocity (m/s)			
	28 d*	56 d*	28 d*	56 d*	7 d†	14 d†	28 d†	56 d*
Control_PC	40.7 70 [0.5] ‡	41.7 [0.4]	3.58 [0.3]	3.68 [0.1]	4565 [22]	4570 [45]	4578 [35]	4609 [7]
Control_FA	23.3 [1.0]	28.6 [1.2]	2.8 [0.4]	3.34 [0.5]	4161 [31]	4260 [51]	4436 [74]	4564 [29]
FA_SF1	19.6 [0.1]	24.5 [0.6]	3.10 [0.2]	3.69 [0.6]	3963 [10]	4007 [44]	4157 [45]	4317 [28]
FA_SF1&SF2	22.8 [0.5]	26.1 [2.0]	3.40 [0.0]	3.82 [0.3]	3970 [42]	4100 [41]	4249 [40]	4383 [88]
FA_SF2	22.5 [2.9]	31.8 [0.8]	3.08 [0.1]	3.23 [0.2]	4142 [109]	4224 [109]	4359 [82]	4506 [114]

*** Tests are performed on 3 specimens**
† Tests are performed on 6 specimens
‡ Numbers in parenthesis are the standard deviations

Ultrasonic pulse velocity (UPV) is used to assess the hardening of the SCC mixes. As seen in Figure 5, as hydration continues the UPVs increased for all the SCC mixes. However, the slope of that curve is quite different for the PC and FA mixes. For the Control-PC mix the slope was much smaller as most of the hydration was complete by 7 days. However, for the mixes with FA the hydration reactions continue after 7 days indicating a higher slope.

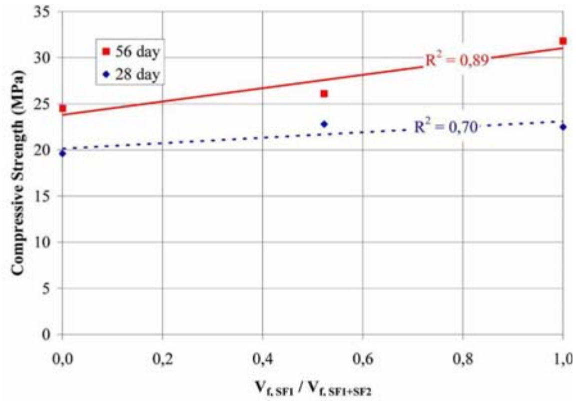

Figure 3. Effect of steel fibers on the compressive strength

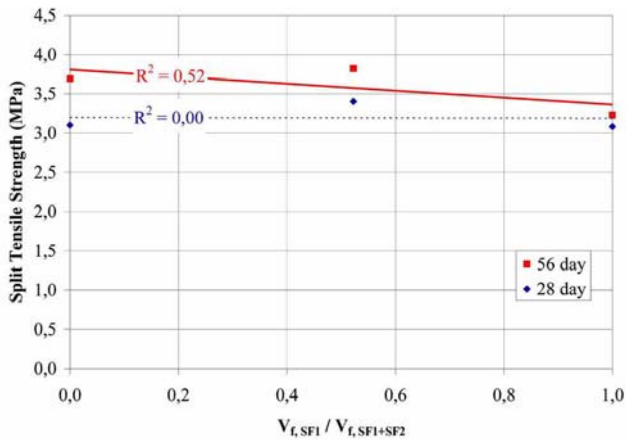

Figure 4. Effect of steel fibers on the split tensile strength

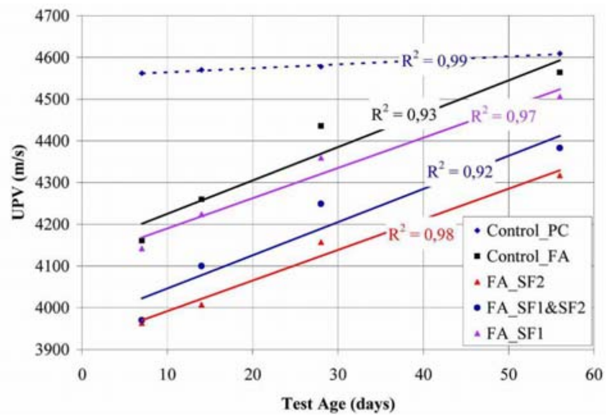

Figure 5. Strength gain of SCC mixes

6. CONCLUSIONS

This paper discusses the part of the results of an experimental program carried out to investigate the effects of incorporation of HVFA, and steel fibers on the flow characteristics of SCC and mechanical properties in the hardened state.

It can be concluded that it is possible to achieve self compaction with considerable fiber inclusion. Incorporation of HVFA may reduce the water requirement of a SCC mix. In other words, using high volumes of coarse FA may increase the workability characteristics of SCC mixes. Therefore the amount of SP and VMA to achieve self compaction could be reduced with proper adjustments to the FA amount. However, it is also seen that using coarse FA may cause significant strength losses to the SCC mixes, since they are used in high volumes. However, the strength reduction due to low pozzolanic activity of the FA was partially off-set by the use of smaller SF2 type steel fibers. It can also be concluded that the SF2 type steel fibers affect the properties of SCC mixes not only in the hardened state but also in the fresh state reducing the water requirement for the same workability measure**.**

ACKNOWLEDGEMENTS

The Atisaz Company has provided this research study for the Concrete Research Center.

REFERENCES

1. H. Okamura, M. Ouchi, Self compacting concrete: development, present use and future. *Proceedings of the First RILEM International Symposium on Self-Compacting Concrete* (1999), pp. 3-14.
2. A. Bilodeau, V. Sivasundaram, K.E. Painter, V.M. Malhotra, Durability of concrete incorporating high volumes of fly ash from sources in U.S. *ACI Mater. J.* **91** (1994), pp. 3-12.
3. A. Bilodeau, V. M. Malhotra, High-volume fly ash system: concrete solution for sustainable development. *ACI Mater. J.* **97** (2000), pp. 41-48.
4. N. Bouzoubaâ, M. H. Zhang, V. M. Malhotra, Mechanical properties and durability of concrete made with high-volume fly ash blended cements using a coarse fly ash. . *Cem. Concr. Res.* **31** (2001), pp. 1393-1402.
5. N. Bouzoubaa, M. Laclemi, Self-Compacting concrete incorporating high volumes of class F fly ash preliminary results. *Cem. Concr. Res.* **31** 3 (2001), pp. 413-420.
6. D.J. Hannant, *Fiber Cements and Fiber Concrete*, Wiley, Chichester, 1987.
7. A. Bentur, S. Mindess, *Fiber Reinforced Cementitious Composites*, Elsevier, London, 1990.
8. B. Mobasher, C.Y. Li, Mechanical properties of hybrid cement-based composites, *ACI Mater. J.* 93 (3) (1996) 284-292.
9. K. H. Khayat, Y. Roussel, Testing and performance of fiber-reinforced, self-consolidating concrete.*Proceedings of the First RILEM International Symposium on Self-Compacting Concrete* (1999), pp.509-521.
10. P. Grouth, D. Nemegeer, The use of steel fibres in self-compacting concrete. *Proceedings of the First RILEM International Symposium on Self-Compacting*

Concrete (1999), pp. 497-507.
11. S. Nagataki and H. Fujiwara, Self-compacting property of highly-flowable concrete. in: V.M. Malhotra (Ed.), *Am. Concr. Inst.* **SP 154** (1995), pp. 301-314.
12. EFNARC, Specification & Guidelines for Self-Compacting Concrete (2002).
13. K. H. Khayat, Z. Guizani, Use of viscosity-modifying admixture to enhance stability of fluid concrete. *ACI Mater. J.* **94** 4 (1997), pp. 332-341.
14. A. Yahia, M. Tanimura, A. Shimabukuro, Y. Shimoyama, Effect of rheological parameters on self compactability of concrete containing various mineral admixtures *Proceedings of the First RILEM International Symposium on Self-Compacting Concrete* (1999), pp. 523-535.

EFFECTS OF POLYPROPYLENE FIBERS ON PHYSICAL AND MECHANICAL PROPERTIES OF CONCRETES

M. Najimi, F.M. Farahani and A.R. Pourkhorshidi
Concrete Department, Building and Housing Research Centre, Tehran, IRAN

ABSTRACT

In this present study, the effects of adding polypropylene fibers on physical and mechanical properties of concretes are investigated. To this end, three concrete mixtures consists of 6 mm, 12 mm and 19 mm polypropylene fibers are made and their physical/ mechanical aspects are studied and compared with control concrete. The results manifest that adding polypropylene fibers increases the flexural strength slightly and decreases the cracks width. Besides, the compressive strength decreases slightly. These properties are improved with increase of fibers length.

Keywords: concrete, polypropylene fibers, crack bridge, flexural strength, impact resistance

1. INTRODUCTION

Nowadays concrete is one of the most applicable materials in construction of structures such as buildings, dams, bridges, tunnels, highway pavements, offshore structures, towers and so on. This material has received great attention because of its desirable performance in compression.

Concrete is considered to be a relatively brittle material, so it is prone to cracking. Many investigations have been carried out in order to overcome this problem. The inclusion of adequate fibers improves tensile strength and provides ductility [1-3]. There are more investigations on the effects of different fibers on concrete properties [4-9].

Some of the important effects of fibers in concrete are: increasing the tensile strength, preventing the crack development and increasing the toughness of concrete. The fundamental advantage of adding fibers to concrete is known as crack bridging [9-14].

In recent years, concrete containing different fibers has been applied in large structures such as highway pavements and airports, huge foundations with large deformations and concrete cover of tunnels. Recently in order to prevent cracking in the covers of the pre-cast tunnels, un-reinforced concrete with the fibers has been used. On the other hand the investigations have shown the compressive strength reduction in fiber concretes. This reduction occurs because of the collection of Calcium-Hydroxide in the interface of hydrated cement and various types of fibers (such as Steel, Carbon, Dacron, Polypropylene fibers, and …) [15].

In recent decades the polypropylene fibers have been widely used in industries. Polypropylene fibers are relatively inexpensive, easy to split into finer sizes, durable in the environment of cement matrix and they don't rust. They have a relatively low modulus of elasticity, relatively poor bond and it is difficult to obtain uniform dispersion with Polypropylene fibers when a sufficiently large volume of fibers is used. In the present study, the effects of adding polypropylene fibers on physical and mechanical properties of concretes are investigated.

2. EXPERIMENTAL PROGRAM

2.1. Materials

2.1.1. Aggregates

Crushed coarse aggregates with maximum nominal size of 19mm and natural fine aggregates were selected. The Physical properties of coarse and fine aggregates are presented in Table 1. The aggregates grading curve is shown in Figures 1, 2.

Table 1: Physical properties of aggregates

Aggregates	Type	SSD Density* (gr/cm^3)	Water absorption (%)	Passing from sieve #200 (%)
Coarse	Crushed	2.53	1.61	0.5
Fine	Natural	2.56	2.46	1.1

SSD: Saturated Surface Dry

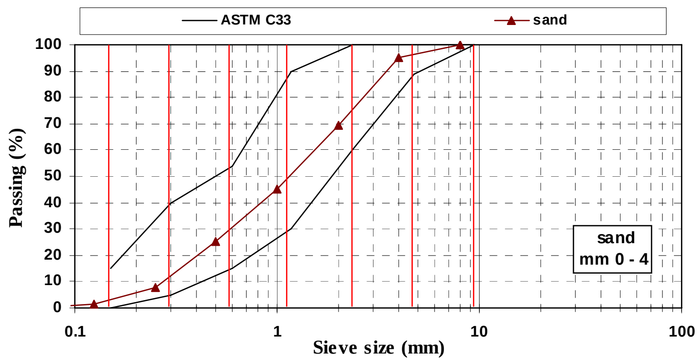

Figure 1. Particle size distribution of fine aggregates

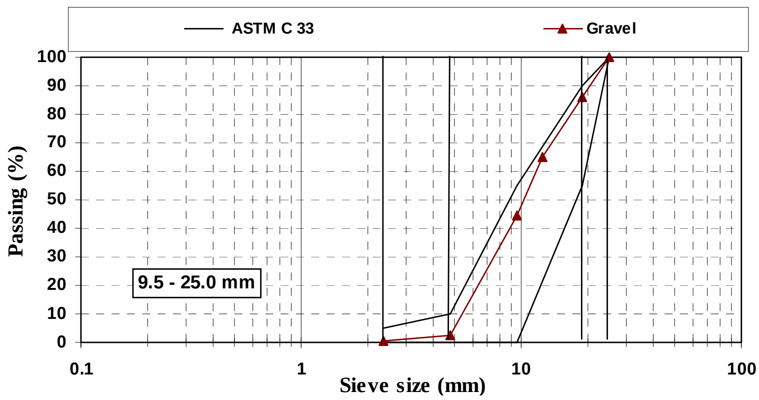

Figure 2. Particle size distribution of coarse aggregates

2.1.2. Cement
Type II Portland cement (according to ASTM C595) produced by Tehran Cement manufactory, was used in this investigation. The chemical and physical properties of this cement are presented in Table 2.

2.1.3. Polypropylene Fibers
The polypropylene fibers in three sizes of 6, 12 and 19 mm were used. A sample of the fibers is shown in Figure 3.

Table 2: Chemical and physical properties of cement

Chemical analysis, %	
Calcium oxide (CaO)	61.9
Silica (SiO_2)	21.1
Alumina (Al_2O_3)	4.2
Iron oxide (Fe_2O_3)	4.6
Magnesia (MgO)	3.4
Sodium oxide (Na_2O)	0.6
Potassium oxide (K_2O)	0.5
Sulfur trioxide (SO_3)	1.79
Bogue potential compound composition, %	
Tri-calcium silicate (C_3S)	52.74
Di-calcium silicate (C_2S)	20.31
Tri-calcium aluminate (C_3A)	3.35
Other properties	
3 days compressive strength, kg/cm^2	223
7 days compressive strength, kg/cm^2	306
28 days compressive strength, kg/cm^2	414
Initial setting time, min	150
Final setting time, min	190
Specific surface, cm^2/gr	3296

Figure 3. Sample of polypropylene fibers (6, 12 and 19 mm)

2.2. Mix Design
The mixtures were made on the basis of a series of experimental mix parameters

such as suitable slump, lack of segregation and bleeding. The mixture proportions are shown in Table 3.

To prevent breaking the fibers, first concrete materials were mixed, and then the fibers were poured in the mixture by hand rapidly in a 1-2 minute period [16].

3. RESULTS AND DISCUSSIONS

3.1. Fresh Concrete

The fresh concrete specifications for each kind of the mixtures are shown in Table 4. The concretes containing polypropylene fibers had lower slump than the control concrete.

Table 3: Mixture proportions (per m^3)

Mixture identification	W/C	Water (kg)	Cement (kg)	Coarse (kg)	Fine (kg)	Polypropylene fibers (kg) 6 mm	12 mm	19 mm
Control mix	0.5	175	350	860	980	--	--	--
Mix 1	0.5	175	350	860	980	2	--	--
Mix 2	0.5	175	350	860	980	--	2	--
Mix 3	0.5	175	350	860	980	--	--	2

Table 4: Fresh concrete specifications

Mixture identification	Density (Kg/m^3)	Slump (cm)	Air percentage	Observations
Control mix	2400	7	4.5	No bleeding-No segregation
Mix 1	2385	3.5	4	
Mix 2	2380	3	4	
Mix 3	2380	3	4	

3.2. Hardened Concrete

In order to determine the physical/ mechanical properties of mixtures, tests of compressive strength, flexural strength, modulus of elasticity, abrasion resistance, impact resistance and shrinkage were performed.

3.2.1. Compressive Strength

The compressive strength of cube specimens was obtained according to the BS 1881 at the ages of 7, 28 and 56 days. The results are presented in Figure 4.

It can be observed that the compressive strength of fiber concretes is less than the control concrete. This strength reduction can be induced by collection of Calcium-Hydroxide in the interface of fibers and hydrated cement. Besides, the compressive strength increased with increase of fibers length. The compressive strength of 19 mm fibers concretes is almost equal to the control concrete.

3.2.2 Flexural Strength

The flexural strength of the specimens was measured according to ASTM C293 at the ages of 7, 28 and 56 days. The results are shown in Figure 5.

As can be seen, the use of fibers increases the flexural strength of the concrete. This increasing trend may have occurred due to crack bridging of the fibers. Besides, the flexural strength increased with an increase in the length of the fibers. It can be concluded that longer fibers (with higher aspect ratio) can bridge the cracks better than other fibers.

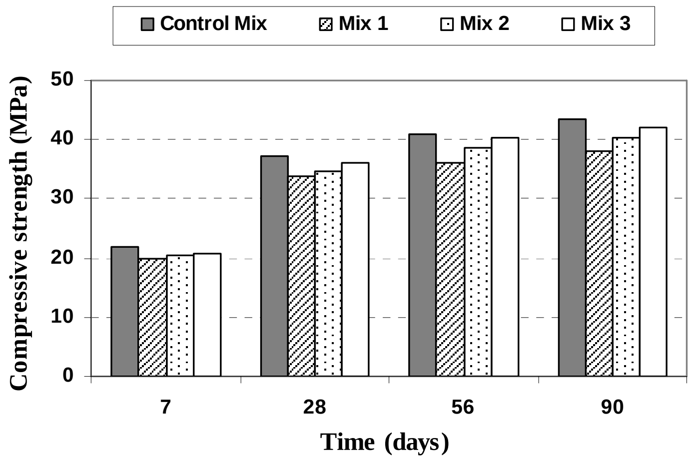

Figure 4. Compressive strength versus age

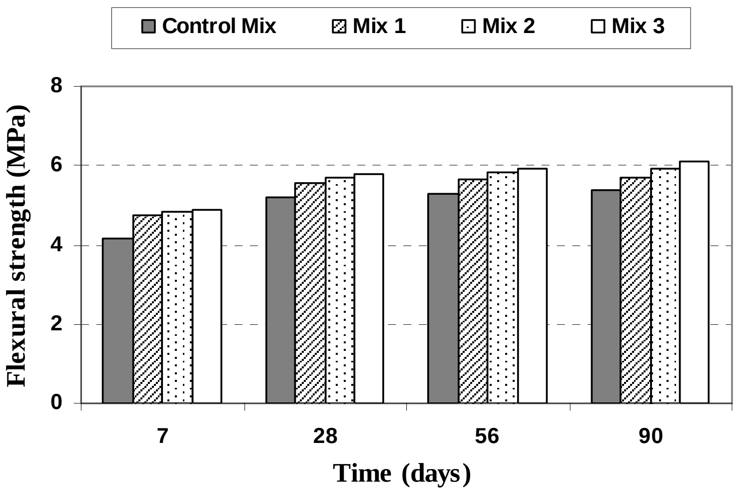

Figure 5. Flexural strength versus age

3.2.3 Modulus Of Elasticity

The modulus of elasticity of the specimens was determined at the ages of 7, 28 and 56 days according to ASTM C469 and the results are shown in Figure 6.

The use of fibers decreases the static modulus of elasticity of the concrete slightly. Besides, the increase in the length of the fibers causes a slight increase in the static modulus of elasticity. This increase may have occurred because of increase in the aspect ratio.

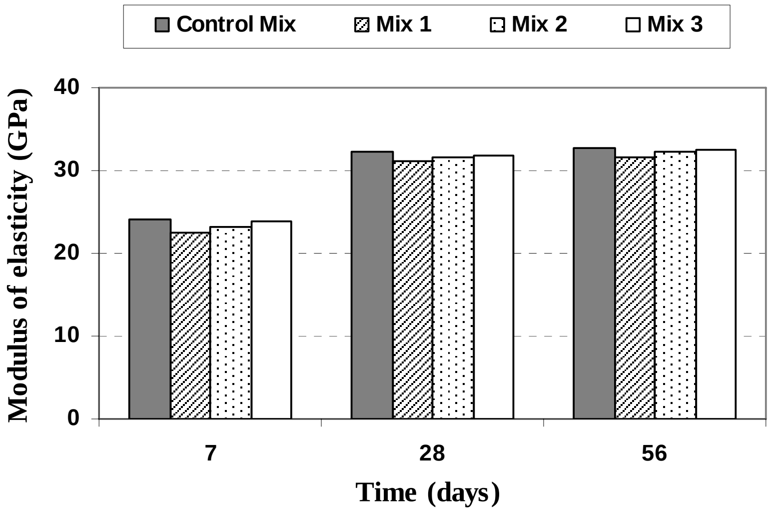

Figure 6. Modulus of elasticity versus age

3.2.4. Abrasion Resistance

The abrasion resistance of the specimens was measured at age of 28 days according to standards ASTM C779 and EN 1338. The results are shown in Table 5.

It can be observed that abrasion resistance of the fiber concretes is better than the control concrete. Besides, the abrasion resistance of the concrete slightly increases with increase in the length of the fibers.

Table 5: Abrasion resistance

Mixture Identification	Abrasion depth according to ASTM C779-89a			Abrasion according to EN 1338	
	After 30 min (mm)	After 60 min (mm)	Variation (%)*	Abrasion (cm)	Variation (%)
Control mix	0.94	1.68	--	2.2	--
Mix 1	0.54	1.09	0.351	2.1	0.045
Mix 2	0.56	1.05	0.375	2.05	0.068
Mix 3	0.52	0.98	0.417	1.85	0.159

*** Variation has been calculated with respect to after 60 min results**

3.2.5. Impact Resistance

One of the important properties of the fiber concretes is the resistance against impact. The test of impact repeat with load drop is one of the valid tests for evaluation of impact resistance of concrete which has been suggested by ACI 544- part 2.

In this test, the number of required impacts which causes to crack and rupture in concrete specimen, is determined and this number implies the qualitative estimation of the absorbed energy by the concrete specimen. In this test the standard hammer (with the weight of 4.5 kg and drop height of 457 mm) drops on the steel sphere of 63.5 mm diameter which has been fixed on the surface of the

concrete, and transfers the impact to the concrete specimen. The specimen shape is cylindrical with 152 mm diameter and 63.5 mm height. The results are shown in Table 6 at the age of 28 days.
Adding fibers to concrete decreases the required number of impacts due to first crack, while it increases the required number of the impacts due to complete rupture. The number of impacts until complete rupture is also increased with the increase of the length of the fibers.

Table 6: Impact resistance in 28 days

Mixture Identification	Required number of impacts due to first crack			Required number of the impacts due to complete rupture		
	Minimum impacts	Maximum impacts	Average	Minimum impacts	Maximum impacts	Average
Control mix	21	25	23	27	27	27
Mix 1	19	21	20	27	28	28
Mix 2	16	18	17	28	29	29
Mix 3	16	18	17	29	31	30

3.2.6. Restrained Shrinkage Test

If the shrinkage of concrete occurs freely, the concrete section doesn't crack, but if it is restrained, the tensile stresses will appear and the concrete becomes more prone to cracking. One of the effective methods of controlling restrained shrinkage cracking is the use of fibers in the concrete mixture. In this research, in order to evaluate the cracking potential caused by restrained shrinkage, the method of cracking in circular specimens which is suggested by ACI 544- part 2 is used. In this test, concrete is molded into a ring formwork with the thickness of approximately 30mm and of 300mm outer diameter. The specimen is subjected to wind blowing and low relative humidity and the procedure of crack development is monitored. A sample of this test is shown in Figure 7. In this test, width of the cracks and the pattern of cracks from the time of cracking were studied up to 90 days. The results of restrained shrinkage up to 90 days are shown in Table 7.
As can be observed, fiber concrete mixtures have less crack width in comparison with control concrete. The time of the first cracking in the fiber concrete has also increased. These results confirm results of the flexural strength test about fiber's crack bridging.

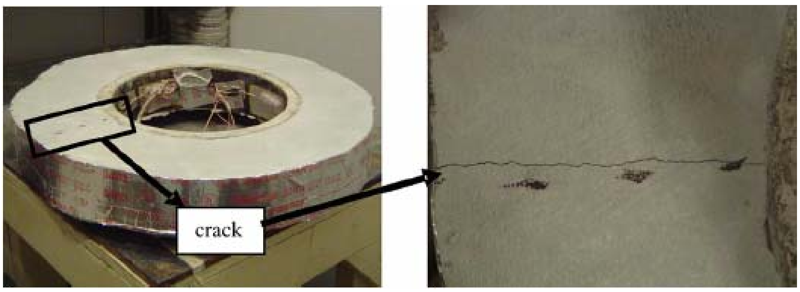

Figure 7. Crack in restrained ring specimen drying from the top and bottom [14]

Table 7: Observed results of restrained shrinkage cracks up to 90 days

Mixture identification	Time of the first cracking after 7 days curing (days)	Maximum crack number	Maximum crack width	Average crack width
Control mix	3	3	0.3	0.27
Mix 1	4	3	0.26	0.21
Mix 2	6	2	0.2	0.18
Mix 3	6	2	0.2	0.17

4. CONCLUSION

From the results of this investigation, the following conclusions can be drawn:

- Adding polypropylene fibers to the concrete has led to a slight decrease in the compressive strength and modulus of elasticity of the specimens. The strength was decreased slightly (up to 10 percent for specimens made of 6 mm length fibers). Besides, the compressive strength has been increased with the increase in the length of the polypropylene fibers. The compressive strength of 19 mm fibers concrete is almost equal to the control concrete.
- According to obtained results of the flexural strength test, adding fibers to concrete has led to increase of flexural strength with respect to the control concrete. Flexural strength also increases with the increase in the length of the fibers. The concrete mixture with 19 mm fibers showed 10 percent higher flexural strength than the control concrete.
- The specimens which contained polypropylene fibers had better abrasion resistance than control concrete. Generally the fibers with different lengths showed equal abrasion resistance.
- Adding fibers to concrete decreased the required number of impacts for the first cracking, but increased it for complete rupture. The number of impacts for complete rupture increases with the increase of the length of the fibers. It can be concluded that adding fibers to concrete has an effective role in reduction of the crack width.
- According to obtained results, polypropylene fibers concretes are useful in control of shrinkage and fine cracks. It is recommended to apply these materials in construction of the concrete floors such as airports and industrial floors.

REFERENCES

1. Konig, G. et al., New concepts for high performance concrete with improved ductility, proceedings of the 12th FIP congress on challenges for concrete in the next millennium, Netherlands, 1998, pp. 49-53.
2. Ramezanianpour, A.A., Najimi, M. and Pourkhorshidi, A., The role of polypropylene fibers on concrete properties, First disaster management symposium, University of Tehran, 2006, pp. 542-549.
3. Breitenbucher, R., High strength concrete C 105 with increased fiber resistance due to polypropylene fibers, 4th international symposium on the utilization of high strength-high performance concrete, Paris, 1996, pp. 571-577.

4. Balaguru, P. and Slattum, K., Test methods for Durability of Polymeric Fibers in Concrete and UV Light Exposure, *In:* Stevens D.J., "Testing of Fiber Reinforced Concrete", ACI SP-155, American Concrete Institute, Detroit, 1995,pp. 115-136.
5. Daniel, J.I., Roller, J.J. and Anderson, E.D., Fiber reinforced Concrete, Portland Cement Association, 1998.
6. Badr, A., Ashour, A.F. and Platten, A.K., Statistical variations in impact resistance of polypropylene fibre-reinforced concrete, International Journal of Impact Engineering, 2006, Vol. 32, pp. 1907-1920.
7. Dave, N.J. and Ellis, D.G., Polypropylene fiber reinforced cement, International Journal of cement and concrete, 1979, Vol. 1, pp.19-28.
8. Yan, L., Jenkins, C.H. and Pendelton, R.L., Polyolefin fiber-reinforced concrete composites, Part I: Damping and frequency characteristics, Cement and Concrete Research, 2000, Vol.30, pp. 391- 401.
9. Nemkumar, B. and Rishi, G., Influence of polypropylene fiber geometry on plastic shrinkage cracking in concrete, Cement and Concrete Research, 2006, Vol. 36, pp. 1263-1267.
10. Hähne, H., Karl, S. and Worner, J.D., Properties of Polyaerylonitrite Fibre reinforced concrete, *In*: S.P. Shah & G.B. Batson, "Fiber Reinforced Concrete Properties and Applications", ACI SP 105, American Concrete Institute, Detroit, 1987, pp. 211-223.
11. Song, P.S., Hwang, S. and Sheu, B.C., Strength properties of nylon and polypropylene fiber reinforced concretes, Cement and Concrete Research, 2005, Vol. 35, pp. 1546-1550.
12. Pye, A.M., A review of asbestos substitute materials in industrial applications, Journal of Hazardous Materials, 1979, pp. 125-147.
13. Keer, J.G. and Throne, A.M., Performance of Polypropylene reinforced cement sheeting elements, *In*: Hoff G.C., "Fiber Reinforced Concrete", ACI SP 81, American Concrete Institute, Detroit, 1984, pp. 213-31.
14. Akhter, B.H. and Jaison, W., The role of specimen geometry and boundary conditions on stress development and cracking in the restrained ring test, Cement and Concrete Research, 2006, Vol. 36, pp. 188-199.
15. Bentur, A., diamond, S. and Mindess, S., The microstructure of the steel fiber-cement interface, Material Science, 1985, Vol. 20, pp. 3610-3620.
16. Tavakoli, M., Tensile and compressive strengths of Polypropylene fibre reinforced concrete, ACI SP-142, Fibre Reinforced Concrete: Developments and Innovations, 1994, pp. 61-72.

CD07-010

OIL PALM SHELL, GROUND PALM OIL FUEL BASED LIGHTWEIGHT CONCRETE

M. Zeinizadeh Jeddi
Department of Civil Engineering, Faculty of Engineering, University Putra Malaysia, 43400 Selangor, Malaysia

ABSTRACT

Compressive strength and water permeability of concretes containing ground palm oil fuel ash (GPOA) and ground rice husk–bark ash (GRBA) were investigated. From the tests, the replacement of Portland cement by both materials resulted in the higher water demand in concrete mixtures as compared to ordinary Portland cement (OPC) concrete with compatible workability. The compressive strengths of concretes containing 20% of GPOA and GRBA were as high as that of OPC concrete and were reduced as the increase in the replacement ratios. Although the compressive strengths of concrete with the replacement of GPOA or GRBA up to 40% were lower than OPC concrete, their water permeabilities were still lower than that of OPC concrete. These results indicate that both of GPOA and GRBA can be applied as new pozzolanic materials to concrete with an acceptable strength as well as permeability.

Keywords: oil palm shell, ground palm oil fuel ash, ground rice, lightweight concrete, permeability.

1. INTRODUCTION

Because of environmental problems and considering the rapid depletion of conventional aggregates, the use of aggregates from by-products and solid waste materials from different industries are highly desirable. One such alternative is oil palm shell (OPS), which is a form of agricultural solid waste.

The bond behaviour of OPS is one such necessary investigation that has to be clearly established. The bond strength between the concrete matrix and the steel reinforcement is one of the most important aspects in structural reinforced concrete. The investigation involved pullout test on both plain and deformed steel bars under two types of curing conditions. In addition, the durability performance is also another important aspect that determines the viability of OPS concrete to be used in practical applications. The permeability of concrete has a high bearing on the concrete durability as it controls the penetration rate of moisture that may contain harmful or chemicals. The absorption characteristics of a concrete is another means of indicating its durability.

The addition of fillers and pozzolanic materials are introduced to improve the strength and other properties of concrete for necessary conditions.

Palm oil fuel ash (POA) is produced from burning of fiber, shell, and empty fruit bunch of palm oil tree as a fuel to heat the steam for electricity generation and palm oil extraction process. The palm oil fuel ash is so disposed in landfills that the amount of ashes increases every year and now becomes a burden. It is estimated that more than 100,000 tons of palm oil fuel ash has been produced every year and increases annually in Thailand. The study of palm oil fuel ash was started by Tay [1] who used it to replace Portland cement with 10-50%. He found that in the range of 20-50% of cement replacement, the decrease in the compressive strength of concrete at various ages was almost proportional to amount of the ash in the concrete mixtures, except when only 10% ash was used. Later, Awal and Hussin [2] reported that palm oil fuel ash had a good potential in suppressing expansion due to sulfate attack. In 2004, it was found that palm oil fuel ash, which contained a substantial amount of silica and was ground to a suitable fineness, could be used as a pozzolanic material to produce high strength concrete as high as 100 MPa at 90 days [3].

Rice husk-bark ash (RBA) is also a waste from electricity generation power plant. In the fluidized bed power plant, two parts of rice husk are used in conjunction with one part of eucalyptus tree bark by weight as fuel. The burning temperature of the materials is between 800 and900-C. The disposal of rice husk–bark ash is also becoming a problem due to its quantity. It is estimated that more than 300,000 tons of rice husk–bark ash has been produced each year in Thailand [4]. Effort has, therefore, been made to utilize this ash. The study revealed that the ground rice husk–bark ash conforms to the Class N pozzolanic material [5] as prescribed by ASTM C 618 [6]. Moreover, the compressive strength of mortar containing very high fineness of rice husk–bark ash is equal or higher than the control mortar. Although some properties of concrete containing rice husk–bark ash have been reported [4], none of them deals with a relationship between the strength and the permeability. The aim of this research is to study the compressive strength and water permeability of concrete containing palm oil fuel ash and rice husk–bark ash. The results are compared to concrete containing fly ash, a well-known pozzolanic material, and also compared to the control concrete as well. The knowledge on the strength and permeability of concrete containing palm oil fuel ash and rice husk–bark ash is and could be beneficial on the utilization of these waste materials in concrete work, especially on the topic of durability.

2. EXPERIMENTAL PROGRAM

2.1. Materials

The properties of the sand and OPS used are illustrated in Table 1. It can be observed that the aggregate impact value (AIV) and aggregate crushing value (ACV) of OPS aggregates were much lower compared to the conventional crushed stone aggregates. The chemical composition of OPS was determined and is presented in Table 2. Before the OPS are used as aggregates, they were sieved and only aggregates passing the 12.5mm sieve were used for mixing. The sieve analysis of the river sand and OPS aggregate is illustrated in Figure 1. Due to the high water absorption of OPS, the aggregates were pre-soaked for 24 h in potable water prior to mixing and were in saturated surface dry (SSD) condition during mixing to prevent absorption from occurring during mixing. The properties of OPS aggregates are different compared to other lightweight aggregates, such as expanded clay, expanded shale and sintered pulverised fuel ash, which are artificially produced.

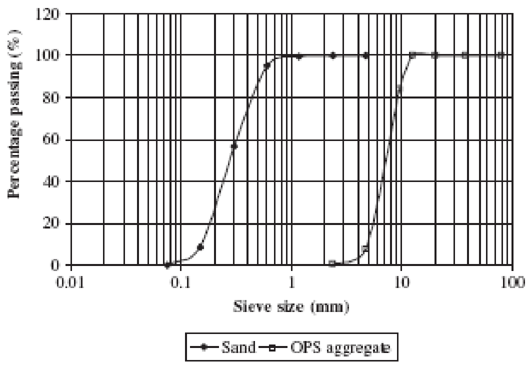

Figure 1: Sieve analysis for river sand and OPS aggregate

Table 1: Properties of river sand and OPS aggregate

Properties	River sand	Oil palm shell (OPS)
Maximum grain size (mm	1.18	12.5
Shell thickness (mm)	-	0.5-3
Specific gravity	2.45	1.17
Bulk unit weight (kg/m^3)	1500-1550	500-600
Fineness modulus	1.40	6.08
Los Angeles abrasion value (%)	-	4.90
Aggregate impact value (%)	-	7.51
Aggregate crushing value (%)	-	8
24-h water absorption (%)	3.89	33

Table 2: Chemical composition of OPS aggregate

Elements	Results (%)
Ash	1.53
Nitrogen (as N)	0.41
Sulphur (as S)	0.000783
Calcium (as CaO	0.0765
Magnesium (as MgO	0.0352
Sodium (as Na_2O	0.00156
Potassium (as K_2O	0.00042
Aluminium (as Al_2O_3	0.130
Iron (as Fe_2O_3)	0.0333
Silica (as SiO_2	0.0146
Chloride (as Cl^-	0.00072
Loss on Ignition	98.5

The mix design for the OPS concrete in this investigation is based on conducting trial mixes and the proportion of these mixes are adjusted to arrive at an optimum mix proportion, which was used throughout the entire investigation. This mix proportion consisted of 510 kg/ m^3 cement, 848 kg/m^3 sand, 308 kg/m^3 OPS with a water/cement ratio of 0.38. The SP added was 1.4 l per 100 kg of cement. The obtained slump, which was between 50 and 70mm showed that OPS concrete has a medium degree of workability and is within the range of a workable concrete. The air content was in the range of 4.8-5.5% and this relatively high air content could be attributed by the highly irregular shapes of the OPS which prevented full compaction to be achieved.

Ordinary Portland cement (OPC) was used for all concrete mixtures. Palm oil fuel ash and rice husk–bark ash were ground by ball mill until the 95% of the particles passed a sieve No. 325 (opening 45 lm) and were assigned as GPOA and GRBA, respectively. Physical properties and chemical compositions of the materials areshown in Tables 3 and 4.

2.2. Aggregates

River sand with fineness modulus of 2.44 and specific gravity of 2.65 was used as fine aggregate. Crushed limestone with the maximum size of 20 mm and having specific gravity of 2.67 was used as coarse aggregate. 2.2. Concrete mixtures OPC was partially replaced by ground palm oil ash (GPOA) and ground rice husk–bark ash (GRBA) at 20%, 40% and 55%, while the replacement of OFA was 20% and 40% by weight of binder. The binder content of concrete was set as a constant of 300 kg/m3 and mix proportions of concrete are presented in Table 3.

Table 3: Materials properties

Materia	Specific gravity	Retained on a sieve #325 (%)	Median particle size, d50 (lm)
OPC	3.14	-	14.7
OFA	2.19	32.1	27.1
GPOA	2.43	1	8
GRBA	2.15	1.9	10.2

Note: OPC = Ordinary Portland cement Type I. OFA = Fly ash.
GPOA = Ground palm oil fuel ash. GRBA = Ground rice husk–bark ash.

3. TESTING

3.1. Compressive Strength and Structural Bond

Concretes cylinders of 100mm in diameter and 200 mm in height were used to determine the compressive strength. The samples were demolded 24 h after casting and cured in water until the testing ages. The compressive strengths of concretes were determined at the ages of 28 and 90 days.

For each specimen, a single reinforcing bar was placed in the centre of the specimen and both ends of the specimen were provided with an unbonded length of 25mm at each end. The unbonded lengths were provided by attaching a plastic sheathing to the bar for obtaining uniform pressure. The short embedment length of 150mm was selected to avoid yielding of the steel bar under pullout load.For the bond strength determination, two types of curing regimes, namely laboratory air-dry curing (CL) and fullwater curing (CC) were considered. Under both curing conditions, the specimens were immediately covered with plastic sheets upon casting to prevent excessive evaporation from the fresh concrete and then demoulded after 24 h. In CL curing, specimens were kept in ambient laboratory conditions (RH of 74–88%; temp. of 2573 1C) until the age of test. For CC curing, the specimens were cured in a water tank (water temp. of 2372 1C) until the age of test. The pull-out test was carried out using the Universal Testing Machine (Shimadzu UH-300kN capacity) complete with a modified loading frame. The load was applied on the top of the concrete surface at a uniform rate as per ASTM standards until failure to obtain the ultimate load. Triplicate specimens were prepared for the pull-out test and the bond strength was reported as an average of three tests.

3.2. Water Permeability

The steady flow method was applied to test the permeability of concrete. The coefficient of water permeability was determined by measuring the amount of water passing through the sample and calculated using Darcy's law and the equation of continuity [7].

Two days before testing the permeability, the samples were prepared by sawing of 40 mm thick slice from the middle of the cylinder. After drying in the laboratory for 24 h, the slice was cast around with 25 mm thick of nonshrinkage epoxy resin to prevent the water leakage. The epoxy resin was allowed to harden and dry for another 24 h. The sample was then installed in the housing cell and then the water pressure of 0.5 MPa was applied. This pressure was recommended and used by Chan and Wu [8]. The time and the amount of water passed through the specimen were monitored until the constant flow rate was obtained.

4. RESULTS AND DISCUSSION

4.1. Properties and Particle Shape of Materials

In Table 4, it revealed that the fly ash and the GRBA can be assigned as class F and class N pozzolan as prescribed by ASTM C 618 [6]. The GPOA cannot be classified as class N pozzolan because the contents of SiO2+Al_2O_3 + - Fe_2O_3 were less than 70%. It should be noted that the loss on ignition (LOI) contents of GPOA and GRBA were rather high as 10.1% and 11.2%, respectively and 74.8% of GRBA was SiO_2. Particle size distribution curves of OPC and the other materials are shown in Figure 4. The median particle size of OFA was 27.1 lm, which was larger than that of the OPC (14.7 lm). Before grinding, palm oil fuel ash and rice husk–bark ash had median particle sizes more than 100 lm. After grinding, the median particle sizes of GPOA and GRBA were reduced to 8.0 and 10.2 lm, respectively. The particle shapes of OPC and the replacement materials are presented in Figure 3. The particle shape of OFA was spherical and smooth surface indicating a rather complete burning. On the other hand, both of GPOA and GRBA had an angular and irregular particle shape, which were similar to that of Portland cement Type I

Table 4: Chemical composition of cement and replacement materials

Chemical Composition (%)	Cement (OPC)	Fly ash (OFA)	Ground palm oil fuel ash (GPOA)	Ground rice husk–bark ash (GRBA
SiO_2	20.9	41.1	57.8	74.8
Al_2O_3	4.8	22.5	4.6	0.2
Fe_2O_3	3.4	11.6	3.3	0.8
CaO	65.4	15.3	6.6	5.9
MgO	1.2	2.8	4.2	0.6
Na_2O	0.2	1.7	0.5	0.2
K2O	0.3	2.9	8.3	2
SO_3	2.7	1.5	0.3	0.5
LOI	0.9	0.2	10.1	11.2
$SiO_2+Al_2O_3 + Fe_2O_3$	-	75.2	65.7	76.8

4.2. Water Requirement in Concrete Mixtures

The water-to-binder (W/B) ratios are shown in Table 4. The W/B ratio of OPC concrete was 0.71. The use of OFA could reduce the W/B ratio in the concrete mixture and the W/B ratio was much lower than OPC concrete as the increase in replacement ratios. This result was affected by the spherical particles of OFA. The W/B ratios of GPOA and GRBA concretes were higher than that OPC concrete and tended to increase with the higher replacement ratios. Because the particles of GPOA and GRBA were angular and irregular with some porous particles, they needed more water to lubricate for maintaining the same workability than OPC concrete. It was noted that the W/B ratios of GRBA concrete were larger than that of GPOA concrete.

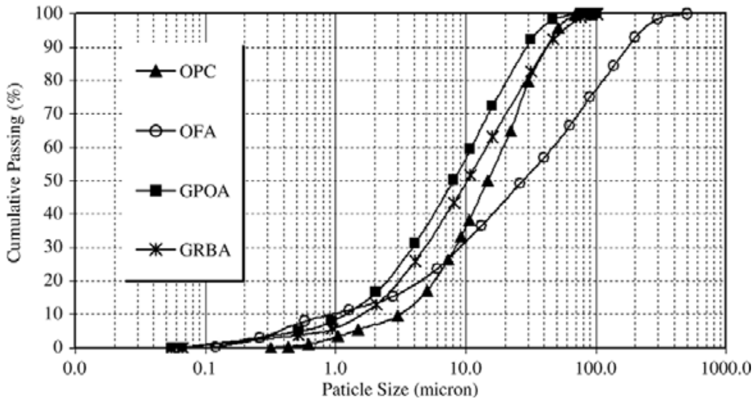

Figure 2. Particle size distribution of materials

4.3. Compressive Strength

At the later age, their strengths slightly increased, therefore, 90-day compressive strengths of these concretes were 29.4, 23.7 and 22.3 MPa or 104%, 84% and 79% of OPC concrete, respectively. It was observed that the compressive strength of GPOA20 concrete at 90 days was slightly higher than that of OPC concrete, although the W/B ratio of GPOA20 concrete was higher. This is due to the filler effects and the pozzolanic reaction of the high fineness of GPOA. Otherwise, the increase in replacement ratio of GPOA to 40% and 55% decreased the strength of concrete. However, the normalized compressive strength of all GPOA concretes increased with the ages. This suggests that the contribution of compressive strength was due to the pozzolanic reaction of GPOA with calcium hydroxide released from hydration of cement.

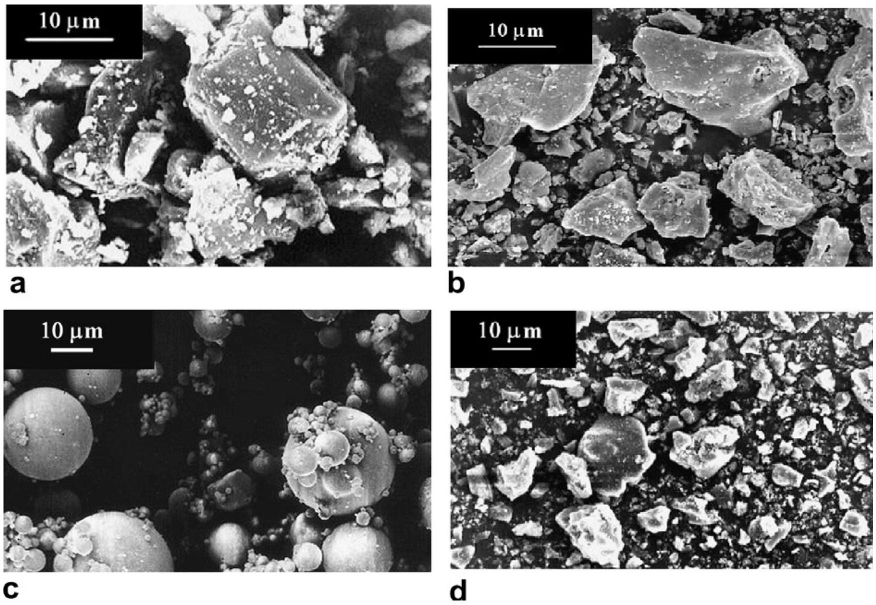

Figure 3. Scanning electron microscopy (SEM) of materials: (a) Portland cement type I (OPC); (b) original fly ash (OFA); (c) ground palm oil fuel ash (GPOA); and (d) ground rice husk–bark ash (GRBA)

From the results, it revealed that the incorporation of 20% of these pozzolans did not adversely affect the strength of concrete. An increase in the replacement ratios to 40% and 55% of binder, however, decreased the strength of concrete. For the same replacement ratio, the strengths of GPOA and GRBA concretes were slightly higher than those of OFA concretes, although their W/B ratios were higher than the OFA concretes. This suggested that the strengths of GPOA and GRBA concretes were affected by the finer particles of GPOA and GRBA as compared to OFA particles. Thus the faster pozzolanic reaction of GPOA and GRBA occurred and the filler effect made the concrete denser. In addition, the strengths of GBRA concretes were slightly higher than the strengths of GPOA concretes, although they needed more water in the concrete mixtures. This indicated that GRBA was more reactive than GPOA. This is due to the rice husk–bark ash contains a large amount of SiO2 (74.8%). It is known that the proper burnt and ground rice husk ash (has the content of SiO2 more than 80%) develops the compressive strength of concrete at the early age [9, 10]. Although, the burning temperature of GRBA was quite high (800–900 _C) and some part of the silica might become crystalline, it had been found that rice husk ash with this high temperature burning could still be successfully used as a good supplementary cementitious material [10, 11].

Table 5: Compressive strength and permeability of concrete

Mixed	W/B	Compressive strength (MPa)-Normalized		Permeability · 10_12, k (m/s) – k/kcontrol	
		28 days	90 days	28 days	90 days
OPC	0.71	26.1 – 100	28.2 – 100	2.89 – 1.00	2.05 – 1.00
OFA20	0.7	26.3 – 101	28.7 – 102	2.22 – 0.77	0.60 – 0.29
OFA40	0.65	20.9 – 80	24.4 – 87	4.67 – 1.62	2.01 – 0.98
GPOA20	0.73	23.9 – 92	29.4 – 104	0.59 – 0.20	0.25 – 0.12
GPOA40	0.74	20.7 – 79	23.7 – 84	0.41 – 0.14	0.26 – 0.13
GPOA55	0.75	18.1 – 69	22.3 – 79	3.30 – 1.14	2.38 – 1.16
GRBA20	0.71	27.5 – 105	29.3 – 104	0.90 – 0.31	0.42 – 0.21
GRBA40	0.76	22.7 – 87	25.6 – 91	1.74 – 0.60	1.33 – 0.65
GRBA55	0.8	20.0 – 77	24.1 – 85	5.48 – 1.90	4.02 – 1.96

Table 6: Mix proportions of concrete

Mixtures	Cement (kg)	OFA (kg	GPOA (kg)	GRBA (kg)	Fine aggregate (kg	Coarse aggregate (kg	Water (kg)	Slump (mm)
OPC	300	-	-	-	915	1080	213	75
OFA20	240	60	-	-	904	1068	215	65
OFA40	180	120	-	-	893	1057	195	60
GPOA20	240	-	60	-	907	1072	220	65
GPOA40	180	-	120	-	900	1064	222	70
GPOA55	135	-	155	-	894	1059	225	90
GRBA20	240	-	-	60	903	1068	214	80
GRBA40	180	-	-	120	891	1055	229	60
GRBA55	135	-	-	155	883	1046	240	70

4.4. Water Permeability of Concretes

The water permeability of concrete and the ratio of permeability are given in Table 6. The ratio of permeability is defined as the permeability of concrete containing pozzolanic materials divided by the permeability of OPC concrete at the same age of testing. At 90 days, the permeability of GPOA concretes decreased as compared to that of 28- day. It is interesting to note that the result showed that GPOA20 and GPOA40 concretes gave the lower perme- ability than the OPC concrete, even though the W/B ratios of the two concretes were higher than the OPC concrete. The permeability of GPOA55 rapidly increased and was higher than the OPC concrete. This may result from the low cement content and the high W/B ratio of GPOA55 concrete [12].

Figures 4 and 5 show the relationship between the permeability of all concretes and the cement replacement levels at 28 and 90 days, respectively. At 28 days, most of concretes had lower permeability than that of OPC concrete, except OFA40 and

GRBA55 concretes and the lowest permeability was observed in GPOA40 concrete. Moreover, the permeabilities of GPOA concretes tended to decrease when the cement replacement ratio increased up to 40%. On the contrary, the permeabilities of OFA and GRBA concretes increased as the cement replacement was more than 20%. At 90 days, the permeabilities of all concretes reduced and were lower than the values at 28 days. The ratios of permeability also had the similar result, except GRBA55 concrete. This suggested that the development of permeation

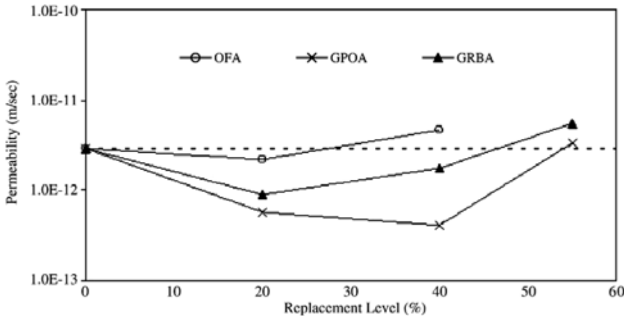

Figure 4. Relationship between the permeability of concretes and the cement replacement ratios at 28 days

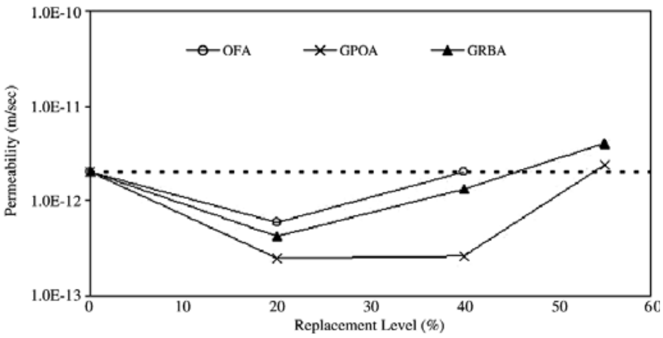

Figure 5. Relationship between the permeability of concretes and the cement replacement ratios at 90 days

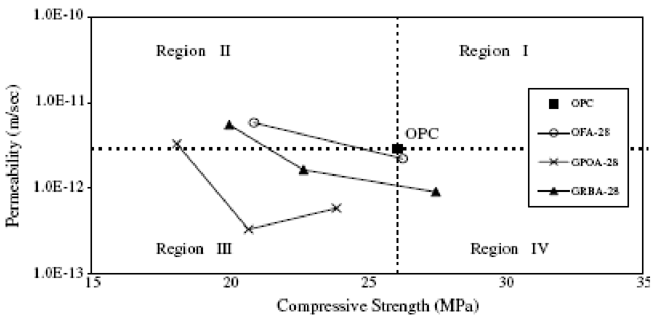

Figure 6. Relationship between water permeability and compressive strength of concretes at 28 days

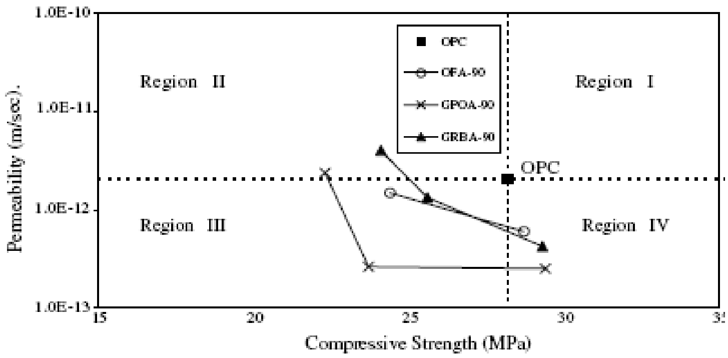

Figure 7. Relationship between water permeability and compressive strength of concretes at 90 days

4.5. Durability Performance

The long-term durability of a structure is highly affected by the permeability of concrete and, therefore, the water permeability can be used as an indicator of the durability of OPS concrete. The water permeability obtained from this investigation is illustrated in Figure 8.

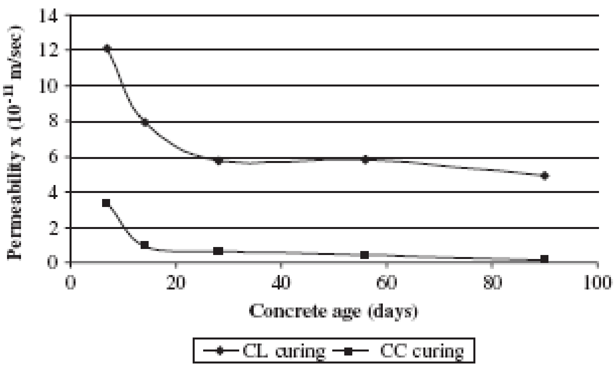

Figure 8. Water permeability of OPS concrete

From the figure, it is observed that the OPS concrete becomes less permeable with time and also it is greatly affected by the curing regime. At the age of 28 days, when cured under CC condition, the water permeability was about 9 times lower compared to that cured under CL condition. This shows when sufficient amount of water is present, the hydration of cement can continue. Consequently, the total porosity of the concrete is reduced as the probability of pores being either blocked or narrowed down by continued formation of hydration products are increased

4.6. Relationship Between Compressive Strength And Water Permeability of Concrete

The relationships between the permeability and the compressive strength of concretes at 28 and 90 days are presented in Figures. 6 and 7, respectively. The permeability of concrete tended to decrease with the increasing in the compressive strength. The figures are divided into four regions in Figures. 6 and 7. Region I represents concretes which have both compressive strength and permeability higher than OPC concrete. Region II indicates concretes which have lower compressive strength but higher permeability as compared to OPC concrete. Region III, which are lower in both of compressive strength and permeability than OPC concrete. Region IV are the preferable concretes, which are more lower permeability and also have higher compressive strength than OPC concrete.

5. CONCLUSIONS

It can be said the following conclusions are understood:
The permeability of GPOA and GRBA concretes depends on the cement replacement ratios, and age of concretes. In general, the permeability of concrete reduces with the increasing in the compressive strength and age of concrete.
The optimum cement replacement by GPOA, GRBA and OFA in this experiment is 20%. The higher replacement than this ratio results in the reduction of compressive strength and tends to give higher permeability of concrete.
Although GPOA and GRBA increased the amount of water in concrete mixture, the compressive strength of concretes containing 20% of these materials as cement replacement were higher than OPC concrete. With 40% of cement replacement, the compressive strength of GPOA and GRBA concretes were more than 84% of OPC concrete at 90 days.
Both GPOA and GRBA are suitable as pozzolanic materials in concrete. This shows a good promise to utilize these waste materials GRBA produces higher compressive strength than GPOA at all cement replacement levels, although lower of permeability of concrete was obtained with GPOA.

REFERENCES

1. Tay, J., *Ash from Oil-Palm Waste as a Concrete Material.* Journal of Materials in Civil Engineering, 1990. **2**(2): p. 94-105.
2. Awal, A. and M.W. Hussin, The Effectiveness of Palm Oil Fuel Ash in Preventing Expansion Due to Alkali-silica Reaction. Cement and Concrete Composites, 1997. **19**(4): p. 367-372.
3. Sata, V., C. Jaturapitakkul, and K. Kiattikomol, *Utilization of Palm Oil Fuel Ash in High-Strength Concrete.* Journal of Materials in Civil Engineering, 2004. **16**: p. 623.
4. Makaratat, N., et al. Utilization of rice husk–bark ash as a cement replacement. 2004.
5. Jaturapitakkul, C., S. Sukantapree, and J. Wongpha. A development of rice husk–bark ash in concrete. in Proceedings of the eighth national convention on civil engineering. 2002. Thailand.
6. Astm, C., 618 Standard Specification for Coal Fly Ash and Raw or Calcined Natural Pozzolan for use as a Mineral Admixture in Portland Cement Concrete. American Society for Testing of Materials, Philadelphia, USA.
7. Khatri, R.P. and V. Sirivivatnanon, *Methods for the Determination of Water*

Permeability of Concrete. ACI Materials Journal, 1997. **94**(3).
8. Chan, W.W.J. and C.M.L. Wu, *Durability of concrete with high cement replacement.* Cement and Concrete Research, 2000. **30**(6): p. 865-879.
9. Nehdi, M., J. Duquette, and A. El Damatty, *Performance of rice husk ash produced using a new technology as a mineral admixture in concrete.* Cement and Concrete Research, 2003. **33**(8): p. 1203-1210.
10. Ismail, M.S. and A.M. Waliuddin, *Effect of rice husk ash on high strength concrete.* Construction and Building Materials, 1996. **10**(7): p. 521-526.
11. Jauberthie, R., et al., *Origin of the pozzolanic effect of rice husks.* Construction and Building Materials, 2000. **14**(8): p. 419-423.
12. Li, Z. and C.K. Chau, *New Water Permeability Test Scheme for Concrete.* ACI Materials Journal, 2000. **97**(1).

CD07-011

HIGH PERFORMANCE CONCRETE FOR REPAIR OF SEWER NETWORK

T. Parhizkar, A.M. Raiss ghasemi, A.R. Pourkhorshidi
Building and Housing Research Center

ABSTRACT
High performance concrete often consists of ternary mixes of silica fume, fly ash or other pozzolans, and Portland cement. However, the specification of the proportions of these components remains uncertain [1-2]. High performance concrete have found their place in construction and compete with other materials for certain features like high strength, long term durability in severe conditions. In fact, high performance concrete has been designed in order to improve durability and provides easy handling, placement and compaction [3-4].
In this research, a high performance concrete with unique specifications has been studied. One of the most important properties of this type of concrete is its low permeability against different aggressive agents, and reduction of cement content in comparison with other high performance concretes.

Keywords: high performance concrete, fly ash, silica fume, permeability

1. INTRODUCTION
Fly ash and silica fume is a by-product. When used in concrete manufacturing, it is truly a "green" building material because it replaces a portion of the Portland cement, and the resulting emissions associated with its production. Fly ash and silica fume have the consistency of fine powder. Due to the shape, size and chemical composition, it imparts a number of benefits to concrete such as reduced water demand, improved durability and increased strength [1-3]. Use of fly ash and silica fume leads to improved workability- hence ease of handling, placing (pumping), and compacting concrete, reduction in bleeding and improvement in cohesiveness of concrete- hence smooth form finished concrete without honey-combing or segregation, reduction in heat of hydration- hence no threat of thermal cracks which makes it ideal for foundations and large sections. It also comes in handy in designing higher grades of concrete, improved resistance to Chloride attack. Chloride attacks lead to corrosion of reinforcing steel and subsequent distress of concrete [5-6].
Considering the optimized specifications of high performance concrete, it is suitable for repair of concrete, in for example, sewer network.
Design of high performance concrete, involves different factors. The most important factors included water-cement ratio, increase in the amount of cement, using mineral and chemical additives and grading curve of particle size for improvement of mixture density [7-9].

2. EXPERIMNTAL PROGRAM

2.1. Materials

Aggregate: Crushed gravel and sand were used as coarse and fine aggregates, respectively. The properties of aggregates are shown in Table 1. Curves of grading are given in Figures. 1 and 2.

Table 1. Aggregate properties

	Specific Gravity	Absorption (%)	Fineness Modulus
Sand	2.53	2.6	2.7
Gravel	2.56	1.46	6.5

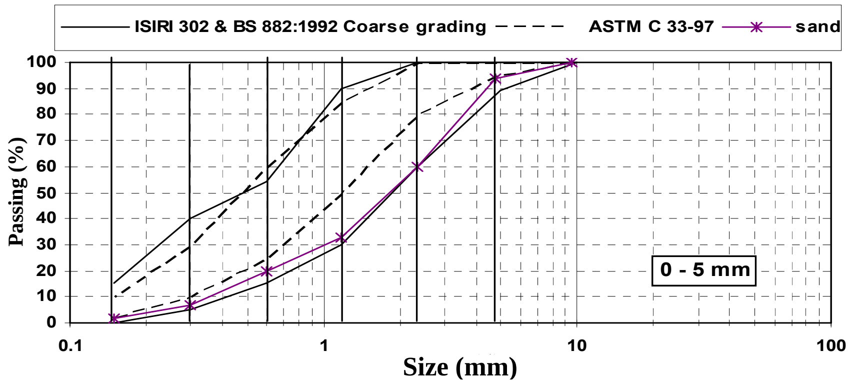

Figure 1. Fine-aggregate grading curve for SN and FSN mixtures

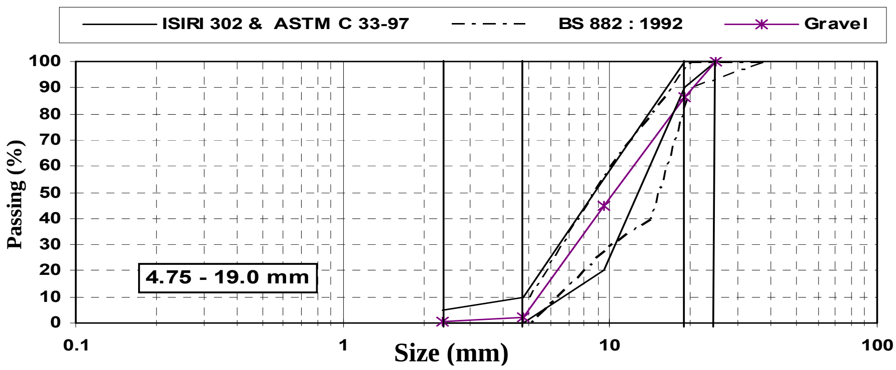

Figure 2. Coarse-aggregate grading curve for SN and FSN mixtures

Cement: ASTM type II Portland cement was used in this investigation. The composition of cement is shown in Table 2.

Fly ash: Fly ash was prepared in Germany. The composition of Fly ash is shown in Table 2.

Silica fume: A locally produced silica fume (in accordance with ASTM C1240) was used. The composition of Silica fume is shown in Table 2.

Grading of binding material is determined by Particle Size Analyzer method and the relative distribution curve is given in Figure 3.
Superplasticizer-The superplasticizer was conventional carbocilate-based. Chemical properties of the superplasticizer are given in Table 3.

Table 2: Chemical compositions of cement, fly ash and silica fume

	Type II	Fly ash	Silica fume
SiO_2	20.96	48	91.10
Al_2O_3	4.2	26	1.55
Fe_2O_3	4.6	9	2.00
MgO	3.4	1.5	0.6
CaO	61.88	2.5	2.24
SO_3	1.79	1	0.45
Na_2O+0.658 K_2O	1.47	2.8	0.80
C_3S	52.74	-	-
C_2S	20.31	-	-
C_3A	7.35	-	-

Table 3: Chemical and physical properties of superplasticizer

Apparent condition	Bright yellow liquid
PH	6.5
Density	1.06 Kg/lit in 20 °C
Quantity of chlorine	Less than 0.1%
Quantity of alkaline	Usually less than 1/5 gr equal to Na_2O per liter

2.2. Grading of Binding Material

As about 80% of cement particles have a diameter in the range of 10 to 100 micrometer, 50% of the particles of Fly ash have the particle size between 5 to 20 micrometer and 60% of silica fume has a size of less than 1 micrometer. This is with regard to the chemical properties of these materials while considering their mechanical and physical properties, as well as their required durability and the particle size distribution of cement. Fly ash and silica fume and also 70% cement, 20% fly ash and 10% silica fume with the combination curve is given in Figures 3 and 4.

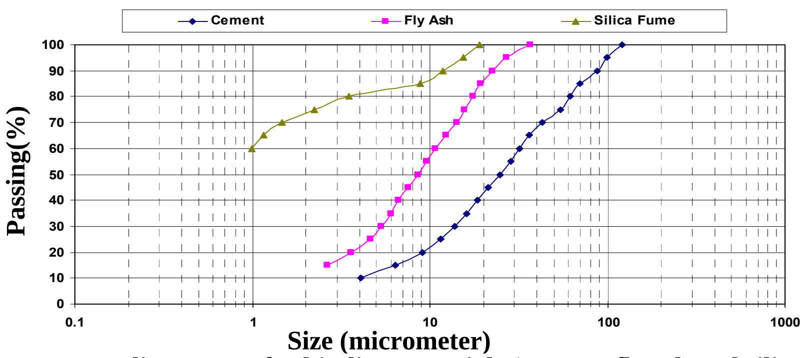

Figure 3. Grading curves for binding materials (cement, fly ash and silica fume)

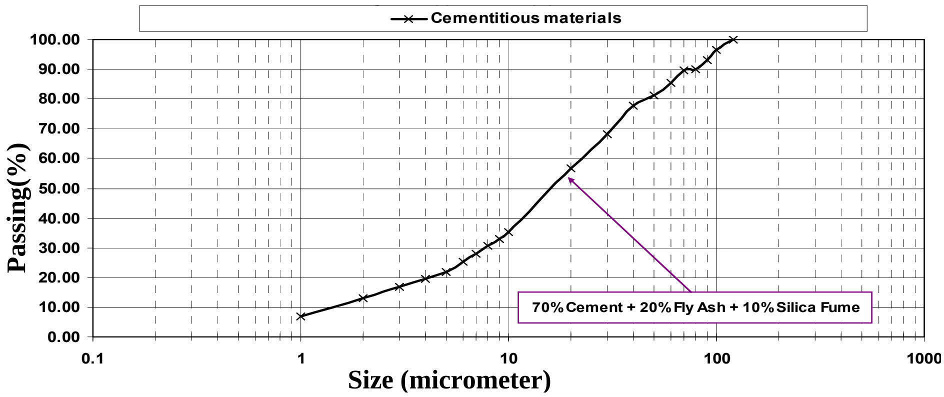

Figure 4. Grading curve for total binding materials

2.3. Concrete Mixtures

Mixture proportions of concrete are summarized in Table 4. Water-cementitious materials ratios(W/Cm) were 0.45. After mixing the concrete, casting performed in the moulds was based on En 12390-2:2000. After one day, under standard conditions, specimens were removed from the moulds and transferred to the standard curing condition until the time of testing.

Table 4: Mixture proportions

Mixture	Water (kg/m^3)	Cement (kg/m^3)	Fly ash (kg/m^3)	Silica fume (kg/m^3)	Fine (0-0.25mm) (kg/m^3)	Coarse (0.25-16mm) (kg/m^3)
SN	170	372	-	30	56	1833
FSN	124	220	63	30	60	1955

2.4. Tests on Fresh Concrete and Results

- Density

Density of fresh concrete was obtained based upon En 12350-6:1999. Results are shown in Table 5.

- Workability

The slump of fresh concrete, was determined based on EN 12350-2:1999 method. Results are shown in Table 5.

- Fluidity in Flow table test

The fluidity of fresh concrete was measured based on EN 12350-5:1997 method. Results are shown in Table 5.

- Air Content

The test performed for measuring air content in concrete was based on per EN 12350-5:1997 method. Results are shown in Table 5.

Table 5: Results of fresh concrete test

Mixture	slump (cm)	Flow consistency (cm)	Density (kg/m3)	Air content (%)
SN	4	37.5	2391	3.8
FSN	-	-	2466	2.0

2.5. Tests on Hardened Concrete and Results

Tests for determination of mechanical properties and durability of concrete, performed on hardened concrete include: Determination of compressive strength, rapid chloride ion permeability, depth of water penetration under pressure, length change of concrete prisms in sulphate solution. To perform the aforesaid test, samples of cubic, cylindrical and prism shapes were prepared upon EN 12390-1:2000. Dimensions and shapes of moulds for the purpose of each test is given in Table 6.

Table 6. Dimensions and shapes of moulds to be used for hardened concrete tests

Type of test	Mould shape	Mould dimensions (mm)
Compressive strength	Cube	100
Depth of water penetration	Cube	150
Rapid chloride permeability test	Cylindrical	100 x200
Length change in sulfate solution	Prism	285x75x75

3. RESULTS

3.1. Compressive strength

Samples (three samples per age) were tested in the age of 7, 28 and 90 days. Compressive strength of samples was measured based on DIN EN 12390-3:2000 and the results are given in Figure 5.

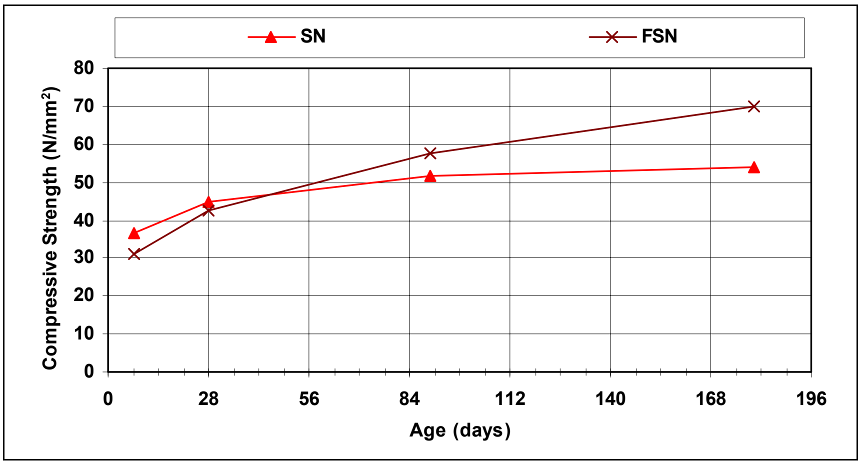

Figure 5. Results of compressive strength test

3.2. Rapid Chloride Permeability

This test is performed on ASTM C 1202-97 method in the age of 28 and 90 days. Test results are given in Figure. 6.

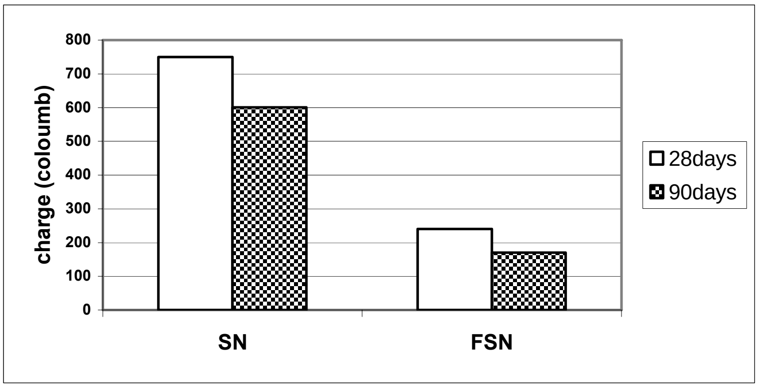

Figure 6. Results of rapid chloride permeability test

3.3. Depth of Water Penetration Test

This test was performed based on EN 12390-9:2000 method at the age of 28 and 90 days and the results are given in Figure. 7.

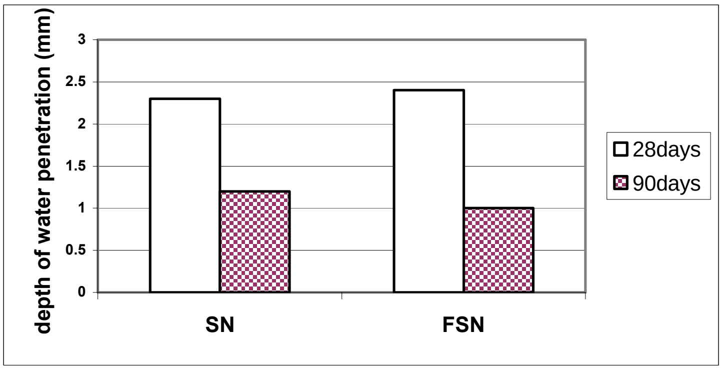

Figure 7. Results of depth of water penetration test

3.5. Length Change of Concrete Prism in Sulphate Solution

To study performance of concrete mixtures in sulphate, the 5% sodium sulphate solution was used. For this purpose, concrete prisms measuring 75x75x285 mm after 28 days of standard curing were placed in sulphate solution. For adjustment of pH and keeping this parameter constant during the process of test, diluted sulphuric acid was used. Meantime and at the early ages, sulphate solution was changed regularly.

Elongation and weight loss of samples at certain intervals and up to 6 months was determined. Results are given in Figure 8.

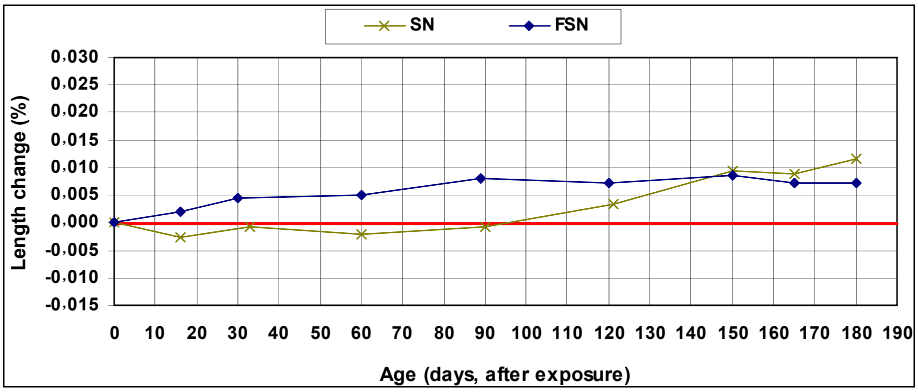

Figure 8. Length change in sulphate

4. CONCLUSIONS

According to the experimental work:

1. The experimental observation showed the effectiveness of Fly Ash on the development of concrete compressive strength and reduction of the chloride permeability.
2. At the early age, the Fly Ash has fewer effects on the properties of concrete, but after 28 days, it could result in a better performance in contrast to the concrete without Fly Ash .

REFERENCES

1. Murat Pala, Erdoğan Özbay, Ahmet Öztaş and M. Ishak Yuce, Appraisal of long-term effects of fly ash and silica fume on compressive strength of concrete by neural networks, Construction and Building Materials, Volume 21, Issue 2, February 2007, Pages 384-394.
2. M. D. A. Thomas, M. H. Shehata, S. G. Shashiprakash, D. S. Hopkins and K. Cail, Use of ternary cementitious systems containing silica fume and fly ash in concrete, Cement and Concrete Research, Volume 29, Issue 8, August 1999, Pages1207-1214.
3. P. Plante and A. Bilodeau, 1989. Rapid Chloride Ion Permeability Test: Data on Concretes Incorporating Supplementary Cementing Materials, ACI SP-114, Vol. 1, American Concrete Institute, Farmington Hills, Mich., pp. 625-644.
4. V.M. Malhotra, G.G. Carette, and V. Sivasundaram, 1992. Role of Silica Fume in Concrete: A Review, Proceedings, International Symposium on Advances in Concrete Technology (CANMET), Ottawa, Ontario, Canada, pp. 915-990.
5. K. Popovics, V. Ukrainic, and A. Djurekovic, 1984. Improvement of mortar and Concrete Durability by the Use of Condensed Silica Fume, in Durability of Building material, Vol.2, Elsevier Science Publishers, Amsterdam, pp. 171-186.
6. A.H. Nilson, 1985. Design Implications of Current research on High

Strength, Concrete, ACI SP-87-7, American Concrete Institute, Farmington Hills, Mich., pp. 85-118.

7. O.E. Gjorv, T. Baerland, and H. R. Ronning, 1993. Abrasion Resistance of High Strength Concrete Pavements, ACI Compilation 17, American Concrete Institute, Farmington hills, Mich., pp. 81-84.
8. L. Lam, Y. L. Wong and C. S. Poon, Effect of Fly Ash and Silica Fume on Compressive and Fracture Behaviors of Concrete, Cement and Concrete Research, Volume 28, Issue 2, February 1998, Pages 271-283.
9. H. Temiz and A. Y. Karakeçi, An investigation on microstructure of cement paste fume, Cement and Concrete Research, Volume 32, Issue 7, July 2002, Pages, 1131-1132.

CD07-012

بررسی اثر منحنی دانه بندی‌های روش ملی طرح مخلوط بتن ایران در رفتار بتن تازه خودتراکم

پرویز قدوسی[1]، رامین دولتیار[2]
۱. عضو هیات علمی‌دانشگاه علم و صنعت ایران
۲. دانشجوی کارشناسی ارشد دانشگاه علم و صنعت ایران

چکیده

پژوهشگران مختلف مدلهایی برای دستیابی به منحنی دانه بندی با کمترین تخلخل و در نتیجه کاهش حجم خمیر سیمان لازم، برای تهیه مخلوط ارائه داده اند.در این مقاله منحنی دانه بندی‌های روش ملی طرح مخلوط بتن ایران با مدلهای ارائه شده توسط محققین دیگر مقایسه شده است. همچنین با استفاده از هر یک از این منحنی دانه بندی‌ها مخلوطهایی ساخته شده است و خصوصیات بتن تازه این مخلوطها مورد بررسی قرار گرفته است. در این مخلوطها این امکان ایجاد شده است که فقط از فیلر برای اصلاح لزجت مخلوط استفاده شود و نیازی به استفاده از VMA نبوده است.در نهایت نتایج آزمایشها نشان داده است که منحنی دانه بندی‌های بین حد وسط و حد بالای منحنی دانه بندیهای روش ملی طرح مخلوط بتن ایران (محدوده ریزدانه)برای ساخت مخلوطهای بتنی خود تراکم مناسب بوده اند و هرچه منحنی دانه بندی مورداستفاده به سمت حدبالا(ریزدانگی) متمایل بوده است، خصوصیات بتن تازه بهتر شده است. دراین تحقیق برای هر یک از منحنی دانه بندی‌های روش ملی طرح مخلوط بتن ایران بازه ای برای حجم خمیرسیمان جهت تهیه مخلوط بتن خود تراکم نیز مشخص گردیده است که در صورت استفاده از فیلر به تنهایی برای اصلاح لزجت، تنها حجم خمیر سیمان در این بازه منجر به تهیه مخلوط بتن خود تراکم می‌شود.

کلیدواژه‌ها: بتن خودتراکم،منحنی دانه بندی،فیلر،ریزدانه،حجم خمیر سیمان.

۱- مقدمه

دانه‌بندی سنگدانه‌ها عامل تعیین کننده ای در مقدار کارآیی مخلوط بتن می‌باشد.کار آیی به نوبه خود بر مقدار آب وسیمان لازم در مخلوط اثر می‌گذارد وجدا شدگی و آب انداختگی بتن را کنترل می‌کند و بر نحوه جایدهی و پرداخت سطح بتن اثر دارد.این عوامل معرف خصوصیات مهم بتن تازه می‌باشند. از طرفی بر خواص بتن سخت شده شامل مقاومت، جمع شدگی دوام و پایداری تاثیر گذار است. بنابر این دانه بندی سنگدانه در تعیین نسبت مواد متشکله مخلوط بتن اهمیت بسیار زیادی دارد.

دانه بندی سنگدانه‌ها به گونه ای باید باشد تا ازبروز پدیده انسداد در هنگام عبور جلوگیری کند، به عبارت دیگر حجم سنگدانه درشت و همچنین حداکثر اندازه سنگدانه را تا حد امکان کاهش داده و برای ایجاد یکپارچگی بین

سنگدانه‌ها از ریز پرکننده‌های مناسب استفاده نمود.در این صورت احتمال انسداد توسط درشت دانه‌ها کاهش پیدا می‌کند و بتن می‌تواند به راحتی تحت اثر وزن خود جاری شده و از بین موانع و آرماتورها عبور کند.
تاثیرات دانه بندی روی خواص بتن تازه ناشی از تراکم سنگدانه‌ها می‌باشد، که این تراکم بستگی به منحنی دانه بندی سنگدانه‌ها دارد.هر چه تراکم سنگدانه‌ها بیشتر باشد و تخلخل ما بین آنها کمتر شود و در نتیجه خمیر سیمان بیشتری برای پوشانیدن دور سنگدانه‌ها و آسوده تر غلتیدن آنها روی یکدیگر، در دسترس خواهد بود. Andreasen&Anderson [۱]با توجه به این مطلب رابطه ای برای به دست آوردن درصد عبوری از هر الک و در نهایت بدست آوردن منحنی دانه‌بندی مناسب ارئه دادند که به صورت زیر می‌باشد:

$$P(D)=(D/Dmax)^q \qquad (۱)$$

که در آن:
P(D)= درصد عبوری از الک با اندازه چشمه D
Dmax= حداکثر اندازه سنگدانه
$0<q<1$
عبارت q، پارامتر توان در معادله (۱) و(۲) می‌باشد که این پارامتر نقش بسیار مهمی‌در تعیین شکل منحنی دانه بندی سنگدانه‌ها دارد که با کاهش آن منحنی دانه بندی سنگدانه‌ها ریز دانه تر، وبا افزایش آن منحنی دانه بندی درشت دانه تر می‌شود.
Andreasen&Anderson [۱]یافتند که اگر q=0.37 باشد تراکم بهینه سنگدانه‌ها به دست می‌آید.زمانیکه q=0.5 باشد منحنی دانه بندی Fuller به دست می‌آید.Funk&Dinger[۲]این مدل را اصلاح نمودند و مدل اصلاح شده را به صورت زیر ارائه دادند:

$$P(D)=(D^q-Dmin^q)/(Dmax^q - Dmin^q) \qquad (۲)$$

که در آن:
Dmin = حداقل اندازه سنگدانه
Browser& Redix[۳]نشان دادند که اگر q=0.25 باشد، منحنی دانه بندی متناظر با این مقدار برای تهیه مخلوط خود تراکم مناسب خواهد بود.در این تحقیق، هدف از مطالعات منحنی‌های دانه بندی و مدلهای مربوطه، به دست آوردن منحنی دانه بندی با کمترین تخلخل و در نتیجه کمترین حجم خمیر سیمان لازم می‌باشد. درگذشته استراتژیهای طراحی بر این اساس بوده اند که منحنی دانه بندی مورد استفاده، نزدیک به یک منحنی دانه بندی ایده آل باشد، که بیشترین تراکم سنگدانه‌ها را منجر شود. دستیابی به منحنی دانه بندی مذکور از طریق سعی و خطا انجام می‌گردید. Larrard [۴]پارامترهایی را ارائه داده است که با استفاده از این پارامترها می‌توان به منحنی دانه بندی ایده آل برای تهیه مخلوط خود تراکم دست یافت.یکی از این پارامترها، پتانسیل جاشدگی می‌باشد که در این تحقیق مورد استفاده قرار گرفته است.
در این تحقیق منحنی دانه بندی‌های روش ملی طرح مخلوط بتن ایران با مدل اصلاح شده Andreasen&Anderson [۱]مقایسه شده است. همچنین پتانسیل جداشدگی این منحنی‌ها مورد مطالعه قرار گرفته و با استفاده از نتایج آزمایشهای انجام شده روی مخلوطهای ساخته شده با استفاده از این منحنی‌ها،

پتانسیل جدا شدگی مورد قبول برای تهیه مخلوط بتن خود تراکم ارائه داده شده است.در نهایت برای هر یک از منحنی دانه بندی‌های مذکور، جهت تهیه مخلوط خود تراکم، یک بازه حجم خمیر سیمان تعریف شده است و مقدار بهینه حجم خمیر سیمان، در این بازه را که منجر به بهترین خواص بتن تازه مخلوط، در مقایسه با سایر مقادیر این بازه شده است، نیز برای هر منحنی دانه بندی مشخص شده است.

۲- برنامه آزمایشگاهی

۲-۱ مصالح مصرفی

سیمان

سیمان مصرفی، سیمان پرتلند معمولی مطابق با ASTM نوع یک با وزن مخصوص ۳,۱۵ می‌باشد.

شن

شن مصرفی با وزن مخصوص ۲,۵۳ و جذب آب۰,۰۱۵ می‌باشد. ماکزیمم اندازه سنگدانه‌های شن مصرفی با توجه به منحنی دانه بندی انتخابی ۱۰ یا ۲۰ میلیمتر می‌باشد.

ماسه

ماسه مصرفی ماسه طبیعی با وزن مخصوص ۲,۵ وجذب آب ۰,۰۴۱ می‌باشد.

منحنی دانه بندی

منحنی دانه بندی‌های به کار برده شده برای شن وماسه مطابق با شکل ۱ متشکل از منحنی‌های A,B,C با حداکثر اندازه ۹,۵و۱۹ میلیمتر می‌باشد.

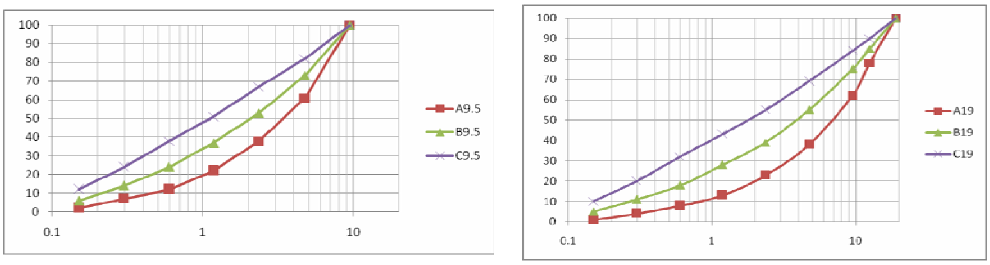

(ب) منحنی دانه بندی سنگدانه با حداکثر اندازه سنگدانه ۹,۵ میلیمتر

(الف) منحنی دانه بندی سنگدانه با حداکثر اندازه سنگدانه ۱۹ میلیمتر

شکل ۱- منحنی دانه بندی‌های روش ملی طرح مخلوط ایران با حداکثر اندازه۹,۵و۱۹میلیمتر

درصد عبوری منحنی دانه بندی‌های سنگدانه روش ملی طرح مخلوط بتن ایران که در شکل ۱ نشان داده شده است، به صورت درصد عبوری حجمی‌می‌باشد. زمانی که جرم حجمی‌سنگدانه‌ها یکسان در نظر گرفته شود درصد عبوری حجمی‌با وزنی تفاوتی ندارد، که این موضوع با مقایسه جدول ۱- ب با شکل ۱ مشخص می‌گردد.اما در این تحقیق به دلیل استفاده از فیلر، مطابق با منحنی دانه بندی سنگدانه مورد استفاده، و متفاوت بودن جرم حجمی‌فیلر با سنگدانه‌ها، درصد عبوری حجمی‌را نمی‌توان برابر با درصد عبوری وزنی دانست.برای بررسی این مطلب ابتدا با توجه به منحنی دانه بندی مورد استفاده، درصد حجمی‌عبوری هر یک از اندازه سنگدانه‌ها و فیلر

مشخص شده و به در صد وزنی عبوری تبدیل گردیده و در جدول ۱– الف نشان داده شده است. با توجه به جدول ۱ بیشترین اختلاف درصد وزنی عبوری با درصد حجمی‌عبوری منحنی‌های دانه بندی همانطور که انتظار می‌رفت، مربوط به منحنی دانه بندی C۹,۵بوده است و مقداراین اختلاف برابر با ۰,۶درصد بوده است.

جدول ۱: الف- درصد وزنی عبوری منحنی‌های دانه بندی روش ملی طرح مخلوط بتن ایران با پودر سنگ

حداکثر اندازه سنگدانه	منحنی دانه بندی	درصد وزنی عبوری								
	اندازه الک (میلیمتر)	۰,۱۵	۰,۳	۰,۶	۱,۱۸	۲,۳۶	۴,۷۵	۹,۵	۱۲,۵	۱۹
۱۹ میلیمتر	۱۹C	۱۰,۶	۲۱,۵	۳۲,۴۳	۴۳,۴	۵۶,۳	۷۰,۲	۸۳,۱	۹۲,۰۵	۱۰۰
	۱۹B	۵,۳	۱۱,۲۸	۱۸,۲۶	۲۸,۲	۳۹,۲	۵۵,۱	۷۵,۱	۸۹,۰۳	۱۰۰
	۱۹A	۲,۱۲	۴,۱۲	۸,۱۱	۱۳,۱	۲۳,۱	۳۸,۱	۶۲,۱	۷۹,۰۲	۱۰۰
۹,۵ میلیمتر	۹,۵C	۱۲,۶	۲۴,۵۷	۳۸,۴۷	۸۱,۴	۹۷,۳	۸۲,۱	۱۰۰		
	۹,۵B	۷,۴	۱۴,۳۸	۲۵,۳۳	۳۷,۳	۵۳,۲	۷۴,۱	۱۰۰		
	۹,۵A	۳,۱۸	۶,۱۸	۱۲,۱۶	۲۲,۲	۳۷,۱	۶۱,۱	۱۰۰		

جدول ۱: ب - درصد وزنی عبوری منحنی‌های دانه بندی روش ملی طرح مخلوط بتن ایران بدون پودر سنگ

حداکثر اندازه سنگدانه	منحنی دانه بندی	درصد وزنی عبوری								
	اندازه الک (میلیمتر)	۰,۱۵	۰,۳	۰,۶	۱,۱۸	۲,۳۶	۴,۷۵	۹,۵	۱۲,۵	۱۹
۱۹ میلیمتر	۱۹C	۱۰	۲۱	۳۲	۴۳	۵۶	۷۰	۸۳	۹۲	۱۰۰
	۱۹B	۵	۱۱	۱۸	۲۸	۳۹	۵۵	۷۵	۸۹	۱۰۰
	۱۹A	۲	۴	۸	۱۳	۲۳	۳۸	۶۲	۷۹	۱۰۰
۹,۵ میلیمتر	۹,۵C	۱۲	۲۴	۳۸	۸۱	۹۷	۸۲	۱۰۰		
	۹,۵B	۷	۱۴	۲۵	۳۷	۵۳	۷۴	۱۰۰		
	۹,۵A	۳	۶	۱۲	۲۲	۳۷	۶۱	۱۰۰		

فیلر

پودر سنگ آهک با وزن مخصوص ۲۶۶۰ به عنوان فیلر استفاده شده است.

فوق روان کننده

فوق روان کننده مورد استفاده بر پایه پلی کربوکسیلاتی و تولید کارخانجات داخل می‌باشد.

۲-۲ نسبتهای مخلوط

در این تحقیق با منحنی‌های B,C طبق شکل ۱ با حداکثر اندازه ۹,۵ و۱۹ که برگرفته از روش ملی طرح مخلـوط بتن ایران می‌باشد، مخلوطهای بتن خود تراکم ساخته شده است. تحقیقات آزمایشگاهی مقدماتی نشان داد که بـا منحنی Aامکان ساخت مخلوط خود تراکم وجود ندارد. در تمامی‌مخلوطهای ساخته شده نسبت آب به سیمان برابر با۰,۴۵ثابت نگهداشته شده و مقدار سیمان برای هر گروه منحنی دانه بندی تغییر داده شده اسـت. همچنـین لازم به ذکر است که در تمامی‌مخلوطهای مذکور به منظور تهیه سنگدانه‌های ریز تر از ۰,۱۵ میلیمتر یعنـی عبـوری از

الک ۰,۱۵ از پودر سنگ عبور داده شده از الک ۰,۱۵ استفاده شده است.
نسبتهای مخلوط‌های ساخته شده با منحنی دانه بندی‌های B,C با حداکثر اندازه سنگدانه ۹,۵و۱۹ میلیمتر در جدول ۲نشان داده شده است.در این تحقیق معرف ۱-C۹,۵ به مفهوم منحنی دانه بندی سنگدانه‌ها C با حداکثر اندازه سنگدانه ۹,۵ میلیمتر و خط تیره و عدد شماره مخلوط ساخته شده می‌باشد. برای سایر معرف مخلوطها نیز به همین صورت می‌باشد.

جدول ۲: نسبتهای مخلوط‌های ساخته شده با منحنی‌های B,C با حداکثر اندازه۹,۵ و۱۹ میلیمتر

معرف مخلوط	منحنی دانه بندی	سیمان (kg/m3)	پودر سنگ (kg/m3)	سنگدانه (kg/m3)	آب (kg/m3)	فوق روان‌کننده (lit/m3)	حجم خمیر (سیمان+آب)m3/1m3
۱-۹,۵C	۹,۵C	۳۵۰	۲۲۳,۸۸	۱۵۴۴,۲۴	۱۵۷,۵	۱,۷۵	۰,۲۶۸
۲-۹,۵C	۹,۵C	۴۰۰	۲۱۱,۶۳	۱۴۶۰,۶۴	۱۸۰	۱,۵	۰,۳۰۷
۳-۹,۵C	۹,۵C	۴۵۰	۱۹۹,۳۹	۱۳۷۲,۹۶	۲۰۲,۵	۱	۰,۳۴۵
۴-۹,۵C	۹,۵C	۵۰۰	۱۸۷,۱۳	۱۲۸۹,۸	۲۲۵	۰,۵	۰,۳۸۳
۵-۹,۵B	۹,۵B	۳۵۰	۱۳۰,۶	۱۶۳۰,۷۳	۱۵۷,۵	۱,۷۵	۰,۲۶۸
۶-۹,۵B	۹,۵B	۴۰۰	۱۲۳,۴۵	۱۵۴۲,۷۸	۱۸۰	۱,۲۵	۰,۳۰۷
۷-۹,۵B	۹,۵B	۴۵۰	۱۱۶,۳۱	۱۴۵۲,۳	۲۰۲,۵	۰,۷۵	۰,۳۴۵
۸-۹,۵B	۹,۵B	۵۰۰	۱۰۹,۱۶	۱۳۶۳,۰۸	۲۲۵	۰,۵	۰,۳۸۳
۹-۱۹C	۱۹C	۳۰۰	۱۹۶,۷۷	۱۶۶۴,۴۶	۱۳۵	۲,۲	۰,۲۳
۱۰-۱۹C	۱۹C	۳۵۰	۱۸۶,۵۷	۱۵۷۸,۱۳	۱۵۷,۵	۱,۷	۰,۲۶۸
۱۱-۱۹C	۱۹C	۴۰۰	۱۷۶,۳۶	۱۴۹۱,۷۹	۱۸۰	۱	۰,۳۰۷
۱۲-۱۹C	۱۹C	۴۵۰	۱۶۶,۱۵	۱۴۰۵,۴۷	۲۰۲,۵	۰,۵	۰,۳۴۵
۱۳-۱۹B	۱۹B	۳۱۱	۹۷,۲۵	۱۷۳۶,۷۷	۱۴۰	۱,۵	۰,۲۳۸
۱۴-۱۹B	۱۹B	۳۶۰	۹۲,۲۶	۱۶۴۷,۵۷	۱۶۲	۱	۰,۲۷۶
۱۵-۱۹B	۱۹B	۴۳۰	۸۵,۱۲	۱۵۱۹,۹۸	۱۹۳,۵	۰,۵	۰,۳۳
۱۶-۱۹B	۱۹B	۴۸۰	۸۰,۰۲	۱۴۲۸,۸۵	۲۱۶	۰,۲	۰,۳۶۸

۲-۳ شرح آزمایش‌ها

آزمایش جریان اسلامپ، قیفV، حلقه J، جعبه L و آزمایش مشاهده VSIمطابق با دستور العمل PCI [۵]انجام شده است.

۳- نتایج آزمایش‌ها و تفسیر

نتایج آزمایش‌های انجام شده روی مخلوط‌ها در جدول ۳ نشان داده شده است.

جدول ۳: نتایج آزمایشهای بتن تازه انجام شده روی مخلوطها

معرف مخلوط	منحنی دانه بندی	حجم خمیر سیمان (m3/1m3)	جریان اسلامپ(cm)	قیف(V(sec	حلقهJ (mm)	جعبه L	VSI*
1-9,5C	9,5C	۰,۲۶۸	۶۹	۳,۳۳	۱۲	۰,۷۵	۱,۵
2-9,5C	9,5C	۰,۳۰۷	۷۳	۳	۴	۱	۰
3-9,5C	9,5C	۰,۳۴۵	۷۱	۲,۴۱	۶	۰,۸۴	۰,۵
4-9,5C	9,5C	۰,۳۸۳	۶۷	۲,۲۵	۹	۰,۸	۱
5-9,5B	9,5B	۰,۲۶۸	۶۶	۵	۱۷	۰,۷۵	۲
6-9,5B	9,5B	۰,۳۰۷	۷۰	۴,۱	۹	۰,۸۵	۱
7-9,5B	9,5B	۰,۳۴۵	۷۴	۳,۸۴	۶	۰,۹۶	۰
8-9,5B	9,5B	۰,۳۸۳	۶۹	۳,۲	۸	۰,۸۹	۰,۵
9-19C	19C	۰,۲۳	۶۷	۵,۹	۱۱	۰,۸۱	۱
10-19C	19C	۰,۲۶۸	۷۵	۳	۳	۰,۸۹	۰
11-19C	19C	۰,۳	۷۲	۲,۵	۵	۰,۸۷	۰,۵
12-19C	19C	۰,۳۴۵	۶۰	۱,۸	۹	۰,۸	۱,۲۵
13-19B	19B	۰,۲۳۸	۵۸	۲۱,۵	۲۷	۰,۱۱	۲
14-19B	19B	۰,۲۷۶	۶۴	۱۱,۸۸	۱۵	۰,۶	۱,۵
15-19B	19B	۰,۳۳	۷۰	۳	۸	۰,۸۸	۰
16-19B	19B	۰,۳۶۸	۶۸	۲	۱۰	۰,۸۳	۰,۵

*** Visual StabilityIndex(VSI): در این تحقیق زمانی که (VSI) بین صفر تا یک بوده است مخلوط به عنوان مخلوط بتن خود تراکم پذیرفته شده است.**

منحنی دانه بندی‌های B,C با حداکثر اندازه سنگدانه ۹,۵ و۱۹ میلیمتر که در این تحقیق استفاده شده است که برگرفته از روش ملی طرح مخلوط بتن ایران می‌باشد.در صورتیکه در مدل اصلاح شده Andreasen&Anderson [۱] که در مقدمه توضیح داده شد Dmax=19 وDmin=0.075 و q=0.1 باشد، منحنی دانه بندی حاصل منطبق بر منحنی دانه بندی C با حداکثر اندازه ۱۹ میلیمتر خواهد بود.اگر در این مدل Dmax=19 وDmin=0.075 و q=0.35 باشد منحنی دانه بندی حاصل منطبق بر منحنی دانه بندی B با حداکثر اندازه سنگدانه ۱۹ میلیمتر خواهد بود.اگر مقدار Dmax در هردو حالت مذکور به ۹,۵ میلیمتر تغییر پیدا کند و سایر مقادیر همان بماند، منحنی دانه بندی‌های حاصل به ترتیب منطبق بر منحنی دانه بندی BوC با حداکثر اندازه سنگدانه ۹,۵ میلیمتر خواهد بود.

با توجه به نتایج آزمایشها برای هر یک از منحنی دانه بندی‌های B,Cبا حداکثر اندازه ۹,۵و۱۹ میلیمتر این امکان ایجاد شد که برای هر یک از این منحنی‌ها یک بازه حجم خمیر سیمان ارائه شود که در صورت قرار گرفتن حجم خمیر سیمان در این محدوده، مخلوط ساخته شده، مخلوط خودتراکم باشد.همچنین در هر بازه یک مقدار بهینه حجم خمیر سیمان وجود داشت که مخلوط ساخته شده با آن مقدار بهینه، خصوصیات بتن تازه

مطلوبتری نسبت به سایر مخلوطهای ساخته شده با مقادیر بازه از خود نشان داد.بازه‌های مذکور به همـراه مقـادیر بهینه برای منحنی دانه بندی‌های مورد بررسی در جدول ۴ ارائه داده شده است.

جدول ۴: بازه حجم خمیرسیمان لازم برای تهیه مخلوط خود تراکم برای منحنی دانه‌بندی‌های روش ملی طرح مخلوط بتن ایران

منحنی دانه بندی	بازه حجم خمیر سیمان	حجم خمیر سیمان بهینه
	(m3/1m3)	(m3/1m3)
۹,۵C	۰,۲۸-۰,۳۸۳	۰۳۰۷
۹,۵B	۰,۳۰۷-۰,۳۹	۰,۳۴۵
۱۹C	۰,۲۳-۰,۳۴	۰,۲۶۸
۱۹B	۰,۳-۰,۳۷	۰,۳۳

با مقایسه نتایج آزمایشهای انجام شده روی مخلوطهای ساخته شده با دو منحنی دانه بندی C,B با حداکثر انـدازه ۱۹ میلیمتر مشخص گردید که حجم خمیر سیمان بهینه لازم برای تهیه مخلوط خود تراکم با منحنی Cبا حداکثر اندازه ۱۹ میلیمتر کمتر از حجم خمیر سیمان بهینه لازم برای تهیه مخلوط خود تـراکم بـا منحنـی B بـا حـداکثر اندازه ۱۹ میلیمتر بوده است.ضمنا خصوصیات بتن تازه ساخته شده با منحنی C۱۹ مطلوبتر از مخلوط ساخته شـده با منحنی B۱۹ بوده است.در نتیجه کلیه منحنـی دانـه بنـدی‌هـای حاصـل از مـدل Andreasen&Anderson [۱]مابین منحنی B,C مناسب برای ساخت مخلوط خودتراکم می‌باشند.در حقیقت منحنی دانه بندی‌هـای متنـاظر با مقادیر q بین ۰,۱ تا ۰,۳۵ مناسب برای تهیه مخلوط خود تـراکم مـی‌باشـد. در صـورتیکه Redix&Browser [۳]مقدار$q=0.25$ مناسب برای ساخت مخلوط خود تراکم دانسته اند.از طرف دیگـر هرچـه منحنـی دانـه بنـدی حاصل از مدل Andreasen&Anderson [۱]به سمت C متمایل باشد یعنی q به سمت ۰,۱ میل کنـد مخلـوط ساخته شده خصوصیات بتن تازه مطلوبتری خواهد داشت.

Larrard [۵]پارامترهایی برای بررسی منحنی دانه بندی‌های مناسب برای تهیه مخلوط ارائه داده است کـه یکـی از این پارامترها، پتانسیل جداشدگی می‌باشد که از رابطه زیر به دست می‌آید:

$$S_i = 1 - \Phi_i/\Phi_i^* \qquad (۳)$$

$$S = S_i(max) \qquad (۴)$$

Φ_i=حجم واقعی ذرات جامد مرتبهi

Φ_i^*= ماکزیمم حجمی‌که ذرات جامد مرتبه iمی‌توانند اشغال کنند

S =پتانسیل جداشدگی

برای محاسبه پتانسیل جداشدگی پارامترΦ_i که در رابطه (۳) و(۴) استفاده شده است از تقسیم جرم ذرات مرتبـه i، که در مرحله به دست آوردن نسبتهای مخلوط به دست آمده است، به جرم حجمی‌ذرات حاصل شده است.پـارامتر Φ_i^* نیز از جمع مقدارΦ_i با تخلخـل موجـود در دانـه بنـدی سـنگدانه‌هـا کـه بـا کمـک دسـتورالعمل ASTM C28,ASTM C29 [۶و۷]محاسبه شده، بدست آمده است.

زمانیکه $S_i=0$ باشدبه این معناست که ذرات مرتبه i به طور کامل متراکم شده اند و امکان جداشدگی وجود نـدارد

وحالت ایده آل می‌باشد که در واقعیت غیر ممکن است.در نتیجه هر چه پتانسیل جدا شدگی منحنی دانه بندی به سمت صفر میل کند مطلوب خواهد بود.

با استفاده ازاین پارامتر نموداری به نام نمودار پرکنندگی ارائه شده است، که این نمودار برای منحنی B,C با حداکثر اندازه سنگدانه ۹٫۵و۱۹ میلیمتر در شکل زیر نشان داده شده است.

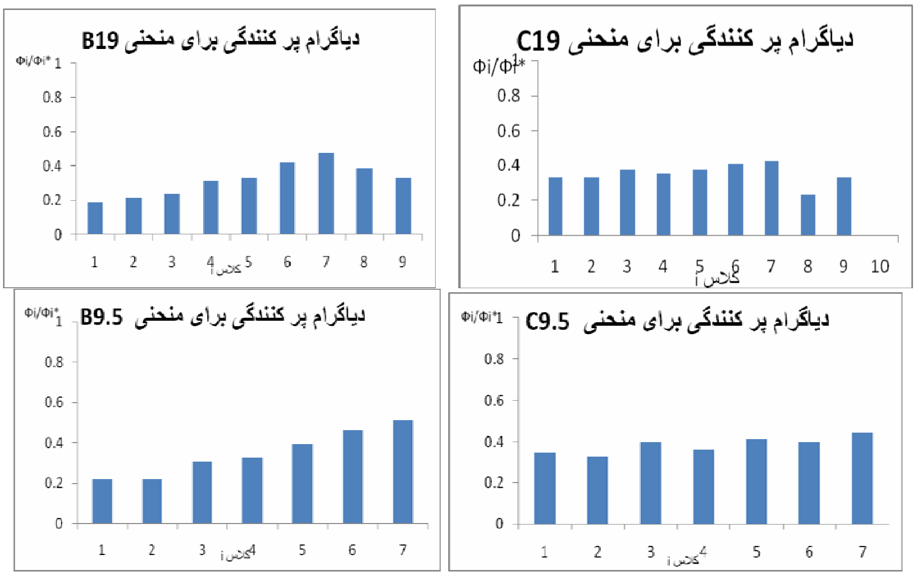

شکل ۲- نمودار پرکنندگی برای منحنی دانه بندی B,C با حداکثر اندازه سنگدانه ۹٫۵ و۱۹ میلیمتر

پتانسیل جداشدگی برای منحنی‌های B,Cبا حداکثر اندازه ۱۹میلیمتر با توجه به شکل ۳ به ترتیب برابر با ۰٫۷۷۱و۰٫۸۱۵ می‌باشد. همچنین برای منحنی‌های B,C با حداکثر اندازه ۹٫۵ میلیمتر به ترتیب برابر با ۰٫۶۷۵و۰٫۷۷۹می‌باشد.

همانطور که بیان شد منحنی دانه بندی‌های بین منحنی‌های B,C برای هر دو حداکثر اندازه ۹٫۵و۱۹ میلیمتر مناسب برای ساخت مخلوط بتن خود تراکم بودند و هر چه منحنی دانه بندی مورد استفاده به منحنی Cنزدیکتر شود خواص بتن تازه مخلوط مطلوبتر بوده است.با توجه به این موضوع و شکل ۳ منحنی دانه بندی‌هایی که پتانسیل جداشدگی آنها بین ۰٫۷۷۱ تا۰٫۸۱۵ برای حداکثر اندازه ۱۹ میلیمتر و۰٫۶۷۵ تا ۰٫۷۷۹ برای حداکثر اندازه ۹٫۵ میلیمتر باشد مناسب برای ساخت مخلوط خود تراکم خواهد بود.هر چه پتانسیل جداشدگی منحنی مورد استفاده به حد پایین بازه‌های ذکر شده متمایل باشد خواص بتن تازه رو به بهبودی خواهد بود.

البته پارامتر پتانسیل جداشدگی به تنهایی کافی برای تعیین منحنی دانه بندی مناسب نمی‌باشد، چرا که منحنی دانه بندی بانمودار پرکنندگی می‌تواند وجود داشته باشد که پتانسیل جداشدگی آن.۷۷۱ باشد ولی مناسب برای تهیه مخلوط نباشد. به این منظور در نمودار پرکنندگی فاکتور دیگری نیز علاوه بر پتانسیل جداشدگی می‌بایست تحت کنترل باشد.این فاکتور تفاضل $S_i(max)$ و $S_i(min)$ در یک نمودار پرکنندگی می‌باشد که هر چه مقدار آن به صفر نزدیکتر باشد نشان دهنده مطلوب تر بودن منحنی دانه بندی می‌باشد.مقدار این تفاضل برای منحنی

دانه بندی B,C با حداکثر اندازه ۱۹ میلیمتر به ترتیب برابر با ۰,۱۹۷ و ۰,۲۹۱ می‌باشد وبرای منحنـی دانـه بنـدی B,C باحداکثر اندازه ۹,۵ میلیمتربه ترتیب برابر با ۰,۱۱۶ و۰,۲۹۲ می‌باشد.در نتیجـه منحنـی دانـه بنـدی مـورد استفاده برای ساخت مخلوط بتن خود تـراکم عـلاوه بـر دارا بـودن پتانـسیل جداشـگی در بـازه‌هـای ذکـر شـده می‌بایست،مقدار تفاضل $S_i(max)$ و $S_i(min)$ در بازه‌های ذکر شده قرارگیرد.

با استفاده از پارامتر پتانسیل جدا شدگی و نمودار پرکنندگی، این امکان ایجاد مـی‌شـود کـه، در صـورت نامناسـب بودن دانه بندی شن و ماسه، با تهیه این نمودار برای شن وماسه موجود، دانه بندی را اصلاح نمود.

۴- نتیجه گیری

- منحنی دانه‌بندی‌های متناظر با مقادیر q بین ۰,۱ تا ۰,۳۵ مناسب برای تهیه مخلوط خود تراکم بوده‌اند.
- هرچه منحنی دانه بندی حاصل از مدل Andreasen&Anderson [1]به سمت C متمایل بوده یعنی q به سمت ۰,۱ میل کرده، مخلوط ساخته شده خصوصیات بتن تازه مطلوبتری داشته است.
- در هرگروه، مخلوطها بر اساس حد اکثر اندازه سنگدانه و منحنی دانه بندی به کـار بـرده شـده، قـرار گرفتـه بودند.با توجه به نتایج آزمایش‌ها، برای هر گروه، یک بازه حجم خمیر سیمان که الزامـات رفتـار بـتن تـازه را تامین می‌نمود، مشخص گردید. هچنین مقدار بهینه حجم خمیر سیمان که بهترین خواص بتن تازه را در هـر یک از بازه‌ها ایجاد نموده است، برای مخلوطهـای گروههـای C۹,۵وB۹,۵وC۱۹وB۱۹ بـه ترتیـب برابـر بـا ۰,۳۰۷و۰,۳۴۵و۰,۲۶۸و۰,۳۳مترمکعب بوده است.
- با توجه به نتایج آزمایش‌ها، منحنی دانه بندی سنگدانه C۱۹ از بین سایر منحنـی‌هـای دانـه بنـدی سـنگدانه استفاده شده در این تحقیق، کمترین حجم خمیر سیمان را برای ساخت مخلوط بـتن خـودتراکم نیـاز داشـته است.
- منحنی دانه بندی‌هایی که پتانسیل جداشـدگی آنهـا بـین۰,۷۷۱ تـا۰,۸۱۵ بـرای حـداکثر انـدازه ۱۹ میلیمتـر و۰,۶۷۵ تا ۰,۷۷۹ برای حداکثر اندازه ۹,۵ میلیمتر بوده است، مناسب برای ساخت مخلوط خود تراکم بوده‌انـد. هر چه پتانسیل جداشدگی منحنی مورد استفاده، به حد پایین بازه‌های ذکر شده، متمایل بوده، خواص بتن تازه رو به بهبودی گذاشته است.
- منحنی دانه بندی مورد استفاده برای ساخت مخلوط بتن خود تراکم علاوه بر دارا بودن پتانسیل جداشـگی در بازه‌های ذکر شده، دارای مقدار تفاضل $S_i(max)$ و $S_i(min)$در بازه ۰,۱۹۷ تا۰,۲۹۱ و ۰,۱۱۶ تا۰,۲۹۲بـرای حداکثر اندازه سنگدانه به ترتیب ۱۹ و۹,۵ میلیمتر بوده است.

مراجع

1. A.H.M. Andreasen, J. Andersen, Ueber die Beziehung zwischen Kornabstufung und Zwischenraum in Produkten aus losen Ko¨ rnern (mit einigen Experimenten), Kolloid-Zeitschrift 50(1930) 217– 22 in German).
2. J.E. Funk, D.R. Dinger, Predictive Process Control of Crowded Particulate Suspension, Applied to Ceramic Manufacturing, Kluwer Academic Press, 1994.
3. H.J.H. Brouwers ,H.J. Radix, Self compacting concrete :theorical and experimental srudy, Cement and concrete research 35(2005)2116-2136.
4. Francois de Larrard, Concrete mixture proportion ,First published 1999 by F:& FN

Spon ,an important of Routledge H New Fetter Lane ,London EC4P 4EE,pp.63-75.

5. Precast/Prestressed Concrete Institute, (PCI), "Interim Guidelines for the use of Self Consolidating Concrete", Chicago, USA, 2003.
6. ASTM C28, 1999,"Standard Specification for Concrete Aggregate", Annual Book of ASTM Standard, PQ.
7. ASTM C29, 1999,"Standard Specification for Concrete Aggregate", Annual Book of ASTM Standard, PQ

CD07-013

مرور طرح‌های اختلاط و خواص بتن‌های خودتراکم

سعید بختیاری[۱]، علی اله وردی[۲]، طیبه پرهیزکار[۳]، مازیار رییس‌قاسمی[۴]
۱. دانشجوی دکترای مهندسی شیمی، دانشگاه علم و صنعت ایران و عضو هیأت علمی‌مرکز تحقیقات ساختمان و مسکن، تهران، ایران
۲. استادیار دانشکده مهندسی شیمی‌دانشگاه علم و صنعت ایران، تهران، ایران
۳. استادیار مرکز تحقیقات ساختمان و مسکن
۴. کارشناس ارشد مرکز تحقیقات ساختمان و مسکن

چکیده

در این مقاله مرور نسبتاً جامعی بر روی ترکیب و خواص مهم بتن‌های خودتراکم ارائه شده است. بتن خودتراکم برای غلبه بر مشکلات عملیات لرزاندن توسعه داده شد و به علت خواص مناسب آن، به سرعت گسترش یافت. خمیر و ملات مورد استفاده در بتن خودتراکم باید دارای لزجت و نیز قابلیت تغییر شکل زیاد باشد و با برقراری تعادل بین این دو، ضمن تأمین قابلیت تغییر شکل و روانی زیاد، از جداشدگی اجزا جلوگیری شود. بنابراین استفاده از مواد افزودنی شیمیایی و پودری مختلف نیاز است. تعین مقادیر و نسبت‌های مناسب مواد مستلزم انجام اختلاط‌های آزمایشی و آزمون‌های خودتراکمی‌نظیر جریان U، جریان اسلامپ و قیف می‌باشد. محدود کردن درصد سنگدانه‌ها به همراه استفاده از مقادیر زیاد پودرهای معدنی و غلظت مناسب فوق‌روان‌کننده‌ها برای دستیابی به این خواص ضروری است. حجم زیاد پودرهای معدنی که در بتن‌های خودتراکم استفاده می‌شود می‌تواند اثرهای متعددی روی خواص آن داشته باشد. پودر سنگ آهک می‌تواند باعث بالا رفتن حرارت هیدراسیون و کاهش قابل ملاحظه دوام بتن در برابر سولفات شود که به علت تشکیل ترکیباتی نظیر گچ، اترنجیت و تاماسیت است. همچنین این پودرها می‌توانند باعث کاهش مقاومت بتن‌های خودتراکم در برابر آتش نسبت به بتن‌های معمولی شود، لذا استفاده از نتایج آزمون و تجربیات موجود روی بتن معمولی را برای این نوع بتن ناممکن می‌سازد.

کلیدواژه‌ها: بتن، خودتراکم، طرح اختلاط، پودر

۱ – مقدمه

یکی از پارامترهای مهم برای رسیدن به بتن با دوام مناسب، متراکم کردن بتن است. برای این منظور اغلب نیاز است تا از عملیات لرزاندن یا ویبره استفاده شود، تا با کاهش تخلخل و هوای درون بتن، مقاومت لازم به دست آمده، دوام افزایش یافته و از شکل‌گیری بتن معیوب جلوگیری شود. عملیات لرزاندن از مشکلات اساسی در این صنعت به شمار می‌رود. مشکلات مختلف مانند کمبود نسبی کارگران ماهر، سهل‌انگاری، مزاحمت‌های جسمی‌و روحی ناشی از لرزاندن و یا دشواری دسترسی مناسب در قالب‌ها و مواضعی که دارای تراکم زیادی از میلگردها هستند، باعث می‌شود تا عمل لرزاندن به طور کامل و صحیح انجام نگرفته و در نهایت مشخصات مطلوبی از بتن

حاصل نشود. بنابراین ساخت بتنی بدون نیاز به لرزاندن، هدف مهمی‌برای متخصصین بتن بوده است که بتوانند با استفاده از مواد افزودنی و تغییر در نسبت اختلاط اجزا، به این هدف دست یابند و نقص‌های بتن در اثر عملیات اجرایی تراکم را برطرف سازند.

ابداع بتن خودتراکم یا SCC نتیجه این تلاش‌ها بوده است. استفاده از این بتن نه تنها به حل مشکلات عدم کارایی و یا ضعف اجرائی کارگران کمک می‌نماید، بلکه موجب صرفه‌جویی‌های چشمگیری از نظر مدت زمان اجرا و به تبع آن در هزینه‌ها می‌تواند بشود [۱ و ۱]. برای ساخت بتن خودتراکم، می‌توان با استفاده از فوق‌روان‌کننده‌های نسل جدید ضمن به دست آوردن روانی زیاد، از بروز جداشدگی نیز جلوگیری نمود. پیش از آن نیز افزایش روانی بتن از طریق مصرف مواد افزودنی روان‌کننده یا فوق‌روان‌کننده امکان‌پذیر بوده است، ولی چنانچه از این طریق روانی بتن بیش از حد معین افزایش یابد، جداشدگی در بتن اتفاق افتاده و به کیفیت بتن صدمه می‌زند. بنابراین باید ضمن استفاده از انواع مناسب فوق‌روان‌کننده‌ها، لزجت مخلوط را در حد مناسبی حفظ کرد تا از جداشدگی ملات از سنگدانه جلوگیری شود. برای این منظور از مقادیر مناسب پودرها و پرکننده‌های معدنی و در صورت لزوم از مواد اصلاح‌کننده لزجت (VMA) استفاده می‌شود.

در این مقاله مرور نسبتاً جامعی بر روی طرح‌های اختلاط و خواص مهم بتن‌های خودتراکم، با استفاده از تعداد زیادی مقالات پژوهشی و سایر مدارک فنی معتبر صورت گرفته است. تعریف، تاریخچه و دلایل گسترش نسبتاً سریع این نوع بتن ارائه شده است. چگالی تراکم، مفهوم مهمی‌در رسیدن به خواص خودتراکمی‌است، که در این خصوص و سنجه‌های مؤثر بر روی آن بحث شده است. روش‌های طرح اختلاط و خواص بتن خودتراکم، از جمله مقاوم فشاری، دوام و مقاومت در برابر آتش با استفاده از ادبیات علمی‌موضوع مورد بحث قرار گرفته است. خصوصاً اثر کلیدی پودرها، که حجم قابل توجهی از بتن خودتراکم را تشکیل می‌دهند، بر روی برخی خواص بتن خودتراکم بحث شده است.

۲- تعریف بتن خودتراکم و دلایل گسترش آن

طبق تعریف بارتوس (Bartos) [2]، بتن خودتراکم بتنی است که تحت وزن خود جاری شده و بدون نیاز به هر نوع لرزاندن، به طور کامل (حتی با وجود میلگردهای متراکم)، قالب‌ها را پرکرده و همگنی خود را حفظ نماید.

طبق تعریف اوزاوا (Ozawa) [3] بتن خود تراکم تازه باید هر سه خاصیت زیر را داشته باشد:

الف ـ توانایی پرکنندگی: جاری شدن بتن خود تراکم درتمام فضاهای قالب تحت وزن خود.

ب ـ توانایی عبور: امکان عبور از فواصل تنگ بین میلگردها و قالب تحت وزن خود.

ج ـ مقاوم در مقابل جداشدگی: شکل و ترکیب یکنواخت خود را در جریان حمل و بتن‌ریزی حفظ نماید.

مزایای چشمگیر بتن خودتراکم موجب گسترش سریع آن در دنیا شده است. از مزایای مهم آن می‌توان حذف عملیات لرزاندن، سهولت بتن‌ریزی، افزایش سرعت اجرا، اطمینان از تراکم مناسب، به خصوص در مقاطع تنگ و یا دارای میلگردهای فشرده، مقاومت خوب در برابر جداشدگی سنگدانه، امکان ایجاد سطوح تمام شده صاف و زیبا و در نتیجه تهیه طرح‌های متنوع معماری در نما و نیز کاهش آلودگی صوتی در محیط کار و محیط‌های شهری را نام برد.

به علاوه حدود ۷٪ از دی اکسیدکربن تولیدی توسط صنایع، مربوط به کارخانه‌های سیمان است [4]. بنابراین

استفاده از بتن‌های توانمند و خودتراکم (به شرطی که عیار سیمان در آن کاهش یابد) یکی از راه‌های مؤثر برای کاهش دی اکسیدکربن، کاهش مشکلات گرم شدن زمین و حفظ محیط زیست است، زیرا در این بتن‌ها سیمان به طور مؤثرتری استفاده شده و نیز جایگزینی درصدی از سیمان به وسیله پرکننده‌ها صورت می‌گیرد.

۳- تاریخچه بتن خودتراکم

بتن خودتراکم نخست در سال ۱۹۸۶ توسط اوکامورا (Okamura) در ژاپن پیشنهاد شد [5 و 6]. در پی آن مطالعات و آزمایش‌های اساسی در دانشگاه توکیو توسط اوزاوا و میکاوا (Meakawa) برای توسعه این بتن صورت گرفت [5-7]. اولین نمونه‌های این نوع بتن در سال ۱۹۸۸ با استفاده از مواد و مصالح موجود در بازار ساخته شد و نتایج مناسبی از نظر جمع‌شدگی ناشی از خشک شدن و سخت شدن، گرمای هیدراسیون، سختی و سایر خواص به دست آمد و در مقاله‌ای منتشر شد [3]. در ابتدا این بتن، بتن توانمند (HPC) نام‌گذاری شد، اما همزمان، آیتسین (Aitcin) و همکارانش [8 و 9]، بتن توانمند را به عنوان بتنی معرفی کردند که دارای مقاومت و دوام بالا در اثر نسبت آب به سیمان پایین باشد. بنابراین نام این نوع بتن توسط اوکامورا و همکارانش تغییر یافت و تحت عنوان "بتن خودتراکم توانمند" یا به طور خلاصه "بتن خودتراکم" خوانده شد [5، 10 و 11]. تفاوت بتن‌های خودتراکم و توانمند در این است که در بتن توانمند، جریان‌پذیری تنها تا حدودی بهبود یافته است، اما نمی‌تواند تحت وزن خود، قالب و یا فواصل بین میلگردها را پر کند، به عبارت دیگر کماکان به عملیات لرزش نیاز دارد.

مقالات اوزاوا و اوکامورا در کنفرانس‌های مختلف بین‌المللی، توجه به بتن خود تراکم را افزایش داد [5، 12 و 13]. در ۱۹۹۶ پروژه‌ای با عنوان "تولید و محیط کاری بهبود یافته با استفاده از بتن خودتراکم" توسط کنسرسیومی‌از کشورهای اروپایی آغاز و باعث گسترش سریع‌تر کاربرد SCC در پروژه‌های ساختمانی و عناصر بتنی پیش‌ساخته شد. در ۲۰۰۵ راهنمای اروپایی بتن خودتراکم توسط "فدراسیون اروپایی متخصصین شیمی‌ساختمان و سیستم‌های بتنی" (EFNARC) [14] منتشر شد. صنعت بتن پیش‌ساخته در امریکا نیز از سال ۲۰۰۰ بتن خودتراکم را برای ساخت عناصر سازه‌ای و غیرسازه‌ای و پانل‌های معماری مورد استفاده قرار داد. کاربرد بتن خودتراکم در ساخت قطعات پیش‌ساخته پیش‌تنیده از حدود ۱ درصد در سال ۲۰۰۰ به تقریباً ۱۵ درصد در سال ۲۰۰۵ افزایش یافت. استفاده از آن در صنایع بتن آمادهٔ امریکا نیز با شتاب کمتری در حال افزایش است [15].

سازه‌های مختلفی با استفاده از بتن خودتراکم در دنیا اجرا شده‌اند که از جمله پل معلق آکاشی-کایکو (Akashi-Kaiko) در ژاپن، دیواره‌های مخازن عظیم LNG شرکت گاز اوزاکا (Ozaka) در ژاپن، بازار بزرگ میدسامر (Midsummer Place) در لندن و پروژه‌های متعدد دیگر در دنیا را می‌توان نام برد [۱ و 16].

در ایران نیز استفاده از بتن خودتراکم از چند سال قبل آغاز شده و از مزایای آن بهره گرفته شده است. برای مثال می‌توان از کاربرد آن در لایه سطحی تونل رسالت تهران، برخی قسمت‌های نما و کتیبه نویسی قرآن در طرح توسعه حرم حضرت معصومه در قم و ساخت قطعات بتنی خاص برای عبور ماشین‌های حفاری تونل در پروژه متروی شیراز را نام برد [17 و ۱۸].

۴- خودتراکمی‌و مفهوم چگالی تراکم

چگالی تراکم مفهومی‌کلیدی برای دستیابی به بتن‌های توانمند و خودتراکم است. چگالی تراکم به معنای «نسبت

حجم مواد جامد به حجم توده‌ای ذرات جامد» است و آن را می‌توان در دو قسمت تراکم سنگدانه و سیمان بحث نمود [۱۹]. تراکم سنگدانه مستقیماً با اندازه‌گیری چگالی انبوهی سنگدانه قابل اندازه‌گیری است و نشان می‌دهد که سنگدانه‌ها به چه میزان به یکدیگر فشرده شده‌اند. به این وسیله حجم حفرات بین سنگدانه‌ها که باید به وسیله خمیر سیمان پر شود، از کم کردن چگالی تراکم از عدد یک به دست می‌آید. روش‌های اندازه‌گیری در استاندارد BS 812-2 [20] آمده است. چنانچه دانه‌های با اندازه‌های مختلف و با نسبت مناسب در مخلوط وجود داشته باشد، دانه‌های کوچک فواصل بین دانه‌های بزرگ را به خوبی پر کرده، فضای خالی کمتری برای پر شدن توسط مواد ریزتر باقی می‌ماند، بنابراین به مقدار کمتری سیمان نیاز خواهد بود. به علاوه، با فرض یک مقدار ثابت مواد سیمانی، خمیری که اضافه بر مقدار لازم برای پر کردن فضای خالی وجود دارد، باعث می‌شود تا دانه‌ها به نحو بهتری با خمیر پوشانده شده، توزیع و جریان بهتری به دست آید. بنابراین دانه‌بندی سنگدانه تأثیر به سزایی در تقاضای خمیر و کارایی مخلوط دارد. کاهش تقاضای خمیر، علاوه بر بهبود کارایی، باعث پایداری ابعادی بهتر بتن می‌شود. چنانچه تمام ابعاد سنگدانه از درشت تا خیلی ریز به طور پیوسته وجود داشته باشد، در عمل دلایلی نظیر عدم وجود تمام اندازه‌های سنگدانه از درشت تا بسیار ریز در مخلوط، شکل هندسی دانه‌ها، زبری دانه‌ها، اصطکاک و مزاحمت‌های فضایی ناشی از اثر جداره‌ها باعث می‌شود تا چگالی تراکم کاهش یابد. استروون (Stroeven) [21] یک مدل کامپیوتری برای تعیین اثر تراکم تصادفی سنگدانه‌ها ارائه کرده است.

مفهوم چگالی تراکم را می‌توان به مواد سیمانی نیز بسط داد. همانگونه که تراکم سنگدانه‌ها تقاضای سیمان را مشخص می‌سازد، تراکم مواد سیمانی نیز تقاضای آب را تعیین می‌کند. مواد سیمانی گوناگون دارای اندازه‌های مختلف هستند، بنابراین پودرهای ریزتر می‌توانند فضاهای خالی بین ذرات درشت‌تر را پر کرده، تقاضای آب را کاهش دهند. فنگ (Feng) و همکاران [22] نشان دادند که مخلوط کردن سرباره با سیمان، جریان‌پذیری خمیر را بهبود می‌بخشد. وانگ و کوان [۱۹] چگالی تراکم سیمان‌های مخلوط را اندازه‌گیری و مشاهده نمودند که افزودن میکروسیلیس به طور قابل توجهی چگالی تراکم سیستم را افزایش می‌دهد. آنها نشان دادند که در یک نسبت آب به سیمان ۰/۲، افزایش میکروسیلیس باعث بهبود چشمگیر قابلیت روانی خمیر سیمان می‌شود. کوان (Kwan) [23] در حین توسعه بتن با مقاومت بالای خودتراکم (HS-SCC) دریافت که در نسبت آب به سیمان ۰/۲۸، با استفاده از میکروسیلیس با اندازه متوسط ۰/۱ میکرون، کارایی بتن به نحو قابل توجهی بهبود می‌یابد. وی این بهبود کارایی را به بسیار ریز بودن میکروسیلیس نسبت داد که با پر کردن فضاهای خالی بین دانه‌های سیمان باعث می‌شود تا آب اضافی بیشتری برای روان کردن خمیر موجود باشد. اوبلا (Obla) [24] نشان داد که مخلوط کردن سیمان با خاکستر بادی بسیار ریز، با اندازه متوسط ۳ میکرون، تقاضای آب را کاهش می‌دهد.

افزایش چگالی تراکم به دلیل کاهش نسبت آب به سیمان و کمتر شدن تقاضای آب، نفوذپذیری و آب انداختگی را کاهش می‌دهد. همچنین در اثر کم شدن فضاهای تخلخلی که به علت اثر دیواره، در مجاورت سنگدانه‌ها ایجاد می‌شود، تخلخل منطقه انتقالی نیز کاهش می‌یابد [۱۹ و 25]. بنابراین کیفیت منطقه انتقالی، که ضعیف‌ترین اتصال در بتن محسوب می‌شود، بهبود می‌یابد [26]. در بتن‌های با مقاومت بالا که چگالی تراکم به وسیله میکروسیلیس در آنها افزایش یافته بود، به طور واضح مشاهده شده که سطح شکست از میان سنگدانه‌ها (و نه از منطقه گذار) عبور نموده است، که نظریه بالا را تائید می‌نماید [27]. لیمن (Leeman) [28] اثر تراکم در کیفیت و نفوذپذیری منطقه انتقالی بتن، برای طرح‌های اختلاط معمولی و خودتراکم را با بهره‌گیری از

میکروسکوپ‌های نوری و الکترونی بررسی کرد. مشاهده شد که تراکم اثر قابل توجهی بر روی تخلخل و پهنـای منطقه انتقالی دارد. بنابراین تخلخل منطقه انتقالی در بتن معمولی لرزانده شده، عموماً بیـشتر از بـتن خـودتراکم است که منجر به مقاومت فشاری کمتر و نفوذ بیشتر اکسیژن می‌شود. در عین حال، مقدار کمتر خمیـر سـیمان و اندازه‌های بزرگتر سنگدانه‌ها در بتن معمولی، این اثرات را کاهش می‌دهد. اثرات توأم پارامترهـای مختلـف، نظیـر نیروی ثقل، کارایی و ناهمگنی منطقه انتقالی، بررسی میکروسکوپی موضوع بـه صـورت یـک روش تکرارپـذیر را دشوار و پیچیده می‌سازد [28].

در مورد اندازه گیری چگالی تراکم سیمان در مراجع مختلف بحث شده است [۱۹، 27–30]. برای بتن‌های توانمند و خودتراکم توصیه شده است که چگالی خمیر با افزودن فوق روان‌کننده، اندازه گیری شود [۱۹].

افزایش چگالی تراکم، علاوه بر مقاومت، باعث بهبود کارایی بتن نیز می‌شود، زیـرا در یـک نـسبت ثابـت آب بـه سیمان، قابلیت جریان یافتن خمیر بهتر می‌شود. همچنین چسبندگی خمیر سیمان بهبود یافته، در نتیجـه مقاومـت بتن در برابر جداشدگی افزایش می‌یابد. این مشخصات، به دستیابی به خاصیت خودتراکمی کمک زیادی می‌نمایـد. آزمایش‌های وانگ [۱۹] بهبود اساسی قابلیت جریان یافتن خمیر سیمان با افزایش چگالی تراکم را، بخـصوص در نسبت‌های پایین آب به سیمان، نشان داد. شکل مقدار جریان اسلامپ را برای نسبت‌های مختلـف مخلـوط و آب به سیمان در آزمایش‌های وی نشان می‌دهد. نسبت‌ها در این شکل حجمی‌هستند. قطر بالایی و پـایینی مخـروط اسلامپ به ترتیب ۶۰ و ۱۰۰ میلی‌متر و ارتفاع آن ۷۰ میلی‌متر بوده است. وی برای بهینه کردن چگـالی تـراکم و اثر آن در بتن، یک طرح اختلاط سه مرحله‌ای شامل مخلوط‌های خمیر سیمان، ملات و بتن را پیشنهاد مـی‌کنـد. در مرحله اول چگالی تراکم مواد سیمانی، تقاضـای آب را تعیـین مـی‌کنـد و آب اضـافی عامـل اثرگـذار بـر روی رئولوژی و چسبندگی خمیر سیمان (مواد سیمانی، آب و فوق‌روان‌کننده) است. در مرحله دوم ملات در نظر گرفتـه می‌شود که شامل خمیر سیمان و سنگدانه‌های ریزتر از ۱/۲ mm است. چگالی تراکم دانـه‌هـای کـوچکتر از mm ۱/۲ تقاضای خمیر را مشخص کرده و خمیر اضافی عامل تعیین‌کنندهٔ جریان‌پذیری ملات اسـت. در مرحلـه سـوم بتن، به معنای ملات به اضافه سنگدانه‌های درشت‌تر از ۱/۲ میلی‌متر، در نظر گرفته مـی‌شـود کـه در آن چگـالی تراکم سنگدانه‌های بزرگتر از ۱/۲ mm تقاضای ملات را مشخص می‌کنـد و مـلات اضـافی عامـل تعیـین‌کننـدهٔ کارایی مخلوط است. وانگ گزارش می‌کند که حتی در آن نمونه‌های بتن که جداشدگی مـشاهده شـد، دانـه‌هـای ریزتر از ۱/۲ میلی‌متر، همراه با خمیر باقی ماندند.

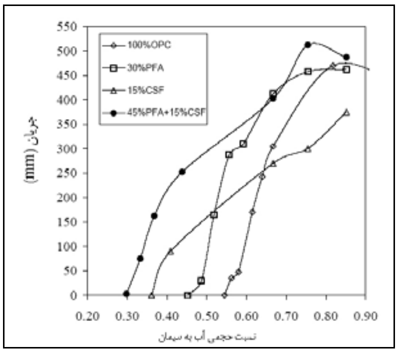

شکل ۱- مقدار جریان خمیر سیمان در نسبت‌های مختلف مواد و آب به سیمان [۱۹]

۵- طرح اختلاط‌های بتن خودتراکم

۵-۱ اصول و روش‌های ارزیابی

اصولاً بتن با توجه به تعدد اجزای آن که دارای چگالی‌های مختلف هستند، مستعد به جداشدگی است. این خطر همواره با افزایش قابلیت تغییر شکل بیشتر می‌شود. به همین علت، در تکنولوژی بتن به طور رایج استفاده از بالاترین لزجتی که قابل کار کردن باشد، توصیه می‌شود. در این صورت قابلیت تغییر شکل کاهش یافته و به عملیات لرزاندن نیاز است. اما برای دستیابی به خاصیت خودتراکمی‌لازم است تا خمیر یا ملات دارای قابلیت تغییر شکل زیاد بوده، به علاوه در هنگام جریان بتن از یک محفظه بسته یا بین میلگردهای تقویت، مقاومت مناسب در برابر جدا شدگی سنگدانه‌های درشت و ملات وجود داشته باشد. قابلیت تغییر شکل به این مفهوم است که انرژی در داخل بتن یا به علت اصطکاک در مرزها، کمتر مصرف شود. در مقابل آن، لزجت بیشتر به معنای افزایش انرژی لازم برای تغییر شکل است. بنابراین نکته کلیدی برای دستیابی به بتن خودتراکم این است که یک تعادل مناسب بین این دو نیاز برقرار شود تا ضمن تأمین قابلیت تغییر شکل و روانی زیاد، از جداشدگی اجزا جلوگیری شود [31].

بدیهی است که طرح اختلاط نهایی بستگی به پارامترهای مختلف، نظیر نوع و کیفیت مواد، مقاومت مورد نیاز، دوام و شرایط محیطی و غیره دارد. مقادیر مناسب مواد را نمی‌توان بدون اختلاط آزمایشی، ثابت در نظر گرفت. بنابراین بلافاصله پس از تعیین نسبت اختلاط، باید خودتراکمی‌را به وسیله آزمون‌های خودتراکمی‌مانند آزمون جعبه، جریان U، جریان اسلامپ و آزمون قیف ارزیابی کرد. روش‌هایی برای قضاوت این که با توجه به نتایج آزمون آیا نسبت آب به پودر یا مقدار روان‌کننده کمتر یا بیشتر ازحد نیاز است، و نیز روش‌هایی برای تخمین مقادیر مناسب مورد نیاز است. روابط بین خواص ملات در بتن خودتراکم و نسبت اختلاط مورد تحقیق قرار گرفته و فرموله شده است. چنانچه خودتراکمی‌بتن به وسیله این آزمایش ناکافی تشخیص داده شود، علت آن باید به طور کمی‌پیدا شود، تا بتوان نسبت اختلاط را تنظیم نمود. آزمایش‌های جریان اسلامپ و قیف به ترتیب برای آزمون قابلیت تغییر شکل و لزجت پیشنهاد شده‌اند و شاخص‌های Γ_C و R_C برای آنها به شرح زیر تعریف شده است [6]:

(معادله ۱) شاخص قابلیت تغییر شکل: $\Gamma_C = (Sfl_1 . Sfl_2 - Sfl_0^2) / Sfl_0^2$

که در آن Sfl_1 و Sfl_2 قطرهای اندازه‌گیری‌شده جریان اسلامپ و Sfl_0^2 قطر مخروط اسلامپ است.

(معادله ۲) شاخص لزجت:

$$R_C = \frac{10}{t}$$

که در آن t زمان اندازه‌گیری شده برحسب ثانیه برای بتنی است که از میان قیف عبور می‌نماید. آزمون‌های جریان و قیف، علاوه بر بتن برای ملات یا خمیر، برای تعیین اثر مواد مورد استفاده در بتن‌های خودتراکم، نظیر مواد پودری، ماسه و فوق‌روان‌کننده‌ها پیشنهاد شده‌اند. این شاخص‌ها می‌توانند برای تعیین یک روش منطقی برای تنظیم نسبت آب به پودر و مقدار فوق‌روان‌کننده و برای به دست آوردن لزجت و قابلیت تغییرشکل مناسب، استفاده شوند. اوکامورا و اوشی [6] ارتباط بین فاکتورهای خودتراکمی‌و نتایج آزمون‌های خودتراکمی‌را بحث کرده‌اند.

۵-۲ روش‌های طرح اختلاط

خودتراکمی‌به طور وسیعی به مشخصات مصالح و طرح اختلاط بستگی دارد. برای افـزایش قابلیـت تغییـر شـکل خمیر، باید نسبت آب به پودر (مجموع پودرهای چسباننده و پرکننده‌های معدنی) را بالا برد و یا از فوق روان‌کننده استفاده کرد. اما در مقابل برای به دست آوردن لزجت زیاد، باید نسبت آب به پودر را کاهش داد یا از افزودنی‌های اصلاح لزجت استفاده کرد. استفاده از مقادیر زیاد مواد اصلاح‌کننده لزجت در سازه‌های بتنی زیر آب رایج است تـا از حل شدن سیمان در آب جلوگیری شود. اما استفاده از چنین مخلـوطی بـرای سـازه‌هـای خـارج از آب مناسـب نیست، زیرا لزجت آن چنان بالا است که هوا از آن خارج نمی‌شود و آن را به راحتی نمی‌توان در قالـب جـای داد. اولین بار تاکشیتا (Takeshita) با چنین روشی به بتن خودتراکم دست یافـت [31 و 32] امـا در ایـن روش حفـظ تعادل بین فوق‌روان‌کننده و مواد اصلاح لزجت بسیار مهم و دشوار است.

اوکامورا و اوزاوا برای حل مشکل فوق فرضیات دیگری را برای طرح اختلاط خود در نظر گرفتند، به ایـن ترتیـب که حجم سنگدانه‌های درشت محدود شود تا از مسدود شدن بتن در پـشت موانـع جلـوگیری شـود. همچنـین بـا استفاده از مقادیر بالای پودر و حفظ نسبت آب به پودر، لزجت بتن تنظیم شود. با توجـه بـه اینکـه مقـادیر بـالای سیمان، باعث مشکلات مختلف در بتن می‌شود، قسمتی از آن با پودرهای خنثی مانند پودر سنگ آهک جـایگزین شد. تفاوت اصلی روش اوکامورا و اوزاوا با روش‌های قبلی برای رسیدن به خودتراکمی‌را باید استفاده از مقادیر زیاد پودر ذکر کرد که اساس طرح اختلاط را تشکیل داده است. استفاده از پودر باعث حذف یـا کـاهش نیـاز بـه مـواد اصلاح کننده لزجت شد.

نکته مهم در طرح اختلاط اوکامورا، درک اثر کلیدی پودر برای دستیابی به خودتراکمی‌است که در چگـالی تـراکم بحث شد. آزمایش‌ها نشان داد که یک رابطه خطی بین مساحت نسبی جریان و نسبت آب به پودر وجـود دارد. بـا استفاده از این رابطه می‌توان نسبت حدی آب به پودر که در آن تغییر شکل خمیر برابر با صفر می‌شود، برون‌یـابی نمود [31] (شکل). در شکل ، F معادل جریان اسلامپ مخلوط پـودر و آب و F0 برابـر بـا انـدازه قطـر مخـروط اسلامپ است. این حد را می‌توان مقدار آب محبوس‌شده توسط پودر در نظر گرفت که بسته به نـوع پـودر، شـکل هندسی و دانه‌بندی ذرات، بین ۰/۷ تا ۱/۰ قرار می‌گیرد. به عبارت دیگر، پودر تقریباً به انـدازه حجـم خـود، آب را محبوس می‌کند. حال برای رسیدن به لزجت مناسب برای خودتراکمی، باید نسبت حجمـی‌آب بـه پـودر را بهینـه کرد. برای پودرهای ریز و با شکل هندسی نزدیک به کروی، این نسبت کوچک است. ضمن این که واکنش پـذیر بودن پودر و گیرش آن نیز بر روی نسبت بهینه تأثیر می‌گذارد. این موضوع برای چند نوع سیمان و پودر مختلـف گزارش شده است [31]. سیمان پرتلند نوع معمولی نسبت به سیمان با حرارت هیدراسیون کم مقدار بیـشتری آب در خود نگاه می‌دارد. همچنین اضافه کردن پودر خاکستر بادی و سرباره، به علت افزایش چگالی تراکم، مقدار آب به دام افتاده را به نحو قابل توجهی کاهش می‌دهد.

جزء مهم دیگر طرح اختلاط، سنگدانه است. معمولاً از نسبت ۱:۱: ۲ برای سیمان: سنگدانه ریز : سنگدانه درشـت به عنوان نسبت مناسب برای رسیدن به مقاومت حداکثر یاد می‌شود و بیشتر شدن مقادیر سنگدانه می‌تواند باعـث کاهش شدید مقاومت شود. توکوجیرو (Tokujiro) [33] در ۱۹۴۰ نشان داد کـه اگـر نـسبت حجمـی‌سـیمان بـه سنگدانه‌های ریز، ۱ به ۱/۵ گرفته شود، آنگاه نسبت حجمی‌بیشتر از ۱ بـه ۱/۵ بـرای سـیمان بـه سـنگدانه‌هـای درشت، منجر به سقوط قابل ملاحظه مقاومت می‌شود. وی اثر تراکم را بـه دقـت مطالعـه نمـود و نـسبت آب بـه

سیمان را در قالب به وسیله فشار و با خارج شدن آب در این حالت، به ۲۲ درصد رساند. نسبت وزنی بهینه آب به سیمان، پیش از قالب‌ریزی و فشار، ۳۱ درصد بود. توکوجیرو برای رسیدن به حداکثر مقاومت، نسبت ۱ به ۲ را برای نسبت حجمی‌سنگدانه‌های ریز به درشت توصیه کرد، اما اوکامورا نسبت کمتر (۱ به ۱) از سنگدانه را برای دستیابی به خودتراکمی‌و قابلیت عبور از موانع موجود در قالب، برای کاربردهای واقعی لازم می‌داند. مقایسه نتایج اوکامورا [31] و توکوجیرو [33] در نسبت برابر سنگدانه‌های درشت و ریز، بیانگر این است که بتن خودتراکم اوکامورا همان بتن با حداکثر مقاومتی است که توکوجیرو به دست آورده و برای دستیابی به خودتراکمی، به آن در حد نیاز فوق‌روان‌کننده اضافه شده است.

آزمایش‌های اوکامورا [31] نتایج مهمی‌در خصوص سنگدانه‌های ریز به دست می‌دهد. مقدار آب نگهداشته شده به وسیله سنگدانه‌های ریز، در یک محدوده مشخص، تقریباً متناسب با حجم آن و در حدود ۲۰ درصد است. این مقدار تقریباً یک پنجم پودرها است. بر اساس نتایج وی سنگدانه‌های ریزتر از ۹۰ میکرون را باید به عنوان پودر در نظر گرفت (و نه سنگدانه). به غیر از تفاوت در مقدار نگه‌داشتن آب، یک تفاوت دیگر نیز بین پودر و سنگدانه ریز وجود دارد: نسبت آب نگه داشته شده توسط سنگدانه ریز، وقتی که مقدار آن از یک حد مشخص فراتر رود، به شدت افزایش می‌یابد (شکل). اوکامورا علت این موضوع را توضیح نداده است، اما دلیل اصلی باید چگالی تراکم باشد. با افزایش درصد ریزدانه‌ها در ملات، تماس این دانه‌ها با یکدیگر افزایش یافته و با کم شدن درصد خمیر، چگالی تراکم کاهش می‌یابد، بنابراین به آب بیشتری برای پر کردن فضای خالی نیاز است. لازم به ذکر است که برای سنگدانه‌های درشت، آب به دام افتاده یا نگه‌داشته توسط آنها عملاً در نظر گرفته نمی‌شود.

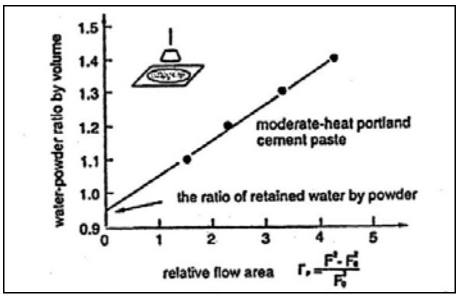

شکل ۲- رابطه بین مساحت جریان نسبی و نسبت حجمی‌آب به پودر

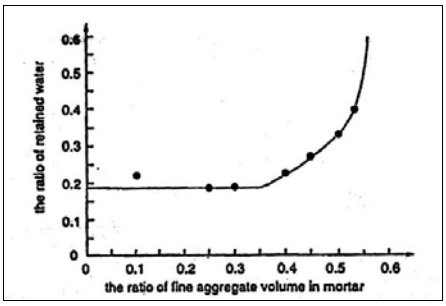

شکل ۳- رابطه بین نسبت آب نگه‌داشته‌شده و نسبت حجمی‌ریزدانه‌ها در ملات

اجزای دیگر مخلوط خودتراکم آب و فوق‌روان‌کننده هستند. نقش اصلی آب در بتن تازه، تأمین قابلیت تغییر شکل به مقدار کافی است. در شکل ۱ و ۵ آب آزاد (به معنای آب موجود در خمیر منهای آب گیر افتاده به وسیله پودر و سنگدانه‌های ریز) بر حسب پارامترهای مساحت جریان نسبی و سرعت نسبی قیف برای خمیر و ملات رسم شده است [31]. در یک مقدار ثابت سنگدانه ریز، مساحت جریان و سرعت قیف برای خمیر و ملات متناسب با نسبت آب آزاد به پودر است. هر چه مقدار سنگدانه‌های ریز افزایش می‌یابد، نسبت تناسب کاهش یافته، مقدار آب آزاد بیشتری برای افزایش مساحت جریان و سرعت قیف لازم است.

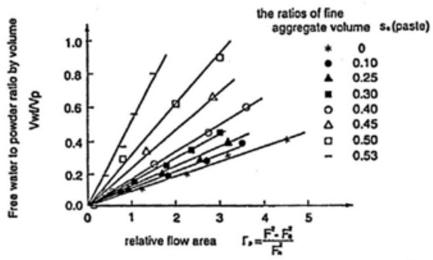

شکل ۱- رابطه بین نسبت آب آزاد به پودر و مساحت جریان نسبی

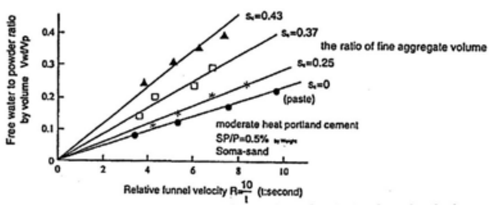

شکل ۵- رابطه بین نسبت آب آزاد به پودر و سرعت نسبی در قیف [31]

نقش فوق‌روان‌کننده نیز مشابه با آب آزاد است، اما مقادیر بسیار کمتری از آن ضروری است. برخلاف آب آزاد، تغییر کم در فوق‌روان‌کننده باعث تغییر زیاد در مساحت جریان می‌شود، اما تغییرات در سرعت قیف به مراتب کمتر است. فوق‌روان‌کننده، بر خلاف آب آزاد، باعث آب انداختگی نمی‌شود، اما ایراد اصلی آنها این است که عملکردشان شدیداً به نوع پودر، دما، گذشت زمان و روش اختلاط بستگی دارد.

اوکامورا و اوزاوا بر اساس مفاهیم و نتایج فوق، اصول طرح اختلاط خود را به شرح زیر ارائه می‌دهند [5، 6 و 31]:

۱- با بالا رفتن درصد سنگدانه درشت، احتمال تماس بین آنها و مسدود شدن فضای بین موانع افزایش می‌یابد. بنابراین درصد سنگدانه‌های درشت را باید محدود کرد. برای این منظور، درصد سنگدانه درشت نسبت به حجم کل جامدات مهم‌تر از مقدار سنگدانه است و آن را باید به ۵۰٪ کل جامد محدود ساخت.

۲- مقدار سنگدانه‌های ریز باید محدود شده و معادل ۴۰٪ حجم ملات باشد. ذرات ریزتر از ۹۰ میکرون موجود در سنگدانه ریز، باید جزو پودر در نظر گرفته شود. اگر از خمیر مناسبی استفاده شود و مقدار سنگدانه ریز به این مقدار محدود شود، برخورد چندانی بین سنگدانه‌های ریز رخ نخواهد داد.

۳ـ نسبت حجمی‌آب به پودر بین ۰/۹ تا ۱/۰، بسته به خواص پودر، درنظر گرفته می‌شود.

۴ـ مقدار فوق‌روان‌کننده و نسبت نهایی آب به پودر به گونه‌ای تنظیم شود که خودتراکمی‌به دست آید.

در طرح اختلاط بتن‌های معمولی، ابتدا نسبت آب به سیمان ثابت گرفته می‌شود تا مقاومت کافی به دست آید. اما در بتن‌های خودتراکم، با توجه به حساسیت و وابستگی شدید خودتراکمی‌به نسبت آب به پودر، این نسبت باید برای رسیدن به خودتراکمی‌تنظیم شود. برای بتن خودتراکم، در اکثر اوقات، مقاومت تعیین‌کنندۀ نسبت آب به پودر نیست، زیرا نسبت آب به پودر جهت دستیابی به مقاومت لازم برای اکثر سازه‌ها، به اندازۀ کافی کم است، مگر این که بیشتر مواد پودری استفاده شده، از نوع غیرواکنش‌زا باشند.

ناگاموتو (Nagamoto) [34] با مطالعات تجربی، صحت روش مذکور در فوق را بررسی کرد. نتایج نشان داد که افزایش مقادیر سنگدانه درشت به بیش از ۵۰ درصد نسبت به مواد جامد، باعث می‌شود تا خواص خودتراکمی‌به شدت و به صورت غیر خطی سقوط کند. تغییر مقدار سنگدانه ریز از ۴۰ درصد حجم ملات به ۴۵ درصد، با ثابت نگاه داشتن درصد سنگدانه درشت، باعث تغییر چندانی در خواص خودتراکمی‌نشد. تغییر سنگدانه‌های درشت، با ثابت نگاه داشتن درصد سنگدانه‌های ریز، تغییری در نسبت آب به پودر ایجاد نکرد، ولی نیاز به تغییر مقدار فوق‌روان‌کننده می‌باشد.

دامون [35] ۶۸ طرح اختلاط بتن خودتراکم استفاده شده در پروژه‌های مختلف را آنالیز کرده است. آنالیز این

طرح‌ها، اصول ارائه شده در طرح اختلاط اوکامورا را تائید می‌نماید. وی اجزای کلیدی مخلوط‌ها، شامل درصد حجمی‌درشت‌دانه‌ها، درصد حجمی‌خمیر، درصد وزنی پودر، نسبت وزنی آب به پودر و حجم ریزدانه‌ها به حجم ملات را بحث و بررسی کرد. بر این اساس میانگین درصد حجمی‌سنگدانه‌های درشت ۳۱/۲، درصد حجمی‌خمیر ۳۴/۸، مقدار پودر ۵۰۰ کیلوگرم بر متر مکعب، نسبت آب به پودر ۰/۳۴ بوده است. به استثنای دو مورد، محتوای پودر در محدودۀ ۶۲۵ـ۴۲۵ کیلوگرم بر مترمکعب و ۸۰٪ آن در محدودۀ ۶۰۵ـ۴۴۵ کیلوگرم برمترمکعب بوده است. حدود نصف مخلوط‌ها دارای VMA بودند که منجر به پایداری مخلوط‌های با درصد کمتر پودر (با یک تفاوت حدود ۳۰ Kg/m^3 در مقدار میانگین) شده است. نسبت‌های آب به پودر در محدودۀ ۰/۲۶ تا ۰/۴۸ بوده است که ۸۰٪ آن در محدودۀ ۰/۴۲–۰/۲۸ قرار می‌گیرد.

نسبت آب به پودر دارای اثرهای قابل توجهی بر روی خواص بتن‌های تازه و سخت شده است، اما در بتن خودتراکم، اغلب این خواص بتن تازه است که محدودکننده این نسبت در مخلوط می‌باشد. برخلاف آن، ترکیب پودر اثر مهمتری روی فرآیند هیدراسیون (و در نتیجه گرمای آزاد شده، مقاومت و غیره) دارد و لذا برای کنترل این خواص به کار می‌رود. از نظر درصد پودر، تفاوت روشنی را برای مخلوط‌های دارای VMA و بدون آن نشان می‌دهد. در هنگام توسعه بتن خودتراکم، مخلوط‌ها بسته به روش به دست آوردن لزجت خمیری مناسب و جلوگیری از جداشدگی، به سه دسته تقسیم می‌شدند [14، 15 و 35]:

۱- برپایه پودر، با نسبت‌های بسیار پایین آب به چسباننده، مقدار بالای پودر و مقادیر بالای فوق روان‌کننده.

۲- برپایه VMA، با نسبت‌های بالاتر آب به چسباننده و مقادیر قابل ملاحظه VMA.

۳- نوع مخلوط دارای مقادیر متوسط این دو (یعنی نسبت متوسط تا پایین آب به چسباننده با مقداری VMA).

مرور دامون [35] نشان داد که عمدۀ بتن‌های خودتراکم یا بر پایه پودر یا از نوع مخلوط بودند و فقط در موارد اندکی از پایۀ VMA استفاده شده است. در عین حال یک امتیاز استفاده از VMAها این است که حساسیت نسبت به برخی تغییرات مخلوط، مانند دانه‌بندی یا درصد رطوبت سنگدانه را کاهش می‌دهند.

ترکیبت ملات برحسب درصد حجمی‌ریزدانه‌ها بین ۰/۳۸ تا ۰/۵۴ متغیر بود که ۸۰ درصد از آن در محدودۀ ۵۲ـ۴۱ درصد قرار می‌گیرد. آنالیز اطلاعات نشان داد که کنترل درصد سنگدانه، خمیر و درصد ریزدانه ملات، مهم‌تر از کنترل درصد پودر و نسبت آب به پودر بوده است.

نان سو [10] نیز یک روش برای طرح اختلاط بتن‌های خودتراکم پیشنهاد داده است که در آن ابتدا مقدار سنگدانه مورد نیاز تعیین و سپس خمیر چسباننده داخل حفرات سنگدانه‌ها پر می‌شود تا از خواص جریان‌پذیری، سایر خواص خودتراکمی‌اطمینان حاصل شود. این روش ساده‌تر از روش‌های قبلی، از جمله روش اوکامورا، بود. نکته اساسی طرح اختلاط سو، این است که خمیر چسباننده به داخل قالبی ریخته شود که سنگدانه‌ها در آن به صورت غیر فشرده ریخته شده‌اند. سو ذکر می‌کند که طبق ASTM C۲۹ انتظار می‌رود که فضای خالی میان سنگدانه‌ها بین ۴۲ تا ۴۸ درصد حجمی‌باشد. مقاومت فشاری SCC به وسیله چسباندن سنگدانه‌ها به وسیله خمیر در حالت سخت‌شده تأمین می‌شود، در حالی‌که کارایی SCC باید به وسیله خمیر چسباننده در حالت تازه به دست آید. سو برای به دست آوردن مناسب خاصیت خودتراکمی‌از راهنمای ارائه شده توسط انجمن مهندسین عمران ژاپن [37] استفاده کرد. (جدول ۱)

جدول ۱: ویژگی‌های بتن خودتراکم، پیشنهادشده توسط انجمن مهندس عمران ژاپن [37]

کلاس قابلیت پرشدن بتن	۱	۲	۳
شرایط ساخت: حداقل فاصله بین تقویت‌کننده‌ها (mm)	۳۰–۶۰	۶۰–۲۰۰	≥۲۰۰
مقدار تقویت‌کننده‌ها (kg/m^3)	≥۳۵۰	۱۰۰–۳۵۰	≤۱۰۰
ارتفاع پرشدن آزمون جعبه U (mm)	≥۳۰۰(RankR۱)	≥۳۰۰(RankR۲)	≥۳۰۰(RankR۳)
حجم مطلق سنگدانه‌های درشت به ازای حجم SCC (m^3/m^3)	۰/۲۸–۰/۳	۰/۳۰–۰/۳۳	۰/۳۰–۰/۳۶
جریان‌پذیری: جریان اسلامپ (mm)	۶۵۰–۷۵۰	۶۰۰–۷۰۰	۵۰۰–۶۵۰
مقاومت به جداشدگی سنگدانه:			
زمان لازم برای جریان از قیف V (s)	۱۰–۲۰	۷–۲۰	۷–۲۰
زمان لازم برای رسیدن جریان اسلامپ به ۵۰۰ mm (s)	۵–۲۵	۳–۱۵	۳–۱۵

در روش سو ابتدا با استفاده از مفهوم درجه تراکم، مقادیر سنگدانه‌های ریز و درشت محاسبه می‌شود. انجمن معماران ژاپن [38] سه گروه ۱۵، ۲۰ و ۲۵ میلی‌متر را برای حداکثر اندازه سنگدانه مشخص می‌کند، که اندازهٔ ۲۰ میلی‌متر از همه رایج‌تر است. همچنین پیشنهاد شده است که مقدار سنگدانه‌های درشت حدود ۵۰ درصد وزن واحد متراکم شدهٔ خشک (طبق ASTM C۲۹) باشد. مقدار هوای لازم بستگی به دما دارد. به عنوان مثال در مناطق سردسیر حدود ۴/۵ درصد و در جاهایی که خطر یخزدگی و آب‌شدن وجود ندارد، حدود ۱/۵ درصد، بسته به روش ساخت و نوع و مقدار فوق‌روان‌کننده، می‌باشد. سپس مقدار سیمان باید محاسبه شود. برای تضمین جریان‌پذیری و مقاومت خوب به جداشدگی، مقدار پودرها نباید کم باشد. براساس راهنمای انجمن مهندسین عمران ژاپن [37]، حداقل مقدار سیمان که برای بتن‌های معمولی و دوام بالا باید استفاده شود، به ترتیب ۲۷۰ و ۲۹۰ کیلوگرم بر مترمکعب است. طبق سو [10] برای سیمان‌های تولیدی در تایوان، هر کیلوگرم سیمان، در بتن‌های خودتراکم و توانمند مقاومت فشاری معادل (MPa) ۰/۱۴ تأمین می‌نماید و از این عدد برای تعیین سیمان لازم استفاده شده است. برای محاسبه مقدار آب اختلاط لازم برای سیمان، مشابه با بتن معمولی، از ACI ۳۱۸ [39] استفاده شد. در مرحله بعد، مقادیر پودرها محاسبه می‌شود. مقادیر زیاد مصالح پودری باید اضافه شود تا جریان‌پذیری و خودتراکمی‌افزایش یابد، اما مقدار اضافی سیمان باعث افزایش هزینه‌ها و جمع‌شدگی ناشی از خشک شدن خواهد شد. به علاوه افت اسلامپ افزایش یافته و مقاومت فشاری نیز بیشتر از مقدار لازم طرح خواهد شد. بنابراین در یک طرح اختلاط مناسب بتن خودتراکم باید مقدار مناسب سیمان و نسبت آب به سیمان را برای رسیدن به مقاومت لازم تنظیم و در کنار آن برای رسیدن به خودتراکمی‌و مقاومت به جداشدگی از مواد پودری دیگر (غیر از سیمان) استفاده کرد. مقادیر فوق‌روان‌کننده و آب در مرحله بعدی تعیین و مخلوط‌های تجربی برای رسیدن به خواص مورد نظر خودتراکمی‌و مقاومت ساخته می‌شود.

ونگالا (Vengala) [40] با آزمایش‌های مختلف، روش ساده زیر را برای طرح اختلاط بتن خودتراکم ارائه کرده است:

۱- ابتدا یک اختلاط معمولی با استفاده از طرح اختلاط ACI یا هر روش پذیرفته شده دیگر با اسلامپ ۱۰۰ میلی‌متر بدون استفاده از فوق‌روان‌کننده تهیه می‌شود.

۲- با افزودن فوق روان‌کننده به طرح اختلاط فوق، یک اسلامپ ۱۶۰ تا ۱۸۰ میلی‌متر به دست می‌آید. در صورت مشاهده هرگونه جداشدگی یا آب انداختگی ظاهری، قسمتی از سنگدانه‌های درشت به وسیله سنگدانه ریز جایگزین شود. درصد جایگزینی اندک و حدود ۵٪ در نظر گرفته می‌شود.

۳- برای رسیدن به بتن خودتراکم، سنگدانه درشت با یک پودر ریز جایگزین می‌شود. برای این کار از افزایش‌های ۵ درصدی استفاده شود تا یک جریان اسلامپ ۵۰۰ تا ۷۰۰ میلی‌متر به دست آید. برای ارزیابی قابلیت عبور باید از آزمون‌های قیف V و جعبه L استفاده شود. آزمون‌ها و شاخص‌های مورد نیاز برای این ارزیابی بحث شده است [40].

۴- در صورت نیاز، افزودنی VMA نیز به مخلوط افزوده شود.

روش‌های اختلاط دیگری نیز توسط پژوهشگران بررسی و ارائه شده است. برخی از این طرح‌ها برای بررسی امکان استفاده از مصالح ارزان محلی ارائه شده‌اند [41 – 44]. برخی دیگر نیز مانند طرح اوزبای (Ozbay) [45] حاوی مطالعات عمیق‌تر با بررسی چندین پارامتر مختلف است. خیاط [46 و 47] برای تعیین نسبت مخلوط بتن خودتراکم، از مدل‌های آماری استفاده و روی آنها بحث نموده است. وی خواص خودتراکمی‌و مقاومت فشاری ۲۸ روزه مخلوط‌ها را بر اساس آزمون‌های متعدد و روش‌های آماری با سنجه‌های مقدار سیمان، نسبت آب به سیمان، غلظت‌های اصلاح‌کننده لزجت و فوق‌روان‌کننده و حجم سنگدانه‌ها همبسته کرده است. ضرایب همبستگی خوبی برای روابط به دست آمده و گزارش شده است [47]. اثرگذاری هر یک از سنجه‌ها نیز بررسی شده است.

۶- مواد فوق‌روان‌کننده و اصلاح‌کننده‌های لزجت

دستیابی به بتن خودتراکم بدون استفاده از مواد افزودنی شیمیایی جدید به این صورت امکان‌پذیر نبود. پژوهش‌های فراوانی روی اثر مواد افزودنی فوق‌روان‌کننده و اصلاح‌کننده‌های لزجت در بتن خودتراکم صورت گرفته است. اوکامورا [6] سه خاصیت زیر را برای فوق‌روان‌کننده لازم می‌شمارد: ۱- اثر پخش‌کنندگی بالا، ۲- حفظ اثر پخش‌کنندگی برای حداقل دو ساعت و ۳-حساسیت کم نسبت به تغییرات دما.

اوزکل و دوگان [36] اثر یک فوق‌روان‌کننده از نوع کوپلیمر N-Vinyl را بر روی خواص بتن‌های تازه و سخت‌شده مطالعه کردند. برای مخلوط‌های با نسبت‌های آب به سیمان بین ۰/۳ تا ۰/۴۵، قطر اسلامپ بین ۵۰۰ و ۷۴۰ میلی‌متر و مقاومت فشاری نمونه‌ها در ۲۸ روز، بین ۵۳ تا ۶۸ مگاپاسکال به دست آمد. اثر فوق‌روان‌کننده روی ایجاد تعادل بین قابلیت جریان‌یافتن و لزجت خمیر در بتن خودتراکم به وسیله اوشی [48] ارزیابی شد. آزمایش‌ها نشان داد که نسبت بین سرعت قیف V به مساحت جریان خمیر سیمان با یک مقدار ثابت فوق‌روان‌کننده تقریباً ثابت بوده، مستقل از نسبت آب به سیمان است. مقدار بالاتر فوق‌روان‌کننده منتج به نسبت پایین‌تری از سرعت قیف V به مساحت جریان شد. این نسبت به عنوان شاخصی برای تعیین اثر فوق‌روان‌کننده روی قابلیت جریان یافتن خمیر سیمان و لزجت آن، از نظر دست یافتن به خودتراکمی‌پیشنهاد شد. رابطه بین مقدار فوق‌روان‌کننده و اثر آن بسته به نوع سیمان یا افزودنی شیمیایی متغیر است. ثابت شده است که نسبت شاخص تغییر شکل به شاخص لزجت برای ملات در نسبت ثابت فوق‌روان‌کننده به پودر، مسقل از نسبت آب به پودر است [6].

سوزا و فلچر [49] عملکرد دو فوق‌روان‌کننده از نوع پلی‌کربوکسیلات اتر و نفتالین‌فرمالدئید سولفونه را در یک بتن ۴۰ مگاپاسکال با یکدیگر مقایسه و گزارش کردند. پلی‌کربوکسیلات اتر فقط به اندازهٔ یک سوم نفتالین‌فرمالدئید سولفونه برای رسیدن اسلامپ از ۴۵ به ۱۵۰ میلی‌متر نیاز بود و تأثیر بسیار بهتری نشان داد.

از طرف دیگر، مواد اصلاح کننده لزجت، پلیمرهای حلال در آب با وزن مولکولی بالا هستند که برای بالا بردن

لزجت آب استفاده می‌شوند. این ترکیبات باعث افزایش پیوستگی بتن تازه شده، زمینه جداشدگی و آب افتادگی را کاهش می‌دهند [51]. اگرچه استفاده از یک طرح اختلاط مناسب با مقدار کافی پودر می‌تواند نیاز به مواد اصلاح کننده لزجت را برطرف سازد، اما در برخی اوقات نیز استفاده از آنها ضروری یا مفید است. تاکادا (Takada) [50]، فراریس (Ferraris) [51]، خیاط (Khayat) [52] و دهن (Dehn) [53] اثر صمغ طبیعی ولان (Welan) (دارای پایه پلی‌ساخارید) بر روی بتن خودتراکم را در شرایط مختلف تحقیق کردند. افزودنی فوق باعث افزایش نسبت آب به سیمان شد و جریان اسلامپ ۳۰±۶۵۰ میلی‌متر و زمان قیف V برابر با ۲±۱۱ ثانیه بر اثر استفاده از ۰/۰۱ تا ۰/۰۲ درصد افزودنی اصلاح‌کننده لزجت و ۰/۰۲۵ تا ۰/۰۳۵ درصد فوق‌روان‌کننده (نسبت به کل مواد سیمانی) به دست آمد که برای دستیابی به خاصیت خودتراکمی‌کافی بود [50]. طبق نتایج دهن [53] پلیمر اصلاح‌کننده لزجت صمغ ولان و پلیمر موجود در فوق‌روان‌کننده، یکدیگر را محدود می‌کنند و این پدیده باعث به دست آمدن یک مقاومت بالاتر در برابر جداشدگی و غلظت بیشتر فوق‌روان‌کننده برای رسیدن به یک تغییر شکل مشخص می‌شود. همچنین رفتار چسبندگی در بتن خودتراکم بهتر از چسبندگی در بتن معمولی به دست آمد [53].

خیاط [54] افزودنی‌های اصلاح‌کننده لزجت برای محصولات پایه سیمانی را مرور کرده است. در این مرور، طبقه‌بندی، نوع و نحوهٔ فعالیت این اصلاح‌کننده‌ها بررسی شده و اثرات آنها بر بهبود خواص رئولوژیکی و چسبندگی سیستم‌های پایه سیمانی و نیز اثر روی خواص بتن تازه و سخت شده، بحث شده است. از جمله طبقه‌بندی‌های میل واگانام (Mailvaganam) [55]، و کاوایی [56] مرور شده است.

۷- حرارت هیدراسیون

بتن‌های خودتراکم نسبت به بتن‌های معمولی دارای مقادیر زیادی پودر هستند. برخی از پودرها خنثی و برخی دارای واکنش هیدراسیون هستند. اگر چه در منابع مختلف، استفاده از پودرهای خنثی برای جلوگیری از توسعهٔ گرمای زیاد در حین هیدراسیون توصیه می‌شود، اما نتایج تجربی نشان داده است که حتی پودرهای خنثی بر روی فرآیند هیدراسیون تأثیر می‌گذارد. بخصوص در مورد بتن‌های خودتراکم کارهای اندکی انجام شده و نیاز به مطالعات و تحقیقات بیشتر در مراجع تأکید شده است [57].

پوپ (Poppe) [57] آزمایش‌های ایزوترمال و آدیاباتیک هیدراسیون را برای ارزیابی حرارت تولیدی از دو نوع بتن خودتراکم انجام داده و نتایج آن را با دو نوع بتن معمولی مقایسه کرده است. آزمایش‌های ایزوترمال روی مخلوط سیمان و دو نوع پرکننده، پودرهای کربنات‌کلسیم و کوارتزیت، با سیمان‌های مختلف انجام شد. توزیع اندازه ذرات شامل سیمان و پودرهای معدنی، برای بالای ۹۰٪ حجمی، زیر ۵۰ میکرون بود. منحنی‌های شدت تولید حرارت برحسب J/g.h به عنوان تابعی از زمان برای آزمون‌های ایزوترمال ارائه شده است. برای تمام انواع سیمان، شدت تولید حرارت نمونه‌های خودتراکم دارای پرکننده پودرسنگ آهک بیش از نمونه معمولی بوده است. هرچه مقدار پودر سنگ آهک بیشتر شده، حداکثر شدت حرارت افزایش یافته و زمان رسیدن به آن نیز کوتاهتر شده است. در مورد نمونه‌های با پودر کوارتزیت، الگوی منحنی‌ها متفاوت است به طوری‌که اولاً در C/P=۰/۳۳ با مقدار آن در حالتی که فقط سیمان موجود باشد، مساوی شده است. یعنی با افزایش پودر کوارتزیت، ابتدا افزایش در شدت تولید حرارت ایجاد شده، و با ادامه افزایش کوارتزیت، مجدداً شدت تولید حرارت کاهش یافته است (شکل‌های ۶ و ۷). ثانیاً زمان رسیدن به حداکثر شدت تولید حرارت در نمونه‌های دارای کوارتزیت نسبتاً بیشتر از نمونه مرجع

می‌باشد. در نمونه‌های خودتراکم دارای پودرسنگ‌آهک، با افزایش پرکننده و نیـز بـا افـزایش دمـا، شـدت تولیـد حرارت افزایش یافت. نتایج آزمایش‌های آدیاباتیک نیز در کل نتایج آزمایش‌های ایزوترمال را تأیید کرد [57].

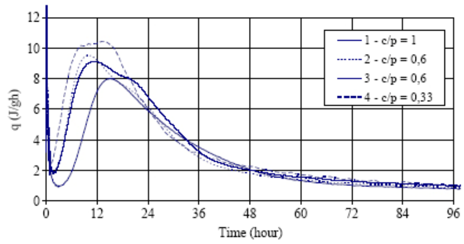

شکل ۶- شدت تولید گرما برای مخلوط سیمان CEM I 42.5 R و پرکننده سنگ آهک در ۲۰ °c

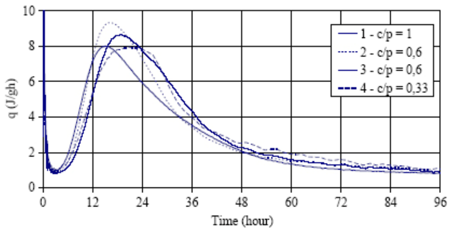

شکل ۷- شدت تولید گرما برای مخلوط سیمان CEM I 42.5 R و کوارتزیت در ۲۰ °c

در ادبیات علمی‌موضوع، اثر پرکننده‌ها و بخصوص پودرسنگ‌آهک در هیدراسیون سیمان، اغلب اوقات بـه اثـر آن در شدت تولید حرارت محدود شده است. برخی نویسندگان بر این قائل هستند که سینتیک گیرش بهبود می‌یابـد، زمان کما یا عدم فعالیت کاهش یافته و فرآیند هیدراسیون در ساعات اولیه تسریع می‌شـود. کـادری و دووال [58] پیشنهاد داده‌اند که دانه‌های پرکننده به عنوان سایت‌های هسته‌سازی غیرهمگن برای رسوب هیدراته‌هـای کـم و بیش بلوری‌شده، عمل کرده و از این طریق هیدارتاسیون را تسریع می‌کند.

در برخی منحنی‌های اصلی پوپ [57] یک پیک دوم نیز مشاهده شد. یک فرض بـرای علـت ظهـور ایـن پیـک، می‌تواند حضور C_3A با مقادیر بیش از ۱۲ درصد در سیمان باشد، ضمن اینکه تبدیل اترینجیت به منوسولفات نیز، حتی در سیمان‌های دارای C_3A پایین (حدود ۷/۵٪) باعث آن می‌شـود. ایـن تبـدیل اترینجیـت بـه منوسـولفات می‌تواند به علت وجود پرکننده پودر سنگ‌آهک فعال شود. نوع سیمان در اینجا نقش مهمی‌دارد، به طـوری‌کـه در سیمان CEM I 52.5 به علت بسیار ریز بودن سیمان، پیک دوم سـریعتر مـشاهده شـده و ایـن موضـوع بـر اثـر پرکننده، غلبه دارد. برای سیمان CEM I 52.5 HSR LA اصلاً پیک دومی‌مشاهده نشده است که به علت مقدار بسیار کم C_3A (۲/۵٪) تحلیل می‌شود. احتمال دیگر عدم خنثی بودن کامل پودر سنگ‌آهـک اسـت. بـه عبـارت دیگر فرض می‌شود که پودر سنگ‌آهک در واکنش هیدراسیون شرکت کرده و واکنش را بهبود مـی‌دهـد. در ایـن فرضیه، ابتدا تشکیل اترینجیت به علت حضور پرکننده تسریع شده و سپس تبدیل آن به منوسولفات تأخیر می‌افتد یا حتی در صورت حضور مقدار خیلی‌زیاد کربنات، حذف می‌شود. پس از ۳ روز منوکربوآلومینات در خمیـر هیدراتـه شده قابل کشف است.

یی (Ye) [59] اثر پودر سنگ آهک بر روی حرارت هیدراسیون در بتن خودتراکم را بررسـی کـرد. مطالعـات وی، نتایج پوپ را تائید می‌کند. وی دو نظریه در مورد علت بالا رفتن حرارت هیدراسیون با افزایش پودر سنگ آهک را مطرح کرد: ایجاد هسته‌های هیدراسیون برای C_2S و C_3S به وسیله ذرات پودر، و یا عدم خنثی بودن پودر سـنگ آهک و واکنش‌دهی آن. مطالعات میکروسکوپی فرضیه اول مبنی بر خنثی بودن پودر را تقویت می‌کند [59].

۸- مقاومت فشاری

رمضانیانپور [60] اثر افزایش پودر سنگ آهک در بتن خودتراکم با عیار سیمان ۴۵۰ کیلوگرم بر متر مکعب و نسبت آب به سیمان ثابت ۰/۴ را بررسی کرد. افزایش مقاومت فشاری، با افزایش پرکننده خنثی تنها تا حد کمی‌مشاهده شد. به طور متوسط با ۶۶٪ افزایش پرکننده، کمتر از ۵٪ افزایش مقاومت فشاری در سنین ۳، ۷ و ۲۸ روزه مشاهده شد. در مطالعات دامون [35] بر روی ۶۸ مورد خاص کاربردهای SCC، خواص مکانیکی مخلوطها نیز بررسی شد. در تمام مقالات مرور شده توسط وی، مقدار مقاومت فشاری ۲۸ روزه ارائه شده بین ۲۰ تا ۱۰۰ مگاپاسکال متغیر بوده‌اند که از این میان حدود ۸۰٪ طرح‌های اختلاط دارای مقاومت بالاتر از ۴۰(MPa) بوده‌اند. به عبارت دیگر، امکان تولید بتن خودتراکم با مقاومت‌های مشابه با انواع بتن‌های معمولی و مقاومت بالا وجود دارد. در اینجا بر خلاف بتن‌های معمولی، مقاومت اساساً به وسیله ترکیب چسباننده، و نه با نسبت آب به چسباننده، کنترل می‌شود. اجزای بتن خودتراکم بسیار مشابه با بتن توانمند است، اما تفاوت اصلی آنها در افزودنی‌های خاصی است که استفاده می‌شود. بنابراین انتظار می‌رود که مشخصات بتن سخت‌شدهٔ خودتراکم نزدیک و مشابه با بتن توانمند باشد.

۹- دوام

دوام سازه‌های بتنی شدیداً وابسته به نفوذپذیری لایه سطح بتن است، جایی که باید ورود مواد مهاجم (مانند کلرید، سولفات، آب، دی‌اکسیدکربن، اکسیژن، قلیایی‌ها، اسیدها و غیره) محدود شود. در عمل دوام بستگی به انتخاب مصالح، ترکیب بتن و نظارت دقیق در بتن‌ریزی، تراکم، پرداخت نهایی و عمل‌آوری دارد. عدم تراکم مناسب لایه سطحی، به علت مشکلات لرزاندن در فضاهای تنگ بین قالب و میلگردها و نظایر آن، عامل اصلی دوام ضعیف بتن تقویت‌شده، در معرض عوامل محیطی مهاجم است [14]. غلبه براین مشکل یکی از دلایل اصلی توسعه SCC در ژاپن بوده است.

در بتن‌های معمولی (یا رایج)، عمل تراکم به وسیله لرزاندن صورت می‌گیرد، که فرآیندی ناپیوسته است. در حالت لرزاندن داخلی، با فرض این که عملیات به خوبی صورت گیرد، حجم بتن در داخل محدوده‌ای که تحت تأثیر لرزاندن است، انرژی تراکم یکسانی دریافت نمی‌کند. به طور مشابه در عملیات لرزاندن خارجی، تراکم به دست آمده اساساً غیرهمگن است و در هر نقطه بستگی به فاصله از منبع لرزاندن دارد. در نتیجه بتنی با تراکم غیریکنواخت و بنابراین با نفوذپذیری‌های متفاوت به دست می‌آید. در چنین حالتی یک نوع ورود انتخابی عوامل مهاجم ایجاد می‌شود، به عبارت دیگر عوامل مهاجم با توجه به اندازهٔ خود، از منافذی که اجازه ورود به آنها را می‌دهد، به بتن نفوذ می‌کنند. عملیات ناقص یا ناصحیح لرزاندن باعث نواقصی مانند لانه زنبوری، جداشدگی، آب انداختن و غیره شده، اثرهای منفی بسیار بیشتری برروی نفوذپذیری و دوام خواهد داشت. انتظار می‌رود که بتن خودتراکم با خواص مناسب، عاری از این نواقص بوده و منجر به بتنی با نفوذپذیری پایین و یکنواخت شده، نقاط ضعف کمتری ایجاد شده و مواد مهاجم کمتر بتوانند اثرات مخرب بر جای بگذارند که به معنای دوام بیشتر می‌باشد.

مقالات اولیه گروه اوکامورا [۶۱] روی بتن خودتراکم (که ابتدا آن را بتن توانمند معرفی کرده بودند)، نشان می‌دهد که به احتمال زیاد، هدف اولیه آنها دستیابی به بتنی با دوام بالا و از جمله همراه با مقداری خواص خودتراکمی‌بوده است. اما به احتمال زیاد پس از اینکه همزمان آیتسین [9] بتن توانمند را معرفی کرد، آنها ادامه

مطالعات خود را بیشتر روی خواص خودتراکمی‌متمرکز نمودند.
با این وجود، نتایج تعدادی از پژوهش‌ها نشان می‌دهد که به علت بالا بودن مقدار پرکننده‌ها در بتن خودتراکم، برخی جنبه‌های دوام در این نوع بتن می‌تواند دچار ضعف‌هایی شود که بستگی به نوع پرکننده دارد. پرشون (Persson) [4] نشان داد که ورود کلرید به بتن‌های خودتراکم دارای پودر سنگ آهک به مقدار قابل توجهی بیشتر از بتن لرزانده شده است که عمدتاً به دلیل مقدار کمتر سیمان در بتن خودتراکم در مقایسه با بتن لرزانده شده است.
استفاده از مقادیر بالای پودرسنگ آهک، کربناسیون را شدت بخشیده و می‌تواند خواص دوام بتن خودتراکم را در مقایسه با بتن لرزانده شده کاهش دهد. در نظر گرفتن یک لایه محافظت کننده بتن معمولی لرزانده شده، روی میلگردهای تقویت کننده در سطح بیرونی بتن‌های خودتراکم در شرایط تهاجمی‌می‌تواند به دوام این نوع بتن کمک نماید. چنانچه بتن خودتراکم با مقدار پودر سنگ آهک زیاد در شرایط تهاجم سولفات تاماسیت (Thaumasite) قرار گیرد، خطر زیادی از نظر کاهش دوام وجود خواهد داشت، زیرا پودر سنگ آهک دارای سطح ویژه بالایی است که می‌تواند منجر به حل CO_2 در آب حفره‌ای، بخصوص در دمای پایین شود. در صورت تهاجم تاماسیت در بتن، ژل C-S-H در خمیر سیمان به یک تودهٔ کم و بیش متخلخل تبدیل شده، باعث تخریب کامل بتن می‌شود. در چنین حالتی نمی‌توان از تهاجم تاماسیت با استفاده از سیمان کم قلیایی مقاوم به سولفات، پیشگیری کرد.
پرشون نمونه‌های مختلف بتن خودتراکم و بتن معمولی لرزانده شده را برای ۹۰۰ روز در معرض محلول سولفات سدیم (g/l) ۱۸ در آب مقطر، قرار داد و دوام آنها را از طریق اندازه گیری وزن و مدول الاستیک، ارزیابی کرد. اثر روش اختلاط نیز، با در نظر گرفتن دو روش مختلف، ارزیابی شد. اول روش معمولی که در آن تمام مصالح خشک با آب برای ۵ دقیقه مخلوط شده و سپس فوق روان کننده اضافه شده و اختلاط برای ۲/۵ دقیقه دیگر ادامه یافت. در روش دوم، اختلاط تمام مصالح به جز پودر سنگ آهک برای ۰/۵ دقیقه و سپس اضافه کردن پودرسنگ آهک و اختلاط بعدی برای ۲/۵ دقیقه مورد استفاده قرار گرفت. روش دوم موفقیت آمیز نبود.
آزمایش‌ها نشان داد که به علت حساسیت بیشتر پودرسنگ آهک به تهاجم سولفات (درمقایسه با سیمان)، در صورت استفاده از بتن خودتراکم با مقادیر زیاد پودرسنگ آهک در مناطق دارای ظرفیت تهاجم سولفات، دوام بتن می‌تواند کاهش یابد. بنابراین بهتر است که در مناطقی که مقدار سولفات در آب‌های زیرزمینی نامعلوم است، از بتن‌های خودتراکم با مقدار بالای پودرسنگ آهک استفاده نشود.
ایراسار (Irassar) [62] اخیراً تهاجم سولفات بر روی مصالح سیمانی حاوی پرکننده سنگ آهک را مرور نموده است. مطالعات آزمایشگاهی روی نمونه‌های خمیر، ملات و بتن با ترکیبات مختلف در برابر تهاجم محلول‌های سولفات سدیم و سولفات منیزیم با غلظت‌های مختلف مرور شده است. پودر سنگ آهک می‌تواند دوام بتن در برابر هجوم سولفات بیرونی را کاهش دهد. در این رابطه، توصیه‌های گروه متخصصین تاماسیت [63] استفاده از سیمان‌های حاوی پودر سنگ آهک در جاهایی که آب زیرزمینی حاوی بیش از ۰/۴ گرم بر لیتر یون سولفات باشد، منع نموده است. مکانیسم و شیمی‌تشکیل تاماسیت و خوردگی ناشی از آن در بتن در مراجع 64 تا 66 بحث شده است. اگرچه در بین کارهای مرور شده توسط ایراسار، بتن خودتراکم نیز وجود داشته است، اما تمرکز بحث وی روی اثر پودر سنگ آهک در دوام در برابر سولفات بوده و بحث دقیقی روی ترکیبات خودتراکم به طور خاص

ارائه نکرده است. ترگارد و کالینووسکی (Trägård and Kalinowski) [67 و 68] روی دوام بتن خودتراکم با پودر سنگ آهک در برابر محیط‌های دارای سولفات و یون منیزیم تحقیق کردند. نمونه‌های دارای پرکننده سنگ آهک دارای دوام کمتری بودند و مخلوط‌های با $50\ kg/m^3$ پودر سنگ آهک ضعیف‌تر از مخلوط‌های با kg/m^3 ۱۰۰و یا بدون آن بود. پس از دوره‌های آزمون (۲۲ و ۴۸ ماه) نمونه‌ها دچار تخریب‌ها و پوستگی‌های سطحی شده و ترکیبات تاماسیت، گچ و اترنجیت در آنها یافت شد.

فریبرت و اشتارک (Friebert and Stark) [69] نیز روی دوام نمونه‌های خودتراکم دارای $200 kg/m^3$ پودر سنگ آهک مطالعه نمودند. نمونه‌ها برای ۴ ماه در معرض محلول سولفات ۳۳/۸ گرم بر لیتر قرار داده شد. نتایج مقاومت کششی نسبی روی نمونه‌های خودتراکم و شاهد مشابه با هم و معادل تقریباً ۰/۷ به دست آمد که به نفوذناپذیری خوب نمونه نسبت داده شد.

نفوذپذیری بیشتر و کمتر نسبت به بتن‌های رایج، هر دو برای بتن خودتراکم گزارش شده است. ژو (Zhu) [7069] دوام بتن خودتراکم را در مقایسه با بتن رایج با مقاومت مشابه، از طریق اندازه‌گیری نفوذپذیری اکسیژن، جذب مویینه و نفوذ کلرید ارزیابی کرده است. وی دو رده C-40 و C-60 را با مقاومت‌های مشخصه ۴۰ و ۶۰ مگاپاسکال، برای آزمونه‌های مکعبی، تهیه کرد. برای هر رده، سه سری متفاوت از مخلوط‌های SCC و دو سری نمونه‌های بتن رایج لرزانده شده، تهیه شد. طرح اختلاط‌های بتن خودتراکم، شامل پودر سنگ‌آهک، خاکستر بادی و یکی هم بدون پودر و فقط با اصلاح‌کننده لزجت بود. برای طرح اختلاط از آزمایش‌های حدس و خطا یا از روش اروپایی استفاده شد. برای نمونه‌های مرجع (بتن رایج) نیز دو نوع نمونه، یکی با سیمان پرتلند و دیگری با سیمان پرتلند و خاکستر بادی با کارایی متوسط (اسلامپ= ۵۰ـ۸۰mm) با استفاده از روش DOE [71] تهیه شد. جریان اسلامپ نمونه‌های SCC و مقدار اسلامپ نمونه مرجع C۶۰ (که دارای خاکستر بادی بود) با تنظیم میزان مصرف فوق‌روان‌کننده تنظیم شد. پودرسنگ آهک بسیار ریز (۳۰ µ>۹۸٪ و ۲ µ>۲۰٪) با خلوص بسیاربالا (۹۹/۳٪ $CaCO_3$) و خاکستر بادی آسیا شده مطابق با استاندارد BS۳۸۹۲ـ۱ به عنوان پودر استفاده شدند. از یک نوع فوق‌روان‌کننده تجاری برای رسیدن به جریان اسلامپ (mm) ۶۵۰ـ۶۰۰ برای بتن‌های خودتراکم بهره‌گیری شد. اصلاح‌کنندهٔ لزجت از نوع صمغ ولان در آن نوع SCC که پودر نداشت، استفاده شد. نمونه‌های مکعب (mm)۱۵۰ و استوانه‌ای Φ۱۵۰×۳۰۰ تهیه شد. نمونه‌ها پس از ۲۴ ساعت از قالب بیرون آورده شده و مطابق استاندارد BS عمل‌آوری شدند. پس از ۷ روز، آزمونه‌های (mm)Φ۱۰۰ از نمونه‌های استوانه‌ای مغزه‌گیری شده، مقطع‌های ۱۵ تا ۲۰ میلی‌متر از دو سرآنها جدا شد. مغزه باقی‌مانده برای آزمایش نفوذپذیری، قابلیت انتشار (diffusivity)، نفوذپذیری اکسیژن، جذب مویینه آب و قابلیت انتشار کلرید استفاده شد. نتایج نفوذپذیری اکسیژن نشان داد که برای نمونه‌های (MPa)۴۰، هر سه نمونه خودتراکم نفوذپذیری کمتری از مخلوط‌های رایج دارند. بخصوص طرح اختلاط‌های خودتراکم که درآنها پودرهای سنگ‌آهک و PFA استفاده شد، ضرایب نفوذی در حد فقط ۳۰ تا ۴۰ درصد طرح‌های مرجع داشتند. نمونه‌های SCC با افزودنی اصلاح‌کننده لزجت که دارای پودر نبودند، به طور قابل ملاحظه‌ای دارای ضریب نفوذپذیری بالاتری بودند. نتایج قابلیت جذب آب نشان داد که در مقاومت (MPa) ۴۰، جذب به طورقابل ملاحظه‌ای در تمام نمونه‌های SCC کمتر از نمونه‌های مرجع بود. درمقاومت (MPa) ۶۰، نمونه مرجع دارای خاکستر بادی، ضریب جذبی تقریباً مشابه با نمونه‌های SCC داشت.

رمضانیانپور [60] آزمون نفوذپذیری یون کلراید طبق استاندارد ASTM C۱۲۰۲ را روی چند نمونه بتن خودتراکم

انجام داد. نتایج حاکی از تأثیر مثبت افزایش پرکننده مصرفی در کاهش نفوذپـذیری یـون کلرایـد بـود. بـه طـور متوسط با ۶۶ درصد افزایش پرکننده مصرفی، ۳۶ درصد نفوذپذیری یون کلراید در نمونه‌ها کاهش یافـت. آهنـگ تغییرات نفوذ یون کلراید نسبت به پرکننده مصرفی تقریباً خطی بود. نتایج رمضانیانپور و ژو تفاوت‌هـایی را نـشان می‌دهند، اما روش مقایسه آنها نیز متفاوت بوده است، زیرا مقاومت فشاری ۲۸ روزه نمونه‌های مرجع و خـودتراکم ساخته شده توسط رمضانیانپور، به طور قابل توجهی متفاوت بوده اسـت. وی نـشان داد کـه بـا افـزایش مقاومـت فشاری نمونه‌ها نفوذپذیری آب و یون کلراید کاهش می‌یابد، که این کاهش با تقریب نسبتاً خوبی خطی است.

در کل باید گفت با توجه به جدید بودن بتن خودتراکم، هنوز نیاز به بررسی‌ها و تحقیقات بسیار بیـشتری بـر روی جوانب متعدد دوام آن وجود دارد.

۱۰- مقاومت در برابر آتش

یکی از مشخصات مهم بتن در ساختمان‌ها، مقاومت آن در برابر آتش اسـت. مقاومـت لازم در برابـر آتـش بـرای اجزای ساختمان توسط مقررات و آیین‌نامه‌های ساختمانی تعیین می‌شود [72]. در مورد مقاومت بتن‌های معمـولی در برابر آتش پژوهش‌ها و آزمایش‌های بـی‌شـماری انجـام شـده اسـت و نتـایج آن در دسـترس اسـت. هرمتـی Harmathy [۷۳-75] تغییرات خواص مختلف بتن‌های معمولی و سبک در شرایط آتـش‌سـوزی و دمـای بـالا را بحث کرده است. نتایج آزمون‌های آتش، تفاوت‌های قابل توجهی را بین رفتـار بـتن‌هـای معمـولی بـا بـتن‌هـای مقاومت بالا (HSC)، توانمند (HPC) و خودتراکم در دمای بالا نشان داده است. تفاوت‌های مهمـی‌نظیـر مقـادیر مختلف پودر، مقدار تراکم و وجود مواد افزودنی، باعث می‌شود تا بتن‌های خودتراکم دارای خواص بسیار متفـاوتی از سایر بتن‌ها در برابر آتش باشد.

یکی از دلایل مهم شکست اجزای بتنی در برابر آتش، پدیـده پوسـته‌شـدن اسـت. پوسـته‌شـدن بـتن در شـرایط آتش‌سوزی، به معنای جدا شدن تکه‌های کوچک و بزرگ بتن از سطح آن در دمای بالا است که در ایـن صـورت پوشش بتنی روی میلگردهای فولادی تقویت نیز از بین می‌رود. این موضوع منجر به گرمایش مستقیم میلگردهـا شده و باعث کاهش سریع ظرفیت باربری بتن می‌شود. گاهی اوقات ابعاد پوسته‌شدن بسیار وسیع است و شکـست فوری سازه را موجب می‌شود. زمینه پوسته‌شدن در بتن‌های متراکم (مانند بتن‌های HPC، HSC و SCC) بـسیار متفاوت از بتن‌های معمولی است. ساختار متراکم در بتن باعث می‌شود تا انتقـال بخـار و رطوبـت در آن دشـوارتر شده و فشار بخار بالایی در نزدیکی سطح بتن ایجاد شود. این به معنای خطر بیشتر پوسته‌شدن در مقایسه با بـتن معمولی است. در بتن معمولی بخار آب با سادگی بیشتری می‌تواند به سطح بتن مهاجرت کنـد و از طـرف دیگـر، رطوبت به قسمت‌های داخلی منتقل شود. اما در نهایت درصد رطوبت می‌تواند بسیار بالا رفته و یک پوسـته‌شـدن انفجاری در ۲۰ تا ۴۰ میلی‌متری سـطح بـتن رخ دهـد. آنـدربرگ [7676] از سـه مکانیـسم اصـلی فـشار بخـار، تنش‌های حرارتی و تغییرات ساختاری سنگدانه‌ها به عنوان عوامل اصلی پدیده پوسته‌شدن نـام مـی‌بـرد. هـرتس [77] چندین عامل دیگر را نیز نام برده و بحث کرده است.

تفاوت‌های بین بتن‌های دارای تراکم بالا و معمولی از نظر رفتار در برابر آتش به میزان زیادی وابسته بـه خـواص ریزساختار آنها است. با این وجود اغلب پژوهش‌های آتش روی آزمونه‌های مقیاس بزرگ متمرکز شده، فقط تعداد اندکی از پژوهش‌ها به پدیده‌های تغییر ریزساختار، مانند تغییرات خلل و فرج، توزیع اندازهٔ منفذها و اتصال منفـذها

پرداخته‌اند. به این دلیل یی (Ye) [78 و 79] تغییرات ریزساختار چند نوع خمیر سیمان، بـا الیـاف پلـی‌پـروپیلن و بدون آن، بر اثر افزایش دما را بررسی کرده است. آزمونه‌های خمیر سـیمان بـتن خـودتراکم، خمیـر سـیمان بـتن توانمند و خمیر سیمان سنتی با نسبت‌های اختلاط یکسان با بتن‌های مربوطه، امـا بـدون سـنگدانه، سـاخته شـد. مخلوط‌های خمیر سیمان SCC استفاده شده در این مطالعه با سـیمان پرتلنـد نـوع CEM I ۵۲/۵ بـا پودرسـنگ آهک اضافه شده به عنوان پرکننده تهیه شد. نتایج این پژوهش، مفید بـودن الیـاف PP بـرای بهبـود رفتـار بـتن خودتراکم در برابر آتش را نشان داد. خواص ریزساختار، یعنی خلل و فرج، توزیع اندازهٔ منفذ و توزیع فاز (تخلخـل، CSH، $Ca(OH)_2$ و مغزه هیدراته نشده سیمان) با اسـتفاده از تخلخـل‌سـنج جیـوه‌ای و میکروسـکوپ الکترونـی روبشی (SEM) بررسی شد. تخریب شیمیایی خمیر سیمان خودتراکم در دماهای مختلف به وسیله آنـالیز حرارتـی وزن‌سنجی (TG) تعیین شد. اثر مقدار الیاف پلی‌پروپیلن روی تغییر ریزساختار بررسی گردید. نتایج تجربـی خمیـر خودتراکم با خمیرهای توانمند و سنتی مقایسه شد. همه نمونه‌ها در معرض دمای بالا در یک کوره الکتریکـی بـا سرعت گرم شدن ۱۰ درجه سلسیوس بر دقیقه قرار داده شدند. حداکثر دمای به دست آمده در کوره ۹۵۰ °C بـود. هیچ‌یک از آزمونه‌ها نشانه‌ای از پوسته‌شدن انفجاری نشان ندادند، اما ترک‌های زیادی در آنها مشاهده شـد. عـدم پوسته‌شدن نمونه‌ها به دلیل اندازه کوچک آزمونه‌ها و مهمتر از آن سرعت کم افزایش دما است. قابـل ذکـر اسـت که در آزمایش‌های استاندارد آتش، دما در دقایق اول با سرعت بسیار زیاد افزایش و در کمتر از ۲۰ دقیقه بـه ۸۰۰ درجه سلسیوس می‌رسد. مشاهده شد که نمونه‌های خمیر خـودتراکم الگـوی متفـاوتی در مقایـسه بـا خمیرهـای توانمند و سنتی نشان می‌دهد.

قبلاً نیز تحقیقات زیادی استفاده از الیاف پلی‌پروپیلن را موفقیت‌آمیز نشان داده بود [80–85]. الیاف پلی‌پروپیلن در ۱۷۰ °C ذوب می‌شوند، درحالی‌که ترکیدن بتن در دمای بین ۱۹۰ °C تا ۲۵۰ °C رخ مـی‌دهـد [86]. ذوب شـدن الیاف و جذب جزئی آن توسط خمیر سیمان باعث می‌شود تا مسیرهایی بـرای عبـور گـاز ایجـاد شـود. بـا ایجـاد شبکه‌ای از این مسیرها، گازهای ایجاد شده در داخل بتن، مـی‌توانـد بـه بیـرون راه یافتـه و از بـالا رفـتن فـشار جلوگیری نماید.

استفاده از الیاف پلی‌پروپیلن برای جلوگیری از ترکیدن بتن‌های توانمند در دماهای بالا، اولین بـار در سـال ۱۹۸۲ توسط هربرت کرشنر (Herbert Krechner) پیشنهاد شده بود، اما هرتس [7777] در آن هنگام، آن را اساساً بـه عنوان یک موضوع تحقیقاتی رد کرد، زیرا بنا به نظر وی اولاً چگونگی خروج فاز مذاب پلی‌پروپیلن از محل آن در بتن جای تردید داشته و ثانیاً با توجه به تئوری‌های موجود، ترکیدن انفجاری از ریزساختار بتن آغاز مـی‌شـود کـه بسیار کوچکتر از فاصله بین الیاف است. معهذا تجربیـات مختلـف، سـودمندی اسـتفاده از الیـاف پلـی‌پـروپیلن در جلوگیری از ترکیدن بتن را نشان داده است و عقیده کلی بر این است که حفرات به جـای مانـده از ذوب شـدن و تجزیه شدن الیاف پلی‌پروپیلن باعث ایجاد حفرات اضافی در بتن می‌شود کـه فـضاهای اضـافی بـرای فـاز بخـار مهاجرت کرده را ایجاد می‌کند.

پژوهش‌ها نشان داده است که در نسبت آب به پودر یکسان، خلـل و فـرج و توزیـع انـدازه منافـذ خمیـر سـیمان خودتراکم شبیه به خمیر سیمان توانمند است. بنابراین به نظر می‌آید که اگر بتن خودتراکم در معرض دماهای بالا قرار گیرد، احتمالاً باید خطر پوسته‌شدن و شکست آن مشابه با بـتن توانمنـد باشـد. بـا ایـن وجـود مـشاهدات بـا میکروسکوپ الکترونی SEM و اندازه‌گیری‌های DTA / TGA نشان داد که ترکیب فاز خمیرهـای خـودتراکم و

توانمند متفاوت است [79].

وجود پودرهای پرکننده، مانند پودر سنگ آهک، از موارد مهمی‌است که باعث تفاوت رفتار بتن خودتراکم در برابر آتش با سایر بتن‌ها می‌گردد [62]. بوستروم [**Error! Reference source not found.**] خواص برخی بتن‌های خودتراکم در برابر آتش را بررسی کرده است. شانزده نمونه بتنی شامل ۴ نمونه معمولی و ۱۲ نمونه خودتراکم تحت آزمون مقیاس بزرگ مطالعه شد. نمونه‌ها به شکل مکعب مستطیلی با ابعاد ۰/۲ × ۰/۲ × ۲ m ساخته و به نحوی در کوره قرار داده شدند که از ۴ طرف جانبی در معرض دمای بالای کوره باشند. نمونه‌ها پیش‌تنیده شدند و بار مکانیکی دیگری در حین آزمون روی آنها وارد نشد. نسبت‌های آب به سیمان معادل ۰/۴، ۰/۵۵ و ۰/۷ بررسی شد. کلیه نمونه‌ها برای ۶ ماه، تعدادی در زیر آب و تعدادی دیگر در هوا، عمل‌آوری شدند. برای نمونه‌های خودتراکم از دو نوع پرکننده، یکی پودر سنگ آهک و دیگری پودر شیشه، استفاده شد. به برخی از نمونه‌ها الیاف پلی‌پروپیلن با مقادیر ۲ و ۴ کیلوگرم بر متر مکعب افزوده شد. ستون‌ها در معرض دو رژیم آتش هیدروکربنی و استاندارد قرار داده شدند.

تمام نمونه‌ها دچار پوسته‌شدگی شدند که موارد زیر از این نظر قابل ذکر است:

۱- پوسته‌شدگی برای تمام نمونه‌ها در همان دقایق ابتدایی (از ۲ تا ۷ دقیقه) رخ داد و بین ۳ تا ۳۴ درصد کاهش وزن در نمونه‌ها مشاهده شد.

۲- مقدار پوسته‌شدگی نمونه‌های خودتراکم بسیار بیشتر از نمونه‌های معمولی بود.

۳- با افزایش نسبت آب به سیمان، پوسته‌شدگی در نمونه‌ها کاهش نشان داد.

۴- با افزایش الیاف، پوسته‌شدگی در نمونه‌ها کاهش نشان داد.

۵- رفتار نمونه‌های پوسته‌شدگی حاوی پرکننده شیشه بهتر از نمونه‌های حاوی پودر سنگ آهک بود.

۶- بدترین رفتار از نظر پوسته‌شدگی، مربوط به نمونه‌های حاوی پودر سنگ آهک با نسبت آب به سیمان ۰/۴ بود.

کلاً به علت جدید بودن موضوع بتن خودتراکم، هنوز تعداد اندکی کارهای پژوهشی بر روی خواص این نوع بتن در برابر آتش صورت گرفته است، که این کارها نیز نیاز به تحقیقات بیشتر بر روی رفتار و مقاومت این بتن در برابر آتش را نشان می‌دهد. آزمایش‌های محدود وجود زمینه پوسته‌شدگی بسیار بیشتر بتن خودتراکم نسبت به بتن‌های معمولی را نشان داده است. اثرات پرکننده، سن بتن، وجود الیاف، نوع الیاف، مقدار رطوبت، شرایط بارهای روی بتن و مسائل متعدد دیگر برای شناخت رفتار بتن خودتراکم در برابر آتش نیاز به تحقیقات وسیع دارد.

نتیجه‌گیری

۱- بتن خودتراکم، به علت خواص عالی آن در بسیاری از زمینه‌ها، شامل هر دو گروه بتن‌های پیش‌ساخته و درجا، گسترش بیشتری در صنعت ساختمان می‌یابد. برای دستیابی به خودتراکمی‌لازم است تا با استفاده از مواد افزودنی و پودرهای معدنی، تعادل مناسب بین جریان‌پذیری و لزجت بتن برقرار نمود.

۲- چگالی تراکم، مفهوم مهمی‌در دستیابی به خودتراکمی‌است. افزایش چگالی تراکم، مقاومت و کارایی بتن را بهبود می‌دهد و قابلیت جریان یافتن خمیر بهتر می‌شود. همچنین چسبندگی خمیر سیمان بهبود یافته، در نتیجه مقاومت بتن در برابر جداشدگی افزایش می‌یابد. این مشخصات، به دستیابی به خاصیت خودتراکمی‌کمک زیادی می‌نماید. استفاده از پودرهای بسیار ریز و با اندازه‌های متفاوت در طرح

اختلاط‌های خودتراکم باعث می‌شود تا چگالی تراکم به نحو قابل توجهی بهبود یافته و در دستیابی به دو خاصیت جریان‌پذیری و عدم جداشدگی تأثیر به سزایی دارد. محدودیت درصد حجمی‌سنگدانه‌های درشت و ریز نیز، علاوه بر تنظیم قابلیت عبور از بین موانع، با مفهوم چگالی تراکم قابل تفسیر است. هر چه مقدار سنگدانه‌های ریز افزایش یابد، مقدار آب آزاد بیشتری برای رسیدن به خودتراکمی‌لازم است.

۳- حجم زیادی از پودرهای معدنی در بتن‌های خودتراکم استفاده می‌شود که اثرهای متعددی روی خواص دارد. حتی پودرهای خنثی مانند پودر سنگ آهک باعث افزایش حرارت هیدراسیون می‌شوند. مقایسه پژوهش‌های افراد مختلف نشان می‌دهد که تئورهای تبدیل ذرات این پودرها به هسته‌های واکنش هیدراسیون قوت بیشتری از احتمال واکنش‌پذیر بودن آنها دارند. پودرها اثر بسیار مهمی‌نیز بر روی دوام به سولفات، کربناسیون و مقاومت در برابر آتش دارند. پودر سنگ آهک می‌تواند باعث کاهش قابل ملاحظه دوام بتن خودتراکم در برابر سولفات شود که به علت تشکیل ترکیباتی نظیر گچ، اترنجیت و تاماسیت است. مقاومت بتن خودتراکم در برابر آتش، متفاوت از بتن‌های معمولی و حتی توانمند است که پودرها در این میان نقش مهمی‌دارند. حساسیت بیشتر بتن‌های خودتراکم نسبت به بتن معمولی باعث می‌شود تا مقاومت این نوع بتن در برابر آتش سریعتر کاهش یافته و استفاده از نتایج آزمون و تجربیات موجود روی بتن معمولی برای این نوع بتن را ناممکن می‌سازد.

۴- به علت جدید بودن بتن خودتراکم، حوزه‌های وسیعی از پژوهش‌ها بر روی آن نیاز است. نیاز به حجم بالای پودر، حوزه‌های وسیعی از پژوهش را برای این نوع بتن باز می‌نماید که از جمله استفاده از انواع پودرهای معدنی محلی و ضایعات صنایع را می‌توان نام برد. بسیاری از خواص بتن خودتراکم متفاوت از بتن‌های معمولی و توانمند است و خصوصاً جنبه‌هایی نظیر دوام به شرایط تهاجمی‌و مقاومت در برابر آتش، بسته به طرح اختلاط و مواد افزودنی پودری مورد استفاده نیاز به پژوهش‌های دقیق دارد.

مراجع

۱. فروغی‌اصل، ع.، فامیلی، هـ «بررسی ویژگی‌های عمومی‌بتن خود تراکم و دلایل گسترش آن در دنیا». شکرچی‌زاده، م.، لیبر، ن. (تدوین‌کنندگان)، مجموعه مقالات اولین کارگاه تخصصی بتن خودتراکم، اسفند ۱۳۸۵، ص ۱-۱۲.

2. Horta, A., "Evaluation of Self-Consolidating Concrete for Bridge Structure Applications", Georgia Institute of Technology, School of Civil & Environmental Engineering, URI:http://hdl.handle.net/1853/7159, 2005.

3. Bartos, P.J.M., Gibbs, J.C. and Zhu, W. "Uniformity of in situ properties of Self-Compacting Concrete in full scale structural elements". Cement and Concrete Composites, 2001.

4. Ozawa K., Maekawa, K., Kunishima, M. and Okamura, H., "Development of High Performance Concrete Based on the Durability Design of Concrete Structures". Proceedings of the 2nd East-Asia and Pacific Conference on Structural Engineering and Construction (EASEC-2), Vol. 1, pp. 445-450, January 1989.

5. Persson, B. "Sulphate resistance of self-compacting concrete". Cement and Concrete Research, Vol. 33, 2003, 1933-1938.

6. Okamura, H., Ouchi, M. "Self-compacting high performance concrete". Concrete construction, Construction Research Communications Ltd., pp. 378-383, 1998.

7. Okamura, H., Ouchi, M. "Self-compacting concrete". Journal of Advanced Concrete Technology, Vol. 1, No. 1, 2003, 5-15.
8. Bartos, P. J. M. and Grauers, M. "Self-Compacting Concrete". Concrete, Vol. 33, No.4, pp. 9-14, 1999.
9. Gagne R., Pigeon M. & Aitcin P. C. "Deicer salt scaling resistance of high performance concrete". Klieger, P. (Ed.), Symposium on Performance of Concrete, Nov. 1989. ACI Report SP-122. Detroit, MI: American Concrete Institute.
10. Aitcin, P. C. "High Performance Concrete". E&FN SPON, London, 1998.
11. Su, N., Hsu, K. Ch., Chai, H. W. "A simple mix design method for self-compacting concrete". Cement and Concrete Research, 31 (2001), 1799–1807.
12. Henry, G. R. "ACI defines high performance concrete". Concrete International, 21(2), 56-57, 1999.
13. Ozawa K., et. al. "Role of materials on the filling capacity of fresh concrete". Proceedings, 4th CANMET & ACI international Conference on Fly Ash, Silica Fume, Slag and Natural Pozzolans in Concrete, Istanbul, May 1992, 121-137.
14. Okamura H. Lecture for 1996 self-compacting high-performance concrete. Concrete international, 1997 19(7): 50-54.
15. The European Federation of Specialist Construction Chemicals and Concrete Systems (EFNARC). "The European Guidelines for Self-Compacting Concrete, Specification, Production and Use", 2005.
16. Ouchi, M., Nakamura, S., Osterberg, Th., Hallberg, S., and Lwin, M., "applications of self-compacting concrete in Japan, Europe and The United States", ISHPC, 2003.
17. Canadian Precast/Prestressed Concrete Institute, www.cpi.ca.

۱۸. شکرچی‌زاده، م. و همکاران. "خصوصیات بتن خودتراکم مورد استفاده در پروژه توسعه حرم حضرت معصومه (س)". شکرچی‌زاده، م.، لیبر، ن. (تدوین‌کنندگان)، مجموعه مقالات اولین کارگاه تخصصی بتن خودتراکم، اسفند ۱۳۸۵، ص ۲۸۵-۲۹۴.

۱۹. شاهیدخت، غ. و جبروتی، م.ر. "طرح اختلاط بتن خودتراکم پروژه تونل بزرگراه رسالت". شکرچی‌زاده، م.، لیبر، ن. (تدوین‌کنندگان)، مجموعه مقالات اولین کارگاه تخصصی بتن خودتراکم، اسفند ۱۳۸۵، ص ۲۹۵-۳۰۴.

20. Wong, H. H. C., Kwan, K. H. "Packing density: a key concept for mix design of high performance concrete". The University of Hong Kong.
21. BS 812-2. "Testing aggregates. Methods for determination of density". British Standard Institute, 1995.
22. Stroeven, P., Stroeven, M. "Assessment of packing characteristics by computer simulation". Cement and Concrete Research, Vol. 29, 1999, 1201–1206.
23. Feng, N.Q., Shi Y.X., Hao T.Y. "Influence of ultrafine powder on the fluidity and strength of cement paste". Advance in Cement Research, Vol.12, No.3, 2000, pp89-95.
24. Kwan, A. K. H. "Use of condensed silica fume for making high strength, selfconsolidating concrete", Canadian Journal of Civil Engineering, Vol.27, No.4, 2000, pp620-627.
25. Obla, K. H., Hill, R.L., Thomas, M. D. A., Shashiprakash, S.G., Perebatova, O. "Properties of concrete containing ultra-fine fly ash". ACI Materials Journal, Vol.100, No.5, 2003, pp 426-433.
26. Trägårdh, J. "Microstructural features and related properties of selfcompacting concrete". in: Skarendahl, A., Petersson, Ö. (Eds.), Proceedings of the 1st

International RILEM Symposium on Self-Compacting Concrete, Stockholm, 1999, 175-186.
27. Mehta, P. K., Aïtcin P. C. "Microstructural basis of selection of materials and mix proportions for high-strength concrete". ACI Special Publication SP-121, 1990, pp 265-86.
28. Kwan, A. K. H., Cai, Y. B., Chan, H. C. "Comparison of granitic and volcanic aggregates for making high strength concrete in Hong Kong". HKIE Transactions, Vol.2, No.2, 1995, pp 1-8.
29. Leeman, A., Münch, B., Gasser, P., Holzer, L. "Influence of compaction on the interfacial transition zone and the permeability of concrete". Cement and Concrete Research, 36, 2006, 1425–1433.
30. De Larrard, F. "Concrete Mixture Proportioning: A Scientific Approach, E&FN Spon, London, 1999.
31. Yu, A. B., Feng, C.L., Zou, R. P., Yang, R. Y. "On the relationship between porosity and interparticle forces". Powder Technology, Vol.130, 2003, 70-76.
32. Okamura, H., Ozawa, K. "Mix-design for self-compacting concrete". Concrete Library of JSCE, 107-120, 1995.
33. Takeshita, H., Sahara, H., Yokota, N. "Fundamental study on super flowing concrete free of compaction". Concrete Research and Technology, Vol. 1, No. 1, 1990 (in Japanese).
34. Yoshida, T. "Production of maximum strength concrete". Journal of JSCE, vol. 26, No. 11, 1940.
35. Nagamoto, N., and Ozawa, K. "Mixture proportions of self-compacting high performance concrete". ACI International, SP-172, 1997, 623-636.
36. Domone, P.L. "Self-compacting concrete: An analysis of 11 years of case studies". Cement & Concrete Composites, 28, 197–208, 2006.
37. Ozkul, M. H., Dogan, H. "Properties of fresh and hardened concretes prepared by N-vinyl copolymers", International Conference on Concretes, Dundee, Scotland 1999.
38. Japanese Society of Civil Engineering. "Guide to Construction of High Flowing Concrete". Gihoudou Pub., Tokyo, 1998 (in Japanese).
39. JASS, Japanese Architectural Standard: Specification for reinforced concrete work (in Japanese), Tokyo, 1986.
40. ACI 318-05. "Building Code Requirements for Structural Concrete and Commentary". ACI Committee 318, 2005.
41. Vengala, J., Sudharshan M. S., Ranganath R. V. "Experimental study for obtaining self-compacting concrete". Indian Concrete J., 77(8), pp. 1261–6, 2003.
42. Alyamac, K. E., Ince, R. "A preliminary concrete mix design for SCC with marble powders". Construction and Building Materials, Vol. 23, 2009, 1201-1210.
43. Bosiljkov, V. B. " SCC mixes with poorly graded aggregate and high volume of limestone filler", Cement and Concrete Research, Vol. 33, 2003, 1279–1286.
44. Ilker Bekir Topçu, I. B., Bilir, T., Uygunoğlu, T. "Effect of waste marble dust content as filler on properties of self-compacting concrete". Construction and Building Materials, Vol. 22, 2008.
45. Akram, T., Memon, S. A., Obaid, H. "Production of low cost self compacting concrete using bagasse ash". Construction and Building Materials, Vol. 23, 2009, 703-712.
46. Ozbay, E., Oztas, A., Baykasoglu. A, Ozbebek, H. "Investigating mix proportions of high strength self compacting concrete by using Taguchi method". Construction and Building Materials, Vol. 23, 2009, 694-702.
47. Khayat, K. H., Ghezal, A., Hadriche, S. "Factorial design models for proportioning

self-consolidating concrete". Materials and Structures, Vol. 32, 1999, 679-686.
48. Khayat, K. H., Ghezal, A., Hadriche, S. "Utility of statistical models for proportioning self-consolidating concrete". Materials and Structures, Vol. 33, 2000, 338-344.
49. Ouchi, M., Hibino, M., Okamura, H. "Effect of Superplasticizer on Self-Compactability of Fresh Concrete". TRR 1574, 1996, 37-40.
50. Souza, B., Fletcher, K. "New generation hyperplasticisers for the new millennium". Degussa Construction Chemicals Australia Pty Ltd.
51. Takada, K. "Influence of chemical admixtures on the mix proportion of general purpose self-compacting concrete". International Conference on Concretes, Dundee, Scotland 1999.
52. Ferraris, C. F., Brower, L., Daczko, J., Ozyldirim, C. "Workability of Self-Compacting Concrete". Journal of Research of NIST, Vol. 104, No. 5, 1999, 461-478.
53. Khayat, K. H., Guizani, Z. "Use of Viscosity-Modifying Admixture to Enhance Stability of Fluid Concrete". ACI Materials Journal, 1997, 332-340.
54. Dehn, F., Holschemacher, K., Weisse, D. "Self-Compacting Concrete - Time Development of the Material Properties and the Bond Behavior". LACER No. 5, 2000, 115-123.
55. Khayat, K. H. "Viscosity-enhancing admixtures for cement-based materials-An overniew". Cement and concrete, Vol. 20, 1998, 171-188.
56. Mailvaganam, N. "Miscellaneous admixtures". Concrete Admixtures Handbook, 2nd edition, ed. V. S. Ramachandran. Noyes Publications, NJ, 1995, Chapter 1.5, pp. 994-995.
57. Kawai, T. "Non-dispersible underwater concrete using polymers". Marine Concrete, International Congress on Polymers in Concrete, Brighton, UK, 1987, Chapter 11.5.
58. Poppe, A. M., De Schutter, G. "Cement hydration in the presence of high filler contents". Cement and Concrete Research, Vol. 35, 2005, 2290 – 2299.
59. Kadri, E. H., Duval, R. "Effect of ultrafine particles on heat of hydration of cement mortars", ACI Mater. J., Vol. 99, No. 2, 2002, 138– 142.
60. Ye, G., Liu, X., De Schutter, G., Poppe, A. M., Taerwea, L. "Influence of limestone powder used as filler in SCC on hydration and microstructure of cement pastes". Cem. Concr. Res., Vol. 29, 2007, 94–102.
۶۱. رمضانیانپور، علی اکبر، بختیاری، یاسر. "بررسی تأثیر افزودن مواد ریز دانه خنثی بر خواص مکانیکی و دوام بتن‌های خودتراز". در شکرچی‌زاده، م.، لیبر، ن. (تدوین‌کنندگان)، مجموعه مقالات اولین کارگاه تخصصی بتن خودتراکم، اسفند ۱۳۸۵، ص ۱۲۴–۱۳۷.
62. Ozawa, K. Meakawa, K., Kunishima, M., Okammura, H. "High performance concrete based on the durability design of concrete structures". Proceeding of the 2nd East Asia-Pacific conference on structural Engineering & construction, Chiang Mai, 11-13 Jan. 1989.
63. Irassar, E. F. "Sulfate attack on cementitious materials containing limestone filler – A review". Cement and Concrete Research, 2009, doi: 10.1016/g.cemconres.2008.11.007.
64. Department of the Environment, Transport and the regions, The Thaumasite form of sulfate attack: risks, diagnosis, remidial works and guidance on new construction, DETR, London, 1999, Report of th Thaumasite Expert Group.
65. Bensted, J. "Thaumasite — background and nature in deterioration of cements, mortars and concretes". Cement and Concrete Composites, Vol. 21, 1999, 117–121.
66. Crammond, N. J. "The thaumasite form of sulfate attack in the UK". Cement and Concrete Composites, Vol. 25, 2003, 809–818.

67. Crammond, N. J., Halliwell, M. A. "The thaumasite form of sulfate attack in concretes containing a source of carbonate ions — a microstructural overview". in: V.M. Malhotra (Ed.), 2nd CANMET/ACI Int. Symp. on Advances in Conc. Tech., ACI SP 154, USA, 1995, pp. 357–380.
68. Trägård, J., Kalinowski, M. "Investigation of the conditions for a thaumasite form of sulfate attack in SCC with limestone filler". in: O. Wallevik, I. Nielsson (Eds.), International RILEM Symposium on Self-Compacting Concrete, 2003, RILEM, Publications 033.
69. Kalinowski, M., Trägård, J. "Thaumasite and gypsum formation in SCC with sulfate resistant cement exposed to a moderate sulfate concentration". 2nd North American Conference on the Design and Use of Self- Consolidating Concrete and 4th International RILEM Symposium on Self-Compacting Concrete, Chicago, USA, 2005, pp. 319–325.
70. Friebert, M., Stark, J. "Investigations to the durability of self compacting concrete". Beton, Vol. 54, 2004, 184–186.
71. Zhu, W., Bartos, P. J. M. "Permeation properties of self-compacting concrete". Cement and Concrete Research, Vol. 33, 2003, 921-926.
72. Teychenne, D. C., Franklin, R. E., Nicholls, J. C., Hobbs, D. W. "Design of normal concrete mixes". Department of the Environment, UK, 1988.
۷۳. آیین‌نامه محافظت ساختمان‌ها در برابر آتش (پیشنهادی)، انتشارات مرکز تحقیقات ساختمان و مسکن، نشریه شماره ض-۴۴۴، ۱۳۸۵.
74. Harmathy, T. Z. "Properties of building materials". In: SFPE handbook of Fire protection engineering, Society of Fire Protection Engineers, Boston, USA, 1995.
75. Harmathy, T. Z., “Properties of building materials at elevated temperatures”. DBR paper No. 1080, NRC 20956, National Research Council of Canada, Ottawa, 1983.
76. Harmathy, T. Z. "Fire safety design and concrete". Longman Scientific and Technical, Harlow, U.K., 1993.
77. Anderberg, Y. "Spalling phenomenon of HPC and OC". In Phan, L. T. (editor), Proceedings of International workshop on fire performance of high strength concrete, NIST, MD, 1997.
78. Hertz, K. D. "Limits of spalling of fire exposed concrete". Fire safety journal, 38, 2003, 103-116.
79. Ye, G., Liu, X., De Schutter, G., Taerwe, L., Vandevelde, P. "Phase distribution and microstructural changes of self-compacting cement paste at elevated temperature". Cement and Concrete Research, Vol. 37, 2007, 978-987.
80. Ye, G., Liu, X., De Schutter, G., Poppe, A. M., Taerwea, L. "Influence of limestone powder used as filler in SCC on hydration and microstructure of cement pastes". Cem. Concr. Res., Vol. 29, 2007, 94–102.
81. Breitenbücker, R. "High strength concrete C 105 with increased fire resistance due to polypropylene fibres". in: F. de Larrad, R. Lacroix, (Eds.), 4th International Symposium on the Utilization of High-Strength/High-Performance Concrete, Paris, France, 1996, 571– 577.
82. Sarvaranta, L., Jarvela, E., Mikkola, E. "Fibre mortar composites under thermal exposure". in: Pluralis (Ed.), Proceedings of 2nd International Symposium on Textile Composites in Building Construction, Lyon, France, 23– 25 June 1992, 47–56.
83. Sarvaranta, L Mikkola, E. "Fibre mortar composites in fire conditions". Fire Mater, 18, 1994, 45-50.
84. Sarvaranta, L Mikkola, E. "Fibre mortar composites under fire conditions: Effects of

ageing and moisture content of specimens, Mater. Struct., 27, 1994, 532–538.

85. Nishida, A., Yamazaki, N., Inoue, H., Schneider, U., Diederichs, U. "Study on the properties of high strength concrete with short polypropylene fibers for spalling resistance". in: K. Sakai, N. Banthia, O.E. Gjorv (Eds.), Proceedings of the Symposium on Concrete Under Severe Environment 2, 1995, 1141–1150.
86. Lennon, T., Clayton, N. "Fire tests on high grade concrete with polypropylene fibres". BRE Report 395, 1999.
87. Kalifa, P. "Spalling and Pore Pressure in HPC at High Temperatures". Cement and Concrete Research, 30, 2000, 1915-1927.
88. Boström, L. "The performance of some self compacting concretes when exposed to fire". SP report 2002:23, SP Swedish National Testing and Research Institute, 2002.

CD07-014

بتن‌های توانمند نسل جدید

طیبه پرهیزکار[1]، امیرمازیار رئیس قاسمی[2]
۱. عضو هئیت علمی‌مرکز تحقیقات ساختمان ومسکن،تهران
۲. پژوهشگر مرکز تحقیقات ساختمان ومسکن، تهران

خلاصه

بتن‌های معمولی که با روش‌های سنتی، طراحی، مخلوط، حمل و عمل‌آوری می‌شوند، نمی‌توانند جهت دستیابی به مشخصات مورد نظر برای کاربردهای ویژه و یا برای دستیابی به الزامات خاص، کاربرد داشته باشند، لذا کاربرد بتن‌های توانمند (HPC)، برای رفع این مشکلات رو به گسترش می‌باشند. برای ساخت این نوع بتن‌های ویژه معمولاً از مصالح رایج ولی با نسبت آب به مواد سیمانی کم و مقدار سیمان زیاد، استفاده می‌کنند.
مواد افزودنی شیمیایی و معدنی (جایگزین سیمان) می‌تواند سبب کاهش عیار سیمان شود. اما از آنجایی‌که روش طرح مخلوط خاصی برای این نوع بتن‌ها وجود ندارد و به دلیل کم بودن نسبت آب به مواد سیمانی، تعیین نقطه بهینه مقدار سیمان و آب و از طرف دیگر تراکم‌پذیری و میزان روانی به سادگی امکان پذیر نبوده و عموماً در این نوع بتن‌ها از مواد سیمانی نسبتاً زیاد استفاده می‌شود که این امرعلاوه بر گران شدن، سبب افزایش جمع‌شدگی و احتمال کاهش دوام نیز می‌شود.
روش پیشنهادی در این مقاله، که بخشی از نتایج تحقیق انجام شده روی نوعی طرح مخلوط بتن می‌باشد، بر اساس فلسفه دستیابی به حداکثر تراکم می‌باشد. در این روش، نحوه توزیع دانه‌ها بگونه‌ای انتخاب می‌شود که بتن دارای نفوذپذیری بسیار کم بوده و در ضمن میزان سیمان نیز (تا ۴۰ درصد)کاهش یابد. کاربرد این روش طرح مخلوط بتن‌های توانمند، نه‌تنها سبب افزایش مقاومت و دوام نسبت به بتن‌های HPC مشابه می‌شود، بلکه سبب کاهش مصرف سیمان نیز می‌گردد.

کلیدواژه: بتن توانمند، مواد جایگزین سیمان، دوام، حداکثر تراکم، نفوذپذیری، منحنی توزیع دانه‌ها

۱- مقدمه

بتن‌های توانمند (High Performance Concrete)، بر اساس مشخصات مواد و مصالح موجود و برای دستیابی به یک‌سری خواص مورد نظر، رویارویی با شرایط محیطی، افزایش دوام و عمر مفید و در نهایت قابل توجیه بودن از نظر اقتصادی، طراحی می‌شوند [۱]. امروزه بتن‌های توانمند کاربردهای متنوعی از جمله استفاده در ساختمان‌هایی که در شرایط اقلیمی‌مهاجم می‌باشند، اسکله‌ها، بنادر، تونل‌ها، قطعات پیش ساخته، پل و غیره، داشته و کاربرد آنها نیز رو به افزایش می‌باشد [۲و۳].
بطور معمول تفاوت بتن توانمند و بتن معمولی، در کاربرد مواد افزودنی شیمیایی و معدنی (جایگزین سیمان) و

کاهش نسبت آب به سیمان می‌باشد. استفاده از این مواد، امکان کاهش نسبت آب به سیمان و مقدار سیمان را بوجود آورده و در حین حال سبب افزایش دوام نیز می‌شوند [۴]. با توجه به اینکه عموماً مواد جایگزین سیمان موادی ارزان قیمت هستند (یا محصول جانبی کارخانه می‌باشند و یا بصورت طبیعی وجود دارند)، استفاده توام مواد جایگزین سیمان و مواد افزودنی شیمیایی سبب اقتصادی شدن نیز می‌گردد [۵].

یکی از مواد جایگزین سیمان که در اکثر بتن‌های توانمند مورد استفاده قرار می‌گیرد، خاکستر بادی می‌باشد. اگر چه این ماده دارای فعالیت پوزولانی زیادی نبوده و به لحاظ خواص و مشخصات گاهاً متغیر می‌باشد، ولی به علت داشتن شکل کروی دانه‌ها و افزایش روانی بتن و همچنین ارزان بودن و در دسترس بودن آن در اکثر نقاط جهان، در بتن‌های توانمند بکار می‌رود [۶]. دوده سیلیس نیز از مواد جایگزین سیمان می‌باشد که برخلاف خاکستر بادی دارای فعالیت زیاد می‌باشد. ریزی بسیار زیاد و شکل دانه‌های دوده سیلیس، سبب می‌شود مقدار آب مورد نیاز برای دستیابی به روانی مناسب، افزایش یابد [۱]. افزایش مقاومت و دوام از یک طرف و افزایش سرعت هیدراسیون و احتمال بروز ترک‌های ناشی از جمع‌شدگی (پلاستیک و ناشی از خشک شدن) در هنگام استفاده از دوده سیلیس باید مورد توجه قرار گیرد.

مهمترین نکته بعد از انتخاب نوع ماده جایگزین سیمان، تعیین درصد اختلاط مواد سیمانی و همچنین دیگر اجزای بتن می‌باشد. استفاده از روش‌های سنتی عموماً نیاز به ساخت مخلوط‌های آزمایشی متعددی دارد و به علت محدودیت‌هایی که دارد نمی‌توانند پاسخگوی نیازها باشند [۱۳]. عمده ترین مشکل این روش‌ها عدم امکان رسیدن به نقطه بهینه مقدار سیمان، مواد جایگزین، نسبت آب به مواد سیمانی و در نهایت دستیابی به روانی و تراکم پذیری مورد نظر، می‌باشد [۴، ۸ و۹]. یکی از کارهای انجام شده، پیشنهاد ضریب تأثیر مواد افزودنی می‌باشد. اسمیت [۷]، برای اصلاح تأثیر مواد جایگزین سیمان، فاکتور k را پیشنهاد داد. با ضرب فاکتور k (که بسته به نوع ماده جایگزین متغیر می‌باشد) در مقدار ماده جایگزین (k.f) در حقیقت مقدار معادل مواد جایگزین سیمان بدست می‌آید که با جمع کردن این مقدار با مقدار سیمان (C+kf)، مقدار سیمان معادل حاصل می‌گردد. از این مقدار برای تعیین نسبت آب به مواد سیمانی استفاده می‌شود. اگرچه محققین و مراجع مختلف مقادیر مختلفی برای k ارائه داده‌اند [۱۰ الی ۱۲] ولی امروزه استفاده از فاکتور تأثیر k مورد توافق همه می‌باشد. در این تحقیق مقدار فاکتور تأثیر بر اساس استاندارد EN 206-1 در نظر گرفته شد.

عامل دیگری که کمتر مورد توجه قرار گرفته ولی عامل بسیار مهمی‌در افزایش تراکم پذیری و دوام می‌باشد، نحوه توزیع دانه‌ها (اعم از سنگدانه‌ها و دیگر مصالح جامد دانه‌ای) می‌باشد. استفاده از منحنی‌های ایده‌آل می‌تواند در افزایش تراکم، کاهش تخلخل و همچنین کارایی بتن بسیار مؤثر باشد. در ادامه انتخاب نحوه توزیع دانه‌ها و فلسفه مورد استفاده به تفصیل ارائه شده است.

۲- مبانی و اصول طرح اختلاط

چنان‌چه اشاره شد، اگر بتوان با افزایش تراکم سنگدانه‌ها، فضای بین دانه‌ها را به حداقل ممکن کاهش داد، نفوذپذیری کاهش پیدا کرده و در نتیجه دوام بتن افزایش خواهد یافت. در این راستا با توجه به تحقیقات هیله مایر [۱۴]، جهت کاهش نفوذپذیری که بر اساس نظریه Fuller & Thompson با استفاده از توزیع دانه‌بندی مصالح سنگی انجام شده‌است، توزیع دانه‌ها به گونه‌ای اصلاح گردید که ضمن حفظ کارآیی ملات و یا بتن، دوام آن در مقابل عوامل شیمیایی مهاجم افزایش یابد.

جهت کاهش ضعف‌های ناحیه انتقال که بیشتر در اطراف سنگدانه‌های درشت دیده می‌شود می‌توان نسبت ریزدانه‌ها را نیز افزایش داد. همزمان به‌منظور کاهش نفوذپذیری در خمیر سیمان، باید ضمن کاهش تخلخل، توزیع حفرات به نحوی اصلاح گردد که دوام بتن یا خمیر، در برابر عوامل مهاجم افزایش یابد. با توجه به اینکه دانه‌بندی سیمان به نحوی است حاوی ذرات بسیار ریز (میکرونی) نمی‌باشد، استفاده از فیلر با قطری کوچکتر از میانگین قطر دانه‌های سیمان جهت بالا بردن جرم حجمی‌خشک، لازم به نظر می‌رسد، چرا که اولاً ذرات ریز اثر پُرکندگی داشته و تخلخل را کاهش می‌دهند، ثانیاً توزیع حفرات مناسب‌تر شده و ثالثاً در صورتی‌که فیلر، دارای سیلیس واکنش‌زا باشد می‌تواند سرعت هیدراسیون را افزایش داده و قسمتی از هیدروکسید کلسیم آزاد را، به مصرف برساند.

منحنی‌های دانه‌بندی مطلوب، عموماً بر اساس آزمایش‌های تجربی و محاسبات تئوری، ارائه گردیده‌اند. از این جمله می‌توان به منحنی‌های Bolomey، Fuller، Graf و Rissel اشاره کرد که در این بین، منحنی Fuller نتایج بهتری را ارائه داده است [۱۵].

از طرف دیگر، برای دستیابی به بتنی با نفوذپذیری کم و دوام زیاد، باید با کاهش خلل و فرج و افزایش تراکم، جرم حجمی‌خشک بتن حداکثر گردد. این موضوع اساس نظریه مورد بررسی در این تحقیق برای دستیابی به بتنی با حداکثر تراکم با استفاده از حداقل میزان مواد چسباننده می‌باشد، به‌گونه‌ای که مقاومت فشاری و کارآیی آن کاهش نیابد. در این راستا با استفاده از روابط ریاضی، توزیع دانه‌ها (اعم از مصالح سنگی و مصالح چسباننده) به‌گونه‌ای انتخاب می‌گردد، که مصالح سنگی ریزدانه و مصالح چسبنده، با پر نمودن فضای خالی بین مصالح سنگی درشت‌دانه باعث تراکم بیشتر مخلوط گردد. شایان ذکر است در عمل منحنی دانه بندی معمول (استاندارد) قسمت ریزدانه (دانه‌های کوچکتر از ۰/۱۵۰ mm) را در بر نمی‌گیرد. در صورتی‌که برای دستیابی به یک دانه‌بندی بهینه و متراکم حائز اهمیت می‌باشد.

استفاده از منحنی دانه بندی Fuller & Thompson اگرچه دارای مزایای اشاره شده در فوق می‌باشد، ولی به‌علت برخی محدودیت‌ها، مانند، عدم گردگوشه بودن کامل تمام دانه‌ها، کاهش کارائی و استفاده از یک منحنی تقریباً گسسته، با اصلاحاتی (توسط هیله مایر [۱۴]) مدنظر قرار گرفت. در شکل ۱ و شکل ۲ منحنی F&T و منحنی اصلاح شده آن در دو حالت (مقیاس خطی و لگاریتمی) نشان داده‌شده‌است. همان‌گونه که مشاهده می‌شود در بخش درشت‌دانه و میان‌دانه (بزرگتر از ۲ میلیمتر) منحنی اصلاح شده دارای مقادیر بیشتری، نسبت به منحنی F&T می‌باشد و بالعکس برای دانه‌های کوچکتر از ۲ میلیمتر دارای مقادیر ریزدانه کمتری نسبت به منحنی F&T می‌باشد [۱۹].

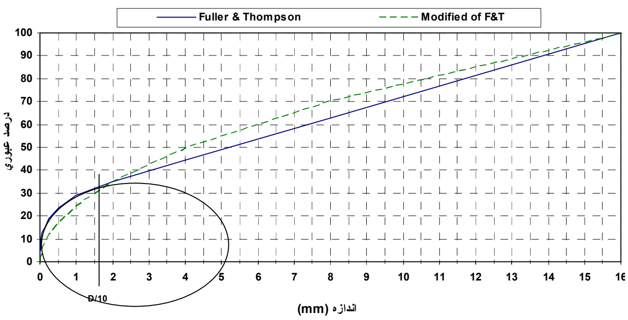

شکل ۱- منحنی‌های دانه‌بندی F&T و اصلاح شده، در مقیاس خطی

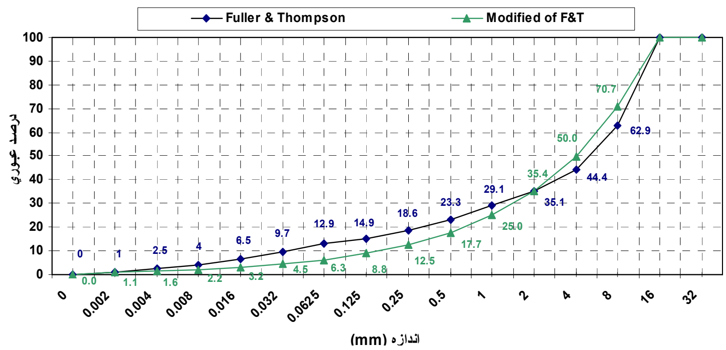

شکل ۲- منحنی‌های دانه‌بندی F&T و اصلاح شده، در مقیاس لگاریتمی

مزایای دانه‌بندی F&T و اصلاح شده آن، به‌شرح زیر می‌باشد [۱۶ الی ۱۹]:

۱. این نوع دانه بندی با مقاومت فشاری برابر در مقایسه با دانه بندی پیوسته نیاز به سیمان کمتری دارد.

۲. در حقیقت با کاهش نسبی قطر سنگدانه مصالح ریزدانه نقش پُرکنندگی از خود نشان می‌دهند.

۳. قابلیت تراکم پذیری مخلوط در اثر کاهش درصد میان دانه‌ها، به‌طور محسوس افزایش می‌یابد. زیرا ریزدانه‌ها با درصد حجمی‌بیشتر، در درشت‌دانه‌ها جابجا می‌شوند. بدین ترتیب با دستگاه لرزاننده، تراکم‌پذیری بیشتری حاصل می‌شود و هوای داخل فضای بین سنگدانه‌ها تخلیه می‌گردد.

۴. قرارگیری سنگدانه‌ها در این نوع مخلوط بتنی قابلیت نگهداری آب را افزایش می‌دهد.

۵. موارد ۲ و ۳، باعث عمل آوری بهتر بتن می‌گردند و درصد آب مورد نیاز نیز متعاقباً کاهش می‌یابد.

۶. از نظر کاهش هزینه‌های کارگاهی نیز کاهش حجم میان دانه‌ها، مناسب بوده زیرا مشکلات حمل، انبار، الک نمودن و عمل آوری بتن تقلیل می‌یابد.

یکی از مهمترین ویژگی استفاده از این منحنی، تعیین نسبت حجمی‌کلیه دانه‌های موجود در بتن، اعم از سنگدانه و مواد چسباننده می‌باشد. بر اساس این منحنی می‌توان سهم هر یک از مواد جامد تشکیل دهنده بتن را تعیین نمود، به‌عنوان مثال درصد مشخص شده برای دانه‌های کوچکتر از ۰/۰۶۳ میلیمتر، بیانگر مقدار مواد چسباننده خواهد بود (به‌علاوه مواد ریزدانه‌ی موجود در سنگدانه‌ها).

۳- مطالعات آزمایشگاهی

۳-۱- مصالح مصرفی

۳-۱-۱- مصالح چسباننده

در انتخاب مواد چسباننده (مواد سیمانی) دو مشخصه مد نظر قرار گرفت. اول از دیدگاه توزیع دانه‌ها در منحنی دانه بندی F&T، که در آن باید تمامی‌مصالح اعم از سنگدانه یا مواد سیمانی بگونه‌ای دانه‌بندی و یا انتخاب شوند که توزیع دانه‌ها تا حد ممکن نزدیک به منحنی ایده‌آل باشد. از جهت دیگر باید مواد سیمانی به‌گونه‌ای انتخاب و با یکدیگر مخلوط گردند که ترکیب شیمیایی آنها خواص مکانیکی و فیزیکی و همچنین دوام خمیر سیمان را برآورده نماید. در این راستا کاهش مقدار آب لازم به حداقل مقدار ممکن (کاهش نسبت آب به مواد سیمانی) نیز یکی از پارامترهای مؤثر باشد.

سیمان : سیمان مصرفی از نوع ۲ و محصول کارخانه سیمان تهران بوده و مشخصات شیمیایی آن در جدول ۱ ارائه شده است. روش انجام آزمون، استاندارد ملی ایران به شماره ۳۸۹ می‌باشد.

خاکستر بادی: با توجه به اینکه در حال حاضر در داخل کشور خاکستر بادی تولید نمی‌شود، خاکستر بادی مورد استفاده در این پروژه از کشور آلمان تهیه گردید. این خاکستر بادی از نوع بسیار ریز (Ultra fine) بوده و دانه بندی آن که به روش particle size analyser انجام شده در نمودار شکل ۳ ارائه شده است. به منظور تعیین خواص مکانیکی، فیزیکی و شیمیایی خاکستر بادی از روش استانداردEN 196-21 و ASTM C 311 استفاده گردید.

دوده سیلیس: دوده سیلیس مصرفی در این پروژه تولید داخل کشور و از کارخانه ازنا تهیه شده است. آزمون‌های مربوط به تعیین خواص شیمیایی دوده سیلیس مورد استفاده که طبق استاندارد ASTM C 1240 انجام گرفته است در جدول ۱ ارائه شده است.

در طرح مخلوط پیشنهادی، که از سیمان، دوده‌سیلیس، خاکستر بادی و فیلر استفاده شده‌است، با توجه به توزیع ذرات سیمان، خاکستر بادی و دوده سیلیس مورد مصرف در این پروژه (حدود ۸۰ درصد ذرات سیمان دارای قطری بین ۱۰ تا ۱۰۰ میکرومتر، ۵۰ درصد ذرات خاکستر بادی بین ۵ تا ۲۰ میکرومتر و ۶۰ درصد ذرات دوده سیلیس دارای قطری کمتر از ۱ میکرومتر، مطابق شکل ۳ بوده‌اند)، و همچنین به‌دلیل خواص شیمیایی هر یک از این مواد و همچنین خواص مکانیکی، فیزیکی و دوام بتن، درصد هر یک از این مواد بشرح ذیل انتخاب گردید:

- سیمان : ۷۰ درصد وزنی
- خاکستر بادی بسیار ریز : ۲۰ درصد وزنی
- دوده سیلیس : ۱۰ درصد وزنی

جدول ۱: تجزیه شیمیایی سیمان و میکروسیلیس

ترکیب شیمیایی (٪)	سیمان	میکروسیلیس	ترکیب شیمیایی (٪)	سیمان	میکروسیلیس	ترکیب شیمیایی (٪)	سیمان
SiO_2	۲۰/۹۶	۹۵/۱	MgO	۳/۴	۰/۶	C_3S	۵۲/۷۴
AL_2O_3	۴/۲	۰/۶	CaO	۶۱/۸۸	۱/۰۲	C_2S	۲۰/۳۱
Fe_2O_3	۴/۶	۱/۱	SO_3	۱/۷۹	۱/۲	C_3A	۳/۳۵
						$Na_2o + O.658\ K_2O$	۱/۴۷

۳-۱-۲- مصالح سنگی

مصالح سنگی مورد استفاده از نوع سیلیسی، با حداکثر اندازه اسمیmm ۱۶ انتخاب شد. سنگدانه‌ها شکسته، و به صورت بخش‌های مجزا روی هر الک تهیه شد. لذا امکان دانه‌بندی براساس منحنی‌های مختلف، با دقت کافی فراهم بود. مشخصات فیزیکی و شیمیائی مصالح فوق در جدول ۲ ارائه شده است.

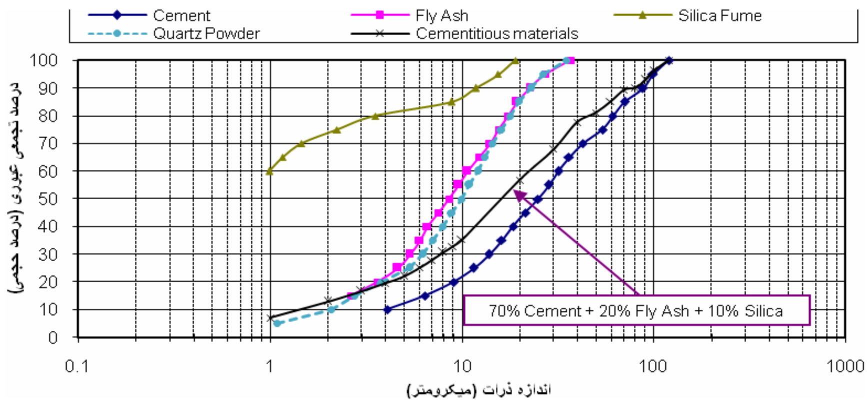

شکل ۳- منحنی‌های توزیع ذرات سیمان، خاکستر بادی، دوده‌سیلیس و پودر کوارتز میکرونیزه

جدول ۲: مشخصات فیزیکی و شیمیایی مصالح سنگی

مصالح سنگی	وزن مخصوص درحالت SSD (g/cm^3)	جذب آب(٪)	عبوری از الک شماره ۲۰۰ (٪)	کلرید (٪)	سولفات (٪)	واکنش قلیایی به روش تسریع شده (درصد انبساط بعداز ۱۴روز)
شن	۲/۵۳	۲/۶۴	۲/۶	۰/۰۰۱	۰/۰۰۱	۰/۰۸۷
ماسه	۲/۵۶	۲/۷۱	۲/۴۶	۰/۰۰۱	۰/۰۰۲	۰/۰۹
فیلر	۲/۵۷	۴/۰	۰/۷	۰/۰۰۲	–	–

۳-۱-۳- ماده افزودنی شیمیایی

فوق روان کننده مصرفی بر پایه کر بوسیلات‌ها و بـا نـام تجـاری structuro 335 بـوده اسـت، ایـن نـوع فـوق روان‌کننده‌ها از نسل جدید مواد افرودنی می‌باشند. از مهمترین مزایای این نوع فوق روان کننده‌ها، افزایش بـسیار زیاد روانی بدون جداشدگی اجزاء بتن می‌باشند، همچنین قابلیت حفظ روانی در مدت زمان طولانی‌تر نیز از جملـه این موارد می‌باشد. مشخصات این فوق‌روان کننده د رجدول ۳ ارائه شده‌است.

جدول ۳: مشخصات فیزیکی و شیمیایی فوق روان کننده

وضعیت ظاهری	مایع با رنگ زرد روشن
pH	۶/۵
وزن حجمی	۱/۰۶ Kg/lit در دمای ۲۰ ^oC
میزان کلر موجود	کمتر از ۰/۱ درصد
میزان قلیایی موجود	بطور معمول کمتر از ۱/۵ گرم معادل Na_2O در هر لیتر

۳-۲- تعیین نسبت اختلاط سنگدانه‌ها (ریز، درشت و فیلر)

همان‌گونه که اشاره شد، یکی از تفاوت‌های اصلی این نوع بتن توانمند با انواع رایج آن، استفاده از روش دسـتیابی به حداکثر تراکم (Dense Packing)، با اصلاح نحوه توزیع دانه‌ها (اعـم از مـصالح سـنگی و مـصالح چـسباننده) می‌باشد، که به این منظور از منحنی اصلاح شده فولر و تامسون استفاده گدیـد. همچنـین جهـت امکـان ارزیـابی

عملکرد این نوع بتن با بتن‌های توانمند رایج، طرح‌هایی نیز بر اساس روش سنتی ساخته شد.
برای طرح پیشنهادی، دو طرح با شناسه‌های FSPD و SPD و برای طرح‌های سنتی نیز دو طرح با شناسه‌های SN و FSN ساخته شد. نسبت اختلاط سنگدانه‌ای دو طرح اول مطابق با منحنی اصلاح شده فولر و تامسون و برای دو طرح سنتی نیز از منحنی ترکیبی استاندارد BS استفاده شده‌است، منحنی دانه‌بندی طرح‌ها در شکل ۴ ارائه شده‌است.

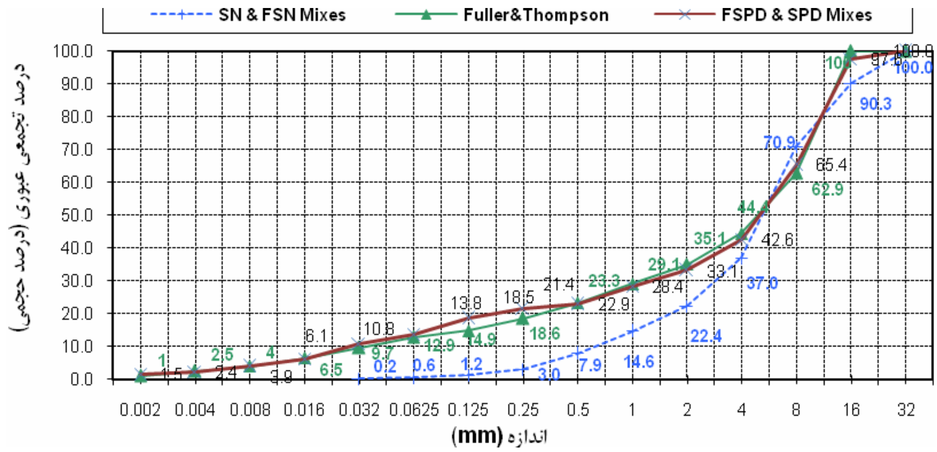

شکل ۴- منحنی دانه‌بندی مجموع سنگدانه‌ها (ریز و درشت)

۳-۳- تعیین نسبت آب به سیمان

با توجه به اینکه در بتن‌های توانمند نسبت آب به مواد سیمانی بسیار پایین می‌باشد، تا دوام بتن در برابر عوامل مهاجم خصوصاً کلرید، سولفات و مواد اسیدی افزایش یابد، و همچنین طبق آیین‌نامه بتن ایران (آبا) حداکثر نسبت آب به سیمان (یا مواد سیمانی) برای شرایطی که احتمال تهاجم کلریدی و خوردگی میلگرد وجود دارد، ۰/۴ و حداقل سیمان ۳۵۰ kg/m3 و در شرایطی که احتمال تهاجم سولفاتی (فوق‌العاده شدید) می‌باشد، برای شالوده‌های بتنی حجیم یا قطعات پیش ساخته، حداکثر نسبت آب به سیمان ۰/۴ و حداقل سیمان ۴۰۰ kg/m^3 توصیه شده است، در این تحقیق نیز سعی شده است نسبت آب به موا سیمان موثر به ۰/۴ محدود شود. البته نسبت آب به سیمان ارائه شده در آبا، نسبت آب به مواد سیمانی موثر نمی‌باشد.

در مواردی است که از مواد افزودنی معدنی (دوده سیلیس یا خاکستر بادی) استفاده می‌شود، برای اصلاح تاثیر این مواد از فاکتور تاثیر استفاده می‌شود. در این تحقیق مقدار فاکتور اصلاح (k) طبق استاندارد EN 206-1:2000 انتخاب گردید. بر این اساس، برای خاکستر بادی (با کیفیت استاندارد مطابق EN 450) در صورت ترکیب شدن با سیمانی با رده مقاومتی **MPa** ۳۲/۵، ضریب k برابر با ۰/۲ و برای سیمانی با مقاومت **MPa** ۴۲/۵ و بیشتر، این ضریب برابر با ۰/۴ در نظر گرفته می‌شود. همچنین برای دوده سیلیس مقدار k برابر با ۲ توصیه شده‌است.
روش اعمال این ضریب در تصحیح نسبت آب به سیمان با کمک رابطه زیر انجام می‌شود:

$$\text{نسبت آب به سیمان مؤثر} = \frac{water}{cement + (K \times (\text{silica fume or fly ash}))}$$

که در آن :

Water : وزن آب آزاد،

Cement : وزن سیمان مصرفی،

Fly ash : وزن خاکستر بادی،

Silica fume : وزن دوده سیلیس می‌باشد.

۳-۴- تعیین نسبت اختلاط

مخلوط‌ها بر اساس دو نظریه طراحی شده‌اند. سری اول، شامل مخلوط‌هایی می‌باشند که حاوی دوده‌سیلیس و خاکستربادی و یا بدون خاکستربادی بوده، و طبق روش‌های طرح مخلوط رایج برای ساخت بتن‌های توانمند، طراحی شده‌اند. سری دوم، مخلوط‌هایی می‌باشند که طبق روش جدید (استفاده از منحنی اصلاح شده فولر و تامسون و اعمال فاکتور اصلاح مواد جایگزین سیمان)، طراحی شده‌اند. در این طرح‌ها از دوده‌سیلیس، فیلر و خاکستربادی و همچنین یک طرح هم بدون خاکستربادی، استفاده شده‌است. علت این‌که دو طرح با خاکستربادی و دو طرح نیز بدون خاکستر بادی ساخته‌شد، این است که، در روش پیشنهادی برای طرح مخلوط بتن‌های توانمند نسل جدید، برای دستیابی به منحنی توزیع ایده‌آل، کارائی مناسب و بتن مقاوم در برابر عوامل مهاجم، نیاز به استفاده از خاکستر بادی نیز می‌باشد، ولی از آنجتیی‌که خاکستربادی در ایران تولید نمی‌شود، طرح‌هایی نیز به‌عنوان جایگزین، بدون خاکستر بادی ساخته‌شد. اگرچه ممکن است این طرح‌های نیز جز بتن‌های توانمند محسوب شوند، ولی طرح بهینه با دوام نمی‌باشند.

در جدول ۴ مشخصات طرح مخلوط‌های ساخته شده ارائه شده است. طرح مخلوط پیشنهادی با شناسه FSPD و طرح بدون خاکستر بادی آن با شناسه SPD، طرح‌های بتن توانمند رایج نیز با شناسه‌های SN و FSN ارائه شده است.

در شناسه مخلوط‌ها حرف "F" نشان دهنده استفاده از خاکستر بادی، حرف "S" معرف استفاده از دوده سیلیس، حرف "P" بیانگر مصرف پودر کوارتز بعنوان فیلر، حرف "N" نشان دهنده منحنی دانه بندی سنگدانه‌ها طبق منحنی معمول و حرف "D" نیز معرف استفاده از منحنی دانه بندی اصلاح شده فولر و تامسون می‌باشد.

جدول ۴ – نسبت اختلاط اجزای بتن در طرح‌های مختلف

شناسه مخلوط	سیمان	خاکستر بادی	دوده سیلیس	نسبت آب به سیمان موثر	سنگدانه (۰/۲۵- ۱۶) م م	فیلر سنگدانه (۰- ۰/۲۵) م م	فیلر پودر سیلیس (۰-۰/۲۵) م م	فوق روان کننده	آب
	Kg/m^3	Kg/m^3	Kg/m^3		Kg/m^3	Kg/m^3	Kg/m^3	(٪ وزن سیمان)	Kg/m^3
SN	۳۷۲	۰	۲۸	۰/۴	۱۸۳۰	۵۶/۵	۰	۰/۶	۱۷۰
FSN	۲۲۰	۶۳	۳۱/۵	۰/۴	۱۹۵۵	۶۰/۵	۰	۰/۶۴	۱۲۴
FSPD	۲۴۵	۷۰	۳۵	۰/۴	۱۸۰۸	۶۱	۱۳۸	۰/۶	۱۳۵
SPD	۳۱۵	۰	۳۵	۰/۴	۱۸۰۸	۶۱	۱۳۸	۰/۶	۱۳۵

۳-۴-۱- اختلاط بتن

پس از اعمال تصحیح مقدار رطوبت موجود در سنگدانه‌ها، هر یک از اجزاء بتن به تفکیک توزین شده و سپس

ابتدا سنگدانه‌ها و بعد مصالح سیمانی، آب و در انتها ماده افزودنی فوق روان کننده به داخل مخلـوط کـن ریختـه شده جهت انجام اختلاط از یک مخلوط‌کن تغاری (Pan mixer) استفاده گردید. ظرفیت اسمی‌مخلوط‌کـن ۲۵۰ لیتر و چرخش تیغه‌های آن بصورت عمودی و در جهت عکس حرکت دیگ بوده است.

۳-۴-۲- ساخت و عمل‌آوری آزمونه‌ها

پس از توزین و اختلاط اجزاء بتن، آمونه‌های بتنی ساخته، نگهداری و عمل‌آوری گردیدند. بر اساس استاندارد EN 12390-2:2000، بتن در قالب‌های مورد نظر جایدهی و متراکم گردید، آزمونه‌هـا پـس از یـک‌روز نگهـداری در شرایط استاندارد (اطاق مرطوب)، از قالب خارج و به داخل حوضچه عمل‌آوری با دمای ۲۳ °C منتقـل و تـا زمـان انجام آزمایش در شرایط مذکور عمل‌آوری شدند.

۳-۵- آزمایش‌های بتن تازه

جهت تعیین خواص بتن تازه (سخت نشده) آزمون‌های تعیین وزن مخصوص، درصد هوای موجود، روانی به روش اسلامپ، و تعیین دمای بتن انجام گردید که نتایج آن در جدول ۵ ارائه شده‌است.

جدول ۵: نتایج آزمایش‌های بتن تازه

شناسه مخلوط	دمای بتن (درجه)	اسلامپ (Cm)	وزن مخصوص (Kg/m^3)	هوای محبوس (٪)
SN	۲۱	۴	۲۳۹۱	۳/۸
FSN	۲۲	۰	۲۴۶۶	۲/۰
FSPD	۲۵	۱۲	۲۵۰۵	۱/۰
SPD	۲۱	۱۰	۲۵۳۳	۱/۵

۳-۶- نتایج آزمایش‌های بتن سخت شده

۳-۶-۱- مقاومت فشاری

به منظور تعیین مقاومت فشاری و بررسی روند افزایش آن، آزمونه‌های مکعبی با ابعاد ۱۰۰ میلی‌متر تهیه گردیدند. آزمونه‌ها (در هر سن، سه آزمونه) در سنین ۷، ۲۸ و۹۰ روز مورد آزمون قرار گرفتند. اندازه‌گیری مقاومـت فـشاری آزمونه‌ها بر اساس استاندارد EN 12390-3:2000 انجام و نتایج آن در شکل ۵ ارائه گردیده است.

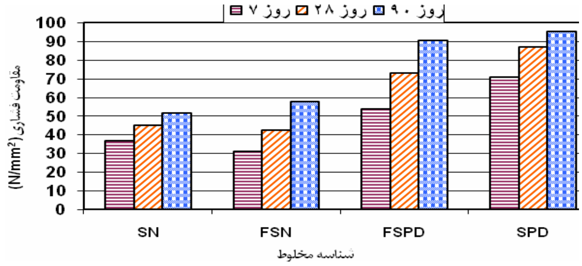

شکل ۵- نتایج آزمایش تعیین مقاومت فشاری

۳-۶-۲- نفوذپذیری یون کلرید به روش تسریع شده

بهبود پارامترهای نفوذپذیری بتن در افزایش دوام آن بسیار حائز اهمیت می‌باشد. آزمون نفوذپذیری کلرید، به منظور طراحی و بررسی عمر مفید (سرویس‌دهی) بتن در مقابل نفوذ یون کلرید مناسب می‌باشد. این آزمون بر اساس استاندارد ASTM C 1202-97 روی آزمونه‌های استوانه‌ای به قطر ۱۰۰ میلیمتر و ضخامت ۵۰ میلیمتر انجام می‌شود، که در این پروژه با استفاده از آزمونه‌های استوانه‌ای ۱۰۰ ×۲۰۰ و برش آنها به ابعاد استاندارد، در سنین ۲۸ و ۹۰ روز مورد آزمون قرار گرفتند. نتایج آزمون در شکل ۶ ارائه گردیده است.

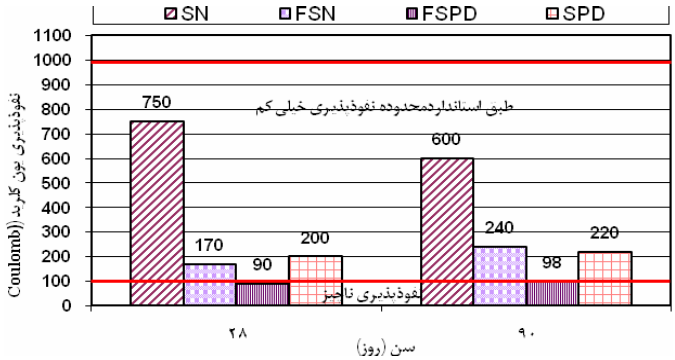

شکل ۶- نتایج آزمایش نفوذپذیری یون کلرید به روش تسریع شده

۳-۶-۳- تعیین عمق نفوذ آب تحت فشار

یکی از مهمترین پارامترهای مؤثر بر افزایش دوام بتن در برابر تهاجم مواد مضر (که از محیط نفوذ می‌نمایند)، کاهش نفوذپذیری بتن می‌باشد. در این راستا آزمون تعیین عمق نفوذ آب، جهت بررسی نفوذپذیری بتن تحت فشار آب می‌باشد. این آزمون طبق استاندارد EN 12390-8:2000 و روی آزمونه‌های مکعبی به ضلع ۱۵۰ میلی‌مترو در سنین ۲۸ و ۹۰ روز انجام گردید که نتایج آن در جدول ۶ ارائه گردیده است.

جدول ۶: نتایج آزمایش تعیین عمق نفوذ آب تحت فشار

شناسه مخلوط	عمق نفوذ آب (mm)	
	۲۸ روز	۹۰ روز
SN	۱۲	۲۳
FSN	۱۰	۲۴
FSPD	۰	۲
SPD	۴	۵

۳-۶-۴- تغییرات طول منشورهای بتنی در معرض محلول سولفات

به منظور بررسی عملکرد مخلوط‌های بتنی در معرض سولفات، از محلول سولفات سدیم ۵ درصد استفاده گردید. بدین منظور منشورهای بتنی بابعاد ۲۸۵×۷۵×۷۵ میلیمتر که در دو انتهای آنها پین‌های مخصوص کار گذاشته شده بود، ساخته و پس از ۲۸ روز عمل‌آوری، در محلول سولفات قرار داده شدند. جهت تنظیم pH و ثابت نگه

داشتن آن در طول زمان آزمایش، از اسید سولفوریک رقیق استفاده گردید، ضـمن آنکـه در سـنین اولیـه محلـول سولفات نیز چندین مرتبه تعویض شد.
تغییر طول و وزن آزمونه‌ها در فواصل زمانی مشخص، تا ۶ ماه بعد از زمان در معرض قرارگیری تعیین گردید، کـه نتایج آن در شکل ۷ ارائه شده است.

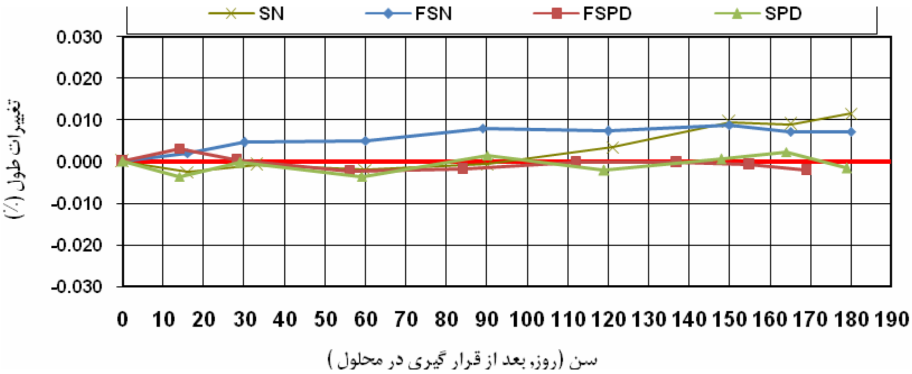

شکل ۷- نتایج انبساط نمونه‌در معرض سولفات سدیم

۴- نتیجه گیری

همانگونه که اشاره گردید، در این تحقیق طرح مخلـوط بـتن توانمنـد نـسل جدیـد کـه بـا تغییـر در دانـه بنـدی سنگدانه‌ها، استفاده از خاکستر بادی و همچنین یک نمونه پودر کوارتز، ارائه شـده اسـت. ایـن نـوع بـتن توانمنـد به‌علت تراکم زیاد و حداقل تخلخل، نفوذپذیری بسیار کم و مقـاوم در برابـر شـرایط مهـاجم (اسـید سـولفوریک، سولفات سدیم، کلرید و...) دارد، ضمن آن‌که میزان سیمان نیز در آن کاهش و کارائی مخلوط افزایش یافته است.
بدین منظور آزمایش‌های تعیین مقاومت فشاری، تعیین عمق نفوذ آب تحت فشار، نفوذپذیری یون کلرید به روش تسریع شده، انبساط ناشی از تهاجم سولفات، بعنوان برنامه آزمایشگاهی مد نظر قرار گرفت.

۱- نتایج آزمایش مقاومت فشاری نشان می‌دهد، نمونه‌هـای مخلـوط SPD کـه در آن از منحنـی دانـه بنـدی اصلاح شده F&T استفاده شده و بدون خاکستر بادی می‌باشد، دارای بیشترین مقاومت در سـنین مختلـف بوده‌اند. طرح FSPD که مشابه طرح SPD بوده و فقط در آن خاکستر بادی نیز (۲۰ درصد بعنوان جایگزین سیمان) استفاده شده است، اگر چه در سنین ۷ و ۲۸ روز دارای مقاومت‌های به نسبت کمتری در مقایسه بـا SPD بوده، ولی در سن ۹۰ روز با آهنگ افزایش مقاومت ۹۰ به ۲۸ روزی معادل ۲۴ درصد، دارای مقاومت ۹۰/۵ N/mm^2 بوده است، در صورتیکه مخلوط SPD با آهنگ افـزایش مقاومـت ۹۰ بـه ۲۸ روزی معـادل ۹/۲ درصد، در سن ۹۰ روز دارای مقاومت ۹۵ N/mm^2 بوده است. این کندی آهنـگ افـزایش مقاومـت در سنین اولیه، در طرح‌های FSN و FSD نیز که دارای خاکستری بادی می‌باشند، مشهود می‌باشد. در مقابـل طرح‌های SN و FSN که به‌عنوان بتن‌های توانمند رایج مورد بررسی قرار گرفته‌اند، اگرچه دارای مقاومـت ۹۰ روزه‌ای بیش از ۵۰ N/mm^2 بوده‌اند ولی نسبت به مقاومت بتن توانمند پیشنهادی دارای افت مقـاومتی حدود ۶۰ درصد می‌باشند.

۲- در خصوص پارامترهای دوام که در این تحقیق مورد بررسی قرار گرفت نیز طرح مخلـوط پیـشنهادی دارای شاخص‌های بسیار بهتری نسبت به بتن‌های توانمند رایج می‌باشد. اگرچه همه مخلوط‌هـا را مـی‌تـوان جـز بتن‌های با دوام تلقی نمود.

۳- طرح SPD، که بر اساس فلسفه حداکثر تراکم طراحی شده، ولی د رآن از خاکستر بـادی اسـتفاده نـشده، از لحاظ پارامترهای دوام کمی‌پایین‌تر از طرح FSPD می‌باشد. شایان ذکر اسـت طـرح SPD دارای مقاومـت فشاری بیشتر می‌باشد.

مراجع

1. Swamy RN, High performance and durability throug design. ACI SP-159, 1996, p.p. 209-230.
2. Shah SP, Ahmad SH, High performance concrete:Properties and application, McGrow Hill 1994.
3. Mittal A, Basu DC, Development of HPC for PC Dome of NPP, Kaiga, Indian Conc J 1999, 73 (3), p.p. 571-579.
4. Hover KC, Concrete mixture proportioning with water reducing admixture to enhance durability : a quantitative model, Cem Concr Compos 1998;20, p.p.113-119.
5. Malhotra VM, Making concrete greener with fly ash, Concrete International, may 1991, p.p. 61-66.
6. Aitcin PC, High-performance concrete, E&FN SPON, new York, 1998.
7. Smith IA, The design of fly ash concrete, Proc Inst Civil Eng., London 1967;36, p.p. 769-790.
8. Rougeron P, Aitcin PC, Optimisation of the composition of high performance concrete, Cem Concr Aggreg 1994;16(2), p.p.115-124.
9. Collepardi M, admixture used to enhance placing characteristics of concrete, Cem Concr Compos 1998;20, p.p.103-112.
10. Din 1045, Beton und Stahlbeton, Beton GMBH, Koln.
11. Schiessl, Hardtle, Efficiency of fly ash in concrete-evaluation of ibac test result, Technical Report of Institute fur Bauforsching, RWTH, Aachen, p.p.1-31.
12. Ganesh Babu K, Siva Nageswara Rao G, Efficiency of fly ash in concrete, Cem Concr compos 1993;15, p.p.223-229.
13. Bharatkumar BH, and et.al, Mix proportioning of high performance concrete, Cement & concrete composion, 2001;23, p.p. 71-80.
14. Hillemeier,B.H.A.," High Performance concrete Specialised for Acid Resistance ", 1st International Conference on Concrete & Development, April 30-May 2,2001,Tehran,Iran.
15. G.Shakhmenko , J.Brish , " Concrete Mix Design and Optimization ", 2nd Int.PhD Symposium in Civil Engineering, 1998, Budapest.

۱۶. پرهیزکار، هیله مایر، رئیس قاسمی، قدوسی، «استفاده از طرح اختلاط بهینـه بـه‌منظـور بهبـود خـواص مکانیکی و کاهش نفوذ پذیری بتن در شرایط آزمایشگاهی و شبیه‌سازی خلیج‌فارس»، ششمین کنفـرانس بین‌المللی مهندسی عمران، اصفهان، ۱۳۸۲.

۱۷. پرهیزکار، رمضانیانپور، رئیس قاسمی، پورخورشیدی، مظفری، «تاثیر کاربرد خاکستر بـادی در افـزایش دوام بتن‌های توانمند با دوام در شرایط محیطی مهاجم»، هفتمین همایش بین‌المللی سواحل، بنادر و سـازه‌هـای

دریائی (ICOPMAS 2006)، تهران، ۱۳۸۵.

۱۸. پرهیزکار، رئیس قاسمی، «بررسی برخی از خواص نوعی بتن توانمند برای تعمیر سازه‌های بتنی در شرایط محیطی حاشیه خلیج فارس»، هفتمین کنگره بین‌المللی مهندسی عمران (ICCE 2006)، تهران، اردیبهشت ۱۳۸۵.

19. Parhizkar, T., Raiss Ghasemi, A.M., Ramezanianpour, A.A., "Properties of The New Type of HPC in Simulated Conditions of Persian Gulf", Sustainable Construction Materials and Technologies, Coventry, U.K., 2007

CD08

Cement Concrete and Environment

CD08-001

ENVIRONMENTAL IMPACT ASSESSMENT OF CONCRETE INDUSTRY IN IRAN

M. Delnavaz[1], H. Famili[2]
[11]Ph.D. Student in environmental engineering, Tarbiat Modares University, Tehran, Iran
[2]Assistant Professor, Iran University of Science and Technology, Tehran, Iran

ABSTRACT
Constructional industry as the largest consumer of natural materials produces the most portion of the wastes in the country. Concrete being the most commonly used building material in Iran that can have pronounced effect on the production of the waste. Concrete is composed of sand, gravel, crushed rock or other aggregates held together by a hardened paste of hydraulic cement and water. Therefore, evaluation of effects of concrete industry on environment is one of the important cases to be considered. In this paper environmental impact assessment (EIA) of concrete industry is performed, and appropriate recommendations to minimize the effect of environmental impact are given.

Keywords: concrete, environmental impact assessment, sustainable development, IRAN

1. INTRODUCTION
Sustainable development involves meeting present needs without compromising the ability of future generations to meet their needs [1].
The ecological criteria for sustainable development are the preservation of biodiversity and adoption of human activities to the natural resources and tolerance of nature [2]. For this purpose there is increasing concern now that the choice of construction materials must also be governed by ecological considerations.
At the beginning of the 20th Century, the world population was 1.5 billion; by the end of that Century it had risen to 6 billion. Considering that it took 10,000 years after the last ice age for the population to rise to the 1.5 billion mark, the rate of growth from 1.5 to 6 billion people is remarkable [1]. Unfortunately, our choices for technology have turned out to be wasteful, because decisions are based on short term and narrow goals of enterprise rather than a holistic view of the full range of consequences from the use of a technology. Only 6% of the total global production of materials, some 500 billion tons a year, actually ends up in consumer products, whereas much of the virgin materials are being returned to the environment in the form of harmful solids, liquids, and gaseous wastes. The greatest environmental challenge today is that of the human-made climate change due to global warming caused by steadily rising concentration of green-house gases in the earth's atmosphere during the past 100 years [3].
An (EIA) is an assessment of the possible impact (positive or negative) that a

project may have on the natural environment. The environmental impact of building products consists of procurement of raw materials, the manufacturing process and also the use of energy resources during transportation – all of which to some extent burden the environment. Environmental burdens of the cement industry consist of limestone quarrying, burning and grinding of clinker. Extraction, excavation, manufacturing and transportation of aggregates and distribution of the final products are elements for EIA of concrete industry [2].
After water, concrete is the second most widely consumed substance on earth. Using concrete minimizes the depletion of our natural resources. Its ingredients come directly from readily available materials: water, aggregate (sand and gravel or crushed stone), and cement. Cement is composed of 75% limestone, the most common mineral on earth. Although extracting any raw material from the earth takes a toll on the environment, extracting the raw materials for concrete has a lower impact than that of other construction materials. Because the ingredients for concrete are so plentiful, supplies are virtually inexhaustible
The goal of this paper is to identify the environmental impacts of concrete and its products which in-turn can lead to determining options for improving environmental effects.

2. EIA OF CONCRETE INDUSTRY IN IRAN

I.R. Iran is located in the center of the Middle East and bridges the Caspian Sea to the Persian Gulf and the east of Asia to the west of Asia. Because of its strategic location it is one of the important countries in the region. Iran has complex climate ranging from subtropical to sub polar and that it is possible at the same time to witness the climatic conditions of all four seasons in the different parts of its territory. The building industry is one of the most important industries in Iran, concrete being the most widely used material. Therefore the concrete industry is very important from the point of view of EIA.

2.1. Concrete Components

Ordinary, concrete typically contains about 12 percent cement, 8 percent mixing water, and 80 percent aggregate by mass. The 11.5 billion tones-a-year concrete industry is thus the largest user of natural resources in the world. The demand for concrete is expected to grow to approximately 18 billion tons (16 billion tones) a year by 2050 [4]. This means that, in addition to 50 million tones of cement (current annual production of cement in Iran), the concrete industry in Iran is consuming annually 137 million tones of fine and coarse aggregate together with 15 billion liters of mixing water.

2.1.1. Cement

The examination of concrete manufacturing shows that the cement, which usually makes up 10–15% of concrete, is the main environmental polluter. Cement manufacturing covers material and energy flows during the extraction of materials, and the production processing such as raw meal, clinker burning, grinding and transportation of the product. Because of the high temperatures used during cement production and the decomposition of calcium carbonate, the cement accounts for over 60% of energy used in concrete manufacturing. The amount of cement production and consumption per capita in Iran is shown in figure 1. Estimated world cement production and CO_2 emission in cement manufactures are shown in figure 2 and 3 respectively [2].

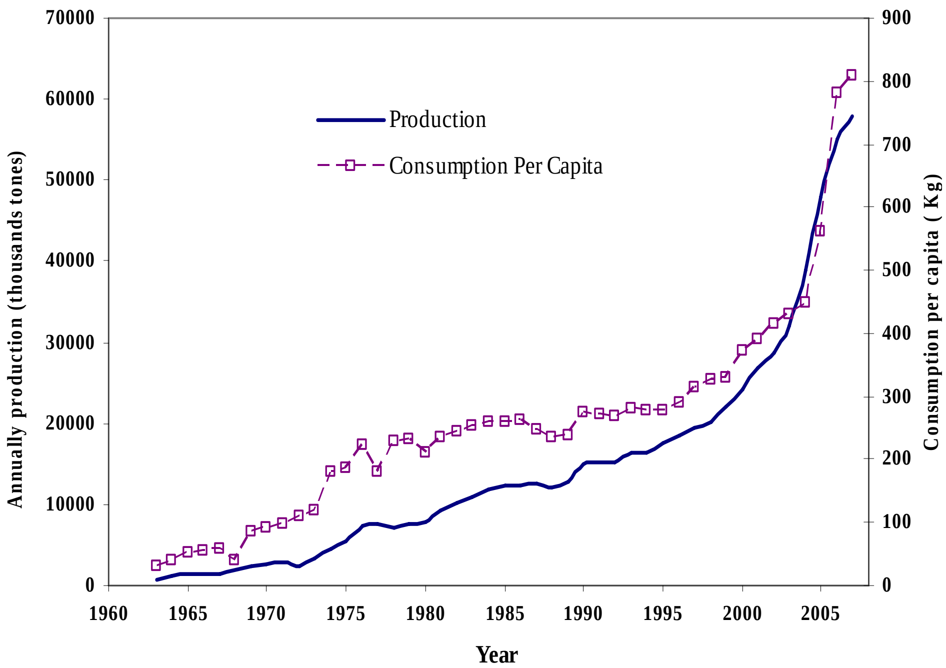

Figure 1. Cement production and consumption per capita in IRAN (1963-2007) [5]

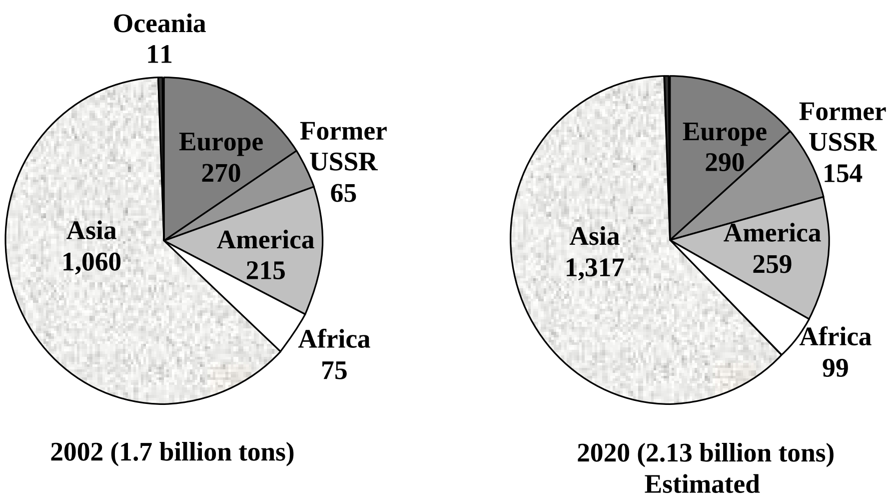

Figure 2. World Cement Production

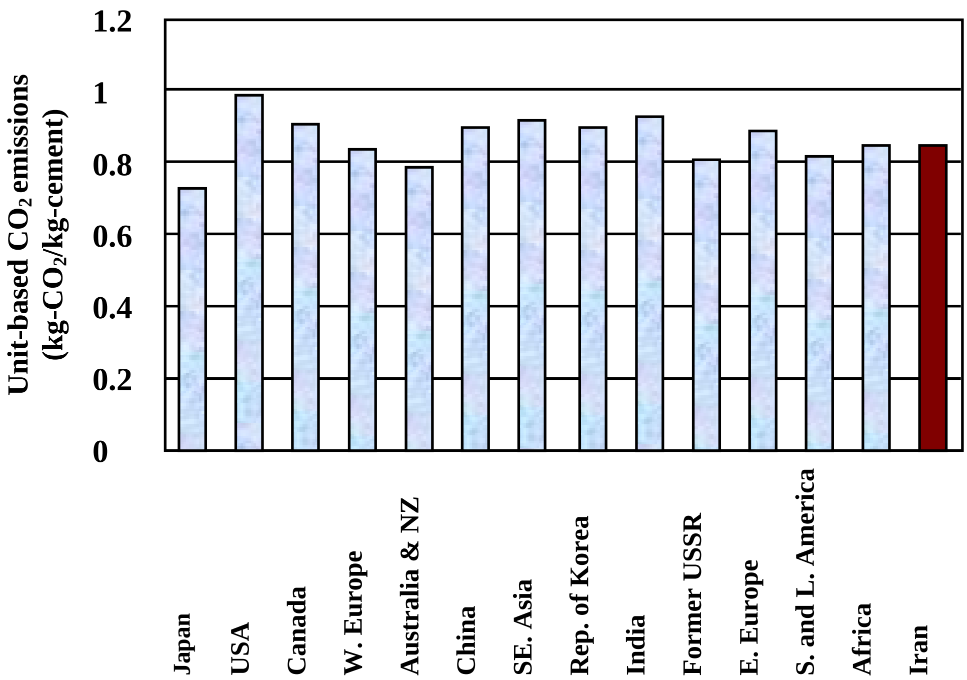

Figure 3. Unit-based CO_2 Emission in Cement Manufactures

The most serious problem with cement industry is that it is a major CO_2 emitter causing global warming. With every ton of cement produced, almost a ton of CO_2 is emitted [6]. About 0.5 tons comes from the decomposition of limestone and the balance is generated by power plant supplying electricity to turn the kiln and ball mills to grind the cement plus the fuel burned to fire the kiln. All other sources of CO_2 emission such as operating ready mix trucks adds only a minor. In terms of conventional concrete mixtures (not containing fly ash, slag or silica fume), about 480 kg of CO_2 is emitted per cubic meter of concrete or 20 kg of CO_2 per 100 kg of concrete produced. All of this amounts to about 7% of the total CO_2 generated worldwide [7]. Enhanced efficiency is not likely to change this but the replacement of some of the cement by a supplementary cementing material not associated with CO_2 emissions can substantially reduce these emissions.

- **Nitrous Oxide Emissions**

Nitrous oxide emissions come from burning gasoline, coal or other fossil fuels. Ozone is formed when nitrogen oxides and volatile organic compounds mix in sunlight. The volatile organic compounds come from sources ranging from industrial solvents to volatile resins in trees. Ozone near the ground can cause a number of health problems such as asthma attack, sore throat, coughing and other health difficulties. In addition, nitrous oxide, carbon dioxide and methane are the most important greenhouse gases [8].

The No_x emissions from Canadian cement kilns range from 1.5 to 9.5 kg/tones of clinker produced with a proposed limit of 2.3 kg of No_x per tone [6]. Using 2.3 kg of No_x per tone, the world release of No_x by the 2130 million tones of cement produced in the year 2020 would be 4.85 million tones of No_x. This is a fifth of the No_x released in all of continental Asia in a year [9]. Reduction in nitrous oxides is normally achieved by reducing the burning temperature or by injecting ammonia compounds into the high temperature exhaust stream [6]. This seems like a good idea but when these actions are taken to reduce the No_x in coal fired electric power generating stations, it adversely affects the quality of the fly ash produced. The fly ash then needs to be treated to remove the unburnt coal and ammonia gas before it can be used in concrete mixtures and several plants doing this are in operation.

- **Particulate Air Emissions**

Particulate emissions from the exhaust gases range from 0.3 to 1.0 kg/tone. It is normally very rich in sodium and potassium which have vaporization temperatures of only 883°C and 774°C respectively. In the past, before there was a concerted effort to capture the particulate emission, the sodium and potassium plume from cement plant chimneys settled over the countryside where it helped to combat acid rain. Now it is mainly carried out in the clinker stream where it creates problems with alkali aggregate reaction [10].

2.1.2. Aggregate

The coarse and fine aggregate content in concrete products is approximately 80% and it covers < 3 % of emissions and energy used. The environmental burdens from procurement of aggregate consist of:

- using raw-materials;
- using land; and
- using energy (in extraction, excavation and crushing of stone materials and in transportation) which causes emissions into air.

Besides these, crushing causes dust emission and quarrying causes land and stone waste. The energy used in gravel excavation and crushing is much less than in production of building materials where heating or grinding is employed (i.e., cement production). Energy used in stone crushing depends on the desired size fraction. Table 1 shows an example of energy used for gravel excavation and Table 2 in quarrying and crushing.

Table 1: Energy used in gravel excavation [2]

Gravel excavation	0.02 MJ/kg	70%
Gravel transport (10 km)	0.01 MJ/kg	30%
Total	0.03 MJ/kg	100 %

Table 2: Energy used in gravel production [2]

Quarrying + Crushing	0.05 MJ/kg	80%
Removal and transportation	0.01 MJ/kg	20%
Total	0.06 MJ/kg	100 %

2.1.3. Water

The water shortage in Iran is a serious problem and this intensified by seasonal rainfalls. Only 10 percent of the country receives adequate rainfall for agriculture; most of this area is in western Iran.

Concrete manufacturing uses normal tap water to make up about 0.06 – 0.10 kg/kg concrete. The total water supply system consumes very little energy for water purifying and delivery so the overall environmental impact remains small [2].

On average of each ready mix about half cubic meter of concrete remains in the truck per day. After concrete is discharged there is still about 300 kg of solids (cement, sand and stone) that it is necessary to washed out, with about 1000 liters of water. In the past the returned concrete and the solids were dumped in a pit at the job site or at the plant. Considering that this represents 2 to 4% of the total concrete produced, it is now considered too valuable to waste and can be recycled or reclaimed as sand and gravel. To reclaim the sand and gravel a "reclaimer" is used. It involves adding water to the returned concrete and then agitating it followed by wet screening to obtain the sand and gravel. Also, the cement-water slurry from the reclaimer, the wash out water, water to clean the outside of the truck, plus any stormwater in the past usually was directed into somewhat inefficient settling basins and then into a local water course [11-12].

2.1.4. Chemical Admixtures

The most common admixtures in concrete are plasticizers and air entrainers. The plasticizers used include lignosulphonate salts, hydroxyl-carboxylic acid, modified melamine, naphthalene and polymers. These are synthetic organic compounds which have a deflocculating and dispersing effect. They act on the forces between solid particles suspended in water by reducing the surface tension of water. Plasticizer content in concrete is typically very low 0.002 – 0.1% (by weight of cement) so their effect on energy use and emissions of concrete products is very low. Plasticizers are non-volatile compounds which mean that their effect on the indoor climate is also inconsequential. Air entraining admixtures are invariably organic substances which help to generate microscopic bubbles of air in the fresh concrete to improve concrete frost resistance. Air entraining agents are based on carboxyl acid salts, alkyl sulphonates, and phenolethoksylates. The most common air entraining agents are made from pine oil and they are alkali metal salts. Pine oil consists of fat and resin acid compounds, which are produced from sulphate pulp processing. Air entraining admixture content in concrete is also typically very low 0.002 – 0.02% (by weight of cement) so their effect on energy use and emissions of concrete products is very low [2].

2.1.5. Mineral Admixtures

- **Fly Ash**

Substitution of cement or natural aggregates with industrial by-products can be done in concrete production. From an environmental point-of-view this result is saving our natural resources and land. It is possible to substitute concrete aggregate with wastes from metal productions, mining industry or mineral stone industry by-

products such as ferrochrome slag or blast-furnace slag. In some cases when using by-products the crushing and transportation can consume more energy than in procurement of the natural resources.
Fly ash from power plants can be used as a substitute for cement or filler. Ash which contains desulphurization products rich in sulphate or sulphite is not suited for making concrete. By using fly ash the environmental profile of concrete or concrete products can be affected only by the ash transport burden. Approximately 10–30% of cement content can be substituted by fly ash without much effect on concrete properties [2]. Currently in Iran fly ash is not produced but natural pozzolanic materials and silica fume are available and can be used.

- **Blast-furnace slag**

Cement can also be substituted by ground granulated blast-furnace slag. Blast-furnace slag is a by-product of crude iron production and its economical value is negligible compared to the crude iron. As such blast-furnace slag is not suited for use as concrete binder because to achieve hydraulic properties it needs to be cooled fast, dried and ground to typical cement fineness. Blast-furnace slag processing uses less energy and causes considerably less emissions than cement manufacturing, so already a small amount of cement substitution with blast-furnace slag lowered environmental burdens. Blast-furnace cement has 10% blast-furnace slag addition but it could be increased to approximately 70% of the total binder content. Compared to concrete composed of 100% cement, the appropriate use of blast-furnace slag in concrete products as a cement substitute decreases environmental effects [2]. The bad quality of blast-furnace slag in Iran limited its content in concrete to 10-15%.

2.2. Durability of Concrete for Eia

One of the most important considerations in the concrete industry is the durability of concrete. When a concrete structure has inadequate durability it causes solid waste generation sooner than it is expected. From an environmental point of view it is essential that every concrete structure should continue to perform its intended functions, which are maintaining its required strength and serviceability during the specified or traditionally expected service life. Improving concrete durability can cause a decrease in solid waste generation in building industry. Therefore quality control of concrete in the Persian Gulf environment has a long record of stigma attached for its harsh climate, desert features and saline waters that do not render the longevity of concrete is very important [13]. Use of supplementary cementitious materials such as silica fume and blast furnace slag with Portland cement has increased durability of concrete in the Persian Gulf region and therefore decreased solid waste form short-lived concrete.

2.3. Recycle of Industrial and Building Wastes for Use in Concrete

Recycled aggregate concrete has become the focus in the past decades due to its great environmental effect. In the USA, about 30 million tons of concrete has to be discarded each year. This number increased from 55 million tons in 1980 to 162 million tons in 2005, approximately tripled in less than 30 years. China faces a more serious problem to cope with discarded concrete with the increasingly rapid urbanization process. For example, Shanghai City alone, wastes concrete 20 million tons annually. Other reasons may also lead to waste concrete. An 8.0 magnitude earthquake in Sichuan province, China on 12th May, 2008 caused collapse of at least four millions houses, which produced tremendous discarded concrete. Similar problems are presented in Iran. Recycling of concrete is, therefore, becoming increasingly important to ensure sustainable development both in world [14].

Waste management and disposal is a major environmental concern in many countries and increasingly becoming a significant environmental, health, and aesthetic problem that is not easily solved [15]. Therefore due to the increasingly serious environmental problems presented by hazardous industrial wastes, the feasibility of burying these materials as aggregate in concrete would be of great interests.

3. CONCLUSION & DISCUSSION

- Constructional industry as the largest consumer of natural materials produces the most portion of the wastes in the country. The concrete industry has potential for environmental pollution.
- With the exception of CO_2 and NO_x emissions, by using our current technology all the perceived environmental problems with concrete can be effectively resolved. The concrete industry needs to focus on these two greenhouse gases.
- In the concrete industry the easiest and most effective way to reduce green house gases is to increase the use of such silica rich by-products as slag and silica fume and natural pozzolanes, thereby reducing the amount of cement used per cubic meter of concrete.
- Concrete industry generates about 7% of the total CO_2 generated globally and if we assume that only 18.5% of the cement can be replaced with slag or fly ash, then the CO_2 reduction would be 300 million tons per year world wide.
- Over the past decade the average annual increase in CO_2 emissions has been 1.3 percent or nearly 300 million tons a year. Therefore our industry could greatly help in easily reducing global warming and at the same time enhance the properties of the concrete.
- Improvement in the durability of concrete in corrosive environments such as the Persian Gulf that has a long record of stigma attached for its harsh climate, desert features and saline waters, can help to reduce solid waste generated from short-lived concrete in these regions.
- The recycling of industrial and building wastes for use in concrete can have significant effect for the environment.

REFERENCES

1. Parrott, Les,. (2002) "Cement, Concrete & Sustainability", Progress of the

UK Cement and Concrete Industry Towards Sustainability.
2. Vares, Sirje,. Häkkinen, Tarja. (2002) "Environmental burdens of concrete and concrete products", Technical Research Centre of Finland.
3. Anon (1991). Protocol to the convention on long-range transboundary air pollution concerning the control of emissions of volatile organic compounds or their transboundary fluxes. United Nations – Economic Commissions for Europe. Geneva.
4. Mehta, P.K. Monteiro, P.J.M., (2000) "Concrete: Microstructure, Properties, and Materials".
5. www.irancement.com
6. Klein, Manfred and Donald Rose, (1998) "Development of CME National Emission Guidelines for Cement Kilns" in CANMET/ACZ International Symposium on Sustainable Development of the Cement and Concrete Industry, editor V.M. Malhotra, Ottawa, pp. 16-30.
7. Malhotra, V.M., (1999)"Making Concrete “Greener” with Fly Ash", in Concrete International, Vol. 21, No. 5, pp. 61-66.
8. Brunner, Borgna, (2001) "Time Almanac ", Time Inc., Boston,p. 594.
9. Clarke, Robin. (2000) "Global Environmental Outlook " United Nations Environment Program, Nairobi, Kenya, , Earthscan Publications Ltd., London, U.K., 398 pp.
10. "CCME National Guidelines for the Use of Hazardous and Non-Hazardous Wastes as Supplementary Fuels in Cement Kilns." (1996) Department of the Environment, Government of Canada, Ottawa,
11. Ruhlin, Douglas, (1995) "Concrete Reclaimers A Tool for Environmental Compliance", Concrete Journal, pp .193-197.
12. Ruhlin, Douglas, "Compliance Matters - Stormwater Permitting for Concrete Producers", Concrete Products Magazine, May 2000, pp. 28-34.
13. Ganjian, Eshmaiel., Sadeghi Pouya, Homayoon., (2009) " The effect of Persian Gulf tidal zone exposure on durability of mixes containing silica fume and blast furnace slag" Construction and Building Materials, 23, pp. 644-652.
14. Li, Jiusu., Xiao, Hanning., Zhou,Yong., (2009) " Influence of coating recycled aggregate surface with pozzolanic powder on properties of recycled aggregate concrete"Construction and Building Materials, 23, pp.1287-1291.
15. Khaloo, Ali R., Dehestani, M., Rahmatabadi, P. (2008) "Mechanical properties of concrete containing a high volume of tire–rubber particles", Waste Management, 28, PP. 2472-2482.

CD08-002

WASTE CEMENT AND CONCRETE MANAGEMENT AS COST-EFFECTIVE AND ENVIRONMENT FRIENDLY: PRINCIPLES AND PERSPECTIVES

I.M. Kelayeh[1], A.A. Mounesan[2], K. Siamardi[3], M.M. Khodavirdi Zanjani[3]
[1] Member of Management Association, Assistant of Technology & Development, Civil
[2]Civil Engineer, Sharif University of Technology, General Manager of Atisaz Company
[3]Civil Engineer, Concrete Research Center, Atisaz Company

ABSTRACT
The use of recycled aggregates in concrete opens a whole new range of possibilities in the reuse of materials in the building industry. The utilization of recycled aggregates is a good solution to the problem of an excess of waste material, provided that the desired final product quality is reached. The studies on the use of recycled aggregates have been going on for 50 years. In fact, none of the results showed that recycled aggregates are unsuitable for structural use. Using the recycled aggregate is a cost-affective and environmental friendly solution which is required general waste concrete management knowledge. This paper is focusing on waste cement and concrete management for optimizing the construction costs. The ways for reducing the green house gases (GHG) at cement and batch plants are suggested. A comparison among Iran industrial utilized cement volume and other countries was performed. Finally, it can be concluded that application of recycling concrete could reduce the costs by reducing truck traffic, providing the Non-Renewable Resource, Better Trucking Utilization (Reduced Costs), Allow down to 10% Deleterious Materials in Iran.

Keywords: waste concrete management, utilized cement volume, cement plants, concrete recycling, GHG reduction.

1. INTRODUCTION
The amount of construction and demolition waste (CDW) has increased considerably over the last few years. The recycling and the reuse of this material is necessary, considering the impact that the use of natural resources and non use of CDW is causing. This would not happen if the use of recycled material were possible.
The largest CDW obtained is concrete [1, 2], and it is the most used construction material nowadays. The studies with respect to the applicability of recycled concrete aggregates (RCA) are extended around the world.
Furthermore, Industrial waste is causing more and more environmental pollution. Dirty water and poisonous gases are released from factories and workplaces in ever increasing quantities. This has led to a new appraisal of a company’s obligation to society. A company is now seen as having as much responsibility for avoiding

environmental pollution outside the factory as for maintaining cleanliness inside. Companies must establish standards for disposing of their waste in a way that will not pollute the environment.
The application of waste materials in cement and concrete industry can improve the ecology cycle and prevent environmental pollution. So, waste cement and aggregate for generating new types of waste concrete is needed to total management.

2. COMPARING IRAN UTILIZED CEMENT AND CONCRETE STATUS WITH OTHER COUNTRIES

Unfortunately, new concrete technology is applied rarely except special or national construction projects in Iran. Existing structures are almost heavy and low strength and advanced concrete knowledge haven't utilized in design and construction of structures that causes in vulnerable structures subjected to ground shaking.
Relation between research centers of universities and construction industry could be optimum alternative for implementation of new concrete technology in real scales.
Used cement is just 10.8 % in Iran Industry. Used cement in ready mixed concrete part is 8.64% of total used cement in Iran. 2.16 % of used cement is subjected to construction of concrete segments while Japan used cement is 86.4% which for ready mix concrete and concrete segments is 73.2 and 13.2% respectively.
United states used cement volume is 66.7% too and according this, 55.7% and 11% of cement is related to ready mix concrete and concrete segments part respectively.
Turkey and Russia used cement volume in industry is 74.4 and 71.3% respectively. 62 and 52 % of used cement in mentioned countries is assigned to ready mix concrete and 12.4 and 19.3% is assigned to concrete segment respectively [3]. Comparison of industrial used cement volumes among countries is shown in figure 1.

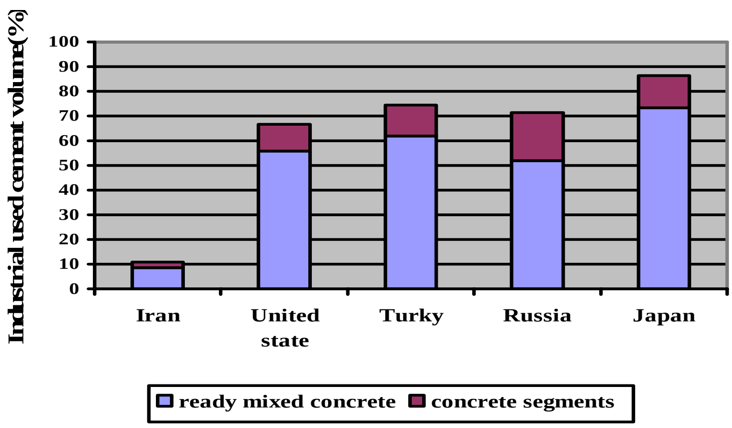

Figure 1. Comparison of industrial used cement volumes among countries

On the other hand, utilized cement infrastructure is still incorrect in Iran. Significant part of utilized cement generate by hand. Failed structures in past strong earthquakes have proved that existing structures is vulnerable especially in Tehran metropolitan. Past Tehran earthquakes have occurred each 150 years. Forcing the ready mixed concrete plants for issuing quality justification is effective solution as more than 75% of ready mixed concrete plants have received standard certificate. In addition, light weight structures construction for improving the seismic performance of structures is important while 20% of light weight building materials utilized in country and remained materials is exported to out of country. Application of light weight concrete in buildings is required the three administration of managers, investors and illuminates cooperation.

3. MANAGEMENT PRNCIPLES IMPORTANCE

3.1. Improves Understanding about Cement and Concrete Industry

From the knowledge of principles managers get indication on how to manage the waste concrete industry. The principles enable managers to decide what should be done to accomplish given tasks and to handle situations which may arise in waste concrete management. These principles make managers more efficient.

3.2. Direction for Training of Managers

Principles of management provide understanding of management process what managers would do to accomplish what. Thus, these are helpful in identifying the areas of management in which existing & future managers should be trained.

3.3. Role of Management

Management principles makes the role of managers sensitive. Therefore these principles act as ready reference to the managers to check whether their decisions are appropriate. Besides these principles define managerial activities in practical terms. They tell what a manager is expected to do in specific situation.

3.4. Guide to Research in Management

The body of management principles indicate lines along which research should be undertaken to make management practical and more effective. The principles guide managers in decision making and action. The researchers can examine whether the guidelines are useful or not. Anything which makes management research more exact & pointed will help improve management practice.

4. CEMENT PRODUCTION RELEASE GHG PROCESS

Cement production generates GHG from two main sources: calcination and fuel combustion. Calcination is the chemical process in which calcium carbonate ($CaCO_3$) is heated to high temperatures, converting it to lime or calcium oxide (CaO), and releasing carbon dioxide (CO_2). So it is not surprising that the main type of GHG from cement production is carbon dioxide (CO_2). The amount of CO_2 released due to the calcination process alone usually varies from 50 to 60 percent the total amount of CO_2 released during cement production. The remaining 40 to 50 percent is mainly due to fuel combustion. The contribution of each of these sources (calcination and fuel combustion) depends on energy efficiency. The percent of CO_2 released from fuel combustion in efficient cement plants tends to be lower since less fuel will be needed to produce the same amount of cement. Figure 2 shows the cement plant.

Figure 2. Cement plant

4.1. Ways to Reduce Cement Ghg at Cement and Batch Plants

4.1.1. Blending SCM at cement plants

Blending cement with Supplementary Cementitious Materials (SCMs) reduces GHG emissions. Common SCMs in use include slag, fly ash, silica fume, and calcined clay. Using two or more SCMs together with portland cement is referred to as a ternary cement mix. Proper use of ternary mixes comprised of fly ash and slag produce not only less but also better quality concrete. The addition of SCM at cement plants has the potential to significantly impact GHG savings.

4.1.2. Environmentally friendly fuel for cement kilns

Use of environmentally friendly fuels would reduce GHG emission by using less carbon intense fuels. Although coal is one of the most efficient and cost effective fuels for heating a kiln, it is also one of the most intense in terms of the CO_2 emissions. Therefore, it is important to use alternative fuels instead, such as recycled materials.

For example, In 2005, fuel combustion from coal constituted about 73 percent of all emissions from fuel combustion by cement plants in California. This number has decreased since 1990 when coal was responsible for about 85 percent of all fuel combustion emissions.

4.1.3. Using of interground limestone

The limestone addition strategy consists of replacing cement with interground limestone. Since interground limestone is added at the end of the cement production line, the cement-related greenhouse gas (GHG) emissions will be reduced proportionally to the amount of limestone added. The GHG savings arise from avoiding GHG emissions associated with cement production during fuel combustion and calcination in the kiln.

The maximum GHG savings generated by this strategy is 5 percent, which is the maximum limestone allowance per American Society of Testing Material (ASTM C 150), a major nationwide cement specification. Since the effect of limestone addition to cement had not been studied in detail, Caltrans sponsored a comprehensive study, use of raw limestone in portland cement, designed to evaluate the three primary indicators of concrete performance: strength, drying shrinkage, and permeability[4]. It was found that limestone improved strength and permeability (at early ages).

Since 2007 Caltrans has been accepting 2.5 percent limestone addition. After concluding the limestone study, Caltrans will accept the full 5 percent but implement a performance-based specification to control shrinkage. Although 5 percent of limestone is allowed per ASTM C 150, it is estimated that the statewide limestone addition may not exceed 3.5 percent based on manufacturing limitations. According to reports from the portland cement association (PCA), the estimated average nationwide is only 2.5 percent [5].

4.1.4. Production efficiency improvements

Significant GHG emission reduction for California is not expected of this particular strategy. One of the reasons being that the cement industry in California is already among the most energy efficient in the world. It has been reported that one of the most recent cement plants built in California has a GHG intensity of only 0.02 below that of the 2005 California average GHG intensity factor of 0.86 ton of CO2 per ton of cementitious material.

All cement plants in California except one have precalcinators. These pre-heaters significantly improve energy efficiency by heating limestone prior to its placement in the cement kiln. Another process-related piece of equipment that significantly improves energy efficiency is the dry kiln compared to wet kiln usage: All cement plants in California have dry kilns. Using one kiln instead of multiple is also recommended to further improve energy efficiency. Only one cement plant in California uses multiple kilns. According to the California Cement Industry (2008), the energy efficiency of California cement plants is 15 percent better than the average U.S. value since 1995.

Another reason for a small GHG emission reduction is the fact that production efficiency improvement only affects 40 percent of the GHG emission from cement production. The other 60 percent of GHG emissions comes from calcination, which is a natural chemical process inherited from the cement production process in which limestone (CaCO3) is converted to calcium oxide (CaO) by releasing carbon dioxide (CO2) in the presence of heat, as follows:

$$CaCO3 + heat \longrightarrow CaO + CO2$$

Since fuel combustion is responsible for only 40 percent of the GHG emissions, a reduction in energy consumption of 4.5 percent accomplished by California Portland, only reduced GHG emissions by 1.8 percent. California Portland was named the 2007 Energy Star Partner of the Year for such energy reduction. This saved the company about $850,000 in operating costs.

4.1.5. Optimizing cement content at batch plants

Optimizing cement content can be prescribed as a strategy to reduce GHG. In some cases, a higher amount of cement is used because of the desired early concrete strength. For instance, a homeowner or general contractor may need concrete with a compressive strength of only 14 MPa. This 14 MPa concrete only needs about 135 Kg of cement to gain this strength at 28 days. That strength requirement can be met if the homeowner or contractor allows more time for concrete to gain strength.

Another option for homeowners and general contractors would be the use of admixtures to accelerate the strength gain of the concrete mix. While there is a cost to these admixtures, they can be used to reduce GHG through the reduction of cement. To optimize the amount of cement, concrete mixes can also reduce the amount of water used since this results in a stronger concrete. Reducing the amount of water would also involve some additional cost for plasticizer or water-reducing admixtures. This cost may be compensated for by cost savings of optimized cement content.

Example: when a mix for a concrete driveway replaces 25 percent of the cement with fly ash, and uses half the normal amount of cement, as much as 5.7 tones of CO_2 can be saved per driveway, assuming each ton of cement emits 0.9 tons of CO_2. This is equivalent to the CO_2 emissions from about one passenger car for the entire year, as the average passenger car emits about 5.2 tones of CO_2, based on data from the Environmental Protection Agency (EPA).

To calculate this emission, it was assumed that each car travels 19,300 Kilometer per year, gets about 8,631 Km per cubic meter and each cubic meter of fuel emits 2,235 tones of CO_2 per cubic meter. To achieve this savings, it may be necessary to keep cars off of the driveway longer. If it is necessary to get strength faster so vehicles can access the driveway, these GHG savings can still be obtained by adding an accelerator to the mix at a concrete cost increase of about 10 percent.

4.1.6. Reducing concrete waste

This strategy seeks to significantly reduce the concrete waste occurring at batch plants. It is estimated that approximately 5-8 percent of the concrete that is made in California every year is returned to the batch plants as waste. Concrete waste (or concrete returned to batch plants) is generated for the following two main reasons: 1) a load of concrete is not completely used, or 2) a load of concrete is rejected by an inspector due to the mix not meeting some specified characteristic. The worst case for a return in terms of GHG is when the plastic concrete is separated back to sand, gravel, and water, and the cement was then truly a waste product.

Concrete is almost always left over at the end of a job. The main reason is because it is more cost-effective to overestimate rather than be short of the material needed. Here are a few ways to reduce waste, and consequently GHG:

1. Better estimating of total concrete requirements.
2. Use of volumetric trucks to handle the exact needs of the last quantities of the day.

3. Design locations to receive the returned or left over concrete. One of the ways to re-use the concrete would be to make concrete blocks for later sale. Another is to use that last truck to make sidewalks that may have been planned for a later placement.

5. APPLICATION OF RECYCLING CONCRETE AS WASTE AGGREGATE IN CONCRETE

5.1. Aggregates are Required for Construction Projects

Aggregates are composed of rock fragments that may be used in their natural state or after mechanical processing such as crushing, washing, and sizing. Natural aggregates consist of both sand and gravel, and crushed stone. Recycled aggregates consist mainly of crushed concrete and crushed asphalt pavement. Construction aggregates make up more than 80 percent of the total aggregates market, and are used mainly for road base, riprap, cement concrete, and asphalt. Aggregates provide bulk, strength, and wear resistance in these applications. Construction aggregates increased from 36 percent of all raw materials used in the United States in 1900 to 70 percent in 1958, a compound annual growth rate of 1.15 percent. From 1958 to 1998, Americans have maintained their use of construction aggregates at 70–73 percent of their total raw material demand [6].

5.2. Concrete Recycling

Aging U.S. infrastructure, decreasing availability of landfill space, and environmental concerns work together to increase concrete recycling. There are two approaches to recycling concrete. One alternative is to haul the concrete debris to a permanent recycling facility, usually close by to minimize transportation costs, for crushing and screening. The other approach is to do the crushing and screening at the demolition site where the aggregate is reused as soon as it is processed. Recycling at the demolition site reduces heavy materials hauling, thereby reducing transportation costs, energy use, and wear and tear on roads and equipment. Figure 3 shows the schematic flow of concrete recycling. Figure 4 shows the stages of concrete recycling [7].

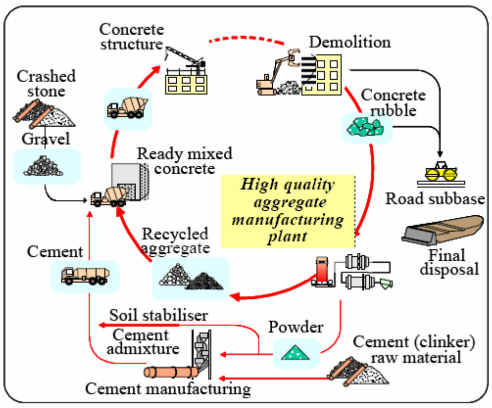

Figure 3. Schematic flow of concrete recycling

Figure 4. Concrete to be Recycled, Concrete Crushing, Processed Concrete

5.3. Recycling-Small Market Share, But Large Tonnage

Construction Materials Recycling Association, Lisle, Illinois, states that about 100 million t of concrete is recycled annually into usable aggregates. Aggregates produced from recycled concrete supply roughly 5 percent of the total aggregates market (more than 2 billion t per year), the rest being supplied by aggregates from natural sources such as crushed stone, sand, and gravel. Preliminary data indicate that in 1998, 3,400 U.S. quarries produced about 1.5 billion tones of crushed stone, of which about 1.2 billion tones was used in construction applications. About 5,300 sand and gravel operations produced more than 1.0 billion t of construction aggregates in 1998. application of recycling concrete could reduce the costs by reducing truck traffic, providing the Non-Renewable Resource, Better Trucking Utilization (Reduced Costs), Allow down to 10% Deleterious Materials in Iran.

5.4. Concrete Recycling Product

The bulk of the aggregates recycled from concrete—an estimated 68 percent—is used as road base. The remainder is used for new concrete mixes (6 percent), asphalt hot mixes (9 percent), high-value riprap (3 percent), low-value products like general fill (7 percent), and other (7 percent) [8]. The low usage rate of recycled aggregates from concrete (15 percent) in high-value new concrete and asphalt hot mixes, compared to the higher usage rates in lower valued products, is related to quality issues, both real and perceived. State agencies have been slow to accept recycled aggregates from concrete for high-quality uses such as road surfacing. Specifications, based on considerable research and favorable in-service experience, have allowed its use mostly as road base material. Some States are experimenting with the conversion of existing worn-out concrete roads to rubble-in-place. The old concrete surface is broken up and compacted, and asphalt pavement is placed over the enhanced base, composed of the original base and the new layer of compacted rubble.

6. LIFE CYCLE ENERGY AND CO2 OF HIGH QUALITY RECYCLED AGGREGATE BY HRM

There is a developed technology for producing high quality aggregate from demolished concrete using a "heating and rubbing method" (HRM) [9]. Using this technology, aggregate can be recycled as raw, material for ready mixed concrete, while fine powder (HRM powder) from cement paste can be recycled as raw material for cement, cement admixture, or soil stabilizer. The HRM uses a considerable amount of energy to heat and rub concrete. Life cycle CO2 and energy of the recycled aggregate are calculated to evaluate this technology. The recycled aggregate is produced from demolished concrete and the HRM powder is used for a soil stabilizer in case 1-1. The HRM powder is used as part of cement raw materials in case 1-2. The production of crashed stone, which is the most popular aggregate, is calculated in case 2. The result of life cycle CO2 is shown in figure 5. In case 1-1 and 1-2, the life cycle CO2 is a negative value because the deduction of CO2 emission during cement manufacturing by the powder is much larger than the emission during recycled aggregate production. In case 2, the CO2 emission from crashed stone production is very small but still positive. This method is proved to be very effective to reduce CO2. As for the life cycle energy, its use of recycled aggregate is greater than that of crashed stone as ordinary aggregate because the deduction of energy consumption during cement manufacturing by the powder is relatively small [9].

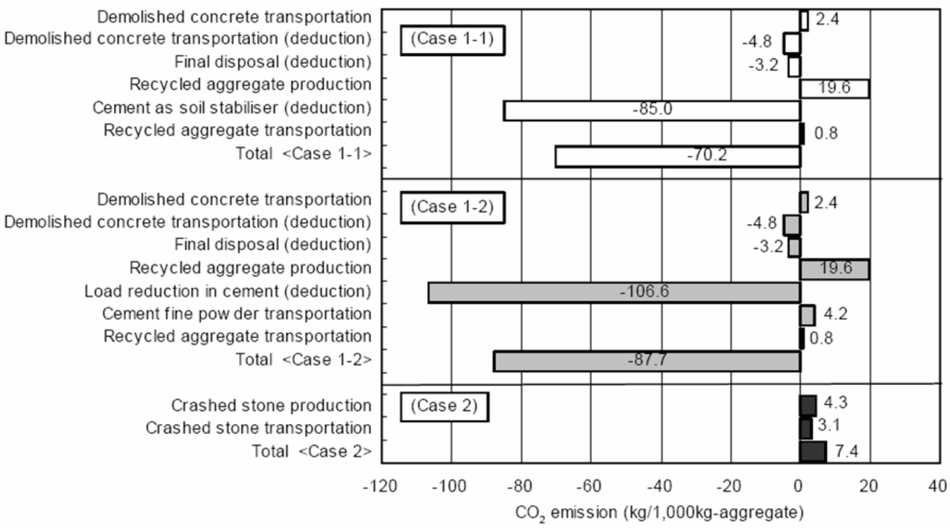

Figure 5. Life cycle CO2 of high-quality recycled aggregate by HRM

7. CONCLUSION

Concrete recycling has proven to be profitable, but its use has limitations. Transportation costs need to be kept low, which forces the market to be urban-oriented. The market for recycled aggregates may be restricted by user specifications and prejudices. Finally, the availability of feedstock into recycling plants is fixed by the amount of demolition taking place, which generally places the activity within older, larger cities. Depending on the size of the recycling facility, entry into the aggregates recycling business requires a capital investment.

Processing costs for the aggregates recycler again depending on the size of the operation. The larger operations distribute costs over more units of output. The average production capacity for a fixed site recycling operation should be determined. Prices for the various aggregate products made from recycled concrete should be evaluated from region to region.

Recyclers often have the opportunity to charge a fee for accepting concrete debris, especially where landfill space is running short and charges for depositing materials into landfills are high. In such cases, the added revenue can compensate for a lower market price for the recycled aggregate product. As natural aggregate producers dominate the market, they tend to set the terms that recyclers can obtain.

The future for recycled aggregates will be driven by reduced landfill availability, greater product acceptance, continuing government recycling mandates, and the continuing decay of a large stock of existing infrastructure, as well as by the demands of a healthy economy.

On the other hand, the industrial utilized cement infrastructure could be improved by observing the ways to reduce cement GHG at cement and batch plants, optimizing cement content at batch plants, reducing concrete waste, application of recycling concrete as waste aggregate in concrete in Iran.

REFERENCES

1. Symonds (1999) European Commission. Construction and demolition waste management practices, and their economics impacts. Report to DGXI, European Commission.
2. Hendriks ChF, Pietersen HS, Fraay AFA (2000) Recycling of building and demolition waste. An Integrated approach, Proceedings of the International Symposium on ‘Sustainable Construction: Use of Recycled Concrete Aggregate’, London, UK, pp 419–431.
3. Mining and development Information service web site: www.news.imidro.org/fa/news.service/categories
4. ASTM C 150. Standard Specification for Portland Cement, 1994. American Society for Testing and Materials.
5. California Department of Transportation (2009), News, Sacramento, CA, USA.
6. Wilburn, D.R., and Goonan, T.G., 1998, Aggregates from natural and recycled sources: U.S. Geological Survey Circular 1176, 36 p.
7. Kelly, T.D., 1998, The substitution of crushed cement concrete for

construction aggregates: U.S. Geological Survey Circular 1177, 15 p.

8. Deal, T.A., 1997, What it costs to recycle concrete: C&D Debris Recycling, September/October, p. 10–13.
9. Shima, H., Matsuhashi, Yoshida, Yoshida, Y. and Tateyashiki, H. (2003a). "Life Cycle Analysis of High Quality Recycled Aggregate Produced by Heating and Rubbing Method." IEEJ Trans. EIS, 123-C (10), 1680-1687.

CD09

Concrete and Architecture

CD09-001

FEASIBILITY OF CONCRETE USAGE IN RURAL HOUSING IN IRAN

G. Raheb[1], A. Tarkashvand[2]
[1]Assistant Professor, Building & Housing Research Center, Tehran, Iran
[2]Ph.D., School of Architecture & Urban Studies, Iran, University of Science & Technology, Tehran, Iran

ABSTRACT

Concrete has been used since the 1970s in construction of rural houses in Iran. Despite extensive use of concrete in rural housing in Iran and the huge allocated budget, the quality of construction is not acceptable. The aim of this paper is to evaluate the influence of using concrete in construction of rural houses in Iran. For this purpose, the effective factors on the development process of rural housing have been identified first. They could be counted as:

1. Efficiency and Effectiveness
2. Compatibility with climate, economy and social aspects
3. Dynamism and Flexibility
4. Stability and Durability
5. Cultural continuity and visual desirability

Then, sample cases -25 villages- have been surveyed through these factors by authors. Minimum of 3 houses have been surveyed in each village. The result of this research recognizes some problems of using concrete in rural housing in Iran. The most common difficulties are providing materials with good quality, lack of technical knowledge in villagers as the main workforces and lack of required equipments.

Keywords: rural housing, feasibility, concrete

1. INTRODUCTION

According to development of rural settlements in Iran, current use of concrete in building construction of rural areas has been begun since the seventieth decade (c.c.). Concrete has been used in the following methods of construction in Iran:

- Bearing wall system with tie beams and columns
- Structural reinforced concrete with beam and column or moment- resisting frame
- Reinforced concrete slab

In the above classification, the first one has the maximum usage in rural settlements of Iran. Despite extensive use of concrete in rural housing in recent years in Iran, the quality of construction has not been acceptable, according to the experts' views. This lack of desirability is related to structural and architectural aspects. However, efforts undertaken in the development of rural housing by making use of new material and methods of construction- such as concrete- have not considered all related aspects of housing development in rural areas.

This paper is going to evaluate use of concrete in building construction by a general and multi-aspect overview considering physical aspects of rural concrete constructions which is related to social, economical and cultural properties of rural housing. The result of this research is to declare the difficulties of making use of concrete in renovation of rural housing in Iran.

2. RESEARCH METHOD

Effective factors on renovation process of rural housing are identified first. Identification of these factors is a process in itself and is not covered in this paper. However, a summarized explanation of steps of exploiting the factors is mentioned in continuation of the report. Final factors and evaluation of the influence of using concrete in Rural Construction by them has been introduced. The factors are based on derivation of a conceptual framework effective on selection of proper rural housing development method, using the existing resources. In this condition, the framework is chosen out of the following domains:

1. Theories including identification of the concept of village and rural housing, theories connected with the way of interfering in man-built environment, especially rural regions (with emphasis on theories relying on dwellers' participation) and theories related to proper technology
2. Internal experiences including macro-policies and programs and experiences on construction and reconstruction of rural housing
3. Experiences of other countries (with emphasis on countries that have similar condition as Iran)

The research is based on surveys in rural samples. The research method is Qualitative and based on observation (profound observation) and interview (focus group). The factors and sub factors have given a checklist for surveying. Each factor has been supported by a question in questionnaire that the surveyor answers by observation.

3. SAMPLING

Sample cases have been selected through a categorized random sampling method. Statistical community consists of villages that have minimum of 15 implemented projects of rural house renovation. Also minimum of three years might have passed from implementation of the projects. In accordance with the sampling method, statistical community has been categorized in a few clusters through the following criteria:

1. Climate categorization of Iran
2. Cooperation of villagers
3. Population

Then, a portion of each cluster has been calculated on the scale of each cluster to the whole amount of final samples. Due to validation of sampling, amount of final samples has been set to 25 villages. Finally, in accordance with the portion of each cluster in statistical community, sample cases have been selected randomly from each cluster. Sample cases have been surveyed by authors with prepared checklists trying not to intervene in the prevailing situation of the villages and houses. A

minimum of 3 houses have been surveyed in each village.
Checklist focuses on five major aspects of renovated rural houses:

1. Efficiency and Effectiveness
2. Compatibility with climate, economy and social aspects
3. Dynamism and Flexibility
4. Stability and Durability
5. Cultural continuity and Visual desirability

Each aspect has been surveyed by a number of correlated indicators mentioned below (refer to 4). Achieved data has been categorized and analyzed. Finally, guidelines are provided in accordance with the results.

4. FINAL FACTORS, MEASUREMENT COMPONENTS AND THEIR EFFECT ON DEVELOPMENT OF HOUSING

Final factors analyzed in the rural settlements of Iran and measuring components of each factor are as the following; In continue, Summarized results of analysis of data are mentioned in accordance with the above mentioned factors:

4.1. Executive Efficiency With Respect To Workforce and Cost

The objective is the complete fulfilment of related necessities by developing the building and providing smooth trend of its implementation in a way that interfering factors do not stop or delay the work trend. In addition, the budget spent to develop the housing and the special procedures taken to reduce spending are the criteria for logicality of the cost with respect to priority needs of the household.
Components for measuring the factor are: speed of implementation [3, 610, 15, 16, 24, 26, 30, 31, 32], independency of expert forces in making [1, 3, 6, 16, 26, 29, 31, 32], repairing and maintaining [1, 5, 6, 19, 23, 24, 26, 29, 30, 31, 32], lack of need for sophisticated and unavailable equipments [1, 3, 4, 5, 11, 15, 16, 19, 23, 32], achieving gradual durability [1, 3, 11, 15, 24, 26, 29, 32], possibility to avoid flaws and mistakes [1, 3, 4, 5, 6, 7, 10, 11, 15, 16, 19, 23, 24], ease of implementation [11, 15, 16, 19, 26, 29, 32], smoothly accessed resources [11, 15, 16, 19, 23, 31, 32], low cost construction and maintenance [1, 10, 16, 19, 23, 24, 26, 32], fair balance between housing budget and credits allocated to it [23, 24, 30, 31, 32], compatibility with current economic conditions and lifestyle, increased self confidence, avoiding luxury [1, 3, 4, 5, 6, 7, 10, 11, 15, 24, 31, 32], desirability to work and to construct a house, convertibility to a capital commodity. [4, 5, 6, 7, 10, 11, 15, 16, 29, 30, 31, 32]
Field studies clearly show a decrease in the quality of concrete constructions. It might be a result of the following reasons:

1. Lack of required equipments and machineries
2. Difficulties in providing high quality material such as mixing water, fine aggregate, coarse aggregate and additives
3. Lack of expert labor in production process.

Also, increasing the cost and time of the construction process has been observed. This is the result of non- industrial process of construction. (Figure 1,2,3,5,6,7)

4.2. Climate adaptation with natural environment

The concern is physical accordance of the building and its construction scheme using climatic elements and employing proper mechanisms to provide comfort relative to the elements used for exploitation of potentials to counteract its negative effects.

- Components for measuring the factors: wind, rain, humidity, sunshine, and temperature. [3,11,15,16,18,20,26,29,30,31,32]

In humid zone, because of high heat capacity of concrete elements, undesirable effect in thermal adjustment, has been seen.

4.3. Physical Effectiveness

- The concern is physical accordance of building with requirements, needs and demands of the residents such that fulfilment of the said needs is predicted in the development method and that physic and spaces created in this method have adequate capability to provide for engineering issues, human factors and are in compliance with human behaviours.

Components for measuring the factor: observance of proportions and dimensional and space criteria from operational efficiency and visional desirability [3,4,6,30,31,32], hygiene [10,11,19,29,30,31,32], caring for tastes and demands of the residents[15,16,19,29,30], compliance with needs [10,11,15,16,19,29,30], avoid shortages [19,29,30,31,32], provide safety [3,4,6,10,11,15,16,19], establish proper relationship between open and closed spaces[3,4,6,10,16,19,29,32], capability to construct infrastructures and facility services.[11,15,16,19,29,30,31,32]

Using concrete increases length of span up to 7 m which improves architectural characteristics of renovated houses. Diversity in interior design and space planning is the result of such structural potentials. Physical effectiveness of renovated concrete structures improves the ability of architectural design in shouldering responsibility to the new style of life, hygienic needs and infrastructures.

4.4. Social Capabilities and Compatibilities

The intention is to create coordination with social under-layer and its expected social functions, such that in proportion with configurations, values, beliefs and traditions, the building would be able to offer a desirable function to the residents relative to other sects of the society.

- Components for measuring the factor: care for social values [1, 3, 4, 5, , 20, 23, 25, 26, 29, 32, 33], coordination with social functions [1, 3, 11, 13, 14, 15, 16, 19, 20, 23, 25, 26, 29], enhancing sense of cooperation and contribution, control and management of the work [6, 10, 11, 13, 14, 30, 31, 32, 33], self-sufficiency, improved quality of the dwellers' life style and culture. [16,19,20,23,25,30,31,32,33]

Vast use of concrete structures decreases capabilities and social compatibilities, because of its need to expert labours. It also results in low proficiency of houses and also, low innovations in the design process by habitants.

4.5. Stability

The intention is the resistance of building against usual, common, unconventional and temporary natural forces and erosion due to withstanding and enduring the environment and its effects and making use of the building all along its life cycle.

- Components for measuring the factor: resistance against earthquake, [6, 10, 24, 29, 30, 31, 32] natural and atmospheric conditions [1, 3, 4, 5, 6, 10, 24, 29, 30, 31, 32] construction quality[1,3,4,5, 32], and durability. [1, 4, 5, 6, 10, 24]

Reinforced concrete structure has a good lateral and vertical stability and also desirable durability, if it has been implemented perfectly. But in rural construction, because of low quality of the process of producing reinforced concrete constructions -such as inappropriate designs, bad curing, missing components portion etc, stability of rural concrete structures could not be guaranteed.

4.6. Dynamism

Dynamism means growth, movement and possibility for optimization of the building based on dwellers' ideas and desires. A dynamic building is the one that is capable of forming a process and a continuous life.

- Components for measuring the factor: partial diversity [1, 3, 10, 11, 29, 30, 31, 32], changeability [4, 5, 6, 10, 11, 26], development possibility. [1, 3, 4, 5, 6, 24, 29, 30, 31, 32]

Lack of expert labours, materials and equipments of concrete construction is a serious limitation for future development and growth of houses. Also, low diversity in design process of building and detailing has been seen. (Figure 8)

4.7. Economic Development

The concern is to measure effects of the chosen approach on economic growth of the region and improvement of economical development factors in the region.

- Components for measuring the factor: expand the native industries and increase production capacity [,7,8,10,11,18,20,24] , improve regional commerce of the area [1,6,7,8,10] , reduce unemployment and train expert men[15,16]

Because of low economic ability of villagers, concrete constructions are not affordable in many rural areas of the country. On the other hand, industrialization of concrete production has had visible effects on growth of economic indicators such as.

4.8. Coordination and Protection of Natural Environment

The intention is to find out how loyal a building development style and the capabilities embedded in a long constructed building during its different utilization steps have been in keeping up with the rules and basics of conserving the environment and how much have they protected the natural resources from getting damaged. In addition, coordination with natural bed, meaning the proportionality of the development procedure, hidden capacities of the structure in its different utilization stages with current environmental conditions, optimum usage of environmental conditions and natural forces must be considered.

- Components for measuring the factor: usage of less basic resources [1, 6, 10 , 15, 16, 17, 18, 24] ,use of renewable resources [6, 10, 15, 16, 17, 18, 19, purification of environmental forces [1, 4, 6, 10, 26], ground slope[1], conservation of environmental view [10, 20, 24, 26]

The most important problem of concrete buildings, according to this factor is recycling. The elements of buildings which have been constructed with concrete could not be recycled or reused in the other way in buildings. It has some visible effects on increasing pollution of closed environment of rural areas.

4.9. Cultural Continuity

The intention is the extent of notice given to the historical bed on which the building is constructed, in a way that the developed building is in logical accordance with construction traditions and that the resulting product does not contradict with the existing physical background.

- Components for measuring the factor: conserving the native identity and laying this building construction tradition [1, 10, 11, 15, 16, 18, 19, 20, 24], conserving appearance of the built environment. [10, 11, 15, 16, 18, 19, 20, 24, 26, 29, 30, 34]

New buildings which have been constructed by new materials and methods –such as concrete- often cannot provide acceptable architectural correlations to their existing context. Because of lack of skill in villagers to use these new methods of building and materials appropriately, the result is not in continuity with vernacular architecture. (Figure 4)

Figure 1. Kushalshad Village- Gilan Province

Figure 2. Shirinsoo Village- Qazvin Province

Figure 3. Jashnabad Village- Fars Province

Figure 4. Ghaesoo Village- Gilan Province

Figure 5. Kolangestan Village- Gilan Province

Figure 6. Abparan Village- Golestan Province

Figure 7. Eivazloo Village- Ardebil Province

Figure 8. AsbMarz Village- Ardebil Province

5. CONCLUSION

Concrete is one of the most important based materials for building construction. In spite of that, difficulties of its implementation in rural areas cause low efficiency. Most of the difficulties encountered can be outlined as the following:

- Difficulties in providing good quality materials, such as water, aggregates and appropriate type of cement.
- Low quality of particle size distribution.
- Lack of technical knowledge of implementation of reinforced concrete.
- Inappropriate curing of concrete.
- Inappropriate structural design.
- Missing standards in time of haulage.

Considering the above achievements, the solutions for increasing the efficiency of concrete usage are:

- Developing vernacular knowledge in concrete construction technology and methods.
- Providing and developing industrialization in concrete construction process and productions.
- Providing appropriate standards for implementation of concrete constructions in rural areas.

REFERENCES

1. Alexander, Christopher(1979),The Secret of Timeless Architecture, Oxford University press.
2. Alalhesabi, Mehran(2007), Architecture of Rural housing in Iran, proceeding of rural housing course, Building &Housing Research Center.
3. Ardam Engineer Group(1984), Reconstruction of seismic area of Tabas (1978), Ministry of Housing &Urban Development, branch in Khorasan region.
4. Alexander, Christopher & others(1977), A pattern language: towns, buildings, construction. New York, Oxford University Press.
5. Alexander, Christopher & others(1975), The Oregon experiment. NewYork, Oxford University Press.
6. Afghanistan. MRRD(2003), "Provision of shelter assistance to vulnerable families in rural Afghanistan-government guidelines for agencies funding, implementing and monitoring shelter activities in rural Afghanistan". Final Draft, 13 April 2003.
7. Broome, John(2005), "Mass housing cannot be sustained". In: Peter Blundel Jones & others (Edt.) Architecture and participation. Spon press.
8. Charles Green (1965), Rural Housing: Some Obstacles to Improving Present Conditions, Editors: David Oakly, K.Ramman Unni, The School Of Planning & Architecture, New Delhi.
9. Dorf, Richard C, (2001), Technology, Human and Society, Toward a Sustainable World, San Diego, Academic Press.
10. ERRA-Pakistan (2006), "Building back better: rural housing reconstruction strategy of earthquake hit districts in NWFP and AJK". Draft policy document rural housing reconstruction for discussion purpose only. February 2006.
11. Fathy, Hasan (1993), An Architecture for the poor, Translate in Farsi by: ashrafi, Ali, Honar Uni. Press.
12. Grout, l. & Wang, D.(2002), Architectural Research Methods, John Wiley & Sons, INC.
13. Habraken, N.J, (1972), Supports; an alternative to mass housing". Translated by B. Valkenburg ARIBA, Architectural Press.
14. Habraken, N.j. (1998), The structure of the ordinary: form and control in the built environment, Cambridge, The MIT Press.
15. Housing Foundation (1992), Quantity and Quality measures of rural housing in Iran.
16. Housing Foundation (2005), Project of Rehabilitation of rural housing in Iran.
17. Complied by: J.K. Varshneya and O.N. Mathur(1968), Hand book: rural housing and village planning, Printed by The General Manager, Government of India Press, India, Dehli.
18. K.R. Uni (1965), Social Factors in Housing, the Rural Habitat, Editors: David Oakly, K. Ramman Unni, The School of Planning & Architecture, New Delhi
19. K.R. Uni (1965), Dimensions of Change in Village Homes and House Groupings, The Rural Habitat, Editors: David Oakly, K.Ramman Unni, The School Of Planning & Architecture, New Delhi.
20. K. Sen (2002), Development and Participation, Oxford University Press, New

Delhi, India.
21. Building & Housing Research Center (2006), Iranian Code for Seismic Resistant Design of Buildings, Standard No. 2800.
22. Marshall Catherine, Rossman, Gretchen (1995), Designing Qualitative Research, Sage Publication.
23. Moatasim, Faiza (2005), Practice of community architecture: a case study of zone of opportunity housing co-operative, Montreal. A research report submitted to the faculty of graduate studies and research in partial fulfillment of the requirements for the degree of master of architecture. School of architecture, McGill University, Montreal.
24. National Buildings Organization and U.N. Regional Housing Center Escap, Demonstration Rural Houses with Inviromental Improvements (1976), Government of India Ministry of Works and Housing, Nirman Bhavan, New Delhi.
25. Pultar, Mustafa (2000), Ethics and the built environment, editor: Fox, Warwick, London: Routledge.
26. Rapoport, Amos, 1969, House Form and Culture, Prentice_Hall, Inc. Englewood Cliffs, N.J.
27. K. Yen. Robert, 1997, Case Study Research, translated by: Parsaeeyan, A. &Arabi, M., Cultural Research Bureau.
28. Raheb, Ghazal (2008), Ph.D. Dissertation, A Method for Identification and specification of factors influential on selection of a proper method for housing development in rural settlements on the southern rim of the Caspian Sea, Iran University of Science & Technology.
29. Rafipour, F. (1997), Researches & Believes, Enteshar.
30. Rafiee Sereshki, B. & Niroomand, M.(1983), Reconstruction of Seismic area in south of Khorasan- Gonabad, Ministry of Housing &Urban Development. (Iran).
31. Rafiee Sereshki, B. & Niroomand, M.(1983), Reconstruction of Seismic area in south of Khorasan- Taybad, Ministry of Housing &Urban Development (Iran).
32. Serlad Engineer Group,(1982), Renovation of Vazrak village, Ghaen.
33. Taheri, M., Alizamani, M.,(2003), Evaluation of reconstruction of damaged Building in The seismic of Ardebil, Housing Foundation, Iran.
34. Turner, John,(1977) Housing By People: Towards Autonomy in Building Environments, Marion Boyars, New York

CD10-001

A LABORATORY INVESTIGATION ON THE EFFECTIVE PARAMETERS OVER THE PENETRABILITY OF ROLLER COMPACTED CONCRETE

V. Khalili Khorram[1], A. Mansouri[2], H.R. Vosoughifar[3]
[1]M.Sc.Student Hydraulic Structures, Islamic Azad University Tehran South Branch
[2]Assistant professor Hydraulic Structures, Islamic Azad University Tehran South Branch
[3]Assistant professor Hydraulic Structures, Islamic Azad University Tehran South Branch

ABSTRACT
Roller Compacted Concrete construction technique has been recently remarkably considered in Iranian academic centers and dam engineering industry. However, research studies can hardly be found in which physico - mechanical properties of RCC have been studied as in a real ongoing project. In this study, permeability of the mass of RCC mixture used in Zirdan RCC dam located in south of Iran, the second large RCC dam in Iran has been investigated. Influences of cementitious material content, water - cement ratio, pozzolan replacement ratio in cementitious material, delay in working time and age of concrete specimens on permeability coefficient have been studied. Moreover, effects of different types of pozzolan on permeability have been examined.results showed that RCC has an equal or even lower permeability coefficient in comparison to an equivalent ordinary concrete. Effect of water content on permeability was considerable and in comparison to cementitious material content, showed a higher degree of importance. The rate of developing permeability coefficient (decreasing) was found faster than the rate of mechanical strength development (increasing). Delay in working time decreased the permeability of RCC. However, decreasing the water content below its optimum limit would result in an excessively high permeability coefficient.
Finally, it was observed that silica fume had a significant effect on permeability coefficient.

Keywords: RCC, permeability coefficient, pozzolan, silica fume, working time

1. INTRODUCTION
Permeability of RCC mass is one of the most important parameters in RCC dams, and also in Roller Compacted Concrete Pavements (RCCP). This is due to direct relationship between this parameter and problems such as water leakage through dam body, pore water pressure, stability in freezing and thawing cycles, and durability requirements. Water leakage may have deteriorating effect on hardened RCC strength by washing away cementitious materials.
Also, freezing and thawing cycles would, have undesirable effects on highly permeable concrete. On the other hand, design of mixtures with sufficient impermeability may lead to omission of several extensive works such as upstream

impermeable faces, resulting in positive effects on. technical and economical aspects ofproject.
Two different aspects of RCC, concrete and soil aspects, have leaded in two different theories about RCC permeability. Considering concrete approach, permeability is related to the content of cementitious material in RCC mixture [1,2]. According to soil approach, on the other hand, increasing the amount of cementitious material will not result in significant change in permeability coefficient in the case designing a suitable RCC mixture proportioning. In fact, it is possible to achieve RCC permeability coefficient as low as a conventional concrete mixture's and using low content of cementitious material [3].
Although a few studies have been formerly conducted on RCC permeability [4,5], our understanding of this vital property of RCC IEemains far from adequate. In addition, pure theoretical researches cannot provide useful, adequate and practical ways to address RCC issues which are currently just the fruit of innovations of contractors and designing engineers.
Having these facts in mind, we were encouraged to investigate the influence of several factors on RCC mixture permeability of Zirdan RCC dam, the second large RCC dam in Iran considering technical, economical and constructional aspects. The dam's study phase test fills of this dam is going on and the placement works is about to start.

2. EXPERIMENTAL WORKS

2.1. Materials

As previously mentioned, materials used in this study were those ones currently used in Zirdan RCC dam. The details are as follows:
Zirdan riverbed materials have been used as aggregates. As it is currently employed in site, two classes of aggregates have been considered: 1- sand (0-4.75 mm) 2- gravel (4.75-37.5 mm), these two classes are mixed in a 40:60 proportion, respectively.
Cement Type II has been used in study. Results of its chemical analysis and physical properties are presented in Table [1]. The main applied pozzolan is Khash pozzolan. A type of silica fume, slag and another natural pozzolan type (Trass) have been employed for comparison. Pozzolan chemical analyses are presented in Table [2].
In order to respond to research questions, several mixture proportions have been applied.
Results obtained from all tested mixtures with their physical and mechanical properties are presented in Table [3].

Table 1: Cement chemical composition

Sio2	Al2O3	Fe2O3	CaO	MgO	SO3	K2O	Na2O	Cl	LOI	C3A	C4AF	C25
21.31	5.24	3.24	63.04	2.49	2.06	0.31	0.52	0.017	0.58	7.44	11.7	0.67

Table 2: Pozzolan composition.

Pozzolan	Na2O	K2O	SO3	MgO	Ca0	Fe2O3	Al2O3	SiO2
Khash	2.72	2.66	0.1	1.7	7.8	4.96	14.54	61.14
Silica Fume	0	0	0	1	2.1	1.5	1.4	90
Trass	0	0	0	1	2.4	0.8	12.3	67
Slag	0	0	1.6	9.06	38	0.71	10.5	35.7

2.2. Test Procedure

Cylindrical specimens have been made according to ASTM C II 76-98 [6], using a modified Ve Be table; the only difference to the mentioned code is that the specimens are made in two 10 cm high layers. Therefore, their height is 20 cm. It means 10 cm shorter than the standard specimens. The specimens have been stored in 20 ± 2°C water.

The measurement of the permeability coefficient was performed by the method shown in Figure [1].During 48 hours before the permeability test the cylindrical specimens were conditioned at 50 % HR and 20°C. Then, the 6 atm water pressure was applied for 24 hours on a circular concrete surface area of 7.5 cm in diameter. Surrounding this circular surface was wate highte by bituminous material. After 24 hours of sustained pressure, the specimen was split and the depth of penetration {d) was obtained. In this case, the permeability coefficient (K_v) was derived from the (Eq. [1]) developed by Valenta [7].

$$K_v = \frac{d^2 V}{2ht} \tag{1}$$

V is the volume voids filled by water in the penetrated zone, (determined by measuring gain), h is the head of water and t is the time to penetrate to depth (d).

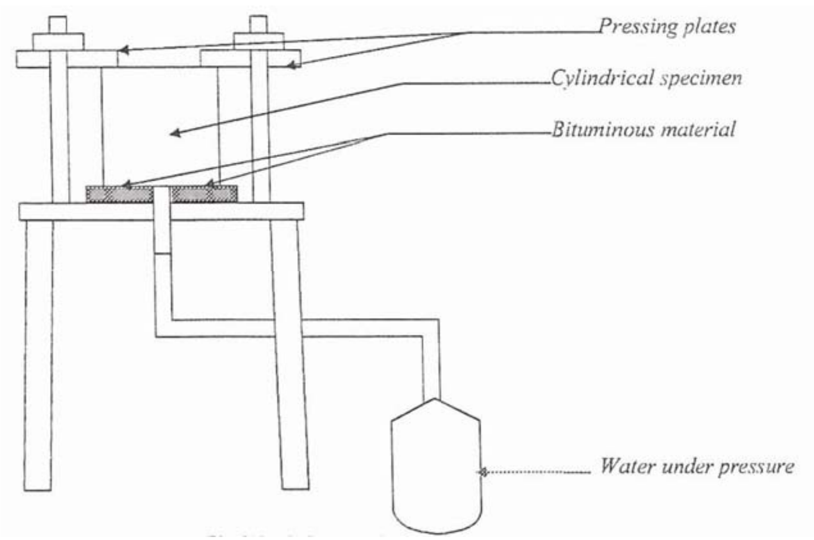

Figure 1. Scheme of permeability test

3. RESULTS AND DISCUSSIONS

The permeability coefficients obtained are presented in Table [3]. Table [3] also includes compressive strength of specimens. Effects of different parameters on permeability are described below [8].

Table 3: Mixture properties and test results

ID	C+P (kg/m^3)	P (kg/m^3)	W (kg/m^3)	W/(C+P)	Pozzolan Type	Consistency (sec)	Age (day)	K (cm/s)	fc (MPa)
A1	200	60	110	0.55	Khash	35	28	2.65E-10	14.3
A2	180	54	110	0.61	Khash	35	28	6.17E-10	13.2
A3	160	48	110	0.69	Khash	35	28	1.21E-09	13.8
A4	140	42	110	0.79	Khash	35	28	1.55E-09	9.4
R1	110	0	110	1	------	40	28	6.14E-09	7.9
R2	110	22	110	1	Khash	38	28	4.38E-09	8.5
R3	110	33	110	1	Khash	36	28	2.89E-10	9.4
R4	110	44	110	1	Khash	34	28	5.04E-09	8.3
R5	110	55	110	1	Khash	30	28	1.95E-08	7.5
R6	110	66	110	1	Khash	26	28	2.37E-08	6.8
W1	130	52	39	0.3	Khash	120	28	1.00E-03	6.5
W2	130	52	65	0.5	Khash	65	28	4.24E-10	12.0
W3	130	52	91	0.7	Khash	30	28	3.13E-09	11.2
W4	130	52	117	0.9	Khash	12	28	7.13E-09	9.8
W5	130	52	143	1.10	Khash	6	28	1.93E-08	6.4
G1	200	80	115	0.58	Khash	30	3	1.78E-08	4.8
G2	200	80	115	0.58	Khash	30	7	3.97E-09	6.7
G3	200	80	115	0.58	Khash	30	14	8.13E-10	9.8
G4	200	80	115	0.58	Khash	30	21	9.25E-10	11.8
G5	200	80	115	0.58	Khash	30	28	3.56E-10	12.1
K1	200	0	115	0.58	------	40	28	7.33E-11	15.0
K2	200	100	115	0.58	Khash	33	28	9.63E-10	12.9
K3	200	100	115	0.58	Trass	32	28	2.38E-08	10.3
K4	200	100	115	0.58	Slag	27	28	2.70E-10	13.4
K5	200	20	115	0.58	SF	29	28	1.16E-11	20.9

C: Cement
P: Pozzolan
W: Water
K: Permeability coefficient
fc: Compressive strength

3.1. Influence of Cementitious Material Content

As can be seen in Figure [2], an increase in cementitious material from 140 to 200 kg/m3 has not shown a significant decrease in permeability coefficient though having a remarkable positive effect on mechanical strength. According to this

Figure, mixtures having acceptable permeability coefficient would be obtained using low cementitious material content.

Although increase of cementitious material would result in a better mechanical strength, no such significant effect is observed for permeability coefficient.

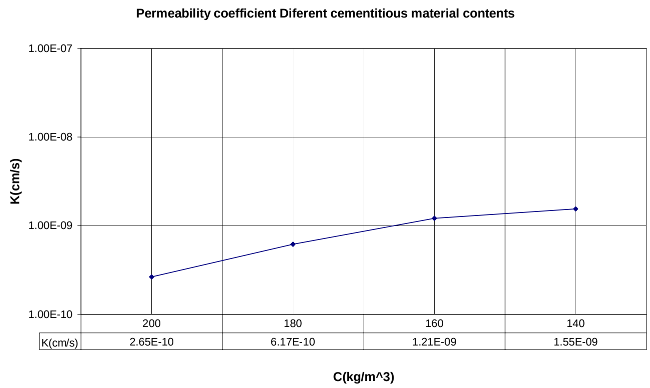

Figure 2. Effect of cementitious material content.

3.2. Influence of Water to Cement Ratio

According to Figure [3], optimum water to cement ratio is estimated 0.55. The diversity of results shows an implication of importance of water content in RCC mixture, instead of water to cement ratio as in ordinary concrete. Another conclusion obtained from Figure 5 is that while water content is increased from its optimum level, insignificant increase in permeability coefficient would be obtained, whereas decreasing water content from the optimum level, even very low content, leads to decrease the compaction factor, and shows an excessive increase in permeability coefficient.

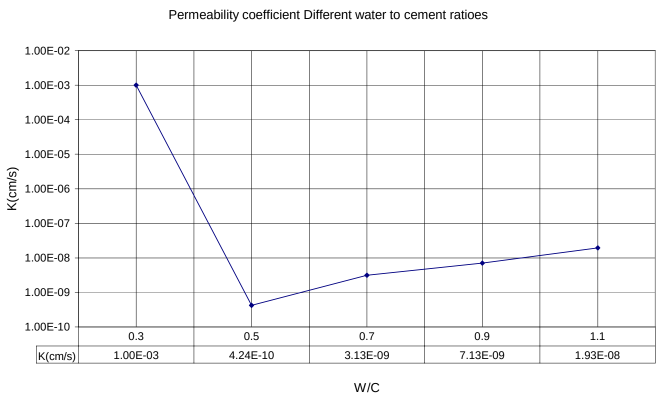

Figure 3. Effect of water to cement ratio.

3.3. Influence of Pozzolan Content

According to Figure [4], the lowest permeability coefficient would be obtained using optimum replacement ratio of pozzolan (in this study, 30% for the main applied pozzolan). Using higher replacement ratio (e.g. 50%), especially in short ages (up to 28 days) would increase permeability coefficient.

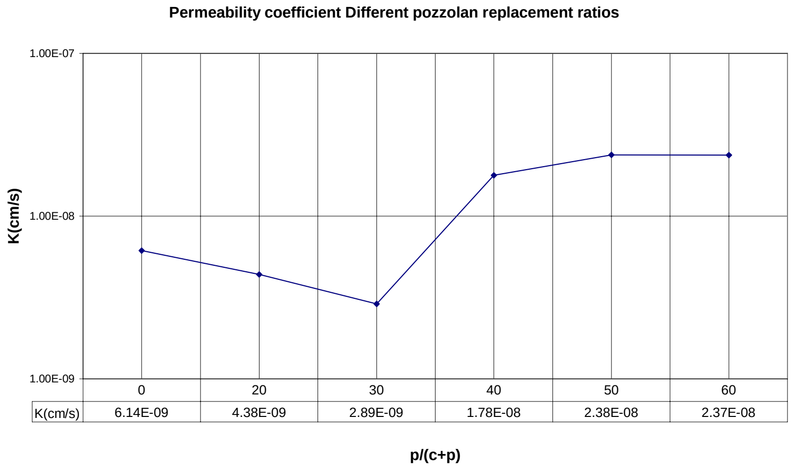

Figure 4. Effect of pozzolan content

3.4. Influences of Age in Working Time

As can be seen in Figure [5], rate of permeability coefficient development shows a different 1· trend to that of for mechanical strength development. Mechanical strength of cemented mixtures as well as RCC increase significantly during the first 28 days, while RCC permeability coefficient do not shows remarkable decrease after 14 days in this study. This is in case that 40% of cementitious material is pozzolan.

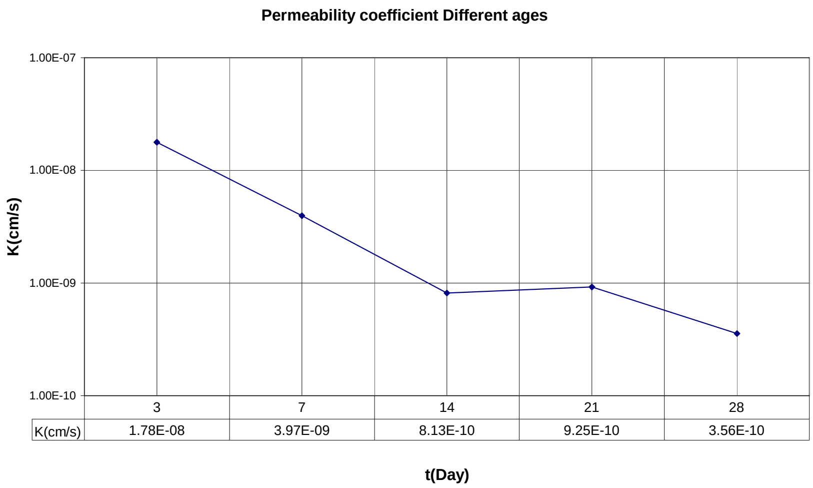

Figure 5. Effect of age

3.5. Influences of Delay in Working Time

Effect of delay in working time (compaction time) is shown in Figure [6]. Dasmeh et al. [9,10] reported that employing pozzolan in cementitious material would extend allowable compaction time. In that study they showed that specimens containing pozzolan in their cementitious material and made after 120 min. delay in compaction time had shown an improve in mechanical strengths. The results obtained from present study on compaction time indicate that it is possible to achieve a lower permeability coefficient for specimens compacted after a delay of up to 110 min. However, the results obtained from specimens compacted with a delay longer than 110 min. illustrate a notable increase of permeability coefficient. It may be due to evaporation of water of mixture. Therefore, decreasing the water content below its optimum limit which would result in an excessively high permeability coefficient.

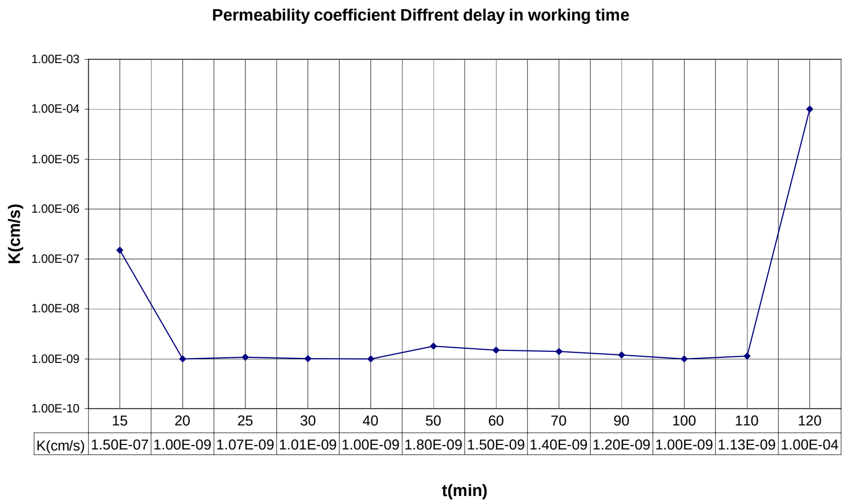

	15	20	25	30	40	50	60	70	90	100	110	120
K(cm/s)	1.50E-07	1.00E-09	1.07E-09	1.01E-09	1.00E-09	1.80E-09	1.50E-09	1.40E-09	1.20E-09	1.00E-09	1.13E-09	1.00E-04

Figure 6. Effect of delay on working time

3.6. Influences of Type Ofpozzolan

The effect of use of silica fume in reduction of the permeability coefficient of Conventional Vibrated Concrete (CVC) has been shown by several authors [11,12]. For Roller Compacted Concrete (RCC), excellent effect of employing silica fume in cementitious material is presented in Figure [7]. In comparison to mixtures containing other types of pozzolan in their cementitious material, and also to mixture without any additive in its cementitious material, a remarkably lower permeability coefficient has been obtained when applying silica fume. The result is due to the fact that using silica fume in the mixtures would improve the "Transition Zone", change capillary pores to gel poreS3 and seal their inter connections. It can also be seen that replacement of slag up to 50% of cement could lead to considerably good results. The main pozzolan applied in this study (obtained from Khash area) has also shown acceptable results regarding permeability coefficient as well as mechanical strength.

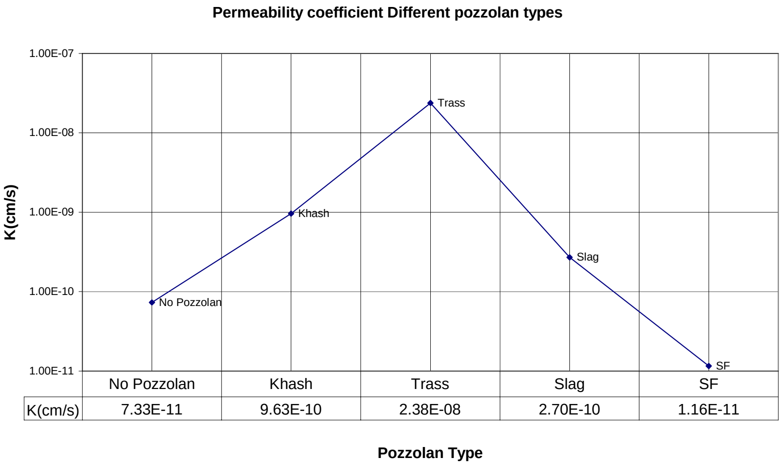

Figure 7. Effect of type of pozzolan

3.7. An Observation: Tortuousity Effect

Some of specimens in this study showed greater values for horizontal permeability coefficient than vertical permeability coefficient. This is an implication of fast evacuation of streamlines through side-walls. The difference between permeability coefficient of two horizontal and vertical directions can be justified as follow: Aggregates including high percentage of flat and elongated particles are allowed to be used in RCC mixtures (coarse aggregate used in this study contains 30% of flat or elongated particles). RCC compaction methods on the other hand, would arrange these particles in horizontal direction. This arrangement of particles is the reason for a phenomenon called "Tortuousity" which increases the length of streamlines in vertical direction. Consequently this increase would result in a lower vertical permeability coefficient and higher value in horizontal direction. This problem should be paid attention when evaluating RCC dam required permeability coefficient. The phenomenon "Tortuousity" is illustrated in Figure [8].

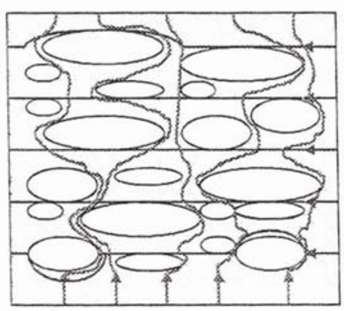

Figure 8. Tortuousity effect

4. CONCLUSION REMARKS

Brief summery of the findings is described below:

1) Influence of water content of RCC mixture on permeability was found vital and

in comparison to cementitious material content has a greater degree of importance.
2) Employing pozzolan up to its optimum replacement ratio in cementitious material decreased the permeability coefficient.
3) Inpite of mechanical strengths, the rate of permeability coefficient improvement was considerable up to first 7 to 14 days.
4) Delay in compaction time would improve permeability coefficient of specimens containing pozzolan in their cementitious material unless it results in a decrease of water content below its optimum limit.
5) Effect of using silica fume in RCC mixture was excellent. Also employing slag in cementitious material had considerable positive effects on the reduction of permeability coefficient. Considering the low price of slag, it is recommended to replace it in great percentages in cementitious material.
6) The RCC permeability coefficient could be much less than 3x10-9 cm/s, a typical value for conventional concrete permeability when using low cement content. In case of using flat and elongated aggregates, different values would be obtained for horizontal and vertical permeability coefficient.

REFERENCES

1. Dunstan, M.R.H. CIRIA Technical Note 106, London, (1981) 94p.
2. Dunstan, M. R. H. International Journal of Hydropower & Dams, Issue one, Volume 6 (1999) 40-45.
3. Schrader E.K. International conference on advanced in concrete technology, Athens, Greece, 2th Edition, CANMET, Ottawa, Canada, (1994).
4. Banthia N., Pigeon M., Marchand J. and Boisvert J. ASCE, vol. 4, No. 1, (1992) 27-40.
5. Bettencourt Ribeiro A. Sixth CANMENT/ACI international Conference on Fly Ash, Silica Fume, Slag and Natural Pozzolan in Concrete, Bangkok, Thailand, Sup. volume (1998) 223-238.
6. ASTM Cl 176-98. Standard Practice for Making Roller Compacted Concrete in Cylinder Molds Using a Vibrated table, (reap proved 1998).
7. Valenta 0. 10th international conference on large dams, Montreal, (1970)103-117.
8. Ghassemi H, MSc. Thesis, University of Tehran, (2002), 215p.
9. Dasmeh A., Fakher A. Shekarchi M. and Gharavi, International Journal of Hydropower and Dam, 7, (2000) 60-63.
10. Dasmeh A., Fakher A., and Shekarchi M., Seventh CANMENT/ACI international conference on fly ash, silica fume, slag and natural pozzolan in concrete, (2001) 341-356.
11. Ayers M.E. and Khan M.S. The need for rational curing standards. Concrete Technology, SP 144-29, (1996) 605-622.
12. Shekarchi M., Debicki G., Clastres P., and Billard Y. 6th CANMET, ACI International Conference on Fly Ash, Silica Fume, Slag and Natural Pozzolan in Concrete, Bangkok, Thailand, (1998) 975-996.

CD10-002

ارائه طرح اختلاط مناسب بتن غلتکی سد زیردان از طریق روش آزمایشگاهی

عباس منصوری[۱]، حمید رضا وثوقی فر[۲]، وحید خلیلی خرّم[۳]
۱. استادیار دانشکده مهندسی عمران، دانشگاه آزاد اسلامی‌واحد تهران جنوب
۲. استادیار دانشکده مهندسی عمران، دانشگاه آزاد اسلامی‌واحد تهران جنوب
۳. دانشجوی کارشناسی ارشد سازه‌های هیدرولیکی، دانشگاه آزاد واحد تهران جنوب

چکیده

یکی از مسایل مهمی‌که در زمینه سدهای RCC مطرح است، تعیین طرح اختلاط بتن غلتکی می‌باشد که با توجه به جدید بودن نسبی بتن RCC و عدم تجربه کافی در ایران، معمولا وقت و هزینـه زیـادی را مـی‌طلبـد. در ایـن مقاله، هدف بررسی عوامل موثر بر خواص بتن غلتکی و ارائه نحوه دستیابی به طرح اختلاط بهینه بتن غلتکـی بـا توجه به سه معیار مقاومت فشاری، کارایی مناسب و عدم جداشدگی دانه‌ها می‌باشد.

در این راستا به این روش عمل شد که تعداد زیادی طرح اختلاط با سنگدانه‌های شکسته و طبیعی سـاخته شـد و اثرات نوع و مقدار سیمان وپوزولان، نوع و دانه بندی مصالح سنگدانه ای، نوع و مقدار مواد افزودنی و مقدار آب بر روی خواص بتن غلتکی خصوصا مقاومت فشاری و کارآیی مورد بررسی قرار گرفته است. سنگدانه‌هـای مـصرفی در چهار گروه طبقه بندی گردیدند و دارای حداکثر اندازه ۵۰ میلیمتر می‌باشند.

یافته‌ها حاکی از آن است که میزان مصالح ریزدانه در حدود ۹ الی ۱۱ درصد حجمـی‌کـل مـصالح مناسـب اسـت. همچنین جداشدگی سنگدانه حساسیت زیادی به تغییرات میزان آب دارد. ضـمنا افـزودن پـوزولان تـا ۳۰ درصـد حجمی‌سبب بهبود خصوصیات بتن سخت شده می‌شود. در ضمن طرحهـای حـاوی افزودنـی منتخـب حـدود ۱۲ درصد مقاومت فشاری بالاتری نسبت به طرحهای دیگر کسب کردند. همچنین با افزایش دوزاج Chrysoplast از ۰٫۶ به ۰٫۸ درصد در شرایط یکسان، حدود ۹ درصد افزایش مقاومت و ۳ درصد نیز کاهنـدگی آب بیـشتر حاصـل شده است. ولی با افزایش دوزاج Conplast برعکس شاهد کاهش در مقاومت هستیم.

نتایج آزمایشات نشان می‌دهد که سنگدانه‌هایی که دارای مقدار زیادی ریزدانه هستند، مقاومـت فـشاری مطلـوبی نتیجه نمی‌دهند و سنگدانه‌هایی که فاقد مقدار کافی ریزدانه هستند از مقاومـت فـشاری خـوبی برخوردارنـد ولـی درآنها جداشدگی دانه‌ها رخ می‌دهد. همچنین مقدار کم آب یا زیاد باعث جداشدگی دانـه‌هـا مـی‌شـود. اسـتفاده از پوزولانها امکان جداشدگی دانه‌ها را کاهش داده و موجب بالا رفتن میزان خمیرمی‌شود.

کلیدواژه‌ها: بتن، RCC، سد وزنی، طرح اختلاط

۱- مقدمه

بتن غلتکی، بزرگترین پیشرفت در ساخت سدهای بتنی، طی ۳۰ سال گذشته می‌باشد و باعث اجرای سریعتر و کم

هزینه‌تر سدهای بتنی شده است. مخلوط‌های بتنی غلتکی در صنعت سد سازی معمولا دارای ۶۰ تا ۲۹۰ کیلوگرم برمتر مکعب مواد سیمانی می‌باشند[3]. میزان متوسط مواد سیمانی در سدهای بتن غلتکی به علت حجیم بودن آن و مشکلات ناشی از گرمای هیدراتاسیون و ملاحظات اقتصادی در آن، در بازه ۷ تا ۱۵ درصد وزن مواد جامد خشک، محدود شده است به طوری که تا پایان سال ۱۹۹۸، مقدار متوسط سیمان مصرفی در کشورهای چین، ژاپن، آمریکا و اسپانیا که از پیشگامان ساخت سد RCC در جهان هستند، ۸۰ کیلوگرم بر متر مکعب و متوسط پوزولان مصرفی در آن در حدود ۸۵ کیلوگرم بر مترمکعب می‌باشد. در سالهای نخستین استفاده از این بتن در سدها، متوسط میزان سیمان مصرفی رو به افزایش بوده که دامنه مصرف مصالح سیمانی از ۶۰ کیلوگرم بر مترمکعب در سد اوراگان درآرژانتین تا ۲۴۸ کیلوگرم بر متر مکعب در سد آپراستیل واتر مشاهده میشود، ولیکن در سالهای اخیر میزان متوسط مواد سیمانی مخلوط‌های بتنی غلتکی در حدود ۱۶۰ کیلوگرم برمتر مکعب می‌باشد که در حدود ۵۵ کیلوگرم بر مترمکعب (درصد وزنی) آن پوزولان می‌باشد.

براین اساس طبقه بندی کلی برای انواع مخلوط‌های بتن غلتکی بر اساس مقدار مواد سیمانی که منظور مجموع سیمان و مواد پوزولانی می‌باشد و به نحوه زیر در مراجع آورده شده است.

بتن غلتکی کم عیار: تعداد قابل توجهی از سدهای بتن غلتکی از مخلوط‌های کم عیار استفاده نموده‌اند که این نوع مخلوطها حاوی مواد سیمانی کمتر از ۱۰۰ کیلوگرم بر متر مکعب می‌باشند به همین علت، اینگونه بتنها دارای نفوذپذیری زیادی بوده و اتصال بین لایه‌ها ضعیف می‌باشد بنابراین برای رفع این نواقص از پوششهای آببند در بالادست استفاده می‌گردد.

بتن غلتکی با عیار متوسط: متوسط مواد سیمانی در آن بین ۱۰۰ تا ۱۵۰ کیلوگرم بر مترمکعب می‌باشد.

بتن غلتکی پرعیار: به منظور بهبود مقاومت درازمدت بتن غلتکی و کنترل چسبندگی و نفوذپذیری لایه‌های بتن غلتکی و نیز امکان طراحی سد با مقاطع کوچکتر، مهندسین انگلیسی برای نخستین بار پیشنهاد کردندکه از مواد سیمانی بیشتری (بیشتر از ۱۵۰ کیلوگرم بر مترمکعب) در بتن غلتکی استفاده شود و نیز برای کنترل تنشهای حرارتی به دلیل افزایش مواد سیمانی، کاربرد زیاد موادپوزولانی مورد نظر قرار گرفت.

بتن غلتکی RCD (ژاپنی): این نوع بتن اولین بار توسط مهندسین ژاپنی در کشور ژاپن توسعه یافت. مقدارمتعارف مواد سیمانی در سدهای RCD، ۱۲۰ کیلوگرم بر متر مکعب در نظر گرفته می‌شود. لیکن در شرایطی که مقاومت بیشتری لازم باشد، نظیر سدها با ارتفاع زیاد، از ۱۳۰ کیلوگرم بر متر مکعب مواد سیمانی استفاده می‌شود[5].

مزایای اقتصادی سدهای RCC نسبت به انواع دیگر سدها به دلیل کاهش در هزینه‌های قالب بندی، مصرف کمتر سیمان، حذف لوله‌های سردکننده بتن در بدنه سد، حذف درزهای طولی، کاهش ابعاد سیستم انحراف آب به علت کوتاه بودن زمان ساخت سد و... می‌باشد[6]. به منظور کسب حداکثر دانسیته با سنگدانه‌های مشخص به یک حداقل خمیر در بخش ملات هر بتن غلتکی نیاز است که این میزان خمیر باعث بهبود چسبندگی بین لایه‌ها نیز می‌شود [12].

۲- روش تحقیق

جهت نیل به چهارچوب طرح اختلاط بهینه، یک برنامه آزمایشگاهی گسترده در آزمایشگاه شرکت جهان کوثر به اجرا درآمد. تعداد زیادی طرح اختلاط با به کارگیری پارامترهایی شامل مصالح کارگاهی در اندازه‌های مختلف

(شن و ماسه) و مقدار درصد آب بتن و همچنین مقدار سیمان و پوزولان و درصد سنگدانه ریز به کل مصالح سنگدانه ای ساخته شد و آزمایشهای روانی و وزن مخصوص با استفاده از دستگاه Vebe و بر اساس استانداردASTM-C1170 انجام پذیرفت[8]. ساخت نمونه‌های بتن غلتکی با استفاده از دستگاه Vebe و مطابق استاندارد ASTM-C1176 صورت پذیرفت[9].

۲-۱ سد زیردان

ساختگاه این سد در ۴۰ کیلومتری شمال غرب روستای پیر سهراب (۱۵۰کیلومتری چابهار از جاده دسترسی مسیر ایرانشهر و انشعابی به طرف پلان) که ازطریق مسیر میان بر حدود ۶۰ کیلومتری شمال چابهار در نزدیکی روستای رگاب و در محلی از رودخانه کاجو که ارتفاعات طرفین به نزدیکترین وضعیت رسیده قرار گرفته است.[2] .

۲-۲ مشخصات فنی سد

نوع سد	وزنی (RCC)
طول تاج	۳۵۰ متر
عرض تاج	۵٫۶ متر
حداکثر ارتفاع سازه ای سد	۶۴٫۵ متر
نوع سر ریز	آزاد، بدون دریچه
طول سرریز	۱۴۶ متر
حداکثر ارتفاع سازه مقطع سرریز	۵۵ متر
حداکثر ظرفیت تخلیه کننده عمقی	۸۵ m3/s
نوع فرازبند	بتنی وزنی
ارتفاع فرازبند	۱۱ متر
ظرفیت سیستم انحراف آب	۶۰۰ m3/s
نحوه انحراف آب	کالورت باسه دهانه در بدنه سد به ابعاد۶*۴ متر

۲-۳ مصالح بتن غلتکی

مصالح مصرفی در بتن غلتکی شامل سیمان (سیمان پرتلند و پوزولان)، سنگدانه (شن و ماسه) و موادافزودنی می‌باشد.

۲-۳-۱ مصالح سیمانی

مصالح سیمانی مورد استفاده در بتن RCC شامل سیمان پرتلند و پوزولان می‌باشد. نوع و مقدار سیمان مصرفی بستگی به اندازه سد، شرایط محیطی و خواص مورد نیاز آن دارد. در سدهای RCC جهت کم کردن اثرات ناشی از حرارت هیداتاسیون سیمان، معمولا از سیمانهای با حرارت زایی کمتر از سیمانهای معمولی (سیمانهای تیپ۱) مانند سیمانهای تیپ۲، سیمان پرتلند پوزولانی و سیمان پرتلند با سرباره کوره آهنگدازی استفاده می‌شود[10]. سیمان مورد استفاده در ساخت طرحهای اختلاط از کارخانه خاش تأمین شده و در مرحله مقدماتی و اول، سیمان

آمیخته تیپ II شامل ۲۲ درصد پوزولان و در مرحله دوم سیمان آمیخته تیپ II شامل ۳۰ درصد پوزولان میباشد. (منطبق با سیمان نوع IP استاندارد595 ASTM).[11]

۲-۳-۲ پوزولان

پودر پوزولان مورد استفاده از نوع طبیعی (منطبق با پوزولان نوع N استاندارد ASTM C618) می‌باشد که در کارخانه خاش تولید گردیده است[9].

۲-۳-۳ آب

پس از تأیید نتایج آزمایشات، از آب رودخانه کاجو که در محل احداث سد جاری است در بتن استفاده شد.

۲-۳-۴ افزودنی

در ساخت طرحهای اختلاط از دو نوع افزودنی تیپ D و یک نوع افزودنی تیپ B مطابق استاندارد ASTM C494 استفاده گردید[12]. همچنین طرحهایی نیز بدون افزودنی جهت مقایسه ساخته شد که در پایان افزودنی تیپ D در طرح منتخب مورد استفاده قرار گرفت.

۲-۳-۴ مصالح درشت دانه

یکی از پارامترهای اساسی در بتن غلتکی، حداکثر اندازه دانه‌ها (M.S.A) می‌باشد. به کار بردن دانه‌های بزرگتر از ۷۶ میلی متر باعث می‌گردد که هم مشکل جداشدگی دانه‌ها به وجود آید و هم کارایی بتن کاهش یابد. به همین دلیل M.N.S.A طرحهای اختلاط ۵۰ میلی متر در نظر گرفته شده است. در مخلوطهایی که با دیدگاه مهندسین بتن تهیه می‌شوند معمولا چهار گروه تقسیم بندی برای سنگدانه‌ها مرسوم است. این چهار بخش مصالح شامل ماسه ۳ ~ ۰ و ۵ ~ ۰، شن ۲۵ ~ ۵ و شن ۵۰ ~ ۲۵ می‌باشد.

۲-۳-۵ مصالح ریزدانه

مصالح ریزدانه یا ماسه به مصالح گذرنده از الک شماره ۴ (سنگدانه‌های کوچکتر از۴٫۷۵ میلی متر) گفته می‌شود. در مخلوط‌های بتن غلتکی که مقدار خاک رس زیادی استفاده شده است، مشاهده می‌شود که پتانسیل ترک خوردگی بتن غلتکی افزایش یافته، در نتیجه مقاومت کاهش پیدا می‌کند. توصیه می‌شود که ریزدانه‌های مصرفی در بتن غلتکی غیر پلاستیک بوده و مقدار آن در حدی باشد که منافذ خالی را پر نموده، مصرف آب را کاهش دهد و باعث تراکم بهتر مصالح گردد[13].

در تولید ماسه ۵ ~ ۰ دو حالت شسته و نشسته بررسی شد. به جهت به دست آوردن بهترین نسبت اختلاط، اقدام به انجام آزمایش وزن مخصوص آزاد میله خورده مصالح گردید. با در نظر گرفتن پارامترهای حداکثر وزن مخصوص میله خورده و کنترل پدیده جداشدگی نسبت اختلاط ۲ به ۱به ترتیب در شن ۲۵ ~ ۵ و ۵۰ ~ ۲۵ نهایی شد. در ماسه نیز پارامترهای مذکور بعلاوه پوش دانه بندی ماسه مخلوط، منجر به نسبت اختلاط ۱ به ۱ در حالت نشسته و ۳ به ۲ در حالت شسته به ترتیب برای ماسه ۳ ~ ۰ و ۵ ~ ۰ گردید. نسبت‌های اختلاط کلی

مصالح نیز با در نظر گرفتن کنترل پدیده جداشدگی، وزن مخصوص میله خورده حداکثر، حداقل میزان خمیـر لازم انتخاب گردید.

۲-۳-۶ دانه‌بندی کلی مصالح سنگی

با توجه به میزان خمیر، در طرحهای حاوی ۱۲۰ تا ۱۵۰ کیلوگرم بر متر مکعـب مـواد سـیمانی ۴۰ درصـد ماسـه، بالاتر از ۱۵۰ کیلوگرم بر متر مکعب ۳۸ درصد و پایین تر از ۱۲۰ کیلوگرم بر متـر مکعـب مـواد سـیمانی نیـز ۴۲ درصد ماسه مناسب بود. در شکل ۱ منحنی دانه بندی کلی مصالح سنگی طرح آمده است.

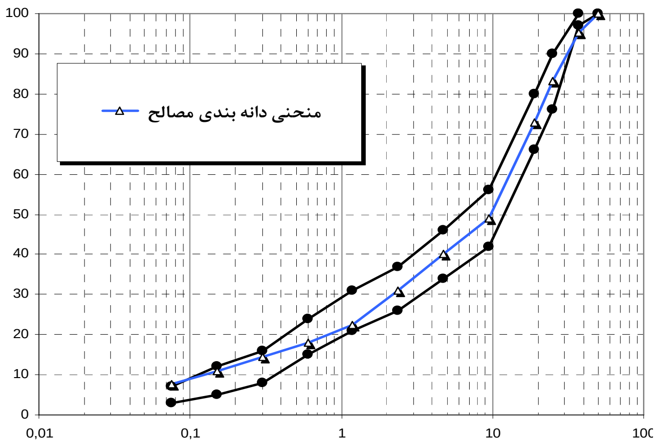

شکل ۱- دانه بندی کلی مصالح سنگی بتن غلتکی

۲-۴ معیارهای طرح بهینه

جهت دستیابی به طرح اختلاط بهینه سه معیار زیر در نظر گرفته شده است.

الف - معیار مقاومت فشاری: برای مقاومت فشاری معیار اصلی رسیدن به مقاومـت فـشاری ۱۲۵ کیلـوگرم برسانتی متر مربع در ۱۸۰ روز قرار داده شده است.

ب - معیار کارآیی: برای اینکه مخلوط کارآیی مناسبی داشته و پیوستگی مطلوب بین لایه‌های متـوالی ایجـاد گردد، معیار زمان ویبی ما بین ۱۴ الی ۲۴ ثانیه در نظر گرفته شده است.

پ - معیار عدم جداشدگی دانه‌ها: جدایی دانه‌ها عمدتا به علت درصد آب خیلی کم و یا خیلـی زیـاد، کـم بودن مقدار ریزدانه و عدم تعادل بین دانه‌های با اندازه‌های مختلف به وجود می‌آید. در طرح بهینه نباید جداشدگی دانه‌هارخ دهد تا ضمن حفظ یکنواختی، مقاومت و دوام مطلوب نتیجه شود.

۳- یافته‌ها

۳-۱ مرحله اول

در این مرحله اقدام به ساخت طرح‌های تکمیلی شد که نمونه‌هایی از این طرح اختلاط‌ها در جدول ۱ آورده شده است.

همچنین نتایج آزمایشات بر روی نمونه‌های ساخته شده به شرح زیر می‌باشند:

۳-۱-۱ مقاومت فشاری

در شکل ۲ رابطه بین نسبت آب به سیمان و مقاومت فشاری ۷، ۲۸، ۹۰ و ۱۸۰ روزه کلیه طرحهـای ایـن مرحلـه نشان داده شده است.

جدول ۱: نمونه‌ای از طرح اختلاط‌های ساخته شده

شماره طرح	نام طرح	0-3 (kg/m³) %	0-5 (kg/m³) %	mai-25 (kg/m³) %	25-50 (kg/m³) %	آب آزاد (kg/m³)	پوزولان خاش (kg/m³)	میزان سیمان (kg/m³)	نوع افزودنی درصد به مجموع مصالح سیمانی	نسبت آب به مصالح سیمانی	زمان ویبی ثانیه	مقاومت فشاری kg/cm² 7	28	90	180
1	R70-30-01	517 23	519 23	822 36	411 18	114	7	63	Chrysoplast CER 0,6	1,630	36	29	33	43	52
2	R80-30-01	492 22	493 22	863 38	409 18	116	8	72	Chrysoplast CER 0,6	1,450	31	33	39	54	64
3	R90-30-01	511 23	513 23	813 36	407 18	117	9	81	Chrysoplast CER 0,6	1,300	20	36	47	57	71
4	R100-30-01	489 22	491 22	858 38	407 18	114	10	90	Chrysoplast CER 0,6	1,140	23	50	63	81	91
5	R110-30-01	608 27,6	407 18,4	806 36	403 18	118	11	99	Chrysoplast CER 0,6	1,068	30	54	81	83	98
6	R120-30-04	500 22,8	335 15,2	914 41	468 21	119	12	108	Chrysoplast CER 0,6	0,991	19	63	85	93	99
7	R126-22-01	570 26,4	381 17,6	843 38	395 18	130	0	126	Chrysoplast CER 0,6	1,033	20	65	90	91	101
8	R130-30-02	545 **25,2**	364 **16,8**	857 **39**	417 **19**	128	13	117	Chrysoplast CER **0,6**	0,983	23	60	93	98	114

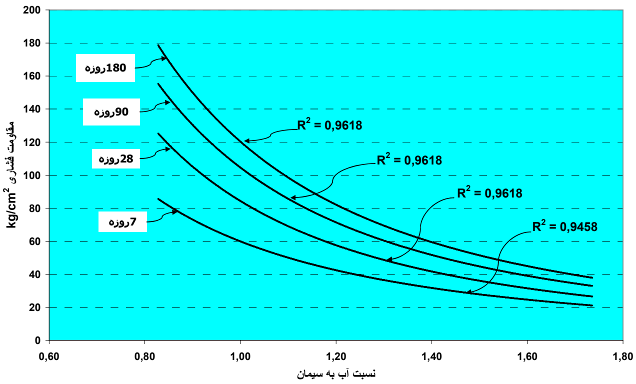

شکل ۲- رابطه نسبت آب به سیمان و مقاومت فشاری

آزمایشات نشان دادند که مقاومت فشاری طرحهای ساخته شده با سنگدانه‌های نشـسته طبیعـی مطلـوب نیـست. همچنین مقدار آب مناسب برای این نوع سنگدانه‌ها زیاد است. علت این امر زیاد بودن مواد ریزدانه خصوصا ذرات

گذرنده از الک نمره ۵۰، ۱۰۰ و ۲۰۰ می‌باشد که مانع عملکرد مطلوب سیمان میگردند.

۳-۱-۲ طرحهای اختلاط شسته و نشسته

پس از ساخت طرحهای حاوی مصالح شسته و نشسته و انجام آزمایشات بر روی آنها نتایج نشان دادند که طرحهای اختلاط شسته و نشسته تفاوت عمده ای بین آنها نیست به طوری که مقاومت طرحهای نشسته کمی‌بالاتر از طرحهای شسته می‌باشد. که دلیل این امر، افزایش نسبت ماسه ۵-۰ در ماسه مخلوط متأثر از نرمتر شدن آن می‌باشد. این موضوع در شکل ۳ به روشنی قابل مشاهده است.

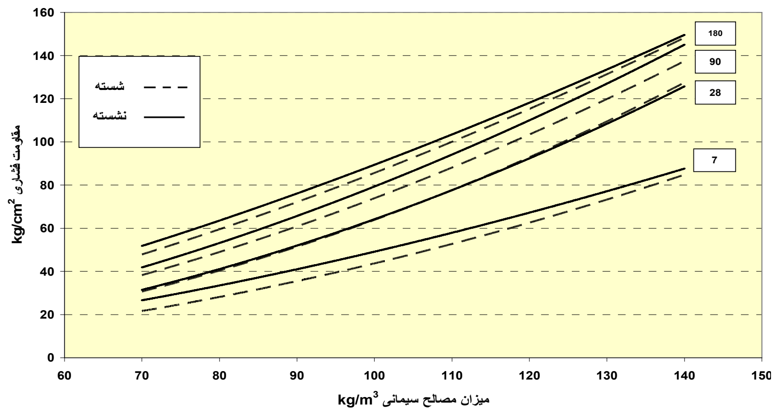

شکل ۳- مقایسه طرحهای اختلاط شسته و نشسته

۳-۱-۳ موادافزودنی

در طرح اختلاط سد بتن غلتکی زیردان از موادافزودنی ChrysoPlast CER و Conplast RP264M و ChrysoTard CHR استفاده شد که طرحهای حاوی افزودنی منتخب (نوع D مطابق استاندارد(ASTM C494 حدود ۱۲ درصد مقاومت فشاری بالاتری نسبت به طرحهای دیگر کسب کردند. در شکل ۴ رابطه بین میزان مصالح سیمانی و مقاومت فشاری ۱۸۰ روزه طرحها با افزودنیهای مختلف نشان داده شده است. همچنین در مورد مخلوط‌های کم سیمان، کاربرد مواد افزودنی روان ساز باعث کاهش در مقدار آب (با زمان Vebe ثابت) می‌شوند ولی با وجود کاهش در نسبت آب به سیمان، مقاومت فشاری به طور محسوسی افزایش نمی‌یابد. لذا در این حالت دلیل عمده برای استفاده از روان ساز، می‌تواند افزایش روانی جهت نیل به زمان Vebe مناسب و بهبود یکنواختی بتن باشد.

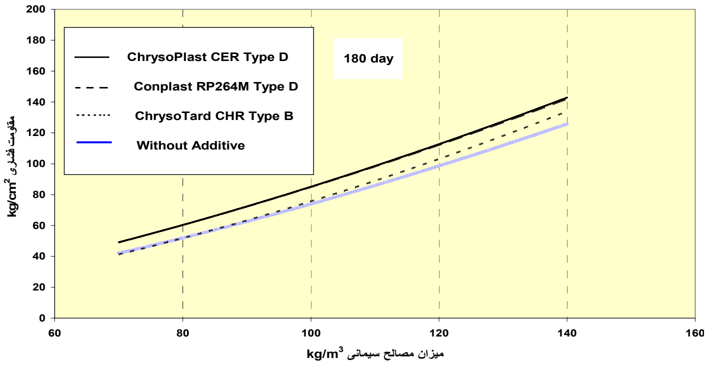

شکل ۴- مقاومت فشاری طرحهای با افزودنی‌های متفاوت

۳-۱-۴ مقدار مختلف مواد افزودنی

با توجه به اینکه حداکثر میزان توصیه شده از سوی سازنده این مواد حدود ۰٫۸ درصد وزنی مواد سیمانی می‌باشد، علاوه بر دوزاج ۰٫۶، سه طرح با دوزاج ۰٫۸ نیز کار شد که برای مقایسه آنها با یکدیگر، ۴ طرح که زمانهای ویبی آنها نزدیک به یکدیگر است به همراه یک طرح که زمان ویبی بالایی دارد، در جدول ۲ آورده شده است.

جدول ۲: طرحهای اختلاط با دوزاج مختلف موادافزودنی

نام طرح	آب آزاد (kg/m3)	افزودنی نوع درصدبه مجموع مصالح سیمانی	زمان ویبی ثانیه	نسبت آب به سیمان	VP / VM %	مقاومت فشاری kg/cm^2 7	میانگین دانسیته (kg/m3)	زمان تراکم ثانیه
R160-30-11	118.7	Conplast RP264M 0.6	16	0.742	46.0	84.5	2508	15
R160-30-12	120.0	Chrysoplast CER 0.6	20	0.750	46.2	97.6	2501	10~15
R160-30-13	116.5	Chrysoplast CER 0.8	18	0.728	45.8	106.0	2507	10~12
R160-30-14	114.3	Conplast RP264M 0.8	45	0.714	45.5	108.9	2517	27~30
R160-30-15	119.2	Conplast RP264M 0.8	18	0.745	46.2	79.7	2474	10~12

چنانچه مشاهده می‌شود با افزایش دوزاج Chrysoplast از ۰٫۶ به ۰٫۸ درصد (مقایسه طرحهای ۱۲ و ۱۳) در شرایط یکسان، حدود ۹ درصد افزایش مقاومت و ۳ درصد نیز کاهندگی آب بیشتر حاصل شده است. ولی با افزایش دوزاج Conplast برعکس شاهد کاهش در مقاومت هستیم. نکته قابل توجه مقاومت یکسان در دو طرح شماره ۱۳ و ۱۴ با زمانهای ویبی متفاوت است که مبین مقاومت بالاتر افزودنی Chrysoplast در شرایط یکسان می‌باشد که این مسئله در طرحهای حاوی ۰٫۶ درصد مواد مذکور نیز به وضوح دیده شد.

۳-۱-۵ مقادیر مختلف پوزولان

با ثابت بودن مجموع مواد سیمانی، افزایش پوزولان کارآیی را بالا خواهد برد. بدین منظور علاوه بر طرحهای حاوی ۳۰ درصد پوزولان، طرحهایی نیز با ۳۵ و ۴۰ درصد پوزولان ساخته شد.
رابطه بین مواد سیمانی با مقاومت فشاری (شکل ۵) و نسبت آب به سیمان و مواد سیمانی با مقاومت (شکل۶ بیانگر مناسبتر بودنِ عملکرد طرحهای حاوی ۳۰ درصد پوزولان است.

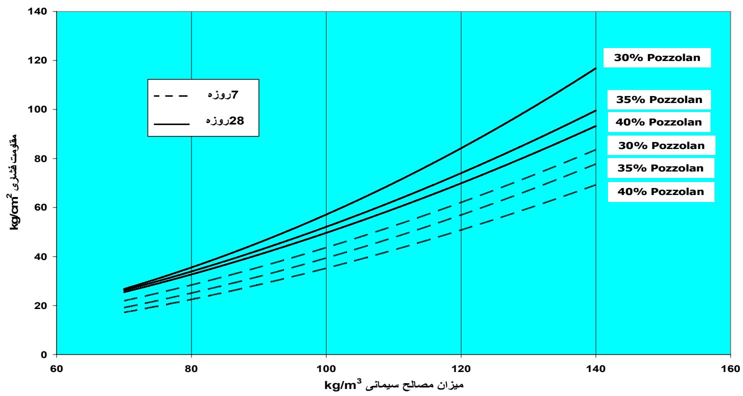

شکل ۵- رابطه بین مواد سیمانی با مقاومت فشاری

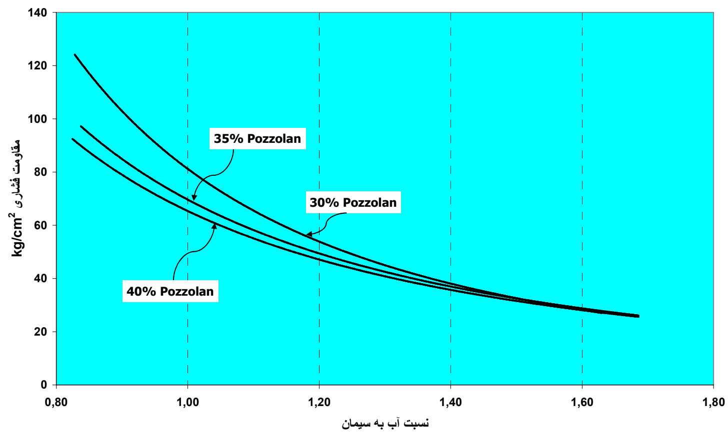

شکل ۶- نسبت آب به سیمان و مواد سیمانی با مقاومت فشاری

۳-۱-۶ مقاومت کششی غیرمستقیم

در زمان ساخت نمونه‌های استوانه‌ای جهت انجام آزمایشات مقاومت فشاری نمونه‌هایی نیز به منظور بررسی مقاومت کششی طرح‌های اختلاط نیزگرفته شد که مقادیر مقاومت کششی برخی نمونه‌های با میزان مصالح سیمانی بیشتر از ۱۵۰ کیلوگرم بر متر مکعب در سنین ۷، ۲۸، ۹۰ و ۱۸۰ روزه آنها در شکل ۷ نشان داده شده است. نتایج نشان‌دهنده این است که مقاومت کششی غیرمستقیم در طرحهای مختلف حدود ۱۰ الی ۱۱ درصد

مقاومت فشاری می‌باشد.

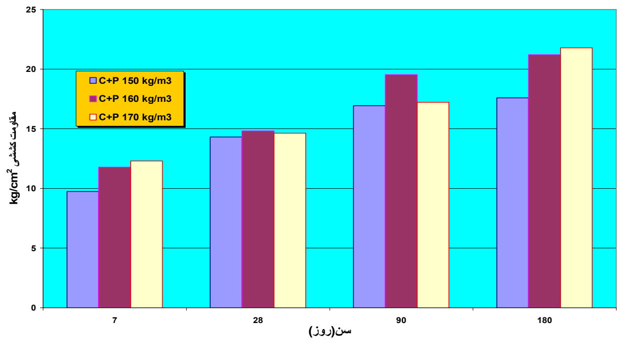

شکل ۷- مقاومت کششی غیر مستقیم طرحهای اختلاط

۳-۲ مرحله دوم

پس از اخذ نتایج طرحهای مرحله اول، ساخت طرحهای نهایی با زمان ویبی واقعی ۱۴ تا ۲۴ ثانیه آغاز شد. همچنین از طرحهای مرحله اول برای مقایسه حالات مختلف (شسته ونشسته، افزودنی‌ها و درصدهای مختلف پوزولان) استفاده شده است. در شکل ۸ ضریب بازده نمونه‌های مختلف ارائه شده است.

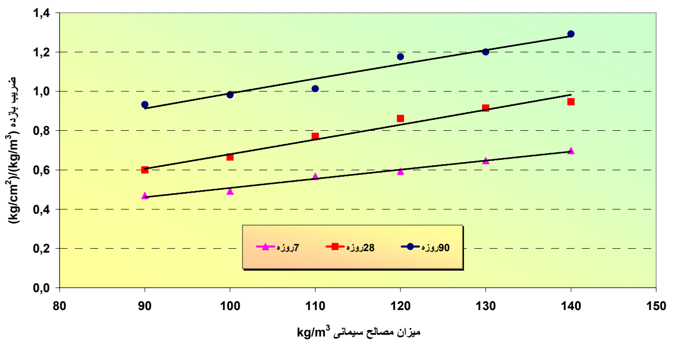

شکل ۸- ضریب بازده طرحهای مرحله دوم

همچنین در شکل ۹ رابطه بین مقدار مصالح سیمانی با توجه به مقاومت ۷، ۲۸ و ۹۰ روزه طرحها آورده شده است.

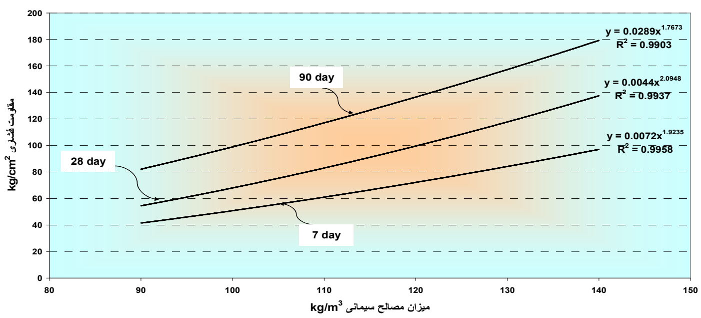

شکل ۹- رابطه نسبت آب به سیمان و مقاومت فشاری

۴- نتیجه گیری و انتخاب طرح اختلاط بهینه

۱- وزن مخلوط طرح‌ها در محدوده ۲۲۸۰ تا ۲۴۸۰ کیلو گرم بر متر مکعب قرار داشتند.

۲- بخش ریزدانه سنگدانه‌های ۵-۰ میلی مترعملکرد دوگانه ای دارند. ازطرفی امکان استفاده از سنگدانه‌های درشت تر بدون آنکه جداشدگی دانه‌ها در مخلوط رخ دهد را میسر می‌سازد و از این طریق مقاومت بتن را افزایش می‌دهند و از طرف دیگر مانع پوشش کامل دانه‌های درشت تر توسط سیمان شده و از این طریق مقاومت را کاهش می‌دهند.

۳- در مخلوط‌های کم سیمان، کاربرد مواد افزودنی روان ساز باعث کاهش در مقدار آب (با زمان vebe ثابت) می‌شوند ولی با وجود کاهش در نسبت آب به سیمان، مقاومت فشاری به طور محسوسی افزایش نمی‌یابد. لذا در این حالت دلیل عمده برای استفاده از روان ساز، می‌تواند افزایش روانی جهت نیل به زمان vebe مناسب و بهبود یکنواختی بتن باشد.

۴- نفوذپذیری مخلوط‌های RCC به اندازه مخلوط‌های بتن معمولی و یا حتی پایین تر می‌باشد[15] که آزمایشات صورت گرفته نیز دلالت بر این موضوع دارد.

۵- استفاده از پوزولانها در بتن هم اقتصادی و هم منجر به اصلاح خصوصیات بتن تازه و سخت شده می‌شود[16] که در آزمایشات انجام گرفته نیز بهبود و رشد خصوصیات بتن غلتکی ازجمله در کارپذیری، مقاومت فشاری، مقاومت سایشی و مسایل حرارتی و جمع شدگی مشاهده شد.

۶- جایگزینی سیمان با ۳۰ درصد پوزولان زمانیکه این مقدار به حالت بهینه در مخلوط باشد منجربه بالاترین مقاومت فشاری بتن غلتکی در سن ۹۰ روزه (۱۳۹ کیلوگرم برمترمکعب) می‌شود[17]. درتحقیقی ازآتیس و همکارانش به جایگزینی بهینه خاکستر بادی در حدود ۲۵ الی ۳۵ درصد وزنی سیمان در مخلوط‌های بتنی دست یافتند[18]. که در مطالعه صورت گرفته نیز با کسب مقاومت فشاری طرح اختلاط بهینه در سن ۹۰ روزه (۱۳۳ کیلوگرم برمترمکعب) دلالت برعملکرد مناسب پوزولان خاش دارد.

۷- مقاومت سایشی و فرسایشی بتنهای ساخته شده با خاکستر بادی و سیمان‌های پرتلند پوزولانی به مراتب بهتر از بتنهای ساخته شده با سیمان پرتلند معمولی می‌باشند[19] که این اثرات در تحقیق صورت گرفته نیز مشاهده شده است.

۸- با توجه به نتایج به دست آمده و برای رسیدن به مقاومت مشخصه طرح (۱۲۵ کیلوگرم بر سانتیمتر مربع در سن ۱۸۰ روز)، طرح اختلاط با مشخصات زیر انتخاب گردید.

میزان مصالح سیمانی	حجم خمیر	حجم ملات	نسبت حجم خمیر به ملات	زمان ویبی	دانسیته	مقاومت فشاری kg/cm^2			
Kg/m3	نسبت حجمی (درصد)		%	ثانیه	Kg/m^3	7روزه	۲۸ روزه	90روزه	180روزه
120	21	49	43	15	2475	65	95	133	133

تشکر و قدردانی

بدینوسیله از مهندس محسن جعفربیگلو و تکنسینهای آزمایشگاه بتن شرکت جهان کوثر (پیمانکار سد زیردان) که در کلیه مراحل ساخت مخلوطهای بتن و انجام آزمایشها، صمیمانه همکاری فراوانی را مبذول داشته اند

سپاسگزاری و قدردانی می‌شود.

مراجع

۱. عرب، داودرضا. «طراحی و ساخت سدهای بتن غلتکی»، پایان نامه کارشناسی ارشد دانشگاه صنعتی شـریف، ۱۳۷۳.

۲. گزارش فنی مهندسین مشاور آبفن و پژوهاب – ۱۳۷۷

3. Hansen,K.D.,"Roller Compacted Concrete",Mc Graw Hill,1991.
4. Dunstan,M.R.H.,The state-of-art of Roller compacted concrete dams Hydropower & dams.March1994.pp.44-45.
5. Compaction of Roller-Compacted Concrete. Reported by ACI Committee 309.5
6. Francisco Rodrigues Andrioli" Roller – Codmpact Concrete on Dams workshop" – IRCOLD – (Tehran – IRAN – june 21 -2007).
7. American concrete Institute committee207 "Roller compacted concrete"207.5R.ACI Materials Jornal1998.
8. ASTM C1170," Standard Test Methods for Determining consistency and Density of Roller- Compacted Concrete Using a Vibrating Table".
9. ASTM C1176,"Standard Practice for Making Roller-Compacted Concrete in Cylinder Molds Using a Vibrating Table".
10. Hansen,K.D.,"Roller Compacted Concrete",Mc GrawHill,1991.
11. M.Dunstan the optimization of the mixture proportion of Rcc Dams 2003
12. ASTM C494"" Standard Specification for Chemical admixtures for concrete".
13. ASCE,"Roller Compacted Concrete",Technical Engineering and Design Guide Adapted from the US Army Corp of Engineers, No.5,American Society Of Civil Engineers,1994.
14. ASTM C595 " Standard Specification for Blended Hydraulic Cements".
15. Schrader, M.R.H.-Roller Concrete for Dams-concrete International, ACI, Chicago, vol.6, May 1984, 38-45.
16. ASTM C618" Standard Specification for Coal Fly Ash and Raw or Calcined Natural Pozzolan for Use as a Mineral Admixture in Concrete".
17. Per-wei Gao,"The characteristics of air voids and frost resistance of RCC with fly ash and expansive agent"2005 Elsevier Science.
18. V.G.Papadakis,S.Tsimas,"Supplementary cementing materials in concrete".2002 elsevier Science.
19. Xie, B.Liu, J.Yin, S.Zhou, "Optimum mix parameters of high strength concrete". Concr. Res. 32(2002) 477-480.
20. C.D.Atis, U.K.Svin, O.Karahan, "Strengh properties of roller compacted concrete contaning a non-standard high calcium fly ash"2003 Elsevier Science.
21. Velu Saraswathy, Ha-Won Song,"Evaluation of corrosion resistance of Portland pozzolana cement andfly ash blended cements in pre-cracked reinforced concrete" 2005 Elsevier Science.

CD11

Nano Technology

CD11-001

INVESTIGATION OF MECHANICAL AND PHYSICAL PROPERTIES OF MORTARS CONTAINING SILICA FUME AND NANO-SIO_2

A. Sadrmomtazi[1], A. Fasihi[2], F. Balalaei[3], A.K. Haghi[4]
[1]Assistant Professor, Dept. of Civil Engg, Faculty of Engg, University of Guilan, Rasht, Iran
[2]M.S. Student, Dept. of Civil Engg, Faculty of Engg, University of Guilan, Rasht, Iran
[3]M.S., Fanavari Park of Guilan, Rasht, Iran
[4]Professor, Dept. of Textile Engg, Faculty of Engg, University of Guilan, Rasht, Iran

ABSTRACT

It has been found that physical properties of concrete, particularly strength and permeability significantly depend on its pore structure. Ultra fine particles of nano-SiO_2 fill the voids of CSH structure and provide more homogenous distribution of hydrated products. This effect of nano-SiO_2 enhances the durability of cement composites as well as the strength. In this paper, influence of nano-SiO_2 on different properties of cement mortar was investigated in comparison with silica fume (SF) as a well-known active pozzolan. Different amounts of nano-SiO_2 (0, 1%, 3%, 5%, 7%and 9%) were incorporated into the ordinary cement mortar. Mechanical properties, shrinkage, water absorption of the specimens were determined. Results showed that the optimal content of Nano-SiO_2 in plain cement mortar was around 7%. Nano-SiO_2 particles were more effective in developing higher mechanical strength and lower water absorption than that of SF. Yet the mortar containing nano-SiO_2 experienced higher shrinkage than that of SF mortar.

Keywords: cement mortar, mechanical properties, nano-SiO_2, silica fume, shrinkage

1. INTRODUCTION

High strength concrete and mortar with high strength and durability properties offer many advantages. They have been gradually replacing normal strength concrete due to their improved mechanical characteristics and low permeability. With such outstanding characteristics they can be utilized in structure, exposed to severe loading or influenced by environmental conditions, for instance large bridges and offshore constructions [1,2].

Silica fume has been widely used as a supplementary cementing material for producing high performance concrete. It is used to enhance the strength and durability of concrete. It has been reported that use of SF as a cement replacement increased sulfate and acid resistance and decreased chloride permeability of concrete. When SF is added to cement/concrete, it acts as a filler to fill the gaps between cement particles resulting in finer pore structure. Also more CSH gel can be formed in SF concrete due to the reaction that occurs between the silica in SF

and the $Ca(OH)_2$ in hydrating cement (pozzolanic reaction)[3,4].
Recently with the help of advanced nanotechnology developments, nano-SiO_2 with finer particles size and higher pozzolanic activity has been introduced. Studies have shown that incorporating nano-SiO_2 into cement based materials improved mechanical properties of the products. Qing Ye [5] reported that nano-SiO_2 improved the bond strength of paste-aggregate interface. Additional studies have also concluded that pozzolanic activity of nano-SiO_2 was much greater than that of silica fume [6]. The abrasion resistance of concrete containing nano-SiO_2 was studied by Hui Li [7]. He suggested that nano-SiO_2 was valuable for enhancing abrasion resistance of pavement. Gengig Li [8] showed that nano-SiO_2 added to high-volume fly ash high-strength concrete could improve short and long term strengths. K. Lin [9] reported that nano-SiO_2 particles could potentially improve the negative influences caused by sewage sludge ash (SSA) replacement mortar. It has been found that when nano-SiO_2 particles are uniformly dispersed in cement paste they will accelerate cement hydration due to their high activity [10].
Owing to the unique properties of nano-SiO_2 it seems that it has a potential to be utilized in production of high strength concrete. Hence more assessments are necessary to ensure usage possibility of nano-SiO_2 in cement based materials. Accordingly, in the present experimental study, Nano-SiO_2 particles were incorporated into ordinary cement mortar and compressive strength, flexural behavior, water absorption and shrinkage of these composites were investigated. Results were compared with mortar containing 10% silica fume.

2. MATERIALS AND METHOD

Materials: In this study, ordinary Portland cement type I, silica fume, nano-SiO_2 particles and tap water were used. SF used in this experiment contained 91.1% SiO_2 with average particles size of 7.38 µm. The chemical compositions of SF and cement were analyzed using an X-ray microprobe analyzer and listed in Table 1. In order to achieve the desire fluidity and better dispersion of nano particles, a polycarboxylate ether based superplastisizer was incorporated into all mixes. Natural river sand was used with the fraction of sand passing through 1.18 mm sieve and retaining on 0.2mm. The specific gravity of sand was 2.51 gr/cm^3. Basic material properties of nano-SiO_2 are given in Table 2.

Table 3: Chemical composition of cement and silica fume

Chemical compositions (%)							Items
L.O.I	**SO_3**	**MgO**	**CaO**	**Fe_2O_3**	**AL_2O_3**	**SiO_2**	
1.35	-	4.8	61.5	2.76	3.68	21.5	O.P.C.
2.1	0.45	.6	2.24	2	1.55	91.1	S.F.

Table 2: Basic material properties of nano-SiO_2

Item	Diameter (nm)	PH value	Composition (mass%)
Target	50	10	SiO_2(30%) + H_2O(70%)

Table 4: Mix proportion of the specimens

No	Sand/Binder	Water/Binder	% Content (by weight)		
			O.P.C.	**N.S.**	**S.F.**
NS0	2.75	0.5	100	0	-
NS1	2.75	0.5	99	1	-
NS3	2.75	0.5	97	3	-
NS5	2.75	0.5	95	5	-
NS7	2.75	0.5	93	7	-
NS9	2.75	0.5	91	9	-
SF10	2. 75	0.5	90	0	10

Methods: Cement mortars containing SF or nano-SiO_2 were prepared with the same flowing capacity through the adjustment of superplastisizer (Table 3). The water/binder and sand/binder ratios of all mixtures were 0.5 and 2.75 respectively, where the binder weight is the total weight of cement, SF or nano-SiO_2. The amount of SF replacement in mortar (SF mortar) was fixed at 10% which is an acceptable range and is used most often. In order to achieve the desired properties, it is essential to disperse nano particles uniformly. Accordingly, mixing was carried out in a rotary mixer as follows:

1. The nano-SiO_2 particles were stirred with 90% of mixing water at high speed and for about 1 min.
2. The Cement and SF were premixed for 30 s. Then dry mixed cement and SF were added to the mixture. After adding, the mixer was allowed to run for 1 min at medium speed.
3. The sand was gradually added at 30s while the mixer was running at medium speed.
4. The superplastisizer and remaining water were added and stirred at high speed for 30s.
5. The mixture was allowed to rest for 90s. Then mixing was continued for 2 min at high speed.

After mixing, the samples were cast into the 50×50×50 mm cubes for compressive and water absorption tests and 50×50×200 beams for flexural and shrinkage tests. The compressive samples were placed in two layers. Each layer was temped 32 times in about 10s using a hard rubber mallet following the procedure of ASTM C-109 [11]. The flexural samples also were placed in two layers and each layer was tamped 12 times in 4 rounds as per ASTM C-348 [12]. After 24 hours the specimens were removed from the molds and cured in water at 23±2 $^{\circ C}$ for 7, 28, 60 and 90 days. The specimens were tested using a hydraulic testing machine under load control at 1350 N/s for compressive test and 44N/s for flexural test. The absorption test was carried out on two 50 mm cubes. Saturated surface dry specimens were kept in an oven at 110$^{\circ C}$ for 72 h. After measuring the initial weight, specimens were immersed in water for 72h. Then the final weight was measured and the absorption was reported to assess the mortar permeability of mortar in this study.

3. RESULTS AND DISCUSSION

Compressive strength: Figure 1 shows the variation in the compressive strength of mortars. It can be seen that the compressive strength of cement mortar with nano-SiO_2 is higher than that of plain cement mortar and gradually increases with an increase in the amount of nano-SiO_2. It is obvious that increase in the nano-SiO_2 content beyond 7% did not change the compressive strength significantly. It is found that large amounts of nano-SiO_2 decrease the compressive strength of the composites instead of improving it. Because when the content of nano-SiO_2 is large, nano particles are difficult to disperse uniformly. Therefore, they create a weak zone in the form of voids, consequently the homogeneous hydrated microstructure can not be formed and a lower strength will be probable [13]. Also it can be observed that the compressive strength of the specimens containing 5%, 7% and 9% nano-SiO_2 (Mixtures NS5, NS7, NS9) are higher than that of the SF mortar. This indicates that nano-SiO_2 has a higher pozzolanic activity and is more valuable in reinforcement of mortar than that of SF.

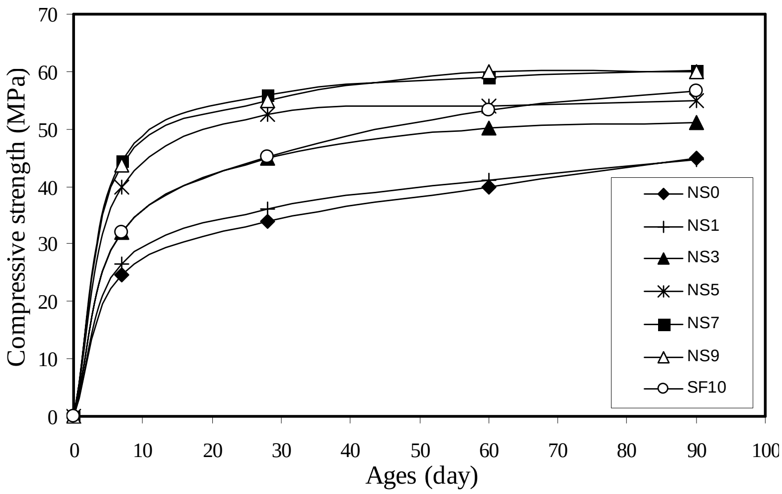

Figure 1. Compressive strength of different cement mortars

Flexural strength: Flexural strength test results are shown in Figure 2. Results show that nano-SiO_2 is more effective in developing flexural strength than that of SF. From the results it can be concluded that the optimum nano-SiO_2 content in ordinary cement mortar ranges between 5% and 7%.

Two fundamental mechanisms can be deduced for strength enhancement by nano-SiO_2:

1) Strength enhancement by matrix densification and paste-aggregate interfacial zone refinement
2) Strength enhancement by reduction in the content of $Ca(OH)_2$.

The first strengthening mechanism is called the filler effect. The micro filling effect of nano-SiO_2 is one of the important factors for the development of dense concrete/mortar with very high strength, because small amount of air content significantly decreases the strength of the mortar. Nano-SiO_2 particles, due to their small size act as a filler to fill into the interstitial spaces inside the skeleton of hardened microstructure of cement paste to increase its density as well as the strength [14]. The filling effect of nano-SiO_2 is also valuable for generating strong transition zone. It has been reported that the microstructure of the transition zone between cement paste and aggregates strongly influences the strength and durability of concrete [15]. Nano-SiO_2 particles reduce the wall effect in the transition zone between the paste and the aggregate and strengthen this weaker zone due to the higher bond between those two phases. It should be mentioned that the silica fume causes reduction in the volume of large pores and increases the mortar strength too, but as the size ratio between filler and the aggregates is one of the main parameters that strongly affects the strengthening caused by filling effect, and thanks to the high size ratio between nano-SiO_2 and cement grains, the filling effect of nano-SiO_2 particles is more obvious. The second strengthening mechanism is the pozzolanic activity. Pozzolans are defined as siliceous or siliceous and aluminous materials that in themselves possess little or no cementing property but in finely dispersed form in the presence of moisture chemically react with calcium hydroxide at ordinary temperature to form compound possessing cementitious properties. Two major products of cement hydration are calcium silicate hydrate (CSH) and calcium hydroxide (CH) respectively. Calcium silicate hydrate which is produced by hydration of C_3S and C2S plays a vital role in mechanical characteristics of cement paste. Whereas calcium hydrate which is also formed by hydration of cement does not have any cementing property. It contains about 20-25% of the volume of the hydration products. Calcium hydrates due to their morphology are relatively weak and brittle. Cracks can easily propagate through regions populated by them, especially at the aggregate cement paste matrix interface [16]. Nano-SiO_2 reacts with Calcium hydrates formed during hydration of cement rapidly and produces calcium silicate hydrate with cementitious properties which is beneficial for enhancement of strength in concrete/mortar.

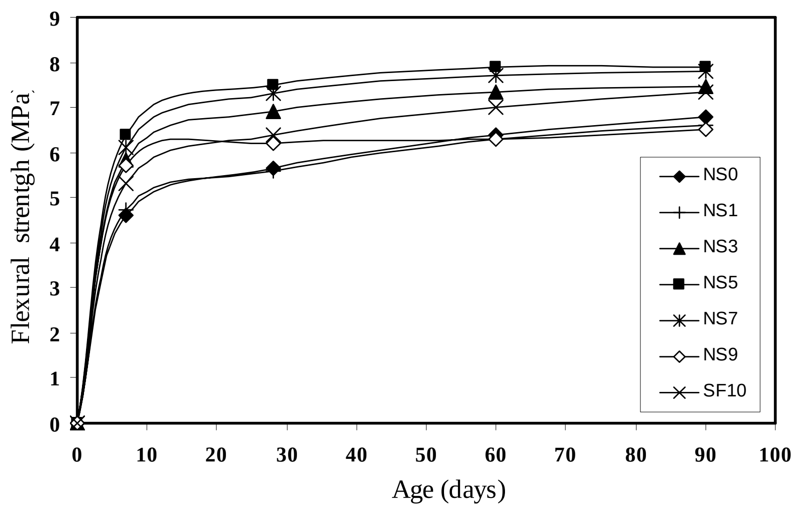

Figure 2. Flexural strength of different cement mortars

Both nano-SiO_2 and SF belong to pozzolanic materials, however results showed that the pozzolanic activity of nano-SiO_2 was much greater than that of SF. A possible reason for this observation could be nucleation effect. Nano-SiO_2 due to its high specific surface serves additional nucleation sites for precipitation of the hydration products whereby chemical reactions are accelerated [17]. Moreover it has been suggested that the surface of pozzolan can adsorb many Ca^{+2} ions and that lowering of the concentration of the calcium ions accelerates the rate of dissolution of C_3 S that increases the rate of hydration [18]. Owing to the higher specific surface of nano particles they adsorb more Ca^{+2} ions and accelerate the rate of hydration more effectively.

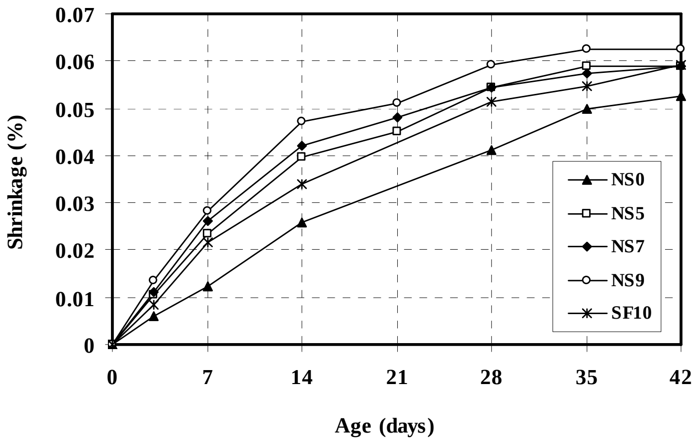

Figure 4. Shrinkage behavior of different cement mortars

Shrinkage: Shrinkage is a common phenomenon generally encountered in almost every cementitious product due to contraction of total mass upon loss of moisture. It is sometimes accompanied by development of cracks specially in such members whose surface area to volume ratio is large [19,20]. These cracks serve as conduits for salt and water. The saline solution comes in contact with reinforcing steel and promotes corrosion. Corrosion causes expansion of steel and inevitably pop-outs occur in the concrete cover, Thereby reducing the strength and service life of the concrete [21]. In view of the importance of the volume changes due to shrinkage this section is devoted to the study of the influence of nano-SiO_2 on the drying shrinkage of ordinary mortars. Prismatic specimens with 50×50×200 mm dimensions were prepared. The first measurement was taken using a length comparator with a precision of 2μm after 24 h of mixing, while the rest of measurements were taken at different ages of 3, 7, 14, 21, 28, 35, 42 days. The specimens were cured in the laboratory environment. The average temperature in the laboratory was 27±3 $^{\circ}$C. The shrinkage behavior of mortars containing different amounts of nano-SiO_2 in comparison with SF mortar is presented in Figure 3. Results showed that both SF mortar and mortar containing nano-SiO_2 experienced higher shrinkage than that of ordinary cement mortar. Moreover it can be seen that the drying shrinkage of mortars with nano-SiO_2 is higher than that of SF mortar and increases with increasing nano-SiO_2 content. The increase in the drying shrinkage of mortar containing nano-SiO_2 might be due mainly to refinement of pore size and increase of mesopores volume which is directly related with the shrinkage due to self desiccation. Moreover nano-SiO_2 particles act as an Activator to accelerate cement hydration, therefore the degree of hydration increases as the amount of nano-SiO_2 increases and the autogenous shrinkage related to chemical shrinkage also increases [22].

Water absorption: The absorption characteristics indirectly represent the porosity through an understanding of the permeable pore volume and its connectivity [23]. In order to investigate the effect of nano-SiO_2 particles on cement mortar permeability, water absorption test was carried out at the curing age of 28 days. The absorption values of mortars are listed in Table 4. It is clear that presence of pozzolanic material in cement mortar decreased the water absorption value. Nano-SiO_2 was more effective in reduction of permeability than that of SF. The increase of impermeability caused by nano-SiO_2 can be attributed to two concomitant phenomena:

i. Nano-SiO_2 particles generate a large number of nucleation sites for the hydration products and induce a more homogenous distribution of CSH and hence less pore structure [24].
ii. Nano-SiO_2 particles block the passages connecting capillary pores and water channels in cement paste [25].

Table 5: Water absorption of mortars

Mixture	Water absorption (%)
NS0	6.12
NS3	5.11
NS5	4.35
NS7	4.23
SF10	5.18

4. CONCLUSIONS

An experimental study was carried out to investigate the effect of nano-SiO_2 on the physical and mechanical properties of mortar. Based on the experimental results, following conclusions can be drawn:

1. Noticeable increase was observed in compressive and flexural strength of ordinary cement mortar upon adding nano-SiO_2, however high amounts of nano-SiO_2 had a negative effect on mechanical properties especially flexural strength. From the results it can be concluded that the optimum nano-SiO_2 content in ordinary cement mortar ranges between 5% and 7%.
2. The effect of nano-SiO_2 on drying shrinkage of mortar was significant. The mortar samples containing nano-SiO_2 experienced higher values of drying shrinkage compared to reference mortars. This effect was more prominent for larger amounts of nano-SiO_2.
3. The absorption characteristics which indirectly reflect the porosity showed that nano-SiO_2 particles decreased the water absorption of cement composites by

pore filling and pozzolanic effects. Also it was observed that nano-SiO_2 particles were more effective in the reduction of permeability than that of SF.

REFERENCES

1. SERDAR A., HALIT Y., BULENT B., High temperature resistance of normal strength and autoclaved high strength mortars incorporated polypropylene and steel fibers, Construction and Building Materials, 2008, 22, 504-512.
2. Toutanji H., Mcneil S., Bayasi Z., Chloride permeability and impact resistance of polypropylene-fiber-reinforced silica fume concrete, Cement and Concrete Research, 1998, 28(7), 961-968.
3. Dotto J.M.R., Deabreu A.G., Dalmolin D.C.C., Muller I.L., Influence of silica fume addition on concretes physical properties and on corrosion behaviour of reinforcement bars, Cement and Concrete Composites, 2004, 26, 31-39.
4. Anderson D., Roy A., Seals R.K., Cartledge F.K., Akhter H., Jones S.C., A preliminary assessment of the use of an amorphous silica residual as a supplementary cementing material, Cement and Concrete Research, 2000, 30, 437-445.
5. Qing Y., Zenan Z., Deyu K., Rong S.C., Influence of nano-SiO_2 addition on properties of hardened cement paste as compared with silica fume, Construction and Building Materials 2007, 21, 539-545.
6. Jo B.W., Kim C.H., Tae G.H., Park J.B., Characteristics of cement mortar with nano-SiO_2 particles, Construction and Building Materials, 2007, 21, 1351-1355.
7. LI H., Zhang M.H., OU J.P., Abrasion resistance of concrete containing nano-particles for pavement, Wear, 2006,260, 1262-1266.
8. Li Gengying, Properties of high-volume fly ash concrete incorporating nano-$SiO_{2,}$ Cement and Concrete Research, 2004, 34, 1043-1049.
9. Lin K.L., Chang W.C., Lin D.F., Luo H.L, Tsai M.C., Effects of nano-SiO_2 and different ash particle sizes on sludge ash–cement mortar, Journal of Environmental Management doi:10.1016./j.jenvman.2007.03.036(2007).
10. LI H., Xiao H.G., Yuan J., OU J.P., Microstructure of cement mortar with nano-particles, Composite part B, 2004, 35(B), 185-189.
11. ASTM C-109, Standard test method for compressive strength of hydraulic cement mortars, Annual book of ASTM standards, 2000, 4.01, 84-89.
12. ASTM C-348, Standard test method for flexural strength of hydraulic cement mortar. Annual book of ASTM standards, 2000, 4.01, 221-226.
13. Li H., Xiao H.G., OU J.P., A study on mechanical and pressure-sensitive properties of cement mortar with nanophase materials, Cement and Concrete Research, 2004, 34, 435-438.
14. Shih J.Y., Chang T.P., Hsiao T.C., Effect of nanosilica on characterization of Portland cement composite, Materials Science and Engineering, 2006, 424(A), 266-274.
15. Yue L., Shuguang H., The microstructure of the interfacial transition zone between steel and cement paste, Cement and Concrete Research, 2001, 31, 385-388.

16. Rao G.A., Investigations on the performance of silica fume-incorporated cement pastes and mortars, Cement and Concrete Research, 2003, 33, 1765-1770.
17. Isaia G.C., Gastaldini A.L.G., Moraes R., Physical and pozzolanic action of mineral addition on the mechanical strength of high-performance concrete, Cement and Concrete Research, 2003, 25, 69-76.
18. Zelic J., Rusic D., Veza D., Krstulovic R., The role of silica fume in the kinetics and mechanisms during the early stage of cement hydration, Cement and Concrete Research, 2000, 30, 1655-1662.
19. RAO G.A., Long-term drying shrinkage of mortar-influence of silica fume and size of fine aggregate, Cement and Concrete Research, 2001, 31, 171-175.
20. RAO G.A., Influence of silica fume replacement of cement on expansion and drying shrinkage, Cement and Concrete Research, 1998, 28, 1505-1509.
21. Toutanji H., Properties of polypropylene fiber reinforced silica fume expansive-cement concrete, Construction and Building Materials, 1999, 13, 171-177.
22. Melo Neto A.A., Cincotto A.M., Repette W., Drying and autogenous shrinkage of pastes and mortars with activated slag cement, Cement and Concrete Research, 2008, 38, 565-574.
23. BABU K.G., BABU D.S., Performance of fly ash concrete containing lightweight EPS aggregates, Cement and Concrete Composites, 2004, 26, 605-611.
24. JI T., Preliminary study on the water permeability and microstructure of concrete incorporating nano-SiO_2, Cement and Concrete Research, 2005, 35, 1943-1947.
25. Benachour Y., Davy C.A., Skoczylas F., Houari H., Effect of high calcite filler addition upon microstructural, mechanical Shrinkage and transport properties of a mortar, Cement and Concrete Research, 2008, 38, 727-736.

CD11-002

EFFECT OF POLYPROPYLENE FIBERS ON MECHANICAL AND PHYSICAL PROPERTIES OF MORTARS CONTAINING NANO-SIO_2

A. Sadrmomtazi[1], A. Fasihi[2], A.K. Haghi[3]
[1]Assistant Professor, Dept. of Civil Engg, Faculty of Engg, University of Guilan, Rasht, Iran
[2]M.S. Student, Dept. of Civil Engg, Faculty of Engg, University of Guilan, Rasht, Iran
[3]Professor, Dept of Textile Engg, Faculty of Engg, University of Guilan, Rasht, Iran

ABSTRACT
It has been demonstrated that the fiber-matrix bond strongly affects the ability of fibers to stabilize crack propagation in the matrix. As the bond between fiber and matrix is mainly mechanical, it seems that incorporating nano-SiO_2 (NS) into fiber reinforced cement composites provides better bond with matrix through pore refinement and better distribution of the hydrated products. Hence in this paper an effort was made to study the effect of polypropylene (PP) fibers on mechanical properties and shrinkage of mortar incorporating NS. Three fiber volume fractions, 0.1%, 0.3% and 0.5% were considered. Compressive and flexural strength, water absorption and shrinkage of mortars were reported. Results showed that NS improved mechanical and water absorption characteristics of mortars significantly. It has been observed that the addition of NS fairly enhanced the fibers effectiveness in improving the mechanical strength of mortars.

Keywords: mortar, nano-SiO_2, compressive strength, flexural strength, shrinkage

1. INTRODUCTION
Nano-particles possess unique physical and chemical properties that can improve the function and properties of many types of materials. Among the nano-particles, nano silica have been used to improve the properties of cement based materials and some efforts on excellent mechanical properties and microstructure of cement composite with NS have been also reported. Studies have shown that application of NS into the production of mortar and concrete can lead to improvement in compressive strength, flexural behavior and abrasion resistance [1-4]. Therefore NS can be applied in production of high performance concrete (HPC) which has been gradually replacing normal strength concrete. As the rate of pozzolanic reaction is proportional to the amount of surface available for reaction and owing to the high specific surface of nano particles, they possess high pozzolanic activity that consume calcium hydroxide (CH) which arrays in the interfacial transition zone between hardened cement paste and aggregates and produce hydrated calcium silicate (CSH) which enhances the strength of cement paste [5]. In addition, due to nano scale size of particles, NS can fill the ultra fine pores in cement matrix. This physical effect of the finer grains leads to reduction in porosity of transition zone in

the fresh concrete. This mechanism strengthens the bond between the matrix and the aggregates and improves the cement microstructure and properties. Furthermore, it has been found that when the small particles of NS uniformly disperse in the paste due to their high activity, they generate a large number of nucleation sites for the precipitation of the hydration products which accelerates cement hydration [6].

Polypropylene fibers have been widely used for the reinforcement of cementitious materials to improve the toughness and energy absorption capability of matrix [7]. They were found to be extremely effective in reducing free plastic shrinkage, in retarding first crack appearance and in controlling crack development [8]. Although effectiveness of PP fibers in shrinkage cracking, impact resistance and ductility of cement matrices has been proved by many researchers, effect of PP fibers on compressive and flexural strength is not quit clear [9]. Studies have shown that there can be little or no chemical adhesion between the fiber and matrix as a result of their chemical inertness [10]. It seems that smooth surface of PP fibers intensifies this effect. Moreover, it has been suggested that the presence of PP fibers in cement paste results in the formation of a water film at the interface of fiber and matrix called wall effect. Due to greater mobility of calcium ions in a water environment, portlandite (calcium hydroxide) macro crystals can easily grow and make the transition zone more pores [11]. This phenomenon has a negative impact on the bond between fiber and matrix. It is clear that in order to utilize the maximum strength of the fiber and improve the composite properties, it is essential to enhance the interfacial bond of pp fibers. It seems that the physical and chemical effects of nano particles can be useful in reduction of wall effect between fiber and matrix. Accordingly, present study focuses on the effect of NS on mechanical and physical properties of fiber reinforced cement composite mortar.

2. EXPERIMENTAL PROCEDURE

Materials and mix proportions: The cement used in all mortar mixes was ordinary Portland cement which corresponds to ASTM type 1. The chemical analysis of Portland cement is shown in Table 1. NS in liquid form with the average particles size of 50 nm was used in this study. In order to achieve desire fluidity and better dispersion of nano particles, a polycarboxylate ether based superplastisizer was utilized. The content of superplastisizer was adjusted for each mixture to keep constant the fluidity of mortars. Ottawa sand conforming to ASTM-C778 [12] was used for mortar preparation. Table 2 reveals the physical properties of PP fibers. All specimens were fabricated with the water/binder and sand/binder ratios of 0.5 and 2.75 respectively. The weight of binder was considered equal to the sum of the weight of cement and NS.

In the initial stage of the present study a total of 6 batches of mortars were prepared to find the optimum amount of NS in ordinary cement mortar (Table 3). According to the initial stage results, in the second stage 0.1%, 0.3%, and 0.5% PP fiber (Compared with the total mortar volume) were added to the ordinary and the optimum mixtures selected in the initial stage with the purpose of evaluating the influence of the PP fibers on the strength and shrinkage properties (Table 4). In all the tests, specimens without fiber were considered reference materials.

Table 6: Chemical compositions of cement

Items	Chemical compositions (%)
SiO_2	21.5
AL_2O_3	3.68
Fe_2O_3	2.76
CaO	61.5
MgO	4.8
SO_3	-
L.O.I	1.35

Table 2: Properties of polypropylene fiber

Property	Polypropylene
Unit weight (gr/cm^3)	0.9-0.91
Reaction with water	Hydrophobic
Tensile strength (MPa)	300-400
Elongation at break (%)	100-600
Melting point	175
Thermal conductivity (W/m/K)	0.12
Length (mm)	6

Test method: In order to achieve desire properties, it is essential to disperse NS and PP fibers uniformly. Accordingly, mixing was carried out in a rotary mixer as follows:

1. The NS particles were stirred with 90% of mixing water at high speed and for about 1 min.
2. The specified amount of fiber was added and mixed for 2 min at medium speed.
3. The cement was added and the mixer was allowed to run for 1 min at medium speed.
4. The sand was gradually added at 30s while the mixer was running at medium speed.
5. The superplastisizer and remaining water were added and stirred at high speed for 30s.
6. The mixture was allowed to rest for 90s. Then mixing was continued for 2 min at high speed.

Fresh mortar was cast into 50×50×50 mm cubes for compressive and water absorption tests and 50×50×200 steel molds for flexural and shrinkage tests. The specimens were tamped using a hard mallet to decrease the amount of the air bulbs. After the feeding operation, each of the specimens was allowed to stand for 24 h. Then the specimens were demolded and kept in water at 23±3 $^{\circ C}$ until they were tested.

Compressive strength test was conducted in accordance with ASTM-C109 [13] using a hydraulic testing machine under load control at 1350N/s. The three-point (i.e. center-point) loading flexural test was carried out with the span of 180mm and at a loading rate of 44N/s. The flexural and compressive strength were determined at 7, 28, 60 and 90 days of curing. Shrinkage test samples were cured in the laboratory environment at 27±3 ℃. Changes in the length of the mortar samples were measured using a length comparator with the precision of 0.002mm. The first measurement was taken after 24h of mixing, while the rest of the measurements were taken at the ages of 3, 7, 14, 21, 28, 35 and 42 days. The water absorption test was carried out at 28 days as follows: Saturated surface dry specimens were kept in an oven at 110℃ for 72 h. After measuring the initial weight, specimens were immersed in water for 72h. Then the final weight was measured and the final absorption was reported to assess the mortar permeability.

Table 3: Mix proportion of the specimens (initial stage)

Batch No	Sand/Binder	Water/Binder	% Content (by weight)	
			O.P.C.	N.S.
NS0	2.75	0.5	100	0
NS1	2.75	0.5	99	1
NS3	2.75	0.5	97	3
NS5	2.75	0.5	95	5
NS7	2.75	0.5	93	7
NS9	2.75	0.5	91	9

Table 4: Mix proportion of the specimens (second stage)

No	S^a/B^b	W^c/B^b	%Content(by weight)		%PP (Vol)	No	S^a/B^b	W^c/B^b	% Content (by weight)		%PP (Vol)
			O.P.C	N.S					O.P.C	N.S	
1	2.75	0.5	100	-	0	5	2.75	0.5	100	-	0.3
2	2.75	0.5	93	7	0	6	2.75	0.5	93	7	0.3
3	2.75	0.5	100	-	0.1	7	2.75	0.5	100	-	0.5
4	2.75	0.5	93	7	0.1	8	2.75	0.5	93	7	0.5

a: Sand b: Binder (Cement +Nano-SiO_2) c: Water

3. EXPERIMENTAL INVESTIGATION AND RESULTS

Compressive strength: The compressive strength of cement mortars with different dosages of NS at four ages are given in figure 1. It is clear that the compressive strength of ordinary cement mortar increases with an increase in the amount of NS. It can be seen that increasing the NS content from 7% to 9% didn’t improve the compressive strength significantly. It seems that a large amount of NS even decreases the strength. According to Hui Li [14] homogeneous hydrated microstructure which is essential for the strength of cement matrix can not be formed because nano particles can not be well dispersed. Strength enhancement of NS can be attributed to reduction in the content of $Ca(OH)_2$ which does not have any cementing property and production of hydrated calcium silicate (CSH) that plays a vital role in mechanical characteristics of cement paste [15,16]. NS particles also generate a large number of nucleation sites for the cement hydration products making the paste microstructure more homogenous and improve its strength and permeability [17]. In the view of the results above, cement mortar with substitution of cement by 7% NS was selected as the optimum mixture. Figure 2 shows the compressive strength of fiber reinforced mortars. Results appearing in this Figure indicate that PP fibers induce a slight modification in the compressive strength. The compressive strength of mortar increased gradually at first with the increase of fiber content but then decreased with the further increasing of fiber content. Almost all the specimens containing 0.1% pp fiber by volume exhibited an increase in compressive strength compared to the target specimens. A possible reason for this may be that PP fibers act as crack arresters.

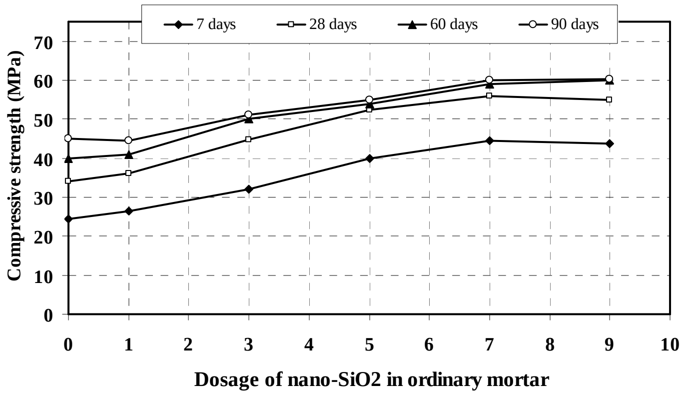

Figure 1. Compressive strength of ordinary mortars at different contents of nano-SiO_2

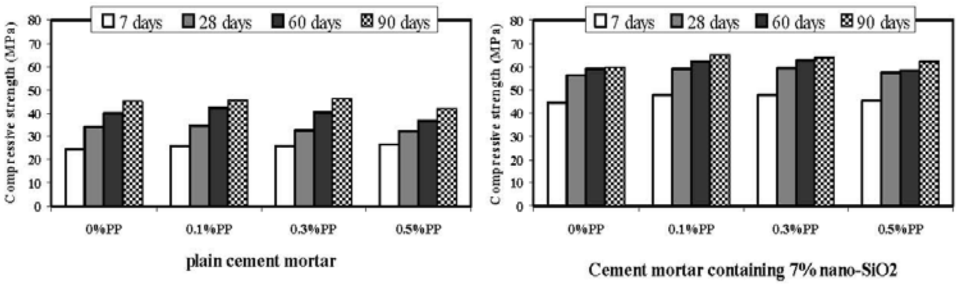

Figure 2. Compressive strength of different mortar mixtures according to the PP content

The uniformly distributed PP fibers reinforce the mortar against disintegration by resisting further opening of initial cracks and disallowing the microcracks from growing into macro cracks [18].

The strength development at 0.1% pp fiber addition varied depending upon the nature of mixtures. The mortar containing 7% NS showed greater average enhancement by 6.49% compared to plain cement mortar by 3.1%. At 0.3% fiber addition, the compressive strength of plain cement mortar decreased contrary to mortar containing 7% NS that still increased. It is obvious that increase in pp dosage beyond 0.3% decreases the compressive strength. This is understandable because large contents of pp fibers are more difficult to disperse uniformly. Therefore fibers form clusters and create more micro-defects in cement matrix which inevitably reduces the compressive strength of mortar.

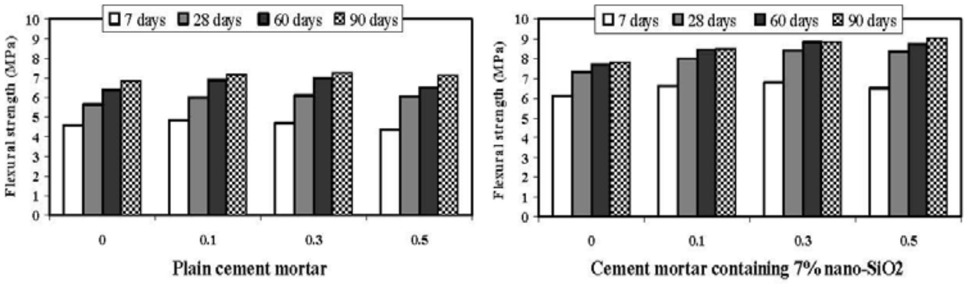

Figure 3. Flexural strength of different mortar mixtures according to the PP content

Flexural strength: The flexural strength of mortar specimens are presented in Figure 3. Comparing the flexural strength of nonfibrous specimens revealed that NS effectively increased the flexural strength of mortar. Results of fiber reinforced specimens showed that the flexural strength in fiber reinforced mortars was slightly higher than that of mortars without fibers. The values of flexural strength of cement composites increased with increasing the fiber content until it reached an optimal amount of 0.3% and then dropped to some lower value at 0.5%, however for mortar containing NS a slight increase of flexural strength was observed beyond 0.3%. It should be noticed that presence of NS in cement matrix improved the effectiveness of fibers in reinforcement of cement mortar. The microstructure of cement paste at the interfacial between fiber and matrix is the most important region influences of the fibers effectiveness. The addition of NS strengthens this weak region through reduction of the internal porosity especially in the transition layer by consumption of porous portlandite crystals which array in the interfacial between fiber and matrix. Therefore, fiber/matrix contact area increases and higher friction can be formed between the two. Typical flexural load deflection response of different mixtures containing 0%, 0.1%, 0.3% and 0.5% PP fibers at 90 days are represented in Figure 4. The test was controlled automatically by computer with a constant cross head movement of 1mm/min. It was found from the figures that for the unreinforced mortar, the materials demonstrated brittle behavior. The samples fully fractured with increase of mid span deflection after peak load while fiber reinforced mortar exhibited some what ductile behavior. A study of the load-deflection graphs showed that mortar containing NS was obviously more brittle than that of plain mortar, however integrating PP fibers somewhat compensated for this shortage. A small effect was noted upon fiber volume fraction of 0.1% and a relatively bigger increase was observed while increasing fiber content to 0.5%. When cracks occur and propagate, fibers are able to bridge across the surface of the cracks and prevent the crack face separation in the tension half of the reinforced beam. The fibers sustain the load until they pullout from the matrix. This mechanism provides an additional energy-absorbing which leads to a stable fracture process and higher fracture energy. The presence of NS enhanced the efficiency of transforming load from matrix to fiber by increasing the friction coefficient between fiber and composite matrix. Hence effect of pp fibers on post-peak resistance was more obvious for mortars containing NS.

Water absorption: The water absorption of specimens is shown in Table 5. A study of the water absorption values of the unreinforced specimens revealed that incorporating NS into cement mortar improved the water absorption properties of the products. The reason for this observation is that the fine particles of pozzolan block the channels connecting capillary pores in cement paste and generate more homogenous distribution of CSH gel resulting in less pore structure and permeable voids [19].

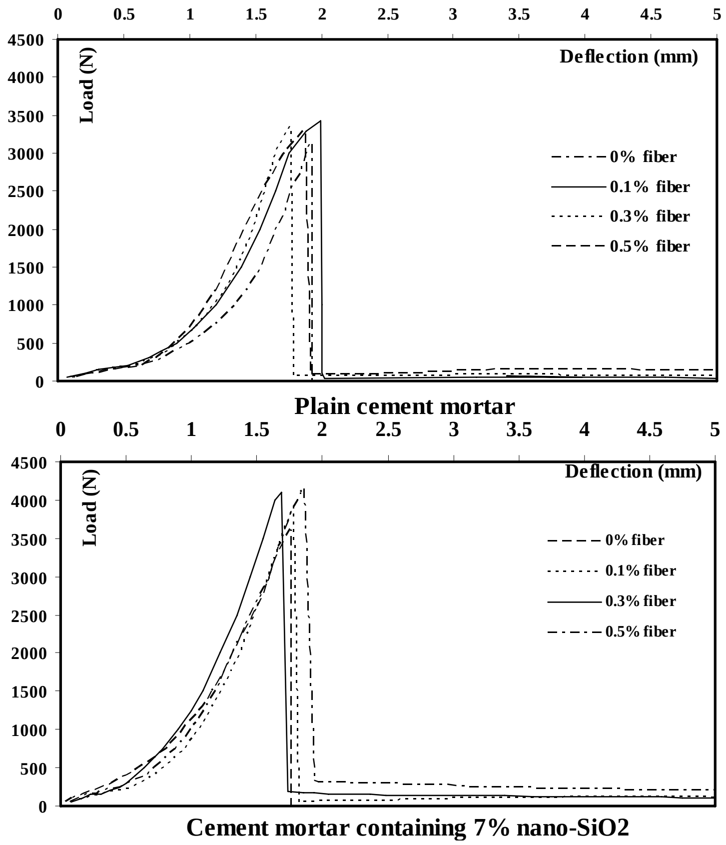

Figure 4. Flexural behavior (load-deflection) of different mixtures

Adding PP fibers changed the water absorption properties. The water absorption values of the mixtures decreased at 0.1% fiber content. It was observed that increasing the fiber percentage increased the water absorption of cement mortars. The reason behind this observation could be the poor dispersion of PP fibers in mortar that consequently increases the pore volume of cement matrix, for plain cement mortar water absorption started to rise up at 0.3% fiber content, while in mortars containing NS at 0.5%. This means that presence of NS in cement matrix provided better fiber dispersion. The reason may be due to an increase in the cohesiveness of the cementitious matrix by NS which is beneficial for better dispersion of PP fibers [20].

Table5: Water absorption of different mixes.

Batch No	Absorption (%)	Batch No	Absorption (%)
1	6.120	5	6.45
2	4.230	6	4.187
3	6.040	7	7.091
4	4.204	8	4.211

Shrinkage behavior: The shrinkage behavior of mortars is presented in figures 5and 6. From the results it can be concluded that presence of NS in mortar increased the drying shrinkage apparently. It may be due to self desiccation caused by pore size refinement of NS [21]. Moreover, from the data presented by the previous researchers it is seen that NS particles act as an activator to accelerate cement hydration [22]. Therefore, the autogenous shrinkage related to chemical shrinkage can be increased.

Results of fiber reinforced specimens demonstrated that small amounts of fiber could contribute positively to moderate the length change caused by drying shrinkage. All the mortars reinforced with 0.1% pp fiber, provided better improvement for shrinkage. Obviously, using higher content of PP fibers (beyond 0.3%) did not work for moderating shrinkage strain. At 0.5% PP content, drying shrinkage of all specimens increased even more than reference mortars. More investigations are needed to explain this effect.

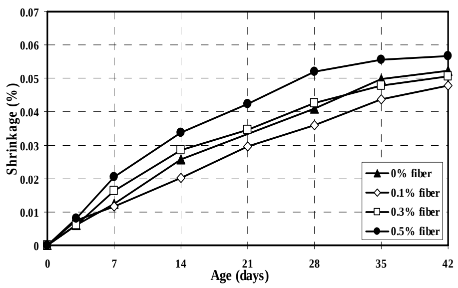

Figure 5. Effect of PP fibers on shrinkage of plain cement mortar

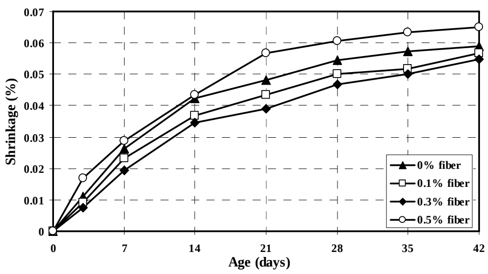

Figure 6. Effect of PP fibers on shrinkage of cement mortar containing 7% nano-SiO_2

4. CONCLUSIONS

A comprehensive experimental investigation was carried out to evaluate the influence of nano-SiO_2 on properties of fiber reinforced cement composite mortars. Based on the test and analysis results the following preliminary conclusions are obtained.

- Utilizing polypropylene fibers in cement matrix caused a slight enhancement in compressive and flexural strength. The contribution of further increase of the fiber content to mechanical strength was not positive. A possible reason for this observation could be the poor dispersion of PP fibers in mortar that increases pore volume and creates more micro defects in cement matrix.
- The fiber reinforced mortar demonstrated higher post-peak flexural strength compared with reference mortars. This effect was more obvious at larger contents of fibers. The effectiveness of the fiber reinforcement on mechanical strength somewhat improved with the incorporation of nano-SiO_2 particles. This can be due to reduction of the internal porosity especially in fiber/matrix transition zone that provides higher contact surface and hence friction between the two.
- Water absorption of ordinary mortar decreased by incorporating nano-SiO_2. Adding small amount of pp fibers resulted in an improvement in water absorption characteristics, however higher amounts of fiber especially in ordinary cement mortar did not have any positive effect.
- Presence of nano-SiO_2 in cement matrix increased the dying shrinkage of mortars. The inclusion of fiber reinforcement within composite cement mortar could moderate this effect. However, utilizing high contents of fiber (beyond 0.3%) didn't have any positive impact on shrinkage strain.

REFERENCES

1. Qing Y., Zenan Z., Deyu K., Rong S.C., Influence of nano-SiO_2 addition on properties of hardened cement paste as compared with silica fume, Construction and Building Materials 2007, 21, 539-545.
2. LI H., Zhang M.H., OU J.P., Abrasion resistance of concrete containing nano-particles for pavement, Wear, 2006,260, 1262-1266.
3. JO B.W., KIM C.H., TAE G.H., PARK J.B., Characteristics of cement mortar with nano-SiO_2 particles, Construction and Building Materials, 2007, 21, 1351-1355.
4. Shih J.Y., Chang T.P., HSIAO T.C., Effect of nanosilica on characterization of Portland cement composite, Materials Science and Engineering, 2006, 424(A), 266-274.
5. Isaia G.C., Gastaldini A.L.G., MORAES R., Physical and pozzolanic action of mineral addition on the mechanical strength of high performance concrete, Cement and Concrete Research, 2003, 25, 69-76.
6. Li H., Xiao H.G., OU J.P., A study on mechanical and pressure-sensitive properties of cement mortar with nano phase materials, Cement and Concrete Research, 2004, 34, 435-438.
7. Sun W., Chen H., Luo X., Qian H., The effect of hybrid fibers and expansive agent on the shrinkage and permeability of high performance concrete, Cement and Concrete Research, 2001, 31,595-601.
8. Toledo Filho R.D., Sanjuan M.A., Effect of low modulus sisal and propylene fibers on the free and restrained shrinkage of mortars at early age, Cement and

Concrete Research, 1999, 29, 1547-1604.
9. Toutanji H.A., Properties of polypropylene fiber reinforced silica fume expansive-cement concrete, Construction and Building Materials, 1999, 13, 171-177.
10. Linfa Y., Pendleton R.L., Jenkins C.H.M., Interface morphologies in polyolefin fiber reinforced concrete composites, Composite Part A, 1998, 29(A), 643-650.
11. Holmer S.J., Vahan A., Transition zone studies of vegetable fiber-cement paste composites, Cement and Concrete Composites, 1999, 21, 49-57.
12. ASTM C-778, Standard specification for standard sand, Annual book of ASTM standards, 2000, 4.01, 360-362.
13. ASTM C-109, Standard test method for compressive strength of hydraulic cement mortars, Annual book of ASTM standards, 2000, 4.01, 84-89.
14. Li H., Xiao H.G., Yuan J., Ou J.P., Microstructure of cement mortar with nano-particles, Composite: part B, 2004, 35(B), 185-189.
15. Gao J.M., Qian C.X., Wang B., Morino K., Experimental study on properties of polymer-modified cement mortars with silica fume, Cement and Concrete Research, 2002, 32, 41-45.
16. RAO G.A., Investigations on the performance of silica fume-incorporated cement pastes and mortars, Cement and Concrete Research 2003, 33, 1765-1770.
17. JI T., Preliminary study on the water permeability and microstructure of concrete incorporating nano-SiO_2, Cement and Concrete Research, 2005, 35, 1943-1947.
18. Song P.S., Hwang S., Sheu B.C., Strength properties of nylon-and polypropylene-fiber reinforced concretes, Cement and Concrete Research, 2005, 35, 1546-1550.
19. Benachour Y., Davy C.A., Skoczylas F., Houari H., Effect of high calcite filler addition upon microstructural, mechanical, Shrinkage and transport properties of a mortar, Cement and Concrete Research, 2008, 38, 727-736.
20. Toutanji H., Mcneil S., BAYASI Z., Chloride permeability and impact resistance of polypropylene-fiber-reinforced silica fume concrete, Cement and Concrete Research, 1998, 28(7), 961-968.
21. RAO G.A., Long-term drying shrinkage of mortar-influence of silica fume and size of fine aggregate, Cement and Concrete Research, 2001, 31, 171-175.
22. Melo Neto A.A., Cincotto A.M., Repette W., Drying and autogenous shrinkage of pastes and mortars with activated slag cement, Cement and Concrete Research, 2008, 38, 565-574.